THE 31TH EUROPEAN MODELING & SIMULATION SYMPOSIUM

SEPTEMBER 18-20, 2019
LISBON, PORTUGAL

EMSS
2019

EDITED BY
MICHAEL AFFENZELLER
AGOSTINO G. BRUZZONE
FRANCESCO LONGO
GUILHERME PEREIRA

PRINTED IN RENDE (CS), ITALY, SEPTEMBER 2019

ISBN 978-88-85741-26-3 (Paperback)
ISBN 978-88-85741-25-6 (PDF)

ISBN 978-88-85741-26-3 (Paperback)
ISBN 978-88-85741-25-6 (PDF)

THE 31TH EUROPEAN MODELING & SIMULATION SYMPOSIUM

SEPTEMBER 18 – 20, 2019

LISBON, PORTUGAL

ORGANIZED BY

DIME – UNIVERSITY OF GENOA

LIOPHANT SIMULATION

SIMULATION TEAM

IMCS – INTERNATIONAL MEDITERRANEAN & LATIN AMERICAN COUNCIL OF SIMULATION

DIMEG, UNIVERSITY OF CALABRIA

MSC-LES, MODELING & SIMULATION CENTER, LABORATORY OF ENTERPRISE SOLUTIONS

HUNGARIAN ACADEMY OF SCIENCES CENTRE FOR ENERGY RESEARCH

AUTONOMOUS UNIVERSITY OF BARCELONA

MODELING AND SIMULATION CENTER OF EXCELLENCE (MSCOE)

LATVIAN SIMULATION CENTER – RIGA TECHNICAL UNIVERSITY

LOGISIM

LSIS – LABORATOIRE DES SCIENCES DE L'INFORMATION ET DES SYSTEMES

MIMOS – MOVIMENTO ITALIANO MODELLAZIONE E SIMULAZIONE

MITIM PERUGIA CENTER – UNIVERSITY OF PERUGIA

BRASILIAN SIMULATION CENTER, LAMCE-COPPE-UFRJ

MITIM - McLeod Institute of Technology and Interoperable Modeling and Simulation – Genoa Center

M&SNet - McLeod Modeling and Simulation Network

Latvian Simulation Society

Ecole Superieure d'Ingenierie en Sciences Appliquees

Facultad de Ciencias Exactas. Ingegneria y Agrimensura

University of La Laguna

CIFASIS: CONICET-UNR-UPCAM

INSTICC - Institute for Systems and Technologies of Information, Control and Communication

National Russian Simulation Society

CEA - IFAC

University of Bordeaux

University of Cyprus

Dutch Benelux Simulation Society

University of Minho

I3M 2019 Industrial Sponsors

CAL-TEK SRL

LIOTECH LTD

MAST SRL

SIM-4-FUTURE

ISBN 978-88-85741-25-6; Affenzeller, Bruzzone, Longo and Pereira Eds.

I3M 2019 Media Partners

Inderscience Publishers – International Journal of Simulation and Process Modeling

Inderscience Publishers – International Journal of Service and Computing Oriented Manufacturing

IGI Global – International Journal of Privacy and Health Information Management (IJPHIM)

Halldale Media Group: The Military Simulation and Training Magazine

Halldale Media Group: The Journal for Healthcare Education, Simulation and Training

SAGE
Simulation Transaction of SCS

De Gruyter
International Journal of Food Engineering

MDPI - Sustainability

Euromerci: The Italian Monthly Logistics Journal

EDITORS

MICHAEL AFFENZELLER
UNIVERSITY OF APPLIED SCIENCES, AUSTRIA
Michael.Affenzeller@fh-hagenberg.at

AGOSTINO G. BRUZZONE
MITIM-DIME, UNIVERSITY OF GENOA, ITALY
agostino@itim.unige.it

FRANCESCO LONGO
DIMEG, UNIVERSITY OF CALABRIA, ITALY
f.longo@unical.it

GUILHERME A. B. PEREIRA
UNIVERSITY OF MINHO, PORTUGAL
gui@dps.uminho.pt

THE INTERNATIONAL MULTIDISCIPLINARY MODELING AND SIMULATION MULTICONFERENCE, I3M 2019

GENERAL CO-CHAIRS

AGOSTINO G. BRUZZONE, *DIME, UNIVERSITY OF GENOA, ITALY*
MIQUEL ANGEL PIERA, *AUTONOMOUS UNIVERSITY OF BARCELONA, SPAIN*

PROGRAM CO-CHAIRS

FRANCESCO LONGO, *DIMEG, UNIVERSITY OF CALABRIA, ITALY*
YURY MERKURYEV, *RIGA TECHNICAL UNIVERSITY, LATVIA*

THE 31TH EUROPEAN MODELING & SIMULATION SYMPOSIUM, EMSS 2019

GENERAL CO-CHAIRS

FRANCESCO LONGO, *DIMEG, UNIVERSITY OF CALABRIA, ITALY*
GUILHERME PEREIRA, *UNIVERSITY OF MINHO, PORTUGAL*

PROGRAM CHAIR

MICHAEL AFFENZELLER, *UPPER AUSTRIA UNIVERSITY OF APPLIED SCIENCES, AUSTRIA*

ISBN 978-88-85741-25-6; Affenzeller, Bruzzone, Longo and Pereira Eds.

EMSS 2019 INTERNATIONAL PROGRAM COMMITTEE

Tracks and Workshop Chairs

Advanced in Discrete and Distributed Simulation
Chairs: Thomas Wiedemann, HTW Dresden FB Informatik, Germany; Gasper Music, University of Ljubljana, Slovenia

Industrial Processes Modeling & Simulation
Chair: Agostino G. Bruzzone, DIME, University of Genoa, Italy

Industrial Engineering
Chair: Francesco Longo, MSC-LES, University of Calabria, Italy

Agent Directed Simulation (ADS)
Chairs: Yu Zhang, Trinity University (USA); Tuncer Ören, University of Ottawa, Canada

Petri Nets based Modelling & Simulation
Chairs: Emilio Jiménez, University of La Rioja, Spain; Juan Ignacio Latorre, Public University of Navarre, Spain

Workshop on Cloud Manufacturing
Chairs: Prof. Lin Zhang, Beihang University, China; Prof. Fei Tao, Beihang University, China;

Simulation Optimization Approaches in Industry, Aviation, Services and Transport
Chairs: Idalia Flores, University of Mexico; Miguel Mújica Mota, Amsterdam University of Applied Sciences, Netherlands

Human-Centred and Human-Focused Modelling and Simulation
Chairs: Agostino G. Bruzzone, DIME, University of Genoa, Italy; Peer Olaf Siebers, University of Nottingham, UK

Workshop on Soft Computing and Modelling & Simulation
Chairs: Michael Affenzeller, Upper Austrian University of Applied Sciences, Austria; Witold Jacak, Upper Austrian University of Applied Sciences, Austria; Stefan Wagner, Upper Austrian University of Applied Sciences (Austria);

Workshop on Cloud Computing
Chair: Chunming Rong, University of Stavanger, Norway

Advanced Simulation for Logistics Systems
Chairs: Maria Pia Fanti, Polytechnic of Bari, Italy; Chrysostomos Stylios, Technological Educational Institute of Epirus, Greece; Walter Ukovich, University of Trieste, Italy

Modelling and Simulation Approaches in and for Education
Chairs: Maja Atanasijevic-Kunc, Univ. Ljubljana, Slovenia; Andreas Körner, Vienna Univ. of Technology, Austria

Modelling and Simulation in Physiology and Medicine (common track EMSS-IWISH)
Chairs: Maja Atanasijevic-Kunc, Univ. Ljubljana, Slovenia; Felix Breitenecker, Vienna Univ. of Technology, Austria

Retail-Oriented Simulation
Chair: Eleonora Pantano, Middlesex University, UK

Computer Simulation for Security
Chairs: Edgar Alonso Lopez-Rojas, Blekinge Institute of Technology, Sweden, Joni A. Amorim, University of Skövde Sweden; Richard Zaluski, Center for Strategic Cyberspace + Security Science, UK

Workshop on Model Engineering for System of Systems
Chairs: Lin Zhang, Beihang University, China; Prof. Bernard P. Zeigler, RTSync Corp, USA; Valdemar Vicente Graciano Neto, Federal University of Goiás, Brazil

Modelling, Computer Simulation and Visualisation of Heritage
Chairs: Galina Merkuryeva, Riga Technical University; Ricardo Gonçalves, Universidade Nova de Lisboa (UNINOVA), Portugal

Modeling and Simulation in Photonics Science and Industrial Technologies
Chairs: Alexander S. Sigov, Moscow Technological University (MIREA), (Moscow, Russian Federation); Mikhail E. Belkin, Moscow State Technological University (MIREA), (Moscow, Russian Federation)

Chairs' Message

Welcome To EMSS 2019!

On behalf of the EMSS 2019 organizing committee we are honored to welcome you to the 31st edition of the European Modelling & Simulation Symposium that takes place in the wonderful city of Lisbon.

Here the natural and historical-monumental beauty permeating the area provides a breathtaking setting for a rich technical program that is meant to provide great opportunities in terms of ideas, applications methodologies and approaches.

In the wake of previous editions, EMSS remains a well-recognized and relevant appointment for the academic community as well as for researchers, engineers and professionals from all over the world. Thanks to such a plethora of contributors EMSS confirms along the years a great impact on research and development in a variety of industrial fields starting from Industry 4.0 paradigms to end up with Transportation, Logistics, Advanced Physics Technologies, Economics and Finance.

The technical program boasts considerable achievements in the area of Simulation, Artificial Intelligence, Optimization, Complex Systems Theory and Applications, Network analysis, Manufacturing and Process Engineering to cite a few. This way EMSS continues to be a unique opportunity for to share ideas, experiences, establish and reinforce relations as well as fruitful collaborations.

So let's thank the many people who made this possible: the authors for their valuable works, the Program Committee for their thorough and timely reviewing of the papers, the sponsors and the Local Organizing Committee members who have all worked extremely hard.

Wishing a memorable event in the appealing and vibrant setting of Lisbon, we are really proud to welcome all of you.

Michael Affenzeller
University of Applied Sciences Upper Austria, Austria

Francesco Longo
DIMEG, University of Calabria, Italy

Guilherme Pereira
University of Minho, Portugal

ISBN 978-88-85741-25-6; Affenzeller, Bruzzone, Longo and Pereira Eds.

ACKNOWLEDGEMENTS

The EMSS 2019 International Program Committee (IPC) has selected the papers for the Conference among many submissions; therefore, based on this effort, a very successful event is expected. The EMSS 2019 IPC would like to thank all the authors as well as the reviewers for their invaluable work.
A special thank goes to all the organizations, institutions and societies that have supported and technically sponsored the event.

I3M 2019 INTERNAL STAFF

AGOSTINO G. BRUZZONE, *DIME, UNIVERSITY OF GENOA, ITALY*
ALESSANDRO CHIURCO, *CAL-TEK SRL, ITALY*
JESSICA FRANGELLA, *DIMEG, UNIVERSITY OF CALABRIA, ITALY*
CATERINA FUSTO, *DIMEG, UNIVERSITY OF CALABRIA, ITALY*
LUCIA GAZZANEO, *DIMEG, UNIVERSITY OF CALABRIA, ITALY*
FRANCESCO LONGO, *DIMEG, UNIVERSITY OF CALABRIA, ITALY*
MARINA MASSEI, *DIME, UNIVERSITY OF GENOA, ITALY*
LETIZIA NICOLETTI, *CAL-TEK SRL, ITALY*
ANTONIO PADOVANO, *DIMEG, UNIVERSITY OF CALABRIA, ITALY*
CATALDO RUSSO, *CAL-TEK SRL, ITALY*
KIRILL SINELSHCHIKOV, *SIMULATION TEAM, ITALY*
MARCO VETRANO, *CAL-TEK SRL, ITALY*

This International Workshop is part of the I3M Multiconference: the Congress leading **Simulation around the World and Along the Years**

Index

REPRESENTATION OF A CONVOLUTIONAL NEURONAL NETWORK AS A HIGH LEVEL PARALEL COMPOSITION APPLIED TO THE RECOGNITION OF DNA SEQUENCES

M. Rossainz-López[a], S. Zúñiga-Herrera[a], M. Capel-Tuñón[b], I. Pineda-Torres[a]

[a] Faculty of Computer Science, Autonomous University of Puebla, San Claudio Avenue and South 14th Street, San Manuel, Puebla, Puebla, 72000, México
[b] Software Engineering Department, College of Informatics and Telecommunications ETSIIT, University of Granada, Daniel Saucedo Aranda s/n, Granada 18071, Spain

[a]rossainz@cs.buap.mx, [a]sarahi.zuhe@gmail.com, [b]manuelcapel@ugr.es, [a]ipineda@cs.buap.mx

ABSTRACT
This work proposes the use of Structured Parallel Programming using the process communication pattern called Pipeline in its version of High-Level Parallel Composition (HLPC) to implement a process composition that represents a convolutional neuronal network or CNN and that is used to solve a specific problem of DNA sequences. The HLPC Pipeline-CNN is then shown, which represents the implementation of a convolutional neural network making use of the three types of parallel objects that make up an HLPC: A manager object, one or more stage objects and a collector object. The manager object represents the HLPC itself and makes an encapsulated abstraction out of it that hides the internal structure, the stage objects are objects of a specific purpose, in charge of encapsulating an client-server type interface that settles down between the manager and the slave-objects and the collector object that is an object in charge of storing the results received from the stage objects to which is connected. To show the usefulness and performance of the HLPC Pipeline-CNN implemented, it was used in the recognition of DNA sequences from a database with 4 types of hepatitis C virus (type 1, 2, 3 and 6). The results of this classification were obtained in terms of percentages of training precision and validation precision, as well as performance results in terms of speedup from 1000 to 4000 training steps with 2, 4, 8, 16 and 32 exclusive processors in one parallel machine of up to 64 processors with shared-distributed memory.

Keywords: High Level Parallel Compositions, HLPC, Convolutional Neuronal Network, CNN, Deep Learning Transfer, DNA Sequences, Parallel Objects, Structured Parallel Programming.

1. INTRODUCTION
The convolutional neural networks (CNN) are like multichannel neural networks, its main advantage is that each part of the network is trained to perform a task, this significantly reduces the number of hidden layers, so training is faster (Calvo 2015). The convolutional neural networks are very powerful for everything that has to do with the image analysis. However, its use is not only restricted to image analysis, it can also be applied to the speech recognition, or to the classification of sentences, with the necessary transformations regarding the type of the input data (Calvo 2015, Vizcayab2018). A convolutional neuronal network is a multilayer network consisting of alternating convolutional and reduction layers, like a pipeline architecture (Calvo 2015). In the convolution, operations of products and sums are carried out between the starting layer and the n filters that a characteristic map (matrix) generates. The extracted characteristics correspond to each possible location of the filter in the original image. The advantage is that the same filter (neuron) serves to extract the same characteristic in any part of the input, with this it is possible to reduce the number of connections and the number of parameters to train in comparison with a multilayer network of total connection (Calvo 2015, Vizcayab2018). In the reduction the number of parameters is reduced by staying with the most common characteristics. The last layer of this network is a sorting layer that will have as many neurons as the number of classes to predict. However, one of the disadvantages of neural networks is the large amount of time needed for training. A direct way to reduce this time is to parallelize the learning algorithms. However, algorithms cannot always be parallelized in a simple way, and in addition, the amount of communication between processors or processes means that most parallel versions of these algorithms can only be executed properly in parallel computers. That is why, in this work, we propose a parallelization of a convolutional neural network under the model of High-Level Parallel Compositions or HLPC as an original and useful proposal to obtain a good performance in the use of a CNN within a concrete problem. HLPC are parallel patterns defined and logically structured that, once identified in terms of their components and of their communication, can be adopted in the practice and be available as high-level abstractions in user applications within an OO-programming environment (Brinch Hansen 1993). The process interconnection structures of parallel execution patterns such as trees can be built using HLPCs, within the work environment of POs that is the one used to detail the structure of a HLPC implementation (Corradi and Leonardi 1991). A structured approach to parallel programming is based on the use of communication/interaction patterns which are predefined structures of user's application processes (Wilkinson and Allen 1999). In such a situation, the

structured parallelism approach provides the interaction-pattern abstraction and describes applications through HLPCs, which are able to implement the pattern mentioned already (Darlington 1993). The encapsulation of a HLPC should follow the modularity principle and it should provide a base to obtain an effective reusability of the parallel behavior to be implemented. When there is the possibility of attaining this, a generic parallel pattern is built, which in its turn provides a possible implementation of the interaction structure between processes of the application, independently of the functionality of these processes. Several significant and reusable parallel patterns of interconnection can be identified in multiple applications and parallel algorithms (Roosta and Séller 1999) which has resulted in a wide library of communication patterns between concurrent processes such as HLPCs whose details are found in (Rossainz and Capel 2008; Rossainz and Capel 2014). In the present work we propose the implementation of HLPC Pipeline-CNN which represents a convolutional neural network using deep learning transfer, as a learning strategy for the neural network and it was used for the recognition of DNA sequences from a database with 4 types of hepatitis C virus (type 1, 2, 3 and 6) taken from the repository available on the ViPR page (https://www.viprbrc.org/brc/home.spg?decorator=vipr) The set of DNA sequences used is the Molecular database (Splice-junction Gene Sequences) Data Set that has 3190 sequences, available on the UCI page (https://archive.ics.uci.edu/ml/index.php), with three classes of sequences: limit exon-intron, limit intronexon and any. For the use of the DNA sequences a representation method was designed where each nitrogenous base is represented in gray scale to form an image. The generated images were used to train the convolutional neuronal network HLCP Pipeline-CNN. The results are shown both of the classification carried out by the HLPC Pipeline-CNN in terms of training precision and validation precision, as well as of parallel performance in its execution obtaining measurements of the law of Amdahl and speedup in a parallel computer with 32 exclusive CPU-SET.

2. DEFINITION OF HIGH-LEVEL PARALLEL COMPOSITIONS (HLPC)

Using an OO-programming environment, the basic idea is implementing any type of parallel communication patterns between the processes of an application or distributed/parallel algorithm. A HLPC comes from the composition of a set three object types: the manager object, the stage objects and the collector object. The object manager (Figure 1) represents the HLPC itself and makes an encapsulated abstraction out of it that hides the internal structure (Rossainz 2005). The object manager controls a set of objects references, which address the object collector and several stage objects and represent the HLPC components whose parallel execution is coordinated by the object manager. The objects stage are objects of a specific purpose, in charge of encapsulating a client-server type interface that settles down between the manager and the slave-objects. The collector object can see an object in charge of storing the results received from the stage objects to which is connected, in parallel with other objects of HLPC composition. During a service request the control flow within the stages of a HLPC depends on the implemented communication pattern. Manager, collector and stages are included in the definition of a PO (Corradi, Leonardo and Zambonelli 1995). POs are active objects, which have intrinsic execution capability. Applications that deploy the PO pattern can exploit the inter-object parallelism as much as the intra-object parallelism (Bacci, Danelutto, Pelagatti, and Vaneschi 1999; Danelutto and Torquati 2014). A PO-instance object has a similar structure to that of an object in C++, and additionally defines a scheduling policy that specifies the way in which one or more operations carried out by the instance synchronize (Danelutto and Torquati 2014). The communication modes used are: The synchronous communication, the asynchronous communication and the asynchronous future (Birrell 1989; Lavander and Kafura 1995). The Synchronization policies are expressed in terms of restrictions; for instance, mutual exclusion in reader/writer processes or the maximum parallelism allowed for writer processes (Andrews 2000).

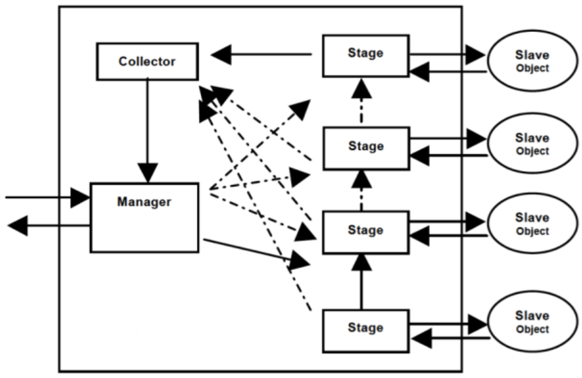

Figure 1: Internal structure of HLPC

The Figure 1 shows the pattern HLPC without defining any explicit parallel communication pattern. The box that includes the components, represents the encapsulated HLPC, internal boxes represent compound objects (collector, manager and objects stages), as long as the circles are the objects slaves associated to the stages. The continuous lines within the HLPC suppose that at least a connection should exist between the manager and some of the component stages. Same thing happens between the stages and the collector. The dotted lines mean more than one connection among components of the HLPC.

2.1. Construction of Communication Patterns between Processes as HLPC

Currently there is a class library that provides the programmer with the three communication patterns between processes most commonly used as HLPC: The

process farm, the process pipeline and the process tree (initially binary process trees), (Liwu 2002). Figure 2, Figure 3 and Figure 4 show the farm, pipeline and tree models as High-Level Parallel Compositions or HLPC.
These models are abstract. The programmer must adapt them to the problem he is trying to solve by making use of the properties of the paradigm of object orientation such as inheritance or polymorphism. The implementation details can be found in (Rossainz and Capel 2008). The structure of the library is shown in the class diagram of Figure 5. The details are in (Rossainz and Capel 2014).

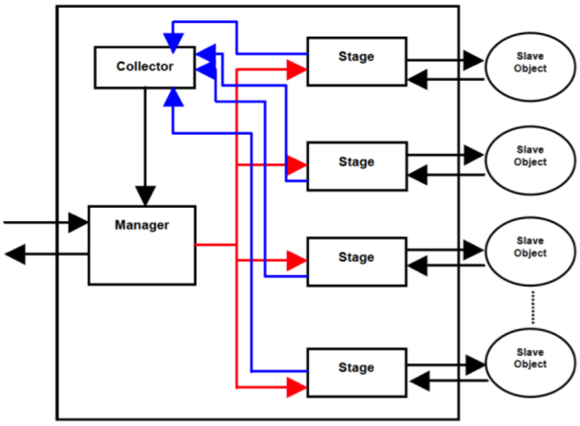

Figure 2: The HLPC of a Farm

With the proposed library it is possible to build concrete HLPCs. To build an HLPC, first it should have made clear the parallel behavior that the user application needs to implement, so that the HLPC becomes this pattern itself. Once identified the parallel behavior, the second step consists of elaborating a graph of its representation. This practice is also good for illustrating the general characteristics of the desired system and will allow us to define its representation with HLPCs later, by following the pattern proposed. When the model of a HLPC has already been made clear, it defines a specific parallel pattern; let's say, for example, a tree, or some other mentioned pattern, and then the following step will be to do its syntactic definition and specify its semantics (Liwu 2002).

Finally, the syntactic definition prior to any programmed HLPC is transformed into the most appropriate programming environment, with the objective of producing its parallel implementation.
The HLPC models of figures 2, 3 and 4 have been used to adapt them and generate farms, pipeline and particular trees, of problems that have been solved with this proposal such as: ordering, search and optimization problems, NP-Complete problems like that of the Traveling Agent, simulation problems such as the movement and attraction of particles in space and more recently with problems that have to do with finding DNA sequences in the construction of GNOMAS.

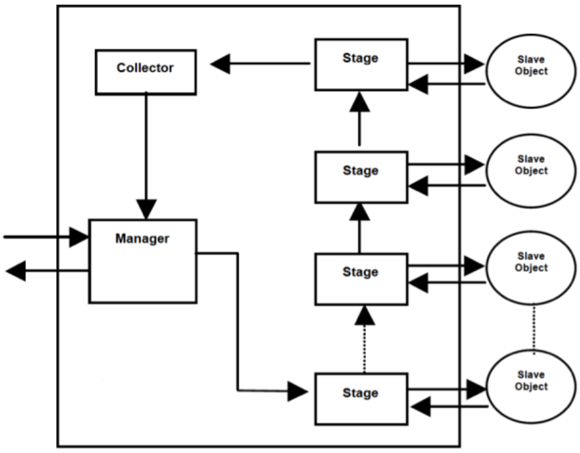

Figure 3: The HLPC of a Pipeline

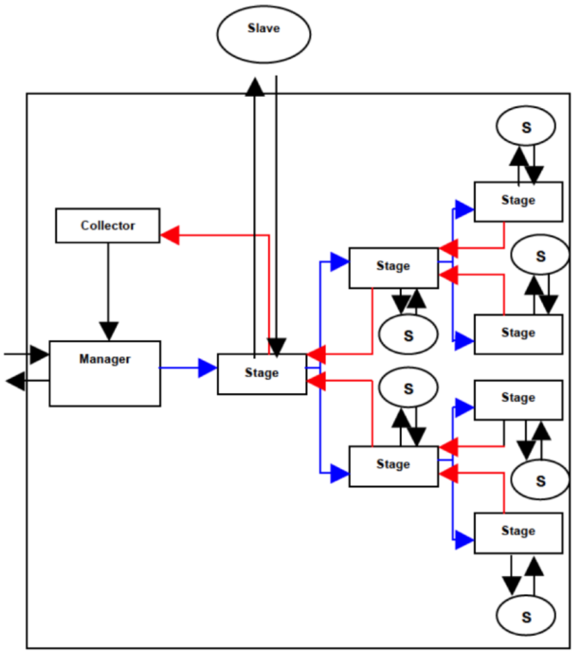

Figure 4: The HLPC of a Tree-Divide & Conquer

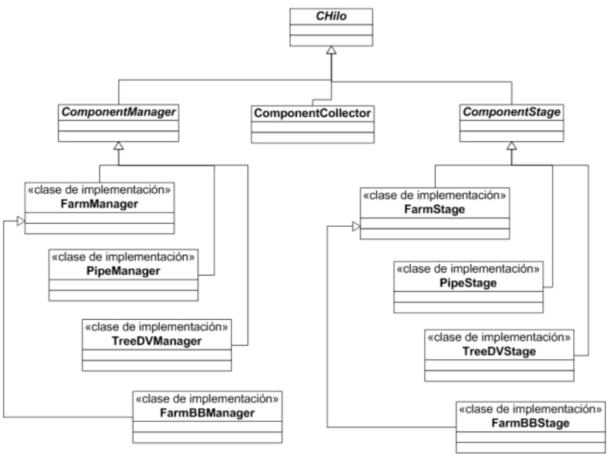

Figure 5: Structure of the HLPC class library

3. CONVOLUTIONAL NEURAL NETWORK (CNN)

In recent years, the field of machine learning has progressed enormously in addressing problems of classification, identification and pattern recognition. In particular, it has been found that a type of model called convolutional neural network or CNN achieves reasonable performance in hardware visual recognition tasks, equaling or exceeding human performance in some domains (Salzberg, Searls and Kasif 1998). A CNN is an algorithm for machine learning in which a model learns to perform classification tasks directly from images, videos or sounds. CNNs are especially useful for locating patterns in images in order to recognize objects, faces and scenes. They learn directly from the image data, using patterns to classify the images and eliminate the need for a manual extraction of features. For a CNN to learn, deep learning models are used. The most common is Inseption-V3 that is designed for the Visual Recognition challenge, this is a standard task in artificial vision, where the models try to classify complete images in 1000 ImageNet classes. This model is available in TensorFlow, which is a tool for machine learning. TensorFlow is designed primarily for deep neural network models (Mathworks. 2018). Modern models of image recognition have millions of parameters; training them from scratch requires a lot of tagged training data and a lot of computing power. Therefore, one of the disadvantages of neural networks is the large amount of time needed for training. A direct way to reduce this time is to parallelize the learning algorithms. However, the algorithms cannot always be parallelized in a simple way, and, the amount of communication between the processes, makes that most of the parallel versions of these algorithms can only be executed in parallel computers (Marcelo, Apolloni, Kavka 2000). Transfer learning is a quick technique that takes a piece from a model that has already been trained in a related task and reuses it in a new model, Figure 6 (taken from) shows an example of a CNN, the filters are applied to each training image with different resolutions, and the output of each convolved image is used as input for the next layer generating a communication pattern of pipeline type and that can be parallelized (Mathworks 2018, Marcelo, Apolloni, Kavka 2000).

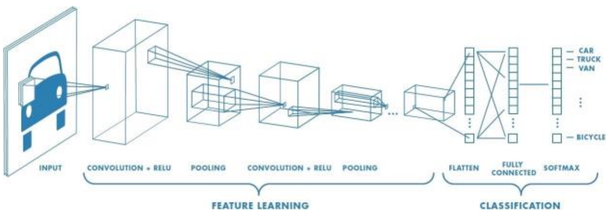

Figure 6: Example of a Convolutional Neural Network (taken from Mathworks 2018)

The transfer learning technique is effective for many applications, works with moderate amounts of training data (thousands, not millions of tagged images) and can be executed sequentially in thirty minutes (Salzberg, Searls and Kasif 1998). In this work, the parallelization of a convoluted neuronal network under the HLPC model is shown. The HLPC Pipeline is adapted to a convoluted neuronal network model to the transfer learning technique; which allows its execution in parallel computers or computers with GPUs.

4. REPRESENTATION OF A CNN AS A HLPC USING DEEP LEARNING TRANSFER

Convolutional networks have characteristics of neural networks such as activation functions or fully connected layers, but also introduce two concepts: the convolutional layer and the grouping or sampling layer. The architectures of convolutional networks are built by stacking these elements, that is why according to the computational and memory use issues of a neural network for image processing (Marturet and Alferez 2018), it is useful and appropriate to represent it through an HLPC pipeline. For the training of a convolutional neuronal network, the transfer of learning by extraction of deep descriptors was used as a way of training and validating the neural network on the set of images of the specific problem to be solved. In this way we obtain the HLPC Pipeline-CNN that is shown in the figure 7, and that will help to solve the case study that is shown in following sections in this article.

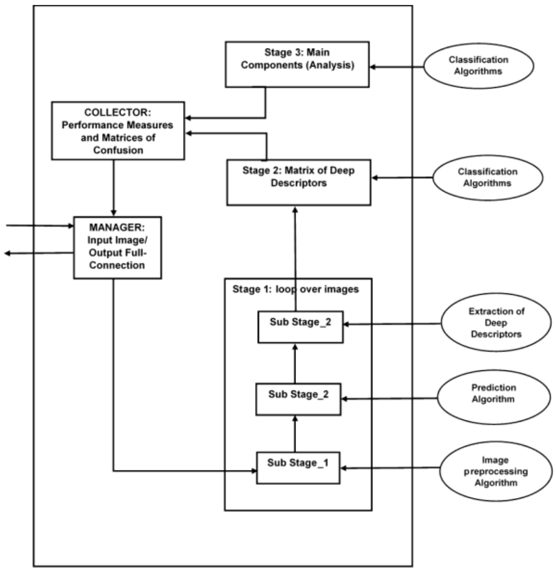

Figure 7: HLPC Pipeline-CNN

In the HLPC Pipeline-CNN of figure 7, in the first convolutional layer, the neurons that make up the CNN connect to a portion of the input image provided by the user in the HLPC manager object and not to the whole of it. When several convolutional layers are concatenated, to a part of the output of a layer, certain neurons of the next layer are connected, but not all of them that make up the second layer. This is carried out in the first stage of the HLPC Pipeline-CNN (loop over images). After several concatenated convolutional layers, details are obtained regarding the characteristics of the image, for example shapes or colors. In each convolutional layer, feature maps are stacked. A feature map is a layer where all its neurons use the same filter and share characteristic parameters. In each convolutional layer as many filters are applied as feature maps are stacked in it. The transfer of learning in the HLPC Pipeline-CNN is produced by describing deep descriptors in the sub-stage2 of the model. This adjustment occurs through training and validation of the set of images of the specific problem that is solved. The work is completed in stage 2 and stage 3 of the HLPC Pipeline-CNN, executing the classification algorithms associated with the slave objects, to generate the matrix of deep descriptors and the analysis of main components, obtaining as results within the collector's object, model performance measures, confusion matrices and the network's classification layer (see figure 6 and figure 7). The internal execution of the parallel objects of the HLPC including the manager, the collector and the stages, as well as the inter-object parallelism of the HLPC, make the solution of the specific problem that is solved obtain a better performance than its sequential counterpart, when working with a large number of images of the order of hundreds of thousands under a hardware architecture that is also parallel.

5. RECOGNITION OF DNA SEQUENCES USING HLPC PIPELINE-CNN

The processes of gene prediction are those that, within the area of computational biology, are used for the algorithmic identification of pieces of genomic DNA sequences (Christos Ouzounis 2012), and that are biologically functional. The identification of genes is an important area to understand the genome of a species once it has been sequenced (Salzberg, Searls and Kasif 1998). DNA is composed of four molecules called nucleotides or nitrogenous bases: adenine, thymine, guanine and cytosine (Panduro 2009). A DNA sequence is composed of an alphabet that contains the letters of the four nitrogenous bases (figure 8).

GTAGTCATGTTGAAAAACTTACGAGTAAATTACGTTGTCGA
GGGCGTGCAAGTAGCGCAACCCGTGACAAGCGCAAATTCG
GAAGTAT**ACGCCAA**TCTACCGCCTCCCGTACCCGCGGAGAC
GTATCAAACCGACGAAGATTACGAGGAAGATGACGGAGG
GTGGGC

Figure 8: A DNA sequence

A DNA sequence can define the characteristics of a living organism, containing all the genetic information in units of inheritance called genes. Splicing junctions are points in a DNA sequence in which "useless" DNA is removed during the process of creating proteins in higher organisms. The problem then is to recognize with a DNA sequence, the boundaries between the exons (the parts of the DNA sequence that are retained after splicing) and the introns (the parts of the DNA sequence that are cut). This problem consists of two subtasks: recognition of exon / intron limits (called “EI” or donor) and recognition of intron / exon boundaries (“IE” sites or acceptor), (Noordewier, Towell and Shavlik 1991). Both tasks are complicated since there is no standard sequence to recognize introns and exons, which is why it is interesting to design tools that help us identify and classify them.

To improve the representation of a DNA chain, sequences are used that can be transformed into representation with numerical or alphabetic values: A (adenine), T (thymine), G (guanine) and C (cytosine), (Genís, Blanco and Guigó 2000), as shows figure 8. However, the representation of large amounts of information as DNA sequences do not make their mathematical analysis easy, this creates the need to find new ways of representing information. It is presented as a case study to generate images from DNA sequences to be analyzed by deep learning techniques, using as a convolutional neuronal network the proposal of the HLPC Pipeline-CNN shown in this research and thus be able to classify images.

The idea is to convert the DNA sequences to graphic representations to train the HLPC Pipeline-CNN. Remember that CNN are used for the recognition of patterns and classification of images. The DNA sequences are represented by letters: A-Adenine, G-Guanine, C-Cytosine and T-Thymine, however, a CNN is not made to process information with this format, so a graphic representation of the sequences was designed.

5.1. Case Study: DNA sequences of the Hepatitis-C virus

We used 1847 DNA sequences from a database with 4 types of hepatitis C virus (type 1, 2, 3 and 6) taken from the repository available on the ViPR page (https://www.viprbrc.org/brc/home.spg?decorator=vipr) and a set of DNA sequences from the Molecular database (Splice-junction Gene Sequences) Data Set that has 3190 sequences, available on the UCI page (https://archive.ics.uci.edu/ml/index.php), with three classes of sequences: limit exon-intron, limit intron-exon and none. The methodology used was the following:

1. A grayscale color was assigned to each of the letters of the DNA sequence (see table 1), which goes from a value of 0 = black to a value of 1 = white, so that the intermediate colors are tones of gray to show a better contrast.
2. The image representing the DNA sequences was created: A matrix of dimension 60 X 60 was used, where the value 60 coincides with the number of nitrogenous bases of all the sequences of the database.

Table 1. Grayscale of nitrogenous bases

Nitrogen base	*Value of gray*
A	0
C	0.3
G	0.7
T	1

Each sequence was placed in the first row and copied in the rest of the rows until it was 60 in total (see figure 9). The result is an image with bars in the grayscale like the one shown in Figure 10, each of the images obtained is specific to each instance of the database shown in Figure 2. In total, 3190 images were obtained.

```
1  CCAGCTGCATCACAGGAGGCCAGCGAGCAGGTCTGTTCCAAGGGCCTTCGAGCCAGTCTG
2  CCAGCTGCATCACAGGAGGCCAGCGAGCAGGTCTGTTCCAAGGGCCTTCGAGCCAGTCTG
3  CCAGCTGCATCACAGGAGGCCAGCGAGCAGGTCTGTTCCAAGGGCCTTCGAGCCAGTCTG
.
.
.
60 CCAGCTGCATCACAGGAGGCCAGCGAGCAGGTCTGTTCCAAGGGCCTTCGAGCCAGTCTG
```

Figure 9: DNA sequences to be encoded

Figure 10: Image of an instance of DNA sequences

3. With the representative images of each sequence, the HLPC Pipeline-CNN was trained. This model of HLPC is based on the CNN InceptionV3 model with deep learning transfer to categorize the recognition of three classes of DNA sequences: recognition of exon/intron limits (EI sites), recognition of intron/exon boundaries (IE sites) and recognition of none of the previous two (N).
4. With the TensorFlow software library, a classification model was constructed and placed as a slave object within the HLPC Pipeline-CNN to be parallelized (see figure 7). This was achieved by categorizing the recognition of a database with four classes of DNA sequences: Hepatitis C virus type 1, 2, 3 and 6 and the recognition of another database with three types of limits: EI, IE and N.
5. With the HLPC Pipeline-CNN the last layers of the networks were trained with instances obtained from the databases, both networks were trained in 4000 steps. First the HLPC Pipeline-CNN was trained to classify the 4 types of Hepatitis virus, then the training was done with 2 classes: IE and IE and finally with all the classes of the database: IE, IE and N to compare the results of the last two neurons.
6. Finally, classification and performance analysis results of the proposed HLPC model were obtained.

6. RESULTS AND PERFORMANCE

The computer equipment used for the training of the HLPC Pipeline-CNN was a parallel computer with 64 processors of which only 32 were exclusive for the tests of this work, 8 GB of main memory with a distributed shared memory architecture and high-speed buses. Regarding classification results for the HLPC Pipeline-CNN trained with the database of the four types of Hepatitis C virus, a precision of 95% was obtained with 145 images tested and at the end of step 4000 the precision training was 94.5% and precision validation 95% (see table 2). When using the HLPC Pipeline-CNN with the classes EI and IE, an evaluation precision of 80.8% was obtained with 177 test images and at the end of step 4000 the precision training was 82% and the precision validation was 75% (see table 3). The results of the training of the HLPC Pipeline-CNN where the three classes of the database were used show a precision of evaluation of 57.5% with 301 images and at the end of step 4000 the precision training was 69% and the precision validation 56% (see table 4).

Table 2. Precision training and precision validation of HLPC Pipeline-CNN with classes of Hepatitis C virus type 1, 2, 3 and 6.

	Training steps (145 images tested)			
	1000 steps	*2000 steps*	*3000 steps*	*4000 steps*
Precision Training	92%	95%	96%	94.5%
Precision Validation	91%	92%	95%	96%

Table 3. Precision training and precision validation of HLPC Pipeline-CNN with IE and EI classes.

	Training steps (177 images tested)			
	1000 steps	*2000 steps*	*3000 steps*	*4000 steps*
Precision Training	77%	80%	81.7	82%
Precision Validation	73%	74.7%	75%	75%

Table 4. Precision training and precision validation of HLPC Pipeline-CNN IE, EI and N classes.

	Training steps (301 images tested)			
	1000 steps	*2000 steps*	*3000 steps*	*4000 steps*
Precision Training	57%	60%	64%	69%
Precision Validation	52%	56%	55%	56%

ISBN 978-88-85741-25-6; Affenzeller, Bruzzone, Longo and Pereira Eds.

Regarding the performance of HLPC Pipeline-CNN for the case study that has been shown, the aim is to show that the performances obtained are "good" based on the model of the HLPC. The graphs in figures 11, 12, 13 and 14 show the performance analysis of the HLCP Pipeline-CNN from 1000 training steps to 4000 training steps respectively. In these graphs the speedup of the precision training and precision validation of HLPC Pipeline-CNN with classes of Hepatitis C virus type 1, 2, 3 and 6, IE and EI classes and IE, EI and N classes is illustrated. In all of them, the speedup shows an acceleration to be incorporating more CPU-SET, always below the law of Amdahl. The execution times in each training vary: For the case of 1000 training steps, of an average sequential execution time of 24 minutes we obtained a decrease with 32 CPU-SET of an average of 11.3 minutes. For the case of 2000 training steps, from an average sequential execution time of 28 minutes we obtained a decrease with 32 CPU-SET of an average of 17 minutes. In the case of 3000 training steps, we obtained an average sequential execution time of 33 minutes while the parallel execution with 32 CPU-SET was an average of 14.8 minutes. Finally, for the case of 4000 training steps, the average sequential execution time was 40 minutes and the parallel execution with 32 CPU-SET decreased it by an average of 20.1 minutes.

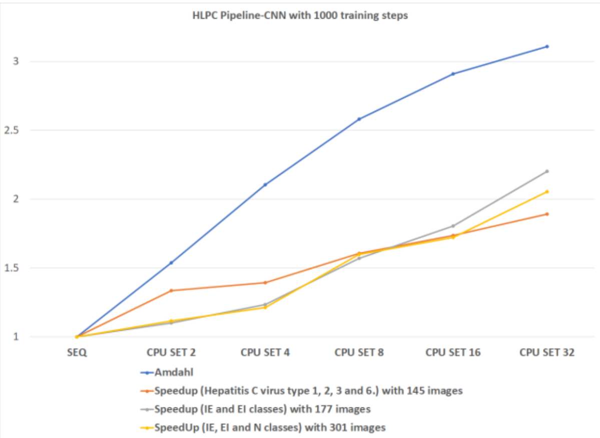

Figure 11: Speedup scalability found for HLPC Pipeline-CNN of Precision training and precision validation with 1000 training steps.

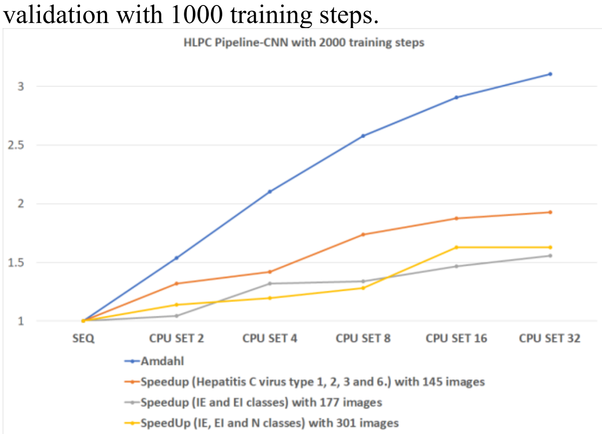

Figure 12: Speedup scalability found for HLPC Pipeline-CNN of Precision training and precision validation with 2000 training steps.

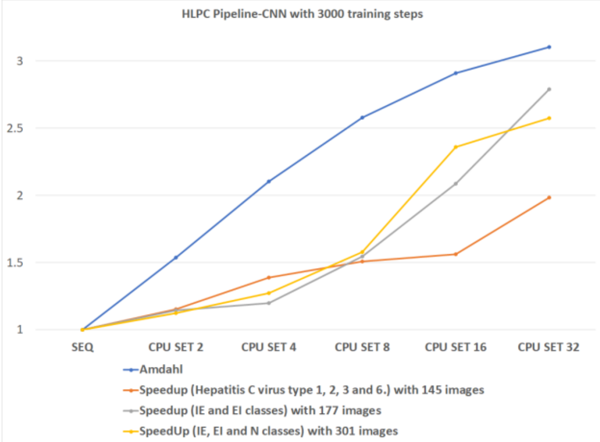

Figure 13: Speedup scalability found for HLPC Pipeline-CNN of Precision training and precision validation with 3000 training steps.

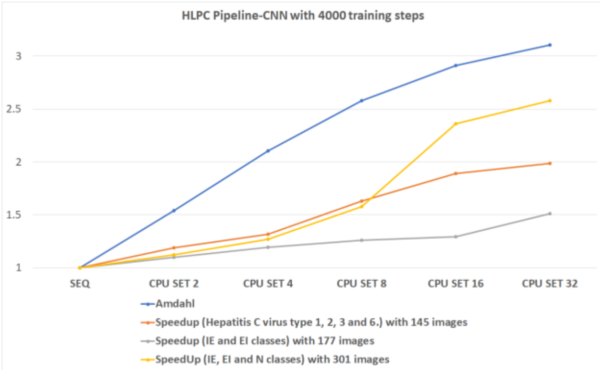

Figure 14: Speedup scalability found for HLPC Pipeline-CNN of Precision training and precision validation with 4000 training steps.

7. CONCLUSIONS

We discuss the implementation of HLPC Pipeline-CNN as generic and reusable communication/interaction patterns between processes which implements a Convolutional Neural Network (CNN) with deep learning transfer, using a pipeline as associated communication pattern. This HLPC can even be used by inexperienced parallel application programmers to obtain efficient code by only programming the **sequential** parts of their applications (slave objects of the model of figure 7). The HLPC Pipeline-CNN was used to be trained in the recognition of DNA sequences through graphic representations and be able to obtain a classification of the different types of hepatitis C virus (type 1, 2, 3 and 6). The results obtained from the HLPC Pipeline-CNN trained with the Hepatitis C virus database suggest that the automatic learning methodology used in this work is suitable for the classification of images generated from DNA sequences. Good percentages of evaluation precision, training precision and validation precision are shown.
The transfer of learning is good when there are few images available to train the HLPC Pipeline-CNN and it

allows to reach acceptable results in most cases (This can be seen in tables 2, 3 and 4), although the results can be improved. On the other hand, the parallel execution of the HLPC Pipeline-CNN shows a good performance comparing its acceleration with respect to its sequential execution. We have also obtained good performance in their executions and speedup scalability compared to Amdahl's law on the number of processors used in training (see figures 11, 12, 13 and 14).

REFERENCES

Andrews G.R., 2000. Foundations of Multithreaded, Parallel, and Distributed Programming, *Addison-Wesley*

Bacci, Danelutto, Pelagatti, Vaneschi, 1999. SklE: A Heterogeneous Environment for HPC Applications. *Parallel Computing 25*.

Birrell A., 1989. An Introduction to Programming with Threads, *Digital Equipment Corporation, Systems Research Center*, Palo Alto California, USA.

Brinch Hansen, 1993. Model Programs for Computational Science: A programming methodology for multicomputers, *Concurrency: Practice and Experience*, Volume 5, Number 5.

Calvo D. (2015). Red Neuronal Convolucional (CNN). Data Scientist. http://www.diegocalvo.es/red-neuronal-convolucional/

Corradi A., Leonardi L., 1991. PO Constraints as tools to synchronize active objects. *Journal Object Oriented Programming* 10, pp. 42-53.

Corradi A, Leonardo L, Zambonelli F., 1995. Experiences toward an Object-Oriented Approach to Structured Parallel Programming. *DEIS technical* report no. DEIS-LIA-95-007.

Christos Ouzounis 2012. Rise and demise of bioinformatics? promise and progress. PLoS computational biology, 8(4):e1002487.

Danelutto M. and Torquati M, 2014. Loop parallelism: a new skeleton perspective on data parallel patterns, *in Proc. of Intl. Euromicro PDP*: Parallel Distributed and Network-based Processing, Torino, Italy.

Darlington et al., 1993, Parallel Programming Using Skeleton Functions. *Proceedings PARLE'93*, Munich (D).

Genís P, Blanco P. and Guigó R., (2000). Geneid in drosophila. Genome research, 10(4):511–515.

Lavander G.R., Kafura D.G. 1995. A Polimorphic Future and First-class Function Type for Concurrent Object-Oriented Programming. *Journal of Object-Oriented Systems*.

Liwu Li, 2002. Java Data Structures and Programming. *Springer Verlag*. Germany. ISBN: 3-540-63763X.

Marcelo A., Apolloni J., Kavka C., et-al. 2000. Entrenamiento de Redes Neuronales. Universidad Nacional de San Luís. WICC 2000. Argentina.

Marturet R., Alferez E.S., 2018. Evaluación de Redes Neuronales Convulcionales para la clasificación de imágenes histológicas de cancer colorrectar mediante transferencia de aprendizaje. Master en Bioinformática y Bioestadística. Universitat Oberta de Catalunya. España.

Mathworks. 2018. Deep learning. https://la.mathworks.com/solutions/deep-learning/convolutional-neural-network.html

Noordewier M, Towell G, and Shavlik Jude, (1991). Training knowledge-based neural networks to recognize genes in DNA sequences. In Advances in neural information processing systems, pages 530–536.

Panduro A, 2009. Biología molecular en la clínica. McGraw-Hill Interamericana.

Roosta, Séller, 1999. Parallel Processing and Parallel Algorithms. *Theory and Computation. Springer*.

Rossainz, M., 2005. Una Metodología de Programación Basada en Composiciones Paralelas de Alto Nivel (HLPCs). Universidad de Granada, PhD dissertation, 02/25/2005.

Rossainz, M., Capel M., 2008. A Parallel Programming Methodology using Communication Patterns named CPANS or Composition of Parallel Object. *20TH European Modeling & Simulation* Symposium.Campora S. Giovanni. Italy.

Rossainz M., Capel M., 2014. Approach class library of high level parallel compositions to implements communication patterns using structured parallel programming. *26TH European Modeling & Simulation* Symposium. Campora Bordeaux, France.

Salzberg SL, Searls DB, and Kasif S., 1998. Computational gene prediction using neural networks and similarity search. Computational Methods in Molecular Biology, pp.32-109.

Vizcaya R., (2018). Deep Learning para la detección de peatones y vehículos sobre FPGA. Disertación de Master. Universidad Autónoma del Estado de México.

Wilkinson B., Allen M., 1999. Parallel Programming Techniques and Applications Using Networked Workstations and Parallel Computers. *Prentice-Hall*. USA.

KNOWLEDGE BASED MODELLING FRAMEWORK FOR FLEXIBLE MANUFACTURING SYSTEM

Syed Imran Shafiq[(a)], Cesar Sanin[(b)] , Edward Szczerbicki[(c)],

[(a)]Faculty of Engineering and Technology, Aligarh Muslim University, Aligarh, India
[(b)] Faculty of Engineering and Built Environment, The University of Newcastle, Callaghan, NSW, Australia, [(c)]Faculty of Management and Economics, Gdansk University of Technology, Gdansk, Poland

[(a)] Sishafiq.bp@amu.ac.in, [(b)] Cesar.Sanin@newcastle.edu.au, [(c)]Edward.szczerbicki@zie.pg.gda.pl

ABSTRACT

This paper proposes knowledge-based modelling framework to manage the storage, analysis, and processing of data, information, and knowledge of a typical Flexible Manufacturing System (FMS). The framework utilizes the concept of virtual engineering object (VEO) and virtual engineering process (VEP) for developing knowledge models of FMS to achieve effective scheduling and manufacturing flexibility. The proposed generic model is capable of capturing in real time the manufacturing data, information and knowledge at every stage of production i.e. at the object level, the process level, and at the factory level. The significance of this study is that it supports decision making by reusing past decisional experience, which will not only help in effective real time data monitoring and processing but also make FMS system more intelligent and ready to function in the virtual Industry 4.0 environment.

Keywords: knowledge representation, knowledge based model, computer integrated manufacturing

1. INTRODUCTION AND BACKGROUND

A flexible manufacturing system (FMS) is a method for producing goods that is readily adaptable to changes in the product being manufactured, both in type and quantity. Machines and computerized systems are configured to manufacture different parts and handle varying levels of production. A flexible manufacturing system (FMS) gives manufacturing firms an advantage to quickly change a manufacturing environment to improve process efficiency and thus lower production cost. FMS is defined as an integrated, computer-controlled complex system of automated material handling devices and numerically controlled tools that can simultaneously process medium-size volumes of medium variety parts (Yadav and Jayswal 2018). Two basic manufacturing flexibility types are proposed: machine flexibility and routing flexibility. Based on these basic flexibility types other types of flexibility like product flexibility, process flexibility, operation flexibility, volume flexibility, expansion flexibility and production flexibility can be derived.

Due to advantages associated with FMS, it is an area of interest from earlier days (Groover 2007). Researchers were working on improving the performance of FMS with application of various techniques. Earlier analytical methods were used for accessing FMS performance (Stecke 1986) but with growing technology, simulation, artificial intelligence, Petri Nets etc. modelling techniques have gained importance too (Yadav and Jayswal 2018).

Investigation of work that are accomplished by using different modelling techniques in FMS like mathematical, artificial intelligence, hierarchical, multi criteria decision-making method, Petri Nets and simulation have some drawbacks as well some advantages. The drawbacks associated with mathematical modelling are the stated assumptions, as they may not be valid in real world. Also the process of computation becomes large with increase in the size of the problem. For analyzing different system performance measures of FMS and seeing how they behave with constraints in particular conditions, the process of modelling and simulation is the best one. For avoiding and protecting the occurrence of deadlock in the FMS system, Petri Net models are used generally. Selection of various machine and parts in FMS can be done effectively by using mathematical and MCDM techniques. FMS control can be done efficiently by using artificial intelligence technique. Selection of best dispatching rule from given alternatives is well evaluated by MCDM and artificial intelligence techniques (Yadav and Jayswal 2018). Thus, general purpose modelling technique for implementation, design and control of FMS is needed.

This paper proposes a multipurpose framework, in which previous knowledge of the FMS along with information communication technology (ICT) features are utilized to induce intelligence to the FMS system. The proposed model enables micro level integration of various FMS components and processes, which in turn will not only facilitate the real-time control and monitoring capabilities but also enhance effective decision making.

2. KNOWLEDGE BASED FMS MODEL

The hypothetical framework for the proposed FSM model is presented in Figure 1. It represents a typical FMS configuration assumed for modelling and research purposes (Ali and Wadhwa 2010).

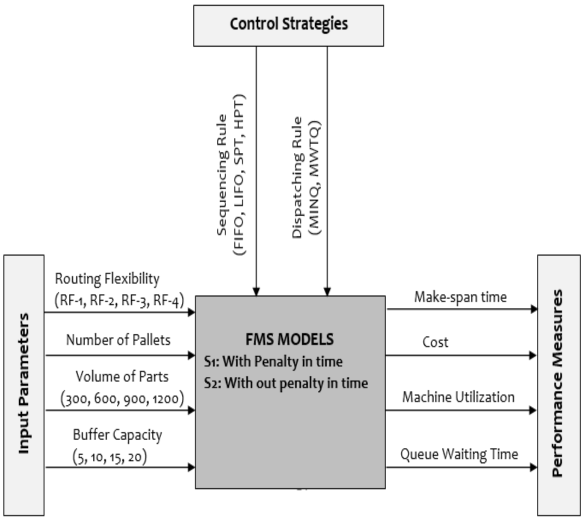

Figure 1: Framework for proposed FMS model

The above FMS framework was modeled using unique knowledge representation technique called Decisional DNA together with the concepts of Virtual Engineering Object and Virtual Engineering Process which are presented next.

2.1. Set of Experience and Decisional DNA

One of the challenges of the Semantic Web society is smart storage of information and knowledge in artificial systems, so it can be unified, enhanced, reused, shared, communicated and distributed between artificial systems (Shabolt et al. 2006). Our DDNA concept introduces one of the key components of addressing the above challenge. This concept stems from the role of deoxyribonucleic acid (DNA) in storing and sharing information and knowledge. The idea behind our approach was to develop an artificial system, an architecture that would support discovering, adding, storing, improving, and sharing information and knowledge among machines, processes and organisations through experience. We proposed a novel Knowledge Representation (KR) approach in which experiential knowledge is represented by Set of Experience (SOE; Figure 2) and is carried into the future by Decisional DNA (DDNA; Figure 3) (Sanin and Szczerbicki 2004, Sanin et al 2009).

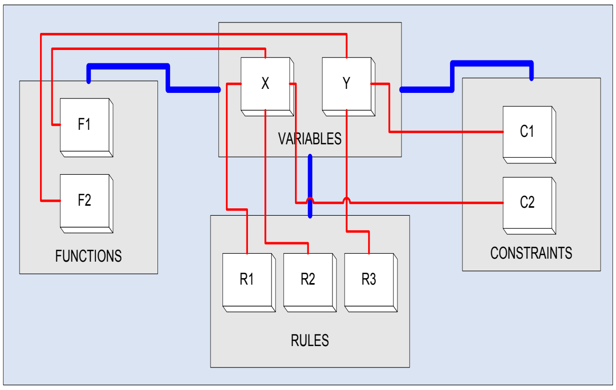

Figure 2: Structure of SOE

As illustrated in Figure 2, SOE is the combination of 4 components that characterise decision making actions (variables V, functions F, constraints C, and rules R) and it comprises a series of mathematical concepts (logical element), together with a set of rules (ruled based element), and it is built upon a specific event of decision-making (frame element).

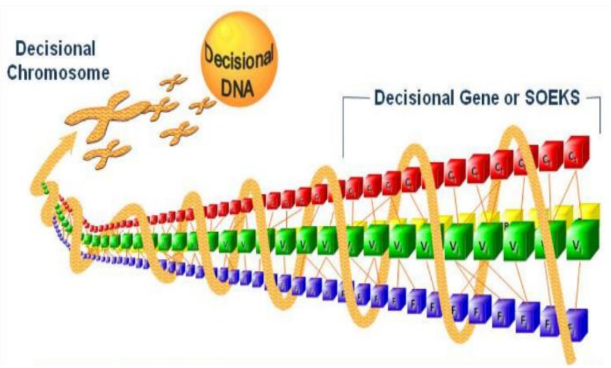

Figure 3: Sets of Experience (Decisional Genes) are grouped according to their phenotype, creating Decisional Chromosomes, and groups of chromosomes create the Decisional DNA

SOE and DDNA can be implemented on various platforms (e.g. ontology, reflexive ontology, software based, fuzzy logic etc.) in multi domains, which makes it a universal approach. We initially developed the concept and coined the expressions of SOE and DDNA in Sanin, Szczerbicki 2008, and Zhang et al 2016. Since then our research efforts resulted in widespread recognition of this innovative KR technique based on DNA metaphor that is presented as multi-technology shareable knowledge structure for decisional experience with proven security and trust in Sanchez et al 2014, Sanin et al 2012a, Shafiq et al 2014a, Sanin et al 2012b, Wang et al 2015. Subsequently, DDNA was used to develop Virtual Engineering Object (VEO) and Virtual Engineering Process (VEP) as presented next.

3. VIRTUAL ENGINEERING OBJECT (VEO)

VEO is developed on the concept of cradle-to-grave approach, which means that the contextual information and decision-making regarding an engineering object right for its inception until its useful life is stored or linked in it. The knowledge representation technique of Set of experience knowledge structure (SOEKS) and Decisional DNA (DDNA) ((Sanin Szczerbicki 2005, 2006, 2009, Sanin et al 2007, Zhang et al 2010) is used for developing this model. SOEKS-DDNA provides dynamicity to VEO to overcome issues related to representation of complex and discrete objects (Shafiq et al 2014b).

VEO of an engineering object implies that knowledge and experience related with that object is stored in a structured manner in a repository. This information not only can be used for decision-making regarding its better operational performance but also can be utilized in areas like maintainability, serviceability and reliability of the object. The concept VEO involves the interlinking of the body of knowledge of connected objects, with the aim of constructing subclasses consistent enough for the purposes of the classification scheme.

A VEO can encapsulate knowledge and experience of every important feature related with an engineering object. This can be achieved by gathering information from six different aspects of an object: *Characteristics, Functionality, Requirements, Connections, Present State*, and *Experience*, as illustrated in Figure 4.

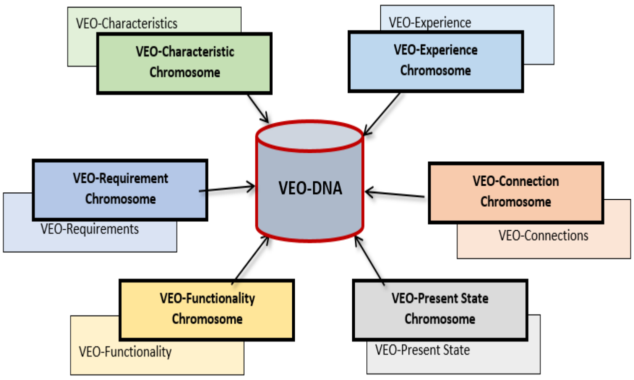

Figure 4: Architecture of a VEO

In each VEO model, the collection of SOEKS combines to form VEO-DNA (see Fiure. 4) Thus, a VEO is knowledge representation of an engineering artefact, and it has three vital features (Shafiq et al 2015a, 2015b)

- the embedding of the decisional model expressed by the set of experience,
- a geometric representation and
- the necessary means to relate such virtualization with the physical object being represented.

4. VIRTUAL ENGINEERING PROCESS (VEP)

The next step in our modelling process is the extension of VEO concept to engineering process or process planning. Dynamic manufacturing environments require a flexible process planning and control system in response to changing manufacturing resource availability, production uncertainty and dynamic machining conditions.

Process planning involves selection of necessary manufacturing processes. It includes determination of manufacturing sequences and the selection of resources needed to 'transform' a design model into a physical component. Therefore, a general, adaptive, resource efficient and experience-based framework with VEP modules comprising VEO is developed. VEP is designed for knowledge representation and decision-making at the shop floor level.

The VEP information model encompasses multiple perspectives of different machining stages and scales, from process planning, machining, to machining feedback which is presented in the next Section.

4.1. Architecture of VEP

Process planning is combination of information regarding the operation required, manufacturing sequence, and machines required. In addition to this, for VEP, information of all the VEOs of the resource associated with the process is also required. Therefore, to encapsulate knowledge of the above-mentioned areas, the VEP is designed having following three main elements or modules (see Figure 5):

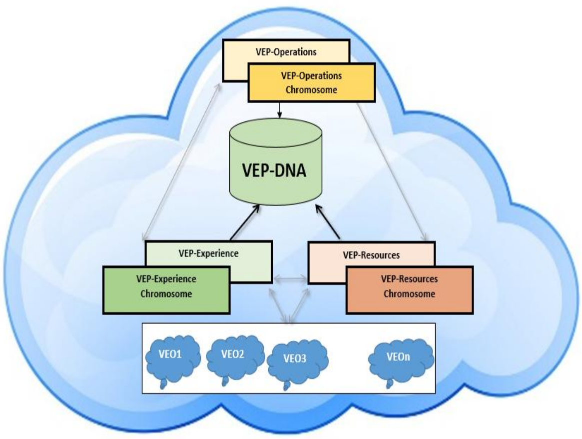

Figure 5: Configuration of a VEP and network with VEOs

(i) Operations - In this module of VEP, all the information related with the operations that are required to manufacture an engineering object is stored. This includes knowledge in the form of SOEKS related to operation process and scheduling. Furthermore, functional dependencies between operations are also part of operations. These are sub categorized and their interaction planning functions are given below:

- Scheduling route – based on global and local geometry.
- Processes – process capabilities, process cost.
- Process parameters – tolerance, surface finish, size, material type, quantity, urgency.

(ii) Resources - Information based on the past experience about resources used to manufacture a component mentioned in operations module of VEP is stored here. The knowledge of the machine level stored in this section is as follows:

- Machine and tool selections –machine availability, cost machine capability, size, length, cut length, shank length, holder, materials, geometry, roughing and finishing.
- Fixture selection – fixture element function, locating, supporting, clamping surfaces, stability.

Furthermore, the information of VEO categorized under *Characteristics, Requirements, Functionality, Present state, Connections, Experience* is also linked in this section

(iii) Experience - In the experience section, links to the SOEKS of VEOs along with VEP having past formal decisions to manufacture engineering components are stored. They represent the links to SOEKS based on past experience on that particular machine to perform given operation along with operational and routing parameter.

As demonstrated in Figure 5, VEP is also envisaged on cloud computing platform to facilitate delivery of compressed information on complex interrelationships within the modelled process.

5. FMS MODELLING FRAMEWORK AND ITS IMPLEMENTATION

The Decisional DNA based FMS is designed and developed to enable the FMS to capture formal decisional events and to capture, extract, reuse, and share knowledge.

As discussed in section 4, that VEO is a knowledge representation of engineering artefacts. In this study each physical component of FMS is considered as a VEO and correspondingly knowledge models are developed for every machine and job i.e. M1-VEO, M2-VEO, M3-VEO, M4-VEO, M5-VEO, M6-VEO, JI-VEO, J2-VEO etc. Each VEO knowledge model having information regarding its *characteristic*, *functionality*, *requirement*, *connections*, *present-state* and *experience* (see Figure 5.) of the physical object. Furthermore, adhering to the structure of SOEKS-DDNA, for each module, information is structured according to variables, function, constant and rules related with every formal decision. On the same pattern information of characteristics, requirement, connections, present state, functionality related to M1-VEO are gathered. CSV files storing SOEKS were generated through arena simulation software for M1-VEO, M2-VEO, M3-VEO, M4-VEO, M5-VEO, M6-VEO, JI-VEO.

Moreover, the routing flexibility is treated as a process and a DDNA based VEP model is developed. SOEKS for VEP elements: *operations*, *resources* and *experience* were also stored in CSV file. For each VEP elements i.e. *operations*, *resources* and *experience*; SOEKS variables, functions constraint and rules are defined. Having these files, a parser is written in Java programming language to read SOEKS stored in the CSV format. Parser looks for CSV file, in that file it looks for the word ‘variables’, then starts reading the first row under variables. Once all the variables of the first row are read then the parser looks for the word ‘functions’, it reads all the rows under functions.

After that it looks for word ‘constraints’ and read all the rows under constraints. This entire information i.e. first row under ‘variables’, all rows under ‘functions’ and ‘constraints’ are stored as one set of experience (SOEKS or SOE).

This cycle is repeated for all rows under ‘variables’, for each row along with functions and constraints, SOEKS are created.

Same procedure is repeated for the all the other CSV files. Each file representing a category, collection of SOEKS of same category forms a chromosome of either of VEO or VEP. Collection of all chromosomes forms a Decisional DNA of a FMS i.e. FMS-DNA as shown in Figure 6. Once the VEO chromosome is constructed, decisional DNA has feature that it can be queried.

Once all the relevant experience of FMS-VEP and associated VEO’s is captured, entire process planning and control of FMS can be virtually represented.

Moreover, this experience can be utilized for future performance evaluation of similar FMS scenario. This approach will not only be beneficial for better resource utilization but also in cost-effective quality production.

Figure 6 shows the proposal for the case study. First, VEOs of machines/resources (M1-VEO, M2-VEO, M3-VEO, M4-VEO, M5-VEO, M6-VEO, J1-VEO etc.) required for the functioning of FMS developed. Then the VEP to decide the routing flexibility is developed based on the case-specific experience of that manufacturing system. VEOs along with experience of engineering process (VEP) form an FMS experience repository. JAVA programming language is used to develop and implement this concept.

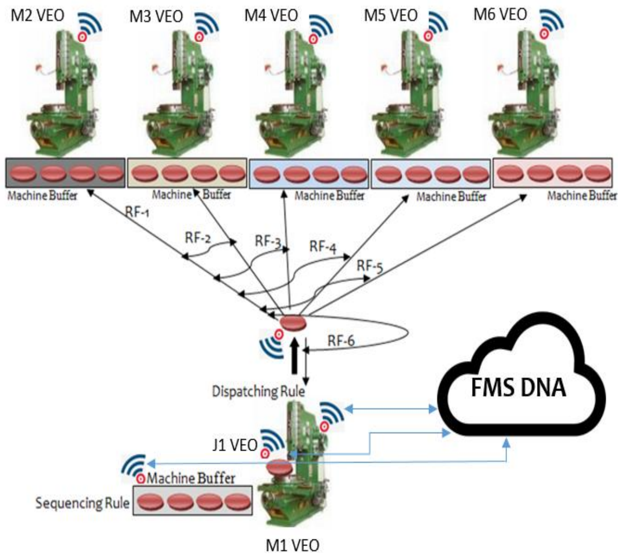

Figure: DDNA based FMS Model

The VEP repository can be queried by the GUI, which makes similarity comparisons with each experience stored and returns the most similar SOEKS. Mechanism for query execution in presented in Figure 7; Euclidean distance is calculated between the query-SOE and each VEP-SOE present in the FMS-DNA repository. SOE with the least value is considered as the best SOE or most similar SOE.

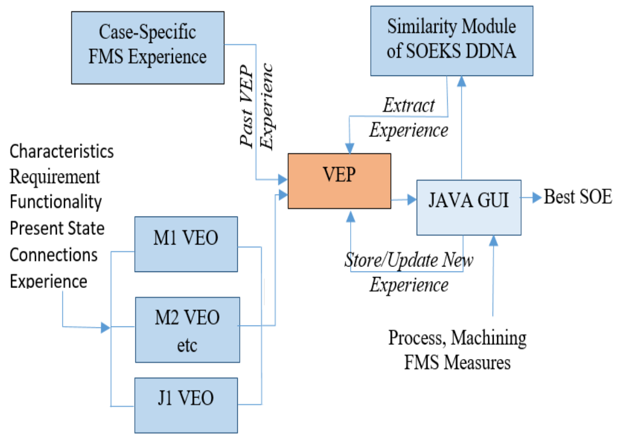

Figure 7: Mechanism for effective decision making

6. EXPERIMENTAL RESULTS

A number of sample queries were executed to find the most similar SOEKS. For example, in query 1, VEP similarity is calculated for a product with RF1 when MST = 4200, cost = 17300, Machine Utilization = 80% and Queue waiting time = 5.3. Figure 8(a) illustrates the outcome of the execution of this query. FMS-DNA returns the top most similar SOEKS which in this particular case is VEP1 having similarity 0.0502. The query also returns the codes of M1-VEO for the most similar VEO-Code. This enables to fetch all the micro level details of Machine 3 at M3-1 code corresponding to most similar VEP- SOEKS. This previous FMS experience of the RF, machines and the jobs can beneficial not only for the design but also in performance evaluation.

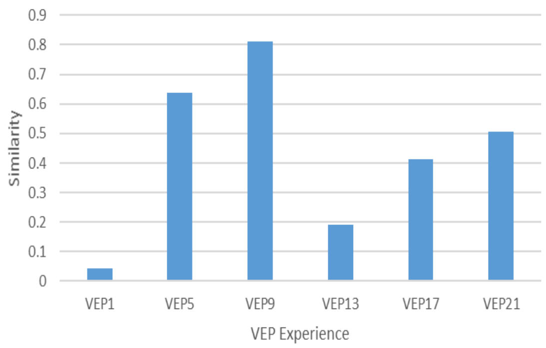

Figure 8(a): Similarity index for query 1 at RF1

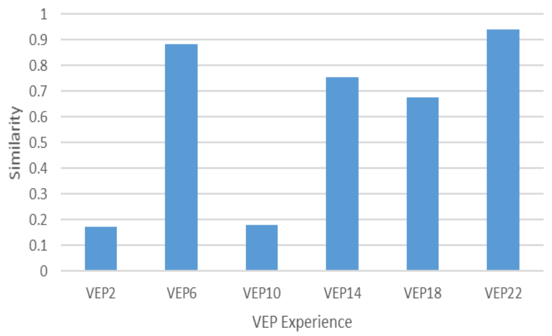

Figure 8(b): Similarity index for query 2 at RF2

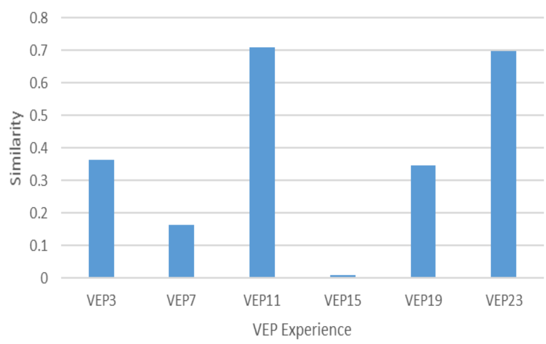

Figure 8(c): Similarity index for query 3 at RF3

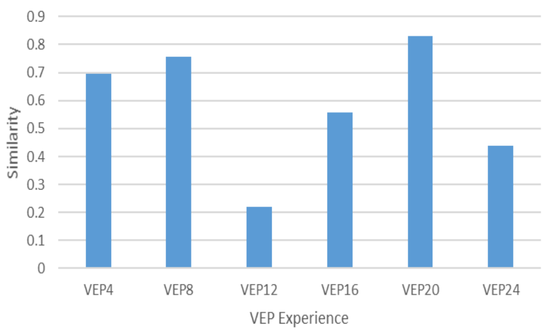

Figure 8(d): Similarity index for query 4 at RF4

Different query 2, 3 and 4 are executed when FMS is executed at RF2, RF3 and RF4 respectively; results are presented in Figures 8(b), 8(c) and 8(d). The output of these queries shows the top most similar VEP experiences along with the experiences of the machines involved. Thus, the entire experience at routing level, machine and job level can be retrieved and can be used to enhance effective decision making and performance evaluation in possible future queries.

7. CONCLUSIONS

Decisional DNA based experience model for a typical FMS is developed, which is capable of capturing and storing formal decisional events both at the process as well as at the object level. Similarity of previous experience is calculated with current requirement. Designing and planning issues of FMS can be solved mainly by this modelling technique. This technique induces intelligence as the database containing information of FMS installation has an interrelation between VEP and VEO features. Moreover, since each component of the FMS has a virtual model and can operate individually and also together with the wider range of production.

REFERENCES

Ali M., Wadhwa S., 2010, The Effect of Routing Flexibility on a Flexible System of Integrated Manufacturing. International Journal of Production Research. 48:5691-709.

Chen W.L., Xie S.Q., Zeng F.F., Li B.M., 2011, A new process knowledge representation approach using parameter flow chart. Computers in Industry. 62:9-22.

Groover M.P., 2007, Automation, Production Systems, and Computer Integrated Manufacturing. Third ed: Upper Saddle River, NJ: Third Edition Prentice Hall Press.

Sanchez E., Peng W., Toro C., Sanin C., Graña M., Szczerbicki E., 2014, Decisional DNA for modeling and reuse of experiential clinical assessments in breast cancer diagnosis and treatment,. Neurocomputing, 146:308-18.

Sanin C., and Szczerbicki E., 2004, Knowledge Supply Chain System: a conceptual model, in Knowledge Management: Selected Issues, A Szuwarzynski (Ed), Gdansk University Press, Gdansk pp. 79-97.

Sanin C., Szczerbicki E., 2005, Set of Experience: A Knowledge Structure for Formal Decision Events. Foundations of Control and Management Sciences. 3:95-113.

Sanin C., Szczerbicki E., 2006, Extending Set of Experience Knowledge Structure into a Transportable Language extensible Markup Language. Cybernetics and Systems. 37:97-117.

Sanin C., Szczerbicki E., 2008, Decisional DNA and the Smart Knowledge Management System: A process of transforming information into knowledge. In: Gunasekaran A, editor. Techniques and Tools for the Design and Implementation of Enterprise Information Systems. New York: IGI Global; p. 149–75.

Sanín C., Szczerbicki E., 2009, Experience-based knowledge representation: SOEKS. Cybernetics and Systems. 40:99-122.

Sanin C., Toro C., Vaquero J., Szczerbicki E., Posada J., 2007, Implementing decisional DNA in industrial maintenance by a knowledge SOUPA extension. Systems Science. 33:61-8.

Sanín C., Mancilla-Amaya L., Szczerbicki E., 2009, CayfordHowell P. Application of a Multi-domain Knowledge Structure: The Decisional DNA. In: Nguyen N, Szczerbicki E, editors. Intelligent Systems for Knowledge Management: Springer Berlin Heidelberg; p. 65-86.

Sanin C., Toro C., Haoxi Z., Sanchez E., Szczerbicki E., Carrasco E., 2012a, Decisional DNA: A multi-technology shareable knowledge structure for decisional experience. Neurocomputing. 88:42-53.

Sanín C., Mancilla-Amaya L., Haoxi Z., Szczerbicki E., 2012b, Decisional DNA: The concept and its implementation platforms. Cybernetics and Systems. 43:67-80

Shadbolt N, Hall W, Berners-Lee T., 2006, The Semantic Web Revisited. IEEE Intelligent Systems Journal. Vol. :96-100.

Shafiq S.I., Sanin C., Szczerbicki E., 2014a, Set of Experience Knowledge Structure (SOEKS) and Decisional DNA (DDNA): Past, Present and Future. Cybernetics and Systems. 45:200-15.

Shafiq S.I., Sanin C., Szczerbicki E., Toro C., 2014b, Virtual Engineering Objects (VEO): Designing, Developing and Testing Models. In: A Grzech LB, J. Swiatek, Z. Wilimowska, editor. System Analysis Approach to the Design,Control and Decision Support. Wroclaw: Wroclaw University of Technology Press; p. 183-92

Shafiq S..I., Sanin C., Szczerbicki E., Toro C., 2015a, Virtual Engineering Object / Virtual Engineering Process: A specialized form of Cyber Physical System for Industrie 4.0. In: Liya Ding CP, Leong Mun Kew, Lakhmi C. Jain, Robert J. Howlet, editor. Knowledge-Based and Intelligent Information & Engineering Systems 19th Annual Conference, KES-2015. Singapore: Procedia Computer Science; p. 1146-55.

Shafiq S.I., Sanin C., Toro C., Szczerbicki E., 2015b, Virtual engineering process (VEP): a knowledge representation approach for building bio-inspired distributed manufacturing DNA. International Journal of Production Research. P. 1-14.

Stecke K.E., 1986, A Hierarchical Approach to Solve Machine Grouping and Loading Problem of FMS. European Journal of Operation Research. 24:369-78.

Wang P., Sanin C., Szczerbicki E., 2015, Evolutionary algorithm and Decisional DNA for multiple

travelling salesman problem, Neurocomputing. 150:50-57.
Yadav A., Jayswal S.C., 2018, Modelling of flexible manufacturing system: a review. International Journal of Production Research. 56:2464-87.
Zhang H., Sanin C., Szczerbicki E., 2016, Towards Neural Knowledge DNA. Journal of Intelligent and Fuzzy Systems.:1-10.
Zhang H., Sanin C., Szczerbicki E., 2010, Gaining knowledge through experience: Developing Decisional DNA applications in robotics. Cybernetics and Systems. 41:628-37.

HYBRID SIMULATION MODEL SUPPORTING EFFICIENT COMPUTATIONS WITHIN RAIL TRAFFIC SIMULATIONS

Radek Novotný[(a)], Antonín Kavička[(b)]

[(a),(b)]Faculty of Electrical Engineering and Informatics, University of Pardubice

[(a)]radek.novotny3@student.upce.cz, [(b)]antonin.kavicka@upce.cz

The contribution deals with the unitary hybrid simulation model of railway traffic, which applies different levels of abstraction (microscopic and macroscopic) to different parts of the simulating system. As a result of applying this approach, simulation experiments can reflect the traffic within a large part of the railway network. The entire computational complexity is supposed to be significantly lower in comparison with an application of a pure microscopic simulator. From this point of view, the hybrid model can also be used to optimize the design of simulators of large and complex railway systems.
Special attention is paid to stochastic simulation experiments (applying random train delays) and to transforming train flows at the interface between pairs of microscopic and macroscopic submodels.

Keywords: scalable simulation model, unitary hybrid model, railway traffic, transformation of traffic flows, random train delays

1. INTRODUCTION

A significant part of the research in the field of optimizations of railway systems represents modelling a railway infrastructure and relevant rail traffic. For these purposes, the experimental research method of computer simulation is utilized. Depending on the required level of details, different simulation models (*microscopic, mesoscopic* or *macroscopic*) can be applied. From the viewpoint of modelling large railways systems, it is necessary to pay attention to their computational-efficient design.
Currently, the standard approach is based on the application of the identical level of details (*granularity*) to the entire simulator. If traffic simulations mirror large railway systems, time-efficient computations are required. That demand can be met by lowering the level of details either within the entire simulating system or within its selected parts. Hence, there is a strong motivation for designers of traffic simulations to use methodologies for building scalable traffic simulators. Those models enable to combine and interconnect various submodels of infrastructure (applying different levels of details) and different traffic submodels reflecting granularities of relevant infrastructural submodels (Hansen and Pachl 2008; Cui, and Martin 2011; Novotny and Kavicka 2016). Certainly, relevant transformations of traffic flows are supposed to be carried out on the boundary between corresponding submodels (Novotny and Kavicka 2017; Novotny and Kavicka 2018).

2. UNITARY HYBRID SIMULATION MODEL

Our presented methodology called *HybridRail* (Novotny and Kavicka 2016) is based on a hybrid simulation model implemented within one simulation tool (*unitary hybrid model*). That methodology supports combining submodels exploiting the microscopic and macroscopic levels of details. Microscopic simulation is connected to particular areas, within the frame of which the details about traffic (and infrastructure) are important for an experimenter. On the other hand, macroscopic simulation is applied to those parts of the simulator, where rough operational/traffic observations are sufficient. Unitary hybrid model enables to adjust the *granularity* of selected individual parts of a simulator. The mentioned parts are connected to relevant traffic submodels operating over corresponding infrastructure submodels. Overall computational demands of a unitary hybrid model (composed of non-homogeneous submodels) are certainly lower than demands related to a corresponding model executing pure microscopic simulation (Novotny and Kavicka 2016).

3. HYBRID INFRASTRUCTURE SUBMODEL

The methodology *HybridRail* (describing hybrid simulator building process) focuses primarily on the construction of a track infrastructure submodel. From the implementation viewpoint, it is necessary to distinguish between *micro-layer* and *hybrid layer*. *Micro-layer* contains a microscopic infrastructure submodel that corresponds to the highest level of details which can be applied to the track infrastructure. On the other hand, the *hybrid-layer* is composed of *micro-segments* and *macro-segments*. *Micro-segments* are directly taken from the micro-layer. *Macro-segments* apply higher degree of granularity (i.e. lower level of details) to relevant parts of the *micro-layer*. Two types of macro-segments (*macro-nodes* and *macro-edges*) are distinguished within the presented methodology. *Macro-edges* typically encapsulate line sequences of edges from micro-layer (typically reflecting rail lines).

Macro-nodes can enclose general continuous micro-layer areas. Constructions of *macro-segments* support constructing variant configurations of hybrid submodels of railway infrastructure (Novotny and Kavicka 2016).
For the purposes of visual deformation of the hybrid infrastructure model (especially around the *macro-segments*), it is necessary to distinguish between schematic visualization of infrastructure and definition of numerical values (parameters) related to metric (topological) and slope properties within the track layout (Novotny and Kavicka 2015).

4. HYBRID TRAFFIC SUBMODEL

Because of combining *micro-* and *macro-segments* within the *hybrid-layer*, it is necessary to apply different traffic submodels (exploiting various levels of abstraction), which are connected to different traffic indicators. From the viewpoint of the implementation of the unitary hybrid model it is necessary to distinguish between traffic submodels carried out over microscopic (*microscopic traffic submodels)* and macroscopic (*macroscopic traffic submodel*s) infrastructure segments. Because several different traffic submodels coexist within a hybrid model, it is necessary to solve transformations of traffic flows, i.e. it is necessary to unambiguously define the information about railway traffic on the interface between each microscopic and macroscopic submodel in order to maintain consistency of data (Burghout 2004; Burghout 2006; Novotny and Kavicka 2016).

5. MICROSCOPIC TRAFFIC SUBMODEL

Microscopic traffic submodel is based on applying realistic calculations connected with the train ride dynamics and train interactions (Salva 2005; Divis and Kavicka 2015). Train rides computations use detailed information about railway infrastructure (real topology/metric and slope properties) defined in *micro*-layer of infrastructure submodel. In other words, the movement of trains on the infrastructure reflects the real driving characteristics with respect to the train, track properties and traffic restrictions (Novotny and Kavicka 2017).

6. MACROSCOPIC TRAFFIC SUBMODEL

The basic idea is that trains do not have to be individually monitored during their movement in *macro-segments* (unlike within the above-mentioned microscopic traffic submodel). In other words, if the train can enter the macroscopic submodel, the moment of the simulation time, when the train leaves the submodel, is individually calculated (certainly, with the respect to railway timetable).

Because of existing differences between *macro-segments* due to the encapsulation of different parts of the microscopic model of infrastructure (railway stations may typically be encapsulated into *macro-nodes* and sections of rail lines to *macro-edges*) within the hybrid model, there are various concepts of realization of macroscopic traffic submodels. Those concepts can be based on an analogy with fluid flow or competition for shared resources (Novotny and Kavicka 2016). Due to the results of simulation experiments (carried out in a deterministic regime) that tested different concepts of macroscopic traffic models, a model based on the competition for shared resources was finally accepted for both types of *macro-segments* (Novotny and Kavicka 2018).
For the needs of stochastic simulation experiments (applying random train delays), it is necessary to specify the following *macro-segment* characteristics:

- the maximum permissible number of trains within the submodel,
- the total train dwell time in the submodel,
- the method of detecting the occupancy of adjacent submodels for the given future time windows and, where applicable,
- the train parameters needed for their movement in adjacent submodel to which they will enter.

6.1. Determination of the maximum permissible number of trains within the macro-segment

Generally, from the viewpoint of the selected macroscopic traffic submodel, the *macro-segment* can be understood as a form of shared resource that is able simultaneously/parallelly to hold only a certain number of trains. The maximum permissible number of trains within this submodel can be calculated on the basis of evaluations applied to selected attributes defined in the *micro*-layer.
In the case that a *macro-edge* consists of only one possible train path, the train input is dependent on the length of the train path, headway distance (determined for example by a table of stopping distances), the length of the train and, of course, the number of trains currently sojourning inside the submodel. On the other hand, the *macro-node* can consist of a set of primary and alternative train paths, which can be allocated to each direction. Thus, it is necessary to divide the station tracks according to all possible directions and then determine the possibility of entering the next train into *macro-node* (the number of currently available station tracks in the given direction and the current number of staying trains within the submodel are considered).

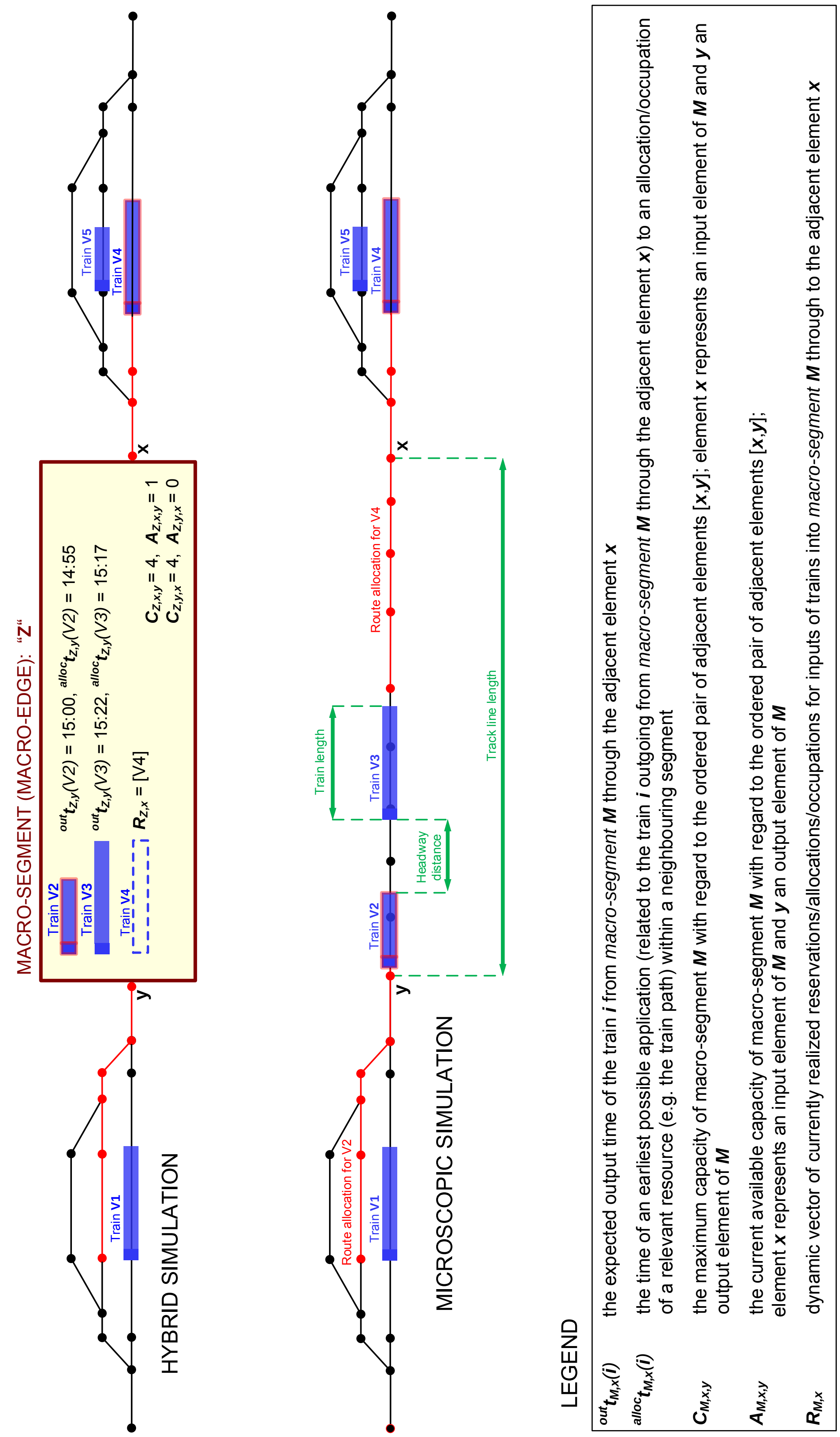

Figure 1 - Hybrid simulation model of railway traffic

In the case of definition *macro-node* capacity by the number of station tracks, it is possible to take into account the occupation of one station track by more trains at the same time. It corresponds to the real situation at the railway station.

Due to the nature of the railway traffic, it is necessary to predict the occupation of the *macro-segment* by a given train (via the dynamic “reservation” vector *R*) before it actually enters the *macro-segment* (*Figure 1*). Of course, this pre-reservation of the *macro-segment* capacity must be feasible not only in the microscopic traffic submodel (adjacent to the *macro-segment*), but also potentially in the macroscopic submodel, especially when is possible to combine *macro-segments* within a hybrid model.

6.2. A priory determination of train dwell time within the macro-segment

Calculation of the instant of simulation time, when the train leaves a given *macro-segment,* is always carried out at the moment when the train enters that segment (thus, a relevant predicted dwell time is determined). The computation of the train dwell time takes into account the following aspects:

- the number of admissible train paths for a given train transit through the *macro-segment*,
- the average lengths of the mentioned paths,
- the average train speed and
- the relevant time addition (e.g. because of stopping a train at a railway station or decelerating in front of a railway station, etc.).

Correct calculation of the time addition ${}^{add}t$ is quite important namely for the realistic determination of overall train running times (including acceleration and deceleration phases of the runnings).

In cases, when the train stops within *macro-node* according to the timetable, the time addition can be calculated as ${}^{add}t = {}^{dec}t + {}^{acc}t + {}^{dwl}t$, where

- ${}^{dec}t$ represents the time addition due to train braking from average speed (defined in the submodel) to complete stop,
- ${}^{acc}t$ represents the time addition due to train acceleration from zero speed to average speed and
- ${}^{dwl}t$ corresponds with the train dwell time at the platform in railway station according to the timetable.

If the train has to brake in front of the railway station in a part of infrastructure that is encapsulated in the *macro-edge,* it is necessary to determine not only the train speed (when leaving the submodel), but again in particular the correct time addition due to braking from the average speed defined in the submodel.

For above mentioned calculations of time additions is applied an approach based on the principle of uniformly accelerated respectively decelerated motion with using acceleration parameter (derived from the traction characteristic according to the average speed in the submodel) and train braking rate.

However, when calculating the train dwell time in the case of a *macro-edge*, it is necessary to consider the fact that train movements follow a FIFO-regime, i.e. they cannot be overtaken like within the *macro-node* (e.g. encapsulating a railway station). From the viewpoint of calculating dwell time of the individual trains and the FIFO-regime, it is important to consider the minimal time interval between trains, i.e. headway distance.

6.3. Determining the occupancy time of the subsequent submodel

Due to the coexistence of different submodels in the hybrid traffic model, the problem of train path occupancy within a relevant adjacent submodel (microscopic or macroscopic) must be potentially dealt. In other words, this means, that even if the train is currently in a given *macro-segment,* the train path or other kind of resource within an adjacent segment must be (reserved and) occupied sufficiently in advance (*Figure 1*). The train enters that adjacent segment later. As an example, the following case can be mentioned: a train plans to move from the *macro-edge* to the adjacent microscopic submodel (reflecting a railway station).

As a result, when the train enters a macro-segment, the moment (${}^{alloc}t$) of a relevant allocation time is calculated. Allocation time represents an earliest possible moment, when a needed occupation within a relevant subsequent segment is launched.

If all required resources are occupied at the given time (${}^{alloc}t$), it is necessary to wait, which will dynamically affect the train dwell time in the current submodel and also the value of the simulation time ${}^{out}t$, when the train will leave this submodel. If the train cannot leave the *macro-edge* for a reason defined above, it is necessary to keep the minimal time interval between trains according to the headway distance. In other words, the dwell time of other trains (which entered to the *macro-edge* behind this train) can be affected.

6.4. Determination of other train parameters for their movement in the subsequent submodel

From the viewpoint of the train leaving the *macro-segment* and its consistent transition to the adjacent submodel (*microscopic* and *macroscopic*), it is necessary to determine the values of other necessary train parameters. These parameters include:

- the current output speed of the train (affected by average speed or acceleration / braking of the train in the *macro-segment* etc.) and
- specific output element/point of the *macro-segment*.

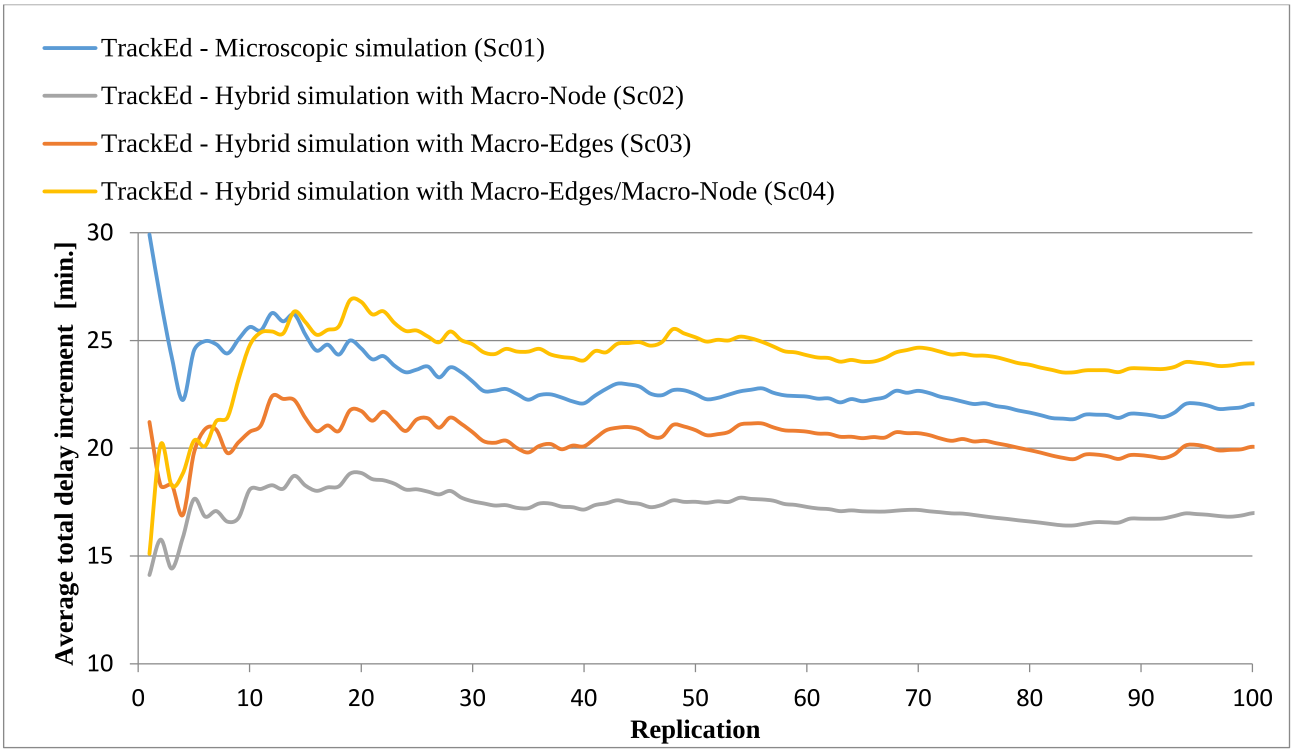

Figure 2 – Comparison of average total delay increments

7. VALIDATION

Regarding applications of a unitary hybrid model in practice, it is necessary that the results of deterministic and especially stochastic simulation experiments are correct and correspond to reality. In order to validate a unitary hybrid simulator, the following comparisons are supposed to be realized. The results of the simulation experiments for different scenarios related to the hybrid simulations are compared with the corresponding results obtained from microscopic simulations (both carried out within the same integrated development environment – e.g. the tool *TrackEd* can be applied). In addition, the comparisons with the results from other simulation tools (specialized in rail traffic simulations) are processed as well (e.g. simulation tool Villon is applied).

The mentioned comparisons will consider achieved running times of trains and their total delay increments. In other words, the desired behavior of hybrid models is that the transformations of traffic flows at the interfaces of the microscopic and macroscopic segments must have a minimal effect on the total train delays (compared with the values obtained from microscopic models). It is also important to compare the computational complexities of the simulation experiments performed within the microscopic and hybrid models.

In order to verify the correctness, the infrastructure of a part of the railway network of the Czech Republic comprised of a prototype station and border stations used for dispatching trains was used. Within the validation of the hybrid simulation model, both deterministic and stochastic simulation experiments were performed, for selected four different scenarios:

- (Sc01) simulation model working exclusively on microscopic level of details,
- (Sc02) hybrid simulation model with prototype station encapsulate in the *macro-node*,
- (Sc03) hybrid simulation model with sections of rail lines (paths between prototype station and the border stations) encapsulate in the *macro-edges*,
- (Sc04) hybrid simulation model with incidents of *macro-edges* and *macro-node* (combination of the previous two scenarios).

Primarily, it was necessary to validate and verify the implementation of train running dynamics and thereby confirm the correctness of used microscopic traffic model. A series of deterministic simulation experiments was performed according to a real timetable (containing several dozen trains in both directions). Basically, it was a comparison of a tachograph compiled from a real environment with a tachograph obtained from simulator results (a series of simulation experiments). Furthermore, the results obtained from the *TrackEd* tool (using the *MesoRail* computational core) were compared with the results from the already validated simulator *Villon*, which represents a simulation tool generally accepted by railroad experts (Divis and Kavicka 2015; Novotny and Kavicka 2017).

In the deterministic mode, both the above-mentioned concepts of macroscopic traffic models (based on an analogy with fluid flow or competition for shared resources) were tested in different scenarios of the hybrid simulation model. From viewpoint of comparison with the results obtained in purely microscopic traffic simulation, the concept of traffic based on the analogy of shared resource was chosen for both types of *macro-segments* (Novotny and Kavicka 2017; Novotny and Kavicka 2018).

As a result of the comprehensive validation of the unitary hybrid model, it was necessary to load railway traffic with random train delays (stochastic mode) and monitor how train delays would change (the most important indicator of interest is the value of the potential increase of delay) when passing through the infrastructure under all of the above scenarios.

Table 1: Parameters of random trains delay

Train category	Probability of train delay [%]	Mean value [s]	Maximum [s]
Express	50	420	7200
Stopping	33	270	7200
Cargo	50	1800	7200

In accordance with the methodology of SŽDC, s.r.o. (Rail Infrastructure Administration of the Czech Republic), the values of random train delays during simulation experiments were driven by exponential distribution of probability with parameter values specified for different train categories (*Table 1*).

Within all of the scenarios mentioned above, 100 replications were carried out with the application of random train delays. Initial testing was focused on the validation of a microscopic traffic model by comparing running times and delay increments achieved in another already validated simulator, Villon (similar as with the deterministic regime). In both cases, almost identical average total running times per replication was achieved - the average total delay increment of all trains (46) in replication then reached about 22 minutes.

In the next validation phase, the above indicators were monitored using *macro-segments* in relation to the results obtained using a simulation model working exclusively on microscopic level of detail (*Figure 2*). In a scenario using only railway station encapsulation into a *macro-node* (Sc02), the average total delay increment per replication was reduced by 5 minutes. This deviation in tens of percent may be due to the fact that in the microscopic traffic submodel, a part of the station (i.e. the track branching) may be occupied when the train is running to the station track, which can delay other trains entering or leaving the railway station.

Conversely, in the scenario using the encapsulation of only sections of rail lines into *macro-edges* (Sc03), the average total replication delay increment was slightly reduced (namely by 2 minutes). This may be due to the application of a different logic in traffic submodels (macroscopic versus microscopic) in cases where the train has to wait in front of a fully occupied railway station.

When comparing the hybrid model, which includes *macro-edges* and *macro-nodes* (Sc04), with a purely microscopic simulation model (Sc01), there was a difference in the achieved average total delay increments on replication. This difference reached about 2 minutes. Due to the many differences between the microscopic and macroscopic traffic submodel of traffic, this result can be assessed as valid.

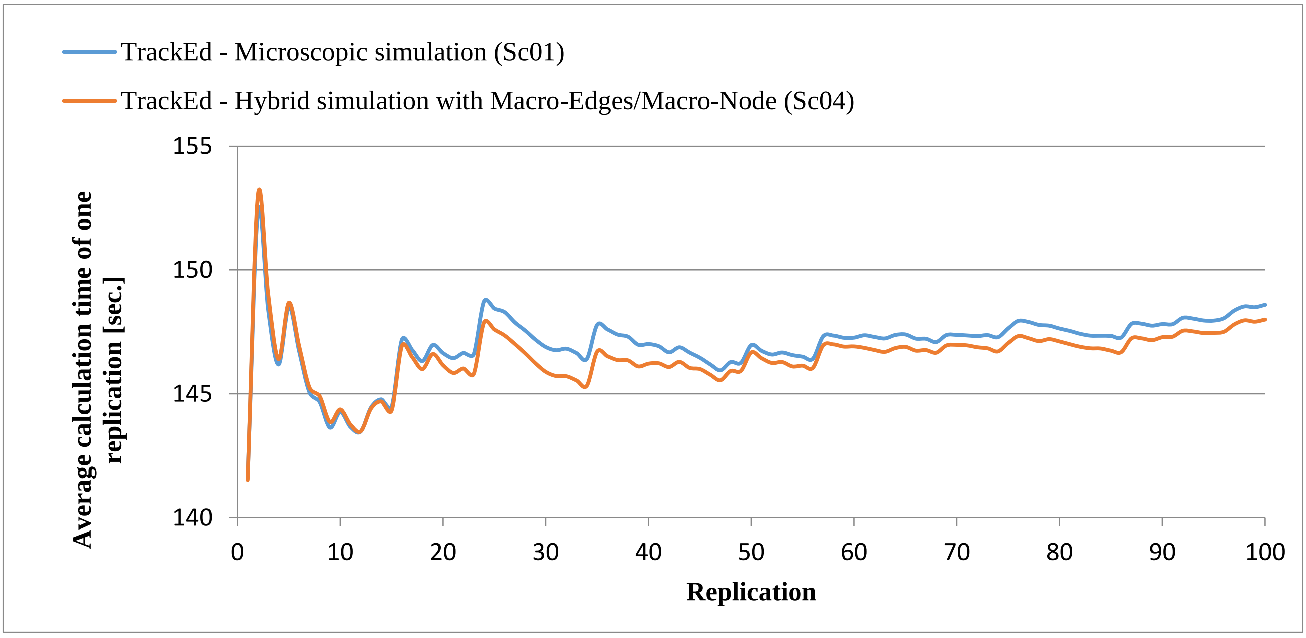

Figure 3 – Comparsion of average calculation time of one replication between hybrid and purely microscopic simulation model

ISBN 978-88-85741-25-6; Affenzeller, Bruzzone, Longo and Pereira Eds.

Despite the detected deviations in average delay increments, the hybrid traffic model (in all scenarios mentioned above) for a specific case study of railway traffic on selected areas of the railway network of the Czech Republic can be considered valid. As part of the experiments, the average length of simulation calculation per replication was compared between a hybrid and a purely microscopic simulation model (*Figure 3*).

The next step will be operational verification of the hybrid traffic model for other areas of the railway network of the Czech Republic. The results of simulation experiments will then lead to establishing a general applicability of the introduced methodology for building a unitary hybrid model of railway traffic.

8. PERSPECTIVES OF FURTHER DEVELOPMENT

Prospective development expects building a hybrid infrastructure model without the need to construct (as a first compulsory step) a microscopic model of the entire railway layout. Extensions can enable modelling of some infrastructure submodels on a higher level of abstraction (macroscopic) and defining only the rough characteristics of the tracks needed for the macroscopic traffic submodel.

9. CONCLUSION

As part of the paper, the original methodical approach (Novotny and Kavicka 2017) to the construction of a unitary hybrid simulation model was verified. The hybrid traffic model combines areas built with varying degrees of *granularity* and thus distinguishes between the microscopic traffic submodel (applying detailed monitoring of train runnings in this submodel) and the macroscopic traffic submodel in which only the gross operating characteristics are monitored.

The hybrid model constructed in this way also brings the problem of solving the transformations of traffic flows at their interfaces. The main emphasis is therefore put on detailed description and implementation of this transformation of traffic flows and on operational verification mainly by means of a series of stochastic simulation experiments, when railway traffic is burdened by random delays.

The described transformation of traffic flows at the interface of microscopic and macroscopic traffic submodels was validated according to the results of deterministic, but mainly stochastic, simulation experiments (implemented in the integrated development environment *TrackEd*). These experiments were carried out within simulation study focused on the investigation of railway traffic in a selected area of the railway network of the Czech Republic.

ACKNOWLEDGEMENT

The work was supported by the funds of University of Pardubice, Czech Republic - *Student grant competition* (SGS_2019_021).

REFERENCES

Cui Y., and Martin U., 2011. Multi-scale Simulation in Railway Planning and Operation. PROMET Traffic. Available from: http://www.fpz.unizg.hr/traffic/index.php/PROMTT/article/view/186 [Accessed 3 March 2019].

Burghout W., 2004. Hybrid microscopic-mesoscopic traffic simulation. Doctoral Dissertation. Royal Institute of Technology.

Burghout W., Koutsopoulos H., and Andreasson I., 2006. A discrete-event mesoscopic traffic simulation model for hybrid traffic simulation. To appear in: Intelligent Transportation Systems Conference. Toronto.

Hansen Ingo, Pachl Jorn, 2008. Railway timetable and traffic. Hamburg: Eurailpress.

Divis R., and Kavicka A., 2015. Design and development of a mesoscopic simulator specialized in investigating capacities of railway nodes. The 27th European Modeling & Simulation Symposium. Bergeggi, Italy.

Novotny R., and Kavicka A., 2015. Model of a railway infrastructure as a part of a mesoscopic traffic simulator. The 27th European Modeling & Simulation Symposium. Bergeggi, Italy.

Novotny R., and Kavicka A., 2016. Scalable simulation models of railway traffic. The 28th European Modeling & Simulation Symposium. Larnaca, Cyprus.

Novotny R., and Kavicka A., 2017. Unitary hybrid model of railway traffic. The 29th European Modeling & Simulation Symposium. Barcelona, Spain.

Novotny R., and Kavicka A., 2018. Different traffic submodels scalable unitary hybrid simulator related to railway systems. The 30th European Modeling & Simulation Symposium. Bucharest, Hungary.

Salva I., 2005. Simulácia pohybu koľajových vozidiel. Doctoral Dissertation. Žilina.

A 0-D MODEL TO PREDICT THE RELATIONSHIP BETWEEN RESISTANCE AND COMPLIANCE IN PULMONARY ARTERIAL HYPERTENSION

Claudio De Lazzari[(a),(b)], Silvia Marconi[(a)], Massimo Capoccia[(c)], Silvia Papa[(d)], Roberto Badagliacca[(d)], Carmine Dario Vizza[(d)]

[(a)]National Research Council, Institute of Clinical Physiology (IFC-CNR), Rome, Italy
[(b)]National Institute for Cardiovascular Research (I.N.R.C.), Bologna, Italy
[(c)]Royal Brompton Hospital, Royal Brompton & Harefield NHS Foundation Trust, London, UK
[(d)]Department of Cardiovascular Respiratory Nephrologic and Geriatric Sciences, Sapienza University of Rome, Italy

[(a),(b)]claudio.delazzari@ifc.cnr.it, [(a)]silvia.marconi@ifc.cnr.it, [(c)]capoccia@doctors.org.uk, [(d)]silvia.papa@uniroma1.it, [(d)]roberto.badagliacca@uniroma1.it, [(d)]dario.vizza@uniroma1.it

ABSTRACT
The inverse relationship between pulmonary vascular resistance and arterial compliance plays a significant role for the treatment of pulmonary arterial hypertension. The hyperbolic relationship between pulmonary vascular resistance and arterial compliance enables to evaluate the percentage of resistance reduction, which ultimately leads to an improvement in compliance. The numerical representation of the pulmonary circulation can help clinicians evaluate these key parameters in relation to therapeutic intervention. In this paper, we present a 0-D numerical model of the pulmonary circulation. The right ventricular pressure is reproduced using a modified time-varying elastance and the pulmonary bed is modelled with RLC elements.
Preliminary results obtained from clinical parameters measured in patients with pulmonary arterial hypertension are discussed in this context. The simulations performed using the 0-D model have been applied to a clinical setting to evaluate the percentage change induced on compliance by a reduction in resistance in fixed circulatory conditions.

Keywords: time-varying elastance, numerical model, pulmonary arterial hypertension, pulmonary compliance

1. INTRODUCTION

The inverse relationship between pulmonary vascular resistance (*PVR*) and arterial compliance (*PVC*) plays a significant role for the treatment of pulmonary arterial hypertension (PAH). Different causes may lead to PAH (Barst 2004) but all of them increase right ventricular (RV) afterload.
Two different analyses provide important information to understand the effects of pharmacological treatment in patients affected by PAH. The first one is the PVRPVC-time (RC-time) analysis in which resistance and compliance are related by an inverse hyperbolic function. In this analysis, it must be kept in mind that the RC-time can be influenced by the pulmonary capillary wedge pressure (*PCWP*). The second one is based on the right ventricular pulmonary arterial coupling defined as the ratio between the pulmonary arterial elastance (E_a) and the slope (E_{es}) of the End-Systolic Pressure-Volume Relationship (ESPVR) of the right ventricle. For the left ventricle, a normally coupled cardiovascular system is characterized by E_a/E_{es} values between 0.5 and 1.5 (Guarracino 2013). A normal value for right ventricular-pulmonary arterial coupling is E_{es}/E_a>1.5 (Kuehne 2004, Tello 2019). The optimal mechanical coupling occurs when the ratio is 1.0. Numerical models of the right circulation may help understand the mechanism of pulmonary arterial hypertension in relation to diagnosis, treatment and prognosis (Lankhaar 2006). CARDIOSIM© software simulator of the cardiovascular system may well be an appropriate tool to address some of the issues related to pulmonary arterial hypertension (De Lazzari 1998, 2009, 2010). In this work we have assembled CARDIOSIM© with two pressure generators for the right atrial pressure and *PACWP*. The right ventricular pressure was simulated with a modified time-varying elastance model. The pulmonary circulation was represented with three different sections: main pulmonary artery, small pulmonary artery and pulmonary arteriole and capillary compartments (De Lazzari 2019).
Preliminary results have been obtained from clinical parameters measured in patients affected by PAH.

2. MATERIALS AND METHODS

CARDIOSIM© is the software package of the cardiovascular simulator developed in the Institute of Clinical Physiology (Rome Section) of the National Research Council (De Lazzari 2011). The software is interactive and capable of reproducing physiological and pathological conditions for clinical decision-making in a controlled environment. This simulation software platform has seven modules: left and right heart (composed by ventricles and atria), systemic and pulmonary arterial sections, systemic and pulmonary venous sections and coronary circulation. Different lumped parameter (0-D) models with variable degree of complexity levels have been implemented for each module. All modules are stored in the CARDIOSIM© library where numerical models of different mechanical circulatory assist devices (MCADs) are also available, which can reproduce the behavior of:

- pneumatic left, right and biventricular assist devices (LVAD, RVAD and BVAD) (De Lazzari 1998);
- intra-arterial, axial-flow pump such as Hemopump (LVAD, RVAD and BVAD) (De Lazzari 2006);
- PUlsatile Catheter Pump (PUCA pump) (Fresiello 2011);
- IntraAortic Balloon Pump (IABP) (De Lazzari 2001, Marconi 2018);
- Berlin Heart INCOR pump (Capoccia 2018);
- biventricular pacemaker (De Lazzari 2013);
- Thoracic Artificial Lung (TAL) (De Lazzari 2014).

Two different modules have been implemented in CARDIOSIM© library to reproduce the native heart behavior. In the first one the ventricles, the atria and the septum have been modelled according to the time-varying elastance theory (De Lazzari 2017) with the aim to reproduce the inter-ventricular (IVS) and the inter-atrial (IAS) septum behavior and the intra-ventricular or inter-ventricular conduction delays. In the second one, described below, the filling and ejection phases of the ventricle are modelled separately using the time-varying elastance concept (De Lazzari 2005).
In CARDIOSIM© the different modules can be assembled according to the need of the simulation with the aim to reproduce physiological and pathological conditions, which can be treated with drugs, MCADs or both. In addition, the effects induced by mechanical ventilation can be simulated during MCADs assistance (De Lazzari 1998, 2001, 2006, 2013, 2014).
Fig. 1 shows the model of the pulmonary circulation assembled and used for this study.

2.1. Electrical analogue of the pulmonary circulation

The right atrial pressure (*Pra*) and the pulmonary capillary wedge pressure (*Wedge*) are modelled with two fixed pressure generators, which can be manually changed throughout the cardiac cycle during the simulations.
The behavior of the main (small) pulmonary artery section is reproduced with a 0-D numerical model implemented using resistance R_{pam} (R_{pas}), inertance L_{pam} (L_{pas}) and compliance C_{pam} (C_{pas}). R_{pac}, L_{pac} and C_{pac} reproduce the pulmonary arteriole and capillary section.
The tricuspid valve is modelled with two resistances (R_{ri} and R_{inv}) and one diode. R_{inv} allows the simulation of tricuspid regurgitation. The valve between the right ventricle and the pulmonary bed is modelled with a resistance (R_{ro}) and a diode.
The variable resistance R_{ap} enables to reproduce the effects of the peripheral pulmonary resistance.

2.2. Right ventricle

Within CARDIOSIM© library, a numerical model reproducing the filling and ejection phases of the right ventricle separately was selected.

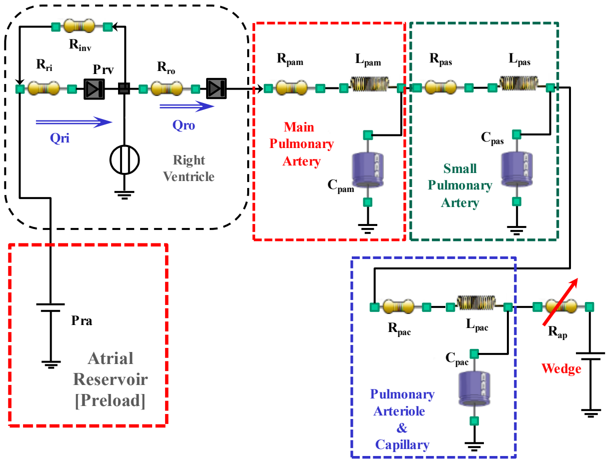

Figure 1: Electrical Analogue of the Pulmonary Circulation.

The contraction and ejection phase can be simulated with the modified time-varying elastance model according to the following equation (De Lazzari 2005):

$$Prv(t) = \left[Vrv(t) - Vrv_0\right] \cdot Erv(t) \cdot \left(1 + a \cdot \frac{dVrv(t)}{dt}\right) \tag{1}$$

Prv(t) is the instantaneous right ventricular pressure, *Vrv(t)* is the instantaneous right ventricular volume, *Erv(t)* is the right ventricular elastance, *a* is a constant and Vrv_0 is the resting right ventricular volume.
The right ventricular filling phase is reproduced by:

$$Prv(t) = C \cdot e^{k \cdot Vrv(t)} + D \cdot e^{-j \cdot Vrv(t)} + E \tag{2}$$

The constants *C*, *D*, *E*, *k* and *j* reproduce the right ventricular filling properties. *C* and *k* modify the right ventricular rigidity. *D* and *j* change the right ventricular aspiration phase. *E*, *k* and *j* vary the resting right ventricular volume (Vrv_0). Eq. (2) describes the End-Diastolic Pressure-Volume Relationship (EDPVR) curve in the pressure-volume (P-V) plane (Fig. 2).
Different EDPVR curves are obtained by changing the values of *C*, *D*, *E*, *k* and *j* (see the box in Fig. 2). In the P-V plane, Eqs. (1) and (2) describe the ventricular loop, the ESPVR and the EDPVR.
In Fig. 2 E_a is the arterial elastance and E_{es} is the ventricular elastance. The ratio between these two variables is the expression of ventricular coupling.
This numerical ventricular representation reproduces Starling's law of the heart.

2.3. Patient description

The software simulator reproduced the patient's basal conditions. The clinically measured parameters are listed in Table 1. The trans-pulmonary gradient (TPG), defined, as the difference between *PAP* and *PCWP*, is 47 mmHg, which is well above the cut-off of 12 mmHg making this patient completely unsuitable for heart transplant. Although attractive, a combined heart and lung transplant is not widely performed, donor availability is more limited and controversy remains.

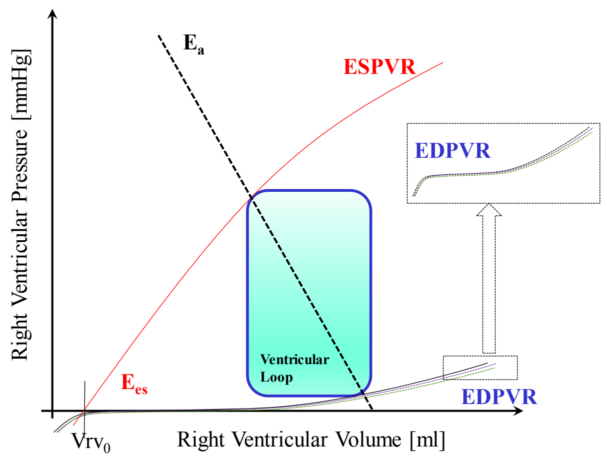

Figure 2: Right Ventricular Loop in the Pressure-Volume Plane.

Table 1: Basal Conditions

NYHA	II-III
Heart Rate (*HR*) [bpm]	70
Body Surface Area (*BSA*) [m^2]	1.97
Right Atrial Pressure (*Pra*) [mmHg]	4.0
Mean Pulmonary Arterial Pressure (*PAP*) [mmHg]	58.0
Mean *PCWP* [mmHg]	11.0
Cardiac Output (*CO*) [$l \cdot min^{-1}$]	5.8
Cardiac Index (*CI*) [$l \cdot min^{-1} \cdot m^{-2}$]	2.94
Total Pulmonary Resistance [Wood Units]	10.2
Pulmonary Arteriolar Resistance [Wood Units]	8.3

Following manual setting of *HR*, *Pra*, *PCWP*, total pulmonary and arteriole resistances, *BSA* and estimated right end-diastolic volume (*EDV*), CARDIOSIM© software automatically adjusts the value of the resistance R_{ap} to reproduce the measured mean *PAP* value. Starting from these conditions the simulator reproduced the other measured parameters (*CO*, *CI*, *PAP*, stroke volume) and estimated the E_{es}/E_a ratio and the RC-time.

Oral combination therapy with a selective endothelin type A receptor antagonist (ambrisentan) and a phosphodiesterase type 5 inhibitor (tadalafil) was continued for six months following which further measurements were recorded and listed in Table 2. Both E_{es}/E_a and RC-time were estimated based on the above measurements using the cardiovascular numerical model in the absence of tricuspid regurgitation.

The results were compared with the previous simulations.

Table 2: Patient's Conditions Following Drug Treatment

NYHA	II-III
Heart Rate (*HR*) [bpm]	72
Body Surface Area (*BSA*) [m^2]	1.93
Right Atrial Pressure (*Pra*) [mmHg]	7.0
Mean Pulmonary Arterial Pressure (*PAP*) [mmHg]	45.0
Mean *PCWP* [mmHg]	12.0
Cardiac Output (*CO*) [$l \cdot min^{-1}$]	6.0
Cardiac Index (*CI*) [$(l \cdot min^{-1}) \cdot m^{-2}$]	3.07
Total Pulmonary Resistance [Wood Units]	7.5
Pulmonary Arteriolar Resistance [Wood Units]	5.5

3. RESULTS

Fig. 3 shows the screenshot produced with the software simulator starting from the baseline parameters reported in Table 1.

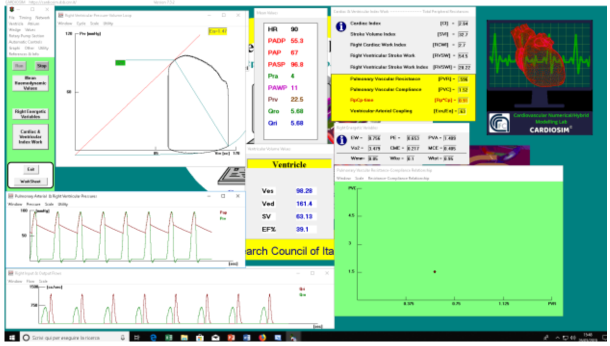

Figure 3: Baseline Conditions: CARDIOSIM© Screenshot.

The right ventricular loop (upper left window), ESPVR, EDPVR and the pulmonary arterial elastance are reproduced in the P-V plane under stationary conditions. The instantaneous ventricular (green waveform) and pulmonary pressures (red waveform) are plotted in the lower left window; both instantaneous right ventricular input/output (*Qri*/*Qro* red/green line) flow waveforms are plotted in the window below (Fig. 3).

The *HR* (90 bpm), the diastolic (*PADP*) and systolic (*PASP*) values for the pulmonary artery pressure, the mean pulmonary arterial pressure (*PAP*), the mean right atrial pressure (*Pra*), the mean pulmonary capillary wedge pressure (*PCWP*), the mean right ventricular pressure (*Prv*) and the mean right ventricular input/output flow (*Qri*/*Qro*) are reported in the upper central box. The lower right window shows the relationship between *PVR* and *PVC* (i.e. the RC-time or RC product). The pair of their values in the considered conditions is represented by the red point in the plane.

The parameter values obtained in stationary conditions (Table 3) can be compared with the measured values (Table 1). Pulmonary vascular resistance is traditionally used to describe pulmonary hemodynamic characteristics. In Fig. 3 *Ves*, *Ved* and *SV* are the end-systolic volume (*ESV*≡*Ves*), the end-diastolic volume (*EDV*≡*Ved*) and the stroke volume (*SV*) respectively. *EW*, *PE* and *PVA* are the external work, the potential energy and the pressure volume area respectively (Sagawa 1988). A comparison between the oxygen consumption (VO_2) of the right ventricle (estimated with the software simulator) and that measured in the whole cardiac muscle is currently being considered by our group.
The new patient's conditions after treatment (Table 2) were reproduced by CARDIOSIM©. The results are reported in Fig. 4 and Table 4.

Table 3: Parameters Obtained Using the Software Simulator (Baseline Conditions)

Heart Rate (*HR*) [bpm]	90
Body Surface Area (*BSA*) [m^2]	1.93
Right Atrial Pressure (*Pra*) [mmHg]	4.0
Mean Pulmonary Arterial Pressure (*PAP*) [mmHg]	66
Mean *PCWP* [mmHg]	11.0
Cardiac Output (*CO*) [$l\cdot min^{-1}$]	5.68
Cardiac Index (*CI*) [$(l\cdot min^{-1})\cdot m^{-2}$]	2.94
Total Pulmonary Resistance (*Rp*) [$mmHg\cdot ml^{-1}\cdot sec$]	0.596
Pulmonary Vascular Compliance (*Cp*) [$mmHg^{-1}\cdot ml$]	1.52
RC-time (*Rp·Cp*) [sec]	0.91
Pulmonary Arterial Elastance (E_a) [$mmHg\cdot ml^{-1}$]	1.47
Right Ventricular ESPVR Slope (E_{es}) [$mmHg\cdot ml^{-1}$]	0.93
Ventricular Arterial Coupling (E_{es}/E_a)	0.63

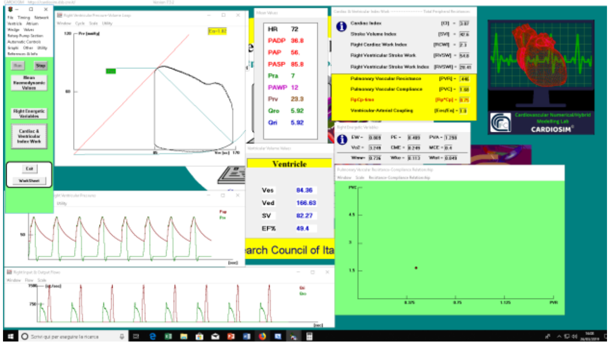

Figure 4: Patient Conditions After Six-Month Drug Treatment: CARDIOSIM© Screenshot.

The effects induced by drug administration can be observed in the *PVR-PVC* plane where the red point shifts to the left and upward with respect to the previous position (see Figs. 3 and 4) confirming a decrease in pulmonary vascular resistance and an increase in pulmonary vascular compliance.
A comparison between the results listed in Table 3 (Fig. 3) with those obtained following drug treatment (Table 4 - Fig. 4) shows a decrease in pulmonary vascular resistance by about 25% (from 0.596 to 0.446 $mmHg\cdot ml^{-1}\cdot sec$).
Simulation results show an increase in pulmonary vascular compliance by about 14% (from 1.52 to 1.68 $mmHg^{-1}\cdot ml$) following drug treatment.
Consequently, RC-time decreases from 0.91 sec to 0.75 sec after a six-month drug treatment.

Table 4: Parameters Obtained Using the Software Simulator (After Six Months)

Heart Rate (*HR*) [bpm]	72
Body Surface Area (*BSA*) [m^2]	1.93
Right Atrial Pressure (*Pra*) [mmHg]	7.0
Mean Pulmonary Arterial Pressure (*PAP*) [mmHg]	56
Mean *PCWP* [mmHg]	12.0
Cardiac Output (*CO*) [$l\cdot min^{-1}$]	5.92
Cardiac Index (*CI*) [$(l\cdot min^{-1})\cdot m^{-2}$]	3.07
Total Pulmonary Resistance (*Rp*) [$mmHg\cdot ml^{-1}\cdot sec$]	0.446
Pulmonary Vascular Compliance (*Cp*) [$mmHg^{-1}\cdot ml$]	1.68
RC-time (*Rp·Cp*) [sec]	0.75
Pulmonary Arterial Elastance (E_a) [$mmHg\cdot ml^{-1}$]	1.02
Right Ventricular ESPVR Slope (E_{es}) [$mmHg\cdot ml^{-1}$]	1.02
Ventricular Arterial Coupling (E_{es}/E_a)	1.0

The inverse coupling of R and C has direct and important hemodynamic consequences. A decrease in R is accompanied by a substantial increase in C in mild pulmonary hypertension (PH) whereas the increase in C is negligible in severe PH.
This may explain the clinical observation that patients with mild PH (moderately increased R) often show a greater hemodynamic improvement following treatment than patients with severe PH (strongly increased R), even if their R decreases by the same amount.
Finally, the simulated pharmacological treatment produced a 59% increase in ventricular arterial coupling (E_{es}/E_a); this effect is mainly attributable to approximately 70% reduction in E_a (from 1.47 to 1.02 $mmHg\cdot ml^{-1}$). An $E_{es}/E_a > 1.0$, normally in the range of 1.5–2.0, allows for right ventricular flow output at minimal energy cost, and thus reflects optimal ventricular-arterial coupling (Sunagawa 1985, Vonk Noordegraaf 2013).
According to literature data E_{es}/E_a in patients with severe forms of pulmonary hypertension such as pulmonary arterial hypertension or chronic thromboembolic PH, shows an adaptative increase in

E_{es} with more or less preserved E_{es}/E_a ratio (Vonk Noordegraaf 2017).

4. CONCLUSIONS

The measurement of pulmonary vascular resistance (*PVR*) is a convenient way to evaluate right ventricular afterload but it may not completely reflect its status because it does not consider the pulsatile component, which is significantly more important in the pulmonary circulation compared to the systemic circulation.

The effect of compliance seems to play a significant role in pulmonary arterial hypertension as addressed by the time constant (RC-time). A simulation approach may give ready information about the two components with a view to patient selection, treatment optimization and outcome prediction.

REFERENCES

Barst R.J., McGoon M., et al. 2004. Diagnosis and differential assessment of pulmonary arterial hypertension. J. Am. Coll. Cardiol., 43, S40-S47.

Guarracino F., Baldassarri R., et al. 2013. Ventriculo-arterial decoupling in acutely hemodynamic states. Crit. Care, 17, 213.

Kuehne T., Yilmaz S., Steendijk P., et al. 2004. Magnetic Resonance Imaging Analysis of Right Ventricular Pressure-Volume Loops. In Vivo Validation and Clinical Application in Patients With Pulmonary Hypertension. Circulation, 110, 2010-2016.

Tello K., Dalmer A., Axmann J., et al. 2019. Reserve of Right Ventricular-Arterial Coupling in the Setting of Chronic Overload. Circulation: Heart Failure, 12(1), e005512.

Lankhaar J.W., Westerof N., Faes T.J.C., et al. 2006. Quantification of right ventricular afterload in patients with and without pulmonary hypertension. Am. J. Phsyol. Heart Circ. Physiol., 291, H1731-H1737.

De Lazzari C., Darowski M., et al. 1998. The influence of left ventricle assist device and ventilatory support on energy-related cardiovascular variables. Med. Engi. & Phys., 20(2), 83-91.

De Lazzari C. Stalteri D. 2011. CARDIOSIM© cardiovascular software simulator. Italy: C.N.R. National Research Council, https://cardiosim.dsb.cnr.it/

De Lazzari C., Neglia D., et al. 2009. Computer simulation of coronary flow waveforms during caval occlusion. Meth. Infor. Med., 48(2), 113-122.

De Lazzari C., D'Ambrosi A., Tufano F., et al. 2010. Cardiac resynchronization therapy: could a numerical simulator be a useful tool in order to predict the response of the biventricular pacemaker synchronization. Eur. Rev. Med. Pharmacol. Sci., 14(11), 969-978.

De Lazzari C., Capoccia M., Marconi S. 2019. How can LVAD support influence ventricular energetics parameters in advanced heart failure patients? A retrospective study. Computer Methods and Programs in Biomedicine, 172, 117-126.

De Lazzari C., Darowski M., Ferrari G., Pisanelli D.M., Tosti G 2006. Modelling in the study of interaction of Hemopump device and artificial ventilation. Computers in Biology and Medicine, 36 (11), 235-1251.

Fresiello L., Gu Y.J., et al. 2011. PUCA pump and IABP comparison: analysis of hemodynamic and energetic effects using a digital computer model of the circulation. Int. J. Artif. Organs, 34 (5), 442-455.

De Lazzari C., Darowski M., Ferrari G., et al. 2001. Ventricular energetics during mechanical ventilation and intraaortic balloon pumping – Computer simulation. Journal of Medical Engineering & Technology, 25 (3), 103-111.

Marconi S., Cappelli C., Capoccia M., et al. 2018. A New Numerical Model of the Intra-aortic Balloon Pump as a Tool for Clinical Simulation and Outcome Prediction. World Congress on Medical Physics and Biomedical Engineering 2018. IFMBE proceedings, Springer, 795-799.

Capoccia M., Marconi S., Singh A.A., et al. 2018. Simulation as a preoperative planning approach in advanced heart failure patients. A retrospective clinical analysis. BioMedical Engineering OnLine, 17:52.

De Lazzari C., Del Prete E., Genuini I., Fedele F. 2013. In silico study of the haemodynamic effects induced by mechanical ventilation and biventricular pacemaker. Computer Methods and Programs in Biomedicine, 110 (3), 519-527.

De Lazzari C., Genuini I., Quatember B., Fedele F. 2014. Mechanical ventilation and thoracic artificial lung assistance during mechanical circulatory support with PUCA pump: In silico study. Computer Methods and Programs in Biomedicine, 113 (2), 642-654.

De Lazzari C., Pirckhalava M. 2017. Cardiovascular and pulmonary artificial organs: educational training simulators. Rome: Consiglio Nazionale delle Ricerche (CNR) Press.

De Lazzari C., Darowski M., Wolski P. 2005. In vivo and simulation study of artificial ventilation effects on energetic variables in cardiosurgical patients. Meth. Infor. Med., 44(1), 98-105.

Sagawa K., Maughan L., Suga H. and Sunagawa K. 1988. Cardiac Contraction and the Pressure-Volume Relationships. Oxford University Press, New York.

Sunagawa K., Maughan W.L., Sagawa K. 1985. Optimal arterial resistance for the maximal stroke work studied in isolated canine left ventricle. Circ. Res. 56, 586-95.

Vonk Noordegraaf A., Haddad F., Chin K.M., et al. 2013. Right heart adaptation to pulmonary arterial hypertension: physiology and pathobiology. J. Am. Coll. Cardiol. 62: Suppl., D22-D33.
Vonk Noordegraaf A., Westerhof B.E., Westerhof N. 2017. The relationship between the right ventricle and its load in pulmonary hypertension. J. Am. Coll. Cardiol. 69, 236-243.

QUICKEST CHANGE-POINT DETECTION IN TIME SERIES WITH UNKNOWN DISTRIBUTIONS

S.M. Pergamenshchikov[a], Tartakovsky, A.G.[b]

[a] LMRS, UMR 6085 CNRS, Université de Rouen Normandie, Saint-Etienne du Rouvray Cedex, France International Laboratory SSP & QF, Tomsk State University
[d] Space Informatics Laboratory, Moscow Institute of Physics and Technology, Moscow, Russia and AGT StatConsult, Los Angeles, California, USA

[a] Serge.Pergamenshchikov@univ-rouen.fr, [b] agt@phystech.edu

ABSTRACT
We consider a problem of sequential detection of changes in general time series, in which case the observations are dependent and non-identically distributed, e.g., follow Markov, hidden Markov or even more general stochastic models. It is assumed that the pre-change model is completely known, but the post-change model contains an unknown (possibly vector) parameter. Imposing a distribution on the unknown post-change parameter, we design a mixture Shiryaev-Roberts change detection procedure in such a way that the maximal local probability of a false alarm (MLPFA) in a prespecified time window does not exceed a given level and show that this procedure is nearly optimal as the MLPFA goes to zero in the sense of minimizing the expected delay to detection uniformly over all points of change under very general conditions. These conditions are formulated in terms of the rate of convergence in the strong law of large numbers for the log-likelihood ratios between the "change" and "no-change" hypotheses. An example related to a multivariate Markov model where these conditions hold is given.

Keywords: asymptotic optimality, change-point detection, composite post-change hypothesis, quickest detection, weighted Shiryaev-Roberts procedure

1. INTRODUCTION

The problem of quick detection of abrupt changes in time series arises in different areas related to automatic control, segmentation of signals, biomedical signal processing, quality control engineering, finance, link failure detection in communication networks, intrusion detection in computer systems, and target detection in surveillance systems. See, e.g., Basseville and Nikiforov (1993), Kent (2000), Page (1954), Tartakovsky, Nikiforov, and Basseville (2015) and references therein. One of a challenging application area is intrusion detection in computer networks [Kent (2000), Tartakovsky et al., Rozovskii, Blažek (2006)]. Large scale attacks, such as denial-of-service attacks, occur at unknown points in time and need to be detected in the early stages by observing abrupt changes in the network traffic.

In the change point analysis, a large variety of observation models is used which include i.i.d. sequences of random variables whose distributions change at the disruption time and also different models with dependent observations. Many papers have been devoted to the problem of detecting abrupt changes of the parameters in autoregression and Markov processes, which are widely used in the statistical analysis of time series and statistics of random processes. There is a vast literature on the detection of abrupt parameter changes in Markov time series with known probabilistic characteristics. See, for example, Basseville and Nikiforov (1993), Lai (1998), Pergamenshchikov and Tartakovsky (2018), Yakir (1994) and references therein.

The present paper addresses a general non-i.i.d. model when the post-change distribution contains an unknown parameter. Using the analytical results obtained in Pergamenshchikov and Tartakovsky (2018), we establish very general conditions under which the mixture Shiryaev-Roberts detection procedure is asymptotically optimal, minimizing the expected delay to detection in the class of change detection procedures with the given maximal local probability of a false alarm when this probability is small.

2. PROBLEM

Consider the change-point problem for the general dependent non-i.i.d. model (time series) $(x_k)_{k\geq 1}$ specified by the conditional densities of x_k given $(x_1,\ldots,x_{k-1})$, denoted as $f_{\theta,k}^{(\nu)}(x_k \mid x_1,\ldots,x_{k-1})$, where θ is an unknown parameter. More precisely, we assume that the conditional density changes from $f_*(x_k \mid x_1,\ldots, x_{k-1})$ to $f_\theta(x_k \mid x_1,\ldots, x_{k-1})$ at a point ν, i.e.

$$f_{\theta,k}^{(\nu)}\left(x_k \mid x_1,\ldots,x_{k-1}\right) = f_*\left(x_k \mid x_1,\ldots,x_{k-1}\right)\mathbf{1}_{\{k\le\nu\}} + f_\theta\left(x_k \mid x_1,\ldots, x_{k-1}\right)\mathbf{1}_{\{k>\nu\}}. \qquad (1)$$

Assume that the conditional densities

$$\left(f_*\left(x_k \mid x_1,\ldots,x_{k-1}\right)\right)_{k\ge1} \qquad (2)$$

are known, the change point ν is a nonrandom unknown integer and one needs to detect the change as soon as possible after it occurs. Introduce the class of detection procedures $\mathbf{M}_{\alpha,m}$ defined by stopping times τ such that

$$\sup_{k\ge1}\mathbf{P}_*\left(k \le \tau \le k+m\right) \le \alpha, \qquad (3)$$

where $\mathbf{P}_*$ is the distribution generated by the family (2), $0<\alpha<1$ is a preassigned upper bound for the false alarm probability and m is a suitably chosen window size. In the sequel, we denote by $\mathbf{P}_{\theta,\nu}$ the distribution of the process $\left(x_k\right)_{k\ge1}$ defined by the family of the conditional densities (1).

Our goal is to find an optimal change-point detection procedure which minimizes the conditional average delay time, i.e.,

$$\inf_{\tau\in\mathbf{M}_{\alpha,m}} \mathbf{E}_{\theta,\nu}\left(\tau-\nu \mid \tau\ge\nu\right) \quad \text{for all } \nu\ge0$$

where $\mathbf{E}_{\theta,\nu}$ is the expectation with respect to the distribution $\mathbf{P}_{\theta,\nu}$. However, finding a strictly optimal detection procedure in the problem (4) is very difficult, if at all possible. For this reason, we consider an asymptotic problem of finding a first-order asymptotically optimal rule that satisfies

$$\lim_{\alpha\to0}\frac{\inf_{\tau\in\mathbf{M}_{\alpha,m}} \mathbf{E}_{\theta,\nu}\left(\tau-\nu \mid \tau>.\nu\right)}{\mathbf{E}_{\theta,\nu}\left(\tau-\nu \mid \tau>\nu\right)} = 1. \qquad (4)$$

3. MAIN RESULTS

3.1. The Information Lower Bound

To study the optimality properties for the detection procedures we use the lower bound obtained in Pergamenshchikov and Tartakovsky (2018):

$$\liminf_{\alpha\to0}\frac{\inf_{\tau\in\mathbf{M}_{\alpha,m}}\mathbf{E}_{\theta,\nu}\left(\tau-\nu \mid \tau\ge\nu\right)}{\left|\ln\alpha\right|} \ge \frac{1}{I(\theta)}, \qquad (5)$$

where $I(\theta)$ is the generalized Kullback-Leibler information number. This asymptotic lower bound holds whenever the log-likelihood ratio (LLR) obeys the strong law of large numbers:

$$\frac{1}{n}\log\sum_{t=k+1}^{k+n}\frac{f_\theta\left(x_t \mid x_1,\ldots,x_{t-1}\right)}{f_*\left(x_t \mid x_1,\ldots,x_{t-1}\right)} \to I(\theta) \qquad (6)$$

as $n\to\infty$ $\mathbf{P}_{\theta,k}$ – a.s.

3.2. The Mixture Shiryaev-Roberts Procedure

Moreover, in this paper using the modified Shiryaev - Roberts procedures proposed in Pergamenshchikov, S. M. and Tartakovsky, A.G. (2018) we construct a special weighted procedure T^* which belongs to the class $\mathbf{M}_{\alpha,m}$.

Let $W(\theta)$ be a distribution on the parameter space Θ. Define the likelihood ratio (LR) mixture as

$$\Lambda_n^k(W) = \int_\Theta\prod_{i=k+1}^{n}\frac{f_{\theta,i}\left(X_i \mid X_1,\ldots,X_{i-1}\right)}{f_{0,i}\left(X_i \mid X_1,\ldots,X_{i-1}\right)}dW(\theta),\ n>k.$$

In what follows, we assume that $W(\theta)$ is quite arbitrary satisfying the condition

$\left(\mathbf{C}_W\right)$ For any $\delta>0$, the measure W is positive on $\left\{u\in\Theta: \left|u-\theta\right|<\delta\right\}$ for any $\theta\in\Theta$, i.e.,

$$W\left\{u\in\Theta: \left|u-\theta\right|<\delta\right\}>0.$$

This condition means that we do not consider parameter values of θ from Θ of the measure null.

Introduce the Shiryaev-Roberts (SR) statistic

$$R_n(\theta) = \sum_{k=1}^{n}\prod_{i=k}^{n}\frac{f_{\theta,i}\left(X_i \mid X_1,\ldots,X_{i-1}\right)}{f_{0,i}\left(X_i \mid X_1,\ldots,X_{i-1}\right)}.$$

Note that it is tuned to $\theta\in\Theta$. In this paper we use the mixture SR statistic

$$R_n^W = \sum_{k=1}^{n}\Lambda_n^k(W) \equiv \int_\Theta R_n(\theta)dW(\theta), \qquad n\ge1,$$

$R_0^W = 0$.

The associated detection procedure, which we will call the *Mixture Shiryaev-Roberts* (MiSR) detection procedure, is given by the stopping time

$$T_a = \inf\left\{n\ge1: \log R_n^W \ge a\right\}, \qquad \inf\{\varnothing\} = +\infty \qquad (7)$$

where $a>-\infty$ is a threshold controlling for the false alarm risk. Write $T^* = T_{a^*}$, where a^* is some function of α which goes to ∞ as $\alpha\to0$. Using a left-tail complete convergence condition in the strong law (6), which usually holds under "concentration" conditions for the LLR process, it can be shown that along with the lower bound (5) the following upper bound holds:

$$\limsup_{\alpha\to 0} \frac{\mathbf{E}_{\theta,\nu}\left(T^* - \nu \mid \tau \ge \nu\right)}{|\ln \alpha|} \le \frac{1}{I(\theta)}. \tag{8}$$

Note that it follows from the bounds (5) and (8) that the proposed MiSR procedure is asymptotically optimal since the asymptotic equality (4) holds for $T = T^*$.

As an example for which we check the strong law of large numbers (6) and "concentration" conditions for the LLR process, we consider the change point detection problem for the autoregressive model. Specifically, assume that $(x_k)_{k\ge 1}$ is the autoregressive process of order p:

$$x_k = a_1 x_{k-1} + \ldots + a_p x_{k-p} + \varepsilon_k, \tag{9}$$

before the change time ν, i.e. for $k \le \nu$, and

$$x_k = \theta_1 x_{k-1} + \ldots + \theta_p x_{k-p} + \varepsilon_k, \tag{10}$$

after ν. Here $(\varepsilon_k)_{k\ge 1}$ is i.i.d. sequence of random Gaussian variables with the parameter (0,1). The parameters $a = (a_1, \ldots, a_p)$ are known and, the parameters $\theta = (\theta_1, \ldots, \theta_p) \ne a$ are unknown. We assume that both processes (9) and (10) are stable, that is all roots of the corresponding characteristic polynomials lie inside the unit circle of complex plane. For this example, the procedure T^* is asymptotically optimal with

$$I(\theta) = \frac{(\theta - a)' F^{-1} (\theta - a)}{2},$$

where F is the covariance matrix of order p for the stationary process (10) which is given in Example 5 in Pergamenshchikov and Tartakovsky (2018).

4. MONTE CARLO SIMULATIONS

In this section, through the Python software we provide Monte Carlo (MC) simulations for the AR(1) model, which is a particular case of (9) – (10) for $p = 1$. Specifically, let the pre-change value $a = 0$ and the post-change value $\theta \in \Theta = \{\theta_1, \ldots, \theta_N\}$, $-1 < \theta_1 < \ldots < \theta_N < 1$, $\theta_i \ne 0$.
We set

$$L_n^{\theta}(X_n, X_{n-1}) = \exp\left\{\theta X_n X_{n-1} - \frac{\theta^2 X_{n-1}^2}{2}\right\}, \; n \ge 1.$$

The MiSR stopping time is written as

$$T_a = \inf\left\{n \ge 1 : \sum_{j=1}^{N} W(\theta_j) R_n(\theta_j) \ge e^a\right\},$$

where the SR statistic $R_n(\theta)$ satisfies the recursion

$$R_{n+1}(\theta) = [1 + R_n(\theta)] L_{n+1}^{\theta}(X_n, X_{n+1}), \; n \ge 1, \; R_0(\theta) = 0.$$

Thus, the MiSR procedure can be easily implemented. The generalized information number $I(\theta) = \theta^2 / [2\,(1 - \theta^2)]$, so the first-order approximation yields the following approximate formula for the average delay to detection $ADD_{\nu,\theta}(T_a) = \mathbf{E}_{\nu,\theta}(T_a - \nu \mid T_a > \nu)$:

$$ADD_{\nu,\theta}(T_a) \approx ADD_{\nu,\theta}^{app}(T_a) = \frac{2(1 - \theta^2)a}{\theta^2}. \tag{11}$$

In the MC simulations, we set

$\Theta = \{$ -0.9, -0.8, -0.7, -0.6, -0.5, -0,4, -0.3, -0.2, -0.1, 0.1, 0.2, 0.3, 0.4, 0.5, 0.6, 0.7, 0.8, 0.9 $\}$

and uniform prior $W(\theta_j) = 1/18$. The results are presented in Table 1 for the upper bound on the maximal local probability of false alarm (LPFA) $\beta = 0.01$ and the number of MC runs 10^5. In the table, we compare operating characteristics of the MiSR rule T_a with that of the SR rule

$$\tau_B = \inf\{n \ge 1 : R_n(\theta) \ge B\}.$$

The thresholds a and B (shown in the table) were selected in such a way that the maximal probabilities of false alarm of both rules ($LPFA(T_a)$ and $LPFA(T_B^*)$) were practically the same.

Table 1: Operating Characteristics of the MiSR and SR Detection Procedures

$\beta = 0.01$, $\nu = 0$			
θ	e^a	$ADD_{\nu,\theta}(T_a)$	$LPFA(T_a)$
0.9	395	11.74	0.0080
0.8	420	14.72	0.0073
0.7	440	18.97	0.0070
0.6	470	25.32	0.0065
0.5	595	36.35	0.0049
0.4	1040	59.57	0.0024

$\nu = 0$, $B = 791$			
θ	$ADD_{\nu,\theta}(\tau_B)$	$LPFA(\tau_B)$	$ADD_{\nu,\theta}^{app}(T_a)$
0.9	11.08	0.0079	2.81
0.8	13.72	0.0073	6.80

0.7	17.52	0.0071	12.67
0.6	23.15	0.0065	21.88
0.5	31.84	0.0049	38.33
0.4	45.88	0.0025	72.94

$\beta = 0.01$, $\nu = 10$			
θ	e^a	$ADD_{\nu,\theta}(T_a)$	$LPFA(T_a)$
0.9	395	10.05	0.0080
0.8	420	12.72	0.0073
0.7	440	16.59	0.0070
0.6	470	22.55	0.0065
0.5	595	32.96	0.0049
0.4	1040	55.34	0.0024

$\nu = 10$, $B = 791$			
θ	$ADD_{\nu,\theta}(\tau_B)$	$LPFA(\tau_B)$	$ADD^{app}_{\nu,\theta}(T_a)$
0.9	9.62	0.0079	2.81
0.8	11.98	0.0073	6.80
0.7	15.30	0.0071	12.67
0.6	20.34	0.0065	21.88
0.5	28.01	0.0049	38.33
0.4	40.83	0.0025	72.94

It is seen that for relatively large values of the post-change parameter, $\theta \geq 0.6$, the SR rule only slightly outperforms the MiSR rule, but for small parameter values (i.e., for close hypotheses) the difference becomes quite substantial. The worst change point is $\nu = 0$, as expected. Also, the first-order approximation (11) is not too accurate, especially for small and large parameter values.

5. REMARKS

1. Despite the fact that the MiSR procedure is first-order asymptotically optimal for practically arbitrary weight function $W(\theta)$ that satisfies condition ($\mathbf{C}_W$), for practical purposes its choice may be important. In fact, selection of the weight W affects higher-order asymptotic performance, and therefore, real performance of the detection procedure. For example, if the set Θ is continuous, one has to avoid $W(\theta)$ that concentrates in the vicinity of a specific parameter value θ_1 since in this case the MiSR procedure will be nearly optimal at and in the vicinity of θ_1 but will not have a good performance for other parameter values. The choice of $W(\theta)$ is also related to the computational issue. It is reasonable to select the weight as to be in the class of conjugate priors, if possible, or to select a uniform prior if Θ is compact. A substantial simplification occurs when $\Theta = \{\theta_1, .., \theta_N\}$ is a finite discrete set. If the observations are i.i.d., then in the discrete case, it is possible to find an optimal (in a certain sense) weight using the approach proposed by Fellouris and Tartakovsky (2013) for the hypothesis testing problem.

2. The traditional constraint on the false alarm risk in minimax changepoint detection problems is the lower bound on the average run length to false alarm (ARL2FA) $\mathbf{E}_\infty[\tau] \geq \gamma \geq 1$. This measure of false alarms makes sense when the distribution of the stopping time τ (in our case of T_a) is approximately geometric. This is typically the case (at least asymptotically as $a \to \infty$) for i.i.d. data models [Pollak and Tartakovsky (2009), Yakir (1995)]. However, apart for the i.i.d. case there is no any result on the asymptotic distribution of the stopping time T_a (as $a \to \infty$), so for general non-i.i.d. models of interest in the present paper this is not necessarily true. Therefore, the usefulness of the ARL2FA is under the question, as discussed in detail in Tartakovsky et al. (2015). In fact, in general, large values of the ARL2FA do not guarantee small values of the maximal local PFA $\sup_{k \geq 1} \mathbf{P}_\infty(\tau < k + m \mid \tau \geq k)$. But the opposite is always true since the maximal local PFA is a more stringent false alarm measure in the sense that if it is small, then the ARL2FA is necessarily large. This argument motivated us considering the maximal local PFA instead of the conventional ARL2FA.

ACKNOWLEDGMENTS

This work was supported by the RSF grant 17-11-01049 (National Research Tomsk State University), by the research project no. 2.3208.2017/4.6 (the Ministry of Education and Science of the Russian Federation). The work of Alexander Tartakovsky was partially supported by the Russian Science Foundation under grant 18-19-00452.

REFERENCES

Basseville, M. and Nikiforov, I.V, 1993. Detection of Abrupt Changes: Theory and Applications. Englewood Cliffs: Prentice Hall.

Girardin, V., Konev, V. and Pergamenshchikov, S. M., 2018. Kullback-Leibler Approach to CUSUM Quickest Detection Rule for Markovian Time Series. Sequential Analysis, 37 (3), 322-341.

Fellouris, G., Tartakovsky, A. G., 2013. Almost optimal sequential tests of discrete composite hypotheses. Statistica Sinica, 23, 1717-1741.

Kent, S., 2000. On the trial of intrusions into information systems. IEEE Spectrum, 37, Issue 12, 52-56.

Lai, T.L., 1998. Information bounds and quick detection of parameters changes in stochastic systems. IEEE Transactions on Information Theory, 44(7), 2917-2929.

Page, E.S., 1954. Continuous inspection schemes. Biometrika, 41, 100-115.

Pollak, M., Tartakovsky, A., 2009. Optimality properties of the Shiryaev-Roberts procedure. Statistica Sinica, 19, 1729-1739.

Pergamenshchikov, S. M., Tartakovsky, A.G., 2018. Asymptotically optimal pointwise and minimax quickest change-point detection for dependent

data. Statistical inference for stochastic processes, 21 (1), 217-259.
Tartakovsky, A.G., Rozovskii, B.L., Blažek, R.B., and Kim, H., 2006. Detection of intrusions in information systems by sequential change-point methods. Statistical Methodology, 3, 252-293.
Tartakovsky, A., Nikiforov, I. and Basseville, M. Sequential Analysis: Hypothesis Testing and Changepoint Detection. Chapman & Hall book, Taylor & Francis Group, 2015.
Yakir, B., 1994. Optimal detection of a change in distribution when observations form a Markov chain with a finite state space. In: Change-Point problems (E. Carlstein, H. Muller and D. Siegmund, Eds), Hayward, CA: Inst. Math. Statist., 346-358.
Yakir, B., 1995. A note on the run length to false alarm of a change-point detection policy. Annals of Statistics, 23, 272-281.

S.M. Pergamenshchikov is professor at Laboratory of Mathematics Rafael Salem of University of Rouen and scientific director of International Laboratory of Statistics of Stochastic processes and Quantitative Finance of Russian National Research Tomsk State University. He works in three fields: statistics, probability and financial mathematics. In statistics his research interests include sequential analysis, nonparametric estimation, model selection, signal and image processing. In probability this is asymptotic analysis for stochastic differential equations, renewal theory for general Markov processes, uniform geometric ergodicity and concentration inequalities. In financial mathematics it is asymptotic hedging problems with transaction costs, optimal investment and consumption and ruin probability problems. During the research work S.M. Pergamenshchikov published more than 100 papers and one monograph in Springer, 72 of them being indexed in the MathSciNet, Web of Science, Scopus databases. He has publications in main high rated journals such as “Annals of Probability”, “Annals of Applied Probability”, “Annals of Statistics”, “Finance and Stochastics”, etc. He obtained several awards, including “Russian Federal Professor in Mathematics” (2016), “Scientific Excellence Award” (2011) in France. He obtained Ph.D (1986) in the Institute of Mathematics, USSR Academy of Sciences in Novosibirsk and Dr. Sci. (1994) in the Institute of Mathematics and Mechanics of Russian Academy of Sciences in Ekaterinburg.

A.G. Tartakovsky is a head of Space Informatics Laboratory at the Moscow Institute of Physics and Technology. His research interests include theoretical and applied statistics; applied probability; sequential analysis; changepoint detection phenomena; and a variety of applications including statistical image and signal processing; video surveillance and object detection and tracking; information integration/fusion; intrusion detection and network security; detection and tracking of malicious activity; and mathematical/engineering finance applications. He is the author of two books (the third is in preparation), several book chapters, and over 150 conference and journal papers. Dr. Tartakovsky is a Fellow of the Institute of Mathematical Statistics and a senior member of IEEE. He obtained several awards, including a 2007 Abraham Wald Award in Sequential Analysis. Dr. Tartakovsky obtained Ph.D. (1981) and Dr. Sci. (1990) degrees from the Moscow Institute of Physics and Technology, Russia (FizTech).

SIMULATION OF THE SPECTRAL CHARACTERISTICS OF THE PHOTOSENSITIVE ELEMENTS BASED ON THE POLYCRYSTALLINE LEAD SULFIDE

B.N. Miroshnikov[(a)], D.A. Zezin[(b)], A.A. Makarov[(c)], A.N. Faulgaber[(d)]

[(a),(b),(c),(d)]National Research University "Moscow Power Engineering Institute", Moscow, Russia
[(a),(b)]Institute of Nanotechnology of Microelectronics of the Russian Academy of Science, Moscow, Russia
[(c)]International Laboratory of Statistics of Stochastic Processes and Quantitative Finance of the National Research Tomsk State University, Tomsk, Russia

[(a)]MiroshnikovBN@mpei.ru, [(b)]ZezinDA@mpei.ru, [(c)]o_v_ch@mail.ru, [(d)]lytaleksandr@mail.ru

ABSTRACT
The results are presented of the simulation of the spectral characteristics of the polycrystalline photosensitive elements based on the lead sulphide. The possible reasons for the experimental data discrepancy are discussed.

Keywords: photoresistors, lead sulfide, carrier lifetime, photosensitivity, spectral dependence

1. INTRODUCTION
Lead sulfide (PbS) is one of the most needed narrow-band-gap semiconductors with the energy-gap width of 0.4 eV at 300 K. The photoresistors based on it are used in registering near infrared radiation (0.6-3.1 microns), i.e. they are integrated into impulse optoelectronic devices, IR detectors, infrared imagers, night viewing devices, etc.
A wide variation of the methods for obtaining the devices mentioned above leads to the production of the patterns of various thicknesses, surface morphology and structure with the result that the spectral characteristics of the devices vary widely.
The objective of this paper is to show the possibility of simulation of these photosensitive elements and to discuss the likely reasons why their theoretical characteristics differ from the experimental curves.

2. SIMULATION OF THE SPECTRAL CHARACTERISTICS OF PHOTORESISTORS
As a basis, the experimental data presented by Ravich, Efimova and Smirnov (1968) are used. Mobility is estimated as 1 $\mathrm{cm}^2/\mathrm{V{\cdot}s}$; carrier (hole) lifetimes τ are chosen to be 50 μs for the "physical" element and 100 and 300 μs for the "chemical" element. The geometrical dimensions are: the photosensitive element area is $1\,\mathrm{cm}\times 1\,\mathrm{cm}$, the thickness is 0.5 micron for the chemical layer and 1 micron for the physical layer. As a radiation source, the absolute black body is used. The temperature of the black body is 500 K, while its radiation spectrum is determined based on the Planck radiation formula. The relationship between the absorption coefficient and the incident radiation energy is taken from the study by Miroshnikov, Miroshnikova and Popov (2018).
In the general case, the dark carrier concentration is determined by the two components. They are: p_1 related to the Auger recombination and carrier lifetime and obeying the ratio $\tau \cdot p_1^2 = (2\ldots3)\cdot 10^{27}\ \mathrm{cm}^{-6}\cdot\mathrm{s}$; and p_2 determined by the concentration of the acceptor-type traps and, especially, by the concentration of both chemically bound oxygen (it forms the deeper traps and increases the surface recombination rate at the crystallite surface) and physically adsorbed oxygen at the crystallite surface (Fig. 1). Our studies (Mohamed, Abdel-Hafiez, Miroshnikov, Barinov and Miroshnikova 2014) show that by heating the patterns up to the temperature of 400 K and degassing the surface, one can minimize the last component and obtain the minimum hole concentration which depends on the shallow trap concentration and is related to the carrier lifetime by the law

$$p_2 = 1.4\cdot 10^{20}\,\tau. \qquad (1)$$

Thus, the dark hole concentration

$$p_{\mathrm{dark}} = p_{\mathrm{dark}}(\tau) = p_1 + p_2 \qquad (2)$$

depends on the carrier lifetime. For example, in Fig. 1, there are presented the dependences p_1, p_2 (1) and p_{dark} (2) as the functions of the carrier lifetime for the lead chalcogenides.
The carrier concentration in the presence of light (p_{gen}) is determined by the generation rate $G(\lambda, x)$ depending on both the radiation wavelength λ and the photon penetration depth x:

$$G(\lambda, x) = \alpha(\lambda)\, N_p(\lambda, T_{\mathrm{ABB}})\,\eta(\lambda)\,\mathrm{d}x\,,$$

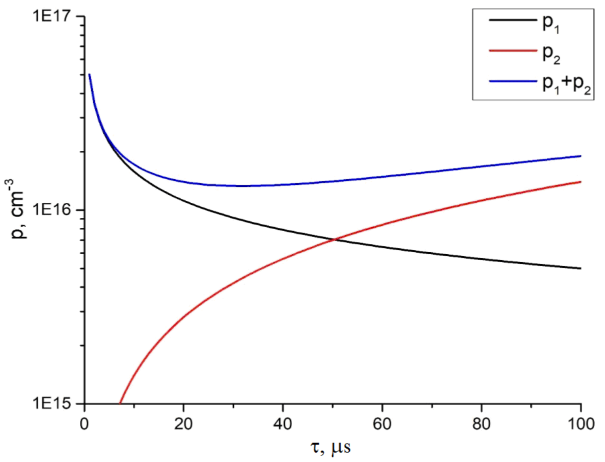

Figure 1: The dependences of the hole concentration in lead chalcogenides upon the carrier lifetime

where $\alpha(\lambda)$ is the radiation absorption coefficient; $N_p(\lambda, T_{\rm ABB})$ is the number of photons incident in a unit of time (second) per unit of area ($\rm cm^2$) and depending on both the radiation wavelength λ and the temperature of the radiation source (absolute black body – ABB); $\eta(\lambda)$ is the quantum efficiency of the photoresistor close to unity. Thus, the total carrier concentration p_{lt} is determined by the sum of the dark carrier concentration $p_{\rm dark}$ (2) and the carrier concentration $p_{\rm gen}$ under the lighting by source (ABB) radiation:

$$p_{lt}(\tau,\lambda) = p_{\rm dark}(\tau) + p_{\rm gen}(\tau,\lambda). \quad (3)$$

And, in turn, $p_{\rm gen}(\tau,\lambda) = G(\lambda, x)\tau$.

In order to find the spectral dependence $S_I(\lambda)$ of the current sensitivity, the following formula is applied:

$$S_I(\lambda) = I_p(\lambda)/F(\lambda, T_{\rm ABB}). \quad (4)$$

In Eq. (4), the designations are: $I_p(\lambda)$ is the photocurrent, $F = N_p h\nu = N_p hc/\lambda$ is the photon flux, N_p is the number of photons, h is the Planck constant, c is the velocity of light in free space, ν is the electromagnetic radiation frequency. For the photocurrent $I_p(\lambda)$, one has:

$$I_p(\lambda) = V_d / R_{lt}(\lambda),$$

where V_d is the bias voltage (which is equal to 15 V) and

$$R_{lt}(\lambda) = \rho_{lt}(\lambda)a/bd = \rho_{lt}(\lambda)/d = 1/\sigma_{lt}(\lambda)d$$

is the incident radiation photoresistor resistance. Here $a \times b$ is the photosensitive element effective area which has been taken as square and equal to 1 $\rm cm^2$ for the calculations; d is the photosensitive layer thickness; $\rho_{lt}(\lambda)$ is the light photosensitive element resistivity; $\sigma_{lt}(\tau,\lambda)$ is the light photosensitive element conductivity.

The conductivity $\sigma_{lt}(\tau,\lambda)$ is primarily determined by the conductivity $\sigma_p(\tau,\lambda)$ due to the majority carriers, that is, holes:

$$\sigma_{lt}(\tau,\lambda) = \sigma_n(\tau,\lambda) + \sigma_p(\tau,\lambda) \approx \sigma_p(\tau,\lambda) = qp_{lt}(\tau,\lambda)\mu_p,$$

where q is an elementary charge, μ_p is the hole mobility close to 1 $\rm cm^2/V\cdot s$ and independent from the light level in the first approximation, while $p_{lt}(\tau,\lambda)$ is determined by the formula (3).

There are two main moses of absorption: near-surface (or non-uniform) absorption and uniform absorption. From the Bouguer-Lambert law, it follows that all the absorption of the radiation incident on the surface occurs at the depth $x = \alpha^{-1}(\lambda)$. Then, when the ratio $\alpha(\lambda)d > 1$ is fulfilled, it was accepted that all the incident radiation is absorbed at a depth less than the film thickness, i.e. on the surface. On the other hand, if the inequality $\alpha(\lambda)d < 1$ is satisfied, then it was assumed that the absorption is uniform.

In the simulation of the lead sulfide thin layers obtained by chemical deposition, it was presupposed that all the absorption is uniform. For thicker physical layers, both types of absorption were taken into account. In addition, the difference in the film technology also influences the efficiency of the radiation absorption by the layers $\eta(\lambda)$. Thus, the chemical layers are characterized by a large energy-gap width, and, therefore, radiation wavelength longer than 3 microns is not absorbed, while for the physical layers, absorption in the near-surface region has less influence due to the thick layer of lanarkite ($\rm PbO \cdot PbSO_4$).

For our low-mobility samples, the condition $L_p << d$ is satisfied, that is, the hole diffuse length L_p is much less than the photosensitive element thickness d, and there can be applied the formula for the concentration under the uniform absorption:

$$p_{\rm gen}(\tau,\lambda) = G(\lambda, x)\tau\left[1 - \frac{2sL_p\tau}{d\left(L_p + s\tau\right)}\right] \approx G(\lambda, x)\tau.$$

where s is surface recombination rate.

For the near-surface absorption, one gets:

$$p_{\rm gen}(\tau,\lambda) = G(\lambda, x)\tau\frac{L_p}{\alpha(\lambda)d\left(L_p + \tau s\right)}\left[\frac{\tau s}{L_p\left(\alpha(\lambda)L_p + 1\right)} + 1\right].$$

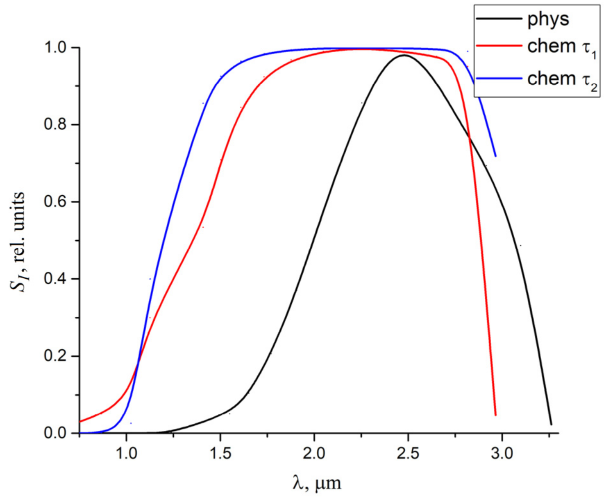

Figure 2: The calculated spectral characteristics for the photosensitive layers with the three lifetimes

In Fig. 2, there are presented the three calculated spectral characteristics of the photosensitive element: *phys* – for the physically deposited layer with $\tau = 50$ μs, *chem* τ_1 – for the chemically deposited layer with $\tau = 100$ μs and *chem* τ_2 – for the chemically deposited layer with $\tau = 300$ μs.

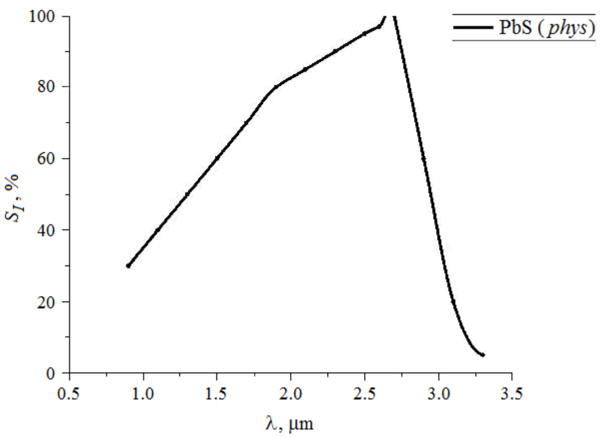

a)

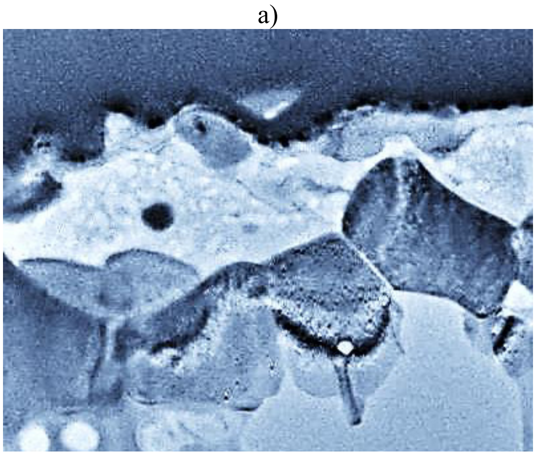

b)

Figure 3: The experimental spectral characteristics (a) and the microphotography of the physical photosensitive element section obtained by means of the transmission high-resolution electron microscope (b)

Our calculations and the comparison with the experimental data show that, for the physical layer, the transition from the near-surface absorption to the uniform one is realized when the value of the incident radiation wavelength is no less than 2 microns (curve *phys* in Fig. 2). If the incident radiation wavelength is bigger than 2.7 microns, then the absorption efficiency near the energies equal to the energy-gap width begins to be influential and the sensitivity begins decreasing. In turn, for the chemical layers (curves *chem* in Fig. 2), the uniform absorption is only taken into account, therefore, in the large wavelength range from 1.5 microns to 2.7 microns, the typical constant high reduced sensitivity is observed. The difference has also been determined under the various values of the lifetime affecting both the dark hole concentration $p_{\text{dark}}(\tau)$ and the generated carrier concentration $p_{\text{gen}}(\tau, \lambda)$.

3. DISCUSSION OF THE RESULTS

For the physically deposited layer, the simulation coincides well with the experimental data (Fig. 3, Morozova and Miroshnikov 2018).

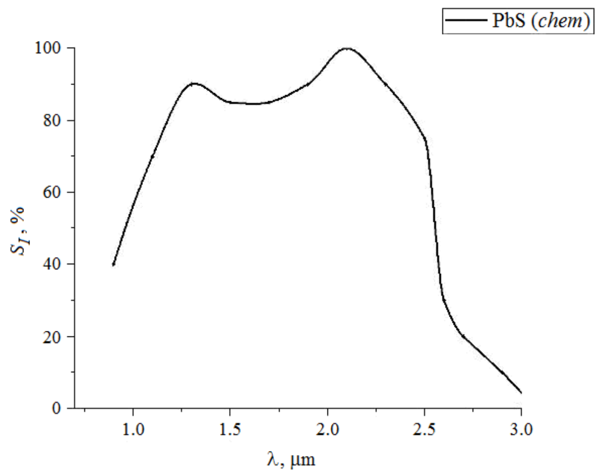

a)

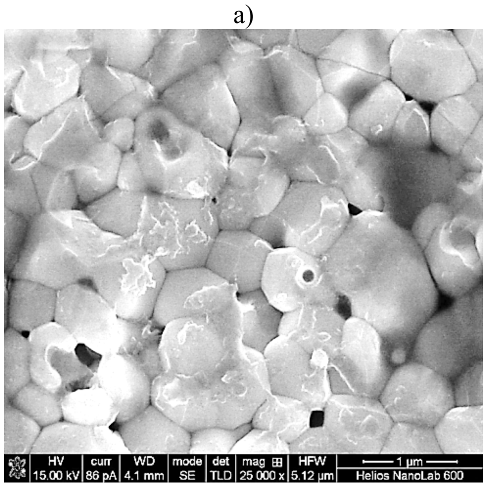

b)

Figure 4: The experimental spectral characteristics (a) and the microphotography of the section of the photosensitive element surface obtained by means of the chemical deposition with the maximum sensitivity (b)

The difference in the slope of the curve in the high-energy spectral region (up to 2.3 microns) is determined by the thickness of the non-photoactive layer of the lead oxides colored by the light colors in Fig. 3b.

The results of the simulation of the spectral characteristics of the photosensitive element obtained by the chemical method also agree well with the experimental data (Fig. 4, Morozova and Miroshnikov 2018). What has not been taken into account in this case is the change in the lead sulfide energy-gap width due to the effect of the oxygen in PbS structure that is the isoenergetic impurity resulting in a local change in the energy-gap width of the material (Morozova and Miroshnikov 2018). This is the first reason for the conformity between the simulation results and the experimental data. Another reason is the small photosensitive element thickness – 0.5 micron, resulting in the long-wavelength (low-energy) radiation part passing through the film without the photo-ionization.

4. CONCLUSION

Thus, it has been established that the simulation can be implemented of such complex structure as the polycrystalline photosensitive element and its results appear to be close to the experimental data.

The simulation takes into account relaxation processes both inside the crystallites (Auger recombination) and the effect of oxygen-containing impurities on the surface, leading to the capture of free electrons, an increase in the hole lifetime and stabilization of the dark conductivity.

ACKNOWLEDGMENTS

This research was financially supported by the Russian Foundation for Basic Research (research project No. 18-29-11051), the Ministry of Education and Science of the Russian Federation (research project No. 2.3208.2017/4.6), and the Council on grants of the President of the Russian Federation (research project No. SP-834.2019.3).

REFERENCES

Ravich Y.I., Efimova B.A. and Smirnov I.A., 1968. Methods for the study of semiconductors as applied to PbTe, PbSe, PbS lead chalcogenides [in Russian]. Moscow: Nauka.

Miroshnikov B.N., Miroshnikova I.N. and Popov A.I., 2018. Optimization of parameters of PbS-based polycrystalline photoresistors. Semiconductors or Physics of the Solid State, 52 (2), 245-249.

Mohamed H.S.H., Abdel-Hafiez M., Miroshnikov B.N., Barinov A.D. and Miroshnikova I.N., 2014. Spectral characteristics and morphology of nanostructured Pb-S-O thin films synthesized via two different methods. Journal of Materials Science in Semiconductor Processing, 27, 725-732.

Morozova N.K. and Miroshnikov B.N., 2018. Isoelectronic oxygen centers and conductivity of CdS in comparison with PbS. Semiconductors or Physics of the Solid State, 52 (3), 295-298.

AUTHORS BIOGRAPHY

Boris N. Miroshnikov was born in Moscow in 1990. He received his Ph.D. in semiconductor physics from the National Research University "Moscow Power Engineering Institute" in 2016. Boris N. Miroshnikov is currently working as an Assistant Professor at the Department of Electronics and Nanoelectronics of the National Research University "Moscow Power Engineering Institute". He also works as a Researcher at the Institute of Nanotechnologies of Microelectronics of the Russian Academy of Science. His main interests are physics and technology of infrared photodetectors based on single- and polycrystals.

Denis A. Zezin was born in 1988. He received his Ph.D. in solid-state electronics from the National Research University "Moscow Power Engineering Institute" in 2014. He is currently working as an Associate Professor at the Department of Electronics and Nanoelectronics of the National Research University "Moscow Power Engineering Institute" as well as a Researcher at the Institute of Nanotechnologies of Microelectronics of the Russian Academy of Science. His research interests relate to the study of the electrophysical visible and infrared radiation-measuring instruments.

Alexander A. Makarov was born in 1993. He received the B.Sc. and the M.Sc. degrees from the National Research University "Moscow Power Engineering Institute" in 2014 and 2016, respectively, both in radio engineering. Presently, Alexander A. Makarov is a PhD student in the Department of Electronics and Nanoelectronics at the National Research University "Moscow Power Engineering Institute" as well as he is working as a Researcher at the International Laboratory of Statistics of Stochastic Processes and Quantitative Finance of the National Research Tomsk State University. His research interests include synthesis, analysis and simulation of the processing algorithms of stochastic processes and fields with unknown parameters.

Alexander N. Faulgaber was born in 1993. He received the B.Sc. and the M.Sc. degrees from the National Research University "Moscow Power Engineering Institute" in 2014 and 2016, respectively, both in radio engineering. Presently, Alexander N. Faulgaber is a PhD student in the Department of Electronics and Nanoelectronics at the National Research University "Moscow Power Engineering Institute". His research interests include synthesis, analysis and simulation of the processing algorithms of stochastic processes and fields with unknown parameters.

THE SIMULATION OF THE TIME CHARACTERISTICS OF THE PHOTORESISTIVE STRUCTURES BASED ON THE CADMIUM LEAD SULFIDES

I.N. Miroshnikova[(a)], B.N. Miroshnikov[(b)], E.V. Zenova[(c)], M.Y. Presnjakov[(d)], A.A. Makarov[(e)]

[(a),(b),(c),(e)]National Research University "Moscow Power Engineering Institute", Moscow, Russia
[(a),(b),(c)]Institute of Nanotechnology of Microelectronics of the Russian Academy of Science, Moscow, Russia
[(d)]National Research Center "Kurchatov Institute", Moscow, Russia
[(e)]International Laboratory of Statistics of Stochastic Processes and Quantitative Finance of the National Research Tomsk State University, Tomsk, Russia

[(a)]MiroshnikovaIN@mpei.ru, [(b)]MiroshnikovBN@mpei.ru, [(c)]ZenovaEV@mpei.ru, [(d)]Presnyakov_MY@nrcki.ru, [(e)]o_v_ch@mail.ru

ABSTRACT
The structures of the lead sulphide and lead selenide based photoresistors are examined. The simulation allowed us to explain the experimentally observed differences in the photoconductivity relaxation time between two different types of photoresistors.

Keywords: photoresistor, lead chalcogenides, Pb_xCd_yS-based structures, carrier lifetime, relaxation time

1. INTRODUCTION

Photoresistors (PRs) on the base of lead chalcogenides (PbS, PbSe, PbTe) have found widespread applications in infrared (1-5 microns) impulse optical-electronic systems (OES) since the 1930s. In order to produce the first PRs, monocrystalline or epitaxial layers were used (Ravich, Efimova, and Smirnov 1968). However, the OES developers encountered two problems then. The first problem was that the layers with a low dark carrier concentration (preferably less than 10^{16} cm^{3}) were required to increase the signal, but the technology of the pure layers was too expensive. The second problem was that in order to increase the sensitivity of PRs, the lifetime must be increased, but in extremely pure PbS crystals the value of τ did not exceed 10 µs.
A special feature of the impulse OES is the fact that the main criterion for the PR quality is not the increment of conductivity $\Delta\sigma$ under the influence of radiation, but the ratio $\Delta\sigma/\sigma_0$ divided by the effective radiation power at the fixed modulation frequency F_e. Here σ_0 is the dark conductivity of PR. Therefore, while the values τ and σ_0 are being simultaneously changed, their ratio remains constant.
It was believed that the recombination processes of the nonequilibrium carriers produced by IR radiation occur mainly according to the Auger process, namely: $\tau p^2 = (2\ldots3)\cdot 10^{27}$ cm$^{-6}\cdot$s for PbS and $\tau n^2 = 4\cdot 10^{27}$ cm$^{-6}\cdot$s for PbSe (Baryshev 2000).
The carrier lifetime in a number of the bulk PbS crystals was measured by T.S. Moss (1953) who managed to obtain the values for the lifetime in the range from $6\cdot 10^{-10}$ to $6\cdot 10^{-6}$ s. In the early 1950s, R.A. Smith (1954) showed that the lifetime of one type of the carrier (electrons or holes) can be extended, if the carriers of another type are localized inside a solid or on its surface. Later, A. Rose (1963) introduced the concept of "attachment level". Creating the system consisting of small crystallites, for which the surface-to-volume ratio is much higher than the one for a single crystal, was a good idea. Therefore, presently there are a large number of PbS- and PbSe-based PR-making technologies applying the vacuum deposition and the chemical deposition of layers (Johnson 1984, Saloniemi 2000).
The purpose of this paper is to show the possibility of the simulation of the carrier lifetime in polycrystalline photosensitive PbSe- and Pb-Cd-S-based layers.
It should be noted that the analysis of the PR parameters based on the lead chalcogenides demonstrates the following regularities: despite of the differences in the energy-gap widths ($E_{g\,\mathrm{PbS}} = 0.4$ eV, $E_{g\,\mathrm{PbSe}} = 0.25$ eV at room temperature), the values of the voltage sensitivity are quite close, while the effective values of the photoconduction relaxation constant differ by 20 times. Namely, there are 15 µs for PbSe and 200...450 µs for PbS. The doping of the PbS films by halogens (I, Br) leads to decreasing the time constant of the PbS-based structures up to 15 µs or less (Maskaeva 2004).
The integration of the lead and cadmium sulfides, which are the substitutional solid solutions ($E_{g\,\mathrm{CdS}} = 2.42$ eV at room temperature), in various proportions allows to conduct broad changes in the energy-gap width of the $Pb_x Cd_y S$ material. These polycrystalline films are obtained by the hydrochemical deposition from the aqueous solutions (Markov, Maskaeva, and Ivanov 2006) as well as by the thermal evaporation

(Aleksandrova, Maksimov, Moshnikov and Chesnakova 2008).

2. THE PHOTOSENSITIVE FILM STRUCTURE

In the case of substitutional solid solutions, the prepared films have varying composition in thickness. The solid solution based on the lead sulfide is formed at the depth of up to 40 nm approximately, while the solid solution based on the cadmium sulfide is formed at the depth of from 70 to 200 nm. In addition, there is a transition region with a thickness of 40-70 nm (Forostyanaya, 2015). During the transition from the PbS to the $Cd_x Pb_{1-x} S$ the conductivity type changes from "*n*" to "*p*", while the carrier concentration decreases by 3-5 orders of magnitude with the time constant τ decreasing up to 15-60 μs.

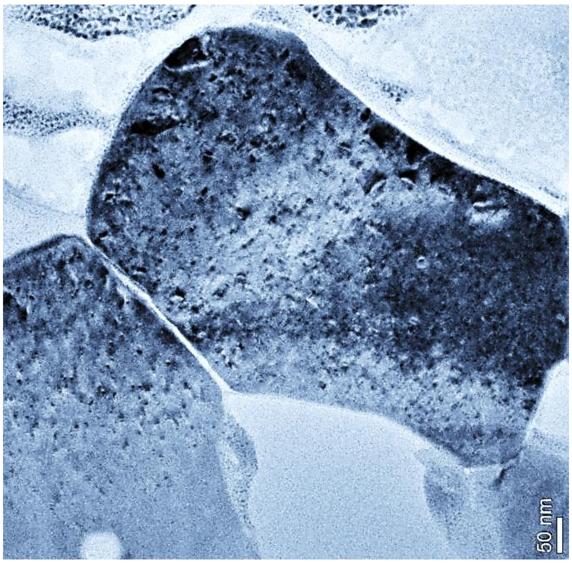

a)

b)

Figure 1: The microphotographs of the cross-section of the physically (a) and chemically (b) deposited PbS-based photoresistors obtained with the help of the high-resolution transmission electron microscopy

Due to the low carrier mobility in polycrystalline films ($1\ \text{cm}^2/(\text{V}\cdot\text{s})$ as it is stated by Petritz (1958)), the sensitivity of PR can be characterized by the ratio τ/p_0 where p_0 is the dark carrier concentration.

The desire to increase the sensitivity of devices by increasing the carrier lifetime and to decrease the dark conductivity σ_0, led to the development process of PR "sensitizing". For this purpose, in the case of the PbS-based structures, oxygen was introduced into the polycrystalline film (Butkevich, Globus and Zalevskaya 1999), that is, either the high-temperature annealing in case of the physical deposition or the addition of the additives in the process of the chemical deposition, while for the PbSe-based structures, oxygen, sulfur, selenium and halogens were used (Humphrey and Scanlon 1957).

The process of conduction in the polycrystalline layers of the lead chalcogenides is greatly influenced by the intergranular barriers as well as by grain structure and size. Therefore, the study of the film morphology is of a particular importance. In Figs. 1 (Mohamed, Abdel-Hafiez, Miroshnikov, Barinov and Miroshnikova 2014) and 2 (Miroshnikova, Miroshnikov, Presnyakov and Mohamed 2018), the microphotographs are presented of the cross-section of the PbS- and PbSe-based structures, respectively, obtained with the help of the high-resolution transmission electron microscopy (HRTEM – STEM/TEM Titan 80-300). In these photographs, the light keys belong to the light elements (primarily, oxygen), the dark color shows the atoms with the big numbers (sulfur, selenium, lead and iodine). It is known (Maraeva, Moshnikov and Tairov 2013) that iodine being a catalyst provides a high sensitivity for the PbSe-based PRs due to the penetration of oxygen into the grain, which originally had *n*-type conductivity.

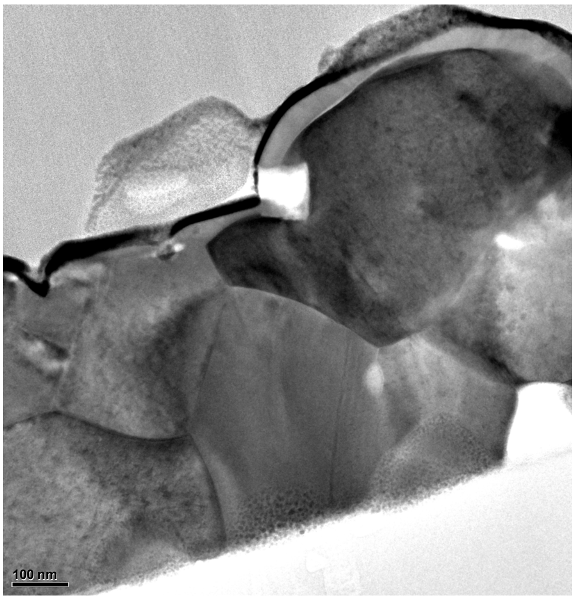

Figure 2: The microphotograph of the cross-section of the chemically deposited PbSe-based photoresistor obtained with the help of the high-resolution transmission electron microscopy

In contrast with the PbSe-based film, in the PbS-based film one can clearly see the oxygen-containing impurities (the term introduced by Butkevich, Globus and Zalevskaya (1999)) at the crystallite boundaries. The introduction of oxygen into the PbS structure leads to the formation of acceptor states in the forbidden band. This, in turn, increases the hole lifetime up to 600 µs, as there takes place the change of the conductivity from *n*- to *p*-type. The dark conductivity σ_0 will also increase in this case.

Based on the analysis of the PR structure, one can presuppose that there are two mechanisms for the overcompensation of the *n*-type conductivity in the lead chalcogenides. Namely, in PbS, the acceptor levels are formed both inside the grain (due to the oxygen diffusion) and on their surface (due to the oxygen-containing impurities), while for PbSe, PbCdS the enhanced oxygen diffusion mainly occurs with iodine and bromine acting as the catalysts for this process. Oxygen as an isoelectron impurity replaces sulfur, while in the PbCdS substitutional solid solution it can have a low concentration of 10^{18} cm^{-3}, approximately.

3. SIMULATION OF THE PHOTORESISTIVE STRUCTURES RELAXATION TIME

The photoresistive structures relaxation time is determined by the majority-carrier lifetime. As it was shown by Miroshnikova, Miroshnikov, Presnyakov, Mohamed (2018), in PbS, the concentration of holes released due to the electron trapping by the oxygen-containing impurities increases linearly with the number of the oxygen-containing impurities (the dependence $p_2(\tau)$ in Fig. 3a) by the law $p_2 = 1.4 \cdot 10^{20}\tau$, while the recombinations by the Auger process leads to the carrier concentration decreasing.

The influence of iodine in PbSe manifests itself in the stronger dependence $p_2 = 2 \cdot 10^{21}\tau$ (Fig. 3b), but in this case there also occurs the overcompensation of the conductivity type (n - p_2 curve in Fig. 3b). As a result, one has a very bounded area of the acceptable values of the carrier lifetime in PbSe that provide the low dark carrier concentration.

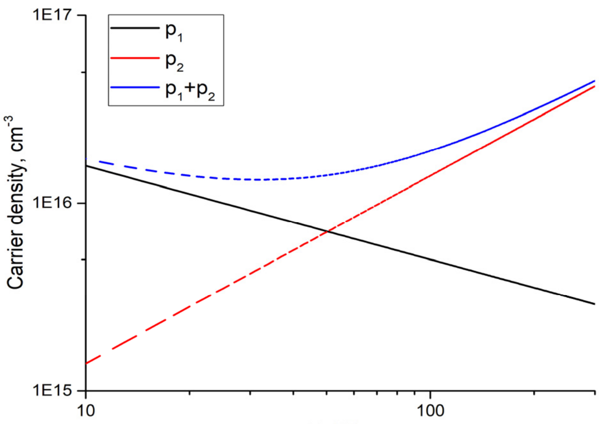

a)

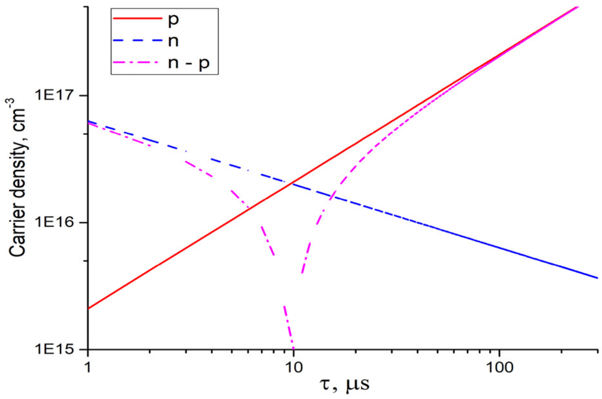

b)

Figure 3: The time dependences of the carrier concentration in the structures based on PbS (a) and PbSe (b)

In $Cd_xPb_{1-x}S$ substitutional solid solution, the oxygen adsorbed by the surface is of a great significance. Our studies using the EDX and AES methods have shown that oxygen is fixed on the surface in the area of lead sulfide. Adsorbed oxygen also creates acceptor traps decreasing the dark resistance.

4. CONCLUSION

Thus, it has been shown that in the case of PbS, there occurs a large variation of τ values acceptable for making the high sensitivity PRs. At the same time, in the case of PbSe and $Cd_xPb_{1-x}S$ substitutional solid solution the area of the acceptable values of the carrier lifetime becomes very bounded due to the superposition of the two processes: the overcompensation of the conductivity polarity and the high rate of the oxygen diffusion deep into the microcrystallites.

ACKNOWLEDGMENTS

This research was financially supported by the Russian Foundation for Basic Research (research project No. 18-29-11051), the Ministry of Education and Science of the Russian Federation (research project No. 2.3208.2017/4.6), and the Council on grants of the President of the Russian Federation (research project No. SP-834.2019.3).

REFERENCES

Ravich Y.I., Efimova B.A. and Smirnov I.A., 1968. Methods for the study of semiconductors as applied to PbTe, PbSe, PbS lead chalcogenides [in Russian]. Moscow: Nauka.

Baryshev N.S., 2000. The properties and the application of the narrow-band-gap semiconductors [in Russian]. Kazan': Unipress.

Moss T.S., 1953. Photoelectromagnetic and photoconductive effect in lead sulphide single crystals. Proceedings of the Physical Society, B66 (12), 993-1002.

Smith R.A., 1954. The electronic and optical properties of lead sulphide group of semiconductors. Physica, 20 (11), 910-929.

Rose A., 1963. Consepts in photoconductivity and allied problems. New York: Wiley.
Johnson T.H., 1984. Lead salt detectors and arrays PbS and PbSe. Proceedings of SPIE 443, pp. 60-94. August 23-25, San Diego (California, USA).
Saloniemi H., 2000. Electrodeposition of PbS, PbSe and PbTe thin films. VTT Publications 423. Espoo: Technical Research Centre of Finland.
Maskaeva L.N., 2004. Hydrochemical synthesis, structure and properties of the films of the supersaturated substitutional solid solutions $Me_xPb_{1-x}S$ (Me-Zn, Cd, Cu, Ag) [in Russian]. Thesis (D.Sc.). Ural State Technical University.
Markov V.F., Maskaeva L.N. and Ivanov P.N., 2006. Hydrochemical deposition of the metal sulfide films: simulation and experiment [in Russian]. Ekaterinburg: Ural Branch of RAS.
Aleksandrova O.A., Maksimov A.I., Moshnikov V.A. and Chesnakova D.B., 2008. Chalcogenides and oxides of the elements of group IV. Obtaining, study, application [in Russian]. St.-Petersburg: Technolit.
Forostyanaya N.A., 2015. Physico-chemical mechanisms of obtaining the solid solutions in the PbS-CdS system by means of the ion-exchange transformations [in Russian]. Thesis (PhD). Ural Federal University.
Petritz R.L., 1958. Theory of an experiment for measuring the mobility and density of carriers in the space-charge area of a semiconductor surface. Physical Review, 110 (6), 1254-1262.
Butkevich V.G., Globus E.R. and Zalevskaya L.N., 1999. Change of the lead sulfide films characteristics by variations of the conditions of chemically deposition from a solution. Applied Physics, (2), 52-56.
Humphrey J.N. and Scanlon W.W., 1957. Photoconductivity in lead selenide. Experimental. Physical Review, 105 (2), 469-475.
Mohamed H.S.H., Abdel-Hafiez M., Miroshnikov B.N., Barinov A.D. and Miroshnikova I.N., 2014. Spectral characteristics and morphology of nanostructured Pb-S-O thin films synthesized via two different methods. Journal of Materials Science in Semiconductor Processing, 27, 725-732.
Miroshnikova I.N., Miroshnikov B.N., Presnyakov M.Y. and Mohamed H.S.H., 2018. The influence of the structure morphology on the relaxation time constant of the lead chalcogenide photoresistors [in Russian]. Proceedings of XXV International Scientific and Technical Conference on Photoelectronics and Night Viewing Devices, vol. 2, pp. 588-591. May 24-26, Moscow (Russia).
Maraeva E.B., Moshnikov V.A. and Tairov Y.M., 2013. The models of oxide phases formation in lead chalcogenide nanostructured layers obtained in oxygen and iodine vapors. Semiconductors or Physics of the Solid State, 47 (10), 1431-1434.

AUTHORS BIOGRAPHY

Irina N. Miroshnikova was born in 1957. She received the Doctor of Technical Sciences degree from the National Research University “MPEI” in 2005. Irina N. Miroshnikova is working as a Director of the Institute of Radio Engineering and Electronics and a Head of the Department of Electronics and Nanoelectronics of the National Research University “MPEI”. She also holds position of Principle Research Scientist at the Institute of Nanotechnologies of Microelectronics of the Russian Academy of Science. Her main interests are physics and technology of infrared photodetectors based on single- and polycrystals.

Boris N. Miroshnikov was born in Moscow in 1990. He received his Ph.D. in semiconductor physics from the National Research University “MPEI” in 2016. Boris N. Miroshnikov is currently working as an Assistant Professor at the Department of Electronics and Nanoelectronics of the National Research University “MPEI” as well as a Researcher at the Institute of Nanotechnologies of Microelectronics of the Russian Academy of Science. His main interests are physics and technology of infrared photodetectors based on single- and polycrystals.

Elena V. Zenova was born in 1966. She received the Doctor of Technical Sciences degree from the Russian Scientific and Research Institute of the Cable Industry in 2013. Presently, she is working as a Head of Laboratory of the Department of Development and Research of Micro- and Nanosystems of the Institute of Nanotechnologies of Microelectronics of the Russian Academy of Science as well as a Professor at the Department of Nanotechnology Microelectronics of the National Research University “MPEI”. Her research interests include physics and technology of nanoelectronic devices and systems.

Mikhail Y. Presnjakov was born in 1988. He received his Ph.D. in semiconductor physics from the National Research University “MPEI” in 2014. Mikhail Y. Presnjakov is currently working as a Head of Probe and Electron Microscopy Resource Center at the National Research Center “Kurchatov Institute”. His main interests are application of transmission electron microscopy methods for materials research.

Alexander A. Makarov was born in 1993. He received the B.Sc. and the M.Sc. degrees from the National Research University “MPEI” in 2014 and 2016, respectively, both in radio engineering. Presently, he is a PhD student in the Department of Electronics and Nanoelectronics at the National Research University “MPEI” as well as a Researcher at the International Laboratory of Statistics of Stochastic Processes and Quantitative Finance of the National Research Tomsk State University. His research interests include synthesis, analysis and simulation of the processing algorithms of stochastic processes and fields with unknown parameters.

PROPERTY CONTROL METHODS OF DIAMOND-LIKE SILICON-CARBON FILMS FOR MICRO- AND NANOELECTRONICS

A.D. Barinov[(a)], A.I. Popov[(b)], A.A. Makarov[(c)]

[(a),(b),(c)]National Research University "Moscow Power Engineering Institute", Moscow, Russia
[(a),(b)]Institute of Nanotechnology of Microelectronics of the Russian Academy of Science, Moscow, Russia
[(c)]International Laboratory of Statistics of Stochastic Processes and Quantitative Finance of the National Research Tomsk State University, Tomsk, Russia

[(a)]barinovad@mpei.ru, [(b)]2009popovai@gmail.com, [(c)]o_v_ch@mail.ru

ABSTRACT
Possible methods for controlling the properties of amorphous diamond-like silicon-carbon films are considered: physical or structural modification, chemical modification, and physical-chemical modification. It is shown that the method of physical modification allows controlling in a wide range the properties of diamond-like silicon-carbon films (electrophysical, mechanical properties and surface morphology) without changing the chemical composition of the material. Chemical modification was carried out by introducing transition metal into diamond-like silicon-carbon films. The dependences of the phase composition, electrophysical and mechanical properties on the content and type of metal are analyzed. The method of physical-chemical modification is considered, when the introduced impurity changes not only the chemical composition, but also the structure of the material.

Keywords: silicon-carbon films, diamond-like structure, modification of properties, phase composition, physical, chemical and physical-chemical modification, transition metals

1. INTRODUCTION

Diamond like amorphous carbon films consist of structural network in which carbon atoms mainly have sp^3 hybridization of electron orbits. These films are widely used in micro- and nanoelectronics, optoelectronics, microelectromechanical systems, aerospace engineering due to their high electrical resistivity, good optical transparency high hardness and low friction (Robertson 2002). At the same time there are some limitations in the application of diamond like amorphous carbon films. These relate to the limited adhesion due to a high intrinsic compressive stress, low thermal stability and material graphitization at high temperatures. In addition, as for all amorphous semiconductors, there are certain difficulties in controlling the properties of the material, due to their weak sensitivity to impurities.

Diamond-like silicon-carbon films are materials that retain the advantages of the amorphous diamond-like carbon films, but are largely free from many of its drawbacks (Mangolinia, Krick et al. 2018). These materials consist of hydrogenated amorphous carbon diamond like network (*a*-C:H) and an amorphous silica network (*a*-Si:O) that mutually stabilize each other. This leads to a significant reduction of the intrinsic stress between films and substrates, improving on the adhesion of the films, as well as to a substantial increase of amorphous state stability of structural network.

The success of micro- and nanoelectronics device creation is largely determined by the capabilities and effectiveness of the material properties control. The generally accepted method of controlling the properties of crystalline semiconductors is the controlled addition of small amounts of donor or acceptor impurities. However, soon after the discovery of non-crystalline (amorphous) semiconductors, a weak sensitivity to the donor and acceptor impurities of these materials was established. It should be noted that alternative methods of controlling properties have been developed for a number of non-crystalline semiconductors. Such methods include chemical modification of properties for chalcogenide glassy semiconductors (CGS), structural modification of properties for amorphous carbon, hydrogenated amorphous silicon and CGS (Popov 2018). However, for other non-crystalline semiconductor materials, this question remains open to the present.

The report discusses the possibilities of controlling the properties of diamond-like silicon-carbon films by the methods of physical (structural) modification, chemical modification, and physical-chemical modification.

2. SAMPLE PREPARATION

Silicon-carbon films were prepared by plasma decomposition of a silicon-containing organic matter (polyphenylmethylsiloxane, PPMS, or polymethylsiloxane, PMS). During the film deposition process negative voltage was applied to the substrate holder. To obtain metal-based nanocomposites metal magnetron sputtering was conducted simultaneously with the growth of the silicon-carbon films. Schematic illustration of sample preparation system is shown in Fig. 1. It provides an opportunity to produce metal-containing films with different metal contents in a single technological process. It gives the opportunity to obtain metal-containing films with different metal content in a single technological process due to fixed position of the substrate holder.

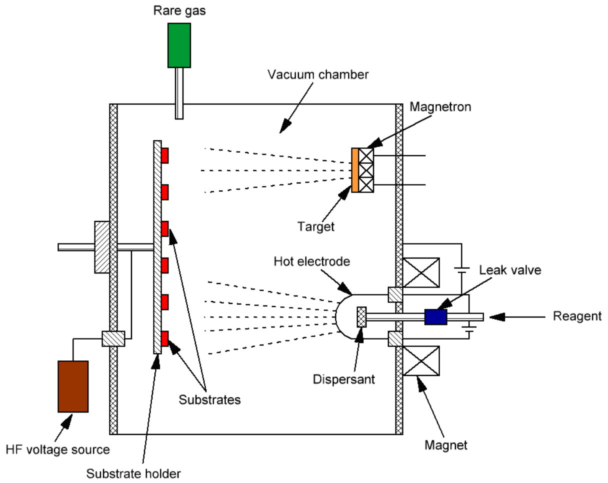

Figure 1: Schematic illustration of sample preparation system

3. METHODS OF MODIFICATION

3.1. Physical modification

The physical (structural) modification of non-crystalline material's properties allows to control properties by changing the material structure without changing its chemical composition. The physical base for the method is the fact that free energy of non-crystalline semiconductors has several minima corresponding to various metastable states of the system. Different structure of the material is obtained by varying the technological regimes and / or conditions of the material preparation. In this work, changes in the structure of amorphous diamond-like silicon-carbon films were achieved by varying the bias voltage on the substrate holder during film growth (from -100 to -1000 V) and bombarding the growing film with argon ions (the partial pressure of argon in the working chamber varied from 0 to $7 \cdot 10^{-4}$ Torr).

The magnitude of the potential on the substrate holder determines the kinetic energy (and hence the mobility) of particles falling on the substrate during the growth of the film. The bombardment of the growth surface with argon ions should affect the film structure. It is shown that the variation of the above parameters leads to a change in the morphology of the sample surface, mechanical properties and electrical conductivity of the material. An increase in the bias potential of the substrate holder leads to a decrease in the surface waviness of the samples by more than 2 times (from 0.9 to 0.4 nm) (Fig. 2). The nanohardness of films increases from 10-13 GPa to 18-24 GPa (Zavedeev et al. 2017) and the electrical conductivity decreases in by at least an order of magnitude (from 10^{-12} to 10^{-13} S/cm at 300 K) (Fig. 3).

Even greater changes in the properties are observed when a growing film is bombarded with argon ions: as the pressure of argon in the chamber increases from 0 to $7 \cdot 10^{-4}$ Torr (with a potential on the substrate holder of -200 V), the waviness of the film surface increases from 0.9 nm to 1.3 nm (Fig. 2), and the electrical conductivity increases by 6 orders of magnitude (from 10^{-12} to 10^{-6} S/cm) (Fig. 3).

To establish the causes of the effect of argon pressure in the chamber on the magnitude and activation energy of the electrical conductivity of silicon-carbon films, spectroscopy of deep levels in the band gap of the material was carried out using charge deep-level transient spectroscopy method (Q-DLTS) (Fig. 4).

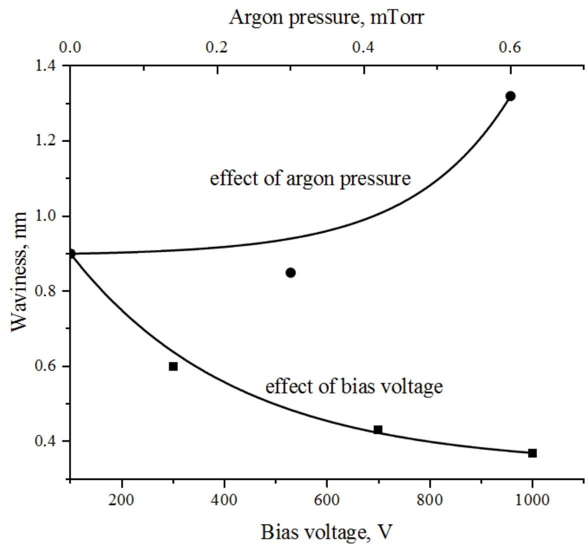

Figure 2: Dependence of the waviness of the film surface on the bias voltage applied to the substrate holder and on partial pressure of argon in the reactor

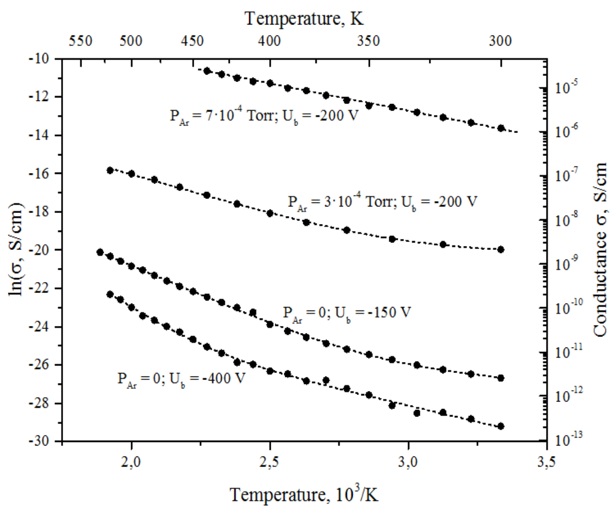

Figure 3: Temperature dependences of the conductivity of silicon-carbon films prepared at different values of bias voltage applied to the substrate holder and on partial pressure of argon in the reactor

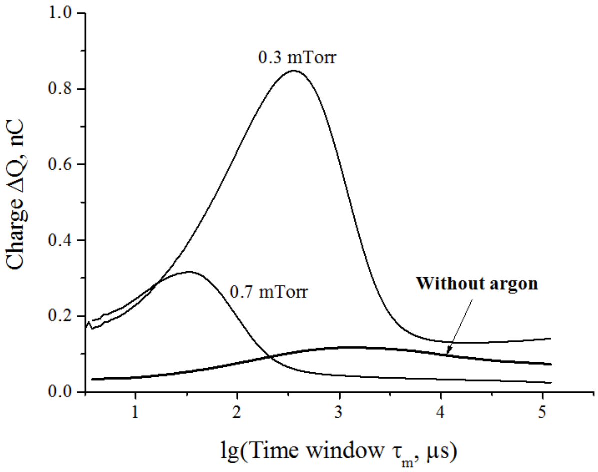

Figure 4: Q-DLTS spectra

Analysis of the Q-DLTS spectra showed that localized states in films prepared both with argon and without argon in the chamber is most likely to have the same nature and is due to the presence of dangling bonds. The concentration of localized states in the film increases with increasing argon pressure in the chamber.

Thus, the method of physical modification makes it possible to control in a significant extent the properties of diamond-like silicon-carbon films without changing their chemical composition. The total changes in electrical conductivity using the above physical modification factors are 7-8 orders of magnitude.

3.2. Chemical modification

The chemical modification of properties involves the introduction of additional chemical elements in the films during their preparation. In this work, metal-containing silicon-carbon films were fabricated by plasma-chemical decomposition of a silicon-organic precursor with simultaneous magnetron sputtering of transition metals (titanium, vanadium, molybdenum, hafnium, tantalum, tungsten). The metal concentration ranged from 4 to 35 at. %. The study of the structure of samples by high-resolution electron microscopy and X-ray photoelectron spectroscopy showed that the introduction of all metals into the silicon-carbon matrix throughout the entire concentration range leads to the formation of a two-phase system: an amorphous matrix with metal carbide nanocrystals embedded in it (Fig. 5). The size of nanocrystals was a few nanometers. No other crystalline inclusions were found in the examined samples. However, X-ray photoelectron spectroscopy spectra obtained in the region of bond energy of metal atoms showed that (at least in some cases) metal-oxygen bonds are present in the samples along with metal-carbon bonds. For example, in the spectra of tungsten-containing samples there are two distinct peaks (Fig. 6), the position of which almost coincides with the energy range of chemical bonds in the tungsten oxide WO3. This indicates that, in these samples, along with the nanocrystalline carbide phase, there is an oxide phase.

However, since high resolution electron microscopy and diffraction analysis reveal only metal carbide nanocrystals in samples, it should be assumed that the oxide phase is in an amorphous state. Simulation of X-ray photoelectron spectroscopy spectra showed approximately equal distribution of tungsten atoms between the carbide and oxide phases.

The carbides of transition metals formed upon the introduction of these metals into the dielectric amorphous silicon-carbon matrix are crystals with high electrical conductivity. In this regard, the use of these metals for the chemical modification of the electrophysical properties of silicon-carbon films seems to be effective. Studies of the concentration dependences of electrical conductivity showed (Fig. 7) that in all cases these dependences are of percolation type, and the value of electrical conductivity with the introduction of metal is up to 30-35 at. % increases by 9 orders of magnitude from 10^{-6} to 10^{3} S/cm.

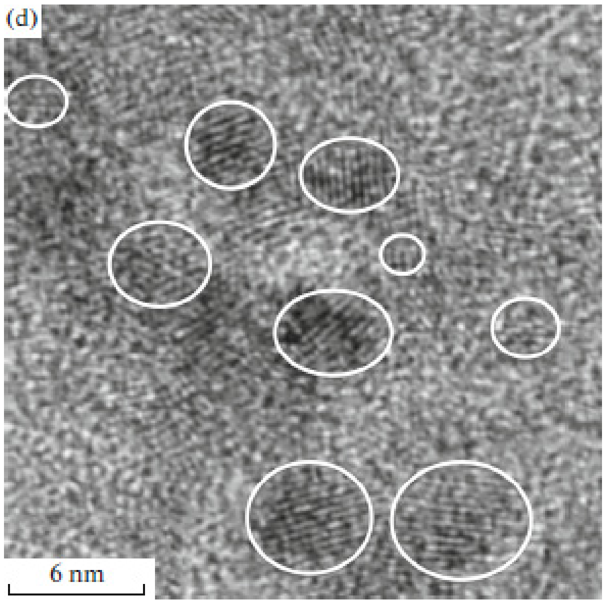

Figure 5: High resolution transition electron microscopy image of tantalum containing silicon-carbon film (Barinov, Popov et al. 2017)

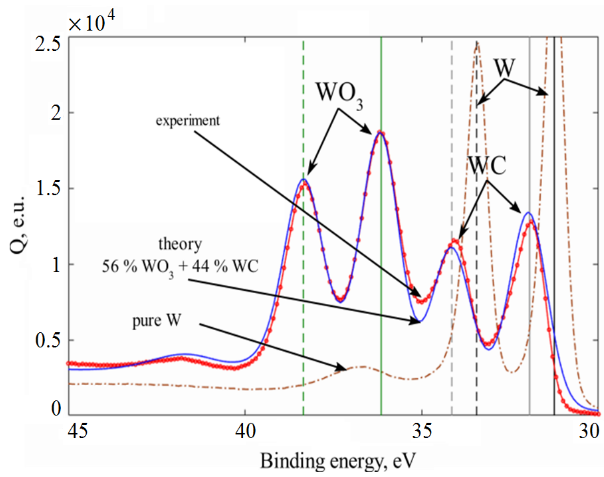

Figure 6: XPS spectra W $4f_{5/2}$ and $4f_{7/2}$

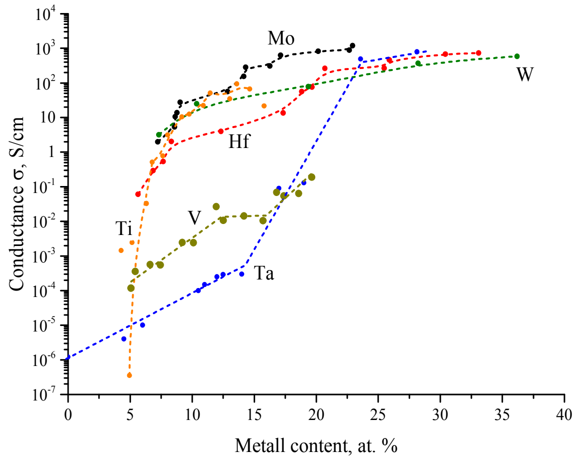

Figure 7: Dependences of silicon-carbon films conductivity on the concentration of metals

3.3. Physical-chemical modification

It should be noted that a number of experimental results obtained when introducing metals into silicon-carbon films are difficult to explain without taking into account changes not only in chemical composition, but also in the structure of the samples. For example, such results are dependencies of mechanical properties on metal concentration. As mentioned above, transition metals in silicon-carbon films form the nanocrystalline phase in the form of carbides. The carbon atoms for the formation of carbides are borrowed from the silicon-carbon matrix. Thus, despite the unchanged total concentration of carbon atoms, it is redistributed between the silicon-carbon amorphous matrix and the carbide nanocrystals of the introduced metal. Based on studies of the concentration dependences of the electrophysical and mechanical properties, it was shown that to correctly explain the dependencies of properties on metal concentration, it is necessary to take into account not only the presence and amount of the nanocrystalline phase, but also changes in the properties of the silicon-carbon matrix due to its structural changes as a result of carbon depletion.

Dependences of microhardness and modulus of elasticity of molybdenum- and tungsten-containing silicon-carbon nanocomposites on the metal concentration are shown in Fig. 8. An increase in the metal content leads to a redistribution of carbon in the nanocomposite: its concentration in the conducting nanocrystalline carbide phase increases, and in the amorphous silicon-carbon matrix it decreases. This leads to the appearance of two competing processes: on the one hand, an increase in the share of the carbide phase increases its contribution to the mechanical properties of the nanocomposite, and on the other hand, the depletion of the matrix with carbon causes a decrease in its contribution to the mechanical properties. These processes cause the appearance of an extremum on the concentration dependences of the mechanical properties (nanohardness and elastic modulus). However, as can be seen from Fig. 8, the minimum is observed only in the case of films with molybdenum, but it is absent in films with tungsten. To explain this fact, it should be noted that the size of nanoparticles in films with molybdenum is about 2.5 nm, and in films with tungsten – about 1 nm (Barinov, Popov et al. 2017). Therefore, with an equal content of the conducting phase (MoC and BC), the amount of tungsten carbide nanoparticles will be larger than that of molybdenum carbide. And this will cause a more rapid increase in the influence of the carbide phase on the mechanical properties of the material and the absence of an extremum on the concentration dependence for samples with tungsten.

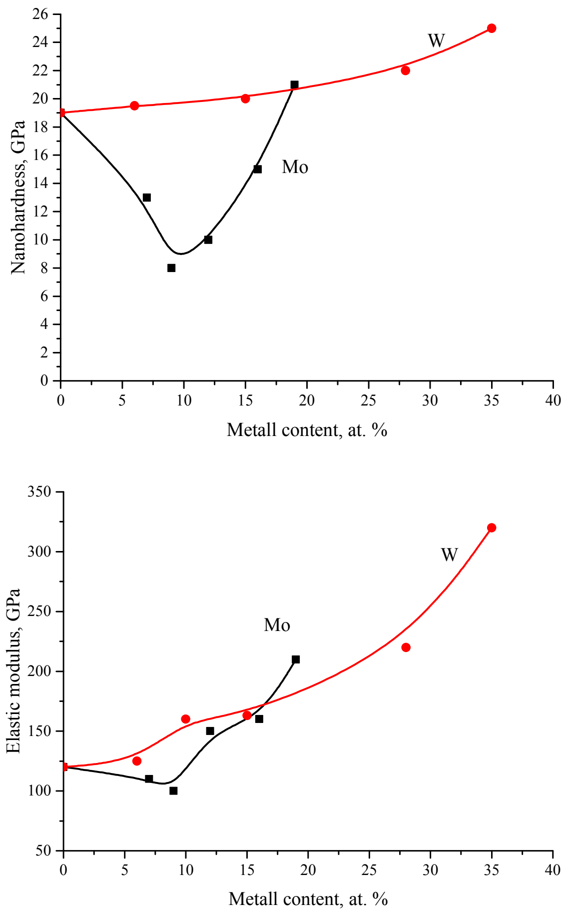

Figure 8: Mechanical properties as functions of metal concentration for the molybdenum- and tungsten-containing nanocomposites (nanohardness – upper and elastic modulus – lower)

4. CONCLUSION

Thus, the proposed methods provide wide possibilities for controlling the physical properties of diamond-like silicon-carbon films. For example, the range of possible changes in electrical conductivity with a combination of different control methods is 16 orders of magnitude. This opens up the possibility of widespread use of these materials in micro- and nanoelectronics.

ACKNOWLEDGMENTS

The authors are grateful to M.L. Shupegin for preparing the samples. This research was financially supported by the Russian Foundation for Basic Research (research project No. 19-07-00021), the Ministry of Education and Science of the Russian Federation (research project No. 2.3208.2017/4.6), and the Council on grants of the President of the Russian Federation (research project No. SP-834.2019.3).

REFERENCES

Barinov A.D., Popov A.I. and Presniakov M.Yu., 2017. Effect of nanophase concentration on the properties of metal-containing silicon-carbon nanocomposites. Inorganic Materials, 53 (7), 690-696.

Mangolinia F., Krick B.A. et al., 2018. Effect of silicon and oxygen dopants on the stability of hydrogenated amorphous carbon under harsh environmental conditions. Carbon, 130, 127-136.

Popov A., 2018. Disordered semiconductors: Physics and applications. 2nd ed. Singapore: Pan Stanford Publishing.

Robertson J., 2002. Diamond-like amorphous carbon. Materials Science and Engineering, 37, 129-281.

Zavedeev E.V., Zilova O.S., Barinov A.D. et al., 2017. Femtosecond laser microstructuring of diamond-like nanocomposite films. Diamond & Related materials, 74, 45-52.

AUTHORS BIOGRAPHY

Alexey D. Barinov was born in Moscow in 1989. After graduating from the Moscow Power Engineering Institute (Technical University) he obtained his PhD degree in the field of semiconductor physics in 2017. He currently works as an Assistant Professor at the same university. In addition, he works as a Researcher at the Institute of Nanotechnology of Microelectronics of the Russian Academy of Science. His research interests relate to the study of the electrophysical and morphological properties of semiconductor and dielectric thin films.

Anatoly I. Popov was born in Moscow, in 1944. After graduating from the Moscow Power Engineering Institute (Technical University) in 1968, he then obtained his PhD and Doctor of Science degrees in physics of semiconductors and insulators from the same university in 1973 and 1984 respectively. He is now a Professor at the National Research University "Moscow Power Engineering Institute" since 1987. He also holds position of Principle Research Scientist at the Institute of Nanotechnology of Microelectronics of the Russian Academy of Science. His scientific interests lie in exploration of the relationship between atomic structure and physical properties of disordered semiconductor materials and in development of optical storage and electrical memory devices based on these materials.

Alexander A. Makarov was born in 1993. He received the B.Sc. and the M.Sc. degrees from the National Research University "Moscow Power Engineering Institute" in 2014 and 2016, respectively, both in radio engineering. Presently, Alexander A. Makarov is a PhD student in the Department of Electronics and Nanoelectronics at the National Research University "Moscow Power Engineering Institute" as well as he is working as a Researcher at the International Laboratory of Statistics of Stochastic Processes and Quantitative Finance of the National Research Tomsk State University. His research interests include synthesis, analysis and simulation of the processing algorithms of stochastic processes and fields with unknown parameters.

INFLUENCE OF EMERGENCY LAY-BYS ON SMOKE STRATIFICATION IN CASE OF FIRE IN BI-DIRECTIONAL TUNNEL: PARALLEL SIMULATION

Weisenpacher, P.[(a)], Valasek, L.[(b)], Glasa, J.[(c)]

[(a),(b),(c)] Institute of Informatics, Slovak Academy of Sciences, Dubravska cesta 9, 84507 Bratislava, Slovakia

[(a)]upsyweis@savba.sk, [(b)]Lukas.Valasek@savba.sk, [(c)]Jan.Glasa@savba.sk

ABSTRACT

The main goal of longitudinal ventilation in case of fire in bi-directional road tunnel is to maintain smoke stratification, which is necessary for safe evacuation of people. This study investigates the influence of emergency lay-bys on smoke stratification in a 900 m long road tunnel by computer simulation using a parallel version of Fire Dynamics Simulator. The calculations were performed on the high performance computer cluster at the Institute of Informatics, Slovak Academy of Sciences in Bratislava (Slovakia). Several scenarios of fire in the tunnel without and with two lay-bys were simulated and compared. The most significant differences between smoke visibilities in both cases can be observed in the area of the lay-by located downstream of the fire. Several other differences are analysed as well.

Keywords: tunnel ventilation system, longitudinal ventilation, Fire Dynamics Simulator, parallel simulation, high-performance computing

1. INTRODUCTION

The concept of smoke stratification is used in fire safety measures in various types of structures with high compartments, for example in atriums and large corridors (Klote and Milke 1992). If upward movement of smoke ceases and the smoke layer does not descend below the level of human head, tenable conditions for human life are maintained and safe evacuation in case of fire is possible. Large dimensions of road tunnels enable to use the concept of smoke stratification for fire ventilation strategy in case of bi-directional tunnels equipped with longitudinal ventilation (Boehm 2008). It is assumed that in case of traffic accident and subsequent car fire, vehicles and people are trapped on both sides of fire. Proper airflow velocity in the tunnel induced by jet fans could maintain the stratification of smoke layer for several minutes to ensure the safe evacuation of people on both sides of fire. If smoke stratification was not maintained, tenable conditions for human life downstream of the fire would disappear.

Capability of maintaining smoke stratification is strongly influenced by tunnel geometry. From the point of view of tunnel geometry complexity, one of the most important features of the tunnel are niches for emergency lay-bys.

Lay-bys in tunnels allow vehicles to stop inside tunnel without blocking the carriageway. This reduces traffic disruption and the risk of collision. It is easier and safer for passengers to get out of their vehicle in a lay-by. Lay-by niches are equipped by various operating and safety installations. They are provided typically every 1000 m in the tunnel (Rattei 2010).

In this study we investigate the influence of lay-bys on smoke stratification in a 900 m long road tunnel using the well-known CFD code Fire Dynamics Simulator (FDS), version 6. Visibility at human head level is considered to be a measure of smoke stratification. In this way, a tunnel without lay-bys and a more realistic tunnel with two lay-bys are considered. Smoke movements in both cases are studied and compared for several selected fire scenarios and the influence of lay-bys on smoke stratification and visibility at head level is evaluated.

2. FDS TUNNEL MODEL

2.1. Fire Dynamics Simulator

FDS is a CFD-based simulation system for modelling fire and fire-driven fluid flows developed by the National Institute of Standards and Technology (NIST), USA in cooperation with the VTT Technical Research Centre of Finland (McGrattan, Hostikka, McDermott, Floyd, Weinschenk, and Overholt 2017). FDS numerically solves a form of conservation equations for low-speed thermally-driven flows with an emphasis on the smoke and heat transport from fire.

The core algorithm is a very efficient explicit predictor-corrector scheme, second order accurate in space and time. FDS also includes models of fire related processes such as turbulence, thermal radiation, pyrolysis, combustion of the pyrolysis products, conductive heat transfer, etc.

Input data for simulation include the rectangular geometry of the scenario (size and shape of compartments, locations and dimensions of all relevant objects), material properties of object surfaces (ignition temperature, thermal conductivity, specific heat, density, emissivity, heat of evaporation, etc.) and the fire HRR.

FDS supports several models of parallelization of calculation (Weisenpacher, Glasa, and Sipkova 2016). The Message Passing Interface (MPI) model was chosen for this study due to its efficiency enabling to deal with significant computational requirements of fire simulation in large tunnel.

The execution of simulation on the HPC (high performance computing) cluster is realized by the invocation of the corresponding FDS manager script accompanied with the input parameters.

The simulations were carried out on the SIVVP HPC cluster at the Institute of Informatics, Slovak Academy of Sciences, Bratislava (Slovakia) (SIVVP). It is an IBM dx360 M3 cluster consisting of 54 computational nodes (23 Intel E5645 @ 2.4 GHz CPU, 48 GB RAM); the total number of cores is 648. The nodes are connected by the Infiniband interconnection network with the bandwidth of 40 Gbit/s per link and direction.

2.2. Tunnel Model Description

The scheme of the tunnel with two lay-bys is shown in Fig. 1. The 900 m long tunnel has a horseshoe cross section of dimensions 10.8 m (width) and 6.8 m (height). The lay-bys are located at 373 m and 635.6 m from the west tunnel portal. The first lay-by is located on the left side of the tunnel, the second one on the right side. The niches are 50 m long and 2.2 m wide with the maximal height of vaulted ceiling of 7.8 m.

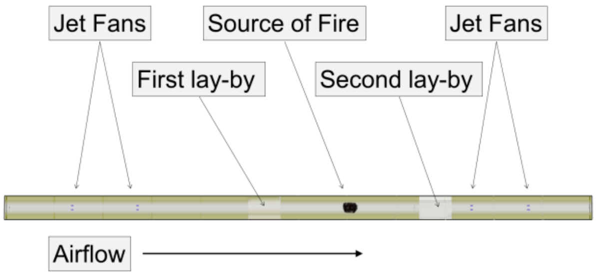

Figure 1: Scheme of the Tunnel with Two Lay-Bys

The tunnel is equipped with four pairs of jet fans located at 101 m, 201 m, 716 m and 801 m. They are modelled using the HVAC feature included in FDS. Two rectangular vents of dimensions 0.6 m x 0.8 m with a prescribed normal velocity are used to model the inlet and outlet of a jet fan. The length of the jet fan shroud is 3.8 m. The maximal volume flow is 18.62 $m^3.s^{-1}$.

The tunnel dimensions as well as the parameters of the jet fans are typical for some tunnels which are currently under construction in Slovakia (Danisovic, Sramek, Hodon, and Hudik 2017).

Fire is located at 530 m, i.e. between the lay-bys. Three different heat release rates (HRR) are considered: 3 MW, 5 MW and 12 MW corresponding to a small passenger car fire, large passenger car fire and truck fire, respectively. The fire soot yield is 0.2.

For each value of HRR four fire scenarios are simulated:

- horizontal tunnel without lay-bys (xMW-0)
- horizontal tunnel with two lay-bys (xMW-0L)
- tunnel with 2° slope without lay-bys (xMW-2)
- tunnel with 2° slope with two lay-bys (xMW-2L),

where x = 3, 5, 12.

The tunnel cross section as well as the jet fans location and performance are the same in all scenarios.

The fire HRR increases linearly since the beginning of the simulation, reaching its maximal value after 40 s of the fire. Jet fans performance is modelled via the RAMP feature in FDS. Adaptive algorithm increases or decreases their performance in order to achieve the prescribed target velocity of 1.2 $m.s^{-1}$ required by Slovak regulation (TP 12/2011).

The computational domain size is 900 m x 18 m x 8 m for all considered tunnels. For 20 cm mesh resolution, the domain consists of 4,500 x 90 x 40 cells. The total number of cells is 16,200,000. In order to deal with significant computational requirements and to increase the simulations performance, the parallel MPI version 6.5.2 of FDS was used. The computational domain was decomposed into 12 meshes, each of them assigned to one MPI process (one CPU core).

The total CPU time strongly depends on specifications of each fire scenario. It varies from 269 hours for 3MW-2 scenario to 993 hours for 12MW-2 scenario.

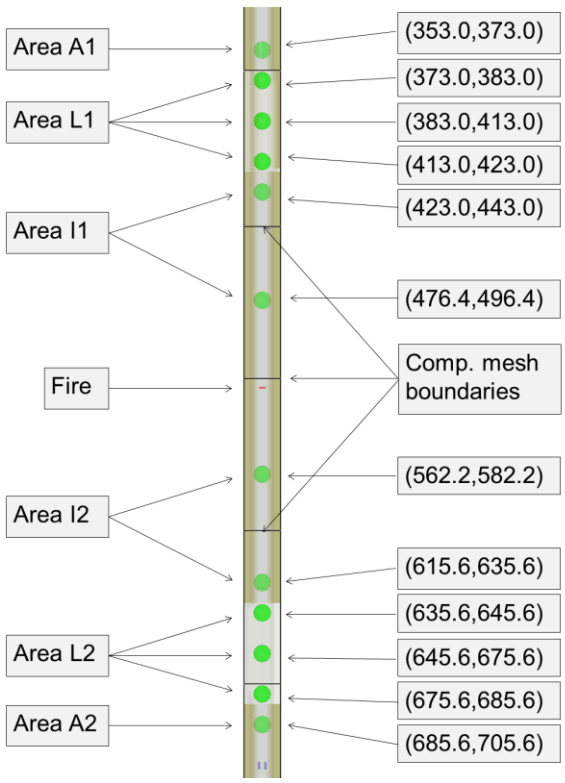

Figure 2: Six Areas of the Tunnel in Which Averaged Visibility Is Evaluated and 12 Sectors Used For Their Definition, Their Location and Dimensions

3. SIMULATION RESULTS

Average visibility at human head level is studied in six areas of the tunnel depicted in Fig. 2: in both lay-bys (L1 and L2), in front of the first lay-by (A1), behind the second lay-by (A2), between the lay-bys upstream and downstream of the fire (I1 and I2, respectively). Because of FDS limitations, averaged quantities must be evaluated within one computational mesh only. Therefore, it is useful to define 12 sectors in which the average visibility is evaluated and to determine the corresponding average quantities for six tested areas via weighted averages of these 12 values according to the scheme in Fig. 2. Finally, we obtain six time-dependent values describing conditions in particular areas of the tunnel from the point of view of smoke distribution.

Main tendencies of smoke movement are similar for all tested scenarios (see Fig. 3). Significant backlayering upstream of the fire increases with increasing HRR and decreases in sloped tunnels. Movement of smoke downstream is accelerated for higher HRR. However, there are several differences that must be analysed.

Figure 3: Smoke Movement for Four 5 MW Fire Scenarios after 100 s to the Fire

3.1. Passenger car fire scenarios

Due to less significant backlayering caused by relatively low HRR there is no visibility drop in any of three areas upstream of the fire (A1, L1 and I1 areas) in passenger car fire scenarios.

Only slight drop of visibility occurs in front of the second lay-by (I2 area, downstream of the fire) for sloped tunnel scenario. However, in the case of horizontal tunnel the drop is considerable and after 200 s to the fire the conditions for human life become untenable (see Fig. 4). Note that the difference is caused by higher air velocity in front of the fire in the case of horizontal tunnel, which disrupts the stratification of the smoke layer downstream of the fire. Due to the higher buoyancy, such effect is attenuated in the sloped tunnel (Weisenpacher, Glasa, and Valasek 2017; Weisenpacher, Glasa, and Valasek 2018).

The similar patterns of visibility decrease can be observed also in the second lay-by (L2 area), although they are shifted in time due to its farther location in the tunnel (see Figs. 5 and 6). In these cases, the first significant differences between scenarios with and without lay-bys can be observed.

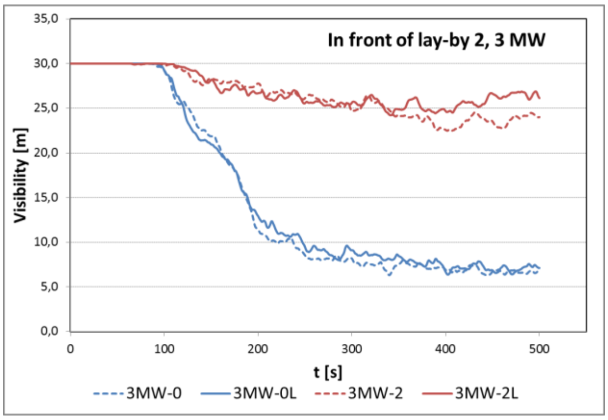

Figure 4: Average Visibility In Front of the Second Lay-By for 3 MW Fires

In the horizontal tunnel the lay-by geometry improves the conditions for people. Untenable conditions occur in all scenarios with horizontal tunnel; however, they occur later in scenarios with lay-bys. The effect is more pronounced for less intensive fire. For 3 MW fire, untenable conditions occur later by more than 2 minutes in the 3MW-0L scenario (with lay-by) than in the 3MW-0 scenario. In 5 MW fire scenarios the corresponding difference is only 49 s.

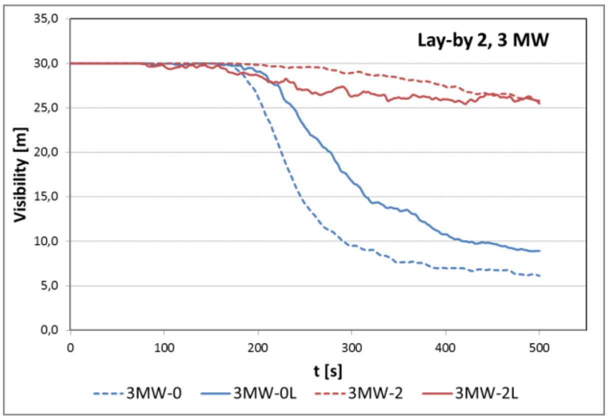

Figure 5: Average Visibility in the Second Lay-By for 3 MW Fires

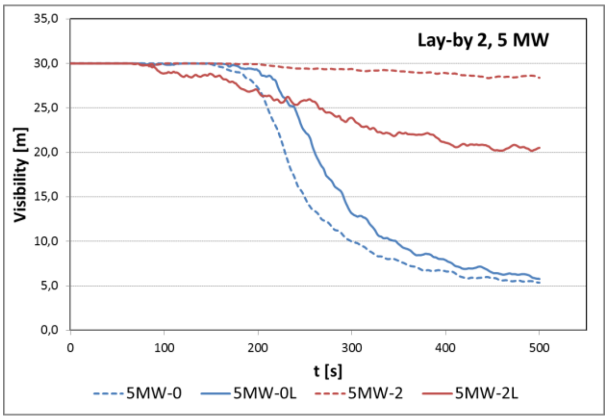

Figure 6: Average Visibility in the Second Lay-By for 5 MW Fires

Note that in horizontal tunnel the visibility decrease starts behind the fire and the region with untenable conditions expands downstream. The higher ceiling in the lay-by enables the ascent of the smoke layer improving conditions at head level. The effect is more significant for thinner smoke layer in 3 MW scenarios.
In the sloped tunnel the visibility decrease is not critical and tenable conditions are maintained. The lay-by deteriorates visibility for both 3 and 5 MW scenarios; however, the effect is very slight in the cases of 3 MW fires (see Fig. 5), while in the cases of 5MW fires the visibility decrease is more pronounced (see Fig. 6). Fig. 3 indicates a considerable visibility decrease occurring in the rear part of the lay-by due to the interaction of the smoke layer with the vertical wall delimiting the end of the lay-by. The smoke is pushed down causing extreme local decrease of the visibility at head level which also decreases the average visibility evaluated within the whole lay-by. The effect is obviously intensified by larger amount of smoke and its higher velocity which is why it is more significant in the case of 5 MW fires. Smoke distribution patterns and their dependence on tunnel geometry and air flows are analysed in detail in the next section.
The vertical wall at the end of the lay-by causes significant drop of visibility in the A2 area (i.e. behind the lay-by) in all scenarios with lay-bys. After 5 – 6 minutes of the fire conditions in the A2 area are untenable in all scenarios with the exception of 3MW-2 and 5MW-2, in which almost perfect visibility is maintained.

3.2. Smoke distribution in the second lay-by

Average visibility depicted in Figs. 5 and 6 does not capture local behaviour of smoke within lay-by. Vertical slices and horizontal slices at head level of visibility for four horizontal tunnel scenarios after 300 s are shown in Figs. 7 and 8. Yellow and red colour mark regions with untenable conditions, green colour marks tenable conditions and blue colour marks the regions with almost perfect visibility. Average visibility in the lay-by at that time is close to 10 m limit for all four considered simulations.

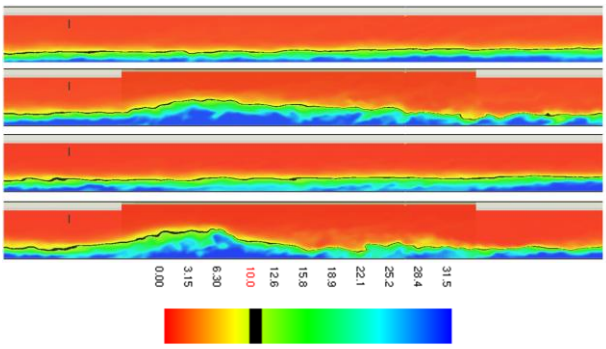

Figure 7: Vertical Slice of Visibility in the Second Lay-By for Horizontal Tunnel Scenarios 3MW-0, 3MW-0L, 5MW-0 and 5MW-0L after 300 s to the Fire

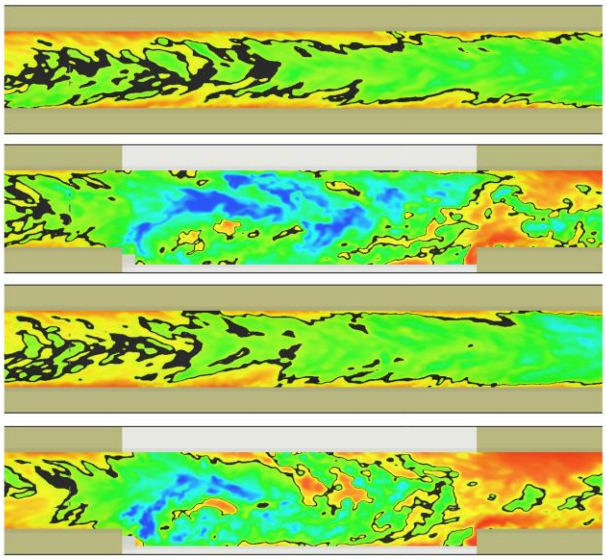

Figure 8: Horizontal Slice of Visibility at Head Level in the Second Lay-By for Horizontal Tunnel Scenarios 3MW-0, 3MW-0L, 5MW-0 and 5MW-0L after 300 s to the Fire

Higher ceiling of the lay-by improves the visibility at head level in the region of lay-by closer to fire, as the smoke ascends higher. The smoke layer becomes thinner. In Fig. 8 large regions with good visibility can be observed. On the other hand, interaction with the vertical wall at the end of the lay-by deteriorates visibility in the rear region of the lay-by, which is worse than in xMW-0 scenarios.

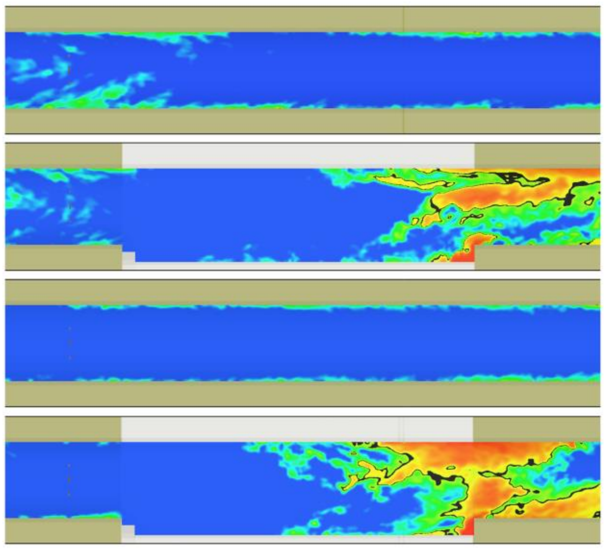

Figure 9: Horizontal Slice of Visibility at Head Level in the Second Lay-By for Sloped Tunnel Scenarios 3MW-2, 3MW-2L, 5MW-2 and 5MW-2L after 300 s to the Fire

At 300 s to the fire conditions in the lay-by become untenable. The visibility drop starts near the tunnel walls and in the lay-by niche at the end of the lay-by. Regions with untenable conditions expand and merge so that they afflict the entire width of the lay-by.

Similar pattern as in horizontal tunnel can be observed also in the case of sloped tunnel (see Fig. 9). The averaged visibility is significantly better than in horizontal tunnel in accordance with Figs. 5 and 6. However, the improvement of visibility at the beginning of the lay-by and deterioration at its end can be observed in this case as well. The visibility drop starts near the walls and lay-by niche.
In horizontal tunnel the increase of the visibility at the beginning of the lay-by improves average visibility which is generally not sufficient. Therefore, the lay-by improves conditions for people. In sloped tunnel the visibility is generally very good, although the lay-by deteriorates conditions for people at some locations.

3.3. Truck fire scenarios

Behaviour of truck fire in sloped tunnel in L2 area is similar as in the case of passenger car fire (see Fig. 10). Lay-bys deteriorate visibility at head level even more significantly, which indicates that deterioration of conditions in the lay-by increases with increasing HRR. For 12 MW fire, the lay-by deteriorates even the conditions in horizontal tunnel slightly (see Fig. 10) which is caused by thick smoke layer in that case.

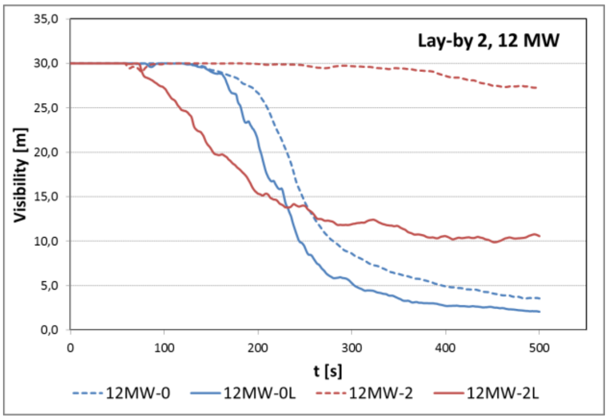

Figure 10: Average Visibility in the Second Lay-By for 12 MW Fires

Higher HRR of the truck fire allows investigating also the smoke behaviour in the first lay-by (L1 area) located upstream. The lay-by is afflicted by smoke due to the more significant backlayering which transfers the smoke upstream farther than in the cases of passenger car fires.
The decrease of visibility at head level starts in the fire vicinity due to cooled smoke entrained from the bottom part of the smoke layer downstream. The region with untenable conditions expands upstream slowly, i.e., for given time the visibility improves with the distance from the fire. The visibility pattern can be seen in Fig. 11.
In the case of horizontal tunnel, the smoke layer covers the entire ceiling of the lay-by and spreads out of the lay-by upstream. However, due to significant distance of the first lay-by, there is only a small decrease of average visibility at head level in it (see Fig. 12). Considerable decrease of visibility occurs locally in lay-by niche at the place for car parking while conditions in the central part of the lay-by are tenable.

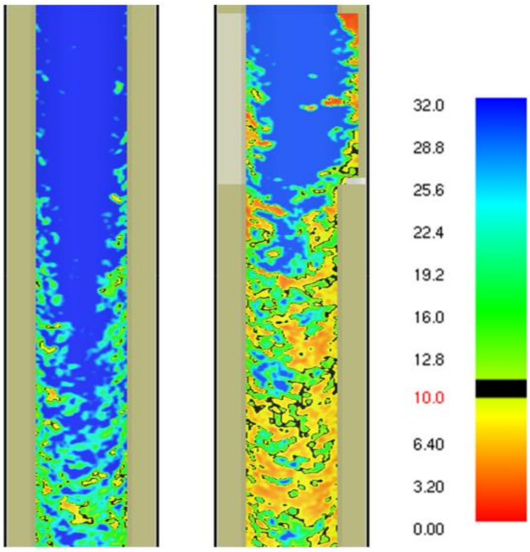

Figure 11: Vertical Slice of Visibility for Horizontal Tunnel Scenarios 12MW-0 and 12MW-0L: Areas L1 and I1 after 400 s to the Fire

The lay-by deteriorates conditions for people. Its geometry influences the spread of smoke in I1 area even more significantly causing enormous decrease of visibility occurring between 300 and 400 s to the fire (see Fig. 11). The vertical wall at the end of the lay-by disrupts the smoke layer intensifying its dissolution. Cooled smoke is entrained towards the fire and descends causing decrease of visibility in the fire vicinity.

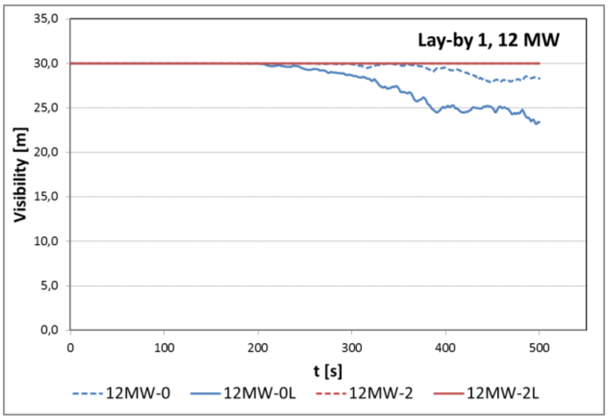

Figure 12: Average Visibility in the First Lay-By for 12 MW Fires

Note that the visibility decrease in the lay-by located upstream in horizontal tunnel may be more significant for shorter distance between the lay-by and the fire. The first lay-by in sloped tunnel is not afflicted by smoke due to the smaller length of smoke backlayering.

3.4. Time-averaged visibilities

The tendencies described above in detail can be presented in a schematic way using time-averaged values of visibility for the last 200 s of simulation. In Fig. 13 the time-averaged visibilities for all scenarios and all six areas of the tunnel are presented.

	A1	L1	I1	I2	L2	A2
3MW-0	30.0	30.0	30.0	7.1	7.4	8.2
3MW-0L	30.0	30.0	30.0	7.6	11.6	5.3
3MW-2	30.0	30.0	30.0	24.0	27.5	28.4
3MW-2L	30.0	30.0	30.0	25.6	26.1	10.0
5MW-0	30.0	30.0	29.8	5.4	6.9	8.2
5MW-0L	30.0	30.0	29.8	5.6	8.3	3.3
5MW-2	30.0	30.0	30.0	25.6	28.8	28.5
5MW-2L	30.0	30.0	30.0	27.5	21.4	9.6
12MW-0	29.9	29.1	23.0	3.4	5.3	6.1
12MW-0L	29.9	25.8	14.0	3.7	3.1	1.3
12MW-2	30.0	30.0	30.0	27.5	28.5	11.1
12MW-2L	30.0	30.0	30.0	27.8	10.9	3.5

Figure 13: Time-Averaged Visibility in Meters for the Last 200 s Period of the Simulations in Six Tested Areas for All Scenarios

The visibility is deteriorated in four types of cases:

- downstream of the fire (I2, L2 and A2 areas) in horizontal tunnels scenarios
- in the second lay-by and behind it (L2, A2) in lay bay sloped tunnel scenarios
- in A2 area for 12 MW fire in sloped tunnel without lay-bys
- upstream of the fire behind the first lay-by (I1 area) for 12 MW fire in horizontal tunnel.

Relative change of the visibility in six tested areas caused by lay-bys can be seen in Fig. 14. Blue colour marks areas in which lay-bys improve the visibility, while red colour indicates deterioration of visibility.

	A1	L1	I1	I2	L2	A2
3MW-0	0.00	0.00	0.00	0.08	0.57	-0.35
3MW-2	0.00	0.00	0.00	0.07	-0.05	-0.65
5MW-0	0.00	0.00	0.00	0.04	0.22	-0.60
5MW-2	0.00	0.00	0.00	0.07	-0.26	-0.66
12MW-0	0.00	-0.11	-0.39	0.08	-0.42	-0.79
12MW-2	0.00	0.00	0.00	0.01	-0.62	-0.68

Figure 14: Relative Change of Time-Averaged Visibility in Six Tested Areas Caused by Lay-Bys Included in the Tunnel

A significant improvement due to lay-by installation occurs in two cases in which conditions are untenable, while a slight improvement occurs in the I2 area in all tested cases.

Deterioration of visibility occurs in the A2 area in all scenarios. For more intensive fires visibility deteriorates also in the second lay-by area (L2) and also behind the first lay-by for 12 MW fire in horizontal tunnel scenario.

4. CONCLUSION

Series of 12 parallel simulations of tunnel fire have been performed by FDS to investigate the influence of emergency lay-bys on smoke stratification in a 900 m long road tunnel.

Specific geometry of the lay-by located downstream improves visibility at head level in the front area of the lay-by and deteriorates it in the rear area. In horizontal tunnel the first mentioned effect prevails and the lay-by improves conditions for people, which would otherwise be untenable after 5 minutes to the fire. In the case of sloped tunnel the conditions are tenable within almost whole tunnel tube and the lay-by causes a local untenability of conditions at the end of the lay-by and behind it which becomes significant for more intensive fires.

Decrease of visibility in the lay-by located upstream occurs only if the length of backlayering is sufficient to achieve its location, i.e., for more intensive fires. In such case only a slight drop of visibility can be observed. However, significant deterioration of visibility occurs in the area between this lay-by and the fire.

In other sections of the tunnel the effect of the lay-by on smoke stratification is very small.

ACKNOWLEDGMENTS

The authors would like to thank Peter Schmidt (National Motorway Company, Slovakia) for information about technical specifications of road tunnels. This paper was partially supported by the Slovak Science Foundation (project VEGA 2/0165/17) and the Slovak Research and Development Agency (project No. APVV-15-0340).

REFERENCES

Boehm M., Fournier L., Truchot B, 2008. Smoke stratification stability: presentation of experiments. Proceedings of 4th International Conference on Tunnel Safety and Ventilation, pp 176–182. April 21-23, Graz (Austria).

Danisovic P., Sramek J., Hodon M., Hudik M., 2017. Testing measurements of airflow velocity in road tunnels. MATEC Web of Conferences, 117, 00035.

Klote J., Milke, J., 1992. Design of smoke management systems. American Society of Heating, Refrigerating and Air Conditioning Engineers. Atlanta, Georgia, USA.

McGrattan K., Hostikka S., McDermott R., Floyd J., Weinschenk C. and Overholt K., 2017. Fire Dynamics Simulator, Technical Reference Guide (sixth edition). National Institute of Standards and Technology. Gaithersburg, Maryland, USA, and VTT Technical Research Centre of Finland, Espoo, Finland.

Rattei G., 2010. Safety installations in road tunnels – are they used in incident cases? Proceedings of 5th International Conference on Tunnel Safety and Ventilation, pp 235–241. May 3-4, Graz (Austria).

SIVVP. Slovak Infrastructure for High Performance Computing. Available from: http://www.sivvp.sk/

TP 12/2011, 2011. Road tunnels ventilation (in Slovak). Ministry of Transport and Construction of the Slovak Republic. Bratislava, Slovakia.

Weisenpacher P., Glasa J., Sipkova V., 2016. Performance of FDS versions 5 and 6 in passenger car fire computer simulation. Proceedings of European Modeling and Simulation Symposium, 2016, pp. 156–161. September 26-28, Larnaca (Cyprus).

Weisenpacher P., Glasa J., Valasek L., 2017. Computer simulation of smoke stratification during fire in bi-directional road tunnel by FDS 6. Proceedings of the MCS-10: Tenth Mediterranean Combustion Symposium. September 17-21, Naples (Italy).

Weisenpacher P., Glasa J., Valasek L., 2018. Influence of slope and external temperature on smoke stratification in case of fire in bi-directional road tunnel. ITM Web of Conferences, 16, 02002.

THE HARDWARE IMPLEMENTATION OF THE MULTI-POSITION SIGNAL DIGITAL DEMODULATORS

O.V. Chernoyarov[(a)], A.N. Glushkov[(b)], V.P. Litvinenko[(c)], A.N. Faulgaber[(d)], A.V. Salnikova[(e)]

[(a),(d),(e)]National Research University “Moscow Power Engineering Institute”, Moscow, Russia
[(a),(e)]International Laboratory of Statistics of Stochastic Processes and Quantitative Finance of the National Research Tomsk State University, Tomsk, Russia
[(a)]Maikop State Technological University, Maikop, Russia
[(b)]Voronezh Institute of the Ministry of Internal Affairs of the Russian Federation, Voronezh, Russia
[(c),(e)]Voronezh State Technical University, Voronezh, Russia

[(a)]chernoyarovov@mpei.ru, [(b)]a.n.glushkov@gmail.com, [(c)]v.p.litvinenko@gmail.com [(c)]lytaleksandr@mail.ru
[(d)]amicus.lat@yandex.ru

ABSTRACT
There are considered the capabilities of the hardware implementation of the digital demodulators when receiving the signals of various modulation formats. It is shown that the multi-position signal processing devices can be implemented by means of the on the relatively inexpensive field programmable gate arrays.

Keywords: workstation design, work measurement, ergonomics, decision support system

1. INTRODUCTION

The digital modulation signals (PSK, QAM, etc.) are widely used in radio communication systems (Feher, 1995; Sklar, 2001; Proakis and Salehi 2007). The application of modern equipment is focused on the digital implementation of phase detectors and demodulators. Hence, in the present paper, devices are introduced requiring performing only a minimum number of simple arithmetic operations over the signal period (Chernoyarov et al. 2015-2018). Yet, software implementation of the algorithms for processing high-frequency digital modulation signals in real time when it is carried out by means of the signal processors requires too significant computational costs. In view of this, the field programmable gate arrays (FPGAs) are considered as more appropriate tools for hardware processing of the high-frequency signals in terms of the specified algorithms. Below, the resources are analyzed that are required for the implementation of the demodulators by means of the FPGAs.

2. THE MAJOR PART

An urgent task in designing the digital demodulators is to estimate hardware resources needed for their FPGA-based implementation. The most resource-intensive receiving devices are the quadrature amplitude modulation (QAM) signal demodulator (Chernoyarov, Glushkov, Litvinenko, Litvinenko and Matveev 2018) and the non-coherent demodulator of the signals phase-shift keyed in toto (Glushkov, Litvinenko, Matveev, Chenoyarov and Kalashnikov 2016; Chernoyarov, Litvinenko, Glushkov, Matveev and Salnikova 2017).

Modern FPGAs (Andina, de la Torre Arnanz and Valdes 2017) provide greater opportunities for the implementation of the digital high-frequency signal demodulators, but in this case, however, there should be designed the processing units requiring minimal computational resources.

In common studies (Chernoyarov O.V. et al. 2015-2018), the basic fast digital algorithms for coherent and noncoherent signal processing are introduced. In Fig. 1, the block diagram of the noncoherent processing algorithm is shown.

The signal from the intermediate frequency section output of the receiver is fed to the input of the 8-to 16-bit analog-to-digital converter (ADC) operated by the clock generator (CG) with the frequency $f_Q = 4f_0$. Here f_0 is the band center of the signal that may have frequency of tens of megahertz. As a result, the four samples s_{1i}, s_{i1}, s_{i2}, s_{i3} are formed over each of the i-th signal period $T_0 = 1/f_0$ as shown in Fig. 2. They are stored in the multi-bit four-cell shifter (MS4), while in the subtractors SUB_0 and SUB_1 the differences are determined of the even and odd samples forming the quadrature processing channels of the signal.

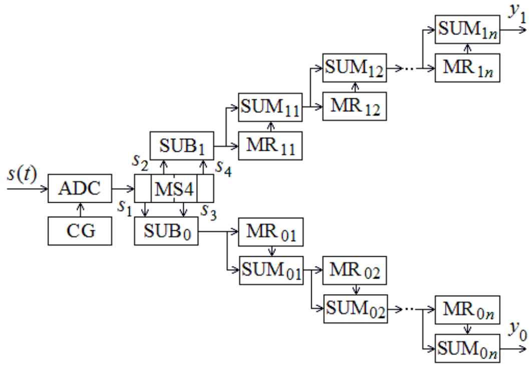

Figure 1: The block diagram of the noncoherent processing algorithm

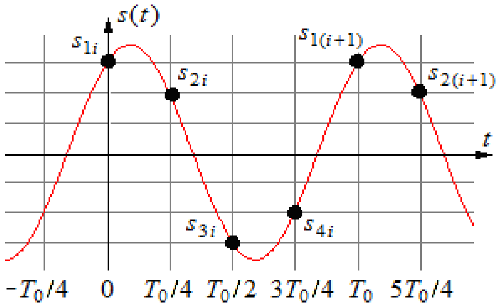

Figure 2: Time quantization diagram

The pairs of even and odd current and previous (stored into multi-bit shift registers MR_{01} and MR_{11}) differences of the samples are summarized in the summators SUM_{01} and SUM_{11}. Further, the obtained sums (two, then four, then eight, etc.) are accumulated in the subsequent summators, so that the responses of the quadrature channels are formed over the interval of the information signal duration $N = 2^n$ (where n is an integer) as follows

$$y_{0i} = \sum_{j=0}^{N-1} \left(s_{1(i-j)} - s_{3(i-j)}\right), \quad y_{1i} = \sum_{j=0}^{N-1} \left(s_{2(i-j)} - s_{4(i-j)}\right).$$

The basic algorithms provide the minimum number $n = \log_2 N$ of the addition operations for accumulating the differences of the signal samples for the sample of the size N in each of the quadrature channels (Fig. 1). This also applies to the coherent algorithm (Glushkov, Litvinenko, Matveev, Chernoyarov and Salnikova 2015; Chernoyarov, Glushkov, Litvinenko, Litvinenko and Matveev B.V. 2017).

Based on these basic and coherent algorithms, various devices can be implemented for demodulating high-frequency phase-shift keyed (PSK) and differential phase-shift keyed (DPSK) radio signals.

In Fig. 3a, the block diagram is shown of the digital binary DPSK signal demodulator, while in Fig. 3b we can see the block diagram of the four-position DPSK signal demodulator (Chernoyarov, Glushkov, Litvinenko, Litvinenko and Matveev 2018).

In comparison with the basic algorithm (Fig. 1) in the demodulator circuit presented in Fig. 3a, there are supplemented the multi-bit N cell shifters $MR_{0(n+1)}$ and $MR_{1(n+1)}$, two additional summators and subtractors, two quadratic blocks (QT) performing the operations

$$z_{0i} = (y_{01i} + y_{0(i-N)})^2 + (y_{1i} + y_{1(i-N)})^2,$$
$$z_{1i} = (y_{01i} - y_{0(i-N)})^2 + (y_{1i} - y_{1(i-N)})^2,$$

as well as the substractor (SUB) and the comparator (C) forming the information symbol S_I.

Similarly, into the four-position DPSK signal demodulator (Fig. 3b), the basic algorithm is supplemented by the computing unit (CU) that performs the operations

$$z_0 = y_{0,i}y_{0,(i-N)} + y_{1,i}y_{1,(i-N)} + y_{1,i}y_{0,(i-N)} - y_{0,i}y_{1,(i-N)},$$
$$z_1 = y_{0,i}y_{0,(i-N)} + y_{1,i}y_{1,(i-N)} - y_{1,i}y_{0,(i-N)} + y_{0,i}y_{1,(i-N)},$$

as well as the two comparators C_1 and C_2 at the outputs of which the symbols S_{I0} and S_{I1} are generated. The block diagrams of the coherent PSK and DPSK signal demodulators are much simpler than those shown in Fig. 3.

Thus, the basic digital algorithm allows us to implement various PSK signal demodulators at relatively low computational costs.

In Fig. 4a, the block diagram is shown of a more complex coherent quadrature amplitude modulation (QAM) signal demodulator (Chernoyarov, Glushkov, Litvinenko, Litvinenko and Matveev B.V. 2018). Here the responses of the quadrature channels (2) and (3) are passed to the threshold devices TD_0 and TD_1 as well as to the normalizing and synchronizing device (NSD) providing clock synchronization and the formation of the thresholds for TDs. According to the output TDs signals, in the resolver (RS) the code words are separated by which the binary code of the received multi-position symbol is formed in the decoder (DC).

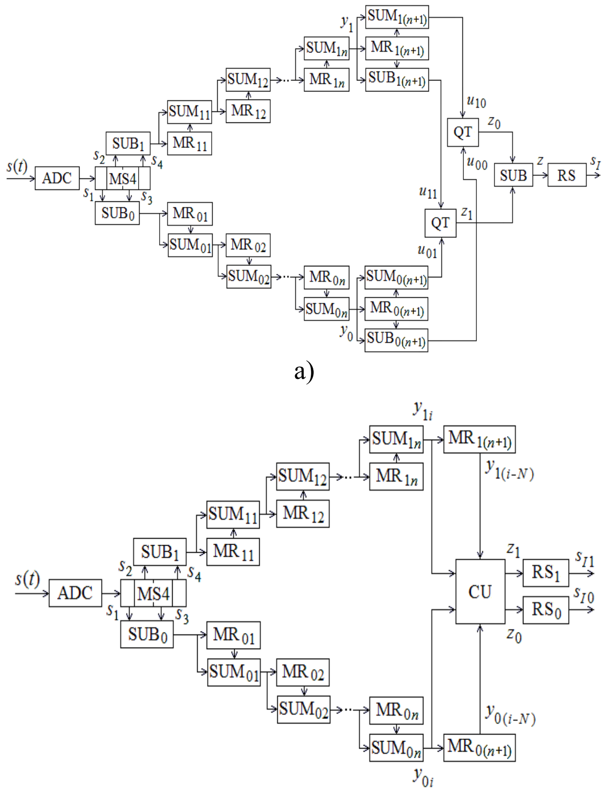

Figure 3: The block diagrams of the fast digital algorithms for noncoherent demodulation of binary (a) and four-position (b) DPSK signals

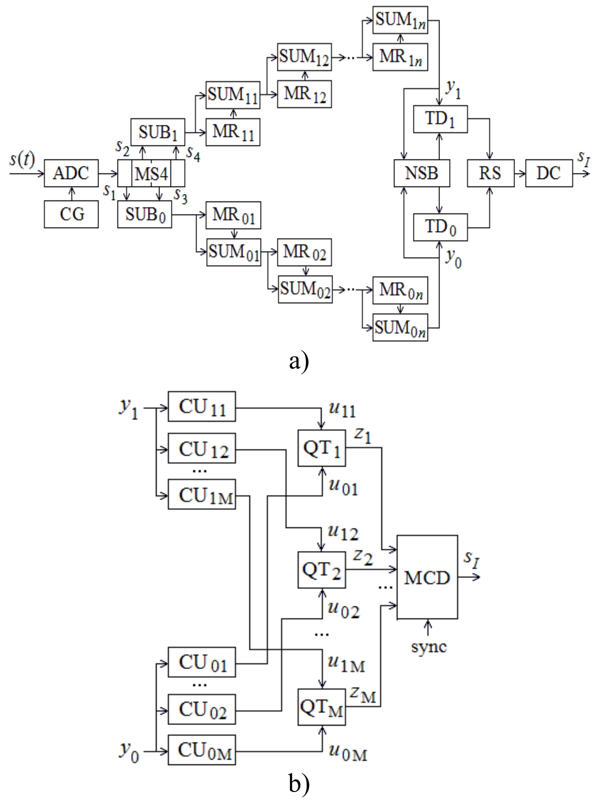

Figure 4: The block diagrams of the fast digital algorithms for noncoherent demodulation of binary (a) and four-position (b) DPSK signals

The digital demodulator of the signals phase-shift keyed in toto (Glushkov, Litvinenko, Matveev, Chenoyarov and Kalashnikov 2016; Chernoyarov, Litvinenko, Glushkov, Matveev and Salnikova 2017) requires the greatest computational cost. The block diagram of its addition to the basic algorithm (Fig. 1) is shown in Fig. 4b.

The values y_{0i}, y_{1i} are moved to the computing units CU_0 and CU_1 generating the responses u_{0m} and u_{1m} to the m-th code combination of K elements length, where $m=\overline{1,M}$ and M is the number of these code words. For the i-th signal period, at the CUs outputs we get

$$u_{0im}=\sum_{k=0}^{K-1} a_{mk} y_{0(i-kN)}, \quad u_{1im}=\sum_{k=0}^{K-1} a_{mk} y_{1(i-kN)},$$

where $a_{mk}=\pm 1$ is the elements of the m-th code word. By the transformation

$$z_{im}=\sqrt{u_{0im}^2+u_{1im}^2}.$$

the demodulator responses are generated for each enabled code combination, and by the largest of these responses a decision on the received code combination S_I is made by the maximum choice device (MCD).

To estimate the possibilities of designing the specified demodulators, FPGAs of various modifications have been considered produced by Xilinx (Xilinx DS160 Spartan-6 family overview 2011; 7 Series FPGAs data sheet: Overview 2018) and Altera (Parab J.S., Gad R.S. and Naik G.M. 2018). The selection criteria are the required hardware resources and the cost.

The results of the FPGA resource estimation for implementing the digital binary DPSK signal demodulator (Fig. 3a) are shown in Table 1, for the case when the ADC width is 8 bits and N=128. As we can see, a relatively simple demodulation algorithm does not require significant computational power.

In order to implement the demodulator of the signals phase-shift keyed in toto and coded by Walsh sequences (Chernoyarov, Litvinenko, Glushkov, Matveev and Salnikova 2017), FPGAs are used produced by the Xilinx, such as XilinxXC6SL25 (Spartan-6), XC7K70T (Kintex-7), XC7A100T (Artix-7). As an example, for each FPGA, an HDL code has been synthesized and implemented with the fixed parameters: the Walsh code sequence length is M = 4, the number of carrier periods is N = 64, the ADC bus width is R = 12. It is established that for the FPGA XC6SL25 the maximum possible carrier signal frequency is 144 MHz, while for the XC7A100T it is 118 MHz and for the XC7K70T – 154 MHz. The power consumption at the signal frequency of 50 MHz lies within the range from 40 to 90 mW. In Table 2, the results are presented of a quantitative estimation (as percentage of the total) of the required hardware FPGA resources.

In Table 3, the similar results are shown produced while implementing the demodulator of the two signals phase shift keyed in toto and coded by M-sequences of K elements length.

As it can be seen, there can be successfully implemented FPGA-based demodulators of the signals with the different digital modulation formats in toto.

Table 1: The estimation of the hardware overhead (per cent) of FPGAs produced by Xilinx for implementing the digital binary DPSK signal demodulator

Elements	Spartan 6	Virtex 5	Kintex 7
Flip Flops	5	<1%	<1%
LUTs	35	2%	<1%
Slices	50	3%	<1%
DSP	25	6%	<1%

Table 2: The estimation of the hardware overhead (per cent) of FPGAs produced by Xilinx for implementing the digital demodulator of the signals phase-shift keyed in toto and coded by Walsh sequences

FPGA	Elements		
	XC6SL25	XC7K70T	XC7A100T
Slice Registers	2.55	0.93	0.6
SliceLUTs	14.26	7.05	4.56
DSP	21.05	3.33	3.33

Table 3: The estimation of the hardware overhead (per cent) of FPGAs produced by Xilinx for implementing the digital demodulator of the signals phase-shift keyed in toto and coded by *M*-sequences

FPGA	Elements			
	K	XC6SL25	XC7K70T	XC7A100T
Slice Regis-ters	15	4.5	1.8	1
	31	6.6	2.5	1.6
	63	12.8	4.4	2.7
Slice LUTs	15	23	8	6
	31	39	13	9
	63	68	26	17

The possibilities of implementing the four-position QAM signal demodulator are considered in relation to Cyclone FPGAs produced by Altera. The results of the hardware cost analysis are shown in Table 4.

Table 4: The estimation of the hardware overhead (per cent) of FPGAs produced by Altera for implementing the digital QAM signal demodulator

FPGA	Elements		
	Cyclone IV E EP4CE22F17 C6	Cyclone V 5CSEBA6 U23I7DK	Cyclone 10 LP 10CL120YF780 C8G
Slice Registers	867/22320 (3.88%)	763/41910 (1.82%)	763/86800 (1.06%)
Slice LUTs	5274/12064 (43.26%)	2891/22000 (13.14%)	2891/42400 (6.81%)
DSP	4/16 (25%)	8/120 (6.66%)	8/260 (30.07%)

3. CONCLUSION

From the analysis of the obtained results, one can conclude that even relatively inexpensive modern FPGAs allow us to implement various devices for demodulating the digital keyed signals while providing rather acceptable, if not promising, technical features. Unused FPGA resources can be applied to solving other technical tasks by the same equipment.

ACKNOWLEDGMENTS

This research was financially supported by the Russian Science Foundation (research project No. 17-11-01049).

REFERENCES

Feher K., 1995. Wireless Digital Communications. Modulation and Spread Spectrum Applications. New Jersey: Prentice-Hall.

Sklar B., 2001. Digital communications: fundamentals and applications. New Jersey: Prentice-Hall.

Proakis J. and Salehi M., 2007. Digital communications. New York: McGraw-Hill.

Chernoyarov O.V., Glushkov A.N., Litvinenko V.P., Litvinenko Yu.V. and Matveev B.V., 2018. Digital demodulator of the quadrature amplitude modulation signals. Measurement Science Review, 18 (6), 236-242.

Glushkov A.N., Litvinenko V.P., Matveev B.V., Chenoyarov O.V. and Kalashnikov K.S., 2016. Hardware implementation of radio signals fast digital detection and demodulation algorithms. Proceedings of the 2016 International Conference on Communications, Information Management and Network Security (CIMNS2016), pp. 303-306, September 25-26, Shanghai (China).

Chernoyarov O.V., Litvinenko V.P., Glushkov A.N., Matveev B.V. and Salnikova A.V., 2017. Digital demodulation of the signals phase-shift keyed in toto and coded by Walsh sequences. Proceedings of IEEE International Conference on Power, Control, Signals & Instrumentation Engineering (ICPCSI), pp. 1-5. September 21-22, Chennai (India).

Glushkov A.N., Litvinenko V.P., Matveev B.V., Chernoyarov O.V. and Salnikova A.V., 2015. Basic algorithm for the coherent digital processing of the radio signals. Proceeding of the 2015 International Conference on Space Science & Communication (IconSpace), pp. 389-392. August 10-12, Langkawi (Malaysia).

Chernoyarov O.V., Glushkov A.N., Litvinenko V.P., Litvinenko Yu.V. and Matveev B.V., 2017. Fast digital algorithms for the coherent demodulation of the phase-shift keyed signals. Proceedings of 2017 IEEE Dynamics of Systems, Mechanisms and Machines (Dynamics), pp. 12-16. November 14-16, Omsk (Russia).

Chernoyarov O.V., Glushkov A.N., Litvinenko V.P., Litvinenko Yu.V. and Matveev B.V., 2018. Fast digital algorithms for the non-coherent demodulation of the differential phase-shift keyed binary signals. International Review of Electrical Engineering, 13 (4), 334-341.

Andina J.J.R., de la Torre Arnanz E. and Valdes M.D., 2017. FPGAs: Fundamentals, advanced features, and applications in industrial electronics. 1st ed. Boca Raton: CRC Press.

Xilinx DS160 Spartan-6 family overview, 2011. San Jose: Xilinx Inc.

7 Series FPGAs data sheet: Overview, 2018. San Jose: Xilinx Inc.

Parab J.S., Gad R.S. and Naik G.M., 2018. Hands-on experience with Altera FPGA development boards. Delhi: Springer India.

AUTHORS BIOGRAPHY

Oleg V. Chernoyarov was born in 1973. He received his M.Sc. and Ph.D. degrees in radio physics from the Voronezh State University, Voronezh, Russia, and the D.Sc. degree in radio physics – from the Moscow Pedagogical State University, Moscow, Russia, in 1996, 2000 and 2011, respectively. Presently, he is working as a Professor at the Department of Electronics and Nanoelectronics of the National Research University "Moscow Power Engineering Institute" as well as a Leading Research Worker of the National Research Tomsk State University (International Laboratory of Statistics of Stochastic Processes and Quantitative Finance) and the Maikop State Technological

University (Department of Higher Mathematics and System Analysis). His main interests are statistical methods for transmission and processing of information.

Alexey N. Glushkov was born in 1975. He received his Ph.D. in radio engineering from the Voronezh Institute of the Ministry of Internal Affairs of the Russian Federation in 2006. Alexey N. Glushkov is currently working as an Associate Professor at the Department of Infocommunication Systems and Technologies of the Voronezh Institute of the Ministry of Internal Affairs of the Russian Federation. His research interests include digital signal processing, as well as development, modeling and hardware implementation of the algorithms for the synchronization of the digital communication signals and their parameters estimation.

Vladimir P. Litvinenko was born in 1949. He received his Ph.D. in radio enginnering from the All-Union Extra-Mural Electrical Institute of Communications, Moscow, Russia, in 1979. Presently, Vladimir P. Litvinenko is working as an Associate Professor at the Department of Radio Engineering of the Voronezh State Technical University. His main interests are statistical radio physics and radio engineering, digital signal processing.

Alexander N. Faulgaber was born in 1993. He received the B.Sc. and the M.Sc. degrees from the National Research University "Moscow Power Engineering Institute" in 2014 and 2016, respectively, both in radio engineering. Presently, Alexander N. Faulgaber is a PhD student in the Department of Electronics and Nanoelectronics at the National Research University "Moscow Power Engineering Institute". His research interests include synthesis, analysis and simulation of the processing algorithms of stochastic processes and fields with unknown parameters.

Alexandra V. Salnikova was born in 1978, graduated in geological and hydrogeological engineering from the Voronezh State University in 2000. Presently, Alexandra V. Salnikova is working as an Assistant Professor at the Department of Management Systems and Information Technologies in Building of the Voronezh State Technical University as well as a Researcher of the National Research Tomsk State University (International Laboratory of Statistics of Stochastic Processes and Quantitative Finance) and the National Research University "Moscow Power Engineering Institute" (RD Department "Scientific Production Center "Design Engineering Bureau of Radio Engineering Devices and Systems"). Her research interests include synthesis, analysis and simulation of the detection and estimation algorithms of stochastic signals and fields with unknown parameters.

MODELING OF SERVICE CORRELATION FOR SERVICE COMPOSITION IN CLOUD MANUFACTURING

Fei Wang [(a)], Yuanjun Laili[(a)], Lin Zhang[(a)], Chi Xing[(b),(c),(d)], Liqin Guo[(b),(c)]

[(a)] School of Automation Science and Electrical Engineering, Beihang University
[(b)] Beijing Complex Product Advanced Manufacturing Engineering Research Center, Beijing Simulation Center
[(c)] State Key Laboratory of Intelligent Manufacturing System Technology, Beijing Institute of Electronic System Engineering
[(d)] Science and Technology on Space System Simulation Laboratory, Beijing Simulation Center

[(a)]wangfeitime@163.com, [(a)]llyj0721@sina.com, [(a)]johnlin9999@163.com, [(b),(c),(d)]xingchi09@163.com, [(b),(c)]guo_96@163.com

ABSTRACT
Cloud manufacturing (CMfg), integrating distributed manufacturing resources as services to cloud center, aims at intelligent, green, and economic customized manufacturing. The optimal composition of services to fulfill particular manufacturing requirement is a core issue to realize efficient cloud manufacturing. Many researchers have studied the problem considering the Quality-of-Service (QoS) of independent services. However, the correlation between services is rarely considered. In this paper, the importance of service correlation is emphasized. Two kinds of service correlation, service exclusion and service collaboration, are modeled for service composition. An improved algorithm DET, which combines Differential Evolution Algorithm (DE) with a Tabu table based on service exclusive and collaborative relationships, is designed to filter composable services and find better solutions for complex tasks. Experiments have shown the effects of service correlation on the quality of composed services and demonstrated the effectiveness of the proposed method DET compared with traditional DE.

Keywords: cloud manufacturing, service correlation, service composition, differential evolution, tabu table

1. INTRODUCTION

Cloud manufacturing (CMfg), as a service-oriented intelligent manufacturing paradigm (Bo-Hu et al. 2010, LinZhang et al. 2014), means to integrate distributed manufacturing resources to produce more complex and flexible products efficiently and economically. Various manufacturing resources and capacities are connected to the CMfg center by using Internet-of-Things (IoT) techniques and are employed flexibly with virtualized cloud computing resources. It offers unified and centralized management for CMfg services (Zhou et al. 2017). Customers are able to acquire on-demand manufacturing services on the Internet (Liu et al. 2018). CMfg services are usually fine-grained and loosely-coupled with simple functions. To accomplish complex manufacturing tasks, service composition is essential to implement more complicated functions. The composed service not only satisfies the functionality requirements of customers, but also ensures good quality, economical price, and efficient process for hybrid manufacturing (Bouzary and Frank Chen 2018). Many services that have same functionality but different Quality-of-Service (QoS) are published by different providers (Cremene et al. 2016). Thus, research on service composition is carried out to find an optimal solution with the best overall QoS (Liu and Zhang 2017, Zhou and Yao 2017, Fazeli, Farjami, and Nickray 2019, Lartigau et al. 2015). Most researches only consider the situation that the services are independent with each other, while the correlation between services is often ignored. Services can be composed arbitrarily as long as they have the required functions (Feng et al. 2017). But in practice, the correlation between different services influences the QoS of services and determines whether these services can be composed in the same solution. Guo et al. investigated three kinds of correlations in services composition including composable relation, business entity relation, statistical relation (Guo et al. 2010). Tao et al. presented a QoS description mode supporting resource service correlation (Tao et al. 2010). Xu et al. considered correlation as one of the main service domain features. But correlation isn't involved in the process of service composition and wasn't analyzed adequately to improve the composition results (Xu et al. 2017).

In this paper, two kinds of service correlation, service exclusion and service collaboration are analyzed. Their models and descriptions are established. In addition, an improved Differential Evolution Algorithm, termed DET, is designed to deal with the correlation between services. DET adopts Tabu table to avoid the coexistence of excusive services in the same the composition solution. Besides, the influence of collaborative services in one solution is calculated in DET to search for optimal solution with the better overall QoS. Finally, the experiment shows the effect of service exclusion and collaboration. The effectiveness of DET is demonstrated.

This paper is organized as follows. Section 2 describes the motivating example of two kinds of service correlation. The model of service correlation and correlation-aware service composition is given in Section 3. Section 4 provides the details of DET to process correlations in service composition. Section 5 reports the effects of two kinds of correlation and the effectiveness of the proposed method by experiments. Section 6 concludes this work.

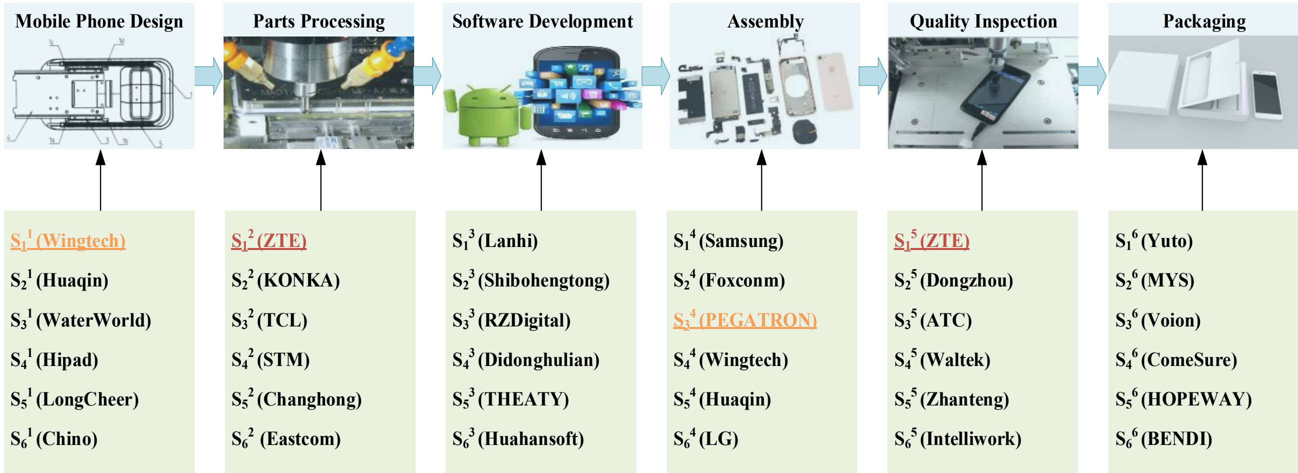

Figure 1: The Example of Mobile Phone Manufacturing

2. MOTIVATING EXAMPLE

Before introducing the main content, an example of mobile phone manufacturing is shown in Figure 1. It contains six subtasks, i.e. design, parts processing, software development, assembly, quality inspection and packaging. Each subtask is accomplished by a service. There are a set of candidate services available for handling each subtask. In Figure 1, the boxes below the corresponding subtasks show their candidate service sets. To finish the task of producing a batch of mobile phones, a group of services are to perform the subtasks. Usually, a good solution of service composition has better individual candidates with better QoS in terms of service cost, time and reliability. But the selection of services for all subtasks are not always independent.

For example, for the mobile phone manufacturing task in Figure 1, a candidate service of parts processing subtask S_1^2 and candidate service of quality inspection subtask S_1^5 are both provided by ZTE. To promote services ZTE, the costs of S_1^2 and S_1^5 are discounted by 10% if both of them are selected for a manufacturing task simultaneously.

On the contrary, if S_1^1 is selected to perform the design subtask, the service for assembly subtask can't be S_3^4. Because the craft of S_1^1 Wingtech is conflict with which of S_3^4 PEGATOR, Wingtech refuses to cooperate with PEGATOR.

These two examples demonstrate two types of correlations. In this paper, the correlation in the first situation is defined as service collaboration, which influences the QoS values of services. The second correlation is called service exclusion, that is, the service selection of one subtask determines whether some services can be selected for another subtask. Both kinds of correlation are modeled in Section 3.2 in detail.

3. A CORRELATION-AWARE SERVICE CORRELATION MODEL

In this section, the basic model of service composition is outlined firstly. Then the influences of two kinds of service correlation are analyzed. The models of the two kinds of service correlations and their effects on service composition are provided. Afterwards, a correlation-aware service composition model is introduced in the next two subsections.

3.1. Basic Service Composition Model

The aim of service composition is to obtain the optimal composition solution with the best non-functionality performance to guarantee high-efficient manufacturing (Bo and Fan 2007). The QoS attributes of a CMfg service, involving time, cost, reliability, and maintainability, measure its non-functional performance quantitatively from different aspects (Fei et al. 2009). Their definitions are as follows:

- Time: The duration of a service for executing a given task.
- Cost: The price that a customer should pay for renting a particular service in a period of time.
- Reliability: The probability that a manufacturing service can execute correctly in a certain time.
- Maintainability: The ease with which a manufacturing service can be maintained in order to recover from failure or to upgrade from current state.
- Trust: The credit of a service in dealing with a particular kind of task

Proceedings of the European Modeling and Simulation Symposium, 2019
ISBN 978-88-85741-25-6; Affenzeller, Bruzzone, Longo and Pereira Eds.

Among the above QoS attributes, time and cost are called negative QoS, whose smaller values indicate better performance. Meanwhile, reliability, maintainability and trust are positive QoS, which means larger values are more desirable.

The notations used in correlation-aware service composition model are listed in Table 1.

Table 1: Notations

Notation	Meaning
T_i	The *i*th subtask of MT
M	The number of subtasks of MT
CSS_i	The candidate service set of T_i
S_j^i	The *j*th service in CSS_i
N_i	The number of services in CSS_i
CS	The composite service composed by *m* candidate services of *m* subtasks from CSS_1, CSS_2,⋯, CSS_m respectively
$T(S_j^i)$	The time value of S_j^i
$C(S_j^i)$	The cost value of S_j^i
$R(S_j^i)$	The reliability value of S_j^i
$M(S_j^i)$	The maintainability value of S_j^i
$Tr(S_j^i)$	The trust value of S_j^i
$TT(CS)$	The overall time value of *CS*
$TC(CS)$	The overall cost value of *CS*
$TR(CS)$	The overall reliability value of *CS*
$TM(CS)$	The overall maintainability value of *CS*
$TTr(CS)$	The overall trust value of *CS*
$SC(S_j^i)$	The exclusive service set of S_j^i
$QC(S_j^i)$	The collaborative service set of S_j^i

The description of CMfg service is the basis of service composition. The basic description of a CMfg service includes its functionality, the provider and the values of all QoS attributes.

$B(S_j^i)$={*Functionality*, *Provider*, *Td*, *Cd*, *Rd*, *Md*, *Trd*}

where $B(S_j^i)$ denotes the basic description of S_j^i. *Td*, *Cd*, *Rd*, *Md* and *Trd* are the default values of the QoS attributes without considering service collaboration. An example is shown as follows:

Basic description of S_1^2:
Functionality: Mobile phone parts processing
Provider: ZTE

Td: 15 Hours
Cd: 100 USD
Rd: 0.92
Md: 0.89
Trd: 0.95

Given a manufacturing task containing *n* subtasks, the CMfg platform provides *n* sets of candidate services that match the functionality requirements of *n* subtasks respectively. Service composition is to select a service from the candidate service set for each subtask to form a composite solution with optimal overall QoS. For a manufacturing task whose subtasks are executed sequentially, a composite service *CS* is composed by m services $\{S_j^1, S_j^2, \ldots, S_j^m\}$. The calculation formula of the overall QoS values of *CS* are as follows:

$$TT(CS) = \sum\nolimits_{i=1}^{m} T(S_j^i) \quad (1)$$

$$TC(CS) = \sum\nolimits_{i=1}^{m} C(S_j^i) \quad (2)$$

$$TR(CS) = \sum\nolimits_{i=1}^{m} R(S_j^i) \quad (3)$$

$$TM(CS) = \sum\nolimits_{i=1}^{m} M(S_j^i) \quad (4)$$

$$TTr(CS) = \sum\nolimits_{i=1}^{m} Tr(S_j^i) \quad (5)$$

The comprehensive utility of a composite service is evaluated by the weighted sum of the above overall QoS values. The QoS values are normalized to real numbers between 0 and 1.

$$\begin{aligned} f(CS) = {} & \omega_1 \bullet \frac{TT(CS) - TT_{\min}}{TT_{\max} - TT_{\min}} + \omega_2 \bullet \frac{TC(CS) - TC_{\min}}{TC_{\max} - TC_{\min}} \\ & + \omega_3 \bullet \frac{TR_{\max} - TR(CS)}{TR_{\max} - TR_{\min}} + \omega_4 \bullet \frac{TM_{\max} - TM(CS)}{TM_{\max} - TM_{\min}} \\ & + \omega_5 \bullet \frac{TTr_{\max} - TTr(CS)}{TTr_{\max} - TTr_{\min}} \end{aligned} \quad (6)$$

where *f*(CS) represents the comprehensive utility of the composite solution *CS* and $\omega_i (i = 1,2, \ldots, 5)$ is the weight of QoS values that satisfies $\sum_{i=1}^{5} \omega_i = 1$. The main objective of service composition is minimizing *f*(*CS*).

3.2. Service Correlation Model

In this paper, two kinds of service correlations, service exclusion and service collaboration, are modelled.

3.2.1. Service Exclusion

The exclusion set of a service S_j^i specifies services that are unable to be composed with S_j^i in the same service composition solution. The exclusion set of S_j^i is expressed as follows:

$$SC\left(S_1^1\right) = \{S_1, S_2, \cdots, S_k\} \quad (7)$$

where $SC(S_j^i)$ is the set of exclusive services of S_j^i and *k* is the number of them.

Taking the second situation of Section 2, the service exclusion description of S_1^1 is shown below:

Service exclusion description of S_1^1:
$SC(S_1^1)$={ S_5^2, S_6^2,S_3^4, S_3^5}

If S_5^2 cooperates with S_1^1 in the same composition solution, their exclusion makes this solution infeasible. Thus, considering service exclusion, candidate services of different subtasks can't compose with other services arbitrarily in case of conflict with their exclusive services.

The selected service of one subtask may constrain the service selection for other subtasks. Service exclusion becomes a constraint for service composition.

3.2.2. Service Collaboration

Service collaboration indicates how other services influence the QoS values of a certain service in the case that they are composed in the same composition solution. Correlation coefficient in the form of percentage is defined to measure the degree of service collaboration. The service collaboration of S_j^i is expressed as follows.

$$QC\left(S_j^{\,i}\right)=\left\{\left(S_1,q_1,c_1\right),\left(S_2,q_2,c_2\right),\cdots,\left(S_k,q_k,c_k\right)\right\} \quad (8)$$

where $QC(S_j^i)$ is the set of tuples that consist of quality correlated service S_i, the influenced QoS attribute q_k and its correlation coefficient c_i. The correlation coefficient c_i could be a positive number or a negative number, which depends on whether the influence is beneficial or not. If S_j^i and S_k are composed in one solution, the actual QoS value of S_j^i is calculated as follows.

$$qa_k\left(S_j^{\,i}\right)=qd_k\left(S_j^{\,i}\right)\bullet\left(1-c_k\right) \quad (9)$$

where $qa_k(S_j^i)$ and $qd_k(S_j^i)$ are the actual and default values of the QoS attribute q_k of S_j^i.
In the first situation of Section 2, the service collaboration description of S_1^2 is shown as follows:

Service collaboration description of S_1^2:
$QC(S_1^2)$={(S_1^5,T,10%)}

According to the service collaboration description and basic description of S_1^2, when S_1^2 and S_1^5 are composed in the same composition solution, the actual cost of S_1^2 $Ca(S_1^2)$ is calculated as follows:

$$Ca(S_1^2)=Cd(S_1^2)\bullet\left(1-c\right)=100\bullet\left(1-10\%\right)=90USD \quad (10)$$

The basic description, service exclusion description and service collaboration description constitute the description of one service together and form the basis of correlation-aware service composition.

4. THE IMPROVED DIFFERENTIAL EVOLUTION ALGORITHM FOR CORRELATION-AWARE SERVICE COMPOSITION

After modeling two kinds of correlation, the method based on Differential Evolution Algorithm (DE) is proposed to solve correlation-aware service composition problem. As a stochastic real-parameter optimization algorithms, DE has been used in QoS-aware service composition problem to implement global optimization (Pop et al. 2011). The proposed method focuses on how to manage service exclusion and service collaboration in the process of service composition.
Considering service correlation, exclusion conflict between services in one solution makes this solution infeasible. Thus correlation-aware service composition is a constrained optimization problem. In this paper, an improved algorithm DET is designed to ensure the feasibility of the obtained solutions. A Tabu table tailored for service exclusion to store the exclusive services, which avoids the exclusion conflict between services in one solution for correlation-aware service composition problem. The Tabu table is maintained according to the service exclusion description of services to filter the composable services.

4.1. Genotype Encoding

In DE of this paper, a genome X_i = (S_{i1}, S_{i2},…, S_{iM}) represents a composition solution that contains the selected services of all subtasks. It is encoded as an array of real number as is shown in Figure 2. The length of the genome array M is the number of subtasks in service composition. S_{ij} in the array refers to the selected service of the subtask T_j. S_k^j is the kth candidate service of T_i. N_i is the number of candidate services of subtask T_i.
The value of S_{ij} is a real number between 0 and 1. It represents the corresponding candidate service S_k^j according to Equation 11.

$$k=\left\lfloor S_{ij}\bullet N_i\right\rfloor \quad (11)$$

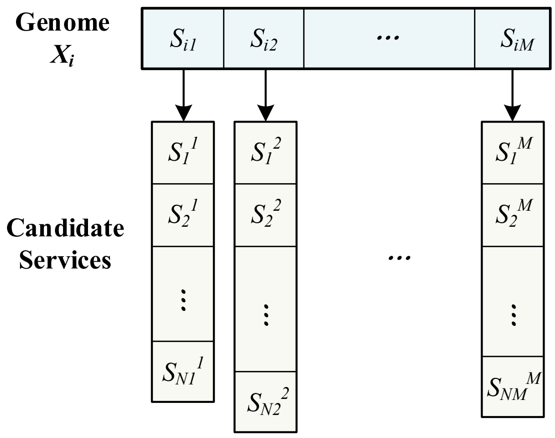

Figure 2: Encoding of Genome

4.2. Main Loop of the Proposed Method

The main loop of DE for correlation-aware service composition is presented in Algorithm 1.

Algorithm 1 Main loop of DE for correlation-aware service composition

Input: Population P, population size L, maximum number of generations $Gmax$
Output: The best solution ind_best

```
initialize population P by selecting n solutions from
  candidate service sets at random
g ← 0
while g ≤ Gmax do
    P′ = Mutation(P)
    P″ = Crossover(P′)
    Fitness Assignment (P″)
    P = P″
    g ← g+1
end while
```

The following introduces the detail of mutation, crossover and selection operators.

4.3. Mutation Operator

Firstly, we use $X_{bg} = (S_{g1}, S_{g2}, \ldots, S_{gM})$ to store the global best solution of all individuals in P during the iteration. And an array $X_{bi} = (S_{bi1}, S_{bi2}, \ldots, S_{biM})$ with the length of L to record the best solution of ith individual in P. In each generation, five individuals (i=1, 2, …, 5) are randomly chosen to conduct mutation operation. $X_w = (S_{w1}, S_{w2}, \ldots, S_{wM})$ is the newly generated genome after mutation. There are 3 kinds of mutation strategies for choice.

$$S_{wj} = S_{gj} + F \bullet \left(S_{1j} - S_{2j} \right) \tag{12}$$

$$S_{wj} = S_{b1j} + F \bullet \left(S_{b2j} - S_{b3j} \right) \tag{13}$$

$$S_{wj} = S_{b1j} + F \bullet \left(S_{b2j} - S_{b3j} \right) + F \bullet \left(S_{b4j} - S_{b5j} \right) \tag{14}$$

Where F is the scaling factor. The first mutation strategy has the priority to be chosen. The mutation of genome bits is executed in sequence. Once S_{w1} is calculated, its exclusive services are recorded in the Tabu table of this solution. Then S_{w2} is calculated according to the first strategy. To avoid exclusion conflict, two conditions need to be checked:

- S_{w2} doesn't exist in the Tabu table;
- S_{w1} isn't in the exclusive service set of S_{w2}.

If these two conditions are satisfied, S_{w2} is accepted and the services that are exclusive with S_{w2} are added into the Tabu table. Otherwise, there is exclusion conflict between S_{w1} and S_{w2}. S_{w2} needs to be recalculated according to the second mutation strategy. If it's still infeasible, the third mutation strategy is adopted. If there is still correlation conflict, S_{w2} is set to a random number whose corresponding service satisfy the above two conditions.

Once a genome bit S_{wj} is generated by a mutation strategy, it is checked whether it is included in the Tabu table and whether the previous services, that is, S_{w1}, S_{w2},a…, $S_{w(j-1)}$ are in the exclusive service set of S_{wj}. If S_{wj} doesn't satisfy these two conditions, it is recalculated by another mutation strategy, until S_{wj} doesn't have conflict with the previous services.

4.4. Crossover Operator

Crossover operator generates the new population based on the results of mutation operator. For the jth gene S_j(t+1) of the individual in (t+1) generation, randomly generate a number r between 0 and 1. If r is less that the probability p_c for X_w, the prior service is S_{w1}. Otherwise, the prior service is S_j(t). Firstly, check whether the prior service satisfies the above two conditions. If so, the prior service is selected. If not, check another alternative and repeat the above steps. If it's also unsatisfying, generate a random service S_r that meet these two conditions.

4.5. Fitness Assignment

The exclusion conflict has been avoided in the mutation and crossover operator by Tabu table. Thus, the obtained individuals are feasible. Firstly, the service collaboration between services in one solution is checked. If there is service collaboration, the actual QoS values of services in the solution are calculated according to Equation 9. Then the actual QoS values is put into Equation 6 to calculate the fitness value of the solution, which is the weighted sum of the normalized QoS values of all services in an individual.

5. EXPERIMENTS

To evaluate the effectiveness of the method proposed in this paper, we carry out two sets of experiments. The first set of experiments verifies the effect of service exclusion. The second set of experiments evaluates the influence of service collaboration and proves the feasibility and effectiveness of the proposed algorithm DET. Simulation experiments are conducted on a PC with Intel Core i7 CPU 3.6 GHz, 8 GB RAM, Windows 10, Microsoft Visual Studio V12.0.

As is shown in the motivating example of Figure 1, the manufacturing task can be decomposed to several subtasks. For every subtask, there are many candidate services that are matched by their functionality. In the two sets of experiments of this paper, the manufacturing task is set with 10 subtasks and 100 candidate services for each subtask. The population size is 20. Their QoS values are random numbers. Their ranges are listed in Table 1.

Table 1: The Ranges of QoS Attributes

QoS Attributes	Ranges of Random Values
Time/Hour	60.0-80.0
Cost/(100USD)	70.0-100.0
Reliability	80.0%-99.9%
Maintainability	80.0%-99.9%
Trust	80.0%-99.9%

The weights of five attributes in Equation 6 are 0.2. The maximum iteration generation of the algorithm is 30000.

5.1. The effect of Service Exclusion

Service exclusion makes some solutions infeasible. To reveal the effect of service exclusion, the ratio of infeasible solutions of each generation is calculated during the iteration of DE without Tabu table. In each generation, the number of infeasible solutions in the population is calculated, which shows the effect of service exclusion. In the first experiment, the number of exclusive services of each candidate service varies from 10 to 200. The exclusive services are randomly chosen from the candidate services of other subtasks. The number of infeasible solutions in every generation is observed. The average ratios of infeasible solutions in 30000 generations are shown in Figure 3. It can be seen that the ratio of infeasible solutions grows remarkably with the increase of exclusive services.

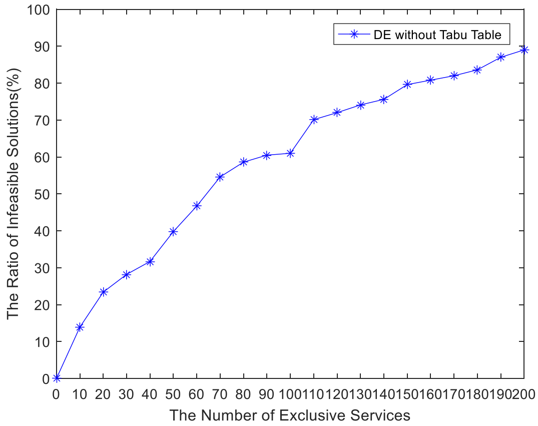

Figure 3: Ratio of Infeasible Solutions w.r.t. Number of Exclusive Services of Each Candidate Service

Figure 3 shows that when the number of exclusive services of each candidate service reach 200, 89% of the solutions on average are infeasible. The above result demonstrates that service exclusion can't be ignored in service composition because not a few solutions are infeasible for this reason. Thus, DE with Tabu table is designed and realized to avoid exclusive services in one solution. The experiment result of DE with Tabu table shows that all solutions in the population of are feasible, which proves the effectiveness of the improved DE for solving service exclusion in correlation-aware service composition.

5.2. The Effect of Service Collaboration

Service Collaboration benefits the QoS performance of collaborative services in the same solution. In the second experiment, the number of collaborative services of each candidate service varies from 0 to 90. The correlation coefficient ranges from 1% to 15%. Meanwhile, the optimal results of DET and DE are recorded and compared. The number of exclusive services of each candidate service is 10. The infeasible solutions of DE are excluded. The results are shown in Figure 4.

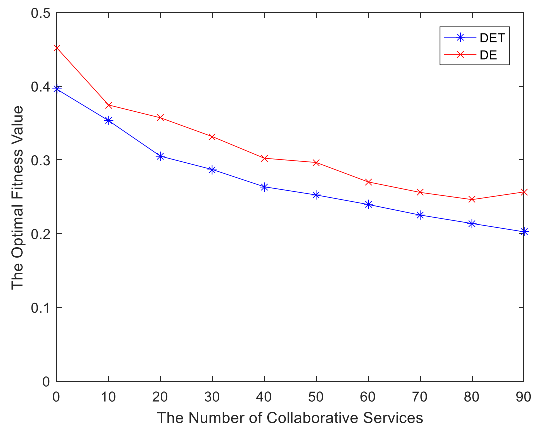

Figure 4: Optimal Fitness Value w.r.t. Number of Collaborative Services of Each Candidate Service

It can be seen from Figure 4 that the optimal fitness value obtained by DET decreases from 0.396 to 0.202 while the number of collaborative services increase to 90. For both DET and DE, the more collaborative services are, the smaller the obtained optimal fitness value is. Because more collaborative services make more solutions whose services are collaborative with each other. Meanwhile, because DET has the ability to tackle service exclusion, the proposed algorithm DET outperforms DE to search solution with optimal overall QoS considering service correlation.

6. CONCLUSION

In this study, service correlation is analyzed, and two kinds of service correlation model are built. An improved Differential Evolution Algorithm is proposed for correlation-aware service composition. The main contributions of this study are as follows.

- The model of two kinds of service correlation describes their effect on service composition, which is the basis of correlation-aware service composition.
- The proposed algorithm DET is employed to handle the above two kinds of service correlation and obtain composition solution with optimal overall QoS.

In future research, more kinds of service correlation will be investigated considering the complex relationship among services in cloud manufacturing. Besides, the method to deal with correlation-aware service composition for CMfg tasks with complex structures will be researched.

ACKNOWLEDGMENTS

The research in this paper was supported by grants 61873014 from the National Natural Science Foundation of China.

REFERENCES

Bo-Hu, L. I., Lin Zhang, Shi Long Wang, Fei Tao, Jun Wei Cao, Xiao Dan Jiang, Xiao Song, and Xu Dong Chai, 2010. Cloud manufacturing:a new service-oriented networked manufacturing model. Computer Integrated Manufacturing Systems, 16 (01), 1-7+16.

Bo, Liu, and Yushun Fan. 2007. "Research on Service-Oriented Workflow and Performance Evaluation." IEEE International Conference on Web Services.

Bouzary, Hamed, and F. Frank Chen, 2018. Service optimal selection and composition in cloud manufacturing: a comprehensive survey. The International Journal of Advanced Manufacturing Technology, 97 (1), 795-808.

Cremene, Marcel, Mihai Suciu, Denis Pallez, and D. Dumitrescu, 2016. Comparative analysis of multi-objective evolutionary algorithms for QoS-aware web service composition. Applied Soft Computing, 39 (C), 124-139.

Fazeli, Mohammad Moein, Yaghoub Farjami, and Mohsen Nickray, 2019. An ensemble optimisation approach to service composition in cloud manufacturing. International Journal of Computer Integrated Manufacturing, 32 (1), 83-91.

Fei, Tao, Yefa Hu, Dongming Zhao, Zude Zhou, Haijun Zhang, and Zhenzhen Lei, 2009. Study on manufacturing grid resource service QoS modeling and evaluation. International Journal of Advanced Manufacturing Technology, 41 (9-10), 1034-1042.

Feng, Li, Zhang Lin, Yongkui Liu, Yuanjun Laili, and Tao Fei, 2017. A clustering network-based approach to service composition in cloud manufacturing. International Journal of Computer Integrated Manufacturing, 30 (3), 1-12.

Guo, Hua, Fei Tao, Lin Zhang, Suiyi Su, and Nan Si, 2010. Correlation-aware web services composition and QoS computation model in virtual enterprise. The International Journal of Advanced Manufacturing Technology, 51 (5-8), 817-827.

Lartigau, Jorick, Xiaofei Xu, Lanshun Nie, and Dechen Zhan, 2015. Cloud manufacturing service composition based on QoS with geo-perspective transportation using an improved Artificial Bee Colony optimisation algorithm. International Journal of Production Research, 53 (14), 4380-4404.

LinZhang, YongliangLuo, FeiTao, Hu Li Bo, LeiRen, XuesongZhang, HuaGuo, YingCheng, AnruiHu, and YongkuiLiu, 2014. Cloud manufacturing: a new manufacturing paradigm. Enterprise Information Systems, 8 (2), 167-187.

Liu, Bo, and Zili Zhang, 2017. QoS-aware service composition for cloud manufacturing based on the optimal construction of synergistic elementary service groups. The International Journal of Advanced Manufacturing Technology, 88 (9), 2757-2771.

Liu, Yongkui, Lihui Wang, Xi Vincent Wang, Xun Xu, and Lin Zhang, 2018. Scheduling in cloud manufacturing: state-of-the-art and research challenges. International Journal of Production Research, 1-26.

Pop, Florin Claudiu, Denis Pallez, Marcel Cremene, Andrea Tettamanzi, Mihai Suciu, and Mircea Florin Vaida. 2011. "QoS-based service optimization using differential evolution." Conference on Genetic & Evolutionary Computation.

Tao, Fei, Dongming Zhao, Hu Yefa, and Zude Zhou, 2010. Correlation-aware resource service composition and optimal-selection in manufacturing grid. European Journal of Operational Research, 201 (1), 129-143.

Xu, Xiaofei, Zhizhong Liu, Zhongjie Wang, Quan Z. Sheng, Jian Yu, and Xianzhi Wang, 2017. S-ABC: A paradigm of service domain-oriented artificial bee colony algorithms for service selection and composition. Future Generation Computer Systems, 68, 304-319.

Zhou, Jiajun, and Xifan Yao, 2017. A hybrid artificial bee colony algorithm for optimal selection of QoS-based cloud manufacturing service composition. The International Journal of Advanced Manufacturing Technology, 88 (9), 3371-3387.

Zhou, Longfei, Zhang Lin, Bhaba R. Sarker, Yuanjun Laili, and Ren Lei, 2017. An event-triggered dynamic scheduling method for randomly arriving tasks in cloud manufacturing. International Journal of Computer Integrated Manufacturing, 31 (3), 1-16.

ANALYSIS OF A UNIVERSITY PARKING LOT SYSTEM THROUGH THE USE OF DISCRETE-EVENT SIMULATION

Ricardo Torres[a] Jenaro Nosedal-Sanchez[b]

[a]Faculty of Engineering, UNAM, Ciudad Universitaria, Ciudad de México, México
[b] Cátedra Conacyt, Facultad de Ingeniería, Universidad Autónoma del Estado de México, Toluca, México

[a] ricardtm@unam.mx, [b]jnosedal@conacyt.mx

ABSTRACT

The management of parking lots in large cities has become one of the most complex problems to solve as this is influenced by many variables, additionally these spaces directly influence the level of service and productivity of many companies. This article proposes the use of the simulation of discrete events to analyze the impact of the changes in the access policies to a pair of parking lots in the Faculty of Engineering of the UNAM in Mexico City, some of the proposed indicators are: number of users not served by saturation (parking spaces not available) , maximum number of users looking for a parking space at the same time, average search time of a parking space in case of saturation and number of parking spaces occupied throughout the day.

Keywords: parking lot, access policies, discrete event simulation, key performance indicators.

1. INTRODUCTION

Parking facilities are usually exposed to long periods of saturation or occupation rates near the maximum along the day due to high demand, this is especially prevalent in busy cities (Barata, 2011). However, in parking facilities that belong to private buildings like universities, the saturation problem has more to do with demand unbalances during specific time frames (peak hours). This problem is directly related to the existence of different schedules of the facilities' users. While some of the users stay in the facilities for long periods, (8 hours or more for full-time staff), other users' activities require them to stay for shorter periods (less than 4 hours, for instance, part-time staff or even shorter for instructors). Furthermore, some users need to transit between different buildings on the campus, which sometimes requires using different parking facilities for convenience, which means the parking spots' occupation fluctuates throughout the day, even when the actual demand for the whole system is the same.

Parking facilities are difficult to manage due to demand fluctuation. Also, it is expensive and difficult to add capacity (Teodorović, 2016), the space in a facility such a university is often better used for other purposes rather than parking facilities. Moreover, increasing parking density (for instance using platforms) is difficult to justify and fund. Thus, parking spaces are a critical resource that requires the adoption of different usage policies to provide the best service possible to their users (Fontaine 2005).

The present research seeks to analyze the current management and performance of the parking facilities that belong to the Faculty of Engineering of UNAM in Mexico City. The parking facilities provide service to full-time professors, part-time teachers, and administrative Faculty Personnel, and has eight parking lots distributed around the Faculty's buildings. The scope of this research is to perform the analysis of two of the eight parking lots that the Faculty has, the ones with the highest and lowest demand. The aiming is to provide an assessment and performance comparison of the current and previous operation of the parking lots, with the ultimate objective of increase the effective utilization of the parking lots and improve the service provided.

2. PROBLEM DESCRIPTION

Currently, there are 594 parking spaces distributed in eight parking lots, during 2018, 1,731 users were served (part-time professors, full-time professors, academic technicians, and administrative staff). Based on empirical observations, the existence of saturation periods had been detected in specific parking lots. These events suggest the existence of demand imbalances that cause some parking lots to become quickly saturated, and others to have low utilization during the same time windows. It is worthy to mention that currently the service is provided free of charge for all the authorized users, so there is no opportunity to modify the demand using push factors like pricing, the approach described in (Sweet, 2019) and also discussed in (Yan, 2019).

This research focuses on the simulation and analysis of two specific parking lots: "South 3" which has the highest demand of all "South" parking lots, and "South 4" which has the lowest demand for the "South" parking lots. These parking lots are located next to each other, as depicted in Figure 1.

Figure 2 shows the demand evolution in terms of the total number of services or events recorded in 2015, 2016 and 2017 for each of the two facilities under analysis. It can be observed that annual demand increases for parking lot "South 3, it can be observed an increase of 5.48% between 2015 and 2017. As for the parking lot "South 4", a percentage demand decrease of 44.35% between 2015 and 2017 is observed.

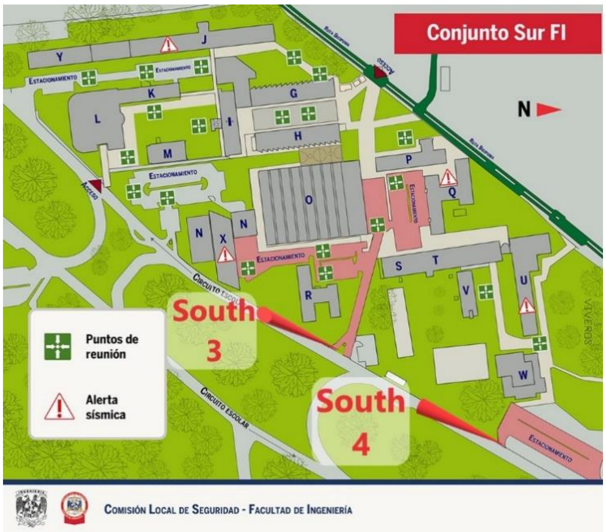

Figure 1: Parking lot locations map. Obtained from the UNAM Faculty of Engineering's Local Safety Commission at http://www.administracion.ingenieria.unam.mx/webcls/paginas/pdf/puntos_reunion_cs.png (April 2019)

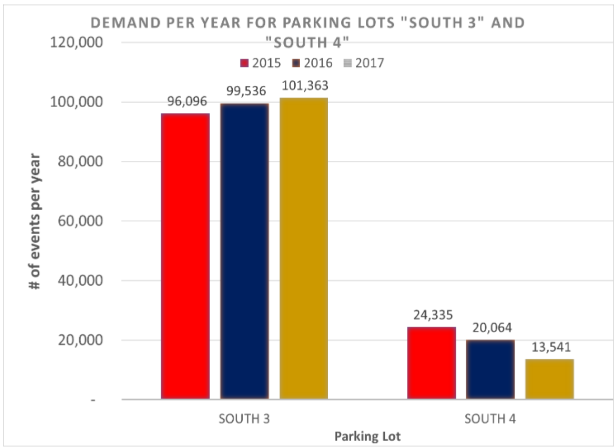

Figure 2: Demand per year for parking lots "South 3" and "South 4", during the years 2015, 2016, and 2017

3. METHODOLOGY

To be able to simulate and analyze the behavior of both parking lots in time, aiming to establish a diagnosis of the periods in which the parking lots are saturated and the magnitude of the capacity shortages, the parking lots will be modeled using a Discrete Event Simulation approach.

This approach allows to analyze the behavior of the system over a period of time, as well as to register the interdependencies between the elements of the system (entrance of the parking lot, spaces of parking and exit of the parking lot), as well as the inherent variability to the types of users that they use parking lot (time spent in the parking lot).
The deployed methodology can be summarized by the following five steps:

1. Process understanding and description,
2. Definition of expected outputs to analyze,
3. Implementation of the process using a discrete event simulation framework (FlexSim 2018),
4. Execution of several experiments to analyze the current operation vs the previous operation on the process, and
5. Discussion of the results considering the performance of the system (service level and utilization rate for the parking facilities).

3.1. Parking lot process and users

The process of parking in the Faculty of Engineering (in their eight parking lots) can be described by three events:

1. Access the parking lot.
2. Use of parking space.
3. Exit the parking lot.

This process is shown in Figure 3.

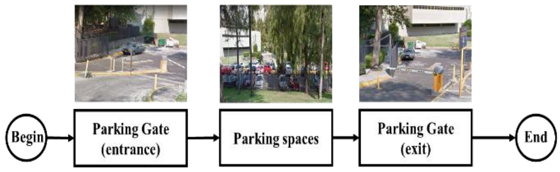

Figure 3: Parking Process in the Faculty of Engineering, UNAM, Mexico City

Both entrances (for South 3 and South 4 parking lots) are located on the same street called Exterior School Circuit, both have a parking gate (for entrance and exit) and independent and fixed capacity (number of parking spaces).
Parking gates (entrance and exit) works with a proximity sensor, for that purpose, one card with a sensor on it is provided to each authorized staff member. Then the cards must be used to have access and to exit the parking lot with a vehicle.
Parking spaces are not assigned to a specific staff member, then all users are entitled to select any of the available places. However, if there is not available space, once in the parking lot, the users can circulate through the parking lot until finding an available space or can drive to the exit gate to leave the parking lot without being served.
The parking lots South 3 and South 4 (and in general the eight parking lots of the Faculty of Engineering at UNAM) serve the following types of users:

- part-time teachers, these users are instructors who teach one or two subjects at the Faculty of Engineering.
- full-time professors, these users, are teaching or research fellows who have to carry out the following activities: teaching, service and research, among other activities, usually each has an assigned office, however they may need to perform some activities in different buildings managed by the Faculty of Engineering.
- academic technicians, these users deal and manage several activities, for instance: support in the management of laboratories, maintenance of equipment and facilities and in some cases teaching; they can be have an office assigned and also develop activities different buildings managed by the Faculty of Engineering.
- administrative staff, these users are responsible for the non-academic support activities of the Faculty of Engineering; they are assigned to offices and normally do not deploy activities in other buildings managed by the Faculty of Engineering.

Due to the imbalanced saturation observed at certain parking lots during specific day time frames, the administration of the parking lots elaborated some rules to restrict the use of the parking lots based on the types of users in July 2016.

These new rules took effect on the second term of the academic year 2016 (August to December 2016), before that, all users were allowed to use of the parking lots any time they needed, without any day or time restriction.

For the new rules, two types of users were identified, those that require access without time restriction (full time professors, academic technicians and administrative staff) and those that should have access to use the parking at specific times (part-time instructors).

Table 1 shows the two time windows established to restrict the use of the parking lots for part-time instructors, part time instructors assigned for morning sessions can use the parking lot from 3 a.m. to 5 p.m., and similarly, instructors assigned for afternoon sessions, can use the parking facilities from 1 p.m. to 12 a.m.

Table 1: Part Time Instructors' parking time windows

Time windows	
Morning	03:00 am to 05:00 pm
Afternoon	01:00 pm to 12:00 am

3.2. Input and output variables

The input variables for the system (parking lots) are the following:

- arrival times of the users to the parking lot,
- time spent by the users in the parking lot,
- service times at the entrances and exits of the parking lot.

The output variables, which in this case also correspond to Key Performance Indicators (KPIs), should help to measure whether the implemented rules had any impact on the saturation and service level of the parking lots, in this paper in specific for South 3 and South 4 parking lots.

One of the KPI's that it would be critical for the impact assessment of the rules implemented, is the parking utilization factor with respect to time, which helps us to see the number of parking places that are occupied (or empty) at throughout the day

Other relevant KPI, is the number of users who cannot find a space to park after crossing the entry gate and, if they are tolerant of waiting, the amount of time it would take to find a place, both measures directly connected with the service level provided.

In summary we have the following output variables:

- Number of users not served because of saturation (parking spaces not available) of the system over a day.
- Maximum number of users waiting for a parking space at the same time (equivalent to a queue after crossing the entrance gate).
- Average search (waiting) time to park in case of saturation.
- Number of parking spaces occupied throughout the day.

3.3. Simulation model

The simulation model is based on the process diagram shown in Figure 3, each of the steps shown in this figure was implemented in the model.

In the present section, the processes that require a greater level of detail are described, these are:

1. Entrance to the parking lot,
2. Search and use of a parking space,
3. Exit from the parking lot.

The process to enter the parking lot consists of the following activities:

- Users' arrival in his/her car to the parking lot.
- If the parking gate entrance is available, then the user taps his/her card to access the parking lot.
- If the parking gate entrance is not available, then the user waits until it is available.

- Once the user has tapped his/her card, he/she enters the parking lot.

The flow diagram for the process to enter the parking lots is provided in Figure 4. As we can see in the diagram, this process concludes with the beginning of the process of searching (waiting inside) and occupation of a parking space, which is denoted by the symbol I.

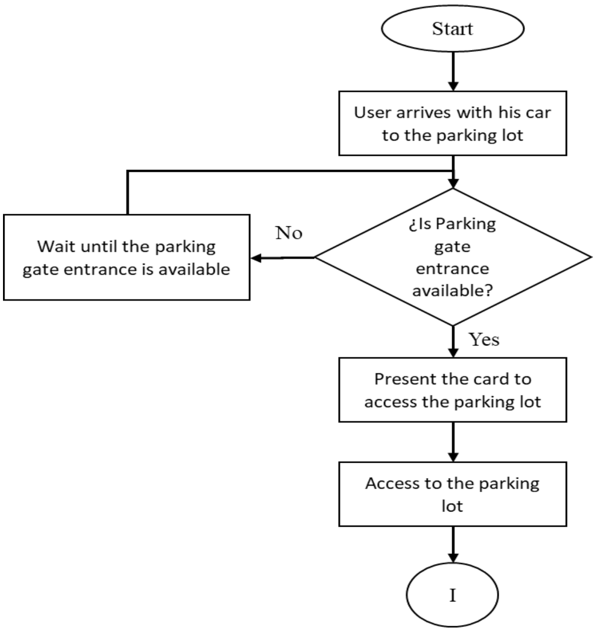

Figure 4: Process flow diagram to enter the parking lots in the Faculty of Engineering, UNAM, Mexico City

The process to search (waiting inside if neeed) and occupy of a parking space, comprises the following activities:

- Search for a parking space.
- If parking space is available, then user occupies the parking space during the required time.
- If parking space is not available, then user wait until a parking space is available.

Process to search and use of a parking space finish with the beginning of process exit from the parking lot.

This can be seen in Figure 5, which shows the activities that make up the process of searching and using a parking space, and the beginning of the parking exit process is denoted by the symbol II.

The process to exit from the parking lot, consists of the following activities:

- Leave the parking space and go to the exit of the parking lot.
- If the parking gate exit is available, then user presents his card to exit of the parking lot.
- If the parking gate entrance is not available, then user waits until it is available.
- Exit to the parking lot.

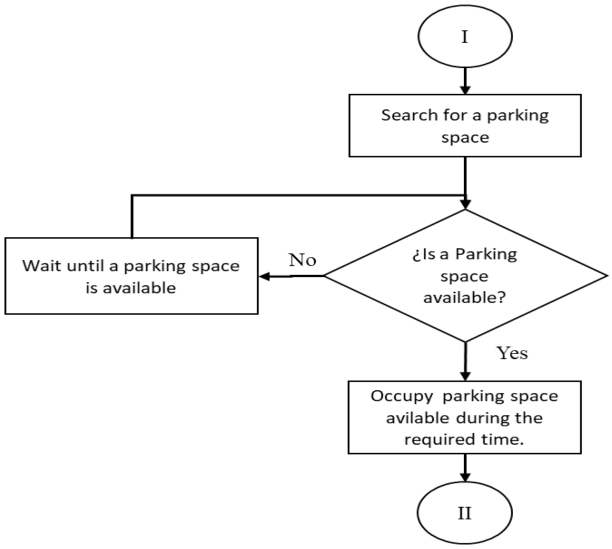

Figure 5: Process flow diagram to search and occupy of a parking space in the Faculty of Engineering, UNAM, Mexico City

The process flow diagram to exit the parking lots is illustrated in Figure 6.

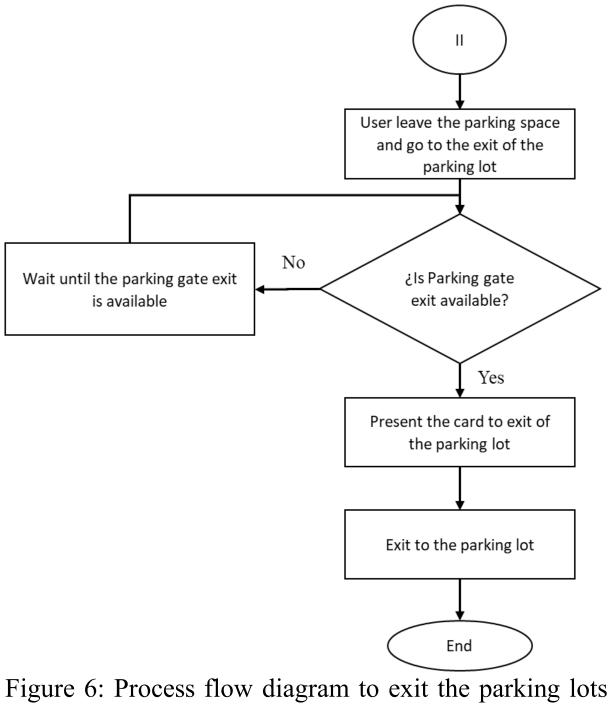

Figure 6: Process flow diagram to exit the parking lots in the Faculty of Engineering, UNAM, Mexico City

Based on the process described above, these processes were modeled under a discrete event simulation approach, then were formalized and implemented in the simulation platform FlexSim®, which among other advantages, has the characteristics required for simulation of discrete event systems, some of these are:

- Model the times between arrivals with distribution functions or with a schedule of arrivals.
- Label the elements that enter the system and differentiate the processing times by type of element.
- Collection of aggregated statistics or time series.

The elements included into the model and its correspondence or meaning to the real system are listed below, the following FlexSim® elements were used:

Source: Used to model the income of the users to the parking lot.

Queues: Used to model the wait of users in cases where the parking gate entrance, parking spaces and the parking gate exit are not available.

Processors: Used to model the service times of the parking gates (entrance and exit) and the dwell times in the parking spaces.

Figure 7 shows the model implemented in FlexSim® in its interface for software's version 2018.

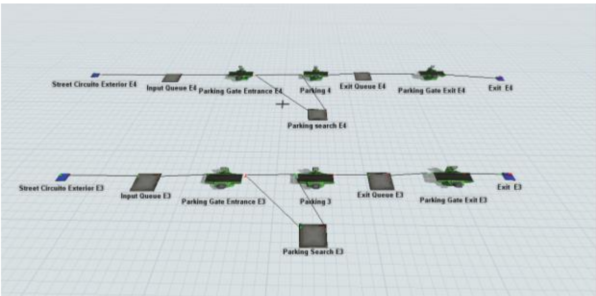

Figure 7: Parking lot model in FlexSim®, for South 3 and South 4 of the Faculty of Engineering, UNAM, Mexico City

3.4. Data collection and analysis

For the data collection, we used the classification proposed by (Harrell, Ghosh and Bowden 2004), which typifies the data in:

- Structural data, these involve all the objects in the system to be modeled.
- Operational data, these data explain how the system operates.
- Numerical data provide quantitative information about the system.

The structural and operational data were obtained through information provided by the parking management and direct observation of the operation of the parking lots. These data correspond to some of the activities reflected in the flow diagrams (Figures 4,5 and 6).

The numerical data to be collected are the following:

- Numbers of parking spaces.
- Service times of the entrance and exit gates.
- Arrival times of the users.
- User dwell times.

The number of parking spaces was provided by the administration of the parking lots, from the information provided, it is worthy to highlight the consideration of parking spaces for users with disabilities, however in this first version of the model this characteristic was not included, additionally during direct observation, it was identified that some users may park in spaces that are not marked as suitable for parking, this information is summarized in Table 2.

Table 2: Parking spaces for parking lots South 3 and South 4 of the Faculty of Engineering, UNAM, Mexico City

Parking lot	Parking spaces		
	All users	Disabled users	Unlabeled spaces
South 3	182	4	5
South 4	54	1	2

The service times of the entry and exit gates were collected, this information was analyzed using independence tests and the data were adjusted through goodness of fit tests, all these tests were applied using the ExpertFit® statistical program. The results of goodness of fit tests are shown in Table 3.

Table 3: Service Time distribution in seconds for parking gates, of the parking lots South 3 and South 4 of the Faculty of Engineering, UNAM, Mexico City

Parking Gate	Service Time distribution (seconds)
South 3 entrance	Loglogistic (4.04842, 6.12395, 2.64871)
South 3 exit	Lognormal (6.0512, 7.87486, 0.57084)
South 4 entrance	Beta (6.894, 47.4926, 1.3725, 6.13798)
South 4 exit	Johnson (9.41334, 56.8009, 2.02019, 0.9954)

Concerning to user's arrival and dwell times, the administration of parking lots provided the information of entrance and exit gates records for each of the eight parking lots, including South 3 and South 4, which comprise years 2015, 2016 and 2017.
Data provided for each event recorded at the entrance and exit gates are:

- Card number
- Date
- Hour (hours, minutes and seconds)

Once these data were obtained, we proceeded to clean the provided databases, during the data cleaning process some of the inconsistencies found were:

- Cards with entry and not exit records.
- Cards with exit and not entry records.
- Duplicate records for both entry and exit.

Once the databases were cleaned and structured for our study, we proceeded to calculate the dwell times by the difference of the time of entry and exit of the cards. Dwell and arrival times were entered the model for each of the users.

The assumptions used in the model are:

- Users wait until they find a parking spot. This assumption allows to determine the capacity shortages along the day.
- The time in which the users present their card to access the parking lots are considered as the arrival time of the users.

3.5. Scenarios and experiments
Scenarios were identified from historical data, since the research aim is to verify the impact of the application of the new restrictions to part time instructor, the scenarios seeks to show the performance before and after the adoption of the rules by means of measuring the KPIs.

That is, since the changes in the operating rules were made in July 2016, the operation of the system for the years 2015 and 2017 will be analyzed.

2015 is analyzed the KPIs when the users had free access independent of the type, and 2017 to analyze the impact after access restrictions by user type took effect.

For both Scenarios (years) an entire week of data (behavior for 5 days) is analyzed, for the election of this week the following steps were followed:

1. Identification of the month with the highest number of events (user occupying the parking lot).
2. Identification of the busiest week among the month, it is, once we have the month with the highest number of events, select the week with the highest number of events.

The number of events per month considering both parking lots (South 3 and South 4) for the years 2015 and 2017 are shown in Table 4.

Table 4: Monthly number of events for parking lots South 3 and South 4 of the Faculty of Engineering, UNAM, Mexico City

Month	Number of events	
	2015	2017
JAN	10,152	8,801
FEB	11,423	10,118
MAR	11,549	11,484
APR	10,211	8,669
MAY	7,628	10,671
JUN	11,635	11,259
JUL	4,728	3,099
AUG	11,832	12,858
SEP	11,870	9,240
OCT	13,021	12,329
NOV	11,137	10,913
DEC	5,245	5,485

For the year 2015, the October has the highest number of events with 13,021, while for 2017, August has the highest number with 12,858.

Weekly events breakdown for selected months (October 2015 and August 2017) are shown in Table 5 and Table 6.

Table 5: Weekly number of events for parking lots South 3 and South 4, October 2015 of the Faculty of Engineering, UNAM, Mexico City

Week October 2015	Number of events
1 to 4	1,165
5 to 11	2,903
12 to 18	2,825
19 to 25	2,925
26 to 31	2,875

Table 6: Weekly number of events for parking lots South 3 and South 4, August 2017 of the Faculty of Engineering, UNAM, Mexico City

Week August 2017	Number of events
1 to 6	1,801
7 to 13	2,698
14 to 20	2,831
21 to 27	2,760
28 to 31	2,232

From the above selection criteria and the numbers, the selected week (days) for October 2015 would be from 19 to 25, 2015, and for the year 2017 from August 14 to 20, 2017.

4. RESULTS

The key performance indicators (KPI´s) for the selected weeks during 2015 and 2017 are shown in Table 7 and 8 respectively. Saturdays and Sundays were excluded, since these days the results of the simulation showed a utilization of less than 50%.

In these tables the following abbreviations are used:

NUNS- Number of users not served due to saturation (parking places not available) of the system over a day.

MNUS- Maximum number of users looking for a parking space at the same time.

AST- Average search time of a parking space in case of saturation.

HSS- It refers to the periods of time (range) in which the utilization of parking was above 95%, this parameter was defined together with the administration of the parking lots.

NA- Not applicable

From the results obtained for the analyzed weeks, there is an increase of saturation level of the South Parking Lot 3, this is observed by comparing year 2015 vs the year 2017, as for the South 4 parking lot, it is detected that never reached a utilization higher that 95%, thus is never saturated.

Another interesting data obtained from the scenarios simulated, is the Average Dwell Time in the South 3 and South 4 parking lots. As is shown in Table 9, this time has decreased from 2015 to 2017 in both parking lots.

The evolution of the utilization of along the day, is illustrated with the time series of the parking spaces occupied for the South 3 and South 4 parking lots. Figure 8 provides an example of this analysis for August 17, 2017. From the plot, is easy to realize that capacity shortages at South 3 parking lot could be avoided by using as supplement the latent capacity of the South 4 parking lot.

Finally, from a straight comparison of the defined KPI's (NUNS, MNUS, AST and HSS), observed in the worse cases for both experiments (2015 and 2017), the numbers for 2015 are systematically lower, which reveals a better service and performance.

From the above, it is questionable to assume a positive effect of those restrictions introduced as improvement actions, it is important to highlight that the demand is growing. Then, unless it is considered an additional adjustment to rebalance the demand, by using both facilities in an integrated way (South 3 and 4), using South 4 as a supplement source of capacity, the service level is predicted to be worsen in the following year of operation.

Table 7: Key Performance Indicators (KPI´s) for parking lots South 3 and South 4 of the Faculty of Engineering, UNAM, Mexico City, October 19 to 23, 2015

October 19 to 23, 2015			
Day	Parking Lot	KPI	Value or Range
October 19	South 3	NUNS	13 users
		MNUS	4 users
		AST	439.7 s
		HSS	11:13 a 13:35 h
	South 4	NUNS	NA
		MNUS	NA
		AST	NA
		HSS	NA
October 20	South 3	NUNS	37 users
		MNUS	7 users
		AST	443.8 s
		HSS	11:08 a 14:21 h
	South 4	NUNS	NA
		MNUS	NA
		AST	NA
		HSS	NA
October 21	South 3	NUNS	NA
		MNUS	NA
		AST	NA
		HSS	11:45 a 12:43 h
	South 4	NUNS	NA
		MNUS	NA
		AST	NA
		HSS	NA
October 22	South 3	NUNS	NA
		MNUS	NA
		AST	NA
		HSS	11:46 a 13:38 h
	South 4	NUNS	NA
		MNUS	NA
		AST	NA
		HSS	NA
October 23	South 3	NUNS	NA
		MNUS	NA
		AST	NA
		HSS	11:00 a 13:04 h
	South 4	NUNS	NA
		MNUS	NA
		AST	NA
		HSS	NA

Table 8: Key Performance Indicators (KPI´s) for parking lots South 3 and South 4 of the Faculty of Engineering, UNAM, Mexico City, August 14 to 18, 2017

August 14 to 20, 2017			
Day	Parking Lot	KPI	Value or Range
August 14	South 3	NUNS	64 users
		MNUS	19 users
		AST	1,400.46 s
		HSS	10:47 a 14:19 h
	South 4	NUNS	NA
		MNUS	NA
		AST	NA
		HSS	NA
August 15	South 3	NUNS	97 users
		MNUS	35 users
		AST	2,222.11 s
		HSS	10:42 a 14:32 h
	South 4	NUNS	NA
		MNUS	NA
		AST	NA
		HSS	NA

August 16	South 3	NUNS	86 users
		MNUS	25 users
		AST	1,439.22 s
		HSS	10:34 a 14:21 h
	South 4	NUNS	NA
		MNUS	NA
		AST	NA
		HSS	NA
August 17	South 3	NUNS	101 users
		MNUS	31 users
		AST	2,881.96 s
		HSS	10:31 a 14:52 h
	South 4	NUNS	NA
		MNUS	NA
		AST	NA
		HSS	NA
August 18	South 3	NUNS	75 users
		MNUS	14 users
		AST	1.075.14 s
		HSS	10:43 a 14:25 h
	South 4	NUNS	NA
		MNUS	NA
		AST	NA
		HSS	NA

Table 9: Average Dwell Time for parking lots South 3 and South 4 of the Faculty of Engineering, UNAM, Mexico City, October 20,2015 & August 17, 2017

Day	Parking Lot	Average Dwell Time (s)
20 October 2015	South 3	15,286.8
	South 4	12,396.6
17 August 2017	South 3	14,880.7
	South 4	11,111.7

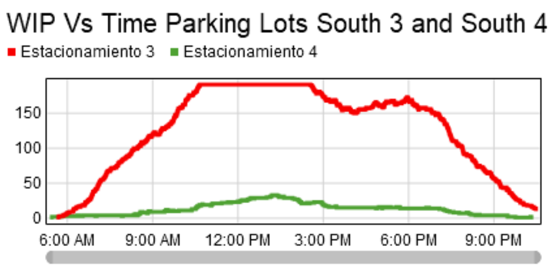

Figure 8: Time series of the parking spaces occupied for the South 3 and South 4 parking lots of the Faculty of Engineering, UNAM, Mexico City, August 17, 2017

5. CONCLUSIONES

The implementation of the discrete event simulation models of the parking lots, allowed to have a better understanding of their operation.

With respect to the analysis of the results obtained with the changes in the access policy by user type. The changes in the policy do not have a positive impact on a decrease of the saturation of the parking lots, although for the South 3 and South 4 parking there is a decrease in the dwell times (Table 9), at the same time there was an increase in the number of users in the case of South 3 parking and a decrease in the number of users in the case of South 4 parking.

For the demand of the week from August 14 to 20, 2017 (Monday to Friday), the period with the highest saturation (occupied parking spaces greater than 95% of the capacity) for parking lot South 3, occurs between 10:30 and 3:00 p.m.

To improve the level of service with respect to the parking utilization factor, it is necessary to establish a policy that allows assigning the parking lots to which users will have access based on the building in which they have their workplace (office, classroom or laboratory), but taking in to account the integrated capacity of the parking lots and not as independent resources. This policy can be tested with the simulation model developed as part of this research paper, its implementations may require minor updated and modifications.

6. FUTURE WORK

The School of Engineering has eight parking lots, these could be divided into two subsystems with four parking lots each, depending on the proximity and the population they serve. Two models should be developed to allow testing and analyzing parking allocation policies based on the location of the workplace (office, classroom or laboratory) and type of user.

ACKNOWLEDGMENTS

This work was supported by UNAM-DGAPA-PAPIME, PAPIME PE102218 “Preparation of didactic material (notes, presentations, exercise series and study cases) and online courses regarding Simulation of Complex Systems and Business Intelligence (Business Intelligence).” Also Dr. Nosedal is supported by the Mexican National Science and Technology Council (CONACYT) (project 2354).

REFERENCES

Barata, E., Cruz, L., & Ferreira, J. P. (2011). Parking at the UC campus: Problems and solutions. Cities, 28(5), 406-413.

FlexSim (2018) https://www.flexsim.com/

Fontaine, Michael & E. Isler, Elizabeth & A. Hoel, Lester. (2005). Innovative Parking Management Strategies for Universities: Accommodating Multiple Objectives in a Constrained Environment.

Harrel C., Gosh B.K., Bowden R. (2004). Simulation Using Promodel, 2nd Edition, Mc Graw-Hill, New York. 128-129.

Sweet, M. N., & Ferguson, M. R. (2019). Parking demand management in a relatively uncongested university setting. Case Studies on Transport Policy.

Teodorović, D., & Lučić, P. (2006). Intelligent parking systems. European Journal of Operational Research, 175(3), 1666-1681.

Yan, X., Levine, J., & Marans, R. (2019). The effectiveness of parking policies to reduce parking demand pressure and car use. Transport Policy, 73, 41-50.

AUTHORS BIOGRAPHY

Ricardo Torres, studied Industrial Engineering, then a Master Financial Optimization and Planning at the Engineering Faculty in UNAM (Mexico). His lines of research are Simulation, and Replenishment systems in Supply Chain.

Jenaro Nosedal-Sanchez holds a Ph.D. in Telecommunications and Systems Engineering from Univesitat Autónoma de Barcelona, Spain. He is currently Research Fellow for the National Science and Technology Council (CONACYT-Mexico), within the "Cátedras Conacyt" program. Since July 2018 was appointed as Lecturer at the Masters in Supply Chain Engineering program at Mexico State Autonomous University. His research interests include modeling and applied simulations, optimization, operations management and humanitarian logistics.

ON ESTIMATION ERRORS WHEN DEALING WITH THE PROBLEMS OF OPTICAL TELECOMMUNICATIONS

O.V. Chernoyarov[(a)], Yu.A. Kutoyants[(b)], A.V. Zyulkov[(c)]

[(a)]National Research University "Moscow Power Engineering Institute", Moscow, Russia
[(a),(b)]International Laboratory of Statistics of Stochastic Processes and Quantitative Finance of the National Research Tomsk State University, Tomsk, Russia
[(a)]Maikop State Technological University, Maikop, Russia
[(b)]Le Mans University, Le Mans, France
[(c)]Voronezh State University, Voronezh, Russia

[(a)]chernoyarovov@mpei.ru, [(b)]kutoyants@univ-lemans.fr, [(c)]zyulkov@phys.vsu.ru

ABSTRACT
The problem is considered of the phase and frequency estimation by the observations of periodic Poisson processes in the cases of different regularity conditions: smooth signals, cusp-type singular signals and change-point type signals. There is described the asymptotic behavior of the mean square errors in all these situations and then the results of numerical simulations are presented.

Keywords: Poisson signal, maximum likelihood estimator, Bayesian estimator, phase modulation, frequency modulation, regular, cusp-type and discontinuous cases, rate of convergence of estimator

1. PROBLEM STATEMENT

1.1. The model of the realization of the observable data

Let us consider the problem of transmission of information ϑ_0 by a Poisson channel with the dark noise having the intensity of $\lambda_N > 0$. It is presupposed that the optical signal (inhomogeneous Poisson process) has an intensity function $S(\vartheta_0, t)$, $0 \le t \le T$, where $S(\vartheta_0, t)$ is periodic function. Therefore, the observations $X^T = (X_t, 0 \le t \le T)$ is Poisson process with the intensity function

$$\lambda(\vartheta_0, t) = S(\vartheta_0, t) + \lambda_N, \quad 0 \le t \le T.$$

The behavior of the mean square error (variance) is studied under $T \to \infty$:

$$\mathbf{E}_\vartheta \left(\overline{\vartheta}_T - \vartheta_0\right)^2 = C / T^\gamma, \qquad (1)$$

where $\overline{\vartheta}_T$ is a certain estimator of the parameter ϑ_0, $C > 0$ is a constant and the value $\gamma > 0$ depends on the regularity of the function $S(\vartheta_0, t)$ with respect to ϑ_0.

1.2. The estimators of the informative parameter

Let us introduce the likelihood ratio function

$$L\left(\vartheta, X^T\right) = \exp\left[\int_0^T \ln\left(1 + \frac{S(\vartheta, t)}{\lambda_N}\right) \mathrm{d}X_t - \int_0^T S(\vartheta, t)\,\mathrm{d}t\right].$$

Then, the two most commonly used estimators of the parameter ϑ_0 can be formed: maximum likelihood estimator (MLE) $\hat{\vartheta}_T$:

$$L\left(\hat{\vartheta}_T, X^T\right) = \sup_{\vartheta \in \Theta} L\left(\vartheta, X^T\right) \qquad (2)$$

and Bayesian estimator (BE)

$$\tilde{\vartheta}_T = \int_\Theta \vartheta p(\vartheta) L\left(\vartheta, X^T\right) \mathrm{d}\vartheta \Big/ \int_\Theta p(\vartheta) L\left(\vartheta, X^T\right) \mathrm{d}\vartheta.$$

Here Θ is the area of possible values, $p(\vartheta)$ is the positive continuous prior probability density of the parameter ϑ_0 and the quadratic loss is presupposed.

1.3. Modulations

P. *Phase modulation*: $S(\vartheta, t) = f(t - \vartheta)$
F. *Frequency modulation*: $S(\vartheta, t) = f(\vartheta t)$
Here and hereinafter $f(t)$ is the periodic function of the known period.

1.4. Regularity

S. *Smooth case*. The function $f(t)$ is continuously differentiable.
C. *Cusp-type case*. The function $f(t)$ has the following representation on the first period: $f(t) = a|t|^\kappa + h(t)$,

where $a > 0$, $\kappa \in (0, 1/2)$, and $h(t) > 0$ is continuously differentiable.

D. *Discontinuous case*. The function $f(t)$ has the following representation on the first period: $f(t) = a\,1_{\{t > \vartheta\}}$.

The following theoretical results have been obtained for the MLE $\hat{\vartheta}_T$ and BE $\tilde{\vartheta}_T$:

PS case, i.e. phase modulation and smooth $f(t)$ (Kutoyants 1979):

$$\mathbf{E}_\vartheta \left(\hat{\vartheta}_T - \vartheta_0\right)^2 \sim C/T, \quad \gamma = 1. \tag{3}$$

PC case, i.e. phase modulation and cusp-type $f(t)$ (Dachian 2003):

$$\mathbf{E}_\vartheta \left(\hat{\vartheta}_T - \vartheta_0\right)^2 \sim C/T^{2/(2\kappa+1)}, \; 1 < \gamma = 2/(2\kappa + 1) < 2. \tag{4}$$

PD case, i.e. phase modulation and discontinuous $f(t)$ (Kutoyants 1979):

$$\mathbf{E}_\vartheta \left(\hat{\vartheta}_T - \vartheta_0\right)^2 \sim C/T^2, \quad \gamma = 2. \tag{5}$$

FS case, i.e. frequency modulation and smooth $f(t)$ (Kutoyants 1979):

$$\mathbf{E}_\vartheta \left(\hat{\vartheta}_T - \vartheta_0\right)^2 \sim C/T^3, \quad \gamma = 3. \tag{6}$$

FC case, i.e. frequency modulation and cusp-type $f(t)$:

$$\mathbf{E}_\vartheta \left(\hat{\vartheta}_T - \vartheta_0\right)^2 \sim \frac{C}{T^{(4\kappa+4)/(2\kappa+1)}}, \; 3 < \gamma = \frac{4\kappa + 4}{2\kappa + 1} < 4. \tag{7}$$

FD case, i.e. frequency modulation and discontinuous $f(t)$ (Kutoyants 1984):

$$\mathbf{E}_\vartheta \left(\hat{\vartheta}_T - \vartheta_0\right)^2 \sim C/T^4, \quad \gamma = 4. \tag{8}$$

With the use of simulations, the convergences

$$\ln \mathbf{E}_\vartheta \left(\hat{\vartheta}_T - \vartheta_0\right)^2 / \ln T \to -\gamma$$

are studied in all the cases specified above. The intensity functions in simulations are always

$$\lambda(\vartheta_0, t) = S(\vartheta_0, t) + 1, \quad 0 \le t \le n \to \infty, \tag{9}$$

where $S(\vartheta, t) = f(t - \vartheta)$ and $S(\vartheta, t) = f(\vartheta t)$ in the cases of phase and frequency modulations, respectively.

The function $f(t)$ in *smooth* **PS** and **FS** cases of the phase and frequency modulations is $f(t) = a\cos^2(2\pi t)$, $a = 2$, $t \ge 0$.

The function $f(t)$ in *cusp* **PC** and **FC** cases is periodic of period 1 and it has the representation on the one period $t \in [-1/2, 1/2]$ as follows

$$f(t) = \frac{a}{2}\left[1 + \operatorname{sgn}(2t + \delta)\left|\frac{2t + \delta}{\delta}\right|^\kappa 1_{\{-\delta < t \le 0\}} - \right.$$
$$\left. - \operatorname{sgn}(2t - \delta)\left|\frac{2t - \delta}{\delta}\right|^\kappa 1_{\{0 < t \le \delta\}}\right] 1_{\{-\delta < t \le \delta\}}. \tag{10}$$

Here $a = 2$, $\delta = 0.25$ and $\kappa = 1/4$.

The function $f(t)$ in *change-point* **PD** and **FD** cases of the phase and frequency modulations is periodic with the period 1:

$$f(t) = a\,1_{\{0 \le t \le \delta\}},$$

where $a = 10$, $\delta = 0.25$ and it is periodically prolonged along the whole line.

In Fig. 1, the qualitative examples are shown of the signals with varying degree of smoothness (different types of singularity of intensity functions (10)) determined by the parameter κ: a) $\kappa = 5/8$; b) $\kappa = 1/2$; c) $\kappa = 1/8$; d) $\kappa = 0$; e) $\kappa = -3/8$.

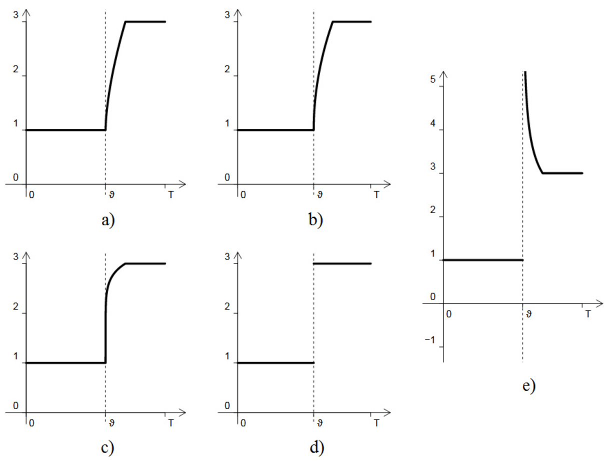

Figure 1: The examples of the signals with different types of singularity of intensity functions

The curve presented in Fig. 1a corresponds to the smooth case. Note that the derivative of this function is unbounded, but nevertheless the Fisher information is finite and this is a regular statistical experiment. The curve presented in Fig. 1b is like the smooth one as well, but the rate of convergence of the mean square error is slightly different: $\mathbf{E}_\vartheta \left(\hat{\vartheta}_T - \vartheta_0\right)^2 \sim C/T \ln T$. The curves presented in Figs. 1c and 1d correspond to cusp-type and change-point type singularities, respectively. Finally, the curve presented in Fig. 1e corresponds to the explosion-type singularity, the properties of the estimators are also known in this case, but this type of singularity is not examined in our present research.

2. RESULTS OF SIMULATIONS

The convergence of the experimental values of the variances of MLE (2) with the asymptotic formulas (3)-(8) have been studied using simulation in programming language R. For non-stationary Poisson process, the simulation is carried out by the method of time scale conversion (Law 2014).

In Figs. 2-6, the log-log plots (1)

$$V = V(\gamma, T) = \ln \mathbf{E}_{\vartheta}\left(\hat{\vartheta}_T - \vartheta_0\right)^2 \sim \ln C - \gamma \ln T, \qquad (11)$$

of the variance of MLE (2) as a function of the number of signal periods N are presented where one can see some results of statistical simulation (circles, squares, pluses) and corresponding theoretical dependences (solid curves). The C parameter is estimated based on the simulation data by the least squares method. Each experimental value is obtained by processing no less than 10^3 realizations of Poisson process with the intensity function (9). Thus, with the probability of 0.9, the confidence intervals boundaries deviate from the experimental values no greater than by 10 %.

In Fig. 2, the dependences (11) are presented for all the three types of regularity in case of the phase modulations (**P**): smooth (3) – curve 1 and circles, cusp-type (4) – curve 2 (if $\gamma = 4/3$) and squares, change-point (5) – curve 3 and pluses.

Fig. 3 describes the similar situations but for the intensities with the frequency modulation (**F**): smooth (6) – curve 1 and circles, cusp-type (7) – curve 2 (if $\gamma = 10/3$) and squares, change-point (8) – curve 3 and pluses.

In the next three figures, there is shown the comparison of the errors (11) occurring in the cases when the same regularity is accompanied with different types of modulations.

In Fig 4, the theoretical and experimental errors (11) are plotted for the cases of the phase (curve 1 and pluses) and frequency (curve 2 and pluses) modulations for smooth intensity functions, i.e. for **PS** and **FS** cases described by the formulas (3) and (6), respectively.

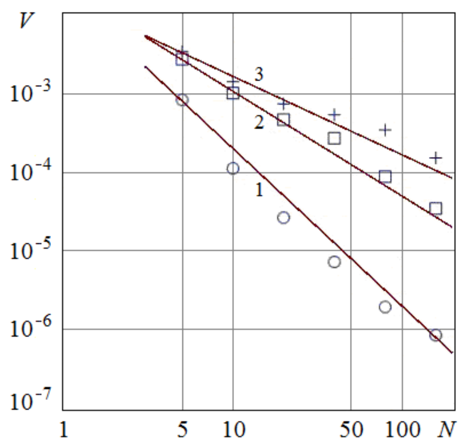

Figure 2: The dependences of the variance of MLE of the Poisson signal in the case of phase modulations

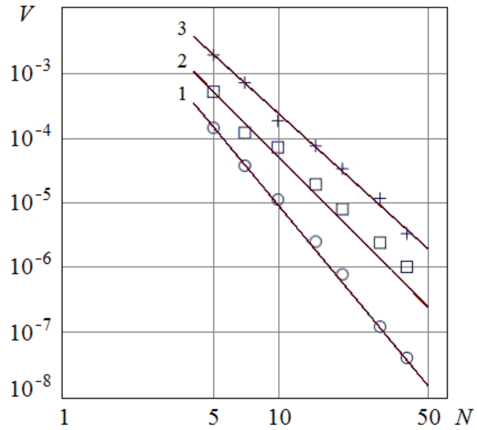

Figure 3: The dependences of the variance of MLE of the Poisson signal in the case of frequency modulations

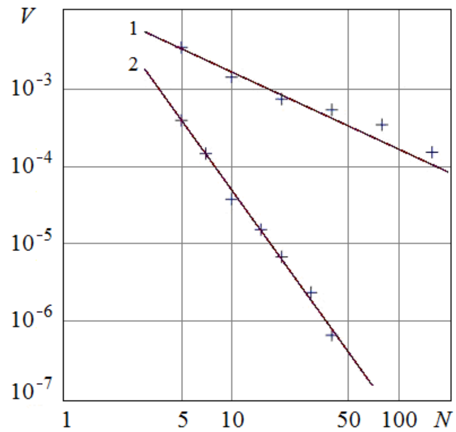

Figure 4: The dependences of the variance of MLE of the Poisson signal with smooth intensity function in the case of phase and frequency modulations

The results presented in Fig. 5 correspond to the phase (curve 1 and squares) and frequency (curve 2 and squares) modulations for the intensities with cusp-type singularity, i.e. for **PC** and **FC** cases described by the formula (3) under $\gamma = 4/3$ and the formula (6) under $\gamma = 10/3$, respectively.

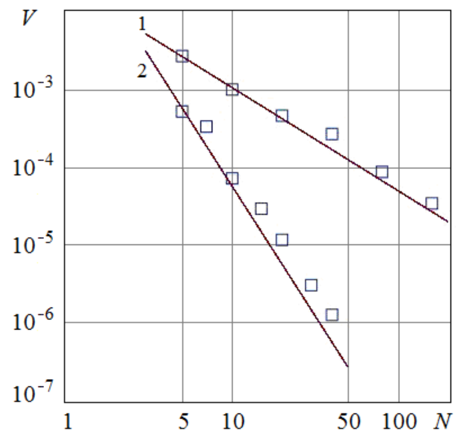

Figure 5: The dependences of the variance of MLE of the Poisson signal with cusp-type intensity function in the case of phase and frequency modulations

And finally, in Fig. 6, the dependences (11) are drawn for the phase-modulated (curve 1 and circles) and frequency-modulated (curve 2 and circles) signals with discontinuous intensities, i.e. for **PD** and **FD** cases described by the formulas (5) and (8), respectively.

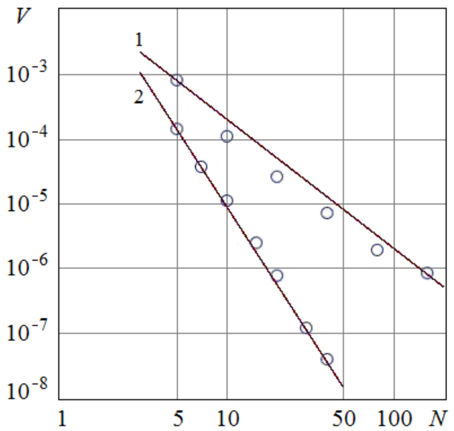

Figure 6: The dependences of the variance of MLE of the Poisson signal with discontinuous intensity function in the case of phase and frequency modulations

One can see that the result of the simulations correspond well to the theoretical properties (3)-(8) of the mean square errors in a wide range of observations' duration.

3. CHOICE OF THE MODEL

Therefore, it is natural to put the following question: *What is the best choice of the intensity function and the estimator and what is the corresponding rate of decay of the mean square error*?

It should be noted that in statistics the observation model is usually presented and the problem is to understand what can be done to identify this model. Here the statement is different and one can choose the model to get less errors.

The problem considered there is, in some sense, inverse. It is presupposed that one can choose any intensity one wants, and the goal is to find such function $\lambda(\vartheta_0, t)$ of $\vartheta_0 \in \Theta = (0,1)$ and $t \in [0,T]$ and the estimator ϑ_T^* that the rate of error decreasing is the best possible. Of course, one has to impose some restrictions on the "energy of the signal" (in terminology coming from telecommunication theory), since, if one allows that $\lambda(\vartheta_0, t) \to \infty$, then one will have any rate wanted.

Let us fix some number $L > 0$ and introduce the class of intensity functions bounded by this constant

$$F(L) = \{\lambda(\cdot):\ 0 \le \lambda(\vartheta, t) \le L,\ 0 \le t \le T\}.$$

Then one gets the following result:

$$\inf_{\lambda \in F(L)} \inf_{\overline{\vartheta}_T} \sup_{\vartheta_0 \in \Theta} \mathbf{E}_{\lambda,\vartheta_0} \left(\overline{\vartheta}_T - \vartheta_0\right)^2 = \exp\left[-\frac{TL}{6}(1 + o(1))\right].$$

This relation contains two different results.

The first one is a lower bound on the risks for all the choices of the intensity function (in $F(L)$) and all the estimators $\overline{\vartheta}_T$:

$$\inf_{\lambda \in F(L)} \sup_{\vartheta_0 \in \Theta} \mathbf{E}_{\lambda,\vartheta_0} \left(\overline{\vartheta}_T - \vartheta_0\right)^2 \ge \exp\left[-\frac{TL}{6}(1 + o(1))\right].$$

The second result is to describe the intensity function $\lambda_*(\cdot)$ and such the estimator ϑ_T^* that (upper bound)

$$\sup_{\vartheta_0 \in \Theta} \mathbf{E}_{\lambda_*,\vartheta_0} \left(\vartheta_T^* - \vartheta_0\right)^2 \le \exp\left[-\frac{TL}{6}(1 + o(1))\right].$$

Proofs can be found in the researches by Burnashev and Kutoyants (1999, 2001). Note that this result follows *the spirit of Information Theory*.

4. CONCLUSION

The goal of this research is to show how the rate of decreasing the mean square error of MLE depends on the regularity of the model. The large diversity of the rates can be seen due to the different types of the smoothness of the signals. There is another important class of problems: what are the errors of the estimators when the regularities of the statistical models real and theoretical are different. It is also proposed to present some results in such situations.

ACKNOWLEDGMENTS

This research was financially supported by the Ministry of Education and Science of the Russian Federation (research project No. 2.3208.2017/4.6).

REFERENCES

Kutoyants Yu.A., 1979. Intensity parameter estimation of an inhomogeneous Poisson process. Problems of Control and Information Theory, 8 (2), 1-13.

Dachian S., 2003. Estimation of cusp location by Poisson observations. Statistical Inference for Stochastic Processes, 6 (1), 1-14.

Kutoyants Yu.A., 1984. Parameter estimation for stochastic processes. Berlin: Heldermann.

Law A.M., 2014. Simulation modeling and analysis. New York: McGrow-Hill Education.

Burnashev M.V. and Kutoyants Yu.A., 1999. On sphere-packing bound, capacity and related results for Poisson channel. Problems of Information Transmission, 35 (2), 3-22.

Burnashev M.V. and Kutoyants Yu.A., 2001. On minimal α-mean error parameter transmission over Poisson channel. IEEE Transactions on Information Theory, 47 (6), 2505-2515.

AUTHORS BIOGRAPHY

Oleg V. Chernoyarov was born in 1973. He received his M.Sc. and Ph.D. degrees in radio physics from the

Voronezh State University, Voronezh, Russia, and the D.Sc. degree in radio physics – from the Moscow Pedagogical State University, Moscow, Russia, in 1996, 2000 and 2011, respectively. Presently, he is working as a Professor at the Department of Electronics and Nanoelectronics of the National Research University "Moscow Power Engineering Institute" as well as a Leading Research Worker of the National Research Tomsk State University (International Laboratory of Statistics of Stochastic Processes and Quantitative Finance) and the Maikop State Technological University (Department of Higher Mathematics and System Analysis). His main interests are statistical methods for transmission and processing of information.

Yury A. Kutoyants was born in 1946. He received his M.Sc. degree in nuclear physics from Moscow Engineering and Physics Institute (MIFI), he defended his Ph.D. degree in information theory from Moscow Institute of Physics and Technology and the D.Sc. degree in mathematics from Leningrad State University in 1970, 1975 and 1988 respectively. Presently he is working as Emeritus Professor at the Le Mans University, France as well as a Leading Research Worker of the National Research Tomsk State University (International Laboratory of Statistics of Stochastic Processes and Quantitative Finance). His main interests are in statistics of continuous time stochastic processes.

Aleksandr V. Zyulkov was born in 1952. He received his M.Sc. and Ph.D. degrees in radio physics from the Voronezh State University, Voronezh, Russia, in 1974 and 1983, respectively. Presently, he is working as an Associate Professor at the Department of Radio Physics of the Voronezh State University. His main interests are statistical methods for transmission and processing of information.

COMPUTATIONAL OPTIMIZATIONS OF NESTED SIMULATIONS UTILIZED FOR DECISION-MAKING SUPPORT

Roman Diviš[(a)], Antonín Kavička[(b)]

[(a),(b)]University of Pardubice, Faculty of Electrical Engineering and Informatics

[(a)]roman.divis@upce.cz, [(b)]antonin.kavicka@upce.cz

ABSTRACT
Nested simulations present a general method suitable for use in realizing a multi-trajectory simulation or as a decision support in a simulator. The principle of nested simulation (as a decision support) is to find a solution to a problem using other time-limited simulations which verify alternative options. After the nested simulations have finished, the solutions of individual alternatives are assessed and the best solution is applied to the main simulation.
The aim of this article is to test various exact and heuristic approaches to reduce the computational complexity of nested multi-simulations. The basic method uses the recorded states from previous simulations to avoid duplicate calculations leading to the same states. Other measures are heuristic and are based on the detection of similar states/replications during the calculation.

Keywords: nested simulations, decision support, rail transport

1. INTRODUCTION

The stochastic simulator requires implementation of some of the decision support techniques. There are a number of ways to solve conflicting situations - from leaving the solution to the user (interactive mode of simulation) through various complex mathematical models (fuzzy logic, artificial neural networks, ...). Even though there are a number of complex decision support techniques, in practice, one of the easiest methods - priority planning - is often implemented in microscopic railway simulators. This method is used in OpenTrack, Villon and other rail simulators.
Nested or recursive simulations represent another methodology that can be used to support decision making in simulators. The principle of the method consists in suspending the actual main simulation at the moment when the conflict situation occurs and the simulation is then cloned into several variants. Individual clones have modified parameterization to allow testing of different options for resolving the conflict situation. These nested/recursive simulations (basically different outlooks for the future within a limited time horizon) are triggered, and after a certain period of time, it is evaluated which one has the best results. The optimal one is then used as a solution and the main simulation continues only with the chosen variant. Nested simulations are implemented and tested as experimental decision support in the developed MesoRail simulation tool (Diviš and Kavička 2015).
The aim of this paper is to describe possible exact and heuristic algorithms designed to optimize nested simulation calculations. The aim of each method is to reduce the machine time required for simulation experiments. The proposed methods use different techniques based mainly on recording reached states during simulations to speed up future calculations.

1.1. Brief overview of the state-of-the-art

It has to be declared that not many authors pay attention to the research of nested/recursive simulations.
The authors Gilmer and Sullivan were focused in several of their articles on the efficiency of higher number of replications in contrast with multi-trajectory simulation (Gilmer and Sullivan 1999). Their main interest is related to the military simulator Eaglet, which simulates the movement of military units of two armies and their mutual interactions.
Eugen Kindler (as a pioneer of nested simulation in Europe) published many articles with the focus on both, the theoretical description of nested simulations (classification, terminology, etc.) and their applications in practice (Kindler 2010).
The issue of a planning support system is discussed by Hill, Surdu, Ragsdale, and Schafer (2000). Those authors were engaged in military planning.
Another area of applied nested simulations is connected with scalable simulation models, which allow applying both a macroscopic and a microscopic level of investigation within the frame of one simulator (Bonté, Duboz, Quesnel and Muller 2009). Another area of exploiting nested simulations is financial a risk management – e.g. Gordy and June (2010).

2. POSSIBLE APPROACHES TO THE USE OF NESTED SIMULATIONS

The method of *nested/recursive simulations* presents a principle of a simulation inside a simulation used to examine the results of multiple alternative scenarios (or developments) of the simulation. One possible use of this method is *decision support in a simulation*. Nested simulations run for a limited time, and after they are completed, their results are evaluated. Subsequently, the nested simulations are merged back into a single instance and the main simulation can continue in a selected manner. The flow chart of a simulation using decision support with the use of nested simulations is shown in figure 1.

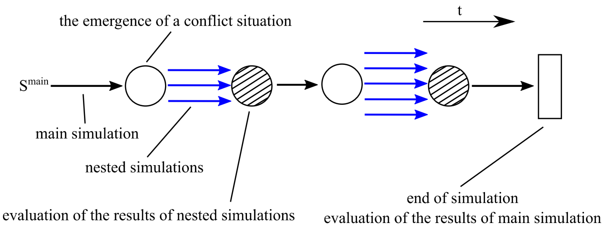

Figure 1: Using nested simulations as simulation decision support technique

Another use of nested simulations can be implemented as a *multi-trajectory simulation* - the simulation experiment is divided into nested simulations at individual points of decision and the simulation is gradually branched more and more and various scenarios are explored. According to the article (Gilmer and Sullivan 1999), this process can be more effective than using a large number of replications of a single simulation scenario. The flow chart of a simulation using a multi-trajectory simulation is shown in figure 2. In addition, attention will be paid to the first method of use – as a decision support in simulation.

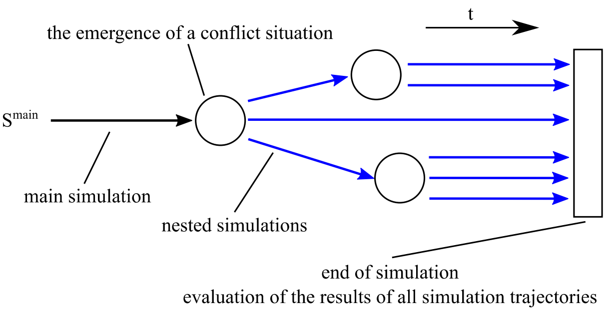

Figure 2: Using nested simulations to implement multi-trajectory simulation

3. NESTED SIMULATION TECHNIQUE

Decision support in the simulator can use the standard simulation engine for both the main simulation and nested simulations.

The method of using nested simulations as a support for decision making is not trivial and its detailed description can be found in the article (Diviš and Kavička 2016). The basic principle consists in pausing the execution of the main simulation at the occurrence of conflict (decision point of simulation). Subsequently, possible variants of the solution are identified, nested replications generated for each variant, and these replications run for a limited time (simulation lookahead). Upon completion, the simulation results are evaluated, and the main simulation continues with the selected solution. The strategy of using nested simulations is shown in figure 3. The whole technique of nested simulations is quite complicated, and for a better understanding of the procedures, several basic functions can be described:

- *simulation* - realizes the progress of one particular simulated replication,
- *solveConflict* - the function is called at the moment of the conflict emergence and decides how to solve it (using nested simulations or other methods),
- *solveUsingNestedSimulations* - performs all necessary steps to create nested simulations, calculate them and collect results,
- *createReplications* - creates specific replications for each possible variant of conflict solution.

The following are the formalizations (using pseudocode) of the above functions. A certain degree of abstraction was chosen with regard to the appropriate demonstration of individual methods leading to a reduction in the computational complexity of the nested simulation method.

```
function simulation(s):
while s.isNotEnd():
    e := s.nextEvent()
    s.processEvent(e)

    if s.isConflictOccured():
        solution := solveConflict(s, s.getConflict())
        s.applySolution(solution)

    s.saveState()
```

```
function solveConflict(s, c):
if simulation.recursionLevel <= REC_LIMIT:
    return solveUsingNestedSimulations(s, c)
else:
    return solveUsingAlternativeMethod(s, c)
```

```
function solveUsingNestedSimulations(s, c):
variants := generateSolutionVariants(s, c)
seeds := generateRandomSeeds(s, REPL_COUNT)
nestedSimulations := createReplications(variants, seeds)

parallel start all nestedSimulations
wait until all finished nestedSimulations

solution := analyseResults(nestedSimulations)
return solution
```

```
function createReplications(variants, seeds):
simulations = {}
for variant in variants:
    for seed in seeds:
        s := createSimulation(baseSimulation, variant,
            seed)
        append s to simulations[variant]

return simulations
```

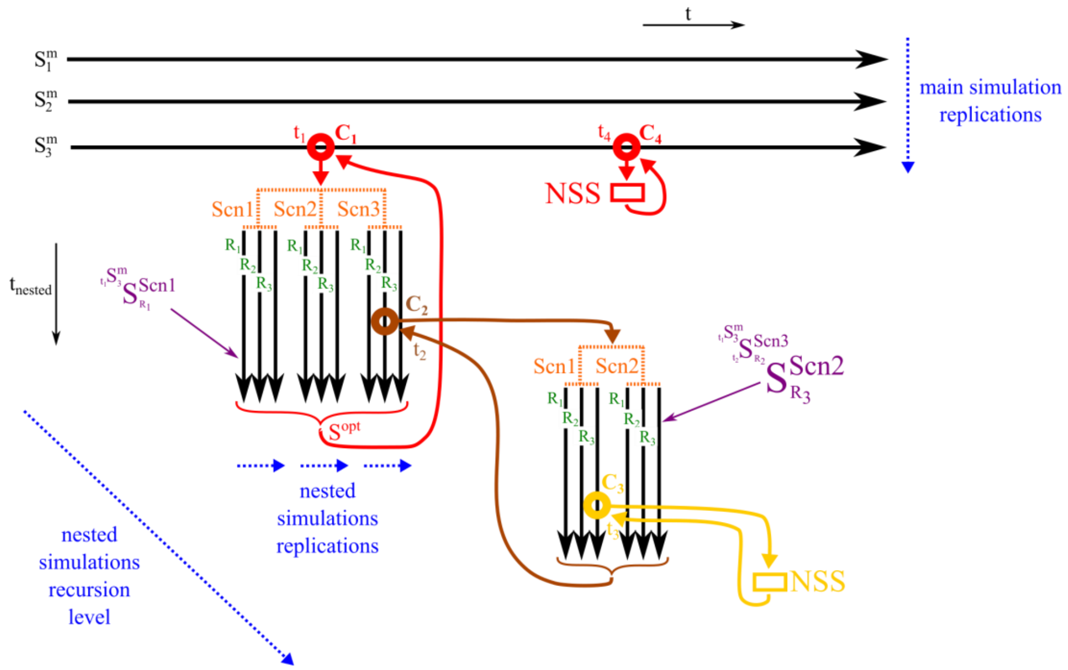

Figure 3: Illustration of occurrence and process of solving one conflict situation in one simulation replication

3.1. Basic parameters of the nested simulations

Before performing the nested simulations, we need to set the parameter group. This set of parameters may vary according to the type of conflict situations to be addressed. Depending on the implementation of decision support using nested simulations, the set of parameters may vary, or some parameters may be implemented differently.

Basic parameter overview:

- *ScnCount* – limit the number of evaluated scenarios (variants),
- *ScnGen* – generator of possible scenarios for solving conflict situation,
- *StopCond* – condition for terminating execution of nested simulations (can be interpreted as a constant value – length of lookahead),
- *CrOpt*, *CrOptComparer* – the functions used to evaluate individual nested simulation results.

Parameters related to multiple replications:

- *ReplCount* – number of evaluated multiple replications for each scenario (variant),
- *ReplResultsAggregateFunction* – function for evaluating results between replications of one scenario.

Parameters related to recursive nested simulations:

- *RecLimit* – maximum depth of recursion of nested simulation calculations,
- *RecStopCondBehaviour* – determines the use of *StopCond* in recursive simulations (extension of lookahead, limitation of lookahead to the original value, ...),
- *RecOnLimitAction* – defines the method (process) for resolving the conflict arising at the maximum recursion depth (no more recursive (nested) simulations are allowed).

More detailed description of individual parameters can be found in the article (Diviš and Kavička 2018).

4. EXACT OPTIMIZATION METHOD OF RECURSIVE CALCULATIONS

A series of simulations are needed to achieve relevant results in the simulation study. Individual simulations differ in the seeds used for pseudorandom number generators and thus affect the run of simulations. During the past investigation of nested simulation behaviour, it was found that the maximum nesting level dominates the quality of the result. A higher nesting level allows for better results. The negative consequence of allowing a high nesting level is a significant increase in the processing complexity of the method. If there is no initial estimate, it is not advisable to run simulations with a higher nesting level. There might also be a situation where the configuration is not computable with the available computing resources (too high computational time and/or memory requirements). An iterative approach to a simulation study can start from the simplest of configurations and continue with more complicated configurations. If recursion is not allowed in the decision-making process at the beginning, the simulations can be completed very quickly. In the next iteration step, one level of recursion would be allowed and computational complexity would increase as expected. This procedure offers a safe way

to get results for all the necessary simulations, even if the available time to perform the study expires at the arbitrary nesting level. The disadvantage of the method is a considerable amount of repetition of previously performed simulations.
As part of our investigation (a case study on rail traffic simulation), it turns out that results do not change significantly between nesting levels. More levels of nesting rather refine decision-making results. It is not yet possible to generalize this behaviour due to the absence of multiple case studies. But for an application class where nested simulations exhibit the above behaviour, it is possible to continually save the progress of the calculation to an external memory (hard disk). Then these simulations are used to speed up calculations of new simulations with a higher nesting level. A more detailed level of simulations will use the capability to skip over already calculated sets of states. These jumps in (simulation) time can be used if a conflict is found whose new solution is identical to the solution from the previous set of simulations. This procedure can be repeated for each partial conflict as long as the simulation progress is the same, and there is no difference between the calculated solutions of the simulation. Each simulation branch (main simulation and individual nested simulations) represents an independent process to which this procedure can be applied.
For a better understanding of the method and the solved situations, the whole simulation strategy is illustrated in the following figures. Figure 4 (case A) shows the basic run of a stochastic simulation where a conflict situation occurred. The depicted situation does not allow nested simulations to be used, and thus conflict is resolved using an alternative method (e.g. priority planning). The selected variant of the solution is represented by a blue text label.

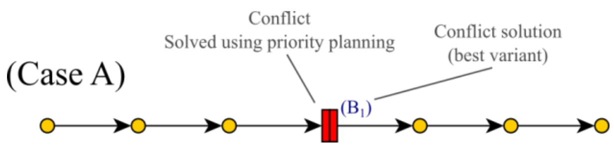

Figure 4: Conflict solved using priority planning (A)

Figure 5 (case B) shows the same simulation with one level of nested simulations allowed. The decision process of nested simulations is shown here as purple rectangles and the solution found is shown in a text label.

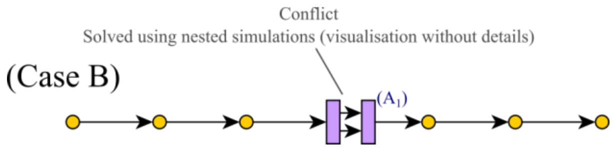

Figure 5: Conflict solved using nested simulations (B)

Figure 6 (case C) extends the previous representation to indicate solution variants that are evaluated by nested simulation. In this illustration, however, the details of the progress of the individual replications of nested simulation variants are omitted.
Figure. 6 (case D) adds a detailed view of each replication in nested simulations. In this representation, the progress of all nested replications is conflict-free and there is no subsequent nested conflict.
Figure 6 (case E) alternates the previous simulation and expands it with possible conflict situations within nested replications. Nested simulations are not allowed to be used as a solution for nested conflicts, but apply the priority planning method. This representation contains all the simulation details that were triggered with the maximum nesting level of 1.
Figure 6 (case F) is based on simulation case E and increases the maximum nesting level to 2. The original nested conflicts are not resolved by priority planning, but by nested simulations.
Figure 6 (case G) completes a detailed view of solving one selected nested conflict. Furthermore, the states and parts of the simulation are highlighted in green, orange, or red. The green colour is used for states that can be skipped (known states from the previous level of simulation; skip is possible to the last state in the green field). These states were already evaluated using a lower nesting level and they are identical to states in the new simulation (with higher nesting level). Orange states are new and related to a higher nesting level. These states need to be newly calculated; data is not available. The red-highlighted states represent changes from the previous simulation. The changes occurred due to the selection of a different solution (variant) to a conflict. These states need to be recalculated, and the corresponding data from the previous simulation cannot be used.
The example shows several possible situations that may occur during the simulation. If the new nesting level provides the same solution as the previous level of simulations - it is possible to effectively skip the following simulation states until the next conflict. Conflicts that have resulted in an alternative solution (as opposed to the previous one) will cause a different state to be created, and therefore the subsequent simulation states needs to be "calculated again". There is also a situation where alternative solutions have occurred within the conflict, but the original (external) solution is the same as in the previous simulation. Therefore, it is not true that the first change in the simulation would prevent further use of data from the previous level of simulation.

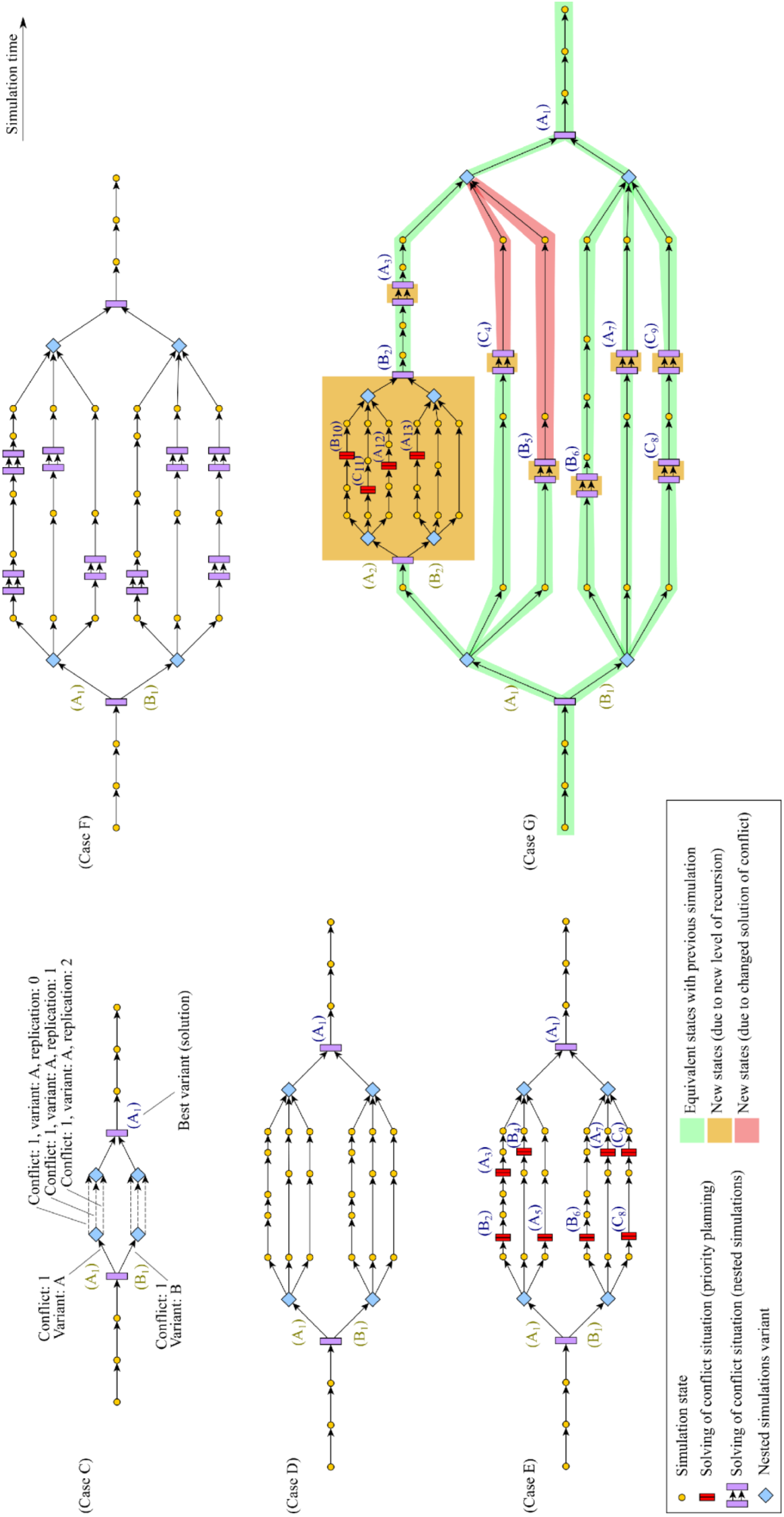

Figure 6: Exact optimization algorithm progress

4.1. Algorithm

To implement the above procedure, it is necessary to change the original *simulation* function. It will now detect possible skips of the already solved states.

```
function simulation(s):
ps := loadPreviousSimulationStates(s)
while s.isNotEnd():
    if ps.isStateCompatible(s):
        state := ps.getStateForNextConflict()
        jumpToState(s, state)
    else:
        e := s.nextEvent()
        s.processEvent(e)

    if s.isConflictOccured():
        solution := solveConflict(s, s.getConflict())
        s.applySolution(solution)

    s.saveState()
```

4.2. Criteria for evaluating results

In order to determine whether this procedure is worthwhile, it is necessary to record the details of the nested simulation calculation progress - the consumed machine time and information about the individual decisions made in nested simulations.

4.2.1. Assessment of the decision-making process

As a first criterion for evaluating this process, it is possible to express the percentage of conflict situations that can be accelerated by this process. That is, to identify the last identical conflict state and to express the value of the ratio of identical conflicts between two calculations of nested simulations.

This criterion is very easy to calculate, but it does not provide a relevant metric for evaluating the actual impact on the required machine time for calculations.

4.2.2. Assesment of time savings

The time-saving criterion is based on the logic of the previous criterion. The criterion is not expressed by the relative number of conflicting states, but by the machine time needed to calculate simulation. Its value corresponds to the actual machine time that can be saved by remembering the previous level of simulations.

4.2.3. Assesment of memory requirements

Nested simulations represent a complex computational task whose computational demands grow exponentially (due to specific parameters). In order to make the simulation faster, it is necessary to remember the state of simulation in all conflicting states in all simulations (not only in the main simulation but also in all nested simulations). The criterion expresses the memory demand for one simulation, respectively the expected memory demands of all simulations. To effectively implement this method, it is necessary to have an external memory (with fast access) with the expected capacity (ideally operating memory, SSD, fast RAID array).

5. HEURISTIC METHOD FOR MERGING IDENTICAL REPLICATIONS

The *createReplications* algorithm method outlines how to create nested replications for each variant. For each variant, there are *ReplCount* simulations that differ by the default random number generator seed.

Heuristic for merging identical replications is based on the capability of prediction that the progress of two selected nested replications will be identical. If the match of two replications can be evaluated in advance, it may be decided to calculate only one replication.

Depending on the particular method of using this heuristic, it is possible to obtain a result whose quality is the same as the original procedure of nested simulations. This is possible when heuristics are used only at a particular level of nested simulations where no further recursion is allowed.

By using a heuristic at all nesting levels, the accuracy of the results can be reduced, and so decision-making process results in suboptimal solutions. In a situation where a conflicting state occurs in a nested simulation and at least one more level of recursion is allowed, using a heuristic may result in a suboptimal solution. Without a heuristic, each replication calculates the nested conflict using a new set of simulations (with different seeds of pseudo-random number generators). The use of a heuristic, limits the nested conflict solution to only one nested calculation and does not examine the complete original set of states.

Figure 7 shows an example of using that heuristic method. Here, the heuristic can be used to merge 2 replications for variant A_1 and 2 replications for variant B_1.

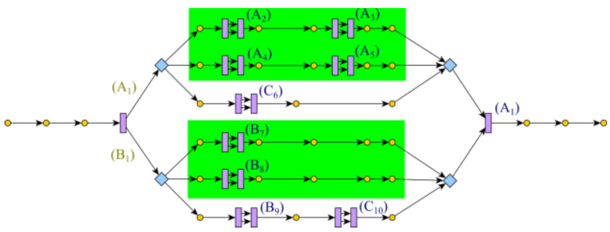

Figure 7: Example of possible replications merge

You can apply this method by modifying the original *createReplications* function:

```
function createReplications(variants, seeds):
simulations = {}
for variant in variants:
    for seed in seeds:
        s := createSimulation(baseSimulation, variant,
            seed)
        if (ss := existSimilarSimulation(s,
           simulations[variant]):
            increment weight simulations[variant][ss]
            delete s
        else:
            append s to simulations[variant]

return simulations
```

In a case study - a train station simulator - it is possible to detect the replication match in a relatively simple way. The nested simulation lookahead (run time) is defined by a constant. Two replications will be the same if the random events during the lookahead are the same. In this case, there is only one stochastic event "train arrival to simulation". It is enough to compare scheduled train arrivals between both replications to evaluate the match.

6. HEURISTIC METHOD FOR SOLVING SUBSEQUENT CONFLICTS

Typically, conflicts that occur during nested simulations (i.e. not in the main simulation), later may emerge in the main simulation (in general in a higher hierarchical level of simulation). This frequently leads to multiple calculations of the same conflict situations (see figure 8). A heuristic allows using results of these conflicts to immediately resolve future (identical) conflicts.

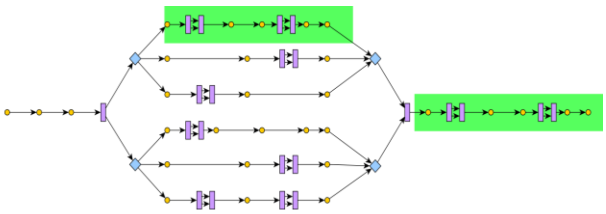

Figure 8: Example of subsequent conflicts

The heuristic can be applied by modifying the original *solveConflict* function:

```
function solveConflict(s, c):
if hasSatisfactoryPreviousSolution(s, c):
    return solveUsingPreviousSolution(s, c)

if simulation.recursionLevel <= REC_LIMIT:
    solution := solveUsingNestedSimulations(s, c)
    saveSolutionDetails(solution, s, c)
    return solution
else:
    return solveUsingAlternativeMethod(s, c)
```

The application of the heuristic is determined by a parameter which defines whether the previous result was calculated in sufficient quality and consequently it can be applied. As an example to select a criterion, the number of recursive levels of nested simulations can be specified. The previous conflict solution will be considered acceptable if the conflict has been solved with at least one nesting level. Thus, if the nested conflicts were allowed to be solved by nested simulations when dealing with a conflict, then previous conflict solution is usable. If nested conflicts were dealt with only by an alternative approach (priority planning), the new conflict would be solved in a standard way, and heuristics would not be applied.

7. TEST SCENARIO

For the purpose of conducting the initial case study (Diviš and Kavička 2017), the infrastructure of a smaller scale prototype railway station with several adjacent track sections (ending with simplified railway station models) was created. In particular, the operation of passenger services and a smaller range of freight transport are expected to take place at the station. In the case study, the behaviour of the station was tested at the arrival of delayed trains. For each train, alternative train paths were defined that use alternate station tracks.

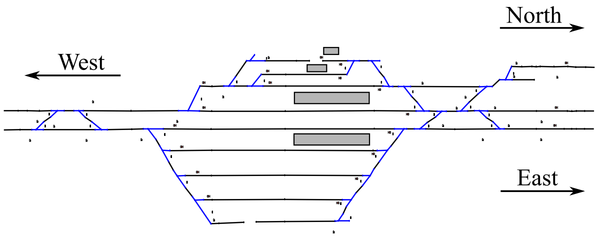

Figure 9: Schematic representation of central station and adjacent tracks

The representation of the main (central) station and the adjacent lines is shown in figure 9. There are two double-track lines (to the stations *West* and *East*) and one single-track line (to the station *North*) leading from the central station. The total distance between the eastern and western stations is about 20 km. The infrastructure is not completely fictional; it is inspired by several railway tracks and stations in the Czech Republic. The track profile contains sections with significant slope and arc ratios.
The simulation study focuses on the station traffic in a two-hour peak period. Passenger and freight trains are included, with the emphasis placed on passenger transport. Passenger transport is divided into two groups: (a) long distance transport - express trains; (b) regional transport - passenger trains. The traffic overview is shown in table 1. Figure 10 shows the occupation of station tracks in the central station under the conditions of deterministic simulation.
In the case study nested simulations are used as decision support. Its task is to select a replacement track for

Table 1: Parameterization of trains in the simulation model

Train type	Locomotive / vagons	Course	Interval between trains [h:mm:ss]	Total train count	Delay prob.	Delay mean time (exponential distribution) [s]
Express	1 / 7	West → Central → East	30:00	5	50 %	420
Express	1 / 7	East → Central → West	30:00	5	50 %	420
Passenger	2 / 4	West → Central → East	10:00	12	33 %	270
Passenger	2 / 4	East → Central → West	10:00	12	33 %	270
Passenger	1 / 2	West → Central → North	30:00	4	33 %	270
Passenger	1 / 2	North → Central → West	30:00	4	33 %	270
Cargo	1 / 22	West → East	1:00:00	2	50 %	1800
Cargo	1 / 22	East → West	1:00:00	2	50 %	1800

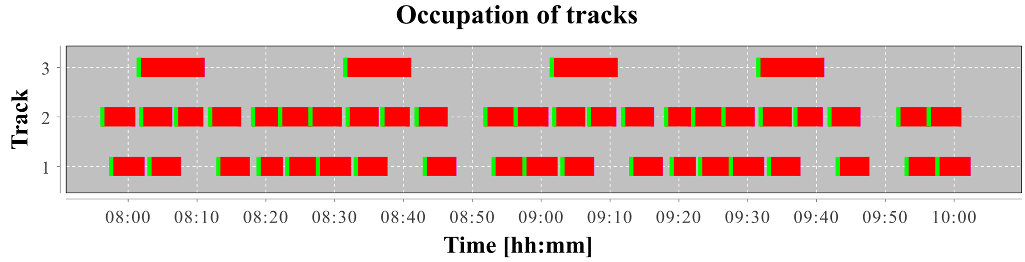

Figure 10: Occupation of station tracks during deterministic simulation

Delayed train, for which originally planned track is occupied.
In the case study, various parameterizations of nested simulations were tested and obtained results were compared. Basic parameterization of nested simulations:

- CrOpt – average weighted increment of train delays
  - weight is defined by a type (priority) of the train,
  - delay increment – the value is defined as the nonnegative portion of the train delay difference when leaving the simulation model minus train's input delay
- *CrOptComparer* – minimum function,
- *ScnCount* – without restriction,
- *ScnGen* – according to the available train paths,
- *ReplPreserveOriginal* – yes,
- *ReplResultsAggregateFunction* – average function,
- *RecStopCondBehaviour* – extension of the simulation time,
- *RecOnLimitAction* – usage of *priority planning* for conflict resolution,
- *FallbackScenarioConflictLimiter* – 15 s.

Varied parameters according to configuration:

- *StopCond* – 5, 15, 30 minutes,
- *ReplCount* – 3, 5 replications
- *RecLimit* – 0, 1, 2 levels of recursion.

For each test configuration was calculated 100 replications of main simulation.

8. SIMULATION RESULTS

Methods were evaluated based on detailed log files from full simulation runs. All methods were evaluated independently, one heuristic method at a time. Complex interactions between methods were not considered and evaluated.
Results are presented in ratio of simulations that are needed to process with heuristics with comparison to simulation without heuristics. Thus, results with lower values are better.

8.1. Exact optimization method

Because exact optimization algorithm is based on fact that you can skip parts of simulations from previous level of recursion, we evaluated effects on level 2 of recursion with information from level 1. From previous simulations, we found out that there is biggest increase in computational difficulty on level 2.
Unfortunately, exact optimization algorithm was evaluated as the worst method. Due to exponential growth of nested simulations, this method is able to save only up to 2 % of all necessary simulations. Method is also highly computationally expensive and requires nontrivial amount of memory. From these first trials this method couldn't be recommended to use.

Results are shown in picture 11. Detail of an analysis of a single replication is shown on picture 12.

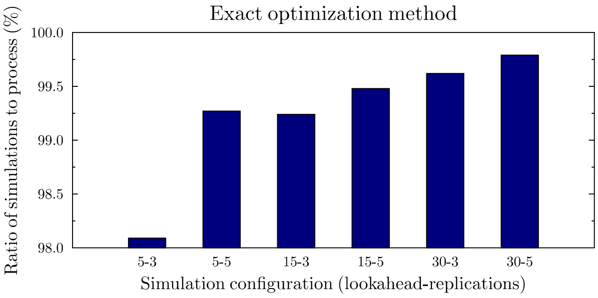

Figure 11: Results of exact optimization algorithm

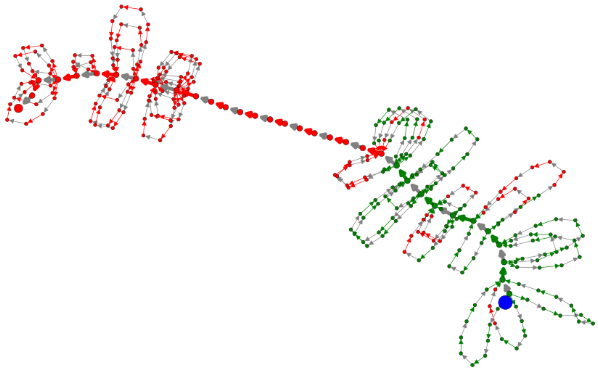
Figure 12: Detail of an analysis of a single replication – lookahead 15 mins, 3 replications, rep. no 38 – visualization shows state chart of the specific replication, blue circle represents starting state of a simulation, simulation of green states used exact algorithm optimization, red states must be recalculated due to state change in simulation

8.2. Heuristics - merging identical replications

Heuristics based on merging of identical replications appears to be very effective. With 5 minute lookahead it eliminated up to 60 % of all simulations, worst result of this method saved 25 % of simulations. With longer lookaheads effectivity of method decreased. With 30 minutes of lookahead it was able to eliminate up to 20 % of simulations.

Method was used and evaluated with 2 different approaches - (a) merging can be performed at all levels of recursion, (b) merging of replications can be performed only at leaf level of recursion. Method (b) should not negatively affect quality of results. Results are shown on picture 13 (method (b) is marked with 'L').

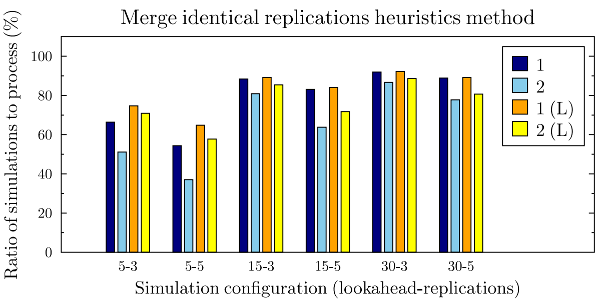

Figure 13: Results of merge identical replications heuristics with different levels of recursion allowed

8.3. Heuristics – solving subsequent conflicts

Heuristics based on solving of subsequent conflicts also appears to be highly effective. It constantly is able to eliminate about 40 % of simulations. Unfortunately, this heuristics method will result in suboptimal solutions. In evaluated scenario it appears that subsequent conflicts result to different solution in 20 % of times. Results of the method and ratio of matched solutions in subsequent conflicts is shown in picture 14.

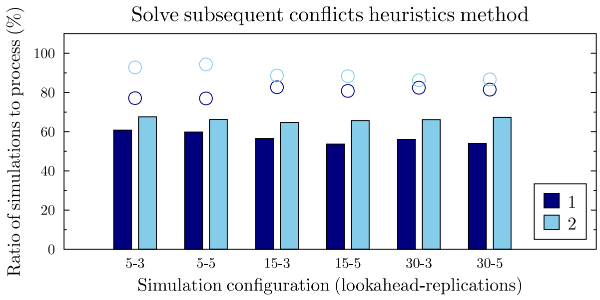

Figure 14: Results of solve subsequent conflicts heuristics with different levels of recursion allowed (bar charts shows actual results, circles show ratio of matched solution)

8.4. Comparison of methods

Results of rough comparison of all proposed methods are presented in picture 15. Numeric results of average value of necessary simulations are presented in table 2.

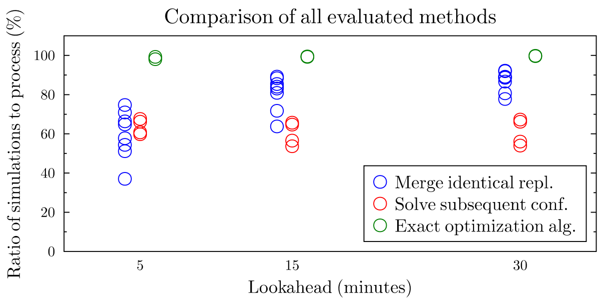

Figure 15: Comparison of all proposed methods

Table 2: Average number of simulations needed to process simulations with usage of specific method

Look-ahead	Repli-cations	Exact opt. alg.	Merge identical	Solve subsequent
5	3	98.1%	65.8%	64.2%
	5	99.3%	53.5%	63.0%
15	3	99.2%	86.0%	60.6%
	5	99.5%	75.7%	59.7%
30	3	99.6%	89.9%	61.1%
	5	99.8%	84.1%	60.7%

9. CONCLUSION

Results shown big differences between proposed methods. The exact optimization algorithm appears to be highly ineffective due to exponential growth of new simulations needed to process in new level of recursion. High complexity of the algorithm, overhead, low effectivity and memory demands rule out this method from real world usage.

Other two heuristics methods appear to be quite usable and results in saving up to 40 % of necessary simulations. Unfortunately, quality of results may decrease due to application of these methods. There are few possibilities how to apply these methods to maintain same quality of results. But extended study of interactions between these methods and how results will be affected, remains as a task to further studies.

ACKNOWLEDGMENTS

The work was supported from ERDF/ESF *Cooperation in Applied Research between the Univ. of Pardubice and companies, in the Field of Positioning, Detection and Simulation Technology for Transport Systems - PosiTrans* (CZ.02.1.01/0.0/0.0/17_049/0008394).

REFERENCES

Bonté B., Duboz R., Quesnel G., Muller J. P., 2009. Recursive simulation and experimental frame for multiscale simulation. In: Proceedings of the 2009 Summer Computer Simulation Conference, 164-172. July 13-16, Istanbul, Turkey.

Diviš R., Kavička A, 2015. Design and development of a mesoscopic simulator specialized in investigating capacities of railway nodes. Proceedings of the European Modeling and Simulation Symposium, 52-57. September 21-23, Bergeggi, Italy.

Diviš R., Kavička A, 2016. The method of nested simulations supporting decision-making process within a mesoscopic railway simulator. Proceedings of the European Modeling and Simulation Symposium, 100-106. September 26-28, Larnaca, Cyprus.

Diviš R., Kavička A, 2018. Complex nested simulations within simulators reflecting railway traffic. Proceedings of the European Modeling and Simulation Symposium, 178-186. September 17-19, Budapest, Hungary.

Gilmer J. B., Sullivan F. J., 1999. Multitrajectory simulation performance for varying scenario sizes [combat simulation]. In: WSC'99. 1999 Winter Simulation Conference Proceedings. 'Simulation - A Bridge to the Future' (Cat. No.99CH37038), 1137-1146. December 5-8, Phoenix, AZ, USA.

Gordy M. B., Juneja S., 2010. Nested Simulation in Protfolio Risk Measurement. Management Science 56:1833-1848.

Hill J. M. D., Surdu J. R., Ragsdale D. J., Schafer J. H., 2000. Anticipatory planning in information operations. In: SMC 2000 Conference Proceedings. 2000 IEEE International Conference on Systems, Man and Cybernetics. 'Cybernetics Evolving to Systems, Humans, Organizations, and their Complex Interactions' (Cat. No.00CH37166), 2350-2355. October 8-11, Nashville, Tennessee, USA.

Kindler E., 2010. Nested Models Implemented in Nested Theories. In: Proceedings of the 12th WSEAS International Conference on Automatic Control, Modelling & Simulation, 150-159. May 29-31, Catania, Sicily, Italy.

MODEL SELECTION METHOD FOR EFFICIENT SIGNALS PROCESSING FROM DISCRETE DATA

Evgeny A. Pchelintsev[(a)], Serguei M. Pergamenshchikov[(b)]

[(a),(b)] International Laboratory of Statistics of Stochastic Processes and Quantitative Finance, Tomsk State University, 36 Lenin Avenue, Tomsk, Russia
[(b)]Laboratory of Mathematics Raphael Salem, University of Rouen Normandy, 12 Avenue de l'Universite, Saint Etienne du Rouvray, France

[(a)]evgen-pch@yandex.ru, [(b)]serge.pergamenchtchikov@univ-rouen.fr

ABSTRACT
The paper considers the problem of robust adaptive efficient estimating of a periodic signal modeled by a continuous time regression model with the dependent noises given by a non-Gaussian Ornstein-Uhlenbeck process with Levy subordinator in the case when continuous observation cannot be provided and only discrete time measurements are available. Adaptive model selection procedure, based on the improved weighted least square estimates, is proposed. Under some conditions on the noise distribution, sharp oracle inequality for the robust risk has been proved and the robust efficiency of the model selection procedure has been established. The numerical analysis results are given.

Keywords: periodic signals, model selection, improved weighted least squares estimates, non-parametric regression, Ornstein-Uhlenbeck process, robust quadratic risk, sharp oracle inequality, asymptotic efficiency

1. INTRODUCTION

In problems of signal processing in the information-communication complexes they successfully use the continuous time models specified by stochastic differential equations

$$dy_t = S(t)\,dt + d\xi_t, \quad 0 \le t \le n, \tag{1}$$

where $S(t)$ is an unknown 1-periodic signal, n is the duration of observation and $(\xi_t)_{0\le t\le n}$ is unobserved colour noise. The development of the identification procedures is most often based on the assumption that the noises in the equations are specified by the Brownian motion processes, i.e. we obtain the well-known "signal+white noise" model which is very popular in statistical radio-physics (see, for example, Ibragimov and Khasminskii 1981; Kassam 1988; Chernoyarov et al. 2015 and etc.). If the noise disturbances acting on the dynamic system are non-Gaussian and include, for example, some pulse component, then the efficiency of identification algorithms may decrease. Therefore, on the condition that the noise disturbances have more complicated nature, the properties of the decision procedures need an additional investigation. This paper considers the problem of estimating the signal S in the continuous time regression from the Equation (1) with the noises of pulse type, specified by a non-Gaussian Ornstein-Uhlenbeck process which obeys the equations

$$\begin{aligned} d\xi_t &= a\xi_t\,dt + du_t, \\ u_t &= \tilde{n}_1 w_t + \tilde{n}_2 z_t \quad \text{and} \quad z_t = x*(\mu-\tilde{\mu})_t, \end{aligned} \tag{2}$$

where a, $\tilde{n}_1$ and $\tilde{n}_2$ are some unknown constants, $(w_t)_{t\ge0}$ is a standard Brownian motion, $\mu(ds\,dx)$ is a jump measure with deterministic compensator $\tilde{\mu}(ds\,dx) = ds\,\Pi(dx)$, $\Pi(\cdot)$ is a Levy measure, i.e. some positive measure on $R_* = R\backslash\{0\}$ such that $\Pi(x^2)=1$ and $\Pi(x^6)<\infty$. Here we use the notation $\Pi(|x|^m) = \int_{R_*}|y|^m\,\Pi(dy)$. Note that the Levy measure $\Pi(R_*)$ could be equal to $+\infty$. We use the notation * for the stochastic integrals with respect to random measures (see Cont and Tankov 2004, Chs. 2 and 3), i.e.

$$x*(\mu-\tilde{\mu})_t = \int_0^t\int_{R_*} y(\mu-\tilde{\mu})(ds,dy). \tag{3}$$

It should be noted that if a=0, then we obtain the Levy regression model considered in (Pchelintsev, Pchelintsev, and Pergamenshchikov 2018). In the case when $\Pi(\cdot)=0$ we obtain the well-known Gaussian Ornstein-Uhlenbeck regression model introduced in (Hopfner and Kutoyants 2009, 2010). The model in the Equations (1) – (2) in which the jump process $(z_t)_{t\ge0}$ defined by the compound Poisson process was studied in (Konev and Pergamenshchikov 2012, 2015). However, the compound Poisson processes can describe only the large noise impulses of small fixed frequency, but the telecommunication and location systems may have the impulse noises with any frequency without any condition. We note also that in the papers (Konev and Pergamenshchikov 2012, 2015) the proposed statistical procedures are based on the classical weighted least square estimators.

The problem is to estimate the unknown signal S in the model (1) on the basis of incomplete observations $(y_{t_j})_{0\le j\le np}$, $t_j=j/p$ and $p>2$ is an odd number depending on n.

The goal of this paper is to develop a new improved adaptive robust efficient signal estimation methods for the non-Gaussian Ornstein-Uhlenbeck noise based on the general Levy processes with unknown distribution Q. We assume that this distribution belongs to the class Q_n^* defined as a family of all these distributions for which the parameters satisfy the inequalities $-a_* \le a < 0$, $\tilde{n}_1 \ge \varsigma_*$ and $\tilde{n}_1^2 + \tilde{n}_2^2 \le \varsigma^*$ with some fixed positive bounds. The quality of an estimate $\hat{S}_n$ of the unknown signal S, i.e. some function of $(y_{t_j})_{0\le j\le np}$, will be measured with the robust quadratic risk

$$\mathrm{R}^*\left(\hat{S}_n, S\right) = \sup_{Q\in Q_n^*} \mathrm{R}_Q\left(\hat{S}_n, S\right), \tag{4}$$

where

$$\mathrm{R}_Q\left(\hat{S}_n, S\right) := \mathbf{E}_{Q,S}\left\|\hat{S}_n - S\right\|^2 \quad \text{and} \quad \|S\|^2 = \int_0^1 S^2(t)\,dt. \tag{5}$$

Here $\mathbf{E}_{Q,S}$ is the expectation with respect to the distribution $\mathbf{P}_{Q,S}$ of the process in the Equation (1) with a fixed distribution Q of the noise $(\xi_t)_{0\le t\le n}$ and a given function S.

2. IMPROVED ESTIMATES

One of the most customarily used methods in the identification theory is the least squares one (LSE). However we can improve (as compared with LSE) the estimation precision using of Stein approach (Stein 1981). This approach to the estimation in the regression models has been developed in (Fourdrinier and Pergamenshchikov 2010, Konev and Pergamenshchikov 2010). At that the gaussianity or spherical symmetricity of distribution of the process under observation plays a key role. In this paper we show that the Stein approach can be used to improve the quality of signal processing observed in the transmission channel with the dependent pulse type noises defined by non-Gaussian Ornstein-Uhlenbeck processes with unknown correlation properties. For this we need to use the modifications of the James – Stein estimators proposed in (Pchelintsev 2013, Konev, Pergamenshchikov, and Pchelintsev 2014) for parametric estimation problems.

For estimating the unknown signal S in the Equation (1) we consider it's Fourier expansion. Let $(\phi_j)_{j\ge1}$ be a trigonometric basis in $\mathbf{L}_2[0,1]$. We extend these functions by the periodic way on R, i.e. $\phi_j(t) = \phi_j(t+1)$ for any $t\in R$. We will use such basis that the restrictions of the functions $\{\phi_j\}_{1\le j\le p}$ on the sampling lattice $T_p=\{t_1,\ldots,t_p\}$, $t_j=j/p$, form an orthonormal basis in the Hilbert space R^{T_p} with the inner product

$$(x,y)_p = \frac{1}{p}\sum_{j=1}^p x(t_j)y(t_j) \text{ for } x,y\in R^{T_p}, \tag{6}$$

i.e. $(\phi_i,\phi_j)_p = 1_{\{i=j\}}$ for any odd $p\ge3$, 1_A is the indicator of the set A. We write the discrete Fourier expansion of the unknown signal S on the lattice T_p in the form

$$S(t) = \sum_{j=1}^p \theta_{j,p}\phi_j(t) \text{ and } \theta_{j,p} = \left(S,\phi_j\right)_p. \tag{7}$$

The first step in estimation procedure consists in estimating the Fourier coefficients $\theta_{j,p}$ from discrete data by the formulae

$$\hat{\theta}_{j,p} = \frac{1}{n}\int_0^n \psi_{j,p}(t)dy_t \text{ with } \psi_{j,p} = \sum_{k=1}^{np}\phi_j(t_k)1_{\{t_{k-1}<t\le t_k\}}. \tag{8}$$

Further, for the first $d\le p$ Fourier coefficients in Equations (7) we use the improved estimation method proposed for parametric models in (Pchelintsev 2013, Konev, Pergamenshchikov, and Pchelintsev 2014). To this end we set $\tilde{\theta}_p = \left(\hat{\theta}_{j,p}\right)_{1\le j\le d}$. In the sequel, we will use the norm $|x|_d^2 = \sum_{j=1}^d x_j^2$ for any vector $x=\left(x_j\right)_{1\le j\le d}$ from R^d. We define the shrinkage estimators as

$$\theta^*_{j,p} = \left(1-g(j)\right)\hat{\theta}_{j,p}, \tag{9}$$

where $g(j) = \frac{c_n}{\left|\tilde{\theta}_p\right|_d}1_{\{1\le j\le d\}}$, c_n is some known parameter such that $c_n \approx d/n$ as $n\to\infty$ (Pchelintsev and Pergamenshchikov 2019). Now we introduce a class of shrinkage weighted least squares estimates for S as

$$S^*_\gamma(t) = \sum_{j=1}^p \gamma(j)\theta^*_{j,p}\psi_{j,p}(t), \tag{10}$$

where the weights $\gamma \in R^n$ belong to some finite set Γ from $[0,1]^p$ defined in (Konev and Pergamenshchikov 2015, Pchelintsev and Pergamenshchikov 2018).

To compare the non-asymptotic accuracy of the proposed shrinkage estimate in Equations (10) and LSE $\hat{S}_\gamma(t)$ from (Konev and Pergamenshchikov 2015, Equation (3.10)) we denote the difference of their quadratic risks as $\Delta_Q(S) := \mathrm{R}_Q(S^*_\gamma, S) - \mathrm{R}_Q(\hat{S}_\gamma, S)$. Now for this deviation, we obtain the following result.

Theorem 1. For any $p > \sqrt{d}\log n / c_n$ and r>0

$$\sup_{Q\in\mathcal{Q}_n}\sup_{\|S\|\le r} \Delta_Q(S) < 0\,. \tag{11}$$

The inequality in Equation (11) means that non-asymptotically, i.e. for any $n \ge n_0$ the estimate in the Equation (10) outperforms in mean square accuracy the LSE.

3. MODEL SELECTION METHOD AND ORACLE INEQUALITY

The model selection procedure for estimating an unknown signal S in the Equation (1) will be constructed on the basis of a family of improved estimates $(S^*_\gamma)_{\gamma\in\Gamma}$. The performance of any estimate S^*_γ will be measured by the empirical squared error

$$\mathrm{Err}_p(\gamma) = \left\|S^*_\gamma - S\right\|^2 . \tag{12}$$

In order to obtain a good estimate, we have to write a rule to choose a weight vector $\gamma \in \Gamma$ in the Equation (10). It is obvious, that the best way is to minimize the empirical squared error with respect to γ. Making use the estimate definition in the Equation (10) and the Fourier transformation of *S* implies

$$\mathrm{Err}_p(\gamma) = \sum_{j=1}^{p} \gamma^2(j)\left(\theta^*_{j,p}\right)^2 - 2\sum_{j=1}^{p}\gamma(j)\theta^*_{j,p}\bar{\theta}_{j,p} + \|S\|^2 , \tag{13}$$

where $\left(\bar{\theta}_{j,p}\right)_{j\ge1}$ are the Fourier coefficients for the signal *S* with respect to the orthonormal system of the functions $\{\psi_{j,p}\}_{1\le j\le p}$. Since these coefficients are unknown, the weight coefficients $\left(\gamma_j\right)_{j\ge1}$ cannot be found by minimizing $\mathrm{Err}_p(\gamma)$. To circumvent this difficulty one needs to replace the terms $\theta^*_{j,p}\bar{\theta}_{j,p}$ by their estimators of the form

$$\tilde{\vartheta}_{j,p} = \theta^*_{j,p}\hat{\theta}_{j,p} - \frac{\hat{\sigma}_n}{n} , \tag{14}$$

where $\hat{\sigma}_n$ is the estimate for the noise variance $\sigma_Q = \mathbf{E}_Q \xi^2_{j,n}$ which we choose in the following form

$$\hat{\sigma}_n = \sum_{j=[\sqrt{n}]+1}^{n} \hat{t}^2_{j,n} \quad \text{and} \quad \hat{t}_{j,n} = \frac{1}{n}\int_0^n \phi_j(t)\, dy_t \;. \tag{15}$$

For this change in the empirical squared error, one has to pay some penalty. Thus, one comes to the cost function of the form

$$J_p(\gamma) = \sum_{j=1}^{p}\gamma^2(j)\left(\theta^*_{j,p}\right)^2 - 2\sum_{j=1}^{p}\gamma(j)\tilde{\vartheta}_{j,p} + \delta\hat{P}(\gamma), \tag{16}$$

where δ is some positive constant, $\hat{P}(\gamma)$ is the penalty term defined as

$$\hat{P}(\gamma) = \frac{\hat{\sigma}_n |\gamma|^2_p}{n} \;. \tag{17}$$

Substituting the weight coefficients, minimizing the cost function

$$\gamma^* = \mathrm{agrmin}_{\gamma\in\Gamma} J_p(\gamma) \tag{18}$$

in the Equation (10) leads to the improved model selection procedure

$$S^* = S^*_{\gamma^*} . \tag{19}$$

It will be noted that γ^* exists because Γ is a finite set. If the minimizing sequence in the Equation (18) γ^* is not unique, one can take any minimizer.

In the case, when the value of σ_Q is known, one can take $\hat{\sigma}_n = \sigma_Q$ and $P(\gamma) = \sigma_Q |\gamma|^2_p n^{-1}$.

Theorem 2. For any $n \ge 2$ and $0 < \delta < 1/2$, the robust risks defined in the Equation (4) of estimate in the Equation (19) for continuously differentiable function S satisfies the oracle inequality

$$\mathrm{R}^*\left(S^*, S\right) \le \frac{1+5\delta}{1-\delta}\min_{\gamma\in\Gamma} \mathrm{R}^*\left(S^*_\gamma, S\right) + \frac{B^*_n}{n\delta}, \tag{20}$$

where the term B^*_n is independent of S and such that $B^*_n n^{-\varepsilon} \to 0$ as $n \to \infty$ for any $\varepsilon > 0$.

The inequality (20) allows us to establish that the procedure in the Equation (19) is optimal in the oracle inequalities sense. This property enables to provide asymptotic efficiency in the adaptive setting, i.e. when information about the signal regularity is unknown.

4. MONTE CARLO SIMULATIONS

In this section we report the results of a Monte Carlo experiment to assess the performance of the proposed model selection procedure in the Equation (19). In the Equation (1) we choose 1-periodic signal S which is defined as $S(t) = t\sin(2\pi t) + t^2(1-t)\cos(2\pi t)$, for $0 \le t \le 1$. We simulate the Equation (1) with the Ornstein-Uhlenbeck noise process defined as

$$d\xi_t = -\xi_t dt + 0.5 dw_t + 0.5 dz_t \,, \qquad (21)$$

where $z_t = \sum_{j=1}^{N_t} Y_j$ N_t is a Poisson process with the intensity λ=1 and $(Y_j)_{j\geq 1}$ is i.i.d. Gaussian (0,1). We use the model selection procedure defined in the Equation (19) with the weights proposed in (Konev and Pergamenshchikov 2015): $k^* = 100 + \sqrt{\ln n}$, $\varepsilon = 1/\ln n$ and $m = [1/\varepsilon^2]$. We used the cost function with $\delta = (3 + \ln n)^{-2}$. We define the empirical risk as $\overline{R}(\tilde{S}, S) = \frac{1}{p}\sum_{j=1}^{p} \hat{\mathbf{E}}\left(\tilde{S}_n(t_j) - S(t_j)\right)^2$ and $\hat{\mathbf{E}}\left(\tilde{S}_n(\cdot) - S(\cdot)\right)^2 = \frac{1}{N}\sum_{l=1}^{N}\left(\tilde{S}_n^l(\cdot) - S(\cdot)\right)^2$ with the frequency of observations p=100001 and numbers of replications N=1000.

Table 1 gives the values for the sample risks of the improved estimate Equation (19) and the model selection procedure based on the weighted LSE from (Konev and Pergamenshchikov 2015) for different numbers of observation period n. Table 2 gives the values for the sample risks of the model selection procedure based on the weighted LSE from (Konev and Pergamenshchikov 2015) and it's improved version for different numbers of observation period n.

Table 1: The sample quadratic risks for different optimal γ

n	100	200	500	1000
$\overline{R}\left(S^*_{\gamma^*}, S\right)$	0.0289	0.0089	0.0021	0.0011
$\overline{R}\left(\hat{S}_{\hat{\gamma}}, S\right)$	0.0457	0.0216	0.0133	0.0098
$\frac{\overline{R}\left(\hat{S}_{\hat{\gamma}}, S\right)}{\overline{R}\left(S^*_{\gamma^*}, S\right)}$	1.6	2.4	6.3	8.9

From the Table 2 for the same weights γ with various observations numbers n we can conclude that theoretical result on the improvement effect is confirmed by the numerical simulations. Moreover, from Table 1 and Figure 1, we can see that the proposed method has the higher estimation quality then LSE.

On the figures the bold line is the signal S, the continuous line is the model selection procedure based on the least squares estimators $\hat{S}$ and the dashed line is the improved model selection procedure S^*.

Table 2: The sample quadratic risks for the same optimal $\hat{\gamma}$

n	100	200	500	1000
$\overline{R}\left(S^*_{\gamma^*}, S\right)$	0.0391	0.0159	0.0098	0.0066
$\overline{R}\left(\hat{S}_{\hat{\gamma}}, S\right)$	0.0457	0.0216	0.0133	0.0098
$\frac{\overline{R}\left(\hat{S}_{\hat{\gamma}}, S\right)}{\overline{R}\left(S^*_{\gamma^*}, S\right)}$	1.2	1.4	1.3	1.5

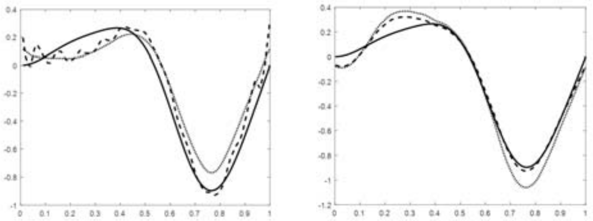

a) n=500 b) n=1000

Figure 1: Behavior of the regression function and its estimates

5. ASYMPTOTIC EFFICIENCY

We define the following functional Sobolev ball

$$W_{k,\mathbf{r}} = \left\{ f \in C_p^k[0,1] : \sum_{i=0}^{k} \left\| f^{(i)} \right\|^2 \le \mathbf{r} \right\}, \qquad (22)$$

where $\mathbf{r} > 0$ and $k \geq 1$ are some unknown parameters, $C_p^k[0,1]$ is the space of k times differentiable 1-periodic functions such that for any $0 \le i \le k-1$: $f^{(i)}(0) = f^{(i)}(1)$. In order to formulate our asymptotic results we set

$$v_n = \frac{n}{\varsigma^*},\; l_k(\mathbf{r}) = \left((2k+1)\mathbf{r}\right)^{1/(2k+1)} \left(\frac{k}{\pi(k+1)}\right)^{2k/(2k+1)} \qquad (23)$$

and we denote by Σ_n of all estimates $\hat{S}_n$ of S from discrete observations of the process in the Equation (1). Also we denote by Q^* the distribution of the process in the Equation (1) with $\xi_t = \varsigma^* w_t$, i.e. white noise model with the intensity ς^*.

Theorem 3. Assume that $Q^* \in Q_n^*$. Then the robust risk defined in the Equation (4) admits the following asymptotic lower bound

$$\liminf_{n\to\infty} \inf_{\hat{S}_n \in \Sigma_n} v_n^{2k/(2k+1)} \sup_{S \in W_{k,\mathbf{r}}} \mathrm{R}^*\left(\hat{S}_n, S\right) \ge l_k(\mathbf{r}) \,. \qquad (24)$$

This lower bound is sharp in the following sense.

Theorem 4. Assume that $Q^* \in Q_n^*$ and there exists $\varepsilon > 0$ such that $\lim_{n\to\infty} n^{5/6+\varepsilon}/p = 0$. Then the robust risk defined in the Equation (4) for the estimating procedure in the Equation (19) has the following asymptotic upper bound

$$\limsup_{n\to\infty} \nu_n^{2k/(2k+1)} \sup_{S\in W_{k,\mathbf{r}}} \mathrm{R}^*\left(S^*, S\right) \le l_k(\mathbf{r}) \ . \qquad (25)$$

Theorems 3 and 4 imply that the model selection procedure S^* is efficient and the parameter $l_k(\mathbf{r})$ defined in the Equations (23) is the Pinsker constant in this case (Pchelintsev and Pergamenshchikov 2018, 2019).

6. CONCLUSION

In this paper, we considered the problem of nonparametric signal processing on the basis of the discrete time observations with the dependent non-Gaussian impulse noises modelled by Ornstein-Uhlenbeck processes. We developed adaptive efficient statistical model selection procedure based on the improved methods which outperforms the LSE in mean square accuracy. The obtained theoretical results are confirmed by the numerical simulation. We obtained the adaptive efficiency property for the proposed statistical method, which means that we provide the best mean square accuracy without using the smoothness information about the form of unknown signal. We studied the accuracy properties for the proposed method on the basis of the robust approach, i.e. uniformly over all possible unknown noise distributions. This allows us to synthesize the statistical algorithms possessing the high noise immunity properties. The results (their satisfactory concordance with the corresponding experimental data) can be used for the estimation of the signals. Such problems are of a great importance in the fields of radio-and-hydroacoustic communications and positioning, radio-and-hydrolocation, etc. (see, for details, Chernoyarov, Kutoyants, and Marcokova 2018 and references therein).

ACKNOWLEDGMENTS

This work was supported by the RSF, research project no. 17-11-01049.

REFERENCES

Chernoyarov O.V., Vaculik M., Shirikyan A. and Salnikova A.V., 2015. Statistical Analysis of Fast Fluctuating Random Signals with Arbitrary - Function Envelope and Unknown Parameters. Communications - Scientific Letters of the University of Zilina, 17 (1a), 35-43.

Chernoyarov O.V., Kutoyants Yu. A. and Marcokova M., 2018. On frequency estimation for partially observed system with small noises in state and observation equations. Communications - Scientific Letters of the University of Zilina, 20 (1), 66-71.

Cont R. and Tankov P., 2004. Financial Modelling with Jump Processes. London: Chapman & Hall.

Fourdrinier D. and Pergamenshchikov S., 2010. Improved selection model method for the regression with dependent noise. Annals of the Institute of Statistical Mathematics, 59 (3), 435–464.

Hopfner R. and Kutoyants Yu.A., 2009. On LAN for parametrized continuous periodic signals in a time-inhomogeneous diffusion. Statistical Decisions, 27 (4), 309-326.

Hopfner R. and Kutoyants Yu.A., 2010. Estimating discontinuous periodic signals in a time-inhomogeneous diffusion. Statistical Inference for Stochastic Processes, 13 (3), 193-230.

Ibragimov I.A. and Khasminskii R.Z., 1981. Statistical Estimation: Asymptotic Theory. New York: Springer.

Kassam S.A., 1988. Signal Detection in Non-Gaussian Noise. New York: Springer.

Konev V.V. and Pergamenshchikov S.M., 2010. General model selection estimation of a periodic regression with a Gaussian noise. Annals of the Institute of Statistical Mathematics, 62, 1083–1111.

Konev V.V. and Pergamenshchikov S.M., 2012. Efficient robust nonparametric estimation in a semimartingale regression model. Annales de l'Institut Henri Poincare (B) Probability and Statistics, 48 (4), 1217-1244.

Konev V.V. and Pergamenshchikov S.M., 2015. Robust model selection for a semimartingale continuous time regression from discrete data. Stochastic Processes and their Applications, 125, 294-326.

Konev V., Pergamenshchikov S. and Pchelintsev E., 2014. Estimation of a regression with the pulse type noise from discrete data. Theory of Probability and Its Applications, 58 (3), 442-457.

Pchelintsev E., 2013. Improved estimation in a non-Gaussian parametric regression. Statistical Inference for Stochastic Processes, 16 (1), 15-28.

Pchelintsev E. and Pergamenshchikov S., 2018. Oracle inequalities for the stochastic differential equations. Statistical Inference for Stochastic Processes, 21 (2), 469–483.

Pchelintsev E. and Pergamenshchikov S., 2019. Improved model selection method for an adaptive estimation in semimartingale regression models. Tomsk State University Journal of Mathematics and Mechanics, 58, 14–31.

Pchelintsev E., Pchelintsev V. and Pergamenshchikov S., 2018. Non asymptotic sharp oracle inequalities for the improved model selection procedures for the adaptive nonparametric signal estimation problem. Communications - Scientific Letters of the University of Zilina, 20 (1), 72-76.

Stein C.M., 1981. Estimation of the mean of a multivariate normal distribution. Ann. Statist., 9 (6), 1135–1151.

AUTHORS BIOGRAPHY

Evgeny PCHELINTSEV was born in Almaty, Kazakhstan. He received his M.Sc. in Mathematics from Tomsk State University in 2009, Ph.D. in Applied Mathematics and Statistics from Tomsk State University and Rouen University in 2012. Since 2012 he worked as a teacher of mathematics at several mathematical departments at Tomsk State University. His research interests include statistical modelling and identification of stochastic dynamic systems, soft computing, and simulation

Serguei PERGAMENSHCHIKOV was born in Tomsk, Russia. He received his M.Sc. from Tomsk State University in 1980, Ph.D. in Probability Theory and statistics from Tomsk State University in 1986, Doctor of Sciences in Mathematics from Central Economics and Mathematics Institute of RAS in 1994. His research interests include statistical modelling and identification of stochastic dynamic systems, stochastic differential equations, optimization, and control.

SOFTWARE FRAMEWORKS FOR ARTIFICIAL INTELLIGENCE: COMPARSION OF LOW-LEVEL AND HIGH-LEVEL APPROACHES

Michael Bogner[a], Florian Weindl[b], Franz Wiesinger[c]

[a], [b], [c] University of Applied Sciences Upper Austria – Department of Embedded Systems Engineering
Softwarepark 11, A-4232 Hagenberg, Austria

[a]michael.bogner@gh-hagenberg.at, [b]florian.weindl@fh-hagenberg.at, [c] franz.wiesinger@fh-hagenberg.at

ABSTRACT
As nearly every artificial intelligence application is based on a framework, using the best fitting one for the task is key in developing an efficient solution quickly. Since there are two main types of frameworks, based on low and high abstraction level approaches, these two types will get compared and evaluated throughout this paper using Tensorflow and Keras as representatives. Key features of artificial intelligence frameworks for industrial applications are performance, expandability, abstraction level and therefore ease of use for rapid prototyping. All those features are major factors to keep development time and costs as low as possible, while maximizing product quality. To evaluate both approaches by these criteria a neural network classifying handwritten digits is implemented.

Keywords: tensorflow, keras, neural network, evaluation

1. INTRODUCTION

Since the middle of the 20^{th} century scientists have been trying to implement forms of artificial intelligence on computer systems. As time went by, those systems have grown from small programs to enormous applications. For each new application of artificial intelligence (AI) a specific neural network was designed and implemented, specifically tailored to the needs of the application. This had to be done since there had not been enough computing power and memory available to develop more general solutions.

Since implementing all basic functionalities each time from scratch is very time consuming and huge amounts of computing power became available year after year, artificial intelligence frameworks have been developed. These frameworks pack useful functionality and a basic environment into a reusable package, making development of bigger and better programs quicker and more convenient. Today nearly all AI applications are based on such software frameworks enabling high flexibility and performance all while keeping development time down to a minimum. Most of the time these generally very basic, reusable software packages are customizable to fit very specific and demanding tasks.

Since artificial intelligence and neural networks are widely used in many commercial products and industrial applications, the number of frameworks being available keeps growing. Based on this fact it is not that easy to choose a fitting framework for a specific task or product. If the wrong software is used, many problems may arise. Those problems may range from slower development and consequently to a longer time to market, to a complete project failure caused by major performance hits.

Some of these artificial intelligence frameworks stand out from the crowd because they are based on a very efficient concept or they are backed and continuously developed by concerns such as Google.

The goal of this paper is to compare the two basic concepts of artificial intelligence frameworks: high- and low-level approaches. Frameworks using a high-level approach do not clutter function interfaces and application programming interfaces (API) with unneeded parameters and details. By using such an approach implementation is done based on more abstract functionality and system blocks, which makes development fast and easier to begin with. Low-level frameworks on the other hand tend to give a very detailed and powerful API, enabling the developers and engineers to tweak and optimize every little setting and element of every component of the complete system. This ability enforces great flexibility and efficient applications but comes with costs of longer development times and more needed know-how of all processes in detail.

As representatives for high- and low-level approaches Tensorflow (Google Inc. 2019) and Keras (Keras Home 2019) have been selected, since both are very widely spread in the research community and in industrial environments as well.

Theano (Theano 2019) would have also been an available option as low-level framework. Based on the NumPy (NumPy 2019) library the software is able to translate all operations into efficient C programming language, enabling high performance.

Another solid choice for a high abstraction level framework would have been Caffe (Berkeley AI Research 2019) due to efficient grafics processing units (GPU) usage and abstract modularization.

The fact that Keras, as high-level framework, is based on Tensorflow ensures the opportunity to compare both frameworks against each other and is the main reason their selection.
For evaluating the performance, the abstraction levels and rapid-prototyping ability a neural network gets implemented using both frameworks and classifying handwritten digits of the MNIST dataset (LeCun Y.L. 1998). This prototype network will consist of 8 layers, transforming the 28- by 28-pixel sized images on its ways through the network and at the end predicting the result.

2. BASICS OF ARTIFICIAL INTELLIGENCE

The main goal of the specialist division of artificial engineers and scientists is to create a system which is capable of making decisions like a real human being would do. To keep the complexity of such systems at a still computable and achievable level an AI or neural network is engineered for one single, very specific application only. Such applications may be daily things such as “face-unlock” on smartphones or customer analytics on online platforms, like amazon.
To enable a computer system to perform such complex tasks they need to be taught and trained. This training phase is a mandatory step and can be done in a few different approaches. In this case supervised learning (Schmidhuber 2015) will be used, where all training data is connotated with the correct answer the system should give. The AI is fed with this dataset repeatedly until it is able to discover different patterns in the data to predict the correct answers for the given information. After each so-called batch, which represents a small subset of the training data, the network is given feedback on its answers, providing possibilities to change its internal parameters to improve its accuracy. Because the system is supervised and feedback is given throughout the complete training process, this method is called supervised learning.
After the network is trained to a sufficient level, which is determined by an error function or error rate, the AI is ready to be deployed on the final product. Training in the beginning plus setting up all different parameters and the datasets is quite time consuming and is therefore mostly done on specific hardware to accelerate these processes. If the network is smaller in most cases the training is done by one graphics processing unit (GPU). For larger scale applications the training phase is done on multiple GPUs or a server farm, sometimes even on cloud servers.

2.1. Neuronal Nets

In case of this prototype where handwritten digits will be classified, image patterns need to be found in the data. For this specific task neural networks (Lunze 2016) provide a perfect fit. Such networks consist of single neurons that try to mimic the functionality of real neurons in the human brain, both give a specific output, if its input connections are stimulated in a certain way. In case of a simulated neuron of a neuronal network these inputs and outputs are not limited in quantity, enabling the neuron to be connected to one or more neurons in its environment. Based on a specific mathematical function like sigmoid, also called the activation function of a neuron, the output is set in a specific way (Gershenson 2003).
The connections between different neurons transporting data from one neuron to another through the network are called edges. These edges may be simply used for transport between neurons, but most certainly will also introduce some weights on the data. By a multiplication with a variable factor the edge values are altered and therefore able to inhibit or constrain the transport of data to specific neurons. By varying those weights of every edge in the network the AI is adapting to given data and optimizing its error rate to a minimum and hence learning (Schmidhuber 2015).
To keep all neurons in a logical and clear order, a neural network consist of different layers, each representing a single functional group of neurons doing simple operations on the given data. A simple network for image recognition may for example involve an input layer, containing one neuron per image pixel, of many intermediate or hidden layers and an output layer, where each neuron is representing one possible outcome of the network. As the tasks of a network get more complex its layer count increases as well as the neuron count per layer, which quickly bursts the limit of network complexity and demonstrates why an AI should be developed for one single application.

2.2. Convolution

A specific type of neural network used in image recognition is called convolutional neural network (LeCun 1995), which uses the concept of convolution to extract features out of the given pictures.
Convolution is done by sliding a filter of a given size over the whole image and calculating the mean value of all pixels within the filter. The calculated value is then set as new pixel value for the next layer. This convolution layer is always paired with a pooling layer, summing up a small area around a pixel or just taking the maximum value and therefore reducing the size of the image. By convoluting and decreasing the image´s size, features and patterns get picked up by the network and overall performance is increased. The combination of a convoluting and a pooling layer is very common in image recognition and is often used more than once to decrease data size further and extract features.

3. METHODOLOGICAL APPROACH

In order to be able to objectively compare high- and low-level frameworks to each other to representatives have been chosen. Both frameworks are based on the same backend software which in this case is Tensorflow.
To compare performance, complexity, usability and rapid-prototyping abilities a prototype convolutional neural network gets implemented using both frameworks. The goal of this prototype is to be

demanding enough to show differences in compute performance but at the same time keep training times to a minimum and get a decent insight in working with the frameworks. For this task classification of handwritten digits of the MNIST dataset was selected since working with 28- by 28-pixel images in multiple layers requires a fair bit of computation power and will show possible bottlenecks or high optimized parts within the framework.
After the implementation the prototypes of both frameworks will get trained and tested on the same datasets to keep errors in accuracy to a minimum.

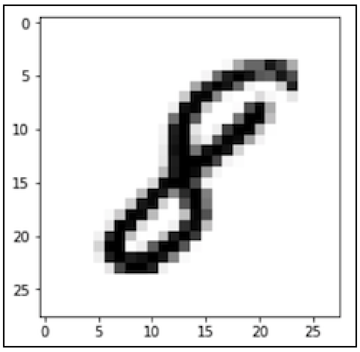

Figure 1: A handwritten digit of the MNIST dataset, representing the digit eight as used in the prototype (Gazi Yalcin O. 2018).

4. PROTOTYPE

As representative for high level frameworks Keras was chosen for its high abstraction level and its current spread on AI topics. On the other hand, Tensorflow was selected as low-level representative based on the high scalability and the opportunity to customize and adapt nearly every process within the framework. Tensorflow may also easily be used as base for Keras to build on, so both frameworks can be objectively compared using the same basic software, regarding data processing and control flow. Both frameworks are supported by big and active communities and are documented very well online making them very attractive to potential users. Also, it is unlikely for them to stop getting frequent support from its developers.

4.1. Concept

To evaluate all pros and cons of both frameworks a prototype network is implemented using both. This convolutional neural network will be developed to classify handwritten digits. The internal structure of the network itself will be explained in detail in the next paragraph. To train both networks to a comparable level the Modified National Institute of Standards and Technology (MNIST) dataset (LeCun Y.L. 1998) will be applied, containing 60,000 images for training and 10,000 images of digits for evaluating the accuracy. All these images were created by 500 different people, offering plenty variation in the dataset to prevent the network from overtraining on special features of unique handwritings. An example for such a handwritten digit may be seen in Figure 1.
This prototype was chosen on the premises of being complex enough to use advanced features of both frameworks and provide long enough training phases to compare the efficiency of both environments. Yet it is quite simple to implement the network with a few basic layers commonly used in many applications working in the same basic principle in both Tensorflow and Keras.

4.2. Network

As mentioned before the best network for such an image recognition task is a convolutional neural network, in this case with eight layers and two stacked cascades of convolution and pooling layers. Figure 2 shows the structure and dimensions of this network, all noted numbers are indications for used neurons in these layers.
At the input layer a 28x28 pixel greyscale image of a handwritten digit gets fed into the network, where the information of each pixel is taken by one neuron. The first cascade of convolution and pooling filter takes the original image, convolutes and resizes it to a dimension of 14 pixels squared. This process is repeated in the next cascade, which resizes the data to 7 pixels squared. This method greatly reduces data inside the network and keeps the number of neurons down, therefore increasing the system's performance in training by a significant amount.
This step is followed by two fully connected layers, in which every neuron is linked to every other neuron within the layer. Such layers are very good in combining all the features detected by predecessor layers. They associate multiple inputs and try to predict the correct digit based on the detected features. Since the data is coming out from the last layer in a 7x7 format with 64 channels or features for the last pooling layer, this layer consists of a great number of neurons. To further optimize and increase accuracy of network predictions, another fully connected layer, this time with 1000 neurons, is added onto the back. The last needed part of the network is an output layer, which consist of the amount of prediction outcomes possible. In this case this layer features ten neurons because there are ten digits from 0 to 9 for the network to predict. At the end each neuron shows an output value from 0 to 1, representing the probability for the picture to be this specific number.

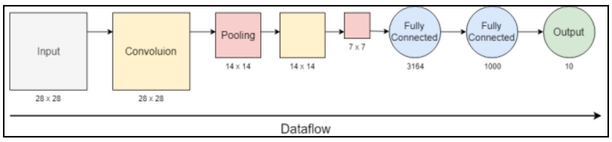

Figure 2: Structure of the Prototype Network, Yellow and Red Layers Represent Convolution and Pooling Layers Respectively.

4.3. Evaluation Criteria

To evaluate both types of frameworks based on objective criteria, they are tested on the following four aspects: Performance or accuracy, rapid-prototyping capability, expandability and training performance. All of these properties are crucial for industrial applications. The most critical point of a neural network is its ability to make accurate decisions and predictions, therefore the performance of the network and its underlying framework is key. Also, very important is the ability of a framework to allow its users to create rapid prototypes for the first evaluation of ideas or new concepts. This also saves a lot of development time and will be mainly evaluated based on the ease of use when implementing the prototypes. This feature makes great difference in project costs, since faster development time directly correlate to less financial effort for companies. Often frameworks do not deliver all needed functionality out of the box, this is where possible expandability of such systems comes into play. If the environment is easily adapted to new functionality and new concepts, much effort can be saved in this stage. The last important criterion is training performance and the ability to upscale the training. Since each neural network nowadays is trained on a GPU, easy and efficient support for such hardware units plays a huge role in an overall performance of the network. This gets tested by training the network on a GPU, since the process as well as the code is nearly the same as for training on specified Tensorflow Processing Units (TPU), explicitly made for training AI. This opens the possibility to further improve AI performance, while still using the same training time, or cutting the training effort and keep the quality of the final network. These options are highly beneficial for commercial or industrial applications.

5. TENSORFLOW

Tensorflow was and still is developed by the Google Brain Team. It is specified in data processing on heterogenic systems, enabling the framework to be very efficient on large multi-core processing units, GPUs und also Google's own Application Specific Integrated Circuit (ASIC) device called TPU. Those TPUs have been solely created to accelerate the training process of neural networks and AI in general (Abadi 2016).

The unique features of Tensorflow are the data flow graph and the so-called tensors. The Dataflow graph is a directed graph, which describes the proceeding of data through the network. Each node of this graph is a representative for a layer in the prototype network and abstracts one or more operations on the data. The term tensor in this case describes an n-dimensional data field, may being one of Tensorflow's base datatypes, such as *int32*, *float32* or *string*. A tensor is always used to hold data between nodes in the graph, there for a node needs at least an input- and output-tensor. The filling state or dimensions of such tensors may vary from operation to operation, since not every operation is based on the same dimensions (Abadi 2016).

A matrix-multiplication of a polling node may, for example, change the dimension of the data based on its input sizes. Such a graph is shown in Figure 3. This graph is automatically generated by the framework and represents the frameworks internal structure of the prototype.

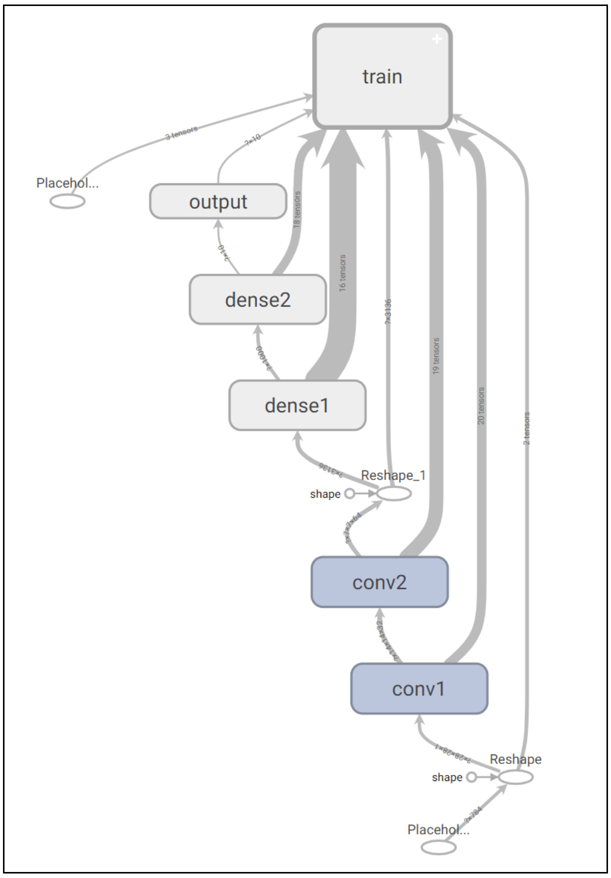

Figure 3: Tensorflow Graph of the Prototype

The major upside of Tensorflow is the ability to scale the systems very efficiently based on hardware acceleration. It is easy to execute parts of the dataflow graph on a GPU or TPU. If needed it is even possible to process the whole graph onto one of these devices. Since Tensorflow is based on a very low abstraction level, every little function can be tweaked and adjusted, which results in an immensely high optimizing potential and if you are willing to spend some time, also in very efficient and nearly infinitely scalable applications. However low abstraction levels are not only positive, they are also Tensorflow's greatest downside. Since rapid-prototyping requires a fast and easy to use environment, it is quite challenging to create a quick prototype of a desired network. Each function needs a specific amount of information about its data and parameters. Those values need to be set in order to achieve a decent accuracy of the network or make it work in the first place. So, a lot of knowledge and a long adjustment period is needed to get the most out of Tensorflow networks. Using Tensorflow is therefore prolonging time to market and development cost by big amounts.

Setting up the environment to use Tensorflow is not challenging and very well documented on the webpage. After installing all needed libraries for GPU support, it is a matter of changing a few lines of code to get Tensorflow to also use available GPUs or TPUs. Tensorflow features a steep learning curve and needs some time to get used to and be productive with the environment. Once you are comfortable with the API there are a lot of useful tools like the included visualizer called TensorBoard. This tool is a great way to double check the correct layout of your neural network and also visually see the ongoing training stats like accuracy and training time in charts.

6. KERAS

Keras is an AI framework for Deep Learning developed by Francois Chollet in 2015. It features a high abstraction level and is available for Open-Source use. Since Keras only is a Python library that needs to be based on a backend software, it can be paired with a few different low-level systems such as Tensorflow, CNTK or Theano. The goal of Keras is to abstract from complex API functions and tons of different tweakable parameters and offer the opportunity to quickly develop a quite powerful neural network out of a few components (Keras 2019). With this approach it is easy to implement first prototypes or react to fast changing specifications. It is also well documented and does not need a lot of special know-how in neural networks to get started with development. Since Keras is based on a low-level framework it inherits much of the performance benefits of its base framework. Due to not having the opportunity to solve all problems in high-level code tuning, some parameters may be necessary at one point. It is possible to write code directly in base-level framework syntax and abstraction to further optimize (Keras 2019).

Because Keras in this case is based on Tensorflow it also uses its dataflow graph mechanisms and therefore generates a visual representation of the internal network, which can be seen in Figure 4. In this figure the ‘train’ node of Figure 3 is decomposed in its subfunctions ‘metrics’ and ‘loss’ shown in the top of the graphic.

The framework and the workflow itself was easy and fast to set up once all required libraries and the background framework was installed. Since Keras is a high-level framework with great abstraction getting used to working with the environment and different abstract layers was fast. An early prototype of the network could be developed within a few hours using the ‘Sequential Model’ offered by the framework, where layers only get added to one another in a sequential fashion. All functionality not available in basic layers and functions may be added or customized in any way. This however needs to be done in the abstraction level of the basic framework, which in this case requires the developer to be able the use Tensorflow as well as Keras. The documentation of the framework is based on very detailed descriptions of all used parameters and settings. This took a while since there are no real examples on how to correctly use the given API functions. But since there is a big community behind Keras it was possible to find all needed information online.

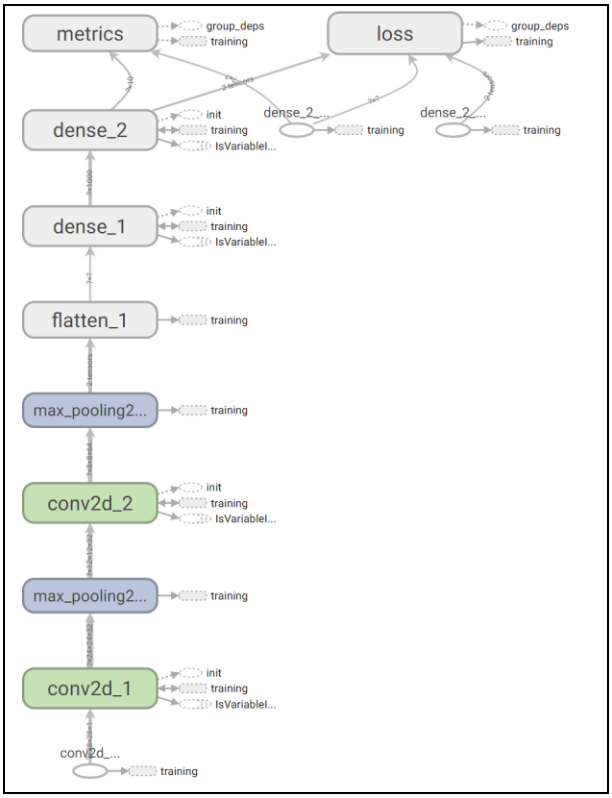

Figure 4: Graph of the Keras Network, Created by Tensorflow Backend Software.

7. TESTING ENVIRONMENT

As testing environment, a computer with a Windows 10 operating system was used. The system is based on an Intel i7 5820k Processor, 16 gigabytes of DDR4 RAM and a Nvidia GTX1080Ti GPU.

For the frameworks a Python environment was needed, which was used in version 3.6.2 and 64 bit. This enabled the test to use Tensorflow version 1.7.0 and Keras version 2.2.0. To test both training performances on CPU and GPU libraries from Nvidia were used. For CUDA support version 9.0.176 was paired with the neural network library cuDNN version 9.0 from Nvidia. At the time of testing an evaluation all the above listed pieces of software had been the latest stable versions.

7.1. Testing Procedure

Both networks were trained on the CPU of the system as well as on the GPU of the system. Each test was conducted 5 times to rule out variances in accuracy or training speed. All results shown further on are averages over these 5 test runs, which were completed with a batch size of 128 images per batch and 20 revolutions of the dataset. One single iteration over all the batches of the dataset is called an epoch further on.

8. TEST RESULTS

All conducted tests have shown that the combination of the network, optimizer and dataset would have also been nearly the same if only half of the epochs had been used for training. After the 10th epoch only minor improvements can be seen in accuracy. In most cases such minor increases in accuracy are not worth extra training time, since accuracy is at this point already at about 98 to 99 percent. Accuracy in this case directly relates to correctly classified digits. However, Keras reaches its final accuracy level a bit faster than the Tensorflow network, which gives the possibility in training even less while reaching the same quality.

8.1. Tensorflow

As shown in Table 1, Tensorflow reaches average accuracy of 0.9880 or 98.80 percent by training the network on the system's CPU, which takes about 16 minutes of training time.

In contrast, using hardware acceleration from the system's GPU an average accuracy of 0.9895 was reached. This took around 40.2 seconds and therefore drastically improves efficiency. By shortening training times more development may be done in the same amount of time, which results in well-defined networks being able to deliver better quality results. Which means the GPU training recognizes digits with an equal precision but does this approximately 25 times faster.

Table 1: Results for Training on CPU and GPU using Tensorflow, all Time Measurements are noted in Seconds.

GPU		CPU		Test number
Accuracy	Time	Accuracy	Time	
0.9896	40	0.9893	980	1
0.9904	40	0.9861	977	2
0.9887	40	0.9890	974	3
0.9899	41	0.9887	970	4
0.9891	40	0.9868	975	5

8.2. Keras

As shown in Table 2 Keras reaches an average accuracy of 0.9989 on the CPU, which takes around 510 seconds. With this accuracy only about 1 in 1000 digits is detected wrong. By training the network on the GPU the same accuracy can be reached. The only difference in this case is the reduced training time needed to 53 seconds on average. In all test runs Keras reached its peak accuracy level a few epochs faster than Tensorflow did, whereas overall training times on GPU based training was longer.

8.3. Comparison of results

By looking at the results one can quickly see the performance and scalability benefit of Tensorflow, being about 31 percent faster when also using the system's available GPU to process data. By looking at the CPU results at first glance there seems to be an error in testing due to the longer training time needed by the more performant framework Tensorflow. But this difference in time is caused by not tuning every little parameter to the best possible value, which represents using the framework in a way an engineer would do when development time is limited and there is no chance to tweak and optimize every little setting. Additionally the Tensorflow code consists mainly of self-implementations, where by using Keras everything for this prototype needed is already provided by the framework environment. This approach also highlights the difference in system modelling between both frameworks. Tensorflow all task and groups need to be modelled quite detailed, whereas Keras enforces a more abstract modelling approach by only needing very abstract process descriptions. Both representatives were used as they would have been in a more complex and bigger industrial environment, to keep objective comparison possible.

Table 2: Results for Training on CPU and GPU using Keras, all Time Measurements are noted in Seconds.

GPU		CPU		Test number
Accuracy	Time	Accuracy	Time	
0.9988	53	0.9986	502	1
0.9994	52	0.9986	506	2
0.9985	54	0.9993	523	3
0.9992	54	0.9993	526	4
0.9988	52	0.9986	525	5

9. CONCLUSION

Although the test series showed performance benefits when using Tensorflow in combination with hardware accelerators, the choice of best framework depends on the intended application and needed key features. If data amounts and complexity stay within average, the high abstraction level of Keras is far superior over the high optimizing potential of Tensorflow. Giving the user the opportunity to develop faster prototypes and test more revisions improves the quality of the final network way more than modelling every single function in detail.

If Keras is then also based on Tensorflow as backend software, they form a great symbiosis where weaknesses of both get covered by the other framework. If an operation is missing in the Keras framework, it is possible to add this functionality in highly optimized Tensorflow native code and keep the rest of the application clearly arranged in high-level code, therefore having the benefit of fast development times combined with great performance.

These features make Keras, and high-level frameworks in general more suited for small to medium sized tasks, where rapid-prototyping is essential and development time advantages weigh more than pure performance and customizability. Therefore, Keras is better in keeping the costs down in development while still delivering good quality results. Although expandability is not as simple as with Tensorflow, all other key features of an efficient AI framework for medium sized projects are covered by the Keras framework, making it great for embedded projects like facial recognition on smartphones or interpreting telemetry data of robots and machines.

Large systems, like customer analyzing, however, suffer performance hits caused by the abstraction level and overhead of Keras where Tensorflow on the other hand is the perfect choice. Due to highly specific and custom modelled processes working with huge amounts of data, Tensorflow is able to deliver the required performance. However, to achieve these results substantial expertise and AI know-how must already be present within the development team. Based on the evaluated key criteria, low-level frameworks like Tensorflow tend to be more useful in scenarios where huge amounts of sensor or image data need to be processed. One example of such an extremely demanding application would be autonomous driving of vehicles, where lots of sensors need to be checked thousand times per second and correct decisions need to be made near instantly. To model such networks the fine granularity and the optimization potential of Tensorflow and low-level frameworks in general is essential in developing efficient and powerful products and keep development effort and therefore product costs as low as possible.

10. REFERENCES

Gershenson C.G., 2003. Artificial Neural Networks for Beginners. Eprint: cs/0308031.

Schmidhuber J, 2015. Deep learning in neural networks: An overview. Available from: http://www.sciencedirect.com/science/article/pii/S0893608014002135 [accessed 10.07.2018].

Lunze J, 2016. Künstliche Intelligenz für Ingenieure: Methoden zur Lösung ingenieurtechnischer Probleme mit Hilfe von Regeln, logischen Formeln und Bayesnetzen. Available from: https://books.google.at/books?id=NqBlCwAAQBAJ [accessed 11.08.2018].

LeCun Y.L., Cortes C.C., Burges C.J.C.B., 1998. THE MNIST DATABASE of handwritten digits. Available from: http://yann.lecun.com/exdb/mnist/ [accessed 13.07.2019].

Abadi M.A., 2016.Tensorflow: A system for large-scale machine learning. Available from: http://arxiv.org/abs/1605.08695 [accessed 06.07.2018].

Keras Home, 2019. Keras Home. Available from: https://keras.io/#keras-the-python-deep-learning-library [accessed 02.08.2018].

Keras, 2019. Keras Why use Keras. Available from: https://keras.io/#why-this-name-keras [accessed 02.08.2018].

Google Inc., 2019. Tensorflow Homepage. Available from: https://www.tensorflow.org/ [accessed 11.07.2019].

LeCun Y.L., Bengio Y., 1995. The Handbook of Brain Theory and Neural Networks.

Theano, 2019. Theano Homepage. Available from: http://deeplearning.net/software/theano/ [accessed 11.07.2019].

Berkeley AI Research, 2019. Caffe webpage. Available from: https://caffe.berkeleyvision.org/ [accessed 11.07.2019]

NumPy, 2019. NumPy Homepage. Available from: https://www.numpy.org/ [accessed 11.07.2019]

Gazi Yalcin O., 2018. Image Classification in 10 Minutes with MNIST Dataset. Available from: https://towardsdatascience.com/image-classification-in-10-minutes-with-mnist-dataset-54c35b77a38d [accessed 10.07.2019]

ARTIFICIAL INTELLIGENCE: CONCEPT OVERVIEW, METHODOLOGICAL APPROACHES AND CHOICE METRICS

Michael Bogner[a], Martin Steiger[b], Franz Wiesinger[c]

[a],[b],[c] University of Applied Sciences Upper Austria – Embedded Systems Design
Softwarepark 11, A-4232 Hagenberg, Austria

[a]michael.bogner@fh-hagenberg.at, [b]Martin.Steiger@fh-hagenberg.at, [c]franz.wiesinger.@fh-hagenberg.at

ABSTRACT
During the last couple of years there has been a renaissance in the field of artificial intelligence, also called AI. A wide diversity of possible concepts to this topic leads to the compulsion to be properly informed about a variety of approaches. This paper focuses on explaining the primary and most relevant theoretical concepts in regard to artificial intelligence and to rate them based on derived criteria. To achieve this, the most significant manifestations of these learning concepts are analyzed to identify their core characteristics. Choice metrics are derived based on this knowledge and selected with regard to an industrial environment. Additionally, a methodical approach is developed to ease the user's choice of an appropriate concept according to the given criteria. The final result of this paper is a set of diagrams that illustrate the different artificial intelligence concepts based on the found criteria.

Keywords: artificial intelligence, deep learning, independent metrics, decision support system

1. INTRODUCTION
The term artificial intelligence, or AI, can be interpreted in many different ways. Due to this, the original meaning describing the process of teaching a system to learn new things, steps into the background slowly but steadily. The overall goal of AI is to create a system which is able to develop solving strategies towards a specific problem based on given examples. In general, a real artificial intelligence has to meet a given set of criteria. On the one hand, it has to be able to generalize problems to operate outside of the given examples. This property is also known as generalization. On the other hand, it is also capable of drawing conclusions from different situations to find appropriate solutions, which is called reasoning. Additionally, a real AI has to perform perception. This describes the ability to perform an analysis of environments and of the relationships regarding objects within those environments. An artificial intelligence is used when a systems purpose is to react to its environment using complex problem-solving strategies.

The rapid developments during the last couple of years and the predominantly positive prognoses for further use cases resulted in a strong public and scientific focus. This has the consequence that a variety of different approaches to the realization of AI applications are pursued, which leads to the question what methodology is the most suitable for a given problem. The motivation of this paper is therefore to support an AI user towards this decision.

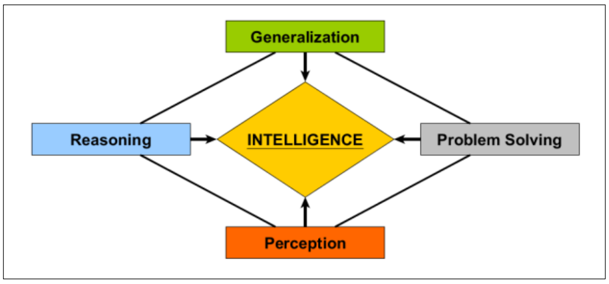

Figure 1: Criteria for a Real AI

To realize this goal, the most commonly used concepts and approaches are analyzed theoretically. To supplement these insights, the concepts are also reviewed with regard to their practical relevance, respectively how they can be utilized for industrial usage. This includes improving processes in companies, emend provided services and advance automatization especially in relation to industry 4.0. The analysis starts at basic machine learning approaches and concludes to artificial neural networks and finishes with the latest large concept called deep learning.

2. RELATED WORK
The artificial intelligence characteristics mentioned in the previous section have different fields of application and limitations. However, all approaches are based on the concept of machine learning. They are therefore only refinements or modifications of the original approach and some models in turn derive from these adaptions. Following this principle, artificial neural networks, for example, are based on the basic approaches of machine learning (Beck 2010) and deep learning is a refinement of these networks. This also leads us to the current state of the art, because the most powerful concepts are currently based on deep learning (Hinton 2007). Convolutional (LeCun 1998) and Long Short-Term Memory Networks (Hochreiter 1997), for example, will be discussed in more detail in the course of this work.

3. MACHINE LEARNING (ML)

To understand what defines machine learning, the model concept has to be clarified first. A so-called model describes the very basic procedure for solving a given problem using AI. What distinguishes a machine learning model from classic solution methods is the used walkthrough. A ML model uses well-known example data of possible solutions, while other methods derive an algorithm based on a given challenge and validate the theory by comparing it with expected values. Consequently, ML approaches are used when the given problem can not be described with a unified algorithm, but with proven examples or when the classical approach is to complicated. The process of learning solutions based on examples is called model training.

Machine learning models can be separated into two different classes. Descriptive models are used to identify or evaluate specific objects and predictive models are used generate forecast based on past knowledge. It is assumed that every problem is deterministic and no random influences occur. Overall there are five main goals of machine learning. To perform classification, a model has to determine, whether a given object can be assigned to a known class based on its attributes. A class describes a set of objects which share common and significant properties that are easy to identify. Regression models try to interpolate a characteristic based on numerical data. It has to be emphasized that such a model does not provide logical statements, but numerical results. Unlike the previous two types, clustering models try to separate an unknown set of data into classes with common attributes. If a model realizes classification or regression, knowledge is gained through examining existing examples. The goal of dimensionality reduction is to compress a large set of data, preserving the characteristic properties. To clarify the issue, an attribute of an object is called dimension in the context of AI. Consequently, dimensionality reduction models try to discard unnecessary attributes and return a cleaned dataset. At last location models are used to find specific data within a large database by trying to estimate the basic structure of the database.

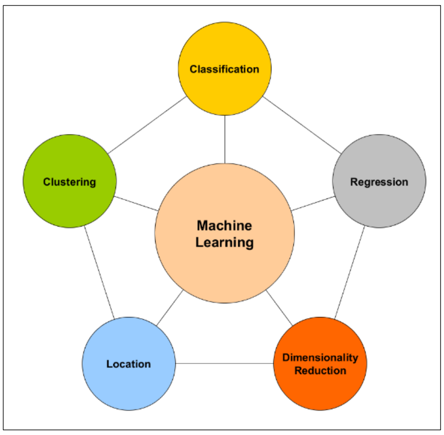

Figure 2: Goals of Machine Learning

To determine the quality of a given model, there are different approaches which are based on four indications. The true positives (TP) describe the number of positive results which are detected as such and the true negatives (TN) determine the number of negative results which have been recognized as such. Additionally, the false positives (FP) display the amount of positive results which have been labeled as negative and the false negatives (FN) act vice versa. Different quality metrics can be derived from these attributes:

- accuracy: $a = \frac{TP + TN}{TP + TN + FP + FN}$
- precision: $p = \frac{TP}{TP + FP}$
- recall: $r = \frac{TP}{TP + FN}$

As already mentioned in the previous chapter machine learning, models can be separated by their goal. But it is also possible to partition them by the used learning paradigm. When supervised learning is used, the models receive labeled training data. The labels abstract the expected output. In contrast to this, unsupervised learning uses training data without any labels, appropriate to the clustering models. This training method results in a black-box where the functionality of the output model is unknown. Mixed forms like semi-supervised learning are also possible. After the definition of the general model concept a few well known approaches will be analyzed.

3.1. Regression Algorithms

As already mentioned within 2.1, regression models, respective regression algorithms have the purpose to interpolate a characteristic based on numeric data. To determine which regression model is appropriate for a given task, one has to consider three aspects. The shape of the regression line is one of those key aspects. Linear regressions can be realized with low effort, but suffer from correlation issues, if the considered dimensions are not statistically independent and are very vulnerable regarding to heteroscedasticity, which describes outliners within the training dataset. To compensate these effects polynomial regression is used as an alternative, which is capable to overcome the heteroscedasticity. This shape has the huge disadvantage of possible over- or underfitting, hence when the chosen polynomial shape fits the training data too exactly, which restricts generalization or too inaccurate to fit the given problem (Sunil 2015). The second key aspect of regression models is the variable type, which can be numeric, discrete or categorical. Lastly the number of independent variables is also crucial for the regression model choice. The more independent variables have to be considered within the model, the more complex it becomes. The independent variables describe the number of data attributes used for a regression. To handle that kind of problems, there are specific approaches available, e.g. stepwise regression models.

The advantages of this approach are a simple implementation for linear and polynomial models and the intuitive selection of the appropriate model type based on training data visualization. In contrast the dimensionality of the model depends on the chosen algorithm, which may result in very large or unhandy models and interferences within the training data can reduce the model accuracy significantly.

3.2. Instance-Based Algorithms

Such models create and maintain databases in which the most significant records from the training data are stored. Due to the fact that instance-based algorithms compare the input data with the generated database, such approaches are commonly used for classification tasks. The input data receives the class which is most similar to its attributes compared with the samples from the database. Particularly noteworthy in such models is the fact that they can still be changed after training by adding or removing records

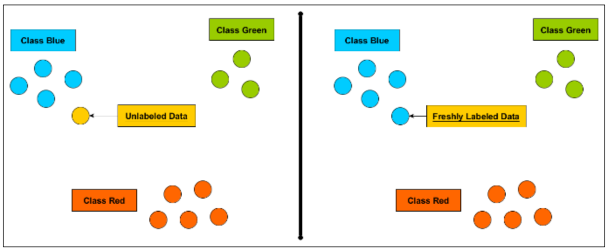

Figure 3: Instance-Based Approach

The advantages of this approach are the simple implementation and the flexible adaption to biased or noisy training data. Major disadvantages of this approach are the high memory consumption for storing the database and the high computation effort, because all records have to be compared with the input sample.

3.3. Regularization Algorithms

Regularization models are approaches which are capable of supporting other models by compensating a possible overfitting during the training process. These algorithms extend existing models to penalize complex developments during the training process, favoring simpler models. Simpler models lead to better generalization. Consequently, regularization methods are often combined with regression algorithms to compensate an over-adaption to the training data.

The training of a model is executed by evaluating the loss function, which describes the deviation of the result of a model from the actual labeled result. Ideally, this value converges to zero. If it becomes too high then the internal parameters of the model have to be changed to compensate this development. By adding certain offsets, so-called regularizations, an attempt is made to influence the loss function and thus also the parameter distribution within the model. The most common regularizations are L1 and L2, which have several advantages and disadvantages.

L1 results in sparse parameters which can be handled efficiently through appropriate algorithms, but is very vulnerable towards outliners within the model which can lead to instability during the training process. L2 loses the sparse parameter property of L1, but is less likely to become unstable.

3.4. Dimensionality Reduction Algorithms

The previously discussed approaches share the common problem that the model size scales with the complexity of the used dataset. Dimensionality reduction algorithms are used to determine whether all dimensions of a given data are necessary, depending on a specific model. Those algorithms can be separated into feature extraction or feature selection methods. Feature extraction tries to generate the best possible subset from a set of given attributes using three different approaches. The filter method calculates the subset which correlates most with the desired output, the wrapper method is capable of a dynamic adaption of the subset during the actual model training and the embedded method combines the other two approaches, also considering the current performance of the model (Kaushik 2016).

Feature extraction uses a different procedure. It does not try to generate a new subset from a given set of attributes, but to map an entire dataset to a new one with a reduced number of dimensions using different mapping rules. The variance, which describes how well the data are scattered, is maximized during this process.

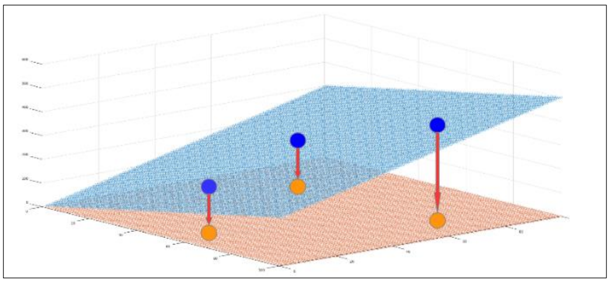

Figure 4: Feature Extraction with PCA

3.5. Summary

Taking the mentioned points from the previous chapters into account, simple machine learning models are easy to implement, but also limited in their performance. In particular, this relationship holds true with regard to the complexity of the considered datasets. If the complexity becomes too high, the models can either be trained poorly or not at all and the consumption of resources also rises sharply in some cases. Additionally, most models are only useful if the input data and the training data are uncorrelated, so each sample can provide a clear information for itself. Nevertheless, those models are recommendable for simple problems because they are very user friendly. Possible fields of industrial application are correcting invalid or noisy data, performing predictive maintenance for production lines through sensor networks and a regression approach or organizing simple databases.

4. ARTIFICIAL NEURAL NETWORKS (ANN)

As already mentioned in section 2, the problems and methodologies with regard to machine learning are generally designed and the proposed solutions can also be applied without comprehensive understanding. But those models are limited by the dimensionality of the datasets, because the training duration or the resource usage is too high. From this point on, artificial neural networks are acting. This approach is capable of handling a high dimensionality.

A neural network consists of a large number of subunits, so-called neurons, which fulfill a similar functionality than their biological counterpart. Figure 5 displays the structure of the neuron subunit. A neuron forwards all input values from external neurons or other information sources individually weighted to the nucleus, where the inputs are summed up. The result of this calculation is the input for the so-called activation function, which represents the activation threshold for the neuron. This output gets forwarded to the next neuron and so on.

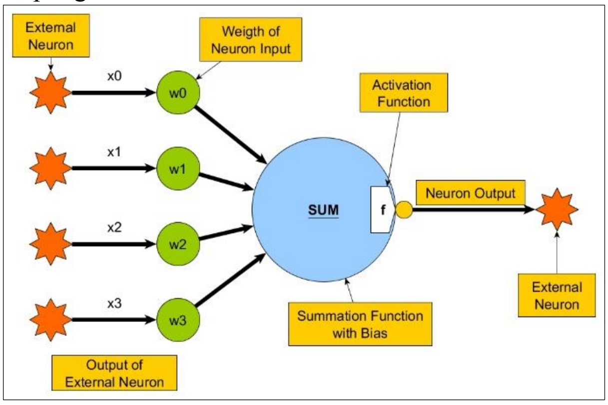

Figure 5: Neuron Structure

To achieve a desired functionality, the neurons need to be organized appropriately, respectively in layers with different tasks, e.g. input layers, hidden layers and output layers. The general structure of layers is displayed in Figure 6, but the functionality of the different layers is strongly determined by the ANN model.

It has to be mentioned that ANNs are a part of machine learning. Consequently, a more detailed comparison between the methodologies is required. Neural networks outperform simple machine learning models with regard to highly nonlinear problems like data with human influence, but suffer a reduced accuracy compared to the ML models if the problem can be described with a unified algorithm. Another notable information is the fact that artificial neural networks may use the local optimum of a problem and not the globally best solution, depending on the training process.

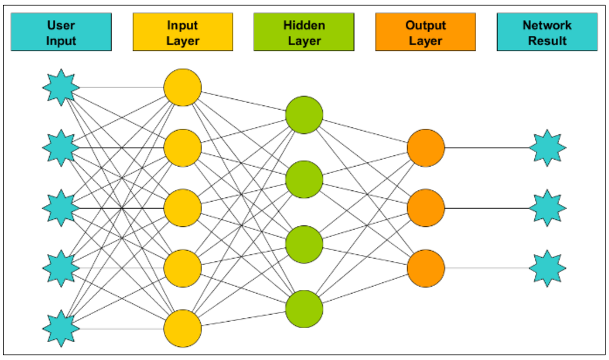

Figure 6: ANN Layer Structure

4.1. Pattern Associator

These neural networks are used for typical classification tasks of uncorrelated data without the need of hidden layers. The lack of layers reduces the model size and training duration significantly. Furthermore, pattern associators provide a solid generalization and tolerance with regard to neuron fading during training. This problem occurs when the input weights of a neuron converge to zero and the subunit is not able to react to input changes any longer. This is even more serious due to the fact that once a weight reached zero during the training process it is likely that it remains zero, which leads to a permanent deactivation of neurons, reducing the overall computation capabilities. Additionally, this model proves very robust against noisy or incomplete input data, but lacks of accuracy. Consequently, it can not be used without any adaptions, to return other then a rough tendency of the input data (Rey 2018).

4.2. Recurrent Neural Networks (RNN)

This type of neural networks differs from the basic pattern associator network by the bidirectional information flow. In general, the information provided to the network gets forwarded straight from the input layer to the output layer. But in this case, there are feedback loops between the layers, which are designed to recognize correlated input data. This functionality appears first within this paper, because every other model mentioned previously is not able to detect and handle correlated data. The type of feedback loop is essential for the functionality. A direct feedback loop describes a coupling between the output and the input of the same neuron, whereas indirect feedback loops act as a connection between the output of a neuron and the input of a neuron in the previous layer (Figure 7). Lateral feedback loops within the same layer and full feedback loops between every neuron are also possible. The purpose of this connections is to provide an internal state or memory within the neural network, which changes based on the last processed sample. Due to this fact, recurrent neural networks are capable of recognizing long-term relationships within the input data (Rey 2018).

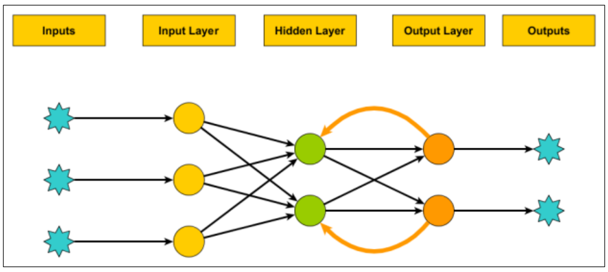

Figure 7: RNN Layer Structure

4.3. Competitive Networks

This type of artificial neural network is similar to the pattern associator model, but uses competitive learning during the training process. This learning paradigm support certain neurons within the ANN during the training that perform very well and optimizes the neighbors towards this neuron by modifying their weights. This circumstance is often used for data prefiltering in combination with other models, because competitive networks perform well with noisy data and can therefore provide clean input data for other models. It is also notable that competitive networks use unsupervised learning during the training process, consequently the most striking features prevail. Due to this fact it is also used for clustering tasks.

4.4. Self-Organizing Maps (SOM)

Self-organizing maps follow an entirely different principle than the other network types. In general, the result of the neurons within the output layer determines also the result of the entire network. But in SOMs the crucial network information follows from the activation states of all neurons. A typical task for self-organizing maps is to map inputs with high dimensionality into a space with low dimensionality. Very helpful in this context is the image of a landscape that is displayed on a map.

4.5. Summary

The decisive advantage of artificial neural networks is the fact that they are able to handle correlated data and to implement memory to recognize long-term dependencies. Also notable is the increased ability to cope with complex datasets. In contrast, the implementation of ANNs is more complicated than the simple machine learning models. To detect errors or possible biases during the training process, special toolsets are necessary. Otherwise the learning remains a black-box. Possible industrial applications are analyzing short-term dependencies in customer data, organizing big data, associative speech detection, creating intelligent inverse kinematics for robotic application or even optimizing delivery routes and other logistic issues.

5. DEEP LEARNING (DL)

As already mentioned in the last section, ANNs are already capable of solving complex problems, but they have got one decisive disadvantage. To perform multiple tasks within one model, a combination of different artificial neural network has to be used, e.g. one network for feature extraction and one for feature detection. Additionally, the mentioned vanishing gradient problem has got a higher impact on networks using a large number of layers, which ensure a better generalization. This problem results in a slow training process. To handle these disadvantages deep learning has been introduced to capsule an automatic feature discovery within the network. In conclusion, a deep learning model uses more hidden layers than a common artificial neural network.

5.1. Convolutional Neural Networks (CNN)

This type of deep learning model is commonly used for image recognition or for processing data with high dimensionality. It consists of three different layer types. The convolutional layer performs the feature extraction using so-called kernels that are generated during the training process. These kernels are often referred as filters, which return a filtered data sample with a possibly reduced dimensionality. After every convolutional layer follows a pooling layer which has the only purpose to reduce the dimensionality of a data sample even further by picking the most significant attribute from the filtered sample and passing it to the next layer. After some pooling and convolutional layers, the dimensionality of the sample has been reduced and it can be processed by classical ANN approaches. The general structure is displayed in Figure 8.

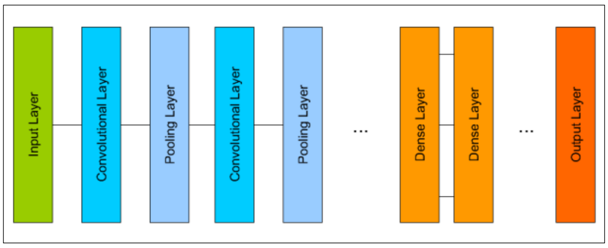

Figure 8: Structure of a CNN

5.2. Long-Short Term Memory Network (LSTM)

LSTM networks are a variation of recurrent neural networks, which leads to the conclusion that it contains a memory due to internal feedback loops. Large RNNs may cause a vast vanishing gradient problem because of their kind of training, called loop unrolling. The more feedback loops exist, the more training layers are resulting. The decisive difference to common RNNs is the kind of neurons used to implement the state capability. So-called LSTM units are operating similar to a computer memory. Data can be extracted, fed or removed from a LSTM unit using gates and the special structure of those units leads to a decreased vanishing gradient problem. Consequently, LSTM networks are used to handle very long-term dependencies within the input data which would lead to a vanishing gradient problem within common RNNs.

5.3. Summary

The reason why common ANNs are mostly used for problems with a medium complexity is the vanishing gradient problem which leads to an excessive training duration. Deep learning approaches are able to compensate this problem, but suffer from a very high implementation complexity. Additionally, there are numerous model variants, which have to be carefully evaluated for a given problem. There exists a large number of possible industrial applications due to the outstanding generalization capabilities of DL approaches. For example, context recognition within video/audio sequences or texts, analyzing long-term dependencies in stock prices, weather forecasting, automated translations in different languages and live image recognition in autonomous driving cars.

6. CHOICE METRICS FOR AI APPROACHES

Taking the previous sections into consideration, a high number of different AI approaches are available to deal with a given problem. To be able to compare models even if the original purpose is different, the further proceeding is problem-oriented. Consequently, the first metric is resource usage, not only considering the physical storage but also training duration and hardware requirements. One has to be aware that a high score in this metric indicates a vast resource usage and should be considered carefully. The second metric is the correlation of the available and expected data, which assesses the ability to recognize and process correlated data. To conclude, data complexity and implementation friendliness also have to be taken into consideration. In Figure 9 an assessment for different types of machine learning approaches is displayed. The same approach has been performed for the artificial neural network types (Figure 10) and some deep learning models in Figure 11.

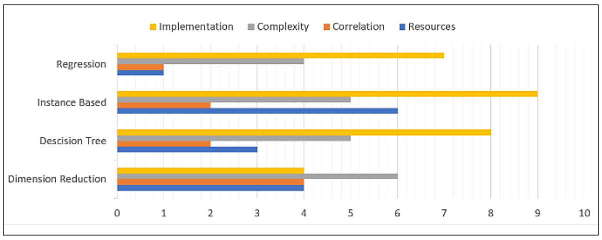

Figure 9: Choice Metrics for Machine Learning

As already mentioned within Section 2, machine learning models provide a high implementation friendliness, but suffer with regard to the correlation and complexity metric. An exception is the dimension reduction approach, but it has to be mentioned that most practical applications are using this approach to pre-filter the dataset for other models. A standalone application of a dimensionality reduction model is very rare.

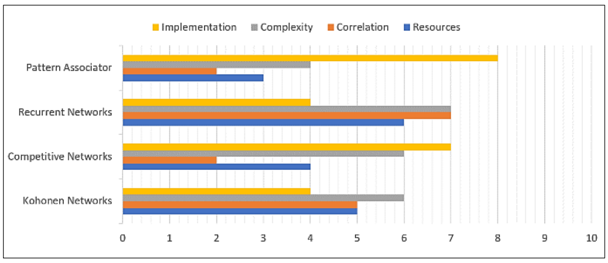

Figure 10: Choice Metrics for ANNs

Artificial neural networks outperform the simple machine learning models with regard to complexity and correlation capabilities, but have got a decisive disadvantage. The resource usage increases significantly and the simplicity of implementation decreases slowly, as described in Section 3.

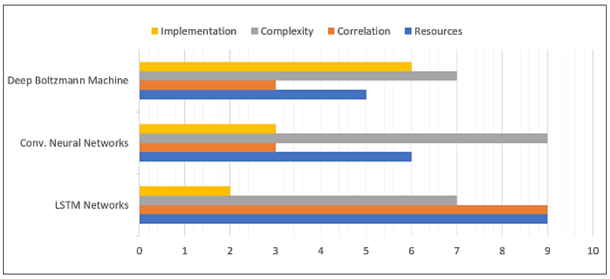

Figure 11: Choice Metrics for DL Examples

Although only a few specific DL model examples are considered, the tendencies are clear. In general, such models are difficult to be realized and therefore need careful consideration. As a balance, they are able to deal with complex data and additional long-term dependencies as displayed through the score with regard to the correlation metric.

7. METHODOLOGICAL SELECTION

After introducing the choice metrics for AI approaches, a methodological selection approach is also provided. At first an AI user has to identify the goal of the model based on Figure 2. Afterwards an inventory of the available data must be carried out to analyze the ground truth used for training and model validation. Above all, the structure and the amount of existing data record is important. For example, in this step, it is evaluated whether it is pixel data of pictures or a time series. Using the gathered information from the previous step, one can estimate the complexity of the dataset, which leads to the macrostructure of the model, respectively whether a simple machine learning approach is appropriate or a deep learning model has to be used. Taking the performed steps into account, one is able to choose a model using the choice metrics introduced in the last section. Afterwards a search for implementation strategies takes place, considering possible programming languages or frameworks, which might simplify the programming process. The next steps are implementation, model training, evaluation and comprehensive practical tests before the model can be considered as finished.

After the actual implementation and validation of the model, however, it must also be maintained and adapted to dynamic customer specifications for industrial applications. To ensure a consistent and reliable model management process Figure 12 introduces the AI lifecycle.

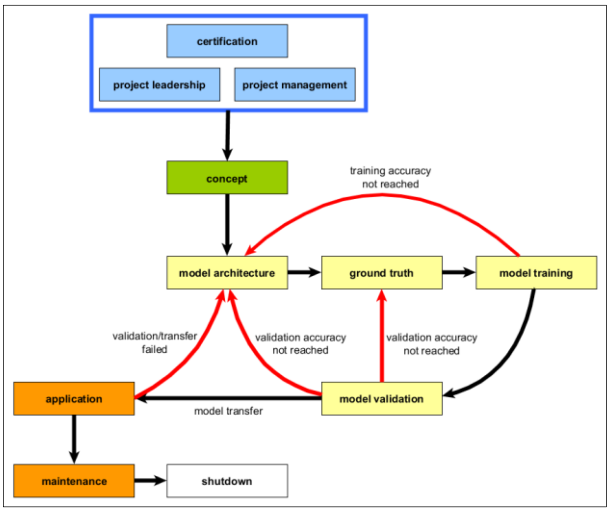

Figure 12: Model Management Lifecycle

8. APPLICATION EXAMPLE

To demonstrate the selection flow, lets assume the following problem. Images from the well-known MNIST dataset (LeCun 1998, MNIST), containing hand-written digits, have to be classified by those numbers. An example for a MNIST data sample is shown in Figure 13. The goal is a classification with regard to Figure 2 and there are 60.000 training examples with a dimensionality of 28x28 pixels available. Even though the resolution of one image if quite low, it will result in a model with high complexity. Therefore, simple machine learning approaches are no option. Remaining are ANNs or deep learning approaches. Most image classification problems are solved using CNNs, due to this it is also used in this example. Additionally, there is no correlation between the data samples. Consequently, the correlation choice metric can be low, the complexity metric has to be high and the resources and implementation are based on personal preferences. That confirms the usage of a CNN. The same choice flow can also be applied to industrial applications. But one has to be aware that it acts mostly as an orientation aid, which means it provides assistance for choosing the general model type and not a specific algorithm.

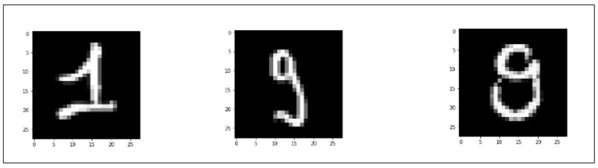

Figure 13: the MNIST dataset (LeCun 1998)

Although the actual implementation of a convolutional neural network is not the main intention of this paper, a possible solution is provided for the sake of this simple application example. As already mentioned, the dimensionality of a MNIST data sample is very small compared to more practical applications like real-image processing from a camera, e.g. in autonomous vehicles. Due to this, less convolutional layers than usual are required. To improve the network performance an additional dropout layer is added. This makes an overadaptation of the model to the training data unlikely. Figure 14 provides a brief overview of the proposed model structure.

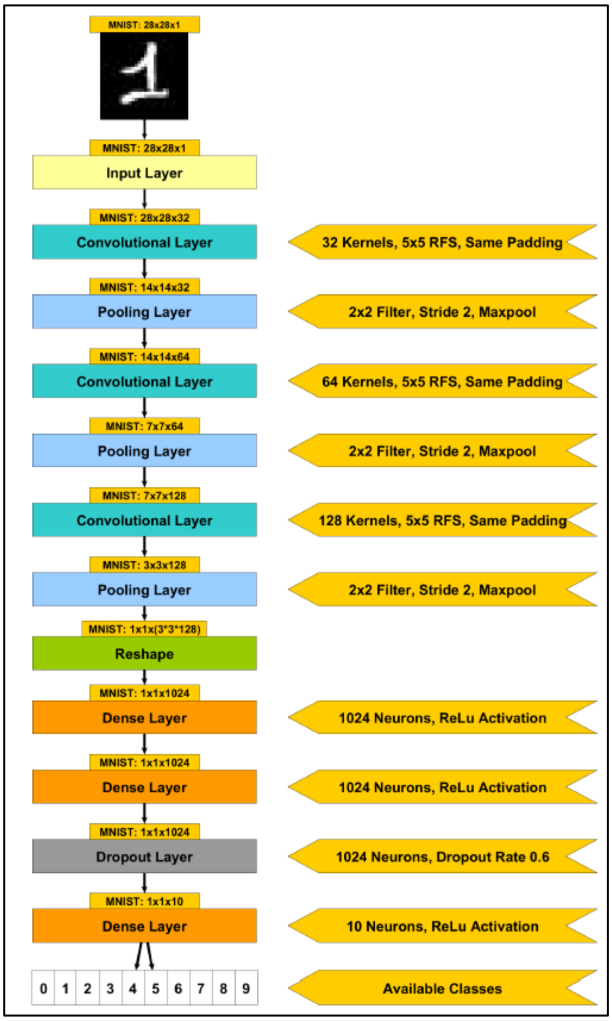

Figure 14: MNIST recognition CNN model structure

The final result of this model is a classification accuracy of approximately 97%. However, it must be taken into account that the example given here is often used as a learning example and that therefore detailed recommendations for the model design already exist. In general, accuracies at this level must be reviewed critically.

Another example for the choice flow would be for example the numerical evaluation of customer data. Due to the fact that information tends to be the most valuable estate of large companies, it can be presumed that a maintained database already exists. It is also assumed that one data sample contains much information, for instance the purchasing behaviour of the customer for different products. The task is to forecast when and which number of independent products will be purchased. With regard to the made assumptions, a simple machine learning model is able to handle this problem. Due to the fact that the data are numeric a regression model seems to me the most appropriate solution. This assumption also confirms the statement that independent products are considered, which results in a low score perquisite with regard to the correlation metric.

9. CONCLUSION

Based on the results of the previous thought models, choosing an appropriate AI algorithm for a given task is still challenging, because is depends strongly on the problem type, the available ground truth and computation resources and also environmental perquisites. But is absolutely possible to take a rough direction based on the above AI choice metrics of resource usage, data complexity, data correlation and implementation friendliness. Also, a basic choice and maintenance flow has been provided, which is tailored to industrial applications.

Due to the fact that economic interaction is increasingly based on services and requires large amounts of information to be handled for this purpose, AI will be inevitable in most industries. Consequently one has to be prepared to be confronted with a tremendous amount of possible AI approaches, whereby the knowledge gained from this paper facilitate the orientation here.

REFERENCES

Sunil R., 2015. 7 Types of Regression Techniques you should know!, available at: https://www.analyticsvidhya.com/blog/2015/08/comprehensive-guide-regression/ [accessed: 16.05.2018]

Kaushik S., 2016. Introduction to Feature Selection methods with an example (or how to select the right variables?), available at: https://www.analyticsvidhya.com/blog/2016/12/introduct on-to-feature-selection-met hods-with-an-example-or how-to-select-the-right-variables/[accessed 16.05.2018].

Rey G. D. and Wender K. F., 2018. Neuronale Netze, Hofrege

Kohonen T., 2007. Self-Organizing Maps (3rd Edition), Berlin: Springer

Patterson D. W., 1996, Artificial neural networks: theory and applications, Singapore: Prentice Hall

Rojas R., 1996, Neural Networks. A systematic introduction, Berlin: Springer

Alpaydin E., 2010. Introduction to Machine Learning – Second Edition, Cambridge, Massachusetts, United States

LeCun Y. and Cortes C. and Burges C., 1998. The MNIST Database, available at: http://yann.lecun.com/exdb/mnist/ [accessed: 09.04.2019]

Hochreiter S. and Schmidhuber J., 1991. Long Short-Term Memory, Neural Computation, 9, 1735-1780

LeCun Y. and Bottou L. and Bengio Y and Haffner P., 1998, Gradient-Based Learning Applied to Document Recognition, Proceedings of the IEEE, vol. 86, no. 11, pp. 2278-2324

Hinton G., 2007, Learning multiple layers of representation, Trends in cognitive sciences, Vol. 11 No. 10

GRASP LAPAROSCOPIC SURGERY BASIC SKILLS: A HIGHLY INTERACTIVE ONLINE COURSE MODEL HERE

Marco Frascio[(a)], Anna Siri[(b)], Francesca Mandolfino[(c)], Marco Chirico[(d)], Gianni Vercelli[(e)]

[(a),(b),(c),(d),(e)] Università degli Studi Genova

[(a)]mfrascio@unige.it, [(b)]anna.siri@unige.it, [(c)] femandolfino@gmail.com
[(d)]marco.chirico@unige.it [(e)]gianni.vercelli@unige.it

ABSTRACT
Recent changes in surgical education and training have made the virtual learning environments more attractive than previously and have created opportunities for new instructional designs of medical curricula.
The aim of this project is to show the results of a novel online elective programme to complement existing surgical undergraduate teaching methods.
The training process was developed to enhance existing skills in the field of minimally invasive surgery among the students of the Bachelor Degree in Medicine and Surgery. Interventions were provided characterised on the one hand by the high quality of content and teaching methods, on the other hand by the strong interaction between teachers and students.
The elective course created was delivered entirely online, password-protected, and was divided into 4 modules.
30 students enrolled in the fifth and sixth-year students of the UNIGE medical schools have significantly improved their knowledge on mini-invasive surgery after the course. The evaluation results demonstrated high levels of course functionality, effectiveness of its online content and high levels of satisfaction among medical students.

Keywords: online teaching and learning model; surgical settings; evaluation model

1. BACKGROUND

Medical educators are facing new challenges in training tomorrow's doctors. The traditional instructor-centered education model, focused on the teacher as both authority and model, is moving to a learner-centered approach that keeps students in control of their own learning [Leung, 2002; Ruiz et al, 2006].
In the last two decades ICT -communication and information technology- have had a rapid advances with important implications and effects for education, also in the medical field [Fornaro et al., 2008; Fornaro et al., 2009; Frascio et al. 2009; Stabilini et al., 2013].
The article will go on look at the implementation of new technologies in one specific context i.e. in an online surgery education program.
Our experience started in 2008 when we organized a comparison between online and standard lessons. Given the positive results obtained by the online class, we decide to propose a completely online course.
In order to increase the number of practical and discussion environment offered to students in the traditional-curriculum scenario, and to create an online community to share knowledge on surgery, we developed and assessed a first online course for undergraduate medical students on minimally invasive surgery at the University of Genoa, Italy.
A group of students was taught online during three months on the theory of minimally invasive surgery through lessons, videos, required readings, collaborative activities using discussion board and asynchronous communication. Pre- and post-tests scores, the students' knowledge gain, their web session variables and the results of the course evaluation were used to support our study.
The primary aim of this novel study was to determine whether the use of an e-learning package about surgical topic was able to improve the knowledge and competence of medical students.
Moreover, in this article we analyzed the students' attitude towards this educational environment.
Testing a methodology for monitoring and evaluating higher-order cognitive skills in online learning was an another key element of this project.
The positive aspects and the restrictions of the model as well as our personal experiences with the implementation of an online education course are discussed.

2. THEORETICAL PERSPECTIVES

2.1 Integrating e-learning into Medical education

E-learning is a new way of teaching that the web to deliver learning contents and to promote collaborative, lerner-centerd learning and it is actually considered a well-founded complement to the traditional instructor-led training, forming part of a blended-learning strategy [Davis & al., 2007], or a valid alternative to it [Chumley-Jones & al., 2002].
In this study, "e-learning refers to the use of Internet technologies to deliver a broad array of solutions that enhance knowledge and performance" [Rosenberg, 2001].
Web-based learning is used with increasing frequency in higher-level and vocational education.

Using e-learning, medical educators can improve educational interventions efficiency and effectiveness [Sadeghi et Al., 2014; Blissitt, 2016]. There have been several studies that have examined the effectiveness of online teaching compared to standard lecture-based approach [Cook & al., 2005; Cook & al., 2008; Davis & al., 2008; Kulier & al., 2009].
Although this teaching format offers many potential advantages, evidence supporting its use in medicine is limited. Some reviews in medical education contexts reveal that its use is highly variable among medical schools and seems to be more common in basic science modules than in internship training [Moberg, & Whitcomb, 1999; Ward & al., 2001; Pettersson & Olofsson, 2015].
The perceived benefits of this learning environment include flexibility in training times, access by geographically dispersed participants, adaptability to learner styles, interactivity, and the opportunity to communicate and collaborate virtually [Harden, & Hart, 2002; Fordis & al., 2005]. This kind of course also allows students to go beyond the content as they learn how to search and take advantage of the huge resources of information available on web network.
The assessment of the quality of an educational process, developed in presence or at a distance is influenced both by the definition that one wants to give of the concept of "quality" as well as by the specific context in which the learning process develops [Warnecke & Pearson, 2011; Siri & Rui, 2015].
If we assume, as stated by Trentin [2000], that "quality" is not synonymous with "excellence", but rather indicates the operation of a continuous process to bridge the gap between the "intended effect" (what should be learned) and "the real effect" (what was learned), it is essential to establish and have in mind the aims and objectives of an educational project in order to compare them with the obtained results.
Therefore, without a doubt, a point of excellence in the training process is represented by the prediction of an integration between the design activity and the monitoring activity and assessment [Lipari, 1995; Means et al., 2009].
This perspective assumes particular significance in distance learning, where the educational process is mainly based on interactive and collaborative dynamics, which involves all members of the learning community and where the tutors are able to observe the dynamics, to monitor the whole process and to redirect it toward the desired effect.
When the interaction between service providers and users is as strong as in training, it is essential to follow a critical or "constructivist" approach, therefore sensitive to the mutual influences between the evaluator, evaluando and social actors involved in the process.
In this perspective, the importance of monitoring teaching activities and the evaluation of their efficacy, not only in terms of achieving the objectives stated in the training project, but also in function to the needs expressed by the students and the skills required by the market work.

3. RESEARCH METHOD

3.1. Learning environment

One of the most used tool in e-learning is the Learning Management System (LMS). It is a web platform that allows us to deliver information in an intuitive way using specific software for the interaction of the users.
The University of Genoa started in 2005 a new system of online teaching called “Aulaweb”, an e-learning system based on the open source platform “Moodle”. This system allows both students and teachers the exchange of information about topics that are uploaded on the system using forums, chats and emails. It is a user-friendly application and it enables the delivery of instructional resources, communication, and collaboration [Siri & Rui, 2011].
In 2010, 22 online classes have been activated, with 38 teachers and 1.219 students registered.
The didactic organization of the Genoa School of Medicine (CLSMC) includes 51 teaching courses, organized in oral classes, practice activities and optional curricula activities (ADE).
The learning process of the student is evaluated using the University Didactic Credits (CFU). One CFU can be obtained after 25 hours of didactic activities.
Every student must acquire 360 CFUs during the six years of medical school in order to obtain the degree. An additional way to obtain CFUs is to attend the ADE.
A combined team of teachers from the Department of Surgery and Department of Anthropological Science of the University of Genoa has recently been built up to realize a web-based optional curricula activity that, added to the already existing web tools, can further develop and improve the University of Genoa e-learning system.
The training process was developed to enhance existing skills in the field of minimally invasive surgery among the students of the Bachelor Degree in Medicine and Surgery. Interventions were provided characterised on the one hand by the high quality of content and teaching methods, on the other hand by the strong interaction between teachers and students.
The elective course created was delivered entirely online, password-protected, and was divided into 4 modules.
The course was coached online by a main tutor; teaching assistants were assigned to help students with their field research and practice.
The course materials were presented through a series of web pages, text documents, and slides. For each topic, there were notes, objectives, assignments, self-assessment quizzes, and links to outside web resources.

3.2. Participants

30 students enrolled in the fifth and sixth-year students of the Genoa medical schools (academic year 2009-2010). Participation in the study was completely voluntary: 50% females and 50% males. The average age of the students was 25 years (± 1.41 ST DEV), with a

minimum age of 23 years and a maximum age of 27 yrs. All the participants were full-time students.

3.3. Learning effectiveness and satisfaction

The entire process was monitored to control the proper development of the planned activities, to make a note of any abnormalities and to identify any changes to be made during the activity. In a wider sense, or rather an instrument of managerial control, the frequency and degree of interactivity for the students, the appreciation of assets and the orderly development of the planned activities, were checked.

Such elements have allowed the analysis of the good progress of the course according to a variety of perspectives and viewpoints, particularly those of the students, through the analysis of the user, teachers and tutors satisfaction, which is a sort of peer review and allows integration of the course feedback given by the students.

Consequently, an assessment of efficacy during the course and a conclusive one, based not only on the achievement their stated objective but also on the needs expressed by students and as a first step, was proceeded by a preliminary identification of the framework of the objectives. The framework of the objectives of the course has been translated into evaluative indicators of a quantitative character. The reconstruction of the objectives perceived by the actors occurred through the partial use of data emerging from the entry questionnaire given to the students and by the teachers considerations. It was then proceeded to analyse the congruence between the objectives of the training project and the students expectations, to then outline some aspects of the validity of the methodology adopted and the internal efficacy.

In the final assessment the tests were performed for these objectives (validity of the methodology and internal efficacy) and a test was performed with respect to the realization and to the results.

More specifically the objectives of the assessment were:

- the adequacy of interventions in relation to the educational context;
- the validity of the methodology, both in relation to particular matters of method and content;
- the internal efficacy of the project, namely the degree in which the activities performed achieved the objectives foreseen;
- the external efficacy of the project, namely the degree in which the project has accomplished the needs initially defined by the students and the educational needs for the course.

The instruments for determination have been perfected since the start of the project to mid-term. Such activity has involved the monitoring group with the support of the scientific coordinator for the project. Participants have been involved in the monitoring project in the first meeting in the presence aimed at presenting the architecture of the course. The overall plan was later approved by the scientific manager.

The activities for the determination for monitoring were as follows:

- Distribution of questionnaires to the participants on the training course.

In particular, the following tools have been developed, for which we briefly report the characteristics and the schedule for distribution:

a) Questionnaires for the assessment of the incoming skills of the participants. The survey, aimed at identifying professional needs and the expected skills, took place after the first meeting in person. Participants were asked to indicate in a nominative questionnaire to what extent, on a scale from 1 to 10, they believe they have mastered each of the six skills listed in the curriculum, the extent to which they consider it useful to the profession and the extent to which they want to improve.

b) Multiple choice test designed to assess specific knowledge in the area at the start of the course

c) Questionnaire assessing the initial satisfaction of the participants. Participants were asked, always on the day of the presentation, to reflect on the expectations of the course, to express their level of satisfaction regarding the information received, the planning of the course as a whole and the usefulness of the proposal.

The questions foresaw an answering method represented by a Likert scale with uneven modality, from 1 to 5 points (avoiding the intermediate position), and a few open answers.

d) Questionnaire for the determination of satisfaction with the training activities. Participants were asked to complete an anonymous questionnaire at the end of the course in which they can express an assessment of the course, of the interaction with the teachers, of the teaching methodology, of the organization and structure.

The questions foresaw an answering method represented by a Likert scale with uneven modality, from 1 to 5 points (avoiding the intermediate position), and a few open answers.

e) Questionnaire for the determination of the participants skills on exiting. The survey, aimed at identifying the expected skills, took place at the end of the course and was conducted in online modality. The participants were asked to indicate in a nominative questionnaire to what extent, on a scale from 1 to 10, did they master each of the 6 skills listed in the teaching schedule. The goal is to get a crossed profile of the perceived competencies at the beginning of the course and those perceived at the end of the course.

f) Multiple-choice test aimed at assessing the specific knowledge in the subject acquired at the end of the course.

- ➢ Observation activities of the tutor (observation of the classroom and individual work, summarized by a report for each student).
- ➢ Observation activities of the teachers (observation of the classroom and of the on-line activities, impressions summarised of the predefined outline).
- ➢ Monitoring activity of the use of the virtual classroom (monitoring access to the site).

Assessment of the project is of great interest, due to its experimental nature and the need to draw insights from the experience to design other similar interventions.
Learning effectiveness was measured in terms of student learning outcomes and satisfaction.
Learning outcomes assessment was based on the student scores on the final tests and in particular on the differential between the results of the pre-test and final test.

4. RESULTS

30 students, on the Degree Course in Medicine (50% females, 50% males) participated in elective educational activities, the 8% of which were registered in the V year of the course and the other 92% in the VI year.
During the first meeting, dedicated to the presentation of the project, with particularly regard to the contents and the teaching aids available (the virtual classroom “Aulaweb”) as well as the "construction of the lecture-hall pact, students were asked to reflect on the expectations regarding the proposed experience, as well as to propose potential suggestions and to express comments on the day of presentation.
The ideas that emerged from the questionnaires in terms of expectations and suggestions, which were taken into account, as mentioned, in the organization of the training course and in the predisposition of the survey instruments, are summarized below:

<u>Expectations about the course contents</u>:

- to improve the technical knowledge of the course according to the latest international standards
- to have a perception which is better than that which is an intervention technique on the patient who today has a much greater potential

<u>Expectations on the innovative methodology used</u>:

- to acquire knowledge by organizing the work according to ones schedules/availability
- to be able to get the same information for a course in which attendance is compulsory
- to have the opportunity to review the lesson again several times so as not to lose details which sometimes escape in one’s presence
- to organize the teaching better to have more time for practical experience
- to have a smoother interaction with the teacher through forums

<u>Comments/suggestions</u>:

- increase the number of ADE structured on virtual classrooms
- improve the computerization of available courses
- apply this process to the examinations
- ensure that teachers are available in person for clarification.

From the above we can see that the initial expectations are very high both in terms of course objectives as well as in relation to the use of innovative teaching methods.
One of the key concepts is the concept of competence, meant as the specific objective of the educational processes.
On the basis of the determination of the competencies at the beginning of the course stated by the participants in the appropriate questionnaire, a form was prepared for each student with the indication of the degree of expertise perceived for each skill, of the level of usefulness for the profession carried out and the interest for improvement. These data were then compared with the values reported in the questionnaire concerning competencies at the end of the course.
From the global analysis of the levels of competence, in particular the degree of expertise and he level of usefulness for the profession perceived by the students, it clearly emerges that the structure of the course has filled gaps in the preparation considered very important for the profession.
A summary of the perception of the participants with respect to each of the six competencies indicated in the course are shown in the chart below.

Graph n. 1: Perception skills at the beginning of the course

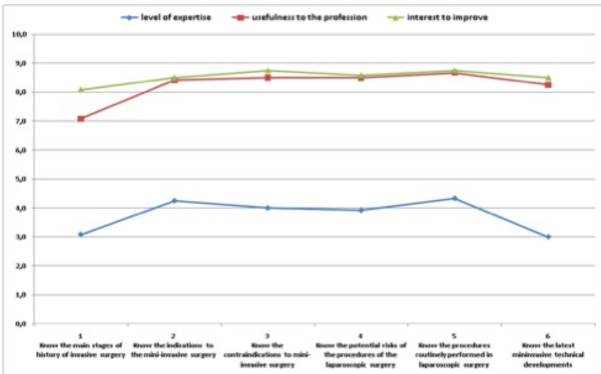

It is important to note that the initial perception on the degree of expertise for each competency at the beginning of the course is always less than the degree in which it is deemed useful for the profession and for which improvement is required/desired.
By cross-referencing the information gleaned from the incoming competency questionnaires with those outgoing, we note first of all that all of the students noticed a marked improvement in the level of expertise at the end of the course in each of the competencies declared at the beginning of the course.
The chart below, comparing the average value of the perception at the beginning and end of the course, clearly highlights the high degree of usefulness perceived by students compared to the proposed training course.

Graph n. 2: Comparison of perception skills on entering and at the end of the course

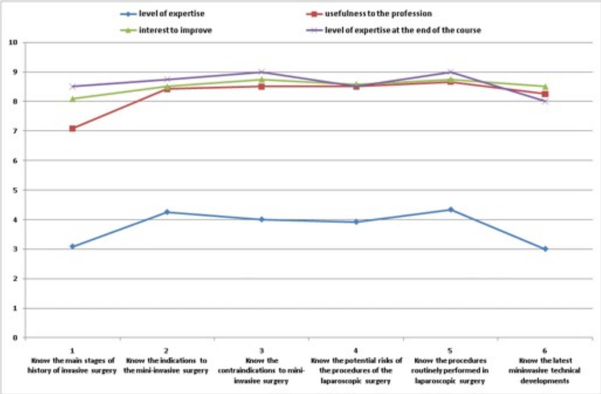

These data correspond to the results of the tests administered at the beginning of the course to assess knowledge in entry and at the end of the course to assess the degree of learning.
The overall pass rate of the enrolled students in the final online tests was 100%. The average university score was 21.7 (± 2.93 ST DEV) in the pretest and 27.3% (± 2.27 ST DEV) in the post test. The data indicate that there was an average improvement in knowledge between the beginning and end of the course equal to 28%.
Students rated all aspects of the course highly and knowledge scores increased significantly at the end of the course.
The comparison, in terms of perceived competence as well as in terms of results achieved also underlines the effectiveness of the course especially from the point of view of the theoretical reinforcement of skills already present among the recipients.
That is, the action proved to be more effective where it was able to confirm, update and sustain competencies already operative among the recipients.
By analysing the overall data obtained from the self-assessment on entering and on exiting, it is possible to advance to a reading of the results for each level of competence.

Objective 1: Know the main stages of history of invasive surgery
In this area of competence the average level of expertise indicated on entry is equal to 3; the average level for the perceived usefulness is 7 and for the interest to improve 8.
Fifty percent (50%) of students claim to know the stages of the history of technology at an insufficient level, 42% at level 1 and 8% at level 2. In a barely adequate manner 25% (level 5), sufficient 17% (level 6) and only 8% have a good knowledge of the topic.
Seventy-five percent (75%) of the students indicated that the knowledge of the topic was useful/very useful for the career, the remaining 25% thought it relatively useful.
At the end of the course the average level indicated in terms of expertise is equal to 9.

It is therefore evident that the decision to begin the ADE with a historical review of the development of the technology was greatly appreciated by the students.

Objective 2: Know the indications to the mini-invasive surgery
In this area of competence the average level of expertise indicated on entry is 4; the average level for the perceived usefulness is 8 and for the interest to improve 8.
Forty-two (42%) of participants claimed to have a sufficient level of knowledge of the technical information at a sufficient level, 17% a good level, the remaining 41% a level very low. All have identified the need to improve this knowledge and 64% indicated that such knowledge is useful to the profession (levels 8, 9 and 10) at level 3 compared to 24% which indicates level 2.
Strong perception of improvement emerges from that stated on exiting, the average level indicated in terms of expertise is equal to 9.

Objective 3: Know the contraindications to mini-invasive surgery
In this area of competence the average level of expertise indicated on entry is 4; the average level for the perceived usefulness is 8 and for the interest to improve 9.
Fifty percent (50%) of the ADE participants remained below level 4 compared to 25% which indicates a sufficient level, the remaining 25% had good knowledge. Eighty-three percent (83%) of the students are aware of the importance of knowing the contraindications of these procedures for the profession. At the end of the course the average level indicated in terms of expertise is equal to 9.

Objective 4: Know the potential risks of the procedures of the laparoscopic surgery
In this area of competence the average level of expertise indicated on entry is 4; the average level for the perceived usefulness is 8 and for the interest to improve 9.
Fifty percent (50%) of the participants believe they have a fair knowledge of the risks of this technique and 83% of students indicate such knowledge as being very important for the profession.
In this area there is a greater percentage of students who master this skill.
In the questionnaires on competencies on exiting a perception of great improvement in knowledge emerges, the average level is 9.

Objective 5: Know the procedures routinely performed in laparoscopic surgery.
In this area of competence the average level of expertise indicated on entry is 4; the average level for the perceived usefulness is 9 and for the interest to improve 9.

Forty-two (42%) of the participants have sufficient knowledge and the remaining wholly inadequate. Ninety-two percent (92%) consider useful the knowledge of the procedures performed routinely in laparoscopic surgery.
Also with regard to this skill, at the end of the course the average level indicated the in terms of expertise is very high, equal to 9.

Objective 6: Know the latest mininvasive technical developments
In this area of competence the average level of expertise indicated on entry is 3; the average level for the perceived usefulness is 8 and for the interest to improve 8.
Ninety-two percent (92%) had an insufficient level of knowledge of the latest technical developments and 75% thought it was very useful to the profession.
In regard to this area, the degree perceived at the end of the course to improve is slightly lower and reaches an average level of 8.

At the beginning of the course the degree of satisfaction, as evidenced by the chart below, in terms of the activities proposed as well as for the innovative methodology used, is globally very high. The information about the course objectives and the organization of training activities resulted satisfactory and comprehensive (respectively, 92% e 95%).
When asked about the usefulness of the introduction of online learning activities within university courses, 93% said yes and 40% specified that they did not consider it possible that courses entirely online risked being confusing. This confirms the view expressed during the first meeting in terms of expectations and suggestions. It has been shown that if teachers are available to clarify in person or actively participate in forums, answering the questions and doubts of students, the fully online mode of training cannot be the cause of confusion and therefore have little effect.
In relation to the educational objectives, to the contents, to the teaching methodologies as well as the tools used, the learners in the questionnaire given at the end of the course on the determination of appreciation of the training activities showed a very high overall mean degree of satisfaction (85%).
However, it should be noted that, even though a higher global level of satisfaction was found, there are some comments on the planning which re-dimension the declared level of appreciation. At the end of the activity only 65% of students recorded that the course was altogether satisfactory. This finding suggests strengthening efforts to make the course clearer and emphasizing the concrete nature of the interventions, in a way which also intensifies the link between the theoretical route object of this assessment with the practical developments foreseen in other clinical training activities.

We can state, from the above, that the students have correctly interpreted the role of investigator at the end of the course, arriving at concrete proposals to implement in the field.

5. CONCLUSIONS

The participants have significantly improved their knowledge on mini-invasive surgery after the course. The evaluation results demonstrated high levels of course functionality, effectiveness of its online content and acceptance among medical students.
This study indicated that an online course for undergraduate students may be successfully developed and implemented also in surgery settings and the students seem to be quite supportive.
<u>Reconstruction of the objectives</u>
The recognition of the framework proposed by the scientific goals of the training and the investigation of the needs expressed by students, has allowed the a comparison to be built in terms of consistency with the objectives of the project submitted at the beginning of the course. In summary the objectives proposed were focused, useful to the profession and for which it caused an improvement of know-how.
<u>Adequacy of the interventions in relation to the training context</u>
With this specific issue in the assessment we aim to analyse the correspondence between the choices made and the characteristics of the reference setting, more specifically between the characteristics of users and the goals of intervention. In regard to this it can be noted that the analysis performed confirm the appropriateness of the selection criteria of the students, namely students belonging to the V or the VI year of the Medicine school appear to be the users who can better respond to the training schedule.
The choice of intervention and its relative use is consistent with the learning needs of students of the medical degree course.
<u>Validity of the adopted methodology</u>
The methodological set-up scheduled in the training project has enhanced the interactive mode and this has allowed the expression of a positive opinion on the chosen method.
The positive assessment was also affected by the usability of proposed educational activities at any time and place, considered a very important element especially in courses that require a large number of activities in person, and the opportunity to review the lessons in order to further elaborate on the topic.
<u>External efficacy</u>
At this level of assessment we can say that the course objectives meet the needs generated by the changes in training methods of the university educational system.
Student participation in the planning of the training has allowed the construction of common objectives and the testing of a new educational model able to integrate with the traditional models.
<u>Internal efficacy</u>

The efficacy was also determined in an indirect manner on the basis of subjective assessments of learners in terms of content and learning experience. This measurement allows us to state that the quality of the operational context of the intervention is good.
Given the experimental nature of the project and the innovation of the training course the results of the survey can be summarized with the following articulations:

- Strong points;
- Critical points;
- Crucial points;
- Indications and suggestions for future editions

Strong points
One of the most interesting aspects of the course is represented by the prospect of integration of the in attendance training and of the online training in highly specialised courses that require a strong coordination between theoretical and practical activities.
The growth of competencies monitored through self-assessment tools, supported by positive data reported in the site of assessment of the perceived quality as well as the assessment of the degree of learning, converges in shaping a totally positive picture of the whole project system and its training program.
Critical points
The only critical aspect indicated by the participants is relative to the planning of the course, most notably in relation to the timing, which therefore requires careful consideration in the new edition.
Crucial points
According to respondents the success of the course focuses on a few significant factors, summarized as follows:

- the opportunity to attend training at times and in places which fit best with other study and work commitments;
- the opportunity to review the teaching activities to capture undertones that may escape during attendance;
- the existence of an online learning assessment that allows the students to self-assess their achievement of the objectives during the course.

REFERENCES

Blissitt AM. Blended learning versus traditional lecture in introductory nursing pathophysiology courses. J Nurs Educ. 2016;55:227–230.

Chumley-Jones HS, Dobbie A, Alford CL. Web-based learning: sound educational method or hype? A review of the evaluation literature. Acad Med. 2002; 77 (10 suppl): S86-S93.

Cook DA, Levinson AJ, Garside S, Dupras DM, Erwin PJ, Montori VM. Internet-based learning in the health professions: a meta-analysis. JAMA 2008; 300:1181–96.

Cook, D. A., D. M. Dupras, W. G. Thompson, and V. S. Pankratz. "Web-based learning in residents' continuity clinics: A randomized, controlled trial." Academic Medicine. 2005; 80 (1): 90–97.

Davis J, Chryssafidou E, Zamora J, Davies D, Khan K, Coomarasamy A: Computer-based teaching is as good as face to face lecture-based teaching of evidence based medicine: a randomised controlled trial. BMC Med Educ 2007, 7:23.

Davis J, Crabb S, Rogers E, Zamora J, Khan KS. Computer-based teaching is as good as face to face lecture-based teaching of evidence based medicine: a randomized controlled trial. Med Teach 2008; 30:302–307.

Fordis M, King JE, Ballantyne CM, Jones PH, Schneider KH, Spann SJ, Greenberg SB, Greisinger AJ. Comparison of the instructional efficacy of Internet-based CME with live interactive CME workshops: A randomized controlled trial. JAMA. 2005; 294:1043–51.

Fornaro R, et al. Chron's disease and cancer. Annali Italiani di Chirurgia 2009; 80(2), pp. 119-125

Fornaro R, et al. Crohn's disease surgery: problems of postoperative recurrence. Chirurgia italiana; 2008, 60(6), pp. 761-781.

Frascio, M., Gervasoni, M., Lazzara, F., (...), Sguanci, M., Vercelli, G. New teaching models for the medical school of medicine. Comparison between oral an online classes. The experience of the Genoa school of medicine. Journal of E-Learning and Knowledge Society 2009 5(3), pp. 43-48

Harden RM, Hart IR. An international virtual medical school (IVIMEDS): the future for medical education? Med Teacher. 2002; 24:261–7.

Kulier R, Coppus S, Zamora J, et al. The effectiveness of a clinically integrated e-learning course in evidence-based medicine: A cluster randomised controlled trial. BMC Medical Education 2009; 9:21.

Leung, W.C.. Competency based medical training: review. BMJ. 2002; 325: 693-696.

Lipari, D. Progettazione e valutazione nei processi formativi, Edizioni Lavoro, Roma, 1995.

Means, B., Toyama, Y., Murphy, R., Bakia, M., Jones, K.. Evaluation of Evidence-Based Practices in Online Learning: A Meta-Analysis and Review of Online Learning Studies, U.S. Department of Education Office of Planning, Evaluation, and Policy Development, Washington, D.C., 2009. Policy and Program Studies Service.

Moberg TF, Whitcomb ME. Educational technology to facilitate medical students' learning: background paper 2 of the medical school objectives project. Acad Med. 1999; 74: 1146-50.

Rosenberg M. E-Learning: Strategies for Delivering Knowledge in the Digital Age. New York: McGraw-Hill, 2001.

Ruiz, J., Mintzer, M.J., Leipzig, R.M.. The Impact of E-Learning in Medical Education. Academic Medicine 2006; 81(3): 207-212.

Siri A, Rui M. (2015). Distance education for health professions' students. International Conference on New Horizons in Education, INTE 2014, 25-27 June 2014, Paris, France. Procedia - Social and Behavioral Sciences, Volume 174, 12 February 2015, pp. 730–738.

Siri A, Rui M (2011). A teachers' training program at the University of Genoa. In: "E-learning innovative models for the integration of education, technology and research. 5th GUIDE International Conference Proceedings". Roma, Italy, 18-19 Novembre 2011, Roma: Guide Association, p. 1-10, ISBN/ISSN: 978-88-97772-00-2.

Stabilini C., Bracale U., Pignata G., Frascio M. Lazzara F., Gianetta E. Laparoscopic bridging vs. anatomic open reconstruction for midline abdominal hernia mesh repair [LABOR]: Single-blinded, multicenter, randomized, controlled trial on long-term functional results. 2013 Trials 14(1), 357.

Trentin G., The Quality-Interactivity Relationship in Distance Education, Educational Technology. 2000; 40, 1, 17-27.

Ward JP, Gordon J, Field MJ, Lehmann HP. Communication and information technology in medical education. Lancet. 2001; 357: 792-96.

Warnecke E, Pearson S. Medical students' perceptions of using e-learning to enhance the acquisition of consulting skills. Australas Med J. 2011;4:300–307.

Sadeghi R, Sedaghat MM, Sha Ahmadi F. Comparison of the effect of lecture and blended teaching methods on students' learning and satisfaction. J Adv Med Educ Prof. 2014;2:146–150.

Pettersson F, Olofsson A. Implementing distance teaching at a large scale in medical education: a struggle between dominant and non-dominant teaching activities. Educ Doc Inf s. 2015;20:359–80.

OPTICAL QUALITY CONTROL USING DEEP LEARNING

Franz Wiesinger[(a)], Daniel Klepatsch[(b)], Michael Bogner[(c)]

[(a),(b),(c)] University of Applied Sciences Upper Austria – Department of Embedded Systems Engineering
Softwarepark 11, A-4232 Hagenberg, Austria

[(a)]franz.wiesinger@fh-hagenberg.at, [(b)]daniel.klepatsch@fh-hagenberg.at, [(c)]michael.bogner@fh-hagenberg.at

ABSTRACT
Optical quality control is still often performed by people and always carries the risk of human error. A modern approach in order to solve this issue is the usage of artificial intelligence to boost performance and reliability.
This paper focuses on implementing a prototype for optical quality control based on the YOLOv3 algorithm. This is a state-of-the-art object detection system that uses deep learning to detect different classes of objects within an image.
Instead of different kinds of objects, the classes in this prototype were different quality levels of a strawberry. The dataset for this task was gathered by taking photos and using images from the internet. The strawberries on these images were labeled and fed to the YOLOv3 algorithm for training.
Despite the poor detection rate, the results showed that it is generally possible to use such systems for detecting different quality levels of products.

Keywords: optical quality control, artificial intelligence, neural networks, deep learning, object detection

1. INTRODUCTION
Artificial intelligence (AI) has been around since the 1960s, but in the past, applications were limited by computing power, algorithms, data or the money invested in research. This has changed over the past years. By utilizing Graphics Processing Units (GPUs) and parallel computation, the available power made it possible to solve problems of higher complexity. Due to ongoing success, funding for AI rose which led to more research and constantly improving algorithms.
Today, there is a lot of data that humans are not able to process anymore. To make use of all the collected data, artificial intelligence and machine learning is used to analyze it, try to find patterns and make predictions, based on the findings. All these systems are highly specialized on one task and are far from being general artificial intelligence. But they can outperform humans in these tasks and therefore improve speed or accuracy of certain processes.
A subfield of AI is machine vision, which enables algorithms to see the world through images and other data. This opens a new field for a broad range of applications. For example autonomous driving, object detection, text analysis as well as generative algorithms. Optical quality control is a task that is performed by humans at the conveyor belt but can be improved by utilizing machine vision.
Implementing such a system is not a trivial task though. It takes a professional approach and a lot of training data to make reliable predictions. These automated systems are meant to reduce costs and improve quality assurance. Mistakes have negative effects on both of these intended advantages. On the one hand, the decision to eliminate a good product leads to higher production costs. On the other hand, shipping a damaged product can cause a bad reputation or even endanger customers in case of unsafe electronics or delivering food. Therefore, a well-conceived and correct modeling of AI systems is required in order to accomplish this task. Tests and simulations in industrial environments will show if the intended results can be achieved.
The objective of this paper was to use a state-of-the-art object detection AI algorithm to not only identify objects within an image, but also determine their optical quality. A custom dataset of images of strawberries with varying quality was used to train the prototype. These quality levels are represented by different classes.

2. ARTIFICIAL INTELLIGENCE BASICS
In order to understand how the algorithm used in this paper and AI algorithms in general work, the following chapters will give a brief overview over some basic building blocks for artificial intelligence.

2.1. Artificial Neuron
The most basic building block of artificial intelligence algorithms is the artificial neuron. It is based on the function of natural neurons in the human brain and is a mathematical approximation that can also be implemented on electronic systems.
A natural neuron consists of three main parts: dendrites, the cell body and the axon. Signals received through the dendrites are forwarded to the cell body, where their processing takes place. After that, they are passed on to the axon, which is the communication channel to other neurons. It can split up into many branches to communicate with more than one neuron. The point

where the axon is connected to the next neurons dendrite is called a synapse. It also processes the incoming signal before forwarding it to the dendrite.
Artificial neurons are based on this simplified function and represented as the following mathematical function:

$$y=f\left(\sum_i \left(x_i w_i\right)+b\right) \tag{1}$$

The incoming signal through one dendrite is called x_i. Its first processing step is modeled by multiplying a weight to the signal, which is called w_i. The weighted signal is then forwarded to the cell body where the final processing takes places. All weighted signals are summed up and a bias b is added. This is the argument for the activation function $f(x)$ (Hijazi S. et al. 2015). The most common activation function is called the Leaky Rectified Linear Unit function (Leaky ReLU) and is depicted in Figure 1.

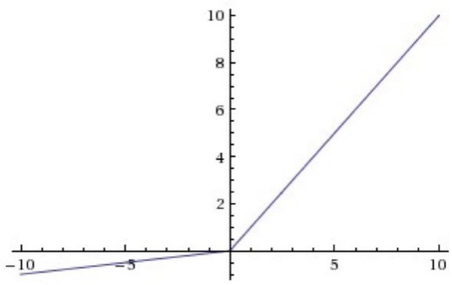

Figure 1: Leaky ReLU function.

The ability of an AI algorithm to learn things is given by adjusting the weights of the incoming signals for each neuron. Every training step calculates the error between the predicted result and the actual result, the ground truth, and the weights of each neuron is modified according to its influence on the error.

2.2. Neural Networks

While neurons in the human brain are connected to other neurons, artificial neural networks are structured in layers, which contain neurons that are not connected to other neurons in the same layer. Basically, there are three types of layers: an input layer, hidden layers and an output layer.
The input layer contains the information about the input data. For example, every neuron could contain the information of one pixel from an image. Usually there is at least one hidden layer, which is used to increase the capacity of the network and the ability to learn more complex functions. In a fully-connected layer, the output of every single neuron is connected to all neuron inputs of the next layer. The output layer determines the classification result (Hijazi S. et al. 2015).
A classification task, for example, would be if a neural network has to determine, if there is a dog or a cat in an image. The input layer would contain the pixels from the image, the hidden layers are required to learn certain characteristics of the images and the output layer would contain two neurons, one for a cat and one for a dog. The network then propagates the input data signals through the network and outputs confidence values to the output neurons. These values are interpreted as how confident the network is whether there is a cat or a dog in the image. This kind of network is depicted in Figure 2.

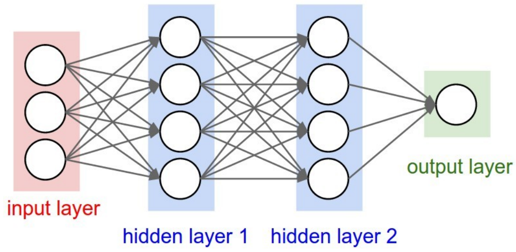

Figure 2: Fully-connected neural network.

2.2.1. Learning Procedure

A neural network is able to learn certain tasks by adjusting the weights of all neurons. In every learning step the output of the network and the ground truth are compared by using a loss function. This function can also take different aspects of the result into consideration and weigh their error value differently. That way, a network can be told what parts of the result are more important to optimize than others.
The target of the learning procedure is to minimize the result of the loss function. The most common way is to use the gradient descent algorithm, which is used to find a local minimum in a function by always going in the direction of the steepest negative gradient. To apply this method to a neural network an additional technique is required: backpropagation.
This method allows the training algorithm to calculate the impact of each neurons weights on the resulting loss by using partial derivation which leads to the gradient. These calculations are used to determine whether the weights are increased or decreased. A parameter called learning rate determines the size of the in- or decrease. If the learning rate is too small, the algorithm might take a very long time to get acceptable results. On the other hand, if it is too large, the optimal result might not be found due to too large changes in the weights (Gschwend D. 2016).

2.3. Deep Learning

Deep learning is a subfield of artificial intelligence and consists of networks with a more complex structure than simple neural networks. One difference is that common networks are rather shallow in terms of number of layers. They often have less than ten layers. In comparison, deep learning networks have up to 1000 layers which increases the capacity of the network as well as the complexity of the task the network can learn. Complex tasks like machine vision and natural language recognition require such deep networks.
The fundamental concept of deep learning algorithms is the idea that the input data have underlying representations, which is composed of various levels of

abstraction. By varying the number of layers, different levels of abstraction can be extracted from the training material which may lead to better accuracy of the network.

2.3.1. Convolutional Neural Network

One of the most important types of deep learning networks is the convolutional neural network (CNN). It is inspired by the way the visual cortex in the brain works and is therefore very much suited for performing image or video processing tasks.
Instead of fully-connected layers with single neurons, the CNN relies heavily on convolutional layers. Each convolutional layer consists of one or more filters, called kernels. A very common example is the Sobel operator which is used for horizontal or vertical edge detection in images. The kernel and the input image are convoluted which results in a two-dimensional feature map. Every kernel in a convolutional layer produces one feature map as output and has usually two or three dimensions, depending on the input data of the current layer. All outputs are stacked and result in a three-dimensional output which can be used by the next layer. Instead of changing the weights of each neuron, the values in the kernels are altered during learning. This results in a great reduction in memory usage.
Pooling layers are used to reduce the dimensions of input data by taking a two-by-two or three-by-three subsets and reduce it to one value by taking the maximum (max-pooling) or the average value (average-pooling).
Fully-connected layers are often used at the end of CNNs where the feature maps are used to perform a classification.
Dropout layers are similar to fully-connected layers and consist of neurons. The only difference is, that during each training step, a certain amount of neurons are deactivated. This helps to prevent the problem of overfitting, where the network memorized all the training data and their solution but is unable to perform well on unseen data (Gschwend D. 2016).

2.4. Types of Algorithms

When it comes to image processing with a neural network there are basically four different tasks that can be performed, which are depicted in Figure 3.

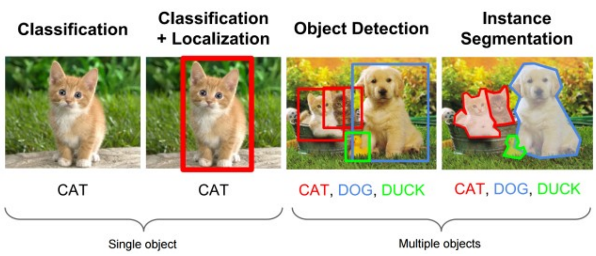

Figure 3: Different types of image processing algorithms.

The classification task is used on images which contain one object. The algorithm tells the user to which of the predefined classes the depicted object belongs to.
Localization extends the classification task by additionally drawing a frame around the object in the image.
Object detection is similar to localization but there is a variable number of objects in the image. The algorithm has to localize the objects and perform a classification on each one (Ng A. 2017).
Segmentation extends the object detection by not only drawing a frame around the object but draw its silhouette.
The prototype in this paper uses an algorithm for object detection since segmentation is significantly more complex but offers no major benefits.

2.5. Quality of Results

To determine the quality of the results, the total loss is insufficient due to problems like overfitting. The loss might be at a minimum but the algorithm does not perform well on unseen data, it just memorized the training data. Therefore, another measure of quality has to be established. This is the mean average precision (mAP). Before calculating the mAP, four result states have to be defined:

- True Positive (TP)
- False Positive (FP)
- True Negative (TN)
- False Negative (FN)

True positive means, that there was a detection and it was right. False positive means, that there was a detection, but it was wrong. True negative means that there was no detection and that this is right. False negative means that there was no detection, but there should have been. A detection is correct if the intersection over union (IoU) between the predicted object and the ground truth, depicted in Figure 4, exceeds a defined threshold.

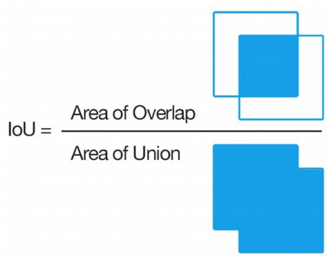

Figure 4: Intersection over union.

Now the precision and the recall of the algorithm can be calculated:

$$precision = \frac{TP}{TP+FP} \tag{2}$$

$$recall = \frac{TP}{TP+FN} \tag{3}$$

By varying the confidence threshold for the object classification, many precision and recall values can be calculated. These are then plotted in the Precision-Recall (PR) curve, where the recall is on the horizontal axis and the precision is on the vertical axis. The integral over that plot is somewhere between 0 and 1 and is called the average precision (AP). To get the mAP, several APs have to be calculated with different IoU thresholds.
The final mAP shows the actual quality of the results the algorithm produces (Henderson P., Ferrari V. 2016).

3. PROTOTYPE

The goal of this paper is to show the possibilities of using a CNN for image processing tasks like optical quality control. Instead of building a custom network, a well established algorithm called You Only Look Once (YOLO) was used. In the original paper it performed very well in comparison to other object detection algorithms of that time in speed as well as accuracy. All comparisons are based on the publicly available "*Common Objects in Context"* (COCO) and Pascal "*Visual Object Classes"* (VOC) image datasets (Redmon J. et al. 2016).
The working environment on the hardware side was as follows:

- Intel Core i5-8400 CPU
- 16 GB RAM
- Gigabyte Nvidia GTX 980 GPU

The software environment consisted of a Windows 10, 64-Bit operating system and the Darknet neural network framework, which was created by the inventor of the YOLO algorithm, Joseph Redmon. Since the framework is not compatible with Windows, an adjusted fork of it was used. This was created by the GitHub-User AlexeyAB. To accelerate the training phase, the Nvidia CUDA and cuDNN techniques were used. These allow the software to speed up all calculation tasks by utilizing the GPU. For generating the image labeling, a tool named Yolo_mark was used. This tool was also created by AlexeyAB.
The actual task, the prototype is supposed to perform, is the optical quality control of strawberries. The quality is categorized in six different classes:

- unripe
- partially ripe
- ripe
- lightly damaged
- heavily damaged
- rotten

If strawberries are totally white, they count as unripe. As soon as there is any red color on the fruit, it is counted as partially ripe. Fruits are ripe, if they are all red and no damage can be found. If there is any light damage or any dry spot, it counts as lightly damaged. Are the strawberries any more than lightly damaged, they count as heavily damaged. As soon as the fruit has any brown spot or signs of mold, it counts as rotten.

3.1. YOLO algorithm

The YOLO algorithm is faster than other systems because it does not use complex pipelines. The deformable parts model, for example, slides a window over the image and performs a classification of the current content of the window at each step. This has to be done in several sizes all over the image. YOLO avoids this by just looking at the image once via the CNN and predicting the objects in it. This also has the advantage, that the algorithm learns to include contextual information, like the background, into the decision making.
The concept of the whole algorithm is, that the input image is split into a S-by-S grid. Each cell is responsible for predicting B frames of objects, which center points are in that cell. In addition to that, each cell predicts C object classes. This means, that each cell outputs two frames and one set of class probabilities. So only one object class can exist in one cell. Before all that, a 24 convolutional layers deep CNN performs the feature extraction and uses several fully-connected layers at the end to map the features to the actual values that represent the object frames and classes. S, B and C can be chosen by the user. A method called non-max suppression is used in post processing to remove low-confidence or overlapping object frames.
The loss function that is going to be optimized during training is the commonly used least squares method but with a few tweaks. First, the error for predicting frames is weighted equally to the class probability. This was changed by giving the error for frame prediction a higher weight, so this becomes more important. Second, errors in predicting the frame size had the same impact on small and big frames. This was changed by predicting the square root of the frame, so the same offset has more impact on small frames than on larger ones (Redmon J. et al. 2016).

3.1.1. YOLOv2

YOLO received two incremental improvements where YOLOv2 was the first one. The accuracy was increased by 15%, the reduction to 19 convolutional layers and the removal of all fully-connected layers made it significantly faster and a combination of classification and detection training made it stronger.
A major change was the change from predicting the whole object frame to predicting offsets to reference frames, called anchor frames. These anchor frames are predefined by the user and their proportions should match the most frequent objects in the dataset. This helps the algorithm while training. This can be automated by a dimension clustering which uses a k-means algorithm to find the optimal proportions.
Additionally, the training of the network was performed with varying image scales. This is possible, since all fully-connected layers were removed. Small scales boost the speed of computation and high scales improve

the accuracy. The variation improves the overall quality, since the network learns to predict objects on several different scales (Redmon J. et al. 2017).

3.1.2. YOLOv3

The third iteration of the YOLO algorithm brings three major changes. Instead of 19 convolutional layers, YOLOv3 uses another base CNN with 53 convolutional layers and 23 residual blocks. In theory, the deeper a network gets, the harder it is to train the whole network. In the worst case, a layer learns its identity function and just forwards the input data instead of having a negative impact on the result. Practical attempts show though, that this negative impact does occur. To solve the problem, residual blocks were introduced which routes a bypass over some layers and sums up the last layers output and the input data.

$$y=F(x)+x \tag{4}$$

That way, the layers only have to learn to set their outputs to zero instead of the identity function.

The second change addresses the class confidence value. In YOLOv2 a softmax function was used to normalize the confidence for all classes for one frame and to pick the best result as detection. Now, a logistic function is used on each confidence value. This makes it possible to determine several classes per frame.

The third improvement is the frame prediction over different scales. While its predecessors directly predicted the object frames, this version predicts only three of the nine frames at the same point. This is now followed by a combination of convolutional layers, residual blocks and an upscaling block, which leads the higher resolution feature maps. After that, the next three frames are predicted and this whole part is repeated once more. This leads to an increase in accuracy, especially on small objects (Redmon J. et al. 2018).

3.2. Dataset generation

The most important part about training an AI is the dataset that is used. The best algorithm is only as good, as the dataset it gets to study.

For this prototype, the whole dataset was acquired in three steps. Custom photos were taken in the first two steps and images from the internet where used during the third step.

3.2.1. Custom photos

A pack of strawberries were picked up at the super market and left alone for four full days. After that time, the fruits had major flaws and also showed signs of mold. The test setup for taking the images consisted of a bright lamp, a white sheet of paper to get a uniform background and a small turntable to spin the fruits around and take images from different angles. 202 photos were taken with this indoor setup using a Samsung Galaxy A5 (2017) smartphone camera. An example image is depicted in Figure 5.

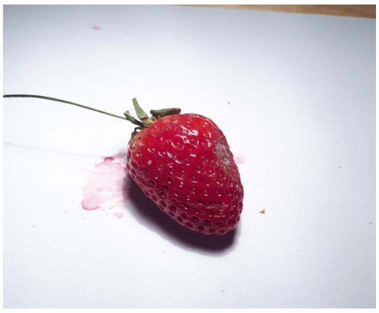

Figure 5: Photo from the first part of the dataset.

For the second step, the current strawberries were left alone for another three days and then a pack with fresh, partially unripe fruits was added. The setup was taken outdoor because using the sunlight led to better quality images. This time, 322 photos were taken by a Canon EOS 600D single-lens reflex camera. An example is depicted in Figure 6.

Figure 6: Photo from the second part of the dataset.

3.2.2. Additional image data

To increase the dataset, additional images from the Google Images were taken. A tool called Google Images Download from GitHub allows it, to automatically download a specific number of images based on a search phrase. For each of the following phrases, 250 images were downloaded:

- new strawberries
- young strawberries
- strawberry
- strawberries
- bad strawberries
- old strawberries
- rotten strawberries
- damaged strawberries

These 2000 images were then numbered and sorted out. Similar images, images with a too low resolution, bad quality images and all non-real pictures (like cartoon strawberries) were deleted. This led to a large dataset with images of strawberries that would be labeled and eventually fed into the algorithm for training.

3.2.3. Labeling

The labeling of the dataset was the most time consuming part in creating the prototype. Every image and every object had to be labeled by hand. This means that a box, which is associated to a pre-defined class,

has to be drawn over every object in an image. The algorithm then uses the labeling data (position, size and class of the box) as ground truth for training the neural network. It takes a training image, tries to predict its objects and classes and compares the result to the ground truth to improve the prediction.
As already mentioned, this task was accomplished by using the Yolo_mark tool. At first, the user defines the classes that the dataset contains. After that, the configuration and a directory containing the training images is passed to the tool. It then shows the user the first image in that folder and a slider to change the displayed image. With the number keys or a second slider, the user can choose a class for which he wants to draw a box on the image. By using the arrow keys, the next or previous image can be displayed.
This way, ever strawberry in the training images was labeled with the corresponding class and box. A screenshot of the tool is depicted in Figure 7.

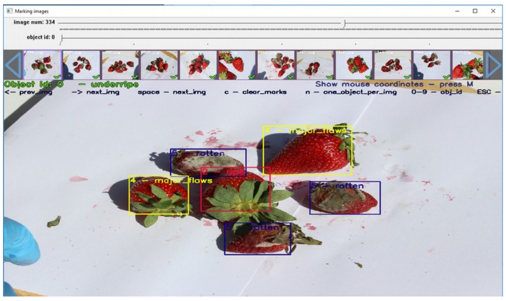

Figure 7: Screenshot of Yolo_mark.

3.2.4. Splitting the dataset

After the labeling was completed, the dataset had to be split into three parts: training data, validation data and testing data. The training data is used by the network to learn how the objects look like and what shapes their frames have. Validation data is used to test the networks performance on unseen data. Based on the validation results, the best model is picked. Test data is then used on this model to determine the actual accuracy. Validation and test data have to be totally independent from the training data.
To split the dataset, a Python script was created. The user passes the folder with all images and the percentages for each part. It then randomly creates the three parts where the images are split according to the percentages. Afterwards, it checks if each part has roughly the same percentage of each object class as the other parts. If these percentages do not match within a user-defined margin, it recreates the three parts with new random picks. This is repeated until the object percentages are within the margin or the user aborts the script. The best split up to that point is then used.

3.3. Training approach

For training the network, an iterative process is used. First, the network is trained by using built-in functions of the Darknet framework. Several parameters like the path to the folder with the training data and the number of batches are passed to the program.
It then executes the training until it completes or the user interrupts the training. Every 100 iterations, the current state of the network is saved so that progress is not lost in case of an error and that the most accurate network can be chosen afterwards.
After the training the results are analyzed. If they are of insufficient accuracy, alternations and optimizations have to be made on the setup. This includes common methods of optimization like increasing the dataset, introduce additional dropout layers or artificially increase the dataset by reusing old images and perform modifications on them.
After the modification of the setup, the training is restarted and the results are once more analyzed.

4. RESULTS

Due to timing limitations, only a total of ten training iterations were executed. The changes and results of every iteration are described in this chapter. Only iterations one and nine are accompanied by figures, because the results did not improve between these two. Therefore, the figures of iteration one show what the general results look like and the figure of iteration nine shows the first improvement in accuracy.
For the first training iteration, the dataset was split in 90% training data and 10% validation data and a standard YOLOv3 network with no modifications was used. The training batch size was 64, which means that the loss of 64 images is averaged and backpropagated. In the following notation a training iteration corresponds to the processing of one batch and a system iteration corresponds to one prototype training iteration. The training took place with pre-trained YOLOv3 weights, which should increase the accuracy of the network. Instead of using a steady learning rate, the default training algorithm also uses a burn-in learning rate, which is depicted in Figure 8.

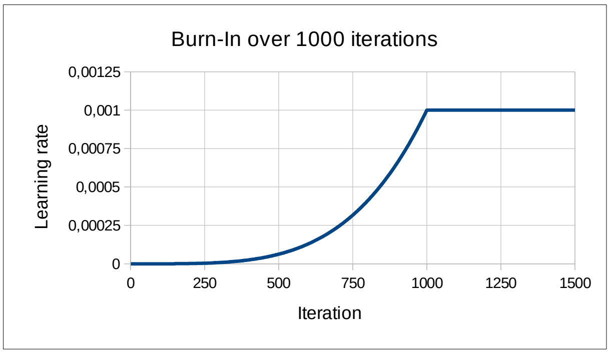

Figure 8: Burn-in learning rate of YOLOv3.

The total loss steadily decreased over the total of 30,000 training iterations, which is depicted in Figure 9 and Figure 10. At first, the loss showed a big variation since the network had no idea of what is depicted on the training images. After about 100 iterations a downward trend established whose slope steadily decreased afterwards. After 30,000 iterations, no significant decrease in loss could be determined and the training was considered to be finished.

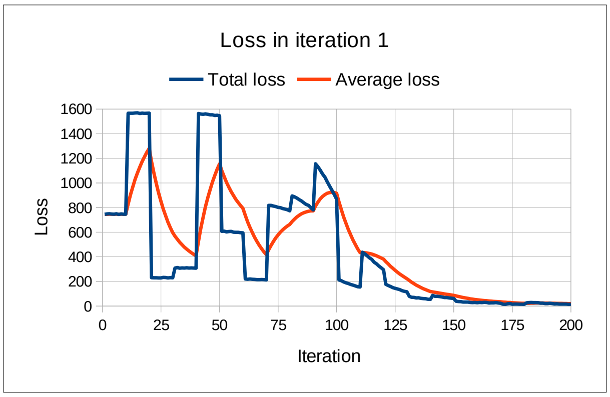

Figure 9: Total and average loss between 0 and 200 iterations.

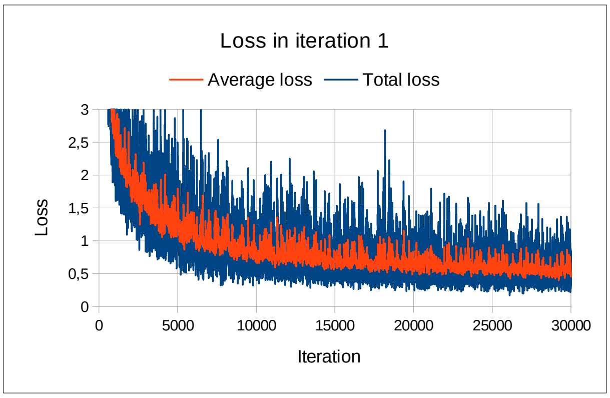

Figure 10: Total loss and average loss over 30,000 iterations.

During the training, the framework stores the weights, which represent the current state of the network every 100 training iterations. These states are then used to calculate the mAP for every 100th iteration. Afterwards, a curve can be drawn to compare the the accuracy of the model using training data and test data. The results of the first system iteration, depicted in Figure 11, show that the mAP curves differ a lot between the training data and the testing data. While the network memorized most of the training data with a maximum mAP of 90%, it had problems identifying objects on unseen images. The highest mAP was about 45%. This means that the network is heavily overfitting.

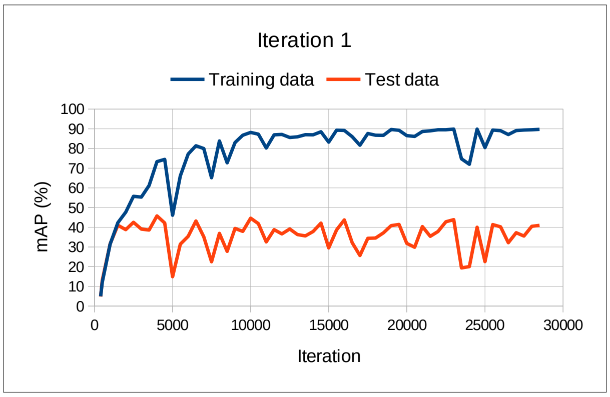

Figure 11: mAP comparison between training data and test data of the first system iteration.

To prevent this problem, an artificial increase of the dataset was performed for the second system iteration. Following techniques were used:

- Image scaling between 75% and 125% per axis
- Moving the image between -40% and +40% per axis
- Rotation between -8° and +8°
- Shearing with an angle between -8° and +8°
- Gaussian blur
- Contrast modification between -20% and +30%

For each original image in the dataset, 20 images were generated. Each image was created with a set of randomized parameters from the above listed. In addition to the artificial increase, the dataset was extended by 100 images from the internet which did not contain any strawberries.
Despite the modification, the mAP was roughly the same as in the first system iteration.
The third system iteration introduced the dimension clustering for the anchor frames, mentioned in the YOLOv2 algorithm. Additionally, less pre-trained layers were used to determine their effect. Only 61 instead of 74 were used.
After 10,000 training iterations, the results were worse than in the second system iteration. The mAP over the training data was only at 70% and the mAP over the validation data was around 40%.
For the fourth system iteration, 74 pre-trained layer weights were used again. Instead, the training on multiple input scales were disabled and the batch size was reduce from 64 to 32.
The results after 10,000 training iterations are the same as the ones from the third iteration.
The Darknet framework features an internal random data augmentation. Brightness and scaling randomization was increased for the fifth system iteration.
This resulted in even worse results, the validation mAP was again around 40% but the training mAP did not exceed 50%.
The sixth system iteration took a different approach. It took the weight from the fifth iteration at 8,000 training iterations. At that point, both the training and the validation mAP were around 40%. Then, the first 80 of the total 107 layers were frozen, so that the weights were not updated. The remaining 27 layers were trained like before. Again, the results did not improve, both mAPs stopped increasing at about 45%.
System iteration seven used a compact YOLOv3 model, the Tiny-YOLOv3, which consists of a total of 23 layers. The eighth system iteration halved the learning rate. Both iterations did not show any improvement.
For the ninth iteration, a modification to the dataset was used. The total of six different quality classes were reduced to just three. Unripe and partly ripe were merged as well as all three damaged classes.

For the first time, an increase in the mAP was achieved. While the training mAP rose up to 95% after 20,000 training iterations, the validation mAP reached up to 65% at one point, depicted in Figure 12. This was an increase of about 15% compared to all previous iterations. An example for what an output looks like is depicted in Figure 13.

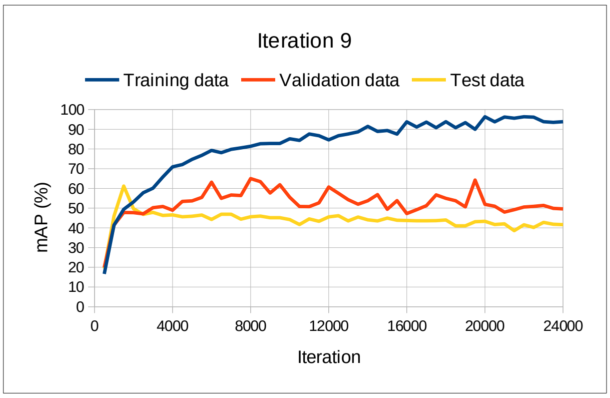

Figure 12: mAP comparison between training data, validation data and test data of the ninth system iteration.

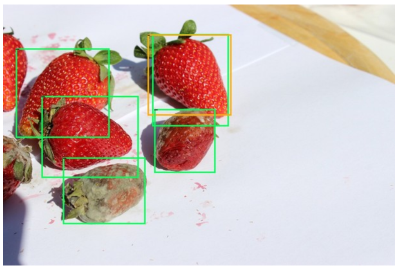

Figure 13: Example of a network prediction after the ninth system iteration. Green frames mark a ripe strawberries and orange frames mark lightly damaged strawberries.

With the additional data augmentation in the tenth system iteration, both mAPs dropped for 5% in comparison to the ninth iteration.
To summarize all results, Figure 14 depicts the comparison of the best validation mAPs of every system iteration. It clearly shows that common methods of optimization did not improve the accuracy but reduction of object classes did.

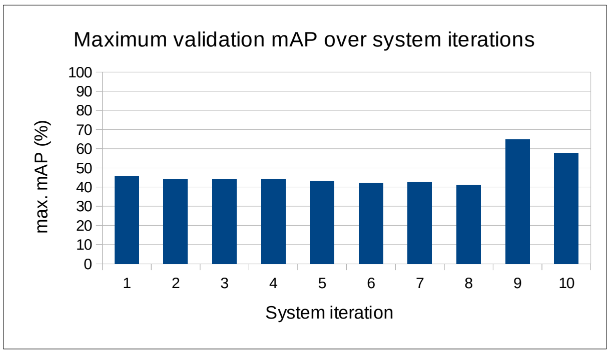

Figure 14: Comparison of the best validation mAPs of every system iteration.

5. CONCLUSION

Based on the ten system iterations performed with the prototype, several conclusions can be made.
Generally, there is no universal optimization technique that instantly boosts the accuracy of a network. It always depends on the task, that should be achieved and many other factors. Optimizing a neural network is done by fine-tuning certain parameter to achieve the best possible result under the given circumstances.
Since YOLOv3 is a reliable algorithm out of the box, there was no need for restructuring the whole network or adding different layers. The opposite can be said about the Darknet framework, which was created by the inventor of the YOLO algorithm. On the one hand, the framework is open source and accessible for everyone. On the other hand, it is lacking a documentation and source code commentary. This makes it difficult to use the framework. Especially if someone’s intention would be to implement a custom network, since the functionality of each available layer has to be looked up in the source code.
The results in this paper show, that the dataset has the most impact and has to be treated with a lot of care. Most likely, inconsistent labeling of the dataset caused rather bad results in terms of accuracy. It was not clear enough defined, whether a strawberry is not, lightly or heavily damaged.

Finally, it can be said that artificial intelligence is generally able to distinct different object from each other. As seen in many other demonstrations, machine vision is becoming better and better at recognizing objects. It comes down to the modelling of the system, which enables a distinction of the same object in different quality levels. This mainly includes the well-conceived creation of the dataset used to train a network. Tests under industrial production conditions show the quality of the system and help the engineers to incrementally improve the system. Also, a reduction to two quality levels is often sufficient and can boost the performance. Companies already collected huge amounts of data about their products which they can use to implement automated quality control systems and profit from their advantages like reliability or cost effectiveness.

REFERENCES

Hijazi S. et al., 2015. Using convolutional neural networks for image recognition. Available from: https://ip.cadence.com/uploads/901/cnn_wp-pdf [accessed 8 April 2019]

Redmon J. et al., 2016. You only look once: Unified, real-time object detection. Proceedings of the IEEE conference on computer vision and pattern recognition, 779-788. June 8-10, Boston, Massachusetts.

Redmon J. et al., 2017. YOLO9000: better, faster, stronger. Proceedings of the IEEE conference on computer vision and pattern recognition, 7263-7271. July 22-25, Honolulu, Hawaii.

Redmon J. et al., 2018. YOLOv3: An Incremental Improvement. Available from: https://arxiv.org/pdf/1804.02767.pdf [accessed 8 April 2019]

Gschwend D., 2016. ZynqNet: An FPGA-Accelerated Embedded Convolutional Neural Network. Master Thesis. ETH Zürich.

Ng A., 2017. C4W3L01 Object Localization. Available from: https://www.youtube.com/watch?v=GSwYGkTfOKk [accessed 8 April 2019]

Henderson P., Ferrari V., 2016. End-to-end training of object class detectors for mean average precision. Proceedings of the Asian Conference on Computer Vision, 198-213. November 21-23, Taipei, Taiwan.

PROACTIVE DEMAND AND CAPACITY MANAGEMENT FOR AUTOMOTIVE LOGISTICS USING AN EFFICIENT INFORMATION MODEL

Lisanne Temur [(a)], Daniel Fruhner [(b)], Katja Klingebiel [(c)]

[(a)] Volkswagen Nutzfahrzeuge
[(b)] IDiAL Institute, Dortmund University of Applied Sciences and Arts
[(c)] Faculty of Business Studies, Dortmund University of Applied Sciences and Arts

[(a)] lisanne.temur@volkswagen.de, [(b)] daniel.fruhner@fh-dortmund.de, [(c)] katja.klingebiel@fh-dortmund.de

ABSTRACT

The increasing technical complexity of cars and the high number of offered options lead to new challenges in the automotive industry and especially the mid-term demand and capacity management (DCM). This requires a procedural adaptation based upon an efficient information model. In this contribution, the state of the art is analysed for both the DCM process and the underlying information models. Promising concepts for managing the steadily increasing requirements in DCM are deducted, and a modular process kit for the procedural adaptation combined into the concept SmartDCM is introduced. Additionally, a new approach of an efficient information model for managing the increasingly complex information is presented.

Keywords: automotive demand and capacity management, information model

1. INTRODUCTION

Technological developments in the automotive industry are increasingly complex (Nagel 2011). They are influenced strongly by continuous derivatisation and an ongoing shortening of the product life cycle (PLC) (Filla and Klingebiel 2014, Hegner 2010, Romberg and Haas 2005). The resulting technical complexity of cars and the decreasing time-to-market lead to a reduced development time (Filla and Klingebiel 2014, Kuhn et al. 2002). Moreover, the possible combinations of different options, which are offered to customers, often account for more than 10^{32} available variants of middle-class cars - roughly the same number as atoms in the human body (Meyr 2004). The amount of data to handle all variants is considered unmanageable (Liebler 2013).

Over the past 30 years, automotive suppliers have taken power over the automotive manufacturing process (Wong 2017). The share of value-added by automotive suppliers in global automotive manufacturing has increased from 56% in 1985 to 85% in 2015 (Wong 2017). The product complexity, in combination with the reduction in vertical integration, leads to a strong dependence of original equipment manufacturers (OEMs) on their supplier networks (Klug 2010).

Foresighted planning is of central importance in a global and resource-optimised value chain. The critical process is the demand and capacity management (DCM): capacities are aligned with demands to avoid later bottlenecks that cause expensive capacity adjustments or production breakdowns (Askar 2008). DCM has to adapt to the changes in external and internal conditions.

This contribution presents the modular process kit SmartDCM supporting a proactive and event-oriented production program evaluation as a key step in the automotive DCM. The concept is based upon a new information model, which effectively transparently unites all required information.

The paper is structured as follows: all relevant terms and concepts, including the automotive DCM process as well as present challenges, are introduced in section 2. The related state of the art and the research gap will be presented subsequently. Section 3 presents a proactive, event-driven approach to DCM and the underlying information model. The paper concludes with the description of the ongoing implementation in industry and an outlook on further research.

2. THE AUTOMOTIVE DCM

This subsection gives an overview of the current management process, the challenges and the state of the art in automotive DCM to deduce the research gap.

2.1. Automotive DCM Processes

Automotive DCM planning process at OEMs can be classified using the Supply Chain Planning Matrix (SCPM): the matrix allocates the planning tasks vertically by planning horizons and horizontally by responsibilities of the OEM departments involved (Dörmer 2013, Fleischmann et al. 2015, Rohde et al. 2000, Schuh and Stich 2012). The automotive planning cycle typically starts with cross-functional strategic network planning. This long-term view typically includes uncertainties (Volling 2009), as the risk of temporary discontinuities in the material supply or the production process tend to make over-deterministic planning unsuitable (Liebler 2013). To handle the increasing number of car models and variants, strategic decisions can only provide the basis for the subsequent more detailed planning tasks in the mid-term horizon. The target of mid-term production planning is the optimisation of personnel and plant capacities. The primary customer demand for the next 12 to 24 months is forecasted in terms of volumes and customer selectable options (in the form of so-called option quotas). The later customer demand depends on the specific configuration of ordered cars. This aggregation reduces the existing complexity (Dörmer 2013, Volling 2009) and results from the possible forecast quality in the mid-term horizon (Dörmer 2013, Volling 2009). Changes in planned demand are triggered by general trends (e.g. urbanisation), scandals or political decisions (e.g. "diesel gate").

Subsequently, DCM processes ensure the availability of materials and resources for the mid-term production plan, even if specific material requirements are difficult to be determined from the aggregated planning volumes (Pawlikowski et al. 2017). If necessary, DCM proposes and initiates capacity adjustments to minimise costs for production, warehousing and human resources (Stadtler 2004). Like this, DCM acts as an essential interface between market demand, production and supply chain capacities (Arnold et al. 2008, Krog et al. 2002). Demand and capacity asynchronies are identified, and appropriate countermeasures are implemented in a reasonable time frame (Pawlikowski et al. 2017).

Then, internal negotiations are usually held in monthly sales meetings to adopt the production program to still necessary changes (Herold 2012). The aggregated procurement plan, production and transport capacities are derived from the identified production demand (Rohde et al. 2000). The result is a plant-dependent production schedule for volumes of defined product groups for each production week in the planning horizon (Dörmer 2013). Economic aspects should be taken into account in these processes (Barthel 2006), but feedback on the economic viability of capacity adjustments is not considered in the mid-term planning (Dörmer 2013).

In contrast, the later following short-term production planning uses customer orders. This deterministic primary demand can be used for the first time for a detailed demand calculation (Liebler 2013).

2.2. Challenges of the Automotive DCM

When central processes, structures and resources are fragmented and geared towards decentralisation, agility and speed (Gehrke 2017, Hompel and Henke 2014), production planning needs to become more flexible, too. For example, the current DCM process is no longer able to cope with the large number of planning impulses and the complexity of demand and capacity information. There is a need for a proactive and event-oriented evaluation of automotive production programs which shall be detailed in the following.

A highly complex set of technical rules describes the compatibility of car models and their potential options. Most of these options can be selected by the customer. Others are driven by marketing considerations, legal and political country-specific requirements and internal restrictions. The technical rules can prohibit or force options for certain models (e.g. no sports seats for a basic model). Because of dependencies among the options, the smallest change in the planned production program may affect greatly the part requirements and associated capacity utilisation of suppliers and other resources.

Moreover, after 125 years, car and drive concepts are fundamentally changing (Kampker et al. 2013). Alternative powertrain technologies are designed to reduce emissions. Electric mobility leads to changes in car architecture and product structure. Additional car variants are introduced within the short to mid-term period to react to changing market demand. At the same time, cars are increasingly connective and become more and more digitised by assistance systems (Gärtner and Heinrich 2018). Especially, the integration of intelligent assistance systems leads to a radical increase in the complexity of parts and car variants (Kampker et al. 2016, Krumm et al. 2014), resulting in a new complexity in the automotive DCM process.

Automotive product life cycles (PLC) amount to about seven years. Assuming a development time of three years, technologies used at the end of the PLC are ten years old (Kampker et al. 2017). Considering the rapid technological development of electronic components, PLCs in the automotive industry are far too long and will have to become shorter (Bundesregierung 2018). The developed markets are increasingly demanding customised products and solutions (Ehrenmann 2015) that adapt to new technological developments during the automobile PLCs. Today, OEMs are incentivised to upgrade electronic functions, components, parts or include numerous new parts within the PLC. In some cases, relationships with new supply chain partners arise (e.g. Apple or Google). On the one hand, the car is continually being redefined as a product, and the entire value chain must continually adapt to these changes (Kampker et al. 2013). On the other hand, it results in greater market dynamism and less predictable customer requirements in the mid-term. A significant flexibilisation of the entire value-added network is required to cope with these challenges.

The processing times for feedback on a production plan or a change within are currently in the range of several weeks. The current DCM process is only slightly automated today and characterised by many participants, iterative planning rounds and data distributed across many systems (MS Excel, SQL-DBs, flat files, etc.). The result is an increasing overload of the responsible human planners, an increasing frequency of bottlenecks as well as the associated costs. The example of a BMW bottleneck in 2017 illustrates how great the threat of a loss in quality and the associated loss of image is (Tagesschau 2017). In sum, the current DCM process is too static, too poorly digitalised and too slow for future automobile production. A more proactive, flexible and fast DCM process and a suitable DCM IT support are necessary.

A suitable degree of automation combined with the support of intelligent planning procedures allows the human planner to plan quickly and validly in an environment of high uncertainty. Today, as a result of the long planning cycles, there is no iterative feedback loop installed between the production plan based on the sales forecast and the production program planning in the mid-term. A real-time capacity check of planned production programs (like a pre-audit) will improve the quality of mid-term production planning by proactively identification of critical capacities.

An integration of continuous iterative feedback loops may increase the economic outcome of the production program when bottlenecks can be identified and avoided proactively. When determining costs for the capacity adjustment, it must be ensured that only the relevant costs are taken into account (Gottschalk 2005) which result from the comparison of planning scenarios (Ewert and Wagenhofer 2008). Costs of capacity adjustments include costs directly related to the provision and use of capacity flexibility (Gottschalk 2005). Additionally, opportunity costs must be considered (Kilger et al. 2012), as a possible profit could probably have been achieved if the capital employed for the measures had been used for a purpose other than that (Gottschalk 2005). An example is the lost contribution margin of car options of which the share decreases as a result of a supply bottleneck (Maiworm 2014). For decision support in medium and short-term sales planning, price limits (Kilger et al. 2012) can be applied for the acceptance of additional orders.

But DCM processes can only be accelerated if the relevant information is fully available in real-time. A prerequisite is the consistency and transparency of all DCM-relevant information.

2.3. State of the Art of the Automotive DCM

A review of relevant literature regarding automotive production program evaluation in the mid-term horizon has been conducted. The aim was to deduct the research gap clearly and understandably using a structured method by Webster and Watson (2002). The research has been based on the keywords “production planning”, “capacity planning”, “planning systems”, “optimisation”, “flexibility”, “supply chain management”, “the automotive industry” and “production and logistics”. A total of 43 relevant publications have been identified. The concepts have been allocated to the planning concepts of the SCPM and been classified into the different horizons. Figure 1 shows the resulting classification of concepts.

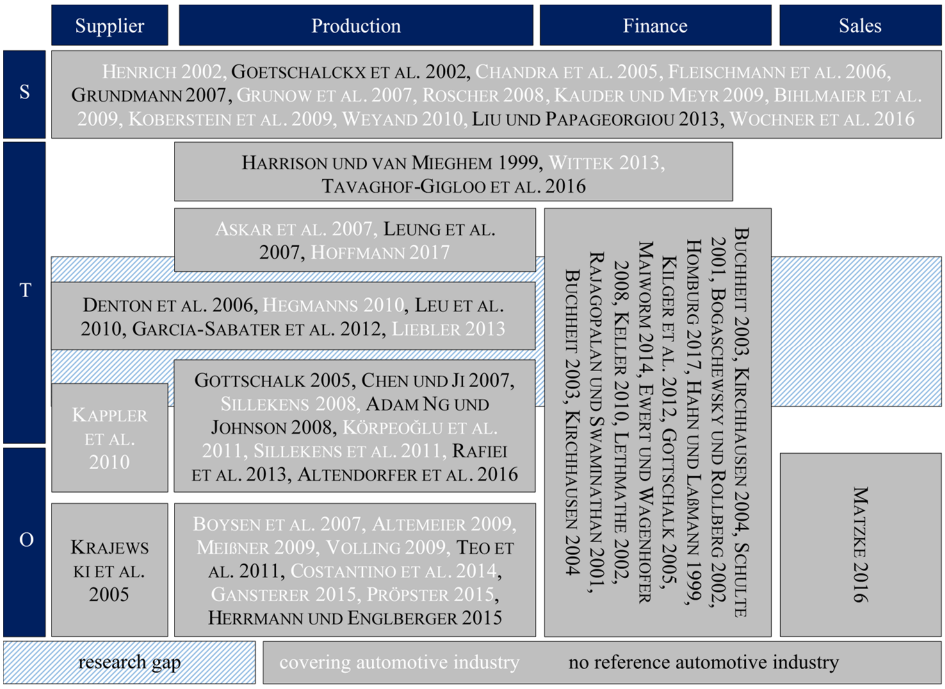

Figure 1: Research gap from the DCM in the mid-term horizon

13 of the 43 authors have been assigned to the strategic horizon, where distributive and capacitive factors of the cross-functional strategic network planning and product allocation are focused. The authors Grunow et al. (2007), Bihlmaier et al. (2009), Koberstein et al. (2009), Liu and Papageorgiou (2013) and Wochner et al. (2016) investigate the collaboration of distribution and production. Goetschalckx et al. (2002), Fleischmann et al. (2006) and Kauder (2008) examine a more holistic perspective and integrate all business areas except sales. Henrich (2002) presents an automotive model for strategic planning for an entire supply chain. The production in the strategic horizon is the focus of the publications of Chandra et al. (2005), Grundmann (2007), Roscher (2008) and Weyand (2010). The authors in the mid-term horizon mainly focus on the OEM production. Only Kappler et al. (2010) work on suppliers and sales by presenting a robust calculation method for determining part requirements using ranges (Kappler et al. 2010). Denton et al. (2006), Leung et al. (2007), Leu

et al. (2010), Körpeoğlu et al. (2011) and Rafiei et al. (2013) analyse the make-to-stock production. The authors Gottschalk (2005), Chen and Ji (2007), Adam Ng and Johnson (2008), Altendorfer et al. (2016) focus the tactical production planning but lack the specifics of the automotive industry. The authors Hegmanns (2010), Garcia-Sabater et al. (2011) and Liebler (2013) provide a holistic view on the mid-term horizon and, in addition, consider production, distribution and suppliers. Askar et al. (2007), Sillekens (2008), Sillekens et al. (2011), Hoffmann (2017) and Tavaghof-Gigloo et al. (2016) focus on the capacities of a production line.

Eleven authors have been assigned to the operative horizon. They focus on the production area of the company and deal with ascertained customer orders and not with demand forecasts or plans. Only Gansterer (2015) and Herrmann and Engelberger (2015) do not rely on orders but examine the transition from tactical to operational horizons. The authors Boysen et al. (2007), Altemeier (2009), Costantino et al. (2014), Pröpster (2015) and Matzke (2016) deal with the capacities of assembly teams. Krajewski et al. (2005), Volling (2009), Meißner (2009) and Teo et al. (2011) evaluate capacity adjustments.

Literature shows that it is not possible to deterministically validate demand plans within the mid-term production planning since the secondary demand can only be determined precisely with specified customer orders. However, for reasons of economy, sales and mid-term production planning are being carried out with a high degree of aggregation. Based on the literature review, there is a need for a new procedural concept which supports the event-oriented review of the production program. The literature review revealed no such concepts. Against the background of increasing market dynamics and globally linked supply networks, it is necessary to present a more integrated and dynamic concept for DCM. Therefore, an integrated, efficient information model is needed. Thus, the following section analyses the state of the art of automotive information models.

2.4. State of the Art of Automotive Information Models

Today, relevant data of automotive logistics is typically kept in several systems using relational data structures. However, a transparent and efficient information model is the key for DCM processes to assess the availability of automotive components. This information model has to depict all dependencies between parts, components and car features in a structured way (Fruhner et al. 2018). An elemental part of this information model is the product structure, which represents a structured form of the product and its components (Schuh and Riesener 2018). However, information on the dependence of planned model volumes, option quotas and material items is also needed as DCM processes synchronise market requirements with capacities and constraints of the supply chain and production system. A detailed analysis of information models in the automotive industry has been conducted in Fruhner et al. (2017). The analysed information models have been evaluated against these requirements which have been identified based on future challenges in the automotive industry: *Integration of new dependencies*, *Integration of cross-functional Information*, *Modularity*, *Management of Comprehensive Data*, and *Transparency* (Fruhner et al. 2017).

The literature review showed that approaches based on relational data structures quickly lead to poor transparency and redundancies as the data is distributed over several database systems (Bockholt 2012). A Design Structure Matrix (DSM) as proposed, for example, by Deng et al. (2012) or Kashkoush and ElMaraghy (2016) could support the representation of complex multidimensional and cross-functional automotive data. However, a DSM only allows to illustrate simple one-dimensional relationships. It is not possible to append additional cross-functional data, as its tabular structure easily becomes intransparent (Kissel 2014). Only similar relationships between two components can be mapped by semantic networks. No kind of hierarchy or at least an overall view can be integrated. Therefore, in complex data environments, the transparency is limited (Yang et al. 2012). Tree structures which have, for example, been presented by Kesper (2012) and Schuh (1988, 2018) do not offer modularity natively. However, an approach with evolving part/product families has been introduced by ElMaraghy et al. (2013). Moreover, it should be noted that tree structures can become very complex (Kesper 2012). With its hierarchical concept, the approach of Vegetti et al. (Vegetti et al. 2011) is a promising development. Two or more components can be joined together and form a more complex (sub-) assembly within the more general graph structure (Luo et al. 2016). Modularity is also supported in this way. Riggs and Hu (2013) introduce a precedence graph for disassembly, which is an especially enhanced graph structure.

Due to the findings of the literature review, a concept based on graph structures (including approaches of ontologies and semantic networks) is most suitable, as graph structures meet the requirements best.

3. INTRODUCTION OF AN APPROACH FOR PROACTIVE AND EVENT-ORIENTED PRODUCTION EVALUATION

A simplified but digitised, proactive DCM planning process is needed. Moreover, an efficient information model, which contains all relevant information, is required. Only the combination of both concepts might exploit the full potential. This section gives an overview of the concept SmartDCM and the new approach for an efficient information model.

3.1. A Modular Process Kit for SmartDCM

The developed qualitative research design addresses the empirical research gap in the automotive DCM and serves to derive the process modules needed for a proactive automotive DCM. It is based on data analysis of 48 guideline-based expert interviews at a plant of a German OEM with private and business customer segments which applies triangulation by combining two methods: the deductive category assignment is supplemented by inductive category formation. According to Mayring (2016), this triangulation improves the quality of research results compared to only one methodical approach. Transcribed text passages of the interviews that could not be assigned to a deductive category have been grouped into inductive categories according to predefined criteria. Three encoders have ensured the quality of the data evaluation in the deductive and inductive coding process. The need for a fast assessment of mid-term production programs to secure the supply of parts and incremental financial change has been validated. In short, it was revealed that an iterative feedback loop between the sales department and capacity providing departments dramatically increases the reaction time. To develop a holistic approach, the processes from literature have been enhanced by the identified requirements of entrepreneurial practice. It could be deduced, that the central vulnerability of today's DCM is reflected by the program approval that is not based on a detailed capacity check: the determination of requirements takes mostly place afterwards. Valuable empirical findings contribute to an application-oriented development of an event-oriented mid-term evaluation of the automotive production-planning program. Table 1 shows the developed modular process kit.

The process kit is divided into three thematic clusters: production program planning, capacitive evaluation and monetary evaluation.

The first thematic cluster production program planning contains nine process modules. The identification of the market requirements takes external parameters and trends into account. The internal requirement identification focuses on the existing restrictions within the OEM's internal production network. Subsequently, the primary requirements planning is carried out as proposed in literature. A comparison is made between the market requirements and the internal requirement identification to determine the production oriented sales planning. The process module for enriching the mid-term primary demand is an alternative to the forecast-based rough planning of resources. It provides the basis for the detailed capacity check of purchased and manufactured parts, containers and OEM internal resources for the mid-term horizon.

The second thematic cluster capacitive evaluation contains eight process modules. The determination of the secondary demand is a relevant process step as proposed by literature. The production requirements planning contains the process steps procurement model assignment, inhouse production planning and external procurement planning. The detailed capacitive evaluation includes capacitive checking within the OEM's internal production network as well as balancing of capacities for purchased and manufactured parts and containers. The capacitive adjustment evaluation relies on relevant information such as marginal cost and capacities, lead times and throughput times for all known measures. If a capacity adjustment is not possible, customer demand may be controlled by demand management. To enable the iterative feedback loop, the capacitive feedback from these processes must be reintegrated into primary demand planning. Finally, the assessment of the overall security of supply summary of the production program takes all capacitive adjustments into account.

Table 1: Modular process kit for a proactive DCM

category	required process modules			
production program planning	PM1	external requirement identification		
	PM2	internal requirement identification		
	PM3	primary requirements planning		
	PM4	analysis of existing restriction		
	PM5	determination of production oriented planning		
	PM6	event-driven production program changes		
	PM7	production program enrichment		
	PM8	production program summary		
	PM9	production program release		
capacitive evaluation	PM10	secondary requirements planning		
	PM11	production requirements planning		
	PM12	interplant capacity evaluation		
	PM13	detailed capacity evaluation	a	internal production plant
			b	purchased parts
			c	manufactured parts
			d	container
	PM14	capacitive adjustment evaluation	a	internal production plant
			b	purchased parts
			c	manufactured parts
			d	container
	PM15	demand management	a	internal production plant
			c	manufactured parts
	PM16	capacitive feedback		
	PM17	security of supply summary	a	internal production plant
			b	purchased parts
			c	manufactured parts
			d	container
monetary evaluation	PM18	contribution marging determination		
	PM19	capacity adjustment costs determination		

The third thematic cluster monetary evaluation includes the financial evaluation and total feasibility check. For a financial comparison of a production program with its predecessor, the respective contribution margins are offset against each other after deduction of relevant costs incurred. To determine the contribution margin, the net cost of sales must be compared with the actual revenue of the planning period by summing up all product types (Hahn and Laßmann 1999, Kilger et al. 2012). Changes in the model mix, option mix or market distribution of the car volumes to be produced can have a positive or negative impact on the contribution margin of the production program.

Figure 2 visualises the proactive DCM process based on the modular process kit. The validation of the process kit is based on workshops to verify the research outcome with the interviewed experts. The workshops took place within each interviewed department at the OEM to ensure the correctness of the process modules within the process kit and to derive requirements for an efficient and user-friendly application development. Underlying requirements are, for example, appropriateness for the task, self-descriptiveness, identification and elimination of faulty customizability and controllability (Deutsches Institut für Normung 2008, Schneider 2008). The appropriateness for the task helps users to do their job effectively and efficiently. The self-descriptiveness ensures that each dialogue step is immediately understandable and that it is explained to the user on request. It is necessary to ensure the identification and elimination of faulty inputs with minimal correction effort as some data is entered by the users themselves (Krcmar 2015). The customizability allows adapting to user-specific needs, such as the choice of the preferred language or the reading direction from left to right. The controllability allows the user to initiate the dialogue process and to influence its direction and speed. To ensure the device-independent applicability of the SmartDCM, a web-based implementation has been recommended.

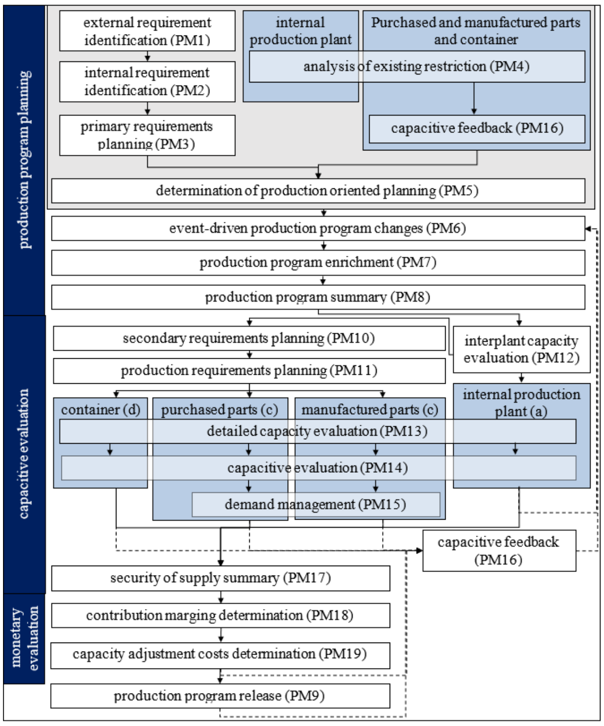

Figure 2: Process for a proactive DCM

3.2. Information Model for Automotive DCM

To implement the described new SmartDCM process, a new information model is needed, which holistically depicts the required information. The literature review revealed that DSMs, even if valuable in development, are not eligible for DCM and its complex cross-functional information. Especially semantic networks, tree structures and generalised graph structures have proven to be promising candidates for a new generation of information models. A graph structure has been chosen as the basis for SmartDCM, as it fulfils the requirements for a future-oriented information model (e.g. parallel component development).

As a next step, it was necessary to analyse what the information model used in the SmartDCM has to contain. For this purpose, data of two middle-class series of a German OEM have been analysed.

Each model of both car series can be sold in several markets, where each market has its own legal rules and customer preferences. Therefore, it is important to differentiate not only between models but also between model-market-combinations.

Each option is typically assigned to an option family (O-Family). This helps, for example, to avoid invalid configurations (e.g. two radios). In DCM processes, the planned volumes of car models and quotas of options are analysed to rule out asynchronicities. In case of a shift in demand, typically model volumes and option quotas are modified in synchronity. So, it is necessary to integrate the volume for model-market-combinations into the information model. All allowed options and the associated option families must also be mapped as well as the planned quota information. The technical and market-specific buildability of any car configuration is a key aspect for the validity of a production program. The highly complex set of technical rules (TECRule) must be integrated as well into the information model to account for this aspect. A car *Type* is divided into several *Models*. Furthermore, each *Model* is connected to several *Markets*. Moreover, within each *Market,* several *Models* can be sold.

For each *Option,* a *Quota* is necessary to anticipate customer orders. The *Quota* is based on the ratio of the occurrence of the *Option* in its *Option-Family* and is considered to be different for each *Market*. Therefore, each *Option* is connected to an *Option-Family*, a *Quota* and a *Market*. The same argumentation is valid for the relation between *Models* or *Model-Market*-combinations and *Volumes*. Furthermore, the *Options* and *Markets* are associated to the *Technical Rules* as those rules might block or force *Options* due to a specific combination of *Options* or *Market*-specific limitation.

The resulting data objects needed can be summarised as follows: *Type*, *Model*, *Market*, *Volume*, *Option Family*, *Option*, *Quota* and *Technical Rules*. Figure 3 shows the identified attributes transferred into a graph structure.

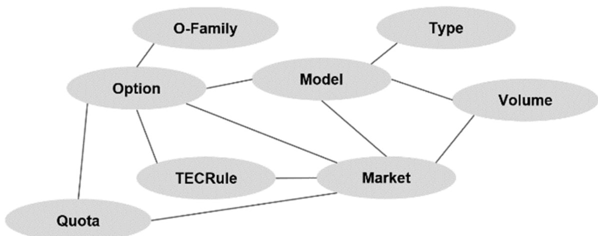

Figure 3: Efficient information model for SmartDCM

For the application, the introduced graph structure has been instantiated at a German OEM. Figure 4 shows the resulting class diagram in the Unified Modeling Language (UML). The model was supplemented within this step by the concept of variant cluster (VCluster). VClusters describe subsets of permitted variants with common characteristics. Each variant cluster inherits all the characteristics of its higher-level cluster. As a result, the model contains an efficient hierarchically linked cluster structure of variants. Thus, an effectively transparently representation of all the required information is given. First tests show that a production program evaluation can be performed efficiently using the developed information model.

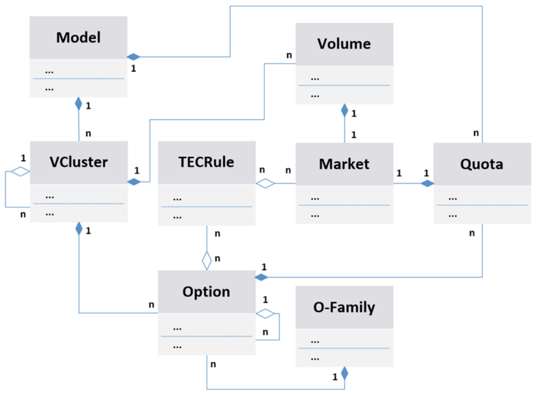

Figure 4: Instantiation of the developed graph structure

4. SUMMARY AND OUTLOOK

Digitisation in the automotive industry and the increasing number of variants are major challenges for future automotive DCM. Additionally, shorter life cycles and development cycles also increase the planning complexity. To overcome these challenges, this paper presents a modular process kit for a proactive automotive DCM which implicates a procedural change and an approach for efficient information model. The SmartDCM modular process kit provides an event-driven capacitive evaluation of an automotive production program that contains country-specific car models and options. The capacitive feedback includes restrictions from manufactured and purchased parts, containers and internal production plants and is communicated to the sales department in iteration loops. To be able to manage the increasingly complex information, the attributes required in the SmartDCM have been identified first. Afterwards, the developed information model, including the required attributes, has been introduced and an instantiation for the prototypical implementation of SmartDCM at a German OEM has been performed.
Currently, a software-suite is being developed, combining both the SmartDCM and the efficient information model. The implementation uses a service-oriented architecture to react as flexible as possible to potential future changes in the DCM process or technological changes (e.g. new deep learning methods). In the next steps, the information model will be extended to include capacity information and especially the new and changed dependencies in automotive products which result from the increasing digitalisation of the car.

REFERENCES

Adam Ng, T. S. and Johnson, E. L., 2008. Production planning with flexible customization using a branch-price-cut method. IIE Transactions vol. 40, 1198–1210.

Altemeier, S., 2009. Kostenoptimale Kapazitätsabstimmung in einer getakteten Variantenfließlinie unter expliziter Berücksichtigung des Unterstützereinsatzes und unterschiedlicher Planungszeiträume. Thesis (PhD). Paderborn University.

Altendorfer, K., Felberbauer, T. and Jodlbauer, H., 2016. Effects of forecast errors on optimal utilisation in aggregate production planning with stochastic customer demand. International Journal of Production Research vol. 54, 3718–3735.

Arnold, D., Isermann, H., Kuhn, A., Tempelmeier, H. and Furmans, K., eds., 2008. Handbuch Logistik[Online], 3rd edn. Berlin: Springer. Available at: http://dx.doi.org/10.1007/978-3-540-72929-7.

Askar, G., 2008. Optimierte Flexibilitätsnutzung in Automobilwerken. Thesis (PhD). Clausthal University of Technology.

Askar, G., Sillekens, T., Suhl, L. and Zimmermann, J., 2007. Flexibility Planning in Automotive Plants. In: Günther, H.-O., Mattfeld, D. C. and Suhl, L., eds. Management logistischer NetzwerkeEntscheidungsunterstützung, Informationssysteme und OR-Tools. Heidelberg: Physica-Verlag Heidelberg, 235–255.

Barthel, H., 2006. Modell zur Analyse und Gestaltung des Bestellverhaltens für die variantenreiche Serienproduktion. Thesis (PhD). Stuttgart. University of Stuttgart[Online]. Available at: http://elib.uni-stuttgart.de/opus/volltexte/2007/2918/pdf/Diss_Barthel_hs.pdf (Accessed 18 October 2017).

Bihlmaier, R., Koberstein, A. and Obst, R., 2009. Modeling and optimizing of strategic and tactical production planning in the automotive industry under uncertainty. OR Spectrum vol. 31, 311–336.

Bockholt, F., 2012. Operatives Störungsmanagement für globale Logistiknetzwerke: Ökonomie- und ökologieorientiertes Referenzmodell für den Einsatz in der Automobilindustrie. Thesis (PhD). TU Dortmund University.

Boysen, N., Fliedner, M. and Scholl, A., 2007. Produktionsplanung bei Variantenfließfertigung: Planungshierarchie und Elemente einer Hierarchischen Planung. Journal of Business Economics vol. 77, 759–793.

Chandra, C., Everson, M. and Grabis, J., 2005. Evaluation of enterprise-level benefits of manufacturing flexibility. Omega vol. 43, 17–31.

Chen, K. and Ji, P., 2007. A mixed integer programming model for advanced planning and scheduling (APS). European Journal of Operational Research vol. 181, 515–522.

Costantino, F., Toni, A. F. de, Di Gravio, G. and Nonino, F., 2014. Scheduling Mixed-Model Production on Multiple Assembly Lines with Shared Resources Using Genetic Algorithms: The Case Study of a Motorbike Company. Advances in Decision Sciences vol. 2014, 1–11.

Deng, X., Huet, G., Tan, S. and Fortin, C., 2012. Product decomposition using design structure matrix for intellectual property protection in supply chain outsourcing. Computers in Industry vol. 63, 632–641.

Denton, B. T., Forrest, J. and Milne, R. J., 2006. IBM Solves a Mixed-Integer Program to Optimize Its Semiconductor Supply Chain. INFORMS Journal on Applied Analytics vol. 36, 383–342.

Deutsches Institut für Normung, 2008 *9241-110:2006: Ergonomie der Mensch-System-Interaktion - Teil 110: Grundsätze der Dialoggestaltung (ISO 9241-110:2006); Deutsche Fassung EN ISO 9241-110:2006*. Berlin: Beuth Verlag GmbH.

Dörmer, J., 2013. Produktionsprogrammplanung bei variantenreicher Fließproduktion: Untersucht am Beispiel der Automobilendmontage. Wiesbaden: Springer.

Ehrenmann, F., 2015. Kosten- und zeiteffizienter Wandel von Produktionssystemen: Ein Ansatz für ein ausgewogenes Change Management von Produktionsnetzwerken. Wiesbaden: Springer Gabler.

ElMaraghy, H., Schuh, G., ElMaraghy, W., Piller, F. T., Schönsleben, P., Tseng, M. and Bernard, A., 2013. Product variety management. CIRP Annals - Manufacturing Technology vol. 62, 629–652.

Ewert, R. and Wagenhofer, A., 2008. Interne unternehmensrechnung. Berlin Heidelberg: Springer-Verlag.

Filla, P. and Klingebiel, K., 2014. Risk profiles for the pre-series logistics in automotive ramp-up processes. Procedia CIRP vol. 20, 44–49.

Fleischmann, B., Ferber, S. and Henrich, P., 2006. Strategic Planning of BMW's Global Production Network. INFORMS Journal on Applied Analytics vol. 36, 191–282.

Fleischmann, B., Meyr, H. and Wagner, M., 2015. Advanced Planning. In: Stadtler, H., Kilger, C. and Meyr, H., eds. Supply chain management and advanced planningConcepts, models, software, and case studies. 5th edn. Berlin Heidelberg: Springer, 71–95.

Fruhner, D., Klingebiel, K., Pawlikowski, K. and Toth, M., 2018. Impacts of the digitalised car on logistics. Proceedings of the 25th International Annual EurOMA Conference, June 24-26. Budapest, Hungary.

Fruhner, D., Pawlikowski, K., Klingebiel, K. and Toth, M., 2017. Efficient Product Representations for Automotive Logistics. Proceedings of the 29th European Modeling and Simulation Symposium (EMSS), 100–109, September 18 - 20. Barcelona, Spain.

Gansterer, M., 2015. Aggregate planning and forecasting in make-to-order production systems. International Journal of Production Economics vol. 170, 521–528.

Garcia-Sabater, J. P., Maheut, J. and Garcia-Sabater, J. J., 2011. A two-stage sequential planning scheme for integrated operations planning and scheduling system using MILP: The case of an engine assembler. Flexible Services and Manufacturing Journal vol. 24, 171–209.

Gärtner, C. and Heinrich, C., eds., 2018. Fallstudien zur Digitalen Transformation: Case Studies für die Lehre und praktische Anwendung[Online]. Wiesbaden: Gabler Verlag. Available at: http://dx.doi.org/10.1007/978-3-658-18745-3.

Gehrke, L., 2017. Entwicklung eines Industrie-4.0-Managementkonzepts als Beitrag zur digitalen Transformation der Logistik und Produktion. Dissertation. TU Dortmund.

Goetschalckx, M., Vidal, C. J. and Dogan, K., 2002. Modeling and design of global logistics systems: A review of integrated strategic and tactical models and design algorithms. European Journal of Operational Research vol. 143, 1–18.

Gottschalk, L. L., 2005. Flexibilitätsprofile: Analyse und Konfiguration von Strategien zur Kapazitätsanpassung in der industriellen Produktion. Zürich: ETH Zurich.

Grundmann, S., 2007. Planung flexibler Produktionskapazitäten im Spannungsfeld logistischer und monetärer Ziele. Dissertation. Gottfried Wilhelm Leibniz.

Grunow, M., Günther, H.-O., Burdenik, H. and Alting, L., 2007. Evolving Production Network Structures. CIRP Annals - Manufacturing Technology vol. 56, 427–430.

Hahn, D. and Laßmann, G., 1999. Produktionswirtschaft - Controlling industrieller Produktion: Band 1 & Band 2: Grundlagen, Führung und Organisation, Produkte und Produktprogramm, Material und Dienstleistungen, Prozesse. Heidelberg: Physica-Verlag HD.

Hegmanns, T., 2010. Dezentrales Planungs- und Prozesskonzept für ein kollaboratives Bedarfs- und Kapazitätsmanagement in Produktionsnetzwerken. Zugl.: Dortmund, Techn. Univ., Diss.

Hegner, C., 2010. Modellbasierte Vernetzung strategischer und operativer Anlaufgrößen von interdependenten Fahrzeugprojekten. Dissertation. Technische Universität Chemnitz.

Henrich, P., 2002. Strategische Gestaltung von Produktionssystemen in der Automobilindustrie. Thesis (PhD). University of Augsburg.

Herold, L., 2012. Kundenorientierte Prozesssteuerung in der Automobilindustrie: Die Rolle von Logistik und Logistikcontrolling im Prozess „vom Kunden bis zum Kunden“[Online]. Wiesbaden: Deutscher Universitätsverlag. Available at: http://dx.doi.org/10.1007/978-3-322-85234-2.

Herrmann, F. and Englberger, J., 2015. Robuste Optimierung zur Produktionsprogrammplanung. In:

Claus, T., Herrmann, F. and Manitz, M., eds. Produktionsplanung und -steuerungForschungsansätze, Methoden und deren Anwendungen. Berlin: Springer Gabler, 25–45.

Hoffmann, U., 2017. Kennzahlenbasierte Entscheidungsunterstützung für die aggregierte Produktionsprogrammplanung. Dissertation. Technische Universität Chemnitz.

Hompel, M. ten and Henke, M., 2014. Logistik 4.0. In: Bauernhansl, T., Hompel, M. ten and Vogel-Heuser, B., eds. Industrie 4.0 in Produktion, Automatisierung und LogistikAnwendung, Technologien, Migration. Wiesbaden: Springer Vieweg, 615–624.

Kampker, A., Deutskens, C., Heimes, H., Ordung, M. and Haunreiter, A., 2016. Using e-mobility as an enabler for a fast and lean product development to optimize the return of engineering with the example of lithium-ion battery. Procedia CIRP vol. 50, 166–172.

Kampker, A., Gerdes, J. and Schuh, G., 2017. Think Big, Start Small: Streetscooter die e-mobile Erfolgsstory: Innovationsprozesse radikal effizienter. Berlin, Heidelberg: Springer.

Kampker, A., Vallée, D. and Schnettler, A., eds., 2013. Elektromobilität: Grundlagen einer Zukunftstechnologie: Springer Vieweg.

Kappler, J., Schütte, A., Jung, H., Arnhold, D. and Bracht, U., 2010. Robuste Primär-und Sekundärbedarfsplanung komplexer und variantenreicher Serienprodukte. Integrationsaspekte der Simulation: Technik, Organisation und Personal. Karlsruhe: KIT Scientific Publishing, 69–76.

Kashkoush, M. and ElMaraghy, H., 2016. Optimum Overall Product Modularity. Procedia CIRP vol. 44, 55–60.

Kauder, S., 2008. Strategische Planung internationaler Produktionsnetzwerke in der Automobilindustrie. Thesis (PhD). Vienna University Of Economics and Business.

Kesper, H., 2012. Gestaltung von Produktvariantenspektren mittels matrixbasierter Methoden. Thesis (PhD). Technical University of Munich.

Kilger, W., Pampel, J. and Vikas, K., 2012. Flexible Plankostenrechnung und Deckungsbeitragsrechnung. Wiesbaden: Gabler Verlag.

Kissel, M., 2014. Mustererkennung in komplexen Produktportfolios. Thesis (PhD). Technical University of Munich.

Klug, F., 2010. Logistikmanagement in der Automobilindustrie: Grundlagen der Logistik im Automobilbau. Berlin: Springer.

Koberstein, A., Bihlmaier, R., Obst, R. and Suhl, L., 2009. Ein Optimierungssystem für die strategische Produktions- und Kapazitätsplanung in der Automobilindustrie. 9. Internationale Tagung Wirtschaftsinformatik, February 25 - 27. Vienna, Austria.

Körpeoğlu, E., Yaman, H. and Aktürk, M. S., 2011. A multi-stage stochastic programming approach in master production scheduling. European Journal of Operational Research vol. 213, 166–179.

Krajewski, L. J., Wei, J. C. and Tang, L.-L., 2005. Responding to schedule changes in build-to-order supply chains. Journal of Operations Management vol. 23, 452–469.

Krcmar, H., 2015. Informationsmanagement. Berlin, Heidelberg: Springer-Verlag Berlin Heidelberg.

Krog, E.-H., Richartz, G., Kanschat, R. and Hemken, M., 2002. Kooperatives Bedarfs- und Kapazitätsmanagement der Automobilhersteller und Systemlieferanten. Logistik Management, 45–51.

Krumm, S., Schopf, K. D. and Rennekamp, M., 2014. Komplexitätsmanagement in der Automobilindustrie – optimaler Fit von Vielfalt am Markt, Produktstruktur, Wertstrom und Ressourcen. In: Ebel, B. and Hofer, M. B., eds. Automotive ManagementStrategie und Marketing in der Automobilwirtschaft. 2nd edn. Berlin: Springer Gabler, 189–205.

Kuhn, A., Wiendahl, H.-P., Eversheim, W. and Schuh, G., 2002. Fast ramp up: schneller Produktionsanlauf von Serienprodukten: Ergebnisbericht der Untersuchung "fast ramp up". Verlag Praxiswissen, Dortmund vol. 6.

Leu, J.-D., Huang, L.-T. and Chen, C.-Y., eds., 2010. A MRP-II based planning method for the TFT-LCD manufacturing: IEEE.

Leung, S. C.H., Tsang, S. O.S., Ng, W. L. and Wu, Y., 2007. A robust optimization model for multi-site production planning problem in an uncertain environment. European Journal of Operational Research vol. 181, 224–238.

Liebler, K. M., 2013. Eine prozess- und IT-gestützte Methode für die Produktionsplanung in der Automobilindustrie. Thesis (PhD). TU Dortmund University.

Liu, S. and Papageorgiou, L. G., 2013. Multiobjective optimisation of production, distribution and capacity planning of global supply chains in the process industry. Omega vol. 41, 369–382.

Luo, Y., Peng, Q. and Gu, P., 2016. Integrated multi-layer representation and ant colony search for product selective disassembly planning. Computers in Industry vol. 75, 13–26.

Maiworm, T., 2014. Lines, Pakete, Sonderausstattungen – Wege der Fahrzeugdifferenzierung und Margenverbesserung durch Upselling. In: Ebel, B. and B. Hofer, M., eds. Automotive Management. Berlin Heidelberg: Springer Gabler, 527–535.

Matzke, A., 2016. Upgrade-Auktionen für die Nachfragesteuerung bei kundenindividueller Auftragsmontage: Mit Beispielen aus der Automobil- und Computerindustrie. Dissertation. Technische Universität Braunschweig.

Mayring, P., 2016. Einführung in die qualitative Sozialforschung: Eine Anleitung zu qualitativem Denken. weinheim, Basel: Beltz.

Meißner, S., 2009. Logistische Stabilität in der automobilen Variantenfließfertigung.

Meyr, H., 2004. Supply chain planning in the German automotive industry. OR Spectrum vol. 26, 447–470.

Nagel, J., 2011. Risikoorientiertes Anlaufmanagement. Wiesbaden: Gabler Verlag.

Pawlikowski, K., Fruhner, D., Klingebiel, K., Toth, M. and Wagenitz, A., 2017. A Motivation and Evaluation of Hierarchical Data Structures for Application in Automotive Demand and Capacity Management. International Journal on Advances in Software, 155–166.

Pröpster, M. H., 2015. Methodik zur kurzfristigen Austaktung variantenreicher Montagelinien am Beispiel des Nutzfahrzeugbaus. Zugl.: Diss., München, Techn. Univ., 2015. Herbert Utz Verlag GmbH.

Rafiei, H., Rabbani, M. and Alimardani, M., 2013. Novel bi-level hierarchical production planning in hybrid MTS/MTO production contexts. International Journal of Production Research vol. 51, 1331–1346.

Riggs, R. J. and Hu, S. J., 2013. Disassembly Liaison Graphs Inspired by Word Clouds. Procedia CIRP vol. 7, 521–526.

Rohde, J., Meyr, H. and Wagner, M., 2000. Die Supply Chain Planning Matrix. PPS-Management, 5 (1) vol. 5.

Romberg, A. and Haas, M., 2005. Der Anlaufmanager: Effizient arbeiten mit Führungssystem und Workflow - von der Produktionsidee bis zur Serie. Stuttgart: LOG X.

Roscher, J., 2008. Bewertung von Flexibilitätsstrategien für die Endmontage in der Automobilindustrie. Thesis (PhD). University of Stuttgart.

Schneider, W., 2008. Ergonomische Gestaltung von Benutzungsschnittstellen: Kommentar zur Grundsatznorm DIN EN ISO 9241-110. Berlin, Wien, Zürich: Beuth Verlag GmbH.

Schuh, G., 1988. Gestaltung und Bewertung von Produktvarianten: Ein Beitrag zur systematischen Planung von Serienprodukten. Thesis (PhD). RWTH Aachen University.

Schuh, G. and Riesener, M., 2018. Produktkomplexität managen: Strategien - Methoden - Tools[Online], 3rd edn. München: Hanser. Available at: http://www.hanser-fachbuch.de/9783446452251.

Schuh, G. and Stich, V., eds., 2012. Produktionsplanung und -steuerung 1: Grundlagen der PPS, 4th edn. Berlin Heidelberg: Springer-Verlag.

Sillekens, T., 2008. Aggregierte Produktionsplanung in der Automobilindustrie unter besonderer Berücksichtigung von Personalflexibilität. Thesis (PhD). Paderborn University.

Sillekens, T., Koberstein, A. and Suhl, L., 2011. Aggregate production planning in the automotive industry with special consideration of workforce flexibility. International Journal of Production Research vol. 49, 5055–5078.

Stadtler, H., 2004. Supply chain management and advanced planning—basics, overview and challenges. European Journal of Operational Research vol. 163, 575–588.

Tagesschau, 2017. BMW wartet auf Bosch-Teile: Engpass in der Produktion[Online]. Available at: https://www.tagesschau.de/wirtschaft/bosch-bmw-produktionsstau-101.html (Accessed 3 May 2018).

Tavaghof-Gigloo, D., Minner, S. and Silbermayr, L., 2016. Mixed integer linear programming formulation for flexibility instruments in capacity planning problems. Computers & Industrial Engineering vol. 97, 101–110.

Teo, C.-C., Bhatnagar, R. and Graves, S. C., 2011. Setting planned lead times for a make-to-order production system with master schedule smoothing. IIE Transactions vol. 43, 399–414.

Vegetti, M., Leone, H. and Henning, G., 2011. PRONTO: An ontology for comprehensive and consistent representation of product information. Engineering Applications of Artificial Intelligence vol. 24, 1305–1327.

Volling, T., 2009. Auftragsbezogene Planung bei variantenreicher Serienproduktion: Eine Untersuchung mit Fallstudien aus der Automobilindustrie. Wiesbaden: Gabler Verlag.

Webster, J. and Watson, R. T., 2002. Analyzing the past to prepare for the future: Writing a literature review. MIS quarterly, xiii–xxiii.

Weyand, L., 2010. Risikoreduzierte Endmontageplanung am Beispiel der Automobilindustrie. Saarbrücken.

Wochner, S., Grunow, M., Staeblein, T. and Stolletz, R., 2016. Planning for ramp-ups and new product introductions in the automotive industry: Extending sales and operations planning. International Journal of Production Economics vol. 182, 372–383.

Wong, W. K. O., 2017. Automotive Global Value Chain: The Rise of Mega Suppliers. London: Taylor and Francis.

Yang, Q., Pan, X., Wei, D. and Wu, K., 2012. Research on Individualized Product Requirement Expression Based on Semantic Network. Physics Procedia vol. 25, 1926–1933.

CLOSED-LOOP-ENGINEERING – ENABLER FOR SWIFT RECONFIGURATION IN PLANT ENGINEERING

Janek Bender[a], Jana Deckers[b], Simon Fritz[c], Jivka Ovtcharova[d]

[a],[b],[c] ,[d] FZI Research Center for Information Technology, Haid-und-Neu-Strasse 10-14, 76135 Karlsruhe, Germany

[a]bender@fzi.de, [b]deckers@fzi.de, [c]fritz@fzi.de, [d]ovtcha@fzi.de

ABSTRACT
Manufacturing industries face increasingly complex customer demands in terms of product customisation and delivery times. At the same time, batch sizes decline and production needs to adapt to flexible demands and highly configurable products. These circumstances pose significant challenges for both plant engineers and process planners. In this work, we explore a novel approach in order to establish a Closed Loop Engineering process chain for the Digital Factory by combining state of the art technologies from the fields of Production and Process Automation, Virtual Reality (VR), and Internet of Things (IoT). As a proof of concept, we developed a VR-demonstrator using the CONTACT Elements for IoT platform in conjunction with a web-based production process planner and Manufacturing Execution System (MES) written by the FZI in Java as well as the Unity game engine for real-time simulation in VR.

Keywords: Digital Twin, Plug&Produce, AutomationML, Virtual Reality

1. INTRODUCTION
Manufacturing industries face increasingly complex customer demands in terms of product customisation and delivery times. At the same time, batch sizes decline and the production needs to adapt to flexible demands and highly configurable products. These circumstances are also known in the literature as Mass Customisation (Tseng et al. 2017). Aside from the implications for product developers, they also pose significant challenges for plant engineers as well as process planners.
Industry, public, and science attempt to meet these challenges by working towards a large-scale transformation of the manufacturing industries, in Germany referred to as Industrie 4.0 (Industry 4.0). Other economic heavyweights employ similar strategies such as Made in China 2025, the Industrial Internet Consortium in the United States of America, or Society 5.0 in Japan.
At the core of the German efforts lies the Smart Factory, for which the Digital Factory forms a key requirement. In this work, we explore a novel approach in order to establish a closed-loop-engineering process chain for said Digital Factory by combining state of the art technologies from the fields of Production and Process Automation, Virtual Reality (VR), and Internet of Things (IoT).
In the following, the state of the art in the key technologies for this paper is reviewed. Then, the concept is described from a theoretical viewpoint leading to a section about the prototypic implementation in form of a research demonstrator. Finally, the results are evaluated and the paper is concluded.

2. STATE OF THE ART
This section gives a brief overview about the concepts and technologies required to describe and implement our approach. Namely we touch on Virtual Reality, (Industrial) Internet of Things, the Digital Twin, Manufacturing Execution Systems, and the Digital Factory as the element that ties everything together.

2.1. Virtual Reality
The idea to leverage Virtual Reality for factory planning and virtual commissioning is not entirely new. (Menck et al. 2012) There have been numerous academic and commercial solutions emerging in recent years like taraVRbuilder (tarakos 2019), IPO.Log (IPO.Plan 2019), R3DT (R3DT 2019), Boxplan (SALT AND PEPPER 2019) or game4automation (in2sight 2019) focussing on different aspects of plant engineering and virtual commissioning in VR, or simple 3D respectively. Choi et al. (2015) present a comprehensive list of VR applications in the manufacturing industries. Our approach however is tightly integrated into existing real-world monitoring and control software and thus provides a lightweight tool for plant engineers to swiftly simulate the impact of layout changes on a process level. Hence we required our own engine capable of VR, for which we employed the commercial game engine Unity (Unity Technologies 2019). It is affordable, accessible, surrounded by a large community, and built executables run on various operating systems including Windows and Linux distributions.

2.2. Industrial Internet of Things
(Boyes et al. 2018) define the Industrial Internet of Things (IIoT) as "*a system comprising networked smart objects, cyber-physical assets, associated generic information technologies and optional cloud or edge computing platforms, which enable real-time, intelligent,*

and autonomous access, collection, analysis, communications, and exchange of process, product and/or service information, within the industrial environment […]". Note that we use the terms IoT and IIoT synonymously in this paper.
The capabilities of such systems provide great opportunities for plant engineers in terms of monitoring and analysis of the production line as well as automated workflows for the staff surrounding it. As such, IoT already needs to be considered during the design phase of a production line. In recent years, numerous commercial and open source IoT platforms have been emerging. For our work, we have been provided with the commercial platform Elements for IoT by CONTACT Software (CONTACT 2019). A key technology for IoT are message exchange protocols such as the publish-subscribe-based Message Queuing Telemetry Transport protocol (MQTT, OASIS 2019) which is used in this work. Originally created for smart home applications, MQTT is easy to integrate into a production context as it is lightweight in comparison to more complex industry standards such as the OPC Unified Architecture (OPC UA, OPC Foundation 2019).

2.3. Digital Twin

A Digital Twin is a digital representation of a real world object. (GI 2017) In the context of production, this could be anything ranging from a sensor, over a machine or a product, up to an entire production line or factory. The Digital Twin is not even tied to the existence of its real world counterpart. In the case of a product or a machine in development, the Digital Twin may be established long before the production of the real world object. It can be used over the entire product lifecycle to track and exchange information. In terms of granularity this information may encompass CAD data, parameters and configurations, meta data, behavioural models, and state information like machine health. The Digital Twin enables users in various roles to view the representation from different perspectives and interact with it without affecting the real world.

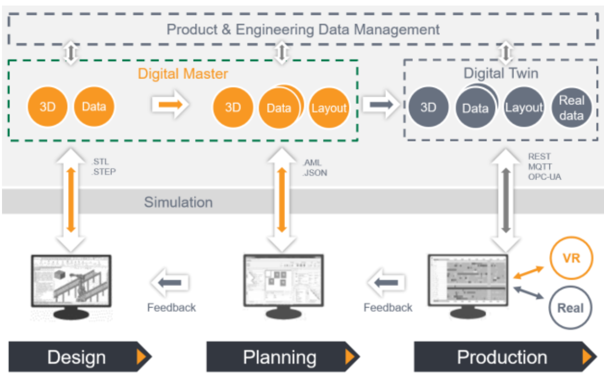

Figure 1: Digital Twin in Product Engineering. Source: Own Illustration

Figure 1 shows how we see the Digital Twin in plant engineering. Already during the early design stage of a machine, a Digital Master is created holding predominantly CAD data, meta data, and parameters. During the planning phase, this is embedded in a layout with other machines leading to the Digital Master of a production line or production centre. When entering production phase, the actual Digital Twin is derived from the Digital Master by deploying the real world objects. The Digital Twin then inherits its Master's information and completes it with information received at runtime, like sensor data or data about the health of the production line. There can be a multitude of Digital Twins derived from a Digital Master. Furthermore, the Digital Twins can be simulated entirely or feed on real world data.

2.4. Manufacturing Execution System

Manufacturing Execution Systems (MES) fill in the gap between Enterprise Resource Planning (ERP) and the shop floor by providing real time planning, monitoring, and control of production processes. According to the VDI (2016), MES provide ten core functions:

1. Detailed Planning and Control
2. Resource Management
3. Material Management
4. Personnel Management
5. Data Collection
6. Performance Analysis
7. Quality Management
8. Information Management
9. Energy Management
10. Order Management

As one can see, there is a slight overlap between MES core functions and the monitoring and analysis aspects of IoT platforms. However, the MES' sophisticated planning and control mechanisms play a key role in being able to realise the Digital Factory. Limits and potentials of these systems must be considered carefully during the process of plant engineering.

2.5. Digital Factory

Originally conceived as aggregation of various planning and simulation approaches for plant engineering (Kuhn 2006), the Digital Factory can be extended by the real time and real world data processing capabilities of the Digital Twin. In our understanding, simulation and planning are only part of the loop that connects engineering and production. The other part is the real world information and knowledge gathered in production being reflected back into the engineering in an iterative development process. Thus, the Digital Factory forms the cornerstone of our efforts.

3. CONCEPT

This section provides a brief introduction into the general ideas behind the Closed Loop Engineering approach by employing a Digital Twin. Figure 2 gives an overview. The illustration is divided into two parts, the production side, i.e. the production line on the shop floor producing goods, and the (re-)engineering side, i.e. the development of new production liens and changes on existing ones.

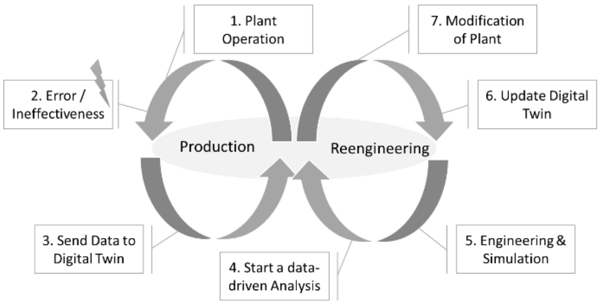

Figure 2: Closed-Loop-Engineering. Source: Own Illustration

Starting on the left side, the Closed Loop process typically assumes there is an existing factory or production line which is already operating (1). Somewhere down the line, an error or inefficiency occurs (2). This could be due to changes in the production process, wear and tear on the machines, or an overlooked mistake during the planning of the production. As data from the real world production line is constantly pushed to its Digital Twin (3), in order to identify the root cause of the problem, analysis can be conducted immediately once an error or inefficiency occurs (4) leading to the right part of the illustration. The results of the analysis are then used to perform re-engineering and simulate the changes, i.e. with methods of virtual commissioning (5). Once a solution has been found and validated through simulation, it is deployed in the Digital Twin (6) and the real world production line (7). In order to realise the concept in form of a demonstrator, we rely on two key approaches, the Product-Process-Resource-Skill model and AutomationML.

3.1. Model of Product-Process-Resource-Skill

To accurately describe our factory model, we employ a Product-Process-Resource-Skill (PPRS) approach. (Pfrommer et al. 2013, Aleksandrov et al. 2014) This allows us to define abstract high-level skills for machines without knowing the implementation details of any specific machine type. For instance, a generic robotic arm could provide the skills transport and assemble. Of course, at some point these high-level skills have to be translated into low-level machine instructions. However, the abstract representation is sufficient to outline machine capabilities and to model the products. A product is understood as defining its own production process in form of a sequence of skills needed to be applied in a certain order on the initial workpiece. At runtime, these required skills (product skills) are mapped onto the skills provided by the machines (resource skills) in the actual layout represented in a graph structure. This allows us to calculate all possible paths for the material flow and derive concrete production sequences in a simple and efficient fashion.

3.2. Exchange Format AutomationML

Both already existing as well as factory layouts still in development are thought to be exchangeable independently of deployed CAD and PLM systems as they come the format of AutomationML (AML, AutomationML 2019). Broadly speaking, AML is an XML-based exchange format for engineering information. (AutomationML 2018) It may contain meta-data and machine parameters but also links to actual CAD files. For simplification purposes, in this paper, AML contains everything required to plan and simulate a simple production process. The four main AML element types are used in our work as follows (note that we do not utilise the AttributeTypeLib yet which was introduced in AutomationML 2.10):

- InterfaceClassLib
  This element stores generic interface types for inter-machine connections.
- RoleClassLib
  This element contains semantic information about the different domain model classes factory, resource (machine), tool, sensor, product, and skill. It also contains descriptions of the various skill types.
- SystemUnitClassLib
  This element defines the generic resource types, i.e. machine, robot, and conveyor. It also defines the product including its skill-based production process using a series of nested nodes.
- InstanceHierarchy
  Finally, this element groups instances of the generic resource types from the SystemUnitClassLib in a defined layout in 3D space. This represents the actual production line on the shop floor.

The AML provides an almost self-contained semantic description of a factory including all its products, processes, and resources. However, we did not include CAD data at this stage of the development. 3D models of the resources and products are directly integrated in Unity.

4. DEMONSTRATOR

As a proof of concept, we developed a VR-demonstrator using the CONTACT Elements for IoT platform (CONTACT 2019) in conjunction with a web-based production process planner and Manufacturing Execution System (MES) written by the FZI Research Center for Information Technology in Java as well as the Unity game engine (Unity Technologies 2019) for real time simulation in VR. This demonstrator is subject of ongoing development and mainly serves as our technological and algorithmic testbed. It also provides an accessible research showcase for both industry and public.

4.1. Use Case

The showcase revolves around a bottling plant in a small enterprise where bottles are filled by a filling machine and then sealed, engraved, and packed for shipping by robot arms with multiple attachable tools at their disposal. As Figure 3 shows, the production line is assembled from one filling machine, two conveyors, up to two robotic arms, one cap stock providing bottle caps, and one box for storing the finished bottles. Parts of this setup were available to us as real world machinery.

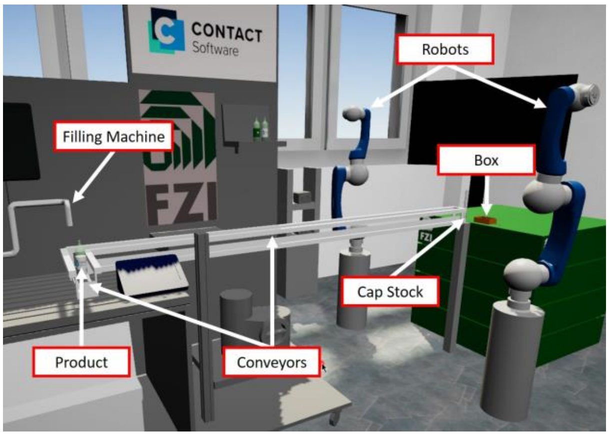

Figure 3: Machines of the Bottling Plant in Unity. Source: Own Illustration

Customer orders are highly customisable and define variable batch sizes, different bottle designs, a variety of fluids, and custom engravings. Thus, production planning and execution complexity rises requiring the MES to adapt to a variety of different circumstances. The subset of the production process illustrated in the demonstrator is thought to run in a fully automated environment. Human interaction in the actual production process is not required in this instance.

4.2. Functions

In order to simulate the use case according to the constraints defined by the concept, i.e. simulating an existing production line encoded in AML, we defined a set of functions the demonstrator has to support:

1. Import Factory Layout
   An existing factory layout encoded in AML is imported and transformed into the system's domain model.
2. Change Factory Layout
   The factory layout is altered by adding, removing, or re-configuring machines.
3. Export Factory Layout
   The factory layout is transformed and exported back into AML.
4. Display Factory Layout
   The factory layout is displayed in 3D and VR. The user can move freely within the scene.
5. Place Order
   An order can be placed containing quantity, desired fluid, and custom engraving.
6. Simulate Production Process
   Based on a placed order, a batch equating the order quantity is scheduled for production. A production plan outlining the specific sequence of machine operations including machine setup is computed and then executed on screen.
7. Simulate Sensors
   Using Unity's physics capabilities, sensor data like weight on the conveyor belts, pull on the robot arms, robot angles, and throughput of the filling machine can be calculated. This data is enriched by information about the internal state of the machines, such as which tools are equipped, at what angles the robot joints are, and what tasks are currently executed.
8. Export Sensor Data
   The simulated sensor data is serialised and pushed to the IoT platform via MQTT in steady intervals.
9. Reset Simulation
   The simulation can be reset and restarted at any given point.

4.3. System Architecture

In order to realise the concept, achieve the necessary functionality, and integrate the IoT platform, an architecture tying together software components from different domains, technologies, and programming languages was required.

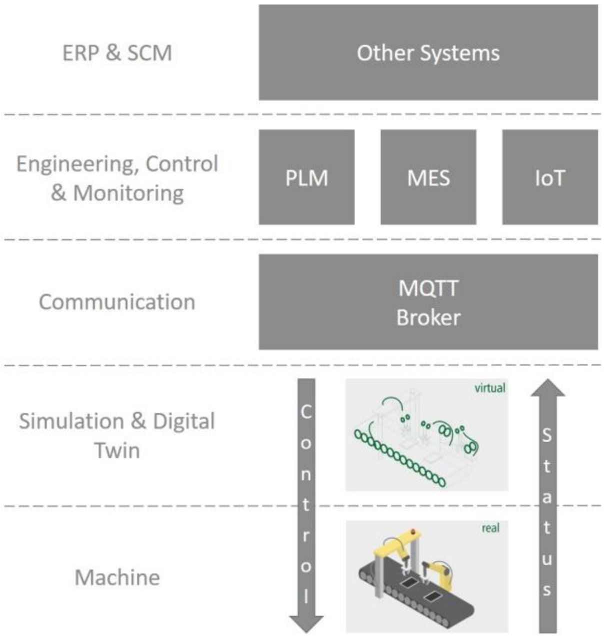

Figure 4: System Architecture & Flow of Information. Source: Own Illustration

As Figure 4 shows, on the very top lie the upstream systems, like Enterprise Resource Planning (ERP) and Supply Chain Management (SCM). These components are not directly integrated in the demonstrator. Instead, data exchange with these systems is mocked using AML files for machine data and JSON strings for order data.

Right below the top level, the actual development and control systems are situated. This encompasses the Product Lifecycle Management (PLM) software for component development, the MES for control of the shop floor, and the IoT for surveillance of the deployed machines. While the PLM system is again not integrated but only mocked through AML files, the other two systems are hooked up to the shop floor via an MQTT Broker. The MQTT Broker serves as central communication hub for all data exchange in the demonstrator across individual system borders. The message format is implemented as JSON strings containing serialised objects.

Downwards of the MQTT Broker lies the shop floor, both virtual and real. The MES is set up to communicate with the Digital Twin which runs in the Unity simulation. This is done by sending instructions from the MES to the Digital Twin which only responds with state reports. Instructions contain the high-level skill to execute, a set of customisable parameters, and a reference to the product it should execute the skill on. State reports contain information about the Digital Twin, whether it is idling, busy, or in error state, which skill it currently executes, its position in 3D space, and a reference to the currently selected tool (if available). These state reports are sent by the Digital Twin when asked for by the MES, an instruction is received or finished, or an error occurs.

The Digital Twin translates the high-level skill references from the instruction into concrete machine code and passes it down to its real world counterpart for execution. In return, the real world machine pushes all its sensor data to the Digital Twin. Hence, the real world machine is capsuled entirely through its Digital Twin. The sensor data as well as data about the internal state of the machine is aggregated by the Digital Twin and sent to the IoT instance periodically. The Digital Twin provides low-level error detection, i.e. when it cannot locate the designated product or execute a given skill, and will report errors to the MES through the state report mechanism. The MES then decides whether it can recover from the error or has to halt production entirely.

4.4. Interaction in 3D and Virtual Reality

The demonstrator can be interacted with through both regular 3D on a monitor plus mouse and keyboard setup as well as in VR using a headset and controller. Users can move freely within the scene and examine all machines in detail. Furthermore, they are able to place orders in-game to start the simulation and stop or reset it at will. Finally, users can deploy new machines from a catalogue and thus try out different factory configurations. At this stage, machines can only be placed at pre-defined locations, however a dynamic placement system is subject to ongoing development.

4.5. An Exemplary Rundown

At this point, an ideal step-by-step rundown of the use-case in the demonstrator is given:

1. In a first step, the PLM system transforms the real world factory and product contained in AML into our domain model.
2. The PLM system then sends the factory over MQTT to our MES and the Unity simulation.
3. The MES calculates a production process graph based on layout information and the product description.
4. Unity renders the 3D scene based on the factory information it received as seen in Figure 5. The Digital Twins connect via MQTT to the MES and to their real world counterparts.

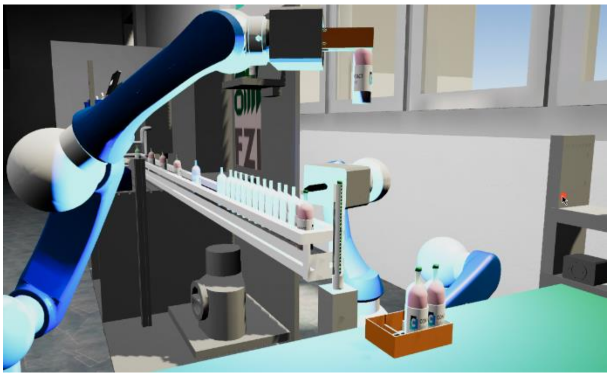

Figure 5: VR-Simulation of the Production Process in Unity. Source: Own Illustration

5. The user places an order either from within Unity or via a webpage provided by the MES.
6. The MES calculates a production plan and starts executing that plan by issuing instructions over MQTT to the Digital Twins.
7. The Digital Twins execute the instructions in the simulation while at the same time translating them to machine code which they send down to their real world counterparts.
8. The real world counterparts execute the orders received from their Digital Twins and send back sensor and machine data in return.
9. The Digital Twins aggregate the incoming sensor and machine data and enrich it with additional information about their own state. This data is periodically pushed to the IoT instance.
10. An error occurs either in the real world or the simulation and is communicated to the MES by the Digital Twins. At the same time, the IoT instance detects inefficiencies based on the incoming sensor data and kicks off a workflow.
11. The MES halts production for the user to review the problem both in the simulation and in the IoT instance as illustrated in Figure 6.

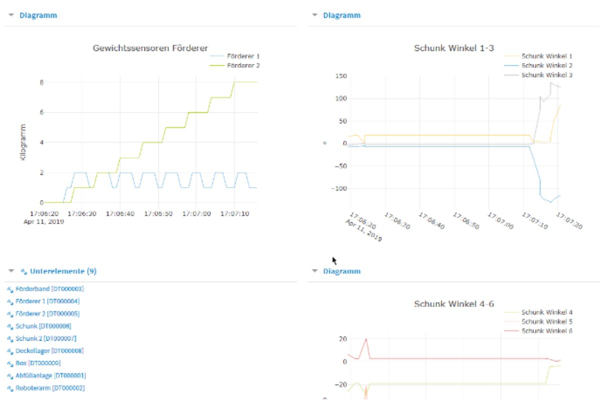

Figure 6: Presentation of Sensor Data in the CONTACT Elements for IoT Platform. Source: Own Illustration

12. The user decides to reconfigure the plant in VR, i.e. by adding an additional robot arm.
13. The user restarts the simulation, this time without connecting to the real world machines and validates the changes made to the layout.
14. The user deploys the additional robot arm in the real world plant and the production starts again.
15. The layout changes are exported back into AML.

The power of the system lies in its flexibility. It can be run in simulation only, or be connected to either the complete or just a subset of the real world machinery. Users can interact with the system via VR, regular 3D, or through a web interface.

5. EVALUATION

Both the demonstrator and the concept work it is based on are still subject to further research and development, hence a final evaluation cannot be given at this point. However, the demonstrator has been exposed to figures from industry and public on several occasions, like visits, trade fairs, and public events. The receptions were positive overall for its ability to demonstrate complex production processes in an immersive format. However, fair criticism was levelled at its physical inaccuracy in contrast to other professional simulation tools which are more focused on accurate physical representations over the process simulation we are interested in. On a positive side, a lightweight version of the demonstrator is used by our partners at CONTACT for training and evaluation purposes.

6. CONCLUSION

In this paper, we presented a novel approach on how to establish a Closed Loop Engineering process chain for the Digital Factory. We did this by combining technologies from the fields of Production and Process Automation, Virtual Reality, and Internet of Things. The approach connects the engineering and simulation aspects of the Digital Factory with the shop floor by exploiting the concept of the Digital Twin. As a proof of concept, we implemented a research demonstrator comprised of multiple software systems integrated through the MQTT protocol. The demonstrator is still subject to ongoing developments and evaluation efforts. However, we are confident our work provides a first step towards the implementation of a widely applicable Closed Loop Engineering approach for plant engineering in the context of the Digital Factory.

7. FUTURE WORK

For the future, we plan to expand the demonstrator hardware by the implementation of a more sophisticated real world miniature production line with support for a wide array of potential production scenarios. This is to be tightly coupled with the virtual environment and serves as a testbed for plug & produce approaches in particular. On the software side, we are mainly interested in driving our model of the Digital Factory more towards the Smart Factory, and use the demonstrator as algorithmic testbed for AI-supported production planning and machine parameter optimisation. Finally, we consider integrating more industry standards, like OPC UA for example, into the showcase.

ACKNOWLEDGMENTS

We would like to thank our partner CONTACT Software GmbH for providing us with both the Elements for IoT platform as well as their in-depth domain knowledge.

REFERENCES

Aleksandrov K., Schubert V., Ovtcharova J., 2014. Skill-Based Asset Management: A PLM-Approach for Reconfigurable Production Systems. In: Fukuda S., Bernard A., Gurumoorthy B., Bouras A., eds. Product Lifecycle Management for a Global Market. PLM 2014. IFIP Advances in Information and Communication Technology, vol 442. Berlin, Heidelberg: Springer.

AutomationML consortium, 2018. Whitepaper AutomationML Edition 2.1. Available from: www.automationml.org/o.red.c/dateien.html [accessed 09 July 2019]

AutomationML e.V., 2019. Homepage. Available from: www.automationml.org [accessed 08 July 2019]

Boyes H., Hallaq B., Cunningham J., Watson T., 2018. The industrial internet of things (IIoT): An analysis framework. Computers in Industry 101: 1-12.

Choi S., Jung K., Noh S.D., 2015. Virtual reality applications in manufacturing industries: Past research, present findings, and future directions. Concurrent Engineering 23(1): 40-63.

CONTACT Software GmbH, 2019. Homepage. Available from: www.contact-software.com/de/produkte/iot-plattform-fuer-digitale-geschaeftsmodelle/ [accessed 08 July 2019]

Gesellschaft für Informatik e.V. (GI), Kuhn T., 2017. Lexikon: Digitaler Zwilling. Available from: www.gi.de/informatiklexikon/digitaler-zwilling/ [accessed 08 July 2019]

Kuhn W., 2006. Digital Factory - Simulation Enhancing the Product and Production Engineering Process.

Proceedings of the 2006 Winter Simulation Conference, 1899-1906. 03.12.2006 - 06.12.2006, Monterey, CA, USA.
in2sight GmbH, 2019. Homepage. Available from: www.game4automation.com [accessed 08 July 2019]
IPO.Plan GmbH, 2019. Homepage. Available from: www.ipoplan.de/software-ipolog/ [accessed 08 July 2019]
Menck N., Yang X., Weidig C., Winkes P., Lauer C., Hagen H., Hamann B., Aurich J.C., 2012. Collaborative Factory Planning in Virtual Reality. Procedia CIRP, Volume 3, 317–322. Athens, Greece.
OPC Foundation, 2019. Homepage. Available from: www.opcfoundation.org [accessed 08 July 2019]
Open Source Robotics Foundation, Inc., 2019. Homepage. Available from: www.ros.org [accessed 08 July 2019]
Organization for the Advancement of Structured Information Standards (OASIS), 2019. MQTT Homepage. Available from: www.mqtt.org [accessed 08 July 2019]
Pfrommer J., Schleipen M., Beyerer J., 2013. PPRS: Production skills and their relation to product, process, and resource. IEEE 18th International Conference on Emerging Technologies and Factory Automation (ETFA), 1-4. 10.09.2013 - 13.09.2013, Cagliari, Italy.
R3DT GmbH, 2019. Homepage. Available from: www.r3dt.com [accessed 08 July 2019]
SALT AND PEPPER Holding GmbH & Co. KG, 2019. Homepage. Available from: www.salt-and-pepper.eu/en/virtualreality/ [accessed 08 July 2019]
tarakos GmbH, 2019. Homepage. Available from: www.tarakos.de/taravrbuilder [accessed 08 July 2019]
Tseng M. M., Wang Y., Jiao R. J., 2017. Mass Customization. In: Laperrière L., Reinhart G., eds. CIRP Encyclopedia of Production Engineering. Berlin, Heidelberg: Springer, 1-8.
Unity Technologies, 2019. Homepage. Available from: www.unity.com [accessed 08 July 2019]
VDI, 2016. Fertigungsmanagementsysteme (Manufacturing Execution Systems - MES). In: VDI 5600 Blatt 1:2016-10. VDI-Gesellschaft Produkt- und Prozessgestaltung.

COMPLEX NETWORK ANALYSIS: MEXICO´S CITY METRO SYSTEM

Olivia Sashiko Shirai Reyna[a], Idalia Flores de la Mota[b]

[a),(b]Posgrado en Ingeniería de Sistemas- Facultad de Ingeniería Edificio Bernardo Quintana 3er, Piso, Departamento de Sistemas, UNAM, Cd. Universitaria, Del. Coyoacán, C.P. 04510, México C.D.M.X

[a]sashikosr@outlook.com , [b] idalia@unam.com

ABSTRACT

The metro system from Mexico City has previously been analyzed, but only by parts, specific case studies to some stations (transfer, transit or terminals) or metro lines (individually) and not to the entire system as such. This study is important since it will give us information about the system that is not yet known, it will help us to correctly identify risks to minimize them, as well as delays in the lines, make improvements to the system, have an adequate planning, establish different policies to improve and satisfy the system needs. Tools such as simulation will be used to create scenarios and search for alternatives for improvement in the system, as well as, where appropriate, other tools such as optimization will be used. This paper uses different techniques such as Complex Networks Methodology, Statistics, Simulation and Risk Analysis.

Keywords: transport system, Complex Networks

1. INTRODUCTION

Currently the Metro System has 12 lines which are distributed within Mexico City and part of the State of Mexico.

Figure 1 México City Metro System

The Metro of Mexico City has a total of 384 convoys, of which 285 are in operation and 99 out of service for the following reasons: 33 for lack of spare parts, 20 for being in reserve, 17 for maintenance, 15 by general review, 7 by revision of breakdowns, 5 by work of modernization, and one more by special works and another by reprofiling of wheels.

2. PROBLEM

During a period of 14 months, from January 2017 to February 2018, the Metro system of México City presented 28,400 breakdowns during its operation. That is, an average of 2 366 failures per month or 77 per day, according to data obtained via transparency request.

The main problems that occurred in that time lapse were braking traction with 5 980; in the door system with 4 169; the automatic piloting with 4 043; the mechanical equipment with 3 144; and the generation of energy with 2 554.

While the lines that presented the highest number of breakdowns in all 2017 and in the first two months of 2018 were the line 3 that goes from Indios Verdes to Universidad with 4 459; line 1 that runs from Observatorio to Pantitlán with 3 631; the line A that travels from Pantitlán to La Paz with 3 394; followed by line 7 that goes from El Rosario to Barranca del Muerto with 2 985; and line 5 that goes from Politécnico to Pantitlán with 2 862 failures.

The subway system has its main problems due to factors such as the elements´wear of the gear change, which has been caused by natural wear, cracks or fractures in lines with greater age, as well as lack of lubrication in rails and settlements differentials caused by the settlements of the subsoil of the city.

While the electronic installations have normal deterioration in the equipment, which affects the Automation and Control systems, then they must operate in safety conditions, over electrical installations. In lines 8 and A were delays due to lack of power of that type due to the failure of a general switch that occurred due to the voltage variation of the CFE (Comisión Federal de Electricidad).

During 2017, the impairment rate in hours due to service faults on all Metro lines was 17.6, while the actual service was 7,454.3, with a service percentage of 99.76, according to the information presented by the Metro.

In January and February of 2018, the hours without service reached 6.8, while the active hours were 1 205. The striking thing about the numbers is that in just two months they have reached almost a third of the total hours of failure that were recorded in all last year, which indicates that the problem is going up.

Only last February there were 4 hours total losses due to faults that have occurred in the service of all Metro lines, which exceeds the highest months of 2017 that were June and December with 3.2 and 3.1, respectively.

The Metro reported different problems: Technical, Operational, Social and Financial problems. The technical problems are those related to the operation of the network such as the control system, braking system, door opening system, capacity of the wagons, lack of spare parts, among others, most of these problems are due to lack of maintenance. Other problems are found in the operation of the system, which are those related to the rules and policies with which the Metro operates, such as the number of trains operating per schedule, action policies within the platforms, such as safety measures, evacuation, action measures in case of mishaps such as earthquakes, fires, terrorist attacks, among others. Another type of problem is the social problems, which are associated with people such as the flow of passengers, crowds, violence inside and outside the wagons, street vendors, among others. Finally, we find the financial or budgetary problems, since the Metro does not have enough money to maintain, buy spare parts of trains, rehabilitation of trains that are out of circulation or put in circulation new trains.

Therefore, the next questions are made: which the most likely failure stations are? how faults will propagate to other lines? how the network connectivity is? which are the alternate routes in case of failures?

So, we will focus this analysis with Complex Networks to identify the stations that have the most important problems and its vulnerability, and we will create different scenarios from which we will have the simulation of the whole system and how it works with the different scenarios.

3. METHODOLOGY

For the methodology we will follow the next steps.

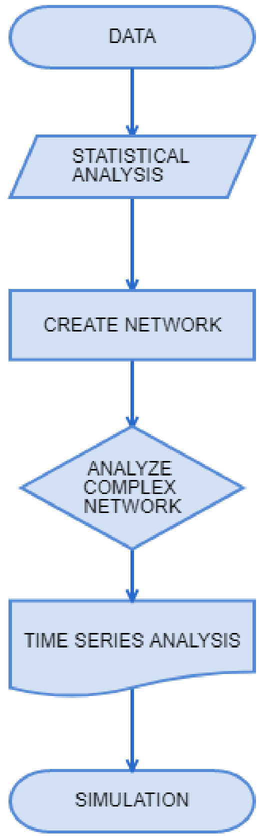

Figure 2 Steps Methodology

For this study we focused on the analysis of the analysis of the metro system to identify as a first approach.

1. **First Step**

This step is maybe one of the most difficult steps because we need to look up for all the data that is relevant for the study.

2. **Second Step**

So, with this information the second step was to analyze the data with basic statistical techniques.

3. **Third Step**

We can create the network in different ways, the most common is with the adjacency matrix. An adjacency matrix is a square matrix used to represent a finite graph or network.

4. **Fourth Step**

Once the network is obtained, we used the methodology of complex networks, specially to analyze the topology or structure of the networks, for example, the clustering, the closeness, betweenness, assortativity, and more metrics of complex networks. Also, we can have the degree distribution of the networks and we can have a good approach of the network’s behavior. With all the metrics and the degree distribution we can classify the networks into one of the different networks model (Random Networks, Small World Networks and Scale-free Networks).

5. Fifth Step

The fifth step consists in translate the information to time series, so we did a decomposition of time series into the three components series (Seasonal, Trend and Random), we obtained the ACF (Auto Correlation Function), PACF (Partial Auto Correlation Function). In this step we also can create time series models like ARIMA (Autoregressive Integrated Moving Average) models to do some forecast of the data.

6. Sixth Step

For the simulation process we will build different scenarios of the network to analyze the different structures and the vulnerability so we can compare which network is better. We can have different scenarios for example what happen if we delete one node or an edge.

4. RESULTS

For the statistical analysis, we used the R software, which is an open source programming language and software environment for statistical computing and graphics. For this work, we used specific R software packages, such as, igraph, networks, tkrplot, sand, sna, forecast, TimeSeries, TSA and others. Software allows us to generate graphs/networks, compute different network metrics like clustering or transitivity, different centrality metrics, plot networks, create mathematical models, forecast data and more functions. Also, we used a BI (Business Intelligence) software that allow us to have some data preparation just like an ETL (Extract, Transform, Load) process and to create reports and visualization of our data.

According to the methodology, at the first step we have the data of the number of passengers by station and trimester from the first trimester from 2011 to the first trimester of 2019.

Computing basic statistics: First, we analyze the number of passengers per line, to have the ranking of the lines with more passengers.

Table 1 Number of Passengers per Line

Line	Passengers	%
Line 2	2,399,777,835	17.87%
Line 1	2,128,428,724	15.85%
Line 3	1,944,304,705	14.47%
Line B	1,313,948,094	9.78%
Line 8	1,129,922,146	8.41%
Line 9	952,297,672	7.09%
Line 5	882,986,511	6.57%
Line 7	828,596,887	6.17%
Line A	794,763,580	5.92%
Line 12	592,338,103	4.41%
Line 4	249,863,002	1.86%
Line 6	215,006,325	1.60%
Total	13,432,233,584	100.00%

Then, we analyze the number of passengers per station to also have a ranking of the station with the highest numbers of passengers.

Table 2 Top 10 Number of Passengers per Station

Line	Station	Passengers
Line 3	Indios Verdes	345,139,908
Line 2	Cuatro Caminos	344,277,759
Line A	Pantitlán A	300,460,361
Line 5	Pantitlán 5	267,067,692
Line 8	Constitución de 1917	259,450,656
Line 2	Tasqueña	259,221,934
Line 9	Pantitlán 9	254,180,021
Line 1	Observatorio	218,684,664
Line 3	Universidad	217,461,690
Line 2	Zócalo	204,023,284

From the table 2 we can see that the station Indios Verdes is the most crowded, but we also can notice that Pantitlán is a hub so, the cumulative number of passengers is higher than at Indios Verdes, this is important because this means that we need to have special attention in this station.

We continue with the methodology and we need to create a network. So, we have the structure of the metro system, characterize these data as an adjacency matrix, in this case, the nodes represent the stations and the edges represent the connections through the line. The next figure shows the structure of the system as a complex network.

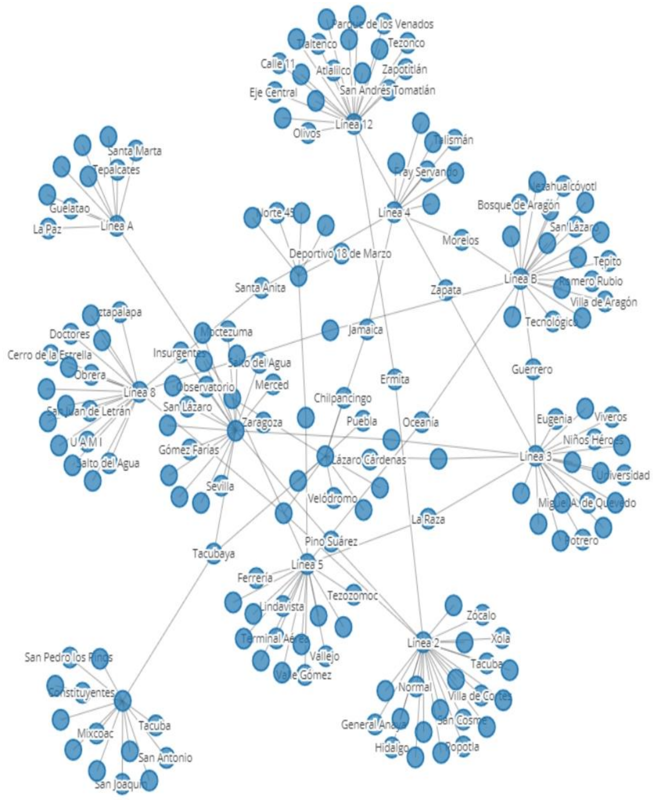

Figure 3 Metro Complex Network

Now, we have the system characterized as a complex network so now we can compute the different complex networks metrics to study the topological structure of our network.

Table 3 Complex network metrics

Results	Total
Nodes	195
Edges	220
Max. Degree	4
Min. Degree	1
Mean Degree	2.25641
Diameter	39
Mean Distance	12.94618
Cliques	4
Density	0.011631
Assortativity	0.245905
Global Clustering	0.056962
Mean Local Clustering	0.017304
Closeness Centrality	0.059484
Degree Centrality	0.008988
Betweenness Centrality	0.144816

The minimum degree corresponds to 1 and it makes sense because they are the terminal stations, the maximum degree is 4 that corresponds to stations like Pantitlán, meanwhile the average grade is 2.25, which tells us that there are very few stations that are transfer.

On the other hand, the density is important, it tells how connected the network is, the real systems modeled with networks, in general, are not very dense, due to the cost of the links. The network has a density of 0.011 which indicates that the connectivity within the network is very low and poor.

Another of the metrics that we use in this analysis is the mean distance, which is the average of the distances between all pair of nodes, so we expect that the networks have a low average distance, which has to do with the small world property, but in this case we have a mean distance of 12.94 that is quit high in comparison with the number of nodes and edges.

In addition to the metrics that are listed above, we are interested in studying the topology of the network so clustering is important and, we start with the global clustering, it means what the tendency of the network is to form triangles or to be transitive, so, the global clustering is very low it is 0.056, so it has a low tendency to form triangles. While, if we look at the mean local clustering, it is very similar to the global clustering but in this case, it is lower (0.017) so we can say that there is no tendency to form small groups, that is, they remain in the whole group.

On the other hand, the betweenness centrality, helps us to identify how important a node is within a network, computing how many short paths pass through the node in question, so we compute the average of the intermediate centrality of each case and we obtained a value of 0.144, the network has a very low betweenness centrality. The closeness centrality focuses on computing the shortest paths of each node to all other nodes in the network, we have that the closeness is relatively high. If we talk about the correlation of nodes, we have the coefficient of assortativity that gives us values between -1 and 1, therefore we can say if a network is assortative or dissortative, so, our network has a value of 0.24 with this we can say that it is assortative.

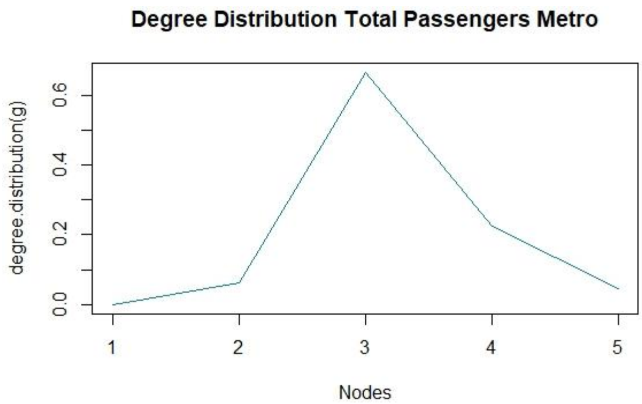

Figure 4 Degree Distribution Total Passengers Metro

We can observe that the distribution of degree seems to be binomial.

With all these results we are able to analyze and compare the behavior of the different stations and lines, in addition, we could analyze the topology of the whole system, which concludes the type of network model is and what specific characteristics and properties they share.

The next step is to perform the time series analysis, so first we organize and sort our date by the date (the most recent date and the end). Then we plot our time series just as the example of the figure 5, where we plot the 12 lines as a time series.

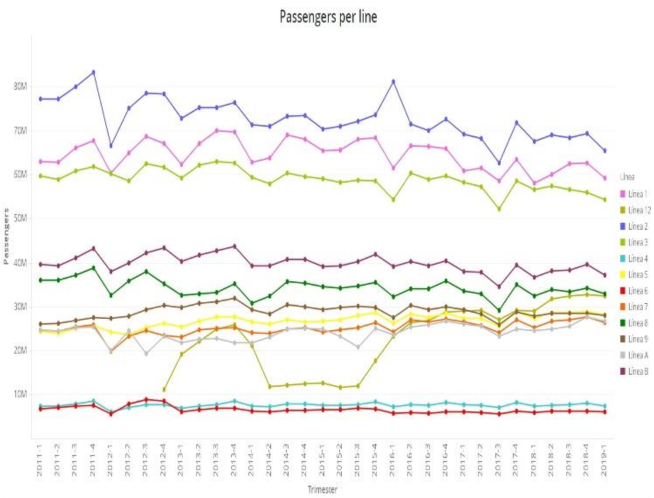

Figure 5 Time Series Passengers per Line

We can see that there are some lines that have the same behavior for example the lines 1,2 and 3, and we can make clusters with the lines that have the same patterns. We have a strange behavior in the line 12 because it was open by the end of October 2012 then the part of the line was close due to technical problems.

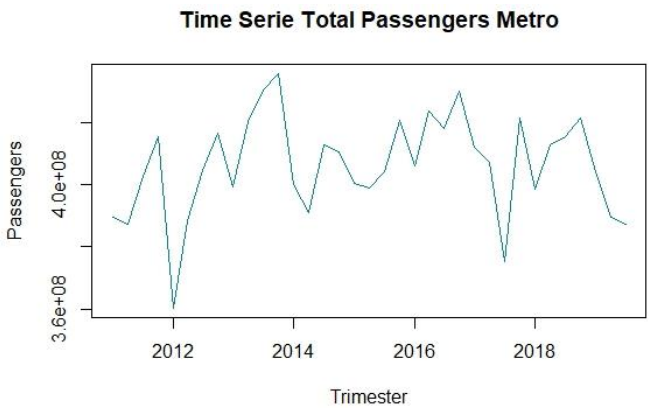

Figure 6 Time Series Total Passengers

On figure 6 we have the time series of all the passengers and the next step is to analyze the time series.

We use the time series decomposition that is a mathematical procedure that transforms a time series into a multiple different time series. The original time series is often split into 3 component series:

- Seasonal: patterns that repeat with a fixed period.
- Trend: The underlaying trend of the metrics.
- Random: also call “noise”, “irregular” or “remainder”, this is the residuals of the original time series after the seasonal and trend series are removed.

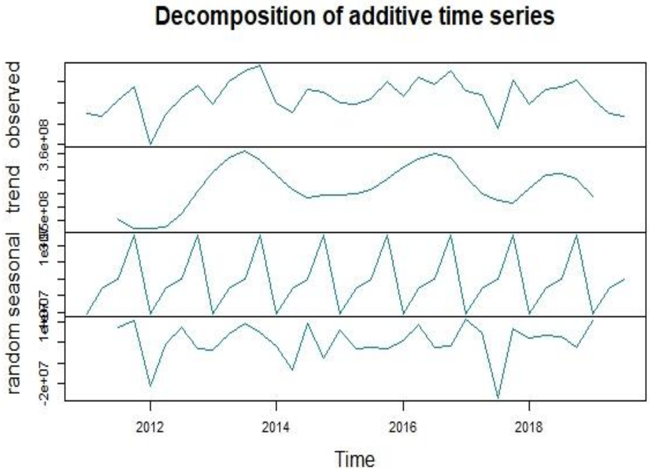

Figure 7 Decomposition Total Passengers Metro

To continue with our analysis, we use the ACF (Auto-Correlation Function) that gives values of autocorrelation of any series with its lagged values. We plot these values along with the confidence. We have an ACF plot. In simple terms, it describes how well the present value of the series is related with its past values. A time series can have components like trend, seasonality, cyclic and residual. ACF considers all these components while finding correlations hence it’s a complete auto-correlation plot.

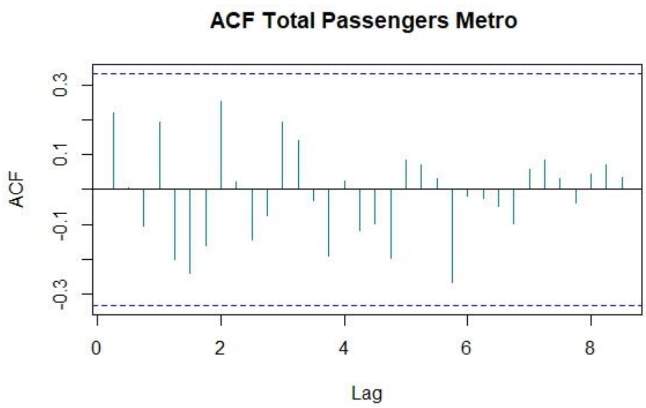

Figure 8 ACF Total Passengers Metro

We also used the PACF (Partial Auto-Correlation Function. Basically, instead of finding correlations of present with lags like ACF, it finds correlation of the residuals (which remains after removing the effects which are already explained by the earlier lag(s)) with the next lag value hence ‘partial’ and not ‘complete’ as we remove already found variations before we find the next correlation. So, if there is any hidden information in the residual which can be modeled by the next lag, we might get a good correlation and we will keep that next lag as a feature while modeling. Remember while modeling we do not want to keep too many features which are correlated as that can create multicollinearity issues. Hence, we need to retain only the relevant features.

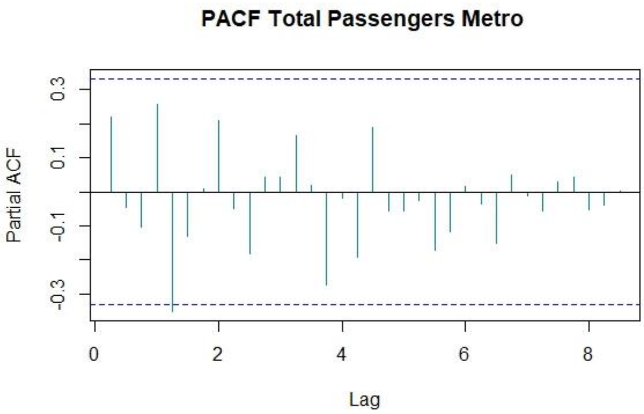

Figure 9 Total Passengers Metro

The ACF and PACF plots are more common used to obtain the values of p and q to feed into the ARIMA model.

All these analyses are important because it show us which are the patterns, seasonality and trend that the passengers follow throughout the time.

For the simulation scenarios we made 2 even more scenarios can be constructed depending on the problem that the network has to face. The first scenario is when we delete Pantitlán (the four stations of the lines 1,5,9, A and it´s connections) station that is one of the most important because of the number of passengers and the connections. The second scenario is when we delete the station with the lowest number of passengers that in this case is Tlaltenco.

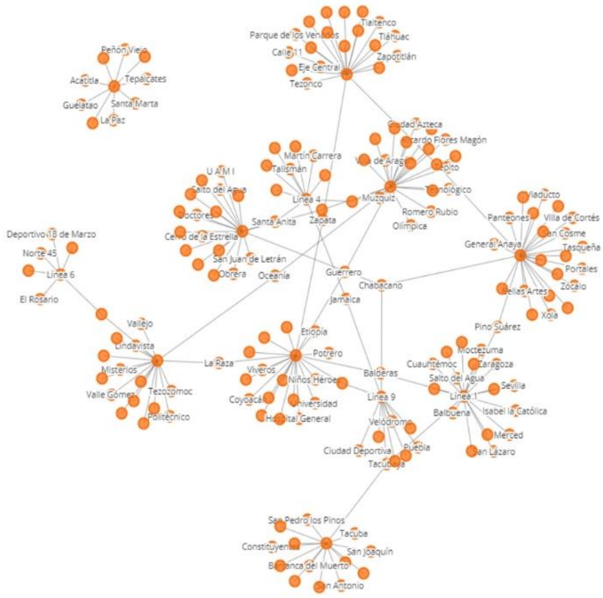

Figure 10 Scenario 1

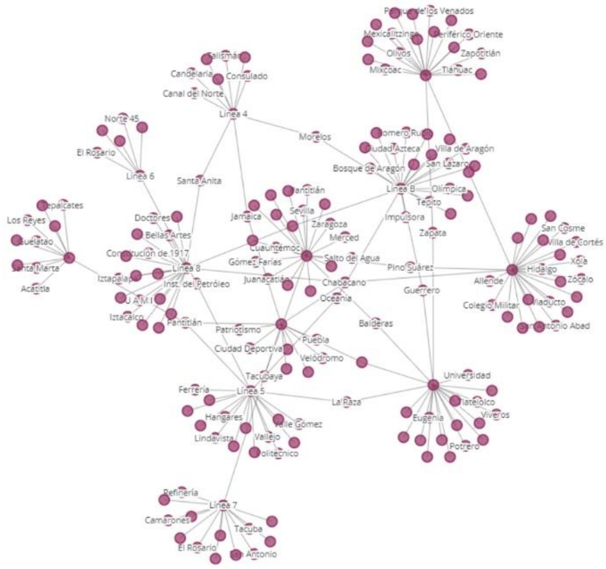

Figure 11 Scenario 2

On the scenario 1 there is a community (all the line A) that is completely disconnected from the whole system and in the case of the scenario 2 we only delete one station and this station is the last one of the line 12 so the only problem here is that the terminal station Tláhuac is completely disconnected from the system.

According with the methodology, we compute the different complex network metrics for both scenarios and then we analyze and compare the results with the original network.

Table 4 Results Scenarios

Results	Total	Scenario 1	Scenario 2
Nodes	195	191	194
Edges	220	212	218
Max. Degree	4	4	4
Min. Degree	1	1	0
Mean Degree	2.25641	2.219895	2.268041
Diameter	39	39	37
Mean Distance	12.94618	28.40568	14.30458
Cliques	4	3	4
Density	0.011631	0.01168366	0.01175151
Assortativity	0.245905	0.1842668	0.24273
Global Clustering	0.056962	0.02006689	0.05538462
Mean Local Clustering	0.017304	0.00571429	0.01657459
Closeness Centrality	0.059484	0.02111135	0.05236912
Degree Centrality	0.008988	0.00936897	0.00897388
Betweenness Centrality	0.144816	0.1533715	0.1566145

Comparing the three-network metrics, we find that the maximum degree is the same but the minimum degree on the scenario 2 is 0 because we delete the node that is the only connection with the terminal Tláhuac, so Tláhuac had 1 degree and when we delete Tlaltenco, Tláhuac remain alone. The mean degree is almost the same, in the case of the diameter on the scenario 2 there is a difference of 2 nodes so is a smaller size, but where we find the greatest difference is on the mean distance because on the scenario 1 it increases a lot so this tell us that Pantitlán station is important in our system and if we delete this station our connectivity decrease so we cannot remove or change this station. On the other hand, the centrality metrics does not change so much, so the scenarios remain with almost the same characteristics of the original network.

We also plot the degree distribution of the scenarios 1 and 2.

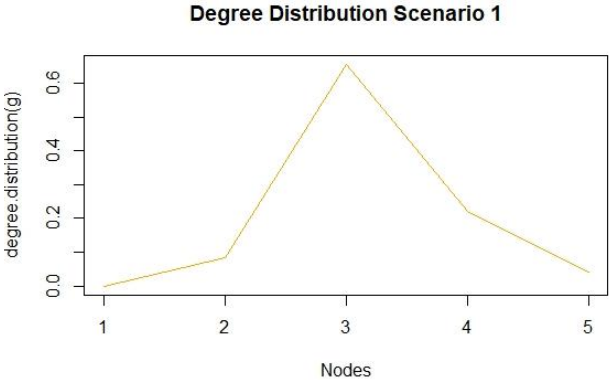

Figure 12 Degree Distribution Scenario 1

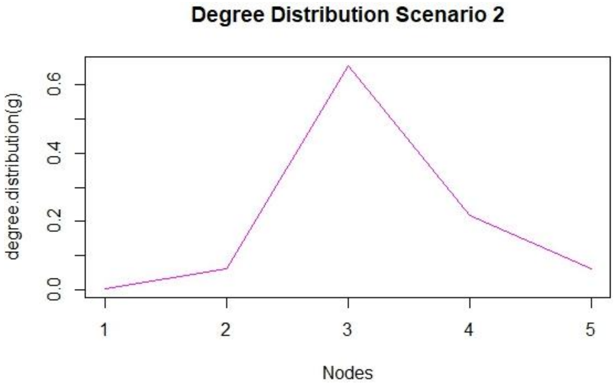

Figure 13 Degree Distribution Scenario 2

Both plots follow a binomial distribution just like the original network.

5. CONCLUSIONS

We conclude that the degree distribution of the network follows a Binomial Distribution, and in this case the network follows a Random Network Model because of the binomial distribution on the degree, the mean distance is high (tends to p ~ logN), the clustering is low (tends to k/N), where k is the average degree of the nodes.

In random networks, the neighbors of a certain node are chosen at random, so there is no correlation between the degree of neighboring nodes. Finally, these networks are more robust to targeted attacks, but at the same time they are vulnerable to internal errors.

After the time series analysis, we concluded that there is no evidence of a growing trend in the number of passengers and we could find some patterns in the seasonal cycles.

It is difficult to find the behavior patterns in a macro level so for the next steps we will do the same analysis but in a medium and micro levels. We will use the same methodology on the stations and lines that are more crowded to find and implement real solutions for this complex system. Also, the simulation will help us to create different scenarios to improve the way the metro works.

ACKNOWLEDGMENT
To the PAPIIT DGAPA project IT102117, UNAM for its support to this research.

REFERENCES

Banks J., **Handbook of Simulation. Principles, Methodology, Advances, Applications, and Practice**, John Wiley & Sons, Inc. pp. 15 - 18. (1998).

Caldarelli G., Catanzaro M., **Networks: A Very Short Introduction**, Oxford University Press, Oxford. (2012).
Camille Roth, S. M. **Evolution of subway networks**. Physics-soc, 1-11. (2012).

Cats O., J. E. **Beyond a complete failure: the impact of partial capacity degradation on.** Transportmetrica B: Transport Dynamics, 77-96.(2018).

Cats, O. **Topological evolution of a metropolitan rail transport network: The case of Stockholm**. Journal of Transport Geography, 62, 172-183. (2017).

Chopra, S., Dillon, T., Billec, M., & Khanna, V. **A network-based framework for assessing infrastructure resilience: a case study of the London metro system**. Journal of the Royal Society Interface, 1-11. Retrieved from http://rsif.royalsocietypublishing.org/content/13/118/20160113. (2016).

Dalgaard P., **Introductory Statistics with R**. Springer. (2008).
Deng, J., Li, Q., Lu, Y., & Yuan, Y. **Topology Vulnerability Analysis and Measure of Urban Metro Network: The case of Nanjing**. Journal of Networks, 8(6), 1350-1356. (2013).

Derrible S., **Network Centrality of Metro Systems,** PLoS ONE 7(7): e40575. doi:10.1371/journal.pone.0040575, (2012).

Derrible, S., & Kennedy, C. **Network Analysis of World Subway Systems Using Updated Graph Theory**. Transportation Research Record: Journal of the Transportation Research Board , 3(2112), 17-25. (2009).

Derrible, S., & Kennedy, C. **Characterizing metro networks: state, form and structure**. Transportation, 37(2), 275-297. (2010).

Dillarza-Andrade, Y, **Medición del tiempo de abordaje de los pasajeros del STC: estación Pantitlán, Line 1**. Tesis UNAM. (2017).

Ding, R., Ujang, N., Hamid, H., & Wu, J. **Complex Network Theory Applied to the Growth of Kuala Lumpur's Public Urban Rail Transit Network**. PLOS one, 10(10), 1-22. (2015).

Drozdowski M., Kowalski D., Mizgajski J., Mokwa D., **Pawlak G., Mind the gap: a heuristic study of subway tours,** J Heuristics 20:561–587, (2014).

Figueras J., **Modelos de Simulación usando simio y redes de Petri**, Universidad Nacional Autónoma de México. pág. 2. (2013).

Flores-De La Mota, I., & Huerta-Barrientos, A. **Simulation-Optimization of the Mexico City Public Transportation Network: A Complex Network Analysis Framework.** En M. Mujica-Mota, & I. Flores-de-la-Mota, Applied Simulation and Optimization (Vol. 2, pp. 43-79). Ciudad de México: Springer. (2017).

Flores-De La Mota, I., Hernández-González, S. **Applying complex network theory to the analysis of metro networks (1969 – 2018)**. Print, Artículo en revisión. (2018).

Fortin P., Morency C., Trépanier M., **Innovative GTFS Data Application for Transit Network Analysis Using a Graph-Oriented Method,** Journal of Public Transportation, Vol. 19, No. 4, (2016).

Gallotti R., Porter M. A., Barthelemy M., **Lost in transportation: Information measures and cognitive limits in multilayer navigation**. Science Advances 2, e1500445, (2016).

Gattusso, D., & Miriello, E. **Compared Analysis of Metro Networks Supported by Graph Theory**. Networks ans Spatial Economics, 5(4), 395-414. (2005).

Guerra E., **Mexico City´s suburban land use and transit connection: The effects of the Line B Metro expansion,** Transport Policy 32, 105–114, (2014).

Háznagy A., Fi I., London A., Németh T., **Complex network analysis of public transportation networks: a comprehensive study,** Models and Technologies for Intelligent Transportation Systems (MT-ITS) 3-5. Junio 2015. Budapest, Hungary, (2015).

Kim H., Song Y**., Examining Accessibility and Reliability in the Evolution of Subway Systems,** Journal of Public Transportation, Vol. 18, No. 3, (2015).

Lara, F., **Teoría, métodos y modelos de la complejidad social I. Seminario de Investigación**, CCADET.

Lara, F., **Metodología para la planeación de sistemas: un enfoque prospectivo**, Dirección General de Planeación, Evaluación y Proyectos Académicos, UNAM. México. (1990).

Latora V., Marchiori M., **Is the Boston subway a small-world network?,** Physica A 314, 109 – 113, (2002).
Leskovec, J., Kleinberg, J., & Faloutsos, C. **Graph Evolution: Densification and Shrinking Diameters**. ACM Transactions on Knowledge Discovery from Data, 1(1), 1-41. (2007).

Louf R., Roth C., Barthelemy M., **Scaling in Transportation Networks**, PLoS ONE 9(7): e102007, (2014).

Mood A., **Introduction to the Theory of Statistics.** McGraw-Hill. (1974).

Negroe, G., **Papel de la planeación en el proceso de conducción**, Universidad Nacional Autónoma de México. pp 10. (1980).

Newman M.E.J., **Networks: An Introduction**, Oxford University Press, Oxford. (2010).

Purdy, G., **ISO 31000:2009 Setting a New Standard for Risk Management**, Society for Risk Analysis, Vol. 30. No. 6, págs. 881-886. (2010).

Shiau T-A., Lee C-H., **Measuring Network-Based Public Transit Performance Using Fuzzy Measures and Fuzzy Integrals,** Sustainability 9, 695, (2017).

Stoilova S., Stoev V., **An Application of the Graph Theory Which Examines the Metro Networks,** Transport Problems Volume 10, Issue 2, (2015).

Sun L., Huang Y., Chen Y., Yaob L., **Vulnerability assessment of urban rail transit based on multi-static weighted method in Beijing, China.** Transportation Research Part A 108, 12–24, (2018).

Swanepoel E., Pretorius L., **A Structured Approach to Risk Identification for Projects in a Research Environment,** Proceedings of PICMET '15: Management of the Technology Age, (2015).
Tarride M., **Complexity and complex systems**, Historia, Ciencias, Salud. Manguinbos, II (1), pp 46-66. (1995).

Vera-Morales, A. E., **Un Modelo de simulación para mejorar los mecanismos de evacuación en el STC Metro**. Tesis UNAM. (2017).

Wang X., Ko Y., Derrible S., Ahmad S-N., Kooji R. E., **Quantifying the robustness of Metro Networks**, *CoRR*, abs/1505.06664, (2015).

Wang X., Ko Y., Derrible S., Ahmad S-N., Pino W. J. A., Kooji R. E., **Multi-criteria robustness analysis of metro networks,** Physica A 474,19–31, (2017).

Wu X., Dong H., Kong Tse C., Ho W. H. I., Lau C. M. F., **A Network Analysis of World's Metro Systems,** 2016 International Symposium on Nonlinear Theory and Its Applications, NOLTA 2016, Yugawara, Japan, 27-30 Noviembre, (2016).

Wu X., Dong H., Kong Tse C., Ho W. H. I., Lau C. M. F., **Analysis of metro network performance from a complex network perspective,** Physica A 492, 553–563, (2018).

Zhang H., **Structural Analysis of Bus Networks Using Indicators of Graph Theory and Complex Network Theory,** The Open Civil Engineering Journal, 11, 92-100, (2017).

ACKNOWLEDGMENTS
To CONACYT scholarship and UNAM scholarship for the first author.

AUTHORS BIOGRAPHY

Sashiko Shirai received a Master in Operation Research in the Faculty of Engineering of the UNAM and she also received her bachelor's in actuarial science in the Faculty of Science of the UNAM. She is studying her PhD in the Instituto de Investigación en Matemáticas Aplicadas y Sistemas (IIMAS) of the UNAM. She is an assistant professor at the Faculty of Engineering and the Faculty of Science. Her research interests lie in complex networks, statistics and operational research.

Idalia Flores received a Master with honors, being awarded with the Gabino Barreda Medal for the best average of her generation, in the Faculty of Engineering of the UNAM, where she also obtained her Ph.D. in Operations Research. Dr. Flores is a referee and a member of various Academic Committees at CONACYT as well as being a referee for journals such as Journal of Applied Research and Technology, the Center of Applied Sciences and Technological Development, UNAM and the Transactions of the Society for Modeling and Simulation International. She is a full-time professor at the Postgraduate Program at UNAM and her

COMPLEXITY ANALYSIS OF THE FUTURE CAR FOR AUTOMOTIVE LOGISTICS

Konrad Pawlikowski[(a)], Michael Toth[(b)]

[(a)]Bochum University of Applied Sciences
[(b)]Department of Business and Management, Bochum University of Applied Sciences

[(a)]konrad.pawlikowski@hs-bochum.de, [(b)]michael.toth@hs-bochum.de

ABSTRACT

The automotive industry has to manage radical changes. Especially, the complexity of parts and variants changed by the technological trends e-mobility and the increasing introduction of intelligent assistance systems that are based on embedded systems. Moreover, not only the car complexity is affected. To realise the impact of change, a holistic complexity analysis of the product car has to be done. Such analysis is particularly relevant for logistics, which acts as a cross-divisional function between technology development, procurement, production, sales and after-sales. Therefore, this contribution presents identified impact areas in the field of the automotive logistics followed by developed indicators to realise an approach for a holistic complexity analysis. This is necessary to identify impacts on logistics processes, e.g. sourcing strategies.

Keywords: automotive logistics, car complexity, e-mobility, embedded systems

1. INTRODUCTION

Since Henry Ford introduced mass production in the early 20th century, the automotive industry is facing the biggest challenge in its history. (Holweg and Pil 2004). The megatrends autonomous driving and the field of e-mobility are becoming increasingly important and will significantly change the car and its production and logistics structures.

Original equipment manufacturers (OEMs) nowadays offer their customers a huge variety of models to compete in international markets. Moreover, those models can be individualised by several hundred options (Dörmer 2013). Among these options are design elements (e.g. car paint), functional components (e.g. gear system) and recently more and more assistance systems (e.g. Adaptive Cruise Control (ACC) as a driver assistance system). Furthermore, the OEMs product range is constantly updated with increasing frequency (Schuberthan and Potrafke 2007).

The management of product variety and the resulting complexity is decisive for the success of the OEMs. Offered variety supports the maintenance of market share, revenue and thus profit. Nevertheless, variety also leads to complexity in the field of product portfolio, product architecture and in supply chain processes. (Götzfried 2013) Especially the mentioned trends e-mobility and the increasing number of embedded systems to integrate intelligent assistance systems have led to a radical increase in complexity of parts and variants (Kampker et al. 2016, Krumm et al. 2014).

Changes within the complexity (increase as well as decrease) in the product architecture and in OEM's portfolio is a challenge itself. Only with a high degree of transparency, the OEMs are able to manage the complexity. For example on the portfolio side, the OEMs are able to identify a non-efficiently level of complexity to handle. (Götzfried 2013) This transparency applies in particular to logistics that has to guarantee material availability and quality under demand uncertainty. In addition, logistics acts as a cross-divisional function between technology developments, procurement, production, sales and after-sales. Therefore, it is essential that the so-called product representation (information basis) depicts all car characteristics (especially dependencies between parts, components and car features) and provides transparent holistic information for all logistics processes. This product representation includes a product structure, its options as well as its components and their dependencies. (Fruhner et al. 2017)

Here, this contribution presents an identification of the impact areas on logistics caused by the future car in the field of the automotive industry. Based on these findings and scientific literature, indicators for a complexity analysis approach are derived. These indicators shall replicate the complexity numerically expressed and therefore be used as a basis for a decision support regarding logistics strategy for example in terms of sourcing strategies.

The paper is structured as follows: relevant terms and concepts will be defined in section 2, attached by a discussion of challenges in the automotive industry. This leads to an identification of impact areas on logistics. Subsequently, complexity indicators are derived related to the identified impact areas in section 3. Moreover, a holistic complexity analysis approach is presented. The contribution concludes with a summary of key insights and an outlook on further research.

2. CHALLENGES FOR THE AUTOMOTIVE INDUSTRY AND CORRESPONDING IMPACT AREAS ON LOGISTICS

After the automotive customer has opted for a car series and a related model, the model can be further individualised by so-called options and option packages. These – sometimes – several hundred options include in addition to exterior, interior and security equipment, nowadays also driving assistance systems (e.g. parking aid) (eVchain 2014). The high degree of individual configuration is a crucial marketing factor for premium OEMs, but it contributes as well significantly to the complexity of the product car. Moreover, automotive customers have to deal with the rapid change of variants and options (Ebel and Hofer 2014).

An effective automotive supply chain logistics management requires the synchronization of resource and component requirements with resource capacities and constraints in the production and supply chain. To achieve this, the logistics planner needs a holistic information set. However, relevant data is typically kept in a highly fragmented information landscape ((Bockholt 2012, Meyr 2004, Stäblein 2008)) and must therefore be integrated into a transparent and efficient form of product representation. This product representation must contain all information that is necessary to grasp the expected or realised needs of the customer (e.g. model volume or option quotas). (Fruhner et al. 2017)

The compatibility of car models and their options is described by a highly complex set of technical rules, while the related material items of the corresponding fully-configured car and the corresponding material items are described by the so-called bill of material (BOM) (Pawlikowski et al. 2016).

Regarding the offered car series variety, the trend of e-mobility leads to radical changes in the car architecture. Electric vehicles differ in various components in comparison to conventional vehicles (vehicles with combustion engines), for example all components related to the exhaust system are obsolete, but the share of electronic components is much higher. The compatibility of the electronic components and the connection of the energy consuming components to the energy source(s) in the car has to be ensured. (Fruhner et al. 2017) In addition, the number of embedded systems and software within the powertrain is generally increasing (Nikowitz 2016). All these facts lead to the impact area "product and production complexity" as an object of this research.

Meanwhile, a shift in the competence of OEMs has been identified and analysed since many years. As the product car includes many simple parts, automotive suppliers produce and develop more and more complex modules (Trojan 2007). OEMs on the other hand focus more and more on the assembly of supplied parts and modules, the coordination of suppliers, the product marketing and the distribution of the product car (Meissner 2009). Today, different supply concepts (e.g. just-in-time delivery), global locations of supplier, long distances, and varying material flow systems increase the complexity (Fruhner et al. 2018).

The OEM's product range will be jointly determined by conventional and electric vehicles in the foreseeable future (Göpfert et al. 2017). Therefore, the effort for supplier selection, triggering and monitoring order processes will increase. Hence, the second impact area on automotive logistics is the field of "supply chain complexity".

The classical product life cycles are seven years in the automotive industry. Rather, the development lead-time is three years, thus the technologies used during this period are ten years old at the end of their life cycle. In comparison to current technology development, such a cycle is far too long and leads to obsolete technologies very quickly. (Kampker et al. 2017) Many electronic components in a car like navigation systems are outdated after a few years of use. Such cars can only be sold to second-hand customers with a great loss of value. This can be countered by updating the components, e.g. by integrating Apple CarPlay into an end-of-life vehicle. (Moynihan 2014). Besides, the share of the electric and electronic components increases within the car (eVchain 2014).

Thus, a continuous update of the vehicles, similar to software, must be enabled to improve sustainability. These effects extend to the after-sales and also spare-part business. Concluding, the "innovation cycles complexity" is a third impact area on automotive logistics.

As summary, the identified impact areas regarding the challenges within the automotive industry are:

- product and production complexity,
- supply chain complexity and
- innovation cycles complexity.

To be able to support decision-making within logistics processes, indicators will be derived in the next section. The aim is to use them as a holistic complexity approach based on the comparison of the "future" and "conventional" car to understand if the automotive logistics is also facing big changes. Moreover, it shall be used to evaluate the complexity of the car in the future and support decisions for example in the field of sourcing strategies.

3. HOLISTIC ANALYSIS APPROACH AND ITS COMPLEXITY INDICATORS

The scientific application of the term "complexity" is interdisciplinary and finds expression in a multitude of sciences (cf. (Kirchhof 2003)). Maguire et al. (2011) emphasized complexity as a significant growing research topic in the field of natural and social sciences. Moreover, the management of complexity represents a crucial managerial challenge in organisation (Morieux 2011, Sargut and McGrath 2011).

An overview of complexity theories and their interpretations is given by Meyer as well as Kirchhoff (Kirchhof 2003, Meyer 2007). For example in the field of systems theory, complexity is defined by the number of elements, their relations, and the change of elements and relations over time (Meyer 2007). Related to the system structure, static or structural complexity arises, whereby dynamic or operative complexity describes the system behavior over time (Schuh 2005).

Another view regarding the management of complexity is the differentiation between external and internal complexity (Kaiser 1995, Schuh and Schwenk 2001). Here, companies try to bridge the gap between customers' demand requirements and the product variety. This results in a certain level of product and process complexity (Marti 2007, Schuh and Schwenk 2001).

As this contribution presents a holistic approach to analyse the complexity of the product car, the opportunities of evaluation are point of interest. Here, two types of complexity evaluation exist: monetary and non-monetary approaches. Both approaches allow manufacturing companies to set and track quantifiable targets. Cost calculations represent monetary approaches, whereby non-monetary approaches are indicators and indices that are not directly transferred to costs. (Götzfried 2013)

Based on this differentiation, a non-monetary evaluation related to the identified impact areas is used as an approach to analyze the car complexity in the field of automotive logistics. It shall consider the changes within the car architecture and the corresponding logistics processes. Hereby, a differentiation between external and internal factors will be considered.

3.1. Product and Production Complexity

The more complex a product to be manufactured is, the more complex are the processes required for production as well as those existing within the remaining value chain (Schaffer 2010).

As the product architecture belongs to the field of product complexity, the following section considers the differentiation between external and internal variety. External variety is the product variety offered to the customer. In the automotive industry, Lechner et al. (2011) refers to 10^{20} different configurations as product variety for several models of German premium OEMs. The total number of variants is responsible for ensuring that within a value-added process, e.g. in mechanical production, assembly or planning, non-value-adding activities are carried out and so-called reactive power is generated (Schaffer 2010).

Therefore, the external variety as a crucial indicator is point of interest. According to Rosenberg (2002) the theoretical variety v^{th}, i.e. the external variety, can be calculated by the multiplication of number of mandatory variety and optional variety (1). Here, x_m is defined as the number of expressions of the mandatory characteristic m and y_k as the number of values of the optional characteristic k. The related amount of the characteristics are *M* and *K*.

$$v^{th} = \prod_{m=1}^{M} x_m * \prod_{k=1}^{K} (y_k + 1) \qquad (1)$$

It shall be highlighted, that v^{th} is a theoretical number. Technical restrictions prohibit options for specific models (e.g. no 17'' tires for convertibles), force specific combinations of options (e.g. LED head light only in combination with LED back lights) or prohibit combinations (e.g. a navigation system rules out all other radios). Schaffer, for example, divides the variety into the practically producible number of variants, the effectively produced number of variants, the technically permissible number of variants and the theoretical number of variants (Schaffer 2010). Scavarda et al. (2010) formulate the producible variety as a subtraction of theoretical variety and restrictions, that affect models and/or bodystyles.

```
// evaluate feasible configurations
FUNCTION evaluateFeasibleVariety(model, originalData, sample size)

   LIST technicalRules      =  get relevant rules for model in originalData
   LIST relevantOptions     =  get relevant options for model in originalData
   reduceOptions()

   WHILE evaluateConfigurations <= sample size

      LIST tempConfig       =  random configutation according option families
      BOOL evalTempConfig   =  valid(tempConfig, technicalRules)
      countFeasible        +=  (evaluatetempConfiguration)

   END WHILE

   RETURN countFeasible

END FUNCTION
```

Pseudocode 1: Evaluate feasible variety

The exact estimation of the feasible variety v^f is not possible in an appropriate time, for example related to the mentioned theoretical variety of $10^{20}$and 60 relevant technical rules, it would result in 60^{21} evaluations. Therefore, the authors approximate the number of feasible configurations v^f (pseudocode 1). Based on the analysed car model random configurations are determined and these configurations are tested if the relevant technical rules are valid. To reduce the amount of calculation, options that will be set independent of the configuration are put in a "basis configuration".

Based on external variety and demands, companies translate into value chain requirements and create internal variety (Pil and Holweg 2004). As the variety of models grows, so does the number of components in the company. This fact leads to an increase in the number of goods to be procured (Kestel 1995).

According to MacDuffie et al. (1996) internal variety can be differentiated in a fundamental, peripheral and intermediate level. The level of fundamental variety is represented by variation of base products, platforms and models. The amount and variation of offered options belongs to the peripheral variety. Intermediate level is characterized by part variety, reflecting product design and the supply chain (e.g. number of suppliers). Accordingly, related to a specific model, p^{mo} represents the intermediate variety with respect to unique parts p^{u} (3).

$$p^{mo} = n(p^{u}(model)) \tag{3}$$

Furthermore, in the context of external variety, the amount of offered options can be indexed as the degree of individualisation. The potential individualisation used by OEMs as a marketing factor affect the "Order Penetration Point" that represents the transition from forecast-driven and customer-neutral to customer order-driven production planning (Klug 2010). Thus, the degree of individualisation d^{i} is calculated by division of the number of choosable (optional) options $op^{o}$and the corresponding total number of options (4).

$$d^{i} = \frac{n(op^{o})}{n(op)} \tag{4}$$

Here, d^{i} is analogous to v^{th} a theoretical indicator. This is caused by the technical rules that prohibit all optional options to be set at the same time. An approximation of a real number of independent optional options ao^{i}can be estimated by (5).

$$ao^{i} = n(op^{o}) - log_2 \frac{v^{th}}{v^{f}} \tag{5}$$

Based on Lechner (2011) the so-called variant density and variant heterogeneity can be used as indications of product complexity. While the density of variants can be determined with regard to the product range, the characteristic number of variant heterogeneity is related to option families (Lechner 2011). The variant density d^{v} can be estimated by counting the base parts p_i^{b} and dividing by the amount of parts for a specific model (6).

$$d^{v} = \sum_{i=1}^{n} p_i^{b} / \sum_{i=1}^{n} p_i \tag{6}$$

The variant heterogeneity h^{v} of an option family is an indicator that shows how strongly variant number changes can affect the logistics system. The result of the value is 1 if a variant family is absolutely heterogeneous and 0 if there are no similarities between the variant characteristics. Therefore, it enables the evaluation regarding scale effects. It is calculated from the sum of attributes a_i, which have the same value ag_j for all variants, in relation to the sum of all characteristics (7).

$$h^{v} = \sum_{j=1}^{m} ag_j / \sum_{i=1}^{n} a_i \tag{7}$$

Regarding to the product architecture not only the physical part of car characteristics has changed. The digitisation of the car has introduced new and changed dependencies among components, e.g. the compatibility of hardware and software. Among other impacts, the compatibility has to be ensured with respect to spare parts and maintenance. Such dependencies are described by the mentioned technical rules. Therefore the next point of interest is the complexity of those. Based on Lechner (2011), the indicator "connectivity of variants" c^{ch} analyses the amount of relations between the option characteristics (8). The amount of characteristic dependencies to other characteristics $m^{ch,re}$ is put in relation to the number of characteristics.

$$c^{ch} = m^{ch,re} / m^{ch} \ \forall \ ch \tag{8}$$

The higher the connectivity, the greater the impact of variant changes. The changes in the number of variants of an existing variant family, e.g. an additional motor, lead to additional variants of other variant families (e.g. transmission).

A similar indicator to evaluate the complexity of the dependencies regarding the characteristics is the analysis of the corresponding technical rules (noted as boolean rules) (9). One indicator is the length of boolean rules $l(r)$. In general, the complexity of boolean rules can be evaluated regarding their depth $d(r)$. It is defined as the maximum number of steps to evaluate from input to output (Paterson 1992). A third part is represented by the average priority of boolean operators $ap(r)$.

$$c^{r} = l(r) * d(r) * ap(r) \ \forall \ r \tag{9}$$

Based on this determination, the average of c^{r} is supposed to imply the complexity of the model under consideration. The effort of logistic processes can be supported, e.g. in the determination of forecasts and demand.

3.2. Innovation Cycle Complexity

As the innovation cycles accelerate, there are some factors that are relevant for the complexity analysis. To be able to manage the short innovation cycles and amount of parts, modularity and platform strategies are used in the automotive industry in the context of variant management. Related to this, the share of part modularity represents an important indicator regarding the question whether the degree of modularity is increasing in the flied of e-mobility. Gross et al. (2007) – for example – describe a degree of modularity, i.e. the number of elements of a modular structure weighted with the production quantities. Based on this idea and under consideration of the changes from the conventional car to the "future" car, the authors decide to measure the product modularity as a share of parts related to the number of suppliers (10).

$$s_m^{pm} = \frac{n(p)}{n(s)} \tag{10}$$

A similar approach to handle such situation is the use of equal parts as far as possible; thus the share of equal parts s_m^{eq} (11) is an indicator for complexity and may support the selection of suppliers and its sourcing strategy (e. g. multiple sourcing).

$$s_m^{eq} = \frac{n(p^{eq})}{n(p)} \tag{11}$$

Moreover, related to electronic parts p^e, the amount of software p^{sw}within the car is significantly increasing (Hammerschmidt 2019). Here, new types of suppliers like Apple or Google are entering the automotive industry. New participants will increase the competition between the OEMs (Bob Heaney 2015). Therefore, the share of electronic parts (12) as well as the share of software elements (13) are points of interest (regarding part complexity and compatibility). The conclusion of more software components is the fact that more software updates have to be managed and the compatibility between those components have to be ensured.

$$s_m^{e} = \frac{n(p^{e})}{n(p)} \tag{12}$$

$$s_m^{sw} = \frac{n(p^{sw})}{n(p)} \tag{13}$$

Not only the innovation cycles accelerate, the product life cycle of the car is getting shorter. Therefore, logistics processes have to handle this, for example the forecast is getting more complex. The indicator "product lifecycle complexity" $plcc^{mo}$ related to the model, is determined by the division 1 by the product life cycle PLC (14).

$$plcc^{mo} = \frac{1}{PLC^{mo}} \tag{14}$$

3.3. Supply Chain Complexity

In general, the third part "supply chain complexity" is crucial influenced by the trend of globalisation. Global suppliers and their competition enable supply chain processes many possibilities. On the one side, the competition between the suppliers is rising, but on the other side, longer delivery times and higher logistics costs are factors for an OEM to be considered. The share of local and the number of global suppliers (15)-(16) shall implicate the complexity, for example regarding the choice of sourcing strategies.

$$s_m^{local} = \frac{n(s^{local})}{n(s)} \tag{15}$$

$$s_m^{global} = n(s^{global}) \tag{16}$$

The increasing electrification of vehicles will shift the value added in the supply chain. Regarding the supply chain of the conventional car, 30% of the value added is generated via the power train, whereby for an electric car it amounts to 60% (caused by the battery). (Bierau et al. 2016, Pieper and Ernst o.J.) In addition, the value added of the battery cell, i.e. raw material supply and production (main part of the costs of batteries) is located outside of Europe (Pawlikowski et al. 2018).

In this context, as a non-monetary approach, the share of produced parts shall be an indicator related to the field of make-or-buy decision (17). Make-or-buy is used to decide on the own depth of value added. Even this basic decision leads to consequences with regard to logistics complexity (such as number of suppliers, variety of incoming goods) and to correspondingly necessary procurement logistics structures (Muchna et al. 2018).

$$s_m^{pr} = \frac{n(p^{pr})}{n(p)} \tag{17}$$

A low vertical range of manufacture tends to lead to the delivery of more complex parts to assemblies. Just-in-time (JIT)/ just-in-sequence (JIS) logistics processes with lower warehousing are more likely to be used here. These are production synchronous strategies, where components for production are delivered on exact dates in coordination with the production or assembly process. (Muchna et al. 2018)

This avoids intermediate stocks and buffers (Kestel 1995). In order to be able to meet the short delivery time, suppliers often locate themselves in close proximity to the automotive plant (Grunewald 2015). Especially if such efficient processes are or can be used, the respective share is derived (18)-(19). Based on this information and in relation to their corresponding number of suppliers, decisions and possible steps shall be assisted.

$$s_m^{local} = \frac{n(p^{local})}{n(p)} \tag{18}$$

$$s_m^{global} = \frac{n(p^{global})}{n(p)} \tag{19}$$

3.4. Holistic Complexity Approach

According to the understanding of complexity in this contribution, complexity is formed by the interplay of many dimensions. For the complete evaluation of complexity it is therefore obvious to consider complexity as a multidimensional quantity, since an adequate quantification of complexity cannot be realised by a single indicator (Scholz-Reiter et al. 2006).

Furthermore, in times of growing modularity, in which the influence of product complexity on the process can be affected by decoupling processes, late configuration, standardization, platform strategies and common parts concepts, it is important to have access to efficient tools and methods with which the influence of product structure and architecture on manufacturing processes and thus on costs can be investigated (Schaffer 2010). This shall support decision-making, which is a central activity in big and complex organisations, thus one of the key tasks and responsibilities of managers. (Götzfried 2013, Nutt and Wilson 2010) Moreover, to manage complexity, the transparency of variety-induced complexity represents a crucial element in order to understand its impact. (Child et al. 1991, Lechner et al. 2011). The effects of product complexity also unfold in a change in procurement complexity. For example, an expansion of the product range also has an effect on the supplier network and leads to additional costs for goods processing in the plant. Product complexity continues to have an internal influence on structural complexity, because structural adjustments must always be made as a result of changes in the product program. (Feldhuetter 2018)

In general, the aim should not be to design a minimal but rather a company complexity adapted to the situation, based on a differentiated selection of measures (Schuh 2005). Regarding the time horizon, three generic strategies for implementing efficient variant management can be distinguished: the strategy of complexity reduction, complexity control and complexity avoidance (Feldhuetter 2018).

Only with such presented holistic complexity analysis, it can be assessed to what extent logistic processes have to adapt and what the future vehicle means for variant management etc. This approach shall support processes and stakeholders in every phase of the product life cycle. Moreover, the integration of new modules, components or software components into an existing vehicle structure as well product representation and into logistics processes shall be assisted.

A visualization of the schema, covering the three impact areas, is shown in figure 1. It is based on a so-called spider chart. The method shall be used to compare the complexity of the conventional car and the “future” car in forthcoming work and enable the identification of impacts on logistics processes.

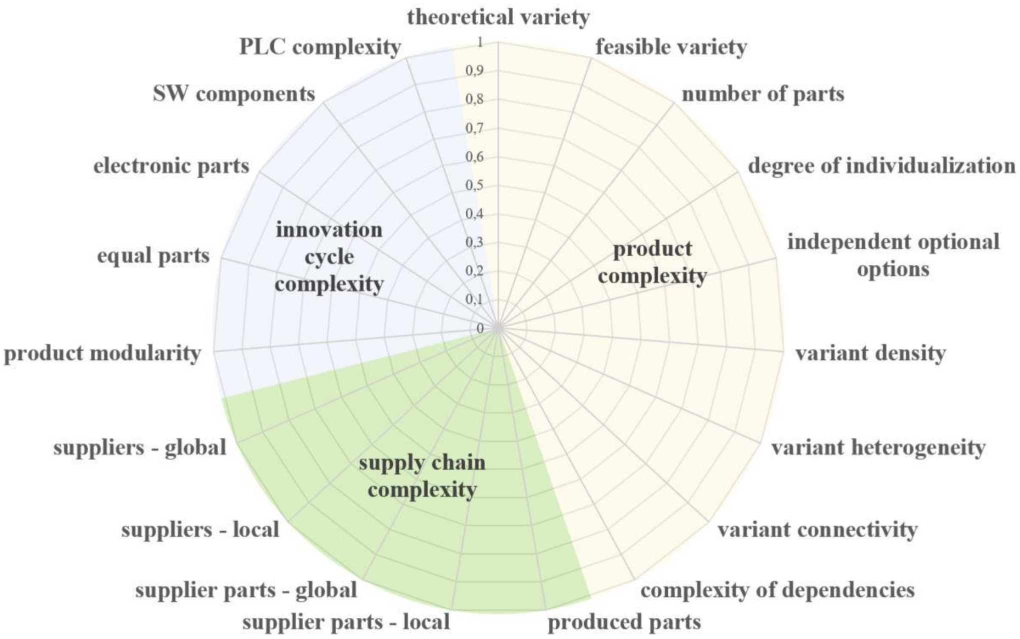

Figure 1: Spider chart for complexity analysis

4. KEY INSIGHTS AND OUTLOOK

The presented contribution is an important starting point, as it shows that not only the car as a product itself radically changes. Moreover, the changes affect the automotive logistics and the corresponding product representation. Hereby, in order to guarantee the availability of components and minimize obsolescence risks, it is essential that the automotive logistics has access to transparent holistic information. Especially, dependencies of technical and electronical components and the compatibility between hardware and software components have to be considered. To realise the impact of change (parts, variants, supplier locations), a holistic complexity analysis has to be done.

Based on this approach, a forthcoming work will be the evaluation of the implemented model and a comparison of the complexity of a conventional model and a “future” car to identify impacts on logistics processes. In addition, this holistic complexity analysis shall help to optimize impacts on logistics processes by simulation (for example by different scenarios within the product development).

REFERENCES

Bierau, F., Perlo, P., Müller, B., Gomez, A. A., Coosemans, T. and Meyer, G., 2016. Opportunities for European SMEs in Global Electric Vehicle Supply Chains in Europe and Beyond. In: Schulze, T., Müller, B. and Meyer, G., eds. Advanced Microsystems for Automotive Applications 2015Smart Systems for Green and Automated Driving: Springer, pp. 223–235.

Bob Heaney, 2015. THE EVOLUTION OF THE SUPPLY CHAIN - SPOTLIGHT ON THE AUTOMOTIVE INDUSTRY.

Bockholt, F., 2012. Operatives Störungsmanagement für globale Logistiknetzwerke: Ökonomie- und ökologieorientiertes Referenzmodell für den Einsatz in der Automobilindustrie. Thesis (PhD). TU Dortmund University.

Child, P., Diederichs, R., Sanders, F.-H., Wisniowski, S. and Cummings, P., 1991. The management of complexity. In: McKinsey Quarterly, pp. 52–68.

Dörmer, J., 2013. Produktionsprogrammplanung bei variantenreicher Fließproduktion: Untersucht am Beispiel der Automobilendmontage. Wiesbaden: Springer.

Ebel, B. and Hofer, M. B., eds., 2014. Automotive Management: Strategie und Marketing in der Automobilwirtschaft, 2nd edn. Berlin: Springer Gabler.

eVchain, 2014. Modellierung der zukünftigen elektromobilen Wertschöpfungskette und Ableitung von Handlungsempfehlungen zur Stärkung des Elektromobilitätsstandortes NRW: (EM1006 – eVchain.NRW).

Feldhuetter, V., 2018. Beitrag zur modellbasierten Bewertung der Komplexität in der Montagelogistik der Automobilindustrie. Thesis (PhD). TU Dortmund University.

Fruhner, D., Klingebiel, K., Pawlikowski, K. and Toth, M., 2018. Impacts of the digitalised car on logistics. Proceedings of the 25th International Annual EurOMA Conference, June 24-26. Budapest, Hungary.

Fruhner, D., Pawlikowski, K., Klingebiel, K. and Toth, M., 2017. Efficient Product Representations for Automotive Logistics. Proceedings of the 29th European Modeling and Simulation Symposium (EMSS), pp. 100–109, September 18 - 20. Barcelona, Spain.

Göpfert, I., Braun, D. and Schulz, M., eds., 2017. Automobillogistik: Stand und Zukunftstrends[Online], 3rd edn: Springer Gabler. Available at: http://dx.doi.org/10.1007/978-3-658-11103-8.

Götzfried, M., 2013. Managing Complexity Induced by Product Variety in Manufacturing Companies Complexity Evaluation and Integration in Decision-Making. Thesis (PhD). University of St. Gallen.

Gross, W., Heimel, J., Kuhn, S. and Schwab, C., 2007. Towards case-based product and network configuration for complex construction machinery. In: Innovative processes and products for mass customization. Berlin, pp. 121–135.

Grunewald, M., 2015. Planung von Milkruns in der Beschaffungslogistik der Automobilindustrie. Wiesbaden: Springer Fachmedien Wiesbaden.

Hammerschmidt, C., 2019. E/E-Architekturen: Frischzellenkur[Online]. Available at: https://www.car-it.com/frischzellenkur/id-0062411?cookie-state-change=1554127222067 (Accessed 14 April 2019).

Holweg, M. and Pil, F. K., 2004. The second century: Reconnecting customer and value chain through build-to-order: moving beyond mass and lean production in the auto industry. Cambridge, MA, USA: MIT Press.

Kaiser, A., 1995. Integriertes Variantenmanagement mit Hilfe der Prozesskostenberechnung. Thesis (PhD). University of St. Gallen.

Kampker, A., Deutskens, C., Heimes, H., Ordung, M. and Haunreiter, A., 2016. Using E-mobility as an Enabler for a Fast and Lean Product Development to Optimize the Return of Engineering with the Example of Lithium-ion Battery. Procedia CIRP vol. 50, pp. 166–172.

Kampker, A., Gerdes, J. and Schuh, G., 2017. Think Big, Start Small: Streetscooter die e-mobile Erfolgsstory: Innovationsprozesse radikal effizienter. Berlin, Heidelberg: Springer.

Kestel, R., 1995. Variantenvielfalt und Logistiksysteme: Ursachen - Auswirkungen - Lösungen[Online]. Wiesbaden, s.l.: Deutscher Universitätsverlag. Available at: http://dx.doi.org/10.1007/978-3-322-99527-8.

Kirchhof, R., 2003. Ganzheitliches Komplexitätsmanagement: Grundlagen und Methodik des Umgangs mit Komplexität im Unternehmen[Online]. Wiesbaden, s.l.: Deutscher Universitätsverlag. Available at: http://dx.doi.org/10.1007/978-3-663-10129-1.

Klug, F., 2010. Logistikmanagement in der Automobilindustrie: Grundlagen der Logistik im Automobilbau. Berlin: Springer.

Krumm, S., Schopf, K. D. and Rennekamp, M., 2014. Komplexitätsmanagement in der Automobilindustrie – optimaler Fit von Vielfalt am Markt, Produktstruktur, Wertstrom und Ressourcen. In: Ebel, B. and Hofer, M. B., eds. Automotive ManagementStrategie und Marketing in der Automobilwirtschaft. 2nd edn. Berlin: Springer Gabler, pp. 189–205.

Lechner, A., 2011. Modellbasierter Ansatz zur Bewertung vielfaltsinduzierter Logistikkomplexität in der variantenreichen Serienfertigung der Automobilindustrie. Thesis (PhD). TU Dortmund University.

Lechner, A., Klingebiel, K. and Wagenitz, A., 2011. Evaluation of product variant-driven complexity costs and performance impacts in the automotive logistics with variety-driven activity-based costing.

International MultiConference of Engineers and Computer Scientists, pp. 1088–1096, March 16 - 18. Hong Kong.

MacDuffie, J. P., Sethuraman, K. and Fisher, M. L., 1996. Product Variety and Manufacturing Performance: Evidence from the International Automotive Assembly Plant Study. Management Science vol. 42, pp. 350–369.

Maguire, S., Allen, P. and McKelvey, B., 2011. Complexity and Management: Introducing the SAGE Handbook. In: S. Maguire, P. Allen and B. McKelvey, eds. The SAGE Handbook of Complexity and Management. London, pp. 1–26.

Marti, M., 2007. Complexity Management: Optimizing Product Architecture of Industrial Products: Springer.

Meissner, S., 2009. Logistische Stabilität in der automobilen Variantenfließfertigung. Thesis (PhD). Technical University of Munich.

Meyer, C. M., 2007. Integration des Komplexitätsmanagements in den strategischen Führungsprozess der Logistik. Bern: Haupt.

Meyr, H., 2004. Supply chain planning in the German automotive industry. OR Spectrum vol. 26, pp. 447–470.

Morieux, Y., 2011. Smart rules: Six ways to get people to solve problems without you. In: Harvard Business Review, pp. 78–86.

Moynihan, T., 2014. Apple's New Car System Turns Your Dashboard Into an iPhone Accessory[Online]. Wired. Available at: https://www.wired.com/2014/03/apple-carplay-system/ (Accessed 5 April 2017).

Muchna, C., Brandenburg, H., Fottner, J. and Gutermuth, J., 2018. Grundlagen der Logistik: Begriffe, Strukturen und Prozesse[Online]. Wiesbaden: Springer Gabler. Available at: http://dx.doi.org/10.1007/978-3-658-18593-0.

Nikowitz, M., ed., 2016. Advanced Hybrid and Electric Vehicles: System Optimization and Vehicle Integration[Online]: Springer. Available at: http://dx.doi.org/10.1007/978-3-319-26305-2.

Nutt, P. C. and Wilson, D. C., 2010. Crucial Trends and Issues in Strategic Decision Making. Handbook of Decision Making.

Paterson, M. S., ed., 1992. Boolean function complexity. Cambridge: Cambridge University Press.

Pawlikowski, K., Fruhner, D., Klingebiel, K., Toth, M. and Wagenitz, A., 2016. Benefits of an Integrated Hierarchical Data Structure for Automotive Demand and Capacity Management. The Eleventh International Multi-Conference on Computing in the Global Information Technology, pp. 20–25. Barcelona, Spain.

Pawlikowski, K., Toth, M., Fruhner, D. and Klingebiel, K., 2018. How electrified car concepts effect automotive logistics. Proceedings of the 25th International Annual EurOMA Conference, June 24-26. Budapest, Hungary.

Pieper, M. and Ernst, C.-S., o.J. Technology, Value Added and Supply Chains of Electric Vehicles[Online]. Available at: http://enevate.eu/4c21c80c-c122-c50a-c386-693b23e00889 (Accessed 27 March 2018).

Pil, F. K. and Holweg, M., 2004. Linking Product Variety to Order-Fulfillment Strategies. Interfaces vol. 34, pp. 394–403.

Rosenberg, O., 2002. Kostensenkung durch Komplexitätsmanagement. In: Kostenmanagement. Wertsteigerung durch systematische Kostensteuerung., pp. 225–246.

Sargut, G. and McGrath, R., 2011. Learning to Live with Complexity. In: Harvard Business Review, pp. 68–76.

Scavarda, L. F., Reichhart, A., Hamacher, S. and Holweg, M., 2010. Managing product variety in emerging markets. International Journal of Operations & Production Management vol. 30, pp. 205–224.

Schaffer, J., 2010. Entwicklung und Optimierung eines treiberbasierten Modells zur Bewertung varianteninduzierter Komplexitätskosten in industriellen Produktionsprozessen. Thesis (PhD). Leuphana University of Lüneburg.

Scholz-Reiter, B., Philipp, T., Beer, C. d., Windt, K. and Freitag, M., 2006. Einfluss der strukturellen Komplexität auf den Einsatz von selbststeuern-den logistischen Prozessen. In: Pfohl, H.-C., ed. Wissenschaft und Praxis im DialogSteuerung von Logistiksystemen - auf dem Weg zur Selbststeuerung ; [3. Wissenschaftssymposium Logistik in Dortmund. Hamburg: Dt. Verkehrs-Verl., pp. 11–25.

Schuberthan, J. and Potrafke, S., 2007. Die Anforderungen des Kunden… In: Gehr, F. and Hellingrath, B., eds. Logistik in der Automobilindustrie: Innovatives Supply Chain Management für wettbewerbsfähige Zulieferstrukturen. Berlin Heidelberg: Springer, pp. 8–18.

Schuh, G., 2005. Produktkomplexität managen: Strategien - Methoden - Tools: Carl Hanser Fachbuchverlag.

Schuh, G. and Schwenk, U., 2001. Produktkomplexität managen: Strategien - Methoden - Tools. München, Wien: Hanser.

Stäblein, T., 2008. Integrierte Planung des Materialbedarfs bei kundenauftragsorientierter Fertigung von komplexen und variantenreichen Serienprodukten. Aachen: Shaker.

DEMAND FORECASTING IN AN AUTOMOTIVE COMPANY: AN ARTIFICIAL NEURAL NETWORK APPROACH

Letizia Tebaldi[(a)], Sara Pindari[(b)], Eleonora Bottani[(c)]

[(a), (b), (c)] Department of Engineering and Architecture, University of Parma, Viale delle Scienze 181/A, 43124 Parma (Italy)

[(a)] letizia.tebaldi@unipr.it, [(b)] sara.pindari@studenti.unipr.it, [(c)] eleonora.bottani@unipr.it

ABSTRACT

This work proposes the development of two Artificial Neural Network (ANN) models for demand forecasting in the automotive industry. The networks are involved for predicting the demand of eighteen car components for a company based in the North of Italy. Statistical Package for Social Sciences (SPSS) was used as software for developing the ANNs, by setting the automatic architecture selection. The structure of the two ANN models is similar; they only differ for the partitioning of the historical data provided by the company itself respectively into training, testing and the optional holdout phases: in the first, which is the one returning the best result, data are simply assigned according to a pre-fixed percentage, while in the second a partitioning variable is introduced.

Keywords: Artificial Neural Network (ANN); demand forecasting; case study; automotive industry; SPSS.

1. INTRODUCTION

Whether the whole production will be employed, the out of stock (OOS) followed by loss of sales or a surplus will occur and many others, are among the main question marks affecting companies in almost any industry field. If the demand forecasting was an exact science, there would probably be no failures, problems, waste or dissatisfactions; but in a stochastic world the variability of the demand is an anchor which necessarily has to be taken into account and this creates a challenge because firms have to make operational decisions before this uncertainty is resolved (Jiang et al., 2016).
The demand forecasting is defined by Fradinata et al. (2014) as the process of using sales history of a determined product and projecting the demand in the future in order to schedule and support purchases, production, resources allocation, level of stocks, sales, workforce and many other items; accordingly, its estimated value is vitally important in business context. Moreover, the customer satisfaction is a direct consequence of an accurate demand forecasting process. Among the main benefits achievable through an accurate forecasting, surely on top fewer missed sales, followed by higher customer-service levels, lower working capital, more efficient manufacturing, less waste and spoilage, reduced effort and raw material/finished goods inventory (Myerholtz and Cafferey, 2014; Croxton et al., 2002).
Several tools can be involved in predicting the demand of a determined product or component, both quantitative (e.g. the renowned autoregressive and integrated moving average, better known as ARIMA, or the exponential smoothing) and qualitative (e.g. Delphi method or life-cycle analogy).
As complexity and dimensions of supply chains are always undergoing changes and development, traditional forecasting techniques such as the aforementioned methods are not always suitable to deal with difficulty and especially nonlinear nature of the problem (Laosiritaworn, 2011). According to that, more reliable and accurate tools were required and among these the Artificial Neural Networks (ANNs) have been widely used in the context of demand forecasting, since the Sixties.
ANNs are machine learning algorithms (Yucesan et al., 2017) aiming at solving classification, optimization, pattern recognition and forecasting problems (Hamzaçebi et al., 2017) by taking inspiration from the natural behaviour of neurons in the human brain. Their main peculiarity is that, just like neurons do, these networks learn from experience and examples, and are able to capture subtle functional relationships among input and output data even if these relationships are unknown or hard to describe (Zhang et al., 1998). To this end, they are firstly trained by providing a sample of input and related output so that they can identify the function connecting these data; secondly, the testing phase inspects whether the output obtained from a set of initial input by applying the model identified in the training phase is in line with the real output; thirdly the optional holdout step repeats the process for a new set of data for verification. The accuracy of findings is measured through the deviation between the output of the ANN and the real output value (i.e. the error).
Specifically, within the context of demand forecasting, input data for the ANN are those factors impacting and affecting the demand, which corresponds to the output.
According to what has been said, the aim of this paper is to present two ANN models developed to predict the demand of car components for a company (for the sake

of privacy the anonymity is respected, and in the following we will generally refer to Company A) operating in the automotive sector, based in the North of Italy. In particular, it produces racing cars by assembling components which can be either supplied or made in-house; typically, cars are directly sold to teams participating to worldwide championships, while for components the market is wider since also other companies or privates are reached.

The two models own the same structure, while they differ for the historical data division respectively into training, testing and the optional holdout phases.

Statistical Package for Social Sciences (SPSS) release 25 for Windows (IBM) was chosen as software for developing the ANNs and simulating the trend in demands.

For an exhaustive and current review of the relevant literature on the use of ANNs for demand forecasting problems see Bottani et al. (2019), demonstrating the versatility and the flexibility of the tool as it is proposed in different contexts. As far as the automotive sector, the only works in line with our specific topic are by Gonazález Vargas and Cortés (2017) and by Shahrabi et al., (2009), in both of which different forecasting methods, including the ANNs, are implemented and compared in predicting the demand of car spare-parts, respectively in Mexico and Iran. Indeed, this very limited number of studies is the reason why the choice fell on this specific industry field; moreover, the automobile supply chain is complicated because of the thousands of components and parts which makes it involving numerous suppliers, distributors and other organizations (Jiantong et al., 2016), and being able to speculate and prevent their demand is a key point for companies' success.

The remainder of the paper is as follows: in section 2 the methodology is described; section 3 provides a general background on the structure of the ANNs; section 4 presents the two models developed, followed by section 5 where results are proposed. Implications and conclusions are finally provided in section 6.

2. METHODOLOGY

The framework proposed by Bottani et al. (2019) has been taken as guideline for the construction of the two networks, properly modified when necessary. The procedure is below depicted (Figure 1) and summarized.

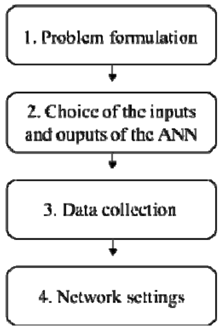

Figure 1 - Adapted framework by Bottani et al., (2019) for the development of an ANN.

1. *Problem formulation*: the context in question has been analyzed together with the management of Company A, as well as the problem to be faced and the inputs of the ANN which influence the requested output results;
2. *Choice of the inputs and outputs of the ANN:* once the main inputs were identified in step 1, the relevant ones were further selected;
3. *Data collection:* three-monthly data from 2013 to 2018 were made available directly from Company A, thanks to meetings and interviews, considering as fiscal year the period 1st July-30th June;
4. *Network setting:* definition of the structure of the network.

In the original framework by Bottani et al., the fourth step was further divided into three sub-steps, namely the identification of the network training algorithm, the transfer function and the termination criterion, and followed by two additional steps, namely the choice of the hidden neurons and layers, and the parameter settings with the final choice of the best ANN configuration: in this case these sub-steps are redundant since an automatic architecture selection by SPSS was set, which already has default settings.

Once the networks were defined, the ANNs were trained with historical data and then tested.

3. BACKGROUND ON THE ARTIFICIAL NEURAL NETWORK STRUCTURE

A neural network has at least two physical components: the processing elements (i.e. neurons) and the connections between them (i.e. links, having a weight parameter associated) (Zhang and Gupta, 2000). Each neuron receives stimuli from the neighboring neurons connected to it, and after processing the information produces outputs. Many configurations are possible; in the following we will refer to the most popular type of neural network, namely the Multilayer Perceptron (MLP), consisting of at least three layers of nodes: an input layer, a hidden layer and an output layer. Input neurons are those receiving stimuli from outside the network; hidden neurons, conversely, capture signals from other neurons, and analogously transmit a signal to

other neurons; these last are the output neurons. This structure is known as *feedforward* architecture, because the information flow starts from input neurons and flows forward to the output layers without any loop.
Each received input is multiplied by the corresponding weight parameter and results are added in order to produce a weighted sum, which passes through an activation function to produce the final output of the neuron.
Figure 2 below outlines the general MLP structure.

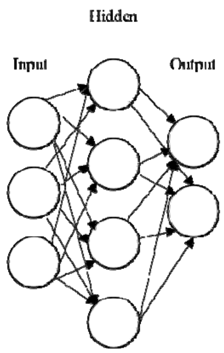

Figure 2 – Structure of a Multilayer Perceptron.

Specifically, the key elements to be defined for the development of an ANN are the following: dependent (i.e. output neurons) and independent (i.e. input neurons) variables; number of hidden layers and their relative activation function linking the weighted sums of units in a layer to the values of units in the succeeding layer, and the number of units in each hidden layer; the output layer with its activation function and the eventual method of rescaling the dependent variables; the measure of the error; the type of training and the optimization algorithm used to estimate the weights, together with the stopping rule determining whether the training should stop or not. Last but not least, the partition dataset has to be set, necessary to divide the available data respectively into training, testing and holdout samples.

4. DEVELOPMENT OF THE ARTIFICIAL NEURAL NETWORKS

4.1. Input and output selection

The aim of the tool is to predict the demand of the following seven car components whose impact in terms of revenue is relevant for Company A: nose, front spoiler, machine structure, arms, brake discs, upright and bearings. Note that some components can be “right” or “left”, “upper” or “lower”; accordingly, the final number of components analyzed is eighteen.
Starting from these desired outputs, the key factors affecting the demands were identified as well; as a result, the following seven elements have been considered as inputs:

1. *Component category*, as many items can be grouped into a main class;
2. *Championship* to which sales data are related, since different championships correspond to different climatic conditions and cultural factors, which may affect accidents or spare parts demand;
3. *Number of machines* competing in each championship, which can also change from year to year;
4. *Number of races* of each championship, which can vary as well from year to year;
5. *Ageing,* simply attributable as YES or NO depending on the component;
6. *Car life cycle,* namely first year of life, interim period and last year of life;
7. *Trimester*, namely July-September, October-December, January-March, April-June. Note that this input was considered only in the first model, as in the second one the partitioning variable imposes a data partitioning in accordance with the reference year, regardless of the trimester.

4.2 Architecture of the models

The automatic architecture selection by SPSS was chosen, procedure which automatically builds the best ANN configuration and includes default settings.
The demand value of the eighteen items corresponds to the dependent variable, while the seven previously mentioned inputs to the independent variables.
In this case, the automatic selection allows only one hidden layer by default, activated by the hyperbolic tangent. Even as far as the activation function for the output layer (containing the dependent variable) the automatic selection led to the only choice of the identity function. The rescaling of scale dependent variables was set as standardized; the error as the sum-of-squares.
Once these key points were fixed, it is the turn of the training. The online training has been selected, mostly used when big data are available; according to SPSS, when this type of training is involved, the optimization algorithm through which the synaptic weight are identified necessarily is the gradient descendent.
The training stops when, after a specified number of steps, there is no decrease in error.
The difference between the two models comes from the breakdown of data for the training-testing-holdout phases. Indeed, SPSS offers the opportunity to choose from two ways, both investigated: to randomly assign percentages (Model 1) or to use a partitioning variable (Model 2). The holdout step is considered only in the first model as the partitioning variable, by attributing value 0 or 1, only divides data in two main groups, namely training and testing.
Table 1 below summarizes the main characteristics of the models.

Table 1: Settings of the models.

DEPENDENT VARIABLES		Demand of the 18 car components
INDEPENDENT VARIABLES		7 input factors
HIDDEN LAYERS	Hidden Layers Number	1
	Units in the Hidden Layers	9
	Activation Function	Hyperbolic Tangent
OUTPUT LAYERS	Number of Units	1
	Rescaling of Scale Dependent Variables	Standardized
	Activation Function	Identity
	Error Function	Sum-of-Squares
TRAINING	Type	Online
	Activation Function	Gradient Descent
PARTITIO-NING	MODEL 1	Pre-fixed Percentages
	MODEL 2	Partitioning Variable

Table 2, instead, shows the exact subdivision of historical data into the three phases.
Specifically, the partitioning variable used in model 2 imposes that data until 2017 are involved in the training phase, while from 2018 onwards for tests. Note that no outlier or missed values were found, probably due to the niche market in which Company A operates.

Table 2: Historical data subdivision into training, testing and holdout phases; in brackets the percentage.

	MODEL 1	MODEL 2
TRAINING PHASE	2.341 (80.6%)	2.660 (91.6%)
TESTING PHASE	282 (9.7%)	245 (8.4%)
HOLDOUT PHASE	282 (9.7%)	-
TOTAL	2.905 (100%)	2.905 (100%)

5. RESULTS

Table 3 below shows the relative errors resulting during first the training phase, then the testing and holdout respectively for Model 1 and Model 2.

Table 3: Relative errors resulting from the two models of ANN.

	MODEL 1	MODEL 2
	RELATIVE ERROR (%)	
TRAINING PHASE	53.7	49.7
TESTING PHASE	35.9	51.5
HOLDOUT PHASE	41.1	-

As can be seen, two opposite situations occur: in Model 1, the testing phase successfully returns a relative error lower than the training phase, while in Model 2 after the training the error increases a bit. According to that, we can argue that Model 1, namely the one in which data were partitioned according to pre-fixed percentages, is more reliable and accurate.

Furthermore, by deepening results, an analysis on the impact of each independent variable was carried out; outcomes are below depicted in percentages (Table 4 for Model 1 and Table 5 for Model 2).

Note that the normalized value is obtained by dividing the impact value itself of each item for the maximum value identified (e.g. for Model 1, the impact of the component category, namely 25.3).

Table 4: Percentages of inputs' effects on outputs for Model 1.

	MODEL 1	
	IMPACT	NORMALIZED IMPACT
Component Category	25.3	100
Championship	14.9	58.9
Number of Machines	6.6	26.3
Number of Races	13.0	51.6
Ageing	23.5	92.7
Car Life Cycle	3.2	12.5
Trimester	13.5	53.5

Table 5: Percentages of inputs' effects on outputs for Model 2.

	MODEL 2	
	IMPACT	NORMALIZED IMPACT
Component Category	28.9	100
Championship	21.0	72.6
Number of Machines	4.9	16.8
Number of Races	26.5	91.9
Ageing	14.0	48.4
Car Life Cycle	4.7	16.6

By modifying the allocation of historical data, the relative importance of the different impact changes.

In both cases, the component category is the item affecting the most the output, followed by, respectively, the ageing for Model 1, and the number of races for Model 2 which, conversely, is not relevant in the first model. The life cycle, instead, turns out to have a low effect on both results.

6. CONCLUSIONS

This paper aimed at presenting two models of artificial neural networks developed in Statistical Package for Social Sciences for the demand forecasting of car components for a company operating in the automotive sector in the North of Italy. The automatic architecture selection was set for both models, including default settings of parameters; accordingly, the two models are similar, differing only for the data allocation into training, testing and holdout phases.

Eighteen car components were analyzed.

Overall, the models were proved to be successful, and can be an effective support for management in their operational decisions and production planning.

Specifically, Model 1, retuning a significant reduction of the relative error during the testing phase, turned out to be the best configuration among the two.

The study contributes in deepening the applications of ANNs in the field of demand forecasting, demonstrating once again the great potential of the tool as a promising alternative approach to traditional linear methods.

For sure, further insights can be considered. For instance, other tools can be tested with the same dataset in order to compare results; more ANNs models can be developed, e.g. by combining the component category, which turned out to be the most impactful input, or by taking into account a different timespan (e.g. annual data). Furthermore, considering applying also genetic programming techniques and benchmark the two approaches would be interesting.

Models can also be implemented in fields other than the automotive, by taking into account different products or components.

REFERENCES

Bottani E., Centobelli P., Gallo M., Kaviani M. A., Jain V., Murino T., 2019. Modelling wholesale distribution operations: an artificial intelligence framework. Industrial Management and Data Systems, 119 (4), 698-718.

Croxton K. L., Lambert D. M., García-Dastugue S. J., Rogers D. S., 2002. The demand management process. The International Journal of Logistics Management, 13 (2), 51-66.

Fradinata E., Suthummanon S., Sirivongpaisal N., Suntiamorntut W., 2014. ANN, ARIMA and MA timeseries model for forecasting in cement manufacturing industry. International Conference of Advanced Informatics: Concept, Theory and Applications (ICAICTA), 39-44. September 20-22, Yogyakarta (Indonesia).

González Vergas C.A., Cortés M.E., 2017. Automobile spare-parts forecasting: A comparative study of time series methods. International Journal of Automotive and Mechanical Engineering, 14 (1), 3898-3912.

Hamzaçebi C., Avni Es H., Çakmak R., 2017. Forecasting of Turkey's monthly electricity demand by seasonal artificial neural network. Neural Computing and Applications, 1-15.

Jiang B., Tian L., Xu Y., Zhang F., 2016. To share or not to share: Demand forecast sharing in a distribution channel. Marketing Science, 35 (5), 800-809.

Jiantong Z., Zhuoqi G., Xiaodong C., 2016. Evaluation of automotive supply chain risks: An empirical research. 13th International Conference on Service Systems and Service Management (ICSSSM). June 24-26, Kunming (China).

Laosiritaworn W.S., 2011. Supply chain forecasting model using computational intelligence techniques. Chiang Mai University Journal of Natural Sciences, 10 (1), 19-28.

Myerholtz B., Caffrey H., 2014. Demand Forecasting – The key to better supply-chain performance. Available from: image-src.bcg.com/Images/Demand_Forecasting_Oct_2014_tcm9-81416.pdf

Shahrabi J., Mousavi S.S., Heydar M., 2009. Supply chain demand forecasting: a comparison of machine learning techniques and traditional methods. Journal of Applied Sciences, 9 (3), 521-527.

Yucesan M., Gul M., Celik E., 2017. Application of Artificial Neural Networks using Bayesian training rule in sales forecasting for furniture industry. Drvna Industrija, 68 (3), 219-228.

Zhang G., Patuwo B.E., Hu M.Y., 1998. Forecasting with artificial neural networks: The state of art. International Journal of Forecasting, 14, 35-62.

Zhang Q.J., Gupta K.C., 2000. Neural Network Structure. In: Artech House, eds. Neural Network for RF and Microwave Design. Norwood, MA, USA, 61-103.

AUTHORS' BIOGRAPHY

Letizia TEBALDI is a first year Ph.D. student in Industrial Engineering at the Department of Engineering and Architecture of the University of Parma. She graduated cum laude in March 2018 in Management Engineering, presenting a dissertation on a systematic literature review on sustainable supply chain and innovation. Her research interests are mainly on logistics and supply chain management; sustainable supply chain; analysis and optimization of supply chain; industry4.0 for operators' safety.

Sara PINDARI graduated in Management Engineering in March 2019 at the University of Parma. She is actually working in Company A in the Sales Operation area.

Eleonora BOTTANI is Associate professor in Mechanical Industrial Plants at the Department of Engineering and Architecture of the University of Parma. She graduated (with distinction) in Industrial Engineering and Management in 2002, and got her Ph.D. in Industrial Engineering in 2006, both at the University of Parma. Her research activities concern logistics and supply chain management issues. She is author (or co-author) of more than 170 scientific papers, referee for more than 60 international journals, editorial board member of five scientific journals, Associate Editor for one of those journals, and editor-in-chief of a scientific journal.

INVESTIGATING THE INFLUENCE OF FIXED ASSIGNMENT OF PLATFORM TRACKS TO TRAINS ON THE RESULTING STATION CAPACITY USING SIMULATION

Michael Bažant[(a)], Josef Bulíček[(b)], Petr Veselý[(c)]

[(a),(c)] Faculty of Electrical Engineering and Informatics, University of Pardubice
[(b)] Faculty of Transport Engineering, University of Pardubice

[(a)]Michael.Bazant@upce.cz, [(b)]Josef.Bulicek@upce.cz, [(c)]Petr.Vesely@upce.cz

ABSTRACT
The paper focuses on the simulation assessment of the operation of a railway station with mixed passenger and freight traffic whereas various options how to assign tracks for considered trains are presented with assessed results. As a base variant of tracks assignments is considered variable tracks assignment that is applied nowadays in the Czech Republic. There are also presented variant with mixed approach – subset of trains is organized with variable tracks assignments, but another subset of trains is organized with fixed assignments and results of various scenarios are presented.

Keywords: capacity, simulation, railway station, platform track

1. INTRODUCTION

Railway transport infrastructure is usually very expensive. Spatial demands of this infrastructure are also high. Demand after as most effective utilization of this infrastructure is based on these reasons. The result is that the extent of infrastructure is sometimes minimized, but regarding operation of all demanded trains.
Transport operation must be effectively scheduled as well to meet these presumptions as well. The issue is if this operation (time schedule and track occupancy plan) will be stable in the case of stochastic conditions, because various train delays and irregularities can occur in practice. Possible lack of additional infrastructure can amplify delays or other operational problems, because this infrastructure is not possible to be applied in the case of irregularities in operation. For example, a train can increase delay by waiting in a station (platform) track, because other empty track can't be reached due to missing of some of switches (replaced due to reduction of infrastructure costs) etc.
Microscopic simulation belongs to usually applied tools for modelling of such issues, including assessment of railway infrastructure capacity. These models are classified as microscopic, because each train with a set of train features is modelled on this resolution level. Principle is that the model simulates train traffic operation on defined part of infrastructure (usually a few stations with line segments interconnecting them). Given time schedule is repeated within individual replication of simulation model with different (stochastic) inputs. For example, input delays on arrivals of individual trains into modelled area can be stochastically changed. Each replication is assessed by a set of output features like increment (change) of delay by individual trains or ratio of time when individual infrastructure elements (e.g. station or line tracks, switch areas etc.) are occupied etc. Collective assessment of a set of replications can be made to make the results more general.
Simulation models are usually applied for assessment of given infrastructure and of given timetables. Operational features can be assessed in this way, but in strictly given situation.
Hypothesis of this research can be stated in following way. It is possible to apply simulation (to get suitable results) for a general case where different configurations of infrastructure will be modelled by application of a different set of operational constraints. The aim is to assess given particular situation, but to assess minimization of infrastructure extent regarding extent of operation as a general feature.
The presumption is that each train will have strictly given position in planned time schedule of operation and adequate extent infrastructure will be reserved for this train. On the other hand, resting (remaining, ineffectively applied) infrastructure will be totally replaced. This situation can be modelled as a time schedule with strict allocation of tracks to trains (or vice versa). Time schedule assessed by simulation must be conflict-less in the case of fully regular operation (according to planned time schedule). The issue is, what can happen in the case of stochastic operation (with train delays) as it is objectively common in practice. Strict allocation of trains to tracks must be ensured any time, including the situation when a train will wait on given track although other tracks can be possibly at disposal as unoccupied. This represents the situation when infrastructure extend will be reduced to minimum according to time schedule (plan). Requirement on conflict-less operation by regular operation is applied. On the other hand, if serious

problem with stability of time schedule will occur, change of track allocation can represent a fact that the station will be equipped by additional infrastructure with no need to change modelled infrastructure. Assessing on the same level is ensured in this way.
Applied stochastic microscopic simulation represents an ideal tool for evaluating this problem because the characteristics of such operation are difficult to detect by the analytical methodologies used (e.g. UIC 406).
This research is part of the PosiTrans project that is focused on the research of aspects affecting the capacity of railway transport infrastructure using simulation and transport modelling tools.

2. LITERATURE OVERVIEW

A considerable number of professional publications are devoted to the planning of train transport and the creation of models for such planning. Most of them, however, devote themselves to the issue of train transport planning very generally and only a few specialize in selected aspects of the issue. For example (Buchmueller1, Weidmann1 and Nash2 2018; Longo and Medeossi 2012), they focus in detail on the determination of sojourn times at the railway station. Although the determination of suitable sojourn times is closely related to the comfort of passengers during transfers and the choice of platform tracks, the issue of assigning platform tracks is not discussed in detail. Typical criteria applied by assigning of tracks to trains are maximizing the utilization rate or increasing efficiency of railway infrastructure.
As stated in (Yuan and Hansen 2007), there must be a compromise when planning a regular (especially passenger) train service between efficient use of infrastructure and improving the reliability and accuracy of the traffic. These objectives can be in a conflict due to fact that railway operation is usually a stochastic process. Systems with high ratio of capacity utilization have limited space (capacity reserves) for solution of irregular situation. Using a new analytical stochastic model, the authors attempt to address the emergence of so-called delays that arise in real rail traffic mainly due to irregularities and differences between planned (presupposed by time schedule) and real “every-day” operation (influenced by stochastic influences). One of the factors influencing the occurrence of subsequent delays and their size is also waiting for the release of the required platform track. It follows from the logic of the case that any tightening of operational conditions in the field of allocation of platform tracks to trains (e.g. strict plan of designated platform tracks without the possibility of any alternative) will contribute to increasing subsequent delays even at the slightest irregularities. It will also mean reducing the robustness of the timetable, i.e. reducing the ability to quickly and effectively absorb the resulting delays. This effect is based on the fact that possible alternative solution cannot be applied (e.g. using of an alternative station track) and the delay can be increased by waiting on tightly assigned infrastructure (track).
Some publications deal with the planning of railway traffic or the creation of models for simulating train traffic and its subsequent evaluation. They always consider certain simplifications which very often concern the issue of the allocation of platform tracks. There is often considered a situation where passenger trains can use all available platform tracks (Jensen, Landex, Nielsen, Kroon and Schmidt, 2017).
A number of publications (e.g. (Yuan and Hansen 2007; Andersson, Peterson and Krasemann 2013)) state that the requirements for the design of platform tracks have a negative impact on the robustness of the planned train schedules and the waiting for the release of the required platform tracks is one of the critical points for increasing delay. It is also the so-called "bottleneck" in the subsequent effort to reduce this delay.
The topic of the allocation of platform tracks is published in (Janosikova, Kavicka, Bažant 2012) on a detail level. The publication deals not only with the subsequent delays due to waiting for the release of the planned platform track but also discusses the impact of any change of platform track on passengers’ comfort. The objective of this study is is the design of a mathematical model for a support of dispatcher decision-making in operational planning. With the support of this tool a dispatcher is able to better decide how to keep the train waiting for the occupied platform track - whether to change the plan of the desired platform track and thus reduce (minimize or not create) the subsequent delay. Or whether the train will continue to wait, for example, to keep comfort from passengers on transfers.

The research published by this paper is based on standard principles of microscopic simulation of railway operation. Such intersections with state-of-art level of research can be found in this field. The novelty is in the fact that the research tries to apply microscopic simulation for examination of given effect (the way of track allocation) despite simulation of given infrastructure as specific part of transport infrastructure. Results of this assessment will be applied in generalized methodology for assessment of capacity. Impacts will be evaluated parallel in two points of view. Time schedule stability is the first one, impacts on operation of connected line segments the second one. Research uncertainty is related to the fact how the results can be influenced by given local conditions. This can be discussed in the paper. On the other hand, transferability of results is invited, because there is an effort to apply simulation in general case and to incorporate results into general methodology for capacity assessment of railway infrastructure. All these aspects will be researched.

3. ADVANTEAGES OF FIXED PLATFORM TRACKS

The main presumptions leading to this research have been stated in the introducing chapter 1. On the other hand, these reasons can be more specified in more detail and some additional reason can be added.

Fixed assignment of platform tracks to trains is a theoretical variant in practice. However, there may be some of the following reasons that may result in at least partial application of such traffic.

3.1. Potential reduction of tracks

One of the most illustrative case is reduction of number of tracks. Each track represents investments for its construction as well as relative serious operation cost (e.g. for maintenance). These effects are characterized in introduction part of the paper.

3.2. Potential reduction of infrastructure elements

Effort to decrease infrastructure cost can be related to some of individual infrastructure elements as well. For example, some of switches (applied by trains minimally) can be replaced. This can be supported by remote way of dispatching. It can be presupposed that a train dispatcher having full information about traffic situation (in “line-wide” point of view) can organize the traffic in such way so this infrastructure elements will not be needed. Replacement of these elements can be compensated in this way.
Limited space can be the second reason for application of this measure in practice. Sometimes not all line tracks are accessible from or to all station tracks due to spatial reasons. For example, construction of some interconnecting track can be impossible in some directions due to spatial reasons.

3.3. Potential reduction of platforms

The third effect related to reduction of infrastructure is reduction of platforms although the track can still exist. State-of-art requirements on platforms and approaching routes to them are high due to reasons of safety and passengers’ comfort. So, establishment and operation of platforms under current conditions represents cost as well. There is also the issue of maintenance, ensuring the equipment is serviceable for people with reduced mobility (lifts, etc.). This can lead to an effort to minimize the number of platforms.

3.4. Facilitating the orientation of passengers

Fixed assignment of platform tracks to passenger trains in railway stations helps passengers to orientate whereas information about departure or arrival tracks (platforms) can be passed on to passengers even in advance. The information may appear in a static information documents, such as tickets or message boards in a station. Passengers can find their pathway at a station in advance, especially passengers can have this information before they arrive at the interchange station and the time for transfer can be reduced by facilitating the orientation of passengers.
Fixed assignments are also common in public bus terminals and passengers are used to it.

3.5. Shortening of transfer times

By placing trains on selected transport tracks, the need to overcome distances and height differences in the station can be significantly reduced, thereby time savings and reducing travel times in a network viewpoint can be reached.

3.6. Shortening of train sojourn times

It is possible to better direct passengers to specific boarding sectors of platform (to a coach with reserved seat) in advance. Possible delays occurred by boarding a train can be avoided and total sojourn time shortened in this way.

4. DISADVANTAGES OF FIXED PLATFORM TRACKS

There has been characterized advantages and motivations of timetable with fixed platform tracks in the chapter 3. It is necessary to mention disadvantages and operational problems occurred by such way of operation for complex solution of this issue.

4.1. Occupancy of planned traffic tracks

The basic drawback is a possible occurrence of a delay by the fact that the planned track will not be available at the given time, another track will not be available, and the train will have to wait at a home signal.

4.2. Transferred delays

For example, due to the need of wait by a train at a home signal for release of a platform track at a station, other trains may be delayed, including freight trains. For freight trains, due to the operating situation (occupation of passenger trains), it may be necessary to use a different transport track and thus slow down these trains (use a slow path at the station, unplanned stops). Delays can also be transmitted to surrounding track sections, especially single-track lines.

4.3. Influencing the connecting trains

Due to the possibility of passenger trains waiting for releasing the planned platform track, the problem can be escalated in case of waiting connecting trains on which the delay is transmitted. Alternatively, the connection link may even be cancelled.

5. MICROSCOPIC STOCHASTIC SIMULATION

To verify this approach, the microscopic simulation model of a railway station is used using the Villon simulation tool, where the generation of train delays on input to the simulation model is used to verify the possibility of using static determination of platform tracks, and the consequences of this approach are examined using multiple replications.
In the simulation model, all the essential details concerning the trains are applied, e.g. train dynamics, possibility to increase power of engine in case of train delay, transfer links between passenger trains, realistic behaviour of interlocking systems, etc.

5.1. Model parametrization

Following parameters were used in simulation experiments:

- *Number of replications* – for every scenario that is considered in simulation is performed 100 replications.
- *Simulation runs calculate with randomly delayed arriving trains*. The utilized train delays match to demands, which are involved in the forthcoming directive of SŽDC: Determining the capacity of railway systems.
- *Value of delay* is generated for each arriving train so that to each train category is applied probability of a delay occurrence (uniform distribution) and the delay value which is obtained from the generator corresponding to the exponential probability distribution.
- *Warming up period* of each replication (applied before collecting data items for relevant statistical analysis) takes *2 hours* of simulation time.

5.2. Evaluation of simulation experiment

The traffic optimization criterion for evaluation is increments of train delays in the modelled area (station). This is the difference between the train exit delay value from the model and the simulated (generated) delay value at the input to the modelled area.

In principle, this value is determined for every single train in each replication. In order to evaluate the simulation, the values of the delay increments thus obtained are processed as follows:

- Average value for each train for all replications.
- Maximum value that is reached for each train in all replicates.
- Average value for all trains in a given replication.
- Maximum value in a given replication.
- Average and maximum values for selected subsets of trains (typically passenger and freight trains, or trains on selected trains, etc.).

6. CASE STUDY

As a case study, a railway station located on a double-tracked line was chosen. One single tracked line is branching at this station as well. The station is an interchange node between passenger trains operated on double-tracked main line and on single-tracked line.

The network taken into a simulation model is extended by neighbouring line segments and by simplified models of 3 neighbouring railway stations. Traffic can be considered in complex point of view also with regard to interface between station and line transport technology.

The core station consists of 8 station tracks, 6 of them are equipped with island platforms with an elevated passenger passageway. It is a common example of railway station in the Czech Republic.

The morning peak hours' time was chosen for testing, when there is the greatest difficulty in organizing the operation of the railway station, especially in cases of passenger train delays.

6.1. Extent of Traffic in Simulation

There is a sample of 30 trains considered. The sample includes 8 passenger trains and 22 freight trains. All passenger trains are obligated to use station track with platform edge, because all of them are stopping for boarding and alighting of passengers. All tracks can be occupied by freight trains. Freight trains are also crossing from main double-tracked line to single-tracked line and vice versa.

6.2. Simulation Scenarios

There are 5 simulation scenarios considered within this simulation study. All of them are based on the same timetable, but they are differing by the way of assignment of a station track to a train. The overview is provided by the Table 1.

Table 1: Simulation Scenarios

Scenario	Description
VA	All trains can use any station track (priority lists of tracks are used for every train).
F6	6 passenger trains have fixed tracks due to passengers' comfort by interchange and time savings.
F8	All 8 passenger trains have fixed tracks. Possible reduction of number of platforms is illustrated (3 tracks are used for passenger traffic in spite of 6).
F8 + 3FT	Scenario based on F8, but extended by fixed assignment of 3 freight trains (for illustration of possible infrastructure limits, e.g. length of trains).
FA	All trains have fixed tracks. It is for illustration of 'rigid' timetables applied e.g. in the case of high capacity utilization.

These scenarios are used for examination of influence of changed operational conditions. The advantage is that the same sample of input delays is applied for all the scenarios. It means that the trains are coming with the same input delay into the modelled area (to the neighbouring stations). The results are comparable in this point of view.

6.3. Delay Increments

The punctuality of timetable is one of the core aspects for the quality level of railway operation. Possible lack of railway infrastructure capacity can be identified by extension of travel times – by increments of delays. On the other hand, for assessment of modelled system –

station and line segments in surroundings the value of input delay (delay occurred by drive on different infrastructure in front of assessed station) is not crucial. Increments of delay in assessed (modelled) area are the core factor.

The values of delay increments are measured in following way. The time when the train leaves the model is reduced by scheduled time and the delay on output is calculated. This value is compared to the value of delay on input and the increment of delay is defined.

There can be three results of this calculation:

- delay increment is equal to 0 – system stability is OK,
- delay increment is less than 0 – system stability is asymptotic (infrastructure is capable to reduce delays due to reserves),
- delay increment is more than 0 – system is increasing values of delays; it can possibly be caused by insufficient capacity of the system.

The third case is the most serious for the railway operation and for that reason this situation is highlighted by simulation assessment if occurs.

6.4. Average Delay Increment

The principle result is average delay increment assessed for all trains in all simulation replications. The results for individual simulation scenarios are in the Table 2. All (positive, zero and negative) values of delay increments are considered in this case (Table 2).

Table 2: Average delay increment per one train [s]

Scenario				
VA	F6	F8	F8 + 3FT	FA
20.9	39.9	39.9	40.1	45.0

The values in the Table 2 show that the average value of delay is increasing by increasing number of trains with fixed assignment of tracks to trains. On the other hand, the same value for scenarios of F6 and F8 refers about the fact that there is a relation to local conditions as well.

The lack of possibilities to solve the traffic situation in an operative way can cause extension of delay. For example, this can be an impact of possible reduction of infrastructure (reduction of number of tracks in station etc.).

Median of delay increments is equal to zero in all cases, because 19.5 – 26.0% of trains (according to scenario) are operated on time in the simulation.

6.5. Average Delay Increment of Delayed Trains Only

Average delay increment of delayed trains represents better feature for assessment of impact e.g. on passengers' comfort. In fact, passengers don't register possible reductions of delay, but they are considering the delay of their train. For that reason, average delay increment for delayed trains in assessed as well.

The term of 'delayed train' must be defined in advance. It is a train with the value of delay increment higher than 30 s. Since 30 s is the 'minimal time step' applied by design of railway timetable (in the Czech Republic), results of simulation are evaluated with precision of 1 s. This measure can compensate possible errors and highlight more serious increment of delay (more than 30 s).

The results are mentioned in the Table 3.

Table 3: Average delay increment per delayed train [s]

Scenario				
VA	F6	F8	F8 + 3FT	FA
289.5	339.9	342.4	338.7	345.0

6.6. Maximal Registered Increment of Delay

Sometimes it if effective to recognize what is the situation in the worst case. Maximal registered increments of delays are assessed due to this in the Table 4. On the other hand, there is no significant relation between the scenario and maximal value in spite of the fact that scenarios with fixed track assignments have slightly worse values.

Table 4: Maximal delay increments [s]

Scenario				
VA	F6	F8	F8 + 3FT	FA
2909	3503	3503	3503	3200

7. CONCLUSIONS

The paper introduces some of other effects that influence quality and reliability of railway traffic and railway infrastructure and these finding were assessed with computer simulation approach.

It is important to note that these findings are find out for just one railway station with one timetable and 5 different scenarios how to organize trains on available tracks within railway station.

The testing of fixed tracks for various variants brings quite surprising results mainly in comparison of variant FA to variants with partial fixed tracks and it could be interesting to test these approaches also for other scenarios or railway stations.

On the other hand, result of variant VA provides better results which is not surprise and this finding support current approach in timetable construction in the Czech Republic where VA variant is almost always used.

Therefore, further research in this area will pay attention to above mentioned aspects of reached results.

ACKNOWLEDGMENTS

The work was supported from ERDF/ESF *Cooperation in Applied Research between the University of Pardubice and companies, in the Field of Positioning, Detection and Simulation Technology for Transport Systems - PosiTrans* (CZ.02.1.01/0.0/0.0/17_049/0008394).

REFERENCES

Buchmueller1 S.,Weidmann1 U. & Nash2 A. Development Of A Dwell Time Calculation Model For Timetable Planning. Computers in Railways XI, 2018. Pages 525–534. ISBN 978-1-84564-126-9.

Longo G. & Medeossi G. Enhancing Timetable Planning With Stochastic Dwell Time Modelling. Computers in Railways XIII, 2012. Pages 461–471. ISBN 978-1-84564-616-5.

Jianxin Yuan, Ingo A. Hansen. Optimizing capacity utilization of stations by estimating knock-on train delays. Elsevier, Transportation Research Part B: Methodological, Volume 41, Issue 2. 2007. Pages 202–217. ISSN: 0191-2615.

Lars Wittrup Jensen, Alex Landex, Otto Anker Nielsen, Leo G. Kroon, Marie Schmidt. Strategic assessment of capacity consumption in railway networks: Framework and model. Elsevier, Transportation Research Part C: Emerging Technologies, Volume 74, 2017. Pages 126–149. ISSN: ISSN: 0968-090X.

Emma V. Andersson, Anders Peterson, Johanna Törnquist Krasemann. Quantifying railway timetable robustness in critical points. Elsevier, Journal of Rail Transport Planning & Management, Volume 3, Issue 3. 2013. Pages 95–110. ISSN: 2210-9706.

Janosikova, Ludmila & Kavicka, Antonin & Bažant, Michael. Optimal operation scheduling and platform track assignment in a passenger railway station. Proceedings of the Institution of Mechanical Engineers Part F Journal of Rail and Rapid Transit. 2012, Pages 228(3): 271–284. DOI: 10.1177/0954409712472275.

AUTHORS BIOGRAPHY

Michael Bažant is a lecturer in Computer Programming and Simulation in the Faculty of Electrical Engineering and Informatics at the University of Pardubice. He completed his PhD in Technology and Management in Transport and Telecommunications. His research interests lie in the areas of decision-making in the simulation models of transportation systems.

Josef Bulíček is a lecturer in Transport Modelling, System Analysis and Capacity of Railway Transport in the Faculty of Transport Engineering at the University of Pardubice. His research interests lie in interconnection of different modes of public passenger transport, including application of modelling in this field.

Petr Veselý is a lecturer in Computer Programming and Computer Graphics in the Faculty of Electrical Engineering and Informatics at the University of Pardubice. His research interests lie in the areas of technological aspects in railway systems.

COMBINING SIMULATION AND OPTIMIZATION MODELS ON A PRODUCTION LINE PROBLEM: A CASE STUDY

António A.C. Vieira[(a)], Edgar Guilherme[(b)], José A. Oliveira[(a)], Luís M.S. Dias[(a)] and Guilherme A.B. Pereira[(a)]

[(a),(b)]University of Minho, Campus Gualtar, 4710-057, Braga, Portugal.
[(a),(b)]ALGORITMI Research Center.

[(a)]{antonio.vieira, zan, lsd, gui}dps.uminho.pt
[(b)]b7542@algoritmi.uminho.pt

ABSTRACT

To improve the performance of a production line of a company of the Bosch Group, an optimization model was developed, which produces the optimum allocation of tasks to workstations and workers, according to a set of constraints. These results can thereafter be used in the simulation model, to estimate performance indicators, which would be difficult to estimate with other approaches, namely: waiting times, times spent with displacements and utilization rates. Thus, the purpose of this paper is twofold. First, it describes the combined use of the optimization and the simulation models. Thereafter, it presents the results obtained for 2 scenarios: one without displacements and another with displacements. The former was used to compare the simulation and the optimization models, whilst the later was used to assess the impact of displacements in the production line. By analyzing the results, it was possible to verify that the displacements increased the total time required to produce the devices in more than 10%. Furthermore, it was shown that the displacements caused considerable changes in the remaining performance indicators, indicating the relevance of considering them. This work also brings insights to the Industry 4.0 by proposing an approach to virtualize a production line system, providing the benefits of the 3D visualization of the simulation tool used in this research.

Keywords: Simulation, Optimization, Simio, Production line, Case Study, Industry 4.0.

1. INTRODUCTION

In production contexts, production lines are used to produce several types of devices. For this purpose, several workstations are used, on which workers perform different operations. In this regard, the optimization of the logistic movements is crucial for these kinds of problems. For instance, it is important to minimize the occurrence of interception between the trajectories performed by each worker, as they change from one workstation to another.

Assembly line production systems are present in different industrial environments and are used to manufacture a large variety of products. Assembly lines were developed for a cost efficient mass-production of standardized products to exploit a high specialization of labor and the associated learning effects (Boysen, Fliedner, and Scholl 2006). The assembly lines can be as follows:

- Modular Assembly (Leisner and Ost 1996) – This is an advanced assembly line method that is designed to improve throughput by increasing the efficiency of parallel subassembly lines feeding into the final assembly line. Modular assembly would involve assembling separate modules on their own assembly lines, then joining them together on a final assembly line.
- Cell Manufacturing (Isa and Tsuru 2002) – This method evolved of the increased ability of machines to perform multiple tasks. Cell operators handle three or four tasks, and robots are used for operations like materials handling and welding. Cells of machines can be run by one operator or a multi-person work cell. In these machine cells it is possible to link older machines with newer ones, thus reducing the investment required for new machinery.
- Team Production (Bukchin, Darel, and Rubinovitz 1997) – Team-oriented production is another development in assembly line methods. Workers used to work at one or two-person work stations and perform repetitive tasks. Now teams of workers can follow a job down the assembly line through its final quality checks. This approach has been hailed by supporters as one that creates greater worker involvement in the manufacturing process and knowledge of the system.
- U-Shaped (Aase, Olson, and Schniederjans 2004) – A line may not be the most efficient shape in which to organize an assembly line. On a U-shaped line, or curve, workers are located on the inside of the curve and communication is easier than in a straight line. Assemblers can see each process; what is coming and how fast; and one person can

perform multiple tasks. Also, workstations along the "line" are able to produce multiple product designs simultaneously, making the facility more flexible. Changeovers are easier in a U-shaped line as well and, with better communication between workers, cross-training is also simplified. The benefits of the U-shaped line have served to increase their use widely.

In the assembly line is also important to know the pace of the work parts moving in it and they can be of three main types (Merengo, Nava, and Pozzetti 1999):

- Moving line – a transport system moves, at a constant speed, the units evenly distributed along the line.
- Paced line – the transport system is periodically moving. When a unit arrives at a station, it remains there for a period of time called cycle time and then it is moved to the following station.
- Unpaced line – is equipped with buffers located between stations. In each station the operator takes a unit from the buffer upstream, performs all the required assembly tasks and then moves the unit to the buffer downstream.

In case of a paced assembly line, the station time of every station is limited to the cycle time as a maximum value for each work piece. Since tasks are indivisible work elements, the cycle time can be no smaller. That situation would be ideal, since it presents no idle time between workstations. What usually happens in real problems is the absence of a common cycle time and it is called an unpaced assembly line, i.e., all stations operate at an individual speed, work pieces may have to wait before they can enter the next station and/or stations may get idle when they have to wait for the next work piece. That situation most of the time cannot be completely solved, instead, the optimization method will try to minimize that idle time.
The standard work is a method that defines how operations should be performed at workstations, preventing operators from performing operations randomly. By describing the operations to be performed, operators can become polyvalent because they have access to all the information and can learn to perform new tasks, which guarantees more flexibility of the production system. Basically, standard work consists of three elements (Lopes 2012):

- Takt-Time – is the rate at which products must be made in a process to meet customer demand.
- Work Sequence – is the precise sequence in which an operator performs tasks within takt-time.
- Standard Inventory – is the parts between operations, including units in machines, required to keep the process operating smoothly.

If applied correctly, the standard work can bring several benefits (Emiliani 2008), such as: the creation of reference points from which is possible to improve continuously, process control, variability reduction, quality and flexibility improvement, stability (i.e. predictable results) and abnormalities predictability.
In light of this problem, a project is being developed at Bosch Car Multimedia Portugal, which consists in optimizing the allocation of an operation to a worker and to a workstation, given a set of requirements and input data, e.g., the duration of each task and number of devices to be produced. Yet, there are other relevant performance metrics, which are difficult to take into consideration by the developed optimization model. Therefore, a simulation model of this problem was also developed, to complement the optimization model with these relevant metrics, i.e., waiting time of devices to produce, per workstation and utilization rates of workers and workstations.
Considering the above exposed, the purpose of this paper is twofold. First, it documents the work conducted to develop both the optimization and the simulation models. The mixed integer linear programming (MILP) model was implemented with AMPL (A Mathematical Programming Language) code, whilst the simulation model was developed in Simio (Dias et al. 2016). Thereafter, it discusses the obtained results emphasizing on the improvement of the production line of the case study. Such work brings insights into the Industry 4.0 agenda (A. A. Vieira et al. 2018; Wang et al. 2016; Uhlemann, Lehmann, and Steinhilper 2017; Longo 2013), namely in the company hosting this research, due to the benefits of the developed solution: virtualization of production line operations in 3D (Turner et al. 2016), testing alternative scenarios, among others. In fact, one of the main contributes of this research is the use of such tool to communicate with customers of the company, while using the tool to illustrate how a given production line will operate. Despite its interest, this topic in out of the scope of this paper.
This paper is organized as follows. Next section presents the MILP optimization model used to improve the performance of the production line, whilst section 3 achieves a similar purpose, for the developed discrete-event simulation model. The results are displayed and analyzed in section 4. Finally, section 5 discusses the main conclusions and some future research directions.

2. THE MILP MODEL

The work sequence optimization can be modelled as a Generalized Assignment Problem (GAP). The GAP under study has the following characteristics:

- Mass-production of one homogeneous product given the production process;
- Paced line with fixed Cycle Time (TCT);

- Deterministic operations time;
- Each task is assigned to only one workstation and only one worker;
- Each workstation has a limited number of workers assigned;
- The workers working time is limited by the assembly line CT;
- The tasks are already assigned to the workstations and the objective is to balance the workers working time;

This GAP problem can be defined by a bipartite graph G=(T,W,A) where T is a set of tasks with size NT, W a set of workers with size NW and A is a set of arcs between tasks and workers. Each task has a processing time and the objective is to balance the work between the workers. The mathematical model for this problem has the following variables, decision variables and constraints:

$$X_{i,k} = \begin{cases} 1, \textit{if task i is assigned to worker k} \\ 0, \textit{otherwise} \end{cases}$$

$$C_i = \begin{cases} 1, & \textit{if worker changes to task } i+1 \\ 0, & \textit{caso contrário} \end{cases}$$

WT_k – *working time of worker k*

Objective function:

$\min \sum_i^{NT} C_i$

Subject to:

$$\sum_k^{NW} X_{i,k} = 1, \ i = 1, \dots, NT \quad (1)$$

$$\sum_i^{NT} T_i * X_{i,k} = WT_k, \ k = 1, \dots, NW \quad (2)$$

$$WT_k \leq CT \quad (3)$$

$$X_{i,k} \leq X_{i+1,k} + C_i, i = 1, \dots, NT-1, k = 1, \dots, NW \quad (4)$$

The objective function minimizes the number of change of workers between tasks aiming to balance the workload for workers. The constraint (1) ensures that each task is assigned to only one worker. The worker working time is calculated in the constraint (2). The constraint (3) ensures that the workers working time is not greater than the cycle time. Finally, the constraint (4) calculates the number of changes. The MILP model was implemented in AMPL and our compact formulation was used to solve the instances using the NEOS Server. The GAP mathematical model was developed in AMPL.

3. SIMULATION MODELLING

To develop the simulation model of this problem, the data provided to the MILP had to be considered. these data are provided by the Neos server and can thereafter be used by regular Excel formulas to obtain data according to what is required by the simulation model, regardless of the output of the MILP model. Thereafter, the tool allows these files to be bound to the simulation model, meaning that whenever a new MILP model is run, the new results can be immediately considered by the simulation model.

This section presents the main steps conducted to develop the simulation model used for this problem. This development was divided in two steps: Data preparation and the development of the main simulation model, covered in the second subsection, which uses the data modelling, described in the first subsection.

3.1. Data Preparation

The data were divided in 3 Excel files, each one concerning the following domains: data of workstations, data of the operations to execute and data of resources involved. After incorporating these data, relationships between them need to be modelled in Simio (A. A. C. Vieira et al. 2017; A. Vieira et al. 2016; A. A. C. Vieira et al. 2018). This allows, for instance, to know which operations are performed by which workers on which workstation. To accomplish this, these relationships were modelled as provided by Figure 1.

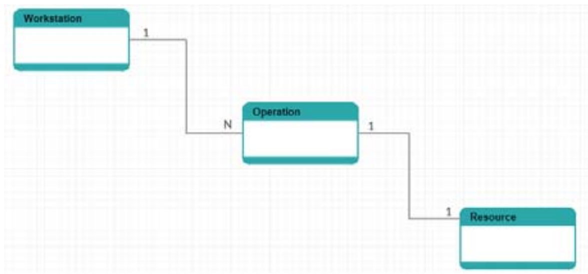

Figure 1: Relationships of data tables.

As the figure suggests, in the problem at hand, at one workstation, there can only be 1 operation at a given time and this operation can only be performed by a single worker. Thus, situation in which, for instance, 2 workers perform the same operation on a given piece, in the same workstation, cannot occur. On the other hand, the same workstation can perform multiple different operations, at different times, therefore there is a one-to-many relationship between the "Workstation" and the "Operation" tables. In this case, the primary key field that identifies a workstation must be incorporated in the "Operation" table, as a foreign key. Lastly, it should be noted that the one-to-one relationship between the "Operation" and the "Resource" tables could be avoided, by merging the content of the two tables in a single one. Yet, this was not adopted, because separating them into 2 tables eased the incorporation of these data into the simulation model. The final of result of incorporating these relationships in Simio is provided in Figure 2, Figure 3 and Figure 4.

	servers_distinct
1	Server1
2	Server1_1
3	Server1_2
4	Server1_3

Data_Table

	Workstation	Starting Process	Ending Process	Operation	Task Sequence	ProcessingTime (Seconds)	Transport
1	Server1_3	StartingProcess	EndingProcess	operation 36	10	3	☐
2	Server1_3	StartingProcess	EndingProcess	operation 37	20	4	☐
3	Server1_3	StartingProcess	EndingProcess	operation 38	30	1,5	☐
4	Server1_3	StartingProcess	EndingProcess	operation 39	40	4	☐
5	Server1_3	StartingProcess	EndingProcess	operation 40	50	1	☐
6	Server1_3	StartingProcess	EndingProcess	operation 41	60	2	☐
7	Server1_3	StartingProcess	EndingProcess	operation 42	70	2	☐
8	Server1_3	StartingProcess	EndingProcess	operation 43	80	1	☐
9	Server1_3	StartingProcess	EndingProcess	operation 44	90	3	☐
10	Server1_3	StartingProcess	EndingProcess	operation 45	100	1	☐
11	Server1_3	StartingProcess	EndingProcess	operation 46	110	2	☐
12	Server1_3	StartingProcess	EndingProcess	operation 47	120	2	☐
13	Server1_3	StartingProcess	EndingProcess	operation 48	130	4	☐

	servers_distinct
5	Server1_4

Figure 2: Data table of workstations.

	Workstation	Starting Process	Ending Process	Operation	Task Sequence	ProcessingTime (Seconds)	Transport
1	Server1	StartingProcess	EndingProcess	operation 1	10	3	☐
2	Server1	StartingProcess	EndingProcess	operation 2	20	1,5	☐
3	Server1	StartingProcess	EndingProcess	operation 3	30	2	☐
4	Server1	StartingProcess	EndingProcess	operation 4	40	2	☐
5	Server1	StartingProcess	EndingProcess	operation 5	50	2	☐
6	Server1	StartingProcess	EndingProcess	operation 6	60	2	☐
7	Server1	StartingProcess	EndingProcess	operation 7	70	1,5	☐
8	Server1	StartingProcess	EndingProcess	operation 8	80	7,5	☐
9	Server1	StartingProcess	EndingProcess	operation 9	90	8	☐
10	Server1	StartingProcess	EndingProcess	operation 10	100	2	☐
11	Server1	StartingProcess	EndingProcess	operation 11	110	1,5	☐
12	Server1	StartingProcess	EndingProcess	operation 12	120	1,5	☑
13	Server1_1	StartingProcess	EndingProcess	operation 13	130	2	☐

Figure 3: Data table of operations.

	Operation	Worker	Reserve	Destination	Reservation Time
1	operation 1	Worker1[1]	True	Input@Server1	Infinity
2	operation 2	Worker1[1]	True	Input@Server1	Infinity
3	operation 3	Worker1[1]	True	Input@Server1	Infinity
4	operation 4	Worker1[1]	True	Input@Server1	Infinity
5	operation 5	Worker1[1]	True	Input@Server1	Infinity
6	operation 6	Worker1[1]	True	Input@Server1	Infinity
7	operation 7	Worker1[1]	True	Input@Server1	Infinity
8	operation 8	Worker1[1]	True	Input@Server1	Infinity
9	operation 9	Worker1[1]	True	Input@Server1	Infinity
10	operation 10	Worker1[1]	True	Input@Server1	Infinity
11	operation 11	Worker1[1]	True	Input@Server1	Infinity
12	operation 12	Worker1[1]	True	Input@Server1	Infinity

Figure 4: Data table of resource allocation settings.

As can be seen, Figure 2 allows to see what operation (from Figure 3) can be performed in which workstation; the server (e.g., Server1 and Server1_1) object of Simio was used to model workstations. Furthermore, it also allows to see other parameters, such as if the piece is to be transported to the next workstation, the processing time, and others. Lastly, Figure 4 shows the resource parameters required to model other behaviors, such as to tell the worker if he needs to keep working on the same piece, or if he can proceed to another one – “Reserve” column.

3.2. Simulation Model Development

After preparing the data, it was necessary to develop the remaining simulation model. The system in question is comprised by 17 workstations and 8 workers. To develop such a system, 17 Simio Server objects were used and their properties were set as described in Figure 5 and Figure 6. In its turn, to consider 8 workers, it was necessary to place a Worker Simio object and edit a specific property which sets the number of workers. Furthermore, it should be noted that the model is prepared to run the simulations without any type of connection between Servers, by using the Free Space concept of Simio. This was accomplished by modelling a sequence table, which specifies the destination sequence that each entity needs to follow. The last modelling step consisted on setting the properties of the Servers. In this regard, the properties of all Servers were set as indicated in Figure 5.

In most of simulation tools, a process is represented as a random distribution specifying the duration of the process. Yet, in this case, each operation has a processing time associated and several can be performed at a single workstation. Therefore, it was necessary to set the "Process Type" property of the Servers to "Task Sequence". Thus, it was necessary to specify the operations' properties, which are specified in two different data tables. Thus, each one was inserted in its corresponding property, i.e., either "Processing Tasks" or "Task Resources". As Figure 6 suggests, each property is assigned to a different field of the already presented data tables.

It should be noted that it is only necessary to indicate the name of the column and the data table, because each row of "Operation_TABLE" is associated to a single operation and the "Process Type" property of all Servers (see Figure 5) is set to "Task Sequence", i.e., one task per row. The final result of the model while running is illustrated in Figure 7, in 3D. As can be seen, the triangles are the entities of the model, which in their turn represent the pieces of the system which are being produced.

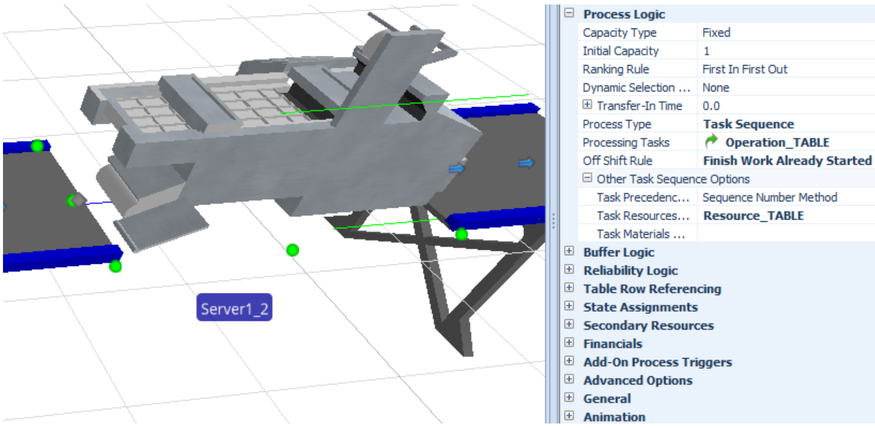

Figure 5: Properties of one workstation of the problem.

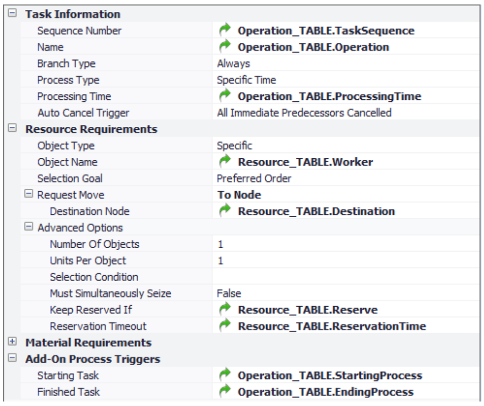

Task Information	
Sequence Number	**Operation_TABLE.TaskSequence**
Name	**Operation_TABLE.Operation**
Branch Type	Always
Process Type	Specific Time
Processing Time	**Operation_TABLE.ProcessingTime**
Auto Cancel Trigger	All Immediate Predecessors Cancelled
Resource Requirements	
Object Type	Specific
Object Name	**Resource_TABLE.Worker**
Selection Goal	Preferred Order
Request Move	**To Node**
Destination Node	**Resource_TABLE.Destination**
Advanced Options	
Number Of Objects	1
Units Per Object	1
Selection Condition	
Must Simultaneously Seize	False
Keep Reserved If	**Resource_TABLE.Reserve**
Reservation Timeout	**Resource_TABLE.ReservationTime**
Material Requirements	
Add-On Process Triggers	
Starting Task	**Operation_TABLE.StartingProcess**
Finished Task	**Operation_TABLE.EndingProcess**

Figure 6: Properties that define the task resource settings.

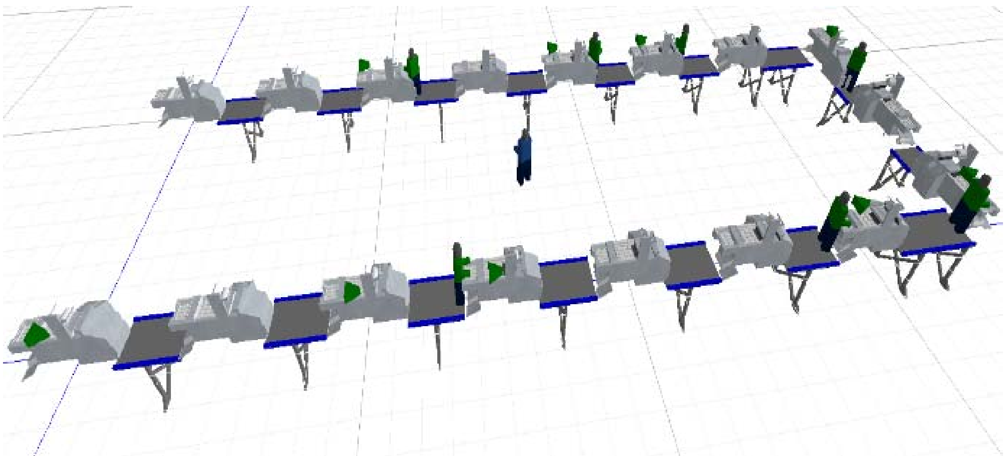

Figure 7: Simulation model running in 3D

4. RESULTS ANALYSIS

This section presents the results of the experiments that were conducted with the purpose of complementing the optimization model with new relevant insights, which are consequence of new Key Performance Indicators (KPI) that the simulation model could obtain, and the optimization model could not. In this regard, 2 experiments were conducted: one which did not consider displacements of workers and materials and a second one which considered them. Whilst the former can be used to compare the performance of both the simulation and the MILP models, the latter is used to obtain the impact of such displacements. The obtained results are displayed in
Table 2, which considered the following KPI:

- KPI1 - Average utilization rates of workstations;
- KPI2 - Average waiting time of devices on each workstation;
- KPI3 - Total simulation time to produce the intended number of devices;
- KPI4 - Average utilization rates of workers;
- KPI5 - Average idle time of workers;

The results of the conducted experiments can be consulted in Table 1 and
Table 2. The former displays the results obtained for KPI1, KPI2 and KPI3. In its turn, the later shows the obtained results for KPI4 and KPI5.

Table 1: Simulation experiments' results for KPI1, KPI2 and KPI3.

	Scenario I (does not consider displacements)		Scenario II (considers displacements)	
Workstation	Utilization Rates (%)	Waiting times (minutes)	Utilization Rates (%)	Waiting times (minutes)
1	92,7	154,6	88,4	174,7
2	31,1	0	26,7	0
3	50,4	0	44,1	0
4	92,2	1,4	87,8	1,6
5	90,8	3,7	88	9,3
6	67,8	0,1	91,8	3,5
7	60,8	0	52,7	0
8	92,4	0,3	85,3	0
9	49,4	0	41,4	0
10	45,1	0	90,7	1,3
11	55,8	0	50,3	0
12	52,8	0	47,5	0
13	77,6	0	71,1	0
14	66,3	0	56	0
15	38,6	0	48,8	0
16	51,9	0	88,2	0
17	90,6	2,1	73	0
Total simulation time (hours)	6,62		7,71	

The first thing to notice from the analysis of both scenarios is the simulation time required to run them, i.e., the time required to produce the specified number of devise (200 in both cases). As expected, this time was higher in the scenario with the displacements – more than 1 hour of difference, indicating its considerable impact on the overall performance of the production line.

Another interesting aspect to notice from this analysis is that some utilization rates dropped when the displacements were considered (all except workstation 6, 10 and 15). Yet, despite this, in some cases – namely workstation 5, 6 and 10 – the average waiting time for these workstations increased. Furthermore, from this analysis, it was also possible to obtain the total waiting time on all workstations, which could not be obtained with the optimization model. In fact, it is possible to verify that 162,3 minutes in scenario I and 190,4 minutes in scenario II, divided by all workstation, are spent waiting for a workstation. However, these values include the first workstation, in which devices are queued in the beginning of the simulation. Thus, if this workstation is excluded, the total waiting times drop to 7,7 and 15,7 minutes for scenarios I and II, respectively. Table 2 shows the obtained results from for the KPI 4 and KPI5.

Table 2. Simulation experiments' results for KPI4 and KPI5.

	Scenario I (does not consider displacements)		Scenario II (considers displacements)	
Worker	Utilization Rates (%)	Idle times (minutes)	Utilization Rates (%)	Idle times (minutes)
1	93,3	26,7	89	50,9
2	89,4	42,1	86,8	61,3
3	78,6	85	75,8	112,1
4	80,9	75,8	81,5	85,8
5	91,6	33,5	96,4	16,8
6	97,2	11,2	95,5	20,8
7	91,1	35,3	88,2	54,5
8	92,4	30,1	85,3	67,8

From the analysis of this table, it is possible to verify that - similarly to the results on Table 1 - in the scenario with the displacements, the utilization rate of some workers also decreased, whilst their idle times increased, which seems to reinforce the importance of including the impact of the displacements on this analysis.
Furthermore, the analysis of both tables also suggests that the capacity of some workstations and workers is not being completely used. For instance, the utilization rates of workstation 2 and worker 5 is 26,7% and 96,4%, respectively. On the other hand, this analysis also showed that the impact of the displacements could be of 50% or more. In fact, workstation 10 presents a utilization rate of 45,1% in scenario I, whilst in scenario II this value increases to 90,7. The same happened with workstation 16, which increased its utilization rate from 51,9% to 88,2%.

5. CONCLUSIONS

Some of the most relevant Key Performance Indicators (KPIs) for the performance of a production line cannot be estimated with analytical methods. In this regard, a project is being conducted in a company of the Bosch Group, which consisted in optimizing the performance of production lines.
In light of this, a MILP model (Generalized Assignment Problem) is under development. Thus, to complement the MILP model, a simulation model of this problem was also developed in Simio, which applies the object-oriented paradigm and is able to incorporate real industrial data. Furthermore, the simulation tool also offers native 3D visualization, enhancing the communication and involvement of stakeholders, during the project execution, which is aligned with the Industry 4.0 agenda.
In a first instance, the MILP is able to determine the optimum allocation of tasks to a workstation and a worker. The resulting allocation can thereafter be inserted in the simulation model, to properly assess the performance of the production line. To conduct this assessment, in this paper, 2 experiments were considered: one without displacements and a second one which considered these displacements.

The obtained results show the importance of the optimization model to consider such displacements by quantifying the differences between both scenarios. In fact, it could be seen that there was more than 1 hour of difference between the time required to produce 200 devices, by the 2 scenarios. Furthermore, the defined KPI for workstations and workers could vary from one scenario to the other, as much as 50%, demonstrating the need to consider displacements, otherwise misleading conclusions can be withdrawn.
Despite the conclusions obtained from this work, the MILP model still needs to be improved. By improving it, the results obtained from the simulation model will change accordingly, since the simulation model receives an output from the optimization model. Thus, the MILP should be complemented to consider displacements and different layouts. Moreover, other KPI can also be considered, for instance the takt time on each workstation and of each worker.

ACKNOWLEDGMENTS

This research was partially sponsored by the Portugal Incentive System for Research and Technological Development. Project in co-promotion nº 002814/2015 (iFACTORY 2015-2018) and has been partially supported by FCT – Fundação para a Ciência e Tecnologia within the Project Scope: UID/CEC/00319/2019.

REFERENCES

Aase, Gerald R., John R. Olson, and Marc J. Schniederjans. 2004. "U-Shaped Assembly Line Layouts and Their Impact on Labor Productivity: An Experimental Study." *European Journal of Operational Research* 156 (3): 698–711. https://doi.org/10.1016/S0377-2217(03)00148-6.

Boysen, Nils, Malte Fliedner, and Armin Scholl. 2006. "A Classification of Assembly Line Balancing Problems." https://doi.org/10.1016/j.ejor.2006.10.010.

Bukchin, Joseph, Ezey Darel, and Jacob Rubinovitz. 1997. "Team-Oriented Assembly System Design: A New Approach." *International Journal of Production Economics* 51 (1–2): 47–57. https://doi.org/10.1016/S0925-5273(97)00060-1.

Dias, Luis M. S., Antonio A. C. Vieira, Guilherme A. B. Pereira, and Jose A. Oliveira. 2016. "Discrete Simulation Software Ranking — A Top List of the Worldwide Most Popular and Used Tools." In *2016 Winter Simulation Conference (WSC)*, 1060–71. IEEE. https://doi.org/10.1109/WSC.2016.7822165.

Emiliani, M.L. 2008. "Standardized Work for Executive Leadership." *Leadership & Organization Development Journal* 29 (1): 24–46. https://doi.org/10.1108/01437730810845289.

Isa, Katsuhide, and Tsuyoshi Tsuru. 2002. "Cell Production and Workplace Innovation in Japan: Toward a New Model for Japanese Manufacturing?" *Industrial Relations* 41 (4): 548–78. https://doi.org/10.1111/1468-232X.00264.

Leisner, Ernst, and Sven Ost. 1996. "Modular Assembly Line System," January.

Longo, F. 2013. "On the Short Period Production Planning in Industrial Plants: A Real Case Study." *International Journal of Simulation and Process Modelling* 8 (1): 17–28. https://doi.org/10.1504/IJSPM.2013.055189.

Lopes, Sara. 2012. "Aplicação de Standard Work e de Outras Ferramentas de Lean Production Numa Empresa de Elevadores." University of Minho.

Merengo, C., F. Nava, and A. Pozzetti. 1999. "Balancing and Sequencing Manual Mixed-Model Assembly Lines." *International Journal of Production Research* 37 (12): 2835–60. https://doi.org/10.1080/002075499190545.

Turner, C.J., W. Hutabarat, J. Oyekan, and A. Tiwari. 2016. "Discrete Event Simulation and Virtual Reality Use in Industry: New Opportunities and Future Trends." *IEEE Transactions on Human-Machine Systems* 46 (6): 882–94. https://doi.org/10.1109/THMS.2016.2596099.

Uhlemann, Thomas H.-J., Christian Lehmann, and Rolf Steinhilper. 2017. "The Digital Twin: Realizing the Cyber-Physical Production System for Industry 4.0." *Procedia CIRP* 61: 335–40. https://doi.org/10.1016/j.procir.2016.11.152.

Vieira, A., L.S. Dias, G.B. Pereira, J.A. Oliveira, M.S. Carvalho, and P. Martins. 2016. "Automatic Simulation Models Generation of Warehouses with Milk Runs and Pickers." In *28th European Modeling and Simulation Symposium, EMSS 2016. Winner of the Best Paper Award*, 231–41.

Vieira, A.A.C., L.M.S. Dias, G.A.B. Pereira, and J.A. Oliveira. 2017. *Agent-Based Simulation to Assess the Performance of Intersections with Pre-Signals: Comparison with Roundabouts*. *Lecture Notes in Computer Science (Including Subseries Lecture Notes in Artificial Intelligence and Lecture Notes in Bioinformatics)*. Vol. 10572 LNCS. https://doi.org/10.1007/978-3-319-68496-3_36.

Vieira, A A C, L M S Dias, G A B Pereira, J A Oliveira, M Do Sameiro Carvalho, and P Martins. 2018. "Simulation Model Generation for Warehouse Management: Case Study to Test Different Storage Strategies." *International Journal of Simulation and Process Modelling* 13 (4): 324–36. https://doi.org/10.1504/IJSPM.2018.093761.

Vieira, António AC, Luís MS Dias, Maribel Y Santos, Guilherme AB Pereira, and José A Oliveira. 2018. "Setting an Industry 4.0 Research and Development Agenda for Simulation – A Literature Review." *International Journal of Simulation Modelling* 17 (3): 377–90. https://doi.org/10.2507/IJSIMM17(3)429.

Wang, Shiyong, Jiafu Wan, Daqiang Zhang, Di Li, and Chunhua Zhang. 2016. "Towards Smart Factory for Industry 4.0: A Self-Organized Multi-Agent System with Big Data Based Feedback and Coordination." *Computer Networks* 101 (June): 158–68. https://doi.org/10.1016/j.comnet.2015.12.017.

A NOVEL APPLICATION OF PRE-SIGNALS TO IMPROVE THE PERFORMANCE OF SIGNALIZED INTERSECTIONS: EVALUATION THROUGH SIMULATION

António A. C. Vieira[a], Luís M. S. Dias[b], Guilherme A. B. Pereira[c], José A. Oliveira[d]

[(a),(b),(c),(d)] University of Minho, 4710-057, Braga, Portugal
ALGORITMI Research Center

[(a)]antonio.vieira@dps.uminho.pt, [(b)]lsd@dps.uminho.pt, [(c)]gui@dps.uminho.pt, [(d)]zan@dps.uminho.pt

ABSTRACT
To ponder less costlier solutions to solve traffic congestion problems at signalized intersections, this paper proposes a novel application consisting of using pre-signals. Hence, an agent-based traffic simulation model was developed, where it is possible to model different types of intersections – including roundabouts of different sizes – and quantify and compare their performance. By analyzing the simulation results, it was found that: on the intersection with pre-signals, an increase in the flow of 10% and 3% was registered, the vehicles spent 1 and 2 less minutes to cross the intersection and the fuel consumption was decreased in 22% and 44%, in comparison to regular intersections and roundabouts, respectively. Concerning the size of queues, it was noted that the queues of the regular intersection were 60 meters longer than the queues on the intersection with pre-signals and on the roundabout. Based on these findings, and by making cost assumptions, a small cost analysis was made, which indicates that at least 1 million € could be yearly saved.

Keywords: Discrete-Event Simulation, Agent Modelling, Signalized Intersection, Pre-signals, Roundabout.

1. INTRODUCTION
Traffic congestion problems are becoming increasingly intense, due to the growing number of vehicles circulating on the roads. Because of this, traffic engineers and academics have been focusing on ways to improve the capacity, and other performance indicators, of traffic intersections, since these are the most common bottlenecks of the traffic congestion problems. Many times, the solutions to these problems are onerous constructions, e.g.: tunnels or bridges.

The purpose of this paper is to propose a novel approach, consisting on using pre-signals on the approaches of a signalized intersection to improve its performance. To evaluate the proposed approach, the authors developed a discrete-event simulation model in Simio (A. Vieira et al. 2015; A. A. C. Vieira et al. 2018), a recent simulation tool that allows the user to build models employing agent-modelling concepts, which consists in individually modelling the behaviour and characteristics of each entity, i.e., each vehicle travelling through the model. Hence, in this paper, the authors will use the developed simulation model to quantify and compare the results obtained by the simulation model, in order to assess the proposed novel approach for pre-signals. In addition, a brief analysis of cost assumptions will be made.

Some of the obtained results have already been published in previous publications. Vieira et al. (2014) firstly compared the performance of regular signalized intersections and intersections applying the proposed pre-signals. The results indicated that both types of intersections performed better for different green light durations and thus a balance between gains and losses, when considering the duration of the green light to use on a regular traffic light intersection, needs to exist. In this type of intersections, durations around 40 to 60 seconds should be used, since increasing it too much would result in a high flow, but also on high waiting times per vehicle and queue sizes, which was also observed by Pan et al. (2010), since the time that the vehicles, on the remaining lanes, wait for the green signal also increases. On the other hand, if low durations of green signal are used, the capacity at a steady level without reducing queue lengths and waiting time. In this regard, it was concluded that the performance increased when low durations of green signal are used. Moreover, the results also showed that for low traffic congestion, the distance between pre-signals and the main traffic lights did not affect the performance of the intersection, while for high congestion scenarios the best performance was achieved for distances of more than 40 meters. In Vieira et al. (2017), the intersection with pre-signals was compared with roundabouts.

For this study, the SIMIO simulation software was used. It should be noted that, of the reviewed studies, none used discrete-event simulation to assess the performance of the proposed implementations. Several studies exist comparing discrete-event simulation tools, considering several factors (Dias et al. 2016; Oueida et al. 2016; António Vieira et al. 2014; V Hlupic and Paul 1999; Vlatka Hlupic 2000).

A pre-signal is an additional traffic signal located upstream of the main traffic signal. The use given to pre-signals found in literature and in practice can be divided in two sets: to increase the capacity of signalized intersections, by giving priority to the left-turn maneuvers, or to give priority to buses. One of the studies the can be fit in the former was proposed by Xuan et al. (2011). The authors proposed a strategy in which the area upstream to the pre-signal is used to separately queue vehicles wanting to make a left turn from the ones wanting to go straight. The pre-signals of these lanes alternatively give green time to these two sets of vehicles, allowing them to enter the area upstream to the main signal and use all lanes for these operations. According to the authors, this way, the capacity of the intersection can be improved. More recently, several studies have demonstrated benefits of this method, in terms of increased capacity, decreased delay and travel time, efficiency of land use, increased safety, and other aspects (Li et al. 2014; Yan, Jiang, and Xie 2014; Yang and Shi 2017; Zhou and Zhuang 2014; Cai et al. 2016).

A similar strategy to the one proposed by Xuan et al. (2011), consists in using an opposite lane to make a left turn, when the convergent flow is with red signal. In this strategy, the pre-signals work as pre-intersections, located at a certain distance upstream to the main intersection, since they regulate the vehicles that want to turn left and the ones that want to access the same approach through an opposing direction (Zhao et al. 2013, 2015; Zhao and Liu 2017; Wu et al. 2016; Kozey, Xuan, and Cassidy 2016; Zhao, Liu, and Di 2016).

One of the first uses given to pre-signals was to give priority to buses in multi lanes with an exclusive bus lane (Oakes, Hellmann, and .Kelly 1994). Whilst buses can advance to the area upstream to the main signal, through their exclusive lane, other vehicles are queued upstream to the pre-signal, thus giving priority to buses.

Guler and Menendez (2014 b) empirically evaluate the use of pre-signals in intersections to give priority to buses. In this implementation of pre-signals, these automatically turn red when a bus arrives to the pre-signal, regardless of the main signal's phase, thus only allowing buses to be queued upstream to the main signal. The same authors (2014 a) also proposed a method to give priority to buses using pre-signals, in which car are alternatively queued in the zones upstream to the pre-signal and the main signal, until the arrival of a bus, which triggers the pre-signal's red phase, allowing the bus to have priority in the main intersection. In both studies, the authors used queuing theory, to quantify and empirically evaluate the delays encountered by cars and buses. With their studies, the authors wanted to demonstrate that their application of pre-signals could significantly reduce the total person hours of delays for both cars and buses.

Guler and Menendez (2016) have also presented an implementation for pre-signals in which these are used to give priority to buses in single-lane intersections, which do not have dedicated bus lanes. In their proposal, on each lane of an intersection, a pre-signal is located upstream and downstream of the main signal, wherein the pre-signal in the opposite lane is nearer to the intersection, than the pre-signal on the remaining lane. This way, buses can bypass vehicles queued on the pre-signal upstream to the intersection, through a bi-directional lane segment, formed as a result of the distance between the pre-signals and located in the lane of the opposite direction. The authors used analytical equations to assess their proposal.

According to Guler and Menendez (2014 b), there is a lack of empirical evaluation on the use of pre-signals, probably due to its scarse implementation across the world. Therefore, simulation could be used to evaluate these novel implementations. Moreover, it allows the modeler to make experiments on the computer, rather than on the field, allowing to thoroughly analyze the proposed pre-signals implementation (A. A. Vieira et al. 2018).

The analyzed researchers agree that these various applications of pre-signals improve the performance of the traffic operations in which they were applied to. In any case, the reviewed applications are either focused on giving priority to buses or improving the capacity of intersections with high left turn demand. However, the purpose of pre-signals proposed in this paper has a different application and purpose. In fact, to the best of the authors' knowledge, is the first time an application of this kind is proposed.

The pre-signals' implementation proposed in this paper is described in the next section. Third section gives a brief contextualization on how the simulation model was developed. The results will be discussed in the fourth section and conclusions, as well as some future work to better cement this new concept, will be addressed in the last section.

2. OPERATION OF PRE-SIGNALS

The pre-signals' implementation proposed in this paper consists on making the space upstream to the main intersection available for all vehicles to accelerate, from their rest state, before the main signal changes to green. To that end, vehicles are queued on the pre-signal and this traffic light changes to green before the main signal, to allow the queued vehicles to notice the change (reaction time) and initiate their start-up acceleration process. With this implementation of pre-signals, an intersection with continuous flow is expected to be achieved, since:

- The reaction time of drivers is eliminated, since when the pre-signal changes to green, the main one is still red;
- The impact of the start-up acceleration is reduced, since the vehicles initiate their start-up acceleration process, while the main signal is still red;
- Whilst the main signal phase of an approaching is ending, the pre-signal of the next approach can change to green, allowing the first vehicle of the second approach to cross the intersection few seconds after the last

of the first approach. This time lag between phases of different approaches should be analyzed for security reasons.

Figure 1 shows an example of the duration of all signals of both pre-signal and main traffic light, in two consecutive approaches of the same intersection. It should be noted that these durations were not used in the intersection modelled with pre-signals in the simulation model; they are just an example.

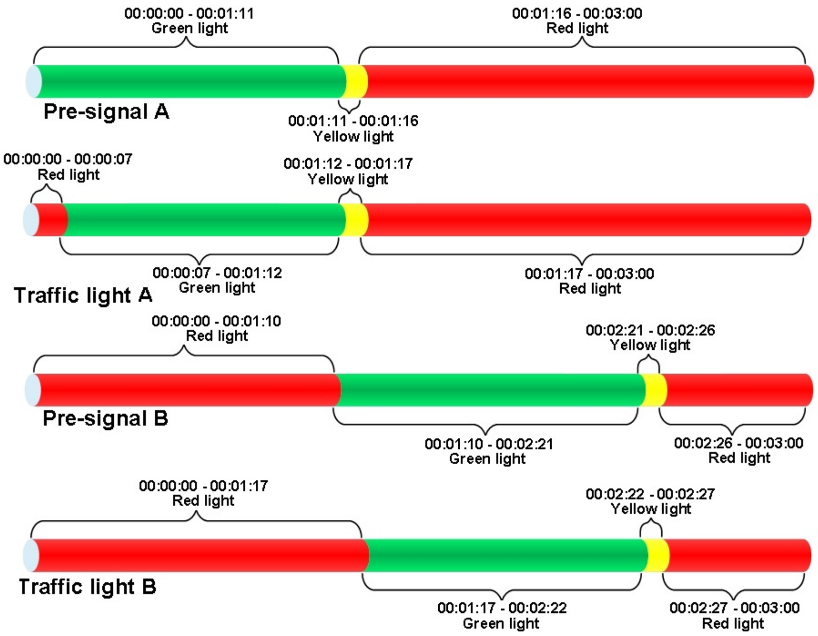

Figure 1: Example of the duration of signals in an intersection with pre-signals (A. Vieira et al. 2014).

The duration of the green phase of the pre-signals is equal to green main signal plus an additional time, before the main green signal and minus another interval duration, before the main green signal. In a case where the first interval is too high, vehicles would reach the main signal, still in red phase, and thus would need to slowdown, or even stop. On the other hand, this interval cannot be too low, otherwise vehicles would not have the sufficient time to reach the main signal with considerable speed, i.e., pre-signals would not serve its purpose of reducing the impact of the reaction time of drivers and start-up acceleration. Regarding the second interval, if it is too high, vehicles would be queued in the pre-signal, with many seconds of main green signal remaining, whereas too low values would result in queued vehicles in the main signal, which would affect the start-up acceleration process of vehicles from the next phase, since these would not have the required space to accelerate.
Besides this, there are also security concerns involved in the phases of the pre-signal. In other words, if its purpose is to allow vehicles from all approaches to cross the intersection at near-to-cruise speed and few seconds of interval between approaches, it still needs to ensure that no accidents occur. The duration of green signa of the pre-signal can be of particular importance in this regard.

3. MODELING

In Simio, the modeler can place and connect 3d objects, which represent the real elements of the system in analysis. Thereafter, additional logic can be added, by using other simulation paradigms, e.g.: processes. Furthermore, concepts of agent modelling are also present in this software, allowing the user to model the individual behaviour of each entity. Thus, in this case, it is possible to have vehicles set their actions, e.g. accelerate and maintain a safety distance to the leading vehicle. Figure 2 shows the 2D representation of the simulation model. Each square represents a distance of 10 meters.

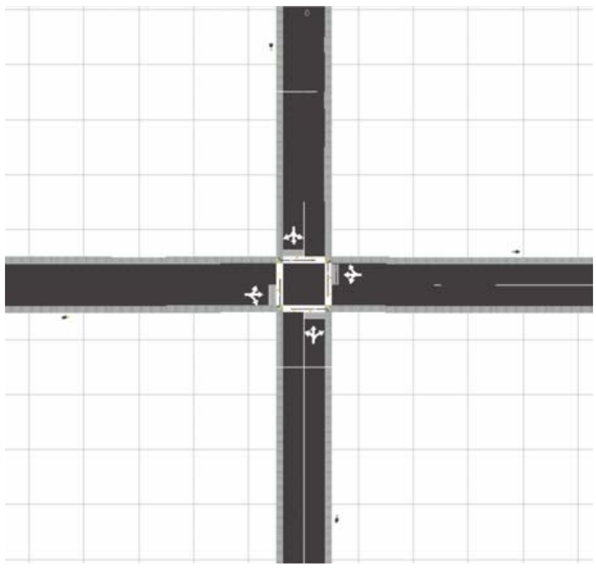
Figure 2: 2D view of the simulation model

As can be seen, the signalized intersection has four approaches, each one with two lanes – one for inflow and another for outflow traffic on the intersection. When the vehicles enter the intersection, regardless of the approach where they are, they can choose the intersection through any exit.

In this simulation model, the traffic lights exist, although merely for animation purposes, since their locations are modelled as geographic coordinates and a data structure, which represents the state of each traffic-light. This way, the position of the signals, including pre-signals, can be easily edited. The signal cycles are processed on a counter clockwise direction, starting with green, changing to yellow and thereafter to red, before repeating the cycle. Only an approach at a time has green signal.

As soon as vehicles are created, they start executing a process that remains active until they cross the intersection, modelling their behaviour according to the situations through which they pass. Some of these processes and the input data used in these models, can be consulted with more detail in the previous publications of this project (A. Vieira et al. 2014; A. A. C. Vieira et al. 2017). Vehicles can even communicate between them to consult, for instance, the speed of the vehicle ahead, the distance to a given object (e.g. traffic-light, stopping line, etc.), or the flasher sign of a vehicle on a roundabout, among others. This modelling paradigm, or philosophy, is known as agent modelling, since entities are modelled as agents, each one being able to make decisions in an independent way, like accelerating or slowing down, considering their surroundings.

To model roundabouts, in Simio, it is possible to add models to a project, using the elements of other models of this project. Thus, in this case, a new model was added to this project, which uses most of the processes that already existed. Thereafter, we only needed to change the design of the intersection and model the rules to access the roundabout. This was of particular importance, since it allowed the modelers to use the same elements in all intersections that would later be compared. For instance, all vehicles in all intersections use the same processes to slowdown or accelerate. Figure 4 and Figure 4 respectively show the simulation models of signalized intersections and roundabouts during runtime.

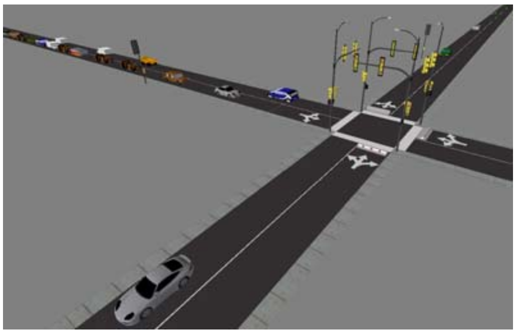

Figure 3: 3D view of the modelled signalized intersection.

Figure 4: 3D view of the modelled roundabout.

4. SIMULATION EXPERIMENTS

In this section, the results obtained in the simulation model will be analysed. The following are parameters of the conducted simulation experiments: frequency with which the vehicles arrive to the system (traffic intensity) and type of intersection, i.e., roundabout or intersection with and without pre-signals. Moreover, the values 4, 8, 13 and 50 seconds were considered, respectively, for the traffic intensity, and hence the following respective levels were considered: very high, high, medium and low traffic. A warm-period of 360 seconds was used, along with a simulation time of 2 hours and 6 replications. As KPI (Key Performance Indicators), the following were defined:

- Average crossing time. This KPI is the elapsed time between the time when a vehicle is created and when it travels an additional distance of 150 meters after having crossed the intersection.
- Average flow of vehicles in vehicles/hour. This KPI is the inverse of the time interval between passages of vehicles through the intersection;
- Average number of vehicles on the queues. This KPI is measured every minute;
- Average flow of vehicles in vehicles/hour. This KPI is the inverse of the time interval between passages of vehicles through the intersection;
- Average total fuel consumed per vehicle in milligrams; and average total emissions of vehicles in milligrams (CO, HC and NOx). These, start being accounted when vehicles are created and are updated every minute. When vehicle cross the intersection, these values are recorded;
- Average number of stops per vehicle.

In this section the performance of each intersection will be analysed in an average day and year perspective. The obtained results can be consulted in Table 1,

Table 2 and Table 3. The displayed values were obtained, considering the formulae given below, in which KPI stands for Key Performance Indicators, θ refers to a number of hours in a traffic intensity and α represents a type of intersection. It should be noted that by using these formulae, the intention is not to exactly determine the respective value, but rather to have an estimation of the what could be the magnitude order of those values, by applying the formulae equally to all analyzed types of intersections. Thus, there is certainly an uncertainty degree associated to these formulae.

$$KPI_\gamma = \begin{cases} Total\ flow\ of\ vehicles\ during\ an\ average\ day & if\ \gamma = 1 \\ Total\ time\ to\ cross\ the\ intersection\ during\ an\ average\ day & if\ \gamma = 2 \\ Total\ fuel\ consumed\ during\ an\ average\ day & if\ \gamma = 3 \\ Total\ CO\ emissions\ during\ an\ average\ day & if\ \gamma = 4 \\ Total\ HC\ emissions\ during\ an\ average\ day & if\ \gamma = 5 \\ Total\ NOx\ emissions\ during\ an\ average\ day & if\ \gamma = 6 \\ Space\ occupied\ by\ a\ queue\ during\ an\ average\ day & if\ \gamma = 7 \end{cases}$$

$$\theta_i = \begin{cases} Hours\ of\ Very\ High\ Traffic\ Intensity & if\ i = 1 \\ Hours\ of\ High\ Traffic\ Intensity & if\ i = 2 \\ Hours\ of\ Medium\ Traffic\ Intensity & if\ i = 3 \\ Hours\ of\ Low\ Traffic\ Intensity & if\ i = 4 \end{cases}$$

$$i \in \begin{cases} Very\ High\ Traffic\ Intensity & if\ i = 1 \\ High\ Traffic\ Intensity & if\ i = 2 \\ Medium\ Traffic\ Intensity & if\ i = 3 \\ Low\ Traffic\ Intensity & if\ i = 4 \end{cases}$$

$$\alpha \in \{Intersection\ with\ Pre-sigals, Regular\ Intersection, Realistic\ Roundabout, Optimistic\ Roundabout\}$$

$$KPI_\gamma^\alpha = \begin{cases} \sum_{i=1}^{4} \theta_i\ KPI_1^{\alpha,i} & if\ \gamma = 1 \\ \frac{\sum_{i=1}^{4} \theta_i\ KPI_1^{\alpha,i}\ KPI_\gamma^{\alpha,i}}{KPI_1^\alpha}\ 30\ 000 & if\ 2 \leq \gamma \leq 6 \\ \frac{\sum_{i=1}^{4} \theta_i\ KPI_1^{\alpha,i}\ KPI_\gamma^{\alpha,i}}{KPI_1^\alpha}\ 7{,}7 + C & if\ \gamma = 7 \end{cases} \tag{1}$$

By applying formula 3 to calculate KPI_1^α, i.e., the total flow of vehicles per day, the registered flow value on each intensity is multiplied by the number of hours of intensity, during a day. The resulting total flow of each intersection is displayed in Table 1.

Table 1: Estimated total flow per day

Intersection	Total flow of vehicles
Pre-signals	32032
Regular Intersection	31167
Roundabout	29149

As can be seen, the intersection with pre-signals was the one to obtain the highest capacity. However, these differences are not very significant, making a total difference of about **3%**, **10%** and **2%**, when compared to the regular intersection, realistic roundabout and the optimistic roundabout, respectively.

For the remaining KPI, apart from the queue size, its values were obtained by applying the respective KPI_γ^α formula. Since different amounts of vehicles entered the system, depending on the modelled intersection and its capacity of handling the income traffic, it was necessary to divide the sum by the total flow of each intersection and, afterwards, multiply it by an average number, i.e. 30 00 vehicles per day. The obtained results can be consulted in Table 2.

Table 2: Estimated total KPI results for an average day and year

	Intersection	Total time wasted (min)	Total fuel consumed (g)	Toal CO emissions (g)	Total HC emissions (g)	Total NOx emissions (g)
Average per cars	Pre-signals	2,96	4,55	0,90	0,07	0,06
	Regular Intersection	3,95	5,84	1,10	0,10	0,07
	Roundabout	4,51	8,62	1,50	0,12	0,10
Average per day (30 000 card)	Pre-signals	88 878	136 371	26 898	2 178	1 770
	Regular Intersection	118 395	175 293	33 099	2 928	2 086
	Roundabout	135 352	258 464	45 094	3 738	2 891
Average per year (30 000 cars * 265 days)	Pre-signals	31 996 172	49 093 409	9 683 422	784 201	637 340
	Regular Intersection	42 622 281	63 105 351	11 915 519	1 054 015	750 787
	Roundabout	48 726 746	93 047 098	16 233 849	1 345 779	1 040 776

As the results illustrate, the vehicles on the intersection with pre-signals were able to cross the intersection in less **25%** time in comparison to the regular intersection and less **34%** in comparison to the roundabout. Moreover, in the intersection with pre-signals, each vehicle could save **1 minute**, in comparison to the regular intersection and **2 minutes**, in comparison to the roundabout.

Regarding the total fuel consumed, the data indicates that, in the intersection modelled with pre-signals, all the vehicles consumed approximately less **22%** of fuel, in comparison to the regular intersection, less **47%** in comparison to the roundabout. Considering all vehicles in a year, these results indicate that there would be a consumption difference of approximately less **14 tons** and **44 tons** of fuel per year, respectively.

To calculate the average space occupied by a queue on each intersection, formula 3 was applied to calculate KPI_7^{α}. In it, after calculating the average queue size on an average day, it is necessary to multiply the queue size by the average space occupied by a vehicle in a queue (Herman, Lam, and Rothery 1971; Bonneson 1992; Messer and Fambro 1977; Zhu 2007) and to sum a constant C, - cf. equation 3, when $\gamma = 7$ - depending of the intersection being considered, i.e. α (these values were also used in the simulation model). In this sense, 20 meters were summed to the values related to the roundabouts, since it is the radius of the modelled roundabouts and 40 meters to the intersection modelled with pre-signals. The results are indicated in Table 3.

Table 3: Average space occupied by a queue on each intersection

Intersection	Total space occupied (meters)
Pre-signals	220,86
Regular Intersection	282,79
Roundabout	226,36

As the table illustrates, the intersection with pre-signals obtained a shorter value than the roundabout, even though the difference is not very significant. It is also possible to verify that its implementation resulted on queues more than **60 meters** shorter that the ones of the regular intersection.

To have an idea of the costs that would be involved in each type of intersection a brief cost analysis was made. It should be noted, however, that these values are estimated, not factual, and their only intention is to give a broad idea of what is the price difference. With this in mind and considering the radius of the roundabouts, i.e. 20 meters, the total area occupied by its infrastructure should be around 1260 m^2. Assuming the size of the roads is around 10 meters, it totalizes an area difference of around 560 m^2. In its turn, considering a cost of 500€ per m^2 a global saving of around **280 000€** is achieved. Moreover, assuming a 5€ cost per hour of a person that is wasted waiting on traffic queues, and a 1.5€ per litre of fuel (1kg ≈ 1l of fuel) Table 4 was built.

Table 4: Cost analysis to the introduction of pre-signals in an intersection

Costs (Difference between intersection with pre-signals and the other intersections)	Comparing intersection with pre-signals and:	Per day	Per year
Extra Time Cost	Regular intersection	2 460 €	885 509 €
	Roundabout	3 873 €	1 394 214 €
Extra Fuel Cost	Regular intersection	58 €	21 018 €
	Roundabout	183 €	65 931 €
Total	Regular intersection	2 518	906 527
	Roundabout	4 056	1 460 145

As the table illustrates, the greater part of the savings is obtained as a consequence of the time saved by drivers. In its turn, the savings related to the fuel consumptions are always beneficial to the intersection with pre-signals. Lastly, considering the total savings per year of the intersection with pre-signals compared to the regular intersection and the roundabout, it can be observed that a global saving of more than **1 million €** per year, summed over all drivers, could be achieved.

It should be noted that, despite the small cost analysis of the impact of introducing pre-signals, these do not include the budgets to build the alternative infrastructures, such as roundabouts, bridges or tunnels. In addition, roundabouts are characterized by increasing the fuel consumption and emission of vehicles, due to the constant stop and start-up processes, through which vehicles trying to access it incur. Thus, the environmental and emissions are also expected to decrease with the proposed approach, even though the limited achieved benefits do not reveal such benefits.

5. CONCLUSIONS

Usually, the solution for most traffic intersection congestion problems consists in building onerous infrastructures e.g.: tunnels or bridges. This paper presents a novel low-cost solution, consisting in using an additional set of traffic-lights situated some meters away from the main ones, working as pre-signals and acting as “launch-pads” for vehicles. To evaluate this new approach, the authors developed a traffic simulation model on Simio. In previous publications (A. Vieira et al. 2014; A. A. C. Vieira et al. 2017) this new approach had already been compared to both regular signalized intersections and roundabouts, albeit considering static traffic intensities. In this paper, all intersections will be compared, considering the traffic intensities during an average day and a brief analysis over assumed costs was establish,

The intersections were compared on average day and year perspectives. It was found that there were no significant differences regarding the maximum flow of vehicles per day, even though the intersections with pre-signals obtained the best flow values, thus increasing the capacity of the intersection. Concerning the time spent on each intersection, it was found that on the intersection modelled with pre-signals, per day, all of the modelled vehicles spent less 25% time than in the regular intersection and less 34% in comparison to the roundabout. Considering the intersection with pre-signals, these results culminate in an average time saving of around 1 minute per vehicle in comparison to the regular intersection and 2 minutes in comparison to the roundabout. Regarding the fuel consumptions, the vehicles modelled in the intersection with pre-signals consumed approximately less 22% of fuel, in comparison to the regular intersection and less 47% of fuel in comparison to the roundabout. These results culminate in a consumption of approximately less 14 tons and 44 tons of fuel per year, respectively. Regarding the average space occupied, it was observed that there were no significant differences between the values recorded of the optimistic roundabout and the intersection with pre-signals. However, the differences registered between the latter and the regular intersection were more than 60 meters. To finalize the study, a small cost analysis was performed by making some cost assumptions. The authors concluded that the area difference between a traffic signalized intersection and a roundabout with 40 meters of diameter, could result in a saving of around 280 000€.By further considering the savings per driver, per year, in both time and fuel consumed, the authors concluded that more than 1 million €, among all drivers, could be saved. Nonetheless, it should be noted that these values do not include the savings that would be obtained by including the budgets to build other infrastructures to improve the intersection, such as bridges or tunnels, as well as the environmental costs associated to the reduction of the emissions, resulted by the reduction of the fuel consumption.

With this paper, the authors believe to have proposed an implementation which, at least, could be pondered by traffic managers, since, the obtained results indicate that it would be possible to considerably increase the performance of a signalized intersection by simply adding pre-signals to its approaches. Whilst building expensive infrastructures in very saturated traffic intersections is still a mandatory option for certain cites, there are cases in which a less expensive option – such as the pre-signals proposed in this paper - could be used. On the other hand, in the author’s view, this paper also contributes to the literature in two ways: firstly, it adds a study that uses a general-purpose discrete-event simulation tool to develop an agent-based traffic micro simulation model – as shows in the first section, most use traffic simulation packages; lastly, it adds a novel implementation for pre-signals in traffic intersections – as shows in the first section, most implementations for pre-signals can be divided in either giving priority to buses or to left-turn maneuvers.

ACKNOWLEDGMENTS

This work has been supported by FCT – Fundação para a Ciência e Tecnologia within the Project Scope: UID/CEC/00319/2019.

REFERENCES

Bonneson, James A. 1992. “Modeling Queued Driver Behavior at Signalized Junctions.” *Transportation Research Record*, 99.

Cai, Zhengyi, Manchu Xiong, Dongfang Ma, and Dianhai Wang. 2016. “Traffic Design and Signal Timing of Staggered Intersections Based on a Sorting Strategy.” *Advances in Mechanical Engineering* 8 (4): 168781401664129. https://doi.org/10.1177/1687814016641292.

Dias, Luis M. S., Antonio A. C. Vieira, Guilherme A. B. Pereira, and Jose A. Oliveira. 2016. “Discrete Simulation Software Ranking — A Top List of the Worldwide Most Popular and Used Tools.” In *2016 Winter Simulation Conference (WSC)*, 1060–71. IEEE. https://doi.org/10.1109/WSC.2016.7822165.

Guler, Lgin, and Monica Menendez. 2014. “Analytical Formulation and Empirical Evaluation of Pre-Signals for Bus Priority.” *Transportation Research Part B: Methodological* 64 (June): 41–53. https://doi.org/10.1016/j.trb.2014.03.004.

Guler, S. Ilgin, Vikash V. Gayah, and Monica

Menendez. 2016. “Bus Priority at Signalized Intersections with Single-Lane Approaches: A Novel Pre-Signal Strategy.” *Transportation Research Part C: Emerging Technologies* 63 (February): 51–70. https://doi.org/10.1016/j.trc.2015.12.005.

Guler, S. Ilgin, and Monica Menendez. 2014. “Evaluation of Presignals at Oversaturated Signalized Intersections.” *Transportation Research Record: Journal of the Transportation Research Board* 2418 (1): 11–19. https://doi.org/10.3141/2418-02.

Herman, Robert, T Lam, and R W Rothery. 1971. “The Starting Characteristics of Automobile Platoons.” *Publication of: Traffic Flow and Transportation*.

Hlupic, V, and R J Paul. 1999. “Guidelines for Selection of Manufacturing Simulation Software.” *IIE Transactions* 31 (1): 21–29. https://doi.org/10.1023/A:1007568516643.

Hlupic, Vlatka. 2000. “Simulation Software: An Operational Research Society Survey of Academic and Industrial Users.” In *Winter Simulation Conference Proceedings*, 2:1676–83.

Kozey, Peter, Yiguang Xuan, and Michael J. Cassidy. 2016. “A Low-Cost Alternative for Higher Capacities at Four-Way Signalized Intersections.” *Transportation Research Part C: Emerging Technologies* 72 (November): 157–67. https://doi.org/10.1016/j.trc.2016.09.012.

Li, Yan, Ke Li, Siran Tao, Xia Wan, and Kuanmin Chen. 2014. “Optimization of the Design of Pre-Signal System Using Improved Cellular Automaton.” *Computational Intelligence and Neuroscience* 2014: 1–11. https://doi.org/10.1155/2014/926371.

Messer, Carroll J, and Daniel B Fambro. 1977. *Effects of Signal Phasing and Length of Left-Turn Bay on Capacity*.

Oakes, J, A. M. Hellmann, and I. T. .Kelly. 1994. “Innovative Bus Priority Measures.” In *Proceedings of Seminar J, Traffic Management and Road Safety, 22nd PTRC European Transport Summer Annual Meeting*, 301–12. Proceedings of Seminar J, Traffic Management and Road Safety, 22nd PTRC European Transport Summer Annual Meeting, University of WARWICK, U.K., vol.381, pp.301-312.

Oueida, Soraia, Pierre Abi Char, Seifeddine Kadry, and Sorin Ionescu. 2016. “Simulation Models for Enhancing the Health Care Systems.” *FAIMA Business & Management Journal* 4 (4): 5–20. http://search.ebscohost.com/login.aspx?direct=true&db=bsu&AN=121321531&site=ehost-live.

Pan, Maolin, Sheng Dong, Jian Sun, and Keping Li. 2010. “Microscopic Simulation Research on Signal Cycle Length of Mixed Traffic Considering Violation.” In *2010 International Conference on Intelligent Computation Technology and Automation*, 674–78. IEEE. https://doi.org/10.1109/ICICTA.2010.658.

Vieira, A., L.S. Dias, G.A.B. Pereira, J.A. Oliveira, M.S. Carvalho, and P. Martins. 2015. “Using Simio to Automatically Create 3d Warehouses and Compare Different Storage Strategies.” *FME Transactions* 43 (4). https://doi.org/10.5937/fmet1504335V.

Vieira, A., L.S. Dias, G.B. Pereira, and J.A. Oliveira. 2014. *Micro Simulation to Evaluate the Impact of Introducing Pre-Signals in Traffic Intersections. Lecture Notes in Computer Science (Including Subseries Lecture Notes in Artificial Intelligence and Lecture Notes in Bioinformatics)*. Vol. 8584 LNCS. https://doi.org/10.1007/978-3-319-09153-2_54.

Vieira, A.A.C., L.M.S. Dias, G.A.B. Pereira, and J.A. Oliveira. 2017. *Agent-Based Simulation to Assess the Performance of Intersections with Pre-Signals: Comparison with Roundabouts. Lecture Notes in Computer Science (Including Subseries Lecture Notes in Artificial Intelligence and Lecture Notes in Bioinformatics)*. Vol. 10572 LNCS. https://doi.org/10.1007/978-3-319-68496-3_36.

Vieira, A A C, L M S Dias, G A B Pereira, J A Oliveira, M Do Sameiro Carvalho, and P Martins. 2018. “Simulation Model Generation for Warehouse Management: Case Study to Test Different Storage Strategies.” *International Journal of Simulation and Process Modelling* 13 (4): 324–36. https://doi.org/10.1504/IJSPM.2018.093761.

Vieira, António AC, Luís MS Dias, Maribel Y Santos, Guilherme AB Pereira, and José A Oliveira. 2018. “Setting an Industry 4.0 Research and Development Agenda for Simulation – A Literature Review.” *International Journal of Simulation Modelling* 17 (3): 377–90. https://doi.org/10.2507/IJSIMM17(3)429.

Vieira, António, Luís M. S. Dias, Guilherme Pereira, and José A. Oliveira. 2014. “Comparison of SIMIO and ARENA Simulation Tools.” In *12th Annual Industrial Simulation Conference (ISC2014)*, 5–13.

Wu, Jiaming, Pan Liu, Zong Z. Tian, and Chengcheng Xu. 2016. “Operational Analysis of the Contraflow Left-Turn Lane Design at Signalized Intersections in China.” *Transportation Research Part C: Emerging Technologies* 69 (August): 228–41. https://doi.org/10.1016/j.trc.2016.06.011.

Xuan, Yiguang, Carlos F. Daganzo, and Michael J. Cassidy. 2011. “Increasing the Capacity of Signalized Intersections with Separate Left Turn Phases.” *Transportation Research Part B: Methodological* 45 (5): 769–81. https://doi.org/10.1016/j.trb.2011.02.009.

Yan, Chiwei, Hai Jiang, and Siyang Xie. 2014. “Capacity Optimization of an Isolated Intersection under the Phase Swap Sorting Strategy.” *Transportation Research Part B: Methodological* 60 (February): 85–106. https://doi.org/10.1016/j.trb.2013.12.001.

Yang, Qiaoli, and Zhongke Shi. 2017. "Performance Analysis of the Phase Swap Sorting Strategy for an Isolated Intersection." *Transportation Research Part C: Emerging Technologies* 77 (April): 366–88. https://doi.org/10.1016/j.trc.2017.01.018.

Zhao, Jing, and Yue Liu. 2017. "Safety Evaluation of Intersections with Dynamic Use of Exit-Lanes for Left-Turn Using Field Data." *Accident Analysis & Prevention* 102 (May): 31–40. https://doi.org/10.1016/j.aap.2017.02.023.

Zhao, Jing, Yue Liu, and Di Di. 2016. "Optimization Model for Layout and Signal Design of Full Continuous Flow Intersections." *Transportation Letters* 8 (4): 194–204. https://doi.org/10.1080/19427867.2015.1109752.

Zhao, Jing, Wanjing Ma, K. Larry Head, and Xiaoguang Yang. 2015. "Optimal Operation of Displaced Left-Turn Intersections: A Lane-Based Approach." *Transportation Research Part C: Emerging Technologies* 61 (December): 29–48. https://doi.org/10.1016/j.trc.2015.10.012.

Zhao, Jing, Wanjing Ma, H. Michael Zhang, and Xiaoguang Yang. 2013. "Increasing the Capacity of Signalized Intersections with Dynamic Use of Exit Lanes for Left-Turn Traffic." *Transportation Research Record: Journal of the Transportation Research Board* 2355 (1): 49–59. https://doi.org/10.3141/2355-06.

Zhou, Yaping, and Hongbin Zhuang. 2014. "The Optimization of Lane Assignment and Signal Timing at the Tandem Intersection with Pre-Signal." *Journal of Advanced Transportation* 48 (4): 362–76. https://doi.org/10.1002/atr.1222.

Zhu, Hong. 2007. "Normal Acceleration Characteristics of the Leading Vehicle in a Queue at Signalized Intersections on Arterial Streets." Master's thesis. Oregon State University.

AUTHORS BIOGRAPHY

António A.C. Vieira is an Invited Assistant Professor and Researcher of the ALGORITMI Research Centre, University of Minho, Portugal. He holds a MSc degree in Systems Engineering at the University of Minho. He is making his doctoral studies in Advanced Engineering Systems for Industry at the University of Minho, in partnership with Bosch Car Multimedia Braga. His research interests include Modelling and Simulation, Logistics and Transportation, and Big Data. His email address is antonio.vieira@dps.uminho.pt.

Luís M.S. Dias is an Auxiliar Professor and Researcher of the ALGORITMI Research Centre, University of Minho, Portugal. He holds a PhD degree in Production and Systems Engineering from the University of Minho, Portugal. His research interests include Simulation, Systems Performance, Operational Research and Systems Visual Modeling. His email address is lsd@dps.uminho.pt.

Guilherme A.B. Pereira is an Associate Professor and Researcher of the ALGORITMI Research Centre, University of Minho (UMinho), in Portugal. He holds a PhD degree in Manufacturing and Mechanical Engineering from the University of Birmingham, UK. His research interests include Operational Research and Simulation. Currently he is Pro-Rector of the University of Minho. His email address is gui@dps.uminho.pt.

José A. Oliveira is an Auxiliar Professor and Researcher of the ALGORITMI Research Centre, University of Minho (UMinho), in Portugal. He holds a PhD degree in Production and Systems Engineering from the University of Minho, Portugal. His research interests include Optimization with Heuristic Methods in Systems Engineering. His email address is zan@dps.uminho.pt.

SIMULATION OF THE DELIVERY SYSTEM FOR THE BICIPUMA BIKE-SHARING SYSTEM IN UNAM-MEXICO

García Cerrud C. [(a)], **Pérez Silva A. M** [(b)], **Olvera Rodríguez V** [(c)], **Soler Anguiano F.I.**[(d)], **Flores de la Mota I**[(e)]

[(a)] Maestría en Ingeniería de Sistemas, UNAM-MÉXICO., [(b)] Maestría en Ingeniería de Sistemas, UNAM-MÉXICO, [(c)] Maestría en Ingeniería de Sistemas, UNAM-MÉXICO, [(d)] Facultad de Ingeniería, UNAM-MÉXICO, [(e)] Facultad de Ingeniería, UNAM-MÉXICO.

[(a)] ank271704ce@gmail.com, [(b)] , moy132.perez@gmail.com [(c)] olvera_veronica@outlook.com [(d)] fisau34@hotmail.com
[(e)] idalia@unam.mx

ABSTRACT
This paper analyzes the delivery of units by the users of Bicipuma so that the accomplishment of this task is done quickly and efficiently for the modules with the highest demand. The aim of the proposal is to create a delivery system by aids of simulation in which the times required are minimal, improving the quality of service to users.

Keywords: delivery, management, simulation.

1. INTRODUCTION

Growing concerns about global motorization and climate change have led to increasing interest in sustainable transportation alternatives such as bikesharing (the shared use of a bicycle fleet). Since Bikesharing's evolution is categorized into three generations: (a) white bikes (or free bike systems), (b) coin-deposit systems, and (c) information technology-based systems.
The principle of bikesharing is simple. Individuals use bicycles as-needed basis without the costs and responsibilities of bike ownership.

1.1. History of bike sharing

Early European bikesharing systems were small scale, operated as nonprofits, and focused on social and environmental issues.

1.1.1. White Bikes (or Free Bike Systems): First Bikesharing Generation

In a free bikesharing system, the bicycle is the main program component.
Other distinguishing characteristics of first-generation bikesharing were that bicycles were usually painted one bright color, unlocked, and placed haphazardly throughout an area for free use (Shahen et al., 2010).

1.1.2. Coin-Deposit Systems: Second Bikesharing Generation

Problems with free bike systems (namely, bike theft) led the city government and the City Bike Foundation of Copenhagen, Denmark, to launch a bikesharing service that was different from any previous system. In January 1995 Bycyken (City Bike) was launched as the first large-scale urban bikesharing program in Europe. Bicycles were unlocked with a 20 DKK (Danish krone) coin deposit (US$3) that was refunded on bicycle return (Shahen et al., 2010).

1.1.3. Third-Generation Bikesharing

The four main components of third-generation bikesharing programs are:

- distinguishable bicycles (either by color, special design, or advertisement);
- docking stations;
- kiosk or user interface technology for check-in and checkout; and
- advanced technology (e.g., magnetic striped card, smartcards).

Third-generation bikesharing programs are distinct because the incorporation of information technology has allowed bikesharing programs to track bicycles and user information. The incorporation of third-generation information technology has helped to deter bike theft, which was a major concern of second-generation coin-deposit systems (Bea, 2009).

1.1.4. Bikesharing: the present

Since 1965 bikesharing activity has expanded to include four continents: Europe, Asia (including Australia), North America, and South America. Not surprisingly, Europe remains the leading hub for bikesharing growth, development, and success.
At present, there are approximately 101 bikesharing programs operating in an estimated 125 cities around the world, with more than 139,000 shared bicycles. As the leader in bikesharing activity today, Europe currently has 19 nations that support bikesharing (Larsen,2013).
The Americas operate programs in Canada, Mexico, the United States, Brazil, and Chile. Asia, which represents the fastest growing bikesharing market, operates programs in China, South Korea, and Taiwan.

1.2. Bikesharing in Mexico

In Mexico City the growth of the demographic density has become exponential and so the need for transportation, because of that the city management needed to look for a sustainable way to help with this mobility issues, as 50% of trips is less than 8 kilometers away, the implementation of a Bikesharing program was viable.

Therefore, the Ecobici program was created as a public bicycle system within the Integral Transportation and Roads Program (2007-2012), which was inaugurated in 2010 with 85 stations served in 6 suburbs of the Cuauhtémoc town hall, that is in the downtown area of the city. In the next years, the program expanded to the historic center of Mexico City and the Polanco neighborhood. This program was promoted as a mobility tool, which allows moving more quickly from one public transport to another or closer to its final or intermediate destinations, seeking to strengthen public transport and improving the time of transfer, road mobility and a healthier lifestyle among the citizens (Pérez López, 2017).

Mexico City launched its Ecobici program with some 1,000 bikes in 2010, it quickly reached its limit of 30,000 annual members and started a waiting list of eager would-be cyclists. The program has quadrupled in size and remains the largest of Latin America's dozen or so programs.

1.3. Bikesharing in UNAM

Currently, the use of alternative forms of transport is booming, especially in school campuses with large volumes of people and routes, so the central campus of the Autonomous University of Mexico created the Bicycle Loan System for those belonging to the university community called: Bicipuma.
The Secretariat of Services to the University Community, through the General Direction of Attention to the University Community, in March of the year 2005 implemented the Alternative Transportation Program "Bicipuma", to promote changes of behavior patterns in our community, directed to improve health, increasing levels of physical activity and well-being. This also reduced the congestion of vehicular traffic and its harmful effects in Ciudad Universitaria and its surroundings.
The objective of the Program is to provide the user, free of charge, the means to transfer to different educational centers and university dependencies, starting from the main accesses to the campus, to carry out their school, administrative or teaching activities, and in the free time as recreational activity. The bicycle not only allows an easy and fast displacement, but also, that the community knows different spaces of the university life is through the 5,980 meters that have of cycle path, fomenting in this way their sense of belonging, coexistence and emotional well-being.
Bicipuma has 14 stations or modules, 5980 meters of cycle path ,1440 unities that serve 4500 users daily (UNAM,2018).

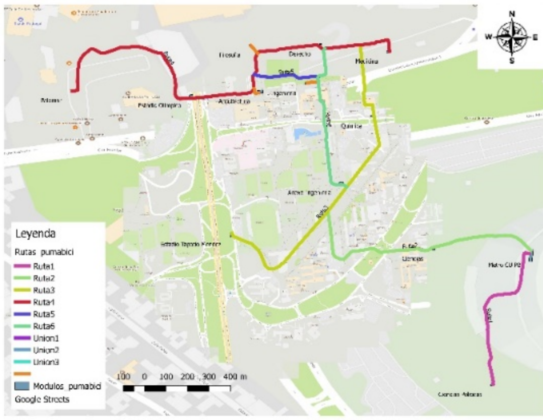

Fig. 1 Bicipuma routes.

The system in use for the loan of the bikes works in the following way: the system records the loan of bicycles, making it by the reading of the bar codes in the students or workers credential and one set on the bicycle; creating through this scan a database with the records of the account number to whom the loan is made, the date, time and exit module; the delivery of the bicycle is corroborated with the scanning of the in the delivery module, thus attaching to the database the delivery time and the module of delivery.
Damaged bicycles are collected every fifteen days for review and maintenance; the damage or wear of the mechanical parts is due to the constant use of the units.
The time spent by the users regarding the delivery of the units causes a delay in the service impacting its quality and operational costs associated to the maintenance of the units.
When observing this problem, the development of a proposal that uses the existing infrastructure for the improvement of the delivery service arise.
By implementing the proposals, the delivery and service times will be improved.
This optimization will not only impact at the operating level of the system but will improve the quality of service and reduce costs associated with the maintenance of the units and modules.
This article was developed in the following way: in section two a literature review is shown. In section three the methodology used such as the data analysis, determination of the problem and determination of the proposed solution is given. Section four shows the results obtained by the followed methodology and in the fifth section conclusions are presented.

2. LITERATURE REVIEW

The bike sharing problem has been deeper studied in the last five years, mostly with optimization methods. In this section some papers are presented.
Maggioni et al (2019) stated that Bike-sharing systems contribute towards obtaining a more sustainable mobility and decreasing traffic and pollution caused by motorized transportation. They considered the problem faced by a bike-sharing service provider who needs to manage a fleet of bikes over a set of bike stations with

given capacities, to serve the stochastic rental demand over space and time. A unit procurement cost is paid for each bike assigned to each station at the beginning of the service. The operational time frame is one day. The delivery of bikes to bike-stations is assumed to be instantaneous (lead time equal to zero), as this operation can be carried out before the start of the service. Backlogging is not allowed. A unit stock-out cost is paid if realized demand exceeds the number of bikes assigned to a station, and a unit transshipment cost is paid at the end of the rentals, when the bike-station inventory levels are rebalanced. The authors objective is to determine the number of bikes to assign to each bike-station at the beginning of the service, to minimize the expected total costs, given by the sum of the procurement costs, the expected stock-out costs for unmet demand, the expected time-waste costs for overflow and the expected transshipment costs for repositioning. According with this problem authors proposed a stochastic optimization model for the rebalancing issue that considers the randomness of user choices and demand over a determined space(infrastructure) and time (service hours) with the two reposition systems that exist: static repositions, and dynamic reposition. A case study is shown in Bergamo (Italy).

For Alvarez-Valdes et al (2016) the most important factor for the success of a public bike sharing system is its ability to satisfy the varying demands of the users and so the patterns of demand that must be identified and estimated and the system has to be planned and managed to maximize the level of customer satisfaction. The authors observed two key factors for this; the availability of bikes at the station and the availability of slots when the users arrive to leave the bicycle. The users must be confident that they will find bicycles to start their trips and available lockers to leave them when the trips are finished wherever and whenever they need them and proposed that for achieving such there are three phases to be considered:

1. Strategic level; the number of stations and their location and size must be decided.
2. Tactical level; the number of bicycles in the system has to be determined.
3. Operational level; a bike repositioning system has to be adopted for moving bicycles from stations with an excess to stations with a shortage in order to satisfy the demands forecast for the next periods.

The problem to be dealt with in this article is based on the second factor delimited by Alvarez-Valdes et al the availability of slots when the users arrive to leave the bicycle and in this particular case the service time associated with it which impacts directly in the system users perceived quality and since the system is meant to provide service to a specific type of users (students and faculty members) that times must be minimized in order to aid them.

Finally H.Si et al (2019) in their review paper Mapping the bike sharing research published from 2010 to 2018: A scientometric review, show an extensive analysis of208 articles about this topic. Based in a scientomatic analysis that can be described as a technology that demonstrates the scientific development process and structure relationship based on the knowledge domain. Based on this analysis the most significant contributions in bike sharing research primarily originated from the US, China, Canada, England and Australia. Major journals also were identified, and eight research clusters as its shown in the next figure 2.

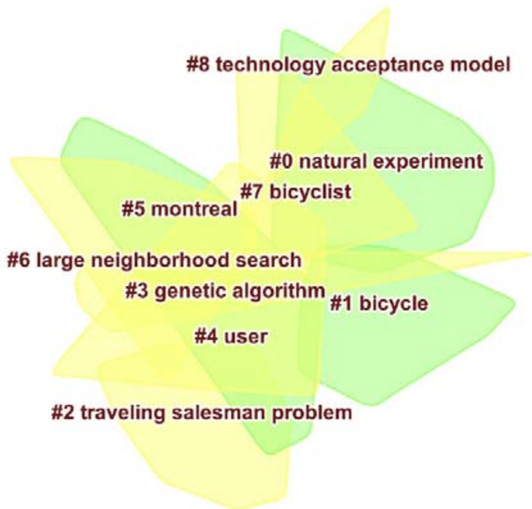

Fig. 2. Cluster analysis in the bike sharing field: 2010-2018. Source H. Si et al (2019)

Authors also identified based on the evolutionary trends of bike sharing research into four stages. The first stage from 2010 to 2012, focused on “safety and policy” issues. From 2013 to 2014, the second stage began to investigate the “benefit, system and impact” of bike sharing programs. Furthermore, the topics were subdivided into “optimization, behavior, built environment, design, and infrastructure”, which are main research themes in the third stage of 2015. The research topics that emerged in the fourth stage (2016-2018) are “demand, rebalancing, redistribution, choice, weather, usage, public transport and attitude”. In terms of knowledge domains, core studies on bike sharing that published from 2010 to 2018 are summarized and classified into five categories in view of different generations of programs. As for the third and fourth generations of programs, the main knowledge domains are divided into: 1) factor & barrier; 2) system optimization; 3) behavior & impact; 4) safety & health. About the fifth generations of programs, the main knowledge domains are divided into: 1) factor & barrier; 2) system optimization; 3) sharing economy.

After this papers review, and mostly the last one, it can be noticed that simulation is not been used, not only for the case of the bikes delivery, but not even for the complete system. That is why is important the use of hybrid methods that consider simulation and optimization.

In the case of our research, after making a bibliographic review of simulation methodologies and a subsequent analysis, it has been possible to develop a simulation model applied in Bicipuma delivery system. The use of discrete simulation was determined due to the fact we can define the state of the Bicipumas delivery system as the number of units in the system at a time in which the system is in state n in the instant t if at that time there are n units in the system, counting those waiting in line to receive service and those who are receiving service at that time.

3. METHODOLOGY

The methodology used for this work is the following:

3.1. Data analysis

The data analyzed consists of the Bicipuma loan records registered during 2016 and 2017.

With the database provided by Bicipuma, the total number of loans registered during the period from 2016 to 2017, the day and month of greatest demand, the highest and lowest demand module.

This information was analyzed with RStudio performing a Pareto analysis and histograms of the demand, with which the modules with greater and lesser demand were determined, as well as the demand by time schedule for each one of them.

This information was used to recognize the modules that need special attention regarding times of pick-ups and deliveries. This research focused in deliveries considering the delays in this activity.

3.2. Problem detection

The detection of problems was carried out first through observation and direct use of the system (field work), to subsequently conduct a series of interviews with the various actors of the system including the Director of Bicipuma module managers and modules operators.

Because of the interviews we obtained that the users find the service of Bicipuma practical even though they indicate that in some cases there´s a considerable delay in the service due to the inefficiency of the delivery system.

While the Director indicates that the system should have a better system in which the times and associated costs are minimized but without making a big investment.

3.3. Determination of the study module

The study module was determined using the data analysis described in this section even though the module is not the number one in destination demand it was selected due to its location.

The location of this module is highly important because of its proximity to one of the main entrances to the campus at the same time is located near Copilco metro station which is one of the most used means of transportation to reach the campus.

The module Medicine was selected to perform a field work in which data of variables of interest such as time of arrival and departure of the users, time in queue and time of service to be used in the simulation were collected.

3.4. Queue theory (manual) and discrete simulation

With the data obtained in the field work two simulations were made: a manual simulation with queue theory using excel and a simulation discrete simulation with SIMIO software, this is to make a comparison and validate the model.

For the discrete simulation it is necessary to identify the type of distribution presented by the data collected for each variable.

4. RESULTS

4.1. Modules with the highest demand

When performing the analysis of the information provided by Bicipuma, it was obtained that the module with the second highest delivery demand is Medicine as shown in the Table 1 and the histogram of these module is shown in Figure 3.

Table 1: Trip distribution for destination modules.

Destination module	Nr of trips	Relative frequency (%)	Accumulated frequency (%)
Anexo de Ingeniería	132318	18.0	18.0
Medicina	114914	15.6	33.7
Bicicentro Pa	7549	10.3	43.9
Ciencias	68692	9.3	53.3
Ingeniería	67546	9.2	62.5
Filosofía	62481	8.5	71.0
Derecho	46289	6.3	77.3
Química	35043	4.7	82.1
Estadio Tapatio	32436	4.4	86.6
Arquitectura	25918	3.5	90.1
Bicicentro Pb	22775	3.1	93.2
Estadio Olímpico	21427	2.9	96.1
Ciencias Políticas	18964	2.6	98.7
Palomar	9583	1.3	100.00
Total	733877		

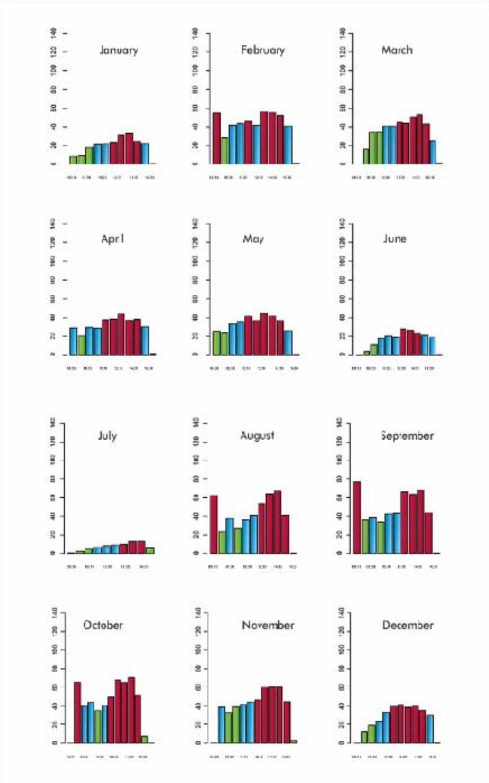

Fig. 3 Medicine module histograms

After classifying the modules, the Medicine module was selected to perform the field work and data recollection due to the reasons listed in section 3.3.

4.2. Description of the delivery system and determination of variables

To determine the variables a description of the delivering process was needed as well as its corresponding process flow diagram.

The delivery process flow diagram is shown in Figure 4, and function as follows: when a user arrives (start), depending on whether the operator is busy because of the demand of the module; he will wait in a queue for the entrance to the station (queuing), as the user enters the module (entering the module) its credential with which the loan of the unit (bicycle) was registered is presented (show ID card).If the credential corresponds to the user the operator scans said credential (scan ID card) and the bar code of the unit (scan Bike),then the operator checks if the unit usage time is between the regulated 20 minutes (time less than 20 min) ;if not, the user is sanctioned (sanction) and if it is within the allowed time then the user proceeds to the return and accommodation of the unit (delivery, accommodation) and that concludes the process (ended service).

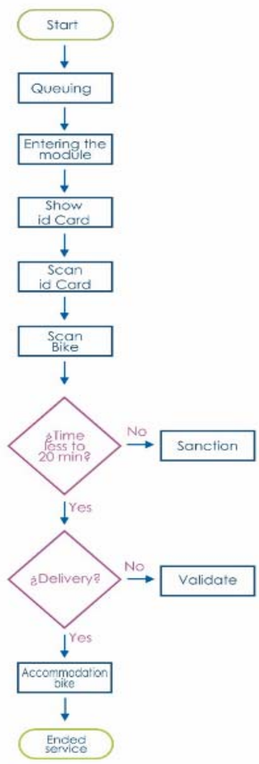

Fig. 4. Delivery process flow diagram

Then the following variables were identified:

- Attention modules.
- Module operator.
- Users.
- Bikes.
- Schedule.
- Times (service, row, arrivals)

4.3. Field work data analysis

Afterwards data collection was carried out and a total of 50 observations were taken which correspond to an hour in the system as shown in Table 2.

Table 2. Collected data from field work

User	Time in queue W	Arrival time	Time between arrivals	Service time	Exit time
1	0	2	0	27	29
2	10	2	0	34	63
3	31	2	0	27	90
4	13	23	21	22	112
5	21	23	0	24	136
6	4	47	24	45	181
7	0	73	26	25	206
8	14	78	5	33	239
9	7	93	15	28	267
10	10	100	7	20	287

The analysis consists of identifying the type of distribution presented by the data collected, the data obtained from the observation was plotted.

4.3.1. Times between arrivals

In Figure 5 the time between arrivals is shown, for those times, the points on the graph follow a straight line within the confidence borders and the p value is greater than the significance level (0.05). For these data, the distributions: normal, lognormal, exponential and Weibull do not provide an adequate fit for the data as shown in Figure 6.

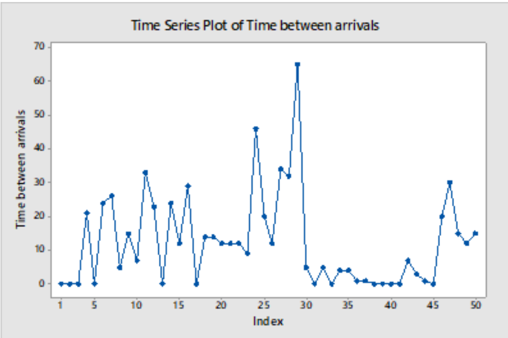

Fig. 5. Time between arrivals plot.

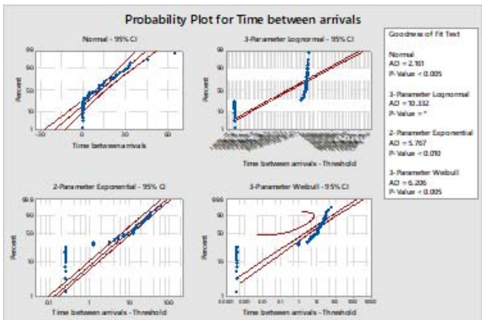

Fig. 6. Time between arrivals probability plot.

4.3.1. Service time

In Figure 7 the service time plot is shown, for this data the distributions: normal, lognormal, exponential and Weibull with a level of significance (0.05) were plotted as shown in Figure 8, the distribution that provides a more adequate fit for the data is the lognormal.

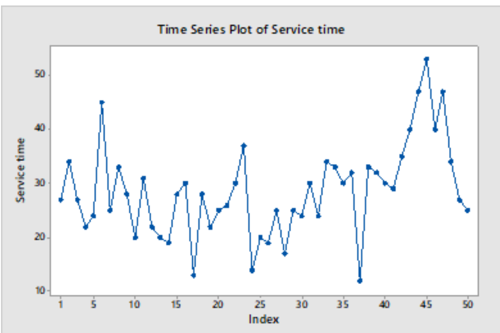

Fig. 7. Service time plot.

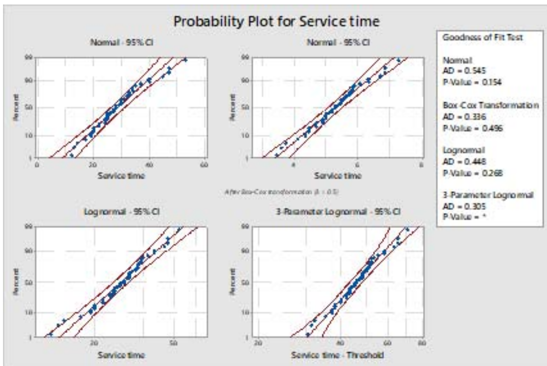

Fig. 8. Service time probability plot.

4.3.1. Arrival time

In Figure 9 the arrival time plot is shown, for this data the distributions: normal, lognormal, exponential and Weibull do not provide an adequate fit for the data as shown in figure 10.

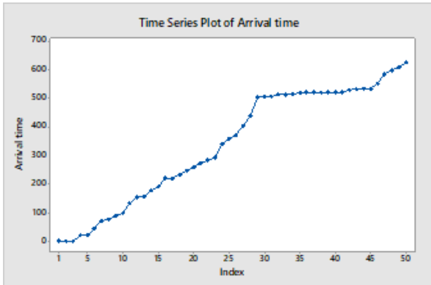

Fig. 9 Arrival time probability plot.

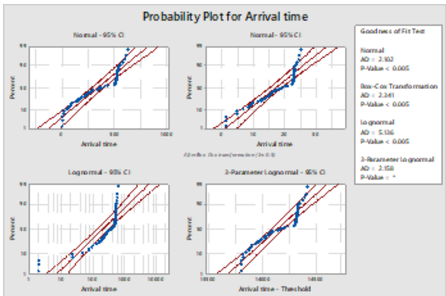

Fig. 10 Arrival time probability plot.

4.4. Queue theory (manual simulation)

Users who require a service (return of bicycles) enter the system and join a waiting queue. At a certain moment, a user of the queue is selected to provide the service the process is shown in Figure 11.

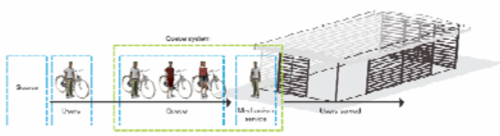

Fig. 11. Delivery service process

The basic components of the queuing process of the Bicipuma system are:

- Input source: Finite, bounded by the number of total bicycles.
- Queue: Finite, bounded by the number of total bicycles that the module can receive.
- Discipline of the queue: The order in which users are selected to receive the service is FIFO (first input first output).
- Service mechanism: Consists of a single service installation, with a single service channel.

The data provided for this queueing process is shown in Table 3 from these the probability that there are exactly n customers in the system(Pn),the expected length of the queue including users who are in service(Lq),the wait time in the queue excluding service time for each client(Wq) and the user in the average system we calculated resulting as shown in Table 4.

Table 3. Collected data from field work

Arrival rate (λ), per hour:	**50**
Service rate (μ), per hour:	**70**
Number of servers or channels	**1**

Table 4. Collected data from field work

$L_s = \frac{\lambda}{\mu - \lambda} =$	2.5	Average users in system
$W_s = \frac{1}{\mu - \lambda} =$	0.05	Hours that the average user spends in the whole system
$L_q = \frac{\lambda^2}{\mu(\mu - \lambda)} =$	1.786	Number of bicycles that are waiting to be served by the server
$W_q = \frac{\lambda}{\mu(\mu - \lambda)} =$	0.036	Average wait time of a user in a queue waiting for the service
$\rho = \frac{\lambda}{\mu} =$	0.71	Percentage of the time the operator is busy attending to users
$P_0 = 1 - \frac{\lambda}{\mu} =$	0.29	Probability that there are no users in the system (who are attending or who are in the queue) at any given time

Figure 12 shows an example of how the manual simulation was carried out which results are shown in Table 5.

40	User 23 arrival	T=	294
41	User 11 departure	T=	318
42	User 12 departure	T=	340

43 Future events actualization

Hour, T[s]	Event
100	User 10 arrival
133	User 11 arrival
156	User 12 arrival
156	User 13 arrival
180	User 14 arrival
192	User 15 arrival
221	User 16 arrival
221	User 17 arrival
235	User 18 arrival
249	User 19 arrival
261	User 20 arrival
273	User 21 arrival
285	User 22 arrival
287	User 10 arrival
294	User 23 arrival
318	User 11 departure
340	User 12 departure

Fig. 12 Manual simulation

Table 5. Results of manual simulation

Average queque time	Average utilization of installation	Average length from the queue
5.2773	99.86004199	11.07907628

4.5. Discrete simulation (Simio Software)

This simulation was carried out in Simio Software with its corresponding distributions:

- Time between arrivals: Poisson (12)
- Arrival rate: Exponential (12)
- Service time: Exponential (12)

The distributions were selected since when testing the different distributions in the simulation those are the ones that best represent the real behavior of the system. Figure 13 shows an image of how the simulation facility was created, the user enters the loan module in which a bike is picked using a combiner both bike and user are matched, then they follow a path to the delivery facility in which by means of a separator the bike is placed in the module and the users ends the process.

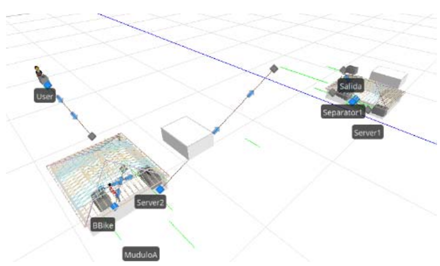

Fig. 13. Simulation facility

After running the simulation for an hour which was the time the data collection and manual simulation was made the results obtained are shown in Table 6.

Table 6. Results of Simio simulation

Average queque time	Average utilization of installation	Average length from the queue
5.2773	99.76	11.07907628

4.6. Comparison of simulations

When comparing the simulations results the difference between simulations results is minimal so we can indicate that the results are valid. The comparison is shown in Table 7.

Table 7. Comparison of simulation results

Simulation Type	Average queque time	Average utilization of installation	Average length from the queue
Manual	5.2773	99.8600419	11.079076
Simio	4.956	99.76	10.965
Difference	.3213	.010004199	.11407628

4.7. Simulation of a second scenario

The final goal is to achieve an economic balance between the cost of service and its associated cost by waiting. The following analysis proposes to determine the number of optimal operators to attend the different schedules in the period of attention to users.

For this particular, the same medicine module will be analyzed taking the following data:

- Hours of service: 6:30 - 4:30
- Salary of the staff that attends the module: $ 33.24 / hour
- User waiting time (one operator): 0.035 h (2.143min), calculated.
- User waiting time (two operators): 0.023h (1.39min). -Estimated- (65%)
- User waiting time (three operators): 0.014H (0.84 min). -Loved- (40%)
- Average number of users: 50

With the information provided, the number of employees to be hired and their associated optimal cost will be determined to minimize the waiting time, this information is shown in Table 8.

Table 8. Information associated to costs

Average users per shift	500
Hours per schedule	10
Average waiting time for user (minutes)	
One operator	2.143
Two operators	1.39
Three operators	.84
Four operators	.73
Operator wage per hour	$33.24
Operator wage per shift	$332.40

Table 9. Associated costs per number of operators

	Number of operators			
Concept	1	2	3	4
Average users number per shift	500	500	500	500
Average queueing time per users	2.143	1.39	0.84	0.72862
Total time of queueing	1071.5	695	420	364.31
Salary cost per shift	$ 332.40	$664.80	$997.20	$1,329.60
Total cost per shift	$ 332.40	$664.80	$997.20	$,329.60

From the previous analysis shown in Table 8 it can be seen that three operators drastically reduce the waiting time of the users of the system, however, due to the cost restriction and the limitation of the registration equipment, it is considered that the optimal number of operators per module is two, which implies a waiting time of 1.39 minutes per user with a cost of $ 664.80 per working hours.

This analysis suggests the opportunity to use two operators at peak times to speed up the service loan to users.

5. CONCLUSIONS

Bicipuma bikesharing system is functional to its users, even though it is not in optimal service conditions due to the long waiting queues for service that occur during peak hours and in high demand modules which generates high associated costs and impacts directly in the quality of the given service.

By carrying out the simulation the problematic in the system became more evident as well as the necessity of implementing a more efficient system for the delivery of the bicycles, so the proposal of adding a second server was considered but due to the lack of resources and the cost associated with this proposal, a lower cost alternative is sought which considers the use of the existing infrastructure.

This proposal analyzes re-defining the layout in such a way that they minimize bottlenecks and, which allow users to reduce the time they perform the delivery service of bicycles, to achieve the certain areas are proposed dedicated to specific activities, these areas are as shown in Figure 14:

- Loading and unloading area: It allows to supply and collect the bicycles to the station (with the truck)

- Bicycle delivery area: Allows the user to deliver the bicycle without "colliding" head-on with the users who come to request the loan service.
- Entry area: Allows the user to request the loan service without "crashing" with the users who deliver the bicycles.
- Exit zone: Allows the user to exit the module without "crashing" with other users (those who request the loan and those who deliver the bicycles).

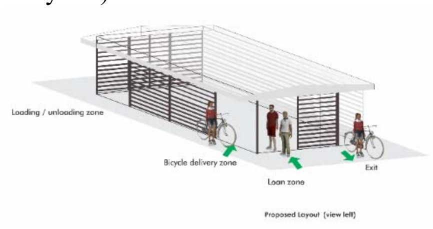

Fig. 14. Outside proposed layout

Another proposal that emerges as part of the analysis consists of the internal distribution of the module which suggests three specific zones as shown in Figure 15:

- Loading and unloading warehouse area: It allows to place the excess of bicycles that are in the module, in addition, this area will allow users who wish to choose between some of the bicycles that are found there.
- Decomposed bicycle zone: Allows the operator to place the decomposed bicycles reported by users, or that are considered to require maintenance. This area is suggested near the loading and unloading warehouse area so that the pickup truck can take them without moving in a considerable way.
- Fast service area: Allows the user to request the loan service without possibility to choose the bicycle that will be carried, the choice will be made in the order in which the bicycles are placed. Aiming to reduce the time it takes for users to choose a bicycle (either for pleasure or necessity).

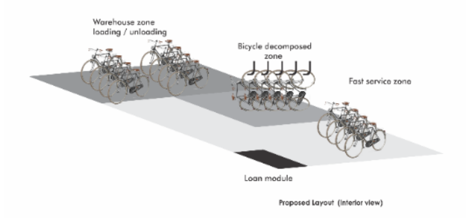

Fig. 15. Inside proposed layout

Also, the service quality will improve by not making the users wait long periods of time when delivering the bicycles and having a continuous service throughout the entire day and in the moment that it is needed.

ACKNOLEDGMENTS

To the PAPIIT DGAPA project IT102117, UNAM for its support to this research.

REFERENCES

Bea Alonso, M., & Pasqual i Robert, J. (2009). Los sistemas de bicicletas públicas urbanas.

Gordillo Sotelo, C. (2016). Estado del Arte. Características y Experiencias de los Sistemas de Bicicletas Público en América Latina y Consideraciones para la Implementación del SBP en Bogotá.

Shahen Susan et al. (2010) Bike sharing in Europe, the Americas, and Asia: Past, Present, and Future.

Larsen Janet. Bike-Sharing Programs Hit the Streets in Over 500 Cities Worldwide (2013), Earth Policy Institute.

Perez López Ruth (2016). Vínculos entre la bicicleta utilitaria, recreativa y deportiva: análisis del impacto de los programas “Ecobici” y “Muévete en Bici” en la Ciudad de México (2006-2012).

Winston WL. Investigación de Operaciones. Aplicaciones y Algoritmos. 4ta ed. Stamford: Editorial Thomson Internacional; 2004.

Chase RB, Jacobs FR, Aquilano RJ. Administración de Operaciones. 12ma ed. México D.F.: McGraw–Hill Interamericana; 2009.

Shortle JF, Thompson JM, Gross D, Harris CM. Fundamentals of Queueing Theory. 5th Edition. New York: John Wiley & Sons, Inc.; 2017.

Aspray, William. John Von Neumann and theOrigins of Modern Computing. Massachusetts. The MIT Press. p. 110-113.

Abu-Taieh, Evon M. and Rahman El Sheikh, Asim Abdel. Handbook of Research on Discrete Event Simulation Environments: Technologies and Applications. New York. Information Science Reference. p. 1.

Chung, Christopher A. Simulation Modeling Handbook, a practical approach. CRC Press. Boca Raton, FL. 2004. P3-20.

Banks, Jerry. Handbook of Simulation, principles, methodology, advances, applications and practice. Engineering & Management Press. Toronto. 1998. P.721-745.esas, PP 208-245.

Maggioni, F. (2019). Stochastic optimization models for a bike-sharing problem with. European Journal of Operational Research, 272-283.

Si, H. (2019). Mapping the bike sharing research published from 2010 to 2018: A scientometric review. Journal of Cleaner Production, 415-427.

Valdes, R. A. (2016). Optimizing the level of service quality of a bike-sharing system. Omega, 163-175.

UNAM (2018). BICIPUMA. Dirección General de Servicios Generales y Movilidad. Retrieved from: http://dgsgm.unam.mx/bicipuma.html, on 22-05-2018.

A RANKING OF THE MOST KNOWN FREEWARE AND OPEN SOURCE DISCRETE-EVENT SIMULATION TOOLS

António A.C. Vieira[(a)], Luís M.S. Dias[(b)], Maribel Y. Santos[(c)], Guilherme A.B. Pereira[(d)], José A. Oliveira[(e)]

[(a),(b),(c),(d),(e)] 4710-057, PORTUGAL
University of Minho
ALGORITMI Research Centre

[(a)]antonio.vieira@dps.uminho.pt, [(b)] lsd@dps.uminho.pt [(c)] maribel@dsi.uminho.pt, [(d)]gui@dps.uminho.pt,
[(e)]zan@dps.uminho.pt

ABSTRACT
Freeware and open source simulation software can be of great relevant when applying simulation in companies that do not possess the required monetary resources to invest in traditional commercial software, since these can be unaffordable Even so, there is a lack of papers that contribute to literature with a comparison of opensource and freeware simulation tools. Furthermore, such existing papers fail to establish a proper assessment of these type of tools. In this regard, this paper proposes a study in which several freeware and open source discrete-event general purpose simulation tools were selected and compared, in order to propose a ranking based on the tools' popularity, considering several criteria. For this purpose, 30 criteria were used to assess the score of each tool, leading to a podium composed by SimPy, JSim and JaamSim. Further conclusion and future work are discussed in the last section.

Keywords: Discrete-Event Simulation, Freeware, Open source, ranking, comparison, review.

1. INTRODUCTION
Discrete-event Simulation (DES), or just simulation, as many times is referred by other authors, is a technique used to run models on computers that represent systems being analyzed (A. A. C. Vieira et al. 2017, 2018). Furthermore, DES deals with stochastic behaviors, uncertainty, thus being appropriate to deal with complex systems that cannot be efficiently and effectively dealt by alternative approaches, e.g. analytical or mathematical models (Park et al. 2010). DES can be used for many objectives and the literature on studies using it is vast. With simulation, users can: study different components of a system and their interactions, communicate better with stakeholders involved in the problem, study alternatives without incurring in unnecessary costs or danger, solve complex problems, help in decision-making, and others (Fowler and Rose 2004; A. Vieira et al. 2014; António Vieira et al. 2014).
Usually, modelers make use of commercial simulation software, such as Arena, Simio, ProModel, FlexSim, WITNESS, PlantSimulation, AnyLogic and others (A. Vieira et al. 2015, 2016). However, while it is true that these tools have helped modelers in adopting and using DES, providing features for modelling, debugging and experimentation, it is also true that such software often are expensive, which many times are prohibitive for some companies, potentially leading to the abandonment of DES.
For the above-exposed reason, freeware and open source simulation tools can be viewed as a solution to implement DES, in specific cases. Open source software is defined by Google as "software for which the original source code is made freely available and may be redistributed and modified" ("Google" 2019). In its turn, Google defines freeware as: "software that is available free of charge" ("Google" 2019). As can be seen, these are two types of software that usually do not entail costs to modelers. In fact, because of this, many times these two concepts are confuse.
There are several simulation freeware and open source tools available on the internet and there are also some studies that compare some of these tools. For instance, Dagkakis and Heavey (2016) considered 44 open source in their study. In this scenario of such large tools' offer, it becomes very hard and non-conclusive to perform a consistent experiment based on features. In fact, most of scientific works related to tools comparison analyze only a small set of features and ultimately avoiding a final judgment, due to the subjectivity of such task.
It is in the light of this that this paper proposes a ranking of the most popular freeware and open source simulation software. "Popularity" was the way that the authors found to overcome the mentioned difficulties. In this sense, choosing a popular simulation tool may bring benefits in two different perspectives:

- If you are with a company, it is easier to find simulation specialists with know-how on a popular tool;
- If you are a simulation specialist, it is easier to find companies working with a popular tool;

Notwithstanding, popularity should not be solely used to select simulation tools. If this was the case, new ones, would never be used. Therefore, popularity may be seen as a significant factor to be used in conjunction with other criteria, such as features comparison.
In this regard, next section addresses the literature review conducted for this study. In its turn, section 3 described the methodology followed to select the tools used in the study and the criteria used to rank them. Section 4 focuses in explaining how the results are obtained, while section 5 shows the obtained classification. Last section presents the main conclusions withdrawn.

2. LITERATURE REVIEW

Several studies exist that compare discrete-event simulation software. For instance, regarding commercial tools' comparison, Hlupic (1999) compared a set of tools, distinguishing between users of software for educational purpose and users in industry. The same author (2000) presented a survey on the use of simulation software for academic and industrial users, which was conducted to discover how users were satisfied with the software and in which ways it could be improved.
Similarly, Abu-Taieh et al. (2007) reviewed 56 simulation tools to find answers for several aspects, such as: modelling approach, reporting features, programming language used, type of animation, simulation approach (i.e. discrete-event, dynamic continuous, etc.) and others.
In its turn, Jadrić et al. (2014) compared some simulation tools by developing the same considered model in the considered tools. Thereafter, the authors compared them, according to specified subjective and objective indicators.
Klingstam and Gullander (1999) outlined most used simulation tools in manufacturing engineering and Computer-Aided Production Engineering. The authors discussed most important features to consider when selecting the most appropriated software.
All these review papers or comparison studies, however, fail to make a judgement, or to somehow rank the considered tools. In this regard, Dias et al. (2007), Dias et al. (2011) and Dias et al. (2016) achieved this by ranking selected discrete-event simulation commercial software according to their "popularity", or presence in several fields, such as social networks, academic digital libraries and many others.
The mentioned studies compared commercial tools, by considering some criteria. However, in the case of open source or freeware simulation tools, there is a lack of such studies, to the best of the authors' knowledge. In fact, and corroborating what was stated by Byrne et al. (2012) there are limited papers considering open source or freeware simulation tools. Moreover, and a fortiori, existing studies fail to rank the considered tools.

3. METHODOLOGY

The methodology followed for this study is adapted from the works of Dias et al. (2007), Dias et al. (2011) and Dias et al. (2016). The main changes are related to the natural difference between commercial software and freeware and open source software, which is the existence of a vendor. Furthermore, some parameters have been removed or added along the years, because they either cease to be relevant, or become relevant, respectively.
This methodology can be divided in 3 groups. The first concerns with obtaining the list of tools that will be used on the ranking. In its turn, the second consists in defining the set of criteria to be used on the study, whilst the last group is related to obtaining the results for each defined criterion. Lastly, it should be stressed that this ranking only considered discrete-event simulation tools that are general purpose.

3.1. Tools Selection

The selection of tools used the following 2 main sources of information:

- Internet sources, such as: Informs ("Informs" 2019), Eurosis (Eurosis. 2019), Wikipedia ("Wikipedia" 2019);
- Available literature, e.g.: Dagkakis and Heavey (2016), King and Harrison (2013) and others.

Whilst the authors also had their own knowledge which allowed them to identify some of these tools, it should be noted that there were no cases of tools identified by own knowledge that could not be identified by the previous identified sources.

3.2. Defined Criteria

For this study, 30 criteria were considered. These can be grouped in the following 6 criteria groups:

- C1: Number of papers published in Winter Simulation Conference (world's largest simulation conference) that refer the simulation tool at hand;
- C2: Number of papers published in digital libraries (Scopus, Science Direct and Google Scholar) that refer to a simulation tool;
- C3: Number of results obtained by searching for the tool at hand in a social network (either Youtube, Facebook, Linkedin, Twitter or Google Plus);
- C4: Number of results obtained by searching for the tool in Google;
- C5: Analysis of the growth evolution of the results obtained in Google for a given tool;
- C6: Number of times a specific tool has been referred in a comparison paper, or a paper that considers several freeware or open source simulation tools;
- C7: Checking if the tool has a web site to disseminate it.

3.3. Obtaining Results

The number of occurrences of a search query may vary from units to several millions. The sum of all of them together leads to irrelevant factors mixed with absorbent ones. To reduce this impact of different orders of magnitude, the use of mathematical functions was studied, in order to "control" big numbers, albeit keeping the relative differences between them. In this regard, square and cubic root, natural and ten base logarithms were the evaluated possibilities. Table 1 shows the values of the parameters' factors adjusted and the corresponding original raw values.

Table 1: Possible Functions to Factors Adjustment.

	^1/2	^1/3	LN	LOG10
1000000	1000	100	14	6
100000	316	46	12	5
10000	100	22	9	4
1000	32	10	7	3
100	10	5	5	2
10	3	2	2	1
1	1	1	0	0

As can be seen, cubic root function considers small and big numbers adequately. Thus, it was used in this study. The use of a cubic root of a number in place of the number itself, is the same as comparing the volume of cubes, using only the value of their width.

4. RESULTS ANALYSIS

The results obtained for this study will be discussed in this section, for each of the defined criteria groups (see section 3). Figure 1 shows the results obtained for WSC (Winter Simulation Conference).

DES Freeware Tools	https://informs-sim.org/	#1 Winter Simulation Conference	
Weight		3	
	Search String	Cubic Root Results	Raw Results
C++Sim	"C++Sim"	5,7	7
cloudes	"cloudes"	4,3	3
CSIM	"CSIM" "simulation" "C" "discrete"	9,8	35
DESMO-J	"DESMO-J"	6,9	12
DEUS	"DEUS" "Discrete Event Universal Simulator"	4,3	3
FreeSML	"FreeSML"	4,3	3
JaamSim	"JaamSim"	6,0	8
jadesim	"jadesim"	0,0	0
japrosim	"japrosim"	3,8	2
javaSim	"javaSim"	8,0	19
JSIM	"JSIM"	9,5	32
khronos DES	"khronos DES"	0,0	0
sharpsim	"sharpsim"	3,0	1
SIM.JS	"SIM.JS"	0,0	0
sim4edu OESjs	"sim4edu OESjs"	0,0	0
SimJ	"simj"	3,0	1
simjava	"simjava"	7,7	17
simkit	"simkit"	11,5	56
simmer	"simmer" "simulation" "R" "discrete"	0,0	0
SimPy	"SimPy"	8,7	24
SSJ	"ssj" "stochastic" "simulation" "java"	9,0	27
Tortuga	"Tortuga"	4,3	3
Yetisim	"Yetisim"	0,0	0

Figure 1: Factor values for WSC

The column "Raw Results" gives the number of results obtained by searching for the "search strings" column values in the WSC website (https://informs-sim.org/). At this point, the cubic root mathematical function is applied and multiplied by the weight factor (3 in this case), in order to obtain "Factor value" column values.

As can be seen, SimKit was the tool that obtained more results. It should also be noted that there are 6 tools that obtained 0 results. Figure 2 illustrates the values obtained for the second criteria (see section 3).

DES Freeware Tools	#2 Google Scholar	#3 Scopus	#4 Science Direct
C++Sim	3,3	2,7	2,4
cloudes	5,3	1,8	0,0
CSIM	12,2	1,9	4,8
DESMO-J	6,7	2,4	1,9
DEUS	1,0	1,0	2,4
FreeSML	2,0	1,0	0,0
JaamSim	3,4	1,6	1,3
jadesim	1,9	0,0	0,0
japrosim	2,6	1,9	0,0
javaSim	8,2	2,2	3,6
JSIM	8,8	2,3	3,6
khronos DES	1,0	0,0	0,0
sharpsim	2,4	1,3	1,0
SIM.JS	0,0	0,0	1,0
sim4edu OESjs	0,0	0,0	0,0
SimJ	7,8	1,3	1,6
simjava	10,6	2,6	3,6
simkit	9,1	2,7	3,5
simmer	1,0	1,8	5,1
SimPy	8,9	2,6	3,9
SSJ	5,9	1,4	1,9
Tortuga	4,1	0,0	0,0
Yetisim	1,4	1,0	0,0

Figure 2: Factor values for Google Scholar, Scopus and Science Direct

The first thing to consider is that for this set of criteria, the weight 1 was used, contrarily to the previous criterion. Regarding the obtained results, the tools with most results are SimPy, SimKit, CSIM and SimJava, whilst SIM.JS, sim4edu, Khronos DES and Jadesim were the ones that obtained less results. Figure 3 shows the results obtained for the social networks criteria (see section 3).

DES Freeware Tools	#5 Youtube	#6 Linkedin	#7 Facebook	#8 Twitter	#9 Google Plus
C++Sim	0,0	1,3	0,0	0,0	0,0
cloudes	2,6	2,2	0,0	1,4	0,0
CSIM	1,0	3,4	0,0	0,0	0,0
DESMO-J	1,7	1,6	1,0	0,0	0,0
DEUS	0,0	1,0	1,0	0,0	0,0
FreeSML	0,0	0,0	0,0	0,0	0,0
JaamSim	5,4	3,2	1,0	1,3	1,7
jadesim	0,0	0,0	0,0	0,0	0,0
japrosim	0,0	0,0	0,0	0,0	0,0
javaSim	0,0	1,6	0,0	0,0	0,0
JSIM	1,9	2,7	0,0	0,0	1,0
khronos DES	0,0	0,0	0,0	0,0	0,0
sharpsim	0,0	1,0	1,3	0,0	0,0
SIM.JS	1,3	2,7	0,0	0,0	0,0
sim4edu OESjs	0,0	0,0	0,0	0,0	0,0
SimJ	0,0	1,6	0,0	0,0	0,0
simjava	1,6	2,2	1,3	0,0	0,0
simkit	1,4	3,3	1,4	0,0	0,0
simmer	2,0	1,4	0,0	1,3	1,4
SimPy	7,5	5,3	1,7	1,6	2,1
SSJ	0,0	0,0	0,0	0,0	0,0
Tortuga	0,0	2,0	4,0	0,0	0,0
Yetisim	0,0	1,0	0,0	1,3	0,0

Figure 3: Factor values for Youtube, Linkedin, Facebook, Twitter and Google Plus

The first thing to notice is that there are many tools without presence in the selected social networks, e.g., SSJ, Sim4edu, Japrosim, FreeSML, Khronos DES, Jadesim and others. These networks are useful for users, for instance, to help members in interacting with the tools. On the other hand, there are only 2 tools without 0 in any of the selected social networks: SimPy and JaamSim. Figure 4 shows the results obtained for the fourth and fifth criteria, i.e., Google results and the growth evolution of the Google results.

For the 2 sets of criteria represented in Figure 4, different weight values were assigned, in order to give more importance to more recent values. In this regard, the raw results are shows in a red (less results) to green (more results) scale. As can be see, all tools are increasing their results along the years. Furthermore, JSIM, Simmer and JaamSim were the tools with most Google results, whilst JSIM, SimPy and CSIM were the tools with most Google results growth. It is also interesting to note that, from the analyzed tools none seems to be decreasing their Google Results, indicating an overall growth of open source and freeware simulation tools. Figure 5 shows the results obtained for the sixth set of criteria (see section3). Regarding this criterion, the following papers were considered:

- Page et al. (1997);
- Sawhney and Mund (1998);
- Sawhney et al. (1999);
- Miller et al. (2000);
- Sawhney et al. (2000);
- L'Ecuyer et al. (2002);
- Weatherly and Page (2004);
- L'Ecuyer and Buist (2005);
- King and Harrison (2013);
- Peixoto et al (2017);
- Dagkakis and Heavey (2016).

By considering Figure 5, it should be noted that, for each selected paper, a weight of 0.5 was assigned. The titles of the chosen papers can be seen in the heading of this figure. SimKit, SimJava, JavaSim and JSIM were the tools with better results, whilst Cloudes, simmer, sim4edu, SimJ, FreeSML and Khronos DES obtained 0 in this criterion. Figure 6 shows the results obtained for the last considered criterion (see section 3).

DES Freeware Tools	#10 Google		#11 2011	Web searches post-2011	#12 2012	Web searches post-2012	#13 2013	Web searches post-2013	#14 2014	Web searches post-2014	#15 2015	Web searches post-2015	#16 2016	Web searches post-2016	#17 2017	Web searches post-2017
C++Sim	3,9	2220	5	0,7	1	0,5	3	0,9	3	1,0	5	1,4	4	1,4	6	1,8
cloudes	4,6	3700	0	0,0	0	0,0	4	1,0	9	1,5	5	1,4	9	1,9	39	3,4
CSIM	6,2	8760	70	1,6	71	2,1	124	3,0	193	4,0	212	4,8	198	5,3	184	5,6
DESMO-J	6,0	8180,0	32	1,3	30	1,6	29	1,8	57	2,7	44	2,8	42	3,1	35	3,3
DEUS	2,7	707	3	0,6	3	0,7	5	1,0	3	1,0	4	1,3	1	0,9	1	1,0
FreeSML	2,5	560	0	0,0	0	0,0	0	0,0	0	0,0	0	0,0	0	0,0	1	1,0
JaamSim	6,5	10200	6	0,7	1	0,5	41	2,1	43	2,5	73	3,3	97	4,1	81	4,3
jadesim	0,6	9	0	0,0	0	0,0	0	0,0	1	0,7	0	0,0	0	0,0	0	0,0
japrosim	2,7	738	1	0,4	0	0,0	8	1,2	5	1,2	3	1,2	2	1,1	2	1,3
javaSim	6,2	8760	37	1,3	29	1,5	49	2,2	52	2,6	78	3,4	62	3,6	121	4,9
JSIM	7,2	14100	172	2,2	156	2,7	271	3,9	285	4,6	345	5,6	356	6,4	293	6,6
khronos DES	1,7	194	0	0,0	1	0,5	0	0,0	2	0,9	4	1,3	0	0,0	0	0,0
sharpsim	2,3	473	4	0,6	0	0,0	1	0,6	2	0,9	1	0,8	1	0,9	0	0,0
SIM.JS	5,1	4870	8	0,8	10	1,1	46	2,1	62	2,8	57	3,1	94	4,1	62	4,0
sim4edu OESjs	2,3	448	0	0,0	0	0,0	0	0,0	0	0,0	0	0,0	6	1,6	8	2,0
SimJ	3,4	1360	3	0,6	1	0,5	1	0,6	3	1,0	0	0,0	1	0,9	0	0,0
simjava	5,1	5020	34	1,3	34	1,6	78	2,6	87	3,1	100	3,7	104	4,2	70	4,1
simkit	5,5	5970	55	1,5	53	1,9	70	2,5	122	3,5	178	4,5	155	4,9	127	5,1
simmer	6,9	11500	41	1,4	36	1,7	76	2,5	94	3,2	104	3,7	110	4,3	172	5,5
SimPy	6,2	8850	64	1,6	70	2,1	143	3,1	155	3,8	179	4,5	204	5,3	267	6,5
SSJ	4,6	3710	5	0,7	20	1,4	9	1,2	8	1,4	39	2,7	30	2,8	23	2,8
Tortuga	5,0	4520	1	0,4	2	0,6	8	1,2	6	1,3	6	1,5	1	0,9	4	1,6
Yetisim	2,1	356	0	0,0	0	0,0	0	0,0	0	0,0	0	0,0	0	0,0	3	1,4

Figure 4: Factor values obtained for Google and the growth evolution of Google factor values

DES Freeware Tools	#18 A review of open source discrete event simulation software for operations research	#19 The JSIM web-based simulation environment	#20 Open-source simulation software jaamsim	#21 Free and open-source simulation software “ururau”	#22 Web-Based Simulation in Simjava Using Remote Method Invocation	#23 Ssj: a framework for stochastic simulation in java	#24 Efficient process interaction simulation in java: implementing co-routines within a single java thread	#25 Simulation in Java with SSJ	#26 simulation based construction management learning system	#27 Javabeans-based framework for construction simulation	#28 Java-based simulation of construction processes using silk	Reviews	
C++Sim												3	7,9
cloudes												0	0,0
CSIM												2	6,9
DESMO-J												4	8,7
DEUS												1	5,5
FreeSML												0	0,0
JaamSim												2	6,9
jadesim												1	5,5
japrosim												1	5,5
javaSim												8	11,0
JSIM												7	10,5
khronos DES												0	0,0
sharpsim												1	5,5
SIM.JS												1	5,5
sim4edu OESjs												0	0,0
SimJ												0	0,0
simjava												8	11,0
simkit												10	11,8
simmer												0	0,0
SimPy												1	5,5
SSJ												3	7,9
Tortuga												3	7,9
Yetisim												1	5,5

Figure 5: Factor values for selected papers

DES Freeware Tools	#30 Web site		
C++Sim		0	0,0
cloudes	https://beta.cloudes.me/	1	2,0
CSIM		0	0,0
DESMO-J	http://desmoj.sourceforge.net/home.html	1	2,0
DEUS		0	0,0
FreeSML		0	0,0
JaamSim	http://jaamsim.com/	1	2,0
jadesim		0	0,0
japrosim		0	0,0
javaSim		0	0,0
JSIM	http://www.physiome.org/jsim/	1	2,0
khronos DES		0	0,0
sharpsim		0	0,0
SIM.JS	http://simjs.com/	1	2,0
sim4edu OESjs	http://sim4edu.com/	1	2,0
SimJ		0	0,0
simjava		0	0,0
simkit		0	0,0
simmer		0	0,0
SimPy	https://simpy.readthedocs.io/en/latest/	1	2,0
SSJ		0	0,0
Tortuga		0	0,0
Yetisim		0	0,0

Figure 6: Factor values for the tools' web site assessment criterion

For this criterion a weight of 2 was considered. Furthermore, tools that have web pages for several types of content, therein including content related to a specific tool (e.g., web page of a university's department which developed a tool, includes reference to a tool in its web page), were not considered. As the figure suggests, only 7 tools were found that match the established restrictions for the web page assessment.

5. RANKING THE SIMULATION TOOLS

This section describes the process of obtaining the final ranking of each assessed tool. In this regard, the steps can be summarized as follows:

- The first step is to sum the values [S] of the criteria of each group (see section 3).
- Thereafter, to neutralize different categories scales, the resulting values were normalized. Thus, the upper ceiling [C] value was calculated. This corresponds to the sum of the average of the sums [A(S)] with the standard deviation of the sums [D(S)], the latter being multiplied by 1.5 [C = A(S)+1.5*D(S)].
- Each criteria group's score is then calculated, by dividing its sum by C [S/C], and multiplying it by 10, truncating the maximum value to 10. As result, all obtained criteria's scores are between 0 and 10.

The obtained values can be seen in Figure 8. The same figure also shows the final score obtained for each tool, which is obtained by calculating a pondered average between the obtained values and the corresponding weights to the criteria. To assign the subjective weights to the sets of criteria the authors formed the following 3 groups:

- Presence in internet, as a whole. (fourth and fifth sets of criteria in section 3, or WWW and Growth in Figure 8);

- presence in academy, in particular (first, second and sixth sets of criteria in section 3, or WSC, Docs and Reviews in Figure 8);
- presence in social networks, in particular (third and seventh sets of criteria in section 3, or Social and Web site in Figure 8).

For each of these 3 groups, 4 weights points were assigned, as described in Figure 8, with the final results specified in the same figure. In its turn, Figure 7 shows the scores grouped by each set of criteria.
With the ranking completed, it can be seen that SimPy was the tool placed in the first position, followed very closely by JSIM, with the podium being finalized with JaamSim. A reference should also be made to Cloudes, which, to the best of the authors' knowledge, is the tool that allows users to work on the cloud that is best placed in this ranking. As indicated by Figure 7 this classification of Cloudes concerns with its lack of presence in academy, namely: in WSC, review papers and selected digital libraries (Google Scholar, Scopus and Science Direct). Khronos DES and Jadesim were tools ranked in the last places. An honorable mention can also be done to other tools that were also considered for this study but did not enter the final ranking, as they did not obtain the minimum score. Those tools including: Simjulia, DSOL, Salabim and XGDESK.

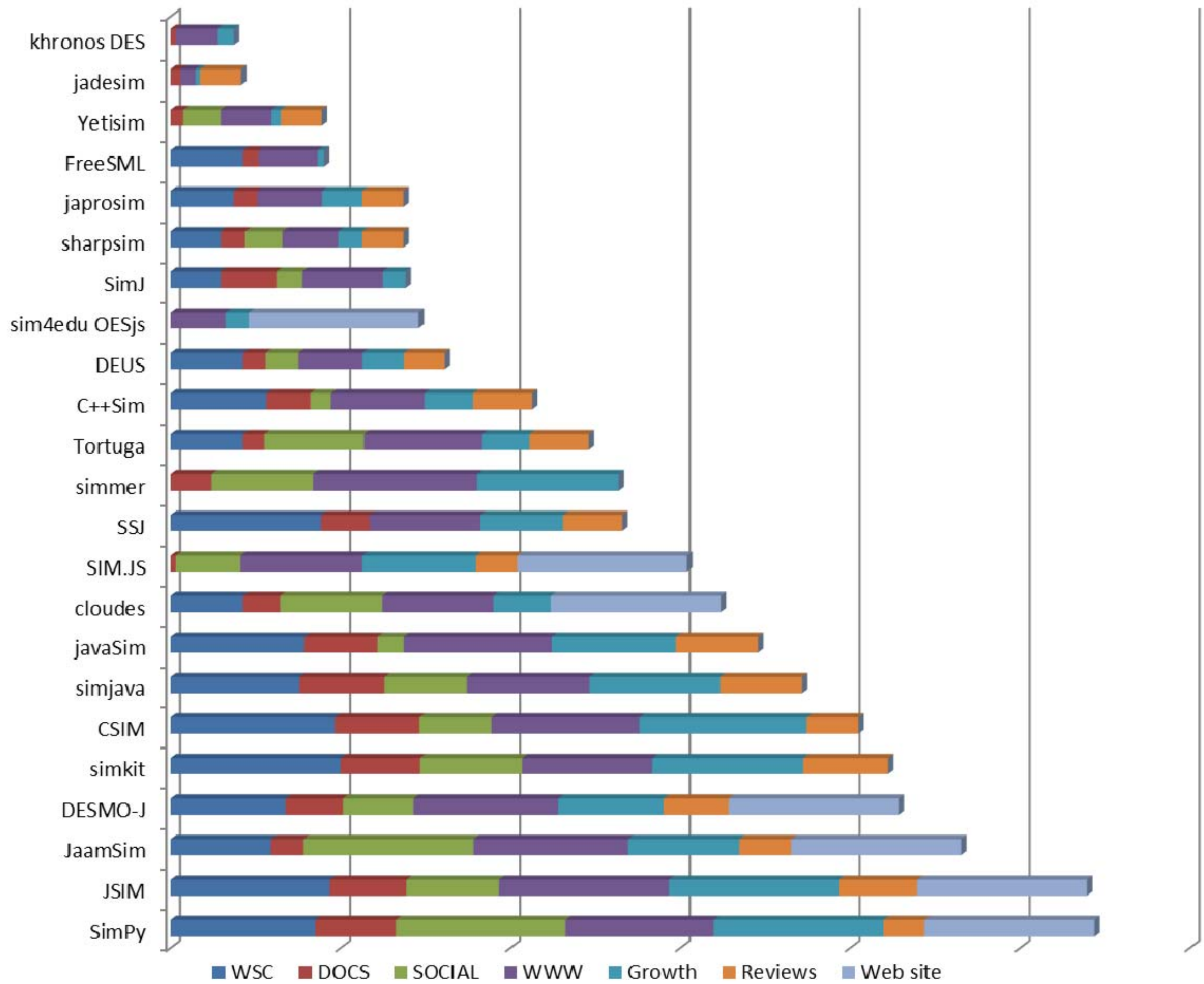

Figure 7: Scores grouped by set of defined criteria

DES Freeware Tools	Σ WSC	Σ DOCS	Σ SOCIAL	Σ WWW	Σ Growth	Σ Reviews	Σ Web site	Σ total score	Ranking Freeware 2018
Weight	2	1	2	2	2	1	2		
SimPy	17	9	20	17	20	5	20	15,54	1
JSIM	19	9	11	20	20	9	20	15,41	2
JaamSim	12	4	20	18	13	6	20	13,29	3
DESMO-J	14	7	8	17	12	8	20	12,24	4
simkit	20	9	12	15	18	10	0	12,07	5
CSIM	19	10	8	17	20	6	0	11,57	6
simjava	15	10	10	14	15	10	0	10,62	7
javaSim	16	9	3	17	15	10	0	9,88	8
cloudes	9	4	12	13	7	0	20	9,25	9
SIM.JS	0	1	8	14	13	5	20	8,69	10
SSJ	18	6	0	13	10	7	0	7,60	11
simmer	0	5	12	19	17	0	0	7,54	12
Tortuga	9	3	12	14	6	7	0	7,03	13
C++Sim	11	5	2	11	6	7	0	6,08	14
DEUS	9	3	4	8	5	5	0	4,61	15
sim4edu OESjs	0	0	0	6	3	0	20	4,17	16
SimJ	6	7	3	9	3	0	0	3,95	17
sharpsim	6	3	4	7	3	5	0	3,91	18
japrosim	7	3	0	8	5	5	0	3,91	19
FreeSML	9	2	0	7	1	0	0	2,58	20
Yetisim	0	1	4	6	1	5	0	2,54	21
jadesim	0	1	0	2	1	5	0	1,18	22
khronos DES	0	1	0	5	2	0	0	1,06	23

Figure 8: Final scores obtained for each set of criteria and for each tool

6. CONCLUSIONS

This paper proposed to rank several open source or freeware simulation tools, according to their popularity. More specifically, according to their presence on academia content, social networks and internet as a whole. The authors used this approach since existing studies that propose to compare freeware and open source simulation tools, ultimately fail to make a judgment or to establish a proper ranking between them. For this purpose, 30 criteria were established and divided among 7 groups, in order to use them to assess each tool. Moreover, the cubic root of the obtained values for each criterion was used, in order to mitigate the different scales of the obtained results. In addition, different weights were assigned to each criterion. Although different weights were used to classify the chosen criteria, the authors believe to have proposed a trustworthy ranking of "popular" open source or freeware simulation tools. Lastly, it should be noted that only tools that address discrete-event simulation and are general purpose, were considered.

After having finalized the study, it is possible to see that SimPy was ranked in first place, closely followed by JSIM, with JaamSim finalizing the podium. Screenshots of some of the considered tools can be consulted in the appendix section. The results obtained by the authors are subject to changes, whether as a consequence of the academic or industry environments. Thus, this study should be regularly updated, by considering new criteria and likewise by pondering on what weight values make sense in the light of more recent trends (e.g., nowadays Facebook may be a relevant social network for simulation users, but in the future, it may cease to be).

By establishing a comparison between the results for WSC (L. M. S. Dias et al. 2016) with the same criteria for this ranking, it is possible to see that the former registered 409 results, which is around 86 % more than the maximum value in freeware and open source tools (SimKit with 56 results). This suggests that, despite the utility of open source and freeware simulation software, their use is still limited.

A last note should be made to emphasize that the authors do not seek to promote freeware or open source tools, or any in specific. In addition, the authors do not want to discourage the use of commercial tools. Rather, this paper recognizes the role and position of freeware and open source simulation tools in the DES community and tried to contribute to literature with a study that assessed and ranked these tools.

ACKNOWLEDGMENTS

This work has been supported by FCT – Fundação para a Ciência e Tecnologia within the Project Scope: UID/CEC/00319/2019 and by the Doctoral scholarship PDE/BDE/114566/2016 funded by FCT, the Portuguese Ministry of Science, Technology and Higher Education, through national funds, and co-financed by the European Social Fund (ESF) through the Operational Programme for Human Capital (POCH).

APPENDIX

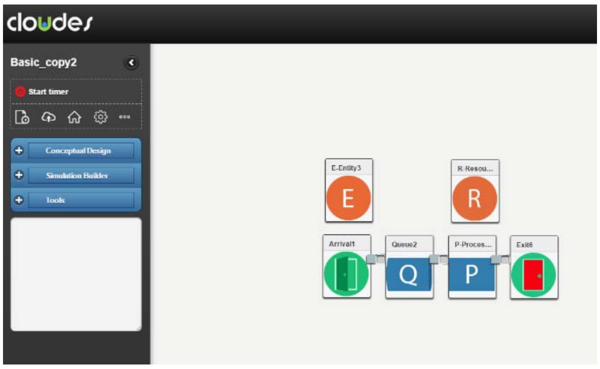

Figure 9: Cloudes screenshot

Figure 10: DESMO-J (3D view) screenshot

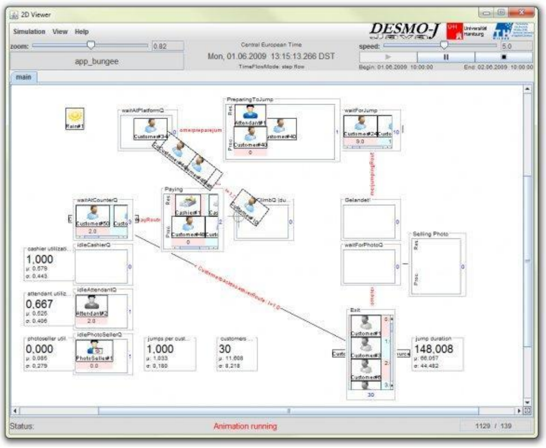

Figure 11: DESMO-J (2D view) screenshot

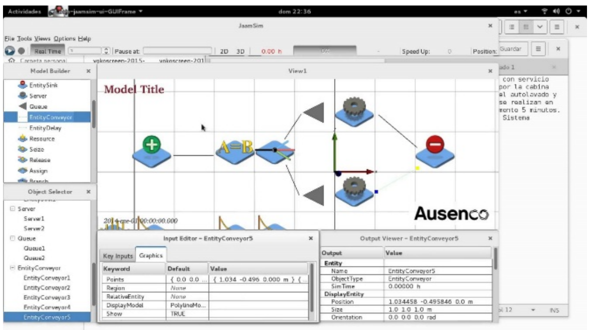

Figure 12: JaamSim screenshot

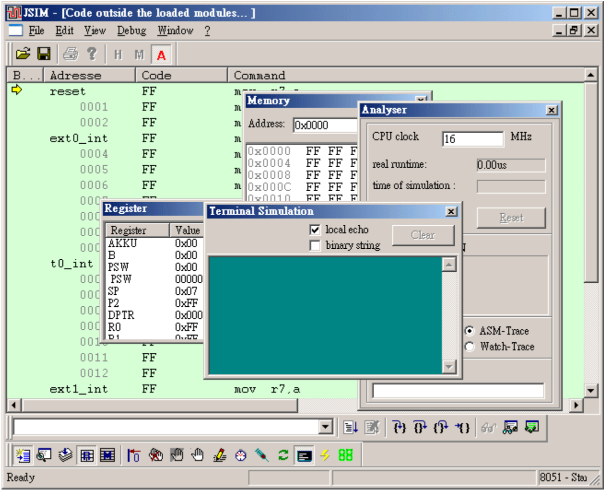

Figure 13: JSIM screenshot

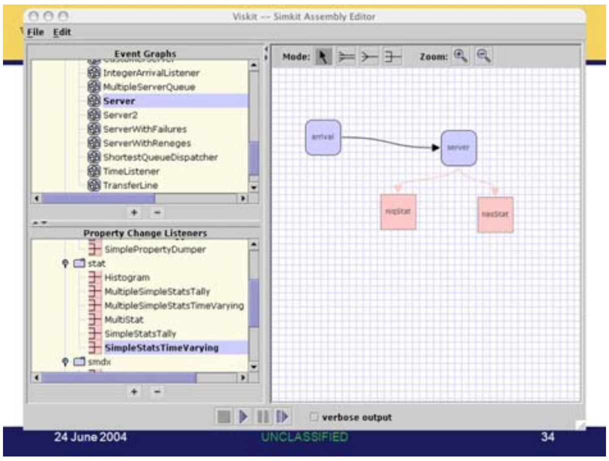

Figure 14: SimKit

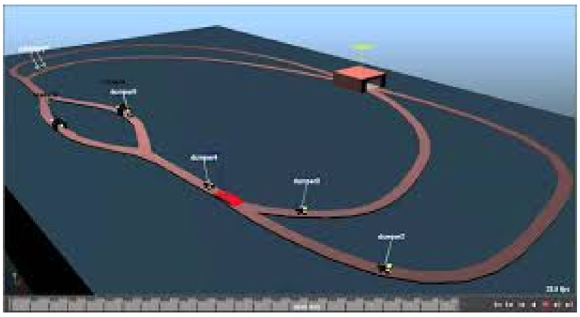

Figure 15: SimPy screenshot

REFERENCES

Abu-Taieh, E M O, and A A R El Sheikh. 2007. “Commercial Simulation Packages: A Comparative Study.” *International Journal of Simulation: Systems, Science and Technology* 8 (2): 66–76.

Byrne, N, P Liston, J Geraghty, and P Young. 2012. “The Potential Role of Open Source Discrete Event Simulation Software in the Manufacturing Sector.” In , 117–26.

Dagkakis, G, and C Heavey. 2016. “A Review of Open Source Discrete Event Simulation Software for Operations Research.” *Journal of Simulation* 10 (3): 193–206. https://doi.org/10.1057/jos.2015.9.

Dias, L., G. Pereira, and G. Rodrigues. 2007. “A Shortlist of the Most Popular Discrete Simulation Tools.” In *Simulation News Europe*, 17,33-36.
Dias, L., G. Pereira, P. Vik, and J. Oliveira. 2011. “Discrete Simulation Tools Ranking: A Commercial Software Packages Comparison Based on Popularity.” In *Industrial Simulation Conference. Venice, Italy*, 6–8.
Dias, Luis M. S., Antonio A. C. Vieira, Guilherme A. B. Pereira, and Jose A. Oliveira. 2016. “Discrete Simulation Software Ranking — A Top List of the Worldwide Most Popular and Used Tools.” In *2016 Winter Simulation Conference (WSC)*, 1060–71. IEEE. https://doi.org/10.1109/WSC.2016.7822165.
Eurosis. 2019. “Simulation and Gaming Software Development Tools and Languages.” https://www.eurosis.org/cms/?q=node/61.
Fowler, J W, and O Rose. 2004. “Grand Challenges in Modeling and Simulation of Complex Manufacturing Systems.” *Simulation* 80 (9): 469–76. https://doi.org/10.1177/0037549704044324.
“Google.” 2019. 2019. https://www.google.com.
Hlupic, V, and R J Paul. 1999. “Guidelines for Selection of Manufacturing Simulation Software.” *IIE Transactions* 31 (1): 21–29. https://doi.org/10.1023/A:1007568516643.
Hlupic, Vlatka. 2000. “Simulation Software: An Operational Research Society Survey of Academic and Industrial Users.” In *Winter Simulation Conference Proceedings*, 2:1676–83.
“Informs.” 2019. 2019. https://pubsonline.informs.org/magazine/orms-today.
Jadrić, Mario, Maja Ćukušić, and Antonia Bralić. 2014. “Comparison of Discrete Event Simulation Tools in an Academic Environment.” *Croatian Operational Research Review* 5 (2): 203–19. https://doi.org/10.17535/crorr.2014.0008.
King, D. H., and Harvey S. Harrison. 2013. “Open-Source Simulation Software “JaamSim”” In *2013 Winter Simulations Conference (WSC)*, 2163–71. IEEE. https://doi.org/10.1109/WSC.2013.6721593.
Klingstam, Pär, and Per Gullander. 1999. “Overview of Simulation Tools for Computer-Aided Production Engineering.” *Computers in Industry* 38 (2): 173–86. https://doi.org/10.1016/S0166-3615(98)00117-1.
L’Ecuyer, P., and E. Buist. 2005. “Simulation in Java with SSJ.” In *Proceedings of the Winter Simulation Conference, 2005.*, 611–20. IEEE. https://doi.org/10.1109/WSC.2005.1574301.
L’Ecuyer, P L, Lakhdar Meliani, and Jean Vaucher. 2002. “SSJ: A Framework for Stochastic Simulation in Java.” In *Simulation Conference, 2002. Proceedings of the Winter*, 1:234–42. IEEE.
Miller, John A, Andrew F Seila, and Xuewei Xiang. 2000. “The JSIM Web-Based Simulation Environment.” *Future Generation Computer Systems* 17 (2): 119–33. https://doi.org/10.1016/S0167-739X(99)00108-9.
Page, Ernest H, Robert L Moose Jr., and Sean P Griffin. 1997. “Web-Based Simulation in Simjava Using Remote Method Invocation.” In , 468–74.
Park, Hyeong-Tae, Jong-Geun Kwak, Gi-Nam Wang, and Sang C. Park. 2010. “Plant Model Generation for PLC Simulation.” *International Journal of Production Research* 48 (5): 1517–29. https://doi.org/10.1080/00207540802577961.
Peixoto, Túlio Almeida, João José de Assis Rangel, Ítalo de Oliveira Matias, Fábio Freitas da Silva, and Eder Reis Tavares. 2017. “Ururau: A Free and Open-Source Discrete Event Simulation Software.” *Journal of Simulation* 11 (4): 303–21. https://doi.org/10.1057/s41273-016-0038-5.
Sawhney, Anil, Hemant Deshpande, and Andre Mund. 2000. “JavaBeans-Based Framework for Construction Simulation.” In , 2:1919–25.
Sawhney, Anil, Jayachandran Manickam, Andre Mund, and Jennifer Marble. 1999. “Java-Based Simulation of Construction Processes Using Silk.” In , 2:985–91.
Sawhney, Anil, and Andre Mund. 1998. “Simulation Based Construction Management Learning System.” In , 2:1319–24.
Vieira, A., L.S. Dias, G.A.B. Pereira, J.A. Oliveira, M.S. Carvalho, and P. Martins. 2015. “Using Simio to Automatically Create 3d Warehouses and Compare Different Storage Strategies.” *FME Transactions* 43 (4). https://doi.org/10.5937/fmet1504335V.
Vieira, A., L.S. Dias, G.B. Pereira, and J.A. Oliveira. 2014. *Micro Simulation to Evaluate the Impact of Introducing Pre-Signals in Traffic Intersections. Lecture Notes in Computer Science (Including Subseries Lecture Notes in Artificial Intelligence and Lecture Notes in Bioinformatics)*. Vol. 8584 LNCS. https://doi.org/10.1007/978-3-319-09153-2_54.
Vieira, A., L.S. Dias, G.B. Pereira, J.A. Oliveira, M.S. Carvalho, and P. Martins. 2016. “Automatic Simulation Models Generation of Warehouses with Milk Runs and Pickers.” In *28th European Modeling and Simulation Symposium, EMSS 2016. Winner of the Best Paper Award*, 231–41.
Vieira, A.A.C., L.M.S. Dias, G.A.B. Pereira, and J.A. Oliveira. 2017. *Agent-Based Simulation to Assess the Performance of Intersections with Pre-Signals: Comparison with Roundabouts. Lecture Notes in Computer Science (Including Subseries Lecture Notes in Artificial Intelligence and Lecture Notes in Bioinformatics)*. Vol. 10572 LNCS. https://doi.org/10.1007/978-3-319-68496-3_36.
Vieira, A A C, L M S Dias, G A B Pereira, J A Oliveira, M Do Sameiro Carvalho, and P Martins. 2018. “Simulation Model Generation for Warehouse Management: Case Study to Test Different Storage Strategies.” *International Journal of*

Simulation and Process Modelling 13 (4): 324–36. https://doi.org/10.1504/IJSPM.2018.093761.

Vieira, António, Luís M. S. Dias, Guilherme Pereira, and José A. Oliveira. 2014. "Comparison of SIMIO and ARENA Simulation Tools." In *12th Annual Industrial Simulation Conference (ISC2014)*, 5–13.

Weatherly, R M, and E H Page. 2004. "Efficient Process Interaction Simulation in Java: Implementing Co-Routines within a Single Java Thread." In , 2:1437–43.

"Wikipedia." 2019. https://en.wikipedia.org/wiki/List_of_discrete_event_simulation_software.

AUTHORS BIOGRAPHY

António A.C. Vieira is an Invited Assistant Professor and Researcher of the ALGORITMI Research Centre, University of Minho, Portugal. He holds a MSc degree in Systems Engineering at the University of Minho. He is making his doctoral studies in Advanced Engineering Systems for Industry at the University of Minho, in partnership with Bosch Car Multimedia Braga. His research interests include Modelling and Simulation, Logistics and Transportation, and Big Data. His email address is antonio.vieira@dps.uminho.pt.

Luís M.S. Dias is an Auxiliar Professor and Researcher of the ALGORITMI Research Centre, University of Minho, Portugal. He holds a PhD degree in Production and Systems Engineering from the University of Minho, Portugal. His research interests include Simulation, Systems Performance, Operational Research and Systems Visual Modeling. His email address is lsd@dps.uminho.pt.

Maribel Y. Santos is an Associate Professor at the Department of Information Systems and Researcher of the ALGORITMI Research Centre, University of Minho (UMinho), in Portugal. She received the Aggregated title (Habilitation) in Information Systems and Technologies (IST) from UMinho in 2012 and a PhD in Information Systems and Technologies from UMinho in 2001. Her research interests include Business Intelligence and Analytics, Big Data and (Big) Data Warehousing. Her email address is maribel@dsi.uminho.pt.

Guilherme A.B. Pereira is an Associate Professor and Researcher of the ALGORITMI Research Centre, University of Minho (UMinho), in Portugal. He holds a PhD degree in Manufacturing and Mechanical Engineering from the University of Birmingham, UK. His research interests include Operational Research and Simulation. Currently he is Pro-Rector of the University of Minho. His email address is gui@dps.uminho.pt.

José A. Oliveira is an Auxiliar Professor and Researcher of the ALGORITMI Research Centre, University of Minho (UMinho), in Portugal. He holds a PhD degree in Production and Systems Engineering from the University of Minho, Portugal. His research interests include Optimization with Heuristic Methods in Systems Engineering. His email address is zan@dps.uminho.pt.

HOUSEHOLDS INCOME-EXPENSES NETWORK SIMULATION

Javier Lara de Paz [(a)], Idalia Flores de la Mota[(b)], Gabriel Policroniades Chipuli[(c)], Sashiko Shirai Reyna [(d)]

[(a),(b),(c),(d)]Facultad de Ingeniería, Universidad Nacional Autónoma de México

[(a)]javier_lara_depaz@comunidad.unam.mx, [(b)]idalia@unam.mx, [(c)]gpolicroniadesch@gmail.com , [(d)]sashikosr@outlook.com

ABSTRACT
Economic systems are recognized as complex systems that can be modeled as complex networks. Analyzing and simulating with the outcoming networks parameters can be obtained the vulnerability and robustness of system's network, assisting the developing of economic policies. In present work we built up an economic weighted directed network between the catalogued labors, the productive sub-sectors, based on 4-digits NAICS-2018, and the eight common household expenses. Weighting edges with total household incomes and total amount paid for each expense. The network is constructed with a sample size of more than one hundred-thirty thousand households. With complex network metrics and adding an inflation rate to each main Expense category, the simulation was performed obtaining key economic properties such as wealth distribution per household and sectors vulnerabilities as well as system robustness.

Keywords: Complex Networks , Complex systems, simulation

1. INTRODUCTION

In many countries, their National Statistical Institutes carry out periodically a demographic survey system, either as a census or as a sampling survey. These surveys are designed to collect information about National Accounts, demographic characteristics, as well as economic behaviors and patterns, among many other information that can be of national interest. In some of these surveys it is described how much population earn, and how much money is spent in principal expenses, or what are the economic activities, even at a household, companies or grand productive sectors level. The information obtained is used by researchers of the academic, public or financial sectors. Even by economists, which by means of econometric, statistical or financial methods, among many others approaches, develop models to estimate either the demographic or financial behaviors. Also, it is possible to estimate the macro-economic information, the GDP, inflation and unemployment rates, economic growth, added values of different productive sectors. It can be considered that the techniques applied can be considered as in a "traditional" framework, which doesn´t allow to visualize robustness of the system. A review of evolution to new trends in economical methods can be seen in (Lara de Paz et al. 2019). Or to find weakly points that risk the system's functionality, or even to obtain clustering formations, leader entities, or structural relations within system. Some of the variables included in the generated metadata from surveys or census, are the economic activities performed by households. Also, information about labor-activities is gathered indicating in which economic productive sectors do these agents work, and how much do they earn as well as in what and how much do they spend. These data is collected through the Households Income-Expenses Survey carried out in Mexico every two years since 1992. The scope in this information provides insight about what trades and crafts are performed per sector. These functional relations can be constructed through a network architecture where economic activities, productive sectors and common expenses become nodes. Wages and amount spent correspond to the edges weight. The network topology constructed with the survey's data provides more information than an analysis performed with traditional econometric and statistical treatments. In present work we constructed a network with the economic-activities per household's variables, productive sectors and the principal expenses. Data were obtained from Mexico´s official surveys about households' expenses, jobs and Economic Census for the year 2016 (ENIGH-2016, Income-Expenses National Survey (INEGI n.d.)). Mexico's National Accounts System (SCNM)(INEGI n.d.) were also consulted. We combined Complex Networks techniques with Simulation approach to obtain more insight about Mexico's socio-economic structure, (Hassani, Saporta, and Silva 2014). Zanin (Zanin et al. 2016) presented in his work some techniques about combining Data Mining methods with Complex Networks theory mainly applied to medical research. They suggested that a network analysis from the system would be an advantage to identify the robustness of the system by identifying single nodes influence over the whole network. Although they also combined Data Mining methods with Complex Networks theory, but one of their strongest points was that complex networks allow representing the system's internal structure of each individual agent relations in a simpler and more understandable way. To represent our system using Network topology let us have an overview of system structure, formation of communities, collective behaviors and to identify the diversity of nodes and its multiple connections, representing the complexity of the system (Silva and Zhao 2016). By applying a simulation methodology allow us to find which instances are more significant to robustness and vulnerability. In the next introductory subsection some Complex Networks theory features are described to understand some of the metrics used as parameters to perform simulations.

1.1. Complex Networks

Interest in complex networks field has grown in many areas from physicists, mathematicians, biologists, engineering, computer scientists, among many others. The structure analysis of many different systems that can be represented as a network, are the Internet, World Wide Web, biological systems together with chemical systems, financial, social, neural, and communication networks. Although these systems can represent artificial or natural systems, they share a main feature, the complexity. Barabási, one of the more active researches in this field (*Network Science by Albert-László Barabási* n.d.) specified that an adequate manner to represent evolution of a complex system, can be through its network topology. Catanzaro and Buchanan (Catanzaro and Buchanan 2013), mentioned some disadvantages of main stream economic theories for preventing an economic crisis like in 2008, and pointed some advantages in developing financial networks. About application of network structures to economic and financial systems, Bouchaud (Bouchaud 2008) addressed to the necessity of the search and applications of different methodologies to aid main stream economic models. Schweitzer et al. (SCHWEITZER et al. 2009), examine the emergence of many economic systems described as networks and the consequences in analyzing through this approach, which is distinguished as a convenient way of data analysis. Caldarelli and Catanzaro (Caldarelli and Catanzaro 2014) made a friendly description about many networks present in Nature. The system involved corresponds to a weighted network constructed as having a branching, treelike topology, like a transportation network with transfer nodes, becoming a directed network as well.

1.1.1. Complex Network Metrics

About the Complex Networks metrics and theory applied to describe our system, Boccaletti (Boccaletti et al. 2006) summarized the sufficient network's features needed for analyzing its behaviors and evolution. Also the work done by Deguchi et al. (Deguchi et al. 2014) was used to estimate HITS metrics. For modularity and community properties, we based on Newman (Newman 2006). In the work reported by Klimkova et. al ((Klimkova, Senkerik, and Zelinka, n.d.), described some methods to detect giant components in directed networks, and Levorato and Petermann (Levorato and Petermann 2011) described some techniques to identify communities in a directed weighted network, based on the modularity, allowing to detect the number of communities or connected subgraphs in network´s system. In this work we calculated the following network metrics (table 1):

Table 1: Network's Metrics calculated at scale-levels

Micro-scale	Nodes degree, in and out degree for a weighted network, eigenvector centrality
Meso-scale	Modularity, strong component number and assortativity
Macro-scale	Average path length

To estimate the system's robustness we performed the simulation adding and removing some high connected nodes according to a percolation model (D'Agostino and Scala 2014) and (Réka Albert and Barabási 2002). In complex systems robustness presents a dynamical component, while representing these systems by its topological structure underlying in complex network, these error tolerance or the vulnerability can be addressed by edges/nodes removal leading to a change on stability of such systems related to error and attack tolerances. In present work we focus only on nodes removal, since some network structures are more robust against random node failures. The node removal mechanism consists in deleting nodes randomly, the second form is by removing highly connected nodes, considering the nodes with highest node degree. Other mechanisms are by cascade or percolation method. The remaining structure allow us to obtain critical vulnerability of the system, (Reka Albert, Jeong, and Barabasi 2000).

2. SYSTEM'S STRUCTURE

The system considered is composed by three different class of elements, agents' activities, which are referred to the diversity of jobs, trends or crafts, registered in corresponding surveys outcomes. These categories are classified based on Mexico's National Catalogue of Jobs and Occupations (SINCO). The other class of elements corresponds to productive subsectors described at 4-digits level based on the North American Industry Classification System (NAICS-2018). The third class are the eight main expenses done per households (housing, shoes & clothing, education, personal care, food, transportation, health care and cleaning-wares). The relation between elements correspond to: between jobs and sectors are total annually incomes. Relation between jobs and expenses are amount spent by household in every expense (Fig. 1). For each household entities considered in the ENIGH-2016 survey, a sample size of more than 130 thousand basic units, it was considered the economic activities (SINCO) the relation with their economic subsector (NAICS 4-digits classification) and the total annual incomes and total annual expenses in 8 main expenses (Table 2).

Table 2: System´s elements for network structure

Productive Subsector (NAICS) 2018 version.	Economic Activity (SINCO) 2011 version	ANNUAL INCOME	ANNUAL SPENT FOR EACH EXPENSES (EDGE WEIGHTS) • HOUSING • FOOD • CLOTHES & SHOES • EDUCATION • TRANSPORT • PERSONAL CARE • HEALTH CARE • CLEANING-WARE
CLASS 1 ENTITIES	CLASS 2 ENTITIES	EDGE WEIGHTS	CLASS 3 ENTITIES

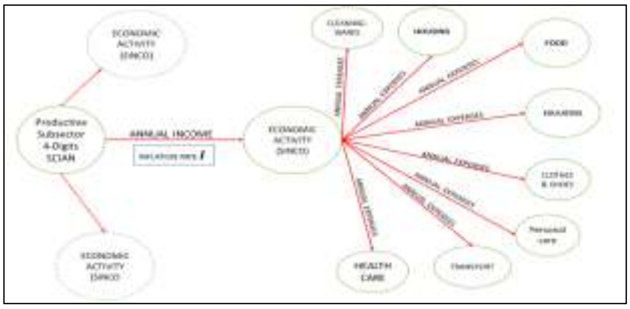

Figure 1: System´s network generated by elements relations

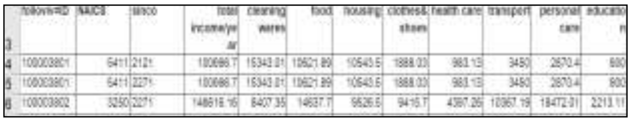

	foliovivID	NAICS	sinco	total income/year	cleaning wares	food	housing	clothes& shoes	health care	transport	personal care	education
3												
4	100003801	6411	2121	100686.7	15343.01	10621.89	10543.5	1888.03	983.13	3450	2670.4	600
5	100003801	6411	2271	100686.7	15343.01	10621.89	10543.5	1888.03	983.13	3450	2670.4	600
6	100003802	3250	2271	148616.16	8407.35	14637.7	9526.5	9416.7	4397.26	10967.19	18472.01	2213.11

Figure 2: Image of first 3 rows CSV Data sheet used to construct system's network.

2.1. Network Structure

To construct the network a directed origin-target layout was applied with origin nodes as Productive Subsectors, first target nodes as the occupational activities and directed to final nodes represented by the eight different categories of expenses. The network obtained is a directed weighted network with edges weights being the annual incomes for first branches and annual spent for second branches. For each household its corresponding branch was constructed:

Subsector → economic activity → expenses
income spent

Network visualization was performed with aids of NETWORK R-package, as well as network metrics calculations. The calculated Metrics are:

- Node degree, in and out degree and weighted in and out degree. For this metric node distribution is estimated. For a weighted directed network this metric is calculated by adding (for in degree) incoming edges weights by node.
- Nodes centralities, eigenvector centrality. This measure indicates importance of each node depending on its connections and weighted links of them.
- Assortativity. This metric indicates capacity of high connected nodes to connect to other high connected nodes (positive assortatvity), or capacity of high connected nodes to connect with low degree nodes (negative assortativity). It is associated to robustness of system, as one high connected node is removed or changed, the remaining structure tends to link whether to a high connected node or to a low connected node in order to network structure to survive (Shizuka and Farine 2016)
- Modularity: this meso scale measure, indicates the formation of communities between similar node categories. It is described with a number related to the subgraphs formed by dividing network in optimal number of communities.
- Strong community number: associated to network's modularity for each node indicates the strongest association of each node to its corresponding community. This metric is obtained implementing the system´s network in GEPHI software released 0.9.2 (https://gephi.org)
- Vulnerability and robus. A removal of nodes is done depending on different mechanism for removing nodes. This measure exhibits systems robustness, and a threshold that indicates when network starts to show fatal errors.

From these metrics simulation performance is carried out to find robustness of the system through complex network approach, which is the main scope of present work.

3. METHODOLOGY

Network construction and parametrization are based on the results of bi-annual Mexico´s Incomes and Expenses per Households National Survey carried out on 2014. Information is available as a metadata ***csv*** format file. The data sheet contains concentrated information of about 130'000 housing with data about location, economic activities, ages, genders, detailed incomes and expenses per households, among many other relevant variables. Out from this information we are interested in economic information about earnings, expenses, economic activities and where do heads of household work. We summarized earnings in total annual incomes and 8 different categories of expenses: housing, food, clothes & shoes, education, transport, personal care, health care and cleaning-ware. Each housing is identified with a unique Id code, by this it is possible to detect same households in different official surveys. Metadata results also show a variable indicating in which productive subsector the head of household works. The coding is based on the NAICS-2013 classification system ("Sistema de Clasificación Industrial de América del Norte, México SCIAN 2013," n.d.). With this information it is possible to match each household in the survey sample with the productive subsector, the economic activity performed, annual and total amount expended in main 8 expenses. Intuitively, this matching generates a directed network (Fig. 1) with 11 different nodes categories for each corresponding column (Fig. 2) and the edges are generated by every row, which correspond to each sampled household. Network structure is constructed under R coding, calculating network metrics, nodes degree (weighted in and out degree distribution, modularity, eigenvector centrality and vulnerability). This information allows us to have a state of the system of how it is behaving. Up to this information we start with simulation process. Network metrics results correspond to 2014 end year's behavior of economic dynamics, with corresponding information of subsequent years (2015, 2016, 2017 and 2018) through simulation, it is possible to estimate the network topology with the corresponding metrics and finally the evolution of robustness of the system. Annual accumulated inflation rate per expense categories is the changing parameter for our simulation performances which affects directly to the expenses branches which go from occupation nodes (identified by the Mexican jobs classification system SINCO) to the 8 categories of expenses. Year 2014 will be our referenced year. About incomes increasing rates, it is assumed that they remain stable through the 4 years period. Inflation rates consider4ed are obtained from the National Consumer Price Indexes (NCPI) for the eight mentioned categories. These are obtained from official databases (Mexican Central Bank, BANXICO). Annual variations between years are multiplied to expenses edges, and network metrics are calculated for each 4 periods with year 2014 as reference. In table 2 variations of the NCPI's of Mexican economy information is showed for years 2014 to end of 2018. Simulation report will show variation of network global weighted in and out degree indicating which productive subsectors or occupations are economically more connected to higher wages or earning nodes. For in-weighted degree, it indicates which occupations or labors are better paid if for a high degree, and for expenses categories which category is more economically significant for households. The eigenvector centrality is also reported indicating what targeted nodes are more important between occupations and expenses categories. Asortativity allows us to identify systems capacity of interacting between sectors and occupations and vulnerability shows robustness of considered system. Fig. 3 shows the process followed by methodology applied.

Table 3 : Annual cumulative Mexican Inflation Rate for years 2014 to 2018*

Year / Expense	End 2014	End 2015	End 2016	End 2017	End 2018
HOUSING	2.02	-0.07	1.11	5.14	2.54
FOOD	6.53	2.32	4.31	7.92	5.39
CLOTHES & SHOES	2.26	2.90	3.26	4.05	2.14
EDUCATION	3.85	3.55	4.23	4.57	3.83
TRANSPORT	4.45	2.43	4.25	11.48	9.36
PERSONALCARE	6.80	4.51	4.89	5.76	5.34
HEALTH CARE	2.87	3.33	4.15	6.13	4.43
CLEANING-WARE	1.58	2.94	2.19	5.06	2.85

*Source: INEGI

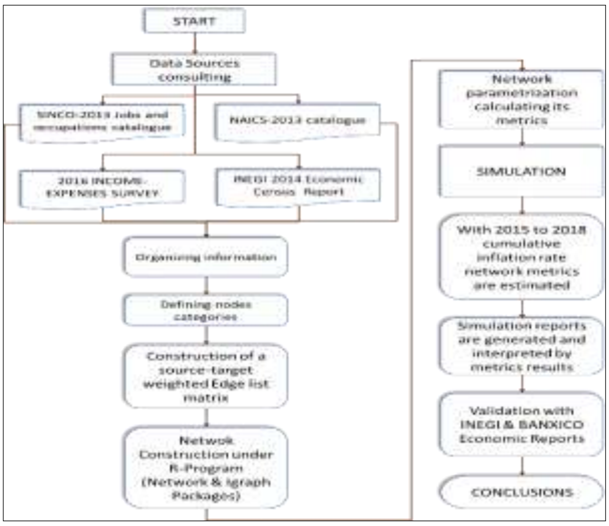

Figure 3: Methodology

4. SIMULATION

To perform the simulation, parametrization of system is carried out by network construction and calculating networks node degree: weighted in and out degree, eigen centrality, assortativity and income distribution. It is identified the productive subsectors with more influence along the network structure, as wages represent edges weights from Subsector nodes to jobs/occupation target nodes, as higher out-weighted node degree a node presents, more economic influence the node has. About weighted in-degree, these correspond to earnings by transfer jobs/occupational nodes and for Expenses category nodes, as higher value it presents, more significant is the node over the network. Edges weights from jobs/occupations nodes to Expenses category nodes, as mentioned, represent the amount each household has paid for respective services. For the simulation, weights values are calculated, with the variation indexes of inflation rates corresponding to this category based on the year and on the node category, constructing four different networks models representing our system. The outcomes of network metrics are calculated in each case and interpreted under robustness insight. To finish with our comparative simulation outcomes, difference between weighted in and out degree distribution by node is analyzed, omitting the 8 nodes expenses categories, resulting only for the jobs/occupation nodes category (Fig. 15). From this distribution the Gini coefficient is obtained as an estimation to understand income distribution after paying for life costs. These metrics are calculated for years 2015-2018. Although consulted source corresponds to the 2016 survey edition (ENIGH_2016), information was collected along 2014 and 2015, hence our base year corresponds to 2014. From this year simulation are performed. In next subsection corresponding to simulation results analysis, it is shown network metrics for each year with respective modifications to inflation rate by product for each year.

4.1. System´s Network parametrization

Fig. 4, shows the system´s network with 594 nodes and 743409 edges. In left frame network is showed without label and nodes are sized based on its node in-degree. Bigger nodes represent the 8 Expenses categories. Right frame represents network with nodes sized based on its node out-degree.

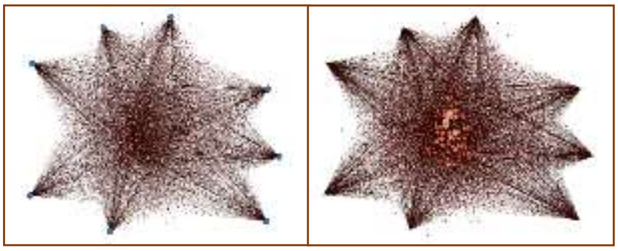

Figure 4: System´s network.

Next the complex networks metrics are shown. Fig. 5 shows the degree distribution plot. This metrics indicates the average links per node. The average node **degree = 15.59** which means that on average every node is linked with 16 different edges to its closest neighbors. It is important to underline that the 8 Expenses Categories nodes have a node **degree = 450**. But as shown in nodes degree distribution histogram (Fig. 6), about 120 nodes present a low connection degree. In Fig. 7, it is shown the distribution of nodes degree by nodes categories. Inside frames indicate the value of the high connected nodes corresponding to productive branch "General Public Administration" with a node **degree of 143**. This means that this productive subsector is the most diversified because of the different kinds of occupations it demands. About jobs/occupations category, the most linked node with a node degree of **101** corresponds to the **9621**classification job. This code is classified in the Mexican National Occupation System Catalogue (SINCO-211), as general cleaner and sweeper (except for hotels and restaurants). This means that this occupation is the most demanded job by a high diversity of productive subsectors. In Fig. 7, nodes vs node degree is plotted omitting the 8 Expenses Category nodes and a power law is fitted. Inside labels shown node degree of most connected nodes by category. In the *x*-axe the node list is labeled, but due to space limitation it is adjusted to the font size and the complete list is not presented. Node degree indicates mainly a topological system's feature, as one of main objectives is to gain more insight on economic dynamics other metrics are considered as weighted node degree. This metric indicates the sum of edge's weight each node has, allowing us to estimate economical significance by node. As higher the value more significant is the node. For a system's directed network representation there are two other metrics related to edges' weight, weighted out and in degree. For Out-degree corresponds to the sum that a node had paid in general, as wages in the case of subsector→job/occupation edges, and for job/occupation→Expenses edges, it correspond to amount paid for living services described as Expenses. For weighted In-degree, it indicates, for the Jobs/Occupations category nodes, the total wages earned from the different subsectors each node is connected to. For the Expenses category nodes, this metric indicates how much is expended in each of the 8 categories by jobs/occupation category nodes. This last metric corresponds to the response to our control parameter inflation rate in simulation performance. Fig. 8 shows weighted node degree distribution. In vertical axis list of nodes are plotted and in horizontal axis it is shown the value of node degree. The node with highest degree (inside label) corresponds to productive subsector category node identified as "Education supporting Services" with a value of 36080309.98. It can be interpreted as this node has paid to its 93 (node degree) different occupations related to this category the mentioned amount (units are in Mexican pesos MXN, 1USD~20MXN). In Fig. 9, a bar plot of weighted in-degree for the 8 Expenses category nodes is presented. In Fig. 10, the distribution of weighted in-degree for Jobs/Occupation Category nodes is plotted. A Power-Law fitting is shown (red dotted line) and an empirical equation with determinant coefficient is shown in upper-right inside frame. With relation to the connectivity, relevance each node presents is expressed through eigencentrality value. In Fig. 11, eigencentrality value is plotted vs Jobs/Occupations category nodes. In both Figures, it can be observed that nodes with the highest respective values are the same for both metrics. In table 4, the more diversified jobs based on mentioned metrics are described. About network metric Modularity class, network can be separated in 9 communities (Fig. 12). Respect to assortativity, the value obtained is **Assortativity = -0.7061681**, this means it has a dissociative behavior by high hubs nodes. Gini coefficient **GN = 68.6** obtained from difference between weighted in and out degree, (distribution is shown in Fig. 13), shows an extremely high value. We assumed two main reasons for such a high GN value. (real one for 2014 GN=45.8), first sample size is not big enough for calculating real income distribution and there are three nodes with a weighted in degree around MXN 360 million a year. But it is able by this technique to manipulate nodes structure to get more insight

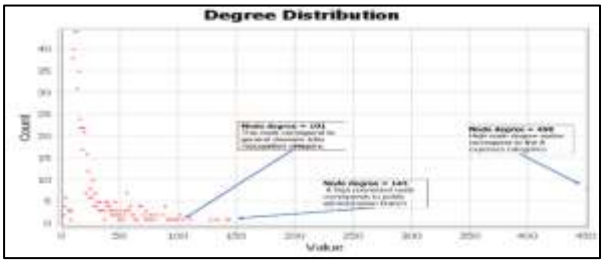

Figure 5: Node degree distribution dot plot. Inside frames indicate node degree of the more connected nodes of the 3 nodes categories.

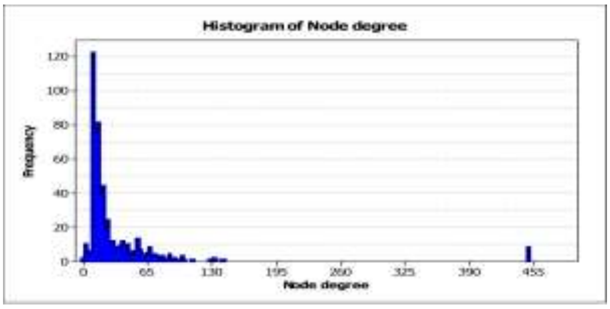

Figure 6: Histogram of node degrees

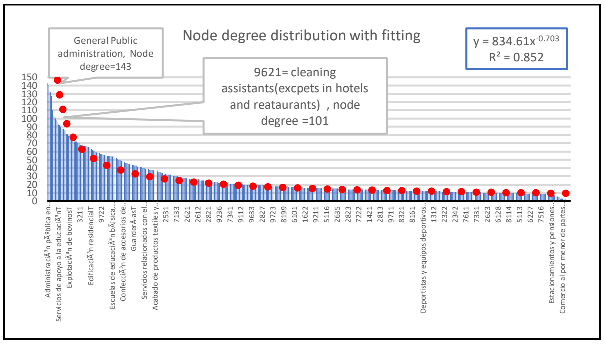

Figure 7: Node degree distribution bar-plot showing all nodes categories, except the 8 expenses category with an potential fit. Inside frames indicate the most connected node corresponding to the productive subsector and the most connected job/occupation category node. Red dot line correspond to a power law fitting and corresponding empirical calculated model with Pearson R^2 coefficient is showed in up right inside frame.

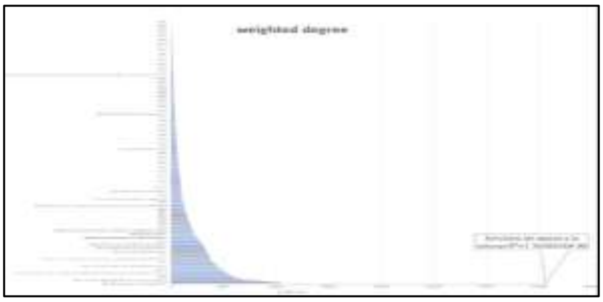

Figure 8: Weighted degree distribution plot. Node with highest degree corresponds to productive subsector “education supporting services” with a node weighted degree of 36080309.98.

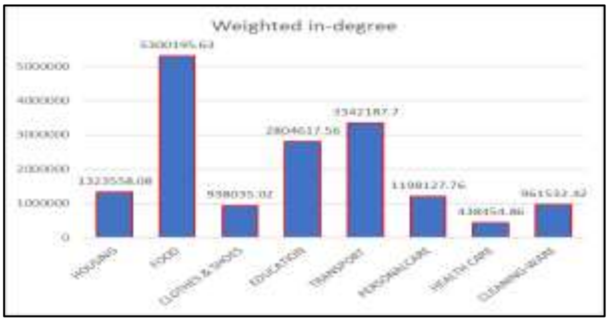

Figure 9: Column plot for weighted In-degree by Expenses (base year 2014).

Figure 10: Distribution of weighted in-degree by jobs/occupations category nodes in horizontal axis. A Power-Law distribution fit was performed, and empirical equation is shown in upper-right frame.

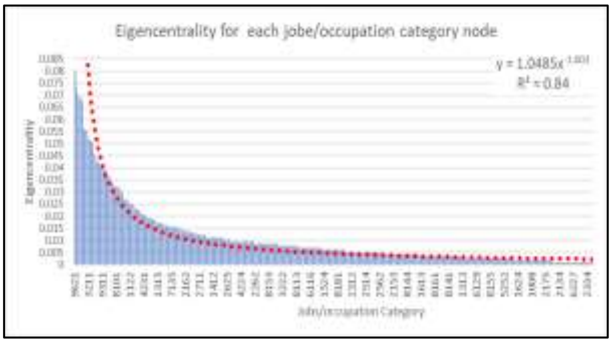

Figure 11: Eigencentrality vs jobs/occupation category nodes plot. Power-Law is fitted with an determinant coefficient of 00.84 is obtained.

Table 4: description of the 6 more diversified jobs

Node Code	Job description
9621	general cleaner and sweeper (except for hotels and restaurants)
2512	auxiliary in accounting economics finance and stockbrokers assistants
3115	Support workers in various administrative activities
3111	Secretaries
2511	Auxiliary in administration, marketing, marketing and foreign trade
5313	Vigilant and guards in establishments

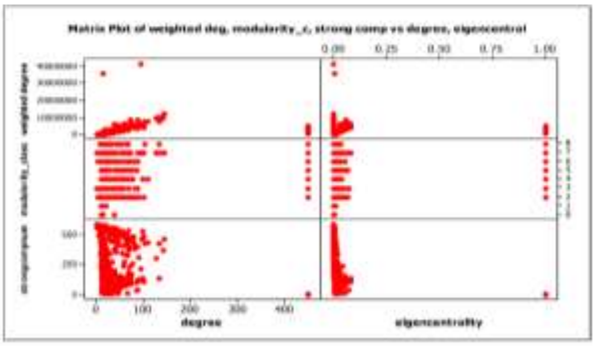

Figure 12: Matrix plot of degree and eigencentrality as horizontal exes and strong, modularity and weighted degree for vertical axis.

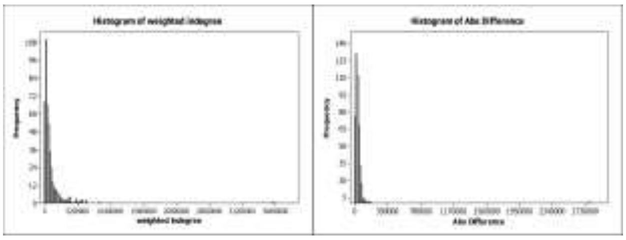

Figure 13: right plot shows weighted in-degree histogram. In right frame shows histogram of the difference between weighted in and out degree by job/occupation category nodes.

4.2. Simulation results

The simulation is performed changing weights of Jobs/occupations Category → Expenses edges for years 2015-2018. The outcomes' analysis are focused only in weighted degree distribution, weighted in-degree distribution and estimation of Gini coefficient. This because other metrics won´t change significantly. Results are summarized in Table 5. In Fig. 15 the annual weighted degree variation for years 2014-2018 is shown, it can be observed that the food category is more significant but transport presents more variation through selected years.

Year / Result	End 2014	End 2015	End 2016	End 2017	End 2018
Gini Coefficient	68.6	72.6	63.54	63.52	63.54
Variation %		5.38	-12.48	-0.031	0.031

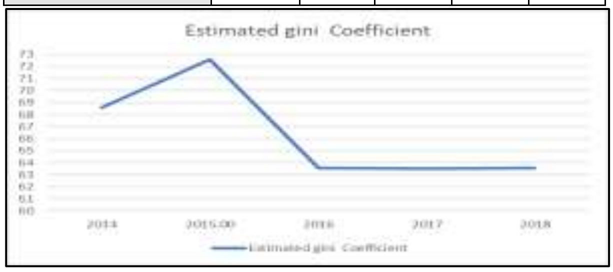

Figure 14:Estimated Gini coefficient from 2014-2016

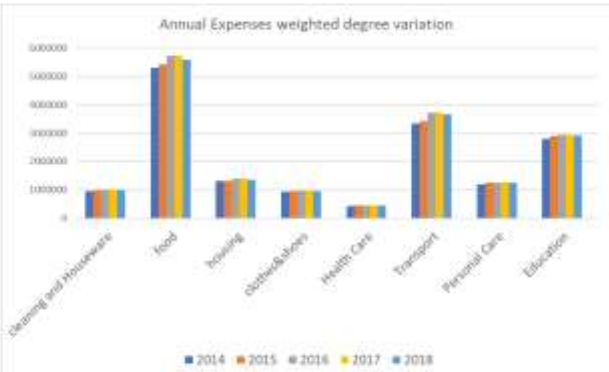

Figure 15: Simulation results for Weighted degree variation when inflation rate was introduced.

4.3. Validation

Our results are validated trough the variation of Gini Coefficient, for corresponding years. It has to be noticed that there is no information available about years 2015 and from 2017 to date. As mentioned, our results have an estimation error of about 49 % in some years, but this can be due to lack of data, and we are only considering the analysis of jobs/occupations category. A further analysis using productive subsector should be improved. Behavior of Gini coefficient responds to shape observed by variation from 2014 to 2016. Our results can be applied to study system's behavior.

2000	2002	2004	2005	2006	2008	2010	2012	2014	2016
51.40	49.00	48.30	48.90	47.70	44.60	45.30	45.40	45.80	43.40
5.54%	-4.67%	-1.43%	1.24%	-2.45%	-6.50%	1.57%	0.22%	0.88%	-5.24%

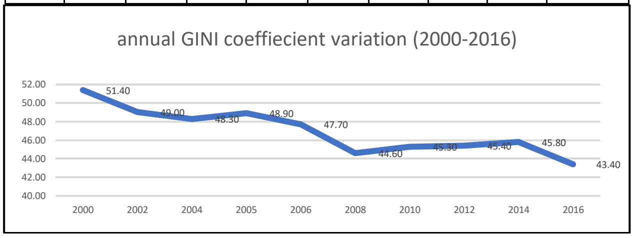

Figure 16: Gini Coefficient values and behavior from years 2000 to 2016. Source INEGI.

5. CONCLUSIONS

Our technique to analyze an economic system by Complex Network approach is suitable to interpret a complex system state, diversity of nodes can be tracked by its diversity of links. Simulation allows us to identify some of key nodes by categories, obtaining an estimated evolution of income distribution using Gini coefficient. A further Modularity metric scope would indicate evolution of system clusters, permitting to identify economic groups aiding to reinforce economic dynamic. Implementation of data mining approach can aid to get more insight of system, by tracking each node and its links. By means of presented method directed attacks or reinforcements of different occupations or jobs, or incentives by expenses or even aiding the design of economic policies directed to specific subsectors can be implemented.

ACKNOWLEDGMENTS

To the PAPIIT DGAPA project IT102117, UNAM for its support to this research.

Javier Lara de Paz is a doctoral student from Programa de Doctorado en Ingeniería, Universidad Nacional Autónoma de México (UNAM) and received fellowship 593341/309027 from CONACYT.

REFERENCES

Albert, Réka, and Albert-László Barabási. 2002. "Statistical Mechanics of Complex Networks." *Reviews of Modern Physics* 74 (1): 47–97. https://doi.org/10.1103/revmodphys.74.47.

Albert, Reka, Hawoong Jeong, and Albert-Laszlo Barabasi. 2000. "Error and Attack Tolerance of Complex Networks." *Nature* 406 (6794): 378–82. https://doi.org/10.1038/35019019.

Boccaletti, S., V. Latora, Y. Moreno, M. Chavez, and D.-U. Hwang. 2006. "Complex Networks: Structure and Dynamics." *Physics Reports* 424

(4): 175–308. https://doi.org/10.1016/j.physrep.2005.10.009.

Bouchaud, Jean-Philippe. 2008. “Economics Needs a Scientific Revolution.” *Nature* 455 (October): 1181.

Caldarelli, Guido, and Michele Catanzaro. 2014. *Redes: Una breve introducción*. Translated by María Hernández Díaz. Edición: edición. Madrid: Alianza.

Catanzaro, Michele, and Mark Buchanan. 2013. “Network Opportunity.” *Nature Physics* 9 (3): 121–123. https://doi.org/10.1038/nphys2570.

Deguchi, Tsuyoshi, Katsuhide Takahashi, Hideki Takayasu, and Misako Takayasu. 2014. “Hubs and Authorities in the World Trade Network Using a Weighted HITS Algorithm.” *PloS One* 9 (7): e100338–e100338. https://doi.org/10.1371/journal.pone.0100338.

Hassani, Hossein, Gilbert Saporta, and Emmanuel Sirimal Silva. 2014. “Data Mining and Official Statistics: The Past, the Present and the Future.” *Big Data* 2 (1): 34–43. https://doi.org/10.1089/big.2013.0038.

INEGI. n.d. “ENIGH 2016.” Accessed May 15, 2019a. https://www.inegi.org.mx/app/biblioteca/ficha.html?upc=702825091934.

———. n.d. “Sistema de Cuentas Nacionales de México. Fuentes y Metodologías. Año Base 2013.” Accessed May 15, 2019b. https://www.inegi.org.mx/app/biblioteca/ficha.html?upc=702825097165.

Klimkova, E., Roman Senkerik, and Ivan Zelinka. n.d. “Topological Structure Analysis in Directed Network.” In .

Lara de Paz, Javier, Idalia Flores de la Mota, Gabriel Policroniades Chipuli, and O. Sashiko Shirai reyna. 2019. “WEALTH AND INCOME DISTRIBUTION: A REVIEW TOWARDS NEW TRENDS” 04 (01): 29.

Levorato, Vincent, and Coralie Petermann. 2011. “Detection of Communities in Directed Networks Based on Strongly P-Connected Components.” In *2011 International Conference on Computational Aspects of Social Networks (CASoN)*, 211–216. IEEE.

Network Science by Albert-László Barabási. n.d. Accessed May 15, 2019. http://networksciencebook.com/.

SCHWEITZER, FRANK, GIORGIO FAGIOLO, DIDIER SORNETTE, FERNANDO VEGA-REDONDO, and DOUGLAS R. WHITE. 2009. “ECONOMIC NETWORKS: WHAT DO WE KNOW AND WHAT DO WE NEED TO KNOW?” *Advances in Complex Systems* 12 (04n05): 407–422. https://doi.org/10.1142/s0219525909002337.

Shizuka, Daizaburo, and Damien R. Farine. 2016. “Measuring the Robustness of Network Community Structure Using Assortativity.” *Animal Behaviour* 112 (February): 237–46. https://doi.org/10.1016/j.anbehav.2015.12.007.

Silva, Thiago Christiano, and Liang Zhao. 2016. “Complex Networks.” In *Machine Learning in Complex Networks*, 15–70. Springer International Publishing. https://doi.org/10.1007/978-3-319-17290-3_2.

“Sistema de Clasificación Industrial de América del Norte, México SCIAN 2013.” n.d., 596.

Zanin, M., D. Papo, P. A. Sousa, E. Menasalvas, A. Nicchi, E. Kubik, and S. Boccaletti. 2016. “Combining Complex Networks and Data Mining: Why and How.” *Physics Reports* 635: 1–44. https://doi.org/10.1016/j.physrep.2016.04.005.

AUTHORS BIOGRAPHY

Javier Lara de Paz studied Physics at the Faculty of Science of National Autonomous University of Mexico (UNAM), a Specialization in Applied Statistics at the UNAM. He studied his Master’s degree in Operation Research at the Faculty of Engineering of the UNAM. He has been professor of Science at the and Operation Research professor at the Engineering School at the UNAM. Currently he is studying a Ph.D. in Operational Research at UNAM.

Idalia Flores de la Mota She received her Ph.D. in Operations Research at the Faculty of Engineering of the UNAM. She graduated Master with honors and received the Gabino Barreda Medal for the best average of her generation. She has been a referee and a member of various Academic Committees at CONACYT. She has been a referee for journals such as Journal of Applied Research and Technology, the Center of Applied Sciences and Technological Development, UNAM and the Transactions of the Society for Modeling and Simulation International. Her research interests are in simulation and optimization of production and service systems. She is a full-time professor at the Postgraduate Program at UNAM.

Gabriel Policroniades Chípuli Studied Industrial Engineering at Technological Institute and Superior Studies of Monterrey, Campus Toluca (ITESM, Campus Toluca), he studied an engineering mastery with operation research orientation and has advanced metrology studies for the calculation of uncertainty, and knowledge of Lean Six Sigma Black Belt and Logistics and supply chain. Currently he is studying a Ph.D. in Operation Research at UNAM.

O. Sashiko Shirai obtained her bachelor’s in actuarial science in the Faculty of Science of the UNAM. She is studying her Master in Operations Research in the Faculty of Engineering of the UNAM with the CONACYT scholarship. She is an assistant professor at the Faculty of Engineering and the Faculty of Science. Her research interests lie in complex networks, statistics and operational research.

FAST APPROXIMATIONS BY MACHINE LEARNING: PREDICTING THE ENERGY OF DIMERS USING CONVOLUTIONAL NEURAL NETWORKS

Dylan Hennessey[(a)], Mariusz Klobukowski[(b)], Paul Lu[(c)]

[(a)]Department of Medicine
[(b)]Department of Chemistry
[(c)]Department of Computing Science
University of Alberta
Edmonton, Alberta, Canada

[(a)]dhenness@ualberta.ca, [(b)]mariusz.klobukowski@ualberta.ca, [(c)]paullu@ualberta.ca

ABSTRACT
We introduce *fast approximations by machine learning (FAML)* to compute the energy of molecular systems. FAML can be six times faster than a traditional quantum chemistry approach for molecular geometry optimisation, at least for a simple dimer. Hardware accelerators for machine learning (ML) can further improve FAML's performance. Since the quantum chemistry calculations show poor algorithmic scaling, faster methods that produce a similar level of accuracy to the more rigorous level of quantum theory are important.

As a FAML proof-of-concept, we use a convolutional neural network (CNN) to make energy predictions on the F_2 molecular dimer system. Training data for the CNN is computed using a quantum chemistry application (i.e., GAMESS) and represented as an image. Using five-fold cross-validation, we find that the predictions made by the CNN provide a good prediction to the theoretical calculations in a fraction of the time.

Keywords: fast approximation, machine learning, molecular geometry optimisation, quantum chemistry

1. INTRODUCTION

Using the mathematical apparatus of quantum physics, quantum chemistry allows for the simulation of molecules, their properties, and chemical reactions in which they participate. From drug design to protein folding, the possibilities are vast. However, it comes with a price tag which is computing time: the Schrödinger equation, which is at the core of quantum chemistry, cannot be solved analytically for any system containing more than one electron, so we must resort to using approximations. To make matters worse, these approximate methods are iterative, with no guarantee of them converging, and even when they do converge there is no guarantee that they have converged to the global minimum of the problem. By far the biggest roadblock is that even the least accurate of a truly quantum theory has a scaling rate of n^4 (n can be loosely thought of as the size of a system, but it might perhaps be better thought of as how accurately we are describing a system). The most accurate level of theory, full configuration interaction, would take an infinite amount of time to compute the first iteration of its solution for just a single helium atom. Modern processors and graphics processing units (GPUs) have helped reduce computing time substantially, but we are still far away from describing large, asymmetrical systems like proteins at the quantum level in any reasonable amount of time. However, there might be a workaround.

Machine-learning (ML) algorithms have been successful in classifying images with high accuracy (Krizhevsky, Sutskever, and Hinton 2012), learning the parameters of data network protocols (Sivaraman *et al.* 2014), and other tasks. The desire for ML performance has spawned specialized hardware (e.g., tensor processing units (TPUs) (Joupii *et al.* 2017)), representing another enticing technology curve for the high-performance computing (HPC) community. As such, it could be beneficial for quantum chemistry if it can make use of ML algorithms.

Most computational quantum chemists are not interested in any arbitrary molecular geometry. They are usually only interested in regions around the most *stable* geometry, which is the one that minimizes the total energy (equal to the sum potential and kinetic energies) of the system. Once the most stable geometry has been found, work can begin on calculating other properties of interest. Algorithm 1 shows the pseudocode for this geometry optimizing process.

We consider an atypical use of ML as part of this larger, generalized molecular geometry optimisation. Instead of using HPC to improve the ML implementation, we consider how ML can improve an HPC computation via *fast approximations by machine learning* (FAML). For example, computing the total energy of a molecule (i.e., lines 3 and 8, Algorithm 1) is both computationally expensive (Schmidt *et al.* 1993) and central to each iteration of the optimisation algorithm. Multiple cores and general-purpose graphics processing units (GPGPU) (Schmidt *et al.* 1993; Abadi *et al.* 2015) can be used to accelerate the energy calculation, but we consider the use of neural networks as a different kind of accelerator.

Algorithm 1: Generalized Molecular Geometry Optimisation, Pseudocode

```
thresh = minimum change in total energy from one geometry
    state to another
current_geo = guess of optimal geometry
current_energy = total energy of current_geo
old_energy = 0

        old_energy = current_energy
        update current_geo based on derivative of the total energy
            with respect to the geometry
        current_energy = total energy of current_geo
end while
return current_energy, current_geo
```

Attempts at this have already been made. von Lilienfeld *et al.* (Montavon *et al.* 2013) made a simple neural network composed of four hidden fully connected (FC) layers and used what they call a "Coulomb matrix" as its input. The Coulomb matrix is given by

$$M_{i,j} = \begin{cases} \frac{Z_i^{2.4}}{2} & \text{if } i = j \\ \frac{Z_i Z_j}{|R_i - R_j|} & \text{if } i \neq j \end{cases} \tag{1}$$

where i and j refer to nuclei, Z_i is the nuclear charge of nuclei i, and $|R_i - R_j|$ is the distance between nuclei i and j. Their network makes predictions on 14 different properties of the system in question. They trained on 5,000 different molecules and tested on 2,211 molecules. The network was able to obtain an accuracy good enough for the predictions to be usable, and that is commendable. However it is worth pointing out that a network made only of FC layers is very simple, and a more complicated type of network could perform much better.

As a proof-of-concept, we show that convolutional neural networks (CNNs) can be used to accurately predict the energy of a molecule with a specific geometry. The CNN-based FAML is six times faster than using a traditional quantum chemistry approach, at least for fluorine dimers (F_2). Quantum chemistry algorithms are still used offline to create the training data for the CNN, training is offline, but when implemented in an actual geometry optimisation calculation, only the pre-trained CNN would need to be used online.

Currently, GPGPUs are used to both train and evaluate the CNNs. For future work, we plan to extend the current results to different dimers, and to larger molecules. Also, in theory, FAML makes it feasible to use specialized ML hardware (e.g., TPUs (Joupii *et al.* 2017)) for higher performance, especially since it is not known how quantum chemistry algorithms can be directly adapted to non-GPGPU accelerators.

1.1. Convolutional Neural Networks (CNNs)

CNNs (LeCun *et al.* 1989) are typically composed of three different layers: convolution layers, pooling layers, and FC layers. How these work on a more technical level can be a bit complex, so we will go over each layer individually, starting with the FC layers.

1) FC Layers: An FC layer is really just a single layer from a multilayer perceptron (Zupan and Gasteiger 1993) [8]. The vector of activations h for the FC hidden layer l is given by the following equation

$$h^l = f\left(\Theta^l h^{l-1} + b^l\right) \tag{2}$$

where Θ^l is a matrix of weights, b^l is a vector of biases, and f is a non-linear function. While the sigmoid function $f(x) = 1/(1 + e^{-x})$ was used extensively in the past, the rectified linear unit (ReLU) function is much more commonly used today. It is given in equation 3.

$$f(x) = \begin{cases} x & \text{if } x \geq 0 \\ 0 & \text{if } x < 0 \end{cases} \tag{3}$$

The first derivative of a ReLU is 1 if $x \geq 0$ and 0 otherwise. This is far simpler than the first derivative of the sigmoid function, which helps greatly during the training process, especially with large CNNs.

2) Convolutional Layers: The convolutional layers are what allows a CNN to become so accurate. Instead of every neuron using all of the data from the previous layer, a neuron in a convolutional layer uses only a subset of the information from the previous layer. This is given mathematically by

$$h_{i,j}^{l,f} = f\left(\left[\sum_{q=1}^{o}\sum_{c=0}^{m-1}\sum_{d=0}^{n-1}\Theta_{c,d}^{l,f,q} h_{x,y}^{l-1,q}\right] + b^{l,f}\right) \tag{4}$$

where i and j are the coordinates of a neuron, m and n are the dimensions of the filter matrix, $x = i\text{-}(m\text{-}1)/2+c$, $y = j\text{-}(n\text{-}1)/2+d$ (here we are assuming that m and n are odd), o is the number of features of the previous layer $l-1$, and f is the feature of the current layer l that we are solving for.

3) Pooling: If we do not stride through the $l-1$ layer, layer l will have the exact same dimensions as layer $l-1$. Typically, we compress the l layer in some way. The most common way of doing this is through *pooling*. This is where we look at one particular neuron and its neighbours and apply some function to them. If we took only the maximum value for a feature of one neuron and its neighbours, this would be *max pooling*. Another common way of doing this is *average pooling*. An example of pooling is as follows. After applying Equation 4, we are left with output that has dimensions of 28 × 28 × 3. For a pooling window of 2 × 2 and for the first feature, we would look at the data in $h_{0,0}^{l,1}$, $h_{1,0}^{l,1}$, $h_{0,1}^{l,1}$, and $h_{1,1}^{l,1}$ (notice how pooling is done with respect to a single feature, so we would have to do three different pooling operations for each where i and j coordinates). In max pooling, we would take the maximum value for these data points, and this would become the value of $h_{0,0}^{l_p,1}$ where l_p is the pooled layer of layer l. We would stride through the un-pooled layer in steps equal to the dimension of the pooling window (so $h_{0,1}^{l_p,1}$ would be the max of $h_{0,2}^{l,1}$, $h_{1,2}^{l,1}$, $h_{0,3}^{l,1}$, and $h_{1,3}^{l,1}$ and so on) until we have gone through the whole of layer l. The output of this pooling operation would compress the input by a factor of four, so the output would have dimensions of 14 × 14 × 3.

Pooling can be thought of as "summarizing" the features of each group of neurons. This allows for layers to specialize the kind of features they look for, and also allows for deeper layers to look for more complex features without needing to greatly expand the window they look at. For instance, the first layer of a CNN might only look for curves and straight lines, the next layer might look for basic shapes like circles, squares, and triangles, and the deepest layers would look for things like faces and other objects.

2. METHODS

The overall goal of this work is to make a CNN that can accurately predict properties of a chemical system. As a first step, we designed a CNN that can predict the total energy of the system, the kinetic energy of the electrons, the potential energy of attraction between electrons and nuclei, the potential energy of repulsion between electrons, and the potential energy of repulsion between nuclei. We chose these because optimizing the geometry of a chemical system requires finding a molecular geometry (i.e., coordinates of atoms in a molecule) where the total energy is at a minimum. This adds a further layer of iterative calculations to an already computationally difficult task and it would be good if there was a method of placing atoms in sensible locations beforehand. Because CNNs work best at image recognition, we need some way to turn a molecule into something that resembles an image. We achieve this in the following way.

2.1. Digitizing Chemical Space

First, we begin by choosing the size of the dimensions of the image to be 512 × 512 × 3. Each pixel of the image represents a $(0.01\text{Å})^2$ area of space. Note that this restricts us to two-dimensional chemical systems. An area of $(0.01\text{Å})^2$ was chosen because changes in molecular geometry smaller than this do not have a strong impact on the properties we want to predict. An image size of 512 × 512 was chosen because this gives us enough room to dissociate dimers, and also to optimize performance on GPUs.

At a simple level, the energy of a molecular system is a function of the nuclear charges present, and the coordinates in space that the nuclei occupy. Everything else can be derived from just these inputs. Because of this, the features of a pixel should at least include the nuclear charge of the nuclei occupying that pixel. For a dimer system, this would produce an image that is completely black except for two white pixels. Even though in theory this should be all that is needed, we are not giving the CNN much to work with. Therefore, we decided to include some additional information to help point the CNN in the right direction.

We thought that it might be helpful to include some information about the attractive and repulsive forces. We did this by including a simplified version of the bonding orbital that would form between the 1s electrons in the system, as well the anti-bonding orbital that would form. These were calculated from Gaussian type orbitals, given by the following equations

$$I_{i,j,2} = \sum_{k=1}^{n} N_k e^{-Z_k r_{ij}^2} \tag{5}$$

$$I_{i,j,3} = \frac{1}{2} \sum_{k=1}^{n} \sum_{l=1}^{n} |N_k e^{-Z_k r_{ij}^2} - N_l e^{-Z_l r_{ij}^2}| \tag{6}$$

where $I_{i,j,x}$ is the x^{th} channel of the pixel at i,j, n is the number of nuclei in the system, r_{ij} is the distance of the pixel i,j, from nuclei k, and N_k is a normalization constant that satisfies

$$N_k^2 \int_0^{\infty} r^2 |e^{-Z_k r^2}|^2 dr = 1 \tag{7}$$

An example of what these images look like is shown in Fig. 1.

Figure 1: The image produced by the Equations 5, 6, and 7. The atoms are F. The green channel is assigned Equation 5, the blue channel is assigned Equation 6, and the red channel is assigned the Z of the nuclei. Note that the image has been normalized such that the maximum value of any channel is 255 and the minimum is 0.

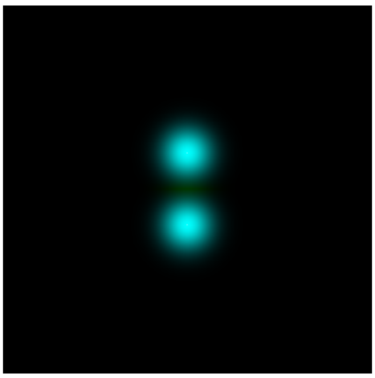

As for the actual training data, we use the results of GAMESS (Schmidt *et al.* 1993) calculations at the CASSCF (Siegbahn *et al.* 1981; Roos, Taylor, and Siegbahn 1980; Siegbahn *et al.* 1980) level of theory and the 6-311+G(2d,2p) basis set (Krishnan *et al.* 1980; Clark *et al.* 1983; Frisch, Pople, and Binkley 1984) on F_2 dimers. The dimers have randomly generated coordinates, so we can be reasonably sure that there are no exact duplicates.

2.2. CNN Architecture

As mentioned, the input layer for our CNN has dimensions of 512 × 512 × 3. We chose a filter with dimensions of 5 × 5 for each hidden layer. The first hidden layer takes in the 3 channels from the input layer, and outputs 32 new features. The value of 32 was chosen for optimisation of the calculations on GPUs. The first hidden layer will have 5×5×3×32 weights and 32 biases. The output of this layer goes through an average pooling operation with a 2 × 2 window and a stride of 2. The output after pooling has dimensions of 256×256×32. Because spatial information is so important to these calculations, each subsequent layer pulls out twice the number of features than the layer before it, in the hopes that this will preserve enough of the information that would get compressed by pooling. In total, there are five convolutional layers and five average pooling operations. The output of the last layer has dimensions of 16 × 16 × 512. This then gets reshaped into a vector with 131072 dimensions, and then goes through the FC layers. There are two FC layers, the first has a weight matrix with dimensions of 131072 × 2048, and the second has dimensions of 2048 × 2048.

In a preliminary study (unpublished), we found that the predictions of total energy were more accurate if we also trained the CNN to predict the electron kinetic energy, the electron-electron repulsion potential energy, the electron-nuclei attraction potential energy, and the nucleus-nucleus repulsion potential energy at the same time. Therefore, the output layer has a weight matrix with dimension of 2048 × 5 and the outputs are the five energy types just described. ReLUs are used for all layers except the output layer, which uses no activation function. A dropout of 50% is also included between the two FC layers, and the output.

2.3. Initialization and Training

The weights and biases are initialized with random numbers from a normal distribution with zero mean and a standard deviation of 0.1. We use the mean absolute error (MAE) as the error function, and we optimize the error using the Adam optimisation algorithm (Kingma and Ba 2014) and a batch size of 32. We performed some initial calculations using 80% of the data to train on and the remaining 20% for testing. We used 5 fold cross-validation for more in-depth experiments. Each fold was constructed by sorting the data by distance between dimers, and then distributing them to each fold round-robin style.

3. EMPIRICAL RESULTS AND DISCUSSION

We generated 100,000 systems ranging in distance from 1.00Å−7.24Å. We found that the energy was skewed in favour of the lower energies, so we added approximately 90,000 more examples that ranged from 1.00Å−1.50Å. We then normalized the energies with the following equation

$$e' = \frac{e - e_{\min}}{e_{\max} - e_{\min}} \tag{8}$$

where e′ is the normalized value of energy *e*, and e_{max} and e_{min} are the maximum and minimum values for the energies of the same type as *e*. This uniformly scales all energies of the same type between zero and one. This helps to reduce the training time, as the CNN does not have to spend as much time trying to find the range of the data. Even so, it can take as long as approximately 40 hours to complete 14 epochs for the F_2 CNN. The results of training for over 14 epochs are given in Table 1.

We can see that the results between folds are all similar. The largest deviations for each energy type is given in Table 2. Scatter plots showing how the predictions line up with their actual values, as well as how the predictions match up to the energy curves are in Figures 2 and 3.

Table 1: The MAE when predicting the total energy (TE), the kinetic energy of electrons (EKE), the potential energy of attraction between electrons and nuclei (ENPE), the potential energy of repulsion between electrons (EEPE), and the potential energy of repulsion between nuclei (NNPE) of a F_2 dimer. Energy is given in Hartree units. Folds 0 to 2 had 37,896 images. Folds 3 and 4 had 37,895 images.

Fold	TE	EKE	ENPE	EEPE	NNPE
0	0.00177	0.0118	0.449	0.207	0.213
1	0.00141	0.0093	0.287	0.163	0.178
2	0.00138	0.0097	0.345	0.219	0.220
3	0.00143	0.0100	0.283	0.209	0.200
4	0.00171	0.0116	0.438	0.195	0.220

Table 2: Largest absolute deviations (LAD) for the predictions of the total energy (TE), the kinetic energy of electrons (EKE), the potential energy of attraction between electrons and nuclei (ENPE), the potential energy of repulsion between electrons (EEPE), and the potential energy of repulsion between nuclei (NNPE) of a F_2 dimer. Energy is given in Hartree units. Distances are given in Å.

Energy Type	LAD	Actual Energy of LAD	Distance of LAD
TE	0.0621	-198.534	1.0008
EKE	0.3181	200.631	1.0024
ENPE	3.2617	-560.249	1.0309
EEPE	2.0255	120.571	1.0066
NNPE	2.2541	42.581	1.0066

Finally, we discuss how the CNN is six times faster than GAMESS in predicting the energy of the dimer molecule. As there is a reduction in the accuracy, there would be little point in using this method if the predictions took longer than using the actual GAMESS program. To make a prediction, the image must first be generated, then the image must be converted into a form TensorFlow can use, and then the data must flow through the CNN.

For the nearly 190,000 molecules used in our experiment, the average time for generating the images is 0.068s per image, the average time for converting the data for TensorFlow is 0.117s per image, and the average time for running the data through the CNN is 0.028s per image. This gives a total time of 0.213s per image. The average time per F_2 calculation using GAMESS is 1.227s. This means that the CNN is almost six times faster. It is also worth pointing out that for anything that will fit into the dimensions of the image we use should require approximately the same amount of time for the CNN to predict, while the time need to calculate larger systems will increase dramatically.

4. CONCLUDING REMARKS

The HPC, ML, and computational science communities are interacting in a variety of interesting ways. First, well-known HPC techniques such as GPGPUs and specialized hardware are improving the performance of ML and scientific computations. Second, ML techniques such as the fast approximations by machine learning (FAML) strategy introduced here, can potentially replace an expensive computation (e.g., quantum chemistry) with a faster ML computation, and stay within acceptable limits of accuracy and error. Using FAML for molecular geometry optimisation (Algorithm 1), the expensive quantum chemistry calculation can be done offline, the ML training can be done offline, so that the cheaper CNN evaluation is all that is done online. Third, FAML provides (in theory) a feasible way to take advantage of a technology trend towards specialized hardware for ML (e.g., TPUs (Joupii *et al.* 2017)) that is less obvious for, say, traditional computational quantum chemistry algorithms. Opportunities to exploit these interactions may provide significant performance benefits, such as the six-fold increase in performance of the CNN-based FAML, for a dimer.

While this study is mostly a proof-of-concept, its findings are promising. We have shown that CNNs offer a viable method of shortening the time needed to predict the energy of a simple molecular system. The predictions made by our CNN have an average of only 0.001 MAE with respect to calculations performed by GAMESS, and are also much faster to obtain. We have shown that we can increase the accuracy of predictions by simultaneously making predictions of related data. We have also shown that generating the training data by randomly generating geometries of molecular systems is valid, so long as the level of theory can dynamically describe the breaking of electron pairs.

In a future study, we will design a CNN that is able to make predictions about dimers with different atoms. It would also be interesting to see if the CNN can make accurate predictions about molecules it has never seen before. For instance, we might train the CNN on the molecules H_2, F_2, Cl_2, FCl, and HF, and then see if the CNN can accurately make predictions on HCl, which is outside of the training set. Finally, we plan on empirically evaluating a CNN-based FAML in an actual, end-to-end, molecular geometry optimisation computation.

ACKNOWLEDGMENTS

This research was funded by the University of Alberta and Natural Sciences and Engineering Research Council (NSERC) of Canada. The NSERC Discovery Grants to Mariusz Klobukowski and Paul Lu are gratefully acknowledged. This research was enabled in part by support provided by Compute Canada (http://www.computecanada.ca).

REFERENCES

Abadi M., A. Agarwal, P. Barham, E. Brevdo, Z. Chen, C. Citro, G.S. Corrado, A. Davis, J. Dean, M. Devin, S. Ghemawat, I. Goodfellow, A. Harp, G. Irving, M. Isard, Y. Jia, R. Jozefowicz, L. Kaiser, M. Kudlur, J. Levenberg, D. Mane, R. Monga, S. Moore, D. Murray, C. Olah, M. Schuster, J. Shlens, B. Steiner, I. Sutskever, K. Talwar, P. Tucker, V. Vanhoucke, V. Vasudevan, F. Viegas, O. Vinyals, P. Warden, M. Wattenberg, M. Wicke, Y. Yu, and X. Zheng, "TensorFlow: Large-scale machine learning on heterogeneous systems," 2015, software available from tensorflow.org. [Online]. Available: https://www.tensorflow.org/

Clark T., J. Chandrasekhar, G. Spitznagel, and P.V. Schleyer, "Efficient diffuse function-augmented basis sets for anion calculations. III. The 3-21+G basis set for first-row elements, Li–F," *J. Comp. Chem.*, vol. 4, pp. 294–301, 1983.

Frisch M.J., J.A. Pople, and J. Binkley, “Self-consistent molecular orbital methods 25. Supplementary functions for Gaussian basis sets,” *J. Chem. Phys.*, vol. 80, pp. 3265–3269, 1984.

Joupii N., C. Young, N. Patil, and D. Patterson, “In-datacenter performance analysis of a tensor processing unit,” in *Proceedings of the 44th Annual International Symposium on Computer Architecture, ISCA 2017, Toronto, ON, Canada, June 24-28, 2017*, 2017, pp. 1–12.

Kingma D.P. and J. Ba, “Adam: A method for stochastic optimization,” *CoRR*, vol. abs/1412.6980, 2014. [Online]. Available: http://arxiv.org/abs/1412.6980

Krishnan R., J. Binkley, R. Seeger, and J.A. Pople, “Self-consistent molecular orbital methods. XX. A basis set for correlated wave functions,” *J. Chem. Phys.*, vol. 72, pp. 650–654, 1980.

Krizhevsky A., I. Sutskever, and G.E. Hinton, “Imagenet classification with deep convolutional neural networks,” in *Advances in Neural Information Processing Systems 25*, F. Pereira, C. J. C. Burges, L. Bottou, and K. Q. Weinberger, Eds. Curran Associates, Inc., 2012, pp. 1097–1105.

LeCun Y., B. Boser, J.S. Denker, D. Henderson, R.E. Howard, W. Hubbard, and L.D. Jackel, “Backpropagation applied to handwritten zip code recognition,” *Neural Comput.*, vol. 1, no. 4, pp. 541–551, Dec. 1989. [Online]. Available: http://dx.doi.org/10.1162/neco.1989.1.4.541

Montavon G., M. Rupp, V. Gobre, A. Vazquez-Mayagoitia, K. Hansen, A. Tkatchenko, K.-R. Moller, and O.A. von Lilienfeld, “Machine learning of molecular electronic properties in chemical compound space,” *New Journal of Physics*, vol. 15, no. 9, p. 095003, 2013. [Online]. Available: http://stacks.iop.org/1367-2630/15/i=9/a=095003

Roos B.O., P. Taylor, and P.E.M. Siegbahn, “A complete active space SCF method (CASSCF) using a density matrix formulated super-CI approach,” *Chem. Phys.*, vol. 48, pp. 157–173, 1980.

Schmidt M.W., K.K. Baldridge, J.A. Boatz, S.T. Elbert, M.S. Gordon, J.H. Jensen, S. Koseki, N. Matsunaga, K.A. Nguyen, S. Su, T.L. Windus, M. Dupuis, and J.A. Montgomery, “General atomic and molecular electronic structure system,” *J. Comput. Chem.*, vol. 14, no. 11, pp. 1347–1363, 1993.

Siegbahn P.E.M., J. Almlof, A. Heiberg, and B.O. Roos, “The complete active space SCF (CASSCF) method in a Newton-Raphson formulation with application to the HNO molecule,” *J. Chem. Phys.*, vol. 74, no. 4, pp. 2384–2396, 1981.

Siegbahn P.E.M., A. Heiberg, B.O. Roos, and B. Levy, “A comparison of the super-CI and the Newton-Raphson scheme in the complete active space SCF method,” *Phys. Scr.*, vol. 21, pp. 323–327, 1980.

Sivaraman A., K. Winstein, P. Thaker, and H. Balakrishnan, “An experimental study of the learnability of congestion control,” in *Proceedings of the 2014 ACM Conference on SIGCOMM*, ser. SIGCOMM ’14. New York, NY, USA: ACM, 2014, pp. 479–490.

Zupan J. and J. Gasteiger, *Neural Networks for Chemists: An Introduction*. New York, NY, USA: John Wiley & Sons, Inc., 1993.

AUTHORS BIOGRAPHY

Dylan Hennessey completed an M.Sc. in Chemistry at the University of Alberta (2018), under the supervision of Mariusz Klobukowski. He is currently engaged in bioinformatics research in the Department of Medicine.

Mariusz Klobukowski is a Professor of Chemistry, Department of Chemistry, University of Alberta. His research program is focused on the development and applications of methods for accurate computational studies of electronic structure, geometry, vibrational spectra, reaction mechanisms, and one-electron properties of organometallic molecules, molecular ions, and molecular clusters in their ground and excited electronic states.

Paul Lu is a Professor of Computing Science, Department of Computing Science, University of Alberta. His research interests are in the area of software systems, including parallel and distributed systems, operating systems, file systems, high-performance computing, and network protocols. He is also one of the co-developers of the “Problem Solving, Python Programming, and Video Games” (PVG) (2018) massive open online course (MOOC) on the Coursera platform.

Figure 2: Scatter plots made from the predictions of the total energy (a), kinetic energy (b), electron-nuclei potential energy (c), electron-electron potential energy (d), and nuclei-nuclei potential energy (e). Results from all folds for the F_2 CNN are shown. Energies are given in Hartree units. The black diagonal line in each plot shows where perfect predictions lie. The green line shows the range of predictions that fall within the MAE. The red line shows the range of predictions that fall within the largest error.

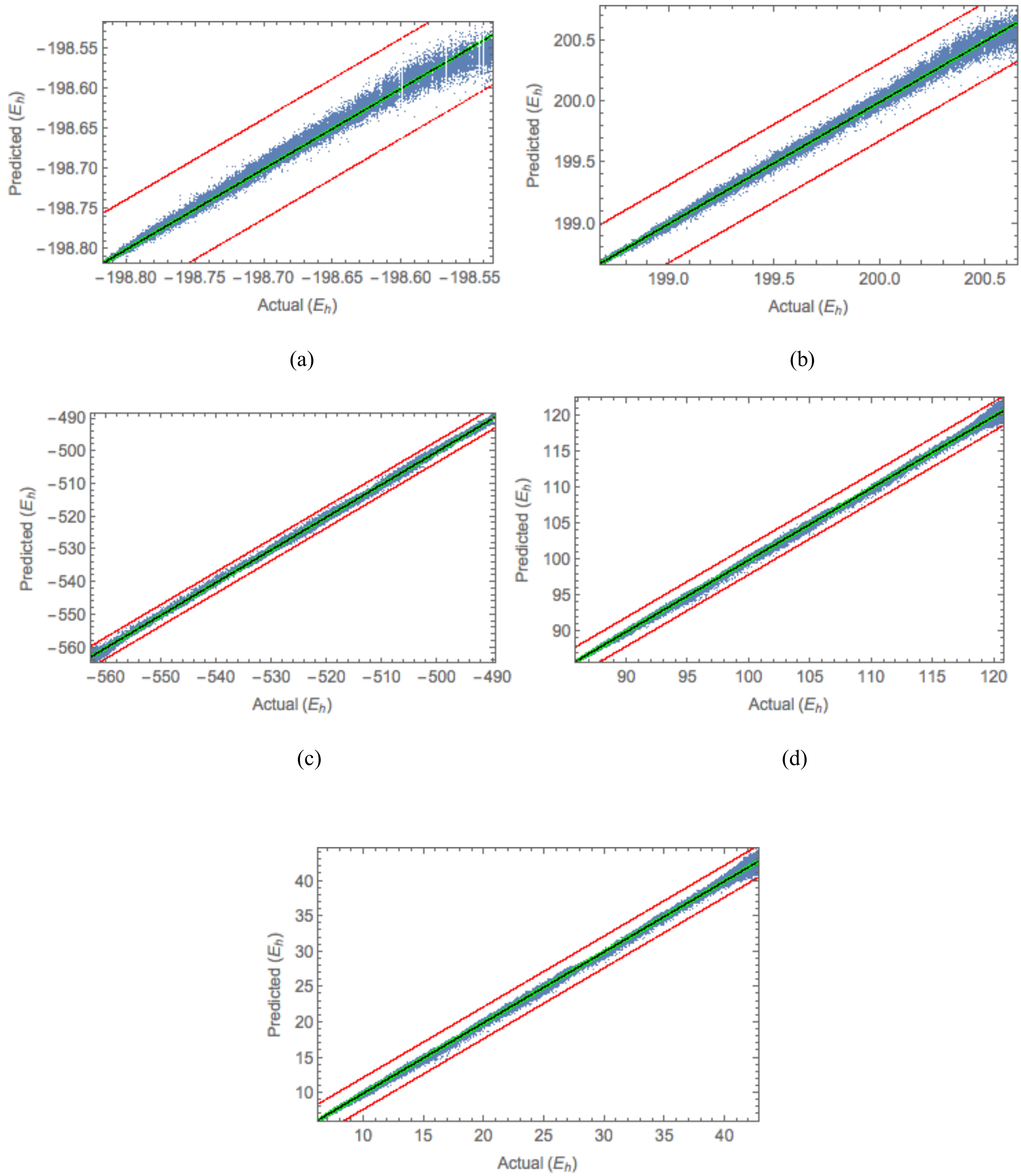

(a)

(b)

(c)

(d)

(e)

Proceedings of the European Modeling and Simulation Symposium, 2019
ISBN 978-88-85741-25-6; Affenzeller, Bruzzone, Longo and Pereira Eds.

Figure 3: The predictions of the energy curves as a function of the distance between dimers for the total energy (a), kinetic energy (b), electron-nuclei potential energy (c), electron-electron potential energy (d), and nuclei-nuclei potential energy (e). Results from all folds for the F_2 CNN are shown. Energies are given in Hartree units and distances are given in Å. The black points in each plot show where perfect predictions lie. The green points show the range of predictions that fall within the MAE. The red points show the range of predictions that fall within the largest error.

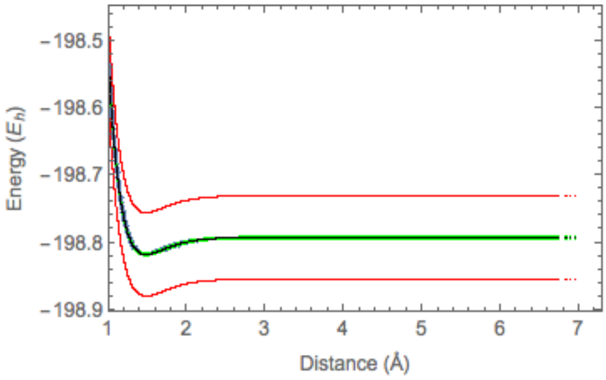

(a)

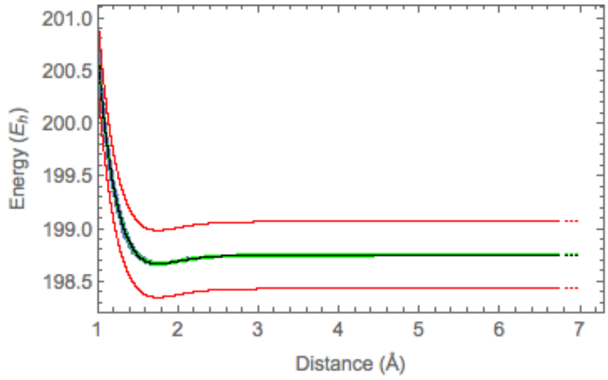

(b)

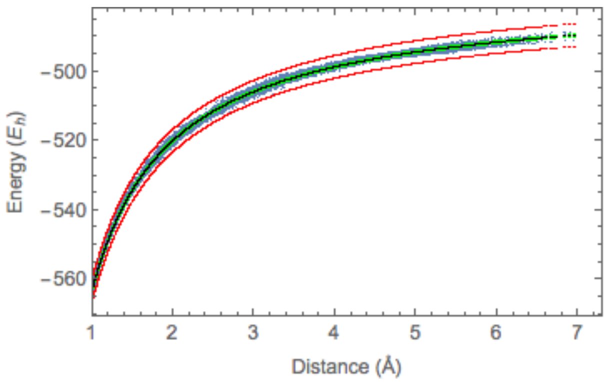

(c)

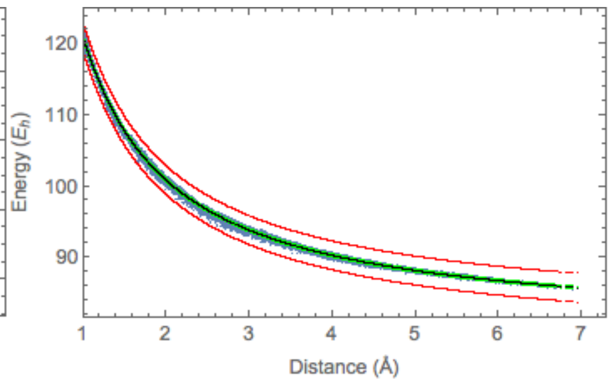

(d)

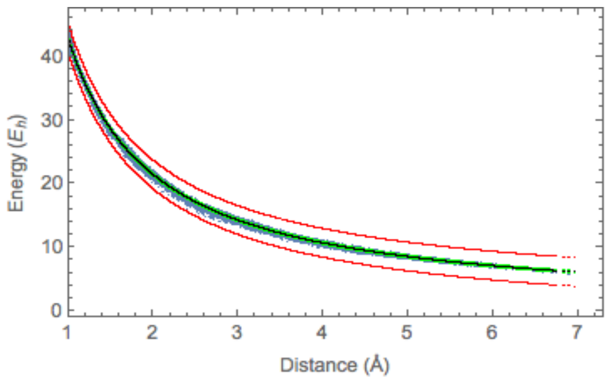

(e)

SUSTAINABLE TECHNOLOGIES FOR HEALTH EDUCATION IN LOW AND MIDDLE INCOME COUNTRIES

Elisa Ferrara [(a)], Silvana Dellepiane [(b)], Marco Frascio [(c)]

[(a),(b)] Dept. of Naval, Electrical, Electronics and Telecommunication Engineering (DITEN), University of Genoa, Via all'Opera Pia, 11a, 16145 Genoa - Italy -
[(c)] Dept. of Surgery Sciences (DISC) University of Genoa, Largo R. Benzi, 8 16132 Genoa - Italy -
[(a)] elisa.ferrara@edu.unige.it, [(b)] silvana.dellepiane@unige.it, [(c)] mfrascio@unige.it

ABSTRACT
Sustainable technologies and collaborative Learning Management Systems (LMS) are investigated according to the Sustainable Development Goals (SDGs), as possible ways to improve, towards distance learning systems, education and towards it, social empowerment and development. Web -based systems, customized for academic teaching in medicine and surgery field, could help the development of cooperation among universities as well as research empowerment and exchange, useful for all the involved stakeholders. Different uses and approaches to the technological solution allow different participants to model and interact with the project despite also difficulties and environmental gaps that could occur in some LMIC.

Keywords: Sustainable technologies, LMS, mHealth, medicine and surgery education.

1. INTRODUCTION
Low and Medium Income Countries (LMIC) are here defined as the World Bank does, under a financial point of view. This means that in the present work we should consider Low-Income economies as those with a GNI per capita of $1,005 or less; Middle-Income countries (MICs) nations with a per-capita gross national income in 2016 between $1,005 and $12,615. Low-Income and Middle-Income economies are collectively referred to as developing economies. [1]
Among the LMIC it is countable the greatest concentration of criticality in terms of poverty, disease and low levels of education and professional education, given mostly by lack of social security as well as a presence of low level political actions and policies.
In order to meet the seventeen Sustainable Development Goals (SDGs) – which range from halving extreme poverty rates to halting the spread of HIV/AIDS and providing universal primary education, all by the target date of 2030 – a blueprint agreed by all the world's countries and all the world's leading development institutions has been exploited. The goals this paper will partially address are goal 3 and 4.
SDG number 3 "Ensure healthy lives and promote well-being for all at all ages" seeks to ensure health and well-being for all, at every stage of life.
The Goal addresses all major health priorities, including:

- reproductive, maternal and child health;
- environmental diseases;
- universal health coverage;
- access for all to safe, effective, quality and affordable medicines and vaccines.

It pushes empowerment in research and development, increased health financing, and strengthened capacity of all countries in health risk reduction and management.
SDG Number 4 "Ensure inclusive and equitable quality education and promote lifelong learning opportunities for all", aims to help in achieving inclusive and equitable quality education for all will require increasing efforts, especially in sub-Saharan Africa and Southern Asia and for vulnerable populations, including persons with disabilities, indigenous people, refugee children and poor children in rural areas. [1]
According to the World Health Organization data, in the world there is a shortage of health care workers for a total amount of 7.2 million people [2]. This is supposed to grow up to 12.8 million in 2035.
This is evident especially for LMIC and, according to the Sustainable Development Goals, promotion of both high education and health is a concrete target to join, that Information and Communications Technology ICT use can easily improve.
In many countries a big effort is made in order to increase health care workforce and to make a coherent distribution in underserved areas but it is a work in progress situation.
In face of severe faculty shortages in resources constrained countries, medical schools look to e-learning systems for improved access to medical education and in this work we will try to analyse some possibilities

2. DEFINITION AND TARGET
In order to improve the quality of education and increase the pool of people who can benefit of it, priority solution should be given to "brain drain" phaenomenon [4]; due to lack of adequate training, people coming from LMICs decide to study in other countries mostly in Europe. After their graduation, they often refuse to return to the land of origin due to an absence of solid social guarantees and the prospect of a salary inadequate to their preparation. In the education of workers in medical area can be strongly and locally supported by the improvement of ICT based solutions in the educational and health care environments.

In such particular contexts like LMICs are, the consideration of infrastructures and technologies to be chosen is fundamental. [5]
The definition of sustainability that has been considered in this work is "the feature of a process that can be maintained at a certain level indefinitely "[3]
A technological system is sustainable when it offers different is the possibility of training locally all the people involved as well as the possibility to find locally al the technical, the simplicity and ease of use and maintenance.
African Countries started a real process of empowerment and recovery already in the last 20 years [6].
The development of communication on a global scale has given rise to the ICT, which is realized through a wide range of infrastructures, services, content and applications, from traditional telecommunications to the Internet, by mass media (such as television) and individual communication media (such as telephone and the computer), to advanced applications of telematics systems. [7][8][9]
Along with this, from the technological point of view, an interesting phenomenon has started to take place, that is the spread of mobile communication and technologies [10].
According to the International Telecommunication Union there are now close to 5 billion mobile phone subscriptions in the world, with over 85% of the world's population now covered by a commercial wireless signal [11].
Communication development and the globalization phenomenon involved also the spread of the diffusion on ICT through an extensive variety of infrastructures, offerings, content material and applications, from conventional telecommunications to the internet, via mass media (which includes television) and personal communication media and tools like the mobile and smartphones and laptops. [7][8][9]
Together with this, from the technological point of view, a thrilling phenomenon has started, this is the unfold of cellular and mobile communication and technologies [10].
In line with the International telecommunication Union at the moment there are close to five billion cellular smartphone in the world, and more than 85% of the global surface is now covered by a wireless signal [11].
The penetration of mobile phone networks in many low- and middle-income countries surpasses other infrastructure such as paved roads and electricity, and dwarfs fixed Internet deployment [10]. The growing sophistication of these networks – offering higher and higher speeds of data transmission alongside cheaper and more powerful handsets – are transforming the way health services and information are accessed, delivered, and managed. With increased accessibility comes the possibility of greater personalization and citizen-focused public health and medical care [12] [13].
ICT has been largely introduced in medicine, both in education [14] and in clinical practice as in surgery and medicine [15]

The unprecedented spread of mobile technologies as well as advancements in their innovative application to address health priorities has evolved into a new field of eHealth, known as mHealth.
mHealth is a component of eHealth. To date, no standardized definition of mHealth has been established. The main definition can consider mHealth or mobile health as medical and public health practice supported by mobile devices, such as mobile phones, patient monitoring devices, personal digital assistants (PDAs), and other wireless devices.
mHealth may involve the use on a mobile phone's core utility of voice and short messaging service (SMS) as well as more complex functionalities and applications including general packet radio service (GPRS), third and fourth generation mobile telecommunications (3G and 4G systems), global positioning system (GPS), and Bluetooth technology[13].
In such an environment, e-learning provides the opportunity to extend new medical courses and reach distant students from the main university centres.
Along with e learning and cooperative learning methods, in such an important field like health education, there are also simulation and remote monitoring systems that can help in improving the service, especially in geographical remote areas and countries.
We will explore these opportunities in the next paragraphs.

3. APPLICATION

We can define different types of e-learning, always considering all the forms of electronically-mediated teaching [8]
It is teaching and learning through ICT inside the classroom or outside. In some cases it could be also included the use of ICT as telemedicine system, allowing students to interact on a real case study session [14].
The e-Learning systems refer to the use of internet technologies and bring to a real collaborative and responsible interaction of the learners who can have a control over content, tailoring their experience in order to meet their personal learning objectives. Individuals are assumed to learn better when they discover things by themselves and when they control the pace of learning. Therefore, it is natural to expect that self-directed, interactive learning would improve learning outcome.
The most common system of e-learning are distance learning systems and computer assisted instruction; both of them have the purpose to increase accessibility to information through the ease of distribution and the standardization of content [15].
E-Learning therefore has become one of the fastest-moving trends [16] and aims to provide a configurable infrastructure that integrates learning material, tools, and services into a single solution to create and deliver training or educational content quickly, effectively, and economically.
It is possible to state that e-Learning is a process that helps in develop, manage, deliver and standardize knowledge contents.

In order to perform a good service through an e learning system we should consider some aspects and components of the entire process of management and release of the content, within the system itself.
Contents: it is possible to define as content all the instructional and digital learning objects, and the digital materials assembled around specific learning lessons or modules.
Management: all the administrative functions (storing, indexing etc.) to make content available to students; this phase could be lead through portals, repositories and libraries;
In this phase the introduction of Learning Management Systems (LMS) could become an effective improvement, since they can help in simplifying and automate teacher tasks, track students' achievement of skills and they finally are repositories available 24h /7. [13]
Linked to this the transport of content material in synchronous and asynchronous manner is an instantaneous effect.
The synchronous mode gives the possibility of an actual time delivery, all novices speak with other inexperienced persons and get hold of the lesson concurrently.
With the asynchronous mode, transmission and receipt aren't simultaneous and freshmen are responsible of their very own training and learning. Communication among instructors and newbies is supplied with the aid of emails or other technologies but not in actual time.
The importance of collaboration within distance getting to know methods, particularly in asynchronous systems has been highlighted already in literature [7]; [8]; [9]; [10] .LMS allow students to communicate with their peers and tutors thus empowering them to socialise and learn together also through remote technological systems helping in participating to their own education.
One example can be the Aquilone Project, ruled by University of Genova; a web-based system, customized for an academic year proposal in medicine and surgery field, has been settled up, in order to help the development of cooperation among universities and research empowerment and exchange: a University in Cameroon has been involved [17][18].
The system has been evaluated useful for both entities and their stakeholders. Different uses and approaches to the technological solution allowed different participants to model and interact with the project despite difficulties and environmental gabs that could occur in some territories for example in Sub-Saharan countries.
Another way to improve a good education in health care studies, is the simulation serious game.
An innovative approach is the application of serious games concepts in supporting and renew the educational processes in Health Care. One of the best way is application of new models of virtual humans to be used as patients in a distributed simulation game together with students to teach them concepts related to the continuous care of patients; the aim could be to create a strong relationship between medical doctor students and their set of personal virtual patients, driven by intelligent agents.

By following this approach, it is possible to reproduce the patient life cycles and teach students on subjects such as pathology evolution, preventive actions, symptoms identification and human relationships. MARIA (Model for Advanced and Realistic patient simulation driven by Intelligent Agents) is one example of solution developed by University of Genova and it has to be regarded as an innovation in the educational programs for health students enabled by new technologies [21].

4. EXPLORING COOPERATIVE AND SUSTAINABLE EDUCATION: TECHNICAL APPROACH

According to the cooperative and sustainable approach to education, many different approaches can be explored; this may help in a collaborative maintenance of the software and of the learning platform itself, giving to the learners the opportunity to adapt and promote their personal knowledge and through an open source, modular, and configurable software solution according to specific needs. A large community that gives information for maintenance and possible evolutions to the educational process of students and users and the participation itself, is a way to stimulate people to care about their own education. A favourable approach is to refer to an environment for the knowledge management, based on the ideology according to which each constructionist learning would be facilitated by the production of tangible objects [17]
The constructionist ideology, from which was born the US "No Child Left Behind Act of 2001" [14] is highlighted by various aspects of development, such as the ability to insert and comment data tables or wiki students, or to deliver tasks over the Internet. It offers a range of modules that enable tutors to create online courses and it tries to empower and address the need for pedagogical support, promoting the definition of constructionist learning, where a student learns from his or her own experiences, giving shape to student-centred learning environment.

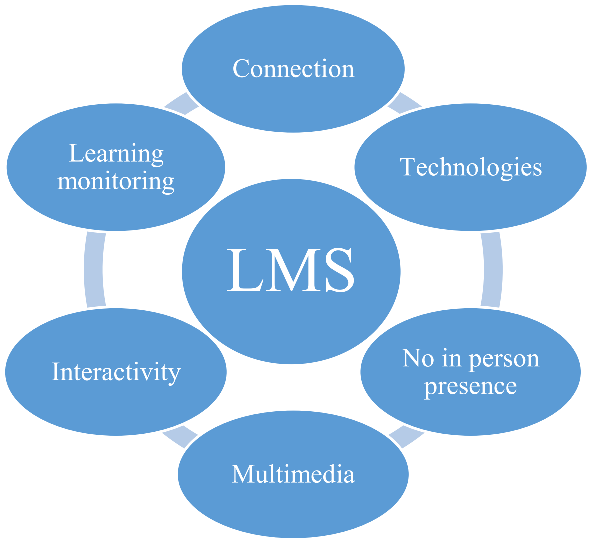

Figure 1: LMS elements

Although e-Learning synchronous systems are preferred, in case of lack of connection or electricity distribution, the asynchronous use and distance learning methods are more reliable and convenient. [18]
The cooperative and sustainable education technique leaves the instructor the possibility to manipulate its personal route, directing it to the success of effects and to manipulate it in a far off manner.
What can be empowered from the pedagogic point of view is particularly noted as follows:

- Provision of lectures within the lecture room adaptable to specific needs of Internet access.
- Teaching materials (ppt and pdf) and video on hand at any time and downloadable
- Availability of extra teaching materials and / or guidelines of deepening: articles, references and other possible sources.
- Forum / chat for interaction with teachers and ask for explanation.
- Archive established and indexed upgradeable, to look for subjects.
- Exams control: the local tutor/teacher learns how to observe, evaluate and corrects the texts.
- Video conference when useful.

These tools can genuinely empower sharing knowledge and help the circulation of people and educational and research topics also from far underdeveloped and deprived areas of the world, empowering the health care service and schooling also in case of bad telecommunications and thanks to low price hardware systems and infrastructures [13].

5. CONCLUSIONS

Use of technologies and LMS is awarded as one of the most effective solutions to empowerment of medical education in LMICs contexts.
In fact, the possibility to access different applications and contents through dedicated applications will allow people completing their career in their local universities, to give their contribution to the society that took care of them since the beginning of their education and to establish a connection with their countries and their people.
Empowering these platforms and apps and customising them according to new advices and needs, helps also in spreading in many fields, and towards it, many other countries and educational systems could benefit of a high quality service at a cheap price. Moreover, digital divide problems that could occur in some areas of the world could be overlapped thanks to the use of open sources but consolidated technologies, able to adapt to different territories and circumstances.
The objective is raising awareness and towards it social empowerment and subsequent policy development.
It will be easier and cheaper for the international community to meet the seventeen Sustainable Development Goals (SDGs), especially those linked to education and health care spread.
The UN reports [20] reveal that SDG number 3 “Ensure healthy lives and promote well-being for all at all ages” already achieved good empowerment, one of the most important achievements is in Global maternal mortality ratio that felt by 37%. 2000 to 2015.
SDG number 4 “Ensure inclusive and equitable quality education and promote lifelong learning opportunities for all” instead, faces some difficulties that can be underlined also as follows.
In 2014, 2 out of 3 children worldwide participated in pre-primary or primary education in the year prior to the official entrance age for primary school, compared to only 4 in 10 children in the poorest countries.
Despite considerable gains in primary school enrolment between 2000 and 2014, 9 % of primary-school-aged children worldwide were out of school in 2014, with little progress since 2008.
Surveys undertaken between 2007 and 2015 in selected countries show that children and adolescents from the richest 20 % of households achieved greater proficiency in reading than those from the poorest 20 % of households, and urban children scored higher in reading than rural children. Data for 2011 indicate that only about one quarter of schools in sub-Saharan Africa had electricity, less than half had access to drinking water, and only 69 % had toilets (with many lacking separate sanitation facilities for girls and boys).
Looking at a transversal SDG 7 “Build resilient infrastructure, promote inclusive and sustainable industrialization and foster innovation” there are encouraging and high level results:

- Global investment in research and development increased at an average annual rate of 4.5 % between 2000 and 2014. It reached 1.8 trillion US dollars (purchasing power parity) in 2014—1.7 per cent of global GDP.
- Coverage by a mobile cellular signal has become almost universal. In 2016, 95% of the world’s population was in range of at least a second-generation (2G) signal and 84 % received at least a third-generation (3G) signal.

This is means that combining new infrastructures empowerment, especially in technical and telecommunication field, can really be effective in empowering the other SDG achievements, and as considered in this paper, in a sustainable and effective way. Following such an approach entities and educational systems, that would like to empower their offer, with concrete approaches to education and participation in education of the stakeholders involved in these processes.

LIST OF ABBREVIATIONS

GPRS general packet radio service
GPS global positioning system
ICTs Information and Communication Technologies
LMIC Low and Middle Income Countries
LMS Learning Management Systems

PDAs personal digital assistants
SDGs Sustainable Development Goals
MICs Middle-Income countries
SMS short messaging service

ACKNOWLEDGMENTS
The basic research of this article derives from the experience of the authors in “Aquilone” project, co-financed by Regione Liguria, Italy, DGR 335/2012.

REFERENCES

1. Bongaarts J. World Health Organization Health in 2015: From MDGs, Millennium Development Goals, to SDGs, Sustainable Development Goals. Geneva: WHO Press; 2016.
2. No Health without a workforce: World Health Organization (WHO); 2013.
3. Bloom DE, Canning D, Chan K. Higher Education and Poverty in Sub-Saharan Africa. Vol 45: Higher Education and Poverty in Sub-Saharan Africa; 2015.
4. Iqbal S, Qureshi IA. M-learning adoption: A perspective from a developing country. The International Review of Research in Open and Distributed Learning. 2012; 13 (3):147-164.
5. Ciegis R, Ramanauskiene J, Martinkus B. The concept of sustainable development and its use for sustainability scenarios. Engineering Economics. 2015; 62 (2).
6. Preece J. Online communities: designing usability, supporting sociability. Chichester: John Wiley & Sons; 2000.
7. Salmon G. E-activities: the key to active online learning. London: Kogan Page; 2002.
8. Hamburg I, Lindecke C, Teh Thij H. Social aspects of distance learning and blending learning methods. Proceedings of the fourth European conference on E-commerce, E-work, Distance learning, E-health, E-banking, E-business, on-line services, virtual institutes, and their influences on the economic and social environment. 2003:11-15.
9. Thurmond VA, Wambach K. Understanding interactions in distance education: a review of the literature. Journal of Instructional Technology and Distance Learning. 2004; 1:9-33.
10. Van de Walle, The impact of multiparty politics in sub Saharan Africa. Forum for Development Studies. 2001; 28(1):5-42.
11. Internet World Stats. Available at: http://www.internetworldstats.com
12 Flynn L, Jalali A, Moreau KA. Learning theory and its application to the use of social media in medical education. Postgraduate medical journal. 2015.
13 Frascio, M., Gervasoni, M., Lazzara, F., (...), Sguanci, M., Vercelli, G. New teaching models for the medical school of medicine: Comparison between oral an online classes. The experience of the Genoa school of medicine Journal of E-Learning and Knowledge Society 2009 5(3), pp. 43-48.
14 Stabilini, C., Bracale, U., Pignata, G., Frascio, M. Lazzara, F., Gianetta, E. Laparoscopic bridging vs. anatomic open reconstruction for midline abdominal hernia mesh repair [LABOR]: Single-blinded, multicenter, randomized, controlled trial on long-term functional results. 2013 Trials 14(1), 357
15. Sife A, Lwoga E, Sanga C. New technologies for teaching and learning: Challenges for higher learning institutions in developing countries. International Journal of Education and Development using ICT [Online]. June 2007; 3(2).
16. Linn RL, Baker EL, Betebenner DW. Accountability systems: Implications of requirements of the no child left behind act of 2001. Educational Researcher. 2002; 31(6):3-16.
17. Monahan T, McArdle G, Bertolotto M. Virtual reality for collaborative distance learning. Computers & Education. 2008; 50(4):1339-1353.
18. Kay M, Santos J, Takane M. mHealth: New horizons for health through mobile technologies. World Health Organization. 2011; 64(7):66-71.
19. Ferrara E, Ponte S, Caputo E, Frascio M, Dellepiane S. Sustainable cooperative distance learning system for education in developing countries. IST-Africa Week Conference. May 2016:1-8.
20. Dellepiane S, Frascio M, Valle V, Bozano E, Ferrara E. E-learning for the medicine students of Ebolowa (Cameroon). Proceedings of the IV Congress of the University Network for Development Cooperation (CUCS). 2015.
21. Bruzzone AG, Frascio M, Longo F, Massei M, Siri A, Tremori A. MARIA: An agent driven simulation for a web based serious game devoted to renew education processes in health care. Paper presented at: International Workshop on Innovative Simulation for Health Care, 2012; Vienna (Austria).
22. The sustainable Development Goals: UN; 2017.

SIMULATION IMPROVES EFFICIENCY AND QUALITY IN SHOE MANUFACTURING

Mohan Mano Hassan[(a)], Sai Priyanka Kalamraju[(a)], Sandeep Dangeti[(a)], Sirisha Pudipeddi[(a)], Edward J Williams[(a)]

[(a)]Business Analytics, College of Business, University of Michigan – Dearborn, Dearborn, MI, USA

[(a)]mohmano@umich.edu, [(a)]kalamraj@umich.edu, [(a)]dvbittu@umich.edu, [(a)]sirishap@umich.edu, [(a)]williame@umich.edu

ABSTRACT

Discrete-event process simulation now has a long and distinguished history of supporting the improvement of manufacturing processes. From those origins, it has expanded its applicability to supply chains, service industries, health care, and public transport. In manufacturing contexts, simulation modeling and analysis regularly helps fine-tune the trade-off between high inventory versus danger of stockout, improve and balance machine utilization, schedule workers more effectively, and improve performance metrics such as average and maximum times in queue and average and maximum length of queues. In the present work, the authors describe a successful application of simulation to the manufacture of footwear. The original manufacturing process was beset by problems including low throughput, high headcount, overly high or low machine utilization, unduly large rejection rates, and ergonomic concerns.

The simulation and analysis project described in this paper guided significant improvements, including doubling the output while reducing worker headcount to two-thirds of its initial value.

Keywords: discrete-event process simulation, footwear manufacture, resource utilization, queueing system performance metrics

1. INTRODUCTION

Historically, discrete-event process simulation was first and very extensively used to improve manufacturing operations; indeed, examples in the literature are numerous. A comprehensive review of progress and challenges in manufacturing simulation appears in (Mourtzis, Doukas, and Bernidaki 2014). There are many potential ways to improve a generic manufacturing operation; e.g., lower inventory while keeping stockouts very rare, improve queue performance metrics (especially average and maximum time in queues, and average and maximum length of queues), keep utilization of expensive equipment high while improving those queue performance metrics, use headcount more efficiently and less extravagantly, and increase throughput. Examples of such simulations abound; for example, (Mirzapourrezaei et al. 2011) applied simulation to improve an assembly process for manufacture of starters.

In the present work, simulation analysis was applied to a manufacturing plant in India which makes shoes. The global footwear market is, according to Allied Market Research, expected to garner $371.8B by 2020. This market is lively, expanding, and volatile, and includes both primary and secondary marketplaces (Weinswig 2016). Footwear manufacture has expanded globally; already prominent in the United States and China, it is rapidly entering India. In this paper, we present a successful simulation study of a shoe manufacturing plant in India. The factory management, already confronting the need to significantly increase production, and having accepted the necessity of payroll and equipment investments to do so, wanted guidance on the best way to proceed in this endeavor. This study has precedents: (Solomon, Jilcha, and Berhan 2014) used simulation to improve lead time prediction at a shoe manufacturer in Ethiopia; (Eryilmaz et al. 2012) analyzed production processes in a shoe manufacturing factory using simulation. The management of this plant presented significant concerns including relatively low throughput relative to high labor headcount, unbalanced utilization of equipment, long queues and waiting times therein, ergonomic concerns, and low throughput.

In the following sections, we (1) present an overview of the shoe-manufacturing operations, (2) describe the collection and analysis of input data, (3) discuss the building, verification, and validation of the simulation model, (4) highlight key results from this model obtained by output analysis, and (5) present conclusions, recommendations to the manufacturing plant's management, and the directions in which likely future work may proceed.

2. OVERVIEW OF SHOE MANUFACTURING OPERATIONS

The overall process of manufacturing shoes comprises the following high-level steps:

1. Procurement of raw materials
2. Cutting materials into shapes specified by design
3. Sewing
4. Assembly of parts
5. Finishing
6. Quality verification
7. Repair/rework or scrap as necessary
8. Packaging and shipping

Repair work may result in scrapping the shoe or selling it at a loss ("seconds"). In this model, manufacture of shoes in the four most common sizes (seven, eight, nine, and ten inches) is considered. Fundamentally, a shoe has four basic components, as shown in Figure 1 below:

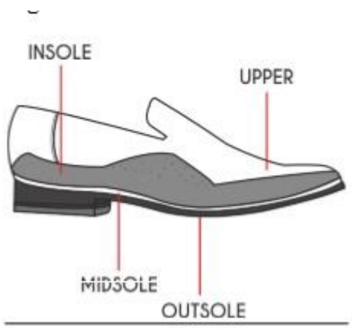

Figure 1: Basic Components of a Shoe

As configured at the beginning of this simulation study, the manufacturing facility comprises 93 workers and 88 worker-run (e.g., manual or semi-automatic, not automatic) machines. Open nine hours per day (9:00am to 6:00pm), the plant produces approximately 225 pairs of shoes daily. Informal industry norms indicate a plant of this size and capitalization investment "ought" to produce approximately 350 pairs of shoes per day. Additionally, manual transfer of shoes from one task to the next is currently giving rise to ergonomic concerns – in particular, cervicobrachial (relating to the neck and arm) disorders, especially on the left side of the body; the importance and etiology of such disorders is documented in (Sällström and Schmidt 1984). Accordingly, the plant management wished to evaluate the feasibility of conveyors to move the shoes.

3. DATA COLLECTION AND ANALYSIS

Various essential input data was willingly and promptly provided to the analysts by plant supervisors and managers in Vellore, India. Arrival rates were 200 per hour during all but the fourth, eighth, and ninth hours of a standard nine-hour shift, with scheduled working time (i.e., less breaks and lunch) of eight hours. Average machine cycle times were provided as shown in Table 1 immediately below, all gathered from raw data.

Table 1: Mean Cycle Time of Operations

Process (Machine)	Avg (min) Time/Piece	Capacity
Cutting	1.26	Variable
Sewing	10.04	Variable
Assembling	10.01	Variable
Inspection	1.50	3
Repairing	116.7	1

After consultation with plant managers, the following assumptions were agreed to:

1. No maintenance is performed during the production period (it is done as necessary off-shift, e.g., at night)
2. At the start of a day's production, sufficient raw material for the day is always available
3. No power interruptions occur
4. Downtimes at the cutting machines occur approximately monthly and take several hours to repair
5. Transportation time is not included in machine cycle time, and is small relative thereto (the longest transport distance in the plant being only ten meters)
6. All workers are assumed equally skilled, and hence produce the same quantity and quality in equal time
7. 2% of production is unsatisfactory and hence sent to repair; of the production sent there, 90% can be repaired and sold as "seconds;" the remaining 10% must be scrapped

Raw data was examined with the Stat::Fit® software (Benneyan 1998). After doing so, and with the precaution of showing plant managers and supervisors the characteristic histogram of distributions, arrivals were modeled as exponential, whereas machine cycle times were modeled as uniform or triangular distributions. As often occurs in practical simulation work, the value added by using distribution-fitting software was not so much advice on the best distribution to use (if indeed there existed a single "best" distribution), but rather cautionary advice on conspicuously inappropriate distributions to avoid (in these cases, the normal, gamma, and lognormal distributions).

4. MODEL DEVELOPMENT, VERIFICATION, AND VALIDATION

The very first model built was entirely conceptual – a flow chart of all paths taken from raw material to completed product: "Now, let put this shoe on your foot, and we'll see if it fits." Drawing and revising this model ensured that the analysts' understanding of the process flows exactly matched the expert knowledge of the plant managers and supervisors. Members of the project team then concurred in the choice of the Simio® software [SIMulation with Intelligent Objects] (Prochaska and Thiesing 2017), (Smith, Sturrock, and Kelton 2018) to construct a model of the salon's operations. Simio® provides constructs such as the Server (to model, for example, the cutting machines for the uppers, middle soles, and "outsoles"), the Worker (design checkers and quality checkers), a Combiner (e.g., gathering and sewing matched components together, and Conveyors (all but one proposed conveyor is to be non-accumulating). These Simio® constructs were used to model the key steps outlined in Table 1:

1. Cutting: the raw materials are cut into both left and right shoes in various sizes. Since the different parts of a shoe are made of different materials, the model considers three different procurement centers for cutting each shoe component.

2. Sewing: The cut components are sent to the assembly section of the manufacturing unit for further processing – all sewing is performed in this phase for all shoe sizes, and for both left and right shoes.
3. Assembly: Unites all parts of the shoe.
4. Inspection: A quality-checking worker examines each shoe for defects.
5. Repair: Low-quality shoes may be sent to rework, if repairable, will be sent to rework. There, they will be repaired for sale at a discounted price. Shoes which cannot feasibly be repaired are scrapped (c.f. assumption 7 above).

The first iteration of the Simio® model deliberately contained only the Simio® default values for parameters such as interarrival times and cycle times. Only *after* verification of correct entity flow in the animation were the values obtained from data collection and analysis (previous section) inserted. A partial two-dimensional screen shot of this model, as completed, is shown in Figure 2, Appendix. From this screen, a three-dimensional animation is only two clicks away.

Verification and validation of the model used the following traditional and time-tested techniques (Sturrock 2018):

- Structured walkthroughs among the analyst team
- Sending one entity (arriving raw material) through the model and tracking, on a time line, every step taken by that entity
- Temporary removal of all stochastic variation of the model, followed by arithmetic checks using Microsoft Excel®
- Ensuring that every routing path placed in the model has non-zero traffic
- Directional variation (e.g., do queue lengths and waiting times increase when the cycle time of a machine is increased -- do they decrease when the capacity of a machine is increased?)

The usual errors were detected and corrected. Indeed, one error resulted in "pairs" of shoes comprising two left shoes or two right shoes! Another error, a routing logic error, was exposed by noticing that one of the routes in the model was never used. After correcting these errors was completed, comparison of model results, pertaining to the current system, with data actually observed during production yielded agreement of performance metrics within 4%, helping the model achieve credibility with the plant management.

5. EXPERIMENTATION AND RESULTS

In keeping with actual policy at the manufacturing plant (production started anew daily), the model was run as a terminating system, hence zero warm-up time. Each replication represented one day's production. Since the facility typically works 25 days per calendar month, and after ensuring that 25 replications yielded sufficiently narrow confidence intervals for performance metrics, the three experimental scenarios were each run for 25 replications. The variance reduction technique (VRT) of common random numbers (CRNs) was used (Nakayama 2003). Simio® conveniently accommodates this technique by allowing the specification of different random number streams for interarrival times, cycle times, times to next failure, and repair times, as was done in this model. Confidence levels for estimation of performance metrics were taken at 95%, and similarly for the confidence level of testing the null hypothesis of equal performance of any two scenarios. Each of these scenarios substituted short conveyors for currently manual transfers. Since management was proposing adding machines as well as workers, the key scenarios addressing one of the major investment decisions to be taken were listed as follows in Table 2:

Table 2. Investment Scenarios Considered

Proposal	#sewing employees	#assembly employees
Smaller invest	27	20
Moderate invest	30	25
Larger invest	33	30

The "moderate" scenario proved the best in this simulation experiment, relative to the performance metrics of machine utilizations, average time in system of a shoe, and most importantly, shoes output per day. The parameters and performance of the current system versus the scenario of moderate investment showed, as summarized in Table 3 immediately below:

Table 3. Proposed System Versus Current System

Current	Planned
15 assembly line workers	25 assembly line workers
25 sewing line workers	30 sewing line workers
18 cutting line workers	3 machines; 3 workers
5 quality checkers	3 quality checkers
Shoe TIS* 2½ hours	Shoe TIS* 1½ hours
225 pairs shoes per day	492 pairs shoes per day

*TIS = time in system

These results were summarized into direct answers of management's initial questions as follows:

Question: Should an investment be made in an automatic cutting machine?

Answer: Yes; this investment will permit the reduction of workers needed in the cutting line from 18 to 3, as shown in Table 3 above.

Question: Does throughput increase?

Answer: Yes, even with fewer workers, it more than doubles, as shown in Table 3 above.

Question: Does the increased throughput from the cutting section affect other sections?

Answer: Yes, more workers will be needed in both the assembly and the sewing sections; these workers can be redeployed from the cutting line workers no longer needed.

Question: With fewer quality checkers, can quality be maintained?

Answer: Yes, because the automated cutting machine will greatly reduce the error rate. However, it is acknowledged that the utilization of the three remaining quality checker will increase – expected to be a plus since inspection workers with too little to do may become bored and complacent – then miss defects (Ramzan, et al 2019)

Management, being highly pleased with and reassured by these results, is now beginning the implementation of machine investments and addition of labor, with conversion of manual transfer to conveyors to follow shortly and largely concurrently.

6. CONCLUSIONS AND FUTURE WORK

Given the promising results of this simulation analysis, ideas for follow-up work are already being considered. These ideas include refinement of the conveyor specifications (lengths, speeds, capacities, and non-accumulating versus accumulating), expansion of the model to accommodate changes in demand mix (for example, one size may be more in demand than another), and adding analysis of different worker skill levels (hence payroll costs, pieces produced per hour, and reject rates).

ACKNOWLEDGMENTS

The authors gratefully acknowledge the cooperation and assistance of the manufacturing plant manager and workers in providing data, explaining details of the plant's processes and operation, and specifying the performance metrics of primary concern. Additionally, suggestions and criticisms from two anonymous referees have provided us significant help in improving this paper.

REFERENCES

Benneyan, C., 1998. Distribution fitting software makes simulation more attractive, viable in many applications. OR/MS Today (98:38,1-10)

Eryilmaz, M., Kuşakci, A., Gavranovic, H., and Findik, F., 2012. Southeast Europe Journal of Soft Computing (1:1, 120-127).

Mirzapourrezaei, S., Lalmazloumian, M., Dargi, A., and Wong, K., 2011. Simulation of a manufacturing assembly line based on WITNESS. Proceedings of the 2011 Third International Conference on Computational Intelligence, Communication Systems, and Networks, 132-137. July 26-28, Bali (Indonesia).

Mourtzis, D., Doukas, M., and Bernidaki, D., 2014. Simulation in manufacturing: Review and challenges. Proceedings of 8th DET International Conference on Digital Enterprise Technology, 213-229. March 25-28, Stuttgart (Germany).

Nakayama, M., 2003. Analysis of simulation output. Proceedings of the 2003 Winter Simulation Conference, Volume 1, 49-58. December 7-10, New Orleans, Louisana (United States of America).

Prochaska, K. and Thiesing, R., 2017. Introduction to Simio. Proceedings of the 2017 Winter Simulation Conference, 4410-4419. December 3-6, Las Vegas, Nevada (United States of America).

Ramzan, M. B., Qureshi, S. M., Mari, S. I., Memon, M. S., Mittal, M., Imran, M., and Iqbal, M. W., 2019. Effect of time-varying factors on optimal combination of quality inspectors for offline inspection station. Mathematics (7:1, 51-68)

Sällström, J. and Schmidt, H., 1984. Cervicobrachial disorders in certain occupations, with special reference to compression in the thoracic outlet. American Journal of Industrial Medicine (6:1, 45-52).

Smith, J., Sturrock, D., and Kelton, W., 2018. Simio and simulation: Modeling, analysis, applications. 5th ed. Sewickley, Pennsylvania (United States of America): Simio LLC.

Solomon, H., Jilcha, K., and Berhan, E., 2014. Lead time prediction using simulation in leather shoe manufacturing. Advances in Intelligent Systems and Computing (334:283-292).

Sturrock, D. 2018., Avoid failures! Tested success tips for simulation product excellence. Proceedings of the 2018 Winter Simulation Conference, 252-260. December 2018, Göteborg (Sweden).

Weinswig, D., 2016. Sneaker culture fuels $1 billion secondary market. 18 March, 22.

AUTHOR BIOGRAPHIES

Mohan Mano Hassan is a graduate student in Business Analytics enrolled with the college of Business at the University of Michigan-Dearborn. He completed a dual degree program at VIT University while earning his MBA. He has gained extensive experience in data analytics and data visualization while doing his Capstone Experience Project and Internship in Italy. He has undertaken projects studying the Flint (Michigan) water crisis, a market research project which enhanced his experience on various tools and technology. He has been awarded "Student of the Year" for his technical skills, leadership skills and helping the society. He helped small-scale and medium-scale companies reduce losses and increase profit with his Data Analysis and Management skills. He also earned a Merit award for his managerial skills while earning his MBA. His mail address is mohmano@umich.edu.

Sai Priyanka Kalamraju is a graduate student in Business Analytics enrolled with the College of Business at the University of Michigan-Dearborn. Prior to this, she studied Information Technology engineering as her first graduate degree program at Osmania University, India and pursued an MBA in Marketing from the Symbiosis Institute of Business Management, India. She has extensive experience in data analytics and data visualization with a keen eye for improving processes for companies large and small. She is a Research Assistant with the iLabs, a center for innovative research at the University of Michigan- Dearborn, where she uses data analysis to advise clients on real-time data. She has also had the opportunity of working with some of India's top companies, including Infosys and Kony Laboratories. At Kony Laboratories, she was instrumental in the automation process of weekly, monthly, quarterly, yearly reporting and helped in deriving metrics, KPIs regarding the profitability of the performance of the services. Due to her excellence in work, she also received the Spot award from the Executive Vice President and the Gem Team Award from Vice President in Kony Laboratories. She is a student member of the Indian Graduate Student Association (IGSA), Student Representative for the Winter Orientation program, and has worked with non-profit organizations like Make a Difference, Shelter Homes, Children's Education, Plant 3 Protection Alliance on the plantation, environmental awareness, and Let's Vote on Voting awareness. She was also the recipient of the Non-Resident Graduate Tuition Differential Scholarship (NRTD) for Fall 2018. Her email address is kalamraj@umich.edu.

Venkata Sandeep Dangeti is a graduate student in Business Analytics enrolled with the college of Business at the University of Michigan-Dearborn. He came through a dual degree program; the first degree is MBA from VIT University in India and he is currently pursuing a second degree. Prior to that he founded a cashback website in India, where he got start-up exposure and practical experience, and where he diversified his entrepreneurial skills, managerial skills, technical skills, and leadership skills. He also worked in a multinational company (Tata Consultancy Services) where he learned how to work in a fast-paced environment. He worked with various tools and technology which made him learn quickly in any given situation. He consistently was in touch with stakeholders to improve and enhance software. He was awarded for a value-added service which saved the company considerable time and money. Apart from having professional experience in simulation, analytics and development, he also has Business Administration skills. He prepared many business plans for start-ups where he forecasted revenue, sales, demand and analyzed market trends. As a part of academic trips, he visited various industries in India and observed how small-scale, medium-scale and large-scale industries perform. He collaborated with many professionals and his friends in wide variety of projects. His email address is dvbittu@umich.edu.

Sirisha Pudipeddi is a graduate student pursuing her Master's in Science with a major in Business Analytics. With a computer science and engineering background, she has founded two start-ups in India. Her forte is in delivering business solutions with the right blend of information systems. She received the "Edex 40 under 40" award from The New Indian Express from the Information Technology Minister of the state of Telangana, India. She volunteers for a student organization named She's the First to help raise awareness and funds for educating girls in developing nations. Sirisha has an avid interest in the field of Analytics and Project Management and is interning at the Global Product Development Center - Ford Motor Company, Dearborn. Her email address is sirishap@umich.edu.

Edward J. Williams holds bachelor's and master's degrees in mathematics (Michigan State University, 1967; University of Wisconsin, 1968). From 1969 to 1971, he did statistical programming and analysis of biomedical data at Walter Reed Army Hospital, Washington, D.C. He joined Ford Motor Company in 1972, where he worked until retirement in December 2001 as a computer software analyst supporting statistical and simulation software. After retirement from Ford, he joined PMC, Dearborn, Michigan, as a senior simulation analyst. Also, since 1980, he has taught classes at the University of Michigan, including both undergraduate and graduate simulation classes using GPSS/H™, SLAM II™, SIMAN™, ProModel®, SIMUL8®, or Arena®. He is a member of the Institute of Industrial Engineers [IIE], the Society for Computer Simulation International [SCS], and the Michigan Simulation Users Group [MSUG]. He serves on the editorial board of the International Journal of Industrial Engineering – Applications and Practice. During the last several years, he has given invited plenary addresses on simulation and statistics at conferences in Monterrey, México; İstanbul, Turkey; Genova, Italy; Rīga, Latvia; and Jyväskylä, Finland. He served as a co-editor of Proceedings of the International Workshop on Harbour, Maritime and Multimodal Logistics Modelling & Simulation 2003, a conference held in Rīga, Latvia. Likewise, he served the Summer Computer Simulation Conferences of 2004, 2005, and 2006 as Proceedings co-editor. He was the Simulation Applications track coordinator for the 2011 Winter Simulation Conference. A paper he co-authored with three of his simulation students won "best paper in track" award at the Fifth International Conference on Industrial Engineering and Operations Management, held in Dubai, United Arab Emirates, in March 2015. His email addresses are ewilliams@pmcorp.com and williame@umich.edu.

APPENDIX A

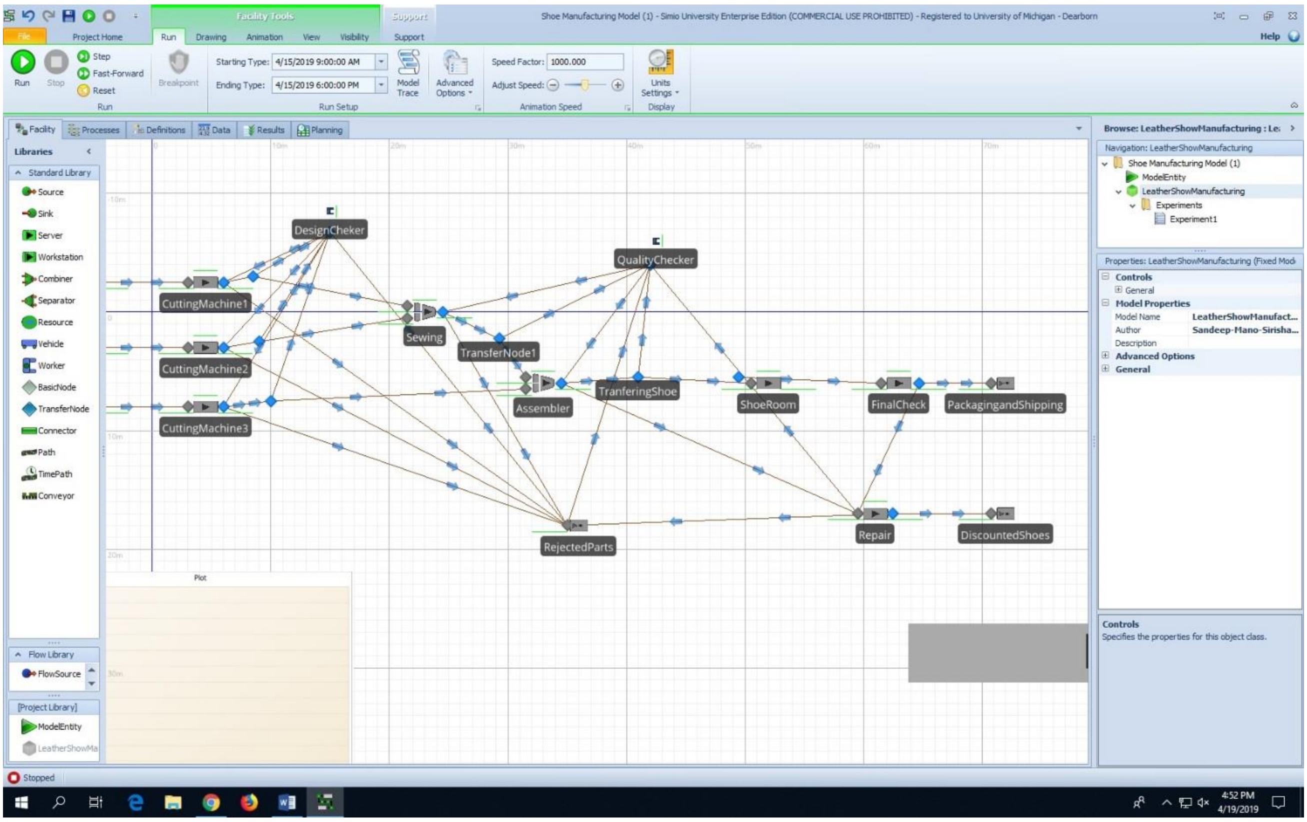

Figure 2: Screen of the Simio® Model Layout

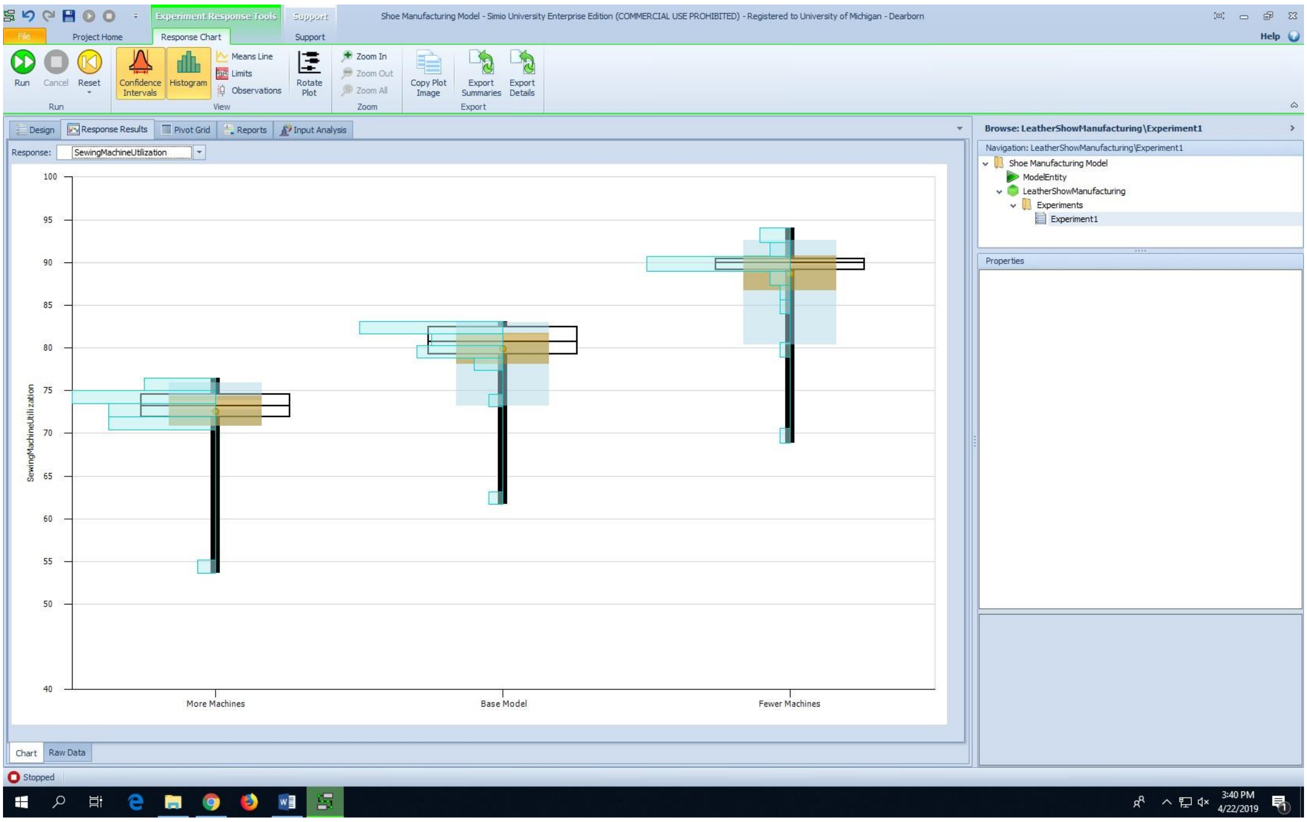

Figure 3: Example of Simio® Graphical Output Across Scenarios

MODELS OF TERAHERTZ AND INFRARED DEVICES BASED ON GRAPHENE/ BLACK-AsP HETEROSTRUCTURES

M. Ryzhii[(a)], T. Otsuji[(b)], V. Ryzhii[(b,c)], V. Leiman[(c)] , V. Mitin[(d)], and M.S. Shur[(e)]

[(a)]University of Aizu, Aizu-Wakamatsu, Japan
[(b)]RIEC, Tohoku University, Sendai, Japan
[(c)]Moscow Institute of Physics and Technology, Dolgoprudny, Russia
[(d)]University at Buffalo, Buffalo, USA
[(e)]Rensselaer Polytechnic Institute, Troy, USA

[(a)]m-ryzhii @ u-aizu.ac.jp

ABSTRACT

The gapless energy spectrum of the graphene layers (GLs) enables the interband absorption and emission of photons and plasmons in the terahertz (THz) and infrared (IR) spectral range. The energy of the emerging the black-phosphorus (b-P), black-arsenic (b-As), and the compounds (b-As_xP_{1-x}) varies from 0.15 to 1.7 eV, depending on the number of the atomic sheets and the component relative content. Due to a strong anisotropy of the b-P and b-As, the ratios of the carrier effective masses in different in-plain directions are very large. One of the crucial properties of the GL heterostructures with the b-P, b-As, and b-As_xP_{1-x} barrier layers are associated with the GL Dirac point corresponding to the energy gap in the barriers. Combination of GLs with the b-P, b-As, and b-As_xP_{1-x} layers opens new prospects for the novel THz and IR devices, in particular, GL-based photodetectors, electro-optical modulators, and sources of THz/IR radiation, including the lasers with the GL active region.

Keywords: black-phosphorus, black-arsenic, graphene, heterostructure, terahertz, infrared

1. INTRODUCTION

In this work, we demonstrate the concepts and models of THz and IR photodetectors, switches, sources, and modulators based on the heterostructures based on the graphene layers (GLs) (Castro Neto 2009) and the black-P (b-P), black-As (b-As), and black-As_xP_{1-x} (b-As_xP_{1-x}) layers (Keyse 1953, Morita 1986, Asashina 1984, Ling 2015, Xia 2014, Guo 2015, Liu 2015, Long 2017, Yuan 2018). Our consideration is based on our recent results (Ryzhii 2017a, Ryzhii 2017b, Ryzhii 2017c, Ryzhii 2018a, Ryzhii 2018b, Ryzhii 2019a, Ryzhii 2019b, Ryzhii 2019c).

In this presentation, we mainly focus on prospective THz/IR sources (including lasers) using the interband transitions in the optically pumped GLs.

We consider also the THz/IR sources based on GL active region with the lateral electron injection from the side contacts and the hole vertical injection via the b-P (b-As) layer.

The optical pumping can be realized using mid- or near-IR light-emitting diodes (LEDs), in particular, integrated with the laser-active GL structure. The main problem is that the electron-hole pairs generated by such LEDs in the GL have fairly large energies. This results in relatively high effective temperature of the electron-hole plasma in the GL that hampers the achievement of the interband population inversion and the possibility of lasing. This obstacle can be avoided introducing the absorbing-cooling layer with the sufficiently narrow energy gap.

The sketch of the band diagram of the GL-based laser structure with the absorbing-cooling layer integrated with the pumping LED is shown in Fig. 1.

The b-As or b-As_xP_{1-x} absorbing-cooling layers can be particularly effective because their energy gap Δ_G rather small (up to 0.15 eV).

This implies that the energy of the electron-hole pairs injected into GL can be about the latter value even in the case of optical pumping with considerably high-energy photons. As shown, if the energy of the injected pairs is smaller than the energy of optical phonons in GLs (about 0.2 eV), the effective temperature of the electron-hole plasma in the laser-active GL can be lower than the ambient (lattice) temperature. This is beneficial for the population inversion in the GL.

2. MODELS AND RESULTS

2.1. Optical pumping via b-AsP absorbing-cooling layer

We developed the model for the THz and FIR lasers with the band diagram of Fig. 1. The device comprises the b-As_xP_{1-x} - GL heterostructure playing the role of the THz active region mounted on the top of the P^+-i-N^+ LED heterostructure. The active region and LED are separated by a wide-gap transparent barrier layer. The IR radiation (with the photon energy $\hbar\Omega$) generated by the LED passes the barrier layer and produces the fairly hot electrons and holes in the b-As_xP_{1-x} absorbing-cooling layer. If the thickness of the b-As_xP_{1-x} layer substantially exceeds the characteristic cooling length,

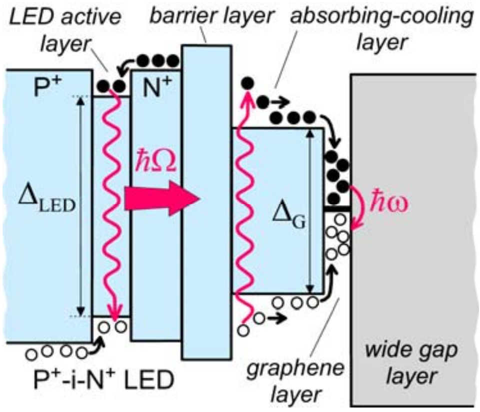

Figure 1: Band diagram of the GL-based laser with an absorbing-cooling layer integrated with a pumping LED.

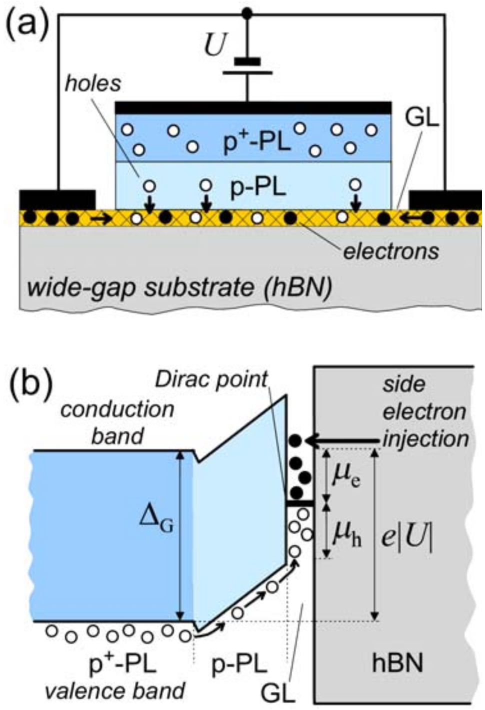

Figure 2: Sketch of the heterostructure with b-P layer (PL) and with lateral electron and vertical hole injection (a), and its energy band diagram (b).

the photogenerated carriers arrive at the GL being efficiently cooled down. The injection into the GL of the carriers with the energy smaller than the energy of optical phonons in the GL can result in reinforcement of the interband population inversion in the GL.

Using the model, we calculated the effective temperature T of the electron-hole plasma and its quasi-Fermi energy μ at different pumping conditions. It is assumed the absorbing-cooling layers constitute the b-As and b-P layers consisting of sufficiently large number of the atomic sheets (> 8), so that the energy gaps Δ_G were set to be 0.15 and 0.3 eV, respectively.

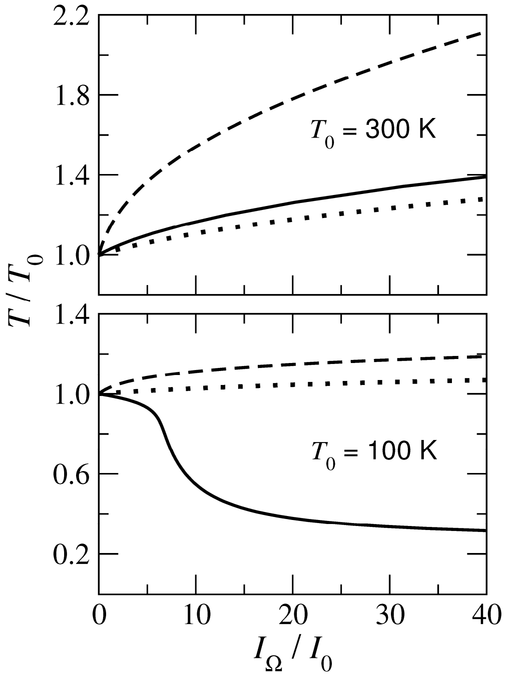

Figure 3: The effective temperature of the electron-hole plasma in the GL normalized by the lattice temperature T_0 as function of the normalized intensity of the pumping radiation I/I_0 calculated for different T_0 for b-As (solid lines) and b-P (dashed lines) absorbing-cooling layers at energy of pumping photons $\hbar\Omega = 0.36$ eV. Dotted lines correspond to the direct pumping (without the absorbing-cooling layer).

Figure 2 shows the heterostructures with relatively narrow-gap p-type b-P (or b-As) layer on a wide-gap substrate and its energy band diagram at the operating voltage U. Different relatively wide-gap materials can be utilized, for example, hexagonal Boron Nitride (hBN).

A wide gap in the hBN substrate provides high energy barrier for the electrons and holes in the GL and blocks their leakage to the substrate. At the applied bias voltage the electrons can freely occupy the GL. Simultaneously, the holes pass vertically from the heavily-doped p^+ region through the undoped or lightly doped b-P layer are vertically injected into the GL. Due to the finite energy spacing between the valence band of the hole injector and the Dirac point in the GL, the injected holes can bring a marked energy into the electron-hole system in the GL. However, the injected energy is effectively removed due to the emission of the high-energy (about 200 meV) optical phonons in the GL. This can result in the cooling of the carrier system injected into the GL.

Figures 3 and 4 demonstrate examples of the calculated dependences of effective temperature of the electron-hole plasma in the GL normalized by the lattice temperature T_0 and the quasi-Fermi energy μ as functions of the normalized intensity of the pumping radiation I/I_0 for the devices with b-As and b-P layers.

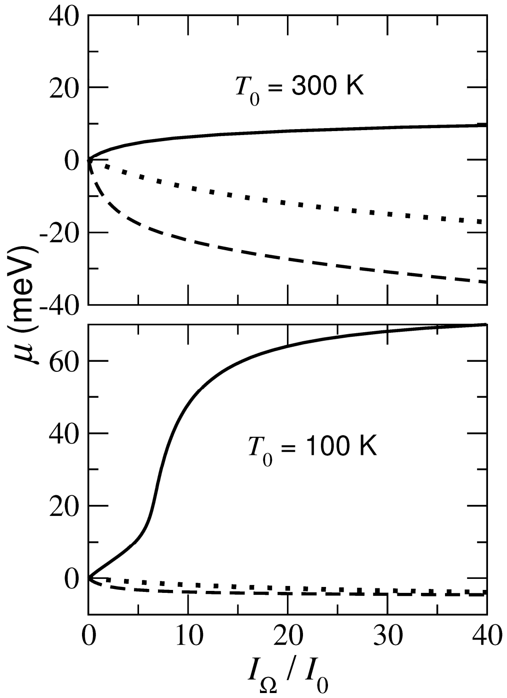

Figure 4: The quasi-Fermi energy as function of the normalized intensity of the pumping radiation I/I_0 calculated for different T_0 for b-As (solid lines) and b-P (dashed lines) absorbing-cooling layers at energy of pumping photons $\hbar\Omega = 0.36$ eV. Dotted lines correspond to the direct pumping (without the absorbing-cooling layer).

In particular, one can see that in the case b-As absorbing-cooling layer at lowered lattice temperatures (see bottom panel of Fig. 3 for $T_0 = 100$ K), the pumping can lead to a marked cooling down of the electron-hole plasma in the GLs. However, in the devices with the b-P absorbing-cooling layer or without the latter (direct optical pumping) $\mu < 0$, i.e., the population inversion is not achieved, at least at the given energies of the pumping photons (Fig. 4).

2.2. Vertical hole pumping via b-As layer

Figure 5 shows the sum of the electron and hole quasi-Fermi energies ($\mu_e + \mu_h$), the effective temperature T of the system, and normalized net quasi-Fermi energy ($\mu_e + \mu_h$)/T calculated as functions of the normalized injection current j/j_G for different relative strengths, s, of the carrier interaction with the GL and substrate surface optical phonons. Small values of s correspond to relatively weak interaction with the substrate surface optical phonons. The energy of these phonons is assumed to be 100 meV. The lattice temperature and the characteristic current density are set T_0 = 25 meV and j_G = 160 A/cm^2, respectively. As seen from Fig. 5, the pumping method under consideration can result in fairly high values of the carrier Fermi energy.

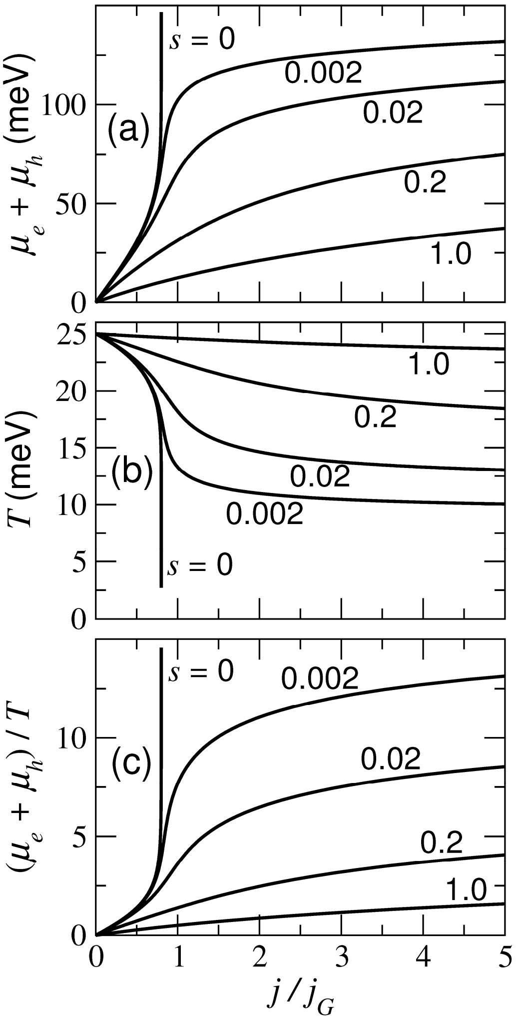

Figure 5: Dependences of (a) the net quasi-Fermi energy ($\mu_e + \mu_h$), (b) carrier effective temperature T, and (c) normalized net quasi-Fermi energy ($\mu_e + \mu_h$)/T as functions of the normalized injection current j/j_G for different relative strengths $s = 0 – 1.0$.

Decrease in the carrier effective temperature T below the lattice temperature T_0, and, therefore, a strong degeneration of the carrier system in the GL are beneficial for the interband THz/IR lasing.

3. CONCLUSIONS

We demonstrated that the combination of GLs with the b-As and b-P layers exhibits a great potential for novel THz and IR devices. In particular, the GL/b-AsP heterostructures are promising for the THz and IR lasers using the interband transitions in the active GLs.

ACKNOWLEDGMENTS

The work was supported by the Japan Society for Promotion of Science, KAKENHI Grant No. 16H06361, RIEC Nation-Wide Collaborative Research Project, and by the Office of Naval Research (Project Monitor Dr. Paul Maki).

REFERENCES

Castro Neto A.H., Guinea F., N. Peres M.R., Novoselov K.S., Geim A.K., 2009. The electronic properties of graphene. Review of Modern Physics, 81, 109-162.

Keyes R.W., 1953. The electrical properties of black phosphorus. Physical Review, 92 (3), 580-584.

Morita A., 1986. Semiconducting black phosphorus. Applied Physics A, 39(4), 227-242.

Asahina H., Morita A., 1984. Band structure and optical properties of black phosphorus. Journal of Physics C: Solid State Physics, 17(11), 1839-1852.

Ling Xi, Wang H., Huang S., Xia F., Dresselhaus M.S., 2015. The renaissance of black phosphorus. Proceedings of the National Academy of Sciences of the USA, 112(15), 4523-4530.

Xia F., Wang H., Jia Y., 2014. Rediscovering black phosphorus as an anisotropic layered material for optoelectronics and electronics. Nature Communications, 5, 4458.

Guo Z., Zhang H., Lu S., Wang Z., Tang S., Shao J., Sun Z., Xie H., Wang H., Yu X.-F., Chu P.K., 2015. From black phosphorus to phosphorene: basic solvent exfoliation, evolution of Raman scattering, and applications to ultrafast photonics. Advanced Functional Materials, 25(45), 6996-7002.

Liu B., Kopf M., Abbas A.N., Wang X., Guo Q., Jia Y., Xia F., Weihrich R., Bachhuber F., Pielnhofer F., Wang H., Dhall R., Cronin S.B., Ge M., Fang X., Nilges T., and Zhou C., 2015. Black arsenic-phosphorus: layered anisotropic infrared semiconductors with highly tunable compositions and properties. Advanced Materials 27(30), 4423-4429.

Long M., Gao A., Wang P., Xia H., Ott C., Pan C., Fu Y., Liu E., Chen X., Lu W., Nilges T., Xu J., Wang X., Hu W., Miao F., 2017. Room temperature high-detectivity mid-infrared photodetectors based on black arsenic phosphorus. Scientific Advances, 3(6), e1700589.

Yuan S., Shen C., Deng B., Chen X., Guo Q., Ma Y., Abbas A., Liu B., Haiges R., Ott C., Nilges T., Watanabe K., Taniguchi T., Sinai O., Naveh D., Zhou C., Xia F., 2018. Air-stable room-temperature mid-infrared photodetectors based on hBN/black arsenic phosphorus/hBN Heterostructures. Nano Letters, 18(5), 3172-3179.

Ryzhii V., Ryzhii M., Svintsov D., Leiman V., Mitin V., Shur M.S., Otsuji T., 2017. Infrared photodetectors based on graphene van der Waals heterostructures. Infrared Physics and Technology, 84, 72-81.

Ryzhii V., Ryzhii M., Leiman V., Mitin V., Shur M. S., Otsuji T., 2017. Effect of doping on the characteristics of infrared photodetectors based on van der Waals heterostructures with multiple graphene layers. Journal of Applied Physics, 122(5), 054505.

Ryzhii V., Ryzhii M., Svintsov D., Leiman V., Mitin V., Shur M. S., Otsuji T., 2017. Nonlinear response of infrared photodetectors based on van der Waals heterostructures with graphene layers. Optics Express, 25(5), 5536.

Ryzhii V., Otsuji T., Karasik V.E., Ryzhii M., Leiman V.G., Mitin V., Shur M.S., 2018. Comparison of intersubband quantum-well and interband graphene-layer infrared photodetectors. IEEE Journal of Quantum Electronics, 54(2), 2797912.

Ryzhii V., Otsuji T., Ryzhii M., Ponomarev D.S., Karasik V.E., Leiman V.G., Mitin V., Shur M.S., 2018. Electrical modulation of terahertz radiation using graphene-phosphorene heterostructures. Semiconductor Science and Technology, 33(12), 124010.

Ryzhii V., Otsuji T., Ryzhii M., Dubinov A.A., Aleshkin V.Ya., Karasik V.E., Shur M.S., 2019. Amplification of surface plasmons in graphene-black phosphorus injection laser heterostructures. arXiv:1901.00580.

Ryzhii V., Ryzhii M., Otsuji T., Karasik V.E., Leiman V.G., Mitin V, Shur M.S., 2019. Negative terahertz conductivity at vertical carrier injection in a black-arsenic-phosphorus-graphene heterostructure integrated with a light-emitting diode. arXiv:1901.10755.

Ryzhii V., Ryzhii M., Ponomarev D.S., Leiman V. G., Mitin V., Shur M.S., Otsuji T., 2019. Negative photoconductivity and hot-carrier bolometric detection of terahertz radiation in graphene-phosphorene hybrid structures. Journal of Applied Physics, 125(15), 151608.

MULTI-OBJECTIVE OPTIMIZATION FOR A SCHEDULING PROBLEM IN THE STEEL INDUSTRY

Viktoria A. Hauder[(a)(b)], Andreas Beham[(a)(c)], Sebastian Raggl[(a)], Michael Affenzeller[(a)(c)]

[(a)] Heuristic and Evolutionary Algorithms Laboratory,
University of Applied Sciences Upper Austria, Hagenberg, Austria

[(b)] Institute for Production and Logistics Management,
Johannes Kepler University Linz, Austria

[(c)] Institute for Formal Models and Verification,
Johannes Kepler University Linz, Austria

[(a)] {viktoria.hauder,andreas.beham,sebastian.raggl,michael.affenzeller}@fh-hagenberg.at

ABSTRACT
Multiple conflicting objectives such as costs versus quality are part of many optimization processes in the area of production and logistics management. Exactly such a case is also examined in this work. For an already existing resource-constrained project scheduling problem, a second objective function, inspired by the steel industry, is taken into account. Together with the presentation of the related mixed integer programming (MIP) and constraint programming (CP) models, the recently developed balanced box method (Boland, Charkhgard, and Savelsbergh 2015) is used to solve this bi-objective optimization problem. Both approaches (MIP and CP) are compared in terms of runtime and solution quality, showing the advantages of using CP.

Keywords: multi-objective optimization, scheduling, balanced box method, steel industry

1. INTRODUCTION
For the successful implementation of real-world logistics optimization problems, more than one objective has to be considered in many cases. In this work, such a multi-objective optimization problem is investigated. The starting point for this examination is the work of Hauder, Beham, Raggl and Affenzeller (2018), where a single-objective scheduling problem of a steel manufacturer is presented. They introduce a resource-constrained multi-project scheduling problem, where one out of multiple alternative production paths has to be selected for the manufacturing of steel lots. The objective is the minimization of the makespan. For the real-world application, however, an additional target criterion has to be taken into account. The company has defined priorities for the selection of the alternative production paths, resulting in a priority function maximization as a second objective (Hauder, Beham, Raggl, Affenzeller 2019b). In order to tackle this multi-objective optimization problem (MOP), the so-called balanced box method (BBM) (Boland, Charkhgard, and Savelsbergh 2015) is regarded. The results of the chosen method are presented for the mixed integer programming (MIP) as well as for the constraint programming (CP) model of the multi-objective optimization problem by solving it with the optimization suite IBM ILOG CPLEX. The achieved solutions are then compared concerning runtime efficiency and solution quality.

The paper is organized as follows. First, related work concerning multi-objective optimization is described in Section 2. Next, the multi-objective industry case models are presented in Section 3. Optimization results are then illustrated in Section 4, followed by concluding remarks and a future outlook in Section 5.

2. RELATED LITERATURE
Many real-world optimization problems involve two or even more conflicting objectives. Typical well-known examples are a maximized quality on the one hand and minimized costs on the other hand. For decision makers, it is very often not easy to prioritize or weight such conflicting goals prior to a necessary optimization process. One possible way out of this challenging target is the generation of all Pareto-optimal solutions, i.e. the set of all optimization solutions in which one objective can no longer be improved without worsening another one (=Pareto-set). Decision makers can then evaluate all generated trade-off solutions and select the one they rate best for their field.
In order to generate the Pareto-set, different heuristic and exact solution methods have already been developed (Bechikh, Datta, and Gupta 2016; Ehrgott 2005). Examples for MOP methods are the weighted sum method (Aneja, Nair 1979; Hauder, Beham, Raggl, Affenzeller 2019b), the ε-constraint method (Haimes 1971) and the non-dominated sorting algorithm (Srinivas, Deb 1994). However, since a full investigation of such methods is outside the scope of this work, the

interested reader is referred to Bechikh, Datta, and Gupta (2016), Deb (2014), and Ehrgott (2005) for a further detailed examination.

One of the most recently developed methods is the balanced box method. This new algorithm for bi-objective optimization problems has been introduced by Boland, Charkhgard, and Savelsbergh (2015). Such as other multi-objective optimization methods, it finds all nondominated points and is described to be very competitive in terms of solution quality and runtime. The BBM is an extension of the Box algorithm (Hamacher, Pedersen, and Ruzika 2007) and always splits the solution space into two parts (bottom and top rectangle). First, the bottom rectangle is searched for a nondominated point by lexicographically optimizing it. Second, the top rectangle is optimized the same way, but already without considering the part which has been identified to be dominated by the first bottom rectangle optimization. This procedure is repeated until all nondominated points are found, always by again splitting the existing boxes and without considering the dominated part of the prior optimization for a speed up of the optimization process (Boland, Charkhgard, and Savelsbergh, 2015).

Project scheduling is known to be a promising modeling approach when limited resources and precedence relations have to be taken into account. The related optimization problem is the so-called resource-constrained project scheduling problem (RCPSP). The basic RCPSP consists of activities which have to be scheduled under consideration of time restrictions, resource constraints and precedence relations (Hartmann and Briskorn 2010). Many real-world applications show that flexibility in the selection of such activities is a necessary extension of this problem (Kellenbrink and Helber 2015; Čapek, Šůcha, and Hanzálek 2012). Hauder, Beham, Raggl and Affenzeller (2018, 2019a) also give two further extensions of the RCPSP where flexibility is considered, based on the work of Tao and Dong (2017). They work on the selection of alternative activities for the production of multiple steel lots in a single-objective environment.

3. MULTI-OBJECTIVE SCHEDULING FOR THE STEEL INDUSTRY

In the following, we first describe the multi-objective problem in detail, including the consideration of a second objective and related additional constraints within a mixed integer programming model in Section 3.1. Thereafter, we present the constraint programming formulation in Section 3.2.

3.1. Steel industry scheduling with multiple objectives: MIP formulation

Our steel industry partner needs an optimized solution for a resource-constrained project scheduling problem allowing flexibility in the selection of activities. This problem arises after the completion of the continuous casting process and ends with customer deliveries. It consists of operations or activities or nodes $i, j \in \{0, \dots, N+1\}$, where nodes $\{0, N+1\}$ represent artificial start and end nodes and all other nodes are real-world activities. Moreover, the subset $L \subset N$ defines the lots and thus, the customer orders considered for the optimization. The adjacency matrix A_{ij} represents the allowed and forbidden connections between all activities. With the flexibility type f_i, flexibility in the selection of alternative production routes is represented. The processing time p_i is defined for every activity and all activities need renewable resources $k \in \{1, \dots, K\}$ with a demand Q_{ik}. We only consider renewable resource capacities C_k, since nonrenewable ones do not exist in the manufacturer´s plant. The time horizon $t \in \{1, \dots, T\}$ gives the maximum planning period. With decision variable y_i, it is decided if an activity is selected for performance ($y_i = 1$) or not ($y_i = 0$) and z_{it} decides if an activity is selected for completion at time slot t ($z_{it} = 1$) or not ($z_{it} = 0$).
The minimization of the makespan is a very well-known objective (Hartmann and Briskorn 2010) and has already been considered in Hauder, Beham, Raggl and Affenzeller (2018). The second goal of priority maximization (Hauder, Beham, Raggl and Affenzeller 2019b) is implemented by the assignment of a priority value $Prio_i$ for the subset P_i which includes all activities with priority values. The higher the priority value is, the more the company wishes to select the corresponding activity and thus, a specific production route. Overall, the presented descriptions result in the following mixed integer programming model:

$Minimize$

$$\sum_{t \in T} t \cdot z_{N+1t} \tag{1a}$$

$Minimize$

$$\sum_{t \in T} \sum_{i \in P} Prio_i \cdot x_i \tag{1b}$$

$subject\ to$

$$y_0 = 1 \tag{2}$$

$$\sum_{t \in T} z_{it} = y_i \qquad \forall\, i \in N, \tag{3}$$

$$\sum_{j \in N} A_{ij} \cdot y_j = y_i \quad \forall\, i \in N, \quad if\ f_i = 0, \tag{4}$$

$$y_j \geq A_{ij} \cdot y_i \qquad \forall\, i, j \in N, \quad if\ f_i = 1, \tag{5}$$

$$\sum_{j \in N} A_{ij} \cdot y_j = y_j \quad \forall\, i \in N, \quad if\ f_j = 2, \tag{6}$$

$$A_{ij}(\sum_{t \in T} t \cdot z_{it}) + (y_j + y_i - 2) \cdot M \leq \sum_{t \in T} t \cdot z_{jt} - p_j \qquad \forall\, i,j \in N, \tag{7}$$

$$\sum_{i \in N} \sum_{\tau = t}^{t+D_i-1} z_{i\tau} \cdot Q_{ik} \leq C_k \qquad \forall\, k \in K, t \in T, \tag{8}$$

$$\sum_{t \in T} \sum_{i \in P} Prio_i \cdot x_i \geq L, \tag{9}$$

$$y_i, z_{it} \in \{0,1\} \qquad \forall\, i \in N, t \in T. \tag{10}$$

Objective (1a) minimizes the overall makespan. Objective (1b) maximizes priority values, i.e. it maximizes the selection of the routes which the company prioritizes the highest. With constraint (2), the production is started and constraints (3) ensure that activities which are selected for performance are exactly finished once. Restrictions (4)-(6) show flexibility possibilities: If an activity is an OR node, exactly one successor must be selected; if an activity is an AND node, more than one successor can be selected. If an activity is an OUT node (=dummy sink node per project), it is guaranteed that no additional nodes of other production routes of the same lot (=project) can be selected. Conditions (7) imply that processing times are met. With constraints (8), capacity restrictions are introduced. Condition (9) serves as a lower bound for the second objective of priority maximization: As for all production routes, a minimum value of 1 is defined in the input, the sum of all priorities must at least correspond with the amount of lots considered for the optimization (since for every lot, one production route has to be selected according to restrictions (4)). Constraints (10) define the decision variables as binary ones.

3.2. Steel industry scheduling with multiple objectives: CP formulation

For the constraint programming model, the formulation, including decision variables and resource utilization, works differently compared to the MIP model. CP in general and also the CP Optimizer of IBM ILOG CPLEX consist of decision variables, functions and expressions for the decision variables, and resource functions (Bockmayr and Hooker 2005; Laborie, Rogerie, Shaw, and Vilím 2018).

For our CP model, we use the decision variable $interval(w_j)$ `optional in 0..T`. It selects one out of multiple alternative activities and decides on the start time of every activity. Moreover, the resource function `cumulFunction` $q_r = \sum_{j \in \mathcal{J}: c_{jr} \geq 0} \texttt{pulse}(w_j, c_{jr})$ decides on the cumulative resource usage of every activity, considering its demand c_{jr}, over time. The resulting optimization model for the BBM implementation is now presented as follows:

$$\mathit{Minimize} \quad \texttt{endOf}(w_{n+1}) \tag{11a}$$

$$\mathit{Minimize} \quad \sum_{i \in P} Prio_i \cdot \texttt{presenceOf}(w_i) \tag{11b}$$

$\mathit{subject\ to}$

$$\texttt{startOf}(w_0) = 1, \tag{12}$$

$$\texttt{presenceOf}(w_0) = 1, \tag{13}$$

$$\texttt{presenceOf}(w_{n+1}) = 1, \tag{14}$$

$$\texttt{presenceOf}(w_i) = 1 \qquad \forall\, i \in \mathcal{L}, \tag{15}$$

$$\texttt{lengthOf}(w_i) = p_i \qquad \forall\, i \in \mathcal{J}, \tag{16}$$

$$\texttt{endOf}(w_i) \geq D_i \qquad \forall\, i \in \mathcal{L}, \tag{17}$$

$$\texttt{endOf}(w_i) \leq T \qquad \forall\, i \in \mathcal{L}, \tag{18}$$

$$\texttt{alternative}(w_i, \{w_a \in S_i\}) \quad \forall\, i \in \mathcal{M}, \tag{19}$$

$$\texttt{endAtStart}(w_i, w_a) \qquad \forall\, i \in \mathcal{M}, a \in E_i, \tag{20}$$

$$\texttt{endBeforeStart}(w_i, w_{n+1}) \quad \forall\, i,j \in \mathcal{L}, \tag{21}$$

$$\texttt{endAtStart}(w_i, w_j) \qquad \forall\, i,j \in \mathcal{A}, \tag{22}$$

$$\texttt{presenceOf}(w_i) = \texttt{presenceOf}(w_j) \qquad \forall\, i,j \in \mathcal{A}, \tag{23}$$

$$\sum_{i \in P} Prio_i \cdot \texttt{presenceOf}(w_i) \geq L, \tag{24}$$

$$q_r \leq C_r \quad \forall\, r \in \mathcal{R}. \tag{25}$$

Objective (11a) minimizes the overall makespan and the objective (11b) maximizes the priority values. Constraints (12)-(14) guarantee the start and end of the whole production cycle. Restrictions (15) ensure the production of all lots. With conditions (16), the processing times have to be adhered to. Constraints (17)-(18) forbid early deliveries and restrict the schedule to the overall project horizon *T*. With restrictions (19)-(20), flexibility in terms of alternative routes is presented. Constraints (21) ensure that all lots have to be produced before the production process is finished. Conditions (23) imply the adherence to existing precedence relations and constraints (24) serve as a lower bound for priority values, as already explained for the MIP model. With constraints (25), capacities cannot be exceeded.

4. COMPUTATIONAL RESULTS

Both models and the corresponding balanced box method are implemented in and solved by IBM ILOG CPLEX 12.9.0 on a virtual machine Intel(R) Xeon(R) CPU E5-2660 v4, 2.00GHz with 28 logical processors, Microsoft Windows 10 Education. The runtime (T) is limited to one hour, since this is the limit set by our steel industry partner. The used benchmark instances are the ones presented in Hauder, Beham, Raggl, Parragh and Affenzeller (2019a) and extended in terms of priority values. The values are defined from 1 to 3 and randomly assigned to all lots. The value 1 corresponds with the highest priority and 3 with the lowest one. The test instances consist of 10, 15, and 20 lots. For every lot size, five instances are randomly generated.

In Table 1, CP and MIP optimization solutions are presented. Column 1 gives the lot size and column 2 the number of activities considered for each instance. The third column shows the runtime in seconds; and the "T" indicates that the runtime limit of 3,600 seconds has been reached. In column 4, the amount of non-dominated points found by the CP optimization is presented. Column 5 and 6 follow the same explanation logic, showing the results of the MIP optimization. Bold letters represent the finding of the whole Pareto-set.

Table 1. CP optimization results with the balanced box method.

		CP		MIP	
Lots	Activi-ties	**Run-time**	**#Non.-dom.**	**Run-time**	**#Non.-dom.**
10	160	2.27	**4**	T	2
	163	15.07	**9**	T	2
	158	16.79	**10**	T	2
	163	15.82	**11**	T	1
	167	35.11	**9**	T	2
15	232	117.30	**6**	T	-
	259	T	12	T	-
	238	T	12	T	-
	252	2459.26	**12**	T	-
	247	T	19	T	-
20	311	T	2	T	-
	340	T	5	T	-
	319	T	3	T	-
	340	T	1	T	-
	306	T	2	T	-

It can be seen in Table 1 that, with the MIP model, it is only possible to generate solutions for the smallest instance size of 10 lots. For bigger instances, it is not even possible to generate a feasible solution. We assume that the reasons for these findings are two-fold. On the one hand, we have a huge amount of nodes already for the smallest lot size 10 (already more than 150 nodes), resulting in a huge amount of decision variables and constraints that have to be considered by the MIP solver in contrary to the CP solver. On the other hand, two objectives have to be regarded, which also seems to make the problem very hard to solve for the MIP solver.

For the CP solution approach, it can be seen that the whole Pareto-front is easily found for small instances. However, the bigger and thus, the more complex the instances become, the harder it is for the CP Optimizer to find even one non-dominated point. Nevertheless, the optimization solutions show that the CP model is more competitive in terms of solution quality and runtime, e.g. having a runtime of under one minute and all optimal solutions for all instances of lot size 10 in contrary to the MIP approach, where only some optimal solutions are found within the allowed time limit T.

5. CONCLUSION

In this work, a multi-objective optimization of an already existing RCPSP with activity selection flexibility has been presented. By applying the balanced box method, it is possible to generate the full Pareto-set for small instances with the developed CP model in contrary to the MIP approach. However, bigger instances show the limit of this approach for the here presented RCPSP. Future work should therefore concentrate on alternative multi-objective algorithms, as for example the NSGA-II, in order to generate exact solutions also for huger instances.

ACKNOWLEDGMENTS

The work described in this paper was done within the project Logistics Optimization in the Steel Industry (LOISI) #855325 within the funding program Smart Mobility 2015, organized by the Austrian Research Promotion Agency (FFG) and funded by the Governments of Styria and Upper Austria.

REFERENCES

Aneja, Y.P. and Nair, K.P., 1979. Bicriteria transportation problem. Management Science, 25(1), pp.73-78.

Bechikh, S., Datta, R. and Gupta, A. eds., 2016. Recent advances in evolutionary multi-objective optimization (Vol. 20). Springer.

Bockmayr, A. and Hooker, J.N., 2005. Constraint programming. Handbooks in Operations Research and Management Science, 12, pp.559-600.

Boland, N., Charkhgard, H. and Savelsbergh, M., 2015. A criterion space search algorithm for biobjective integer programming: The balanced box method. INFORMS Journal on Computing, 27(4), pp.735-754.

Čapek, R., Šůcha, P. and Hanzálek, Z., 2012. Production scheduling with alternative process plans. European Journal of Operational Research, 217(2), pp.300-311.

Deb, K., 2014. Multi-objective optimization. In Search methodologies (pp. 403-449). Springer, Boston, MA.

Ehrgott, M., 2005. Multicriteria optimization (Vol. 491). Springer Science & Business Media.

Haimes, Y.V., 1971. On a bicriterion formulation of the problems of integrated system identification and system optimization. IEEE transactions on systems, man, and cybernetics, 1(3), pp.296-297.

Hamacher, H.W., Pedersen, C.R. and Ruzika, S., 2007. Finding representative systems for discrete bicriterion optimization problems. Operations Research Letters, 35(3), pp.336-344.

Hartmann, S. and Briskorn, D., 2010. A survey of variants and extensions of the resource-constrained project scheduling problem. European Journal of operational research, 207(1), pp.1-14.

Hauder, V.A., Beham A., Raggl S., Affenzeller M., 2018. Resource constrained project scheduling: a real-world extension for steel industry - Proceedings of the 30th European Modeling and Simulation Symposium EMSS2018, Budapest, Hungary.

Hauder, V.A., Beham, A., Raggl, S., Parragh, S.N. and Affenzeller, M., 2019a. On constraint programming for a new flexible project scheduling problem with resource constraints. arXiv preprint arXiv:1902.09244.

Hauder, V.A., Beham, A., Raggl, S. and Affenzeller, M., 2019b. Solving a flexible resource-constrained project scheduling problem under consideration of activity priorities. International Conference on Computer Aided Systems Theory. Accepted for Publication.

Kellenbrink, C. and Helber, S., 2015. Scheduling resource-constrained projects with a flexible project structure. European Journal of Operational Research, 246(2), pp.379-391.

Laborie, P., Rogerie, J., Shaw, P. and Vilím, P., 2018. IBM ILOG CP optimizer for scheduling. Constraints, 23(2), pp.210-250.

Srinivas, N. and Deb, K., 1994. Multiobjective optimization using nondominated sorting in genetic algorithms. Evolutionary computation, 2(3), pp.221-248.

Tao, S. and Dong, Z.S., 2017. Scheduling resource-constrained project problem with alternative activity chains. Computers & Industrial Engineering, 114, pp.288-296.

AUTHORS BIOGRAPHY

VIKTORIA HAUDER obtained her master´s degree in social and economic sciences with a major in production and logistics management from the Johannes Kepler University Linz, Austria, in 2014. After gaining practical experience as a logistics manager, she has started working as a research associate in the research group HEAL. Her research interests focus on operations research, production planning and logistics optimization, respectively. In 2017, she has started with her doctoral studies with the working title "Integrated Logistics Optimization".

ANDREAS BEHAM received his master's degree in computer science in 2007 and his PhD in engineering sciences in 2019 from the Johannes Kepler University in Linz, Austria, and is a research associate in the Heuristic and Evolutionary Algorithms Laboratory at the research center in Hagenberg. His research interests include metaheuristic methods applied to combinatorial and simulation-based problems. He is a member of the HeuristicLab architects team.

SEBASTIAN RAGGL received his Master of Science in Bioinformatics in 2014 from the University of Applied Sciences Upper Austria, and is a research associate at the Research Center Hagenberg in the Heuristic and Evolutionary Algorithms Laboratory. His research interests include metaheuristic methods applied to combinatorial and simulation-based problems.

MICHAEL AFFENZELLER has published several papers, journal articles and books dealing with theoretical and practical aspects of evolutionary computation, genetic algorithms, and metaheuristics in general. In 2001 he received his PhD in engineering sciences and in 2004 he received his habilitation in applied systems engineering, both from the Johannes Kepler University in Linz, Austria. He is a professor at the University of Applied Sciences Upper Austria and head of the Heuristic and Evolutionary Algorithms Laboratory.

MODELING FOR COMPONENT RELATIONS IN ROBOTIC DISASSMEBLY

Xiang Li[(a)], Yuanjun Laili[(b)], Lin Zhang[(c)], Lei Ren[(d)]

[(a),(b),(c),(d)]School of Automation and Electrical Engineering, Beihang University

[(a)]lllixxxiang@buaa.edu.cn, [(b)]lailiyuanjun@buaa.edu.cn, [(c)]zhanglin@buaa.edu.cn, [(d)]renlei@buaa.edu.cn

ABSTRACT
Robotic disassembly is a critical technology to achieve automatic disassembly in remanufacturing. However, industrial robots cannot recognize component relations of specific products with various unpredictable states. Therefore, a model for component relations is of great necessity for disassembly optimization problems like Disassembly Sequence Planning (DSP) and Disassembly Line Balancing Problems (DLBP). This paper first introduces the most commonly used models of component relations in three categories. The characteristics of different models are analyzed and compared from the aspects of transformational relations and applications. Finally, suggestions are given as a reference for choosing a suitable component relation model.

Keywords: modeling of component relations, robotic disassembly, disassembly sequence planning, disassembly line balancing

1. INTRODUCTION

Remanufacturing refers to the process of rebuilding end-of-life (EoL) products to their original quality standard (Ilgin and Gupta 2016). It has gained great attention due to both the economic and ecological benefits it creates (Guide Jr 2000). Product disassembly is regarded as the core step of remanufacturing (Tang, et al 2004). However, traditional disassembly process relies on many human workers, which results in great labor costs.

Research efforts in robotic disassembly have been made to increasingly replace manual disassembly. They can execute batch disassembly of easy products independently. The introduction of robots raises several disassembly optimization problems, such as disassembly sequence planning (DSP) and disassembly line balancing (DLB), which are aimed at achieving high efficiency and low time consumption by robots. The preliminary of optimizing those problems is to obtain the internal structure information of EoL product with various unpredictable states. Nevertheless, merely a CAD model is insufficient for getting these component relations.

In order to model the inner structure of products for robotic disassembly, researchers have presented several models. One of the most natural way to represent the connection information between components of a product is liaison graph (Bourjault 1984). Each node of the graph defines a component, while an edge between two nodes indicates that the two components contact to each other. Then matrix-based model of liaisons called interference matrix was presented by Dini and Santochi (1992). To simplify the matrix, Huang, et al (2002) introduced disassembly matrix, which is the integration of interference matrices in all disassembly directions. Except these matrix-based models, graph-based models are also used in representing component relations, like joint precedence graph (Riggs, et al. 2015), AND/OR graph (De Mello and Sanderson 1990) and connector-based precedence graph (Tseng, et al. 2004). Matrix-based and graph-based models are combined by some researchers to convey more information of products. Zhang and Kuo (1997) designed a component fastener graph accompanied with two matrices, adjacency matrix and fasten matrix. Disassembly Petri net is also a popular hybrid-based model with many variations in models of component relations (Zhou and Venkatesh 1999; Guo, et al. 2015). A lot of models are provided but a new issue arises that there are so many models that researchers are confused of choosing a more appropriate one for their problems.

Therefore, this paper compares the most frequently used models of component relations and provides a reference for researchers. Section 2 is devoted to introducing three categories of product model. A discussion of these models from the perspective of transformation and application comparison is shown in Section 3. Finally, section 4 concludes this paper and summarizes the future works.

2. TYPICAL MODELS OF COMPONENT RELATIONS

To obtain feasible sequences from a more comprehensive model, researchers have proposed several kinds of matrices and graphs as the preliminaries of disassembly planning. These models can be clarified as three categories, i.e., matrix-based model, graph-based model, hybrid-based model, as shown in Table 1.

Table 1: Typical Models of Component Relations

No.	Category	Name	References
1	Matrix	Interference matrix (IM)	Dini and Santochi (1992) Huang and Huang (2002)
2		Disassembly precedence matrix (DPM) (Static DPM & Dynamic DPM)	Güngör and Gupta (2001) Tao, et al. (2018)
3		Immediate preceded matrix (IPM)	Kalayci and Gupta (2013)
4	Graph	Task precedence diagram (TPD)	Prenting and Battaglin (1964)
5		Joint precedence graph (JPG)	Riggs, et al. (2015)
6		AND/OR Graph (AOG)	De Mello and Sanderson (1990)
7		Transformed AND/OR Graph (TAOG)	Koc, et al. (2009)
8		Connector-based precedence graph (CPG)	Tseng, et al. (2004)
9		Disassembly constraint graph (DCG)	Li, et al. (2005)
10	Hybrid	Component-fastener graph (CFG)	Zhang and Kuo (1997)
11		Disassembly hybrid graph model (DHGM)	Zhang and Zhang (2010)
12		Disassembly Petri net (DPN)	Zhou and Venkatesh (1999) Guo, et al. (2015)

2.1. Matrix-based Models

Commonly used matrix-based models include interference matrix, disassembly precedence matrix and immediate preceded matrix.

(1) Interference Matrix

Interference matrix expresses the interference relations between two components along one or more principal directions.

Assume a product composed of n components $E=\{e_1,e_2,\cdots,e_n\}$, the integrated interference matrix in direction (X-, X+, Y-, Y+) is a square matrix of order n as defined in Eq. (1).

The variable $h_{ijk}=1$ means that e_i impedes e_j in direction k, otherwise $h_{ijk}=0$. As no component interferes with itself, h_{mmk}, $m\in[1,n]$ equals 0. The interference matrix can be automatically extracted from CAD model of the product (Zhang, et al. 2017).

Huang, et al. (2002) proposed to use the Boolean OR operator to check each component that if there exists one direction in which no precedent component hinders its removal. An example product and its interference matrix are given in Figure 1.

$$\mathbf{H}_{\text{integ}}=\begin{bmatrix} h_{11x-}h_{11x+}h_{11y-}h_{11y+} & h_{12x-}h_{12x+}h_{12y-}h_{12y+} & \cdots & h_{1nx-}h_{1nx+}h_{1ny-}h_{1ny+} \\ h_{21x-}h_{21x+}h_{21y-}h_{21y+} & h_{22x-}h_{22x+}h_{22y-}h_{22y+} & \cdots & h_{2nx-}h_{2nx+}h_{2ny-}h_{2ny+} \\ \vdots & \vdots & \ddots & \vdots \\ h_{n1x-}h_{n1x+}h_{n1y-}h_{n1y+} & h_{n2x-}h_{n2x+}h_{n2y-}h_{n2y+} & \cdots & h_{nnx-}h_{nnx+}h_{nny-}h_{nny+} \end{bmatrix} \quad (1)$$

In addition, interference matrix is usually used together with many complementary matrices such as contact matrix and connection matrix proposed by Dini and Santochi (1992).

(2) Disassembly Precedence Matrix

There are two types of disassembly precedence matrix (DPM) to show the precedence relations, static DPM and dynamic DPM. Static DPM and its variations mentioned in later references (Tseng, et al. 2011; González and Adenso-Díaz, 2006) somehow has more similarities to interference matrix.

As the precedence relations vary during the disassembly process, dynamic DPM is established by Tao, et al (2018) to reflect these changes.

Dynamic DPM consists of four sub-matrices, a connection matrix between components and fasteners (CFM), a motion constraint matrix for fasteners (FCM), a motion constraint matrix for components (CCM), and a precedence matrix between fasteners (FFM). Element in these matrices represents the disassembly precedence between fasteners and components.

If some components and fasteners can be dismantled as a subassembly, dynamic DPM will be divided into several sub-DPMs. Dynamic characteristic here refers to dimensionality reduction of the disassembly sequencing, and therefore reduces computing cost and difficulty of searching feasible solutions.

(3) Immediate Preceded Matrix

Immediate preceded matrix (IPM) is also termed as immediately preceding matrix (Kalayci and Polat 2014). Each element in an IPM defines a disassembly operation/task instead of a component/fastener. Therefore, the task precedence relations are shown by IPM$[y_{ij}]_{n\times n}$, where y_{ij} is equal to 1 if task i should be executed after task j, otherwise it is 0.

Using IPM alone is not enough for disassembly line balancing. It is usually accompanied with an assignment matrix $[x_{ij}]_{n\times m}$ to state the partition of total tasks, where *m* denotes the number of workstations (Kalayci and Polat 2014; Kalayci and Gupta 2013). If part *j* is assigned to station k, corresponding element x_{jk} equals to 1, otherwise it is 0.

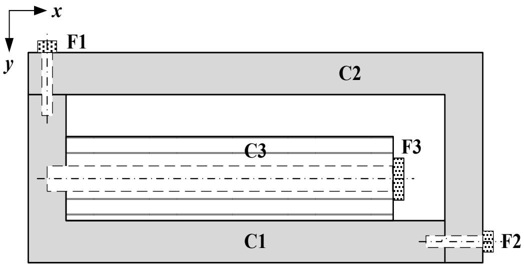

(a)

	C1	C2	C3	F1	F2	F3	OR
C1	0000	0110	0110	1111	1111	1111	1111
C2	1001	0000	1001	1111	1111	1001	1111
C3	1001	0110	0000	0000	0000	1111	1111
F1	1101	1101	0000	0000	0000	0000	1101
F2	1011	1011	0000	0000	0000	0000	1011
F3	1011	0110	1011	0000	0000	0000	1111

(b)

Figure 1. A simple product example and its interference matrix

2.2. Graph-based Model

Typical graph-based models are task precedence diagram, joint precedence graph, AND/OR graph, Transformed AND/OR graph, connector-based precedence graph and disassembly constraint graph.

(1) Task Precedence Diagram

Task precedence diagram (TPD) is proposed mainly in solving assembly/disassembly line balancing problem. Each node in the graph represents a task required in assembly/disassembly. Each connecting arc with a specific direction demonstrates the precedence relationship between the two connected nodes.

The advantages of TPD are its simplicity and elimination of redundancies (Lu and Li 2003). As a task-based diagram, it can be regarded as the graph-based model of IPM and derived from other graphs such as AND/OR graph. The topology of TPD for the same product may vary due to different choices of disassembly tasks. Hence, it is used to represent the assembly/disassembly of products with fixed tasks. (Koc, et al. 2009)

(2) Joint Precedence Graph

JPG is originally used for assembly line balancing. Riggs, et al. (2015) validates its usability in disassembly line balancing. It is an acyclic graph which can be seen as a composition of a TPD and a group of node weights representing the weighted average processing time of each task respectively. It is denoted as $G=(V,E,\overline{\mathbf{t}})$ with the definitions that the node set V contains all tasks for disassembling a product, the directed arc set E reflects the precedence relations between each two nodes. A vector $\overline{\mathbf{t}}$ represents the average processing times of these nodes, which can be obtained in Eq. (2).

$$t_i=\sum_{q\in Q} p_q t_{iq} \quad \forall i\in I \tag{2}$$

There are in total of *Q* models. t_{iq} represents the processing time of the i^{th} task. p_q is defined as a demand portion to represent the weight of the q^{th} model. These weights satisfy $\sum_{q\in Q} p_q=1$. Therefore, t_i is the resultant average processing time of node *i*. The nodes of the resultant graph are the union set of the sub-graphs correspond to different models. An example JPG is shown in Figure 2. The arcs of the resultant graph are obtained by Eq. (3). Redundant arcs are defined as the ones that not exist in the critical path of a process.

$$E=\bigcup_{q\in Q} E_q \setminus \{\text{redundant arcs}\} \tag{3}$$

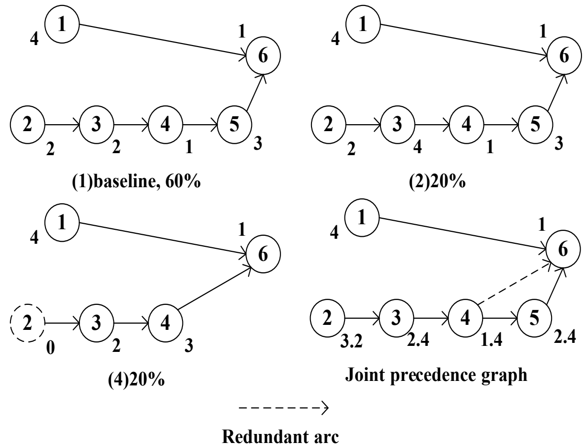

Figure 2: An Example JPG

(3) AND/OR Graph

AND/OR graph (AOG) is introduced by De Mello and Sanderson (1990) to connect disassembly task, components and subassemblies. Nodes in AOG indicate possible subassemblies and components. Parent and children subassemblies are connected by a pair of directed arcs representing disassembly tasks. The arcs are AND-type. If there are multiple optional operations for a parent node, OR-type relation is used between different pairs of AND-type-arcs to show possible disassembly processes. A disassembly sequence will be generated by choosing OR-type-arcs with connected sub-graphs.

AOG enumerates all possible operations for disassembling a product. One can traverse the graph to find the optimal disassembly sequence (Ghandi and Masehian 2015), but it is not practical. In order to avoid excessively complex graph search, Lambert (1999) proposed to use hyper-arcs to avoid repeated nodes and

Proceedings of the European Modeling and Simulation Symposium, 2019
ISBN 978-88-85741-25-6; Affenzeller, Bruzzone, Longo and Pereira Eds.

simplify the graph. An improved AOG of the sample product of Figure 1(a) is given in Figure 3.

(4) Transformed AND/OR Graph

Transformed AND/OR graph (TAOG) is introduced by Koc, et al. (2009). It is a clearer and more efficient model than AOG.

There are two types of nodes in a TAOG, i.e., artificial node and normal node. Artificial node A_i defines subassembly or component to be disassembled, while normal node B_i represents possible disassembly operation. Therefore, the two kinds of nodes are connected alternately. A group of OR-type arcs points from an artificial node to normal nodes defines optional operations. Only one of these operations can be executed at one time. A set of AND-type arcs that start from a normal node and end at several artificial nodes indicates the resultant parts by the specific operation.

With the precedence relations still satisfied and nodes connected by the two kinds of arcs, a TAOG can be formed or transformed from an AOG.

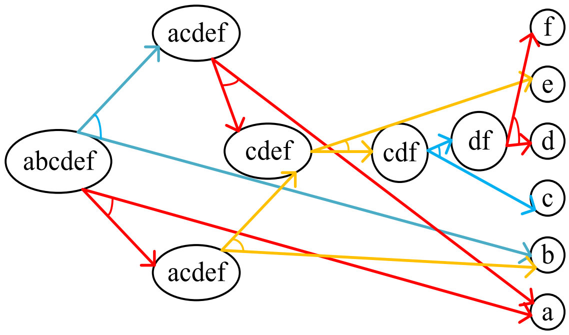

Figure 3: Hyper-arc AND/OR Graph of the Product in Figure 1(a). a to c and d to f Correspond to F1 to F3 and C1 to C3 Respectively

(5) Connector-based Precedence Graph

Connector-based precedence graph (CPG) is originally proposed to deal with assembly sequence planning by Tseng, et al. (2004). Considering the definition of connectors provided in the paper, a product can be decomposed into a set of connector-based elements, thus the graph is also applicable in disassembly problems. A node in CPG refers to a connector or fastener, with its assembly/disassembly information, such as disassembly directions, tools, and precedence constraints. In assembly problems, CPG has a start point representing the state that all connectors are not assembled yet and a terminal point representing full product. Directed arc between two nodes shows their precedence relations.

(6) Disassembly Constraint Graph

Disassembly constraint graph (DCG) introduced by Li, et al. (2005) minimizes model complexity and simplifies the process of generating disassembly sequences for selective disassembly.

A DCG is defined as a triple $M=\{V,E,DE\}$. V is a node set containing components and subassemblies which cannot be dismantled further. E is an undirected edge set containing disassembly contact constraints between components and also represent the disassembly operations. DE is a directed edge set describing precedence information between components. Li, et al. (2005) have developed a method to identify non-contact adjacent nodes and subassemblies in a DCG within a short time.

2.3. Hybrid-based Model

By hybridizing matrix and graphs, models like component-fastener graph, disassembly hybrid graph model and disassembly Petri net, can extract more information from CAD model.

(1) Component-fastener Graph

Component-fastener graph, denoted as $G_c=(V,E)$, is presented by Zhang and Kuo (1997).

It can be retrieved from a CAD model providing required information, like the name of components, disassembly method and connection relationship between components. The n components are labeled as $\{v_1,v_2,\cdots,v_n\}$ in the vertex set V. The relations between these vertices are indicated as a set of undirected edges $E=\{e_1,e_2,\cdots,e_m\}$. All the component and fastener information in need is included in the vertex, such as its name, weight and material type.

Elements in two auxiliary matrix, adjacency matrix E_c and fasten matrix F_c are defined respectively in Eq. (4) and Eq. (5).

$$E_{i,j}=\begin{cases}1, & \textit{if the component } i \textit{ is connected} \\ & \textit{with component } j \\ 0, & \textit{otherwise}\end{cases} \tag{4}$$

$$F_{i,j}=\begin{cases}k, & \textit{if the component } i \textit{ is connected with} \\ & \textit{component } j \textit{ by } k \textit{ fasteners } (k>0) \\ 0, & \textit{otherwize}\end{cases} \tag{5}$$

(2) Disassembly Hybrid Graph Model

Disassembly hybrid graph model (DHGM) is proposed by Zhang, et al (2010) to record both mating contact and noncontact precedence relationships among components. A DHGM is denoted as $G=\{V,E_f,E_{fc},E_c\}$, where node set V contains the minimal disassembly units (components or subassemblies). E_f contains undirected edges that denotes contact constraints. E_{fc} is a directed solid edge set in which the edges represent both contact constraints and precedence relations. Directed dotted edges in E_c define the priority relationships between two units. A DHGM of sample product in Figure 1(a) is shown in Figure 4.

(3) Disassembly Petri Net

Disassembly Petri net (DPN) varies in different definitions. In this paper, an 8-tuple Petri net presented by Guo, et al. (2015) is introduced. DPN can be defined as $\text{DPN} = (S,T,I,O,M,c,\tau,w)$, where defines a place set containing n disassembly parts (the number of components or subassemblies). T records a set of transitions representing disassembly operations. I is an input function that defines a set of directed arcs from T to S. O is an output function defining arcs from S to T. $M = \{M_0,\cdots,M_n\}$ is a mark set. Each element M_i represents the number of tokens in place S_i, $i = 1,2,\ldots,n$. c is disassembly cost associated with each disassembly operations. τ is corresponding recycling/reuse value of each place. w is a set of weight functions corresponding to the transitions. A DPN of sample product in Figure 2(a) is shown in Figure 5.

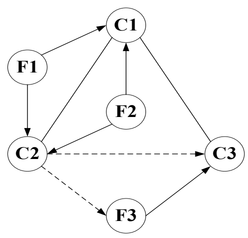

Figure 4: DHGM of Sample Product in Figure 2(a)

Two matrices, precedence matrix $\mathbf{U} = [u_{ij}]$ and disassembly matrix $\mathbf{D} = [d_{ij}]$, are also adopted (Guo, et al. 2015) and specified in Eq.(6) and (7).

$$u_{ij} = \begin{cases} 1, \ \textit{if operation } t_j \textit{ need to be} \\ \quad \textit{performed after } t_i \\ 0, \ \textit{otherwise} \end{cases} \tag{6}$$

$$d_{ij} = \begin{cases} 1, \quad \textit{if disassembly unit } s_i \textit{ is obtained} \\ \qquad \textit{via operation } t_j \\ -1, \ \textit{if } s_i \textit{ is disassembled via } t_j \\ 0, \quad \textit{otherwise} \end{cases} \tag{7}$$

3. TRANSFORMATION AND COMPARISON BETWEEN DIFFERENT MODELS

Twelve frequently used models of component relations are already introduced hereinbefore, although it is possible that there are still some remarkable ones not mentioned. Although those models vary, all of them are able to provide essential information for solving disassembly optimization problems such as DLP and DLBP. This section aims at offering a reference for those confused of choosing the model better for their problems.

A comparison between the models is given in Table 3 and the transformational relations are also included. As shown in the table, it is noticeable that three categories of models can be converted to each other in some ways. However, differences still exist between those models. By contrast, matrix-based models like IM, DPM is easier to extract from others, while hybrid ones like DHGM, DPN are more informative therefore difficult to obtain. Almost all models based on components can be derived from a CAD model. Without definitions of each task and other necessary information, a component-based model cannot be transformed directly to a task-based one. Apart from those based on either components or tasks, models based on both of them, such as AOG and TAOG, are commonly applied to solve disassembly problems as well. The two models can be converted to each other. To replace repeated and long-hour manual work, some automatic generating methods are presented. Zhang, et al. (2016) proposed an algorithm to generate improved IMs.

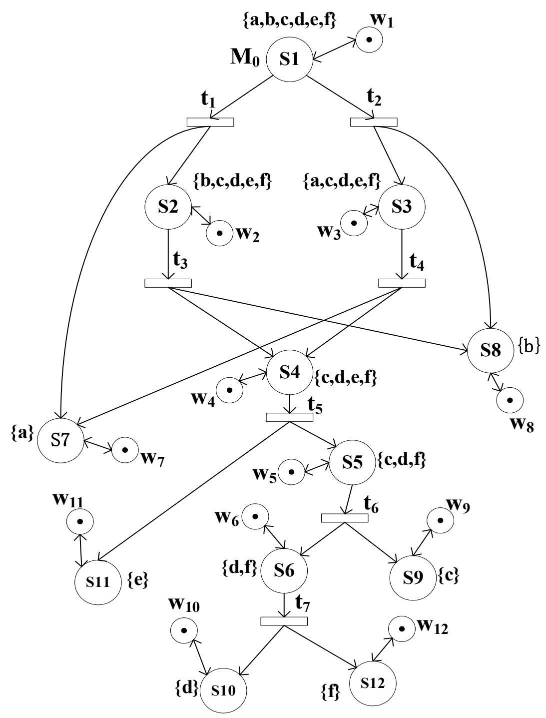

Figure 5: Disassembly Petri Net of the Sample Product Shown in Figure 1(a)

To clarify the application of each model, the conclusion is shown in the following Table 4. N, T, D and C are assumed as the number of indecomposable elements, tasks, operation directions and connectors respectively.

Combined with the former table, it can be concluded that task-based models are mostly used on solving DLBP while component-based ones on solving DSP. Therefore task-and-component-based model, AOG and TAOG, can be applied in both cases (Altekin 2016; Ren, et al. 2017; Bentaha, et al. 2014). Space complexity refers to the storage that the model takes up after formation. The complexity of hybrid-based models is relatively high due to abundant information they contain. That of AOG and DPN is uncertain because it depends on total number of disassembly choices during sequence generation.

Table 2: Transformation

No.	Category	Name	Task-based model or component-based	Transformable from CAD model?	Can be transformed to	Can be generated from
1	Matrix	IM	Component-based	YES	DPM	DPM, CPG, DCG, DHGM, DPN
2		DPM	Component-based	YES	IM	IM, CPG, DCG, DHGM, DPN
3		IPM	Task-based	NO	TPD	TPD, JPG, AOG, DPN
4	Graph	TPD	Task-based	NO	IPM	IPM, JPG, AOG, DPN
5		JPG	Task-based	NO	IPM, TPD	/
6		AOG	Task-and-component based	YES	TAOG	TAOG, DPN
7		TAOG	Task-and-component based	YES	AOG	AOG, DPN
8		CPG	Component-based	YES	IM, DPM, CFG	CFG
9		DCG	Component-based	YES	IM, DPM	DHGM
10	Hybrid	CFG	Component-based	YES	CPG	CPG
11		DHGM	Component-based	YES	IM, DPM, DCG	/
12		DPN	Task-and-component based	YES	IM, DPM, IPM, TPD, AOG, TAOG	/

Furthermore, all of the above models are capable of recording disassembly state and assisting with real-time updates, which is not mentioned in the table. Some of them works by modifying the model to eliminate the dismantled part immediately, like IM, dynamic DPM and so on. Some label the current separated progress at the node of component or task, instead of changing the original model of component relations.

Table 3: Applications

No.	Category	Name	Space(model) complexity	Disassembly sequence planning	Disassembly line balancing
1	Matrix	IM	$O(N^2D)$	√	
2		DPM	$O(N^2 D)$	√	
3		IPM	$O(T^2)$		√
4	Graph	TPD	$O(T^2)$		√
5		JPG	$O(T^2)$		√
6		AOG	Uncertain	√	√
7		TAOG	$O[(2N)^2]$	√	√
8		CPG	$O(C^2)$	√	
9		DCG	$O(N^2)$	√	
10	Hybrid	CFG	$O(N^2)$	√	
11		DHGM	$O(N^2)$	√	
12		DPN	Uncertain	√	

From the perspective of disassembly completion, there are three types of disassembly, complete disassembly, selective disassembly and partial disassembly. Most researches about modeling for component relations are devoted to completely disassembly. Only a few of them have been applied to solve two incomplete separations, such as IM and DCG. Nevertheless, not all parts of EoL products are valuable and reusable. What really matters for manufacturers is how to collect those components of high recovery value within the least time duration. Therefore, the latter two disassembly problems are supposed to be paid more attention.

4. CONCLUSIONS

Rapid development of remanufacturing brings challenges and opportunities for product manufacturing industry. Compared with those other new fields, there is no doubt that robotic disassembly attracts more attention. Most optimization problems in this field start with modeling for component relations. Therefore, this paper concludes three typical categories of component relation models, matrix-based model, graph-based model and hybrid-based model. Model comparison from perspectives of transformation and application were also discussed, which provides a reference for choosing more suitable component relation models in robotic disassembly optimization problems.

So far, most of the existing models of component relations are designed for completely disassembly. However, it usually takes plenty of time for robot to dismantle unnecessary parts in this kind of disassembly process. Modeling for selective and partial disassembly would be a fruitful area for future work.

CAD model of an EoL product contains various information of products. Only several models of component relations can be obtained with automatic generating algorithms if CAD models are provided. To make use of other models, manual work is still required, which undoubtably will take a lot of time. Future research can be conducted to reduce human involvement in model generation process.

ACKNOWLEDGMENTS

This work is supported by the National Natural Science Foundation of China (NSFC) (Grant No. 61703015) and the Fundamental Research Funds for the Central Universities.

REFERENCES

Ilgin M.A. and Gupta S.M., 2016. Remanufacturing modeling and analysis. CRC Press.

Guide Jr V.D.R., 2000. Production planning and control for remanufacturing: industry practice and research needs. Journal of operations Management, 18(4), 467-483.

Tang O., Grubbström R.W. and Zanoni S., 2004. Economic evaluation of disassembly processes in remanufacturing systems. International Journal of Production Research, 42(17), 3603-3617.

Bourjault A., 1984. Contribution à une approche méthodologique de l'assemblage automatisé: élaboration automatique des séquences opératoires. Thesis (PhD). Université de Franche-Comté.

Dini G. and Santochi M., 1992. Automated sequencing and subassembly detection in assembly planning. CIRP annals, 41(1), 1-4.

Huang Y.M. and Huang C.T., 2002. Disassembly matrix for disassembly processes of products. International Journal of Production Research, 40(2), 255-273.

Riggs R.J., Battaïa O. and Hu S.J., 2015. Disassembly line balancing under high variety of end of life states using a joint precedence graph approach. Journal of Manufacturing Systems, 37, 638-648.

De Mello L.S.H. and Sanderson A.C., 1990. AND/OR graph representation of assembly plans. IEEE Transactions on robotics and automation, 6(2), 188-199.

Tseng H.E., Li J.D. and Chang Y.H., 2004. Connector-based approach to assembly planning using a genetic algorithm. International Journal of Production Research, 42(11), 2243-2261.

Zhang H.C. and Kuo T.C., 1997. A graph-based disassembly sequence planning for EOL product recycling. Twenty First IEEE/CPMT International Electronics Manufacturing Technology Symposium Proceedings 1997 IEMT Symposium. 140-151. Oct 13-15, Austin (Texas, USA).

Zhou M.C. and Venkatesh K., 1999. Modeling, simulation, and control of flexible manufacturing systems: A Petri net approach. World Scientific.

Guo X., Liu S., Zhou M.C. and Tian G., 2016. Disassembly sequence optimization for large-scale products with multiresource constraints using scatter search and Petri nets.. IEEE transactions on cybernetics, .46(11), 2435-2446.

Güngör A., Gupta S.M., 2001. Disassembly sequence plan generation using a branch-and-bound algorithm. International Journal of Production Research, 39(3), 481-509.

Tao F., Bi L., Zuo Y. and Nee A.T.C., 2018. Partial/parallel disassembly sequence planning for complex products. Journal of Manufacturing Science and Engineering, 140(1), 011016.

Kalayci C.B., Gupta S.M., 2013. Ant colony optimization for sequence-dependent disassembly line balancing problem. Journal of Manufacturing Technology Management, 24(3), 413-427.

Prenting T.O., Battaglin R.M., 1964. The precedence diagram: A tool for analysis in assembly line balancing. Journal of Industrial Engineering, 15(4), 208-213.

Koc A., Sabuncuoglu I., Erel E., 2009. Two exact formulations for disassembly line balancing problems with task precedence diagram construction using an AND/OR graph. Iie Transactions, 41(10), 866-881.

Li J.R., Khoo L.P., Tor S.B., 2005. An object-oriented intelligent disassembly sequence planner for maintenance. Computers in Industry, 56(7), 699-718.

Zhang X.F., Zhang S.Y., 2010. Product cooperative disassembly sequence planning based on branch-and-bound algorithm. The International Journal of Advanced Manufacturing Technology, 51(9-12), 1139-1147.

Zhang W., Ma M., Li H., Yu J., 2017. Generating interference matrices for automatic assembly sequence planning. The International Journal of Advanced Manufacturing Technology, 90(1-4), 1187-1201.

Lu M., Li H., 2003. Resource-activity critical-path method for construction planning. Journal of construction engineering and management, 129(4), 412-420.

Ghandi S., Masehian E., 2014. Review and taxonomies of assembly and disassembly path planning problems and approaches. Computer-Aided Design, 67, 58-86.

Lambert A.J.D., 1999. Linear programming in disassembly/clustering sequence generation. Computers & Industrial Engineering, 36(4), 723-738.
Altekin F.T., 2016. A Piecewise Linear Model for Stochastic Disassembly Line Balancing. IFAC-PapersOnLine, 49(12), 932-937.
Ren Y., Yu D., Zhang C., et al, 2017. An improved gravitational search algorithm for profit-oriented partial disassembly line balancing problem. International Journal of Production Research, 55(24), 7302-7316.
Bentaha M.L., Battaïa O., Dolgui A., 2014. Disassembly line balancing and sequencing under uncertainty. Procedia CIRP, 15, 239-244.

AUTHORS BIOGRAPHY

Xiang Li received the BS Degree from the School of Automation Science and Electrical Engineering at Beihang University. Now she is studying as a postgraduate in the School of Automation Science and Electrical Engineering at Beihang University. Her research interests include evolutionary optimization for large-scale cloud computing system and robotic disassembly for remanufacturing.

Yuanjun Laili received the BS, MS, and Ph.D Degree from the School of Automation Science and Electrical Engineering at Beihang University. She is an assistant Professor of the School of Automation Science and Electrical Engineering in Beihang University. She is also a member of SCS (The Society For Modeling and Simulation International) and an Associate Editor of "*International Journal of Modeling, Simulation, and Scientific Computing*". Her main research interests are in the areas of intelligent optimization, modeling and simulation of manufacturing.

Lin Zhang received the B.S. degree in 1986 from the Department of Computer and System Science at Nankai University, China. He received the M.S. degree and the Ph.D. degree in 1989 and 1992 from the Department of Automation at Tsinghua University, China, where he worked as an associate professor from 1994. He served as the director of CIMS Office, National 863 Program, China Ministry of Science and Technology, from December 1997 to August 2001. From 2002 to 2005 he worked at the US Naval Postgraduate School as a senior research associate of the US National Research Council. Now he is a full professor in Beihang University. He is an associate Editor-in-Chief of "*International Journal of Modeling, Simulation, and Scientific Computing*". His research interests include integrated manufacturing systems, system modeling and simulation, and software engineering. Prof. Zhang is an IEEE senior member and a director of baord of SCS.

Lei Ren is an associate professor and the deputy head of Cloud Manufacturing Research Center at School of Automation Science and Electrical Engineering in Beihang University, and a senior research scientist at Engineering Researching Center of Complex Product Advanced Manufacturing Systems, Ministry of Education, China. He received a Ph.D degree in computer science from the Institute of Software, Chinese Academy of Sciences in 2009. His research interests include big data analytics and applications. He has published 50+ papers and got 2000+ citations according to Google Scholar. He edited a book entitled "Challenges and Opportunity with Big Data" published by Springer LNCS. He served as an associate editor of SIMULATION: Transactions of the Society for Modeling and Simulation International, and reviewers for journals such as IEEE TII, TSMC, ACM TCC. He also served as a TPC co-chair for the 19th Monterey Workshop on Big Data, 5th International Conference on Enterprise Systems, etc. He is a member of IEEE, ACM, ASME and SCS.

A NEW SOLUTION ENCODING FOR SIMULATION-BASED MULTI-OBJECTIVE WORKFORCE QUALIFICATION OPTIMIZATION

Johannes Karder[(a)], Viktoria A. Hauder[(b)], Andreas Beham[(c)], Klaus Altendorfer[(d)], Michael Affenzeller[(e)]

[(a),(b),(c),(e)]Heuristic and Evolutionary Algorithms Laboratory,
University of Applied Sciences Upper Austria, Softwarepark 11, 4232 Hagenberg, Austria
[(d)]Department of Operations Management,
University of Applied Sciences Upper Austria, Wehrgrabengasse 1–3, 4400 Steyr, Austria
[(a),(c),(e)]Institute for Formal Models and Verification
Johannes Kepler University, Altenberger Straße 69, 4040 Linz, Austria
[(b)]Institute for Production and Logistics Management,
Johannes Kepler University, Altenberger Straße 69, 4040 Linz, Austria

[(a)]johannes.karder@fh-hagenberg.at, [(b)]viktoria.hauder@fh-hagenberg.at, [(c)]andreas.beham@fh-hagenberg.at, [(d)]klaus.altendorfer@fh-steyr.at, [(e)]michael.affenzeller@fh-hagenberg.at

ABSTRACT
Solutions for combinatorial problems can be represented by simple encodings, e.g. vectors of binary or integer values or permutations. For such encodings, various specialized operators have been proposed and implemented. In workforce qualification optimization, qualification matrices can for example be encoded in the form of binary vectors. Though simple, this encoding is rather general and existing operators might not work too well considering the genotype is a binary vector, whereas the phenotype is a qualification matrix. Therefore, a new solution encoding that assigns a number of workers to qualification groups is implemented. By conducting experiments with NSGA-II and the newly developed encoding, we show that having an appropriate mapping between genotype and phenotype, as well as more specialized genetic operators, helps the overall multi-objective search process. Solutions found using the specialized encoding mostly dominate the ones found using a binary vector encoding.

Keywords: workforce qualification, encoding, multi-objective optimization, NSGA-II, simulation

1. INTRODUCTION

One of the main key factors for the success of manufacturing companies is qualified staff. Only if a company's personnel is qualified in such a way that all necessary production steps can be carried out on time, a high customer service level with an associated maximized high customer satisfaction is achievable. At the same time, Europe and thus, the European industry, is facing skills shortage, i.e. there is an increasing amount of vacant jobs for which no qualified human resources are available (OECD 2018). This problem, also referred to as skill gap, can of course be counteracted by raising qualification through internal or external trainings which leads to an increased flexibility in the assignment possibilities of workers (De Bruecker, Van den Bergh, Beliën, and Demeulemeester 2015). However, in many cases there is not even enough workforce available that could be hired and then trained, resulting in a major economic challenge for European companies (EUROCHAMBRES 2019; OECD 2018). As a result, the flexibility should be achieved with the smallest possible amount of necessary qualifications.

Precisely these two contradictory objectives, a maximized service level on the one hand and a minimized sum of necessary qualifications on the other hand represent the two major challenges in the long-term production planning of the flow shop system of our company partner. In order to tackle these problems, we propose a simulation-based multi-objective optimization approach with the optimization framework HeuristicLab (HL), consisting of an innovative encoding for the elitist non-dominated sorting genetic algorithm (NSGA-II) (Deb, Pratap, Agarwal, and Meyarivan 2002) and the simulation framework Sim#.

The paper is structured as follows. In Section 2, we give an overview of the related scientific literature. Next, we present our solution method in Section 3, involving the developed new encoding for the applied multi-objective algorithm and the simulation model. In Section 4, we evaluate our proposed method, showing the potentials of our solution encoding for the NSGA-II as an appropriate algorithm for the presented problem. Finally, we conclude our work and give directions for further research in Section 5.

2. RELATED LITERATURE

Workforce planning is a well-researched topic in the area of operations research. It defines how many workers should be hired or dismissed at which point in time and when they should work for how many periods of time. As a result, workforce planning can consist of staffing and scheduling decisions (De Bruecker, Van den Bergh,

Beliën, and Demeulemeester 2015). Related to this, it is also defined that if a worker is able to perform one specific task, he has one specific skill. There are different determinants which influence skills, such as the qualification, the experience or the age of a worker. Moreover, it is noted that skill determinants have a direct impact on so-called skill consequences, such as the quality of work. However, the link between skill determinants and consequences has rarely been observed up to now (De Bruecker, Van den Bergh, Beliën, and Demeulemeester 2015). Exactly this missing link complies with our object of investigation. We present a simulation-based optimization approach to study the impact of worker qualifications (skill determinant) on the customer service level of a company (skill consequence), assuming that the quality of work is expressed by the customer service level of the partner company. For this purpose we develop an innovative new solution encoding and corresponding variation operators that are able to screen the space of possible workforce qualifications. It is noted that we concentrate on the qualifications of workers, since this is the determining skill factor defined by our company partners.
As we consider the two objectives of service level maximization and qualification minimization, we work on a multi-objective optimization problem. Besides well-known solution methods such as the ε-constraint method (Haimes, 1971) or the recently established Balanced Box Method (Boland, Charkhgard, and Savelsbergh 2015), there is the NSGA-II, proposed by Deb, Pratap, Agarwal, and Meyarivan (2002). This algorithm is the method of choice for many multi-objective optimization problems, including a wide variety of real-world applications (Hu, Bie, Ding, and Lin 2016; Wang, Fu, Huang, Huang, and Wang 2017). Although it is a generic metaheuristic solution approach, depending on the specific problem definition, new solution encodings have to be developed. The combination of a simulation model with a metaheuristic optimization method results in the so-called simulation-based optimization or simulation optimization (Gosavi, 2015). With simulation-based optimization, a simulation model can be used as an objective function for approximating the performance of a real-world system. However, it is also possible to use optimization methods during the execution of a simulation. In general, simulation-based optimization is very often used to get an increased real-world system performance (Affenzeller et al. 2015; Kück, Broda, Freitag, Hildebrandt, and Frazzon, 2017; Lin, Chiu, and Chang 2019).

3. MULTI-OBJECTIVE SIMULATION-BASED WORKFORCE OPTIMIZATION

In the following, we explain our developed method. The optimization part takes responsibility for the assignment of workers to qualifications. The simulation part then simulates the flow shop by integrating the optimization solution candidates and evaluates the corresponding customer service level. The new solution encoding for the implemented NSGA-II is presented in Section 3.1. The simulation model is described in Section 3.2.

3.1. New Solution Encoding

In order to optimize the workforce qualifications, we use the optimization framework HeuristicLab (see https://dev.heuristiclab.com), where we implement a new solution encoding. The *Qualification Encoding* consists of two main properties that define the number of possible qualification configurations: i) the number of qualifications Q and ii) the number of workers W that are present in the system that has to be optimized. A configuration is specified by a variable amount of distinct qualification groups and a number of workers assigned to each group. Qualification groups define which qualifications are present. Each worker w must be assigned to exactly one group and each qualification must be present in at least one qualification group. An example of a qualification configuration is shown in Figure 1. In this example, a total of 6 qualifications need to be distributed among 20 workers. Each qualification group is represented as a Boolean vector in which 1 indicates the presence of a qualification and 0 indicates its absence. In this configuration, 3 workers have been assigned to the first qualification group and therefore possess qualifications 2 and 5.

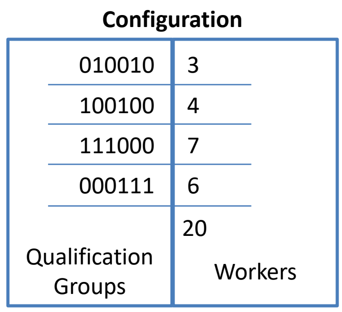

Figure 1: Example qualification configuration.

The encoding also provides 11 operators to create, cross, and manipulate such qualification configurations. Metaheuristic algorithms can use these operators in their implementations, e.g. to initialize populations or create offspring. All operators are described in Section 3.1.1. Furthermore, the feasibility of configurations is validated and a repair procedure is devised to correct infeasible configurations, as shown in Section 3.1.2.

3.1.1. Operators

In this section, the implemented operators, i.e. 1 solution creator, 5 crossover operators and 5 mutation operators, are presented.

1) Random Qualification Creator (RQC)

This operator is used to create qualification configurations in a random fashion. A configuration contains at least 1 and a maximum of Q different qualification groups. A qualification group is a set of qualifications that are available for all workers in this group. All qualification groups within one configuration must be unique. Furthermore, all workers must be assigned to a qualification group and one worker must not be present in more than one group. On average, each qualification group created contains one qualification. Initially, one worker is assigned to each group, all remaining workers are then distributed among the groups randomly.

2) Union Average Crossover (UAX)
This crossover creates offspring that contain all groups from its parents by averaging and rounding up or down the number of workers in each group. Rounding up and down is done in an alternating fashion.

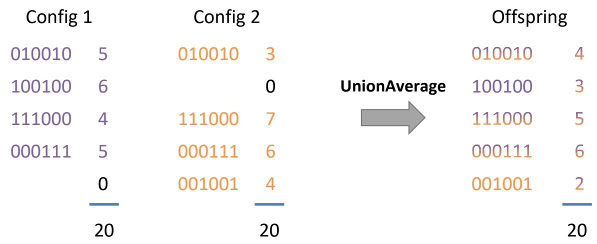

Figure 2: The UAX.

3) Overlap Average Crossover (OAX)
Compared to the UAX, this crossover creates offspring that only contain groups occurring in both parents. For such groups, the number of workers inside these groups is averaged. Workers assigned to groups that are not present in both parents are “lost”, i.e. a repair procedure distributes the missing workers among the groups that are present in the offspring. If no common groups are found, a discrete crossover, explained in the following paragraph, is applied.

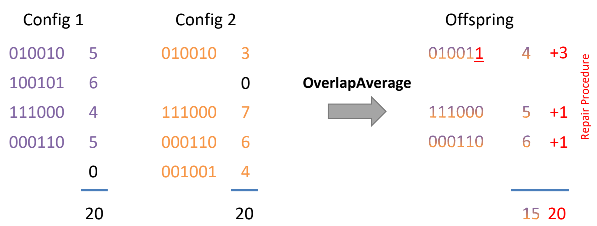

Figure 3: The OAX.

4) Discrete Crossover (DX)
This crossover randomly selects groups from either parent and introduces them in the offspring. A resulting offspring configuration has the same amount of groups as the parent with the least groups. The last group taken from either parent is assigned the number of workers that have not been assigned yet.

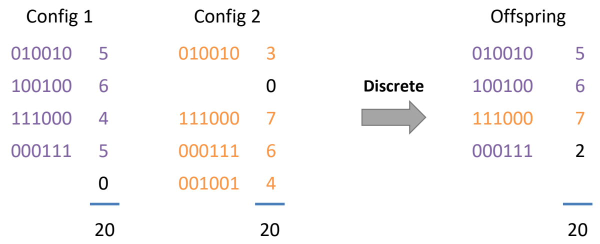

Figure 4: The DX.

5) Set Cover Crossover (SCX)
This crossover aims to find the minimal set of pools present in the parents that covers all qualifications. This so called *Set Cover Problem* is an NP-complete problem itself (Karp 1972). Therefore, a construction heuristic, including a branch & bound algorithm have been implemented to tackle this problem. If the generated offspring is identical to either parent, the DX, as explained before, is applied.

Figure 5: The SCX.

6) Set Pack Crossover (SPX)
The SPX aims to select the greatest number of groups that do not intersect, i.e. that do not have the same qualifications. Finding such sets is equal to the *Set Packing Problem*, which is also NP-complete (Karp 1972). Again, a construction heuristic has been implemented to solve this problem and if the offspring equals either parent, the DX is executed.

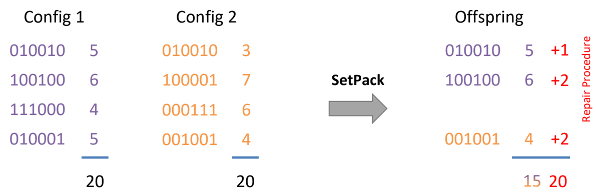

Figure 6: The SPX.

7) Add-Qualification-To-Group Manipulator
This manipulator first selects one group randomly, checks for unset qualifications and aborts if there are none. If unset qualifications are available, one qualification is randomly chosen and set. Finally, the manipulator decides how many workers should be removed from the old group and moved to the new group.

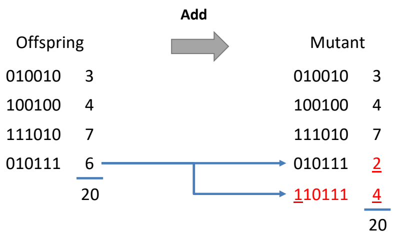

Figure 7: The Add-Qualification-To-Group manipulator.

8) Remove-Qualification-From-Group Manipulator
This manipulator works in principle in the same fashion as the previous one. However, instead of adding a new qualification, it randomly removes one. Again, the number of workers to be transferred from the old to the new group is randomly chosen.

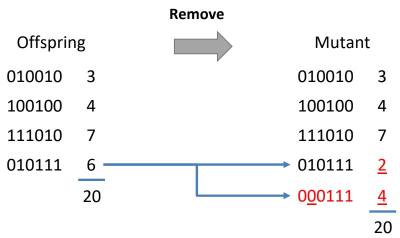

Figure 8: The Remove-Qualification-From-Group manipulator.

9) Swap-Qualification-Within-Group Manipulator
Here, one set and one unset qualification within a randomly chosen group are swapped. The qualifications are chosen randomly and if there are no unset qualifications, the chosen set qualification is removed.

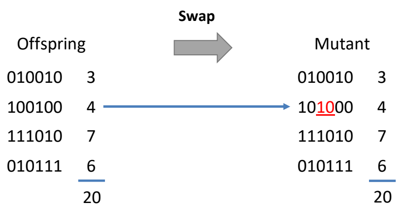

Figure 9: The Swap-Qualification-Within-Group manipulator.

10) Split-Qualification-Group Manipulator
This manipulator splits a randomly chosen qualification group into two disjoint groups. The number of workers are split randomly between the two new groups.

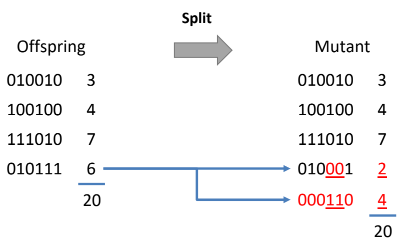

Figure 10: The Split-Qualification-Group manipulator.

11) Merge-Qualification-Group Manipulator
Using this manipulator, qualifications of two randomly chosen groups are merged. All workers from both groups are transferred to the merged group.

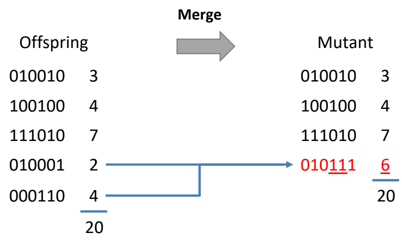

Figure 11: The Merge-Qualification-Group manipulator.

3.1.2. Repair Procedure

The implemented solution encoding also has some constraints that need to be adhered to. First, each qualification must be set in at least one qualification group (see Figure 12).

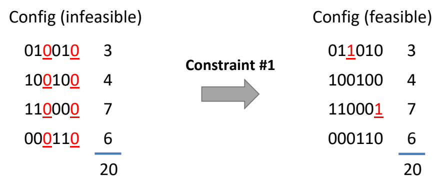

Figure 12: An infeasible configuration, where two qualifications are not present in any qualification group, is repaired.

Second, each worker must have at least one qualification, i.e. each worker must be assigned to exactly one qualification group (see Figure 13).

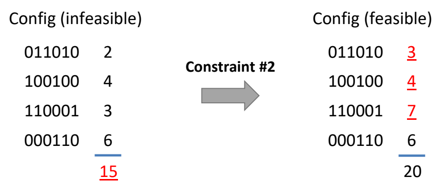

Figure 13: An infeasible configuration, where 5 out of 20 workers are not assigned to any qualification group, is repaired.

Furthermore, a configuration must have unique qualification groups and an empty qualification group (i.e. a group which has either no workers or no qualifications assigned) is not allowed. To ensure these properties, a repair procedure has been implemented and is applied after every solution creation, crossover and mutation operation (except in case of the Merge-Qualification-Group manipulation, which should never yield infeasible configurations).

3.2. Simulated Production System

The simulated production system has been first described by Schober, Altendorfer, Karder, and Beham (2019). We have created an implementation of the described model with the help of the Sim# simulation kernel (see https://github.com/abeham/SimSharp). An overview of this model is depicted in Figure 14.

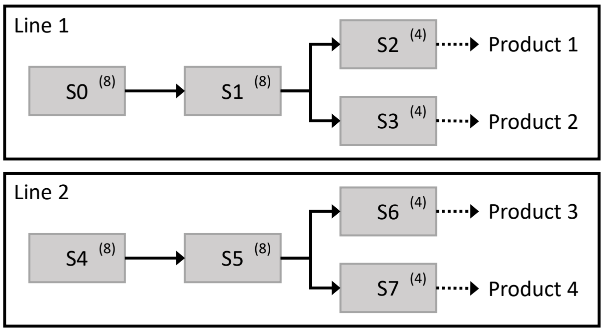

Figure 14: The simulated production system with 2 lines and 4 stations per line, producing 4 different types of products.

Figure 14 shows the production system. All products have to sequentially pass stations from left to right and are split up after the second station between the third and fourth in each line. Each station has its own capacity, i.e. how many workers can process jobs on this particular station at once, depicted in parenthesis. The inter-arrival time of production orders is log-normal distributed and a fixed customer-required lead time is used. The system has been designed for a total of 48 workers. Workers are in a pool, which means that they are idle, and are assigned to stations when required, using a first come first serve (FCFS) dispatching policy. FCFS assigns the first worker that is available and capable of operating the respective machine as determined by the worker's qualifications. Switching between stations costs time. After a machine has been operated by a specific worker, this worker is idle again. For a further detailed examination of the implemented simulation model, the interested reader is referred to the C# source code, which is available on GitHub (see https://github.com/abeham/qualification-model).

4. EXPERIMENTS & RESULTS

This section first discusses the experimental setup in Section 4.1 and then presents and discusses the observed optimization results in Section 4.2.

4.1. Experimental Setup

As already explained, an NSGA-II has been used to optimize the qualification configurations, where the service level is maximized and the total number of required qualifications is minimized. Two experiments (EB1+2) use the binary vector encoding, whereas three other experiments (EQ1–3) use the newly implemented qualification encoding. For statistical significance, all experiments are conducted with 10 repetitions. Table 1 lists the parameters that were used to configure the NSGA-II. Values marked with *EB* are used in all binary vector encoding experiments, *EQ* defines parameter values used in all qualification encoding experiments.

Table 1: The NSGA-II parameters for binary vector and qualification encoding experiments.

Name	Value
PopulationSize	100
Selector	CrowdedTournament
CrossoverProbability	0.5
Crossover	Multi
MutationProbability	0.5
Mutator (Manipulator)	*EB1*: SinglePositionBitflip *EB2*: SomePositionsBitflip (Mut.Prob.: $\frac{1}{6}$) *EQ*: Multi
MaximumGenerations	100
SelectedParents	200

HL supports so called multi-operators, e.g. a multi-crossover or multi-manipulator, which apply 1 of n specified operators randomly. The experiment using the binary vector encoding uses all crossovers available for this encoding, whereas the three experiments that use the qualification encoding utilize different sets of crossover operators:

- EQ1: All proposed crossovers are enabled.
- EQ2: Only the DX is enabled.
- EQ3: Only the DX, UAX and OAX are enabled.

Furthermore, all experiments involving the qualification encoding apply a multi-manipulator, which chooses and executes one of all proposed manipulators randomly every time a mutation operation should be carried out. The binary vector encoding only offers two manipulators, which are evaluated separately (EB1+2). In case of the SomePositionsBitflip manipulator, the operators probability of flipping a bit has been set to $\frac{1}{Q}$, where $Q = 6$, which is the number of qualifications. This means that on average, every 6^{th} bit should be flipped, which corresponds to one qualification per worker.
Each qualification configuration is simulated 20 times. Table 2 shows the used simulation parameters. In the tested scenario, only 46 workers are available, although the system is designed for a total of 48 workers. This makes it harder to find high quality solutions, more specifically, to find solutions that have high service levels. Furthermore, switching stations between lanes costs twice as much as switching stations within a lane.

Table 2: The parameters of the simulation model.

Name	Value
Change Time Ratio	10 %
Cost FGI Inventory	1.0
Cost Tardiness	19.0
Cost WIP Inventory	0.5
Dispatch Strategy	FirstComeFirstServe
Due Date (Fix)	1.0
Due Date (Var)	100.0
Due Date (CV)	0.0
Interarrival Time (CV)	1.0

Line Change Factor	2.0
Observation Time	3600.0
Order Amount Factor	5.0
Personnel Ratio	50 %
Processing Time (CV)	0.25
Qualifications	6
Utilization	95 %
Warmup Time	600.0
Workers	46

A total of 6 qualifications are required to operate all stations of the production system. Stations S0, S1, S2 and S3 are mapped to indices 0, 1 and 2 within a qualification group, S4, S5, S6 andS7 to indices 3, 4 and 5, as shown in Figure 15.

S01 2/3 45 6/7

010010 10

100100 11

110001 12

001000 13

46

Figure 15: A valid qualification configuration.

This solution is interpreted as follows:

- Group 1: 10 workers that can operate S1 and S5.
- Group 2: 11 workers that can operate S0 and S4.
- Group 3: 12 workers that can operate S0, S1 and S6+S7.
- Group 4: 13 workers that can operate S2+S3.

4.2. Optimization Results

Figure 16 shows the achieved qualities of all binary vector experiments (EB) and the experiments involving the specialized encoding (EQ).

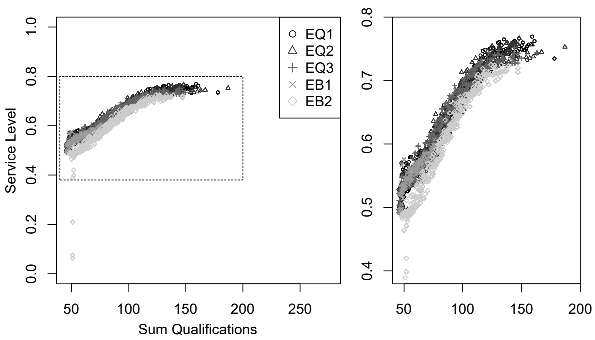

Figure 16: The achieved solution qualities from all conducted experiments.

The sum of qualifications can range from 46 (i.e. one qualification per worker) to 276 (every worker is qualified for every station), the service level ranges from 0.0 to 1.0 (100 %). The dashed box marks the zoomed-in area which is depicted again on the right side of the figure. A visual inspection of this result suggests that that the experiments that use the qualification encoding (EQ1–3) yield better results, compared to the binary vector encoding experiments (EB1+2). When looking at the solutions with the highest service level that where found by EB, one can observe that EQ found solutions with approximately the same service level, but significantly lower sums of qualifications. EB cannot reach the service levels found by EQ. Both sets of experiments found the solution with the minimal number of qualifications, i.e. 46 qualifications, which corresponds to 1 qualification per worker.

The following empirical attainment function plots (López-Ibáñez, Paquete, and Stützle 2010) compare the dominated area of each experiment and thus show how the specialized encoding is able to outperform the binary vector encoding. Figure 17 indicates that there is a significant difference between EB1 and EB2. EB1 finds more solutions with qualities that reside in the lower left corner of the objective space, the upper right corner is dominated by EB2.

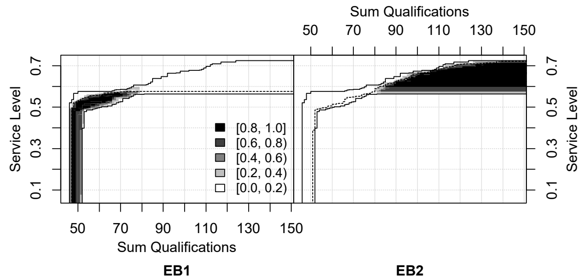

Figure 17: EB1 vs. EB2.

When comparing EB1 to EQ1–3, it is obvious that EQ is dominant in almost all areas of the objective space (see Figure 18; only EQ1 is shown here, comparisons with EQ2+3 look alike).

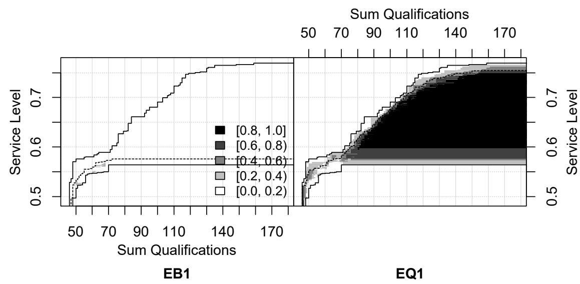

Figure 18: EB1 vs. EQ1.

Even though EB2 reaches higher quality levels than EB1, it is still dominated by EQ in all cases (see Figure 19; again, only EQ1 is shown here, comparisons with EQ2+3 look alike). The highest service levels that are achieved by EB2 are also achieved by EQ, but with significantly less qualifications.

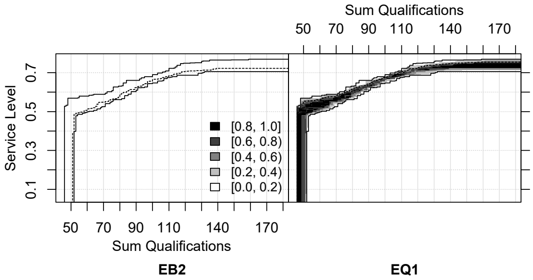

Figure 19: EB2 vs. EQ1.

Finally, there are no significant differences between all EQ experiments, but EQ1 and EQ2 are slightly dominating EQ3 in the upper right area of the objective space (see Figures Figure 20, Figure 21 and Figure 22).

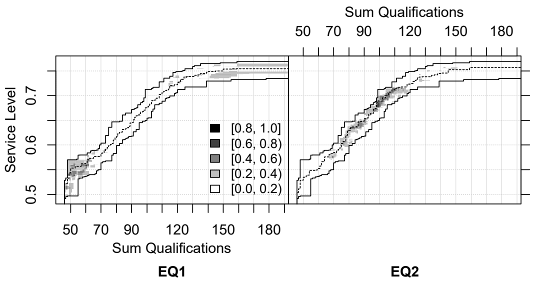

Figure 20: EQ1 vs. EQ2.

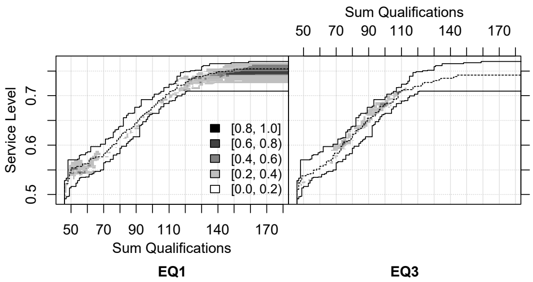

Figure 21: EQ1 vs. EQ3.

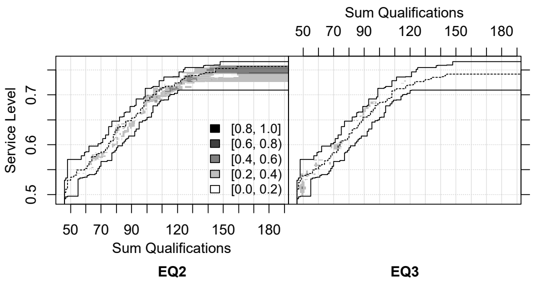

Figure 22: EQ2 vs. EQ3.

For EQ1–3, the chosen crossover and mutation operators have also been analysed with respect to their achieved success ratios. The success ratio $\Psi(c)$ of crossover c in one generation is defined as

$$\Psi(c) = \frac{x_c}{y}$$

, where x_c is the number of offspring that was created by crossover c and y is the overall number of offspring that was created by all crossovers in this generation. The same success ratio can also be calculated for mutation operators. For EQ1, the UAX yielded the most offspring, followed by OAX and DX operators, as can be seen in Figure 23. When inspecting the success ratios of the mutation operators, all success ratios are smaller compared to crossover success ratios and the most successful operator seems to be the Remove-Qualification-From-Group manipulator, as shown in Figure 24 for EQ1.

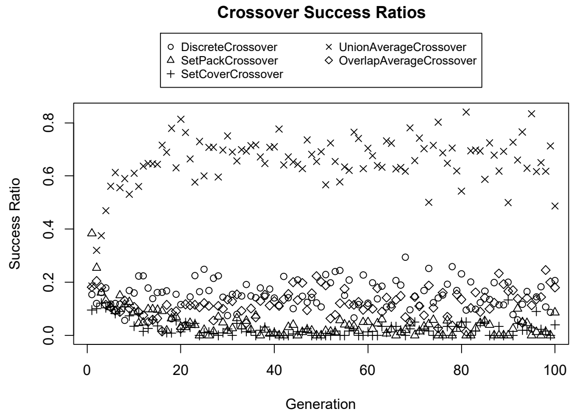

Figure 23: The success ratios of all crossovers used in EQ1 throughout all generations.

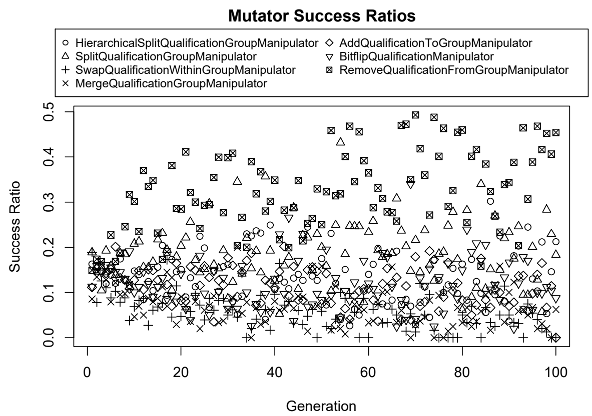

Figure 24: The success ratios of all manipulators used in EQ1 throughout all generations.

5. CONCLUSION & OUTLOOK

First tests with the new encoding show promising results. We conducted multiple experiments with NSGA-II using our new solution encoding and a simpler binary vector encoding. The obtained results show that using the new encoding, solutions with the same amount of qualifications, but higher service levels can be found. Furthermore, the algorithms are able to achieve higher service levels in general. Three different sets of crossovers have been used for testing the new solution encoding. EQ1–3 do not differ much in achieved solution qualities, which indicates that the respective crossover sets are all able to transfer the necessary building blocks to achieve high quality solutions. However, when analyzing crossover success ratios of EQ1, one can observe that the UAX was the most successful crossover in this set.

The proposed encoding can be extended in various ways. An idea is to introduce more solution creators which follow other strategies for constructing solutions. Specialized solution creators could for example use construction heuristics or introduce qualification groups according to predefined patterns, where e.g. a group is qualified for all stations within a line. Such predefined patterns have already been simulated in the aforementioned paper by Schober, Altendorfer, Karder, and Beham (2019), and some manually crafted configurations were even better than solutions optimized by NSGA-II. Another way to extend the proposed encoding is by adding more crossover or manipulation operators.

Finally, the objectives that are optimized can be extended. So far, the only objectives that have been considered were service level and number of qualifications. In the future, we will also take the number of qualification groups into account in order to find good configurations with as few groups as possible.

ACKNOWLEDGMENTS

The work described in this paper was done within the project *Digitale Methoden für verbesserte Personal-qualifizierungsstrategien* (OPTIMAL WORKFORCE, #862008), funded by the Austrian Research Promotion Agency (FFG) and the Government of Upper Austria.

REFERENCES

Affenzeller, M., Beham, A., Vonolfen, S., Pitzer, E., Winkler, S.M., Hutterer, S., Kommenda, M., Kofler, M., Kronberger, G., Wagner, S., 2015. Simulation-Based Optimization with HeuristicLab: Practical Guidelines and Real-World Applications. In: Mujica Mota, M., De La Mota, I.F., Guimarans Serrano, D., eds. Applied Simulation and Optimization: In Logistics, Industrial and Aeronautical Practice. Cham Springer International Publishing, pp.3–38.

Boland, N., Charkhgard, H., Savelsbergh, M., 2015. A criterion space search algorithm for biobjective integer programming: The balanced box method. INFORMS Journal on Computing, 27(4), pp.735–754.

De Bruecker, P., Van den Bergh, J., Beliën, J., Demeulemeester, E., 2015. Workforce planning incorporating skills: State of the art. European Journal of Operational Research, 243(1), pp.1–16.

Deb, K., Pratap, A., Agarwal, S., Meyarivan, T.A.M.T., 2002. A fast and elitist multiobjective genetic algorithm: NSGA-II. IEEE transactions on evolutionary computation, 6(2), pp.182–197.

EUROCHAMBRES, 2019. EUROCHAMBRES Economic Survey 2019. Available from: https://issuu.com/eurochambres/docs/ees_2019_report_3.0 [Accessed May 2019].

Gosavi, A., 2015. Simulation-based optimization. Berlin: Springer.

Haimes, Y.V., 1971. On a bicriterion formulation of the problems of integrated system identification and system optimization. IEEE transactions on systems, man, and cybernetics, 1(3), pp.296–297.

Hu, Y., Bie, Z., Ding, T., Lin, Y., 2016. An NSGA-II based multi-objective optimization for combined gas and electricity network expansion planning. Applied energy, 167, pp.280–293.

Karp, R.M., 1972. Reducibility Among Combinatorial Problems. In: Miller, R.E., Thatcher, J.W., Bohlinger, J.D., eds. Complexity of Computer Computations. New York Plenum, pp.85–103.

Kück, M., Broda, E., Freitag, M., Hildebrandt, T., Frazzon, E.M., 2017, December. Towards adaptive simulation-based optimization to select individual dispatching rules for production control. In 2017 Winter Simulation Conference (WSC) (pp. 3852–3863). IEEE.

Lin, J.T., Chiu, C.C., Chang, Y.H., 2019. Simulation-based optimization approach for simultaneous scheduling of vehicles and machines with processing time uncertainty in FMS. Flexible Services and Manufacturing Journal, 31(1), pp.104–141.

López-Ibáñez, M., Paquete, L., Stützle, T., 2010. Exploratory Analysis of Stochastic Local Search Algorithms in Biobjective Optimization. In: Bartz-Beielstein, T., Chiarandini, M., Paquete, L., Preuss, M., eds. Experimental Methods for the Analysis of Optimization Algorithms, Berlin Springer, pp.209–222.

OECD, 2018. Skills for jobs. Organisation for Economic Co-operation and Development. Available from: https://www.oecdskillsforjobsdatabase.org/data/Skills%20SfJ_PDF%20for%20WEBSITE%20final.pdf [Accessed March 2019].

Schober, A., Altendorfer, K., Karder, J., Beham, A., 2019. Influence of Workforce Qualification on Service Level in a Flow Shop with two Lines. 9th IFAC Conference on Manufacturing Modelling, Management and Control. Berlin, Germany [accepted].

Wang, H., Fu, Y., Huang, M., Huang, G.Q., Wang, J., 2017. A NSGA-II based memetic algorithm for multiobjective parallel flowshop scheduling problem. Computers & Industrial Engineering, 113, pp.185–194.

A SIMULATION MODEL FOR ESTIMATING HUMAN ERROR PROBABILITY

Anastasia Angelopoulou [(a)], Konstantinos Mykoniatis [(b)], Nithisha Reddy Boyapati [(c)]

[(a),(c)] Columbus State University
[(b)]Auburn University

[(a)] angelopoulou_anastasia@columbusstate.edu, [(b)] kmykoniatis@gmail.com,
[(c)] boyapati_nithishareddy@columbusstate.edu

ABSTRACT

This paper describes the system dynamics architecture of a simulation model which estimates human error probability for humans performing certain tasks in a given scenario. Human error probability is estimated as a function of the type of tasks performed and the number of performance shaping factors. In this work, the Standardized Plant Analysis Risk-Human (SPAR-H) reliability analysis method is utilized for estimating the probability of human error. The system dynamics simulation model captures the cause and effect relationships of the SPAR-H defined performance shaping factors that affect human error and uses them to assess the overall human error probability of the system. The present work is a continuation of our previous work on task analysis, workload and human reliability assessment simulation and aims to evaluate the system dynamics simulation as a potential approach to assess human reliability.

Keywords: Simulation; Modeling; System Dynamics; Human Error

1. INTRODUCTION

Human error is one of the main contributing factors in accidents and disasters in various industries and accounts for more than 90% in nuclear industries and 80% in chemical industries (Ramondo et al. 2012). Human error is also one of the primary causes of some of the most shocking industrial accidents that occurred around the world such as the Texaco refinery accident in Wales (1994), the Chernobyl nuclear disaster in Ukraine (1986), the Piper Alpha accident in United Kingdom (1988) and the Bhopal gas disaster in India (1984) (Johnson 1999). Therefore, human error prevention is seen as a major contribution to the safety, maintenance, and reliability of systems.

Modeling and Simulation (M&S) is a tool that can address the dynamic nature and progression of human behavior and provides a way to estimate and/or predict the human error probability (HEP) when humans perform tasks. Estimating or predicting the HEP can help determine policies to be applied in order to avoid errors and/or reduce the likelihood of errors, especially if the tasks are critical. Policies may include but are not limited to adding more operators to perform certain tasks and manage critical constraints; reconfiguring the layout and/or testing alternative working environments; training the operator to improve his/her skills for critical tasks; applying risk-based planning and scheduling (i.e. by changing shifts or taking a break before starting a certain task).

M&S has been used in the past to analyze human behavior in order to assess human reliability. Different models and simulation paradigms have been used for human reliability assessment. More specifically, Discrete Event Simulation (DES) has been utilized to model human behavior and to predict the error probability for given scenarios (Di Pasquale et al. 2015), as well as to improve a production process considering the availability and reliability of machines, operators, and robots as stochastic parameters (Kampa et al. 2017). Agent Based (AB) simulation models have focused on evaluating human performance and behavior (Deadman 1999; Pritchett et al. 2002; Bonabeau 2002). Bayesian Belief Network (Belkacem et al. 2011; Gregoriades 2018) and Petri-nets have also application in safety, reliability, and risk assessments (Kabi and Papadopoulos 2019). Finally, System Dynamics (SD) simulation models have been utilized as a tool to assess human performance and human reliability (Block and Pickl 2014; Angelopoulou 2015; Angelopoulou and Mykoniatis 2017; Gregoriades 2018).

The current paper focuses on the description of the SD module of a "work-in-progress" hybrid simulation model for the estimation of HEP by utilizing the SPAR-H method's Performance Shaping Factors (PSFs). The model is a continuation of our previous work (Angelopoulou 2015; Mykoniatis 2015; Angelopoulou and Mykoniatis 2017; Angelopoulou and Mykoniatis 2018; Mykoniatis and Angelopoulou 2019).

The remainder of the paper is organized as follows: Section 2 provides an overview of the SPAR-H human reliability assessment method and the defined PSFs, while Section 3 describes the SD architecture of our hybrid AB-SD model and the cause and effect relationships of the SD model components. Finally, in Section 4 we discuss conclusions and future work.

2. HUMAN RELIABILITY ASSESSMENT

A hybrid AB-SD simulation model has been developed for estimating the human error probability (HEP). In this work, the SPAR-H method is utilized as a basis to build the SD module of the hybrid model for estimating the HEP of the system. The SPAR-H method (Boring and Blackman 2007; US Nuclear Regulatory Commission 2005) was developed for assessing human error probabilities in the nuclear industry but shows promise for wider application in other domains (Boring and Gertman 2005; Bell and Holroyd 2009). The SPAR-H method utilizes eight PSFs: Available Time, Stress, Complexity, Experience, Procedure, Ergonomics, Fitness for Duty, and Work processes.

Each PSF has different levels and each level is associated with a multiplier that increases or decreases the likelihood of errors. For example, a high multiplier (greater than 1) increases the likelihood of human error and a low multiplier (less than 1) decreases it. The list of the multiplier scale used in the SD model for the HEP estimation is presented in Table 1.

Table 1
PSF Multipliers used in the system dynamics model for the HEP estimation (Boring and Blackman 2007)

PSF	PSF Level	Multiplier
Available Time	Inadequate time	No multiplier
	Barely Adequate time	10
	Nominal Time	1
	Extra Time	0.1
Stress	Extreme	5
	High	2
	Nominal	1
Complexity	High	5
	Moderate	2
	Nominal	1
	Obvious	0.1
Experience	Low	10
	Nominal	1
	High	0.5
Procedures	Not available	50
	Incomplete	20
	Poor	5
	Nominal	1
	Good	0.5
Work process	Poor	2
	Nominal	1
	Good	0.8
Ergonomics	Missing	50
	Poor	10
	Nominal	1
	Good	0.5
Fitness for Duty	Unfit	No multiplier
	Degraded	5
	Nominal	1

If there is no information available in order to provide a judgment for the PSF level, the PSF level is assumed to be nominal (equal to 1). Once the levels of each PSF are assigned, the final HEP is estimated as the product of the PSF multipliers and the base error rate, as in (1).

$$HEP = NHEP \times PSFc \qquad (1)$$
$$PSFc = \pi \; PSFs$$

The base error rate or nominal human error probability (NHEP) is equal to 0.001 for action tasks and 0.01 for diagnosis tasks.

PSFs may increase, decrease or have no effect on human error probability. If three or more PSFs have a negative effect on HEP, a correction process of SPAR-H is applied, as in (2).

$$HEP = \frac{NHEP \times PSFc}{NHEP\,(PSFc - 1) + 1} \qquad (2)$$

This HEP provides a quantitative basis to the system's evaluation. Based on the HEP, each task will be further classified as critical or not in order to aid analysts in determining which areas of the system may need redesign or caution.

3. SYSTEM DYNAMICS SIMULATION MODEL

The hybrid AB-SD model consists of agents that represent the human operators performing a task. A SD model is incorporated within each agent in order to estimate the probability that each individual will make an error while performing a task. The model presented in this paper discusses the SD module of the hybrid simulation model.

The simulation model is developed in Anylogic™ , reads inputs from a database and estimates the probability of the errors to occur based on the type of the task (action vs. diagnosis task) and the performance shaping factors. The SD model is depicted in Figure 1 and the model variables are presented in Table 2. Subsection 3.1 describes the SD model variables in more detail, while subsection 3.2 focuses on the description of the causal loops and the HEP correction process.

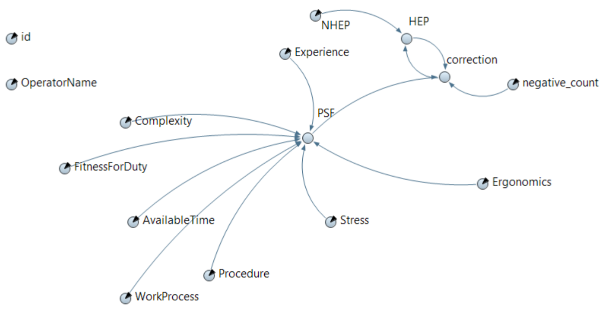

Figure 1: System Dynamics Model

Table 2
Description of System Dynamics Model Variables

Properties	Definition	Model Variable
ID	Unique identifier	id (integer)
Operator Name	The name of the operator performing the task	OperatorName (String)
Available Time	The time for which an operator will be available for performing the task.	AvailableTime (double)
Stress	Stress levels of an operator during the task performance.	Stress (double)
Complexity	States the complexity of a task to be performed.	Complexity (double)
Experience	Experience level of each operator while performing the task.	Experience (double)
Procedure	Describes the knowledge of an operator on a specific task.	Procedure (double)
Ergonomics	States the efficiency of an operator while performing the task.	Ergonomics (double)
Fitness for Duty	Fitness level of an operator during the task performance.	FitnessForDuty (double)
Work processes	States the process of work of an operator	WorkProcesses (double)
NHEP	Nominal Human Error Probability whose values are 0.01 and 0.001	NHEP (double)
HEP	Human Error Probability	HEP (double)
Correction	Applies the HEP correction when there are 3 or more negative PSF factor.	correction (double)
Negative Count	Counts the number of negative factors. It is used to apply the HEP correction.	negative_count (integer)

3.1. System Dynamics Model Variables

A unique identifier (ID) is assigned to each simulated agent upon creation. The model then reads the database inputs and assigns the operator name to each agent, as well as values to each of the PSF factors.

The **available time** is generally referred to as the amount of time that a crew or an operator must act and diagnose upon an abnormal event (Gertman et al. 2005; Boring and Blackman 2007; Blackman, Gertman and Boring 2008; Whaley et al. 2012). In the SD model, the PSF "AvailableTime" denotes the amount of time available for the task relative to the time that is required to complete a task. The HEP and the availability of the worker during the time of performing the tasks are inversely proportional to each other. In other words, if the worker is unavailable to perform an operation, the probability that he/she might commit an error will be high and approximately 1. The HEP will be reduced if the worker is available most of the time to perform the task, even during an emergency.

In the SPAR-H context, **stress** refers to the level of undesirable circumstances and conditions that impede an operator to complete the task (Gertman et al. 2005; Boring and Blackman 2007; Blackman, Gertman and Boring 2008; Whaley et al. 2012). The effect of stress on the performance is curvilinear, which indicates that even small amounts of stress can improve the performance and consider it as nominal, while extreme and high stress levels may affect the human performance in a negative way. The HEP is assumed to be approximately 1 if the worker's stress levels are high before or at the time of performing a task.

The **complexity** refers to the difficulty of the task to be performed in a certain context considering both the environment and the task (Gertman et al. 2005; Boring and Blackman 2007; Blackman, Gertman and Boring 2008; Whaley et al. 2012). As the complexity of the task increases, the probability of human error will also increase since they are directly proportional to each other. At the same time a more ambiguous task may have a higher chance for human error. Boring, Griffith and Joe (2007) defined complexity as indirect as it cannot be directly measured. Due to this reason, the complexity value cannot be directly assigned but it depends on the input factor from various elements such as parallel tasks general complexity, need for mental errors, physical effort needed from the activity type and the level of precision for the activity. These elements will be incorporated in the model in the future.

The **experience** refers to the operator's experience involved in a task (Gertman et al. 2005; Boring and Blackman 2007; Blackman, Gertman and Boring 2008; Whaley et al. 2012). The experience level is defined based on the operator's years of experience, whether the operator has been trained or not on the type of accident, the amount of time spent on the training and its frequency, involvement of system in the scenario and task. The three levels of the "Experience" variable are defined as follows:

- High: Demonstrated master; extensively experienced.
- Nominal: More than 6 months of training or/and experience.
- Low: Less than 6 months of training or/and experience.

More experienced workers present reduced probability to commit an error. If the worker has less or no experience then the probability of the worker to commit an error will be extremely high. As Duffey and Saull (2004) state: "*Human error probability is dynamic and evolves with experience*".

For the tasks under consideration, **procedure** refers to the use and existence of formal operating procedures (Gertman et al. 2005; Boring and Blackman 2007; Blackman, Gertman and Boring 2008; Whaley et al. 2012). Most common problems in event investigations of procedures involve situations where inadequate or wrong data are provided regarding a certain sequence of control. Ambiguity of steps is seen as another common problem. The HEP will be reduced if the worker uses and follows the existence of operating procedures while performing the task. Therefore, the HEP and the procedure to be followed by the worker during the time of performing the tasks are inversely proportional to each other. In other words, if the worker does not follow the procedure during the performance of an operation, the HEP will be high and approximately 1.

Ergonomics refer to the interaction of the operator/crew with the equipment in carrying out the tasks, to the layout, equipment, controls and displays, as well as to the quality and quantity of available information from the instrumentation (Gertman et al. 2005; Boring and Blackman 2007; Blackman, Gertman and Boring 2008; Whaley et al. 2012). Human machine interface aspects as well as inadequacy or adequacy of the computer software are involved in this category. The HEP will be reduced if the operator has prior knowledge on the usage of the tools and equipment before performing the task. Therefore, there is an inversely proportional relationship between HEP and ergonomics. For example, if the operator/crew has no knowledge on the instrumentation information before performing an operation, the probability that he/she might commit a mistake will be extremely high.

Fitness for duty refers to whether the individual/crew is mentally and physically fit to perform the task or not (Gertman et al. 2005; Boring and Blackman 2007; Blackman, Gertman and Boring 2008; Whaley et al. 2012). This includes legal or illegal usage of drugs, distractions, personal problems, sickness, overconfidence, and fatigue, and contains factors that are associated with the individuals, but are not related to experience, training or stress. The levels for the "Fitness for duty" variable are defined as follows:

- Nominal: Individual can perform tasks; It should be used when the judgment is made by the analyst for the PSF and not as a performance driver.
- Degraded fitness: Even though performance is affected negatively, the individual can perform the tasks. For example, if an individual is sick, physical and mental performance will be affected. If individuals are inappropriately overconfident in their abilities to a task, they may exhibit degraded performance.
- Unfit: Individual cannot perform the tasks due to physical or mental incapacitation or other illness.

The HEP and fitness for duty are inversely proportional to each other. For example, if a worker is unfit to perform an operation, the probability that he/she might commit a mistake will be high and approximately 1.

Finally, **work processes** refer to the work aspects such as work planning, safety culture, communication and management support, inter-organizational factors and policies (Gertman et al. 2005; Boring and Blackman 2007; Blackman, Gertman and Boring 2008; Whaley et al. 2012). The individual and crew performance can be affected based on how the work is planned, communicated and executed. If the communication and planning are poor, an individual may not understand the requirement of the work, which will lead to an increase in HEP. The HEP will be high if the operator/crew is not aware of how the work is planned, communicated and executed before performing an operation. This indicates that the HEP and work processes are indirectly proportional to each other. In other words, if an operator has no knowledge on the requirements of the work to be done prior to performing an operation, the probability that the worker might commit a mistake will be very high.

3.2. Causal Loops

The SD model is composed of causal loops that show the interrelations among the parameters/variables and expose feedback loops within the system. Causal loops are developed by correlating pairs of variables where one is dependent and the other independent.

A causal loop diagram is defined as the simple map of interactions along with all its constituent components of a system. The diagram consists of a set of edges and nodes. Edges are the links that define a relation or a connection between two variables, while nodes define the variables. The polarity of the edges or causal links is indicated by "+" for a positive link or "-" for a negative link. A positive link indicates that the two nodes are directly proportional to each other or change in the same direction, i.e. if the link in one node increases, the other node will also increase. A negative link indicates that the two nodes are inversely proportional to each other or change in the opposite direction i.e. if the link in one node increases, the other node will decrease.

A causal loop diagram reveals the system structure by capturing the consequent feedback loops interactions. Causal loops can be categorized as reinforcing or balancing. Reinforcing loops reinforce and influence the same state or action thus resulting in growth or decline. Balancing loops compare the actual state to the goal and then initiate a corrective action in response to the discrepancy between the two. In our model, a balancing loop is present (Figure 2).

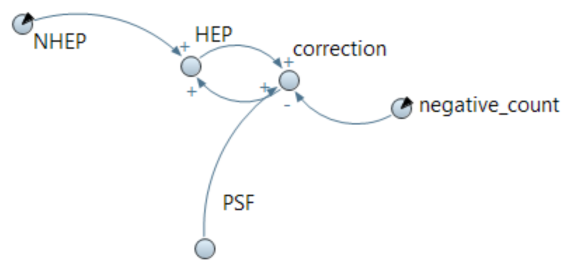

Figure 2. Balancing causal loop for applying the HEP correction. The number of negative links is odd.

The balancing loop affects the human error probability: If the number of negative PSFs increases to three or more (negative_count≥3), a correction is initiated to correct the HEP, if it is not within the appropriate range (0≤HEP≤1). In this paper, the HEP is the product of NHEP and the correction value. If the correction value increases, the value of HEP also increases and vice versa. The correction value is calculated based on the following condition: if three or more PSFs have a negative impact to HEP (negative_count≥3), then the value of PSFs is adjusted according to the correction formula (3). The correction formula ensures that the final individual HEP will not exceed the probability limit of 1.

$$\frac{\mathrm{PSF}}{(\mathrm{PSF}-1)+\frac{1}{\mathrm{NHEP}}} \tag{3}$$

4. DISCUSSION AND FUTURE WORK

This paper presented the components of a SD model for estimating human error probability when performing specific tasks in a given scenario. The simulation model takes as input the eight PSFs and the type of the task (NHEP) and outputs the estimation of the HEP for the total task and the HEP for each subtask. The factors that affect human error (PSFs) as well as the cause-effect relationships and feedback loops were also presented.

Future work will consist of the model validation using real-world case studies and will be compared with other HRA methods for accuracy. The model will be further developed to include more factors that affect human error and to provide suggestions that will decrease the likelihood of errors for the tasks with the higher error probabilities. An interface will also be created to allow the user to experiment with and compare alternative scenarios.

REFERENCES

Angelopoulou A., 2015. A Simulation-Based Task Analysis Using Agent-Based, Discrete Event and System Dynamics Simulation. Ph.D. Dissertation. University of Central Florida, Orlando, FL.

Angelopoulou A. and Mykoniatis K., 2017. The system dynamics architecture of UTASiMo: a simulation-based task analysis tool to predict human error probability. 2017 IEEE conference on cognitive and computational aspects of situation management (CogSIMA). Savannah, GA, USA, 27-31.

Angelopoulou A. and Mykoniatis K., 2018. UTASiMo: a simulation-based tool for task analysis. In: Simulation, 94(1), 43-54.

Belkacem O, Yang Z, Rochdi M, Wang J, 2011. Bayesian modelling for human error probability analysis in CREAM. Proceedings for the international conference on quality, reliability, risk, maintenance, and safety engineering. Xi'an, China. June 17-19.

Bell J. and J. Holroyd, 2009. Review of human reliability assessment methods. Health & Safety Laboratory.

Blackman H. S., Gertman D. I., and Boring R. L., 2008. Human error quantification using performance shaping factors in the SPAR-H method. In: Proceedings of the human factors and ergonomics society annual meeting, 52(21), 1733-1737.

Block J. and Pickl S., 2014. The mystery of job performance: a system dynamics model of human behavior. Proceedings of the 32nd international conference of the System Dynamics Society, Delft, Netherlands, 20-24.

Bonabeau E., 2002. Agent-based modeling: Methods and techniques for simulating human systems. Proceedings of the national academy of sciences, 99 (suppl 3), 7280-7287.

Boring R. L., and Blackman H. S., 2007. The origins of the SPAR-H method's performance shaping factor multipliers. In: 2007 IEEE 8th Human Factors and Power Plants and HPRCT 13th Annual Meeting, 177-184.

Boring R. L. and Gertman D. I., 2005. Advancing Usability Evaluation through Human Reliability Analysis. Proceedings of HCI International.

Boring R. L., Griffith C. D., and Joe J. C., 2007. The measure of human error: Direct and indirect performance shaping factors. In *2007 IEEE 8th Human Factors and Power Plants and HPRCT 13th Annual Meeting*, 170-176.

Deadman, P. J., 1999. Modelling individual behaviour and group performance in an intelligent agent-based simulation of the tragedy of the commons. Journal of Environmental Management, 56(3), 159-172.

Di Pasquale V., Miranda S., Iannone R., and Riemma S., 2015. A simulator for human error probability analysis (SHERPA). Reliability Engineering & System Safety, 139, 17-32.

Duffey R. B. and Saull J. W., 2004. The probability and management of human error. In Proc. 12th Int. Conf. Nucl. Engineering (ICONE12), 3, 133-137.

Gertman D., Blackman H., Marble J., Byers J., and Smith C., 2005. The SPAR-H human reliability analysis method. US Nuclear Regulatory Commission, 230.

Gregoriades A., 2008. Human error assessment in complex socio-technical systems-system dynamic versus Bayesian belief network. In System Dynamics Conference, Manchester.

Johnson C, 1999. Why human error modeling has failed to help systems development. Interact Comput.

Kabir S., and Papadopoulos Y., 2019. Applications of Bayesian networks and Petri nets in safety, reliability, and risk assessments: A review. Safety science, 115, 154-175.

Kampa A., Gołda G., Paprocka I., 2017. Discrete event simulation method as a tool for improvement of manufacturing systems. Computers, 6(1), 10.

Mykoniatis K., 2015. A Generic Framework For Multi-Method Modeling and Simulation of Complex Systems Using Discrete Event, System Dynamics and Agent Based Approaches. Ph.D. Dissertation. University of Central Florida, Orlando, FL.

Mykoniatis K., and Angelopoulou A., 2019. A modeling framework for the application of multi-paradigm simulation methods. *SIMULATION*, in press.

Ramondo A, De Felice F, Carlomusto A, Petrillo A., 2012. Human reliability analysis: a review of the state of the art. IRACST – Int J Res Manage Technol (IJRMT) 2, 35-41.

Pritchett A. R., Lee S., Abkin M., Gilgur A. Z., Bea R. C., Corker K. M., ... and Jadhav, A., 2002. Examining air transportation safety issues through agent-based simulation incorporating human performance models. In: The 21st Digital Avionics Systems Conference, 2, 7A5-7A5.

US Nuclear Regulatory Commission, 2005. The SPAR-H human reliability analysis method.

Whaley A. M., Kelly D. L., Boring R. L., and Galyean W. J., 2012. SPAR-H step-by-step guidance (No. INL/CON-12-24693). Idaho National Laboratory (INL).

SIMULATION OF BAGGAGE DELIVERY MANAGEMENT FOR AN INCREASE IN DEMAND IN A MEXICAN AIRPORT

Karla Elizabeth Brambila Loza[a], Ann Godelieve Wellens[b], Sonia Karina Pérez Juárez[c]
Universidad Nacional Autónoma de México, Posgrado de Ingeniería

[a]karla.brambila.0399@gmail.com, [b]wann@unam.mx, [c]ing.karinaperezj@gmail.com

ABSTRACT

One of the airport operations that define customer satisfaction is baggage handling. This document analyzes baggage logistics once the plane lands. We used SIMIO® to construct a simulation model for the baggage delivery process in a Mexican airport, used to assess the associated degree of comfort and processing time.

In this preliminary study, IATA performance indicators were used to determine the service classification for the baggage claim unit and the overall baggage processing time for two scenarios. The first one considers the arrival of two A320 arriving a few minutes apart; the second one considers two A321 aircraft in the same conditions. Simulation results confirm that PBC's current operating conditions, aircraft types and flight frequencies allow the airport to have an acceptable service and comfort level in the baggage claim area. However, an increase in passenger demand can lower passenger comfort significantly, as the current baggage claim band violates IATA standards and is under-dimensioned.

Keywords: simulation model, baggage management, occupation level, IATA

1. INTRODUCTION

The saturation of Mexico City airport and its impossibility of growth have been identified since the 1990s. For over 15 years, the airport authorities and federal government have been proposing alternatives for the development of a new airport or the implementation of a Metropolitan Airports System (SMA: Sistema Metropolitano de Aeropuertos) to cover the current demand (ASA, 2006). The government of President Peña Nieto (2012-2018) agreed in 2014 on the construction of a new airport in Texcoco. However, at the start of the new federal government (2018-2024), this initiative was suspended in favor of the expansion of the military airport in Santa Lucía, which has required substantial changes in the original expansion proposals (La Jornada, 2019). A renewed interest arose in one of the earlier proposals to cover the demand with a network of metropolitan airports (Excelsior, 2016; Milenio, 2016; A21MX, 2019; América vuela, 2018), including those of Puebla, Querétaro, Toluca and Cuernavaca, which are close to Mexico City and already have the necessary infrastructure (Galindo López and Nava Figueroa, 2011; ASA, 2006). It should be mentioned that some of the secondary or regional airports could generate losses instead of being profitable (Doganis, 1995). In the case of the Metropolitan Airports System, only the Cuernavaca airport generates losses.

This type of airport system has been used in several big cities where the main airport has a very high occupation, however, operates efficiently supported by secondary airports. This is the case of for example London, where a set of six airports meet the demand of the entire city (Cantera, 2018), Paris, where four airports are used or New York that is integrated with three nearby airports (Neufville, 2013).

The Metropolitan Airports System includes Mexico City Airport, as well as the airports described in table 1. All four secondary airports are owned partially by the federal government, represented by ASA (Aeropuertos y Servicios Auxiliares), and the local government (Aeropuertos de México, 2013); in the case of TLC airport, also private participation exists. Figure 1 shows the Metropolitan Airports System.

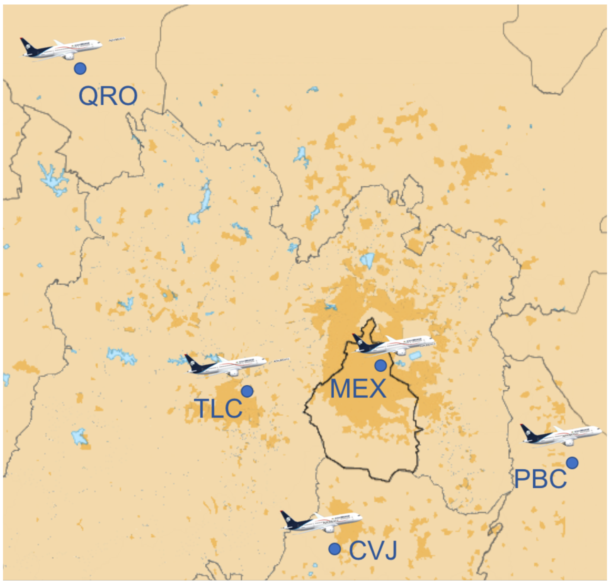

Figure 1. Central Mexico network of metropolitan airports

Not all airports in the Metropolitan Airports System have the right infrastructure for viable growth. CVJ started operations in 1988 and can handle an hourly rate of 1000 passenger; however, it currently does not handle commercial flights and no operator offers line services to this airport (low-cost carrier Volaris ceased operations in CVJ in 2017).

Table 1. Characteristics of metropolitan airports (Galindo López and Nava Figueroa, 2011; Excelsior, 2016).

	Cuernavaca	Toluca	Puebla	Querétaro
IATA	CVJ	TLC	PBC	QRO
Distance to MEX (km)	110	68	103	213
Main use	General services	Commercial	Commercial, industry and special services	Commercial and industry
Terminal building area (m^2)	1,200	28,300	6,800	5,241
Passengers in 2018	7,735	691,712	685,583	1,024,023
Capacity (pax/h)	240	1,850	450	400
Roadway capacity (ops/h)	14	36	20	45
Nr of operating airlines	-	2	6	8

The main competitive disadvantage of TLC is its altitude and meteorological conditions, which do not allow large passenger planes to leave with a full fuel tank (Expansión 2016; Alfadiario, 2019). For long journeys, this implies a departure with restricted weight and needing at least one stopover in the Caribbean, which considerably increases costs and makes the route less competitive. Although TLC has the capacity to serve eight million passengers a year, demand decreased from 4.3 million travelers in 2008 to less than 700,000 in 2018 (Milenio, 2016).

For both PBC and QRO, approximately half of the flights correspond to cargo and business flights. The large proportion of cargo flights are due to the presence of important industrial parks, including aeronautical and automotive industry in QRO and automotive industry in PBC. Despite its proximity to the Popocatepetl volcano, PBC has grown in recent years.

The increase in the occupation of secondary airports that were not originally designed to serve a high flow of passengers brings challenges in terms of service logistics to maintain the level of customer satisfaction, including baggage and its handling, very valuable for the passenger.

This article describes the evaluation, for PBC airport, of the degree to which the currently installed baggage reception capacity is sufficient to cover possible future increases in demand, if the airport absorbs part of the demand from Mexico City.

1.1. PBC Airport

The Puebla International Airport (IATA Code: PBC, ICAO code: MMPB) or Huejotzingo Airport, officially named Hermanos Serdán International Airport, is located in the municipality of Huejotzingo, 25 km from downtown Puebla; operated by ASA, it serves flights from Puebla to major cities in Mexico and abroad (figure 2).

PBC airport has a 16,400 m^2 platform with 6 loading positions and a terminal building with capacity for approximately 450 passengers per hour (Red ASA, 2019). PBC's platform is classified to be 4D according to the ICAO Aerodrome Reference Code (wingspans between 36 and 52 m and outer main gear wheel span between 9 and 14 m). However, the characteristics of the airport runway support the arrival of B747 (up to 412 passengers), A380 (up to 550 passengers) or AN124 (up to 150 tons of cargo) aircraft; the latter has been used for cargo transport in PBC.

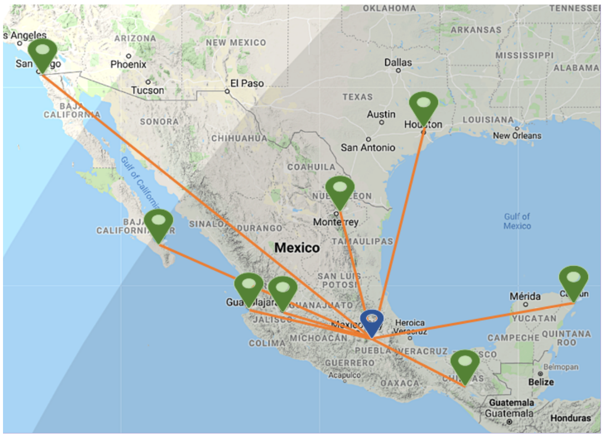

Figure 2. Commercial flights from PBC airport

The majority of commercial flights arriving at PBC are operated by low-cost carriers (Volaris 32%, VivaAerobus 15%, Aeromar 15%). Aeromexico, the only Mexican full-service carrier, is responsible for another 15% of the PBC demand. The remaining 23% is divided into four other low-cost airlines, of which two are from the USA.

Average annual growth has been approximately 10% since 2014, due to an increased airline participation and renewed terminal infrastructure. Puebla has become a reference airport and the presence of automotive assembly plants in the surroundings still offers opportunities for growth. Passenger demand is presented in figure 3.

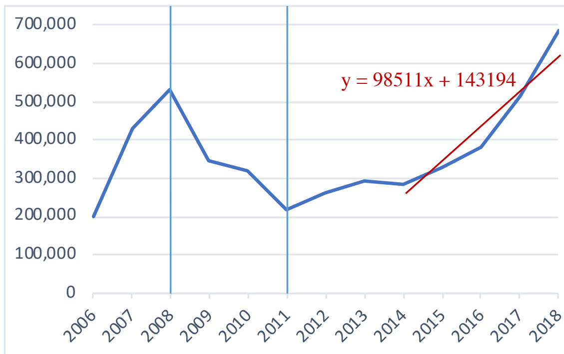

Figure 3. Yearly number of passengers served in PBC

Before 2008, PBC showed significant growth, mainly due to demand from the automotive sector. However, due to the poor physical conditions of the runway, some airlines withdrew their flights and demand dropped significantly. After a change of administration and a major remodeling of the facilities in 2011, demand started to grow again. As of 2014, the growth rate becomes very similar to that between 2006 and 2008; that rate was used to estimate future demand by linear regression, as shown in Table 2.

Table 2. Passenger number forecasts for PBC

Year	Future periods (x)	Forecast (y)	Growth (%)
2019	7	832,771	
2020	8	931,282	11.83
2021	9	1,029,793	10.58
2022	10	1,128,304	9.57
		Average	10.18

Demand is expected to stabilize in a few years. In case of using BPC as a secondary airport to MEX within the Metropolitan Airports System, the forecast might need to be adjusted. At the moment, mainly small aircraft (A319 and A320) arrive to PBC, although the runway also supports B757 and B767 aircraft.

Although the airline is the responsible entity, the baggage handling of the PBC airport is outsourced to an independent company, while the physical facilities are owned by the airport. Baggage handling international regulations consider that it should be done exclusively by trained and supervised personnel, and that the delivery of the baggage to the passenger must occur in maximum 30 minutes.

2. LITERATURE REVIEW

Passenger baggage travels along a logistic path at the airport until it is loaded on or removed from the airplane. Baggage problems constitute one of the main causes of passenger's complaints and baggage handling is an important indicator of customer satisfaction (Frey, 2014; Cavada et al., 2017). Due to the increase in congestion, baggage handling is becoming increasingly complex at international airports and one of the biggest management problems of airports worldwide (ABC viajar, 2015), ranging from late delivery to loss and damage to suitcases.

The concept of "service level" was introduced by the US Highway Capacity Manual in 1965. Given a certain demand and maximum process capacity, the service level of an infrastructure can be determined, indicating some degree of user satisfaction. Lemer (1992) mentions different performance factors for passenger satisfaction in airport terminals, emphasizing, however, the overall performance. Based on Lemer's formulation, Correira and Wirashinge (2010) propose operational indicators that should be considered when measuring the level of passenger satisfaction regarding the airport baggage claim service (see table 3). Ronzani and Correia (2015) use an index of service based on the IATA performance indicators used in this paper, specifically for the baggage claim unit.

As baggage handling performance depends on the volume and flow rate of baggage from incoming and departing flights, busy flight schedules can overload the system, extending bag in-system time (Le et al., 2012).

Table 3. Airport baggage claim operational indicators (from Correira and Wirashinge, 2010)

Factor	Description
Equipment configuration and claim area	Type, layout, feed mechanism, and rate of baggage display: space available for waiting passenger; relation of wait area to display frontage; access to and amount of feed belt available
Staffing practices	Availability of porters (sometimes called "sky caps") and inspection of baggage at exit; rate of baggage loading/unloading from cart to feed belt
Baggage load	Number of bags per passengers, fraction of passengers with baggage, time of baggage arrival from aircraft
Passenger characteristics	Rate of arrival from gate, ability to handle luggage, use of carts, number of visitors

As baggage handling performance depends on the volume and flow rate of baggage from incoming and departing flights, busy flight schedules can overload the system, extending bag in-system time (Le et al., 2012).

Several tools can be used for airport analysis, depending on the required level of detail and observed process complexity. For example, Ghobrial (1982) presents an interesting paper describing an empirical model that, for different demand and device conditions, can predict the performance of a claim device. However, when stochasticity plays an important role, mathematical models may not be applicable and simulation tools can help to identify the critical points of the system and the viability of the improvement proposals.

Different authors have applied simulation tools to analyze the baggage handling process. One of the first authors to simulate baggage handling systems was Robinson (1969). He focused on delays suffered by passengers and assessed the problem with a computer code written in GPSS III. More recently, modeling systems such as ARENA have been used to analyze the need for a baggage carousel to serve demand created by a large aircraft (Eller et al., 2002) or to predict human behavior and its influence on the check-in system (Appelt et al., 2007). Automated baggage handling systems have been simulated in ExtendSim for Riga airport (Savrasovs et al., 2009), adapting the traffic software package Quadstone Paramics to simulate the baggage handling system of Santiago de Chile airport (Cavada et al. 2017), using Delmia Quest to analyze two merging conveyor lines in a conveyer-based baggage handling system (Johnstone et al., 2015) or using ProModel to assess passenger congestion in an Indonesian airport (Novrisal et al., 2013).

SIMIO® is a discrete event modelling system that has supported several airport-related investigations, such as the simulation of Mexico City airport's air traffic and the associated congestion problems (Mendoza et al., 2015), or the development of a model to increase the productivity of Amsterdam airport (Mota et al., 2017).

This document analyzes baggage logistics once the plane lands. We used SIMIO® to construct a simulation model for the baggage delivery process in a Mexican airport, used to assess the associated degree of comfort and processing time by means of different simulation scenarios.

3. METHODOLOGICAL APPROACH

In this section, we describe the methodology of this paper, including the simulation approach and corresponding determination of input data.

The simulation was carried out using Discrete Event Systems (DES), which is a modelling approach where the state of the system variables changes only at discrete instants of time; the term "event" is used to represent the occurrence of discontinuous changes at possibly unknown intervals (Flores de la Mota et al. 2017). Figure 4 describes the methodology that was used.

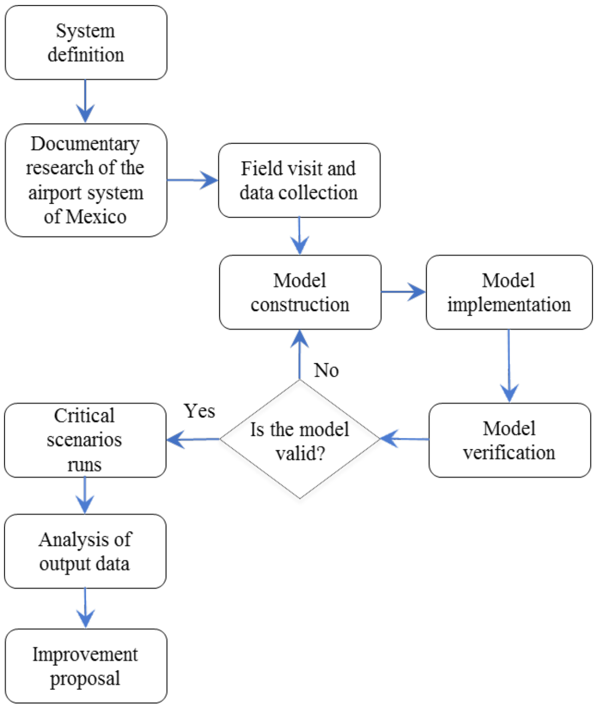

Figure 4. Methodology

Simulation requires modeling, model validation, selection of probability distributions, design and analysis of simulation experiments, as well as the analysis and discussion of results. The simulation consists of the different runs or replicas of the system to analyze different scenarios (Flores de la Mota et al. 2017), considering uncertainty in several model variables. In our case, uncertainty mainly affects the number of passengers and documented bags, as well as the bag processing time and time when passengers arrive to the baggage claim area; however, the structure of operations is fixed. SIMIO® was used, which is a flexible software that uses intelligent objects and requires little or no programming (Simio LLC, 2019). It has an attractive graphic environment and good computation times, making it efficient for simulating different industrial environments (Mujica, 2013).

PBC airport's baggage delivery service is analyzed to identify the characteristics of its operation and the processes that involve customer satisfaction in baggage management. A field visit was made to the PBC airport, where information was obtained on the baggage delivery process, including the unloading of the baggage from the plane, the transfer by cart to the delivery band and a timely collection of the baggage by the passenger. The data taken was analyzed to characterize the required probability distributions and average process times. In addition, the current conditions of the baggage claim room were evaluated, in accordance with the international IATA regulations.

The starting time of the corresponding simulation process depends on the arrival time of the flight (Frey, 2014). The arrival data to PBC was obtained from the *flightradar24.com* platform; the resulting database was cleaned and analyzed with the R software.

The evaluation of the results of two scenarios allowed us to analyze whether the configuration of the band supports an increase in the flight frequency, the arrival of larger aircraft and the decrease in arrival interval time. Possible problems of delayed baggage delivery, bottlenecks and system response to changes in flight frequency were observed.

Based on the simulation results, required changes in the baggage claim area configuration are proposed to improve the delivery process.

3.1. Comfort standards

The International Air Transport Association (IATA, 1995) uses the following international comfort indicators:

1. *Required baggage claim area*

$$A\,[\mathrm{m}^2] = 0.9\,\boldsymbol{e}\ (+10\%) \quad (1)$$

where $\boldsymbol{e}$ is the maximum hourly number of passengers in the terminal

2. *Number of baggage claim devices for narrow-body aircraft*

$$n = \frac{er}{300} \quad (2)$$

where $\boldsymbol{e}$ is the maximum hourly number of passengers in the terminal (m^2) and $\boldsymbol{r}$ is the proportion of passengers arriving by narrow-body aircraft (0.2; IATA, 1995).

3. *Length of the claim band*
For narrow-body aircraft: 30 – 40 m
For wide-body aircraft: 60 – 70 m

To collect the baggage around the baggage claim band, each individual is considered to need a space of approximately 50 cm, which is slightly larger than the standard width between the shoulders of men, aged 18 to 65 (41.43 cm; Ávila et al., 2007). Considering the effective perimeter in the current T-configuration of the baggage claim band (it has a 20 m length, which is below the recommended value), 32 passengers can be at the same time waiting for their baggage on the perimeter of the band.

Table 4 compares the information of the claim area determined for PBC airport from the above-mentioned comfort indicators, as compared to the observed situation.

Table 4. Information on PBC's baggage delivery service (Consultation year 2018)

Variable	Determined/observed value
Declared capacity (pax/h)	450
Required number of baggage claim devices	1 (30 m minimum – equation 2)
Installed number of baggage claim devices	2 (1 inactive)
Length of the claim band	Device 1: 20 m Device 2: 8 m
Number of passengers waiting simultaneously	Device 1: 32 passengers Device 2: Inactive
Required baggage claim area	405 m² – equation 1
Installed baggage claim area	374 m² – visual inspection

Considering that PBC airport receives mostly A320 aircraft, that baggage delivery takes on average 30 min and that, at present, the baggage of aircraft is served sequentially, a maximum of 180 simultaneous passengers is expected in the baggage claim room. It's size of 374 m^2 indicates that the present service level in the baggage claiming area corresponds to 2 m^2 per passenger (an A-classification; IATA, 1995). IATA considers this an excellent level of comfort or conditions of free flow. As only one claiming device is used at the moment, an increase in flight frequency might lower this classification considerably.

3.2. Baggage claim system

PBC airport has a semi-automatic system for unloading baggage for A320 aircraft, but for smaller planes unloading is done manually; that is, the use of the auxiliary belt to lower the baggage to the transport cart is omitted. Figure 5 shows the manual unloading procedure.

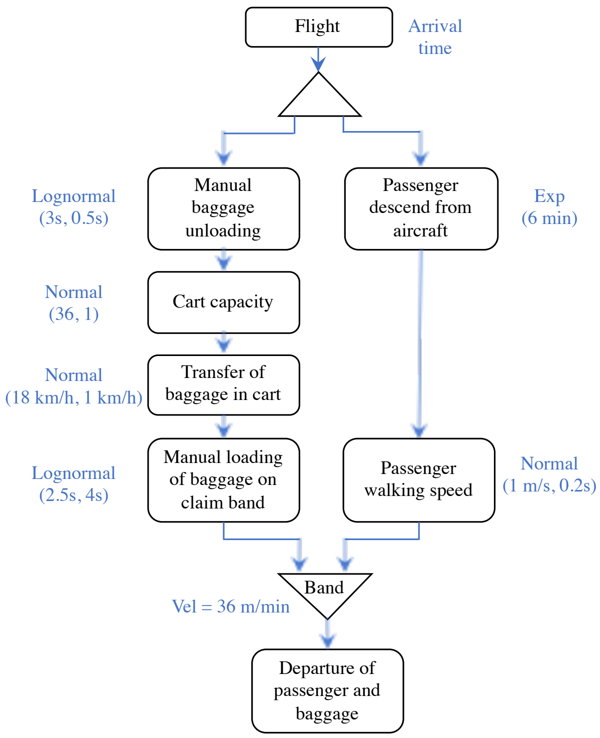

Figure 5. Manual baggage unloading at PBC airport

The human factor is an essential part of the baggage delivery process, since 90% of the operations are carried out by individuals. PBC has a current baggage claim area of 374 m^2, a 20-meter main baggage band and an 8-meter auxiliary band, with a configuration like the one shown in Figure 6.

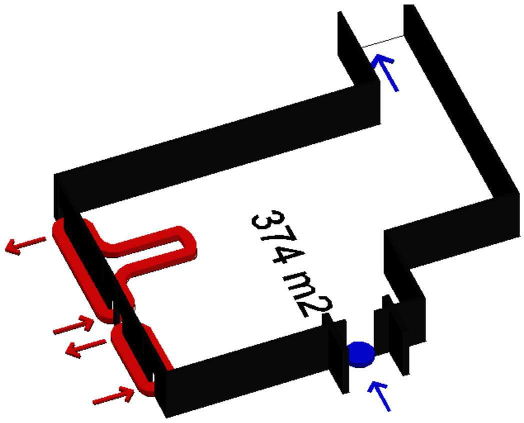

Figure 6. Configuration of the claim band and waiting room

3.3. Check-in system

In an interview, boot personnel of Volaris and Calafia Airlines informed us that approximately 80% of passengers document baggage and, most commonly, only one suitcase. Based on the above, the simulation model considers that, for passengers on an A320 aircraft, on average 144 of the 180 passengers document their baggage. The corresponding standard deviation was fixed at 8 (+/- 5%). Other assumptions are that only one suitcase per person is considered and that oversized bags are unlikely to be transported to PBC.

3.4. Input variables and probability distributions

Table 5 shows the probability distributions used for different model variables.

Different considerations were made: a passenger was assumed to be waiting on average 6 minutes before being able to descend from the plane, for both A320 and A321 aircraft. An exponential distribution was used, expressing passenger descent as an interarrival time. Walking and driving speeds were considered to follow a normal distribution. For walking speed, a speed slightly slower than the standard speed of approximately 90 m/minute (Causa directa, 2013) was considered. For the cart moving speed, we considered that, in general, the carts are driven at speeds very close to the speed allowed in the airside part of the terminal (20 km/h).

The lognormal distribution is used to model a multiplicative sequence of operations that presents variations in time with respect to the average; in our simulation it is used to model the time required for the bag unloading and loading processes. The used baggage carts have a maximum capacity of 900 kg, or, on average, 36 bags of 25 kg each. Finally, the baggage claim velocity is fixed by normativity at 36 m/min.

Table 5. Distribuciones por módulo de simulación

Model variable	Distribution	Parameters
Passenger descent from aircraft	Exponential	λ = 6 min = 300 s
Passenger walking speed	Normal	μ = 1 m/s σ = 0.2s
Passenger picking up baggage item	Uniform	[10s; 20 s]
Manual baggage unloading from aircraft	Lognormal	μ = 3s σ = 0.5s
Cart capacity	Normal	μ = 36 σ = 1
Baggage cart moving speed	Normal	μ = 18 km/h σ = 1 km/h
Manual loading of baggage on claim band	Lognormal	μ = 2s σ = 0.3s
Baggage claim band velocity	Constant	36 m/min

4. MODEL DEVELOPMENT AND RESULTS

The simulation model represents the current conditions of the airport in terms of the baggage delivery service. Currently, PBC receives almost only narrow-body aircraft, and with a relatively low flight frequency. Under these conditions, an excellent level of service is maintained with little damage to suitcases (approximately 1 in 200) and with baggage delivery times under 30 min.

However, poorly controlled factors (basically those performed manually, such as baggage unloading from the aircraft) add a significant portion of uncertainty and variability to the process.

The simulation considers the current conditions of the airport, using the probability distributions specified in table 5 for the different modules of the baggage delivery process. Passengers move on foot to the terminal building. Approximate passenger transfer speed within the system, baggage cart transfer speed and routes from the plane to the baggage claim band were obtained from the field visit. The corresponding distance was obtained with Google maps, according to the arrival position of the aircraft (table 6).

Table 6. Distance to the baggage claim area from different aircraft positions

Position	Passenger route (m)	Baggage route (m)
1	80	140
2	50	100
3	90	60
4	130	60
5	180	100
6	241	150

The simulation considers that each passenger must take his own baggage from the claim band. Fallen or damaged baggage was taken to be 1 piece per flight, according to information obtained from airport personnel; this is considered in the model as a failure of the server with a restauration time of on average 2 min.

The model does not include the handling of special baggage (sports equipment, musical instruments, ...) due to the type of passenger demand, mainly industrial in PBC.

PBC airport has sufficient baggage delivery capacity for current demand. However, the airport continues to grow, as seen in table 2. As a member of the Metropolitan Airports System, it might also receive larger aircraft in the future, such as those included in Table 7, typical for low-cost airlines.

Table 7. Most common aircraft used by low-cost carriers

Aircraft	Max. number of passengers
A319	144
A320	180
A321	220
B737	215
B757	280
B767	375

Based on the previous information, two scenarios were considered in this preliminary stage of the project:

- *Scenario 1, 360 passengers served*
  Baggage unloading from two A320 aircraft (maximum capacity 180 passengers) arriving a few minutes apart in positions two and three. The A320 is currently the critical aircraft in PBC. Although its simultaneous arrival is not currently scheduled, this scenario is viable if the demand for PBC as a secondary airport within the Metropolitan Airports System increases; in this case, also bigger aircraft could be expected.
- *Scenario 2, 440 passengers served*
  Baggage unloading from two A321 aircraft (maximum capacity 220 passengers) arriving a few minutes apart in positions two and three.

Figure 7 visualizes the simulation model developed in SIMIO® for the analysis of baggage delivery, using the data specified in figure 5 and table 5.

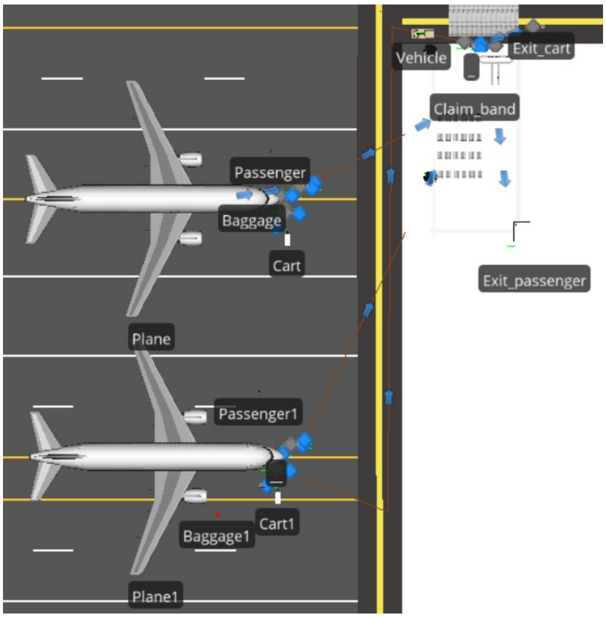

Figure 7. View of the simulation model.

The number of replications was determined to be 100. Simulation results include the length of passenger and baggage queues, bottlenecks, failures and possible system collapses, as well as the current comfort level of the baggage delivery service of PBC airport. The flexibility of the model allows to easily introduce different aircraft types and occupation levels, as well as to include different baggage types and to increase cart or personnel capacity. Also, the arrival logic can be replicated to include a larger number of aircraft. Therefore, it can be generalized to other semi-manual baggage claiming services or airports without too much effort.

Table 8 shows the required conditions of the room and the baggage claim band to meet the IATA comfort requirements in each of the simulated scenarios.

Table 8. Comparison of IATA comfort requirements

Variable	Existing	Required according to IATA	
		Scenario 1	Scenario 2
Baggage claim area	374	356 m^2	436 m^2
Maximum number of pax in the claim area	180	183	221
Comfort classification	A	A	C

In addition to the decrease in comfort classification for de baggage claim area, also baggage delivery process time increased from 28.5 minutes on average for an A320 aircraft to 43.1 minutes when a second A320 arrives within 15 minutes. For the second scenario, baggage delivery time was 41.2 minutes when one aircraft A321 arrives, while this increased to 65.4 minutes for the second aircraft. The main problem is that baggage delivery is performed sequentially with a claim band that is too short according to IATA standards.
The process time increased by 51.2% for the first scenario, and by 58.7% for the second.

5. CONCLUSIONS

Simulation is a useful analysis tool in short, medium, and long-term decision making. Its results are based on the analysis of different scenarios that will not necessarily be implemented in the real system.

In this study, the simulation was implemented to analyze possible problems in the baggage delivery service of PBC airport, and that can only be studied in virtual environments close to reality. In our case, SIMIO® provides the necessary conditions for an appropriate approach of the problem and the corresponding result determination.

Given the current problem of air traffic and saturation of Mexico City airport, questions arise about the way in which the airports of the Metropolitan Airports System can be enhanced, according to their characteristics and without negatively affecting the passenger.

In this study we analyzed PBC airport, located in the southeast of Mexico City. It's expected increase in demand suggest areas for improvement, while passenger's comfort level should be maintained within international standards. The analyzed subsystem was the baggage delivery service, that should finish processing all flight's baggage within a 30-minute interval after arrival.

PBC's current operating conditions, aircraft types and flight frequencies allow the airport to have an acceptable service and comfort level in the baggage claim area. However, the simulation showed that the simultaneous arrival of different aircraft, as well as the arrival of larger aircraft, means a decrease in the service quality. Preliminary results show that, depending on the aircraft occupation, baggage delivery times can increase from 31.2 minutes on average for an A320 aircraft to 47.1 minutes when a second A320 arrives within 15 minutes, increasing the process time by almost 50%. For larger aircraft such as the A321, this delay in baggage delivery increases considerably.

The main problem detected is that the baggage claim band violates IATA standards and that baggage delivery occurs sequentially. If similar situations to the presented scenarios arise in the future, an increase in band length as well as a configuration change should be considered. Other possible improvements to the baggage delivery process may include a more careful baggage handling by the personnel, as well as an increase in the baggage cart capacity.

ACKNOWLEDGMENTS

The authors want to thank MSc. María de Lourdes Arrellano Bolio for kindly providing advice and support, as well as data to develop and test the simulation model.

REFERENCES

A21MX (2019). Buscan que Querétaro libere carga aérea al AICM. Retrieved from: https://a21.com.mx/aeropuertos/2019/01/17/buscan-que-queretaro-libere-carga-aerea-al-aicm

ABC Viajar (2015). Problemas en el aeropuerto: cuales son los más habituales y cómo reclamar. Retrieved from: https://www.abc.es/viajar/20140408/abci-reclamar-aerolineas-semanasanta-201404071333.html

Aeropuertos de México. (2013). Aeropuerto Internacional de Toluca. Retrieved from http://www.aeropuertosmexico.com/content/view/280/380/

Alfadiario (2019). El Aeropuerto Internacional de Toluca sin reactivación visible. Retrieved from: http://www.alfadiario.com.mx/articulo/2019-02-08/1025694/el-aeropuerto-internacional-de-toluca-sin-reactivacion-visible

América vuela (2018). Próximo gobierno analiza el Sistema Metropolitano de Aeropuertos. Retrieved from: https://vuela.com.mx/am/aeropuertos/4784-proximo-gobierno-analiza-el-concepto-del-sistema-aeroportuario-metropolitano.html

Appelt S., Batta R., Lin L., Drury C. (2007). Simulation of passengers check-in at a medium-sized us airport. *Proceedings of the Winter Simulation Conference*, pp. 1252-1260.

ASA (2006). *Aeropuertos para la competitividad y desarrollo*. Colección editorial del gobierno del cambio, ASA-México, 299 p.

Ávila-Chaurand R., Prado-León L., González-Muñoz E. L. (2007). Dimensiones antropométrica de la población latinoamericana: México, Cuba, Colombia, Chile. Centro

Universitario de Arte, Arquitectura y Diseño, *Universidad de Guadalajara*. 281 p.
Cantera S. (2018). Operar en aeropuertos alternos duplica el gasto para las aerolíneas. *El Universal*. Retrieved from: https://www.eluniversal.com.mx/cartera/finanzas/operar-en-aeropuertos-alternos-duplica-el-gasto-para-las-aerolineas-canaero
Causa directa (2013). Tabla-relación velocidad de peatones caminando. Retrieved from: https://causadirecta.com/especial/calculo-de-velocidades/tablas/tabla-relacion-velocidad-de-peatones-caminando
Cavada J. P., Cortés C., Rey P. (2017). A simulation approach to modelling baggage handling systems at an international airport. *Simulation Modelling Practice and Theory 75*, pp. 146-164.
Correira A., Wirashinge S. (2010). Level of service analysis for airport baggage claim with case study of the Calgary International Airport. *Journal of Advanced Transportation* 44, pp. 103-112.
Doganis R. (1995). La empresa aeroportuaria. Paraninfo. ISBN 978-84-283213-9-6, 257 p.
El financiero (2018). Aeropuerto de Querétaro podría liberar carga al AICM. Retrieved from: https://www.elfinanciero.com.mx/bajio/aeropuerto-de-queretaro-podria-liberar-de-carga-al-aicm
Eller R.A.G., Feitosa M.V.M., Porto P.P. (2002). Simulation model of a baggage claim device coping with a new large aircraft. *Journal of Transport Literature* 5, pp. 63–72.
Excelsior (2016). El ABC del Sistema Metropolitano de Aeropuertos; conectividad en México. Retrieved from: https://www.excelsior.com.mx/comunidad/2016/05/14/1092523
Expansión (2016). El gobierno quiere revivir el aeropuerto de Toluca ante saturación del AICM. Retrieved from: https://expansion.mx/empresas/2016/09/14/el-gobierno-quiere-revivir-el-aeropuerto-de-toluca-ante-saturacion-del-aicm
Figueras, J., Guasch, A., Mujica, M. A., Narciso, M., & Piera, M. A. (2013). *Modelos de simulación*. UNAM, 179 p.
Flores de la Mota I., Guasch A., Mujica Mota M.A., Piera M.A. (2017). Robust Modelling and Simulation: Integration of SIMIO with Petri nets. *Springer*, 1st Ed., pp. 162.
Frey M.M. (2014). Models and methods for optimizing baggage handling at airports. PhD thesis, Lehrstuhl für Operations Management. *Technische Universität München*. 145 p. Retrieved from: https://mediatum.ub.tum.de/doc/1232183/1232183.pdf
Galindo López D., Nava Figueroa B. (2011). El sistema metropolitano de aeropuertos a seis años de su establecimiento, Asociación Mexicana de Ingeniería de Vías Terrestres A.C. (AMIVTAC). México, 157 p.
Ghobrial A., Daganzo C.F., Kazimi T. (1982). Baggage Claim Area Congestion at Airports: An Empirical Model of Mechanized Claim Device Performance, *Transportation Science* 16, pp. 246-260.
IATA (1995). *Airport development reference manual*. International Air Transport Association, Montreal. ISBN 92-9035-729-0.
Johnstone M., Creighton D., Nahavandi S. (2015). Simulation-based baggage handling system merge analysis. *Simulation Modelling Practice and Theory* 53, pp. 45–59.
La Jornada (2019). IATA: es inviable el esquema de los tres aeropuertos. Retrieved from: https://www.jornada.com.mx/ultimas/2019/03/01/iata-es-inviable-el-esquema-de-los-tres-aeropuertos-2461.html
Le V.T., Zhang J., Johnstone M., Nahavandi S., Creighton D. (2012). A Generalised Data Analysis Approach for Baggage Handling Systems Simulation. *Proceedings of the IEEE International Conference on Systems, Man, and Cybernetics*, pp. 1681-1678.
Lemer, Andrew, (1992). Measuring performance of airport passenger terminals. *Transportation research part A: policy and practice* 26A, pp. 37-45.
Mendoza E., Zúñiga C.A., Mujica M.A., Delahaye D. (2015). Simulating airport capacity: Mexico City airport case. Conferences in Air Transport & Operations. In *Proceedings of the 3rd International Conference on Interdisciplinary Science for Innovative Air Traffic Management.*
Milenio (2016). Aeropuertos desaprovechados. Retrieved from: https://www.milenio.com/negocios/aeropuertos-desaprovechados
Mujica Mota M.A., Scala P., Delahaye D. (2017). Improving Airport Performance Through a Model Based Analysis and Optimization Approach. In *Applied Simulation and Optimization New Applications in Logistics, Industrial and Aeronautical Practice*, Springer, pp. 109-129.
Neufville (2013). Airport Systems Planning, Design, and Management. McGraw-Hill, 2nd edition. ISBN 978-0071770583.
Novrisal D., Hamani N., El Mhamedi A., Soemardi T. P. (2013). Simulation of departure terminal in Soekarno-Hatta International airport. *IEEE International Conference on Industrial Engineering and Engineering Management.*
Red ASA (2019). Aeropuerto Internacional de Puebla. Retrieved from: https://www.aeropuertosasa.mx/aeropuerto_de_puebla.php
Robinson G.L. (1969). Simulation Models for Evaluation of Airport Baggage-Handling Systems, *Winter Simulation Conference Proceedings,* Institute of Electrical and Electronics Engineers (IEEE), pp. 226 – 235.
Savrasovs M., Medvedev A., Sincova E. (2009). Riga airport baggage handling system simulation. *23rd European Conference on Modelling and Simulation.* Retrieved from: https://pdfs.semanticscholar.org/45ad/bc003a6952ce3f50b7a4b6e33f16d24abd5e.pdf
Simio LLC (2019). What is Simio? Retrieved from: https://www.simio.com/about-simio/what-is-simio-simulation-software.php

NEITHER PUSH NOR PULL: STATE-FEEDBACK CONTROL FOR PRODUCTION SYSTEMS

Gašper Mušič[(a)], Juliana Keiko Sagawa[(b)]

[(a)]University of Ljubljana, Faculty of Electrical Engineering, Tržaška 25, 1000, Ljubljana, Slovenia
[(b)]Federal University of São Carlos, Production Engineering Department, Rodovia Washington Luís, Km 235, 13565-905, São Carlos - SP, Brazil

[(a)]gasper.music@fe.uni-lj.si, [(b)]juliana@dep.ufscar.br

ABSTRACT

Operations management techniques can benefit from integration of control theory methods when dealing with production and supply chain networks dynamics. In this context, we revisit a bond-graph based mathematical model that is able to capture the dynamics of multi-workstation production systems, and propose a state feedback control design to maintain work in process at desired levels. The closed loop performance of this real case inspired model was explored and simulations with the introduction of a disturbance in the production system were carried out. The proposed control design results in a disturbance-oriented behaviour that has advantages over pure push or pull systems commonly used in Production Planning and Control (PPC). In the given case, the results revealed that the model can provide prescriptive capacity adjustments and can help to define appropriate reference levels for the work in process in dynamic production environments.

Keywords: state feedback control; production planning and control; operations management

1. INTRODUCTION

Supply chain and production managers are faced with increased decision-making complexity, caused, among others, by the large variety of offered products, wide network of customers and suppliers, distributed production facilities, and customer demands on reduced delivery times.

From the operations perspective, it is known that the delivery performance is related to work in process (WIP) and throughput time (Lödding 2013). The trade-off between throughput rate and throughput time, and the direct relation of both with the WIP must be incorporated in any reasonable model of manufacturing systems (Lefeber 2012).

Various modelling approaches were proposed to cope with this trade-off in the context of production dynamics. The application of control theory principles, using feedback loops, control laws and transfer functions is one of the alternatives for this purpose (Duffie and Falu 2002). Another less explored option for dynamic modelling of production systems is the use of bond graphs (Ferney 2000).

An advantage of the bond graph methodology is its modular structure, i.e., once a set of graphs and elements is defined to represent basic entities (such as a machine or a buffer), several of these elements may be linked together into a more complex model to form different configurations. This makes the methodology attractive to be used by production managers and practitioners.

Adaptations of the bond graph methodology for modelling production systems (Ferney 2000) result in formal models that do not comply with the standard control theoretic synthesis methods. Thus, the design of good controllers for these models presents a substantial challenge. Hence, this paper aims to revisit a bond graph model of a multiproduct production system (Sagawa, Nagano, and Speranza Neto 2017) and presents a solution for the design of controllers for this system.

2. BOND GRAPH MODELLING OF PRODUCTION SYSTEM

The model of production system used in this paper was presented in Sagawa and Nagano (2015a,b), Sagawa, Nagano, and Speranza Neto (2017). The model depicts the dynamics of multi-product manufacturing system and was developed based on bond graph methodology. It is based on analogies between the manufacturing entities and electrical components, and involves the approximation of discrete systems as continuous systems (Ferney 2000). In terms of analogies, the machines are represented as resistors while the intermediate buffers are characterised as capacitors. The well-known expressions from electrical circuits are applied to form equations of these elements. A single workstation in this model comprises a machine and its precedent buffer, and is obtained from the combination of a capacitor, a resistor and a source of effort, as proposed by Ferney (2000).

In order to represent a multi-workstation system, Sagawa, Nagano, and Speranza Neto (2017) employ the concept of a material flow matrix (MFM) or probability flow matrix (PFM). When normalized, this matrix expresses the percentage of work content that flows from a workstation of a job shop to another one. In addition, ideal electrical transformers are introduced in the bond graph model to represent divergent junctions, where the output flow of a given workstation is split up into k different inputs to downstream workstations.

This approach was applied to an 11-workstation system of a textile company with complex material flow (Sagawa and Nagano 2015). The production process starts with the extrusion of polymer to produce polypropylene thread, and continues with weaving in circular looms. After that, the various products go through different finishing operations, such as lamination, printing, cutting and stitching, according to the required customizations. The system may be classified as a unidirectional job shop or a general flow shop, since the products have different routings where operations might be skipped, but there are no reentry-order-flows.

The related model is described in detail in Sagawa, Nagano, and Speranza Neto (2017). Here, only the main equations and resulting matrix model are presented. The input to machine i comes from a subset S of machines upstream machine i, whose outputs feed machine i to some extent. The rate of work in process (WIP) generation $\dot{q}_i$ on a given workstation is described by:

$$\dot{q}_i(t) = \sum_{s \in S} \varphi_{is} U_s \min(1, q_s(t)) - U_i \min(1, q_i(t)), \qquad (1)$$

where $s \in S$ and φ_{is} may be defined as the non-zero elements of a characteristic material flow matrix φ for the production system, out of its main diagonal. Parameter U_i is associated to the processing frequency of a given machine, and q_i is production volume stored in the machine preceding buffer. The min function is related to the approximation of discrete systems as continuous systems (Ferney 2000).

For the system under analysis, the matrix φ is shown in Eq. (2).

$$\boldsymbol{\varphi} = \begin{bmatrix} -1 & 0 & 0 & 0 & 0 & 0 & 0 & 0 & 0 & 0 & 0 \\ 1 & -1 & 0 & 0 & 0 & 0 & 0 & 0 & 0 & 0 & 0 \\ 0 & 0{,}4300 & -1 & 0 & 0 & 0 & 0 & 0 & 0 & 0 & 0 \\ 0 & 0{,}2508 & 0{,}5118 & -1 & 0 & 0 & 0 & 0 & 0 & 0 & 0 \\ 0 & 0{,}1538 & 0{,}3140 & 0 & -1 & 0 & 0 & 0 & 0 & 0 & 0 \\ 0 & 0{,}0170 & 0{,}0347 & 0 & 0 & -1 & 0 & 0 & 0 & 0 & 0 \\ 0 & 0{,}0175 & 0{,}0020 & 0{,}2811 & 0{,}2811 & 0 & -1 & 0 & 0 & 0 & 0 \\ 0 & 0{,}0087 & 0{,}0010 & 0{,}1399 & 0{,}1399 & 0 & 0 & -1 & 0 & 0 & 0 \\ 0 & 0{,}0161 & 0{,}0018 & 0{,}2588 & 0{,}2588 & 0 & 0 & 0 & -1 & 0 & 0 \\ 0 & 0{,}0200 & 0{,}0023 & 0{,}3204 & 0{,}3204 & 0 & 0 & 0 & 0 & -1 & 0 \\ 0 & 0 & 0 & 0 & 0 & 0 & 0{,}2407 & 0{,}2407 & 0{,}2407 & 0{,}2407 & -1 \end{bmatrix}$$

(2)

Some elements of this flow matrix directly correspond to the percentages of work content flowing from a workstation of a job shop to another one. For the cases where the input flow of a given machine is ruled by a combination of convergent and divergent junctions, then the coefficients of the flow matrix are appropriate products of these percentages (for details, see Sagawa, Nagano, and Speranza Neto (2017)). The matrix is lower triangular since there are no re-entry flows.

The only exception for the application of Eq. (1) regards to the first machine of the system (the extruder), whose input flow comes from the source of raw material, U_{01}. Adjusting Eq. (1) to it yields:

$$\dot{q}_1(t) = U_{01} - U_1 min(1, q_1(t)). \qquad (3)$$

Using the flow matrix φ, Eqs. (1) and (3) may be rewritten in matrix form, yielding the state model of the system:

$$\dot{\mathbf{q}}(t) = \boldsymbol{\varphi} \cdot diag(\mathbf{U}(t)) \cdot min(1, \mathbf{q}(t)) + \mathbf{0}_1 U_{01}(t), \qquad (4)$$

where system state $\mathbf{q}(t)$ is a 11x1 a vector of momentary production volumes stored in the system buffers, $\dot{\mathbf{q}}(t)$ is the corresponding vector of volume rates, φ is material flow matrix defined by Eq. (2), and $\mathbf{U}(t)$ is a column vector of workstation processing frequencies. Expression $diag(\mathbf{U}(t))$ denotes a 11x11 diagonal matrix whose non-zero elements are the elements of vector $\mathbf{U}(t)$, $U_{01}(t)$ is the processing frequency of the source of raw material that feeds the system, and $\mathbf{0}_1$ is a 11x1 vector filled with zeros except at the first position, which contains 1 ($\mathbf{0}_1$ = $[1\ 0\ 0\ ...\ 0]^T$). This state space model was used as the basis for the controller design proposed in the sequel.

3. CONTROL DESIGN

The main goal of the presented approach is WIP control, and WIP in the system corresponds to the material in the buffers of the stations. The related amounts of WIP in the buffers are the controlled variables of the system and the processing frequencies of the stations are the manipulated variables with additional manipulated input representing the source of material flow. Reference levels for the buffers are set so that there is enough material to process (to prevent starvation) but also the throughput times remain within acceptable range. The level of the buffers is monitored and the implemented controller performs capacity adjustments (i.e. it regulates the processing frequencies of the stations) in order to keep the material in the buffers at desired levels. To some extent, input control (order release) and output control (capacity control) are performed simultaneously, since input flow U_{01} is also adjusted by the controller.

3.1. Model linearization

The standard state space controller design methods require a linear model. As the derived production model is nonlinear, it has to be adjusted.

First, the nonlinear expressions $min(1, q_j)$ are omitted. In this way, the model only correctly describes the operation in the high production volume regime, which should be taken into account when setting the reference values for the buffer levels.

The corresponding linearized model is

$$\dot{\mathbf{q}}(t) = \boldsymbol{\varphi} \cdot \mathbf{U}(t) + \mathbf{0}_1 U_{01}(t), \qquad (5)$$

The workstation processing frequency U_i can be expressed as

$$U_i = U_{ip}(1 + u_i), \qquad (6)$$

where U_{ip} denotes the steady state processing frequency of machine i, and u_i is the relative processing frequency deviation from the steady state. A similar transformation is applied to the material input flow U_{01}. The deviation u_i will represent a control input in the linearized model.
The formulation (6) emphasises the fact that controller-adjusted processing frequencies will vary around the nominal steady state processing frequencies. These are calculated based on the average demand for each product family, and thus define the steady-state operation regime, which will be able to meet the demand for each product family.
The model (5) is further simplified by introducing an extended vector of processing frequencies $\mathbf{U^1} = [U_1, \dots, U_{11}, U_{01}]^T$. Similarly, the diagonal matrix of processing frequencies is extended to $diag(\mathbf{U^1})$. Taking (6) into account, the processing frequencies are expressed in vector form as

$$\mathbf{U^1} = \mathbf{U_p^1} + diag(\mathbf{U_p^1}) \cdot \mathbf{u_f}. \tag{7}$$

It should be noted here that $\mathbf{U_p^1}$ is determined by the steady state relation $\boldsymbol{\varphi} \cdot \mathbf{U_p} + U_{01p}\mathbf{0}_1 = [\boldsymbol{\varphi}, \mathbf{0}_1] \cdot \mathbf{U_p^1} = \mathbf{0}$ and has a unique solution for a given U_{01p}.
Considering (7) and the steady state relation, the model (5) is rewritten as

$$\dot{\mathbf{q}}(t) = [\boldsymbol{\varphi}, \mathbf{0}_1] \cdot diag(\mathbf{U_p^1}) \cdot \mathbf{u_f}(t), \tag{8}$$

which can be interpreted as a linear state space model with zero state matrix $\mathbf{A} = 0$ and input matrix $\mathbf{B}$, such that

$$\mathbf{B} = [\boldsymbol{\varphi}, \mathbf{0}_1] \cdot diag(\mathbf{U_p^1}).$$

3.2. Control synthesis

The basic full state feedback control law for the given case is

$$\mathbf{u}_f = -\mathbf{K} \cdot \mathbf{q}, \tag{9}$$

where $\mathbf{K}$ is a matrix of $(n+1) \times n$ feedback gains, n representing the number of workstations.
As the goal of the controller is to maintain reference levels for the buffers, i.e., reference tracking, the state feedback control has to be modified to settle at nonzero q values. This can be achieved by standard technique of adding integral action in state feedback control (Franklin, Powell, and Emami-Naeini 1994). To this end, the state vector $\mathbf{q}$ is augmented with additional n state variables q_{jI}. These will maintain the desired operating point by acting as internal states of an integral controller. The integral action is implemented as a part of the full state feedback control law for the augmented system. The added state variables are related to deviation from the reference levels:

$$q'_{jI} = -e_j = q_j - r_j,$$

where e_j is the control error, and r_j is the reference value for buffer level q_j. Negative integral gain is assumed to comply with the negative sign in the state feedback equation.
For the case with zero state matrix, $\mathbf{A} = 0$, the augmented system model is

$$\begin{bmatrix} \dot{\mathbf{q}}_I \\ \dot{\mathbf{q}} \end{bmatrix} = \begin{bmatrix} 0 & \mathbf{I}_n \\ 0 & 0 \end{bmatrix} \cdot \begin{bmatrix} \mathbf{q}_I \\ \mathbf{q} \end{bmatrix} + \begin{bmatrix} 0 \\ \mathbf{B} \end{bmatrix} \mathbf{u}_f - \begin{bmatrix} \mathbf{I}_n \\ 0 \end{bmatrix} \mathbf{r}, \tag{10}$$

and the corresponding control law is

$$\mathbf{u}_f = -[\mathbf{K}_I \quad \mathbf{K}] \begin{bmatrix} \mathbf{q}_I \\ \mathbf{q} \end{bmatrix}. \tag{11}$$

Note that the closed loop dynamics is determined by augmented system matrices $\mathbf{A}_a = \begin{bmatrix} 0 & \mathbf{I}_n \\ 0 & 0 \end{bmatrix}, \mathbf{B}_a = \begin{bmatrix} 0 \\ \mathbf{B} \end{bmatrix}$, $\mathbf{C}_a = [0 \quad \mathbf{I}_n]$, $\mathbf{D}_a = 0$, and the extended feedback gain matrix $\mathbf{K}_a = [\mathbf{K}_I \quad \mathbf{K}]$.
The variations in the processing frequencies imposed by the controller represent in fact capacity adjustments, which cannot be performed in a continuous manner. In practice, a corresponding control action is applied in a discrete manner, by means of overtime or extra shifts, for instance. In order to better represent that, the continuous processing frequency adjustments provided by the controller should be converted into discrete adjustments in specified time intervals, such as one day, five days or ten days.
Conversion to discrete-time control adjustments is straightforward. The continuous state space model (8) has to be discretized to

$$\mathbf{q}(k+1) = \mathbf{A}_d \mathbf{q}(k) + \mathbf{B}_d \mathbf{u}_f(k), \tag{12}$$

with a chosen sampling time T_s, $t = kT_s$. Sampling time should be relatively short in comparison to the expected system settling time.
When the control inputs are piecewise constant over the sample time T_s, matrices $\mathbf{A}_d$ and $\mathbf{B}_d$ can be expressed as $\mathbf{A}_d = e^{\mathbf{A}T_s}$, $\mathbf{B}_d = \int_0^{T_s} e^{\mathbf{A}T_s}\mathbf{B}dt$. For the system under analysis, $\mathbf{A} = 0$, therefore $\mathbf{A}_d = \mathbf{I}_n$ (with n equal to the number of workstations) and $\mathbf{B}_d = \mathbf{B}T_s$. As in the continuous case, $\mathbf{C}_d = \mathbf{I}_n$ and $\mathbf{D}_d = 0$. Similarly to (10), the augmented model for the reference tracking is composed as

$$\begin{bmatrix} \mathbf{q}_I(k+1) \\ \mathbf{q}(k+1) \end{bmatrix} = \mathbf{A}_{ad} \cdot \begin{bmatrix} \mathbf{q}_I(k) \\ \mathbf{q}(k) \end{bmatrix} + \mathbf{B}_{ad}\mathbf{u}_f(k) - \begin{bmatrix} \mathbf{I}_n \\ 0 \end{bmatrix} \mathbf{r}(k), \tag{13}$$

where $\mathbf{A}_{ad} = \begin{bmatrix} \mathbf{I}_n & \mathbf{I}_n \\ 0 & \mathbf{I}_n \end{bmatrix}, \mathbf{B}_{ad} = \begin{bmatrix} 0 \\ \mathbf{B}_d \end{bmatrix}$ and, additionally, $\mathbf{C}_{ad} = [0 \quad \mathbf{I}_n], \mathbf{D}_{ad} = 0$.
Then, the specific values of the gain matrix for a given case can be derived by various synthesis methods.
In the following, the control matrix K can be derived by a discrete-time version of LQR method, which minimizes the quadratic cost function

$$J(\mathbf{u}_f) = \sum_{k=1}^{\infty}(\mathbf{q}(k)^T\mathbf{Q}\mathbf{q}(k) + \mathbf{u}_f(k)^T\mathbf{R}\mathbf{u}_f(k) + 2\mathbf{q}(k)^T\mathbf{N}\mathbf{u}_f(k)). \quad (14)$$

Matrices **Q**, **R** and **N** in (14) weigh the contribution of various terms to the cost function value. The **Q** matrix determines the relative importance of different combinations of the product of states, **R** defines the contribution of terms related to manipulated variables (control input), and **N** determines the importance of mixed terms.

Commonly, only squared states and squared inputs are taken into account, meaning that the **Q** and **R** matrices become diagonal, and **N**=0. Appropriate coefficient ratios are chosen to compensate for differences in the signal magnitudes. A well-known rule of thumb (Bryson's Rule, see Franklin, Powell, and Emami-Naeini 1994) is to weight signal s_i by $\omega_i^2/(s_i)_{max}^2$ with $\sum_i \omega_i = 1$ for signals related to **Q** and **R**, respectively. Weights ω_i add additional relative weighting on the various components of the state/control vector. Additionally, the balance between the influence of state deviations and the influence of control effort to the cost function is achieved by scaling matrix **R** with constant ρ. In the investigated case, the state vector was scaled based on reference buffer levels, and the same scaling was used for both integrator states and buffer levels. No additional relative weighting was used, and we have no additional information that could be used for control signal scaling, therefore:

$$\mathbf{Q} = \begin{bmatrix} diag(1/r_i^2) & 0 \\ 0 & diag(1/r_i^2) \end{bmatrix}, \quad \mathbf{R} = \rho \cdot \mathbf{I}_{nu}, \quad \mathbf{N} = 0. \quad (15)$$

The relative weight between state and control vector components was set to $\rho = 100$.

4. SIMULATION RESULTS

The closed loop control system with state feedback was initially simulated under a scenario, where all buffers are initially empty, and the desired reference levels are set to 0.1 times the benchmark levels adopted in Sagawa and Nagano (2015). Sampling period of 1 day was chosen, which corresponds to daily changes of the prescribed capacity levels. Three months of production are simulated.

A partial breakdown of station 2 occurs after a month of operation, i.e. at time 30. The station consists of 12 parallel looms, and the partial breakdown corresponds to the malfunction of one of these looms. The repair time was artificially extended to 20 days before the looms are set back into operation, in order to have a clearer picture of the system's response to such a disturbance. The corresponding controller signal is shown in Fig. 1.

The controller response shows that the workstations 1, 2 and 3 start to operate with processing frequencies above the respective steady state frequencies, in order to fill the initially empty buffers. Simultaneously, the stations downstream station 3 (i.e., station 4 to station 11) process material with a frequency below the steady state frequency until there is enough WIP in the buffers to be processed (see U4 to U11 at Fig. 1). After circa 20 days, the system reaches steady state with the WIP at the reference levels (the relative errors close to zero correspond to relative processing frequencies close to 1 in Fig. 1).

It can be observed that controller responds to a disturbance (partial failure of the station, i.e. breakdown of one of the looms on day 30), by gradually increasing the capacity of the remaining functioning part to approximately 111% in the first few days after the disturbance, and then decreasing it to 108% until the machine recovery, to keep the WIP at required levels. After the recovery, the capacity is set back to normal, after a few days of transient adjustments.

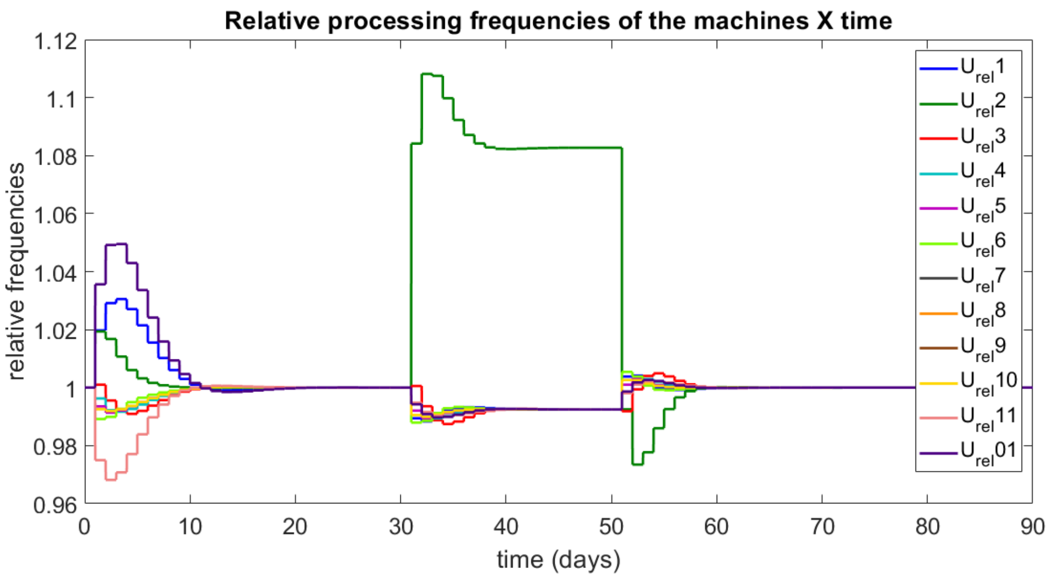

Figure 1: Discretization of the controller signal for 1 day intervals (i.e. recommended capacity adjustments for the stations)

4.1. Testing scenarios

A set of testing scenarios were defined in order to test the ability of the proposed production control strategy to respond to disturbances. Simulations with the synthesised discrete-time controller were carried out under the following scenarios:

1. The same scenario used in the simulation already presented, but with reference levels set as 0.2 and 0.05 times the benchmark levels (to verify the impact of the variation of the reference buffer levels);
2. A scenario with reference levels set as 0.2 times the benchmark levels and the breakdown of station 8 from day 30 to day 32;
3. A scenario with reference levels set as 0.2 times the benchmark levels and the breakdown of station 4 from day 30 to day 32.

The results are shown in: Fig. 2-3, for the first scenario; Fig. 4-5, for the second scenario; Fig. 6-7, for the third scenario.

One remark regarding Fig. 5b and 7 is that the processing frequencies of the broken stations 4 and 8 from day 30 to 32 shown in the figures correspond to how the controller would intend to react, but not to the actual processing frequency of the broken station. In fact, the processing frequencies of these stations during the breakdown are kept at zero.

The tests with scenario 1 showed that, with too low reference levels for the WIP, some buffers become empty (this corresponds to relative errors equal to -1, as in Fig. 3b). This means that the local work in process is not sufficient to absorb the disturbance occurred, and some machines starve. Buffers work as a safety "cushion" against the interruption of production flow, and the simulations with the proposed model may help to define adequate reference levels for this cushion.

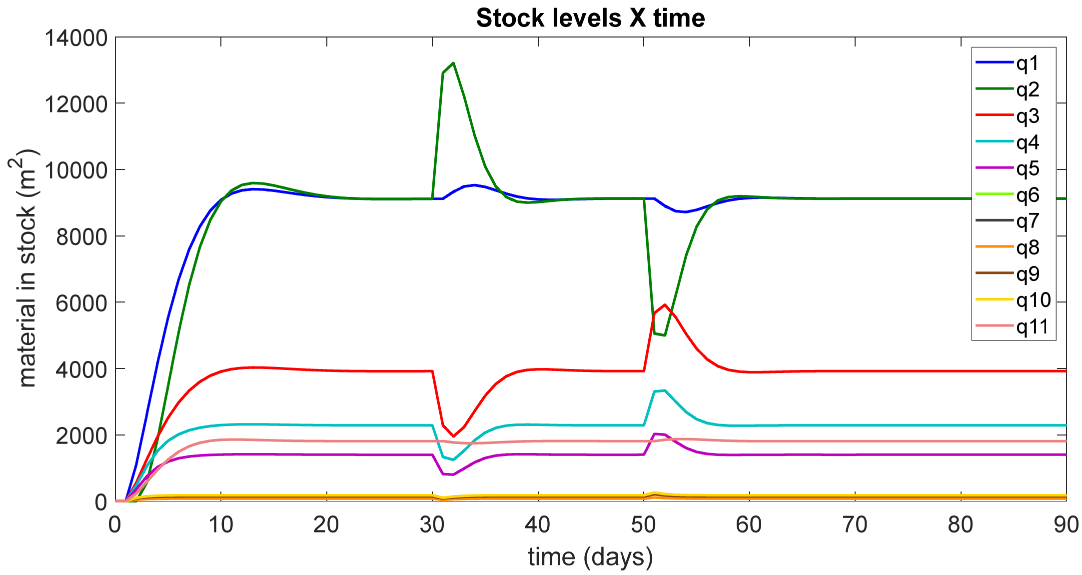

Figure 2: Simulation results for scenario 1 (discrete-time LQR), with reference levels equal to 0.2 x the benchmark levels and partial breakdown of the looms (station 2) – stock levels

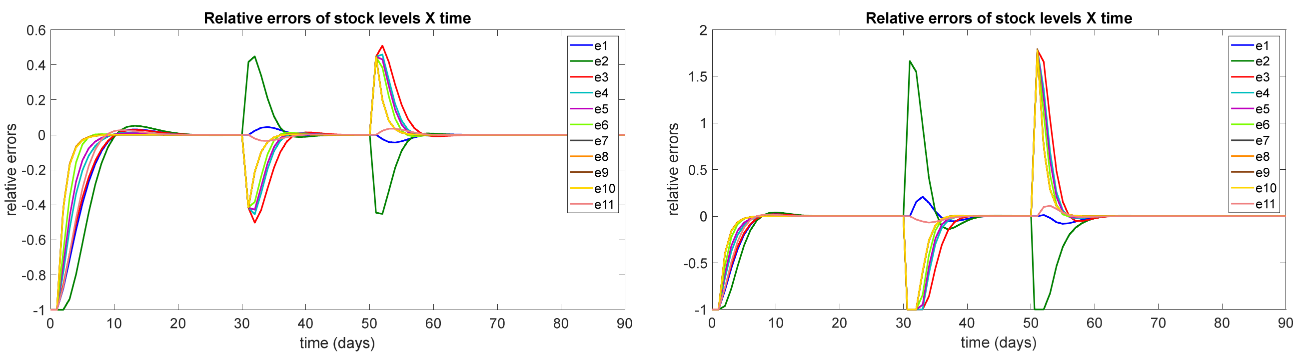

Figure 3 - Simulation results for scenario 1 (discrete-time LQR) - relative errors in the stock levels: a) with reference levels as 0.2 times benchmark values; b) with reference levels as 0.05 times benchmark values.

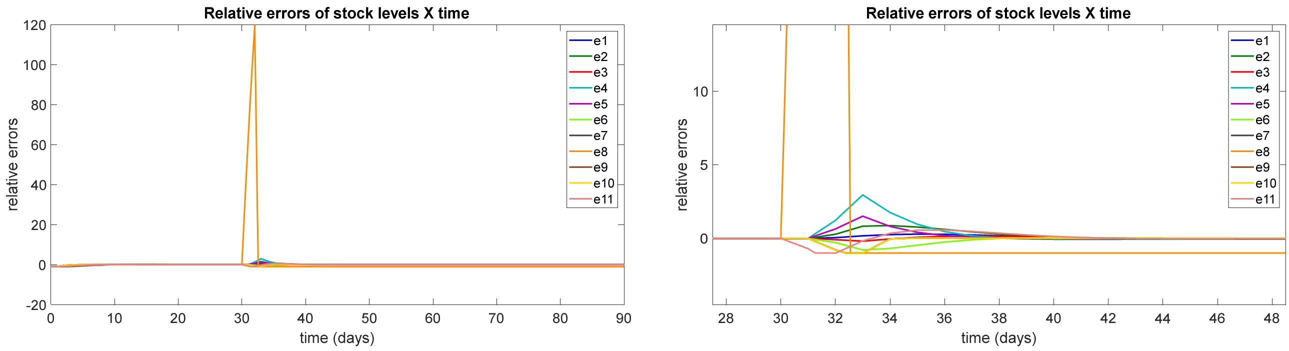

Figure 4 - Simulation results for scenario 2 (discrete-time LQR) - relative errors in the stock levels: a) overview; b) view of the detail

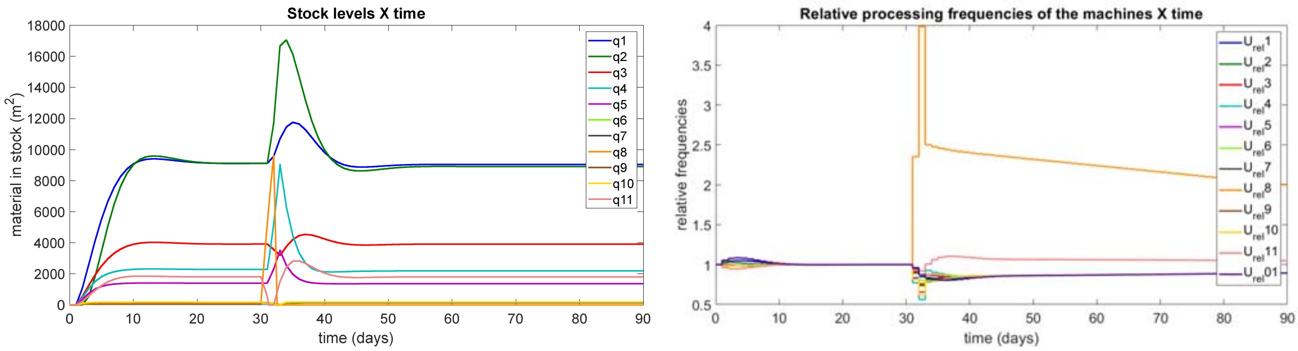

Figure 5 - Simulation results for scenario 2: a) stock levels; b) relative processing frequencies

In scenario 2, the breakdown of machine 8 causes a temporary increase of WIP around 9500 m^2 of material (q_8 in Fig. 5a). This peak of seems to be very pronounced in relative terms (Fig. 4a) because the reference level for buffer 8 is significantly lower than the levels of other buffers. This level was defined as a function of the total volume of material that is processed in each station. Station 8 is parallel to 3 other stations with similar function (stations 7, 9 and 10) and performs a finishing operation. As the products of four families do not require this finishing, it processes a relatively low volume of material. After 3 days, when the station 8 has already recovered, the material is totally consumed and the buffer becomes empty. The significant increase in the processing frequency of station 8 (Fig. 5b) represents how the controller would intend to react (in fact, the processing frequency of the station is kept at zero during days 30 to 32). After the disturbance, the station 8 should work 2.5 times more (Fig. 5b). The remaining stations decrease their rate of operation during the breakdown. With this reaction, after the disturbance, the buffer levels tend to get back to the reference levels.

In Fig. 6b, depicting scenario 3, it is possible to see that the starvation of the stations 7, 8, 9 and 10 occurs just during the breakdown, i.e. during 2 days (curves are superposed). As soon as machine 4 restarts to operate with 1.4 times its capacity, then the downstream buffers start to be filled again; after an overshoot, they stabilize close to the desired levels. It takes longer for the buffer of machine 4 to reach its desired level, but it doesn't mean that the production is interrupted: it just means that all its production is feeding the downstream machines, in order to keep delivering the desired output flows.

The controller decreases the processing frequencies of the stations upstream station 4 in order not to aggravate the build-up of WIP at station 4 (Fig. 7). On the other hand, the processing frequency of the stations immediately downstream (stations 5 and 6) is also decreased to respond to a lower incoming flow from machine 4. This shows that some stations react looking downstream (i.e. looking at the customer process, as in a pull system) and some stations react looking upstream (i.e. looking at the supplier process). This means that the system is neither pulled nor pushed; the control is centralized and rather focused on responding to the disturbance.

5. DISCUSSION

In the push system, the scheduling/sequencing of tasks in each station is defined according to a centralized strategy and based on exogenous information. The stations keep producing independently of the situation downstream in the process. In the pull systems, on the contrary, the material and information flows are in the opposite directions, i.e. the consumption of the downstream stations determines the amount and sequence of production of a given station. Thus, in the pull system, this reaction is based on endogenous information and is

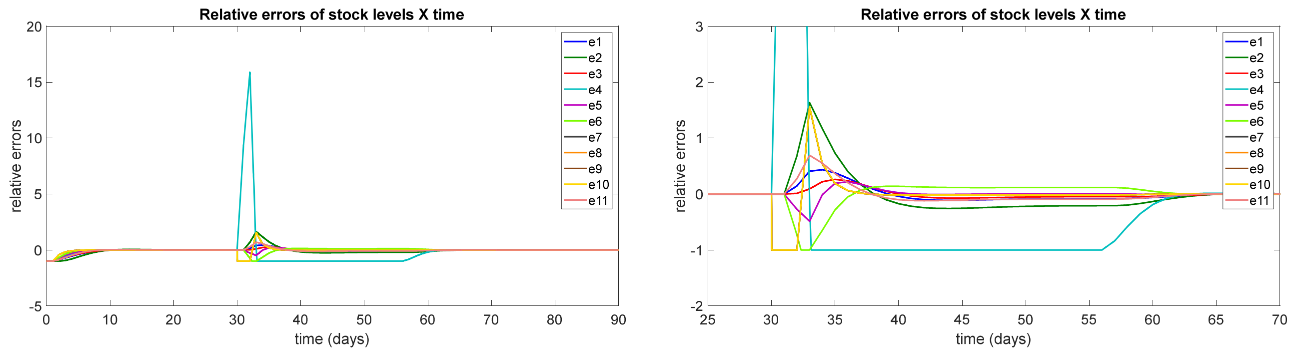

Figure 6: Simulation results for scenario 3 (discrete-time LQR) - relative errors in the stock levels: a) overview; b) detail

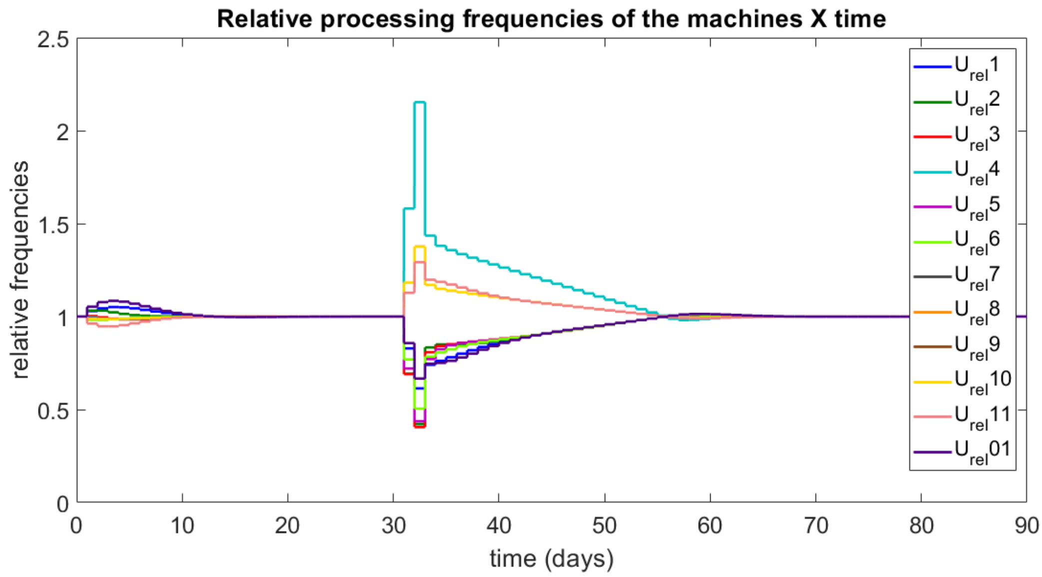

Figure 7: Simulation results for scenario 3 (discrete-time LQR) – relative processing frequencies

local, i.e. driven by the immediately subsequent station. As a result, a pull production system explicitly limits the amount of WIP that can reside in the system (Hopp and Spearman 2004).

In previous studies (Sagawa and Nagano, 2015; Sagawa, Nagano, and Speranza Neto 2017), feedback control was implemented to simulate a pull system, where the controller of each station just reacted based on the error of the buffer downstream, i.e. the buffer of the next station. This local approach based on proportional (P) controllers proved not to be so effective, since a high overshoot (i.e. surplus of material) in some buffers was observed. When the system was subjected to machine breakdowns, significant peaks were observed, even when a local Proportional Integral (PI) controller was used (Sagawa and Freitag 2016).

In the proposed model, instead of being local, the control is centralized, in the sense that a holistic view of the system is considered in order to define the reaction of each station. As observed in the simulation of scenario 3, if the disturbance occurs in the middle of the system, some stations react by looking upstream and some stations react by looking downstream; in fact, they react to the disturbance itself. This is an alternative operation mode that can be more effective in some situations than a pure "push" or "pull" system, see also Sagawa and Mušič (2019).

6. CONCLUSIONS

This paper presented a production control strategy for a dynamic multi-product production system, and the synthesis of the corresponding production controller that improves the system's operation. This approach based on state feedback control design techniques is novel in the sense that it had not been applied in prior studies concerning bond graph models that depict the shop floor of a manufacturing system.

The choice of the modelling framework and the application of control synthesis techniques open the way to use the simulation of production systems in a prescriptive rather than descriptive manner. The controllers of the workstations suggest necessary capacity adjustments in order to achieve specific goals, e.g. to keep the WIP under control, even in the presence of disturbances. Other relevant goals might be set, such as attending fluctuating demand levels, for instance.

One of the possible directions to be explored in future works is to investigate the combination of advanced control techniques with discrete-event simulation.

ACKNOWLEDGMENTS

The authors acknowledge the financial support from the Slovenian Research Agency (research core funding No. P2-0219).

REFERENCES

Duffie N., Falu, I., 2002. Control-Theoretic Analysis of a Closed-Loop PPC System. CIRP Annals - Manufacturing Technology, 51 (1), 379-382. doi: 10.1016/s0007-8506(07)61541-8.

Ferney M., 2000. Modelling and Controlling product manufacturing systems using bond-graphs and state equations: continuous systems and discrete systems which can be represented by continuous models. Production Planning & Control, 11 (1), 7-19.

Franklin G.F., Powell, J.D., Emami-Naeini, A., 1994). Feedback control of dynamic systems (3rd ed.). Reading, MA: Addison-Wesley.

Hopp, W.J., Spearman, M.L., 2004. To pull or not to pull: what is the question? Manufacturing & service operations management, 6 (2), 133-148.

Lefeber, E., 2012. Modeling and Control of Manufacturing Systems. In: Armbruster, D., Kempf, K.G. (Eds.). Decision Policies for Production Networks, Springer-Verlag London, 9-30. doi: 10.1007/978-0-85729-644-3_2

Lödding, H., 2013. Handbook of Manufacturing Control: Fundamentals, Description, Configuration. Springer-Verlag Berlin Heidelberg.

Sagawa, J.K., Nagano, M.S., 2015a. Applying bond graphs for modelling the manufacturing dynamics. IFAC-PapersOnLine 48 (3), 2047-2052.

Sagawa, J.K., Nagano, M.S., 2015b. Modeling the dynamics of a multi-product manufacturing system: A real case application. European Journal of Operational Research, 244 (2), 624-636. doi: 10.1016/j.ejor.2015.01.017.

Sagawa, J.K., Freitag, M., 2016. A simulation model for the closed-loop control of a multi-workstation production system. Proceedings of the 9th EUROSIM Congress on Modelling and Simulation, Oulu. Linköping: Linköping University Press.

Sagawa, J.K., Nagano, M.S., Speranza Neto, M., 2017. A closed-loop model of a multi-station and multi-product manufacturing system using bond graphs and hybrid controllers. European Journal of Operational Research, 258 (2), 677-691. doi: 10.1016/j.ejor.2016.08.056.

Sagawa, J.K., Mušič, G., 2019. Towards the use of bond graphs for manufacturing control: Design of controllers, International Journal of Production Economics, 214, 53-72. doi: 10.1016/j.ijpe.2019.03.017.

AUTHORS BIOGRAPHY

JULIANA KEIKO SAGAWA received B.Sc., M.Sc. and Ph.D. degrees in production engineering from the University of São Paulo, Brazil in 2006, 2008, and 2013, respectively. She is Adjunct Professor at the Faculty of Production Engineering of the Federal University of São Carlos. Her research interests include dynamic modelling of production systems, planning, scheduling and some organizational topics such as integration and servitization. More information can be found at: http://lattes.cnpq.br/6549481623896786.

GAŠPER MUŠIČ received B.Sc., M.Sc. and Ph.D. degrees in electrical engineering from the University of Ljubljana, Slovenia in 1992, 1995, and 1998, respectively. He is Full Professor at the Faculty of Electrical Engineering, University of Ljubljana. His research interests are in discrete event and hybrid dynamical systems, supervisory control, planning, scheduling, and industrial informatics. His Web page can be found at http://msc.fe.uni-lj.si/Staff.asp.

A SIMULATOR FOR STUDYING AUTOMATED BLOCK TRADING ON A COUPLED DARK/LIT FINANCIAL EXCHANGE WITH REPUTATION TRACKING

George Church[a] & Dave Cliff[b]

Department of Computer Science
University of Bristol, Bristol BS8 1UB, UK.

[a]gc14768@my.bristol.ac.uk, [b]csdtc@bristol.ac.uk

ABSTRACT
We describe a novel simulation of a contemporary real-world financial exchange: *London Stock Exchange (LSE) Turquoise*, and we also introduce a newly-created adaptive automated trading strategy called *ISHV*, which exhibits realistic behavior in situations where large orders can radically shift prices before transactions occur. LSE Turquoise is a recently-introduced platform where buying and selling takes place on a pair of coupled trading pools: a *lit* pool that is visible to all traders; and a *dark* pool where large "block" orders are hidden from sight until they are automatically matched with a counterparty, after which the transaction is then revealed. Orders from traders are routed to the lit or dark pool depending on their size, and on the reputation of the trader issuing the order. Unlike all other public-domain adaptive trading strategies, ISHV can alter the prices it quotes in anticipation of adverse price changes that are likely to occur when orders for block-trades are publicly visible: so-called *market impact*. LSE Turquoise is intended to reduce the negative effects of market impact; something that we test with our simulator. We extend the existing *BSE* open-source exchange simulator to incorporate coupled lit and dark pools, naming the new system BSELD. We show ISHV exhibiting market impact in a lit-only pool, and discuss how a Turquoise-style coupled dark pool reduces or eliminates that impact. We also show results from a Turquoise-style reputation-tracking mechanism, which can be used for modulating trader access control to the dark pool.

Keywords: financial markets, automated trading, dark pools, economic simulation.

1. INTRODUCTION

In contemporary global financial markets, traders routinely interact by remotely accessing an electronic trading venue, an online financial exchange, where they can post various types of order that indicate the prices at which they seek to sell or to buy some quantity of a particular tradable asset. They do this in the hope of finding one or more counterparties, other traders from whom they can buy, or to whom they can sell; interaction mediated via the trading venue allows potential counterparties to negotiate and agree a fair price for each transaction. In this minimally simple characterization, electronic exchanges are nothing more than digital implementations of the open-outcry trading pits that most major financial exchanges operated before the advent of computerized trading. And, in turn, those trading pits were strikingly similar to the impromptu haggling between gatherings of buyers and sellers that has been an everyday occurrence at public markets and exchanges and souks and bazaars for many centuries.

However, once major financial exchanges had switched from physical trading floors to virtual ones, opportunities then opened up for novel structures of market, for bringing buyers and sellers together to identify counterparties and for them to jointly agree a fair price for their transactions, in ways that are different from, or would simply not have been possible, if the exchange had not virtualized. That is, electronic markets can sometimes be created to offer trading-venue functionality that would have been difficult or impossible to achieve in a traditional bricks-and-mortar exchange.

This is already trivially the case in major financial-trading centers such as New York, London, Tokyo, and Hong Kong, where a few decades ago there would be only one major national exchange for trading equities (stocks and shares) and yet where today a trader typically has a choice of several venues on which any one trade could be executed (and, in some countries, where the venues are required by law to pass a trader's order to competitor-venues if that gives the trader a better price for her deal). Many of the new alternative trading venues have been created post-virtualization, after the economic and regulatory barriers to entry were lowered by making it feasible for trading venues to be operated from out-of-town data-centers rather than prime real-estate in the center of major-city financial districts. However, such developments only scratch the surface of the new opportunities offered by fully electronic trading venues.

Less trivially, in recent years innovative operators have offered new forms of online exchanges that are designed specifically to counteract aspects of traditional markets that had previously made business difficult for traders. Traders working for investment banks or major fund-management companies, where their jobs require them to routinely handle "block orders", i.e. individual orders for very large quantities of an asset, face a particular problem known as *market impact*. A single order to buy 100,000 shares in IBM will often not affect the price of IBM stock in the same way that 100 bids for 1,000 shares of IBM do. Major venue-operators such as the London Stock Exchange (LSE) now operate electronic markets that are custom-designed to reduce or eliminate the negative effects of market impact for block traders.

In brief, market impact is the name given to the effect experienced by traders when they try to execute a block (i.e., bulk) order, an order with a quantity so large that the sudden increase in supply (for sell orders, i.e. *asks*) or in demand (for buy orders, i.e. *bids*) means that other traders in the market — potential counterparties to the trade — recognize that the order is so big that it will shift the price of the asset in question: those potential counterparties then (entirely rationally) adjust the prices that they are willing to trade at, in a direction that is less attractive to the trader trying to initiate the block trade. This can be thought of as the counterparties guessing or estimating what price the asset will shift to and trade at *after* the block transaction has executed, and then setting that price for the transaction with the block trader *before* the price has actually shifted.

An example will help to illustrate this. Say that the current price for a tradeable asset with ticker-symbol WXYZ is roughly $10, and that the usual size of a deal, the usual quantity traded in WXYZ, is 100 units. Then say that our trader Anne is looking to sell 20,000 units — 200 times bigger than a regular-sized order: this definitely qualifies Anne as a block trader, for this particular deal. Before she does anything, Anne checks her trading screen and sees buy orders on the exchange from Bob, Carrie, and Dee: they are bidding at $9.98, $9.97, and $9.95, respectively. Anne asks these three potential buyers for their price on 20,000 WXYZ and they immediately respond with lowered prices of $7.03, $6.95, and $7.02, respectively. This means that Anne has seen a 30% reduction in the price she could get for her sale, merely because she revealed the size of her intended trade: the size caused her potential counterparties to factor into the deal their expectations of how the price would fall as a consequence of the sudden major increase in supply of WXYZ that would result from Anne's deal executing. This 30% fall when selling is the *market impact*, the price moving against Anne. If Anne had instead been buying a similarly bulk deal, she would very likely have suffered impact in the other direction: the quoted price would have moved up, as the potential counterparties priced-in the effects of increased demand.

If instead Anne had a way to signal her desire to trade but without fully revealing the size of her deal, and had waited for a while, maybe she could have found a willing counterparty, another block-trader looking to buy a big block who was happy with Anne's asking price.

That issue, of matching big block-traders (to their mutual advantage) without giving away details of the full size of each block-trader's intended deal is something that has been addressed by exchange and trading-venue operators who offer what are known as *dark pool* exchange facilities. Dark pools offer access to financial liquidity, 'darkened' so that key details of trader's orders are concealed from the pool's participants and observers, with only the trading-venue operator knowing the full details of the position of each trader in the pool. The venue operator matches bids and offers in the pool against those from willing counterparties, notifies the buyer and the seller that they have matched, and details of the trade are then made public after it has executed. Market impact is avoided because no-one can see in what quantity a participant is seeking to trade, until the trade is agreed and goes through. In contrast, traditional trading venues, exchanges with full transparency on quantities, are now known as *lit* trading pools.

In the past 15 years much of the trading activity on electronic markets has become highly automated. That is, many or all of the entities trading on the exchange are no longer human traders, but instead are autonomous algorithmic trading systems buying and selling with little or no direct human control. Automated trading systems running on electronic markets typically process such vast quantities of data, and have such very short reaction times, that no human could ever hope to match their performance. Financial institutions that operate profitable trading desks treat details of their automated algorithmic trading systems as tightly-guarded commercial secrets, for the obvious reason that this is how they make their money, their competitive advantage.

Nevertheless, there is a body of published work, a series of peer-reviewed academic papers and reputable university-level textbooks, that gives some insight on how adaptive automated trading systems are constructed. Since the mid-1990s researchers in universities and in the research labs of major corporations such as IBM and Hewlett-Packard have published details of various forms of trading strategy, often incorporating machine learning methods so that the automated trader can adapt its behaviors to prevailing market conditions. Notable trading strategies in this body of literature include the MGD and GDX automated traders developed by IBM researchers (Tesauro & Das, 2001; Tesauro & Bredin, 2002); the ZIP strategy developed at Hewlett-Packard (Cliff, 1997); HBL (Gjerstad, 2003); AA (Vytelingum, 2006; Vytelingum *et al*., 2008); Roth-Erev (e.g. Pentapalli, 2008); and ASAD (Stotter *et al.* 2013). However, for reasons discussed at length in a recent review of key papers in the field (Cliff, 2019) this sequence of publications concentrated on the issue of developing trading strategies for regular-sized orders: none of the key papers explored in (Cliff, 2019) look at trading strategies for outsize block orders, and none of them directly explore the issue of how an automated trader can best deal with, or avoid, market impact.

The lack of prior studies of automated trading strategies for block orders may be due to the complexity of the test-environment that is required to evaluate such strategies. An automated block trader needs to act and interact in a market environment in which there are other traders, potential counterparties, that are capable of making reasonable guesses or estimates for where the price of the tradeable asset will shift to after the block trade has gone through: that is, the other traders need to react to block orders by exhibiting behavior that is reasonably describable as market impact in response to the arrival of a block order, and none of the public-domain algorithms listed above does that. Second, the trading venue in which the various traders are interacting needs to support the processing of orders that vary over a significant range of sizes, so that some orders are "small" and others "large" — large enough to have an impact effect.

We report here on automated-trading experiments that are novel on two fronts, and which directly address that complexity. First, we show how an existing trading strategy can be modified in such a way that impact effects are exhibited when a block order is submitted to a market populated by those traders. For our market environment, we use the free public-domain open-source BSE exchange simulator (BSE, 2012) which provides much of the functionality of a traditional trading venue and comes with pre-coded versions of a variety of automated trading strategies. We then report on our work altering and extending BSE so that it is a model of the *Turquoise Plato* trading venue recently announced by the London Stock Exchange (LSE). Turquoise is a trading platform founded in 2008 and is now majority owned by the London Stock Exchange Group (LSEG). Turquoise features a lit order book called Turquoise Lit™ and a coupled dark order book called Turquoise Plato™. Turquoise Plato incorporates a novel reputation-tracking mechanism to encourage desirable behaviors in the traders using the dark pool. We refer to the extended BSE as *BSELD*: *BSE* with *L*it and *D*ark venues. The experiments we report here are the first to demonstrate that populations of automated traders can exhibit market impact effects in a traditional venue like BSE, and that the impact effect is reduced when the BSELD venue structure is used instead. Our simulator allows us to explore the effects that different aspects of the BSELD architecture have on the overall market dynamics, and to evaluate trading algorithms designed to operate in such a contemporary trading environment.

In Section 2 we review the motivations for our work and relevant previous literature. In Section 3 we demonstrate the way in which automated traders can alter their quote-prices in response to the arrival of individual block orders, which is a useful model of large-block market impact, and we show results that illustrate the impact effects in trading sessions on the traditional lit-only BSE. In Section 4 we compare and contrast the outcomes for block traders in the paired lit/dark market structure offered in BSELD: via a simple argument, it can be seen that the addition of an appropriately coupled dark pool will indeed greatly reduce (or eliminate) size impact effects. Section 5 then describes the reputation system.

2. BACKGROUND: FINANCIAL MARKETS

In contemporary global financial markets, traders routinely interact by remotely accessing an electronic trading venue, an online financial exchange. Financial exchanges typically allow traders to buy or sell varying quantities of any of a large number of tradeable assets, and different exchanges specialize in different asset-classes: for example, in London the primary market for equities (stocks and shares) is the London Stock Exchange; the primary market for metals is the London Metal Exchange; and the primary market for derivatives (tradeable options and futures contracts) is the ICE Futures Europe Exchange (originally founded as the London International Financial Futures Exchange, LIFFE, with its name subsequently changing as a result of a succession of corporate acquisitions and mergers). Exchanges typically operate as a venue in which buyers and sellers can interact, typically via buyers submitting *bids* and sellers submitting *asks* (also known as *offers*) with the exchange accepting the buyers' bid orders and the sellers' ask orders, and implementing some kind of matching process that enables traders to identify a willing counterparty for a transaction that then takes place at an agreed price, one which both parties consider fair.

Without loss of generality, we will consider here the market for only a single, anonymous, tradeable asset, and we will concentrate on the data-structure at the heart of operating an exchange in almost any class of tradable asset: that data-structure is the *Limit Order Book* (LOB). The LOB is typically published by the exchange and distributed to all traders simultaneously any time it changes. At any one time the LOB shows a summary of unexecuted orders that have been submitted by traders active in that market. The orders summarized on the LOB are of a specific type, known technically as *limit orders*. A trader in a market can typically chose to submit an order to the exchange either to buy or sell at whatever the current best available price is, this order-type is known as a *market order;* or a trader can choose to submit a *limit order,* one that specifies a *limit price*, a price that the asset is not yet trading at. When a trader submits a limit order to the exchange, that order is then held on the exchange's books until a counterparty can be identified that is willing to trade at a price that is equal or better than the order's indicated limit price: the book on which the limit orders are recorded at the exchange is the LOB. Because orders are fundamentally either bids or asks, the LOB is routinely spoken about as being divided into two sides: the bid side and the ask side. The best bid on the LOB is the one with the highest limit price, and the best ask is the one with the lowest limit price: the LOB is usually shown with the best bid and ask at the top, and with less competitively priced orders arranged below them in numeric order of price (descending for bids, ascending for asks). The quantity of the asset available at each price is also indicated on each side of the LOB, although the identities of the traders behind each order are typically not shown, so the LOB acts an aggregator and an anonymizer of individual orders.

The difference between the best bid price P_b and the best ask price P_a is known as the *spread*, and the mid-point of the spread (i.e., the arithmetic mean, $(P_a + P_b)/2$) is the *midprice*, which is very commonly used in situations where a single price value is required to summarize the state of the market for that asset. An illustration of a LOB is provided in Figure 1. Prices are usually quantized to some atomic resolution known as the tick-size: in very many exchanges the tick size is one cent or one penny, i.e. 1/100th of a unit of fiat currency. For further details of exchanges and the LOB see e.g. Harris (2002) or Cartea *et al.* (2015),

When a trader submits an order to the exchange, if it is a bid with a price greater than the current best ask-price, or an ask with a price lower than the current best bid-price, then the order is said to *cross the spread*, and that is interpreted as an indication that the trader submitting the order wishes to trade at the best price on the counterparty side of the LOB – known as *lifting the ask* (for an incoming bid that crosses the spread) or *hitting the bid* (for an incoming ask that crosses the spread). That is, a spread-crossing limit order is effectively a market order.

Because any spread-crossing quote issued by a trader is immediately executed (i.e., immediately results in a transaction occurring, consuming some quantity of the limit orders on the counterparty side of the LOB), the best bid and best ask on the LOB at any one time will always be different values and hence values for the spread are bounded from below by the tick-size.

	BID	ASK	
Qty	Price	Price	Qty
1	100	200	1
1	99	201	1
1	98	202	1
1	97	203	1
1	96	204	1
1	95	205	1
1	94	206	1

Figure 1: a Limit Order Book (LOB) presented in the conventional format: the left-hand side of the LOB is the Bid-book, the right hand side is the Ask-book. Prices are displayed as integer numbers of cents, so the *tick-size* is \$0.01. On each side of the LOB, prices are arranged top-to-bottom in order best to worst, so the highest bid price and the lowest ask price are at the top of the book. The columns at outside left and right, labelled "Qty", show the quantity of items available at that price. In this example the *spread* is \$2.00-\$1.00=\$1.00, and the *midprice* is (\$1.00+\$2.00)/2 = \$150.

Over the course of the 20th Century, trading activity on major exchanges transitioned from open-outcry trading pits to remote, electronically mediated communications. In the trading pits, which had often operated for well over 100 years, human traders gathered in close physical proximity and shouted and gestured at one another to directly signal their bids and offers. As relevant technology became cheap and reliable, traders no longer gathered at the exchange but instead communicated remotely: first by telephone; then via dedicated computer networks; and latterly using Internet and Web channels. Nevertheless, at the turn of the 21st Century, almost all traders active in any one major financial market would be human. In the past 15 years, that situation has changed significantly and now most trades in "spot" (immediate-execution) financial markets for a wide range of assets are dominated by *robot traders*, automated software systems using artificial intelligence (AI) and machine learning (ML) techniques that have replaced the human traders because trading machines are much faster, much more reliable, and much cheaper than human employees. This development, the rise of automated trading (and its potential ill effects) has been documented and discussed by various authors including Arnuk & Saluzzi (2012), Bodek & Dolgopolov (2015), Narang (2013), Patterson (2013), and Rodgers (2016).

For the purposes of this discussion, a key initial academic paper was the surprising set of results published in the prestigious *Journal of Political Economy* by Gode & Sunder (1993): this introduced a minimally simple automated trading algorithm now commonly referred to as *ZIC*. Four years later two closely related research papers were published independently and at roughly the same time, each written without knowledge of the other: the first was by Cliff (1997) describing the adaptive trading-agent strategy known as the *ZIP* algorithm; the second by Gjerstad & Dickhaut (1998), describing an adaptive trading algorithm now widely known as *GD*.

Gjerstad later moved to IBM's TJ Watson Labs where he helped set up a laboratory facility that was used in a study that generated world-wide media coverage when the results were published by Das *et al.* at IJCAI-2001, the prestigious *International Joint Conference on Artificial Intelligence*. This paper presented results from experiments exploring the behavior of human traders interacting with GD and ZIP robot traders, in a LOB-based financial exchange, and demonstrated that both GD and ZIP reliably outperformed human traders. Neither GD nor ZIP had been designed to work with the LOB, so the IBM team modified both strategies for their study. A follow-on 2001 paper by Tesauro & Das (two co-authors of the IBM IJCAI paper) described a more extensively *Modified GD* (MGD) strategy, and later Tesauro & Bredin (2002) described the *GD eXtended* (GDX) strategy. Both MGD and GDX were each claimed to be the strongest-known public-domain trading strategies at the times of their publication.

Subsequently, Vytelingum's 2006 thesis introduced the *Adaptive Aggressive* (AA) strategy which, in a paper published in the *Artificial Intelligence* journal (Vytelingum *et al.*, 2007), and in later AI conference papers (De Luca & Cliff 2012a, 2012b), was argued to be dominant over ZIP, GDX, and human traders, and hence the strongest-known public-domain robot trader. Recent work (Vach, 2015; Cliff, 2019) has called into question the supposed dominance of AA over GDX and ZIP, but all three of these trading algorithms can outperform human traders.

3. MODELLING MARKET IMPACT

The essence of market impact was sketched in the example story involving Anne, Bob, Carrie, and Dee that was given in Section 1. For the purposes of the discussion in this paper, here we will more precisely define *market impact* as the situation in which the market mechanism (e.g., the LOB) for some tradeable asset A shows the best price $B(t)$ available from potential counterparties at time t, and where at time t_1 a trader T signals an intent to transact a large quantity Q of asset A at a price equal to or better than $B(t_1)$, and this immediately results in $B(t_1+\Delta t)$ worsening with respect to the transaction intended by T, *before any actual transaction has yet taken place.* Here "better than $B(t)$" means a *higher* price if T is buying, and a *lower* price if T is selling; and "worsening" means the price B *increasing* if T is intending to buy, and *decreasing* if T is intending to sell. Similarly, "a large quantity Q" can be interpreted as any quantity sufficiently large, relative to the quantity previously available at the then-current best counterparty price, to cause a significant shift in B: a factor of 10 or more is usually sufficient.

From this definition, it is clear that the quantities bid or offered at various prices in the auction are the driving factors of market impact. However, to the best of our knowledge, none of the automated trading strategies mentioned in Section 2 incorporate any reasoning about order-quantity effects: neither in the original publications that introduce each strategy, nor in any later publications that describe subsequent use of those strategies. Because of this, one novel aspect of our work described here is our demonstration of size impact effects in markets populated by artificial trading agents: we are not aware of any previous publications that have demonstrated this.

In this paper we focus initially on exploring impact effects in markets populated by traders running an adapted form of the SHVR strategy that is built-in to BSE (see BSE 2012, Cliff 2018a). SHVR operates by attempting to always beat the best bid or offer: if a SHVR is selling, it will issue a quote that shaves one cent off the best ask price on the LOB so long as it is able to do so; and if SHVR is buying it will issue a quote adding one cent to the LOB's best bid price (thereby shaving one cent off its potential profit). SHVR is an attractive first choice because of its simplicity; extending the methods and results presented here to working with other more sophisticated adaptive strategies such as ZIP, GDX and AA are obvious topics for further work.

We extended the open-source code for SHVR traders such that their quote prices will, in appropriate circumstances, be determined by a function, an algorithm, that takes order-quantity into account. Our alteration involves making the traders sensitive to the market's current *microprice*. The microprice (see e.g. Cartea *et al.* 2015) is a statistic that is related to the midprice but whereas the midprice is calculated only from price data, the microprice is a quantity-weighted calculation. If the LOB's current best bid price and quantity are denoted by P_b and Q_b respectively, and the current besk ask price and quantity by P_a and Q_a respectively, then the microprice P_μ is given by:

$$P_\mu = P_a\,(Q_b\,/\,(Q_a{+}Q_b)) + P_b\,(Q_a\,/\,(Q_a{+}Q_b))$$

When $Q_a = Q_b$ this reduces to the equation for the midprice P_m, but as the difference or *imbalance* between Q_a and Q_b grows so the difference between P_μ and P_m increases, with P_m remaining constant but P_μ moving in the direction that subsequent transaction prices can reasonably expect to head in, given the current imbalance in supply and demand and assuming all other things remain equal. This captures the intuitive notion that, in times of excess demand, competition among buyers is likely to push prices up toward the best ask price, while in times of excess supply, competition among sellers is likely to push prices down toward the best bid price: in each case, the microprice moves in the corresponding direction. An important factor to note here is that the microprice gives an indication of the expected direction of change in transaction prices, *before* any transactions affected by market impact have actually taken place. Figure 2 illustrates the effect that size imbalances at the top of the LOB can have on the microprice: The left-hand table illustrates the case where there is excess demand; the right-hand table shows a situation with excess supply. The midprice is the same in each case, but the size imbalance skews the microprice either down or up, depending on whether there is an excess of supply or demand. The Δ value indicated above each table is the difference between the midprice and the microprice.

To distinguish the original SHVR from the adapted/extended version, we will refer to the latter as ISHV (pronounced *eye-shave*; the *I* can stand for *imbalance*, or for *impact*).

	midprice=	150.0	
	microprice=	190.9	
	Δ=	40.9	
	BID	ASK	
Qty	Price	Price	Qty
10	100	200	1
1	99	201	1
1	98	202	1
1	97	203	1
1	96	204	1
1	95	205	1
1	94	206	1

	midprice=	150.0	
	microprice=	109.1	
	Δ=	40.9	
	BID	ASK	
Qty	Price	Price	Qty
1	100	200	10
1	99	201	1
1	98	202	1
1	97	203	1
1	96	204	1
1	95	205	1
1	94	206	1

Figure 2: effects of size imbalances on the microprice.

In the current version of ISHV, the amount that the trader shaves off the current best counterparty price on the LOB (denoted by Δs, and which in the original SHVR was a constant, equal to the exchange's tick-size Δp) is determined by the imbalance at the top of the LOB, the difference between the midprice and the microprice, which we refer to as Δm:

$$\Delta m = P_\mu - P_m$$

Intuitively, if there is no imbalance, $\Delta m{\sim}0$; if $\Delta m{>>}0$, the imbalance indicates that subsequent transaction prices will increase; and if $\Delta m{<<}0$, the indication is that prices will subsequently fall. This can be formalized in ISHV by defining an *impact function, F,* that maps from Δm to Δs, i.e. $\Delta s{=}F(\Delta m)$. We have explored a number of forms for the impact function, and the results that we present here have been generated from a simple linear form expressed as pseudocode in Figure 3.

The rationale for this impact function is straightforward: at the macro level buyers and sellers react in symmetrically complementary ways; if the imbalance indicates that the price will be worsening for a trader, the trader reacts by attempting to shave a proportionately larger amount off of the best price on the LOB, thereby lowering its potential profit on the trade, but at least trying to "stay in the game", maintaining its chances of actually getting a deal. Conversely, if the imbalance indicates that prices will be improving for the trader (i.e., prices are likely to move in favor of the trader, because of excess quantity on the counterparty side of the book), the ISHV trader reduces the amount it shaves off the best price: here, it sets the shave-amount to the smallest possible, the exchange's tick-size Δp. Finally, for that reduction in shaving when the price is moving in the trader's favor to be meaningful, ISHV's "default" shave-amount at $\Delta m = 0$ (which was uniformly Δp for the original SHVR) the constant C should be >1: here we use C=2. In the current impact function, for both buyers and sellers, the scaling of Δs as $|\Delta m|$ increases is linear with M=1: avenues for further research include studying the effects of varying the values of C and M, and/or using a nonlinear form for $F(\Delta m)$.

To explore the extent to which a BSE market populated with ISHV traders can act as a reasonable model of market impact, we devised experiments that are somewhat artificial in comparison to the dynamics of real markets, but in which the artificial constraints have been introduced to help clarify any market impact effects. We create a market with N buyers and N sellers, and initially all buyers and sellers are given assignments to trade in maximum quantities of one (so, after traders have issued quotes to the exchange, the quantity columns in the LOB resemble those of Figure 1), and with prices according to a fixed supply and demand schedule with a known underlying theoretical equilibrium price, denoted by P_0. Traders are given a period of time to interact via the exchange's LOB-based auction mechanism, settling to a steady state, and then at a specific time a lone trader is given an assignment to either buy or sell a large quantity of the asset at a price which places that trader's order at the top of the LOB (creating a situation on the LOB much like those illustrated in Figure 2). This single large order can be thought of as a step-change "shock" to the market; albeit a quantity-shock rather than a price-shock. We then monitor what happens to the prices quoted on the LOB, and to any subsequent transaction prices, as the traders in the market respond and adapt to the post-shock conditions.

```
if (buying)
then if Δm < 0
        then Δs = Δp
        else Δs = CΔp + M.Δm.Δp
        if P_b + Δs <= p_lim
        then q = P_b + Δs
        else q = p_lim

if (selling)
then if Δm > 0
        then Δs = Δp
        else Δs = CΔp – M.Δm.Δp
        if P_a – Δs >= p_lim
        then q = P_a – Δs
        else q = p_lim
```

Figure 3: pseudocode for the ISHV imbalance-sensitive decision tree that sets Δs, the amount an ISHV attempts to shave off the current best price on the LOB, and then uses that to set q, the price that the trader quotes in the market. Δm is the difference between the microprice and the midprice; Δp is the exchange's tick-size; p_{lim} is the limit price on the current assignment (i.e., the customer order being worked); P_a is the price of the best ask on the LOB; P_b is the price of the best bid; and the constants C and M are parameters that determine the ISHV's linear response to the imbalance.

It is important to note that our work differs from the norm in studies of market dynamics because we are primarily focused here on changes in the prices that are quoted by the traders in response to an imbalance occurring at the top of the LOB, *before* the next transaction takes place, rather than on the nature of the longer-term time series of a sequence of successive transactions in that market. Because the system is inherently stochastic, we repeat this basic shock-test some number of times, and then generate relevant visualizations and calculate summary statistics.

Figure 4 shows the typical price dynamics of a market populated homogeneously by 20 ISHV traders (i.e., N=10) and in which no quantity shock occurs. Fresh customer orders (i.e, exogenous commands to either buy or to sell a specified quantity of the asset, with an associated maximum-purchase-price or minimum-sale-price) are assigned to the 10 buyers and the 10 sellers every 20 seconds, starting at t=20: the graph shows the prices quoted by each of the 10 buyers and 10 sellers. For each ISHV trader, after it has been assigned a customer order, it then quotes a price when prompted to: if its side of the LOB is empty, the price it quotes is based on the limit price for its current assignment; but if its side of the LOB does already show a best price, then ISHV attempts to improve on that price by calculating its own value for Δs according to the method shown in Figure 3, and then adding that Δs to the best price (when the assignment is to buy) or subtracting it (when the assignment is to sell). As can be seen from Figure 4, the prices quoted by a population of ISHV buyers and sellers converge and meet at a value close to (but not necessarily exactly equal to) P_0, and transactions then occur when the prices quoted by the traders start to cross the spread. The convergence is steady and stable (i.e., once converged, the transaction prices remain close to P_0), and repeats once every 20 seconds as fresh assignments are distributed to the traders. Figure 5 shows the market impact effects of a single buy order suddenly increasing the quantity supplied, pushing the prices up rapidly *before* a transaction occurs; for brevity we do not show here a similar figure illustrating the corresponding market impact effect of a single sell order suddenly increasing the quantity demanded, but the dynamics in that case are very similar: arrival of a sell block order pushes the prices down *before* a transaction occurs. In both cases, arrival of a block order triggers a a price move against the block trader: when trying to execute a large buy order, quoted prices rise; when trying to execute a large sell order, quoted prices fall; and in both cases the price shift occurs before any transaction takes place. These results demonstrate that, in the single lit-pool version of BSE populated by ISHV traders, market impact is as genuine a concern as in real markets: that is, the dynamics of our model market do capture size impact effects, and so can function as a valuable first approximation for studying impact effects in real-world markets. Having established that our simulated market traders can now demonstrate market impact effects, the next section briefly describes our extension of BSE to incorporate a coupled dark pool, and discusses its effectiveness in reducing market impact.

4. DARK POOL CUTS MARKET IMPACT

We altered the public-domain source-code of BSE, extending its functionality to include a coupled pair of dark and lit pools. In the first instance, the two pools are identical objects: each has the full LOB functionality of the original BSE lit-only trading pool, except that that details of orders sat on the dark pool are not published by the exchange, i.e. the traders do not know any details of orders sat on the dark LOB, other than their own orders. A very simple order-routing mechanism was implemented whereby, when the exchange receives an order, if the size of the order is below a threshold value then the order is "small" and is sent to the lit pool for processing, whereas orders larger than the threshold are "block" sized and hence processed by the dark pool.

Because ISHV traders use only the lit-pool microprice, this simple mechanism is sufficient to eliminate market impact effects for orders sized above the block threshold: now larger orders do not appear on the lit LOB, and so the prices quoted by the population of ISHV traders are now unaffected by the arrival of any such block orders.

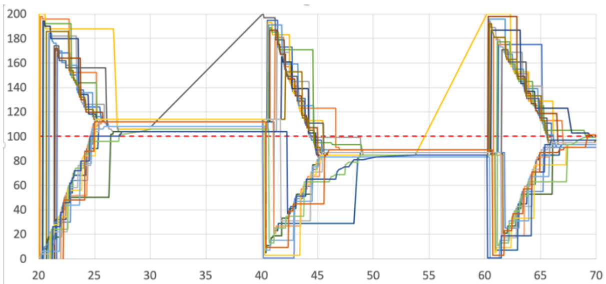

Figure 4 time-series of the prices being quoted by 20 ISHV traders (10 buyers and 10 sellers) across three successive batch assignments of customer orders: horizontal axis is time; vertical axis is price; each trader's current quote-price is represented by a single line. Fresh customer orders, one order per trader and each order for a quantity of one, are redistributed every 20 seconds: price competition among the sellers and buyers results in convergence toward prices close to the P_0 value of \$1.00 (indicated by the horizontal dashed line). After each batch of assignments, the actual price converged to varies slightly from the underlying P_0 value, but the deviation is never large.

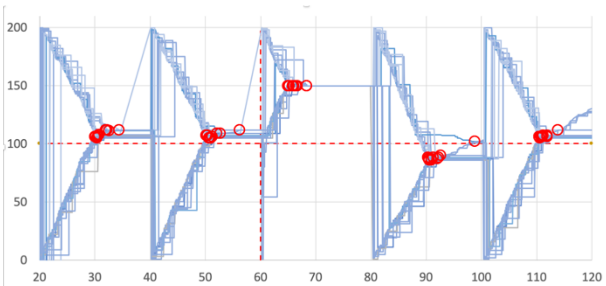

Figure 5: quote-prices and transaction prices showing quantity-impact effect in a market populated entirely by ISHV traders. These data come from the same structure of experiment as described in the caption to Figure 4, but here all the traders' individual quote-prices are the same pale blue colour, and the time and price of individual transactions are illustrated as red circles. At time t=60 (indicated by the vertical dashed line), a single large buy order (quantity=200) is assigned to one trader, imposing a step-change quantity shock on the market's demand schedule. The ISHV strategy detects the imbalance between supply and demand at the top of the LOB and reacts by rapidly increasing buyer's quote prices before any transactions take place: transactions then occur at prices around \$1.50, a large deviation from P_0. After that, the large order is removed from the market and prices return to the previous equilibrium.

It is important to note that, in practice, the effectiveness of such a simple coupled lit/dark pair of pools is potentially open to exploitation by unscrupulous traders who deliberately submit orders with sizes large enough to be routed to the dark pool, but who then delete those orders once they have partially completed (i.e., once they have been matched with one or more smaller orders). To guard against this, LSE Turquoise has mechanisms for tracking the "reputation" of traders who use the dark pool, and only traders with a sufficiently high reputation are permitted ongoing use. Our simulation of the LSE Turquoise reputation-based access system, described in detail in (Church, 2019), is discussed in the next section.

5. REPUTATIONAL DARK POOL ACCESS

Turquoise Lit is a LOB-based exchange in which the LOB is made visible to all participants, and hence Turquoise Lit can be simulated by the existing BSE functionality as documented by Cliff (2018a, 2018b) and does not need to be discussed further here. However, BSE does not have any dark-pool functionality, nor any reputation-scoring system, and so the focus in this section is on describing those two aspects of LSE Turquoise. In Section 5.1 we introduce the Plato dark pool, and then in Sections 5.2 to 5.6 we introduce various aspects of the Plato operation that are involved in the reputational scoring, which is described in Section 5.7.

5.1. The Turquoise Plato Dark Pool

Plato is the dark pool service offered by Turquoise. Orders submitted to Turquoise Plato are added to the Turquoise Plato Order Book, which we refer to here as TPOB. TPOB is not made visible to the participants in Turquoise Plato, as is expected of a dark pool trading venue; however, the details of each trade that takes place are subsequently made public, after the trade completes. The Turquoise documentation refers to bids as *buy orders* and asks as *sell orders,* so we use that terminology here. Buy orders rest on the buy side of TPOB and sell orders rest on the sell side of TPOB. All trades that take place within Turquoise Plato execute at the midprice of the LOB on the primary (i.e., lit) market for the financial instrument being traded. The primary market is the trading venue where the financial instrument was first admitted to trading. Orders submitted to Turquoise Plato can specify an optional limit price. For an order with a limit price to be able execute, the limit price must be better than the current primary market midprice. Orders can also specify an optional Minimum Execution Size (MES). The MES specifies the minimum quantity that can be traded in that order. For example, say that a trader submits a buy order X with a quantity of 20 and a MES of 10. Say that another trader submits a sell order Y with a quantity of 15 and a MES of 12. These orders can be matched for a trade since the quantity of each order is greater than the MES of the other order. A quantity of 15 will be traded in this case. Now, let's say that instead of sell order Y, a sell order Z was submitted with a quantity of 9 and a MES of 5. In this case the buy order X and sell order Z will not be matched for a trade since the quantity of Z is less than the MES of X. Orders also have a duration attribute which determines how long the order will rest on TPOB, if at all. The duration can be set as *Fill-or-Kill* (FOK), which means that the order must be able to execute immediately and in full or it will not be executed at all, and will not be added to TPOB. The duration can also be set as *Immediate-or-Cancel* (IOC), meaning that the order must be able to execute immediately either fully or partially otherwise it will be cancelled; if the order is only partially executed then the remaining quantity of the order will not be added to TPOB. The duration of an order may also be specified as an expiration time which will cause the order to rest on TPOB until either it is fully executed or the expiration time is reached. Orders that lie on TPOB until execution or expiry are known as *persistent* orders.

Persistent orders with larger quantities are given a higher priority when order-matching occurs. If two orders have the same quantity, then the order with the earlier arrival time is given the higher priority. If an order is only partially executed, the remaining unexecuted portion of that order maintains the priority that the whole order was first assigned on the basis of its initial quantity.

When trying to match persistent orders, matching starts with the highest-priority buy order. The sell orders are then checked in priority order, from highest to lowest, to see if they can match with the buy order for a trade. If no match is found for this buy order, then the next highest priority buy order is selected for matching, and the process is repeated. When a match is found between a buy order and a sell order, the trade is executed. This process of matching orders and executing trades operates continuously and is referred to as *continuous matching mode*.

5.2. Block Discovery

Turquoise Plato offers an additional service called Block Discovery which is intended to be used by traders that wish to place block orders. Block Discovery allows a trader to first tentatively identify if there are any counterparties that can match their block order before they commit to submitting a firm order. This is done by the trader first submitting a Block Indication (BI). A BI is an indication to the exchange that a trader wants to place a block order, but this is not yet a firm order. Within the BI, the trader specifies the details of the firm order that they are interested in submitting. This includes the quantity, the limit price, the MES, and the duration. Turquoise’s matching logic then attempts to match the trader's BI with another BI submitted by a different trader. Once a match between two BIs is found, the traders that submitted the BIs are each sent an Order Submission Request (OSR) notifying them of the match. The OSRs ask the traders to convert their BIs into firm orders by sending a Qualifying Block Order (QBO). The QBO specifies the final details of the firm order that the trader will now be submitting. The details that a trader specifies in a QBO can be different from the original details specified in the BI. Each trader has a reputational score, and if the details specified in the submitted QBO are different from the corresponding BI, then the trader's reputational score may be negatively affected. Once the QBOs are received from both traders, the firm orders specified in the QBOs are submitted to the TPOB. The matching of these orders and the execution of the trade will then take place. To summarize, the main steps that occur in the Block Discovery process are: (1) a trader submits a BI; (2) if a match is found for that BI, then the trader is sent an OSR to notify them; (3) the trader places a firm order by submitting a QBO; (4) the firm order is added to the TPOB and the trade takes place; (5) the trader's reputational score is updated.

5.3. Block Indication (BI)

A BI is not a firm order, but an indication to the Block Discovery service that the trader is interested in placing a firm order. The trader first wants to see if any counterparty can match their order. The BI contains details about the firm order that the trader would like to place, such as the quantity, the limit price, the MES, and the duration. The limit price and the MES are optional and can be omitted. The quantity specified in the BI must be greater than the Minimum Indication Value (MIV) for the financial instrument being traded. If the quantity is not greater than the MIV, then the BI will be rejected by the Block Discovery service. Whenever a BI is added to the exchange, a check is performed to see if any submitted BIs can be matched for trading. The priority of each BI in the matching process is determined in the same way as it is for orders. If the BI specifies an MES and/or a limit price, then these values are considered in the matching process. Once a match is found for a BI, then the trader is sent an OSR to notify them.

5.4. Order Submission Request (OSR)

An Order Submission Request is sent to a trader to notify them when a match is found for a BI that they submitted. The OSR does not include any details about the counterparty or the counterparty's BI that it was matched with. The OSR is also used to notify the trader of their reputational score. Upon receiving an OSR, a trader is expected to respond with a QBO in order to submit a firm order.

5.5. Qualifying Block Order (QBO)

A Qualifying Block Order is sent by a trader to the exchange upon receipt of an OSR. The OSR tells the trader that their BI has been matched with another BI on the exchange. The QBO is a confirmation of their BI; turning their indication into a firm order. The details specified in the QBO may be different from the details specified in the original BI. This recognizes that sometimes a trader's preferences or circumstances change after a BI is submitted. For example, the QBO could specify a smaller quantity or a higher limit price that in the original BI. The differing details between a QBO and the corresponding BI will affect the trader's reputational score. If a QBO's details are sufficiently different from the original BI that the trade becomes impossible, this will have a negative impact on the trader's reputational score. Once the QBOs are received from both traders, the firm orders are added to the TPOB and the trade can take place.

5.6. Block Discovery Notification (BDN)

When a trader submits an order, they can specify whether the order is a Block Discovery Notification (BDN). If an order is a BDN, then the order is eligible for participation in the Block Discovery service. This means that the order may end up getting matched with a BI. An order can only be a BDN if the quantity of the order is greater than the Minimum Notification Value for the financial instrument being traded. If the order is matched with a BI, then the trader that submitted the BI is notified with an OSR as usual. The trader that submitted the BI is not made aware that they have been matched with a BDN order.

5.7. Reputational Scoring

The Block Discovery service monitors each trader’s conversion from BIs to QBOs with a reputational scoring system. A trader is given an event reputational score (ERS) every time they convert a BI into a QBO. A QBO should be *marketable* in comparison to its corresponding

BI. In relation to price, a QBO is marketable if it meets any of the following criteria:

- The BI does not specify a limit price and the QBO does not specify a limit price.
- The BI specifies a limit price and the QBO does not specify a limit price.
- The BI specifies a limit price and the QBO specifies a more marketable limit price. When buying, this means that the QBO limit price must be greater than the BI limit price. When selling, this means that the QBO limit price must be less than the BI limit price.

In relation to the MES, a QBO is marketable if it meets any of the following criteria:

- The BI does not specify an MES and the QBO does not specify an MES.
- The BI specifies an MES and the QBO does not specify an MES.
- The BI specifies an MES, and the QBO specifies an MES that is less than or equal to the BI's MES.

If a QBO is not marketable, then the ERS given to the trader is zero. If the QBO is marketable, then the ERS is calculated by considering the difference in the quantity specified in the BI and the quantity specified in the QBO. The resulting ERS will be between 50 and 100. The exact formula used to calculate the score in this case is not explicitly specified in the public documentation for Turquoise Plato, so in our simulation we have a heuristic rule that can be edited to explore different approaches.

A trader's composite reputational score (CRS) is calculated from a weighted sum of their last 50 individual ERSs, with more recent scores having higher weights. A trader is notified of their CRS in every OSR that they receive. If a trader's CRS falls below the exchange's Reputational Score Threshold (RST), then the trader will no longer have access to the Block Discovery service. A trader's CRS persists from one day to the next; any trader with a CRS less than the RST can in principle increase it over time by issuing a succession of BIs and matching QBOs where each QBO does meet the commitments of the corresponding BI.

Figure 6, from Church (2019), shows how an individual trader's CRS changes over time when the trader consistently responds with a QBO having the exact same details as the corresponding originally submitted BI. The trader receives an ERS of 100 every time they convert a BI into a QBO which results in the trader's CRS rising over time.

Figure 7, also from Church (2019), shows how an individual trader's CRS changes over time when it consistently returns a QBO with a quantity half that of the originally submitted BI. This results in the trader receiving an ERS of 50 every time they convert a BI into a QBO. This causes the trader's CRS to fall from its initial value over time. Eventually, the trader's CRS falls below the RST: at this point, the trader is no longer allowed to participate in the Block Discovery service.

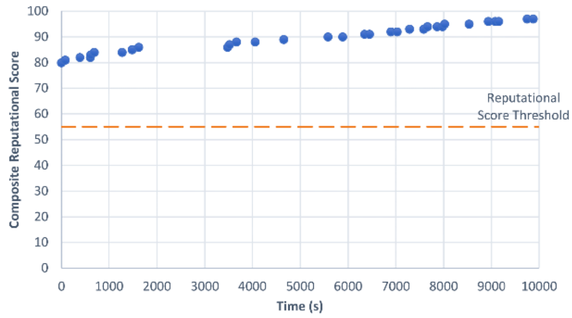

Figure 6: rise in a single trader's composite reputational score over time, when the trader is consistently responding with QBOs that match the corresponding BIs.

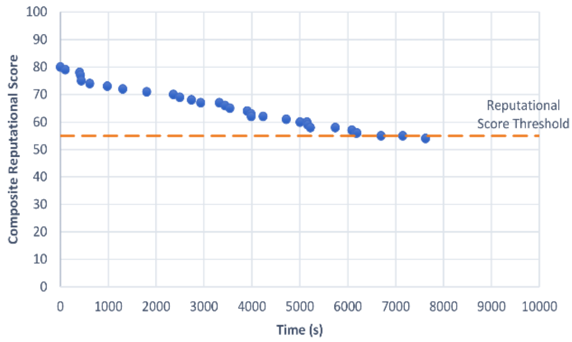

Figure 7: fall in a single trader's composite reputational score over time, when the trader is consistently responding with QBOs that are under-sized with respect to the corresponding BIs: eventually the composite reputational score falls below the system's RST and the trader can no longer access the Block Discovery service.

6. FUTURE WORK

Currently one aspect of our BSELD simulator that requires further work is the implementation of functionality that models *Turquoise Plato Uncross.* Uncross events occur many times in each trading day. These events are triggered by the matching of block indications, or at random time intervals if no triggers have fired for a sufficiently long time.

Further work could also be devoted to taking ISHV's use of the difference between the market's midprice and microprice as an indicator of order-book imbalance likely to have an impact effect, and incorporating that or a similar mechanism into well-known high-performing trading strategies such as AA, GDX, or ZIP.

7. SUMMARY AND CONCLUSIONS

To the best of our knowledge, this is the first published account of a functional simulation of the LSE Turquoise coupled lit/dark pools and associated reputation-based order management system. For us to demonstrate the utility of BSELD, it was necessary to create a new type of automated trading agent, one that is sensitive to imbalances in the quantities on the limit order book and which in consequence exhibits market impact behaviors in its pricing: we have done that with ISHV, presented here for the first time, and as far as we are aware ISHV is the only public-domain automated trader that can be used in this way, to explore market impact issues. Thus the two primary contributions of this paper are the first-ever demonstration of size-related impact effects in markets populated by automated traders, via our introduction of the ISHV strategy; and the reduction (to the point of elimination) of those impact effects via the introduction of mechanisms in BSELD that are closely modelled on the LSE Turquoise trading platform.

By adding the code for our BSELD simulator, and the ISHV trader, to the public-domain BSE repository on GitHub we are providing a tool that can be widely used as the platform for a large range of further research in experimental economics, market microstructure, automated trading, and computational finance. Providing BSELD as a freely-available shared common platform for such research is intended to facilitate replication and extension of results, and to ease the work of researchers wanting to study the behavior of automated trading systems in truly contemporary market environments.

8. REFERENCES

Arnuk, S., & Saluzzi, J., 2012. *Broken Market: How High-Frequency Trading and Predatory Practices on Wall St are Destroying Investor Confidence and your Portfolio.* Financial Times / Prentice Hall.

Bodek, H. & Dolgopolov, S, 2015. *The Market Structure Crisis: Electronic Stock Markets, High Frequency Trading, and Dark Pools.* CreateSpace Publishing.

BSE, 2012. *The Bristol Stock Exchange*. On GitHub at github.com/davecliff/BristolStockExchange

Cartea, A., Jaimungal, S., & Penalva, J., 2015. *Algorithmic and High-Frequency Trading*. Cambridge University Press.

Church, G., 2019. *Extending the Bristol Stock Exchange with a Dark Pool.* Master's Thesis, Department of Computer Science, University of Bristol.

Cliff, D., 1997. *Minimal-Intelligence Agents for Bargaining Behaviours in Market-Based Environments.* Hewlett-Packard Labs Technical Report HPL-97-91.

Cliff, D., 2018a. BSE: A Minimal Simulation of a Limit-Order-Book Stock Exchange. In: M. Affenzeller, A. Bruzzone, *et al.* (eds) *Proceedings. of the European Modelling and Simulation Symposium (EMSS2018)*, pp.194–203.

Cliff, D., 2018b. "An Open-Source Limit-Order-Book Exchange for Teaching and Research." *Proc. IEEE Symposium on Computational Intelligence in Financial Engineering (CIFEr)*, pp.1853–1860.

Cliff, D., 2019. "Exhaustive Testing of Trader-agents in Realistically Dynamic Continuous Double Auction Markets: AA Does Not Dominate". In: *Proceedings ICAART 2019*, Vol.2: 224–236; ScitePress.

Das, R., Hanson, J., Kephart, J., & Tesauro, G., 2001. "Agent-Human Interactions in the Continuous Double Auction". *Proc. International Joint Conference on AI.* (IJCAI'01), pp.1169–1176.

De Luca, M., & Cliff, D., 2011. Human-Agent Auction Interactions Adaptive-Aggressive Agents Dominate. *Proceedings of the International Joint Conference on AI* (IJCAI-2011), pp.178–185.

De Luca, M., 2015. *Adaptive Algorithmic Trading Systems.* PhD Thesis, Department of Computer Science, University of Bristol, UK.

Gjerstad, S. & Dickhaut, J., 1998. Price Formation in Double Auctions. *Games & Economic Behavior*, 22(1):1–29.

Gjerstad, S., 2003. *The Impact of Pace in Double Auction Bargaining.* Working Paper, Department of Economics, University of Arizona.

Gode, D. & Sunder, S., 1993. Allocative efficiency of markets with zero-intelligence traders: Market as a partial substitute for individual rationality. *Journal of Political Economy*, 101 (1):119–137.

Harris, L., 2002. *Trading and Exchanges: Market Microstructure for Practitioners*. Oxford University Press.

London Stock Exchange Group, 2019a. *Turquoise Plato Block Discovery (V2.26.2)*: bit.ly/2ZPJAi0.

London Stock Exchange Group, 2019b. *Turquoise Trading Service Description (V3.34.9j)*: bit.ly/2Y1jWFi.

Narang, R., 2013. *Inside the Black Box: The Simple Truth about Quantitative Trading.* Second Edition. Wiley Finance.

Palmer R., Rust, J., & Miller, J. 1992. Behavior of Trading Automata in a Computerized Double Auction Market. In D. Friedman, & J. Rust (Eds.), *Double Auction Markets: Theory, Institutions, Laboratory Evidence.* Addison Wesley.

Patterson, S., 2013. *Dark Pools: The Rise of AI Trading Machines.* Random House.

Pentapalli, M., 2008. *A comparative study of Roth-Erev and Modified Roth-Erev reinforcement learning algorithms for uniform-price double auctions.* PhD Thesis, Iowa State University.

Rodgers, K. 2016. *Why Aren't They Shouting? A Banker's Tale of Change, Computers, and Perpetual Crisis.* RH Business Books.

Stotter, S., Cartlidge, J., and Cliff, D. 2013. "Exploring assignment-adaptive (ASAD) trading agents in financial market experiments", *Proceedings ICAART2013*, 1:77–88.

Tesauro, G. and Das, R. 2001. "High-performance Bidding Agents for the Continuous Double Auction". *Proceedings of the 3rd ACM Conference on Electronic Commerce,* pp.206–209.

Tesauro, G. and Bredin, J., 2002. "Sequential Strategic Bidding in Auctions using Dynamic Programming". In *Proceedings AAMAS 2002*.

Vach, D., 2015. *Comparison of Double Auction Bidding Strategies for Automated Trading Agents.* Master's Thesis, Charles University in Prague.

Vytelingum,P., 2006. *The Structure and Behaviour of the Continuous Double Auction.* PhD Thesis, University of Southampton.

Vytelingum, P., Cliff, D., & Jennings, N., 2008. "Strategic Bidding in Continuous Double Auctions". *Artificial Intelligence*, 172(**14**):1700–1729.

A CLOUD-NATIVE GLOBALLY DISTRIBUTED FINANCIAL EXCHANGE SIMULATOR FOR STUDYING REAL-WORLD TRADING-LATENCY ISSUES AT PLANETARY SCALE

Bradley Miles[(a)] **Dave Cliff**[(b)]

Department of Computer Science
University of Bristol, Bristol, BS8 1UB, U.K.

[(a)]bm15731.2015@my.bristol.ac.uk, [(b)]csdtc@bristol.ac.uk,

ABSTRACT

We describe a new public-domain open-source simulator of an electronic financial exchange, and of the traders that interact with the exchange, which is a truly distributed and cloud-native system that been designed to run on widely available commercial cloud-computing services, and in which various components can be placed in specified geographic regions around the world, thereby enabling the study of planetary-scale latencies in contemporary automated trading systems. The speed at which a trader can react to changes in the market is a key concern in current financial markets but is difficult to study latency issues using conventional market simulators, and is extremely difficult to study "in the wild" because of the financial and regulatory barriers to entry in conducting experimental work on real financial exchanges. Our simulator allows an exchange server to be launched in the cloud, specifying a particular geographic zone for the cloud hosting service; automated-trading clients which attach to the exchange can then also be launched in the cloud, in the same geographic zone and/or in different zones anywhere else on the planet, and those clients are then subject to the real-world latencies introduced by planetary-scale cloud communication interconnections. In this paper we describe the design and implementation of our simulator, called DBSE, which is based on a previous public-domain simulator, extended in ways that are partly inspired by the architecture of the real-world Jane Street Exchange. DBSE relies fundamentally on UDP and TCP network communications protocols and implements a subset of the FIX *de facto* standard protocol for financial information exchange. We show results from an example in which the exchange server is remotely launched on a cloud facility located in London (UK), with trader clients running in Ohio (USA) and Sydney (Australia). We close with discussion of how our simulator could be further used to study planetary-scale latency arbitrage in financial markets.

Keywords: cloud-based simulations, financial exchanges, electronic markets, automated trading.

1. INTRODUCTION AND MOTIVATION

1.1 Algorithmic Trading & Experimental Economics

Since the dawn of the first financial exchange – the Amsterdam Stock Exchange in 1602 – until the introduction of computer aided trading in the 1970s, the buying and selling of financial products, such as shares and bonds were executed by the verbose shouting of highly-paid individuals on the floors of major financial exchanges. By today's standards, these interactions between skilled human traders were slow, inefficient, and often error prone. Consequently, as soon as the relevant technologies were available, the buying and selling of financial products became a digital interaction and the traditional trading floors in national financial exchanges around the world were gradually closed. Modern-day electronic financial exchanges are highly sophisticated and complicated distributed computational systems that enable institutions, such as investment banks, fund managers, brokers, and insurance companies, to remotely connect and trade on the world's open markets. Although the transition from physical to electronic markets was largely complete (or, at least, inevitable) by the end of the 20th Century, at the turn of the millennium most trades were still executed by humans. Since then, as computer hardware capabilities improved and as regulatory barriers were lowered, the financial markets underwent a second technological revolution: the widespread introduction of automated software systems that replace human traders.

In many major present-day markets, the majority of trades are executed by sophisticated autonomous adaptive computational systems. These automated systems (known variously within the industry as *trading agents*, *algo traders*, or *robot traders*) can be responsible at any one major investment bank for weekly trading flows of $100Bn or more. Early automated trading systems failed to match the behavior of human traders, but in 2001 a research team at IBM's TJ Watson Labs published results (Das *et al.* 2001) from an experiment that tested the effectiveness of two adaptive trading algorithms, known as GD (Gjerstad & Dickhaut 1998) and ZIP (Cliff 1997). Using heterogeneous populations of humans and agents, the IBM researchers discovered that the GD and ZIP trading algorithms could consistently outperform human traders with respect both to efficiency and to profitability. In the past 15 years, the rising penetration of this technology has transformed the financial markets into a world of predominantly robotic traders, not necessarily a change for the better, as documented by Arnuk & Saluzzi (2012), Bodek & Dolgopolov (2015), Cartea *et al.* (2015), Narang (2013), Patterson (2013), and Rodgers (2016). For a comprehensive introduction to exchanges and trading, see Harris (2002).

Robot traders are capable of processing vast amounts of data and can react to market changes at millisecond speeds. Consequently, trading agents are considered by some to be vastly superior to human traders because not only are they more profitable, but also their operating costs are often substantially cheaper. Now, rather than hiring lots of human traders, a trading house can instead clone robotic agents and deploy them to multiple servers, with the primary operational costs no longer being salaries and bonuses but instead being those associated with maintaining the trading software, and the server-hardware that it runs on. Many financial institutions and proprietary trading firms now focus solely on the research and development of more intelligent, faster, and more profitable advanced trading algorithms. However, investing in algorithms that can quickly make intelligent trading decisions is not all that is required: many trading houses also make major investments in reduction and mitigation of telecommunications latency. The reason for this concentration on latency is best illustrated by an example: if two competing, identical agents are listening to market events from the same exchange, the one which can receive and respond the quickest will be the most profitable, because its actions in the market may well require the slower agent to re-think, i.e. to re-start the process of deciding what to do next. Hence being the cleverest trader is not necessarily a guarantee of riches: if a slightly less clever, but much faster, trader is active in the market, that trader's sheer speed may be enough for it to outperform the greater brainpower of the cleverer trader. The industry in recent years has been focused on a battle to minimize latency between robotic agents and exchanges (see e.g. Haldane 2011). This enables trades to be fulfilled electronically at super-human speeds, potentially trading multiple times per second, a practice known as High Frequency Trading (HFT).

In conjunction with these real-world developments, academics have been exploring the profitability of both human and robotic traders with experiments and simulations for decades. In 2002, the Nobel Prize in Economics was awarded to Vernon Smith, for his ground-breaking work in establishing a new field of research now known as *Experimental Economics*. Starting in the late 1950's, Smith worked on a series of laboratory experiments which demonstrated that the behavior of human traders could be studied empirically under controlled and repeatable laboratory conditions: see e.g. Smith (1992), and Kagel & Roth (1997, 2016).

In 2012, a minimal simulation of a modern-day electronic financial market was released as free open-source software, as a tool for teaching and research on automated trading algorithms: this software is the *Bristol Stock Exchange* (BSE), documented in (BSE, 2012) and in (Cliff 2018a, 2018b). BSE allows experiments in the style pioneered by Smith to be run in simulation on a standard laptop or desktop computer. A simulated market requires virtual traders, and BSE includes source-code for a number of robot-trading strategies, including: *Giveaway* (Cliff, 2018a); *Zero-Intelligence-Constrained* (ZIC: see Gode & Sunder 1993); *Shaver* (Cliff, 2018a); *Sniper* (inspired by Kaplan's Sniper strategy described by Palmer *et al.* 1992); and *Zero-Intelligence-Plus* (ZIP: Cliff 1997). Within the BSE documentation, these strategies are referred to via three- or four-letter codes: GVWY; ZIC; SHVR; SNPR; and ZIP, respectively. Despite BSE's success as an introductory teaching aid, it has significant limitations compared to real-world distributed financial exchanges: the most notable of which, like many other financial exchange simulations, is that BSE is only a minimal approximation to a fully distributed real-time system, and therefore critically it assumes absolutely zero latency in the communications between trader and exchange. Yet, as noted above, minimizing the latency of robotic agents is an integral part of their design and operation, and thus simulating robot traders without also modelling latency is a major limitation to using BSE as a platform for leading-edge research. This paper addresses that limitation.

In the text that follows, we introduce a significantly extended and truly *distributed* version of BSE, referred to as DBSE. Like BSE, DBSE implements a financial exchange simulation that can be used with robotic agents; unlike BSE, DBSE allows for the creation of truly distributed experimental systems that operate asynchronously in real-time, and with real communications latencies. DBSE has been written as a cloud-native simulator: it has been designed from the outset so that constituents of DBSE can be launched in cloud data-centers around the world, enabling the user of DBSE to set up a truly planetary-scale distributed system consisting of an exchange server that provides connectivity to trading clients at various disparate locations on the planet. This allows for the study of mechanisms to deal with real-world communications latency, rather than simulated approximations of it. Practical use of DBSE is only possible because of the availability of low-cost remotely-accessible cloud-computing services: the example we give here (and for which we have released the code as open-source on GitHub) runs on Amazon Web Services but adapting it to any other major cloud provider would be trivial work. The ultimate output of the work reported here is our release of the DBSE code-base as open-source, that can be used by researchers and practitioners as a common platform for exploration of many other key questions within Experimental Economics.

1.2 Testing Robot Traders with Realistic Latency

A fundamental challenge with testing robot traders is answering the question of where you can test them. Running a prototype algorithm on a real-world financial exchange would be the most realistic test, however this carries a manifest risk of serious financial consequences if anything were to go wrong. Even if the losses were bearable, there are often significant regulatory barriers to also overcome. Consequently, it is preferable to test new agents in controlled simulations that accurately imitate real markets. Many organizations choose to use playback simulations, a process of replaying legacy real market data and recording how agents react to the changes in market events. These simulations are fundamentally flawed as the agent is not able to influence the change in market prices with its own activity: regardless of what the agent does, the prices on the simulated market immediately after the trader has sold or bought a large quantity of some asset will remain the same as if the trader had instead done nothing at all. The alternative is to build your own market simulator, one in which the actions of an individual trader really can have an immediate effect on the rest of the market, and the Bristol Stock Exchange (BSE) is an example of such a simulator.

BSE allows the user to configure how the supply and demand for a tradeable asset will change over time: this influences (but does not exclusively determine) the market price of that asset; critically, the actions of individual traders also influence prices on a moment-by-moment basis. The disadvantage however is that the trading agent is operating on data from a synthetic market. Whether a market simulator is based on legacy-data playback or on dynamically determined market prices, these simulations are very often designed to run on a single machine. In the case of BSE, the simulator runs in a single thread, with the operations of the exchange and all the active traders running via time-sliced simulation techniques operating in the application's sole thread. This results in absolute-zero latency between the traders and exchange because the agents continuously have perfect knowledge of the data broadcast by the exchange, and because their messages back to the exchange take exactly zero seconds to get there, significantly limiting the realism of the simulation. Other public-domain exchange/market simulators, such as De Luca's *Open Exchange* (De Luca & Cliff 2011; De Luca 2015) do run as distributed systems across a local-area network (LAN): in these there will be fundamentally non-zero latencies as network packets are communicated around the LAN, but at the level of the practitioners running the experiments these latencies are so small as to be treated as negligible, i.e. as effectively zero.

For these reasons, there is a strong requirement for better simulations, both in the academic and professional world: both academic researchers and professional industry practitioners care about latency not only as a source of frustrating delays, but also as an aspect of the market that could potentially be profitably exploited, via what is known as *latency arbitrage*.

Latency arbitrage involves exploiting time disparities in the market. The disparity may be between the public price of a stock and the latest market update, or it could be that one of several available trading venues (i.e., exchanges) is particularly faster or slower at processing and responding to orders than other venues, in which case there are ways of profitably exploiting the speed difference. High frequency trading (HFT) firms pay very large amounts of money for their computer systems to be as physically close to their target financial exchanges as possible and to have direct access to the market data publishing feeds. Latency arbitrage can be exploited when multiple exchanges are selling the same commodity, for example let's assume both the NASDAQ and the New York Stock Exchange (NYSE) are selling a stock XYZ. At time, t=0, the price of XYZ throughout America is constant. This is governed by the Securities Information Processor (SIP), which links all U.S. markets by processing and consolidating all quotes and trades from every trading venue into a single data feed (CTA, 2018). If a large trade was to occur on the NYSE, thus changing the price of XYZ on that exchange, market data would be published to both the SIP and along the direct data feeds to HFT firms. Due to the SIP consolidating market data, it is slightly slower than a direct feed to a HFT firm and so for a few fractions of a second, the price of XYZ on the NYSE is different to the NASDAQ. HFT firms can react to this disparity in price and buy or sell XYZ accordingly between the NYSE and the NASDAQ, before the NASDAQ even learns about the changed price from the SIP. Although perhaps a morally questionable practice, this is a technique that trading firms routinely use to make significant profits. Most market simulations, including BSE, have no concept of latency and thus it is impossible to simulate this style of trading. Understanding and developing techniques to minimize or exploit latency arbitrage is a constant demand in industry, and has also been the topic of academic research (see e.g. Wah & Wellman 2013; Duffin & Cartlidge 2018).

In this paper, which summarizes (Miles, 2019), we describe the design and construction of a distributed financial exchange that can test the profitability of trading agents in real-time with real latency. This work explores how real-world financial institutions and exchanges build their systems and communicate with each other across a distributed network for order placements, execution reports, and market data publications at scale, all whilst minimizing latency across the globe. Although our DBSE simulator was originally based on the publicly available BSE source-code, that code was extensively rewritten to provide more functionality to the executing agents, as well as removing the assumption of zero-latency. With suitable network configuration, users of this simulation will be able to remotely host a financial exchange at any location in the world where a cloud-hosting service is situated, and to connect numerous trading agents running on servers that are sited in regions that are geographically local or remote with respect to the server on which the exchange is running. Here we demonstrate the capabilities of this simulation deployed on the cloud compute and networking infrastructure provided by Amazon Web Services (AWS). Our work enables researchers and educators to design and evaluate new trading agents on a more realistic test-bed that utilizes the same communication technologies as real-world financial exchanges. DBSE has been designed and implemented with scalability in mind. This paper is our first description of DBSE, and there remain many opportunities to extend the project in various ways: we aim for the code-base to be accessible to all of those who wish to improve and work with it. The goal is to enhance the research and teaching capabilities of our software and for it to become a common platform: to the best of our knowledge DBSE is the first such globally distributable freely available open-source financial exchange simulation.

2. CASE STUDY: JANE STREET EXCHANGE

Running a successful electronic financial exchange can be a lucrative business, and technical details of commercially sensitive computer systems are rarely placed in the public domain. It is generally extremely difficult to find detailed information on the architectural designs of financial exchanges and even more challenging to find fine-grained descriptions of how trading firms organize their automated systems to place orders and use subscriptions to market data sources.

Nevertheless, on the 2nd February 2017, Jane Street Inc, a global liquidly provider and market-making company, published a technical presentation outlining a high-level overview of the design and development of their own financial exchange known as JX (Jane Street, 2017). Jane Street develop in-house proprietary models and use quantitative analysis to trade over $13 billion in equities worldwide in a single day. The motivation for the development of JX was due to their necessity to test new algorithms and financial models – much like the motivation for our work presented here. The JX exchange is based on the design of the American NASDAQ exchange and serves as a perfect exemplar for a real-world distributed financial exchange.

JX has been designed to satisfy many of the underlying requirements of a modern exchange, including dealing with high transaction rates, and aiming for consistently low response times, while maintaining fairness and reliability. It has been reported to handle messages rates in the 500k/second range with latencies in the single-digit microseconds. Below we summarize key roles and responsibilities of the individual micro-services on the JX internal private network and outline the key technologies that enable such high performance.

Figure 1 outlines the key components of the JX distributed limit order book financial exchange. The network backbone is represented by the thick purple line; any component above this line has no direct communication with the outside world and can be assumed to sit within a private subnet of the network.

All components below the network backbone are public facing and can connect to external clients either via the Internet or a paid private connection, at the exchange owner's discretion.

2.1. The Matching Engine (ME)

The matching engine (ME) is the heart of the exchange. It is a single, monolithic machine that holds all the current orders on the exchange in a Limit Order Book (LOB) data structure, as discussed by e.g. Harris (2002), Cartea *et al.* (2015), and Cliff (2018a, 2018b). These orders are kept in memory and the matching engine is responsible for identifying the buy and sell orders that can be matched to give each counterparty a transaction that satisfies their order. The JX Matching Engine sits within a strictly managed internal private network and receives and publishes message to a wide variety of other services on the client side of the network.

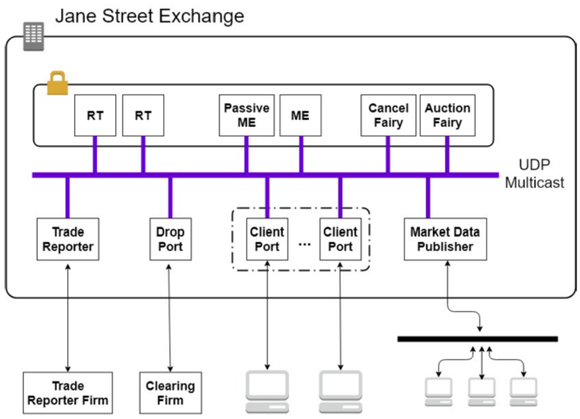

Figure 1: Architecture of the Jane Street Exchange.

Adjacent to the active Matching Engine is a passive copy that listens to all output of the active matching engine: this *Passive ME* is used as a fail-safe if the active engine has a system failure and goes offline, at which point the passive engine immediately takes control. In real-world exchanges this failover process is close to instantaneous to limit impact to clients and to the wider financial world.

2.2. Cancel Fairy & Auction Fairy

As previously stated, the ME is the critical component of a financial exchange and must losslessly deal with receiving thousands of messages a second. A large proportion of these messages however are not relevant to the live activities of the exchange; an example of which is the *cancel order* request message. At the end of a market session, it is common for clients to cancel all their live orders. Clients would send cancel order requests throughout the trading day but set a delay so that each of them is only executed at market close.

Historically, it was the responsibility of the ME to keep track of all these delayed cancel order requests. This however added noise to the matching engine, and thus modern exchanges offload this responsibility to an independent application, known as the *Cancel Fairy*. When a delayed cancel order request hits the ME, it would be acknowledged by the ME and then picked up by the Cancel Fairy. Once it is time for the order to be legitimately cancelled on the exchange, the Cancel Fairy would send a new cancel request that would be executed immediately by the ME.

In other non-continuous exchanges, there exists an additional process known as the *Auction Fairy*. It is used to aggregate many orders, often with overlapping prices, and runs an optimization to find a price that maximizes the shares traded. This process takes time and so is run independently. Once complete, the results are returned to the ME; another example of how modern distributed exchanges strive to limit the work done by the ME.

2.3. Re-Transmitter (RT)

In order to make communication across the network efficient and fair, all components communicate with each other via a technology known as UDP Multicast, discussed in more detail in Section 3.2. Critically this technology does not include guaranteed message delivery or acknowledgement and so messages can be lost during transmission. To account for this, a series of processes known as re-transmitters are added to the network. Their sole purpose it to record all the messages that have been seen on the network and to resend any message that was subsequently lost by a micro-service. Multiple re-transmitters are used in the event that one of them did not receive a message and thus they can communicate and reach consensus about the current state of the messages transmitted. In the unlikely event that all of the re-transmitters did not receive a message, they can request it from the ME, which maintains an in-memory copy of all messages sent in the current market day.

2.4. Client Port

Each Client Port is the main connection point for external financial institutions, such as brokers, investment banks, and fund managers wanting to trade on the exchange. The client ports accept connections to individual clients and provide a mechanism for them to perform transactions with the matching engine. This includes placing, amending and cancelling orders, requesting quotes and receiving execution reports on any trades that resulted from that client's orders.

2.5. Drop Port

The Drop Port is very similar to a Client Port, however it accepts connections from institutions known as clearing firms instead of clients. When a trade occurs, an independent third party is needed to take responsibility for "clearing" the trade, i.e. managing the transmission of money and transfer of ownership between the two trading parties. This is the responsibility of clearing firms, and thus they require information about the activities of both clients. As such, when a trade occurs and the execution reports are sent to the corresponding client ports; both execution reports are sent to and aggregated by the Drop Port and then sent to the relevant clearing firm.

2.6. Trade Reporter

The Trade Reporter is the public-facing data feed for all trade activities on the exchange. It listens to all trades that occurred on the matching engine, anonymizes the data, and publishes it to an external trade reporting firm.

2.7. Market Data Publisher

Similar to a trade reporter, a Market Data Publisher (MDP) listens to and anonymizes all market data on the matching engine. Instead of broadcasting to an external trade reporting facility however, the market data publisher uses UDP multicast technology to transmit the data to a network of clients, both human and robotic. The fees to access these MDPs are very expensive; this is how many HFT firms take advantage of latency arbitrage, using an MDP to know the exchange's activity before any competitors reliant on the Trade Reporter do.

3. DBSE IMPLEMENTATION DETAILS

3.1 FIX for Financial Information eXchange

A major design commitment was our decision to use the Financial Information eXchange (FIX) Protocol (see FIX, 1992) as DBSE's inter-process communication language for order placement and execution reports. FIX is unarguably the communication protocol of choice in real-world finance; it is used as a *de facto* standard by thousands of financial institutions and exchanges daily to facilitate trading data exchange. Understandably, for the FIX protocol to handle all aspects of financial trading in the real world, it supports a large and complex language of different messages. This is a noticeable disadvantage for its use within DBSE because FIX's messaging capabilities are far more extensive than what is required for DBSE in its current form. In the latest versions of FIX, the protocol supports messages for all aspects of stock trading as well as other financial asset classes, including bonds and foreign exchange.

As a result, it could be argued that the FIX protocol provides too much functionality that complicates the development of DBSE. Instead, a more simplistic protocol could have been used and the messaging language customized for DBSE's needs. The counterargument is that using FIX enriches DBSE as a teaching platform because it presents to users the real-world language and mechanisms that facilitate worldwide financial trading. Moreover, people who desire to do so can view the DBSE source-code to observe how the protocol operates and is implemented within the exchange, and in teaching contexts using DBSE provides an opportunity for students to experience creating FIX-compliant trading clients of their own as a potential coursework assignment. From a realism perspective, the decision to use FIX undoubtedly enhances DBSE. FIX is the global trading protocol and thus the time required to send FIX messages on the DBSE should be close if not equivalent to that of real-world financial institutions: although precise data on such timings is generally not publicly available. Use of FIX supports DBSE's overarching goal of being real-time and using real world tools wherever possible. Finally, regardless of whether FIX is too extensive or not, the selected protocol for DBSE had to fulfil three main characteristics. It had to be bi-directional, full-duplex, and able to communicate over a single constant TCP connection. Unsurprisingly, the FIX protocol supports all three of these characteristics, because it was designed to support financial communication, and that made it a natural choice.

3.2. UDP Unicast

Our final deployment of DBSE uses the UDP protocol with the unicast addressing method for publication of market data from the exchange to trading clients. This combination is close to, but not an exact copy of, what is used in the Jane Street Exchange and on other real-world financial exchanges. Ideally, the market data would be published using UDP multicast rather than unicast, to ensure efficient, non-duplicated traffic throughout the network. A compromise unfortunately had to be made because currently AWS does not support the multicast addressing method. Because of this, TCP was a consideration to replace UDP as it would guarantee message delivery. Upon detailed evaluation however, TCP would require the exchange to manage connections between all trading clients, increasing its computational overhead. Moreover, in the event of a lost packet during UDP transmission, it does not cause a major issue to clients as they will just update their market data when a future packet is received. Despite the compromise of using UDP unicast rather than multicast, DBSE still publishes market data successfully to clients positioned in cloud data centers across the globe. The only slight negative consequence is that the exchange's publisher must iterate though each client in turn sending them their market data. This does not cause any issues at the current scale of our DBSE deployments: in the next section we show DBSE supporting four trading clients at various locations around the world, with each trading client playing host to multiple robot traders. In any case, DBSE maintains an implementation of both unicast and multicast transmission so if at a later date AWS starts to support multicast, or a user wishes to buy and maintain their own networking hardware for larger-scale tests, the multicast functionality built into DBSE can be brought into use.

4. TESTS AND EVALUATIONS

4.1. Latency Tests

To demonstrate and evaluate the UDP unicast market data publisher and the distributed nature of DBSE, we conducted an investigation into the varying latencies for clients positioned around the globe. Specifically, with a DBSE exchange-server hosted in London, we timed how long it takes for trading clients in London, Ohio and Sydney to receive market data. We wanted to ensure that there was a disparity in latency depending on how far from the exchange a client was hosted. This was crucial because without distance-dependent variations in latency, it would be impossible to test whether the profitability of a trading agent is dependent on its ability to race-to-market. To test the latency, we ran DBSE with some additional timing code. When the exchange publishes market data it timestamps the message before sending it through the network. Thus, when each respective trading client receives the message it can perform a comparison between the time of arrival and the timestamp for when the message was sent: that timestamp is located within the message. By utilizing the network atomic clocks provided by the Amazon Time Sync Service we could guarantee that all time on the network would be synchronized and thus the results would be accurate. Results presented below are from an experiment that ran for ten minutes, recording the latency to transmit market data from a DBSE exchange-server in London to four trading clients under otherwise routine simulation conditions.

During the ten-minute experiment, DBSE published market data 491 times. Table 1 summarizes the minimum, first quartile, median, third quartile and maximum latency timings, in milliseconds, for each of the four clients. CLNT1 and CLNT2 are both located in the London, UK region; CLNT3 is positioned in Ohio, USA; and CLNT4 is hosted in Sydney, Australia. As expected, the results show that as geographical distance increases from the DBSE exchange server, so does the latency. Consequently, clients located in Australia receive market data from the exchange in a median time of 135.3ms compared to London's 0.8ms and 0.9ms. Interestingly, market data is consistently received by CLNT2 0.1ms slower than CLNT1, even though they are located within the same region. This is likely because of using the unicast addressing method instead of multicast, as a result of the exchange sending data to each client sequentially; thus, CLNT2 is usually sent data fractions of a millisecond after CLNT1.

	Latency (ms)			
	CLNT1	**CLNT2**	**CLNT3**	**CLNT4**
MIN	0.4	0.5	43.7	134.9
Q1	0.7	0.8	44.0	135.2
MEDIAN	0.8	0.9	44.1	135.3
Q3	1.0	1.1	44.3	135.5
MAX	2.9	1.8	55.0	138.5

Table 1: Results for the latency experiment. The DBSE exchange server is located in London, as are clients CLNT1 and CLNT2. Clients CLNT3 and CLNT4 are in USE and Australia, respectively.

The spread of the latency timings is relatively consistent amongst all four clients, although there are a couple of outliers that result in the high maximum values of 2.9ms and 55ms for CLNT1 and CLNT3 respectively. Figure 2 shows the distributions of each client's latency, binned into 0.1ms intervals.

All four graphs in Figure 2 have approximately the same left-skewed shape and in each the majority of latency is clustered within a 0.5ms spread. Table 2 presents the mean, variance and standard deviation of the timing experiment. These results show that CLNT1, CLNT2 CLNT3 and CLNT4 each on average receive market data 0.9ms, 1.0ms, 44.2ms and 135.4ms after the exchange publishes it. This was to be expected, as transmitting messages over increasingly greater distances should take longer amounts of time.

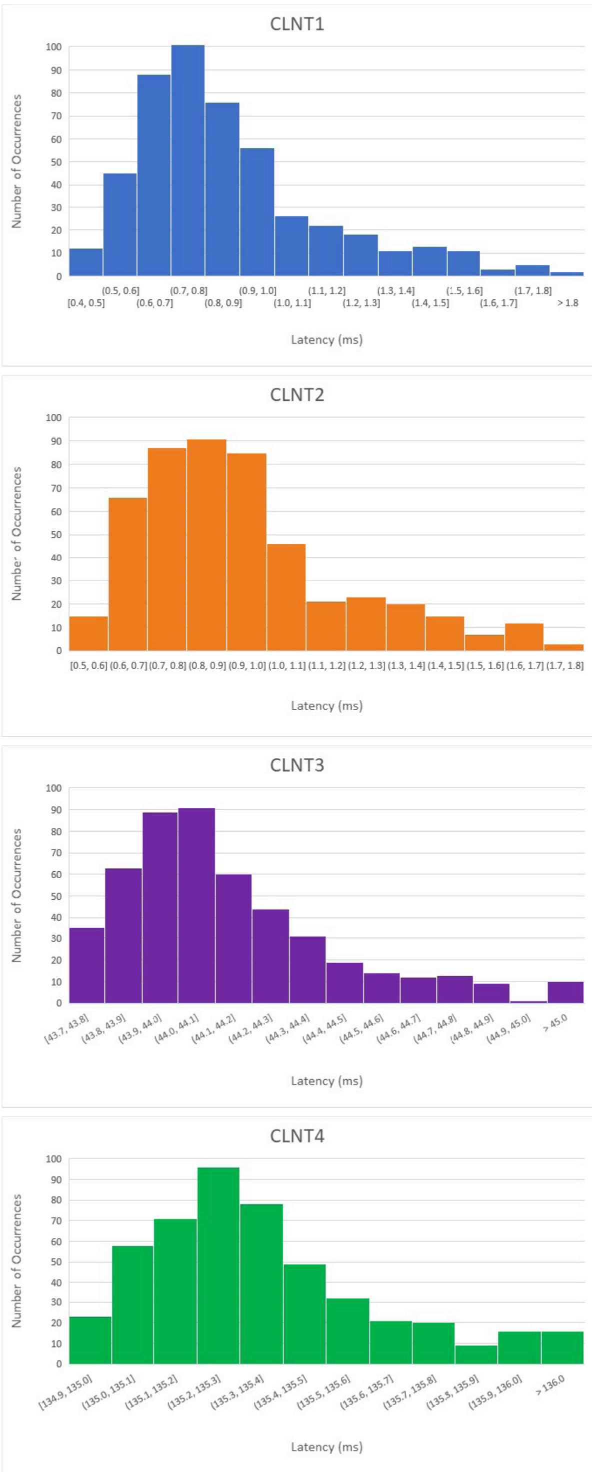

Figure 2: Latency distributions for four clients.

However, the values for the variance and standard deviation of CLNT3, positioned in America, were unexpected compared to the other clients. Since all communication traffic was occurring within AWS's internal network, we would have expected the variance and standard deviation of latency across clients to be consistent. Upon further analysis of the timing data, the larger spread of CLNT3 was caused because of a few outliers, the largest of which was 55ms. This gives insight into the amount of traffic AWS's internal network is handling between London and Ohio: these increased latencies suggest that Amazon handles more spikes in traffic between London and Ohio.

	Latency (ms)			
	CLNT1	CLNT2	CLNT3	CLNT4
MEAN	0.9	1.0	44.2	135.4
VARIANCE	0.1	0.1	0.4	0.1
STANDARD DEVIATION	0.3	0.3	0.7	0.3

Table 2: Spread of the latency experiment.

These results demonstrate that UDP unicast definitely is a perfectly viable option for transmitting market data within Amazon's network to clients positioned across the globe. UDP was the logical choice, compared to TCP, as it is fast, requires little computational overhead, and is the protocol used by real world exchanges. Despite being restricted to the unicast addressing method, DBSE successfully handles it role at millisecond speeds with the current configuration of trading clients.

4.2. Race-to-Market Experiment

To demonstrate the capability of DBSE as a real-time and real-latency simulation we conducted a race-to-market experiment. As discussed earlier in this paper, race-to-market is a concept by which a trader can "steal the deal" if they learn about and respond to a market change before a competitor. Therefore, in a real-world scenario, if a trading client is positioned further away from the exchange than a competitor's trading client, then it will take longer for that client to receive market data. Consequently, the closer of the two clients can react faster to market events and therefore should be more profitable. We explored this in DBSE.

We constructed an experiment on the globally deployed DBSE with four configured trading clients, two in London, one in Ohio and one in Sydney. The experiment would consist of a total of 160 trading agents across the four clients. These trading agents were split 50/50 between supply and demand as well as 25/25/25/25 between four of BSE's built-in trading algorithms, Giveaway (GVWY), Shaver (SHVR), Sniper (SNPR) and Zero-Intelligence Constrained (ZIC). For each trading client, there were five agents of each robot type on the supply side and five agents of each robot type on the demand side, hence a total of 40 trading robots per client, and 160 agents for the simulation across four clients.

Each of the four trading clients were given equivalent order scheduling configuration that ran for a total of three minutes. The order schedulers were configured to distribute new orders to the traders, for them each to either buy or sell some number of units of the exchange's tradeable commodity, at 30 second intervals: inter-arrival times of orders were set to follow a Poisson distribution (this functionality is built-in to the original BSE, via BSE's `drip-poisson` update mode). Within each three-minute simulation, the range of prices for both the supply and the demand are configured to change every minute. Initially, at time t=0, the supply and demand are configured to sit in the range \$1.00–\$2.00; at time t=60, the range increases to \$1.50–\$2.50; before returning to the initial range, \$1.00–\$2.00, at time t=120. We set the parameter `stepmode` of each range to be fixed, this results in DBSE creating an even spread of orders across the price range, resulting in a theoretical equilibrium price P_0 of \$1.50, \$2.00 and \$1.50 cents for each minute of the simulation respectively: if the market is functioning as would be expected, then transaction prices should converge to the relevant P_0 within each one-minute period. It is common practice in experimental economics to configure simulations in this way; changing the P_0 value at a set point in time via a shock change in the market's supply and demand, and transaction prices are expected to reflect the market adapting to each shock change; this is an accepted way to test the reactiveness of trading agents -- in the real world, transaction prices are constantly changing depending on the world's events. If the supply and demand curves of the simulation were configured to be constant then the P_0 value would also be static, and thus the market dynamics would be somewhat stale. The full simulation configuration for this experiment can be found in Appendix B of (Miles, 2019). We repeated the three-minute experiment ten times and for each run recorded the total profit of each trader type. Figure 3 shows the average profits per client for each type of robot trader over the ten runs. For this specific order scheduling configuration, the results show that the GVWY, SHVR and SNPR traders all performed roughly equivalently across clients, with the ZIC algorithm performing the poorest. These results show that regardless of distance from the exchange, each algorithm performs equivalently in each region compared to its counterparts.

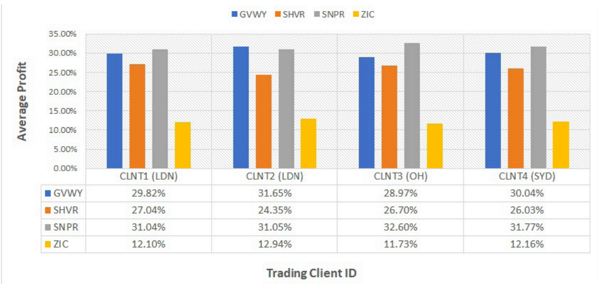

Figure 3: Ratios of total profit per trader type for each client.

Figure 4 on the other hand compares the total profits of all of the algorithms per client. The results presented here are particularly interesting as they indicate that on average CLNT1 and CLNT2 outperformed CLNT3, which in turn outperformed CLNT4. This supports our argument that increasing distance-related latency will degrade the performance trading agents of because CLNT1 and CLNT2 are positioned closest to exchange, followed by CLNT3, followed by CLNT4. Although the average profits of each client are close, there is a significant difference with CLNT2 in London earning 25.72% of profit compared to CLNT4 in Sydney earning 24.10% profit. If latency did not affect the profitability of trading agents and their ability to race-to-market, then we would have expected each client to perform equivalently and each earn 25% of profit across the simulation. These results show that latency can be a limiting factor in the profitability of agents. Designing new trading agents involves a challenging trade-off between adding more "intelligence" (which is typically more computationally demanding, in time and space) and keeping their total processing times low enough that the traders' reaction times keep them in contention in the race-to-market. The trading agents currently available in DBSE are all relatively computationally undemanding. Further work, discussed in Section 5, can be devoted to testing more sophisticated trading agents such as AA (Vytelingum, 2006), GDX (Tesauro & Bredin, 2002) or ZIP60 (Cliff, 2009) to determine whether the computational demands of their extra intelligence comes at the cost of their reactiveness to market events.

The results presented in this section have demonstrated that there is much to explore about algorithmic trading when one has access to a simulator that can offer real-time and real-latency analysis. DBSE enables such analysis and can be configured to enable researchers to uncover new insights into latency driven simulations.

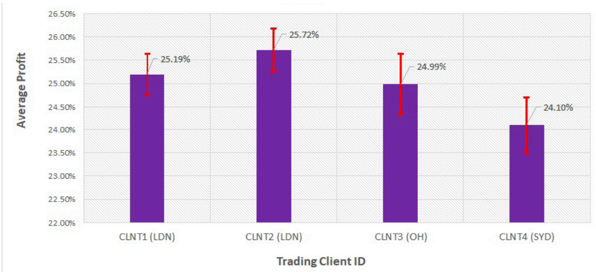

Figure 4: Ratios of total profit across clients.

5. FURTHER WORK

The ultimate aim of the work described here is to develop a distributed simulation platform that could fully model current multi-venue trading systems, and the opportunities for latency arbitrage between different venues. This would require extensive work, implementing multiple exchanges, a trade reporting facility between exchanges, and an entirely new trading client that could connect to and place orders on multiple exchanges simultaneously. Included in this work would be an expansion of the FIX messages that the current

DBSE exchange supports, such as the *Order Replace Request,* <G>*,* used to amend orders that are live on the exchange. Moreover, a persistent storage mechanism, such as a relational database, would benefit the exchange enabling it to be hosted permanently in the cloud. Such additional work could potentially consume many person-months of concentrated effort.

As a part of any future work, we propose a new high-level AWS architecture, as shown in Figure 5. This diagram does not include networking infrastructure but shows the simulator's compute hardware and introduces a new proposed application, the web client. Currently, it is inconvenient for users of DBSE to be required to SSH onto the simulation's hardware to run experiments. The web client would be a web-based application that acts as a simulation controller, hosted permanently in the cloud, that has the permission to orchestrate the instantiation, termination and synchronization of trading clients across the network. Protected behind a user access control system, such as that provided by Amazon Cognito (AWS, 2019), the web client would enable easy and efficient configuration of simulation runs in a graphical interface. Upon completion of a simulation session, it would amalgamate the results, terminate the unneeded trading clients, and provide suitable tools for analyzing the results.

Another obvious avenue for future work, already touched upon earlier in this paper, is the addition of more sophisticated automated trading agents implementing various of the strategies that have been described in public-domain literature, such as: AA (Vytelingum 2006, Vytelingum *et al.* 2008); ASAD (Stotter *et al.* 2013); GDX (Tesauro & Bredin 2002); HBL (Gjerstad, 2003), MGD (Tsauro & Das 2001); Roth-Erev (e.g. Pentapalli, 2008); and ZIP60 (Cliff, 2009).

DBSE has the potential to be an easy-to-use simulation for non-developers, both in the academic and business worlds, and we are intrigued to see how it is developed and used by the wider community in the future.

6. CONCLUSION

The Distributed Bristol Stock Exchange (DBSE) is a globally distributable financial exchange simulation for research and teaching. Its source-code consists of two independent applications, `dbse_exchange` and `dbse_trading-client`, both available for download from:

- `github.com/bradleymiles17/dbse_exchange`
- `github.com/bradleymiles17/dbse_trading-client`

The codebase has been written in Python 3.7 (currently the latest version of this programming language) and all function/method declarations have been typed to assist readability for new users of the DBSE. Both applications use an argument parser when executing, and when attempting to run the application a user can view the required and optional parameters via the help, `-h`, flag.

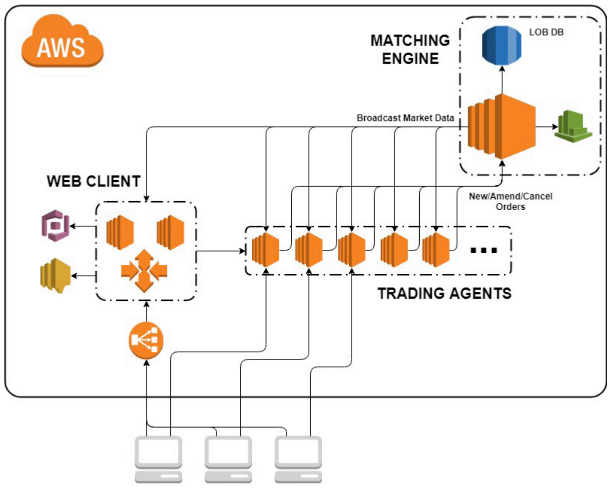

Figure 5: Proposed AWS architecture for future DBSE.

DBSE is significantly revised and expanded from the original work described in (BSE, 2012; Cliff 2018a, 2018b): it has extended the concepts embodied in the original Bristol Stock Exchange and taken BSE from a single-source-file single-threaded application into a fully distributed and cloud-native simulation that can readily be run on widely available commercial cloud-computing services. Trading clients can be configured and positioned around the globe and set trading simultaneously on a single stock exchange. Where BSE naively assumed absolutely zero-latency, DBSE operates using real-world financial communication protocols that are designed to minimize latency but which do not disregard it, and can be distributed at planetary scale for unavoidable real-world latencies. The results presented here demonstrate DBSE's capability in enabling research aimed at understanding race-to-market trading. DBSE is now offered to the global community of researchers and practitioners as a common platform for further exploration and tuition in how latency affects trading in contemporary markets, and in particular DBSE enables repeatable planetary-scale studies of latency arbitrage, a heavily under-researched topic in financial trading; it also serves as an open-source exemplar for teaching distributed systems architecture and design. We look forward to watching how the community makes use of this platform.

REFERENCES

Arnuk, S., & Saluzzi, J., 2012. *Broken Markets: How High-Frequency Trading and Predatory Practices on Wall St are Destroying Investor Confidence and your Portfolio.* Financial Times / Prentice Hall.

AWS, 2019. Amazon Web Services: *Amazon Cognito.* https://aws.amazon.com/cognito/.

Bodek, H. & Dolgopolov, S, 2015. *The Market Structure Crisis: Electronic Stock Markets, High Frequency Trading, and Dark Pools.* CreateSpace Publishing.

Cartea, A., Jaimungal, S., & Penalva, J., 2015. *Algorithmic and High-Frequency Trading*. Cambridge University Press.

BSE, 2012. *The Bristol Stock Exchange*. On GitHub at github.com/davecliff/BristolStockExchange

Cliff, D., 1997. *Minimal-Intelligence Agents for Bargaining Behaviours in Market-Based Environments.* Hewlett-Packard Labs Technical Report HPL-97-91.

Cliff, D. 2009. ZIP60: Further explorations in the evolutionary design of trader agents and online auction-market mechanisms. *IEEE Transactions in Evolutionary Computation*, 13(1): 3-18.

Cliff, D., 2018a. BSE: A Minimal Simulation of a Limit-Order-Book Stock Exchange. In: M. Affenzeller, A. Bruzzone, *et al.* (eds) *Proceedings of the European Modelling and Simulation Symposium (EMSS2018)*, pp.194-203.

Cliff, D., 2018b. "An Open-Source Limit-Order-Book Exchange for Teaching and Research." *Proc. IEEE Symposium on Computational Intelligence in Financial Engineering (CIFEr)*, pp.1853--1860.

Cliff, D., 2019. "Exhaustive Testing of Trader-agents in Realistically Dynamic Continuous Double Auction Markets: AA Does Not Dominate". In: A. Rocha *et al.* (eds) *Proceedings of the 11th International Conference on Agents and Artificial Intelligence (ICAART 2019)*, Vol.2: 224-236; ScitePress.

CTA, 2018. Securities Information Processor. https://www.ctaplan.com/index, 2018.

Das, R., Hanson, J., Kephart, J., & Tesauro, G., 2001. "Agent-Human Interactions in the Continuous Double Auction". *Proc. International Joint Conference on AI.* (IJCAI'01)*,* pp.1169-1176.

De Luca, M., & Cliff, D., 2011. Human-Agent Auction Interactions Adaptive-Aggressive Agents Dominate. *Proceedings of the International Joint Conference on AI* (IJCAI-2011), pp.178-185.

De Luca, M., 2015. *Adaptive Algorithmic Trading Systems.* PhD Thesis, University of Bristol, UK.

Duffin, M., & Cartlidge, J., 2018. Agent-Based Model Exploration of Latency Arbitrage in Fragmented Financial Markets. In *Proc. 2018 IEEE Symposium on Computational Intelligence for Financial Engineering and Economics (CIFEr-2018)*.

FIX, 1992. *Financial Information Exchange Protocol*. https://www.fixtrading.org.

Gjerstad, S. & Dickhaut, J., 1998. Price Formation in Double Auctions. *Games & Economic Behavior*, 22(1):1-29.

Gjerstad, S., 2003. *The Impact of Pace in Double Auction Bargaining.* Working Paper, Department of Economics, University of Arizona.

Gode, D. & Sunder, S., 1993. Allocative efficiency of markets with zero-intelligence traders: Market as a partial substitute for individual rationality. *Journal of Political Economy*, 101(1):119-137.

Haldane, A., 2011. *The Race to Zero.* Transcript of a speech given to International Economic Association Sixteenth World Congress. Available from https://www.bis.org/review/r110720a.pdf

Harris, L., 2002. *Trading and Exchanges: Market Microstructure for Practitioners*. Oxford University Press.

Jane Street, 2017. *How to Build an Exchange.* https://www.janestreet.com/tech-talks/

Kagel, A., & Roth, J., 1997. *The Handbook of Experimental Economics*. Princeton University Press.

Kagel, A., & Roth, J., 2016. *The Handbook of Experimental Economics, Volume 2*. Princeton University Press.

Miles, B., 2019. *Architecting and Implementing a Globally Distributed Limit Order Book Financial Exchange for Research and Teaching.* MEng Thesis, University of Bristol.

Narang, R., 2013. *Inside the Black Box: The Simple Truth about Quantitative Trading.* 2nd Ed. Wiley Finance.

Palmer R., Rust, J., & Miller, J. 1992. Behavior of Trading Automata in a Computerized Double Auction Market. In D. Friedman, & J. Rust (Eds.), *Double Auction Markets: Theory, Institutions, Laboratory Evidence.* Addison Wesley.

Patterson, S., 2013. *Dark Pools: The Rise of AI Trading Machines.* Random House.

Pentapalli, M., 2008. *A comparative study of Roth-Erev and Modified Roth-Erev reinforcement learning algorithms for uniform-price double auctions.* PhD Thesis, Iowa State University.

Rodgers, K., 2016. *Why Aren't They Shouting? A Banker's Tale of Change, Computers, and Perpetual Crisis.* RH Business Books / Cornerstone Digital.

Smith, V., 1992. *Papers in Experimental Economics.* Cambridge University Press.

Stotter, S., Cartlidge, J., and Cliff, D. 2013. "Exploring assignment-adaptive (ASAD) trading agents in financial market experiments", *Proceedings ICAART2013*, 1:77-88.

Tesauro, G. and Das, R. 2001. "High-performance Bidding Agents for the Continuous Double Auction". *Proceedings of the 3rd ACM Conference on Electronic Commerce,* pp.206-209.

Tesauro, G. and Bredin, J., 2002. "Sequential Strategic Bidding in Auctions using Dynamic Programming". In *Proceedings AAMAS 2002*.

Vytelingum,P., 2006. *The Structure and Behaviour of the Continuous Double Auction.* PhD Thesis, University of Southampton.

Vytelingum, P., Cliff, D., & Jennings, N., 2008. "Strategic Bidding in Continuous Double Auctions". *Artificial Intelligence*, 172(**14**):1700-1729.

Wah, E. & Wellman, M., 2013 "Latency arbitrage, market fragmentation, and efficiency: a two-market model," in *Proc. 14th ACM Conference on Electronic Commerce,* pp. 855–872.

SELECTING AN OPTIMAL COMPUTER SOFTWARE TO DESIGN MICROWAVE-BANDWIDTH OPTOELECTRONIC DEVICES OF A FIBER-OPTICS LINK

M. E. Belkin[(a)], T. Bakhvalova[(a)], V. Golovin[(b)], Y. Tyschuk[(b)], and A.S. Sigov[(a)]

[(a)]Scientific and Technological Center "Integrated Microwave Photonics" MIREA - Russian Technological University Moscow, Russian Federation
[(b)]Sevastopol State University (SevSU) Sevastopol, Russian Federation

[(a)]belkin@mirea.ru

ABSTRACT
Selecting an optimal program mean, we compare in detail two off-the-shelf computer-aided design software: optoelectronic VPIphotonics Design Suite and microwave-electronic NI AWRDE by designing a realistic microwave-photonics-based fiber-optics link including two widespread microwave-bandwidth optoelectronic devices at the transmitting end such as direct intensity modulating semiconductor laser and external intensity modulating electro-absorption modulator. In the result, the qualitative comparison of possibilities showed that NI AWRDE-based approach generally provides broader and deeper functionality, and the single critical shortcoming of it is the absence of any built-in photonic models. Nevertheless, the quantitative comparison on the example of transmitting 2.5 Gbit/s 16-QAM signals at radio-frequency carrier of 25 GHz along the same fiber-optics link showed a relatively close coincidence for the quality of digital radio signal transmission, which indicates the possibility of modeling in any of the software environments.

Keywords: microwave photonics, fiber-optic link, computer-aided design, directly modulated semiconductor laser, electro-absorption modulator

1. INTRODUCTION

It is well-known that Radio-over-Fiber technology, RoF (Al-Raweshidy, Komaki 2002; Novak, Waterhouse, Nirmalathas, Lim, Gamage, Clark, Dennis and Nanzer 2016; Bakhvalova, Belkin, Fofanov 2018) should find the most extensive dissemination to architect an access network in the incoming mobile communication systems of fifth generation, 5G NR (Andrews, Buzzi, Choi, Hanly, Lozano, Soong, Zhang 2014; Chen, Zhao 2014; Waterhouse and Novak 2015), and a microwave-photonics-based (Seeds and Williams 2006; Capmany and Novak 2007.) fiber-optics link (MP-FOL) is a requisite part of this technology. Devices of microwave photonics (MWP) operate concurrently in microwave and near infrared (optical) bands, thanks to it they are finding a widespread occurrence in modern radio engineering means related with information traveling, monitoring of environment and technological parameters of production, radar supervision, etc. Nowadays there are specialized optoelectronic computer-added design (OE-CAD) tools allowing to develop and simulate both radio-frequency (RF) and optical circuits separately or in common. However, in the latter case, which is inherent for MP-FOLs, the structural, functional, and parametric restrictions of either optical or RF range are inevitable. For example, by well-known OE-CAD environment VPI Photonics Design Suite a developer is able to execute in precision manner the design of a fiber-optic link with detailed study of optical units' characteristics, but RF, especially microwave and millimeter-wave functional devices or units are designed without paying attention to specialties of microwave band. On the other hand, operating at symbolic level modern high-power microwave electronic CAD (E-CAD) tool is able simply and with high precision to solve this problem but there are completely no models of active optoelectronic devices in its libraries.

Recently, we proposed and described a way to overcome this problem and encourage an accurate design of MWP-based radio-electronic devices and systems using, for example off-the-shelf E-CAD tool NI AWRDE (Belkin, Golovin, Tyschuk, Vasil'ev, and Sigov 2018). Following it, in this paper we compare E-CAD and OE-CAD tools by designing a realistic MP-FOL including two widespread microwave-bandwidth optoelectronic devices at the transmitting end such as direct intensity modulating semiconductor laser (DIM-SL) and external intensity modulating electro-absorption modulator (EIM-EAM). So, the remainder of the paper is organized in such a way. First, the microwave photonics approach and the available OE-CAD and E-CAD software are highlighted shortly in sections 2 and 3, correspondingly. Then in section 4, the models and setups for simulation using VPI Photonics Design Suite and NI AWRDE software are proposed and discussed. Section 5 represents the simulation experiments and results referred to transmitting 2.5 Gbit/s 16-QAM signals at RF carrier of 25 GHz over MP-FOL using the single-mode optical fiber of various distances. Section 6 concludes the paper.

2. MICROWAVE PHOTONICS APPROACH

Microwave photonics is an interdisciplinary scientific and technological area that combines the domains of microwave and RF engineering and photonics (Urick, McKinney, Williams 2015). This direction in the last 40 years has attracted ever-increasing interest and generated many newer R&Ds from both the scientific community and the commercial sector. Emerging applications for 5G NR networks based on RoF architecture, sub-terahertz wireless systems, radar, and electronic warfare means indicate that MWP approach is set to be a subject of great importance. Generally, MWP devices are the examples of an intimate integration of photonics, microwave electronics, and antenna array technologies for producing a complicated functional module in a multichannel analog environment. In particular, MWP technique opens the way to super-wide bandwidth transmitting characteristics at lower size, weight, and power as compared with traditional electronics (Paolella, De Salvo, Middleton, and Logan 2015). As an example, in a typical arrangement of MWP-based fiber optics link (Figure 1), a photonic area is inserted between two microwave-electronic areas. The first one includes RF transmitter unit that typically consists of a digitally modulated data source, RF up-converter, and RF power amplifier, while the second one includes RF receiver unit that typically consists of a low-noise RF amplifier, RF down-converter, and data detector. For forward and reverse transformations of microwave and optical signals there are two interfacing units at their bounds: electrical-to-optical (E/O) and optical-to-electrical (O/E) converters. E/O-converted microwave signals are distantly transported in optical domain through optical fiber.

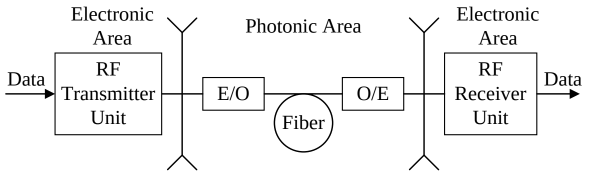

Figure 1: A Typical Arrangement of MWP-Based Fiber-Optics Link

3. AVAILABLE OPTOELECTRONIC AND MICROWAVE ELECTRONIC SOFTWARE

The developer of new MWP devices is facing a problem of choosing an appropriate computer tool for their modeling and design. As of today, a system designer is forced to use means of several computer-aided design tools because the existing OE-CAD are not as developed as compared with the E-CAD tools intended for modeling of microwave devices (Leijtens, Le Lourec, Smit 1996). Table 1 lists detailed comparison of two off-the-shelf software: OE-CAD tool VPI Photonics Design Suite of VPI Photonics and well-known E-CAD tool AWRDE of National Instruments. As one can see from the Table, the second approach generally provides broader and deeper functionality; and the single critical shortcoming of E-CAD tool is the absence of any built-in models of photonics area interfacing elements (see Figure 1).

Table 1: Comparison of Modern Off-The-Shelf E-CAD and OE-CAD Tools

#	Feature	Realization		Comments
		By E-CAD (NI AWRDE)	By OE-CAD (VPI Photonics Design Suite)	
1	Analysis approach	Building Blocks, 3D electromagnetic analysis	Building Blocks	Broader and deeper functionalities of E-CAD
2	Simulation methods: - Linear circuits -Nonlinear circuits	S-,Y- matrix, equivalent circuits Harmonic Balance Engine, ALPAC, 3D planar electromagnetic simulator, AXIEM modeling	S-matrix S-matrix, combination of time-and-frequency domain modeling	Broader and deeper functionalities of E-CAD
3	Element representation: - active microwave elements - active MWP elements - passive elements	Multirate harmonic balance, HSPICE, Volterra, measured characteristics-based models ABSENT Lumped and distribution, microwave-band specialties	Ideal or data file-based models Rate equation-based, transmission line models Lumped, ideal	Broader and deeper functionalities of E-CAD excluding active MWP elements and modules (laser, photodiode, optical modulator)

4	Possibility for calculating the key parameters of MWP circuits and links	By one-click operation	By user-created complicated schemes	Large-signal transmission gain, Noise figure, Phase noise, Intermodulation distortion, Intercept points, etc.
5	IC Layout design and analysis	Yes	No	Broader and deeper functionalities of E-CAD for more sophisticated investigations
6	Built-in design kits from the main foundries	Yes	No	
7	Parameter optimization	Yes	No	
8	Sensitivity analysis	Yes	No	
9	Design of tolerance	Yes	No	
10	Statistical design	Yes	No	
11	Yield optimization routine	Yes	No	
12	Built-in library of producer specifics models	Yes	No	

To overcome this shortcoming, we have developed by NI AWRDE E-CAD tool a number of the models for active MWP elements, such as semiconductor laser, p-i-n photodetector, single- and multi-core optical fiber, and for rather simple MWP devices, such as optoelectronic microwave oscillator, optoelectronic microwave-frequency mixer, and optical delay lines. The results of the work are summarized in (Belkin, Golovin, Tyschuk, and Sigov 2018a; Belkin, Golovin, Tyschuk, Vasil'ev, and Sigov 2018). However, it is of considerable interest to compare the results of calculations using E-CAD and OE-CAD tools, which is presented below on the example of MP-FOL using two key active MPW elements: semiconductor laser and optical electro-absorption modulator performing E/O conversion operation (see Figure 1). The concept proposed by us consists in a comparative assessment of the quality for propagation of a digital RF signal along the same MP-FOL, in the transmission chain of which one of the tested devices is entered.

4. THE MODELS AND SETUPS FOR SIMULATION

4.1. Use of the DIL-SL

A semiconductor laser performing the function of E/O conversion is one of the most important circuit elements for both fiber optics and integrated MWP devices including the MP-FOL under research. Its important advantage in comparison with other types of optical sources is the possibility of direct modulation by RF signals, which greatly simplifies the design of the optical transmitter.

4.1.1. Modeling in VPI

Figure 2 depicts VPIphotonics Design Suite's setup of MP-FOL using a directly modulated semiconductor laser for the simulation experiments that consist of the library models of C-band DIM-SL, standard single-mode optical fiber and pin-photodiode followed by the electrical amplifier model. One can see their relevant parameters in Tables 2 and 3. To control DC bias current of a laser the setup includes the library model of DC Source. There are two instrumental modules in the setup. The first one imitates 2.5 Gbit/s, 16-QAM RF transmitter containing library models of QAM generator, output unit for power control, electrical amplifier, and a device setting the desired signal-to-noise ratio (SNR). This module generates an electrical M-QAM signal up-converted at a given RF carrier frequency of 25 GHz with a user-defined output SNR. In addition, the Electrical 16-QAM Receiver is included in Figure 2. This module detects RF signal, decodes an electrical 16-QAM signal and evaluates the error-vector magnitude (EVM) of the received QAM signal. The model of Numerical 2D Analyzer is used for two-dimensional graphical representation of the data from the QAM Receiver output.

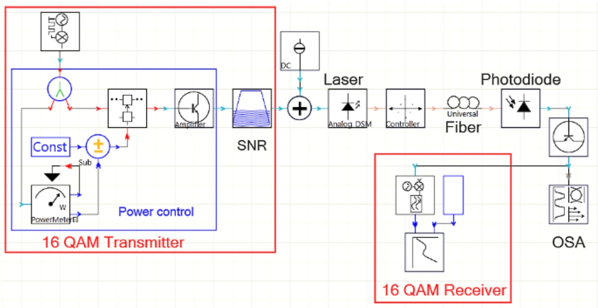

Figure 2: VPIphotonics Design Suite's setup of MP-FOL using a directly modulated semiconductor laser

4.1.2. Modeling in NI AWRDE

Figure 3 depicts NI AWRDE's setup of MP-FOL using a directly modulated semiconductor laser for the simulation experiments. The setup has the same block diagram as in Figure 2 including in-series models of 16-QAM transmitter, MP-FOL, and 16-QAM receiver, but the built-in modules are realized in a different way. In particular, the first one contains the library model of 16

QAM source, the output signal of which is up-converted on the RF carrier of 25 GHz using the models of RF tone generator and RF multiplexer. Besides, the library model of the Noise Generator to set the desired SNR is entered at its end. The second one consists of proposed early double-carrier laser model (Belkin, Golovin, Tyschuk, Vasil'ev, and Sigov 2018) including a passive sub-circuit representing frequency response of the laser under test in S2P format, library model of quasi-optical tone generator imitating laser carrier, and library model of multiplexer that performs the operation of up-converting signal to the optical range. In addition, according to the block diagram of the MP-FOL under study, the previously described (Belkin, Golovin, Tyschuk, Vasil'ev, and Sigov 2018) equivalent models of optical fiber and photodetector were introduced, followed by library models of an electric amplifier and a RF signal delay compensator. The third unit is a laboratory model of a vector signal analyzer to measure EVM values.

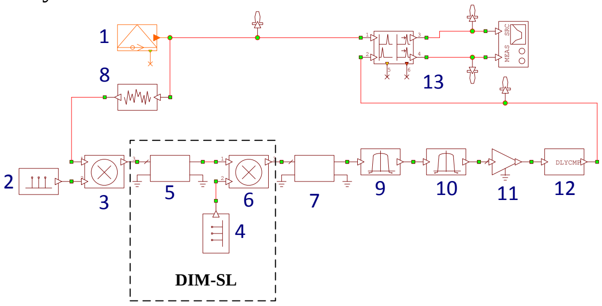

Figure 3: NI AWRDE's setup of MP-FOL using a directly modulated semiconductor laser: 1 – QAM generator; 2 – RF tone generator; 3, 6 – multiplexer; 4 – quasi-optical signal generator; 5 – frequency-modulation response block; 7 – optical frequencies splitter; 8 – RF noise generator; 9 – model of single-mode fiber as sub-circuit; 10 - model of photodetector as sub-circuit; 11 – RF amplifier; 12 – signal delay compensator; 13 – vector signal analyzer

4.2. Use of the EIM-EAM

To The operation of an electro-absorption modulator (EAM) that has recently appeared on the worldwide market is referred to the effect of increasing absorption in a quantum-size region based on quantum wells with an electric field applied. Its main advantages compared to the Mach-Zehnder modulator traditionally used for external intensity modulation of optical radiation are compactness, increased electro-optical conversion efficiency, suitability for photonic integrated circuits, and the ability to work in transceiver mode.

4.2.1. Modeling in VPI

Figure 4 depicts VPIphotonics Design Suite's setup of MP-FOL using an electro-absorption modulator (EAM) under test. The setup has the same block diagram as in Fig. 2 (see sub-section 4.1) excluding the transmitting part of MP-FOL that contains the library models of unmodulated continuous-wave laser source and EAM under test.

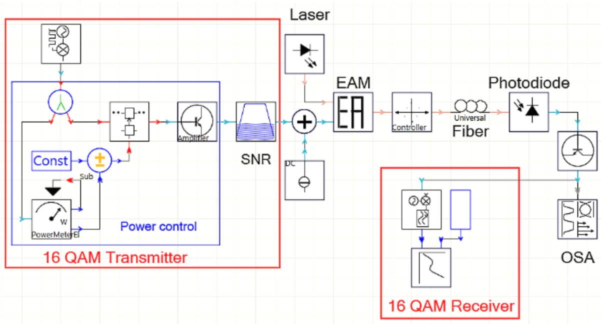

Figure 4: VPIphotonics Design Suite's setup of MP-FOL using an electro-absorption modulator

4.2.2. Modeling in NI AWRDE

Figure 5 depicts NI AWRDE's setup of MP-FOL using an externally modulated electro-absorption modulator for the simulation experiments. The setup has the same block diagram as in Fig. 4 excluding the transmitting part of MP-FOL that contains the library model of quasi-optical tone generator imitating laser carrier, the library model of multiplexer that performs the operation of up-converting signal to the optical range, and a passive sub-circuit representing frequency response of the EAM under test in S2P format. Notice that earlier, we proposed and described in detail (Belkin, Golovin, Tyschuk, and Sigov 2018b) a non-structural nonlinear model of the EAM suitable for developers of local telecommunication systems based on RoF technology. However, its simplified model is used here.

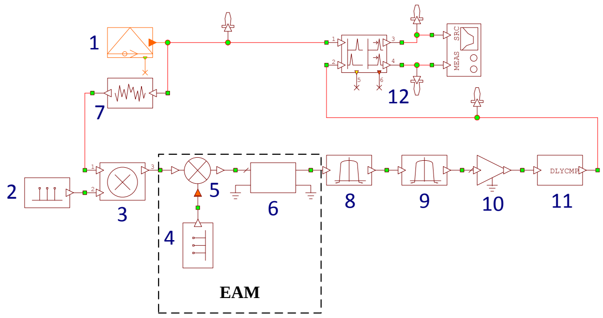

Figure 5: NI AWRDE's setup of MP-FOL using an electro-absorption modulator: 1 – QAM generator; 2 – RF tone generator; 3 – multiplexer; 4 – quasi-optical signal generator; 5 – behavioral mixer; 6 – optical frequencies splitter; 7 – RF noise generator; 8 – model of single-mode fiber as sub-circuit; 9 - model of photodetector as sub-circuit; 10 – RF amplifier; 11 – signal delay compensator; 12 – vector signal analyzer

5. SIMULATION EXPERIMENTS

5.1. Reference Data

In this work, the subject of the study is a microwave-photonics fiber-optic link (MP-FOL); the devices of study are directly modulated semiconductor laser, an electro-absorption modulator for external modulation, and standard single-mode fiber (SMF). The tools for the computer simulation are two well-known commercial program environments such as OE-CAD VPIPhotonics

Design Suite™ and E-CAD NI AWRDE. The study took into account two key distortion sources of the transmitted signal: a chirp of laser and modulator as well as losses and chromatic dispersion of the fiber. To eliminate the influence of nonlinear effects during modulation and signal transmission through the fiber, RF and optical signal levels were selected so that the modulation index did not exceed 30%, and the optical power in the fiber was not more than 5 mW. Table 2 lists the common reference data for the MP-FOL under study. In addition, Table 3 and 4 list the reference data for the DIM-SL and EIM-EAM, correspondingly.

Table 2: Common Reference Data for the MP-FOL under Study

Parameter		Value
Length of pseudo-random bit sequence		2^{15}-1
Bitrate		2.5 Gbit/s
RF Carrier Frequency		25 GHz
Input RF Power		-11 …-26 dBm
Type of RF modulation		16-QAM
Optical Carrier		C-band (1552.52 nm)
Type of optical modulation		Intensity
PIN-Photodiode	Responsivity	0.92 A/W
	Dark current	100 nA
	3dB Bandwidth	20 GHz
	Optical Input Power	<3 mW
Post-amplifier	Gain	40 dB
	Noise Spectral Density	$20\cdot10^{-12}$ A/Hz$^{1/2}$
Optical Fiber	Type	SMF-28e+
	Length	up to 20 km
	Attenuation	0.2 dB/km
	Dispersion	$17e^{-6}$ s/m^2
	Dispersion Slope	80 s/m^3

Table 3: Reference Data for Direct Intensity Modulated Semiconductor Laser

Parameter	Value
Operating current	50 mA
Linewidth	500 kHz
Relative intensity noise	-160 dB/Hz
Threshold current	10 mA
Slope efficiency	0.14 W/A
Linewidth enhancement factor (α)	4.6
Adiabatic chirp factor (*k*)	3.2 GHz/mW

Table 4: Reference Data for External Intensity Modulated Electro-Absorption Modulator

Parameter	Value
Operating voltage	-0.5 V
Extinction ratio	14 dB
Slope efficiency	0.14 W/V
Linewidth enhancement factor (α)	1.0
Adiabatic chirp factor	0

5.2. Simulation results

In preparation for the simulation experiments, the modulation index of each device under study was optimized in such a way as to ensure the maximum output RF carrier-to-noise ratio while maintaining the low-signal mode at the modulating frequency. . Figures 6, 7 depict examples of simulating EVM vs fiber length characteristics for the devices under study during transmission of 2.5 Gbit/s, 16-QAM RF signal at the frequency of 25 GHz using RF signal-to-noise ratio (SNR) of 50 and 25 dB. For the best vision, there are the insets in the Figures showing constellation diagrams at fiber length of 10 km. In addition, in the Figures, the dotted lines indicate the standard limit of the EVM during transmission of the 16-QAM signal, which is 12.5% (ETSI 2017).

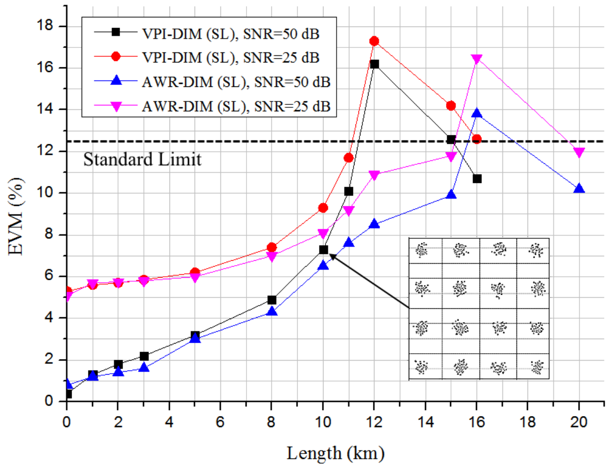

Figure 6: EVM vs fiber length characteristics based on MP-FOL simulation including DIM-SL

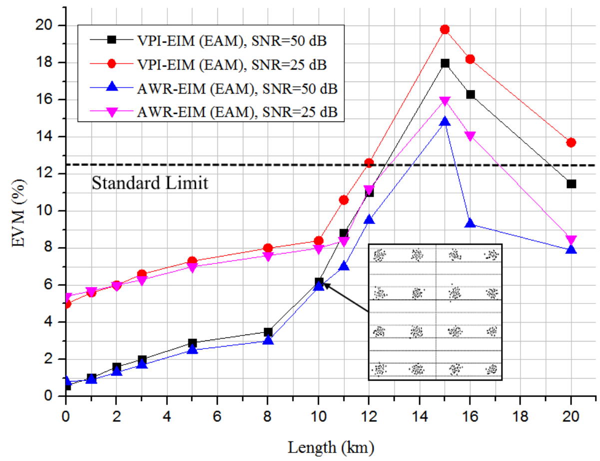

Figure 7: EVM vs fiber length characteristics based on MP-FOL simulation including EIM-EAM

The following outputs can be derived from our study:

- the EVM vs fiber length characteristics simulated by the both software closely coincide with each other at the signal-to-noise ratio of 50 and 25 dB within the FOL distance of up to 10 km;
- for longer FOL lengths, all characteristics show a peak that exceeds the standard limit, caused by the effect

of dispersion in the fiber (Urick 2015). Figure 8 exemplifies the photodiode's output spectrum explaining the dispersion effect, which is remarkably reduces SNR and therefore increases EVM value. To eliminate it in order to increase the length of the FOL, it is required to introduce at its end a dispersion corrector, which is a standard element in fiber-optic communication systems;

- the fiber distance for the FOL under study including a directly modulated semiconductor laser reaches within standard limit of 12.5% up to 11 km for VPI simulation and up to 15 km for AWRDE simulation ;
- the fiber distance for the FOL under study including a externally modulated electro-absorption reaches within standard limit of 12.5% up to 12-14 km for the simulations by the both software tools;
- The most likely reason for this behavior is the effect of an electro-optical converter chirp, which is much greater with a laser than with a modulator (see α- and k-factors in Tables 3 and 4). However, this parameter is not included in the proposed AWRDE's laser and modulator models.

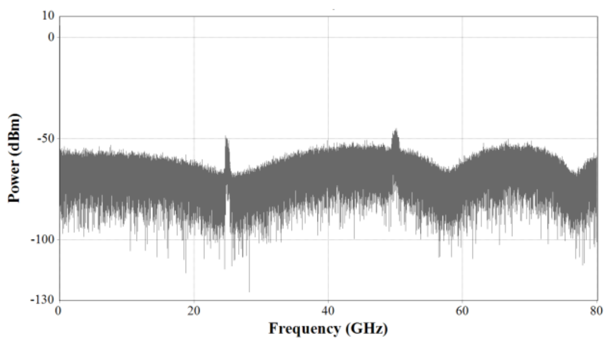

Figure 8. Photodiode's output spectrum explaining the dispersion effect

CONCLUSION

In the paper, we compared two off-the-shelf computer-aided design software: VPIphotonics Design Suite for the simulation of photonics circuits and NI AWRDE for the simulation of microwave-electronics circuits on the example of a microwave-photonics-based fiber-optics link using two key active microwave-bandwidth optoelectronic devices: semiconductor laser or optical electro-absorption modulator performing electro-optic conversion operation. The concept proposed consists in a comparative assessment of the quality for propagation of a digital radio-frequency signal along the same fiber-optics link, in the transmission chain of which one of the tested devices is entered. The result was a relatively close coincidence for the quality of digital radio signal transmission, which indicates the possibility of modeling in any of the software environments. Therefore, the designer depending on the requirements for the fiber-optics link being developed should make the choice of suitable software. In this case, the absence of library models of optical and optoelectronic devices in the NI AWRDE program's current version should be taken into account. Nevertheless, the problem is simplified due to the possibility of using the previously developed models of these devices in the form of sub-circuits.

ACKNOWLEDGMENTS

This work was supported by the Russian Foundation for Basic Research, Grant No. 18-29-20083.

REFERENCES

Al-Raweshidy H., Komaki S., 2002. Radio over Fiber Technologies for Mobile Communications Networks: 436 pp., Artech House.

Andrews J. G., Buzzi S., Choi W., Hanly S. V., Lozano A., Soong A. C. K., Zhang J. C., 2014. What Will 5G Be? IEEE Journal on Selected Areas in Communications, 32 (6): 1065 – 1082.

Bakhvalova T., Belkin M., Fofanov D., 2018. Advances in Fiber-Wireless Network Architecture Approach to the Next-Generation Communication Systems. Proceedings of the Seventh International Conference on Advances in Computing, Communication and Information Technology - CCIT 2018, pp. 62-67, Oct. 27-28, Rome, Italy.

Belkin M.E., Golovin V., Tyschuk Y., and Sigov A.S., 2018a. A simulation technique for designing next-generation information and communication systems based on off-the-shelf microwave electronics computer tool. International Journal of Simulation and Process Modelling, 13 (3): 238-254.

Belkin M.E., Golovin V., Tyschuk Y., and Sigov A.S., 2018b. Modeling Electroabsorption Modulated Laser for Digital Optical Transmission. Proceedings of the 1st IEEE British and Irish Conference on Optics and Photonics (BICOP 2018), 4 pp. December 12 – 14, London, UK.

Belkin M.E., Golovin V., Tyschuk Y., Vasil'ev M., and Sigov A.S., 2018. Computer-Aided Design of Microwave-Photonics-based RF Circuits and Systems. Chapter in book IntechOpen "RF Systems, Circuits and Components". 21 pp. Available from: https://www.intechopen.com/online-first/computer-aided-design-of-microwave-photonics-based-rf-circuits-and-systems [accessed 5 November 2018]

Capmany J., Novak D., 2007. Microwave photonics combines two worlds. Nature Photonics, 1 (1): 319-330.

Chen S., Zhao J., 2014. The requirements, challenges and technologies for 5G of terrestrial mobile telecommunication. IEEE Communications Magazine, 52 (5): 36–43.

ETSI, 2017. Minimum requirements for Error Vector Magnitude. TECHNICAL SPECIFICATION, LTE; Evolved Universal Terrestrial Radio Access (E-UTRA); User Equipment (UE) radio transmission and reception (3GPP TS 36.101 version 14.3.0 Release 14), pp. 215.

Leijtens X. J. M., Le Lourec P., Smit M. K., 1996. S-Matrix Oriented CAD-Tool for Simulating Complex Integrated Optical Circuits. IEEE Journal

of Selected Topics in Quantum Electronics, 2 (2): 257-262.
Novak D., Waterhouse R. B., Nirmalathas A., Lim C., Gamage P. A., Clark T. R., Dennis M. L., and Nanzer J. A., 2016. Radio-Over-Fiber Technologies for Emerging Wireless Systems. IEEE Journal of Quantum Electronics, 52 (1): 1-11 (0600311).
Paolella, A.C., De Salvo, R., Middleton, C. and Logan, C., 2015. Direction in radio frequency photonic systems. Proceedings of the IEEE 16th Annual Wireless and Microwave Technology Conference (WAMICON), pp. 1-6. April 13-15, Cocoa Beach, FL, USA.
Seeds J., Williams K. J., 2006. Microwave Photonics. IEEE/OSA Journal of Lightwave Technology, 24(12): 4628-4641.
Urick V. J., McKinney J. D., Williams K. J., 2015. Fundamentals of Microwave Photonics, Hoboken, New Jersey.
Waterhouse R., Novak D., 2015. Realizing 5G. IEEE Microwave Magazine, 16 (8): 84-92.

MIXED DISCRETE-EVENTS AND AGENT-BASED MODELING OF A COMPLEX AUTOMATIC WAREHOUSE FOR COPPER TUBES BUNDLES

Braglia Marcello[a], Frosolini Marco*[b], Gabbrielli Roberto[c], Marrazzini Leonardo[d], Padellini Luca[e]

[a], [b], [c], [d] Dipartimento di Ingegneria Civile e Industriale - Università di Pisa, Largo Lucio Lazzarino 2, 56126 Pisa (Italy)

[e] Dipartimento di Ingegneria dell'Informazione - Università di Pisa, Via Girolamo Caruso 16, 56122 Pisa (Italy)

[a] m.braglia@ing.unipi.it, [b] marco.frosolini@ing.unipi.it, [c] r.gabbrielli@ing.unipi.it, [d] leonardo.marrazzini@ing.unipi.it

[e] luca.padellini@phd.unipi.it

*corresponding author

ABSTRACT

The use of simulation modelling in science and engineering is today well established. Three methods exist that allow to build complex simulation models in many different contexts: Discrete Event Simulation, System Dynamics, and Agent Based Simulation. Despite the interesting results obtained, what has really limited the parallel and combined application of the three currently used paradigms was the lack of integrated simulation tools. This paper presents the outcomes of a complex plant simulation that has been carried out by means of the parallel and combined application of Discrete Event Simulation and Agent Based Simulation, while using a well-structured modular approach. This presents the advantage of simplifying the building, the debugging and the validation of the whole simulation model, while, at the same time, it offers the unquestionable benefit of allowing a widespread reusability of the simulation code.

Keywords: Industry 4.0; Discrete event simulation; Agents; Object-oriented programming.

1. INTRODUCTION

In the Industry 4.0 era, simulation modelling is a growing and attractive solution to reduce costs, shorten development cycles, increase the quality of products and processes, and greatly facilitate knowledge management. Nowadays, the use of simulation modelling in science and engineering is well established. A great body of scientific and professional literature on various aspects of Simulation modelling, especially in an object-oriented environment, is available, from original works such as Zeigler (1987) and Zeigler (1990) to newer publications, for example Piccinini et al. (2018). Among the simulation techniques, Discrete Event Simulation, System Dynamics, and Agent Based Simulation, are probably the most used and discussed. The recent framework of Sumari, Ibrahim, Zakaria, and Hamid (2013) compares all these three methods in terms of features, advantages, disadvantages and tools being used in each simulation method.

Despite the interesting results obtained, what has really limited the parallel and combined application of the three currently used paradigms was the lack of integrated simulation tools. In response, this paper presents the outcomes of a significantly complex plant simulation that has been carried out by means of the parallel and combined application of Discrete Event Simulation and Agent Based Simulation, while using a well-structured modular approach. Whilst the method is not new at all, as many authors have stated (Zeigler 1987, Zeigler 1990), its importance over time since the last decade of the last century, the availability of improved simulation tools makes it easily usable today.

The remaining part of this paper is organized as follows. Section 2 presents the literature review. In Section 3, we deeply explain the purpose of the study and its related approach. In order to show the operating principles and potential results of this novel approach, a real industrial implementation is presented in Section 4. Section 5 introduces and explains the verification and the validation of the model. In the last section, we summarise the key findings of the study and suggest future research directions.

2. LITERATURE REVIEW

The efficiency and effectiveness of logistics activities and of distribution networks in particular is largely determined by the operation of the nodes of the network, i.e. the warehouses. Warehouses are important links in the supply chain; here, products are temporarily stored and retrieved subsequently from storage locations to fulfil customer' orders (Rouwenhorst et al. 2000).

Assessing the performance of a warehouse in terms of cost, throughput, space utilization, and service provides feedback about how a specific design or operational policy performs compared with the requirements, and how it can be improved (Calzavara et al. 2017, Guo, Yu, and De Koster 2015). Furthermore, a good performance evaluation model can help the designer to quickly evaluate many design alternatives and narrow down the design space during the early design stage. Performance evaluation methods include benchmarking, analytical

models, and simulation models (Gu, Goetschalckx, and McGinnis 2010). However, this should not obscure the fact that simulation is, nowadays, the most widely used technique for warehouse performance evaluation in the academic literature as well as in practice.
Specifically, simulation models have recently appeared as useful tools for analyzing specific issues related to warehouses in terms of, among the others, inventory management, logistics and layout design (Krenczyk, Davidrajuh, and Skolud 2019; Smith and Srinivas 2019; Vieira et al. 2018). The main reason for adopting simulation is that, in many practical cases, the definition of exact analytic models for managing a warehouse could be a complex task, especially when numerous factors, such as inventory policies, number of items, physical layout should be considered.
On the basis of the premise above, our study tries to contribute to the literature on "warehouse simulation modelling" in the following ways:

- To begin with, this paper presents the outcomes of a significantly complex plant simulation that has been carried out by means of the parallel and combined application of Discrete Event Simulation, System Dynamics and Agent Based Simulation, while using a well-structured modular approach. Specifically, a very complex model dealing with the automatic warehouse management of a plant for copper tubes production, has been effectively decomposed into a hierarchical, modular structure that is easy to develop, test, validate, modify and maintain.
- The single components that constitute the model can be effortlessly adapted to different situations and, thanks to a fully parametric approach, they can be effectively used to simplify the modelling phase and to optimize the model itself.

3. THE PURPOSE OF THE WORK AND APPROACH

As stated above, in the paper we present a combined approach which presents the advantage of simplifying the building and the debugging of the whole simulation model, while, at the same time, it offers the unquestionable benefit of allowing a widespread reusability of the simulation code. Indeed, during the initial assessment of the real-world application under analysis, that will be briefly described in the following, two major key points emerged clearly:

1. The complete process presents a great complexity, due to the large number of physical elements, rules and exceptions, that characterize the different material flows.
2. The actual model presents many repeated sub-processes (with limited or no modifications) and similar equipment and facilities.

The first point testifies the necessity of opportunely divide the simulation into smaller pieces of code, that can be put together when needed to build the complete picture. Small pieces mean, after all, less errors and easy maintenance of the simulation model, in particular with respect to the testing phase, as well as future enhancements and modifications. The presence of many commonalities makes this method even more convenient, in that many small pieces of code can be easily reused and adapted to different parts of the model itself. Further, the adoption of the agent modelling approach permits to transform each single sub-model into a standalone, autonomous and fully recyclable object. Indeed, by means of a consistent amount of opportunely chosen parameters, the single modules can be copied, pasted and set up in place with few modifications, making the model construction fast and straightforward. We could almost venture a similitude with the well-known "plug & play" systems.
Therefore, while the discrete events modelling still continues to constitute the backbone of the whole simulation model, small object-oriented autonomous agents are used both to characterize the products flowing within the plant, the orders and the equipment (cranes, shuttles, machines and stores, for example) as well as the flows themselves.
The inner structure of each single agent is in turn characterized by a varied mix of simulation techniques. Again, discrete events have been widely used to represents logic flows, when applicable. On the contrary, some other logic behaviors have been extensively modelled by means of state charts (often, making the most of the communication skills of the single agents) and pure object-oriented java programming techniques. The final outcome is a complete set of reusable components that can be linked together within the main application body.
It can be said, briefly, that hundreds different objects have been correctly and effectively reproduced by means of no more than a dozen of agents. Owing to this, the main body of the simulation model acts as a true control system, that addresses the different products to the correct destinations, whereas the management of the single sub-processes is completely delegated to the above mentioned quasi-intelligent agents.
Specificities, that often occur within the real-world application, can be easily introduced within the simulation by making the most of the Object-oriented programming (OOP) linked concepts of inheritance and polymorphism (Armstrong 2006, Kindler and Krivy 2011). Indeed, an entire sub-model can be derived to build a new entity, that inherits the complete functionalities of the ancestor and that can be subsequently modified and adapted to specific requirements.
As already mentioned, the validation stage, usually difficult and cumbersome, and certainly highly time-consuming, can be reduced consistently both in terms of complexity and duration, in that each single agent needs to be tested only once. Besides, small pieces of code are

easier to be effectively validated with respect to a large, monolithic application

4. THE INDUSTRIAL CASE STUDY

The studied model mimics the behavior of a complex, high-intensity automatic warehouse where thousands copper tubes (having different lengths, weights and characteristics) are stored, handled and moved each day. The warehouse represents the main buffer between the production site, constituted by a foundry and a drawing plant, and the outgoing interface, where heavy load trucks are prepared continuously, in order to serve customers all over the world (Figure 1).

Figure 1: The automatic bundles warehouse

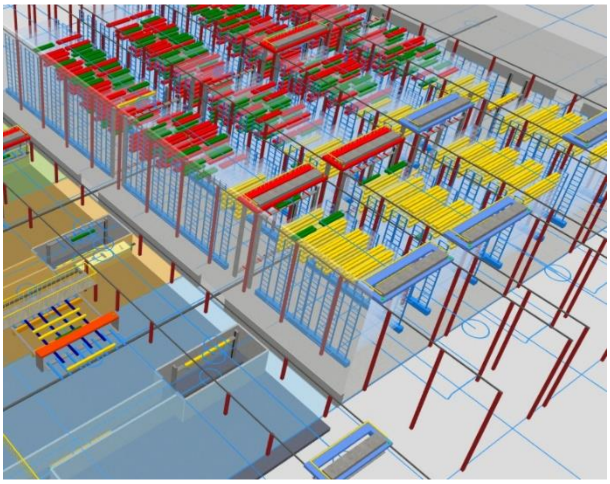

Figure 2: Simulation model of the automatic bundles warehouse

Products exiting the drawing plant are moved towards the warehouse, that is several meters far from the production site, by means of a few underground shuttles (whose end stations are partially visible in the simulated 3D model of Figure 2). Loading and unloading of the shuttles is performed by means of dedicated lifters and, in order to reduce the transferral time in presence of extraordinarily long paths, intermediate stations and duplicate shuttles may be present. The incoming tube bundles are then loaded by two different middle-height cranes, depending on the incoming lane and the destination location, that serve as distributors for the following stations (their number may vary depending on the site dimensions). These, in turn, are used to control the bundles, removing defective elements prior to store and expedite them, and to send them to the warehouse shelves by means of a different set of ground shuttles. The high intensity warehouse is constituted by a variable number of parallel shelves (about 10 meters high, with double depth and the possibility of accommodating a variable number of bundles depending on their length, as evidenced in Figure 1), forming long lanes, and it can contain up to tens of thousands bundles at the same time. The different lanes are served by means of lifters (that move the bundles from the incoming shuttles up to the cranes) and upper cranes that have three different purposes:

1. To insert the incoming bundles.
2. The actual model presents many repeated sub-processes (with limited or no modifications) and similar equipment and facilities.
3. To pick-up the required outgoing bundles.

Outgoing bundles are moved again down to the ground shuttles (the same that operate the incoming flow) and are transferred to the loading stations, where the trucks are prepared for the final destinations.
This process presents some interesting complexities. Among them, it is important to highlight that:

- Bottlenecks are not known a priori and cannot be easily determined. Optimization opportunities remain almost hidden and difficult to be evaluated.
- The distributor cranes shall be programmed to avoid overlapping and to minimize the travelled distance.
- The ground shuttles, serving the warehouse both with respect to the incoming and the outgoing flows, shall be programmed carefully to optimize the two flows.
- The warehouse cranes shall be programmed to avoid overlapping, to minimize the travelled distance and to effectively allocate the bundles in order to optimize the subsequent handling stages.

As soon as the initial analysis had been completed, it emerged clearly that the process was too complex to be modelled by a standard, monolithic discrete events simulation (Figure 3).

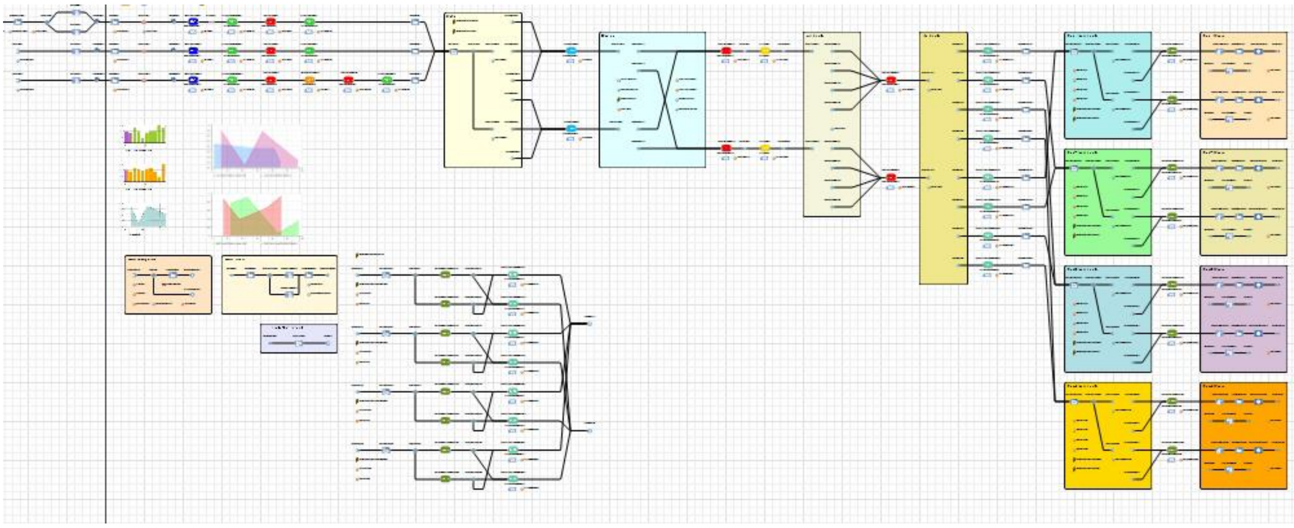

Figure 3: The main flow and its complexity (small blocks represent complex sub-processes).

Therefore, we immediately looked for a simulation environment in which we could use different methodologies and a modular approach at the same time. Thus, our final choice was that of adopting the Anylogic® Professional simulation package, that allows modellers to build applications with a fully working mix of Discrete Event Simulation, System Dynamics and Agent Based Simulation.

As stated, these requirements have been modelled making use of OOP techniques and a hierarchical modular approach aimed at simplifying the whole process. In particular, the most important elements have been carefully isolated and modelled as independent, intelligent agents that can interact and communicate with each other. These agents represent, among the various entities, the incoming and the outgoing orders, the end-line machines, the lifters (those used to load-unload the underground shuttles and those used within the warehouse as well), the underground and ground shuttles, the controller stations, the middle-height distributor cranes and the warehouse cranes (Figure 4)

Figure 4: OOP components within the main flow (partial view)

The OOP paradigm has been extensively adopted to inherit and modify single entities, when needed. For instance, underground and ground shuttles, though differently managed, are almost similar.

Therefore, they have been derived from a common ancestor and have been later specialized to perform their own tasks adequately. The middle-height cranes and the warehouse cranes are different both with respect to the functioning and to the exterior appearance, yet they have a common parent that provide them with the basic functionalities (Figure 5 and Figure 6 show the crane class constituting elements, along with the corresponding flow management class).

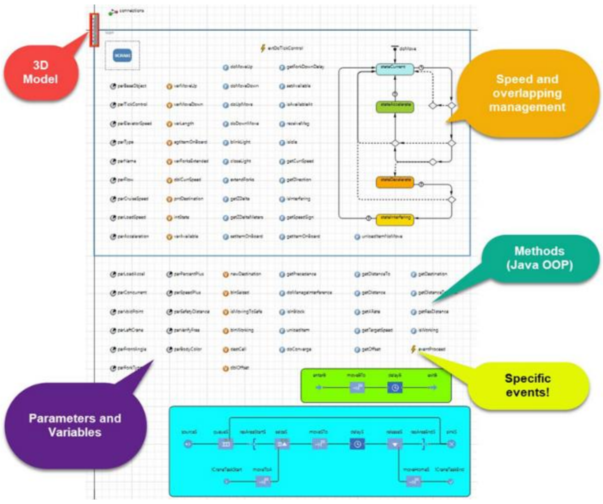

Figure 5: Crane agent structure (HCrane agent)

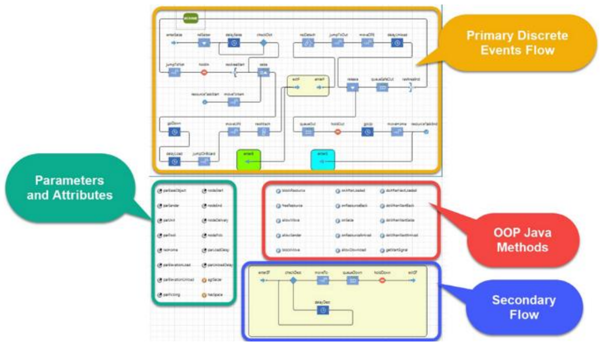

Figure 6: Crane agent flow structure (HCraneFlow agent)

5. VERIFICATION AND VALIDATION

One of the major concerns when modeling and simulating a real case deals with the subsequent verification and validation. Following Sargent (2011), verification ensures that the model and its implementation are correct, whereas validation grants that the model "possesses a satisfactory range of accuracy, consistent with the intended application of the model". Naturally, we may need many different experimental conditions to define the model intended applicability. Therefore, due to costs and time, it is often impossible and/or inconvenient to look for absolute validity.

Following this approach, we performed the conceptual model validation, the implementation validation and, finally, the operational validation. In particular, we used animations, events validation, and historical data to ensure that both the conceptual model and the corresponding computer translation were good enough to satisfy the end-user requirements.

Finally, we performed a set of experimental runs to optimize the parameters and a parameter-based sensitivity analysis to determine the effect of variability on the obtained outcomes. Results of this activity were good enough to ensure that the model was correct with enough degree of confidence. With respect to the available historical data, that however lacked of information about specific breakdowns and warnings from sensors (these were not available and should be collected punctually in the future), the model followed the real data with a small deviation (the error between the real and the simulated warehouse consistency resulted lower than 7.5%) and both the performance and the saturation level of the simulated equipment was comparable with that of the real shuttles and cranes.

6. RESULTS AND CONCLUSIONS

In conclusion, a very complex model dealing with the automatic warehouse management of a plant for copper tubes production, has been effectively decomposed into a hierarchical, modular structure that is easy to develop, test, validate, modify and maintain. The single components that constitute the model can be effortlessly adapted to different situations and, thanks to a fully parametric approach, they can be effectively used to simplify the modelling phase and to optimize the model itself, for instance, using experiments that may vary several parameters at the same time. Further, the OOP paradigm along with the agent modelling methodology has allowed to build complex entities that are able to deal autonomously with specific, often intricate issues (for example, the cranes are able to deal with speed and overlapping control by themselves). Finally, the case study has shown that the possibility of integrating agents modelling and discrete events gives an enormous advantage in that it allows to make the most of the in-depth knowledge of flows and procedure (typical of the discrete event simulation), while, at the same time, all those aspects that cannot ne mimicked with the classical discrete events programming are introduced within the agents by means of state charts and pure java OOP. The model is therefore a valuable tool to verify the current productivity of the warehouse (identifying issues and bottlenecks, for example) and to analyse potential improvements and future modifications.

ACKNOWLEDGMENTS

The authors would like to thank the Consorzio Quinn (https://www.consorzioquinn.it/) for allowing us the use of the licensed version of the Anylogic® Professional simulation package, without which this research paper would not have been possible.

REFERENCES

Armstrong D.J., 2006. The Quarks of Object-Oriented Development. Communications of the ACM, 49 (2), 123-128.

Calzavara M., Glock C.H., Grosse E.H., Persona A., Sgarbossa F. 2017. Analysis of economic and ergonomic performance measures of different rack layouts in an order picking warehouse. Computers & Industrial Engineering, 111, 527–536.

Gu J., Goetschalckx M., McGinnis L.F., 2010. Research on warehouse design and performance evaluation: A comprehensive review. European Journal of Operational Research, 203 (3), 539-549.

Guo X., Yu Y., De Koster R.B.M. 2015. Impact of required storage space on storage policy performance in a unit-load warehouse. International Journal of Production Research, 54 (8), 2405–2418.

Kindler E., Krivy I., 2011. Object-Oriented Simulation of systems with sophisticated control. International Journal of General Systems, 40 (3), 313-343.

Krenczyk D., Davidrajuh R., Skolud B., 2019. Comparing Two Methodologies for Modeling and Simulation of Discrete-Event Based Automated Warehouses Systems. In: Hamrol A., Kujawińska A., Barraza M., eds. MANUFACTURING 2019: Advances in Manufacturing II. Cham: Springler, 161-175.

Piccinini A., Previdi F., Cimini C., Pinto R., Pirola F., 2018. Discrete event simulation for the reconfiguration of a flexible manufacturing plant. 16th IFAC Symposium on Information Control Problems in Manufacturing, pp. 465-470 June 11-13, Bergamo (Italy).

Rouwenhorst B., Reuter B., Stockrahm V., van Houtum G.J., Mantel R.J., Zijm W.H.M., 2000. Warehouse design and control: framework and literature review. European Journal of Operational Research, 122, 515–533.
Sargent R.G., 2013. Verification and validation of simulation models. Journal of Simulation, 7(1), 12-24.
Smith D., Srinivas S., 2019. A Simulation-based Evaluation of Warehouse Check-in Strategies for Improving Inbound Logistics Operations. Simulation Modelling Practice and Theory, 94, 303-320.
Sumari S., Ibrahim R., Zakaria N.H., Hamid A.H.A., 2013. Comparing three simulation model using taxonomy: system dynamic simulation, discrete event simulation and agent-based simulation. International Journal of Management Excellence, 1, pp. 54-59.
Vieira A.A.C., Dias L.M.S., Pereira G.A.B., Oliveira, J.A., Carvalho M.D.S., Martins P, 2018. Simulation model generation for warehouse management: case study to test different storage strategies. International Journal of Simulation and Process Modelling, 13 (4), 324-336.
Zeigler B.P., 1987. Hierarchical, modular discrete-event modelling in an object-oriented environment. Simulation, 49 (5), 219–230.
Zeigler B.P., 1990. Object Oriented Simulation with Hierarchical Modular Models. 1st ed. Cambridge: Academic Press.

AUTHORS BIOGRAPHY

Marcello Braglia graduated (with distinction) in 1988 in Electronic Engineering at Politecnico di Milano. Since 1995, he has been a Researcher in Mechanical Technology and Production Systems at the Università degli Studi di Brescia. Since 1998, he has been employed as a researcher and since 2002, as a Full Professor, in Industrial Plants at the Università di Pisa. His research activities mainly concern maintenance, reliability, production planning, lean production, logistics and statistical quality control. He is the author of about 180 technical papers published in national and international journals and conference proceedings. He is a member of ANIMP (National Association on Industrial Plants) and AIDI (National Association of Academicians on Industrial Plants).

Marco Frosolini graduated in Mechanical Engineering at the Università di Pisa and obtained a PhD in Mechanical Engineering in 2005. He is currently a researcher in Industrial Plants within the same University. His research activities mainly concern equipment maintenance and reliability, production planning, logistics and project management. He is also interested in industrial information systems. He is author of more than 30 technical papers, published in national and international journals and conference proceedings. He is a member of AIDI (National Association of Academicians on Industrial Plants).

Roberto Gabbrielli graduated with honours in Mechanical Engineering, specializing in Energy, at the University of Pisa (Italy). He has a PhD in Energy Power Systems and is Associate Professor in Industrial Systems Engineering at the Department of Civil and Industrial Engineering of the University of Pisa (Italy). His current research concerns production planning and control, development of decision support systems for industrial investments, occupational safety, energy saving, energy storage and the reduction of the environmental impact in industrial systems. He authored more than 25 papers published in international scientific journals.

Leonardo Marrazzini graduated (110/110) in 2016 in Mechanical Engineering at the University of Pisa. In the same year, he began his PhD studies in Industrial Plants within the same university. His research activities mainly concern the adaptation of Lean Manufacturing principles to engineering-to-order (ETO) production environments. His research focuses on models and techniques to support various company operations.

Luca Padellini
Luca Padellini graduated in 2018 in Mechanical Engineering at the University of Pisa. In the same year, he began his PhD studies in Smart Industry within the same University. His research activities mainly concern the digitalization of the supply chain in the Tuscan Fashion district. His research focuses on models and techniques able to improve the communication and the transfer of information between the members of the supply chain.

MODELLING AND SIMULATION TOOLS FOR INTEGRATING FORWARD AND REVERSE LOGISTICS: A LITERATURE REVIEW

Giulio Paolo Agnusdei[(a)], Maria Grazia Gnoni[(b)], Fabiana Tornese [(c)]

[(a),(b),(c)]Department of Innovation Engineering, University of Salento, Lecce

[(a)]giuliopaolo@agnusdei@studenti.unisalento.it, [(b)]mariagrazia.gnoni@unisalento.it, [(c)]fabiana.tornese@unisalento.it

ABSTRACT

The scientific and technical interest towards sustainability issues is increasing in the industrial sector; thus, closed-loop supply chains are getting more and more diffused. As recycling and remanufacturing strategies are becoming a common practice, the importance of reverse logistics is nowadays increasing. Practitioners need to face with both strategic and operational level decisions related to the coordination of direct and reverse logistic flows. While several reviews are available on reverse logistics and closed-loop supply chains, a summary of scientific literature on integrated forward and reverse logistics is still missing. This paper proposes a review of the literature focused on how to integrate forward and reverse logistics in the industrial sector. The main purpose is to identify advantages and criticalities of current tools highlighted by researchers on this topic, with particular attention to modelling and simulation tools. A critical analysis on the benefits and challenges of the main methods identified is proposed. A discussion about potentialities provided by simulation modelling is also discussed.

Keywords: integrated forward-reverse logistics, simulation modelling, closed-loop supply chains, literature review.

1. INTRODUCTION

In the last 20 years, reverse logistics flows have been growingly integrated in supply chains to guarantee the recovery of products and materials at the end of their useful life (Islam and Huda 2018). Reverse logistics (RL) involve activities in the waste management sectors as well as product recovery in industrial supply chains. On one side, legislations worldwide are pushing towards waste reduction and material recovery, especially in specific sectors (such as the waste from Electronic and Electric Equipment, EEE), lately promoting Circular Economy (CE) models to replace consumption-based linear systems (Govindan et al. 2015). The CE paradigm strongly relies on the integration of direct and reverse logistics to keep materials in the economic system and prevent them from becoming waste (Elia et al. 2016; Ellen MacArthur Foundation 2013). On the other side, material recovery and remanufacturing activities are proving to be potentially profitable for companies in the manufacturing sector (Guide and Van Wassenhove 2009). In this scenario, the problem of the integration of forward and reverse (F/R) logistics in a closed-loop supply chain (CLSC) is being studied from researchers with different modelling approaches, in order to optimize the performance of the CLSC and maximize profits for the company. While scientific literature has been focusing on CLSC and reverse logistics for two decades, and several reviews are already available on the topic, highlighting the main challenges and opportunities, a specific focus on the integration of F/R flows is still missing. This paper tries to fill this gap, providing a literature review about the main modelling and simulation methodologies used to design and manage integrated F/R flows. In the next section, a background on the main contexts and issues in the integration of F/R flows is provided. Section 3 shows the methodology followed, while the literature review is provided in section 4. Section 5 offers a discussion about the use of simulation modelling in this sector, while conclusions are drawn in Section 6.

2. THE INTEGRATION OF FORWARD AND REVERSE LOGISTICS IN A CLOSED-LOOP SUPPLY CHAIN

A traditional supply chain involves all the actors that participate in the process of value creation for the final customer, from suppliers, manufacturers, to distributors, wholesalers, retailers and logistics operators, including all the activities traditionally indicated as forward logistics. In the last decades, RLs became more and more important, allowing to recover products and materials from the end customer and send them back to different echelons of the supply chain, enabling several possible end-of-life (EOL) scenarios, such as reuse, repair, remanufacturing, recycling.
A CLSC integrates both the forward and the reverse logistics flows, designing and managing the operations with the aim of maximizing the value creation (Coenen et al. 2018; Govindan et al. 2015). An example of a generic CLSC is given in Figure 1. The coexistence of these two flows increases the system complexity and pose some challenges in logistics, related to network design, production planning, fleet management, operations management. Two main issues can be

identified: the first problem is to address is the possibility of *coordinating forward and reverse flows in last-mile logistics*, combining the delivery to the final customer with the collection of EOL products, which can be convenient if both the operations are managed by the same actor. This coordination is already in place in several business-to-business (B2B) contexts: to name a few examples, new tires distribution to mechanic's workshops is often combined with the collection of used ones; a similar dynamic can be found in pallet management models where direct interchange of new and used pallets is put in place (Elia and Gnoni 2015). The "one-to-one" service operated by retailers of electric and electronic equipment for big devices (e.g. white goods) that collect the used device when the customer buys a new one, is another example of simultaneous delivery and pickup (SDP), in the business-to-consumer (B2C) context.

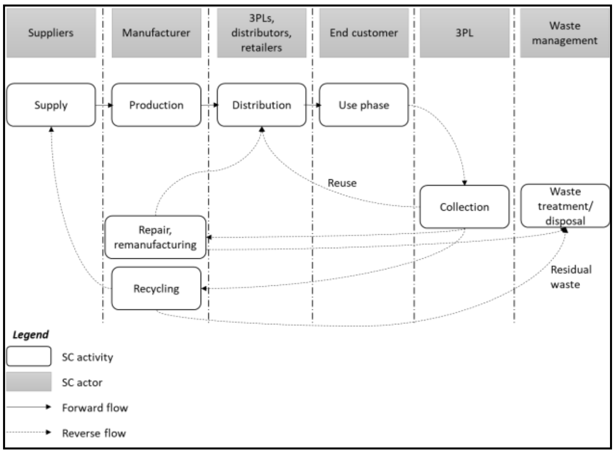

Figure 1: A generic closed-loop supply chain

The second main problem is related to the high *uncertainty of return flows* in a CLSC (Ponte et al. 2019). While forward flows are usually managed based on more or less accurate forecasts of the end customer's demand, considering the production capacity of the manufacturer and planning production and distribution accordingly, it is not always simple to collect data about returned or EOL products. First of all, different types of reverse flows can coexist in a SC, according to the nature of the unit returned. The main types are summarized as follows:

- *New returned products*: this category includes new items that have been bought by the customer but never been used, and returned for different possible reasons (e.g. wrong size, customer's dissatisfaction, etc.). This flow is particularly relevant in e-commerce, but is also present in traditional retail. New returned products are usually inspected for quality and then restocked, if compliant.
- *Defective products*: this includes the used products that are returned for maintenance to the manufacturer. They usually undergo repair/refurbishment (according to the level of damage) and are shipped back to the customer, or can be replaced with new ones while they are remanufactured/recycled or disposed.
- *EOL products*: used products at the end of their life that the customer does not use anymore. Like defective products, these products can be reused, repaired, remanufactured or recycled according to their state and functionality, and can get back in the forward SC.
- *Waste materials*: this includes all products and materials that are not recoverable and undergo waste treatment or disposal.

For each flow type, the return rate during time can vary sensitively according to several factors, e.g. users' habits and behavior, market fluctuations that can foster (or limit) the sales of new products substituting used ones, defectiveness of new products that are sent back to the manufacturers, etc. For example, the amount of new returned products can vary from an average of 8-10% in brick-and-mortar to 20-30% in e-commerce: one common example is represented by the apparel sector, where often customers buy online, try the items at home and ship back those they do not like (Orendorff 2019; Saarijärvi et al. 2017). This type of customer behavior is not easily predictable, although it can be more prominent in specific sectors. Consequently, a high uncertainty and variability of return flows can increase the SC complexity, since a full coordination of forward and reverse flows cannot easily be reached. To cite a few examples, a high percentage of new products returns would require an adjustment of the data about sales, therefore of the actual demand of customers. The flow of repaired and remanufactured products has to be matched with the customer demand for repaired or remanufactured products, and a perfect correspondence between demand and offer is not always the case. Similarly, recycled materials have to find space in the secondary material market. All these issues make the uncertainty of reverse flows a critical point to address, and the coordination of forward and reverse flows one possible way to address it.
The two issues described can occur differently in different contexts: we propose in this section three examples to better contextualize the problem, summarized in Table 1.

2.1. Integration of F/R in Remanufacturing
Remanufacturing is one of the most diffused contexts in which F/R logistics need to be integrated in a CLSC. It represents not only a material recovery strategy that can benefit the environment, but also a business strategy that can potentially increase a manufacturer's revenue. Moreover, in the last decade it's been acknowledged to be one of the mail pillars of CE, this increasing its adoption as a more effective alternative strategy to waste management that keeps the value of products and materials inside the SC (Jensen et al. 2019). In this context, new circular business models based on the use of a product more than its consumption and the

recovery of components and materials at the end of its useful life (e.g. leasing) are growingly being studied and implemented by manufacturers (van Loon et al. 2019).
The main return flows involved in remanufacturing are EOL products and defective products, which can be repaired or remanufactured and placed back to market. Considering the two main issues illustrated about CLSC, remanufacturing has its peculiarities.
By analyzing the coordination of F/R flows, the most relevant factor to be evaluated is the logistics organization, starting from the identification of collection points, which often correspond to point of sales. As previously mentioned, this condition occurs especially when use-based business models are applied (Gnoni et al. 2017) as for retailers of large EEE. When retailers are also collection points, F/R flows can be managed simultaneously, resulting in a vehicle routing with SDP. When collection points are not part of the forward logistic network, the vehicle routing problem (VRP) is with mixed deliveries and pickups (MDP) (Wassan and Nagy 2014).
Regarding the uncertainty of return flows, this is a crucial issue for business models based on remanufacturing, since not only the logistics operations have to be planned according to the actual return flow, but also the remanufacturing operations, that need to be matched with the demand of remanufactured products from the secondary market. This issue can be partly overcome through accurate sales forecasts of new products, that allow to estimate substitutions of used products, while it is even more controlled in use-based business models, where usually the contract with the customer establishes the period of time after which the product can be returned or substituted.

Table 1: Main features of the three contexts analyzed

Context	Flow involved	Coordination F/R logistics	Uncertainty
Remanufacturing	EOL products, defective products	SDP or MDP models	coordination of new and remanufactured products
WEEE	EOL products	Not possible	High variability of return flows
E-commerce	New returned products, defective products	SDP or MDP models	Extreme variability of return flows

2.2. Integration of F/R in Waste of Electronic and Electric Equipment (WEEE) logistic

Another specific context in which the management of return flows is crucial is the WEEE sector. WEEE is different than other waste flows for its composition and value: EOL electronic products often contain both hazardous materials that need to be properly processed and precious materials that can be recovered with profit. The EU directive on WEEE establishes some collection channels, together with recycling targets: the "one-to-one" policy guarantees to consumers that buy a new device the possibility to leave the old one to the retailer. The "one-to-zero" policy requires big retailers to collect small electronic devices from customers, even when they do not buy a new one. In both scenarios, the retailer has to manage the stock of returned products as a temporary collection point, from which the WEEE is then collected by specialized logistic service providers. Therefore, retailers act both as a delivery point for forward flows and collection point for reverse flows. Next to them, other collection points are often established by municipalities, where users can deliver their waste, including WEEE (Elia et al. 2018).
Since legislation in most countries (e.g. Italy) does not allow to manage products and waste simultaneously, the collection problem in WEEE reverse logistics is not related to the coordination with forward flows, but to collection planning. The complexity of the network, with multiple collection points that have different functions, capacities and WEE generation rates, requires flexible and adaptive models that can monitor the state of each collection point, in order to plan the routing and scheduling accordingly. The main issue in WEEE collection systems is the uncertainty of reverse flows, which depends on customers' behavior, on the different collection models available in the system, on the existence of informal secondary markets where users often sell or give their used EEE. For these reasons, traditional and static collection schemes do not fit the needs of WEEE, while dynamic schemes based on internet-of-things technologies can be much more effective (Elia et al. 2019).

2.3. Integration of F/R in e-commerce

The e-commerce sector has been growing considerably in the last years, and last-mile logistics operators have been facing the challenges related to this context (Cárdenas et al. 2017). The reverse logistics of new and defective products is one of these challenges. Product returns in e-commerce can be driven by many different reasons, according to the customer's habits and behavior: Saarijärvi et al. (2017) identified ten types of returning reasons (e.g. a mistake in the type or size of the product, a quality issue, the same product has been found cheaper on another on-line store, etc.). This, of course, increases sensitively the variability of return flows in e-commerce, that can represent up to 30% of the sales. Another peculiarity of this context is that the delivery point in last-mile logistics varies from case to case: there are not fixed delivery points, since the good is shipped singularly to the buyer's location (instead of being sent in batches to retailers' stores). On the other hand, pickup points for returned products can be fixed locations (like collection points of the logistics operators, or physical retail stores when cross-channel strategies are in place (Radhi and Zhang 2019)) or variable ones, when the service include the home-pickup from the customer's location. Since often both pickup and delivery are managed by the same 3PL operator, the coordination of F/R flows in last-mile logistics can be realized, addressing the VRP with SDP or MDP, according to the nature of shipments. Scheduling and routing need to be dynamic, since both the locations and the delivery/pickup frequency are variable.

3. METHODOLOGY

A systematic literature review has been performed to analyze what have been the main methodologies and tools to study the integration of F/R logistic flows. The scientific databases Web of Science and Scopus were searched for the review, using different combinations of keywords: “integrated forward reverse logistics”, “reverse logistics + last-mile delivery”, “forward reverse logistics + simulation”. Of the 121 articles found, a first selection was made based on the title and the abstract, including only those that addressed the issue of the integration of F/R logistics flows in a CLSC. The second screening was based on the content of the articles, resulting in a final sample of 78 papers (including publications on international journals and conference proceedings) published until June 2019.
After the selection, articles have been classified according to the year and journal of publication, the problem addressed, the methodology used, the nature of the variables analyzed (stochastic or deterministic) and the objectives pursued (where applicable). This allowed to perform a deeper analysis whose results are presented in the next section.

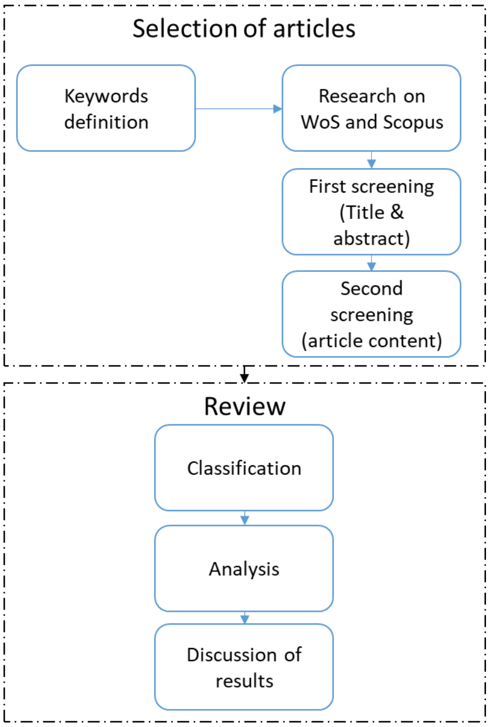

Figure 2: The methodology followed

4. THE LITERATURE REVIEW

The 78 papers analyzed were published on a wide variety of sources, including 45 international journals and 16 conference proceedings. Of these, only 14 international journals included more than one of the selected papers: just 3 of them (the *Annals of Operations Research*, the *International Journal of Production Economics* and *Scientia Iranica*) included three articles each. This shows that the problem in analysis invests different fields and is studied from different perspectives, from logistics to economics, from transportation science to mathematical modelling.
Concerning the publication period, all of the articles found were published in the last 12 years (2007-2019), as shown in Fig. 3. No trend has been identified, with a number of publications per year ranging from a minimum of two (in 2011) and a maximum of nine (in 2016), and an average of six. This shows a continuous interest in the topic from the scientific community in the last decade that is likely to go on, given the growing diffusion of CLSCs worldwide.

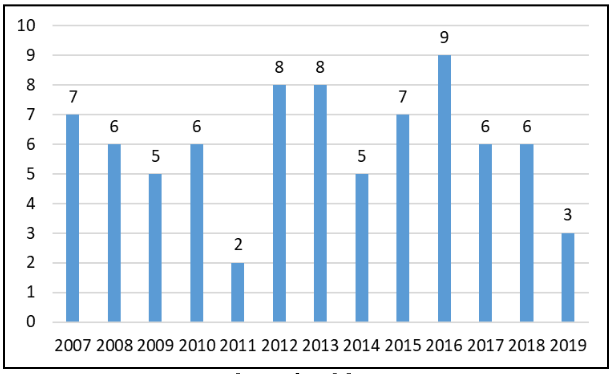

Figure 3: Number of publications per year

The first analyzed factor is the type of *main problem addressed* in the study. As shown in Table 2, almost half of the articles are focused on a network design and operations problem, while 13 focus only on network design and 10 only on operations in a CLSC. Together, these three clusters include about 75% of the papers reviewed, listed in Table 3.

Table 2: Focus of the articles analyzed

Focus	Frequency
Network design and operations	37
Network design	13
CLSC operations	10
Inventory model	4
VRP	3
VRP with SDP	3
Long-term behavior analysis	3
Other	5
Total	78

Other 4 works are focused specifically on inventory management in the CLSC, elaborating optimal replenishment policies (Chung et al. 2008; Mitra 2012), lot sizing policies (Kim et al. 2013) and recovery policies (Niknejad and Petrovic 2014) to maximize the profit. Seven papers address the vehicle routing problem (VRP), focusing on different aspects of the well-known problem, such as the simultaneous delivery and pickup (SDP) (Gajpal and Abad 2010; Xie et al. 2007; Zhang et al. 2014), the presence of cross-docking facilities (Kaboudani et al. 2018), the coordination of F/R flows (Chang and Liao 2011; Dondo and Méndez 2016).

Table 3: Articles focused on network design and/or operations.

Focus	Articles
Network design and operations	(Al-Salem et al. 2016; Choudhary et al. 2015; De Rosa et al. 2013; Elahi and Franchetti 2014; Fattahi and Govindan 2017; Garg et al. 2014; Guo et al. 2018; Hatefi et al. 2016; S.M. Hatefi et al. 2015; S. M. Hatefi et al. 2015; Hatefi and Jolai 2015, 2014; Ko and Evans 2007; Lee et al. 2007a, 2007b, 2013, 2012; Lee and Dong 2008; Lee and Lee 2012; Lin et al. 2009; Lu and Zhao 2010; Nobari and Kheirkhah 2017; Pedram et al. 2017; Peng and Yao 2007; Pishvaee et al. 2010, 2009; Rezaei and Kheirkhah 2017; Roghanian and Kamandanipour 2013; Ross et al. 2017; Soleimani et al. 2016; L.-C. Wang et al. 2013; Wang and Di 2010; Wang and Zhao 2009; Y. Wang et al. 2013; Yazdi and Honarvar 2015; Zhou and Xu 2009; Zohal and Soleimani 2016)
Network design	(Afshari et al. 2016, 2014; Barker and Zabinsky 2008; Behmanesh and Pannek 2018, 2016; Chen et al. 2017; Cilacı Tombuş et al. 2017; Ding 2010; Djikanovic et al. 2015; Djikanovic and Vujosević 2016; Easwaran and Üster 2010; Faccio et al. 2011; Sahyouni et al. 2007)
CLSC operations	(Chen et al. 2008; Gu and Ji 2008; Habibi et al. 2019; Jalil et al. 2019; Jayant and Kumar 2012; Jinlan and Ni 2007; Keyvanshokooh et al. 2013; Mehdizadeh et al. 2013; Porkar et al. 2018; Zhou 2015)

Three works from the same research group study the long-term behavior of an integrated F/R logistic system under different managerial scenarios (Das and Dutta 2013a, 2013b, 2012). Finally, the last five works address other aspects characterizing an integrated F/R logistics system, adopting qualitative approaches to frame the context (de la Fuente et al. 2008; Jaaron and Backhouse 2016), focusing on restocking and fee policies (Shulman et al. 2009), on government policies influencing the recycling quality (Tan and Guo 2019), or on the selection of third party forward and reverse logistics providers (Govindan et al. 2019).

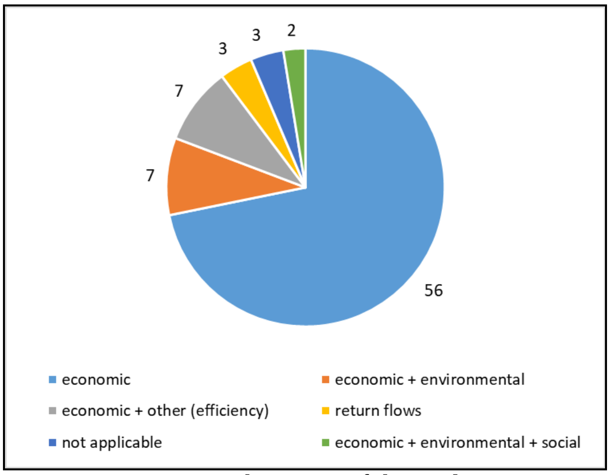

Figure 4: Objectives of the studies

Regarding the *main objectives* considered in the studies analyzed, Figure 4 shows that research so far has been mostly focused on the optimization of economic objectives, either alone or combined with other performance measures, such as customer satisfaction (Afshari et al. 2016, 2014), entity of return flows (Lee et al. 2007b; Niknejad and Petrovic 2014), time (Lee et al. 2013), responsiveness (Pishvaee et al. 2010), efficiency (Jayant and Kumar 2012). Seven works focus on two dimensions of sustainability, looking at both the economic and the environmental performance (Chen et al. 2017; Choudhary et al. 2015; Garg et al. 2014; Porkar et al. 2018; L.-C. Wang et al. 2013; Y. Wang et al. 2013; Zohal and Soleimani 2016), while only two include also the social dimension (Govindan et al. 2019; Nobari and Kheirkhah 2017). Finally, three of the articles reviewed measured the return flows in the CLSC as main key performance indicator (KPI) (Das and Dutta 2013a, 2013b, 2012).

Table 4: Use of deterministic and stochastic models in the methodologies applied

Methodology	Deterministic models	Stochastic models
Analytical model (71)	52	19
Simulation model (4)	0	4
Qualitative framework (3)	--	--

Considering the *methodology* adopted for the study, most of the articles reviewed were based on an analytical model (71), four of them used simulation to investigate the problem and only three were based on some kind of qualitative framework (Table 4). This show a clear prevalence of analytical models used to address different kinds of problems in the design and management of a CLSC with the integration of F/R logistics. A variety of methods has been applied (e.g. mixed integer linear and non-linear models, multi-objective models, fuzzy linear programming models, etc.), which in 73% of cases are deterministic models, but also 19 stochastic programming models have been found. In the case of simulation modelling, the most applied technique is System Dynamics (SD), used to model the long-term behavior of the system (Das and Dutta, 2013a, 2013b, 2012), while in one case the Discrete Event Simulation (DES) has been used to model the whole SC and its flows (Jayant and Kumar 2012).

5. THE USE OF SIMULATION FOR THE DESIGN AND MANAGEMENT OF INTEGRATED F/R LOGISTICS

We can notice from the review that simulation modelling is not widely adopted in the context of F/R logistics integration, and it has been applied so far only in works focusing on CLSC operations or on long-term behavioral analysis, while in all other cases an analytical model has been preferred. In particular, analytical models have been mostly applied to optimize the performance of the CLSC (mainly economic, but also from other perspectives), while simulation models to explore the behavior of the system in the future and the interactions between the actors and the variables analyzed. Therefore, despite the higher complexity of contexts with integrated F/R logistics, most researchers are still adopting classic analytical tools typically employed in SCM (e.g. MILP models, VRP, etc.) to analyze systems with higher variability and uncertainty, leaving the potential contribution of simulation methodologies mostly unexplored.

Each of the three main simulation methodologies available has some peculiarities that entail some strengths and weaknesses, which can make them more suitable to some kinds of problems than the others. DES models the system based on passive entities that flow through a process (a sequence of activities employing different resources). The model advances with a discrete time following a sequence of events. It is most suitable to capture low abstraction levels of a system, given its process-centric nature. On the contrary, SD is mostly used for high abstraction levels, aiming at capturing the complex dynamics resulting in a system from the interactions of entities and variables modelled as stocks and flows, with feedback structures. The model is based on a continuous time-scale through differential equations that define the causal relationships between variables. Finally, Agent Based Modelling (ABM) allows the representation of complex systems through the interaction of single intelligent entities (agents) with personal behavioral rules. Their interaction results in the final behavior of the whole system. This bottom-up approach allows reaching a wider range of abstraction, from the low level (agents' behavior) to the high level (system behavior), according to the specific needs and objectives of the modeler (Galvão Scheidegger et al. 2018). The features briefly described can be beneficial to model a context where F/R logistic flows are integrated in a closed-loop system. Table 5 summarizes some advantages of the three techniques, related to the two main modelling problems described in section 2: the necessity to coordinate direct and reverse flows and the high uncertainty of return flows in CLSCs.

Table 5: Advantages of simulation techniques in modelling integrated F/R logistic systems

Technique	F/R flows coordination	Uncertainty of return flows
DES	Captures entity flows and low-level processes	Allows using stochastic variables
SD	Captures high-level evolution of the system	Captures causal relationships between variables
ABM	Captures complexity due to interactions among individuals	Allows using stochastic variables

One of the strengths of DES is the ease of modelling processes based on activities and resources. This allows capturing the dynamics of a logistic process with a low level of abstraction, focusing on resource utilization, which is often a KPI for the process efficiency. Moreover, DES allows modelling both inputs and variables as stochastic, which gives the modeler the possibility to represent the inner uncertainty related to return flows and analyzing different possible scenarios, which is much harder to realize in an analytical model.

This can also be done with ABM, which is very effective in capturing the system evolution resulting from individuals' behavior and their interactions. This can be useful in a system where complexity arises from different entities, not just from the process represented.

On the other side, SD can be more suitable when the objective is to focus on the evolution of the system during time on a high-level. The possibility to model causal loops with positive and negative feedbacks highlights the impact on the system of variations due to one or more variables. This can facilitate the representation of return flows when uncertainty is related to the interactions between variables.

One more possibility for the modeler is to adopt a hybrid simulation approach: this allows integrating different techniques, exploiting the advantages of each particular methodology where they are needed, and overcoming their limits (Brailsford et al. 2019).

6. CONCLUSIONS

This work focuses on how to deal with the complexity of integrated F/R logistic systems, and how simulation could support the design and management of such systems. After a brief description of the main issues to face, illustrated through three typical examples of CL systems that require the integration of F/R flows, a literature review has pointed out what are the main problems addressed by researchers in this area, what are the most applied methodologies and what are the

objectives commonly involved. The review shows, among other results, that analytical approaches are still prevalent in this area, while a few works apply simulation to support the integration of F/R logistic flows, mainly to predict the system behavior in the future and its performance according to different scenarios. Starting from the analysis of the main benefits of each simulation technique, this work shows the potential of simulation methods in supporting the design and management of CLSC with integrated flows, underlining the possible advantages of this approach compared to traditional analytical ones.
Further research will be oriented to analyze each of the specific sectors identified (remanufacturing, e-commerce and WEEE) to understand how simulation can be beneficial in each of these contexts, according to their peculiarities.

REFERENCES

Afshari, H., Sharafi, M., ElMekkawy, T.Y., Peng, Q., 2016. Multi-objective optimisation of facility location decisions within integrated forward/reverse logistics under uncertainty. Int. J. Bus. Perform. Supply Chain Model. 8, 250.

Afshari, H., Sharifi, M., ElMekkawy, T.Y., Peng, Q., 2014. Facility Location Decisions within Integrated Forward/Reverse Logistics under Uncertainty. Procedia CIRP, Variety Management in Manufacturing 17, 606–610.

Al-Salem, M., Diabat, A., Dalalah, D., Alrefaei, M., 2016. A closed-loop supply chain management problem: Reformulation and piecewise linearization. J. Manuf. Syst. 40, 1–8.

Barker, T.J., Zabinsky, Z.B., 2008. Reverse Logistics Network Design: A Framework for Decision Making, in: Proceedings of the 2008 Industrial Engineering Research Conference. pp. 1290–1295.

Behmanesh, E., Pannek, J., 2018. The Effect of Various Parameters of Solution Methodology on a Flexible Integrated Supply Chain Model. Math. Probl. Eng. 2018, 1–14.

Behmanesh, E., Pannek, J., 2016. A memetic algorithm with extended random path encoding for a closed-loop supply chain model with flexible delivery. Logist. Res. 9, 22.

Brailsford, S.C., Eldabi, T., Kunc, M., Mustafee, N., Osorio, A.F., 2019. Hybrid simulation modelling in operational research: A state-of-the-art review. Eur. J. Oper. Res. 278, 721–737.

Cárdenas, I., Beckers, J., Vanelslander, T., 2017. E-commerce last-mile in Belgium: Developing an external cost delivery index. Res. Transp. Bus. Manag. 24, 123–129.

Chang, T.-S., Liao, Y.-F., 2011. Routing strategies for integrating forward distribution and reverse collection. J. Oper. Res. Soc. 62, 971–981.

Chen, Y., Liu, D., Mao, H., Tian, Y., 2008. Uncertain programming of the distribution/recovery center in forward/reverse hybrid logistics system, in: 2008 IEEE International Conference on Service Operations and Logistics, and Informatics, pp. 3057–3062. Beijing (China).

Chen, Y.-W., Wang, L.-C., Wang, A., Chen, T.-L., 2017. A particle swarm approach for optimizing a multi-stage closed loop supply chain for the solar cell industry. Robot. Comput. Integr. Manuf. 43, 111–123.

Choudhary, A., Sarkar, S., Settur, S., Tiwari, M.K., 2015. A carbon market sensitive optimization model for integrated forward–reverse logistics. Int. J. Prod. Econ. 164, 433–444.

Chung, S.-L., Wee, H.-M., Yang, P.-C., 2008. Optimal policy for a closed-loop supply chain inventory system with remanufacturing. Math. Comput. Model. 48, 867–881.

Cilacı Tombuş, A., Aras, N., Verter, V., 2017. Designing distribution systems with reverse flows. J. Remanufacturing 7, 113–137.

Coenen, J., van der Heijden, R.E.C.M., van Riel, A.C.R., 2018. Understanding approaches to complexity and uncertainty in closed-loop supply chain management: Past findings and future directions. J. Clean. Prod. 201, 1–13.

Das, D., Dutta, P., 2013a. Simulation Study of an Integrated Reverse Logistics in Fuzzy Environment, in: Yang, G.-C., Ao, S.-I., Huang, X., Castillo, O., IAENG Transactions on Engineering Technologies: Special Issue of the International MultiConference of Engineers and Computer Scientists 2012. Springer Netherlands, Dordrecht, 151–165.

Das, D., Dutta, P., 2013b. A system dynamics framework for integrated reverse supply chain with three way recovery and product exchange policy. Comput. Ind. Eng. 66, 720–733.

Das, D., Dutta, P., 2012. A System Dynamics Framework for an Integrated Forward-Reverse Supply Chain with Fuzzy Demand and Fuzzy Collection Rate under Possibility Constraints, in: Proceedings of the International MultiConference of Engineers and Computer Scientists (Hong Kong).

de la Fuente, M.V., Ros, L., Cardós, M., 2008. Integrating Forward and Reverse Supply Chains: Application to a metal-mechanic company. Int. J. Prod. Econ. 111, 782–792.

De Rosa, V., Gebhard, M., Hartmann, E., Wollenweber, J., 2013. Robust sustainable bi-directional logistics network design under uncertainty. Int. J. Prod. Econ. 145, 184–198.

Ding, S., 2010. Logistics Network Design and Optimization Based on Fuzzy Adaptive Differential Evolution Algorithm, in: International Conference on Biomedical Engineering and Computer Science, 1–4. IEEE, (Wuhan, China).

Djikanovic, J., Joksimovic, D., Vujosevic, M., 2015. Application of Variable Neighbourhood Search Method for Vehicle-Routing Problems in an Integrated Forward and Reverse Logistic Chain. Acta Polytech. Hung. 12, 51–70.

Djikanovic, J., Vujosević, M., 2016. A new integrated forward and reverse logistics model: A case study. Int. J. Comput. Intell. Syst. 9, 25–35.

Dondo, R.G., Méndez, C.A., 2016. Operational planning of forward and reverse logistic activities on multi-echelon supply-chain networks. Comput. Chem. Eng. 88, 170–184.

Easwaran, G., Üster, H., 2010. A closed-loop supply chain network design problem with integrated forward and reverse channel decisions. IIE Trans. 42, 779–792.

Elahi, B., Franchetti, M., 2014. A new optimization model for closed-loop supply chain networks, in: 2014 IEEE International Technology Management Conference, 1–9. (Chicago, IL, USA).

Elia, V., Gnoni, M.G., 2015. Designing an effective closed loop system for pallet management. Int. J. Prod. Econ. 170, 730–740.

Elia, V., Gnoni, M.G., Tornese, F., 2019. Designing a sustainable dynamic collection service for WEEE: an economic and environmental analysis through simulation. Waste Manag. Res. 37, 402–411.

Elia, V., Gnoni, M.G., Tornese, F., 2018. Improving logistic efficiency of WEEE collection through dynamic scheduling using simulation modeling. Waste Manag. 72, 78–86.

Elia, V., Gnoni, M.G., Tornese, F., 2016. Measuring circular economy strategies through index methods: A critical analysis. J. Clean. Prod.

Ellen MacArthur Foundation, 2013. Towards the Circular Economy - Economic and business rationale for an accelerated transition.

Faccio, M., Persona, A., Sgarbossa, F., Zanin, G., 2011. Multi-stage supply network design in case of reverse flows: a closed-loop approach. Int. J. Oper. Res. 12, 157.

Fattahi, M., Govindan, K., 2017. Integrated forward/reverse logistics network design under uncertainty with pricing for collection of used products. Ann. Oper. Res. 253, 193–225.

Gajpal, Y., Abad, P.L., 2010. Checking the feasibility of a vehicle route in integrated supply chain transportation model. Int. J. Bus. Perform. Supply Chain Model. 2, 258–281.

Galvão Scheidegger, A.P., Fernandes Pereira, T., Moura de Oliveira, M.L., Banerjee, A., Barra Montevechi, J.A., 2018. An introductory guide for hybrid simulation modelers on the primary simulation methods in industrial engineering identified through a systematic review of the literature. Comput. Ind. Eng. 124, 474–492.

Garg, K., Sanjam, Jain, A., Jha, P.C., 2014. Designing a Closed-Loop Logistic Network in Supply Chain by Reducing its Unfriendly Consequences on Environment, in: Babu, B.V., Nagar, A., Deep, K., Pant, M., Bansal, J.C., Ray, K., Gupta, U., Proceedings of the Second International Conference on Soft Computing for Problem Solving, 1483–1498, December 28-30, 2012. New Delhi (India).

Gnoni, M.G., Mossa, G., Mummolo, G., Tornese, F., Verriello, R., 2017. Circular economy strategies for electric and electronic equipment: a fuzzy cognitive map. Environ. Eng. Manag. J. 16, 1807–1817.

Govindan, K., Agarwal, V., Darbari, J.D., Jha, P.C., 2019. An integrated decision making model for the selection of sustainable forward and reverse logistic providers. Ann. Oper. Res. 273, 607–650.

Govindan, K., Soleimani, H., Kannan, D., 2015. Reverse logistics and closed-loop supply chain: A comprehensive review to explore the future. Eur. J. Oper. Res. 240, 603–626.

Gu, Q.L., Ji, J.H., 2008. An integrated logistics operational model for Remanufacturing/Manufacturing system based on the consumer market. Int. J. Logist. Syst. Manag. 4, 21.

Guide, V.D.R., Van Wassenhove, L.N., 2009. OR FORUM—The Evolution of Closed-Loop Supply Chain Research. Oper. Res. 57, 10–18.

Guo, H., Li, C., Zhang, Y., Zhang, C., Wang, Y., 2018. A Nonlinear Integer Programming Model for Integrated Location, Inventory, and Routing Decisions in a Closed-Loop Supply Chain. Complexity 2018, 1–17.

Habibi, Muh.K.K., Battaïa, O., Cung, V.-D., Dolgui, A., Tiwari, M.K., 2019. Sample average approximation for multi-vehicle collection–disassembly problem under uncertainty. Int. J. Prod. Res. 57, 2409–2428.

Hatefi, S.M., Jolai, F., 2015. Reliable forward-reverse logistics network design under partial and complete facility disruptions. Int. J. Logist. Syst. Manag. 20, 370.

Hatefi, S.M., Jolai, F., 2014. Robust and reliable forward–reverse logistics network design under demand uncertainty and facility disruptions. Appl. Math. Model. 38, 2630–2647.

Hatefi, S.M., Jolai, F., Torabi, S.A., Tavakkoli-Moghaddam, R., 2016. Integrated forward-reverse logistics network design under uncertainty and reliability consideration. Sci. Iran. 23, 721–735.

Hatefi, S.M., Jolai, F., Torabi, S.A., Tavakkoli-Moghaddam, R., 2015. A credibility-constrained programming for reliable forward–reverse logistics network design under uncertainty and facility disruptions. Int. J. Comput. Integr. Manuf. 28, 664–678.

Hatefi, S. M., Jolai, F., Torabi, S.A., Tavakkoli-Moghaddam, R., 2015. Reliable design of an integrated forward-revere logistics network under uncertainty and facility disruptions: A fuzzy possibilistic programing model. KSCE J. Civ. Eng. 19, 1117–1128.

Islam, M.T., Huda, N., 2018. Reverse logistics and closed-loop supply chain of Waste Electrical and Electronic Equipment (WEEE)/E-waste: A comprehensive literature review. Resour. Conserv. Recycl. 137, 48–75.

Jaaron, A.A.M., Backhouse, C., 2016. A systems approach for forward and reverse logistics design. Int. J. Logist. Manag.
Jalil, S.A., Hashmi, N., Asim, Z., Javaid, S., 2019. A de-centralized bi-level multi-objective model for integrated production and transportation problems in closed-loop supply chain networks. Int. J. Manag. Sci. Eng. Manag. 14, 206–217.
Jayant, A., Kumar, S., 2012. Simulation Modeling of Integrated Supply Chain Logistics Networks, in: Deep, K., Nagar, A., Pant, M., Bansal, J.C. (Eds.), Proceedings of the International Conference on Soft Computing for Problem Solving, December 20-22, 2011, Advances in Intelligent and Soft Computing. Springer India, 101–111.
Jensen, J.P., Prendeville, S.M., Bocken, N.M.P., Peck, D., 2019. Creating sustainable value through remanufacturing: Three industry cases. J. Clean. Prod. 218, 304–314.
Jinlan, L., Ni, J., 2007. A Hybrid Immune Genetic Algorithm Approach to Optimize the Integrated Forward/Reverse Logistics Network for 3PLs, in: Third International Conference on Natural Computation (ICNC 2007), IEEE, 609–613. Haikou (China).
Kaboudani, Y., Ghodsypour, S.H., Kia, H., Shahmardan, A., 2018. Vehicle routing and scheduling in cross docks with forward and reverse logistics. Oper. Res.
Keyvanshokooh, E., Fattahi, M., Seyed-Hosseini, S.M., Tavakkoli-Moghaddam, R., 2013. A dynamic pricing approach for returned products in integrated forward/reverse logistics network design. Appl. Math. Model. 37, 10182–10202.
Kim, T., Goyal, S.K., Kim, C.-H., 2013. Lot-streaming policy for forward–reverse logistics with recovery capacity investment. Int. J. Adv. Manuf. Technol. 68, 509–522.
Ko, H.J., Evans, G.W., 2007. A genetic algorithm-based heuristic for the dynamic integrated forward/reverse logistics network for 3PLs. Comput. Oper. Res. 34, 346–366.
Lee, D.-H., Bian, W., Dong, M., 2007a. Multiproduct Distribution Network Design of Third-Party Logistics Providers with Reverse Logistics Operations. Transp. Res. Rec. J. Transp. Res. Board 2008, 26–33.
Lee, D.-H., Bian, W., Dong, M., 2007b. Multiobjective Model and Solution Method for Integrated Forward and Reverse Logistics Network Design for Third-Party Logistics Providers. Transp. Res. Rec. J. Transp. Res. Board 2032, 43–52.
Lee, D.-H., Dong, M., 2008. A heuristic approach to logistics network design for end-of-lease computer products recovery. Transp. Res. Part E Logist. Transp. Rev. 44, 455–474.
Lee, H., Zhang, T., Boile, M., Theofanis, S., Choo, S., 2013. Designing an integrated logistics network in a supply chain system. KSCE J. Civ. Eng. 17, 806–814.
Lee, J.-E., Lee, K.-D., 2012. Integrated forward and reverse logistics model: a case study in distilling and sale company in Korea. Int. J. Innov. Comput. Inf. Control 8, 4483–4495.
Lee, Y.J., Baker, T., Jayaraman, V., 2012. Redesigning an integrated forward–reverse logistics system for a third party service provider: an empirical study. Int. J. Prod. Res. 50, 5615–5634.
Lin, L., Gen, M., Wang, X., 2009. Integrated multistage logistics network design by using hybrid evolutionary algorithm. Comput. Ind. Eng. 56, 854–873.
Lu, T., Zhao, X., 2010. Reverse Logistics Network Design with Consideration of Forward and Reverse Facility Integration, in: 2010 International Conference on E-Business and E-Government. IEEE, 3271–3274. Guangzhou (China).
Mehdizadeh, E., Afrabandpei, F., Mohaselafshar, S., Afshar-Nadjafi, B., 2013. Design of a multi-stage transportation network in a supply chain system: Formulation and efficient solution procedure. Sci. Iran. 20, 2188–2200.
Mitra, S., 2012. Inventory management in a two-echelon closed-loop supply chain with correlated demands and returns. Comput. Ind. Eng. 62, 870–879.
Niknejad, A., Petrovic, D., 2014. Optimisation of integrated reverse logistics networks with different product recovery routes. Eur. J. Oper. Res. 238, 143–154.
Nobari, A., Kheirkhah, A., 2017. Integrated and Dynamic Design of Sustainable Closed-loop Supply Chain Network Considering Pricing. Sci. Iran. 6(25), 410–430.
Orendorff, A., 2019. The plague of Ecommerce return rates and how to maintain profitability. Shopify. URL:https://www.shopify.com/enterprise/ecommerce-returns (accessed 7.3.19).
Pedram, A., Yusoff, N.B., Udoncy, O.E., Mahat, A.B., Pedram, P., Babalola, A., 2017. Integrated forward and reverse supply chain: A tire case study. Waste Manag. 60, 460–470.
Peng, Y., Yao, H., 2007. Integrated Networks of Third Party Logistics Service Providers, in: International Conference on Transportation Engineering 2007, 1530–1535. Chengdu (China).
Pishvaee, M.S., Farahani, R.Z., Dullaert, W., 2010. A memetic algorithm for bi-objective integrated forward/reverse logistics network design. Comput. Oper. Res. 37, 1100–1112.
Pishvaee, M.S., Jolai, F., Razmi, J., 2009. A stochastic optimization model for integrated forward/reverse logistics network design. J. Manuf. Syst. 28, 107–114.
Ponte, B., Naim, M.M., Syntetos, A.A., 2019. The value of regulating returns for enhancing the dynamic behaviour of hybrid manufacturing-remanufacturing systems. Eur. J. Oper. Res. 278, 629–645.

Porkar, S., Mahdavi, I., Maleki Vishkaei, B., Hematian, M., 2018. Green supply chain flow analysis with multi-attribute demand in a multi-period product development environment. Oper. Res.

Radhi, M., Zhang, G., 2019. Optimal cross-channel return policy in dual-channel retailing systems. Int. J. Prod. Econ. 210, 184–198.

Rezaei, S., Kheirkhah, A., 2017. Applying forward and reverse cross-docking in a multi-product integrated supply chain network. Prod. Eng. 11, 495–509.

Roghanian, E., Kamandanipour, K., 2013. A fuzzy-random programming for integrated closed-loop logistics network design by using priority-based genetic algorithm. Int. J. Ind. Eng. Comput. 4, 139–154.

Ross, A., Khajehnezhad, M., Otieno, W., Aydas, O., 2017. Integrated location-inventory modelling under forward and reverse product flows in the used merchandise retail sector: A multi-echelon formulation. Eur. J. Oper. Res. 259, 664–676.

Saarijärvi, H., Sutinen, U.-M., Harris, L.C., 2017. Uncovering consumers' returning behaviour: a study of fashion e-commerce. Int. Rev. Retail Distrib. Consum. Res. 27, 284–299.

Sahyouni, K., Savaskan, R.C., Daskin, M.S., 2007. A Facility Location Model for Bidirectional Flows. Transp. Sci. 41, 484–499.

Shulman, J.D., Coughlan, A.T., Savaskan, R.C., 2009. Optimal Restocking Fees and Information Provision in an Integrated Demand-Supply Model of Product Returns. Manuf. Serv. Oper. Manag. 11, 577–594.

Soleimani, H., Seyyed-Esfahani, M., Shirazi, M.A., 2016. A new multi-criteria scenario-based solution approach for stochastic forward/reverse supply chain network design. Ann. Oper. Res. 242, 399–421.

Tan, Y., Guo, C., 2019. Research on Two-Way Logistics Operation with Uncertain Recycling Quality in Government Multi-Policy Environment. Sustainability 11, 882.

van Loon, P., Delagarde, C., Van Wassenhove, L.N., Mihelič, A., 2019. Leasing or buying white goods: comparing manufacturer profitability versus cost to consumer. Int. J. Prod. Res. 1–15.

Wang, L.-C., Chen, T.-L., Chen, Y.-Y., Chen, Y.-W., Wang, A., 2013. Closed-Loop Sustainable Supply Chain Design Under Uncertainties, in: Azevedo, A. (Ed.), Advances in Sustainable and Competitive Manufacturing Systems. Springer International Publishing, Heidelberg, 799–812.

Wang, M., Di, W.-M., 2010. A location-inventory model for integrated forward/reverse logistics network design, in: 2010 International Conference on Management Science & Engineering 17th Annual Conference Proceedings, IEEE, 299–304, Melbourne (Australia).

Wang, X., Zhao, L., 2009. Network Design of Reverse Logistics Intergrated with Forward Logictics, in: 2009 Asia-Pacific Power and Energy Engineering Conference, IEEE, 1–4, Wuhan (China).

Wang, Y., Lu, T., Zhang, C., 2013. Integrated Logistics Network Design in Hybrid Manufacturing/ Remanufacturing System Under Low-Carbon Restriction, in: Zhang, Z., Zhang, R., Zhang, J., LISS 2012. Springer Berlin Heidelberg, 111–121.

Wassan, N., Nagy, G., 2014. Vehicle Routing Problem with Deliveries and Pickups: Modelling Issues and Meta-heuristics Solution Approaches. Int. J. Transp. 2, 95–110.

Xie, R.H., Qiu, Z.Q., Zhang, Y.Y., 2007. A New Heuristics for VRP with Simultaneous Delivery and Pick-Up. Presented at the International Conference on Transportation Engineering, Southwest Jiaotong University, Chengdu (China).

Yazdi, A.A., Honarvar, M., 2015. A Two Stage Stochastic Programming Model of the Price Decision Problem in the Dual-channel Closed-loop Supply Chain. Int. J. Eng. 28.

Zhang, T., Chaovalitwongse, W.A., Zhang, Y., 2014. Integrated Ant Colony and Tabu Search approach for time dependent vehicle routing problems with simultaneous pickup and delivery. J. Comb. Optim. 28, 288–309.

Zhou, X., 2015. A Random Multi-objective Model on Integrated Logistics. World J. Model. Simul. 11, 3–15.

Zhou, X., Xu, J., 2009. A class of integrated logistics network model under random fuzzy environment and its application to Chinese beer company. Int. J. Uncertain. Fuzziness Knowl. Based Syst. 17, 807–831.

Zohal, M., Soleimani, H., 2016. Developing an ant colony approach for green closed-loop supply chain network design: a case study in gold industry. J. Clean. Prod. 133, 314–337.

AUTHORS BIOGRAPHY

Giulio Paolo Agnusdei is a graduate student at the Department of Innovation Engineering of the University of Salento. His research focuses on the design and management of last-mile logistic systems.

Maria Grazia Gnoni, PhD, is an Assistant Professor at the Department of Innovation Engineering of University of Salento. Her research interests focus on designing sustainable waste management systems, green supply chain and processes and lean safety.

Fabiana Tornese, PhD, is a post-doctoral researcher in the Department of Innovation Engineering in the University of Salento. Her research focuses on supply chain management and logistics, in particular on the impact of circular economy models on reverse logistics in the industrial and service sector.

TOWARDS MORE EFFICIENT MULTICLASS AUC COMPUTATIONS

S. Dreiseitl[(a)]

[(a)]University of Applied Sciences Upper Austria, Campus Hagenberg, Austria
[(a)]stephan.dreiseitl@fh-hagenberg.at

ABSTRACT

The area under the receiver operating characteristics curve (AUC) can be used to assess the discriminatory power of a dichotomous classifier model. Extending this measure to more than two classes is not obvious, and a number of variants have been proposed in the literature. We investigate a heuristic approximation to a method that generalizes the notion of probabilities being correctly ordered, which is equivalent to AUC, to an arbitrary number of classes. While the exact method is computationally complex, we propose a much simpler heuristic that is linear in the number of classes for every combination of data points. Using one artificial and one real-world data set, we demonstrate empirically that this simple heuristic can provide good approximations to the exact method, with Pearson correlation coefficients between 0.85 and 0.998 across all data sets.

Keywords: multiclass AUC, multiclass ROC, classifier performance assessment

1. INTRODUCTION

Receiver operating characteristics (*ROC*) *curves* have a long and storied history as tools for evaluating classification performance of predictive models, in particular in the application domain of biomedicine (Metz 1978; Lusted 1978; Lasko et al. 2005). At around the new millenium, machine learning researchers also discovered the usefulness of ROC curves for the analysis of their models (Flach 2003; Fürnkranz and Flach 2005; Fawcett 2006; Davis and Goadrich 2006).

ROC curves provide a graphical visualization of false positive rate (1− specificity) vs. true positive rate (sensitivity) across a spectrum of thresholds for any two-class discriminatory task based on a linearly ordered measurement. The *area under ROC curve* (*AUC*) is therefore indicative of how well two classes can be distinguished from one another, regardless of the chosen threshold (Hanley and McNeil 1982, 1983; Bradley 1997). AUC can be shown to be equivalent to the c-index $P(X < Y)$ (Bamber 1975), the probability that two randomly chosen measurements X and Y from two classes are correctly arranged on a linear scale. For a classifier that outputs posterior class membership probabilities, AUC is thus an alternative to accuracy, which is generally thresholded

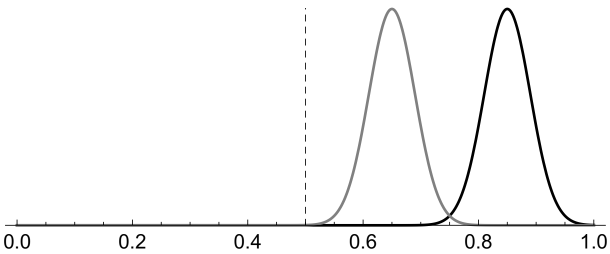

Figure 1: Hypothetical distribution of classifier outputs for a two-class problem. The left normal distribution represents outputs for true class 0, and the right normal distribution represents outputs for true class 1. If these outputs are thresholded at 0.5 (smaller values are considered to belong to class 0, larger values to belong to class 1), all the cases of true class 0 are misclassified. Nevertheless, the classifier achieves almost perfect discrimination between the two classes, with a corresponding AUC value of close to 1.

at 0.5. A classifier that is not well calibrated (possibly owing to changes in class distributions between training and test set) may therefore achieve an accuracy of only 50%, although its AUC may be close to 100%. This situation is shown graphically in Figure 1.

Deep learning problem settings, architectures and training techniques have brought a renewed interest in extending the use of AUC as a discriminatory measure to the multiclass case. There has been some work on constructing and interpreting ROC curves in multiclass settings (Edwards et al. 2004, 2005; He et al. 2006; He and Frey 2006). Previous work on extending the discriminatory measure AUC to N classes has focused either on combining multiple AUCs from one-vs-all classifiers (Hand and Till 2001; Landgrebe and Duin 2007), or on directly generalizing the equivalence of AUC to c-index and the underlying notion of what it means for class-membership probabilities to be “correctly ordered”. Here, we will pursue this second direction of reasoning.

The obvious starting point is to consider three classes. Mossman (1999) advocated a geometric argument to generalize the notion of a changing threshold; a more involved derivation of a similar argument is given by He and Frey (2008). Dreiseitl et al. (2000) argued for a broader interpretation of the notion of “correctly ordered” to the three-class case. This latter idea,

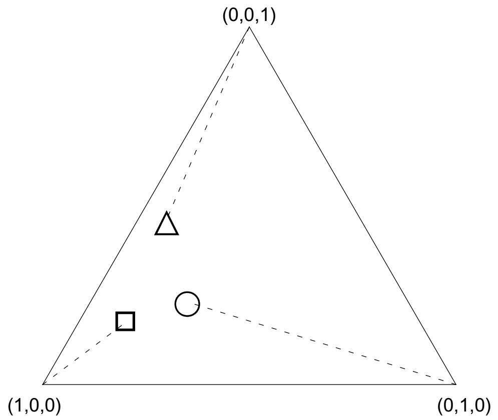

Figure 2: Three probability estimate triplets $\triangle$ (for an element of class 0), $\bigcirc$ (for an element of class 1) and $\square$ (for an element of class 2) on the triangle $\{(x, y, z) \in \mathbb{R}^3 \,|\, x + y + z = 1\}$. The three triplets are considered correctly ordered if the sum of distances between triplets and true-class corners is smaller than the sum of distances between triplets and all permutations of corners.

which will form the basis for the following argument, rests on viewing a traditional two-class pair of probabilities $p_0 = P(\text{class is 1} \,|\, \text{case is class 0})$ and $p_1 = P(\text{class is 1} \,|\, \text{case is class 1})$ as correctly ordered if $p_0 < p_1$. For the three-class case, a classifier output is a probability triplet (p_0, p_1, p_2), with the p_i being posterior class-membership probabilities for each of the three classes. One possible way of considering three probability triplets $p_0 = (p_{00}, p_{01}, p_{02})$, $p_1 = (p_{10}, p_{11}, p_{12})$ and $p_2 = (p_{20}, p_{21}, p_{22})$ to be correctly ordered is if the sum of distances of the p_i to their true-class corners of the convex set $\{(x, y, z) \in \mathbb{R}^3 \,|\, x + y + z = 1\}$ is smaller than all other possible distances of triplets to corners. This idea is expressed graphically in Figure 2. Note that this notion of "correctly ordered" depends only on the positioning of the three symbols relative to one another, and not on *where* on the triangle the three symbols are placed, as long as their relative positioning is the same. It is thus possible to transfer the property of AUCs of being invariant to monotonic transformations to the three-class case.
In the three-class case, the equivalent to AUC is the *volume under the surface*, which is calculated as the fraction of all triplet combinations, one each from the three classes c_0, c_1 and c_2, that are correctly ordered in the sense above:

$$\mathrm{VUS}(c_0, c_1, c_2) := \frac{1}{|c_0|\,|c_1|\,|c_2|} \sum_{p_0 \in c_0} \sum_{p_1 \in c_1} \sum_{p_2 \in c_2} \mathrm{co}(p_0, p_1, p_2)\,,$$

where co is a Boolean indicator function that returns 1 iff its arguments are correctly ordered.
Due to the combinatorial nature of the problem, an exact VUS calculation is possible only for small cardinalities of the data sets involved. Approximations, however, are feasible, as sampling theory ensures that the error of an approximation will decrease with the square root of the data set cardinalities.
The derivations above are sufficiently general to be applicable in the $N > 3$-class case. We will use the term *probability vector* to denote the generalization of class membership probability triplets to an arbitrary number of classes. Extending the VUS calculations from three classes to the general N-class case, however, is hampered not only by the exponential growth of having to compare all $n_1 n_2 \cdots n_N$ possible combinations of N-class probability vectors (with the n_i denoting the cardinalities of the data sets from class i), but by the $O(N!)$ complexity of computing all possible distances of probability vectors to corners for every combination of probability vectors. This latter calculation cannot be approximated by sampling, because *all* of the $N! - 1$ other sums of distances have to be smaller than the sums of distances to the "true" corners for a combination of probability vectors to be correctly ordered.
This paper thus addresses the question of how to efficiently substitute for the factorial problem of computing all sums of distances between probability vectors and corners. The approach considered here is based on computing angles to the true-class corners of the estimate space, and only grows as $O(N)$ instead of $O(N!)$. Details of this approach are given in Section 2; experimental results in Section 3 demonstrate its feasibility.

2. METHODS

The approach presented here was inspired by the notion of varying thresholds in ROC curve construction first presented by Mossman (1999), although no explicit thresholds are required for AUC and VUS computations. As a heuristic approximation to N-dimensional probability vectors being correctly ordered (which would require $N!$ distance computations for an N-class problem), we compute only N angles between the lines formed by the centers of mass of N probability vectors, the individual probability vectors, and their corresponding "true" corners. A graphical representation of this idea is shown in Figure 3. As a visual aid, the figure also shows the grey lines obtained by orthogonal projections of the center of mass onto the triangle sides. These lines illustrate that for three classes, an arrangement of points can be considered to be correctly ordered if every point is in its own (correct) portion of the triangle; this translates to a restriction of $|\cos\alpha| \leq \frac{1}{2}$ for the angle α between center of mass, point and corresponding corner. One can show that for the general situation with N classes, this restriction is $|\cos\alpha| \leq \frac{1}{N-1}$, thus approaching an angle of $\alpha = 90°$ in the limit $N \to \infty$.
Preliminary experiments, however, revealed this limit to be too restrictive, as some situations that were correctly ordered in the computationally expensive distances-to-corners sense were not identified as such in the angles sense introduced here. The limit was therefore set to a constant $\alpha \leq 90°$, which gave reasonable results that were computationally cheap approximations to the much

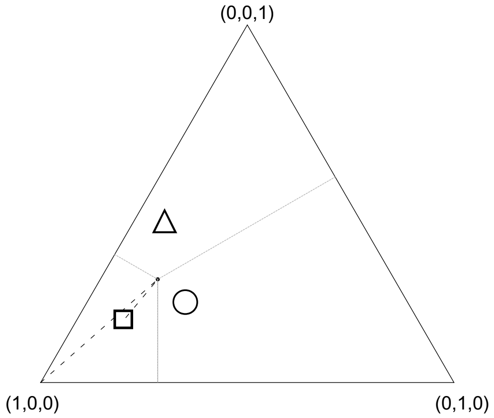

Figure 3: Three probability estimate triplets △ (for an element of class 0), ○ (for an element of class 1) and □ (for an element of class 2) on the triangle $\{(x, y, z) \in \mathbb{R}^3 \mid x + y + z = 1\}$. For clarity, only one line connecting the center of mass of these three triplets to one of the triplets and its corresponding corner are shown. The grey lines connect the center of mass to the triangle sides at right angles.

more expensive distances-to-corners calculations.

3. EXPERIMENTS

We investigated the effect of substituting a heuristic approximation for an exact computation using two data sets, one artificial, and one from the wide range of publically available machine learning data sets.

3.1. Artificial data set

For the artificial data set, we used random variates from multivariate Gaussians, one for each class, with spherical covariance matrices $C = \sigma I$, with I the identity matrix. To obtain probability vectors, we passed these random variates through the softmax function. Changing the distances between the distribution means relative to the σ values allows to increase or decrease VUS values as desired.

As there are two sources of computational complexity in N-class VUS calculation, we initially isolated only the first source, i.e., sampling from the data sets, while keeping the more complex distances-to-corners definition of "correctly ordered". For a three-class VUS value in the intermediate range of around 0.85, Figure 4 shows how increasing the data set size leads to more and more accurate estimates of the VUS value. The distribution of data points in this artificial data set is shown in Figure 5.

Because the proposed approach of substituting the angles calculation introduced in Section 2 for the distances-to-corners definition is only a heuristic approximation, it is of primary interest to evaluate how much results obtained using these two approaches match. For the three-class case, we placed the means of three Gaussians at equal distances from one another, and varied the values of σ to create more or less overlap between the classes. A scat-

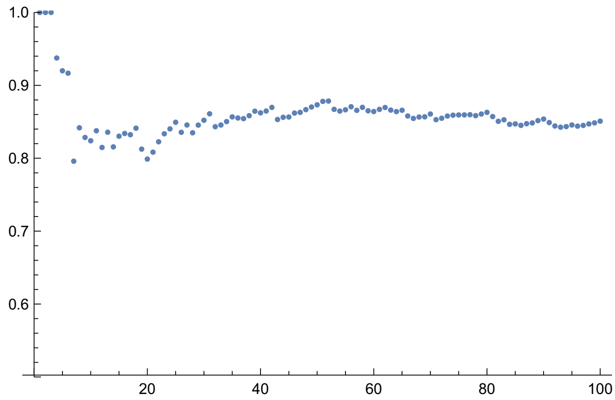

Figure 4: VUS values as function of data set size, for sizes from 1 to 100, on the artificial three-dimensional set of probability vectors shown in Figure 5.

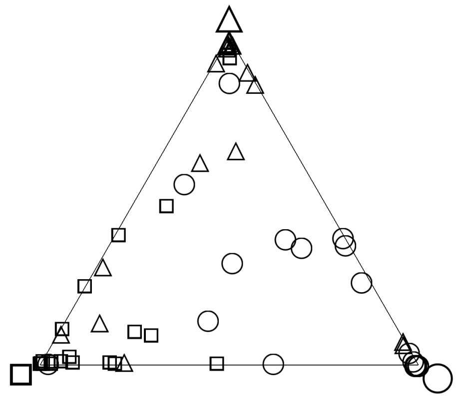

Figure 5: The distribution of the three-dimensional probability vectors used for generating the VUS values shown in Figure 4. For clarity of presentation, only 20 points from each data set are shown. The "true corners" of each class are marked with the corresponding symbol.

terplot of the VUS values obtained from exact and approximate approaches is shown in Figure 6. One can observe that the heuristic calculation using angles provides a good approximation to the exact, but more computationally complex distances-to-angles VUS values. The Pearson correlation coefficient between both sets of values is 0.998.

Moving from three to four classes, we observed the same agreement between exact calculation and heuristic approximation (Pearson correlation coefficient again at 0.995), leading us to believe that the agreement might extend to $N > 4$, for which the exact calculation is all but infeasible. The probability vectors were generated as described above; the result of a scatterplot between the two sets of results is given in Figure 6.

3.2. CIFAR-10 data set

The CIFAR-10 data set (Krizhevsky 2009) is one of the most widely-used data sets in machine learning. It consists of 50 000 training and 10 000 test color images at a

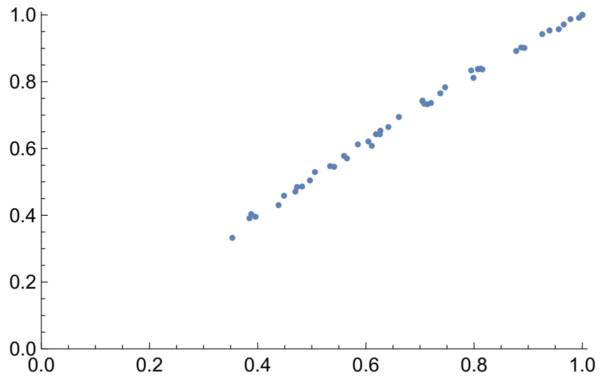

Figure 6: Scatterplot of the 50 VUS values obtained by the traditional distances-to-corner method (on the x-axis) vs. the proposed angles heuristic (on the y-axis), for $N = 3$ classes on the artificial data set. All values were obtained with 50 probability vectors in each of the three classes.

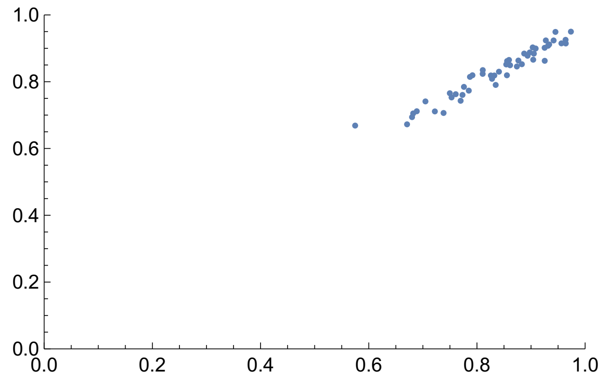

Figure 8: Scatterplot of the 50 VUS values obtained by the traditional distances-to-corner method (on the x-axis) vs. the proposed angles heuristic (on the y-axis), for $N = 3$ classes on the CIFAR-10 set. All values were obtained with 50 probability vectors in each of the three classes.

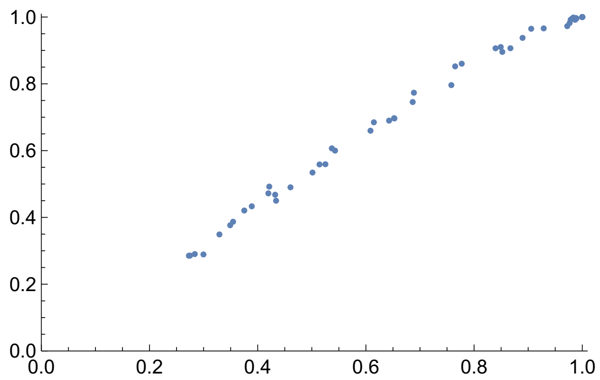

Figure 7: Scatterplot of the 50 VUS values obtained by the traditional distances-to-corner method (on the x-axis) vs. the proposed angles heuristic (on the y-axis), for $N = 4$ classes on the artificial data set. All values were obtained with 50 probability vectors in each of the four classes.

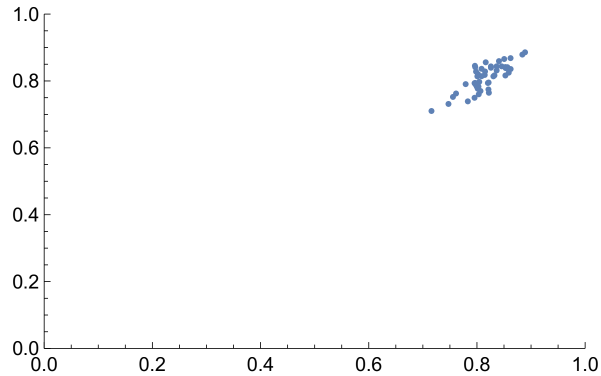

Figure 9: Scatterplot of the 50 VUS values obtained by the traditional distances-to-corner method (on the x-axis) vs. the proposed angles heuristic (on the y-axis), for $N = 4$ classes on the CIFAR-10 set. All values were obtained with 15 probability vectors in each of the four classes.

resolution of 32×32 pixels from ten different classes, ranging from airplanes and automobiles to cats and dogs. We used a Tensorflow implementation of a deep neural network with four convolutional and two fully connected layers to train a classifier for distinguishing between all ten classes. To obtain results across a more generally representative range of VUS values (and not just close to 1), we trained the neural network model for only one iteration through all 50 000 training instances. Already in this one iteration, we achieved an accuracy value of 61.65% on the test set.

For the experiments reported here, we picked arbitrary three or four classes and renormalized the corresponding vector components to turn them into probability vectors. This choice of classes was repeated 10 times; for each such data set, we sampled 5 instances of 50 probability vectors in each class. The scatterplot comparing the angles heuristics with the distances-to-corners method for three classes is shown in Figure 8. One can observe that the VUS values are rather high, with most in the range of 0.9 to 1. The Pearson correlation coefficient between both the angles heuristic and the distances-to-corners method was 0.968. The corresponding plot for four classes is shown in Figure 9, with a similar appearance, but a more narrow range of VUS values, and more dispersion of points and a correspondingly lower Pearson correlation coefficient of 0.797. We speculate, however, that this lower value may be due to the more narrow range of VUS values.

4. CONCLUSION

The area under the ROC curve, and its multiclass variant, the volume under the ROC surface, provide alternatives to accuracy as a measure of classifier performance. We demonstrated empirically that a simple $O(N)$ heuristic approximation to a prohibitively computationally expensive $O(N!)$ calculation for N classes is able to achieve similar results.

REFERENCES

Bamber D., 1975. The area above the ordinal dominance graph and the area below the receiver operating characteristic graph. *Journal of Mathematical Psychology*, 12:387–415.

Bradley A., 1997. The use of the area under the ROC curve in the evaluation of machine learning algorithms. *Pattern Recognition*, 30:1145–1159.

Davis J. and Goadrich M., 2006. The relationship between Precision-Recall and roc curves. In *Proceedings of the 23rd International Conference on Machine Learning (ICML-2006)*, pages 233–240.

Dreiseitl S., Ohno-Machado L., and Binder M., 2000. Comparing three-class diagnostic tests by three-way ROC analysis. *Medical Decision Making*, 20:323–331.

Edwards D., Metz C., and Kupinski M., 2004. Ideal observers and optimal ROC hypersurfaces in N-class classification. *IEEE Transactions on Medical Imaging*, 23:891–895.

Edwards D., Metz C., and Naishikawa R., 2005. The hypervolume under the ROC hypersurface of "near-guessing" and "near-perfect" observers in N-class classification tasks. *IEEE Transactions on Medical Imaging*, 24:293–299.

Fawcett T., 2006. An introduction to ROC analysis. *Pattern Recognition Letters*, 27(8):861–874.

Flach P., 2003. The geometry of ROC space: Understanding machine learning metrics through ROC isometrics. In *Proceedings of the 20th International Conference on Machine Learning (ICML-2003)*, pages 226–233.

Fürnkranz J. and Flach P., 2005. ROC 'n' rule learning—towards a better understanding of covering algorithms. *Machine Learning*, 58:39–77.

Hand D. and Till R., 2001. A simple generalisation of the area under the ROC curve for multiple class classification problems. *Machine Learning*, 45:171–186.

Hanley J. and McNeil B., 1982. The meaning and use of the area under the receiver operating characteristic (ROC) curve. *Radiology*, 143:29–36.

Hanley J. and McNeil B., 1983. A method of comparing the areas under receiver operating characteristic curves derived from the same cases. *Radiology*, 148:839–843.

He X. and Frey E., 2006. Three-class ROC analysis—the equal error utility assumption and the optimality of three-class roc surface using the ideal observer. *IEEE Transactions on Medical Imaging*, 25:979–986.

He X. and Frey E., 2008. The meaning and use of the volume under a three-class ROC surface (VUS). *IEEE Transactions on Medical Imaging*, 28:577–588.

He X., Metz C., Tsui B., Links J., and Frey E., 2006. Three-class ROC analysis—a decision theoretic approach under the ideal observer framework. *IEEE Transactions on Medical Imaging*, 25:571–581.

Krizhevsky A., 2009. Learning multiple layers of features from tiny images. Technical report, Computer Science Department, University of Toronto.

Landgrebe T. and Duin R., 2007. Approximating the multiclass roc by pairwise analysis. *Pattern Recognition Letters*, 28:1747–1758.

Lasko T., Bhagwat J., Zhou K., and Ohno-Machado L., 2005. The use of receiver operating characteristic curves in biomedical informatics. *Journal of Biomedical Informatics*, 38(5):404–415.

Lusted L., 1978. General problems in medical decision making with comments on ROC analysis. *Seminars in Nuclear Medicine*, 8:299–306.

Metz C., 1978. Basic principles of ROC analysis. *Seminars in Nuclear Medicine*, 8:283–298.

Mossman D., 1999. Three-way ROCs. *Medical Decision Making*, 19:78–89.

AUTHOR BIOGRAPHIES

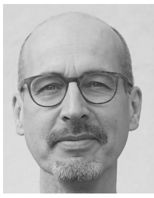

STEPHAN DREISEITL received his MSc and PhD degrees from the University of Linz, Austria, in 1993 and 1997, respectively. He worked as a visiting researcher at the Decision Systems Group/Harvard Medical School before accepting a post as professor at the Upper Austria University of Applied Sciences in Hagenberg, Austria, in 2000. His research interests lie in the development of machine learning models and their application as decision support tools in biomedicine.

EVALUATION OF A SELF-ORGANIZING MIGRATING ALGORITHM APPLIED TO DISCRETE EVENT SIMULATION OPTIMIZATION

Pavel Raska[(a)], Zdenek Ulrych[(b)]

[(a)] Department of Industrial Engineering - Faculty of Mechanical Engineering, University of West Bohemia, Univerzitni 22, 306 14 Pilsen
[(b)] Department of Industrial Engineering - Faculty of Mechanical Engineering, University of West Bohemia, Univerzitni 22, 306 14 Pilsen

[(a)]praska@kpv.zcu.cz, [(b)] ulrychz@kpv.zcu.cz,

ABSTRACT

The paper deals with testing and evaluation of a modified Self-Organizing Migrating Algorithm (SOMA) applied to a discrete event simulation model reflecting the supply of production lines using automated guided vehicles. The SOMA heuristic optimization method is derived from the Differential Evolution method. We test all the SOMA strategies under the same conditions of the simulation experiments – the same termination criteria, number of repetitions in the optimization experiments, and the same setting of the basic parameters of the SOMA. We propose a methodology using different evaluation criteria to analyse the different SOMA strategies behaviour of finding the optimum of an objective function specified for each discrete event simulation model.

Keywords: SOMA, Self-Organizing Migrating Algorithm, Discrete Event Simulation Model, AGV, Evaluation

1. INTRODUCTION

Many of today's industrial companies are large complex systems affected by a host of internal and external factors. An important thing is effective management of company resources and processes. We can use a digital replica of a physical system – a digital twin. This simulation model can answer the question "What happens if …". The simulation of different scenarios can avoid bad human decision-making and also prevent system errors in the company before they occur e.g. timely identification of bottlenecks, mapping and increasing the utilization of company resources, effective scheduling and resource allocation, bin packing problems (Koblasa, Vavrousek, and Manlig 2017), transport distances (Bučková, Krajčovič, and Edl 2017), etc. Another problem is we cannot often calculate and evaluate each possible scenario because of the large number of possible solutions in the search space – NP hard problem. The search space is usually boundary-constrained and it represents the domain of the input parameters of the discrete event simulation model. The search space is defined as follows:

$$\tilde{X} = \prod_{j=1}^{n} \tilde{X}_j = \prod_{j=1}^{n} [a_j, b_j],\ a_j \leq b_j, a_j, b_j \in \mathbb{R} \qquad (1)$$

Where symbols denote: $\tilde{X}$ denotes the search space; j denotes the j-th decision variable of the simulation model; n denotes the dimension of the search space; a_j denotes the lower bound of the interval of j-th decision variable; b_j denotes the upper bound of the interval of j-th decision variable.

The goal of using the simulation optimization is to find the best quality solution (represented by the objective function value) according to the other possible solutions.

We proposed the simulation optimizer with different (heuristic, metaheuristic, etc.) optimization methods that vary the discrete event simulation model input parameters to find the optimal solution of the modelled problem. The possible solution containing the settings of each simulation model input parameter is defined as follows:

$$\mathbf{X}[j] = x_j \forall j: j = \{1,2,\dots,n\} \qquad (2)$$

where $\mathbf{X}[j]$ denotes a possible solution – the vector of the values for each decision variable; x_j denotes the value of the j-th decision variable; j denotes the index of the decision variable.
If we minimize the objective function values, the global optimum is defined as follows:

$$\breve{\mathbf{X}} = \mathrm{argmin}_{\mathbf{X}\in\tilde{X}}\, F(\mathbf{X}) = \{\breve{\mathbf{X}} \in \tilde{X}: F(\breve{\mathbf{X}}) \leq F(\mathbf{X}) \forall \mathbf{X} \in \tilde{X}\} \qquad (3)$$

where $\breve{\mathbf{X}}$ denotes the global minimum of the objective function; $F(\mathbf{X})$ denotes the objective function value of the candidate solution – the range includes real numbers, i.e. $F(\mathbf{X}) \subseteq \mathbb{R}$; $\tilde{X}$ denotes the search space.
The function maximization can be converted to function minimization by multiplying the objective function value by -1.

The simulation optimizer provides a candidate solution (best found feasible solution of the modelled problem) or a list of candidate solutions. The problem is that we cannot confirm that the candidate solution provided by the optimization method is the real optimum of the objective function because we cannot evaluate all possible solutions in the search space - NP hard problem. Another problem is that the optimization method is prone to bad settings of its parameters. Hence, we proposed a methodology using different evaluation criteria to analyse the SOMA behaviour of finding the optimum of an objective function.

2. SELF-ORGANIZING MIGRATING ALGORITHM - SOMA

SOMA is based on the self-organizing behaviour of groups of individuals in a 'social environment'. It can also be classified as an evolutionary algorithm, even though no new generations of individuals are created during the search. Only the positions of the individuals in the search space are changed during a generation, called a 'migration loop'. Individuals are generated at random according to what is called the 'specimen of the individual' principle. The specimen is in a vector, which comprises an exact definition of all these parameters that together lead to the creation of such individuals, including the appropriate constraints of the given parameters. SOMA is not based on the philosophy of evolution (two parents create one new individual – the offspring), but on the behaviour of a social group of individuals. (Zelinka 2016)

The SOMA optimization method is derived from Differential Evolution. There are different modifications of the Differential Evolution e.g. (Elsayed, Sarker, and Essam 2013; Li et al. 2015)

The original source code in different programming languages of the tested SOMA can be downloaded at (Zelinka 2005).

2.1. The SOMA parameters

The *Mass* parameter denotes how far the currently selected individual stops from the leader individual (if $Mass = 1$ then the currently selected individual stops at the position of the leader, if $Mass = 2$ then the currently selected individual stops behind the position of the leader, which equals the distance of the initial position of the currently selected individual and the position of the leader). If $Mass < 1$ then the currently selected individual stops in front of the leader which leads to degradation of the migration process (the algorithm finds only local extremes). Hence it is recommended to use $Mass > 1$. It is also recommended to use the following lower and upper boundary of the parameter $Mass \in [1.1,3]$.

The *Step* parameter denotes the resolution of mapping the path of the currently selected individual. It is possible to use a larger value for this parameter to accelerate the searching of the algorithm if the objective function is unimodal (convex function, few local extremes, etc.). If the objective function landscape is not known, it is recommended to use a low value for this parameter. The search space will be scanned in more detail and this increases the probability of finding the global extreme. It is also important to set the *Step* parameter in a way that the distance of the currently selected individual and the leader is not an integer multiple of this parameter (the diversity of the population is reduced because each individual could be pulled to the leader and the process of searching for the optimum could stop at a local extreme). Hence it is recommended to use $Step = 0.11$ instead of $Step = 0.1$. The setting of e.g. $Step = 0.11$ also rapidly increases the effectiveness of SOMA Strategy All To All.

The PRT parameter denotes the perturbation. The Perturbation vector contains the information whether the movement of the currently selected individual toward the leader should be performed. It is one of the most important parameters of this optimization method and it is very sensitive. It is recommended to use $PRT = 0.1$. If the value of this parameter increases, then the convergence of the SOMA algorithm to local extremes also rapidly increases. It is possible to set this parameter to $PRT \in [0.7,1.0]$ if many individuals are generated and if in the dimension of the search space the objective function is low. If $PRT = 1$ then the stochastic part of the behaviour of SOMA is cancelled and the algorithm behaves according to deterministic rules (local optimization of the multimodal objective function).

The *NP* parameter denotes how many individuals are generated in a population. If this parameter is set to $NP = 2$ the SOMA algorithm behaves like a traditional deterministic method.

Generally if n (where n denotes the dimension of the search space) is a higher number, then this parameter can be set to $NP = [0.2,0.5] \times n$. If the objective function landscape is simple we can use a lower number of generated individuals. If the objective function is complicated we can set this parameter $NP = n$. It is recommended to use $NP \geq 10$.

This parameter is equivalent to the 'Generation' parameter used in other evolutionary algorithms. This parameter denotes the number of population regenerations. (Volna 2012; Zelinka 2016; Zelinka et al. 2013;

2.2. Strategy of Individual Movements

There are several variants of the basic SOMA optimization method – strategies of individual movements. The principle is to distinguish the cooperation of the individuals and the migration of the population in the search space. The strategies are: AllToOne – all the individuals in the population migrate to the leader, except the leader. The leader remains at its position during a migration loop - strategy index: 0; AllToAll – in this strategy, there is no leader. All individuals move towards the other individuals. The individual comes back to the best found solution after finishing the *NP*-1 individual migrations. This strategy is more time consuming, but the probability of finding the global extreme is higher, because the individuals can explore a bigger area of the search space - strategy index: 1; AllToAllAdaptive – this strategy is similar to AllToAll strategy. The difference between the AlltoAll strategy is that individuals do not begin a new migration form the same old position, but from the last best position found during the last migration to the previous individual - strategy index: 2; AllToRand – this is a strategy where all individuals move towards a randomly selected individual during the migration loop, no matter what cost value this individual has. It is up to the user to decide how many randomly selected individuals there should be - strategy index: 3. (Zelinka 2016)

3. AGV TRANSPORT MODEL

This practical discrete event simulation model deals with supplying the production lines using automated guided vehicles (AGVs). Large parts are supplied by the trailers and it is not possible to load a big number of these parts to satisfy the needs of the production line for a longer time. Hence more trailers must be used for the transport at once. It is also not possible to control the supply in a way that if the supply falls below a certain level there would be generated a requirement for transport from the warehouse (except for a limited number of some parts). This is caused by the transport time which is longer than the time of consumption of the parts transported to the production line.

The whole system of supplying the production lines is based on a simple principle: a tractor with trailers continually transports the parts and after the unloading of the transported parts it goes to the warehouse or to pre-production for new parts and then transports them immediately to the production lines – see Figure 1.

Limited capacity of the buffer (parts storage) on the production line is a regulation in this case. Each tractor has a defined path using different loading and unloading stations which must be passed. The various types of parts are loaded and unloaded at different stations in the company. The parts can be loaded on the trailer at the loading stations in the warehouse or at the various production departments in the company. Each production line has several unloading stations for various parts. A schematic layout of the loading and unloading stations is shown in Figure 2. The decision variables are the number of each AGV type. The following illustrates a situation where a collapse of the whole transport system occurred (because of the blockage of one AGV by another AGV) – see Figure 2.

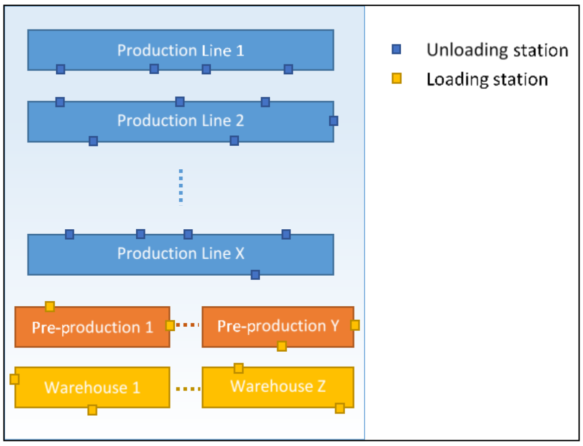

Figure 1: Simple Layout of Loading/Unloading Stations for AGV

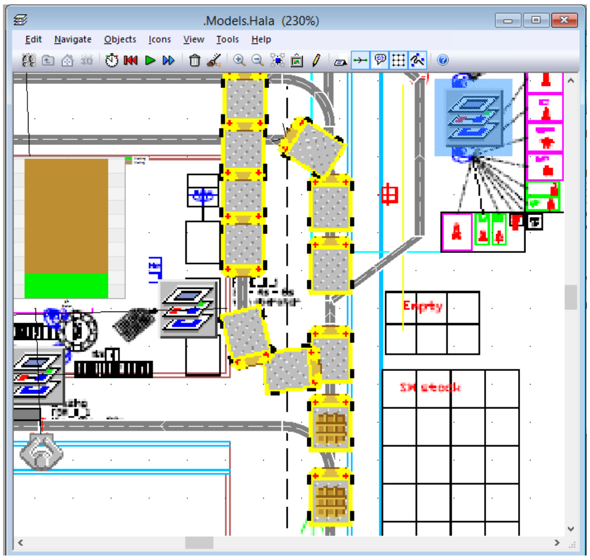

Figure 2: Sample of AGV Collapse in the Simulation Model

The objective function reflects the average use of AGV (tractor with trailers). The objective function also reflects the overall average utilization of the production lines. The average use of the production lines is superior to average use of the trains using the coefficients in the objective function. The objective function is maximized. (Raska and Ulrych 2014)

The objective functions definitions:

$$F_1(\mathbf{X}) = \sum_{i=1}^{n} U_i\,(\mathbf{X}) \tag{4}$$

where U_i denotes the utilization of the i-th production line; n denotes the number of production lines.

$$F_2(\mathbf{X}) = \frac{\sum_{i=1}^{m}(10 - N_i(\mathbf{X}))}{1000} \tag{5}$$

where N_i denotes the number of AGV of the same type; m denotes the number of AGV of different types.

ISBN 978-88-85741-25-6; Affenzeller, Bruzzone, Longo and Pereira Eds.

$$F(\mathbf{X}) = F_1(\mathbf{X}) + F_2(\mathbf{X}) \tag{6}$$

where $F(\mathbf{X})$ denotes the resulting objective function.

4. OPTIMIZATION EXPERIMENTS

We have to repeat the simulation optimization experiments. This replication ensures the reduction of the influence of random implemented in the optimization algorithm. We divide the number of the simulation experiments as follows:

- Simulation experiment – simulation run of the simulation model
- Optimization experiment – performed with a specific optimization method setting to find the optimum of the objective function
- Series – replication of optimization experiments with a specific optimization method setting

We tested 2,304 different settings of the SOMA optimization method. Table 1 shows the defined step and lower and upper boundaries for the SOMA parameters.

Table 1: Settings of SOMA Parameters

Parameter	Step	Lower Bound	Upper Bound
Mass	0.5	1.1	2.6
Step	0.4	0.11	1.31
PRT	0.1	0.1	0.6
NP	1×n	1×n	6×n
Migrations	10	10	10
Strategy index (strategy type)	1	0	3

We designed our own simulation optimizer based on Client - Server architecture. This architecture allows us to reduce the time of the optimization experiment because the series - replication of optimization experiments with a specific optimization method setting - can be performed on many remote simulation optimizers - servers.
We tested all the items - possible solutions - of the discrete event simulation model search space. We selected only feasible solutions. These feasible solutions represent the feasible settings of the simulation model input parameters under specified constraints. We created a database containing these solutions and their objective function values. Each feasible solution and its objective function value is encoded into one number to accelerate the searching of the database. A remote simulation optimizer on the servers downloads this database from the client to local computer memory before performing the simulation runs. The simulation optimizer does not have to perform the simulation run in simulation software, but it only searches for the possible solution in the internal memory. If the local memory on the server does not contain the possible solution, the optimizer asks for this solution from the client's external database. All the servers are connected to this remote database and if the local memory of the simulation optimizer does not contain this new generated possible solution by the optimizer, the simulation optimizer performs the simulation experiment with the settings of the simulation model input parameters and calculates its objective function value. Then it saves the possible solution and its objective function value in its own local server and in the external database of the client. This user option increases the speed of the simulation optimization experiment.

4.1. Termination Criteria

The same termination criteria were satisfied for each tested series. We specified the first termination criterion – Value to Reach - because we mapped all the solution candidates in the search space. The found value of Value to Reach is the global optimum/maximum of the objective function (the objective function maximization):

$$\widehat{\boldsymbol{X}} = \text{argmax}_{\mathbf{X}\in\tilde{X}}\, F(\mathbf{X}) = \left\{\widehat{\boldsymbol{X}} \in \tilde{X} : F\left(\widehat{\boldsymbol{X}}\right) \geq F(\mathbf{X}) \forall \mathbf{X} \in \tilde{X}\right\} \tag{7}$$

where $\widehat{\boldsymbol{X}}$ denotes the global maximum of the objective function; $F\left(\widehat{\boldsymbol{X}}\right)$ denotes the objective function value of the global maximum; $F(\mathbf{X})$ denotes the objective function value of the possible solution – the range includes real numbers, i.e. $F(\mathbf{X}) \subseteq \mathbb{R}$; $\tilde{X}$ denotes the search space.

Because we know the global optimum of the objective function we could specify the tolerated deviation ($\varepsilon = 0.001$ in our case) from the objective function value of the global optimum. The optimization methods also stop searching for the global optimum if they find a possible solution whose objective function value is within the defined tolerance.

$$\left|F(\mathbf{X}) - F(\widehat{\boldsymbol{X}})\right| \leq \varepsilon \tag{8}$$

where $F(\mathbf{X})$ denotes the objective function of the found possible solution in the optimization experiment with concrete settings of the optimization method parameters; $F\left(\widehat{\boldsymbol{X}}\right)$ denotes the objective function value of the global maximum.
The second termination criterion is the maximum number of simulation runs that the simulation optimizer can perform in the optimization. We performed many optimization experiments in the initial stage of testing.
We confirmed that the settings of the optimization method could significantly affect the performance of the optimization method. Hence we tested many different settings of the optimization methods to reduce the number of bad settings of the optimization methods parameters. Another reason for repeating the optimization experiments is reduction of the random nature of the optimization method (SOMA uses random distribution).
We calculated this maximum number using information entropy - Shannon Entropy. The number of all possible solutions in the search space is reduced using information entropy. (Borda 2011)

The reduction coefficient:

$$\delta = \max\{0,1 - \beta \cdot log\tilde{X}\}, \delta \in [0,1] \quad (9)$$

Where $\tilde{X}$ denotes the size of the search space – the number of all possible solutions in the search space; β denotes the coefficient of search space reduction.

$\tilde{X}_H$ denotes the maximum number of simulation runs that the optimization method can perform in each optimization experiment. It is defined as follows:

$$\tilde{X}_H = \lfloor 2^{\delta \cdot log_2 \tilde{X}} \rfloor \quad (10)$$

The following table shows the specifications of the tested discrete event simulation model – the global minimum, the global maximum, the dimensions of the search space, the number of possible solutions in the search space, the maximum number of simulation runs that the simulation optimizer can perform in the optimization using information entropy. We set the coefficient $\beta = 0.05$ according to our initial optimization experiments – see Table 2.

Table 2: Specifications of the Discrete Event Simulation Model

Discrete Event Simulation Model	$F(\check{\mathbf{X}})$	$F(\hat{\mathbf{X}})$	n	$\tilde{X}$	$\tilde{X}_H$
AGV Transport Model	0.1368983	9,1	15	14,515,200	39,558

5. EVALUATION CRITERIA

Many research papers use the average or the standard deviation to evaluate the performance of the optimization methods. This evaluation criterion is sufficient for commonly used testing functions, e.g. De Jong's, Rosenbrock's, Ackley's function, etc. (Pohlheim 2006)
We proposed different evaluation criteria which express the success or the failure of the optimization method in different ways. Each criterion value is between [0, 1]:

$$f_i \in [0,1] \forall i: i = \{1,2,\ldots,5\} \quad (11)$$

If the failure is 100[%], the criterion equals 1, therefore we try to minimize all specified evaluation criteria. The second and the third criteria are calculated from the Box plot characteristics - the smallest observation – sample minimum Q_1, lower quartile Q_2, median Q_3, upper quartile Q_4, and largest observation - sample maximum Q_5. These characteristics are calculated for each performed series – the setting of the optimization method parameters.

We calculated the quality of each series which comprises all the proposed evaluation criteria. We calculated the quartile characteristics – the minimum, the first quartile, the median, the third quartile and the maximum of the whole range of values representing the quality – the weighted sum for all other proposed criteria. The following boxplot charts show the main criteria calculated for each series sorted according to the calculated weighted sum of all the proposed criteria:

$$f = f_1 \cdot w_{f_1} + f_2 \cdot w_{f_2} + f_3 \cdot w_{f_3} + f_4 \cdot w_{f_4} + f_5 \cdot w_{f_5} \quad (12)$$

where f denotes the weighted sum of all criteria; f_1 denotes the value of the first criterion – The Optimization Method Success; w_{f_1} denotes the weight of the first criterion; f_2 denotes the value of the second criterion - The Difference Between Optimum and Local Extreme; w_{f_2} denotes the weight of the second criterion; f_3 denotes the value of the third criterion - The Distances of Quartiles; w_{f_3} denotes the weight of the third criterion; f_4 denotes the value of the third criterion - The Number of Simulation Experiments Until the Optimum Was Found; w_{f_4} denotes the weight of the fourth criterion; f_5 denotes the value of the fifth criterion - Convergence to the Optimum (objective function values of the possible solutions generated in series by the optimization algorithm).
Table 3 shows the value specified for each weight. The sum of the weights equals one.

Table 3: Specifications of The Weights for Each Criterion

Weight	Value
w_{f_1}	0.35
w_{f_2}	0.25
w_{f_3}	0.2
w_{f_4}	0.15
w_{f_5}	0.05

5.1. Optimization Method Success

If we know the global minimum and the global maximum in the search space we can calculate the range of the objective function values:

$$F_{\tilde{X}} = |F(\check{\mathbf{X}}) - F(\hat{\mathbf{X}})| \quad (13)$$

where $F(\check{\mathbf{X}})$ denotes the objective function value of the global minimum in the search space; $F(\hat{\mathbf{X}})$ denotes the objective function value of the global maximum in the search space.
The problem is to define the global minimum or maximum where we cannot test all the possible solutions in the search space – NP-hard problem. This is a common situation in industrial simulation optimization. We can only calculate the difference between the objective function value of the found best solution candidates in the search space in all series (we cannot confirm that the

found best solution candidate is the global optimum) - and the objective function value of the worst found possible solution of the search space (the maximum if the objective function is minimized):

$$\Delta F_{\tilde{X}} = F(\mathbf{X}^*) - F(X_{Worst}) \tag{14}$$

where $F(\mathbf{X}^*)$ denotes the objective function value of the found best candidate solution of the search space in all series; $F(X_{Worst})$ denotes the objective function value of the worst found possible solution (element) of the search space.

The value of the first criterion represents the failure of finding the best solution candidates in the search space in one series performed by the optimization method – value minimization. This criterion is expressed by Pseudo Pascal code – see Figure 3:

begin
  $n_{Succ} \longleftarrow 0$;
  (*browse all the items of the list*)
  for $i \longleftarrow 0$ **to** Length$(X^*) - 1$ **do**
    (*optimum or acceptable candidate solution was found*)
    if $|F(X^*[i]) - F(\mathbf{X}^*)| \leq \varepsilon$ **then**
      $n_{Succ} \longleftarrow n_{Succ} + 1$;
    (*standardization - % share of unsuccessful series*)
    result $\longleftarrow \frac{\text{Length}(X^*) - n_{Succ}}{\text{Length}(X^*)}$;
end;

Figure 3: Pseudo Pascal Algorithm of the First Criterion Calculated for One Series – Finding the Global Optimum or Suboptimum

where X^* denotes the list of found best feasible solutions - candidate solutions – for all the optimization experiments performed in one series; Length(X^*) denotes the length of the list of the candidate solutions - number of found global/local optima with the concrete settings of the optimization method parameters; $\mathbf{X}^*$ denotes the found best candidate solution (global maximum if we mapped all the possible solutions in the search space) in all series; ε denotes the tolerated deviation from the value of the objective function value of the found best candidate solution in the search space in all series; $F(\,)$ denotes the objective function value; n_{Succ} denotes the counter of successful finding of the found best candidate solutions in the search space in all series.

The average method success of finding the best solution candidates in the search space from all the series (if we know the optimum) can be formulated as follows:

$$f_{1AVG} = \left(1 - \frac{\sum_{i=1}^{s} f_{1_i}}{s}\right) \cdot 100[\%] \tag{15}$$

where f_{1AVG} denotes the average method success of finding the optimum of the objective function (criterion maximization), i denotes the index of one series; f_{1_i} denotes the standardised scalar value of the i-th series (the optimization method failure – minimization of the criterion), s denotes the number of performed series.

We calculated the average success of all the SOMA strategies of finding the optimum of the objective function – see Figure 4.

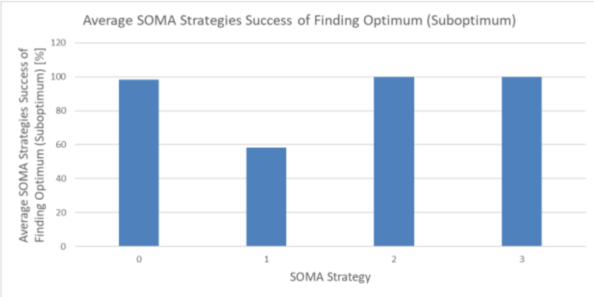

Figure 4: Average SOMA Strategies Success of Finding Optimum (Suboptimum)

We calculated the quality of each series which comprises all the proposed evaluation criteria using the weighted sum as the main criterion. We sorted these series using their values of the weighted sum. We calculated the minimum, the first quartile, the median, the third quartile and the maximum of the whole interval of the weighted sums.

We selected the series that represent the calculated boxplot characteristics. The next box plot chart shows the success of each SOMA strategy from the worst to the best series (concrete settings of the SOMA optimization method parameters) – see Figure 5.

The AllToAllAdaptive strategy (index 2) and AllToRand (index 3) is prone to wrong optimization method parameters settings in our case of a discrete event simulation model. This strategy is followed by the SOMA strategy AllToOne strategy (index 0). The worst strategy AllToAll (index 1) for setting the wrong optimization method parameters.

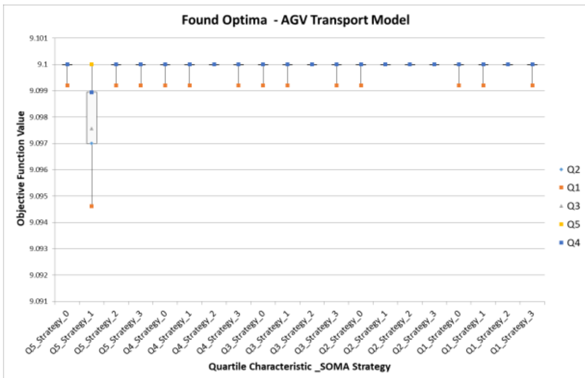

Figure 5: Found Optima for Different Strategies of Individual Movements - Objective Function Maximization

5.2. The Difference between Optimum and Local Extreme

The second criterion is useful when there is no series which contains any optimum or a best solution whose objective function value is within the tolerance of the optimum objective function value. The first criterion equals zero in this case. The output of the function can take value $f_2 \in [0,1]$. This function evaluates the difference between the objective function value of the found best solution in the series and the optimum of the objective function value. The task is to minimize this evaluation function. The list of found optima considering objective function value is sorted in ascending order. This sorting can be performed using the comparator function, which compares the quality (objective function values) of two possible solutions. If we maximize the objective function:

$$\mathrm{CF}_{F(\mathbf{X})}(\mathbf{X}_1, \mathbf{X}_2) = \begin{cases} -1 & \text{if } F(\mathbf{X}_1) > F(\mathbf{X}_2) \\ 1 & \text{if } F(\mathbf{X}_1) < F(\mathbf{X}_2) \\ 0 & \text{else} \end{cases} \qquad (16)$$

where $\mathrm{CF}_{F(\mathbf{X})}$ denotes the comparator function comparing the objective function values of two possible solutions; $F(\mathbf{X}_1)$ denotes the objective function value of first possible solution.

After that the value of the second criterion is calculated using the formula:

$$f_2 = \left(\frac{F(\mathbf{X}^*) - F(X_{Best})}{F_{\tilde{X}}}\right) \qquad (17)$$

where $F(\mathbf{X}^*)$ denotes the objective function value of the optimum of the search space in all series; $F(X_{Best})$ denotes the objective function value of the best solution candidate found in a concrete series; $F_{\tilde{X}}$ denotes the difference between the objective function value of the global minimum and the global maximum in the search space.

5.3. The Distances of Quartiles

The third criterion expresses the distance between the quartiles of a concrete series. The output of the function can take value $f_3 \in [0,1]$. If the first criterion equals zero then the third criterion equals zero – an absolutely successful series. The task is to minimize this evaluation function. Weights are used for evaluation purposes. These weights penalize the solutions placed in quartiles. The values of the weights are defined based on the results of the simulation experiments. The user can define the weight value. The sum of weights equals one. The third criterion when the objective function is minimized can be formulated as follows:

$$f_3 = \frac{f_{3w1} + f_{3w2} + f_{3w2} + f_{3w4} + f_{3w5}}{F_{\tilde{X}}} \qquad (18)$$

$$f_{3w5} = |Q_1 - F(\mathbf{X}^*)| \qquad (19)$$
$$f_{3w4} = w_{4_{f_3}}|Q_1 - Q_2| \qquad (20)$$
$$f_{3w3} = w_{3_{f_3}}|Q_2 - Q_3| \qquad (21)$$
$$f_{3w2} = w_{2_{f_3}}|Q_3 - Q_4| \qquad (22)$$
$$f_{3w1} = w_{1_{f_3}}|Q_4 - Q_5| \qquad (23)$$

Where $F(\mathbf{X}^*)$ denotes the objective function value of the global optimum of the search space; $w_{4_{f_3}}$ denotes the weight (penalty) of objective function values between sample minimum Q_1 and lower quartile Q_2; $w_{3_{f_3}}$ denotes the weight of objective function values between lower quartile Q_2 and median Q_3; $w_{2_{f_3}}$ denotes the weight of objective function values between median Q_3 and upper quartile Q_4; $w_{1_{f_3}}$ denotes the weight of objective function values between upper quartile Q_4 and largest observation - sample maximum Q_5.

If the objective function is maximized the parts of the third criterion are calculated as follows:

$$f_{3w5} = |F(\mathbf{X}^*) - Q_5| \qquad (24)$$
$$f_{3w4} = w_{4\mathfrak{f}_3}|Q_4 - Q_5| \qquad (25)$$
$$f_{3w3} = w_{3\mathfrak{f}_3}|Q_3 - Q_4| \qquad (26)$$
$$f_{3w2} = w_{2\mathfrak{f}_3}|Q_2 - Q_3| \qquad (27)$$
$$f_{3w1} = w_{1\mathfrak{f}_3}|Q_1 - Q_2| \qquad (28)$$

Table 4 shows the value specified for each weight for the third, fourth and the fifth criterion The sum of the weights equals one.

Table 4: Specifications of Weights for The Third, Fourth and The Fifth Criterion

Weight	Value
$w_{1\mathfrak{f}_i}$	0.05
$w_{2\mathfrak{f}_i}$	0.1
$w_{3\mathfrak{f}_i}$	0.25
$w_{4\mathfrak{f}_i}$	0.6

5.4. The Number of Simulation Experiments Until the Optimum Was Found

The fourth criterion evaluates the speed of finding the optimum – the number of performed simulation experiments until the optimum/best solution was found in each series. The output of the function can take the value $f_4 \in [0,1]$. The task is to minimize this evaluation function. The fourth criterion when the objective function is minimized or minimized can be formulated as follows:

$$f_4 = \frac{f_{4w1} + f_{4w2} + f_{4w2} + f_{4w4} + f_{4w5}}{m_{\tilde{X}}} \qquad (29)$$

$$f_{4w5} = |Q_1 - 1| \qquad (30)$$
$$f_{4w4} = w_{4_{f_4}}|Q_1 - Q_2| \qquad (31)$$
$$f_{4w3} = w_{3_{f_4}}|Q_2 - Q_3| \qquad (32)$$
$$f_{4w2} = w_{2_{f_4}}|Q_3 - Q_4| \qquad (33)$$

$$f_{4w1} = w_{1_{f_4}}|Q_4 - Q_5| \quad (34)$$

The next box plot shows the number of simulation experiments until the optimum (suboptimum) was found. The task is to minimize the chart values – see Figure 6. High chart values of the strategy AllToAll (index 1) show that this strategy has a problem to find the optimum of the objective function. The leader of the fastest finding of the optimum is AllToOne strategy (index 0).
The AllToRand (index 3) is a little bit faster than the AllToAllAdaptive strategy (index 2).

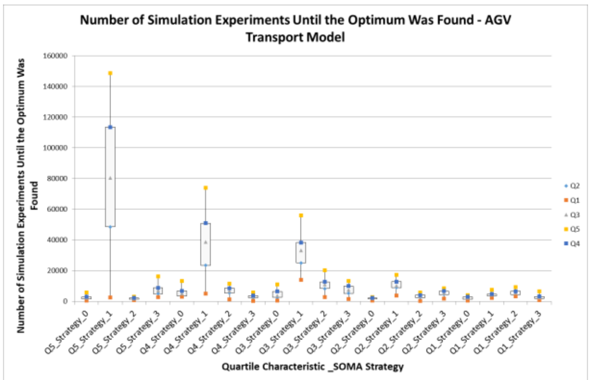

Figure 6: Number of Simulation Experiments Until the Optimum Was Found – Value Minimization

The AllToAll strategy (index 1) is not useful when the second termination allows a small number of simulation experiments to be performed. We tested this strategy with a higher number of simulation experiments, which SOMA can perform in the series. This strategy was better than other strategies of SOMA.

5.5. Convergence to the Optimum

The fifth criterion evaluates the convergence to the optimum. We store the objective function values of all feasible solutions generated by the optimization method in the optimization experiments in the series. The output of the function can take the value $f_5 \in [0,1]$. The task is to minimize this evaluation function. The fifth criterion when the objective function is minimized can be formulated as follows:

$$f_5 = \frac{f_{5w1} + f_{5w2} + f_{5w2} + f_{5w4} + f_{5w5}}{F_{\tilde{X}}} \quad (35)$$

$$f_{5w5} = |Q_1 - F(\mathbf{X}^*)| \quad (36)$$
$$f_{5w4} = w_{4f_5}|Q_1 - Q_2| \quad (37)$$
$$f_{5w3} = w_{3f_5}|Q_2 - Q_3| \quad (38)$$
$$f_{5w2} = w_{2f_5}|Q_3 - Q_4| \quad (39)$$
$$f_{5w1} = w_{1f_5}|Q_4 - Q_5| \quad (40)$$

If the objective function is maximized, the parts of the fifth criterion are calculated as follows:

$$f_{5w5} = |F(\mathbf{X}^*) - Q_5| \quad (41)$$
$$f_{5w4} = w_{4f_5}|Q_4 - Q_5| \quad (42)$$
$$f_{5w3} = w_{3f_5}|Q_3 - Q_4| \quad (43)$$
$$f_{5w2} = w_{2f_5}|Q_2 - Q_3| \quad (44)$$
$$f_{5w1} = w_{1f_5}|Q_1 - Q_2| \quad (45)$$

The next box plot shows the boxplot characteristics of the intervals of the objective function values of the generated feasible solution by the SOMA strategies. The task is to maximize the chart values – see Figure 7.
The leaders of the process of generating quality solutions are the AllToAllAdaptive strategy (index 2) and the AllToOne strategy (index 0) in our model. The AllToRand strategy (index 3) is worse than the previous strategies. The low chart values of the strategy AllToAll (index 1) show that this strategy has a problem to generate quality individuals in a small number of simulation experiments. This strategy supports the exploration and it needs to perform more simulation experiments to find the global optimum.
In the context of optimization, exploration means finding new points in areas of the search space which have not been investigated before. Since computers have only limited memory, already evaluated solution candidates usually have to be discarded in order to accommodate new ones. Exploration is a metaphor for the procedure which allows search operations to find novel and maybe better solution structures.
Exploitation, on the other hand, is the process of improving and combining the traits of the currently known solutions, as done by the crossover operator in evolutionary algorithms, for instance. Exploitation operations often incorporate small changes into already tested individuals leading to new, very similar solution candidates or try to merge building blocks of different, promising individuals. They usually have the disadvantage that other, possibly better, solutions located in distant areas of the problem space will not be discovered.(Weise 2009)

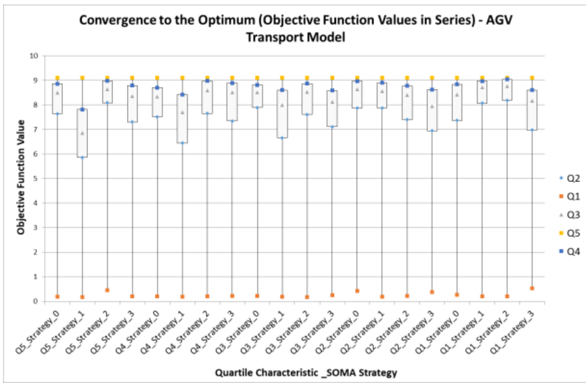

Figure 7: Convergence to the Optimum (Objective Function Values in Series) - Objective Function Maximization

5.6. The Frequency of Using the Database Records

Because we mapped all the possible solutions and their objective function values in the search space and found the lower and upper bounds of the objective function of the simulation model we could count the relative frequencies of the feasible solutions objective function values between the specified range. We divided the whole interval of objective function values into 100 smaller parts - intervals ($n = 100$) with the same step:

$$\varepsilon_F = \frac{|F(\hat{\boldsymbol{X}}) - F(\check{\boldsymbol{X}})|}{n} \tag{46}$$

where n denotes the number of smaller intervals of the objective function values of feasible solutions with the defined size of the interval - ε_F.

We calculated how often the objective function values occur within different ranges of objective function values:

$$FR_j, j \in [1, n] \tag{47}$$
$$= \begin{cases} FR_j + 1 \text{ if}\left(F(\boldsymbol{X}_i) \geq \varepsilon_F * (j-1) + F(\check{\boldsymbol{X}})\right) \\ \quad \wedge \left(F(\boldsymbol{X}_i) < F(\check{\boldsymbol{X}}) + \varepsilon_F * (j-1) + \varepsilon_F\right), \\ \quad i \in [1, NCS] \\ FR_j + 0 \quad \text{else} \end{cases}$$

Where FR_j denotes the frequency of the feasible solutions' objective function values; j denotes the index of the small interval of the objective function value, $F(\boldsymbol{X}_i)$ denotes the objective function value of the i-th feasible solution belonging to the interval of the objective function; NCS denotes the number of feasible solutions in the interval of the objective function value; ε_F denotes the size of the range of the smaller interval.

We calculated the percentage relative frequency of each smaller interval.

Figure 8 shows the percentage of the calculated relative frequencies of the mapped objective function values of the discrete event simulation model considering the intervals of the objective function values. These data series reflect the quality of the feasible solutions in the search space of the modelled problem.

We also tested the series of the boxplot characteristics of the weighted sum to obtain and compare their quality due to their relative frequency of using the database records. Other charts show the percentage of relative frequencies of the objective function values found by the different SOMA strategies using the boxplot characteristics series – see Figure 9.

If we compare the relative frequencies of the mapped objective function values of the discrete event simulation model and the relative frequencies of the objective function values found by the optimization method, the strategies tend towards a strong convergence on the global optimum. If we select less suitable optimization method settings the relative proportion starts to increase in other areas of the interval. Appropriate setting of the optimization method leads to a lower number of optimization experiments to find the global optimum (a steeper convergence on the global optimum and a lower relative frequency in the area of global extremes of the objective function values).

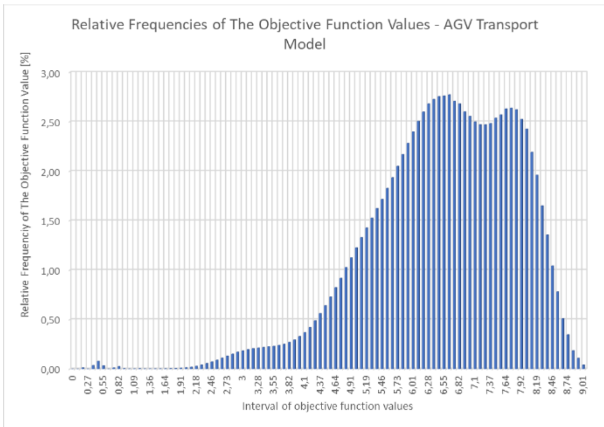

Figure 8: Relative Frequencies of The Objective Function Values – Objective Function Maximization

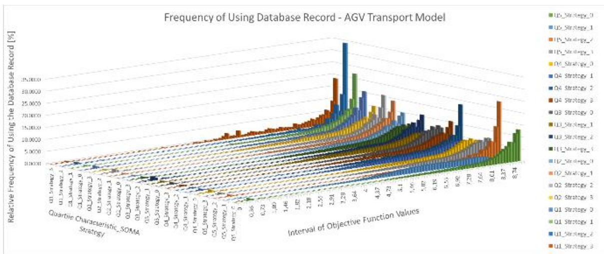

Figure 9: Frequency of Using Database Record - Objective Function Maximization

6. CONCLUSION

The testing of the SOMA optimization method confirmed that it is quite a successful and generic optimization method according to the different objective function landscapes of our tested AGV Transport model. This method found the global optimum or candidate solutions even in the case of the worst settings of this optimization method.

If we focus on the optimization method success and the convergence to the optimum during the optimization process, the AllToAllAdaptive strategy and AllToRand are successful strategies of the SOMA optimization method. These strategies are prone to wrong optimization method parameters settings in our discrete event simulation model. These strategies are followed by the SOMA strategy AllToOne.

The AllToAll strategy is not useful when the second termination allows a small number of simulation experiments to be performed. This strategy supports the exploration and it needs to perform more simulation experiments to find the global optimum We tested this strategy with a higher number of simulation experiments, which SOMA can perform in the series.

ACKNOWLEDGMENTS
This contribution has been prepared within the project LO1502 'Development of the Regional Technological Institute' under the auspices of the National Sustainability Programme I of the Ministry of Education of the Czech Republic aimed at supporting research, experimental development and innovation.

REFERENCES

Bučková M., Krajčovič M., Edl M., 2017. Computer Simulation and Optimization of Transport Distances of Order Picking Processes. Procedia Engineering, 192, 69-74.

Borda, M., 2011. Fundamentals in Information Theory and Coding. Berlin: Springer Berlin Heidelberg.

Elsayed, S. M., Ruhul A. S., Daryl L. E., 2013. An Improved Self-Adaptive Differential Evolution Algorithm for Optimization Problems. IEEE Transactions on Industrial Informatics, 9 (1), 89-99.

Koblasa, F., Vavrousek, M., Manlig, F., 2017. Three-dimensional Bin Packing Problem with heterogeneous batch constraints. In: P. Prazak, ed. Mathematical Methods in Economics, 330–335.

Li Y. L., Zhan Z. H., Gong Y. J., Chen W. N., Zhang J., Li, Y. 2015. Differential Evolution with an Evolution Path: A DEEP Evolutionary Algorithm. IEEE Transactions on Cybernetics, 45(9), 1798–1810.

Pohlheim, H., 2006. GEATbx: Example Functions. Available from: http://www.geatbx.com/docu/fcnindex-01.html#P204_10395 [accessed 20 November 2011]

Raska, P., and Ulrych, Z., 2014. Hierarchical approach to developing a logistic discrete event simulation model using Automated Guided Vehicles. 26th European Modeling and Simulation Symposium, pp. 205-211. Bordeaux (France).

Volna, E., 2012. Evolutionary Algorithms and Neural Networks (in Czech language: Evolucni algoritmy a neuronove site). University of Ostrava. Available from: http://www1.osu.cz/~volna/Evolucni_algoritmy_a_neuronove_site.pdf [accessed 5 March 2016]

Weise, T., 2009. E-Book "Global Optimization Algorithms - Theory and Application" 2nd Edition. Available from: http://www.it-weise.de/projects/book.pdf [accessed 2 February 2011]

Zelinka, I., 2016. SOMA—Self-organizing Migrating Algorithm. In: Studies in Computational Intelligence. Springer Verlag, 3–49.

Zelinka, I., Snasel, V. and Abraham, A., 2013. Handbook of Optimization: From Classical to Modern Approach. Intelligent Systems Reference Library, Berlin: Springer.

Zelinka, I., Vybíral J., 2005. SOMA - Source Codes. Tomas Bata University in Zlín. Available from: http://www.ft.utb.cz/people/zelinka/soma/ [accessed 6 March 2012]

ABOUT THE AUTHORS

Pavel Raska is a Doctor at the Department of Industrial Engineering and Management at the University of West Bohemia in Pilsen (Czech Republic). He holds M.Sc., and Ph.D. in Mechanical Engineering at the same university. His research interests are oriented towards discrete event simulation, simulation optimization, modelling and simulation tools (ARENA, Plant Simulation) and working on practical simulation projects for companies.

Zdenek Ulrych is Associate Professor at the Department of Industrial Engineering and Management at the University of West Bohemia in Plzen and he is also a researcher in the Regional Technological Institute at the University of West Bohemia in Plzen (Czech Republic). He holds M.Sc., Ph.D. and doc. in Mechanical Engineering at the same university. His research interests are oriented towards discrete event simulation, optimization in simulation, modelling and simulation tools (ARENA, Plant Simulation), design and development of software and working on practical simulation projects for companies.

VRP COMPLEX NETWORK ANALYSIS AND SIMULATION

Gabriel Policroniades Chípuli[(a)], Idalia Flores de la Mota[(b)], Author3[(c)], Javier Lara de Paz[(d)] Sashiko Sihirai Reyna[(e)]

[(a),(b),(c),(d),(e)] Universidad Nacional Autónoma de México

[(a)]gpolicroniadesch@gmail.com, [(d)]idalia@unam.mx, [(c)]jlaradepaz@gmail.com, [(b)] sashikosr@outlook.com

ABSTRACT

When carrying out a systemic analysis of a distribution network, it is possible to identify controllable and non-controllable factors for decision makers, when the system being disaggregated into greater levels of detail, which may affect compliance with a deterministic routing plan. Some of these factors, to mention a few, may include late deliveries of raw material, unexpected transportation failures, unexpected closures of some distribution center; among others. If this type of analysis is combined with a topological analysis of the network as complex one, then it will be possible to develop more robust networks that can deal with a greater number of adversities. Identifying the topological analysis as an opportunity niche for the elaboration of possible scenarios to improve the flow through the entire network. These scenarios have been simulated in SIMIO. One way to mix both principles, is possible to find in the method proposed by authors. A case study is shown in the automotive industry.

Keywords: VRP, Complex Networks, Simulation

1. INTRODUCTION

The main objective of a vehicle routing problem (VRP) is the design of routes assigned to vehicles that distribute product to a group of customers; with the characteristic that each route starts and ends in the same central warehouse. This type of problem is considered as a classic problem of combinatorial optimization and due to its complexity, it is cataloged in the literature as a NP-Hard type problem as is mentioned in(Braekers, Ramaekers, & Van Nieuwenhuyse, 2016; Cordeau, Laporte, Savelsbergh, & Vigo, 2007; Mohammed et al., 2017; Parragh, Doerner, & Hartl, 2008a, 2008b). This type of models can be solved by heuristic, metaheuristic or exact techniques; However, because one of its objectives is the optimization of resources for obtaining solutions, the preferred method is usually metaheuristic techniques; due to its quality of solution and execution time; compared to the exact techniques that provide optimal solutions at a high cost of time (Cordeau et al., 2007). An application of these models to solve a problem within a distribution network considers the clients how the vertices of the network and the arcs will rep-resent the travel or tour sections, to each of these arcs, it is assigned a cost that represents travel time or distance.

The VRP as is mentioned in (Policroniades & Flores de la Mota, 2016; Policroniades, G., Flores de la Mota, I., Sihirai Reyna, O. S., & Lara de Paz, J., 2018) has been mainly concerned with solving problems of combinatorial optimization routing, seeking to optimize the resources used in a general way to obtain a solution. This principle can go so far as to undermine transportation models, by eliminating relationships and significant variables of reality; in order to make efficient models that can be executed in a brief moment; considering most of the time deterministic models. However, reality is not always usually this way; and stochastic events, which are not controllable for decision makers, usually occur. In many cases, within the systems, or in their environments, there are factors that are usually omitted when performing a modeling, due to the increase in complexity; both computationally and systemically. A tool that allows analyzing the system and identifying possible critical points in the distribution network, are the metrics provided by complex networks; because they allow to know and characterize the topology of a distribution network. Some of these metrics are clustering coefficients, centrality analysis, grade distribution and vulnerability analysis; among other; which will allow for example to identify where to place a Distribution Center closer to a set of customers, group customers or warehouses by common characteristics, etc. Knowing these metrics will allow the generation of scenarios that can be tested by means of simulation; to which an optimization process will be applied to identify the ideal input parameters for its correct operation. All this process is based on the methodology proposed by (Policroniades, G. et al., 2018); shown in figure 1. In this way, it can be said that the main objective of this work is to show an application of the methodology.

2. THE PROPOSED METHODOLOGY, DESCRIPTION AND BACKGROUND

The methodology is composed of nine stages; among which there is a process of verification and validation of the information; as shown in the figure 1. The validation process is done both to validate the conceptual model and the simulation model. The process is shown as a cyclical process in which the main objective is the continuous improvement of the distribution system. The following methodology is based on (C. M. Banks, 2010; J. Banks, 1998; Barceló, Grzybowska, & Pardo, 2007; Carson & Maria, 1997).

Figure 1: Proposed methodology

In general terms, it can be said that the methodology begins by identifying the problem as a vehicle routing problem by means of company indicators; subsequently, a systemic analysis stage is carried out; Once the systemic analysis is obtained, the conceptual model is constructed, and the distribution network is analyzed. With these stages, we proceed to carry out the simulation process and generate the scenarios to improve the topology of the network; just like the improvement of the process is executed. Once this stage is obtained, we proceed to simulation-optimization, the results are presented, and the solution is implemented. The process must be under constant supervision, and if possible, failures are detected, the methodology must be applied again.

The proposed methodology is made up of different methodological and technical approaches; as shown in figure 2.

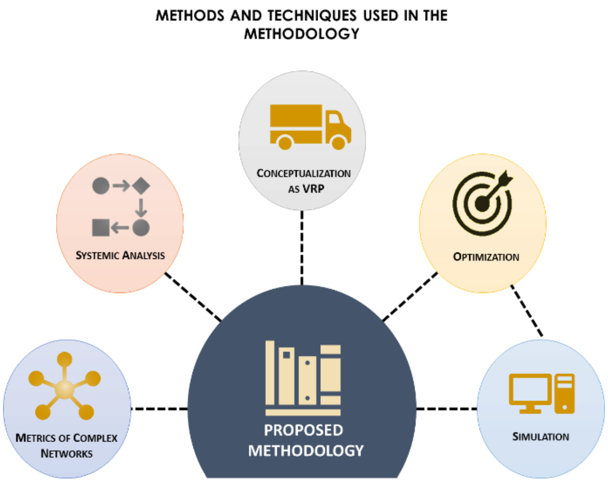

Figure 2: Proposed methodology, own design.

From left to right, it can be identified the following methods and techniques:

- ***Complex Networks***: The objective of this approach is based on the topological analysis of the distribution network; mainly aimed at identifying the vulnerability and efficiency of the network, in the face of possible attacks that may generate blockages of routes, or elimination of nodes within the network; together with an analysis of metrics that allow to quantify the coefficients of centrality, clustering, assortativity; among others (Casasnovas, 2012; Estrada, 2015).
- ***General systems theory***: The use of this approach allows a systemic analysis to identify the restrictions, relationships, variables and functions that exist within the system. During this process, it is possible to identify internal or external elements of the system that may affect the distribution of the product throughout the network (Prawda, J., 1991; Von Bertalanffy, L., 1976).
- ***Vehicle Routing Problem***: The core part of the methodology is to solve vehicle routing problems; for which, the specific characteristics and restrictions that allow classifying the type of vehicle routing detected in the company must be identified.
- ***Simulation – Optimization***: This selected solution technique allows the integration of environmental or stochastic factors that cannot be integrated into deterministic models; Some of these factors may be vehicle failures, stochastic customers, stochastic demands, change of routes due to unexpected closures; among others (Berhan, Beshah, Kitaw, & Abraham, 2014; Bertsimas, 1992; Huang, Wu, & Ardiansyah, 2018). The concept of optimization, is linked to the VRP to find the best route that minimizes the cost function determined (Fan, Xu, & Xu, 2009; Juan, Faulin, Pérez-Bernabeu, & Domínguez, 2013).

In terms of the methodology approach of companies related to the automotive sector; can be mentioned the work done by (Lei, Mingfang, & Lijun, 2012). However, when it is desired to perform a combination of the approach of the vehicle routing problem with a complex network approach; applied in a manufacturing sector, it is important to mention that the linearity of the process does not allow the existence of bifurcations in the roads, as found in other works such as (Aleta, Meloni, & Moreno, 2016; Gallotti, Porter, & Barthelemy, 2016); thus preventing the traditional vision of a complex network with multilayer structure as proposed (Boccaletti et al., 2014). Against this, it is proposed to use the metrics of a complex network to analyze the distribution network a company in this sector; emphasizing the vulnerability and efficiency metrics of the network against possible failures in nodes and arcs. These last concepts, as mentioned in (Holme, Kim, Yoon, & Han, 2002), they can be measured through attacks directed to certain arcs or nodes

A problem of vehicle routing, as identified in (Cordeau et al., 2007) it is structured by means of a complete network; which indicates that all the elements or nodes of the network are connected to each other by means of arcs; showing an assortativity of 100%. When analyzing the distribution network of a company with respect to its customers; it can be observed that this can be composed of a set of different complete networks; the way to identify each of them, lies in finding the central or regional stores that comprise it. Each of them has a specific portfolio of interconnected customers, which are served by a fleet of vehicles, forming a complete network. However, what happens in the case of one or two regional stores and a central warehouse? As shown in the following figure:

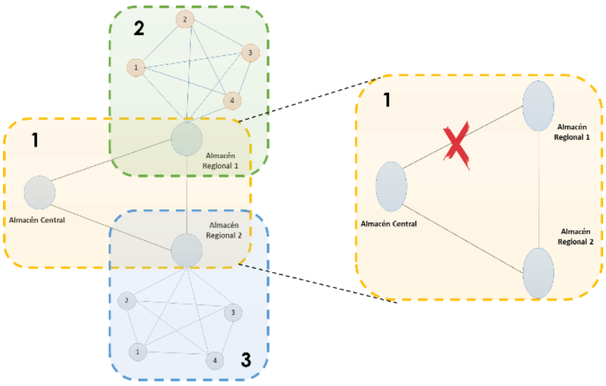

Figure 3: Example of the elimination of an arc in the distribution network, own design.

In Figure 3, there is greater vulnerability in the VRP 1 network, because there are only two different ways to get from the central warehouse to one of the other two warehouses, against the case that one of these two roads fail.

Another possible scenario to which the distribution networks are exposed, are the possible partial closures of its important nodes, as distribution warehouses or regional warehouses. When this happens, as mentioned (Cartledge & Nelson, 2011), the arcs belonging to the failure node are disabled within the network until after the contingency causing a drastic loss of connectivity within the network.

However, it can be said that within the chain, a lower level supplier can supply its product to multiple clients with different levels within the chain; as in the case of finished products for meals; which goes directly to a dealership or automotive agency, jumping to the same OEM or manufacturer of vehicles (Braese, Niklas, 2005). In this way, it can be said that, depending on the capacity of production and distribution of the manufacturer, the product can reach a previous step to the final customer.

Each of the companies that make up the distribution chain of the automotive sector has a specific structure of its distribution network; which, depending on the consolidation mode, can be: Milk-Run, Consolidation at the Transfer Point, or Supplier Consolidation; as mentioned in (Policroniades & Flores de la Mota, 2016). Each of these modes may vary from company to company depending on the type of contract with its customers and its facilities. However, these distribution networks due to the volume of product they handle, and the high globalization and search for emerging markets present in the same sector, make them vulnerable to possible supplier failures, change of routes, partial closure of warehouses, elimination and annexation of new clients; between another factors (Braese, Niklas, 2005).

According with all these considerations, the proposed methodology is in the process of being developed as part of a doctoral thesis project, then it will be shown the most relevant in terms of the respective progress; applied to a small case that belongs to the application case.

3. CASE STUDY, DESCRIPTION AND APPLICATION

The case study presented in this section is part of the distribution system of a real company of the automotive sector; which will be called as Company X due to confidentiality issues.

3.1. Description of the case

Company X has a Portfolio of 8 clients; which are cataloged in two regions according to their percentage of sale and distance from the central warehouse. However, despite the regions customers are served by this single store. Figure 4 shows the structure of the distribution network of company X

The consumption behavior of these customers is determined by different statistical distributions depending on each client. The statistical distribution of the time between orders arrivals of the clients is known. These customers can be classified into three types; the first the assemblers, the second the automotive agencies and the third, the service workshops.

It has a manufacturing cell with the capacity to produce a safety belt every 4 minutes on average. In this way it can be said that a total of 15 belts can be produced for one hour; in an 8-hour working day, there will be a total production of 120 seat belts.

It has a warehouse with a maximum capacity for 250 seat belts.

It has a fleet of two vehicles with a capacity for 4 packed products; considering that each packaged product can carry 4 belts inside.

It has a sales department with a person responsible for this activity.

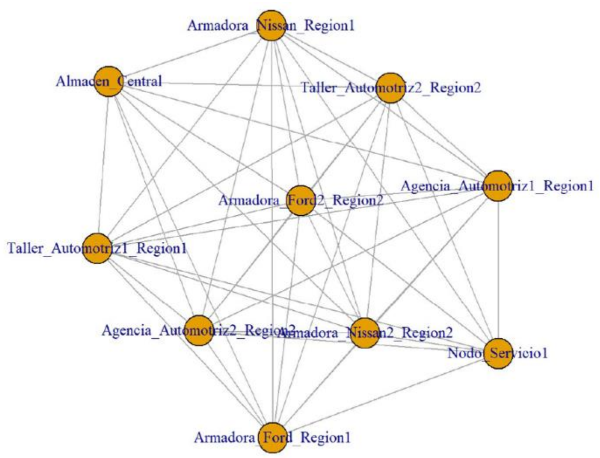

Figure 4: Company X distribution network, obtained through software R.

As can be observed in the first instance, there are three types of customers that depend on the central warehouse: Automotive Agencies, Service Workshops and Shippers. Each of these client's groups has their own characteristics. For example, the assembly companies, as mentioned previously, usually present a uniform behavior regarding their orders, while the other two types of clients, usually present a stochastic behavior.
Regarding to the problem; this can be classified in the following three ways:

- Shortage of Raw Material: Throughout the last 7 months the company has presented a shortage in the delivery of its raw material, despite the talks with its suppliers, this problem can be extended indefinitely due to the lack of components for its elaboration. The company has tried to find new suppliers; but it is the only provider of that type of product.
- Demand and Arrival of Orders: Because customer demand and order arrivals are stochastic, the company does not have a method to identify the best routing sequence; before which, once the loading of the vehicle is carried out, the delivery of the product begins at random, sometimes generating a greater travel distance than expected.
- Lack of Suppliers: Faced with the growing failure on the part of suppliers for the timely delivery of their product, the company considers the installation of one or two regional warehouses that can deal with possible shortages in its production area. With this alternative the warehouses must be close to the customers and source of supply; reducing the distances traveled through the entire system.

As for its routing system, each warehouse that exists in the system will control its own fleet of vehicles; an optimization must be carried out separately for each one of them. Also, it is important to mention the following characteristics of the routing problem:

- The vehicles wait for their loading capacity to be completed to start the journey to the corresponding customers. The capacity of the vehicles is maximum of 15 pallets.
- The demands that exceed the capacities of the vehicles can be divided to be sent in several vehicles.
- Each vehicle has a specific schedule; regarding the driver's workday. During the leisure periods, the vehicle returns to the corresponding warehouse to wait for the new start of its journey.
- Each vehicle has a failure time, due to breakdowns. Similarly, there is a repair time.

From this information, it can be said that the main objective of the company and the research to be carried out is possible to define it in the following two points:

- Find the best configuration of the network to reduce vulnerability to possible failures of the central warehouse, by annexing one or two regional warehouses strategically seeking to minimize the distance traveled in the network.
- Obtain by means of simulation - optimization a routing sequence for the vehicles that minimizes the distance traveled during the delivery process.

3.2. Application of the Methodology

Next, each of the stages applied to the case will be described very generally; likewise, that some of its deliverables will be addressed; mainly, with emphasis on stage III.

It is important to mention that some of the stages are carried out several times as the methodology advances to obtain their deliverables for later stages.

3.2.1. Stage I

The objective of the first stage is to justify the application of the methodology through the consideration of two aspects; the first of them, detecting the problem as a vehicle routing problem, through the analysis of the company's transport indicators. The second, if there is a company´s goal, that implies a modification to the structure of the company's distribution network. Another important aspect of this stage is the identification of the vehicle routing problem model of the company under study.
In the case of company X, a main interest is seen in the reduction of its operational vulnerability by adding one or two regional warehouses to its distribution network. Then it is possible to define the following objectives:

- Find the best network configuration to reduce vulnerability to possible failures of the central warehouse; annexing to the system one or two regional warehouses strategically seeking to minimize the distance traveled to the interior of the network.

- Obtain by means of simulation - optimization a routing sequence for your vehicles that minimizes the distance traveled during your delivery process.

The VRP model of company X can be defined as:

- A routing problem with vehicle capacity restriction (CVRP).
- Stochastic Clients.
- Stochastic Customer Demand.
- And with an inventory problem.

Once defined the objectives and the VRP model of the company; It is advisable to define a work team responsible for the application of the methodology; With these defined aspects, it is possible to carry out stage II.

3.2.2. Stage II

During this stage the systemic analysis of the original network and the proposed network is carried out. In the case of the proposed network, the analysis must be made to the new elements annexed to the network; as they can be: warehouses regions / Local. The objective of this stage is to identify the variables, functions, relationships and constraints of the different elements of the system. Another important aspect during this section is the adjustment and analysis of the data.

As an example of this section, table 1 is shown, where the customer's demands can be identified, and their respective distribution can be determined from the corresponding adjustment obtained through the @Risk software. It is important to mention that integer values will be considered because they represent demand values.

Table 1: Example of the parameters of the statistical distributions for the demand data obtained by the @risk software when fitting the data.

Client	Distribution	Parameters
Automotive assembler Ford 1	Uniform Distribution	$\alpha = 3$ $\beta = 7$
Automotive assembler Nissan 2	Uniform Distribution	$\alpha = 2$ $\beta = 4$
Automotive assembler Ford 3	Uniform Distribution	$\alpha = 2$ $\beta = 7$
Automotive assembler Nissan 4	Uniform Distribution	$\alpha = 1$ $\beta = 6$
Automotive workshop 1	Gamma Distribution	$\alpha = 2.39$ $\beta = 5.2$
Automotive workshop 2	Gamma Distribution	$\alpha = 2.21$ $\beta = 2.11$
Automotive Agency Ford 1	Gamma Distribution	$\alpha = 2.7$ $\beta = 3.6$
Automotive Agency Nissan 2	Gamma Distribution	$\alpha = 2.9$ $\beta = 4.3$

In the figure 5 the inventory process is observed and how a set of variables behaves as a function.

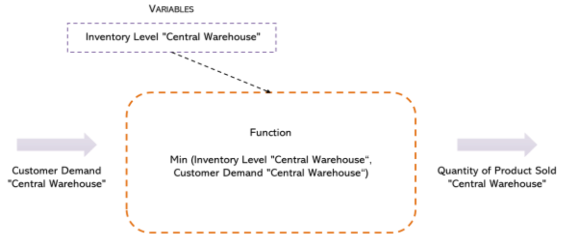

Figure 5: Example of the relationship between the variables and the calculation of a function

3.2.3. Stage III

This stage is divided into two main sections: in the first one, is the conceptual model. The second one is the analysis of the distribution network as well as the analysis of the different scenarios defined in stage IV when we have already one iteration. Once the analysis of the metrics is done, is time to select the best scenario that matches the objective of the project and the objective of the analysis of the metrics. With the distribution network selected, stage II is carried out to carry out the systemic analysis of the new elements of the network and the conceptual model of the first section of stage III is updated considering the new modifications of the network.

Table 2 shows the characteristics of the different scenarios obtained in stage IV, to improve the topology of the network.

Table 2: Description of the different scenarios

Scenery	Description
Scenery 1	Equivalent to the original network of the company.
Scenery 2	The existence of the two regional warehouses is considered: each of which serves its four closest customers. Each region has its service node for vehicles.
Scenery 3	The two regional stores are considered; so that customers are divided into two distinct groups and assigned to the nearest store. Subsequently, each one of the warehouses, including the central warehouse, comprises two closest customers assigned to other warehouses.
Scenery 4	Clients are accommodated by type of demand; customers with more stable demand are assigned to the central warehouse; while the other clients are assigned to the other two warehouses.
Scenary 5	The use of a single regional warehouse is proposed; customers with stable demand are assigned central warehouse; while the other clients are assigned to the new warehouse.

Next, the corresponding summary of this stage equivalent to the original network of the company will be shown, as well as the respective scenarios generated in stage IV.

If the central warehouse stops working, the total distribution in the network is lost; even when in topological terms, due to the high connectivity of all the elements, vulnerability is low. Therefore, it can be said that this structure presents an operational vulnerability; which, should be minimized by means of the analysis of the different scenarios proposed in stage IV. See figure 6.

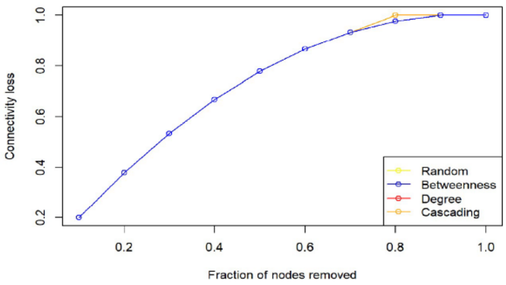

Figure 6: Company X distribution network, obtained through software R.

Vulnerability can be analyzed considering two scenarios: First eliminate two arcs randomly, see figure 7, and in the second case, the elimination of the client nodes in the network of figure 8. As can be seen with these two possible hypothetical cases, the greatest impact on the efficiency of the network occurs with the elimination of arcs randomly since in the second place, the elimination of a node does not affect the network.

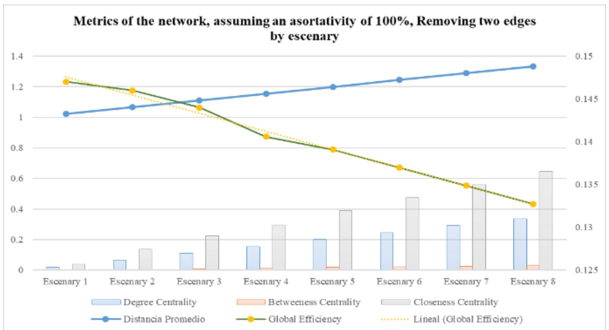

Figure 7: Behavior of the metrics of the real network, by eliminating edges from the network

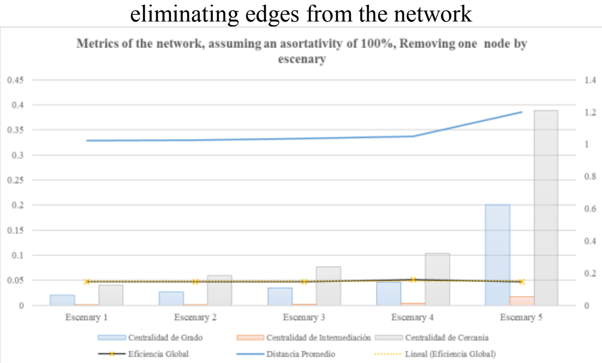

Figure 8: Behavior of the metrics of the real network, by eliminating nodes from the network

When the different scenarios generated in stage IV are analyzed, defined in table 2; Figure 9 is obtained; in which, the main metrics of each of them are represented.

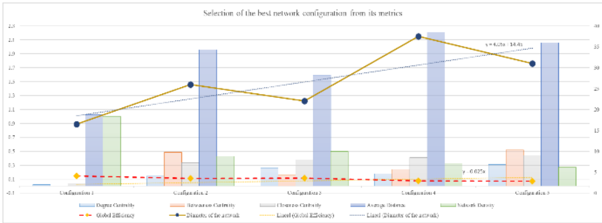

Figure 9: Metric comparison by scenario

From this figure 9, it can be said that the best selected scenario is scenario 3; because, if there is a failure of any of the supply nodes of the network, the overall impact on customers will be the minimum; this is achieved, through the concept of density.

Figure 10: Proposed network of scenario 3

An important aspect to consider of the density concept; is that as a customer is attached to a new distribution warehouse; this warehouse must have enough capacity to provide the requested product. Therefore, the more connectivity there is in a network, the distribution nodes should be specialized in more customers.

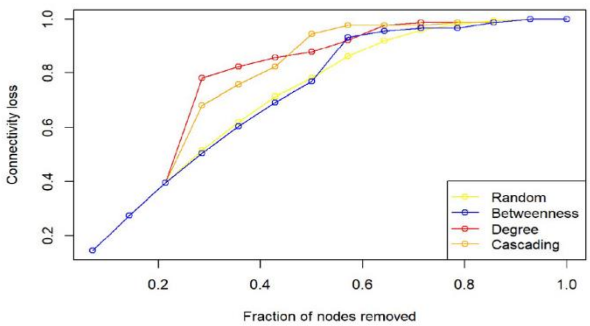

Figure 11: Vulnerability analysis for the scenario 3 network

As shown in Figure 11, when 30% of the nodes of the network are removed, it is observed how network connectivity begins to be lost; mainly because there are few connection arcs between the central warehouse and the regional warehouses. By the time one of the warehouses or the two regional stores is eliminated, all the arcs that depend on them are eliminated.

With this selected scenario and the current distribution network; we proceed to simulate the model and then to optimize and compare the results to verify the improvement of the distribution process.

In the research shown in this article; only the simulation reports of each of the two models will be displayed.

3.2.4. Stage IV

The progress of the methodology is shown until stage 4; the process of Simulation - Optimization for the proposed network and the current network is pending. The simulation was executed in Simio - Simulation software version 10.181; on a PC with an Intel core i7, 8th Generation processor.

3.2.4.1 Analysis of the Original Network

The simulation was executed considering a work week; equivalent to a total of 168 hours. During this period, it was detected that the percentages of utilization of the entities were as follows: the central depot was used during 1.58% of the time due to production; which can be observed in the following percentages:

- Production Area: 1.58% of total time.
- Waiting Area: 0.46% of total time.
- Inventory Area: 0.16% of total time.

The percentage of time of use of the vehicles is as follows: Vehicles were available 73% of the time; with respect to the 27% that elapsed in driver's rest time This percentage is because while one vehicle rests, another performs the operation; which gives a period of 84 hours per week per vehicle. This is explained as follows:

- Vehicle 1: Use 54% of time to deliver the product; the remaining time is divided between the driver's rest time and the vehicle failure time. Travel a total of 124,604 km.
- Vehicle 2: Use 63% of total time for product delivery. The total route was 98.32 km, practically 84 km less than the vehicle 1.

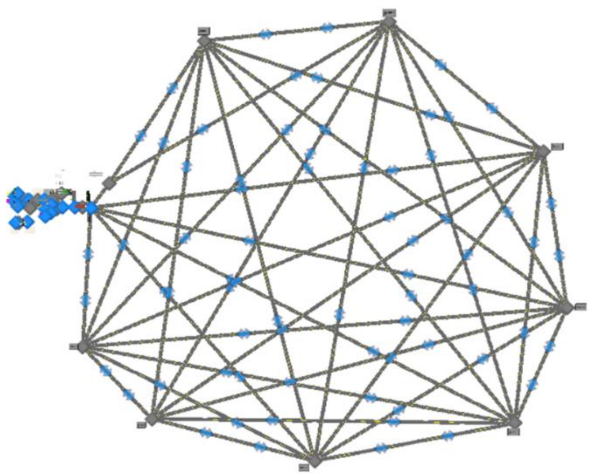

Figure 12: Current distribution network done with Simio

A total of 63 orders were received; equivalent to a total of 375 pieces of product. The entire product was delivered to the customer.

3.2.4.2 Analysis of the Proposed Network

For the following case, the same criteria were considered as in the original network; with the difference that, for each existing warehouse in the network, there is a fleet of two vehicles available with their respective work and rest hours.

Regarding the proposed network, executed during the same period, the following characteristics are detected by warehouse:

Central Depot:

- Production Area: 0.93% of total time.
- Waiting Area: 0.14% of total time.
- Inventory Area: 0.01% of total time.

The percentage of use of their vehicles is lower than that of the regional stores because this warehouse only makes deliveries when the product in the regional warehouses is exhausted; which gives a utilization of 18% with respect to 82% in leisure. As for the distance traveled on average by the two vehicles was 54 km.

Regional Warehouse 1:

- Waiting Area: 1.32% of total time.
- Inventory Area: 0.12% of total time.

The percentage of use of their vehicles is greater than that of the central warehouse; with 61% of transport activity.

Regional Warehouse2:

- Waiting Area: 0.46% of total time.
- Inventory Area: 0.16% of total time.

The percentage of use of its vehicles is like that of regional warehouse 1; with the united difference that this warehouse made an average use of 67% for the transport activity.

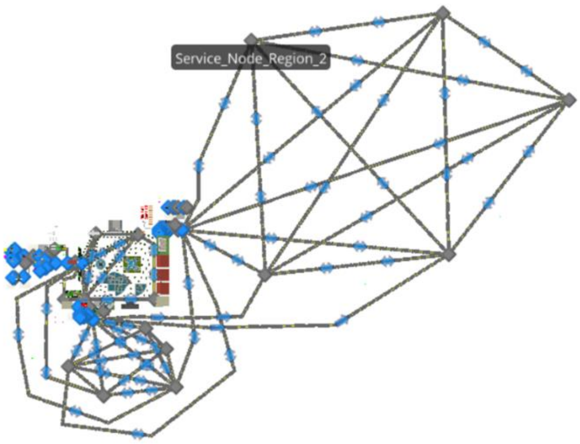

Figure 13: Proposed methodology

A total of 56 orders were received; with a total of 302 ordered products in total to the two regional warehouses. As a partial conclusion so far, it can be said that the proposed methodology allows the mixture of two approaches; the first of them, using the metrics of complex networks to analyze and reduce the vulnerability of the network, identifying the impact on customers and the operation of the network. The second approach where simulation is combined with the problem of vehicle routing through simulation optimization; allowing integrating the complexity of the environment to routing problems. An example of this in the case is the integration of the vehicles breakdowns, as well as the driver's rest time.

4. CONCLUSIONS, EXPECTED RESULTS AND ACTIVITIES TO BE CARRIED OUT

As a conclusion of the application of the methodology until the fourth stage, to the case of company X; it can be said that it is important to study the metrics of the network, if these are contrasted with the operational and strategic aspects of the companies. As it could be seen in the case, the analysis of vulnerability can generate confusion when there is a high connectivity and a single central warehouse.

However, what would happen to the network if that central warehouse were to fail operationally; the entire distribution chain would collapse, even when there is a high level of connectivity; because all the other nodes are client nodes and would not have the capacity to distribute the input between them. However, this controversy can be eliminated if scenarios are generated that consider these two aspects.

As advantages when performing this type of analysis; it can be mentioned that it allows to decrease the average distance traveled to the interior of the network; and explore unexplored roads or routes to reduce vulnerability through the concept of assortativity of the network.

Another measure of complex networks, for example, is the intermediation coefficient, which can be obtained globally or locally; in the case of being local, it quantifies the frequency or the number of times a node acts as a bridge along the shortest path between two other nodes. This measure can support for the location of local stores. There is a wide variety of metrics that describe the topology of the network; and its strategic use for network analysis; can help improve the performance of vehicle routing problems.

Among the activities to be carried out are the following:

- Perform a more complete analysis of the company's distribution network, including a clustering analysis for the classification and assignment of customers to regional warehouses. In the same way, through this analysis, analyze the impact of the vulnerability of the network for each of these subgroups generated.
- Execute the optimization of the network to validate the improvement of the process.
- Include all the company's clients in the study.

The expected results can be classified into:

- The methodology is expected to improve the performance of the distribution network of any company; combining two aspects: Topological and Operational.
- It will also offer the ability to integrate elements of the environment that may influence the performance of vehicle routing; as in the case of company X, with vehicle failures.
- It will allow by means of the Simulation - Optimization to obtain routing programs that improve the assignments of the vehicles to the routes established for the reduction of the costs derived from the distribution.

ACKNOWLEDGMENTS

We are grateful for the support to CONACYT for its support, likewise, we greatly thank to our advisor Ph.D. Idalia Flores de la Mota whom we greatly esteem, and we admire.

To the PAPIIT DGAPA project IT102117, UNAM for its support to this research.

REFERENCES

Aleta, A., Meloni, S., & Moreno, Y. (2016). A multilayer perspective for the analysis of urban transportation systems. *arXiv:1607.00072 [cond-mat, physics:physics]*. Recuperado de http://arxiv.org/abs/1607.00072

Banks, C. M. (2010). Introduction to Modeling and Simulation. En *Modeling and Simulation Fundamentals* (pp. 1-24). https://doi.org/10.1002/9780470590621.ch1

Banks, J. (1998). *Wiley: Handbook of Simulation: Principles, Methodology, Advances, Applications, and Practice - Jerry Banks*. Recuperado de

http://www.wiley.com/WileyCDA/WileyTitle/productCd-0471134031.html
Barceló, J., Grzybowska, H., & Pardo, S. (2007). Vehicle Routing And Scheduling Models, Simulation And City Logistics. En *Operations Research/Computer Science Interfaces Series*. *Dynamic Fleet Management* (pp. 163-195). https://doi.org/10.1007/978-0-387-71722-7_8
Berhan, E., Beshah, B., Kitaw, D., & Abraham, A. (2014). Stochastic Vehicle Routing Problem: A Literature Survey. *Journal of Information & Knowledge Management*, *13*(03), 1450022. https://doi.org/10.1142/S0219649214500221
Bertsimas, D. J. (1992). A Vehicle Routing Problem with Stochastic Demand. *Operations Research*, *40*(3), 574-585. https://doi.org/10.1287/opre.40.3.574
Boccaletti, S., Bianconi, G., Criado, R., del Genio, C. I., Gómez-Gardeñes, J., Romance, M., … Zanin, M. (2014). The structure and dynamics of multilayer networks. *Physics Reports*, *544*(1), 1-122. https://doi.org/10.1016/j.physrep.2014.07.001
Braekers, K., Ramaekers, K., & Van Nieuwenhuyse, I. (2016). The vehicle routing problem: State of the art classification and review. *Computers & Industrial Engineering*, *99*, 300-313. https://doi.org/10.1016/j.cie.2015.12.007
Braese, Niklas. (2005). *The Dynamics of Supply Chains in the Automotive Industry*. Massachusetts Institute of Technology.
Carson, Y., & Maria, A. (1997). *Simulation Optimization: Methods And Applications*. 118-126. Recuperado de https://www.computer.org/csdl/proceedings/wsc/1997/4278/00/42780118.pdf
Cartledge, C. L., & Nelson, M. L. (2011). Connectivity Damage to a Graph by the Removal of an Edge or a Vertex. *arXiv:1103.3075 [cs]*. Recuperado de http://arxiv.org/abs/1103.3075
Casasnovas, D. J. P. (2012). Some Basic Concepts on Complex Networks and Games. En *Springer Theses*. *Evolutionary Games in Complex Topologies* (pp. 9-46). https://doi.org/10.1007/978-3-642-30117-9_2
Cordeau, J.-F., Laporte, G., Savelsbergh, M. W. P., & Vigo, D. (2007). Chapter 6 Vehicle Routing. En C. B. and G. Laporte (Ed.), *Handbooks in Operations Research and Management Science* (pp. 367-428). https://doi.org/10.1016/S0927-0507(06)14006-2
Estrada, E. (2015). Introduction to Complex Networks: Structure and Dynamics. En J. Banasiak & M. Mokhtar-Kharroubi (Eds.), *Evolutionary Equations with Applications in Natural Sciences* (pp. 93-131). https://doi.org/10.1007/978-3-319-11322-7_3
Fan, W., Xu, H., & Xu, X. (2009). Simulation on vehicle routing problems in logistics distribution. *COMPEL - The international journal for computation and mathematics in electrical and electronic engineering*, *28*(6), 1516-1531. https://doi.org/10.1108/03321640910992056
Gallotti, R., Porter, M. A., & Barthelemy, M. (2016). Lost in transportation: Information measures and cognitive limits in multilayer navigation. *Science Advances*, *2*(2), e1500445. https://doi.org/10.1126/sciadv.1500445
Holme, P., Kim, B. J., Yoon, C. N., & Han, S. K. (2002). Attack vulnerability of complex networks. *Physical Review. E, Statistical, Nonlinear, and Soft Matter Physics*, *65*(5 Pt 2), 056109. https://doi.org/10.1103/PhysRevE.65.056109
Huang, K., Wu, K.-F., & Ardiansyah, M. N. (2018). A stochastic dairy transportation problem considering collection and delivery phases. *Transportation Research Part E: Logistics and Transportation Review*. https://doi.org/10.1016/j.tre.2018.01.018
Juan, A. A., Faulin, J., Pérez-Bernabeu, E., & Domínguez, O. (2013). Simulation-Optimization Methods in Vehicle Routing Problems: A Literature Review and an Example. En *Lecture Notes in Business Information Processing*. *Modeling and Simulation in Engineering, Economics, and Management* (pp. 115-124). https://doi.org/10.1007/978-3-642-38279-6_13
Lei, W., Mingfang, G., & Lijun, W. (2012). The Directed Complex Network Application in the Supply Chain. *2012 Third International Conference on Digital Manufacturing Automation*, 911-914. https://doi.org/10.1109/ICDMA.2012.215
Mohammed, M. A., Ghani, M. K. A., Hamed, R. I., Mostafa, S. A., Ahmad, M. S., & Ibrahim, D. A. (2017). Solving Vehicle Routing Problem by Using Improved Genetic Algorithm for Optimal Solution. *Journal of Computational Science*. https://doi.org/10.1016/j.jocs.2017.04.003
Parragh, S. N., Doerner, K. F., & Hartl, R. F. (2008a). A survey on pickup and delivery problems. *Journal Für Betriebswirtschaft*, *58*(2), 81-117. https://doi.org/10.1007/s11301-008-0036-4
Parragh, S. N., Doerner, K. F., & Hartl, R. F. (2008b). A survey on pickup and delivery problems. *Journal Für Betriebswirtschaft*, *58*(1), 21-51. https://doi.org/10.1007/s11301-008-0033-7
Policroniades, G., & Flores de la Mota, I. (2016). State of the Art of the Different Models of Transportation Most Used in the Supply Chain of Automotive Industry. *International Journal of Combinatorial Optimization Problems and Informatics*, *7*(3), 44-53.
Policroniades, G., Flores de la Mota, I., Sihirai Reyna, O. S., & Lara de Paz, J. (2018). The Vehicle Routing Problem Complex Network Analysis. *Journal of Applied Mathematics and Computation*, *2*(12). https://doi.org/10.26855/jamc.2018.12.001

Prawda, J. (1991). *Metodos y modelos de investigacion de operaciones . Vol I-II* (Decima). Recuperado de https://www.iberlibro.com/Metodos-modelos-investigacion-operaciones-Vol-I-II/10051661077/bd

Von Bertalanffy, L. (1976). *TEORIA GENERAL DE LOS SISTEMAS*. Recuperado de http://www.gandhi.com.mx/teoria-general-de-los-sistemas

AUTHORS BIOGRAPHY

Gabriel Policroniades Chípuli Studied Industrial Engineering at Technological Institute and Superior Studies of Monterrey, Campus Toluca (ITESM, Campus Toluca), he studied an engineering mastery with operation research orientation and has advanced metrology studies for the calculation of uncertainty, and knowledge of Lean Six Sigma Black Belt and Logistics and supply chain Currently he is studying a Ph.D. in Operation Research at UNAM.

Idalia Flores de la Mota She received her Ph.D. in Operations Research at the Faculty of Engineering of the UNAM. She graduated Master with honors and received the Gabino Barreda Medal for the best average of her generation. She has been a referee and a member of various Academic Committees at CONACYT. She has been a referee for journals such as Journal of Applied Research and Technology, the Center of Applied Sciences and Technological Development, UNAM and the Transactions of the Society for Modeling and Simulation International. Her research interests are in simulation and optimization of production and service systems. She is a full-time professor at the Postgraduate Program at UNAM.

Javier Lara de Paz studied Physics at the Faculty of Science of National Autonomous University of Mexico (UNAM), a Specialization in Applied Statistics at the UNAM. He studied his Master's degree in Operation Research at the Faculty of Engineering of the UNAM. He has been professor of Science at the and Operation Research professor at the Engineering School at the UNAM. Currently he is studying a Ph.D. in Operational Research at UNAM.

Sashiko Shirai obtained her bachelor's in actuarial science in the Faculty of Science of the UNAM. She is studying her Master in Operations Research in the Faculty of Engineering of the UNAM with the CONACYT scholarship. She is an assistant professor at the Faculty of Engineering and the Faculty of Science. Her research interests lie in complex networks, statistics and operational research.

UTILIZATION OF COMPUTER SIMULATION FOR DETECTION NON-STANDARD SITUATIONS WITHIN SINGLE-TRACK LINES

Jan Fikejz[(a)], Jan Merta[(b)]

[(a,b)] Department of Software Technologies, FEI, University of Pardubice, Pardubice, Czech Republic

[(a)] Jan.Fikejz@upce.cz ,[(b)] Jan.Merta@student.upce.cz,

ABSTRACT
This article deals with the use of computer simulation for induction and detection of non-standard/crisis situations within single-track railways. First, attention is paid to the collection and evaluation of historical data, which are then used for the designed simulator. The article then focuses on the design of a simulation tool for inducing non-standard/crisis situations within a monitored segment of a railway network. Simulation tool is then used for selected experiments.

Keywords: Railway infrastructure models, train positioning, railway traffic simulation

1 INTRODUCTION

One of the areas of rail transport is the positioning of rolling stock. Localization of these transport elements can be looked at differently. Depending on the importance and utilization of the line, localization systems with different reliability and accuracy can be deployed. Regional lines are not such an object of interest compared to major or international corridors, but in each country, regional lines form a significant part of the railway network. These lines have their own specifics, such as the fact that they often consist of single-track lines, have lower utilization ratio, lower speed limits, but also lower demands on security and localisation systems. In 2011, the European Commission published a White Paper (Kom 2011), which sets out objectives and actions for the transport sector with an outlook to 2050. The White Paper sets out, among other things, a roadmap for a unified European transport area — the creation of a competitive, resource-efficient transport system. From the perspective of rail transport, it is mainly the strengthening of rail transport on main and regional lines and the introduction of intelligent systems using, for example, *ERTMS* or *GNSS*. From this perspective, regional lines should be given appropriate attention, too.

2 STATE OF ART

There are a number of different national solutions around the world that deal with the localisation of rolling stock on regional lines, most of which use *GNSS*, balises, or odometers. Wireless information transmission is then done mainly via mobile networks *GSM-R* (Global System for Mobile - Railway) or classic *GSM* technology. Let us mention at least some national systems focused on regional lines.

2.1 ERTMS *Regional* – Švédsko

This system was developed in cooperation with the International Union of Railways *(UIC*), Swedish Transport Administration (Trafikverket) and the company Bombardier (Low cost ERTMS 2014). *ERTMS Regional* is a simpler and cheaper variant of the *ERTMS/ETCS* L1 to L2 system as a suitable option for lines with lower traffic density. The designed system is operated on a single-track line with a total length of 143 km with five stations and a traffic density of sixteen trains per day, with planned further extension to lines in total length of 565 km. The basic principle lies in the periodic sending (every 6 seconds) of position information to the Train Control Centre (*TCC*), which issues a running permit. Information about the position of RS (rolling stock) is obtained from the odometer, while the accuracy of the position is done by means of *balises* installed in stations and on the track with fixed spacing of five kilometres. The *GSM-R* and *GSM* mobile networks are used for the transmission of information.

2.2 LOCOPROL – Francie

Another system used in France is the *LOCOPROL* technological solution (Libbrecht and Sturesson 2005), based on the name **Lo**w **Co**st Satellite based train location system for signalling and train **Pro**tection for **L**ow density traffic railway lines. The system was developed under the leadership of the company *ALSTOM* and other partners from Belgium, Germany and France as part of a research project focusing on the use of satellite navigation for low-density traffic railway lines. The *LOCOPROL* system is used on a single-track regional line of 35 km. The basic principle again uses radio block centre (*RBC*) to which information about the location of the RS on the line is sent and information about the running permit is also received from *RBC*. The information about the location of the RS is collected by satellite navigation (*GPS, Gleans*, *Galileo* in the future) and the odometer. Refining the position in critical places (usually in stations and station throats or in places of radio shadow) is realized using installed *balises*. The position locator is integrated directly into the on-board *ETCS* and the mobile network of the public operator is used to transmit information. The integrity of the train is under the control of the driver.

2.3 3InSat – Itálie

In Italy, a system called *3InSat* (Train Integrated Safety Satellite System) was developed under the auspices of *Ansaldo STS* in cooperation with other foreign partners. The project was completed in 2014 and the resulting system is used on a single-track regional line in Sardinia with a total length of 50 km. Again, it uses *RCB* to collect location data and issues running permits. Location information of the RS is obtained from satellite navigation (*GPS EGNOS*, *Galileo*) and the odometer. The mobile network *GSM*, *TETRA* (**T**rans-**E**uropean **T**runked **R**adio) and satellite communication to transmit the information. The architecture of the solution is based on *ETCS* L2 (Mouna 2013).

2.4 SATLOC – Rumunsko

The *SATLOC* system was established under the auspices of *UIC* in cooperation with eleven organizations from six countries around the world with the support of the European Space Agency (*ESA*). The project focuses and the development and innovative use of *GNSS* to support rail traffic management within regional lines. Furthermore, the objectives of the project are focused on the design of new operational standards, software and hardware solutions and services.

Currently, the *SATLOC* system is operated in test mode on a single-track line of 27 km. The designed and tested system meets *ETCS* L2 standards (Redding 2014).

2.4.1 Status in the Czech Republic

The infrastructure of the Czech railway network currently has over nine and a half thousand kilometres of lines, which are divided into four categories (see Figure 1):

- Corridor lines registered in the European railway system with a total length of 1402 km — pink colour,
- National lines registered on the European railway system with a total length of 1189 km — green colour;
- National lines not registered on the European railway system with a total length of 3748 km — red colour;
- Regional lines not registered on the European railway system with a total length of 3232 km —blue colour.

Single-track lines account for approximately 7607 km, which corresponds to approximately **80%** of the total length of all lines. The regional lines as such account for over 33% of the lines (Kolář 2014, Dorazil 2008).

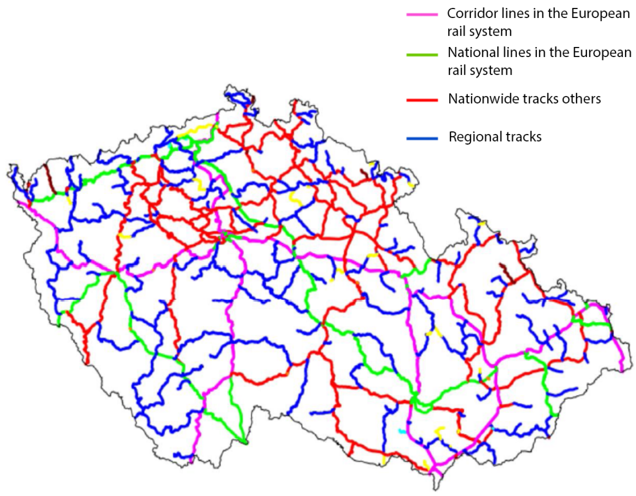

Figure 1: Structure of lines in ČR.

Single-track and, above all, regional lines are perceived as less important for reasons of lower utilization, and this corresponds to a lower level of safety. On these lines it is often possible to register only that the train left the station or arrived at the station. Yet hundreds of emergency events have occurred over the last decade.

3 LOCALIZATION

Generally, localisation is prone to a wide range of approaches on how to identify the position of trains on a track. Put simply, localisation may be divided into the following three groups:

- localization without the use of GNSS,
- GNSS using localization,
- GNSS-based, involving further support systems.

Our approach of trains localisation access to tracks is based on the correct pairing up of GPS information on position, provided by communication terminals, with the nearest vertex or edge of the graph (Fikejz and Kavička, 2011; Fikejz and Řezanina 2014.). The discovered vertex/hectometre post disposes not only of a multi-dimensional key in the form of a GPS coordinate, it is also linked, through definition sections, to further information concerning the railway network infrastructure.

View of the situation that the model of railway infrastructure is stored in the database Oracle we can use the native database functions and operators (Kothuri et al. 2007). The `SDO_NN` (*nearest neighbor*) operator was selected in view of realising this unique trains localisation approach. The aforementioned operator searches for a geometric object that is closest to the object entered (like a point, for example). In other words, it is possible to find the nearest vertex, or more precisely edge in a model, from the current position trains, Figure 2.

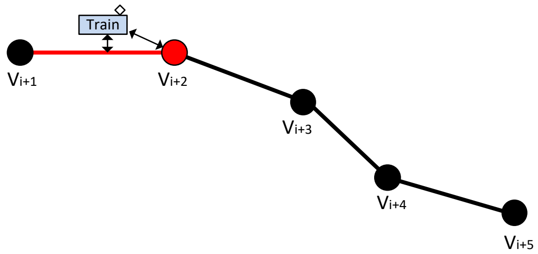

Figure 2: Main concept of localization

The actual detection of the current position of the trains can be divided into the following steps:

1. **Finding the nearest vertex and edge of the graph** – from the current position of the trains given the three-layer railway network model
2. **Assessment of the relevancy of incoming GPS information from the communication terminal** – verification whether the current position is not burdened by a disproportionate error (like, for example, that the distance of the trains from the nearest vertex/edge is a mere few meters or tens of metres, or that the trains is still assigned to the same super-edge, provided that it should still be located on it)
3. **Calculation of the exact position of the trains on the edge of the model** – using perpendicular projection of the point (current trains position) onto the line

The trains position data are collected from the communication terminals. These communication terminals sent position information to the central from 10 to 60 second (depends on configuration), Figure 3

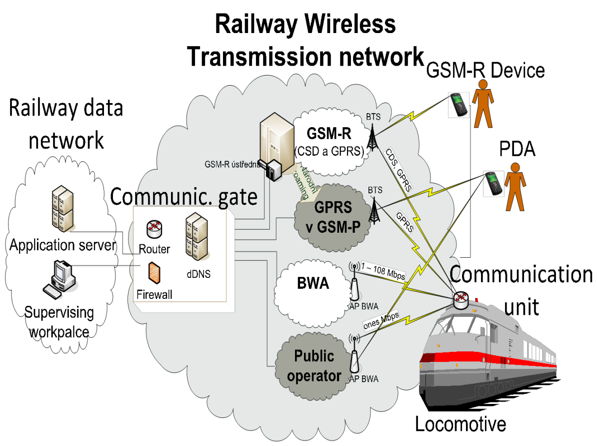

Figure 3 : Communication between the rail vehicle and dispatching centre

4 RAILWAY NETWORK MODEL

Undirected graph, as defined graph theory, is a natural candidate for a railway network model. Based on an analysis of data provided by the company SŽDC-TUDC (consisting of service regulations, passports, and codebooks), sets of algorithms were subsequently created, with which it was possible to generate a three-layer model of the rail network (Fikejz and Kavička, 2011). Roughly speaking, the track can be divided into individual so called supertracks, which consist of definition supra-sections (TDNU), where each supra-section contains track definition sections (TUDU) with mileposts (in hectometres). Basic aspects of the description of the rail network are collectively shown in Figure 4.

Mileposts (in hectometres) are shown in Figure with the distance in kilometres and are graphically represented using gray points. TUDU is recorded using a six-digit code (163105, 163106, 16307, 173202) and are graphically represented using solid lines (red, black, orange, brown). Individual supra-sections (CLS 007, CLS008, REG023) are shown in light blue and supertracks (B421021 1 and B421021 1A) are shown in dashed lines. A place significant in terms of transportation (branch line) is symbolized by a green square.

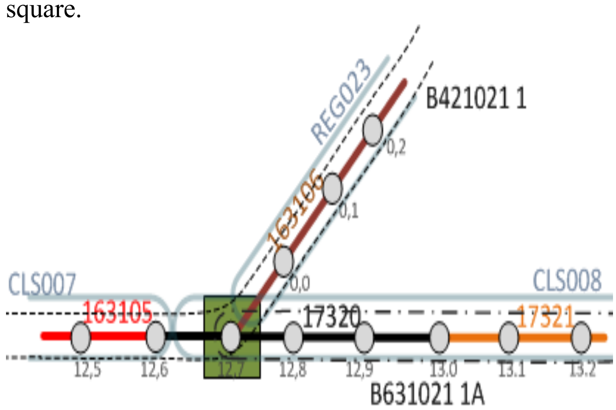

Figure 4: Basic aspects of the description of the rail network

The algorithm of railway network model (Fikejz and Kavička, 2011; Fikejz and Řezanina 2014.) was implemented directly on the database level using PL/SQL language. However, the algorithm had to be adjusted and generalized several times since there are various nonstandard conditions in the data, such as jumps in the mileposts (nonlinear growth of the kilometre succession between the mileposts) or change of an increasing kilometre sequence into a decreasing one and vice versa. The final model includes three data layers:

- **Data-Micro**, consisting of vertices and edges,
- **Data-Mezo**, include mezo-vertices and mezo-edges
- **Data-Macro**, containing super-vertices and super-edges.

Figure 5 presents the overall concept of a complete three-layer railway network model.

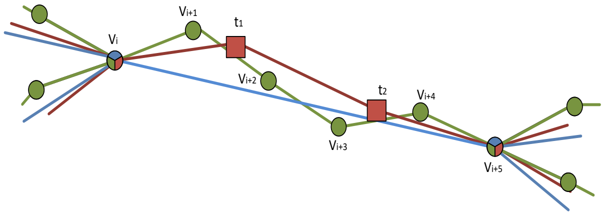

Figure 5: Illustration overall concept of a three-layer module

The data structure non-oriented graph was finally implemented directly in the ORCLE database using the ORACLE Spatial Network Data Model (Kothuri et al. 2007) technology. This technology enables the user to build a various network representation, involving also the object scheme and the communication interface API.

The objects scheme includes metadata and network tables. The interface contains on the server-side PL/SQL API (an SDO_NET packet) for the creation, control and analysis of the database network, and a middle layer Java API (on client´s side) for the network analysis. The actual network is then defined by means of two compulsory tables:

- Node table,
- Link table.

For the work with spatial data, ORACLE with Spatial technology defines a special object data type SDO_GEOMETRY, which enables its user to store a number of spatial information and geometric types, such as various points, arcs, linear chains or polygons.

5 EVALUATION OF HISTORICAL POSITIONS OF TRAINS

In order to create realistic conditions of future experiments, data of real trains were evaluated with a period of:

- 5 seconds,
- 10 seconds,
- 30 seconds,
- 60 seconds.

Individual records of train positions were subsequently processed by statistics. The current position of the train has always been evaluated from the point of view of the perpendicular projection of the nearest track of the observed route, see Figure 6.

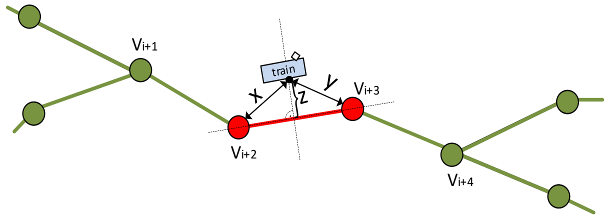

Figure 6: Illustration of the distances of the current RS position from the nearest vertices and edge of the infrastructure.

The database operator SDO_NN (nearest neighbours for a geometry) was used to find the nearest track and its distance. Overall, the following basic statistical indicators were evaluated:

- Average distance
- Minimum/Maximum Distance
- Median
- Standard deviation

Table 1: Resulting distance values from peaks and edges

	Distance from vertex [m]	Distance from edge [m]
Average	26.54	7.03
Min	0.41	0.1
Max	80.26	69.17
Median	26.53	3.69
Standard deviation	14.67	11.45

However, the table above does not consider situations in which the rolling stock is located/ is not located on the open line or in the railway station. The designed model does not fully reflect the reality of the track infrastructure in railway stations that can have a high number of shut-down tracks. These tracks are not considered by the model and are replaced by one or more continuous tracks. Therefore, it is clear that at stations the calculated distances of the current position of the rolling stock to the vertices and edges will be considerably higher.
Further experiments focus on two other subvariants, in which the rolling stock was located on the wide line or in the perimeter of the railway station. The resulting assessment is shown in Tables 2 and 3

Table 2: Result values of distances from vertices in railway station and on the wide line

	Distance from vertex in station [m]	Distance from vertex on the wide line [m]
Average	28.68	24.63
Min	1.68	0.44
Max	80.26	50.68
Median	28.09	26.53
Standard deviation	15.40	14.67

Table 3: Resulting values of distances from the edges in the railway station and on the wide line.

	Distance from edge in station [m]	Distance from edge on wide line [m]
Average	11.33	3.25
Min	0.01	0.1
Max	69.15	24.63
Median	6.11	2.50
Standard deviation	15.37	2.93

The tables show how the distance values of the current position of the rolling stock on the wide line differ from the distance in stations. If we focus on Table 8, which is of the highest importance for us from the point of view of monitoring train on regional lines, then we can note significant differences between the values of distances in station and outside it. When observing the median, whose value divides the observed set in half, the distance difference is more than double.
From the point of view of evaluating the accuracy of the calculation of the position of the rolling stock relative to the model of the railway network, for the overall monitored set of input data (railway station + wide line) the distance from model edges is up to 10 meters in 88% of cases. If we then focus only on wide single-track lines, then the distance of the rolling stock position from the edge of the model up to 10 meters occurs in **98,5%** of cases.

6 DETECTION OF NON-STANDARD STATES

A situation where two rolling stock (trains) occur below a defined boundary distance can be considered as a non-standard or a crisis within single-track lines. From the point of view of the movement of the rolling stock, we can follow:

- the opposite running of trains;
- parallel running of trains
    - a faster vehicle approaching a slower moving vehicle

In the simplest case, it would be possible to test great circle distance, however, this solution has limitations, for example, when crossing lines or in non-linear course of the line, see Figure 7.

Figure 7: Real vs. great circle distance

The above example illustrates the problem of accessing great circle distance in relation to the track profile. The real distance (grey curve) is 2.251 m, whereas the great circle distance of the track objects (red dashed line) corresponds to 1.514 m which is almost 1.5 times the real length.
For a more realistic calculation of distances of two rolling stock, the described multi-layered model of the railway network reflecting an non-oriented graph is used, in combination of data layers Data-Micro and Data-Mezo. The data layer is used to detect non-standard situations, i.e. when two rolling stock occurs on:

- an identical edge,
- adjacent edges.

Both approaches can be seen in Figure. 8 and 9.

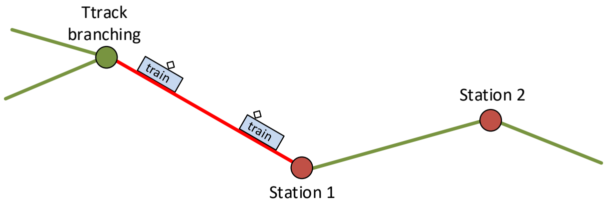

Figure 8: Illustration of detection of two rolling stock on identical edge

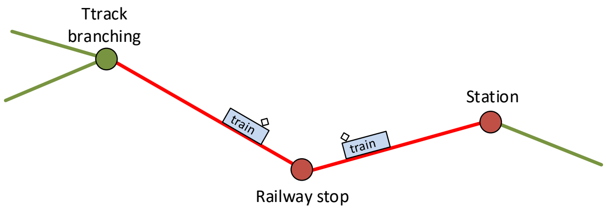

Figure 9: Illustration of detection of two rolling stock on two edges.

The Data-Micro data layer is then used to calculate the distance of two observed rolling stock. The data layer has the smallest degree of abstraction, with each edge being 100 m long.

7 EXPERIMENTS

A computer simulation, which induces the operation of the rolling stock, was used for the detection of non-standard situations. The simulator used data based on real conditions which were based on historical data processing of trains.
Individual experiments of non-standard situations can be divided into three groups:

- The opposite running of trains;
- Simultaneous train running,
- One train is on halt, the other is moving.

and further it is possible to distinguish between situations where two trains occur on:

- Single/identical edge
- Two adjacent edges.

In the following experiment, attention was focused on the opposite direction running of two trains, and it was observed how far apart they are at the time of detection of each train set when the train location is transmitted every:

- 5 seconds,
- 10 seconds,
- 30 seconds,
- 60 seconds.

7.1 Results of experiments

If we focus on detecting the opposite direction running on an identical rail/edge (as shown in Figure 8), then their distances at the time of detection can be statistically expressed according to Table 4.

Table 4: Resulting distances [m] at the time of detection of two trains on an identical edge.

	Period 5 [s]	Period 10 [s]	Period 30 [s]	Period 60 [s]
Min	1000	1000	600	0
Max	2500	2500	2400	2400
Average	2016	1968	1628	1140
Median	2100	2100	1800	900
Standard deviation	396,67	413,49	519,63	726,64

The table above shows that both average and median decrease with increasing time frequency, while the standard deviation increases. The frequency of 60 seconds is unequivocally unsatisfactory, when in two cases a collision has already occurred. The 30-second period also appears unsatisfactory for single-track regional lines where the train speed is lower than on the main routes.
In the latter case, the detections of opposite direction running on two adjacent rails/edges were evaluated according to the approach shown in Figure 9. The results can be seen in Table 5.

Table 5 : Resulting distances [m] at the time of detection of two trains on two adjacent edges.

	Period 5 [s]	Period 10 [s]	Period 30 [s]	Period 60 [s]
Min	2500	2500	2000	1400
Max	3900	3900	3600	3600
Average	3084	3064	2776	2624
Median	3000	3000	2700	2700
Standard deviation	402,67	418,45	443,87	612,32

Table 5 shows that compared to the results of the first experiment (Table 4), where the values of median and standard deviations were approximately double, significantly lower distance differences, namely in all monitored parameters, can be seen in this case.

CONCLUSION

This article was primarily focused the use of computer simulation for induction and detection of non-standard/crisis situations within regional and single-track lines. First, attention is paid to data collection of real passes within the selected segment of the railway network. Subsequently, this data was processed statistically. The evaluated results of the distances of the current position of the rolling stock from the edge and vertices showed the same parameters/deviations as historical data from another segment of the railway network.
The results of the analysed data were then used for parametrization of the designed simulator, allowing for the simulation of rolling stock operation. The simulator was used in the next phase for experiments involving induction of non-standard/crisis situations within the selected segment of the railway infrastructure model. The experiments included different running scenarios, and at this stage of the research, the distance within which the rolling stock is located was initially observed when the crisis/non-standard situation was detected.

ACKNOWLEDGMENTS

The work was supported from ERDF/ESF " Cooperation in Applied Research between the University of Pardubice and companies, in the Field of Positioning, Detection and

Simulation Technology for Transport Systems (PosiTrans)" (No. CZ.02.1.01/0.0/0.0/17_049/0008394)

REFERENCES

Dorazil, P. Základní vlastnosti kolejových obvodů bez izolovaných styků. Pardubice, 2008. Bachelor thesis. University of Pardubice. Supervisor: Milan Kunhart.

Fikejz, J. and A. Kavička. Utilisation of computer simulation for testing additional support for dispatching rail traffic. In: European Simulation and Modelling Conference, 2011. Ostende: EUROSIS - ETI, 2011. p. 225-231. ISBN 978-90-77381-66-3.

Fikejz, J. and E. Řezanina, Utilization of computer simulation for detection non-standard situations within the new data layer of railway network model. In: The 26th European Modeling & Simulation Symposium. Bordeaux, 2014s. 371-377, ISBN 978-88-97999-32-4

Kolář, P. *Řízení provozu na vedlejších železničních tratích.* Seminář ZČU Plzeň-Fakulta elektrotechnická [online]. 2014 [cit. 2014-12-12]. http://old.fel.zcu.cz/Data/documents/sem_de_2014/5-RB_Kolar.pdf

KOM 2011) 144 - WHITE PAPER - A Roadmap to a Single European Transport Area - Creating a competitive and resource efficient transport system.

Kothuri, R. et al. Pro Oracle Spatial for Oracle database 11g. New York, NY: Distributed to the book trade worldwideby Springer-Verlag New York, c2007, xxxiv, 787 p. ISBN 15-905-9899-7.

Libbrecht, R. and H. Sturesson. *LOCOPROL: Final Report* [online]. 2005 [cit. 2015-06-10].: http://www.transport- research.info/Upload/Documents/200607/20060727_153639_69273_LOCOPROL_Final_Report.pdf

Low cost ERTMS implementation: ERTMS Regional. *Railwaysignalling* [online]. 2014 [cit. 2016-01-02]. http://www.railwaysignalling.eu/ertms-regional

Mouna L. Integrated Applications Promotion Programme: Train Integrated Safety Satellite System *(3InSat) Demonstration project*, Rome 2013,[online]. [cit. 2015-06-10]. https://artes-apps.esa.int/sites/default/files/1-IAP%20ASTS%203InSat_18-04-2013.pdf

Redding, L. Satloc: a high-tech saviour for low-density lines. *Railjournal* [online]. UK, 2014 [cit. 2016-01-02]. http://www.railjournal.com/index.php/telecoms/satloc-a-high-tech-saviour-for-low-density-lines.html?channel=533

UTILIZATION OF COMPUTER SIMULATION FOR SOLUTION OF FLOOD-CONTROL RESEVOIR PROTECTION FUNCTION

Jan Fikejz[a], Ladislav Roušar[b], Tomáš Zachoval[c]

[a,c] Department of Software Technologies, FEI, University of Pardubice, Pardubice, Czech Republic
[b] VHRoušar, s.r.o., Pardubice, Czech Republic

[a] Jan.Fikejz@upce.cz , [c] rousar@vhrousar.cz, [c] Tomas.Zachoval@student.upce.cz,

ABSTRACT
This article deals with the use of a computer simulation to solve the protective function of a flood-control reservoir as a support tool for flood wave transformation. Attention is primarily focused on the design and implementation of a simulation tool enabling to implement selected mathematical approach for numerical solution of the balance equation of inflow, outflow and retention of water in the reservoir. The designed software tool is then used for the selected experiment of transformation of theoretical flood wave by flood-control reservoir.

Keywords: computer simulation, flood-control reservoir, flood wave transformation

1. INTRODUCTION
Flood-control reservoir or polders are hydraulic structures designed to protect human health, property and the environment from the effects of floods. Due to global climate change, there have been changes in the approach in the field of protection against extreme and torrential floods in recent decades. These are reservoirs with design parameters corresponding to small water reservoirs, i.e. with volume up to 2 million m^3 and the largest reservoir depth of 9 m (Doležal et al., 2011). The purpose of the reservoir is to reduce the peak flow rate of the flood and distribute the volume of the flood wave to a longer time interval by temporary water retention. After the flood subsides, the reservoir is emptied. Outside the flood, the reservoir can be dry, without water, or partially filled, the it is so-called semi-dry reservoir, which then has a landscape design and ecological function outside flood events (Ministry of Agriculture, 2005).
To ensure the maximum transformation effect of the reservoirs it is necessary to ensure that the protective space is filled only during the period of the culminating flood wave. Its premature filling in the period of onset of the flood can significantly reduce the retention effect. Therefore, in order to function properly and ensure the greatest transformation effect, it is necessary to design the optimal capacity of the bottom outlets and the emergency spillway parameters in relation to the expected inflow in flood and to the level of flood protection downstream the reservoir.

2. STATE OF ART
The transformation of the flood wave can be solved by complex rainfall-runoff model (HYDROG, AquaLog), hydrodynamic numerical model for surface water flow (HEC-RAS, MIKE), graphical Klemeš's method, or mathematical interpretation of the differential equation of the law of mass preservation (balance equation).
The rainfall-runoff models include partial models for the solution of flood wave transformation (Marton, Starý, 2018), but from the point of view of their complexity of solved hydrological phenomena, difficulty in inputting data, and restricted access to the program are not used. Hydrodynamic models of surface water flow solve the transformation of the flood wave by reservoirs by calculating the unsteady flow. To assemble the numerical model, you need to specify the morphology of the reservoir bottom and the parameters of functional objects. To build the model, however, it is assumed that the user is well versed in the field of hydrodynamic modelling of surface water and has basic knowledge in the field of numerics. Graphic Klemeš's method is the simplest of methods (Starý, 2006), but its construction is time-consuming and is not suitable for optimization tasks. The mathematical interpretation of the differential balance equation can be done by tabular calculation e.g. in a spreadsheet, but the accuracy of the calculation is mainly limited by the length of the time step (Doležal et al., 2011). Therefore, the authors of the article develop their own simulation program interpreting the differential balance equation (Roušar, 2015) without the limitation of the time step, with a friendly user interface (Zachoval, 2019) enabling a clear input of data and a choice of contemporary hydraulic relations for optimization of functional objects and solutions of protective function of flood-control reservoir (Yaraghi et al. 2019).

3. FLOOD WAVE TRANSFORMATION
To solve the transformation of a flood wave, a mathematical apparatus based on the balance equation of inflow, outflow and retention of water in the reservoir is

used. This equation is mathematically expressed as ordinary differential equation (relationship 1),

$$\frac{dV}{dt} = Q - O \tag{1}$$

where the left element of the equation denotes the change in volume V for time t, Q is the inflow, and O is the outflow. The inflow represents the hydrograph of the flood wave, where $Q = f(t)$. The outflow depends on the current water level, the parameters of functional objects and, if necessary, the manipulation rules of the reservoir.

Equation (1) is further approximated by Euler's explicit scheme (*Moin, 2010*) according to relation (2).

$$V_{i+1} - V_i = (Q_i - O_i)\Delta t \tag{2}$$

with an approximation error in the time step Δt. To solve equation (2), an initial condition representing the filling of the reservoir is necessary

$$V(i = 0) = V_0 \tag{3}$$

3.1. Bathygraphy

In order to solve equations (2) and (3) it is necessary to specify the characteristics of the reservoir in the form of bathygraphy. This is a description of the flooded area of the reservoir expressed by the dependence of the position of the water level and its corresponding flooded area or the corresponding total volume of water in the reservoir. Bathygraphy expressed in volume and area of water is shown in Figure 1.

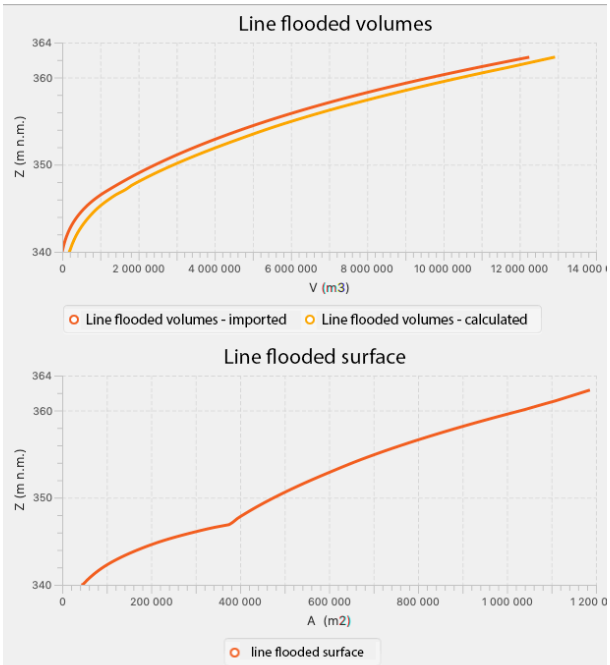

Figure1: Bathygraphy of the reservoir

3.2. Hydrograph

The flood wave hydrograph represents the volume of water poured into the reservoir for the duration of the wave. The flood wave is evaluated for individual N-years, which differ from each other not only by the volume and duration of the wave, but also by the maximum peak flow and shape of the hydrograph. The hydrograph is entered in the program as a flow dependency for the corresponding time step of the flood wave, see Figure 2.

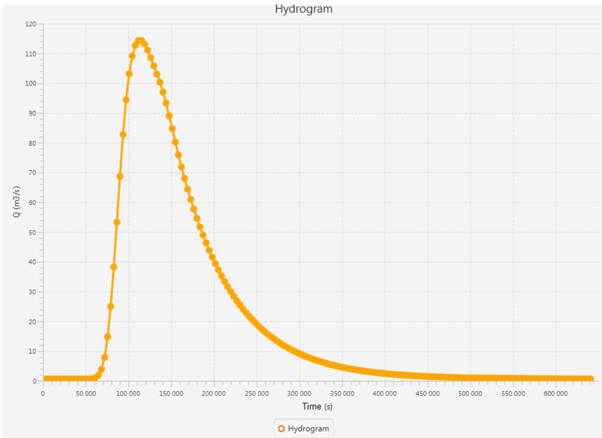

Figure 2: Hydrograph of a flood wave

The outflow of water from the reservoir is determined as the sum of the sub-outflows of the bottom outlets and emergency spillways. In the program it is possible to specify different parameters for up to three objects from each. It is assumed that the bottom outlet is still open. The outflow through the emergency spillway shall only take place until the position of the water level in the reservoir exceeds overflow edge level of the emergency spillway.

The bottom outlet discharge O_s is

$$O_s = \mu A\sqrt{2gH} \tag{4}$$

where μ is the bottom outlet discharge coefficient, A is the cross-sectional area at the end of the outlet, g is the gravity acceleration, and H is the difference between the upstream water level and the outlet axis.

The emergency spillway discharge O_p is

$$O_p = mb_0\sqrt{2g}h^{\frac{3}{2}} \tag{5}$$

where m is the discharge coefficient, b_0 is the effective spillway width and h is the head on the spillway crest.

4. DESIGN OF A SIMULATION TOOL

A simulation software tool was designed for the purposes of the flood-control reservoir simulation, which enables a wide range of parameterization of functional objects (outlets and spillways). Some parameters of functional objects can be entered as input constants, or they can be calculated using appropriate mathematical relationships based on the physical parameters of the given object. The

designed simulation software tool contains a core of discrete simulation, which, according to the simulation time step, performs individual iterations of the calculation.
The simulation tool allows to simulate the behaviour of the flood-control reservoir based on input parameters according to selected simulation scenarios. These include three areas of inputs:

- Flood wave — entered using a hydrograph
- Shape of the valley of the situated dam — according to the bathygraphy curves
- Functional object group:
    - Outlets
    - Spillways

4.1. Outputs

Each simulation scenario compiles the results in text and graphical form. Simulation output data are the values of the quantities observed at the reservoir at a specific time, observing the following values:

- Δt — time step (s)
- Q — inflow (m^3/s)
- H — water level (above sea level)
- V — volume (m^3)
- O — outflow of individual functional objects (m^3/s)
- dV/dt — volume change over time
- dV — volume change

5. THE CONCEPT OF THE CALCULATION ALGORITHM

The simulation core uses a designed calculation algorithm that can be divided into several steps:

1. The calculation time step (Δt) is determined based on the parameter specified by the user before starting the calculation. In practice, this step corresponds to a range of 1-100 seconds.
2. The inflow (Q) is taken from the hydrograph based on time. If the required time is not present in the hydrograph, then the inflow Q is interpolated by linear interpolation from the closest two values.
3. The volume (V) for the initialization time t_0 based on the height of the water level in the reservoir is determined from the bathygraphy curves. In other simulation times, the volume is calculated from the flow and outflow difference.
4. The water level (H) at the time t_0 is determined from the parameter specified by the user before starting the calculation. In other simulation times it is determined from the bathygraphy curves, based on the current volume. If the given volume value is not found in the bathygraphy curves, then the water level is linear interpolated from the closest two values.
5. The outflow of outlet/outlets (O_s) is calculated based on the parameters of the particular outlet and the height of the water level in the reservoir, always for the current time point of the simulation calculation.
6. Outflow of spillway/spillways (O_P) is calculated based on the parameters of the specific spillway, always for the current time point of the simulation calculation.
7. Then the calculation of volume difference (dV) according to relation (7) is performed as a ratio of the sum of outflows from functional objects ($\sum O$ relation 6) and inflow (Q). This difference is then multiplied by the time step value (t). Negative difference indicates that the inflow is larger than the outflow, and vice versa.

$$\sum O = \sum O_S + \sum O_P \tag{6}$$

$$dV = \left(\sum O - Q\right)\Delta t \tag{7}$$

8. The water volume in the flood-control reservoir for the next simulation step ($V(i+1)$) is given by the sum of the current volume value ($V(i)$) and the volume difference in the observed time step (dV), relationship 8.

$$V(i+1) = V(i) + dV \tag{8}$$

9. If the simulation calculation was implemented for all time moments, then it can be declared completed. However, if during the simulation there is a situation where the value of volume of water in the flood-control reservoir is greater than its maximum volume indicated in the bathygraphy curves then the flood-control reservoir overflows and the simulation is terminated.

5.1. Verification and validation

For the verification and validation of design approach for simulation of balance equation of inflow, outflow and retention of water in the reservoir was used verification calculations on historical data of selected dams. The sub-parts of implemented equations were vitrificated and consulted by expert on hydrogeology. As technical software tools were utilized MS Excel and Matlab.

6. EXPERIMENTS

As part of the experiments, an already existing flood-control reservoir was tested from the perspective of potential reconstruction and reconfiguration of the

current spillway, which in conditions of changing climate and nature of precipitation may appear as no longer satisfactory in the future.
The simulation was considered for the flood wave, which is described by the hydrograph, see Figure 3

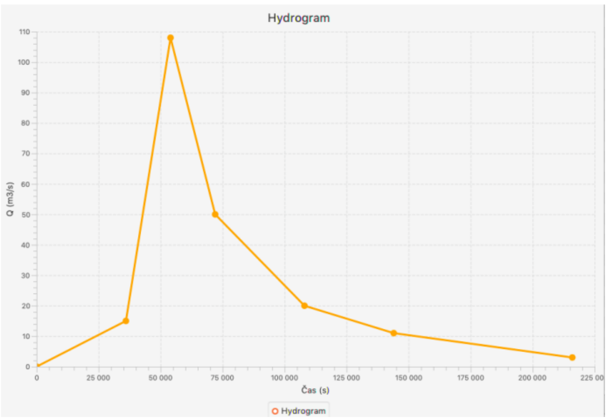

Figure 3: Input hydrograph

The shape and capacity of the flood-control reservoir is described in the bathygraphy curve shown in Figure 4.

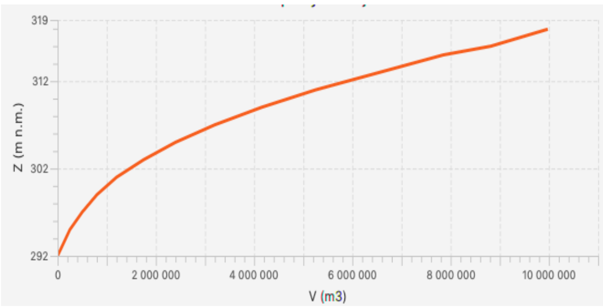

Figure 4: Bathygraphy curve of the flood-control reservoir

The longitudinal profile of the observed flood-control reservoir is shown in Figure 5 (Kratochvíl and Stara 1987)

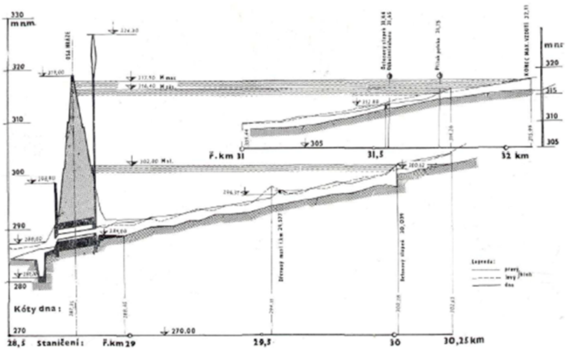
Figure 5: Longitudinal profile of the dam

and it has the following parameters:

- Crest of the dam: 319 m above sea level
- Maximum level (*Hmax*): 317.9 m above sea level
- Maximum storage space: 316.4 m above sea level
- Level before the arrival of the flood wave: 315.5 m above sea level

The flood-control reservoir will have two functional objects, namely:

- Outlet:
  - Outlet diameter: 0.8 m
  - Outlet bottom dimension: 288.1 m above sea level
  - Outflow factor μ: 0.416
- Spillway
  - Spillway dimension: 316.4 m above sea level
  - Spillway width: subject to simulation
  - Spillway factor m: 0.51

The aim of this selected simulation was to examine various variations in the of spillway width so as to avoid uncontrolled overflow of the flood-control reservoir, as well as to ensure that the total water outflow through functional objects was less than 40 m^3/s. With a total outflow larger than 40 m^3/s, the residential area under the flood-control reservoir would already be flooded. The range of the checked spillway width was established to be from 4 to 35 metres. In Figure 7, we can see the partial results of the simulation experiment for a spillway width of 10 meters.
The final results of the experiment are then shown in Figure 6. From these values it is clear that for the tested flood wave it is possible to consider the spillway width of 6-17 meters. For the spillway width of less than 6 meters, there is already an uncontrolled overflow of the flood-control reservoir. For a spillway width of more than 17 metres, the flow is already above 40 m^3/s, which would already result in flooding of residential and industrial premises under the flood-control reservoir.

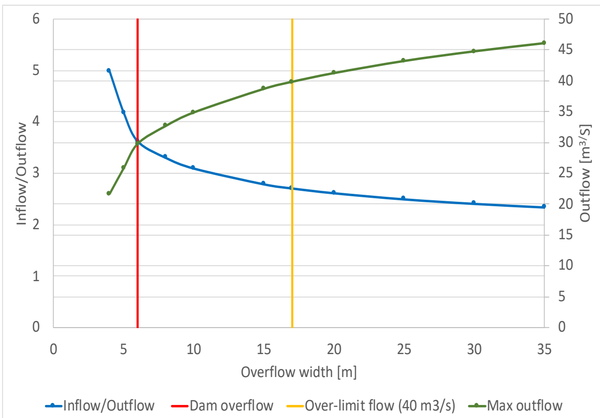

Figure 6: Experiment Results

CONCLUSION

As the climate changes, the nature of rainfall that affects our landscape changes as well. A part of the solution of flood control measures is the construction and utilisation of flood-control reservoirs. These allow to transform flood waves to protect human health, property and the environment. It is therefore important to have software tools available for the design and reconstruction of flood-control reservoirs to help us examine various flood situations and propose functional changes. The primary goal was to design and implement a simulation tool enabling to implement selected mathematical approach for numerical solution of balance equation of inflow, outflow and flood-control of water in the reservoir.

The designed software tool was then used for experiments in the transformation of a flood wave by a flood-control reservoir. As part of the experiment, an already existing flood-control reservoir was tested from the perspective of potential reconstruction and reconfiguration of the current spillway, which in conditions of changing climate and nature of precipitation may appear as unsatisfactory in the future. The results of the experiment were then transferred into a graphic form. From these values it is clear that for the tested flood wave it is possible to consider the spillway width of 6-17 meters. For the spillway width of less than 6 meters, there is already an uncontrolled overflow of the flood-control reservoir. For a spillway width of more than 17 metres, the flow is already above the boundary 40 m^3/s, which would already result in flooding of residential and industrial premises under the flood-control reservoir.

ACKNOWLEDGMENTS

The work was supported by the funds of the University of Pardubice, Czech Republic – *Student grant competition* (SGS_2019_021)

REFERENCES

ČSN 75 2935 Posuzování bezpečnosti vodních děl při povodních. Leden 2014. 16 str.

Doležal, P., Golík, P, Říha, J., Torner, V., Žatecký, S. *Malé vodní a suché nádrže*. Technická pomůcka k činnosti autorizovaných osob, TP 1.19. Praha, 2011. Str. 108. ISBN 978-80-86364-16-2.

Kratochvíl, J., Stara, V. Projektování přehrad, Komplexní projket HT. ES VUT scripts, 1987 101paages.

Marton, D., Starý M. *Posouzení funkčních objemů vodního díla Vír I na aktualizovaná vstupní data*. VTEI, 2018, 2. ISSN 1805-6555.

Ministerstvo zemědělství. *Suché a polosuché poldry*. Katalog opatření 35. Prosinec 2005. 5 str.

Moin, P. *Fundamentals of engineering numerical analysis*. Second edition. Cambridge university press, 2010. ISBN 978-0-521-26967-4.

Roušar, L. *Studie odtokových poměrů – Horní Bradlo. Hydrotechnické výpočty*. Červen, 2015. 18 str.

Starý, M. *Nádrže a vodohospodářské soustavy*. Modul 01. VUT Brno, 2006. 120 str.

TNV 75 2415 *Suché nádrže*. Leden 2013. 19 str.

Yaraghi, N, Ronkanen, A., Darabi, H., Kløve B., and Torabi Haghighi, A. Impact of managed aquifer recharge structure on river flow regimes in arid and semi-arid climates. Science of The Total Environment [online]. 2019, 675, 429-438 ISSN 00489697.

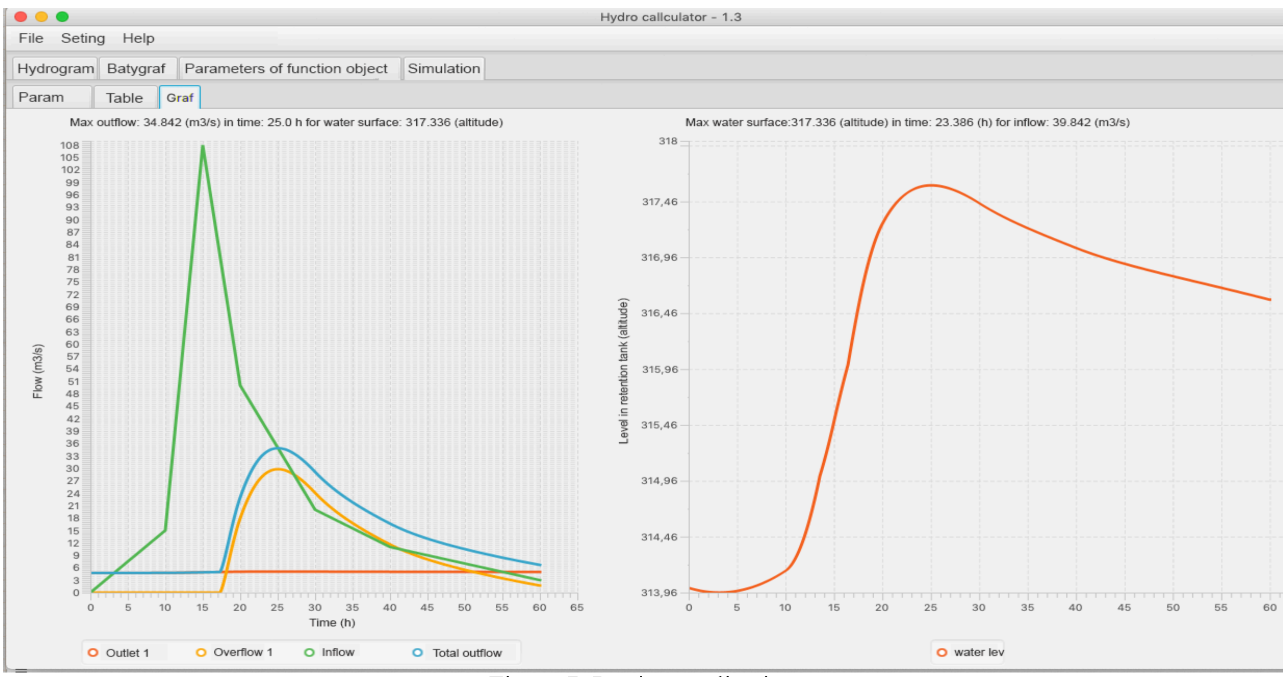

Figure 7: Runing application

ESTIMATES OF UNKNOWN TRANSFORMATION PARAMETERS IN TERRESTRIAL MEASUREMENTS: ONE SIMULATED PROBLEM

Nedvědová Marie[(a)], Marek Jaroslav[(b)], Chmelař Pavel[(c)]

[(a),(b),(c)] University of Pardubice, Faculty of Electrical Engineering and Informatics, Studentská 95, 532 10 Pardubice, Czech republic

[(a)] marie.nedvedova@student.upce.cz, [(b)] jaroslav.marek@upce.cz, [(c)] st19544@student.upce.cz

ABSTRACT
In connection with the expansion of 3D scanners, 3D object modeling has become highly studied in recent years. Many methods are currently available to solve the registration problem, whereby unknown transformation parameters need to be estimated when targeting a 3D object in multiple scans from different locations. Two different problems are encountered in the practice of targeting 3D objects in geodesy or construction. In the first variant, the measurement of the coordinates of the points of the 3D object is realized in several scans on tens of points marked with targets on a reflective surface. In the second variant, measurements of the coordinates of "clouds of hundreds or thousands of points" are available in several scans from different coordinate systems. In clouds it is necessary to find matching pairs of points, called identical points, based on their color match. In both versions, the coordinates of identical points from different coordinate systems must be recalculated to the selected coordinate system during data fusion. The problem leads to finding unknown shift and rotation transformation parameters. The aim of this article is to simulate the measurement of identical points in multiple scans. We will create a test task that can be used to test the methods proposed to solve the registration problem.

Keywords: registration problem, 3D range scanning, transformation of coordinates, point clouds

1. INTRODUCTION

The 3D range scans fusion is called registration. If the localization in a space or user's measurements are precise, the registration could be done directly by individual measurement connection into one group. However, due to inaccuracy of measurement sensors and the erroneous self-localization, the registration has to be considered.

In recent years, many methods have been developed to solve the registration problem that occurs in 3D scanning of objects. 3D cameras are sources of a large set of measurement points. When needed to recognize a 3D model of an object from the point clouds, an efficient method for identifying identical points is required. Obtained identical points are measured in different coordinate systems and it is necessary to find unbiased estimates of these transformation parameters.

The most commonly used algorithms are: ICP Algorithm (He, Liang, Yang, Li, and He 2017), Normal distribution transform (Magnusson 2013), Feature based registration (Nüchter 2009), Iterative dual correspondences (Lu and Milios 1997), Probabilistic iterative correspondence method (Montesano, Minguez, and Montano 2005), Quadratic patches (Mitra, Gelfand, Pottmann, and Guibas 2004), Likelihood-field matching (Burguera, Gonzalez, and Oliver 2008), Conditional random fields (Bataineh, Bahillo, Díez, Onieva, and Bataineh 2016), PointReg (Olsen, Johnstone, Kuester, Driscoll, and Ashford 2011). These method ensembles exhibit a lot of interesting properties, and required accuracy of estimation is widely met. Helmert transformation plays a key role, cf. (Amiri-Simkooei 2018). Three dimensional (3D) coordinate transformations are generally given by three origin shifts, three axes rotations, three scale changes and three skew parameters.

Unfortunately, in literature there exists no dataset with a simple testing problem with known solution of such a problem. Therefore, we will try to prepare such a test problem.

In this paper, the ICP algorithm will be presented in a very general manner without any assumptions of the point clouds feature to be assigned. A semi-automatic procedure for identic point segmentation, outlier elimination and transformation parameters estimation in point clouds will be explored on our testing problem.

2.1. Basic ideas of ICP algorithm

During the last years researchers used ICP very often, see (He, Liang, Yang, Li, and He 2017). The first reason is its easy feasibility. The second reason is almost no limits on point cloud size.

The algorithm calculates the optimal rotation and translation for the model to minimize the distances between the corresponding points.

In the first step, the algorithm tries to find matching pairs of points from both clouds.

In the second step, it updates the rotation matrix and the shift vector based on the initial point assignment.

Then, according to the rotation matrix and the shift vector, it transforms a point cloud.
Given two independently acquired sets of 3D points from position P_1 and P_2, we want to find the transformation $(\boldsymbol{R}, \boldsymbol{t})$ consisting of a rotation matrix $\boldsymbol{R}$ and a translation vector $\boldsymbol{t}$ which minimizes the following cost function

$$E(\boldsymbol{R}, \boldsymbol{t}) = \sum_{i=1}^{N_m} \sum_{j=1}^{N_d} w_{i,j} \left\| \widehat{m}_i - \left(\boldsymbol{R}\widehat{d}_j + \boldsymbol{t} \right) \right\|^2 . \qquad (1)$$

$w_{i,j}$ is assigned 1 if the i-th point of $\widehat{m}_i$ describes the same point in space as the j-th point of $\hat{d}$. Otherwise $w_{i,j}$ is 0. Two things have to be calculated: First, the corresponding points, and second, the transformation $(\boldsymbol{R}, \boldsymbol{t})$ that minimizes $E(\boldsymbol{R}, \boldsymbol{t})$ on the base of the corresponding points. The ICP algorithm calculates iteratively the point correspondences. In each iteration step, the algorithm selects the closest points as correspondences and calculates the transformation $(\boldsymbol{R}, \boldsymbol{t})$ for minimizing equation $E(\boldsymbol{R}, \boldsymbol{t})$.
Indeed, on one hand, the quality of results is affected essentially by the camera accuracy. On the other hand, the number of correctly identified points in different scans is important.
Therefore, there are still many interesting open questions.

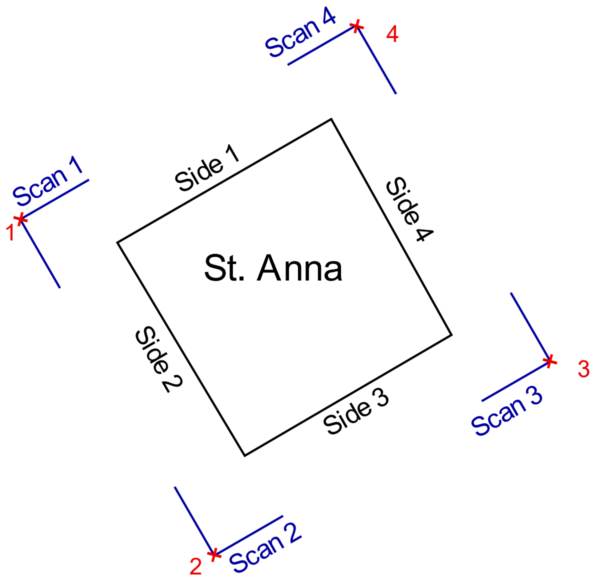

Figure 1: Chapel's plan and four coordinate systems

2. ONE SIMULATED PROBLEM

In the following subchapters we will present one simulated problem, the solution of which appears in Chapter 3.
We base our example on the 3D description of the Chapel of Saint Anna in Pardubice.
Consider that the actual geometric shape of the chapel's plan is an equilateral trapezoid. Next, let's work with measurements in four coordinate systems. See Fig. 1.
Next, we will prepare X, Y, Z, and HSV color simulations of point clouds in 4 scans that will contain identical and non-identical points.
However, collecting of theoretical true values and noisy data are our interest.
Studies of covariance matrices of HSV are well suited for the investigation of color transformation of the same point between scans.

2.1. The first step: coordinate simulation

The similar numerical example with two scans is given in (Marek, Rak 2015) that is focused on simulating only 3D coordinates in two scans.
Let us denote the northwest wall as side 1, the southwest wall as side 2, the southeast wall as side 3 and the northeast wall as side 4. See Fig. 1.
We simulate point cloud measurements in 4 scans (two sides 1-2, 2-3, 3-4, 4-1 are scanned in each scan).
In this task, we simulate the positions of several thousand points in clouds for these scans.
We have the model given by

$$\boldsymbol{Y} = \begin{bmatrix} \boldsymbol{Y}_1^{I} \\ \boldsymbol{Y}_2^{I} \\ \boldsymbol{Y}_2^{II} \\ \boldsymbol{Y}_3^{II} \\ \boldsymbol{Y}_3^{III} \\ \boldsymbol{Y}_4^{III} \\ \boldsymbol{Y}_4^{IV} \\ \boldsymbol{Y}_1^{IV} \end{bmatrix} = \begin{bmatrix} \boldsymbol{a}_1^{I} \\ \boldsymbol{a}_2^{I} \\ \boldsymbol{a}_2^{II} \\ \boldsymbol{a}_3^{II} \\ \boldsymbol{a}_3^{III} \\ \boldsymbol{a}_4^{III} \\ \boldsymbol{a}_4^{IV} \\ \boldsymbol{a}_1^{IV} \end{bmatrix} + \boldsymbol{\varepsilon}, \qquad (2)$$

$$\boldsymbol{\varepsilon} \sim N(\boldsymbol{0}, \boldsymbol{\Sigma}),\ \boldsymbol{\Sigma} = \begin{pmatrix} \boldsymbol{\Sigma}_1 & 0 & 0 & 0 \\ 0 & \boldsymbol{\Sigma}_2 & 0 & 0 \\ 0 & 0 & \boldsymbol{\Sigma}_3 & 0 \\ 0 & 0 & 0 & \boldsymbol{\Sigma}_4 \end{pmatrix} \qquad (3)$$

Notation of model $\boldsymbol{Y} = \boldsymbol{a} + \boldsymbol{\varepsilon} \sim N\left[\,\boldsymbol{0} + \boldsymbol{a},\ \boldsymbol{\Sigma}\,\right]$ means that observation vector $\mathbf{Y}$ (with elements $\boldsymbol{Y}_1^{I}$ and $\boldsymbol{Y}_1^{IV}$) has (symbol ~) multinomial normal distribution with mean value $(\boldsymbol{a}_1^{I}, \dots, \boldsymbol{a}_1^{IV})$ and with covariance matrix $\boldsymbol{\Sigma}$.
3ni-dimensional vector $\boldsymbol{a}_1^{I}$ is the vector of true coordinates n_i points on i-th side of object in a coordinate system of i-th device position. Analogous $\boldsymbol{a}_1^{I}$ is 3 n_{i+1}-dimensional vector of n_{i+1} points on (i + 1)-th side of an object in a coordinate system of i-th device position.
From layout of measurement we can obtain constraint function

$$\boldsymbol{g} = \begin{bmatrix} \boldsymbol{g}_2^{II}(\boldsymbol{\gamma}_2, \boldsymbol{T}_2) \\ \boldsymbol{g}_3^{II}(\boldsymbol{\gamma}_2, \boldsymbol{T}_2) \\ \boldsymbol{g}_3^{III}(\boldsymbol{\gamma}_3, \boldsymbol{T}_3) \\ \boldsymbol{g}_4^{III}(\boldsymbol{\gamma}_3, \boldsymbol{T}_3) \\ \boldsymbol{g}_4^{IV}(\boldsymbol{\gamma}_4, \boldsymbol{T}_3) \\ \boldsymbol{g}_1^{IV}(\boldsymbol{\gamma}_4, \boldsymbol{T}_3) \end{bmatrix} = \begin{bmatrix} \boldsymbol{a}_2^{II} - \boldsymbol{\gamma}_2 - \boldsymbol{T}_2\boldsymbol{a}_2^{I} \\ \boldsymbol{a}_3^{II} - \boldsymbol{\gamma}_2 - \boldsymbol{T}_2\boldsymbol{a}_3^{I} \\ \boldsymbol{a}_3^{III} - \boldsymbol{\gamma}_3 - \boldsymbol{T}_3\boldsymbol{a}_3^{I} \\ \boldsymbol{a}_4^{III} - \boldsymbol{\gamma}_3 - \boldsymbol{T}_3\boldsymbol{a}_4^{I} \\ \boldsymbol{a}_4^{IV} - \boldsymbol{\gamma}_4 - \boldsymbol{T}_4\boldsymbol{a}_4^{I} \\ \boldsymbol{a}_1^{IV} - \boldsymbol{\gamma}_4 - \boldsymbol{T}_4\boldsymbol{a}_1^{I} \end{bmatrix} = 0 \qquad (4)$$

Notation of model $\boldsymbol{Y} = \boldsymbol{a} + \boldsymbol{\varepsilon} \sim N\left[\,\boldsymbol{0} + \boldsymbol{a},\ \boldsymbol{\Sigma}\,\right]$ means that observation vector $\mathbf{Y}$ (with elements $\boldsymbol{Y}_1^{I}$ and $\boldsymbol{Y}_1^{IV}$) has (symbol ~) multinomial normal distribution with mean value $(\boldsymbol{a}_1^{I}, \dots, \boldsymbol{a}_1^{IV})$ and with covariance matrix $\boldsymbol{\Sigma}$.

a) 1st and 2nd sides (scan 1)

b) 2nd and 3rd sides (scan 2)

c) 3rd and 4th sides (scan 3)

d) 4th and 1st sides (scan 4)

Figure 2: Scans of the chapel

3-dimensional vector $\boldsymbol{a}_1^I$ is the vector of true coordinates n_i points on i-th side of object in a coordinate system of i-th device position. Analogous $\boldsymbol{a}_1^I$ is 3 n_{i+1}-dimensional vector of n_{i+1} points on (i + 1)-th side of an object in a coordinate system of i-th device position.
From layout of measurement we can obtain constraint function

$$\boldsymbol{g} = \begin{bmatrix} \boldsymbol{g}_2^{II}(\boldsymbol{\gamma}_2, \boldsymbol{T}_2) \\ \boldsymbol{g}_3^{II}(\boldsymbol{\gamma}_2, \boldsymbol{T}_2) \\ \boldsymbol{g}_3^{III}(\boldsymbol{\gamma}_3, \boldsymbol{T}_3) \\ \boldsymbol{g}_4^{III}(\boldsymbol{\gamma}_3, \boldsymbol{T}_3) \\ \boldsymbol{g}_4^{IV}(\boldsymbol{\gamma}_4, \boldsymbol{T}_3) \\ \boldsymbol{g}_1^{IV}(\boldsymbol{\gamma}_4, \boldsymbol{T}_3) \end{bmatrix} = \begin{bmatrix} \boldsymbol{a}_2^{II} - \boldsymbol{\gamma}_2 - \boldsymbol{T}_2\boldsymbol{a}_2^I \\ \boldsymbol{a}_3^{II} - \boldsymbol{\gamma}_2 - \boldsymbol{T}_2\boldsymbol{a}_3^I \\ \boldsymbol{a}_3^{III} - \boldsymbol{\gamma}_3 - \boldsymbol{T}_3\boldsymbol{a}_3^I \\ \boldsymbol{a}_4^{III} - \boldsymbol{\gamma}_3 - \boldsymbol{T}_3\boldsymbol{a}_4^I \\ \boldsymbol{a}_4^{IV} - \boldsymbol{\gamma}_4 - \boldsymbol{T}_4\boldsymbol{a}_4^I \\ \boldsymbol{a}_1^{IV} - \boldsymbol{\gamma}_4 - \boldsymbol{T}_4\boldsymbol{a}_1^I \end{bmatrix} = 0 \qquad (4)$$

Let the true model of our chapel in coordinate system S_0 be given. We will consider that the base of our chapel is is an equilateral trapezoid with length of sides 4.500 m, 4.300 m and 5.051 m. Now we will set origins of coordinate systems S_2, S_3, and S_4, see Tab. 1.
Further, we consider that matrices T_2, T_3, T_4 are given as

$$\boldsymbol{T}_i = \begin{pmatrix} \boldsymbol{R}_i & 0 \\ 0 & 1 \end{pmatrix}, \quad \boldsymbol{R}_i = \begin{pmatrix} c_i & s_i \\ -s_i & c_i \end{pmatrix}, \qquad (5)$$

where $c_i = \cos(\theta_i)$, $s_i = \sin(\theta_i)$ e.g. transformation do not change vertical position of chapel.
According to our experiment and obvious uncertainty of 3D camera, we consider that the standard deviation $\sigma_d = 2$ cm. Of course such value is large measurement error.
A following numerical study will be made. Firstly we transform coordinates $\boldsymbol{a}_0$ of points on true trapezoid model from coordinate system S_0 to S_1.
We will use transformation: $\boldsymbol{a}_1 = \boldsymbol{\gamma}_1 + \boldsymbol{T}_1\boldsymbol{a}_0$.
We set $\gamma_1 = [44.000, 90.000]'$ and $\theta_i = \frac{4}{3}\pi \Rightarrow$ $\boldsymbol{R}_1 = \begin{pmatrix} \cos(240°), \sin(240°) \\ -\sin(-240°), \cos(240°) \end{pmatrix}$.
Using formulas $\boldsymbol{a}_2 = \boldsymbol{\gamma}_2 + \boldsymbol{T}_2\boldsymbol{a}_1$, $\boldsymbol{a}_3 = \boldsymbol{\gamma}_3 + \boldsymbol{T}_3\boldsymbol{a}_2$, $\boldsymbol{a}_4 = \boldsymbol{\gamma}_4 + \boldsymbol{T}_4\boldsymbol{a}_3$ we obtained coordintes of points in every coordinate system S_1, S_2, S_3, S_4. From data $\boldsymbol{a}_1$, $\boldsymbol{a}_2$, $\boldsymbol{a}_3$, $\boldsymbol{a}_4$ it is possible to obtained only points $\boldsymbol{a}_1^I$, $\boldsymbol{a}_2^I$, $\boldsymbol{a}_3^I$, $\boldsymbol{a}_4^I$ that lie only on first, second, third or fourth side of our object.
To these exact coordinates we add measurement errors by generating independent epsilon errors. With respect to the origins of coordinate systems we then extracted the simulated (measured) values of $\mathbf{Y}$, cf. model (1).
The simulated values are available on the website (Nedvědová 2019).
Table 1 presents the transformation parameters between start and target coordinate systems.
Part of the coordinates of identical points are given in Table 3.

Table 1: True transformation parameters

	Sides		
Scans	1,2 to 2,3	2,3 to 3,4	4,1 to 1,2
Shift	-50, 30	65, 125	118, 38
θ_i	65°	148°	244°
Rotation	$\begin{matrix} 0.42 & 0.91 \\ -0.91 & 0.42 \end{matrix}$	$\begin{matrix} -0.85 & 0.53 \\ -0.53 & -0.85 \end{matrix}$	$\begin{matrix} -0.44 & -0.90 \\ 0.90 & -0.44 \end{matrix}$

2.2. The second step: HSV simulation

First, we select points of the same type that appear in photos taken from different locations.
For 12 color groups with ten-point color, we obtained HSV measurements in two scans for every chaple's side. For example, the fifth color group was created from points on the stone plinth of the chapel. Points were focused in the 1st and 2nd scans.
The diagram in the figure 3 shows information about in which scans the color groups were selected and targeted. By analyzing data containing 12 times 10 points, we estimate the variability of HSV components. Averages and standard deviations of HSV measurement for all color group are given in Tab. 2.

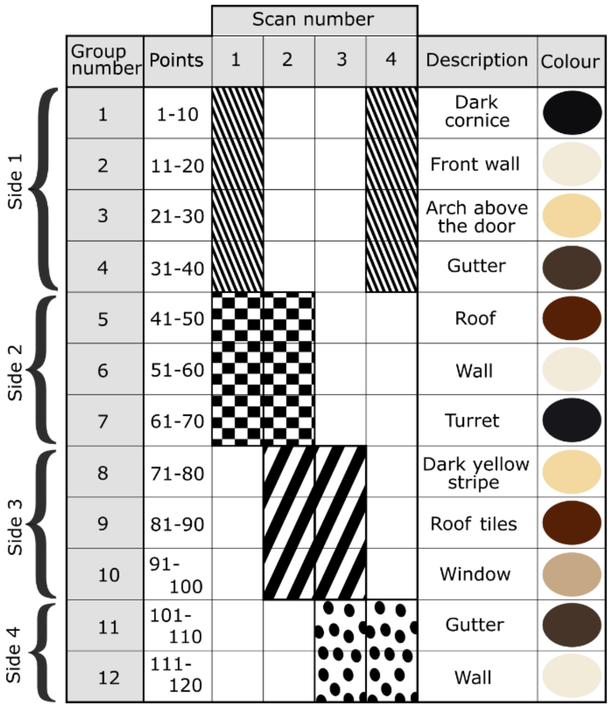

Figure 3: Group diagram

Table 2: Pairs of HSV measurements

	Average HSV		
	H	S	V
Group 5, Scan 1	49.2156	26.7981	3.3147
Group 5, Scan 2	73.9066	26.1388	3.3262
Group 6, Scan 1	48.3860	25.6160	5.2158
Group 6, Scan 2	72.6436	26.8238	5.2061
	Standard deviation		
	H	S	V
Group 5, Scan 1	0.3631	0.5231	0.1314
Group 5, Scan 2	0.5552	0.2982	0.1328
Group 6, Scan 1	0.2376	0.3285	0.7499
Group 6, Scan 2	0.3480	0.1971	0.7570

We created a matrix of differences in HSV values in these two scans, which has a dimension of 120x3. For these measurements, we have obtained a 3x3 covariance matrix that describes the variability and dependence of HSV components. This matrix is shown in formula (6).

$$V(H,S,V) = \begin{pmatrix} 0.14 & 0.0004 & 0.003 \\ 0.0004 & 0.0142 & 0.0014 \\ 0.003 & 0.0014 & 0.0016 \end{pmatrix} \tag{6}$$

However, we did not use this matrix for simulation. For all 12 color groups, we determined the variance matrices using 10 points measured in two scans:

$$V_1(H,S,V) = \begin{pmatrix} 0.0665 & 0.0028 & 0.0040 \\ 0.0028 & 0.0199 & 0.0020 \\ 0.0040 & 0.0020 & 0.0005 \end{pmatrix} \tag{7}$$

$$V_2(H,S,V) = \begin{pmatrix} 0.2086 & 0.0943 & 0.0587 \\ 0.0943 & 0.4476 & 0.1554 \\ 0.0587 & 0.1554 & 0.0959 \end{pmatrix} \cdot 10^{-3}$$

$$V_3(H,S,V) = \begin{pmatrix} 0.0055 & -0.0001 & -0.0002 \\ -0.0001 & 0.0007 & -0.0003 \\ -0.0002 & -0.0003 & 0.0002 \end{pmatrix}$$

$$V_4(H,S,V) = \begin{pmatrix} 0.5728 & -0.0153 & 0.0033 \\ -0.0153 & 0.0052 & 0.0004 \\ 0.0033 & 0.0004 & 0.0002 \end{pmatrix}$$

$$V_5(H,S,V) = \begin{pmatrix} 0.0003 & 0.0007 & 0.0000 \\ 0.0007 & 0.0059 & 0.0008 \\ 0.0000 & 0.0008 & 0.0003 \end{pmatrix}$$

$$V_6(H,S,V) = \begin{pmatrix} 0.0027 & -0.0011 & -0.0004 \\ -0.0011 & 0.0006 & 0.0003 \\ -0.0004 & 0.0003 & 0.0002 \end{pmatrix}$$

$$V_7(H,S,V) = \begin{pmatrix} 0.0005 & -0.0004 & -0.0000 \\ -0.0004 & 0.0034 & 0.0003 \\ -0.0000 & 0.0003 & 0.0001 \end{pmatrix}$$

$$V_8(H,S,V) = \begin{pmatrix} 0.0034 & 0.0111 & -0.0088 \\ 0.0111 & 0.2452 & -0.0339 \\ -0.0088 & -0.0339 & 0.0446 \end{pmatrix} \cdot 10^{-3}$$

$$V_9(H,S,V) = \begin{pmatrix} 0.0062 & -0.0212 & -0.0022 \\ -0.0212 & 0.5339 & -0.0983 \\ -0.0022 & -0.0983 & 0.4110 \end{pmatrix} \cdot 10^{-3}$$

$$V_{10}(H,S,V) = \begin{pmatrix} 0.0001 & -0.0002 & -0.0000 \\ -0.0002 & 0.0010 & -0.0006 \\ -0.0000 & -0.0006 & 0.0012 \end{pmatrix}$$

$$V_{11}(H,S,V) = \begin{pmatrix} 0.0002 & 0.0001 & -0.0000 \\ 0.0001 & 0.0060 & -0.0017 \\ -0.0000 & -0.0017 & 0.0009 \end{pmatrix}$$

$$V_{12}(H,S,V) = \begin{pmatrix} 0.0513 & -0.0375 & 0.0122 \\ -0.0375 & 0.2651 & -0.1361 \\ 0.0122 & -0.1361 & 0.1053 \end{pmatrix} \cdot 10^{-3}$$

We can proceed as follows.
To the points simulated by transformation parameters given in Table 1, HSV values simulation was added. We selected the exact HSV value for any point on our object. We randomly selected one of the 12 covariance matrices V_1 to V_{12}. Using this randomly chosen covariance matrix, we simulated measurements for two different scans twice. During the simulation we assumed normal error distribution of HSV and chosen covariance matrix V. We used simple simulation technique for normal data with estimated prespecified covariance matrix. For detail see (Kaiser, 1962).
We use funcction R = mvnrnd($\boldsymbol{\mu}$, $\boldsymbol{\Sigma}$), that returns an N-by-D matrix $\boldsymbol{R}$ of random vectors chosen from the multivariate normal distribution with mean vector $\boldsymbol{\mu}$, and covariance matrix $\boldsymbol{\Sigma}$.

3. NUMERICAL STUDIES

3.1. Estimation in our test problem

The ICP method is applied to our data set. The estimated parameters are presented on the website (Nedvědová 2019).
According to the articles (Amiri-Simkooei 2018) and (Marek 2015) we calculate the transformation parameters for the task. We applied the ICP method from Point Cloud Library (Rusu and Cousins 2011) to find pairs of identical points between scans based on the similarity of HSV values to estimate the transformation parameters.
We just decide to use the HSV color model on base of our previous research (Chmelar and Benkrid 2014) and (Chmelar, Beran and Kudriavtseva 2015), where for a color detection form static frames the HSV model overcomes standard used color models. Its advantage lies in color description by only one channel. Other channels describes a concrete color's properties.
The following figure shows comparison between RGB Fig. 4 (a) and HSV Fig. 4 (b) color space for the exact color. When we match similar color from different chapel's sides the bigger color span in the color space it is more suitable, but when the ICP algorithm's parameters are properly set, than the precise match is achieved.

Table 3: Simulation of HSV: identical points

	Point: X, Y, Z H, S, V		
No 51: Scan 1	60.6841 48.7407	7.1315 26.1132	47.2399 4.2658
No 51: Scan 2	10.8373 73.4339	27.6623 26.4070	84.1735 2.6310
No 52: Scan 1	68.2305 48.4720	3.1235 25.7026	46.3298 4.5565
No 52: Scan 2	11.1249 73.4181	27.2490 26.4010	86.7095 2.7851
No 53: Scan 1	59.4553 48.1522	5.6575 25.3072	47.4210 4.2163
No 53: Scan 2	10.3987 73.1719	31.7112 26.5519	86.7758 2.8363
No 54: Scan 1	63.3525 48.0840	4.0797 25.1802	47.2996 4.9363
No 54: Scan 2	9.0201 73.4261	35.0025 26.3800	85.3573 3.1580
No 55: Scan 1	65.6075 48.6650	3.1142 25.9867	46.2436 5.0952
No 55: Scan 2	11.7636 73.2439	23.8849 26.5146	88.5562 3.1231
No 56: Scan 1	56.8741 48.3353	5.8002 25.5887	47.3855 5.1940
No 56: Scan 2	10.1819 73.1590	26.9011 26.5272	88.6639 3.2359
No 57: Scan 1	54.3685 48.6171	11.6568 25.9424	51.7027 5.6725
No 57: Scan 2	10.9817 73.3495	28.4105 26.4477	83.5378 3.2783
No 58: Scan 1	66.4225 48.1491	0.5393 25.3256	44.5333 5.7490
No 58: Scan 2	11.7224 73.4699	26.7111 26.3413	88.0017 2.9403
No 59: Scan 1	64.3876 48.4461	4.5814 25.7048	46.5366 6.0703
No 59: Scan 2	11.3594 73.2436	27.9017 26.4897	87.5473 2.7728
No 60: Scan 1	59.5184 48.1983	6.1586 25.3090	46.3937 6.4026
No 60: Scan 2	10.0160 73.1467	27.1193 26.5443	89.3212 2.6745

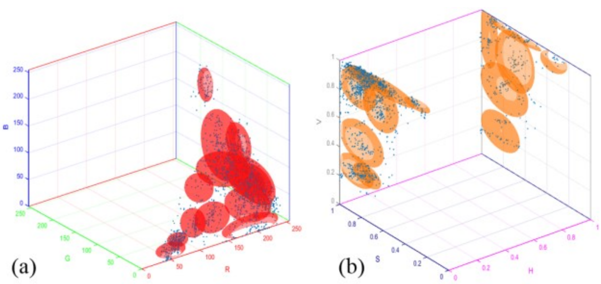

Figure 4: Color space span for exact color, (a) RGB model, (b) HSV model

The testing dataset includes four registration cases. Each case describes registration of two chapel's sides with identical points, sides 1-2, 2-3, 3-4 and 4-1.

4. CONCLUSION

In this paper, we presented the process of simulation of data for a registration problem. We designed the testing example for multi-stage 3D coordinate transformations.

ACKNOWLEDGMENTS

The paper was supported by grant SGS_2019_021 of the University of Pardubice.

REFERENCES

Amiri-Simkooei, A. R., 2018. Parameter estimation in 3D affine and similarity transformation: implementation of variance component estimation. Journal of Geodesy, 92 (11), 1285–1297.

Bataineh, S., Bahillo, A., Díez, L., Onieva, E., and Bataineh, I., 2016. Conditional Random Field-Based Offline Map Matching for Indoor Environments. Sensors, 16(8).

Burguera, A., Gonzalez, Y., and Oliver, G., 2008. The likelihood field approach to sonar scan matching. IEEE/RSJ International Conference on Intelligent Robots and Systems, pp. 2977-2982.

He, Y., Liang, B., Yang, J., Li, S., and He, J. 2017. An Iterative Closest Points Algorithm for Registration of 3D Laser Scanner Point Clouds with Geometric Features. Sensors, 17(8).

Chmelar, P., and Benkrid, A., 2014. Efficiency of HSV over RGB Gaussian Mixture Model for fire detection. 24th International Conference Radioelektronika, pp. 1-4

Chmelar, P., Beran, L. and Kudriavtseva, N. 2015. The laser color detection for 3D range scanning using Gaussian mixture model. 25th International Conference Radioelektronika pp. 248-253

Lu, F., and Milios E., 1997. Robot pose estimation in unknown environments by matching 2D range scans. Journal of Intelligent and Robotic Systems [online]. 18(3), 249-275.

Kaiser, H. F., & Dickman, K., 1962. Sample and Population Score Matrices and Sample Correlation Matrices from an Arbitrary Population Correlation Matrix, Psychometrika, 27 (2), 179-182.

Magnusson, M., 2013. The three-dimensional normal-distributions transform: an efficient representation for registration, surface analysis, and loop detection. Dissertation thesis. Örebro university.

Marek J., Rak J., and Jetensky P., 2015. Statistical solution of 3D transformation problem. In: V. Skala, ed. Proceedings of 23rd International Conference in Central Europe on Computer Graphics, Visualization and Computer Vision, WSCG 2015, pp. 85-90. Jun 8-13, Pilsner (Czech republic).

Mitra, N. J., Gelfand, N., Pottmann, H., and Guibas, L., 2004. Registration of point cloud data from a geometric optimization perspective.

Eurographics/ACM SIGGRAPH symposium on Geometry processing - SGP 04, p. 22.
Montesano, L., Minguez, J., and Montano, L., 2005. Probabilistic scan matching for motion estimation in unstructured environments. IEEE/RSJ International Conference on Intelligent Robots and Systems, pp. 3499-3504
Nedvědová, M., 2019. Estimates of unknown transformation parameters in terrestrial measurements: One simulated problem. Available from: http://hsv-transform.esteticke-charakteristiky.eu [Accessed 10 July 2019]
Nüchter, A., 2009. 3D robotic mapping: the simultaneous localization and mapping problem with six degrees of freedom. Heidelberg: Springer.
Olsen, M. J., Johnstone, E., Kuester, F., Driscoll, N., and Ashford, S. A., 2011. New Automated Point-Cloud Alignment for Ground-Based Light Detection and Ranging Data of Long Coastal Sections. Journal Of Surveying Engineering, 137(1), 14-25.
Rusu, R., and Cousins, S., 2011. 3D is here: Point Cloud Library (PCL). IEEE International Conference on Robotics and Automation, pp. 1-4

COMPARATIVE COMPUTER-AIDED DESIGN OF MILLIMETER-WAVE-TO-OPTICAL CONVERTERS FOR FIFTH-GENERATION COMMUNICATION NETWORK

M. E. Belkin[(a)], T. Bakhvalova[(a)], and A.S. Sigov[(a)]

[(a)]Scientific and Technological Center "Integrated Microwave Photonics" MIREA - Russian Technological University
Moscow, Russian Federation

[(a)]belkin@mirea.ru

ABSTRACT
Using well-known off-the-shelf optoelectronic software, we compare in detail three most prospective types of external optical modulators as millimeter-wave-to-optical converters in fiber-optics link of fiber-wireless fronthaul network for fifth-generation communication network based on Radio-over-Fiber technology. In all cases, the same 1.25 Gbit/s 16-position quadrature amplitude modulated signal at the radio-frequency carrier in intermediate-band (15 GHz) or millimeter-wave band (40 GHz) propagates over fiber-optics link under study. In the result, it is shown that the use of a signal transmission scheme at the radio frequency of intermediate band (between "Low Range" and "High Range" of 5G network) allows a significant increase in the length for the fiber-optics section of a fiber-wireless fronthaul network. However, this leads to a complication of the base station scheme, since additional up/down-conversion of the radio-frequency carrier is required.

Keywords: 5G communication network, quadrature-amplitude-modulation signal transmission, electro-optical modulator

1. INTRODUCTION

In the last decade, the global telecommunications industry is experiencing a stage of violent development associated with the becoming of fifth-generation mobile telecommunications networks (5G NR) (Andrews, Buzzi, Choi, Hanly, Lozano, Soong and Zhang 2014; Browne 2018; Chen and Zhao 2014; Munn 2016; Waterhouse and Novak 2015). The serious activity of the world telecommunication community in this direction began in the first half of the current decade. This statement is easily confirmed by the world's largest scientific database IEEE Xplore. In particular, when typing the keywords "5G" and "communication" in the search box, the number of publications increased 210 times from 2010 to 2018. Table 1 lists the search results in more detail.

One of the key distinctive feature of 5G NR in comparison with the previous generations is to overcome the 5 GHz ceiling in a mobile network (5G Americas 2017). Following this tendency, which is reflected in a vast number of publications, currently, the local telecommunications commissions of various countries are proposing and harmonizing the plans for mobile communication in millimeter-wave (MMW) band (24.5-86 GHz), which will be reviewed this year at the World Radio Conference (WRC-2019) (Resolution 238 2017).

Table 1: Publications Referred to 5G Communication

Year	Number of publications
2010	23
2011	30
2013	680
2015	1332
2018	4831 including 3321 in conference proceedings, 1409 in journals and magazines, and 58 in monographs

Another milestone of great importance is the development of access network. In this direction, well-known Radio-over-Fiber (RoF) technology (Al-Raweshidy and Komaki 2002; Novak, Waterhouse, Nirmalathas, Lim, Gamage, Clark, Dennis and Nanzer 2016; Sauer, Kobyakov and George 2007) is considered as the most promising approach, which is implemented based on fiber-wireless architecture. A typical configuration of a RoF-based communication network includes central office (CO), set of base stations (BS), which are a key element of a RoF-based fiber-wireless fronthaul network (FWFN) that interactively (using downlink and uplink) connects the CO and each BS using fiber-optic links (FOL), and microwave or millimeter-wave band user radio terminals. As is known, for the transmission of signals through a FOL, direct and inverse electro-optical conversions are required. The first one in the RoF-based communication system is usually performed with the help of an external electro-optical modulator (EOM), and the second with a photodetector.

Taking part in the studies recently we have proposed and previously investigated photonics-based beamforming networks for ultra-wide MMW-band antenna arrays (Belkin, Fofanov, Golovin, Tyschuk and Sigov 2018), optimal approaches to design next-generation combined fiber-wireless telecom systems (Belkin, Golovin, Tyschuk and Sigov 2018; Bakhvalova, Belkin, Fofanov 2018), and to distribute signals through FWFN (Belkin, Bakhvalova, Sigov 2019), as well as have studied fiber distribution networks with direct and external modulation in the "Low Range" of 5G NR system (Bakhvalova, Fofanov, Alyoshin and Belkin 2019). Nevertheless, in the cited, as well as in the works of other authors referred to this direction, there is no specific consideration related to the choice of the optimal frequency range for signal transmission over the FOL included in the FWFN. This choice, in principle can be made on the basis of one of three transmission options (Belkin, Bakhvalova, Sigov 2019): in the baseband, in the intermediate frequency (IF) band, and in the millimeter-wave radio frequency (RF) band. Meeting this shortcoming, the remainder of the paper is organized as follows. Section 2 presents the reference data for the further simulation. Section 3 demonstrates the models and setups for simulation of a FOL with three types of EOM using well-known software tool VPIphotonics Design Suit™. Leveraging the application of these EOMs for a realistic case in Section 4 the results of the simulation experiment by the same computer tool imitating transmission of quadrature amplitude modulated RF signals of 40 GHz ("High Range" of a wireless cell) or 15 GHz (IF-band) through a FOL connected CO and BS, are discussed. Section 5 concludes the paper.

2. REFERENCE DATA FOR THE SIMULATION

In this work, the subject of the study is the FOL of FWFN; the devices of test are three widespread types of electro-optic modulators for an external modulation of optical carrier including double-sideband Mach-Zehnder modulator (DSB MZM), carrier suppressed single-sideband Mach-Zehnder modulator (CS-SSB MZM), and electro-absorption modulator (EAM), and standard single-mode fiber (SMF). A tool for the computer simulation is well-known commercial software VPIphotonics Design Suit™. The study took into account two key distortion sources of the transmitted signal: a chirp of modulators and chromatic dispersion of the fiber. To eliminate the influence of nonlinear effects during modulation and signal transmission through the fiber, RF and optical signal levels were selected so that the modulation index did not exceed 40%, and the optical power in the fiber was not more than 5 mW. Table 2 lists the common reference data for the FOL under study. In addition, Table 3 lists the reference data for the modulators under test.

Table 2: Common Reference Data for the FOL under Study

Parameter		Value
Length of pseudo-random bit sequence		2^{15}-1
Bitrate		1.25 Gbit/s
RF Carrier Frequency		15 or 40 GHz
Input RF Power		-10…0 dBm
Type of RF modulation		16-QAM
Optical Carrier		C-band (1552.52 nm)
Type of optical modulation		Intensity
PIN-Photodiode	Responsivity	0.7 A/W
	Dark current	100 nA
	3dB Bandwidth	50 GHz
	Optical Input Power	<5 mW
Post-amplifier	Gain	30 dB
	Noise Spectral Density	20•10-12 A/Hz1/2
Optical Fiber	Type	SMF-28e+
	Length	up to 70 km
	Attenuation	0.2 dB/km
	Dispersion	$17e^{-6}$ s/m^2
	Dispersion Slope	80 s/m^3

Table 3: Reference Data for the Modulators under Test

Parameter	DSB MZM	CS-SSB MZM	EAM
Optical Insertion Loss	4 dB	6 dB	3 dB
Optical Extinction ratio	20 dB	20 dB	14 dB
Slope efficiency	-	-	0.14 W/V
RF π-Bias Voltage	5.5 V	7.5 V	-
Electro-Optical Bandwidth	40 GHz	40 GHz	40 GHz
Linewidth enhancement factor (α)	0 (X-cut)	0 (X-cut)	1.0

3. CAD MODEL AND SETUP

Figure 1 shows VPIphotonics Design Suite's externally modulated/direct detection FOL model and setup for the simulation experiments that consist of the library models of unmodulated continuous-wave laser, EOM under test, single-mode optical fiber and photodiode followed by the electrical amplifier model. One can see their relevant parameters in Tables 2 and 3. Besides, there are two instrumental library models in the setup. The first one imitates 1.25 Gbit/s, 16-QAM RF transmitter containing library models of QAM generator, output unit for power control, electrical amplifier, and a device setting the desired signal-to-noise ratio (SNR). This module generates an electrical M-QAM signal up-converted at a given RF carrier frequency. The second one is the

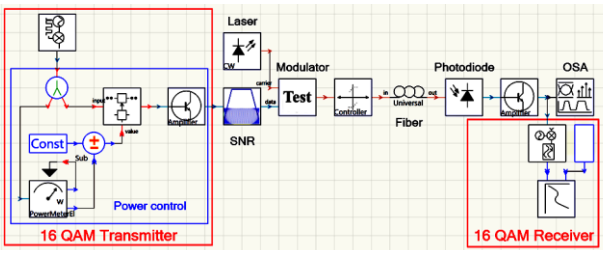

Figure 1. VPIphotonics Design Suite's Setup for the FOL with External Modulation by QAM-signals

16-QAM RF Receiver. This module detects RF signal, decodes an electrical 16-QAM signal and evaluates the error vector magnitude (EVM) of the QAM signal. The model of Numerical 2D Analyzer is used for two-dimensional graphical representation of the data from the Receiver output.

4. SIMULATION RESULTS

In preparation for the simulation experiments, the intensity-modulation index of each modulator under test was optimized in such a way as to ensure the maximum output RF carrier-to-noise ratio while maintaining the linear-signal mode of the modulators at all modulating frequencies. Figures 2, 3, and 4 depict examples of simulating EVM vs fiber length characteristics for the modulator under test during optical modulation by 1.25 Gbit/s, 16-QAM, 15 GHz (transmission in IF-band) or 40 GHz (transmission in MMW-band) RF signal, correspondingly. For the best vision, there are some insets in the Figures showing constellation diagrams in specific points. In addition, in the Figures, the dotted lines indicate the standard limit of the EVM during transmission of the 16-QAM signal, which is 12.5% (ETSI 2017).

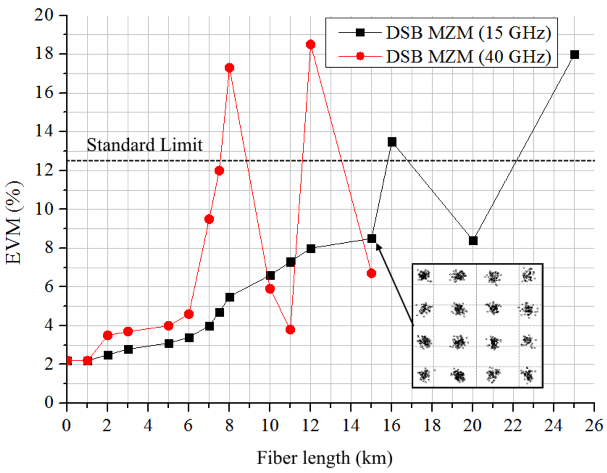

Figure 2. Example of simulating EVM vs fiber length characteristic for a FOL with DSB MZM under test

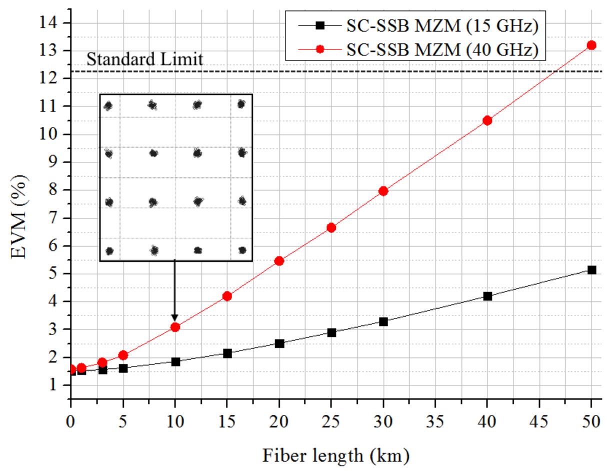

Figure 3. Example of simulating EVM vs fiber length characteristic for a FOL with CS-SSB MZM under test

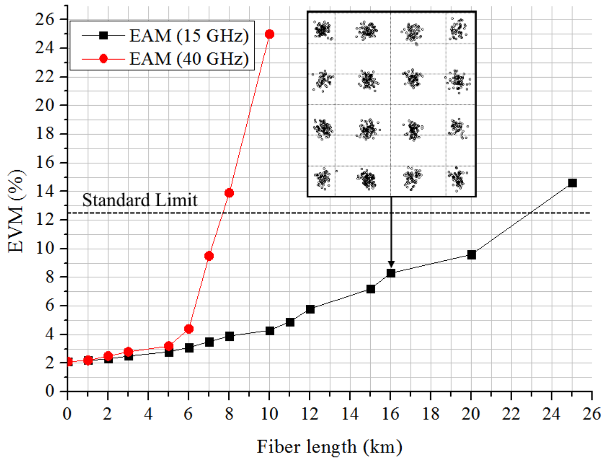

Figure 4. Example of simulating EVM vs fiber length characteristic for a FOL with EAM under test

The results of the simulation for the fiber-optics link under study within fiber-wireless fronthaul network of 5G NR system are summarized in Table 4.

Table 4: The Results of the Simulation

Device under test	RF carrier (GHz)	Allowable Distance of FOL (km)
DSB MZM	15	16
	40	7.3
SC-SSB MZM	15	Much more than 50
	40	47
EAM	15	23
	40	8

The following outputs can be derived from our study:

- the minimum values of EVM were obtained for external modulation using CS-SSB MZM, which, nevertheless, requires the most complex control schematic, accordingly, has the greatest value;
- the slope of the EVM characteristic increases with distance from SC-SSB MZM to DSB MZM through EAM, which corresponds to the known data (Kim, Bae, Kim and Chung 2018; Salvatore, Sahara, Bock and Libenzon 2002);
- the following from Fig. 2 significant fluctuations in the values of the EVM are characterized by the effect of dispersion in an extended optical fiber. To eliminate it in order to increase the length of the FOL, it is required to introduce at its end a dispersion corrector, which is a standard element in fiber-optic communication systems.

CONCLUSION

Using off-the-shelf photonic computer-aided design tool VPIphotonics Design Suite a methodical analysis for the model of fiber-optics link within fiber-wireless fronthaul network with external intensity modulations by 1.25-Gbit/s 16-QAM signal for 5G NR-oriented networks based on analog RoF system, was conducted. For a comprehensive analysis, all prospective electro-optical converting devices including a DSB MZM, SC-SSB MZM, and EAM, were comparatively investigated. The results of simulating the error vector magnitude coincide in trend with the known calculation and experimental data, however, differ quantitatively, which is associated with a large number of device parameters used in the process of transmitting the QAM-modulated radio-frequency signal over the fiber-optic link. The use of a signal transmission scheme at the radio frequency of intermediate band (between "Low Range" and "High Range") allows a significant increase in the length for the fiber-optics section of a fiber-wireless fronthaul network. However, this leads to a complication of the base station scheme, since additional up/down-conversion of the radio-frequency carrier is required. Therefore, to make a final decision, more thorough research in the framework of a specific RoF-based network is needed.

ACKNOWLEDGMENTS

This work was supported by the Russian Foundation for Basic Research, Grant No. 18-29-20083.

REFERENCES

5G Americas: White Paper on 5G Spectrum Recommendations. Apr. 2017. 28 pp.

Al-Raweshidy H., Komaki S., 2002. Radio over Fiber Technologies for Mobile Communications Networks: 436 pp., Artech House.

Andrews J. G., Buzzi S., Choi W., Hanly S. V., Lozano A., Soong A. C. K., Zhang J. C., 2014. What Will 5G Be? IEEE Journal on Selected Areas in Communications, 32 (6): 1065 – 1082.

Bakhvalova T., Belkin M., Fofanov D., 2018. Advances in Fiber-Wireless Network Architecture Approach to the Next-Generation Communication Systems. Proceedings of the Seventh International Conference on Advances in Computing, Communication and Information Technology - CCIT 2018, pp. 62-67, October 27-28, Rome, Italy.

Bakhvalova T.N., Fofanov D.A., Alyoshin A.V. and Belkin M.E., 2019. Fiber Distribution Networks with Direct and External Modulation by Digital QAM-Signals. Proceedings of the 2019 42nd International Conference on Telecommunications and Signal Processing (TSP2019), 4 pp., July 1-3, in Budapest, Hungary, Accepted.

Belkin M E., Golovin V., Tyschuk Y. and Sigov A. S., 2018. Studying an Optimal Approach to Design Combined Fiber-Wireless Telecom Systems. Proceedings of the 41-st International Conference on Telecommunications and Signal Processing (TSP2018), pp. 43-46, July 4-6, Athens, Greece.

Belkin M., Bakhvalova T., Sigov A.S., 2019. Studying an Optimal Approach to Distribute Signals through Fiber-Wireless Fronthaul Network. Proceedings of the International IEEE Conference on Microwaves, Communications, Antennas and Electronic Systems (COMCAS-2019), 4 pp., November 4-6, Tel Aviv, Israel, Submitted.

Belkin M.E., Fofanov D., Golovin V., Tyschuk Y. and Sigov A.S., 2018. Design and optimization of photonics-based beamforming networks for ultra-wide mmWave-band antenna arrays. Chapter in book IntechOpen "Antenna Array Optimization". 21 pp. Available from: https://www.intechopen.com/books/array-pattern-optimization/design-and-optimization-of-photonics-based-beamforming-networks-for-ultra-wide-mmwave-band-antenna-a [accessed November 5, 2018]

Belkin M.E., Golovin V., Tyschuk Y., and Sigov A.S., 2018. Modeling Electroabsorption Modulated Laser for Digital Optical Transmission. Proceedings of the 1st IEEE British and Irish Conference on Optics and Photonics (BICOP 2018), 4 pp. December 12 – 14, London, UK.

Browne J., 2018. What Role Will Millimeter Waves Play in 5G Wireless Systems? Microwaves & RF, pp. 38-42. Available from: https://www.mwrf.com/systems/what-role-will-millimeter-waves-play-5g-wireless-systems [accessed April 10, 2018]

Chen S., Zhao J., 2014. The requirements, challenges and technologies for 5G of terrestrial mobile telecommunication. IEEE Communications Magazine, 52 (5): 36–43.

ETSI, 2017. Minimum requirements for Error Vector Magnitude. TECHNICAL SPECIFICATION, LTE; Evolved Universal Terrestrial Radio Access (E-UTRA); User Equipment (UE) radio transmission and reception (3GPP TS 36.101 version 14.3.0 Release 14), pp. 215.

Kim B. G., Bae S. H., Kim H., Chung Y. C., 2018. RoF-Based Mobile Fronthaul Networks Implemented by Using DML and EML for 5G Wireless Communication Systems. IEEE Journal of Lightwave Technology, 36 (14): 2874-2881.

Munn J., 2016. Our 5G Future: In the Fast Lane with Numerical Simulation. Microwaves & RF, pp. 48-50. Available from: https://www.mwrf.com/software/our-5g-future-fast-lane-numerical-simulation [accessed November 16, 2016]

Novak D., Waterhouse R. B., Nirmalathas A., Lim C., Gamage P. A., Clark T. R., Dennis M. L., and Nanzer J. A., 2016. Radio-Over-Fiber Technologies for Emerging Wireless Systems. IEEE Journal of Quantum Electronics, 52 (1): 1-11 (0600311).

Resolution 238, 2017. International Telecommunication Union, World Radiocommunication Conference 2019, Agenda and Relevant Resolutions, 92 pp.

Salvatore R. A., Sahara R. T., Bock M. A. and Libenzon I., 2002. Electroabsorption Modulated Laser for Long Transmission Spans. IEEE Journal on Quantum Electronics, 38 (5): 464- 476.

Sauer M., Kobyakov A., George J., 2007. Radio over Fiber for Picocellular Network Architectures. IEEE Journal of Lightwave Technology, 25 (11): 3301-3320.

Waterhouse R., Novak D., 2015. Realizing 5G. IEEE Microwave Magazine, 16 (8): 84-92.

MODELLING THE GROUND CONNECTION BETWEEN TWO AIRPORTS IN A MULTI-AIRPORT SYSTEM: CASE SANTA LUCIA-MEXICO CITY

Miguel Mujica Mota[(a)], Paolo Scala[(b)], Danny Spit[(c)], Reyhan Tasdelen[(d)]

[(a),(c),(d)]Aviation Academy, Amsterdam University of Applied Sciences
[(b)]Amsterdam School of International Business, Amsterdam University of Applied Sciences

[(a)]m.mujica.mota@hva.nl, [(d)]p.m.scala@hva.nl,[(b)]danny.spit@hva.nl, [(c)]reyhan.tasdelen@hva.nl

ABSTRACT
This study presents a model-based analysis of the ground connectivity performance of the future Santa Lucia-Mexico City multi-airport system. The plan of the current government is to connect the two airports by a dedicated line, either by bus or other transport so that passengers and airlines can get the benefit of a coordinated operation. Performance indicators such as minimum connecting time, vehicle utilization and passenger waiting time are used to evaluate the future performance. Results reveal that when all passengers are allowed to use the connection, a big number of vehicles are required for providing a good level of service while in the case of a restricted use to only transfer passengers the operation with Bus would have a good performance.

Keywords: multi-airport system, connectivity, congestion, AIMC, transport

1. INTRODUCTION

Benito Juárez International Airport, better known as Mexico City International Airport, has faced rapid growth of air traffic in the last decade, witnessing a passenger growth of 61% in a decade, going from 25.8 million in 2007 to 41.7 million in 2016 (AICM 2019).
On the other hand, the infrastructures at Mexico City airport have not seen any major upgrade/expansion in recent years, with the consequence of saturation and congestion. One of the main indicators of congestion is represented by the high number of delayed flights, which in turn affects airport operations and, above all, the level of service to the passengers.
In order to cope with this problem, the first action taken by the airport authority was to set a limit to the hourly operations (landings and take offs), to a maximum of 61Atm/hr (DOF 2014). Although, this solution restricted the traffic to the airport, the system operated in most part of the day at the edge of its capacity with some periods of the day exceeding his declared capacity (see Figure 1).
Recently, the government authority of Mexico proposed to develop a Mexico City multi-airport system. This multi-airport system, composed by three airports, Mexico City (MEX), Toluca (TLC), and Santa Lucia (NLU), should relieve Mexico City airport from congestion by sharing the air traffic demand amongst the three airports. Toluca and Santa Lucia airports, are located around 100 and 40 km from Mexico City airport, respectively. Toluca airport is currently operating commercial traffic, while Santa Lucia airport is currently operating only military operations.

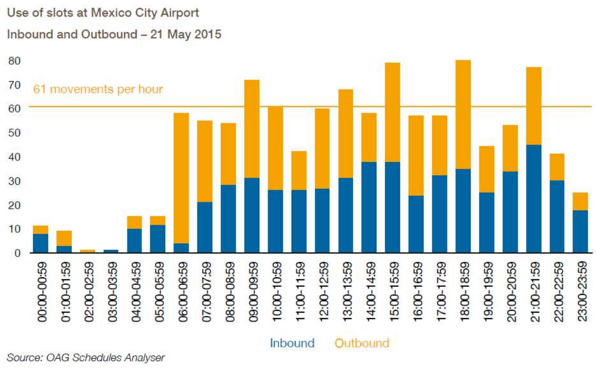

Figure 1: Daily trend of the air traffic at Mexico City airport (AOG 2019)

The proposal of the government is to upgrade and expand the facilities at Santa Lucia airport for accommodating commercial traffic. To this end, the investment in Santa Lucia airport will clearly bring the needed extra capacity to the Mexico City catchment area.
This work, is part of a study performed by the authors which focuses on the feasibility of the multi-airport system Santa Lucia-Mexico City, the current paper focuses only on the connectivity of the two airports.
Multi-airport systems (MAS) are comprised by a number of airports that provide service to metropolitan areas, where secondary airports give support to a main airport and altogether satisfy the air traffic demand. Two typical cases of MAS are New York City, where three principal airports give service to the NYC metropolitan area, composed by John F. Kennedy Airport, Newark and LaGuardia, or London whose MAS is composed by 5 airports.
The management of MASs presents a variety of operational difficulties, irrespective of political, technical and economic difficulties (de Neufville 1995). For instance, estimating the maximum and operating capacity of a MAS could be more complicated than estimating the capacity of a single airport, which is already a demanding task (Gilbo 1993), because the interactions between the operations at different airports could make it infeasible to concurrently operate all the airports at their operating capacity (Ramanujam and Balakrishnan 2009). A crucial aspect when developing a multi-airport system is to consider the connectivity between the airports and the region to be served as it was suggested by Fasone et al. (2012) and Yang et al. (2016).
The current aim of the authorities who are working on the development of the multi-airport system Santa Lucia-

Mexico City, is to develop a flexible environment where passengers that arrive at one of the two airports can be transferred to the other airport with a minimum (acceptable) connecting time.
Due to the big investments at stake for the development of Santa Lucia airport and its connectivity with Mexico city airport, it is important to properly design the infrastructures. In this context, it becomes critical the use of the right tools for evaluating the performance of the system, so that infrastructures can be designed in the most optimal way. Modeling and simulation techniques have been widely used for planning activities in various fields, from logistics to manufacturing (Banks 1998; Brunner et al. 1998; Negahban and Smith 2014), and lately some authors have also used them for airport planning purposes (Mujica et al. 2018; Mujica and Scala 2019).
Considering the previously issues regarding the multi-airport planning and design, the aim of this study is to identify and understand the limitations and impact of the connecting infrastructure in the performance of the system Santa Lucia-Mexico City. Moreover, this study will give an indication of the resources needed for the smooth connectivity operations between the two airports.
The remaining of the paper is as follows. In the next section a literature review about multi-airport system is presented. In section 3, the methodology employed in this study is described while at section 4, experiments are conducted and results shown. Lastly in the final section, conclusions are drawn.

2. LITERATURE REVIEW

Scientific community has paid attention to multi-airport systems since they are a valid alternative for absorbing the demand as current facilities are not able to cope with the growing rates of traffic.
As defined by de Neufville and Odoni (2013): “a multi-airport system is the set of significant airports that serve commercial transport in a metropolitan region, without regard to ownership or political control of the individual airports”. All multi-airport systems have a primary airport with one or more secondary airports which have less traffic than the primary airport.
The topic of MASs has been gaining some attention the last few years as many issues regarding complex airport systems have been studied. For example, the subject of the main factors involved in airport selection among customers has been extensively studied using statistical methods (Hess and Polak, 2005; Loo 2008; Ishii et al. 2009; Marcucci and Gatta 2011; de Luca 2012; Fuellhart et al. 2013; Nesset and Helgesen 2014). These papers found that air fare, access time, flight frequency, the number of airlines and the availability of particular airport–airline combinations were statistically significant factors in customer choice of airport. Interestingly, airport access time was found to be more important for business travelers than for leisure travelers. In contrast, leisure travelers were found to be more sensitive to price changes than business travelers.
The seminal paper of De Neufville (1995) introduced the analysis of the viability of MASs by identifying that air traffic of a metropolitan area should exceed 10 million originating passengers per year to make a MAS economical and operationally viable. The previous value has changed with time, and De Neufville and Odoni (2013) updated it as 15 million passengers per year. They also mentioned that this is not the only necessary condition to make a MAS economical and operationally viable, since customer and airline preferences for a primary airport is difficult to change and this might cause an underutilization of secondary airports. Furthermore, Fasone et al. (2012) and Yang et al. (2016) suggest that the viability of a MAS is intertwined with the development of other transport infrastructure, such as, railways, roads and bus services, that connects customers and cargo with the various airports in the system so that customers of the MAS could have accessible options to use any of the airports in the system and change their initial preference regarding the primary airport.
To the knowledge of the authors, none of the previous studies have analyzed the operational viability of a system using a model-based approach. In the current work this gap is partially fulfilled by simulating the connection transport line between the two airports and evaluating its performance in terms of connecting time, and other indicators related to passengers’ level of service.

3. METHODOLOGY

The methodology followed in this work, is the one presented by Mujica et al. (2018) for developing a multi model system in which a combination of models are developed in order to create one that minimizes the uncertainty associated with the modelling process (Figure 2). By using this methodology an integral model of the multi-airport is developed considering all the different components such as: terminal facilities of the two airports and the connection between them. Moreover, the different components were modeled by applying different level of abstractions, the airports were modeled in low-detailed version, while the connection between the two airports was modeled in a high-detailed version. The approach allows identifying potential problems of the future system as well as increasing the situational awareness during the planning process of the airport facilities. A more detailed description of the methodology can be found in the paper of Mujica et al. (2018).

3.1. The simulation model

The model created for this study is an extension of the model created by the group of Mujica et al. (2019). In the existing model, the two airports under study are connected to each other by a transport line (following the plan of the current

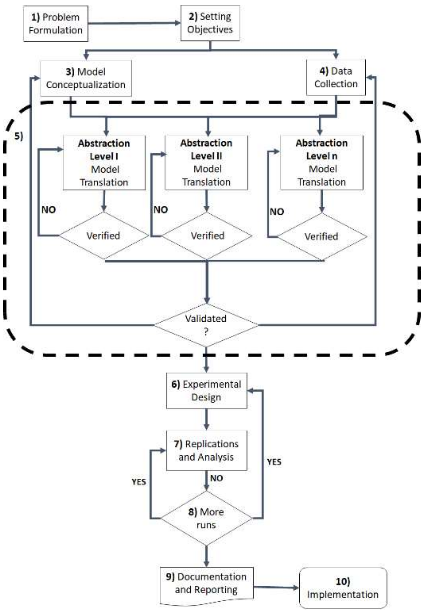

Figure 2: n-model simulation methodology

government) allowing passengers move between the two airports. The model was built considering public information from the government. Key elements were included and some assumptions were made for developing the conceptual model of the system. In addition, the boundaries of the model were set; in this case the complete airport operations were not considered, only some important processes like check-in and security in both airports were modeled as high-level models leaving some particularities out of scope. A network model was developed for simulating the flow of entities in the correspondent network. One set of entities represented passengers, another set was representing luggage while other entities represented vehicles that transport passengers and bags. It is worth to note that there can be different types of passengers making use of the connection: passengers that can check-in in one airport and then depart from the other one; passengers that arrive at one of the two airports and then transfer to the other airport in order to catch a connecting flight. These characteristics raise questions like how to handle different types of passengers and also the impact of restricting the utilization of connection only to transfer passengers. These scenarios are considered in the experimental design. Table 1 presents some of the assumptions made for the current approach. A commercial simulation software was used for translating the methodology into an integral model. Figure 3 illustrates the model developed.

Several scenarios were developed in which different options were compared, considering different demand levels, types of vehicles, share of traffic between the two airports and also the amount of bags the passengers are carrying among others.

Some of the elements that have been considered for this model are:

- Arrival and departure flights to and from Mexico City International Airport
- Arrival and departure flights to and from Santa Lucia Airport
- Transfer passengers between Mexico City and Santa Lucia airports
- A highway that connects the two airports
- Alternative vehicles for passengers transportation between the two airports
- Current and Future demand

Table 1: Model assumptions

Assumption	Value
Speed of baggage system within airport	15km/h
Distance between check-in and bus/rail station NLU	450m
Distance between check in and bus/rail station MEX	1050m
Number of active check-in desks MEX/NLU	100/100
Number of active security gates MEX/NLU	30/30
Duration of security process	Random Triangular(3,4,7) min
Vehicle boarding time per passenger	1.15 sec
Vehicle deboarding time per passenger	1 sec

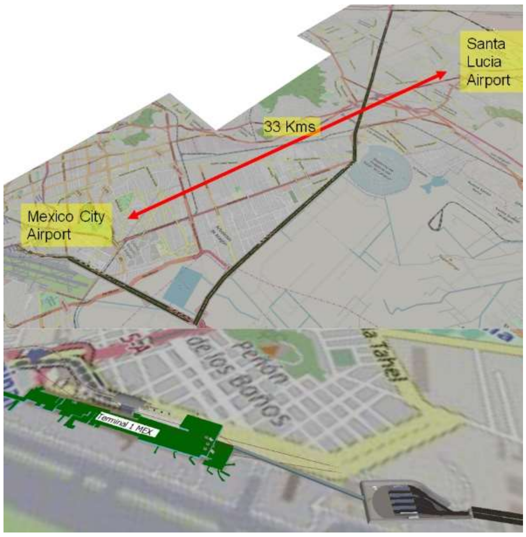

Figure 3: Simulation model snapshot for the connection

4. EXPERIMENTS AND RESULTS

In order to evaluate the performance of the multi-airport system we have constructed different scenarios and measured specific performance indicators. The scenarios were based on the following factors:

- Passengers configuration. Two configurations were considered. One where all passengers are allowed to use connection between the two airports; and a second one where only transfer passengers are allowed to use the connection.

Proceedings of the European Modeling and Simulation Symposium, 2019
ISBN 978-88-85741-25-6; Affenzeller, Bruzzone, Longo and Pereira Eds.

- Traffic scenario. Two different traffic scenarios were analyzed; short term traffic development (10% traffic increase, Scenario 2021) and medium term traffic development (60% traffic increase, Scenario 2030). The traffic increase was based on the assumption that traffic would have increased with a constant growth rate per year of 5.4% since 2014.

- Vehicle used for transporting passengers. Three different types of vehicle were tested. The first one represents a regular Bus (capacity 95 seats) (Volvo 2019a), the second one represents a BRT biarticulated bus (capacity 240 seats) (Volvo 2019b), and the last one represents an innovative mode of transport, a tram that does not require a track for moving (capacity 300 seats) (Lipeng 2018). In Table 2 the main characteristics of these transport modes are described.

Table 2: Characteristics of the vehicles utilized

Vehicle	Speed	Capacity
Bus	80 Km/h	95 pax
BRT	72 Km/h	240 pax
Trackless tram	70 Km/h	300 pax

- Number of vehicles used. For each transport mode, three different options in terms of number of vehicles were evaluated. For the scenarios where all passengers are allowed to connect between the two airports we considered the following ones:
    - Bus: [35, 40, 45]
    - BRT:[24,27, 30]
    - Tram [21,24, 27]

For the scenarios where only transfer passengers are allowed:

- Bus: [4, 8, 12]
- BRT, Tram:[3, 6, 9]

In total 36 different scenarios were evaluated for each of the two passengers configurations. The PIs measured were: minimum connecting time (MCT); vehicle utilization (VU); and passengers waiting time (WT) at the stations. MCT is the most important and representative of the multi-airport connectivity performance. It represents an indicator of the travel efficiency between the two airports and is key for the airlines to decide whether to operate in one airport or another. VU tells how efficiently the vehicles are utilized given the traffic configuration and it is directly related to the cost of operation. The WT tells how long passengers need to wait before getting to the vehicles that take them to the other terminal. It impacts directly in the level of service of passengers.

Simulations were run for a period of one day for each scenario, 50 replications were conducted in order to obtain accurate results. The PIs consider the 95 percentile of the observations.

4.1. Non restricted Scenarios

In this section, results are shown by analyzing each PI and evaluating different transport modes. This scenarios assume passengers can use the connecting vehicles indistinctly no matter if they are flying from MEX or NLU.

4.1.1. Scenario 2021

This scenario represents a short-term prediction of the future air traffic growth at Santa Lucia-Mexico City multi airport system. The main assumption behind this scenario is that the traffic will be increased by 10% compared to the current year. MCT is calculated from gate to gate between the two airports, therefore, it becomes relevant to specify from which terminal the passengers are transferring, since Mexico City has two terminals. Figure 4 and 5 are graphs of MCT versus VU for the case where passengers are transferring from Mexico City to Santa Lucia, and vice versa. Each graph shows the results according to the different options in terms of type of vehicle and number of vehicles utilized. The bars in the graph represent MCT, while the lines represent the VU. As the blue and orange bars show, the use of Busses generate a big MCT when compared to other transport mode, regardless the direction of transfer.

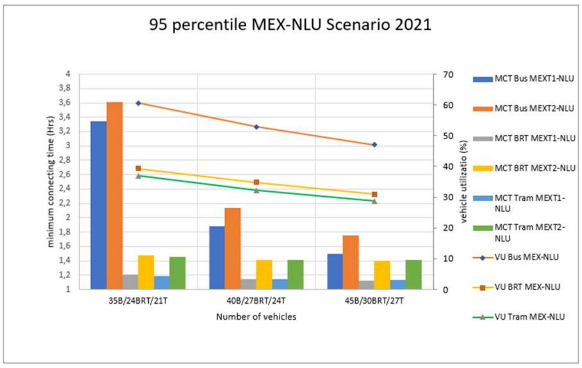

Figure 4: 95 percentile MCT vs VU from MEX to NLU for scenario 2021

We notice that for any of the options, MCT for Mexico City Airport terminal 2 are higher than Mexico city airport terminal 1, this is because terminal 2 is located in a more remote location compared to terminal1.

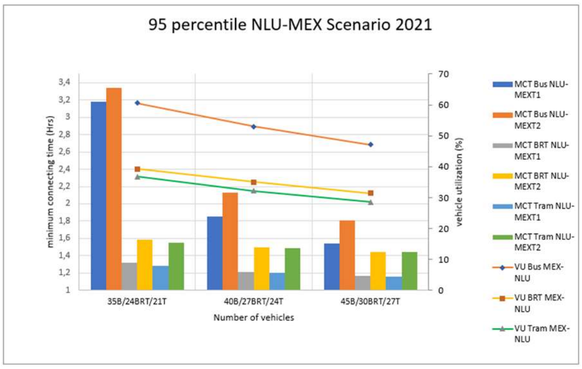

Figure 5: 95 percentile MCT vs VU from NLU to MEX for scenario 2021

The highest MCT for Buses is around 3.6 hours and it relates to the case from Mexico City airport to Santa Lucia airport with 35 vehicles utilized. The lowest MCT for the Buses was found in the scenario with 45 vehicles utilized with value of 1.5 hours, for both transfer directions. BRT and Tram show similar results, ranging from 1.4 to 1.2 hours when passengers transfer from Mexico City airport, and from 1.6 to 1.2 hours for passengers that transfer from Santa Lucia airport. Increasing the number of vehicles has a small impact of the MCT for BRT and Tram. The dependency on Buses numbers is stronger as it can be seen from the previous figures.

VU is higher for the Buses compared to BRT and Tram. It ranges between 60% and 45% for Buses, between 40% and 30% for BRT and between 35% and 28% for Tram. These results suggest that BRT and Tram provide a good level of service, however, they might be underutilized in times of the day.

Figure 6, shows the passengers WT at the stations of Mexico City and Santa Lucia for this scenario.

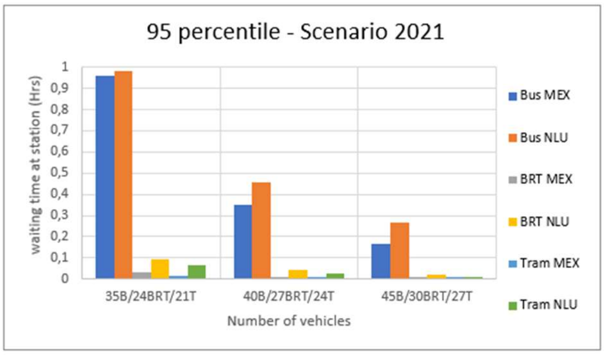

Figure 6: 95 percentile WT at station for scenario 2021

Buses have the longest WT, which is almost one hour in the worst situation. BRT and Tram show very short WT in both stations under the current numbers of vehicles, with highest values of 0,1 hours (6 minutes). Regarding Buses, they present a negative correlation with waiting times of passengers. In the best scenarios, using 45 Buses, passengers are expected to wait 0,15 hours (9 minutes) for Mexico City and 0,25 hours (15 minutes) for Santa Lucia.

4.1.2. Scenario 2030

This scenario represents a medium-term analysis of the future air traffic. The assumption is that the traffic will be increased by 60% compared to 2019. Figure 7 and 8, plot MCT versus VU for the case where passengers are transferring from Mexico City airport to Santa Lucia airport, and vice versa. In this scenario, it can be noted that in all of the scenarios analyzed, the utilization of only Buses is prohibitive, since MCT would be of several hours.

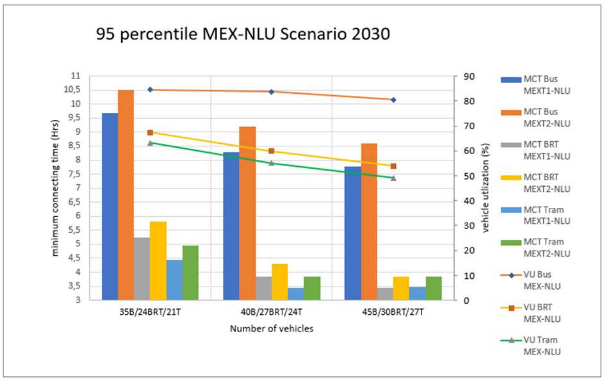

Figure 7: 95 percentile MCT vs VU from MEX to NLU for scenario 2030

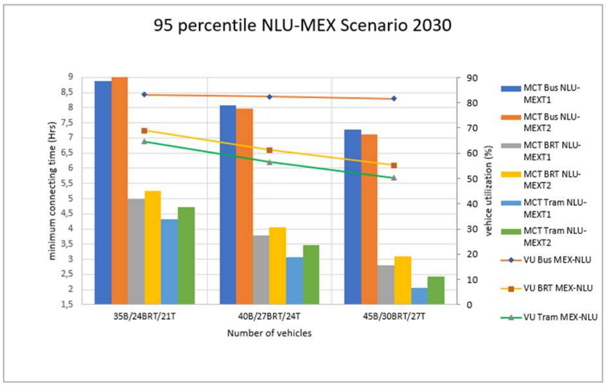

Figure 8: 95 percentile MCT vs VU from NLU to MEX for scenario 2030

For the other vehicles the amount of hours for MCT make them also unfeasible. This is an indication that other scenarios with a bigger amount of vehicles should be evaluated for the long term and also the impact of other elements in the system like security filters or check-in desks.

Regarding the scenario with the biggest amount of vehicles, Tram presents the best performance.

Regarding the WT, as Figure 9 shows, the Buses have the highest value, with peak of almost around 7 hours when 35 vehicles are utilized, and the lower value of 4 hours when 45 vehicles are utilized.

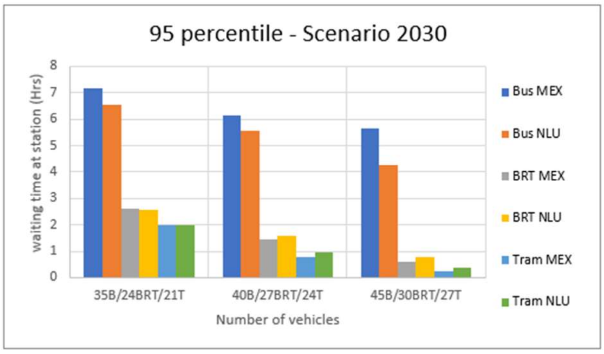

Figure 9: 95 percentile WT at station for scenario 2030

Tram show the lowest WT in both stations compared with Buses and BRT Buses, with values of 0,1 hours (6 minutes) and 0,18 hours (10,8 minutes) for Mexico City airport station and Santa Lucia airport station, respectively.

4.2. Restricted Scenarios

In these additional scenarios, only transfer passengers will use the connection between the two airports. The authors assumed that around 4% of passengers will transfer from one airport to the other. Due to the lower amount of transfer passengers considered in these scenarios, we have analyzed the scenarios considering an small amount of vehicles.

As with the previous scenarios, we evaluated the two traffic scenarios, short-term (2021) and medium-term traffic (2030).

4.2.1. Scenario 2021

Figure 10 and 11, present MCT versus VU for the case where passengers are transferring from Mexico City airport to Santa Lucia airport, and vice versa.

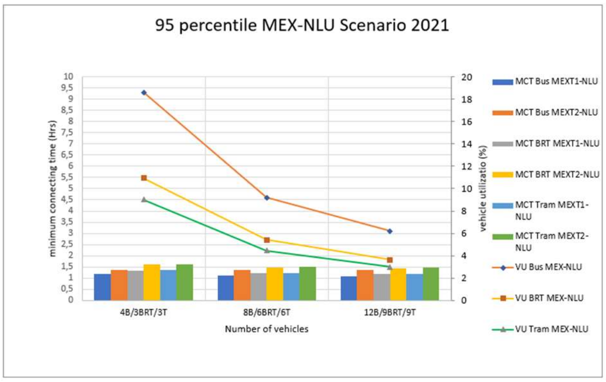

Figure 10: 95 percentile MCT vs VU from MEX to NLU, Scenario 2021 (transfer passengers)

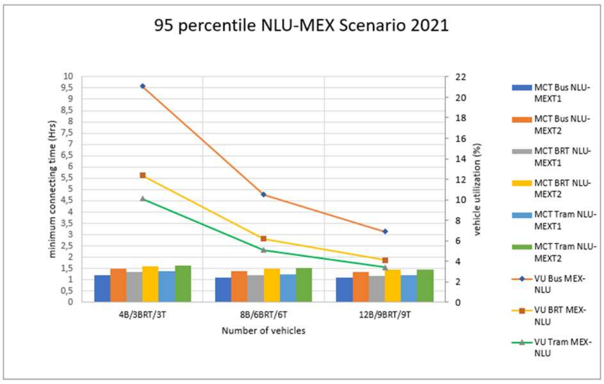

Figure 11: 95 percentile MCT vs VU from NLU to MEX, Scenario 2021 (transfer passengers)

As in the previous scenarios, the bars in the graph represent MCT, while the lines represent the VU. We notice that the use of Buses slightly outperforms the other two transportation modes. However, all of them have similar MCTs, ranging between 1.2 and 1.5 hours. Same results are obtained regardless the direction of the passengers. VU in this scenario is low, with maximum values obtained by Bus with 21% when using 4 vehicles. The use of BRT and Tram generate low vehicle utilization, almost the half compared to Buses, having 12% and 10% for BRT and Tram, respectively. These values suggest that the situation of only transfer passengers is prone to optimization of the amount of vehicles used.

As it can be noted, as the number of vehicles are increased, the vehicle utilization decreases for all the different transportation modes, while connecting times stay steady. Under this circumstance, the best scenarios would be with the operation using a minimum amount of vehicles.

Figure 12, shows passengers' WT at the stations of Mexico City and Santa Lucia. Even by testing the lowest amount of vehicles for the different transport modes, waiting times are not high, as they range between 0.18 hours (10.8 minutes), 0.9 hours (5.4 minutes). The lowest values have been found in the scenario where 12 Bus vehicles were tested, obtaining values under 0,02 hours (1,2 minutes) in both stations. However, these values do not significantly differ from the ones obtained by using less vehicles, as 0.1 hours (6 minutes) were obtained when 4 Bus vehicles were evaluated.

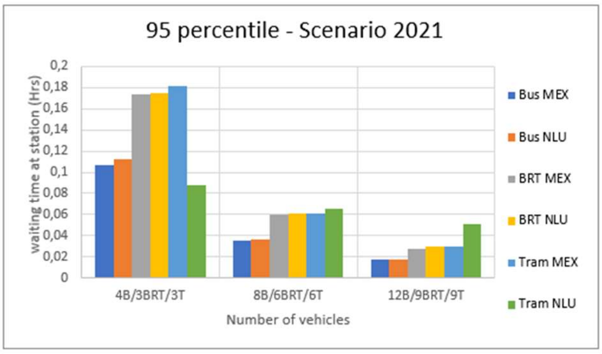

Figure 12: 95 percentile WT, Scenario 2021 (transfer passengers)

4.2.2. Scenario 2030

Figure 13 and 14, present MCT versus VU for the scenario with high demand and where only transfer passengers are allowed to use the connection between the two airports. The results obtained show similar values for the short-term scenario (low traffic amount), with values between 1.2 and 1.5 hours of connecting times regardless of the transport mode, number of vehicle utilized, and direction. In Figure 13, it can be seen that VU, show values up to 28% for Buses, 16% for BRT, and 13% for Tram. Figure 14, which represents values of passengers flow from Santa Lucia airport to Mexico City airport, show higher values of VU, with a peak, found for scenario using 4 Buses, of 38%. BRT and Tram have their peak of VU when 3 vehicles are utilized, obtaining 22% and 18%, respectively.

Figure 15 shows the values of WT at the station, where it can be noticed that similarly as the previous scenario depicted in Figure 12, values of waiting time do not vary significantly between the different use of transport mode and the amount of vehicles. Maximum values are obtained when the minimum number of vehicles is utilized, with a high peak of almost 0.27 hours (16.2 minutes) and a low peak of 0.13 hours (7,8 minutes). Minimum values of WT are obtained when the maximum number of vehicle is utilized, with a high peak of almost 0.03 hours (1.8 minutes) and a low peak of 0.02 hours (1.2 minutes).

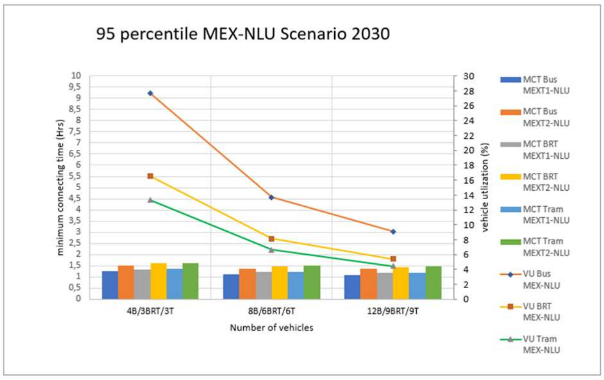

Figure 13: 95 percentile MCT vs VU from MEX to NLU, Scenario 2030 (only transfer passengers)

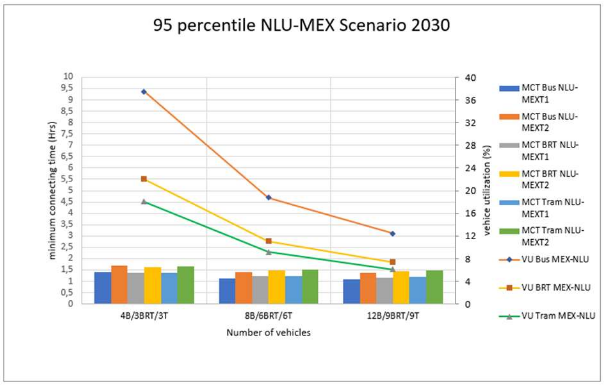

Figure 14: 95 percentile MCT vs VU from NLU to MEX, Scenario 2030 (transfer passengers)

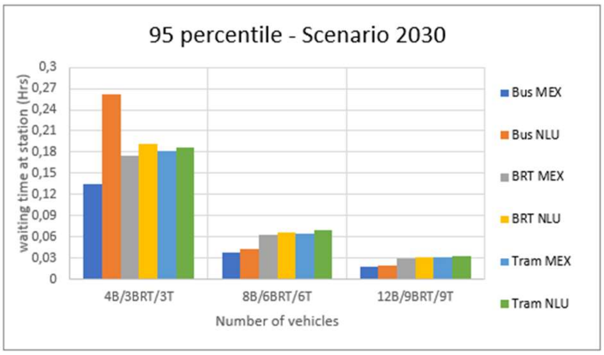

Figure 15: 95 percentile WT at station for scenario 2030 (only transfer passengers)

5. CONCLUSIONS

In this study, a simulation-based analysis has been conducted to evaluate the passenger ground connectivity between Santa Lucia and Mexico City airports which will be part of the Multi-airport system of Mexico. Different transportation vehicles were evaluated such as Bus, BRT and Tram considering minimum connecting time, vehicle utilization and passenger waiting time as the main performance indicators. Different sets of vehicles were considered for different time horizons and restrictions of use. Regarding the non-restricted scenario, the expected minimum connecting times and the amount of vehicles required to provide good service is big and highly dependent on demand. On regard to a scenario restricted to use by only transfer/transit passengers, the results clearly show that the amount of required vehicles are much less than the one of the previous scenario. For this scenario, all the performance indicators show good values with an expected MCT around 1.5 hrs in most of the cases.

It is important to remark that the study revealed that the non-restricted use of the transport connection by passengers might lead to a rapid saturation of the system when more passengers use it in the future. On the other hand, a restricted use to only transfer or transit passengers will keep the system operating at good levels even under scenarios of high demand.

Apart from the potential problems identified, it was possible to have an initial estimation of the performance of the system once it is up and running with real demand, revealing the importance of using simulation techniques.

As future work, the analysis will be further extended by considering other amounts of vehicles to find the optimal set under a multi-objective approach for balancing indicators like efficiency, service, cost and eventually environmental aspects.

ACKNOWLEDGEMENT
The authors would like to thank the Amsterdam University of Applied Sciences for the support in this research, as well as the Dutch Benelux Simulation Society (www.dutchBSS.org) and EUROSIM for disseminating the results of this work. Moreover, the authors would like to mention the support given by the International Group on Aviation and Multimodal Transport Research (IGAMT).

REFERENCES
AICM, 2019. Statistics and Flight-Schedules, Mexico City International Airport. https://www.aicm.com.mx. Accessed on April 2019.
AOG, 2019. https://www.oag.com/. Accessed on April 2019.
Banks, J., 1998. Handbook of Simulation. John Wiley $ Sons, Inc.
Brunner, D.T., Cross, G., McGhee, C., Levis, J., Whitney, D., 1998. Toward increase use of simulation in transportation. In the Proceedings of the 1998 Winter Simulation Conference, pp. 1169-1176. Dec. 13-16, Washington, DC, USA.
DOF, 2014. Declaratory: Saturation at the Mexico City International Airport. Official Newspaper of the Federation (DOF), Mexico.
de Luca, S., 2012. Modelling airport choice behaviour for direct flights, connecting flights and different travel plans. Journal of Transport Geography, vol. 22, pp. 148-163. doi: http://dx.doi.org/10.1016/j.jtrangeo.2011.12.006.
de Neufville, R., 1995. Management of multi-airport systems. Journal of Air Transport Management, Vol. 2. Issue 2, pp. 99-110. doi:http://dx.doi.org/10.1016/0969-6997(95)00035-6.
de Neufville, R., Odoni, A.R., 2013. Airport Systems: Planning, Design, and Management, 2nd eds, McGraw-Hill Education, New York.
Fasone, V., Giuffre, T., Maggiore, P., 2012. Multi-Airport System as a Way of Sustainability for Airport Development: Evidence from an Italian Case Study. Procedia – Social and Behavioral Sciences, Vol. 53 (2012), pp. 95-105. doi: https://doi.org/10.1016/j.sbspro.2012.09.863.
Fuellhart, K., O'Connor, K., Woltemade, C., 2013. Route-level passenger variation within three multi-airport regions in the USA. Journal of Transport Geography, vol. 31, pp. 171-180. doi: http://dx.doi.org/10.1016/j.jtrangeo.2013.06.012.
Gilbo, E. P., 1993. Airport capacity: representation, estimation, optimization. IEEE Transactions on Control Systems Technology, vol. 1, no. 3, pp. 144-154. doi: 10.1109/87.251882.
Hess, S., Polak, J.W., 2005. Mixed logit modelling of airport choice in multi-airport regions. Journal of Air Transport Management, vol. 11, no. 2, pp. 59-68. doi: http://dx.doi.org/10.1016/j.jairtraman.2004.09.001.
Ishii, J., Jun, S., Van Dender, K., 2009. Air travel choices in multi-airport markets. Journal of Urban Economics, Vol. 65, Issue 2, pp. 216-227. doi:http://dx.doi.org/10.1016/j.jue.2008.12.001.
Lipeng, Z., 2018. The world's ART demonstration line runs today! http://www.crrcgc.cc/en/g7389/s13996/t292853.aspx. Accessed on July 2019.
Loo, B.P.Y., 2008. Passengers' airport choice within multi-airport regions (MARs): some insights from a stated preference survey at Hong Kong International Airport. Journal of Transport Geography, vol. 16, no. 2, pp. 117-125. doi: http://dx.doi.org/10.1016/j.jtrangeo.2007.05.003.
Marcucci, E., Gatta, V., 2011. Regional airport choice: Consumer behaviour and policy implications. Journal of Transport Geography, vol. 19, no. 1, pp. 70-84. doi: http://dx.doi.org/10.1016/j.jtrangeo.2009.10.001.
Mujica Mota, M., Di Bernardi, A., Scala, P., Ramirez-Diaz, G., 2018. Simulation-based Virtual Cycle for Multi-level Airport Analysis. Aerospace, Vol 5, No. 2, pp.1-18.
Mujica Mota, M., Scala, P., 2019. Simulation of a remote runway solution for a congested airport: Mexico City Airport. Int. J. Simulation and Process Modelling (in press).
Mujica Mota, M., Di Bernardi, A., Scala, P., Delahaye, D., 2019. Simulation-Based analysis of capacity for a multi-airport system: Mexico case study. In the Proceedings of the Air Transport Research Society Conference 2019, Jul. 2-5, Amsterdam, The Netherlands.
Negahban, A., Smith, J.S., 2014. Simulation for manufacturing system design and operation: Literature review and analysis. Journal of Manufacturing Systems, Vol. 33, pp. 241-261.
Nesset, E., Helgesen, Ø., 2014. Effects of switching costs on customer attitude loyalty to an airport in a multi-airport region. Transportation Research Part A: Policy and Practice, vol. 67, pp. 240-253. doi: http://dx.doi.org/10.1016/j.tra.2014.07.003.
Ramanujam, V., Balakrishnan, H., 2009. Estimation of arrival-departure capacity tradeoffs in multi-airport systems. Proceedings of the 48h IEEE Conference on Decision and Control (CDC) held jointly with 2009 28th Chinese Control Conference. Dec. 15-18, Shanghai, China. doi: 10.1109/CDC.2009.5400462.
Volvo, 2019a. Volvo 7700 Híbrido para la Línea 4 del Metrobús. https://www.volvobuses.mx/es-

mx/news/2011/sep/news-109386.html. Accessed on May 2019.

Volvo, 2019b. Volvo 7300 Descripción general | Volvo Buses. https://www.volvobuses.mx/es-mx/our-offering/buses/volvo-7300.html. Accessed on May 2019.

Yang, Z., Yu, S., Notteboom, T., 2016. Airport location in multiple airport regions (MARs): The role of land and airside accessibility. Journal of Transport Geography, vol. 52, pp. 98-110. doi: http://dx.doi.org/10.1016/j.jtrangeo.2016.03.007.

IMPROVING DATA CONSISTENCY IN INDUSTRY 4.0: AN APPLICATION OF DIGITAL LEAN TO THE MAINTENANCE RECORD PROCESS

Francesco Longo[(a)], Letizia Nicoletti[(b)], Antonio Padovano[(c)], Agostino Bruzzone[(d)], Giovanni Mirabelli[(e)], Adriano Solis[(f)], Caterina Fusto[(g)], Jessica Frangella[(h)], Lucia Gazzaneo[(i)]

[(a)(c)(e)(g)(h)(i)] DIMEG, University of Calabria, Arcavacata di Rende (CS), Italy
[(b)]Cal-Tek S.r.l., Rende (CS), Italy
[(d)]DIME-University of Genoa, Italy
[(f)]York University, Toronto (ON), Canada

[(a)]f.longo@unical.it, [(b)]l.nicoletti@cal-tek.eu, [(c)]antonio.padovano@unical.it, [(d)]agostino@itim.unige.it
[(e)]giovanni.mirabelli@unical.it, [(f)]asolis@yorku.ca, [(g)]caterina.fusto@unical.it, [(h)]jessica.frangella@unical.it,
[(i)]lucia.gazzaneo@unical.it

ABSTRACT
Being competitive in today's global business environment requires an even higher productivity, quality, flexibility and service levels in the perspective of the new era of industrial systems based on an augmented knowledge. As a result, many companies have focused their attention on better management of their asset and equipment. In this perspective, some factories have turned to Lean Management guidelines, while others, have tried to become "smart", following the principles of Industry 4.0 paradigm. Although a positive correlation has been established between them, the integration of lean practices and Industry 4.0 remains an open question that needs to be further explored and analyzed. The paper will give a contribute to the topic, investigating this relation within asset management perspective. In particular, a 4.0 solution will be used to evaluate if and to what extent Industry 4.0 is able to implement the lean principles of Poka-Yoke. The developed tool will prove its effectiveness in solving problems related to the maintenance record management of a firm.

Keywords: Industry 4.0; Digital Lean; Poka-Yoke; Asset Management; Maintenance

1. INTRODUCTION
The survival of a company on the market depends on its capability to satisfy customers' needs in a competitive way. Market forces such as globalization and customization have exacerbated this competition, retrieving industries attention to improving their performance. Increasing productivity, reducing costs, improving quality and service levels are some of the aspects that contribute to the purpose. In this perspective, some industries have turned to lean management guidelines, while others, have started to become "smart", following the principles of Industry 4.0 paradigm. Thus, the question of evaluating the relationship between the domains arose. As a matter of facts, a positive correlation has been identified (Sanders, et al., 2016) by virtue of the Industry 4.0's capability to implement the concept of "Jidoka" (that means "automation with a human touch" or "autonomation"). Nevertheless, integrating Lean Manufacturing and Industry 4.0 is a research field that needs to be further explored (Sanders, et al., 2016), evaluating the effects also in areas such as asset management which has proved to be of fundamental importance to improve the competitiveness of a company. Therefore, the paper aims to analyze the aspects of lean manufacturing and industry 4.0 relative to asset management activities. In particular, the article will integrate the lean methodology of Poka-Yoke and the technologies of Industry 4.0 in a 4.0 mistake proofing solution that will be used to modify the maintenance management process of a firm. The introduction of the tool will eliminate the errors that currently affect machine maintenance records and will facilitate performance analysis activities.

The article is organized as follows: section 2 presents a literature review; section 3 describes the methodology adopted; section 4 introduces the case study; Sections 5 summarizes findings and results.

2. LITERATURE REVIEW
The term Industry 4.0 describes the current development phase of Industry also called Fourth Industrial Revolution which has produced a new company dimension known as the "Cyber-Physical-System" where real objects are enriched with a digital component. People and machines are interconnected, produce, share and use data that allows both to know the current situation of the system, foresee and analyze possible future scenarios and support decision making process. Industry 4.0 is the smart factories era whose advent is made possible by the so-called key enabling

technologies such as simulation, big data and analytics, cloud, additive manufacturing and augmented reality.

Lean manufacturing stems from the Japanese industrial practices of Toyota Production System. It could be referred as a philosophy, a set of principles, a manufacturing paradigm that is adopted for separating the Value-Added Activities from the Non-Value-Added ones in order to identify “muda” (or wastes) caused by the latter. Lean implementation started in automotive industry, but soon its application extended to many other industrial sectors, including textile, construction, service, food and medical sectors (Bhamu & Sangwan, 2014; Sundar, et al., 2014).

There are several tools and approach to implement lean principles whose selection depends on the purpose to be achieved. For instance, if the purpose is to eliminate defects caused by human, a good methodology is that of Poka-Yoke. Errors are eliminated by preventing, correcting or drawing attention to human errors as they occur, promoting the principles described in Table 1.

Poka-Yoke (or “mistake proofing”) can take prevention or detection forms. Depending on the severity, frequency or downstream consequences, prevention-based mechanisms signal or halt processing when abnormalities are about to happen. The detection-based forms, instead, are used when is not possible or economically feasible to prevent defects. Poka-Yoke should be simple objects and devices used all the time by all the operators where mistakes occur in order to cheaply eliminate defects. Each approach is achieved through a specific method. In particular, the detection form of Poka-Yoke can use the contact-method, which tests the characteristics of a product in order to identify a defect; the fixed value-method which ensures that all parts of a product are available in the right quantities; and the motion-step-method, which ensures that the activities needed to obtain an output are performed in the right number and sequence (Malega, 2018).

Table 1: Basic principles of Poka-Yoke

Principle	Objective	Way
Elimination	Eliminating the possibility of error	Redesigning the process/product
Replacement	Replacing the process with a more reliable one	Using automation
Facilitation	Making the work easier to perform	Color coding
Detection	Detecting the error before further processing	Developing software which notifies a worker when a wrong input is made

Both Industry 4.0 and Lean Manufacturing aim to increase flexibility and productivity of a firm. While Lean is a well-established methodology, Industry 4.0 is a relatively new paradigm, thus there is a shortage of studies exploring their link (Buer, et al., 2018). Nevertheless, a positive relationship has been identified (Sanders, et al., 2016). In particular, the technologies and concepts of the Fourth Industrial Revolution seem to act as enablers of Lean dimensions, increasing the technical feasibility and the related benefits. For instance, by producing Smart Products and giving the possibility to collect and analyze a huge amount of data, Industry 4.0 allows a strong involvement and integration of customers in the business process where the data collected are used to anticipate their needs and can be instantaneously shared along the entire supply chain; while the use of tags and wireless tracking promotes JIT delivery of goods by suppliers. As regards Asset Management, the most obvious implications concern maintenance operations. Indeed, data collection, data interchange and (big) data analysis of CPS support the principles of Total Productive Maintenance, including monitoring and improvement of the Global Plant Efficiency, development of autonomous preventive maintenance and predictive maintenance. On the other hand, Augmented Reality has proven a great potential for maintenance operations, providing augmented contents on one side and enriching maintenance experience on the other side. The classic lean tools are changing as well. As a matter of facts, there are many empirical applications showing how Lean tools are losing some of their initial edge (Behrendt et al., 2017). Striking examples are that of Virtual Kanban used to replace physical cards for order-oriented production control and inventory control (Filho & Lage, 2010) or the iBin System for Kanban bins where a camera is used to detect the charging level of the bin and the iBin reports the information to the inventory control system and automatically sends order to suppliers (Würth Industrie Service GmbH & Co. KG, 2013).

The implementation of lean principles through Industry 4.0 technologies offers many opportunities, but also challenges. Indeed, rush in automation without analyzing and identifying the sources of wastes will led to digitize inefficiencies (Nafais, 2017). In a nutshell, while lean approach could be seen as the lynchpin of operational improvements, process standardization, and promotion of kaizen, Industry 4.0 should be seen as a provider of advanced technologies and solutions that are selected and adopted to implement the lean guidelines. In this perspective “Industry 4.0 is just the topping on the cake” (Rüttimann & Stöckli, 2016).

3. METHODOLOGY

In order to achieve the aims of this study, the traditional maintenance process in manufacturing industries has been analyzed. The current process has been then redesigned by introducing an ad-hoc tool integrating Industry 4.0 key enabling technologies and Lean manufacturing principles, i.e. the Poka-Yoke practice.

The developed mobile application is presented and later deployed in an industrial case study.

3.1. Initial maintenance management process

In order to identify the underlying reasons of the problem, a traditional maintenance process in manufacturing industries has been analyzed. The maintenance process usually involves three different actors: the operator, the Head of Maintenance and the Maintenance operator. Maintenance operations are also frequently outsourced; thus, both the Head Maintenance and the Maintenance Operator are external to the company. When an abnormality or a failure occurs (e.g. vibration of the axis, head locking, refrigerant leakage, etc.) the asset puts out a signal. The operator is in charge of detecting the signal and filling a maintenance job request. In particular, he fills the request manually, entering on a sheet the following information: plant location, identification number of the maintenance job request, alarm code, the description of the alarm code, the description and the details of the alarm, the ID of the asset, the location of the asset, the signalman's ID, and the reporting date. The sheet constitutes the maintenance record of the asset. Once completed the filling, he sends a copy of this maintenance job request to the head of maintenance. The head of maintenance takes the request in charge, analyses it and, considering also the maintenance orders previously scheduled, draws-up and updates the maintenance plan. According to the scheduled interventions, a maintenance operator will perform the maintenance operations. Hereafter, the Head of Maintenance will check if the cause of the alarm has been solved (eventually, a second intervention could be rescheduled). Both the Head of Maintenance and the maintenance operator are required to fill the remaining fields of the maintenance record. In particular, the Head of Maintenance will enter the references of maintenance operators (ID and name), the expected starting and closing dates for maintenance operations, and the check period, while maintenance operator will enter the information about the effective starting and closing dates. The entire process is resumed in Figure 3.

Due to the manual filling of maintenance records carried out by the maintenance personnel, a high delay in managing breakdowns or alarms occurs. Furthermore, since the data are not structured and incomplete, this slows down the process. In particular, the data inconsistency errors can be classified as follow:

1. data are incomplete;
2. data are affected by typos;
3. the terminology used to describe the same type of error is not uniform.

The consequences of maintenance data inconsistency errors are the following:

1. there are no records of a performed maintenance task or of an executed intervention on machines;
2. it is not possible to trace back to the person in charge of a maintenance track or the person who performed maintenance tasks;
3. it is not possible to evaluate delays with respect to the maintenance plan;
4. it is not possible to analyze and improve the maintenance process or to assess the performance of the third-party company in charge of the maintenance activities.

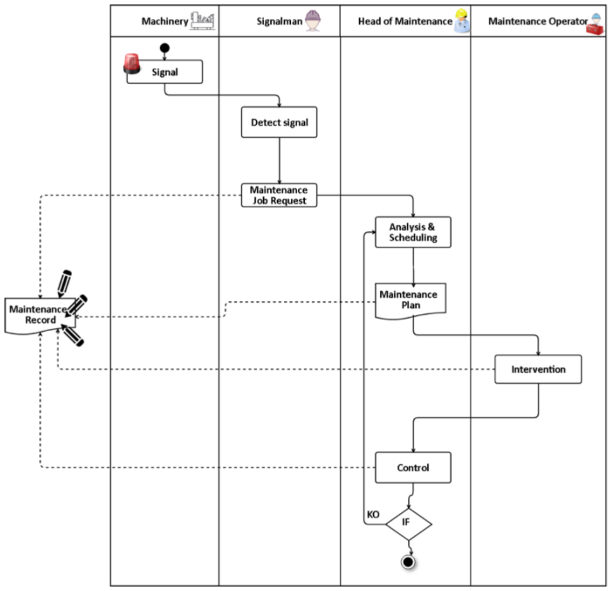

Figure 1: The initial maintenance management process

3.2. An Industry 4.0 driven Poka-Yoke approach

The above described process can benefit from an Industry 4.0 driven Poka-Yoke approach, which is aimed at solving data inconsistency errors in maintenance. The process can be indeed re-designed as in Figure 4. Once a signal has been notified by an equipment, the signalman is in charge to detect it and fill a job request. The operator will be allowed to send the job request to maintenance office if and only if he will complete all the required fields. By scanning a QR code or by selecting the machine among the list of the available ones, the operator will identify the machine where the failure has occurred. All the information about the machinery (e.g. plant, location, production orders) will be automatically reported on the job request. Then, the signalman will be required to select (or insert) the alarm code notified by the machine. Once again, the description of the error will be automatically reported on the job request. The operator will be allowed to send the job request only when the two fields (alarm code and machinery ID) will be filled. Once received the request, the head of maintenance will prepare the maintenance plan. The order will be not saved and notified until the required fields (e.g. estimated times and dates, maintenance operator reference). Similar considerations can be made with respect to the remaining operations (maintenance intervention and equipment control).

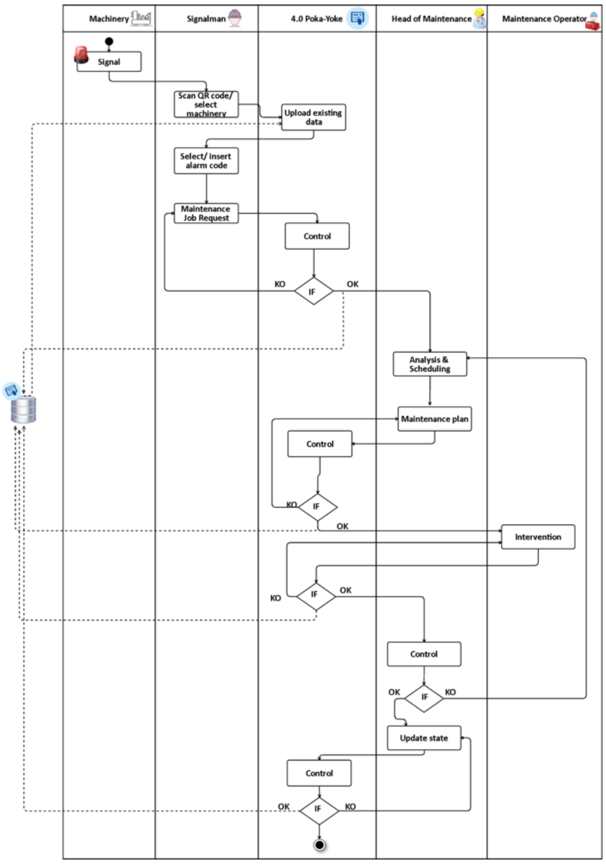

Figure 2: The maintenance management process after the introduction of the 4.0 Poka-Yoke

3.3. A new 4.0 application to implement Poka-Yoke in the maintenance process

A new 4.0 application to implement Poka-Yoke in the maintenance process has been developed. It uses the Industry 4.0 technologies on one hand, embedding and implementing the Poka-Yoke tenets on the other. Basically, the solution allows Knowledge creation and Knowledge Management. the architecture of the system could be described as the set of two collaborative parts: the contents manager and the contents user. The former, cloud-based, provides a series of functionalities for implementing the contents, the data and metadata (e.g. name, ID, description, QR code, 3D model, AR contents, etc.as shown) related to a particular object (e.g. a plant or an equipment) as shown in Figure 1, while the latter allows to access data and contents and to enter data as well, as shown in Figure 2. The underlying architecture is developed by using the Laravel framework and includes a relational MySQL DB, the Java-based Apache Solr open source research framework (containing a non-relational database) that uses the Lucene Java search library for full text search and indexing; HTTP / XML APIs (e.g. REST and JSON) for data search. The system is provided on web/mobile applications that make the platform easy to use.

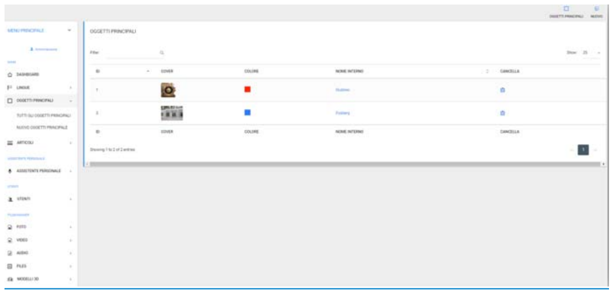

Figure 3: Contents creation

Figure 4: Contents fruition

The capability of the solution to implement the principles of Poka-Yoke has been tested within maintenance process of a firm. To this end, the maintenance process of the company has been evaluated and formalized through the use of flow charts. Then, the maintenance records collected by maintenance personnel have been analyzed allowing to reveal problems in data consistency due to the manual filling of records performed by operators. The solution has been customized to address these problems, entering the objects needed to prevent errors (such as alarm codes, machineries ID and operators ID). Finally, this application has been deployed into a real industrial environment and changes introduced by poka-yoke in the maintenance process and in maintenance records have been analyzed.

3.4. Case study

The application study involved an enterprise that is active in the Oil & Gas industry and produces heat exchangers. Currently, the company pursues two maintenance strategies: corrective maintenance and preventive maintenance. The former is performed when assets break down. The latter is performed to lessen the likelihood of equipment failing. Preventive maintenance is performed while the equipment is still working; it can be scheduled on a time or usage-based trigger. Actually, there is a substantial difference between the moment when a failure or a problem has been detected and the moment when the problem is solved, and this causes wastes and delays on product delivery. Additionally, the company is not aware whether excessive preventive maintenance is performed, whether the adopted maintenance intervals could be reduced or increased. Finally, the enterprise can’t easily carry out analysis of performance.

4. RESULTS AND DISCUSSION

Analyzing the data collected during the period June 2017 until June 2018 in the company under study, it has been noticed that the delay in maintenance scheduling is attributable to the manual filling of maintenance records carried out by the maintenance personnel and the data kept therein. Indeed, the scheduling is based on the analysis of information included in the maintenance records and, since the data are not structured and incomplete, this slow down the process. Considering the "closed" maintenance orders and assuming that the expected start dates coincide with the effective dates when maintenance operations are performed, it is possible to observe how on 758 maintenance job requests, the 43% has been turned to maintenance orders between 12 and 15 months, while the remaining 57% between 6 and 12 months. Considering the average case, the total time required to schedule the maintenance orders could be estimated as a percentage of the time required to turn the maintenance job requests in maintenance orders. Assuming a percentage of 10%, the total time required to schedule the maintenance orders is 1 month. This time is due to the errors that affect data.

Using the data inconsistency categories to characterize the data collected during the reference time, the errors made by the operators have been classified as shown in Table 2.

Table 2: Errors performed by the signalman

	Missing Data	Typos	Heterogeneous Terminology
Plant	0,26%	5%	0%
Maintenance Job Request ID	0,13%	3%	0%
Alarm code	99,6%	0%	0%
Alarm description	0,13%	65%	40%
Signalman ID	0,26%	0%	0%
Signalman's name	43,27%	10%	0%
Reporting date	0,78%	13%	10%

The alarm code that allows to identify the root causes of the problem, the resource to use and the solution to be adopted, lacks 99% of the time. From the other hand, the description that could replace the use of the alarm code is affected by typos (65%) or the same problem is described in different ways.

Moving the attention on analysis of performance, it is affected by the same problems. Over the errors performed by the internal operators, the ones performed by the maintenance officers are noticed (Table 3 and Table 4). For instance, the expected start and end dates lack the 90,5% of times, as well as the information related to the maintenance operator lacks the 43,27% of time.

Table 3: Errors performed by the head of maintenance

	Missing Data	Typos	Heterogeneous Terminology
Maintenance Job Order ID	90,5%	10%	0%
State of the Order	0,26%	30%	0%
Maintenance Operator ID	43,27%	10%	0%
Maintenance Operator name	43,27%	10%	0%
Expected start time	67,15%	0%	0%
Expected end time	65,3%	10%	0%
Expected start day	90,5%	12%	19%
Expected end day	90,5%	10%	23%
Check period	0,26%	7%	23%

Table 4: Errors performed by the maintenance operator

	Missing Data	Typos	Heterogeneous Terminology
Effective start time	90,5 %	7%	3%
Effective end time	90,5%	2%	0%
Effective start day	12,8%	10%	15%
Effective end day	12,93%	14%	20%

The following observation can be done.

1. The 4.0 tool could be described as a process standardization that embeds and implements the elimination, replacement and facilitation principles of Poka-Yoke. Indeed, by substituting the sheet with the application, the possibility of make error has been eliminated.
2. By inserting check points on data structure and completeness and providing a list of predefined information, the possibility to have unstructured or missing data has been avoided. Thus, the process is more reliable.
3. In addition, it is possible to say that the process has been facilitated. Indeed, having a digital DB with structured and integral data instead of sheets, allows head of maintenance to schedule

more quickly the maintenance orders and plans. The previously estimated time (e.g. 1 month) has been eliminated. This means providing a better level of service to the customer. On the other hand, the possibility to have data aligned and updated between parts, allows firm to perform evaluation both on the plants and maintenance personnel.

The 4.0 tool assumes the prevention form of Poka-Yoke. As stated before, the structure prevents all the human errors resumed in Table 2, Table 3 and Table 4. It implements the motion-step method, because ensure that all the activities necessary to fill the maintenance records will be performed by personnel.

5. CONCLUSIONS AND FURTHER RESEARCH

Issues related to the collection, use and store of accurate and reliable data are currently very common among industries (Christiansen, 2018). The proposed paper discusses about the relationship between Industry 4.0 and Lean Manufacturing within Asset Management area. Since Lean Principles should shape the relation, the lean methodology of Poka-Yoke has been selected and a 4.0 solution has been implemented. The ability of the solution to embed and implement the lean tenets and provide clear benefits to the maintenance process has been evaluated in a firm operating the Oil & Gas industry. Further research will be devoted to assess the impact of the developed tool on the firm's productivity, to integrate the tool with other company management systems and extend its use to other processes.

REFERENCES

Alkhoraif, A., Rashidb, H. & McLaughlin, P., s.d. Lean implementation in small and medium enterprises: Literature review. Operation Research Perspectives, Issue https://doi.org/10.1016/j.orp.2018.100089.

Bhamu, J. & Sangwan, K. S., 2014. Lean manufacturing: Literature review and research issue. International Journal of Operations & Production Management, July, pp. 876-940.

Buer, S.-V., Strandhagen, J. O. & Chan, F. T. S., 2018. The link between Industry 4.0 and lean manufacturing: mapping current research and establishing a research agenda. The International Journal of production Research, 56(4), pp. 1-17.

Christiansen, B., 2018. 4 Biggest Building Maintenance Challenges and Solutions.

Filho, G. & Lage, J. M., 2010. Variations of the kanban system: literature review and classification. Int J Prod Econ, Volume 125, p. 13–21.

Malega, P., 2018. Poka-Yoke - solution to human errors in the production process. The International Journal of Business Management and Technology, 2(5), pp. 207-213.

Nafais, S., 2017. Manufacturing, Automated Lean. Kingston University London.

Rüttimann, B. G. & Stöckli, M. T., 2016. Lean and Industry 4.0—Twins, Partners, or Contenders? A Due Clarification Regarding the Supposed Clash of Two Production Systems. Journal of Service Science and Management, Volume 9, pp. 485-500.

Sanders, A., Elangeswaran, C. & Wulfsberg, J. P., 2016. Industry 4.0 implies lean manufacturing: Research activities in industry 4.0 function as enablers for lean manufacturing. Journal of Industrial Engineering and Management (JIEM), 9(3), pp. 811-833.

Shrimali, A. K. & Soni, K. V., 2017. A Review on Issue of Lean manufacturing Implementation by Small and Medium Enterprises. International Journal of Mechanical and Production Engineering Research and Development, 7(3), pp. 283-300.

Sundar, R., Balaji, A. N. & SatheeshKumar, R. M., 2014. A Review on Lean Manufacturing Implementation Techniques. Procedia Engineering, 97(12th GCMM), pp. 1875-1885.

Würth Industrie Service GmbH & Co. KG, 2013. iBin(R) stocks in focus—the first intelligent bin

MACHINE LEARNING TO SUPPORT INDUSTRIAL DIGITALIZATION AND BUSINESS TRANSFORMATION

Agostino G. Bruzzone[(a)], **Marina Massei**[(b)], **Kirill Sinelshchikov**[(c)], **Giuliano Fabbrini**[(d)], **Marco Gotelli**[(e)], **Alberto Molinari**[(f)]

[(a), (b), (c)] Simulation Team, Genoa University
[(d), (e)] SIM4Future
[(f)] Liophant Simulation

(a), (b), (c) {agostino.bruzzone, marina.massei, kirill}@simulationteam.com
[(d), (e)] {giuliano.fabbrini, marco.gotelli}@sim4future.com
[(f)] alberto.molinari@liophant.org

ABSTRACT
This paper addresses use of Artificial Intelligence (AI) and in particular Intelligent Agents (IA) in order to evaluate efficiency of information exchange and awareness in Small and Medium Enterprise (SME), with particular attention to digital transformation. To perform required experimentation, the authors have developed a Serious Game (SG) named JANUS, in which the player interacts with intelligent agents representing a virtual company and its actions aim to acquire as much as possible data about the organization.

Keywords: Modeling, Simulation, AI, IA, ANN, Data analytics, CPM, CRM, Digitalization

1 INTRODUCTION

Given the evolution in business processes as well as the rising of technological enablers, digital transformation is one of the main trends in development of modern business along these day. For instance, modern software packages and solutions are used to support activities for a variety of different fields and industries, such as supply chain management, customer management, organization support, production, service and maintenance.

Based on the state-of-the-art, it is confirmed that data analytics and business intelligence are some of the main pillars of digital transformation because allows to provide valuable information to the people to support decisions as well as guide effective management. At the same time, particular attention should be focused on aspects such as digital marketing operations and corporate performance management. Hence, these sectors are very promising in terms of potential business improvement through innovative solutions able to react promptly to situation evolution and to capture expectations and behaviors of existing and potential customers. All these potential achievements are strongly related, not only to the capability to properly redesign business processes, but also to human resources attitudes and capabilities and from this point of view it is evident the necessity to develop the cultural background in the companies to get full advantage of these technologies. At the same time there is a significant need for introducing new people and to train them to become familiar with the concepts as well as with the software solutions and new organizational processes.

2 NEEDS AND CHALLENGES

Due to these reasons, it was decided to develop a serious game devoted to test ability of a young engineer or consultant to face the challenge of a transformation project within a company and to study the potential of this kind of application as well as the different further development that could be enabled by integrating it with Intelligent Agents. So this study focuses on the different approaches devoted to design and deliver new solution enabling cutting-edge services based on available big data and related capabilities in checking, validating and mining them. This opportunity (innovative business models and management) is very attractive to industries, but obviously requires a clear understanding of capabilities, constraints and critical issues in introducing, activating and using modern integrated solutions such as CRM (Customer Relationship Management) and CPM (Corporate Performance Management) (Bohling et al. 2006). Indeed, a crucial aspect identified during the business experiences matching with research results, it was that digital transformation and big data analysis allow both redesigning business models and change also the roles of those working in business analysis and business management. Obviously, introducing systems which integrate company information may cause new possible vulnerability and point of failure. Indeed, if compromising a single computer typically was not an issue for stand-alone systems, for today's integrated systems the risk to lost all information at once creates a lot of concerns in companies (Bruzzone, 2017b).

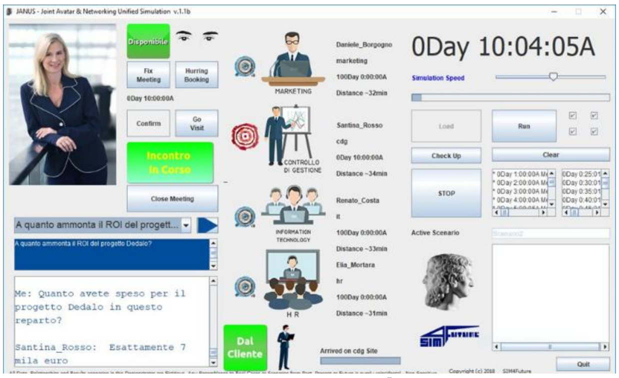

Figure 1: Janus Simulation

3 DIGITAL TRANSFORMATION PROJECTS

It was decided to consider the transformation projects as the mission environments to be used to develop this new capability and the scenario for the serious games. Among the different ones, considering current business development and in reference to previously mentioned aspect the focus was on transformation initiatives based on adoption of CPM and CRM solutions. Indeed, these kind of systems are expected to be able to improve the efficiency of company management and reactivity to external and internal stimulations; therefore to achieve these results it is fundamental to properly develop, implement and use these tools and it is not rare to observe projects of transformation that fall into a deadlock or that don't perform as expected. Due to these reasons the use of serious games to train, evaluate and even learn new correlations on resources involved in these initiatives resulted very interesting. Indeed, the spectrum of cases is pretty wide; in some case the companies do not have the resources (in terms of finance or people) to guarantee the possibility to introduce new systems all over the processes, hence, they keep using "legacy" applications, sometime quite obsolete; otherwise spreadsheets are extremely popular and result often the preferred office package to support business processes with all flexibility advantages, but also strong limitations for common work, reliability, reuse, sharing, updates, etc; these situations are quite typical for small companies, but also big companies are afflicted by these cases with the additional aspect to have a galaxy of different solutions with very limited and "unreliable" integration (Krumbholz et al. 2001; Gérpm 2017). In some other cases, problems are related to improper systems configuration and use, which is often caused by not skilled, or not motivated, personnel, which result often into not being capable to benefit from the potential of valuable solutions. Among the multiple critical issue, it should be mentioned, that the development and implementation team often are not very well amalgamated and could have different specific goals that tend to increase project duration, unnecessary customization, twisted processes and so on. In any case, in order to improve overall efficiency in one of this projects, it is necessary to understand quickly all possible pitfalls of the business process, define where and how to introduce digitalization and check what kind of risks are related to the introduction and utilization of new systems considering both ICT, business and human factors (Bruzzone et al. 2004).

4 JANUS

Due to the above mentioned issue the Simulation Team have developed JANUS (Joint Avatar & Networking Unified Simulation), a discreet event stochastic engine acting as a Serious Game capable to reproduce human behaviors and reactions. JANUS is specifically designed to be adopted in scenarios related to business digitalization. In order to improve involvement and motivation of the players it was decided to adopt the MS2G approach (Modeling, interoperable Simulation and Serious Games) that guarantee the engagement of user and modularity of the models (Bruzzone, 2018; De Gloria et al., 2012). In fact, the creation of interesting and immersive scenarios allows to achieve multiple objectives, for instance to acquire more data by stimulating player to perform more simulation runs; in this way it is possible to use the serious games not only for training of people assessment, but also to capture emergent tactics and effective playing strategies by the multiple users based on crowdsourcing approach (Massei et al. 2014; Bruzzone et al.2017c). In JANUS, it was created a set of predefined data for basic playing, therefore, the system is fully open to be further integrated with other models and data, modifying information accordingly to the parallel evolution of the scenario thanks to the flexibility of the proposed interoperable models. Indeed, JANUS is a Serious Game (SG) devoted to address multiple business and consulting issues including among the others virtual interview with avatars controlled by Intelligent Agents (IA), as well as time management and meeting scheduling considering human behavior modifiers (HBM). In this case study, the intelligent agents represent key figures of a company (i.e. managers of different divisions) that play their specific roles while demonstrating their individuality due to their cultural heritage or background (Bruzzone et al., 2015; Bruzzone, 2017a). Indeed, every avatar is characterized by a set of individual characteristics including among the others: cultural, educational and professional background, as well as social network in the company; in addition the avatar is characterized by its openness to change, hostility to consultants, smartness, laziness, punctuality, precision, aggressiveness, stress, fatigue, fear, reliability and honesty. The use of intelligent agents as sparring partners allows not only to challenge the player, but also to improve the quality of interactions during the game, making the entire experimentation immersive and engaging (Bruzzone et al., 2014). As demonstration of this fact, the authors observing neutrally the users at "play" with JANUES collected evidence of emotional engagement by laughing, snorting and swearing at the computer based on the IA reactions. In facts, the JANUS scenario evolves in time as well as based on actions of the player. For example, delays on meetings or improper behaviors influence the avatars and make them more hostile and less available in providing reliable and precise feedback and values on the company's Key Performance Indicators (KPI). This may reach extreme outcomes (i.e. avatars refuse the meeting or lie to the human player). By the way the incorrect data provided by avatar could be identified by data mining different virtual managers reports and simulated project evolution during the game by smart players that pay attention to the general situation. Indeed, player's actions impact on the perception of the avatar, which could become friendly and open or hostile and aggressive. In order to conduct the experimentation, it was selected a set of professionals working in the field of interest, mostly from consulting companies, as well as university students in management and engineering. During the experimentation, these players had the possibility to run multiple time JANUS analyzing each time a different scenario generated stochastically by the game, with different virtual managers and digitalization projects. For each run it was possible to collect logs and data regarding the evolution of the scenario and the state of the virtual environment, such as company's data, avatars' parameters, players' interactions, etc. The application logs have been collected, filtered and analyzed in order to assess also players' skills in terms of evaluation capability in various cases, such as in with or without presence of new valid CPM and CRM solutions. In order to analyze experimental results, the authors have decided to developed an Artificial Neural Network, (ANN) able to assess the performance enhancement caused by using the CRM/CPM solutions on the specific digitalization project and, at the same time, discriminate various capabilities of human players based on their interviews with avatars. Indeed, each player has to plan the interviews with avatars, develop time schedule for visiting offices and departments avoiding delays, time slot overlapping and, finally, conduct interviews selecting available questions (fig.1)

4.1 IMPLEMENTATION DETAILS

From the beginning of the study, it was planned to involve large number of people in the experimentation phase; typically, in such situations participants use different versions of distinct operation systems. To guarantee portability, flexibility easy use and compatibility issues, the authors have adopted Java programming language to make the Serious Game platform independent; indeed even the Graphic User Interface (GUI) is implemented in simple, but reliable, way by Java Swing toolkit. Given this architecture, many professional consultants, as well as students within these fields of interest, were able to be easily involved in the experimentation and to provide the authors with sufficient data sets for analysis.

5 DATA ANALYTICS AND AI

Obviously, there are numerous possibilities to analyze experimental data, starting from basic statistical analysis up to artificial intelligence; often, it is convenient to adopt more than one (Montgomery, 2017). Indeed, the authors have used different techniques for different datasets; for instance, the duration of tests and percentage of errors performed by the players was compared based on their statistical distribution. At the same time, the performance of the virtual company and avatars, in the different scenarios (with or without information management solutions), was assessed using ANN (Artificial Neural Network).

Obviously the proposed results in this paper represents only a preliminary demonstration of a potential ability to develop a support system for assessment sessions, meetings and interviews with experts. In order to perform data classification, the authors have developed an application using Tensorflow library for Python.

According to the number of variables to be taken into account and number of possible categories for classification, input and output layers of the neural network have been experimented with 14 and 4 neurons each. At the same time, a specific analysis was carried out to identify the optimal numbers of neurons in the hidden layer for this case and experimentally it resulted to be equal to 20.

Furthermore, the authors tested different types of activation functions and type of gradient based optimization, finding that in the case of interest Hyperbolic Tangent Activation Function (tanh) and Root Mean Square Propagation (RMSProp) are most suitable candidates (Géron, 2017). It is possible to state that developed ANN allowed to achieve almost 96% precision in classification after 1000 cycles of training just over the testing data set.

6 MODELS AND PLAYING MODES

As mentioned, in order to perform experimentation, the authors have developed multiple scenarios, characterized by different sets of parameters to be identified, possible questions and answers as well as behavior of the avatars.

The players are able to plan meeting with the departments' representatives in order to interview them and collect the desired information. Due to the stochastic nature of the simulation, the participant could face partial or complete overlapping of meetings times, as proposed by the avatars, hence, being forced to choose between delays or postponing some meetings. Obviously, in such circumstances, some avatars could become less friendly to the user, or even hostile. Another possibility to face unfriendly behavior is to arrange multiple meetings with the same persons, each time obtaining only partial information.

Based on the perception of the avatar, the dialog options could differ, while provided information could be more or less precise. Indeed, the participants were required to run the simulation multiple times, performing required set of interviews with IA and indicating their guesses about values of the parameters of interest at the end of each run; data acquired at each step of the game was saved in dedicated log files to be consequently analyzed by the authors.

7 RESULTS

By applying ANN to the data from the log files, it was confirmed a strong correlation between level of digitalization of the virtual company and error level made by the player while guessing parameters values during the simulation; the precision of estimation highly depends on such systems as CPM and CRM. As anticipated, the ANN is capable to identify presence of new reliable software solutions with precision almost 96% (this based only on the estimation of error values) confirming importance of employment of such systems in companies. Another interesting data was obtained by analyzing logs corresponding to multiple sequential simulation runs performed by the same player. Indeed, while large part of the participants conducted only 2 simulations, many players did 4 or more runs. In such cases it was found that precision of human players typically demonstrates notable improvement after the second run, when estimation error of correct values decreases by almost 20%. More significant difference is observed in case of comparison of simulation duration. In this case, typical duration of runs decreased by more than 50% after the 3rd tentative, which is likely related to the familiarization with the software.

8 CONCLUSIONS

The proposed approach made possible to finalize a general analysis on digitalization solutions and methodologies in relation with actual case studies.

A simulation engine has been developed and implemented into a serious game able to engage users into challenging scenarios related to company digitalization projects.

In facts, the experimentation conducted with professionals from consulting companies, led to validate the system for this operating context.

Therefore just preliminary results of the experimentation carried out on these models is proposed within this paper, therefore the authors are active in conducting additional tests and experimentations as well as extending the simulation engine and IA capabilities.

A basic artificial neural network has been developed, then its ability to learn correlations and classify the different cases has been assessed, evaluating its generalization capacity. These experimental results are obviously only a starting point, a demonstration of a potential capacity which, based on the results, looks promising. In the future, the author expect also to further develop similar games to be applied extensively in consulting and digitalization projects to support actors in this field and to assess the skills of potential new resources.

REFERENCES

Bohling, T., Bowman, D., LaValle, S., Mittal, V., Narayandas, D., Ramani, G., & Varadarajan, R. (2006). CRM implementation: Effectiveness issues and insights. Journal of Service Research, 9(2), 184-194.

Bruzzone A.G. (2018). MS2G as pillar for developing strategic engineering as a new discipline for complex problem solving. In proceedings of 30th European Modeling and Simulation Symposium, EMSS 2018 pp. 405-411.

Bruzzone A.G. (2017a). Smart Simulation: Intelligent Agents, Simulation and Serious Games as enablers for Creating New Solutions in Engineering, Industry and Service of the Society. Keynote Speech at International Top-level Forum on Engineering Science and Technology Development Strategy- Artificial intelligence and simulation, Hangzhou, China.

Bruzzone, A.G. (2017b). Information Security: Threats & Opportunities in a Safeguarding Perspective. Keynote speech at World Engineering Forum, Rome, Italy.

Bruzzone, A. G., & Massei, M. (2017c). Simulation-based military training. In Guide to Simulation-Based Disciplines (pp. 315-361). Springer, Cham.

Bruzzone A.G., Massei M., Poggi S., Bartolucci C., Ferrando A.(2015) Intelligent agents for human behavior modeling as support to operation. Simulation and Modeling Methodologies, Technologies and Applications, Springer, pp. 119-132.

Bruzzone A.G., Massei, M., Longo, F., Poggi, S., Agresta, M., Bartolucci, C., & Nicoletti, L. (2014). Human Behavior Simulation for Complex Scenarios based on Intelligent Agents. Proceedings of the 2014 Annual Simulation Symposium, SCS, San Diego, CA, April.

Bruzzone, A. G., Viazzo, S., Briano, C., & Massei, M. (2004). Modelling Human Behaviour in Industrial Facilities & Business Processes. SIMULATION SERIES, 36(2), 15.

De Gloria, A., Bellotti, F., & Berta, R. (2012). Building a comprehensive R&D community on serious games. Procedia Computer Science, 15, 1-3.

Gargeya, V. B., & Brady, C. (2005). Success and failure factors of adopting SAP in ERP system implementation. Business process management journal, 11(5), 501-516.

Géron, A. (2017). Hands-on machine learning with Scikit-Learn and TensorFlow: concepts, tools, and techniques to build intelligent systems. "O'Reilly Media, Inc.".

Krumbholz, M., & Maiden, N. (2001). The implementation of enterprise resource planning packages in different organisational and national cultures. Information systems, 26(3), 185-204.

Massei, M., Poggi, S., Agresta, M., & Ferrando, A. (2014). Development planning based on interoperable agent driven simulation. Journal of Computational Science, 5(3), 395-407.

Montgomery, D. C. (2017). Design and analysis of experiments. John Wiley & Sons, NYC.

Author's Index

ISBN 978-88-85741-25-6; Affenzeller, Bruzzone, Longo and Pereira Eds

ISBN 978-88-85741-25-6; Affenzeller, Bruzzone, Longo and Pereira Eds

ISBN 978-88-85741-25-6; Affenzeller, Bruzzone, Longo and Pereira Eds